



ASTES

Advances in Science, Technology & Engineering Systems Journal



VOLUME 4-ISSUE 6 | NOV-DEC 2019

www.astesj.com

ISSN: 2415-6698

EDITORIAL BOARD

Editor-in-Chief

Prof. Passerini Kazmerski
University of Chicago, USA

Editorial Board Members

Prof. Rehan Ullah Khan
Qassim University, Saudi Arabia

Prof. María Jesús Espinosa
Universidad Tecnológica
Metropolitana, Mexico

Dr. Hongbo Du
Prairie View A&M University, USA

Dr. Nguyen Tung Linh
Electric Power University,
Vietnam

Tariq Kamal
University of Nottingham, UK

Sakarya University, Turkey

**Dr. Mohmaed Abdel Fattah
Ashabrawy**
Prince Sattam bin Abdulaziz
University, Saudi Arabia

**Mohamed Mohamed Abdel-
Daim**
Suez Canal University, Egypt

Dr. Omeje Maxwell
Covenant University, Nigeria

Prof. Majida Ali Abed Meshari
Tikrit University Campus, Iraq

Dr. Heba Afify
MTI university, Cairo, Egypt

Regional Editors

Dr. Hung-Wei Wu
Kun Shan University, Taiwan

Dr. Maryam Asghari
Shahid Ashrafi Esfahani, Iran

Dr. Shakir Ali
Aligarh Muslim University, India

Dr. Ahmet Kayabasi
Karamanoglu Mehmetbey
University, Turkey

Dr. Ebubekir Altuntas
Gaziosmanpasa University,
Turkey

Dr. Sabry Ali Abdallah El-Naggar
Tanta University, Egypt

Aamir Nawaz
Gomal University, Pakistan

Dr. Gomathi Periasamy
Mekelle University, Ethiopia

Dr. Walid Wafik Mohamed Badawy
National Organization for Drug Control
and Research, Egypt

Dr. Abhishek Shukla
R.D. Engineering College,
India

Abdullah El-Bayoumi
Cairo University, Egypt

Ayham Hassan Abazid
Jordan university of science and
technology, Jordan

Editorial

Advances in Science, Technology and Engineering Systems Journal (ASTESJ) is an online-only journal dedicated to publishing significant advances covering all aspects of technology relevant to the physical science and engineering communities. The journal regularly publishes articles covering specific topics of interest.

Current Issue features key papers related to multidisciplinary domains involving complex system stemming from numerous disciplines; this is exactly how this journal differs from other interdisciplinary and multidisciplinary engineering journals. This issue contains 55 accepted papers in Computer Science and Artificial Intelligence domains.

Editor-in-chief

Prof. Passerini Kazmersk

ADVANCES IN SCIENCE, TECHNOLOGY AND ENGINEERING SYSTEMS JOURNAL

Volume 4 Issue 6

November-December 2019

CONTENTS

- Q² YouTube: Quantitative and Qualitative Information Analysis based Influencer-aware YouTube Channel Ranking Scheme* 01
Ji Hyeon Lee, Hayoung Oh
- A Proposal of TCP Fairness Control Method for Two-Host Concurrent Communications in Elastic WLAN System Using Raspberry Pi Access-Point* 10
Rahardhita Widayatra Sudibyo, Nobuo Funabiki, Minoru Kuribayashi, Kwenga Ismael Munene, Md. Manowarul Islam, Wen-Chung Kao
- An ML-optimized dRRM Solution for IEEE 802.11 Enterprise Wlan Networks* 19
Mehdi Guessous, Lahbib Zenkour
- Monitoring System Using GPS for Logistic's Key Performance Indicator* 32
Abba Suganda Girsang, Triadi Prabowo
- Optimization of Power Balance Transaction Based on Renewable Energy Sources Using Artificial Salmon Tracking Algorithm for Modeling the Interconnected Grid Development* 38
Arif Nur Afandi, Aripriharta, Yuni Rahmawati
- The Relationship of Coalition on Employee Spiritual Engagement: Interplay of Organisational Politics* 45
Isaac Onyeyirichukwu Chukwuma, Emmanuel Kalu Agbaeze, Nkiru Peace Nwakoby, Gertrude Chinelo Ugwuja, Fidelis Odinakachukwu Alaefule, Ifeanyi Leo Madu
- Creating a Digital Twin: Simulation of a Business Model Design Tool* 53
Kira Rambow-Hoeschele, Nick Giani Rambow, Matthias Michael Hampel, David Keith Harrison, Bruce MacLeod Wood
- Fast Determination of Tsunami Source Parameters* 61
Mikhail Lavrentiev, Dmitry Kuzakov, Andrey Marchuk
- Multi Biometric Thermal Face Recognition Using FWT and LDA Feature Extraction Methods with RBM DBN and FFNN Classifier Algorithms* 67
Evan Hurwitz, Chigozie Orji
- The Influence of Adhesive on Roof Tiles Product from Water Hyacinth Fiber Residues* 91
Arkorn Pasilo, Umphisak Teeboonma

<i>Intelligent Wireless System for PV Supervision Based on The Raspberry Pi</i>	94
Youssef Bikrat, Khalid Salmi, Kamal Azghiou, Ahmad Benlghazi, Abdelhamid Benali, and Driss Moussaid	
<i>A Word Spotting Method for Arabic Manuscripts Based on Speeded Up Robust Features Technique</i>	99
Noureddine El Makhfi	
<i>Discriminant Analysis of Diminished Attentiveness State Due to Mental Fatigue by Using P300</i>	108
Kosuke Fujita, Kazuya Miyanaga, Fumiya Kinoshita, Hideaki Touyama	
<i>Learning Literary Style End-to-end with Artificial Neural Networks</i>	115
Ivan P. Yamshchikov, Alexey Tikhonov	
<i>The Potential of Ocean Current as Electrical Power Sources Alternatives in Karimunjawa Islands Indonesia</i>	126
Aris Ismanto, Dwi Haryo Ismunarti, Denny Nugroho Sugianto, Siti Maisyarah, Petrus Subardjo, Agus Anugroho Dwi Suryoputro, Hendry Siagian	
<i>Spiral Curve for Revocable Touchless Fingerprint Template Securitisation</i>	134
Tahirou Djara, Boris Sourou Zannou, Antoine Vianou	
<i>A New Wire Optimization Approach for Power Reduction in Advanced Technology Nodes</i>	140
Jalal Benallal, Lekbir Cherif, Mohamed Chentouf, Mohammed Darmi, Rachid Elgouri, Nabil Hmina	
<i>Coordination between Heterogeneous Models Using a Meta-model Composition Approach</i>	147
Naima Essadi, Adil Anwar	
<i>Simulation and Reproduction of a Manipulator According to Classical Arm Representation and Trajectory Planning</i>	158
Ahmad Yusairi Bani Hashim, Silah Hayati Kamsani, Mahasan Mat Ali, Syamimi Shamsuddin, Ahmad Zaki Shukor	
<i>Evaluation of Classroom Furniture Design for Ecuadorian University Students: An Anthropometry-Based Approach</i>	163
Pablo Pérez-Gosende	
<i>Quranic Reciter Recognition: A Machine Learning Approach</i>	173
Rehan Ullah Khan, Ali Mustafa Qamar, Mohammed Hadwan	
<i>Data Dashboard for Decision Support Systems for Intrapreneurship in A Company</i>	177
Evaristus Didik Madyatmadja, Evaristus Didik Madyatmadja, Alvi Sasqia Putri, Siti Sabilul Hiqna, Wigna Pratita	

<i>A Joint Source Channel Decoding for Image Transmission</i> Slim Chaoui, Osama Ouda, Chafaa Hamrouni	183
<i>Integration of Third-Party Routing Stack to NetScaler CPX</i> Shreyas K K, Abhishek H P, Sneha M, Shobha G, Deepak Kumar	192
<i>The Correlation of the Specific and Global Performance of Teachers in UNTELS Engineering Schools</i> Omar Freddy Chamorro Atalaya, Dora Yvonne Arce Santillan, Jorge Isaac Castro Bedriñana, Yesica Pamela Leandro Chacón, Martin Díaz Choque	196
<i>Comparative Analysis of Student Dissatisfaction of the Continuing Academic Semesters at UNTELS</i> Omar Freddy Chamorro Atalaya, Dora Yvonne Arce Santillan, Jorge Isaac Castro Bedriñana, Teodoro Neri Díaz Leyva, Denisse Marie Barrientos Pichilingue	203
<i>Eye Feature Extraction with Calibration Model using Viola-Jones and Neural Network Algorithms</i> Farah Nadia Ibrahim, Zalhan Mohd Zin, Norazlin Ibrahim	208
<i>Development of Evaluation Metrics for Learners in Unplugged Activity</i> Woochun Jun	216
<i>SCMS: Tool for Assessing a Novel Taxonomy of Complexity Metrics for any Java Project at the Class and Method Levels based on Statement Level Metrics</i> Issar Arab, Bouchaib Falah, Kenneth Magel	220
<i>Attacks classification and security mechanisms in Wireless Sensor Networks</i> Amine Kardi, Rachid Zagrouba	229
<i>Current Trends and Challenges in Link Prediction Methods in Dynamic Social Networks: A Literature Review</i> Elfadil Abdalla Mohameds, Nazar Zakis2, Mohammad Marjans	244
<i>Optimization of the Electrical Discharge Machining of Powdered Metallurgical High-Speed Steel Alloy using Genetic Algorithms</i> Mohd Razif Idris, Imad Mokhtar Mosrati	255
<i>Prediction of Demersal Fishing Ground Associated with Coral Reefs in the Coastal Jepara Regency, Central Java, Indonesia Based on Sentinel 2a Imagery</i> Kunarso, Muhammad Zainuri, Denny Nugroho Sugianto, Jarot Marwoto, Hariyadi, Muslim	263
<i>Multiscale Texture Analysis and Color Coherence Vector Based Feature Descriptor for Multispectral Image Retrieval</i> Devulapalli Sudheer, Rajakumar Krishnan	270

<i>Smart Ambulance: Speed Clearance in the Internet of Things paradigm using Voice Chat</i>	280
Noor A.Hussein, Mohamed Ibrahim.Shujaa	
<i>Designing and Using a MySQL Database for Human Resource Management</i>	285
Evaristus Didik Madyatmadja, Chelsea Adora	
<i>Fuzzy Modelling using Firefly Algorithm for Phishing Detection</i>	291
Noor Syahirah Nordin, Mohd Arfian Ismail, Vitaliy Mezhuyev, Shahreen Kasim, Mohd Saberi Mohamad, Ashraf Osman Ibrahim	
<i>BPMN4 Collaboration: An Extension for collaborative Business Process</i>	297
Leila Amdah, Adil Anwar	
<i>A Comparative Study of Safety Leading and Lagging Indicators Measuring Project Safety Performance</i>	306
Sevar Dilkhaz Salahaddin Neamat	
<i>Fabrication of Glaze Material from Recycled Bottle Glass and Kaolin</i>	313
Agus Dwi Anggono, Elkana Bilak Lopo, Joko Sedyono, Tri Widodo Besar Riyadi	
<i>MIMO Fractional Order Control of a Water Tank Plant</i>	321
Arturo Rojas–Moreno, Juan Hernandez–Garagatti	
<i>A Method for Mosaicking Aerial Images based on Flight Trajectory and the Calculation of Symmetric Transfer Error per Inlier</i>	328
Daniel Arteaga, Guillermo Kemper, Samuel G. Huaman Bustamante, Joel Telles, Leon Bendayan, Jose Sanjurjo	
<i>Study of MX/M/1 Queueing System with Vacation, Two kinds of Repair facilities and Server Timeout</i>	339
Naga Rama Devi Vedala, Yadla Saritha, Ankam Ankamma Rao, Gaddam Sridhar	
<i>Multi-Stage Enhancement Approach for Image Dehazing</i>	343
Madallah Alruwaili	
<i>Fire System for an Automated Electrical Substation via Programmable Logic Controller</i>	353
Omar Freddy Chamorro Atalaya, Dora Yvonne Arce Santillan, Martin Diaz Choque	
<i>Experimental Analysis in Alternate Current and Direct Current of the Operating Parameters of a Universal Single-Phase Engine</i>	360
Omar Freddy Chamorro Atalaya, Nel Yuri Huaita Ccallo, Luis Enrique Rojas Vicuña, Rudy Jesús Capa Ilizarbe, José Arturo Pillco Torres, José Jean Franco Ramos Rupay	

<i>Design and Analysis of Frequency Reconfigurable Antenna Embedding Varactor Diodes</i>	371
El Mustapha Iftissane, Moulay Driss Belrhiti, Seddik Bri, Jaouad Foshi, Nawfal Jebbor	
<i>A Multi-Objective Voltage Optimization Technique in Distribution Feeders with High Photovoltaic Penetration</i>	377
Temitayo Olayemi Olowu, Mohamadsaleh Jafari, Arif Sarwat	
<i>Novel Cost Function based Motion-planning Method for Robotic Manipulators</i>	386
Daniel Szabo, Emese Gincsaïne Szadeczky-Kardoss	
<i>Multi-period Quadratic Programming Model for Sewon-Bantul Facultative Ponds Optimization</i>	397
Sunarsih, Sutrisno	
<i>Performance Analysis of Routing Protocols in Resource-Constrained Opportunistic Networks</i>	402
Aref Hassan Kurd Ali, Halikul Lenando, Mohamad Alrfaay, Slim Chaoui, Haithem Ben Chikha, Akram Ajouli	
<i>An Exploratory Qualitative Study of the Influence of Hospital Logistics Factors on Quality of Care and Patient Satisfaction at Public Hospitals in Morocco</i>	414
Youness Frichi, Fouad Jawab, Said Boutahari	
<i>Alleviation of Nonlinear Impact Using PAPR Hybrid Technique in CO-OFDM Systems</i>	423
Liqaa A. Al-Hashime, Sinan M. Abdul Satar, Ghaida A. Al-Suhail, Osama Saied	
<i>Linear Logic Synthesis of Multi-Valued Sequential Circuits</i>	430
Nikolay Butyrlagin, Nikolay Chernov, Nikolay Prokopenko, Vladislav Yugai	
<i>CSFs for the Implementation of the Hybrid Lean ERP System. Stakeholders Interactions</i>	443
Mariam Houti, Laila El Abbadi, Abdellah Abouabdellah	

Q²YouTube: Quantitative and Qualitative Information Analysis based Influencer-aware YouTube Channel Ranking Scheme

Ji Hyeon Lee¹, Hayoung Oh^{*2}

¹Ajou University, Department of English Language and Literature, Suwon, Korea

²Ajou University, DASAN University College, Suwon, Korea

ARTICLE INFO

Article history:

Received: 14 June, 2019

Accepted: 08 October, 2019

Online: 20 November, 2019

Keywords:

Quality aware YouTube
Ranking scheme

Flipped learning maximiza-
tion

Influencer Analysis

Data analysis

ABSTRACT

With the development of big data, artificial intelligence and deep learning, various social information networks are becoming exponentially intelligent. Of all the various social networks, YouTube is so popular that it is called the YouTube era. Not only video viewers, but also actual video producers, influencer youtubers, are increasing, allowing individuals as well as operators to use and market contents on various topics. As the number of users and contents increases, the choice of information increases, but it is more difficult for individual and business owners to select information that meets their needs. Therefore, this study aims to analyze the channel of the subject that the user needs from various angles and provide the ranking of the channel to individuals and businesses. We crawl the channels and measure the average awareness and influencer youtuber of channels and channel videos by analyzing the qualitative data of quantitative data and comments which are statistical information. As a final case study, we recommend the English learning channel to individual users based on numerical data statistics and emotional analysis results to show the maximum of flipped learning effect regardless of time and space. Plus, we prove the maximum of the effectiveness of marketing by influencer channel which is influential to operators in the medium and long term.

1 Introduction

There are about 3.4 billion people using social media (SNS) among 7.6 billion people worldwide. Compared with the year 2018, about 280 million people started the SNS within a year. Especially with the development of big data, artificial intelligence and deep learning, various social information networks are becoming exponentially intelligent. One of them, YouTube is the most famous social platform for satisfying various objects such as users as well as businesses on top of the recommender system. However, as the development of technology and the emergence of big data have caused the exponential growth of YouTube channels, users are having difficulties in selecting personalized videos. In other words, users have difficulty in selecting a channel on top of the basic recommendation of YouTube, and they spend additional time searching for a good channel or comparing contents directly [1]–[4]. In aspects of the business operator, the new influencer marketing on top of YouTube data analysis is also emerging as a new and successful marketing strategy. Influencers are

influential individuals, which can include the general public as well as entertainers and SNS stars. Using the recommendation on top of the influencer aware YouTube data analysis, the general public can easily consume the contents and at the same time be satisfied with the content.

As the application case studies based on influencer aware YouTube data analysis, in this paper we introduce the possibility of the flipped learning maximization of user education as well as business marketing satisfaction.

Regardless of age, interest in lifelong education has increased in various fields such as English and Chinese, and various contents based on smartphone such as internet lecture, radio, and learning application are attracting attention. As the number of smartphone users increases, demand for online content is growing more than offline. However, since the above-mentioned online service requires the motivation of the user to voluntarily learn, the more the time passes, the less motivated and the less interested in learning.

The popularity of the YouTube-based beyond time and space learning is increasing due to the characteristics of these

*Corresponding Author: Hayoung Oh, Address, Contact No & hyoh79@gmail.com

online learners. Internet lectures are similar to flipping learning in pedagogy, which is not an existing concept of 'off-line class', but can be learned anytime and anywhere by transcending time and space. In particular, Youtube provides big data that can be analyzed statistically of videos that are composed by influencer Youtuber in a free environment and have lots of choices in social network, so it can maximize the effect of flipped learning education. In other words, influencer aware YouTube video ranking based education does not require as much concentration as text-oriented education, and users can use it for free time very effectively. In particular, influencer aware YouTube video ranking based online education can maximize the effectiveness of education because it shows the candid reviews of ordinary users and the cases that are natural but helpful in real life on top of big data analysis quantitatively and qualitatively. Similar to the general online education methodologies, the influencer YouTube aware flipped learning education can solve the physical limitations and anyone can be educated in real time or streaming (pre-recorded streaming).

In aspects of the business operators, influencer aware YouTube data analysis based the marketing has become a new and solid strategy. As of February 2017, people spent 25.7 billion minutes on YouTube, a video platform. This shows that YouTube spending time has more than tripled in the past two years compared to 2015. In other words, research in video and photo-based YouTube influencers analysis techniques is critical in aspects of users and businesses, as it indicates that people are more interested in video content than text content over time. Specifically, if the business operators recommend the personalized video to the users by referring the features of influencer Youtuber with high quantitative and qualitative data analysis, the satisfactions of the users as well as businesses can be maximized. Different from the previous related schemes of YouTube big data analysis, we consider velocity, veracity(Truth), value as well as volume and variety among five characteristics of big data.

As a result, in this paper, we propose an influencer aware YouTube ranking scheme for the channel recommendation technique to maximize the satisfaction of users as well as the businesses. As mentioned before, we show the flipped learning effect through explicit and implicit analysis of various data of the influencer provided by YouTube centering on the YouTube English learning channel. Based on numerical data such as the number of views and likes of channels collected by using Google and R's tuber package for four channels with the same ranking of the social channel. The primary statistic is given and those of positive and negative are calculated through emotional analysis of the comment. Finally, based on the numerical data statistics and emotional analysis results, the English learning channel is recommended to the user to maximize the flipped learning effect and the business satisfaction regardless of time and space. In future, the proposed method can be used for flipped learning of various contents because it can be used for analysis of big data of influencer aware YouTube channel in various fields as well as language field.

2 Related Work

Recently, in an environment where big data has grown exponentially, personalized recommendations are a great way to efficiently search for information and discover content with high satisfaction.

2.1 Recommender system

Based on how designing recommender systems, the recommendation systems are usually classified into the following categories [5]–[8]: Collaborative recommendation systems; Content-based recommendation systems; and Hybrid recommendation systems.

Collaborative filtering is currently the most wise and popular approach because of focusing more on rating-based recommendations. The collaborative methods predict the utility, preference or taste of items per a particular user using the items previously rated by other users as shown in figure 1.

On the other hand, content-based approaches are generally based on classical information retrieval such as keywords as content descriptors. Therefore, the content-based methods are very popular for recommending documents, news articles or web pages. Lastly, the hybrid systems [9, 10] is to combine two or more different approaches to maximize desirable properties.

	Item ₁	Item ₂	Item ₃	...	Item _n
User ₁	0	3	4	...	5
User ₂	1	1	2	...	?
:	:	:	:	...	:
User _m	4	?	5	...	4

Figure 1: Collaborative recommendation systems

2.2 Social Network aware Recommender system

Youtube, which efficiently provides dynamic data such as video among various contents, is gaining popularity around the world. Although a basic recommendation system on the YouTube platform is installed to recommend high-profile videos, personal satisfaction is not high. Three factors can be used to determine ranking of recommendation systems. These are each of video quality, user specificity and diversity. The quality of the video includes quantitative information such as views, comments, favorites, upload time, and so on. User specificity is related to individual taste and preference. The way to check this is to consider the number of views or watch time of the watch record. Thereafter, in order to maintain the diversity of the video, there is a method of limiting the number of videos of the same channel [11]. In [12], the authors designed the recommendation system in consideration of the factors. In [13]–[16], different studies have attempted to verify the significance of influencer decision through R-based data analysis rather than heuristic

judgment. In this case, the data commonly used are nine characteristics (i.e., features) such as total number of views of the channel, number of videos of the channel, average number of videos views of the channel, number of channel subscribers, likes and dislikes of each video. In [13], the authors tried to normalize covariance of each variable and analyzed the correlation between each variable with views of the subordination variable. Plus, they proved that the average number of views on the channel and the number of subscribers on the channel had a positive relationship with the number of views. However, the degree of correlation was insufficient, and the statistical data alone have limitations in producing significant results, such as the determination of video recognition, etc. In [14], the authors first focused on the influencer YouTube data analysis with accompanying the 50 channels made using the blind date app 'swipe'. With the data, the release date of the video, likes, dislikes, the number, video length, hash tag count, total number of views of channels, number of videos of channels, average number of video views of channels, number of channel subscribers were analyzed as variables, and Principal Component Analysis and Multiple Regression Analysis were performed as well as R-based data analysis. The cumulative contribution rate of PCA1 and PCA2 was more than 80% of the total to compared these two factors to determine the importance of each variable. For the first component, the average number of views on the channel, comments on swipe videos, views on swipe videos, and likes of videos were -1.25, -2.6, -2.49, and -2.83, respectively, showing a strong negative value, while the video length of swipe video and the hashtags of swipe video were 3.31 and 1.95, respectively, showing a strong positive value. The second component showed a negative value with the number of views and video subscribers, and a weak positive value with the length of the video and tag count. In addition, author concluded that the number of videos of the channel is most influential on the influencer attribute decision model among the variables when the two components are judged synthetically. In Multiple Regression Analysis, only the number of videos reveals significance. However, the limitation of the Principal Component Analysis was that the differences among the variables were large, and for Multiple Regression Analysis, there is a mismatch with the Principal Component Analysis results, therefore the study also has a limit. In [15], the authors analyzed the comment of each video with time to demonstrate the continuing influence of YouTube Influencer. The group is classified as "Large group" and "Small group" based on the total number of comments. In the case of "Large group", the number of comments per an hour is similar and the decreasing width is constant over time. In the case of "small group" is assumed that the number of comments per an hour is irregular, and that the decreasing width is not constant over time. Accordingly, the paper selected the "Big3" of the group and used the decreasing width and consistency obtained through the existing "Large group" and "Small group" as an evaluation indicator. In the case of decreasing width, the smallest percentage was 3% and the largest percentage 2%. For consistency, the standard deviation was used, and

the results were derived that the standard deviation of the "Large group" was relatively small compared to the standard deviation of the "Small group." This has proven that "Large group"'s influencer continues to receive people's attention in a stable manner. However, the limitations still exist because of the lack of connectivity with the recommendation system of YouTube through high-profile video analysis.

In [16], the authors proposed the importance of the analysis of the comments quantified through the questionnaire and suggested the link between the analysis of the comments and the generation of profits. According to the survey, 12 percent of users post their opinions on a regular basis, which means about 96 million people are actively writing their opinions, considering the size of the YouTube community is estimated at 800 million. Also, 34 % of the respondent of investigation read comments frequently and read comments 2-3 times after watching 53 % of the video. In the case of comments, those received a lot of likes if those were reasonable, practical and content-customized, and eventually showed that it could be used to increase the popularity of the videos and make profits. However, the existing study also has limitations due to the lack of connectivity with the recommendation system of YouTube through high-profile video analysis, and there is a limit to analyzing human contradictory behavior. In [17] the authors used YouTube comment analysis, TF-IDF (term frequency inverse document frequency) and Association Rule Analysis to select influencers. Comment analysis used the B-rated YouTube channel when searching for "English study", "English education" and "English learn" on the social blades that provide the YouTube ranking system. The comparison of TF (Terminal Frequency) and TF-IDF analysis then demonstrated that the TF-IDF analysis elicited more significant words. For example, when word analysis was conducted with the frequency of words (TF), common words related to learning such as "learn" and "lesson" or words that had nothing to do with the video content such as "love," "video" and "channel" were heavily weighted. In contrast, for TF-IDF analysis, words related to video content such as "resort," "plan," "proposal," "vegan," and "vegetarian" are expected to be talking about travel first and vegetarian second. Compared to TF analysis, TF-IDF extracts features of each video content and shows them well. Finally, the association among words was analyzed through the Association Rule Analysis. As a result of the Association Rule Analysis, the authors can see that words with high TF are generally generated as rules. In case of using TF-IDF, there is a limit to judge the association among words heuristically. In the case of Association Rule Analysis, the rules are generated based on the frequency of words in general, so that only meaningless words are repeated in the YouTube environment. However, the paper is considered to provide a cornerstone of the proposed technique because it found that the two methods can be only applied to select the influencers. Recommender systems of [18] collects information about users and businesses and how they are related. The recommender systems let users share their reviews about products, places, establishments or services. If a product receives more votes or reviews, it

becomes more popular among customers.

It is expected that higher number of positive reviews is beneficial for marketing's success of the product. Interactions based on user's followers are usually allowed by recommender systems. A user is considered a fan of another user when there's no personal relationship between them but still the former wants to see the latter's posts in his or her own main page. This type of social link is based on interests and affinities with celebrities, special products, places or common interests. When a review is posted, it is seen by the submitter's friends and followers, increasing its chances of readings about the reviewed product or place. The more social links a user has, the more persons will likely read the review. This social component has become an interesting aspect of recommender systems because it allows an increase of popularity of a product or place. In the case of the recommendation system mentioned in the thesis, the user-to-user social network is formed through the follow, and is also distinguished by the user-user fan through the interaction relationship. In general, reviews by users with many social networks (users with many fans) are more likely to be accessed by more users. These characteristics are an interesting part of the recommendation system, and many businesses approach these users for satisfaction. This proves that the existing research direction of recommending to companies for profit generation is reasonable. The current model excludes text analysis, but acknowledges that the analysis of comments exerts an influence on Influencer's numerical data.

3 System Model

The data used for the proposed scheme was based on 54 channels of influence, which produced promotional videos on the "Enligh Education" related channel. The videos are easy to use influencer attribute analysis because general public influencer can directly produce video and observe other users' reactions in various formats such as numerical information and comments on YouTube. YouTube's visible numerical data shows the date of creation of each video, likes, dislikes, length of the videos, number of hash tags, total number of views on the channel, the number of videos on channel, average number of views on the channel's video, and number of channel subscribers. The primary analysis of suggested techniques is to look at their correlation using various numerical data provided on YouTube quantitatively. At this time, the set hypothesis is that "if the correlation of each numerical data is high, can it be judged unconditionally that the recognition of the corresponding video is high?" In general, it is easy for general users to judge the quality of channel and video by trusting only the numerical data based ranking system of YouTube. However, since the average number of views of a channel is increased with only single click of a YouTube video, the actual playback time is unknown, such as whether the user actually viewed the videos, which parts of the videos were particularly popular, or whether they stayed for a certain period of time, rather than simply clicking them. In

addition, YouTube does not provide access to statistics and visualization information (e.g., demographics information) of the audience, such as age, gender, etc., which videos are usually viewed highly by which user class. Therefore, we simultaneously analyze influencer YouTube data quantitatively and qualitatively as shown in figure 2

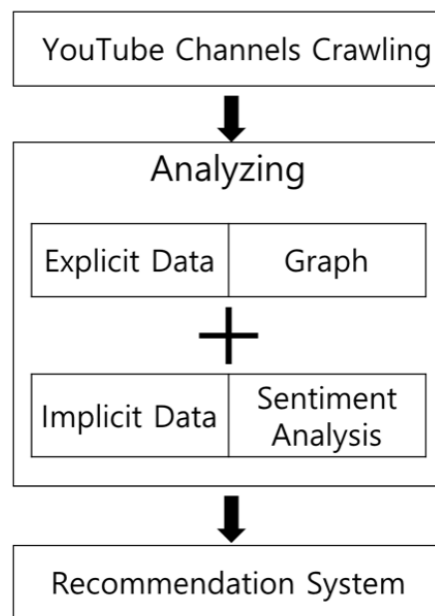


Figure 2: Recommendation System analysis flowchart

In detail, the English learning channels corresponding to B level, which is the self-rating of the social blade, were filtered based on the influencer criteria of the social network data. Those are the number of subscribers, English learning channels, which have a much higher number of views and likes, generally have a higher level awareness of videos as well as the number of videos with the long days of channel opening. We chose channels that were opened between 2016 and 2018 to allow for the latest videos of channel. The YouTube channel has its own concept, and English learning channels are largely divided into lecture type and talker type. One of the reasons that users prefer YouTube over Internet lectures is because they can learn English through content that is not formal and has a free atmosphere. Therefore, focusing on the talker-type channel except for the lecture type, we conducted research on ETK English, Interactive English, JForrest English and Real English With Real Teachers.

The study method used the statistical analysis software R tuber package. There are research [10] that used the chrome extension tool SelectorGadget. However, due to the limitations of the crawlable area due to the manual selection of the user and lack of real time property, considering the characteristics of R in which various packages exist, a tuber package for YouTube is used. We crawled the data on YouTube and explicitly extracted a statistical graph for the primary numerical social network data. Afterwards, we crawled the comment big data for each video on each channel through the package

for YouTube data access only and the Google open API, and performed the YouTube data qualitative analysis.

The overall research process is shown in figure 2

After crawling YouTube channel data in the Tuber package, we set up different research methods for each data type quantitatively and qualitatively. The social numeric data such as the number of likes and subscribers extracts the graph based on the mutual relationship and applies the qualitative approach through the emotional analysis to the comment data in which the opinions of actual users are reflected on the channel.

4 Proposed scheme

4.1 Research technique

YouTube provides statistics on channel and channel video. In this study, channel information and channel video information are distinguished from each other because channel and channel video are different. We use the number of subscribers to measure channel itself awareness. The recognition of channel videos is based on qualitative data analysis using comment data analysis as well as quantitative data such as number of views, likes, and comments. Therefore, the recognition of one channel, that is, the number of subscribers, is not popular and highly rated. After analyzing the quantitative and qualitative data of the channel and the channel video, the channels are ranked by synthesizing them.

4.1.1 Crawling

After selecting the influencer channels to be ranked, call the channel ID from the YouTube url address as follows and use the R tuber package to crawl the statistical information like followings. <https://www.youtube.com/channel/> (Channel ID). When we enter the YouTube channel main screen, the above url address is generated, and the last part is the channel ID. The channel information is coded by entering the channel ID into the `get_channel_stats` function of the tuber package. The `yt_search` function calls up the video list of the channel, and the video statistics information is also retrieved using the ID of each video in the same manner as above. In order to organize the crawled statistical information by video and channel, the title and channel name are added to the same row and stored as a data frame. Each channel is refined in the same manner as described above, and then organized into one data frame. Then, column names such as "Title", "Likes", "Views", "Subscriptions", "Channel" The video title defines character type, number of likes, number of views, number of subscribers as integer type, and channel name as factor type.

The comment data corresponding to the qualitative data also uses the tuber package. A comment on the video is called up to generate a comment data frame for each channel, which consists of a comment and an video ID in one row. This identifies channel names as well as quantitative data.

4.1.2 Quantitative Data Analysis

The results of quantitative data analysis are graphically displayed for visualization. Quantitative data is a measure of channel awareness and channel video awareness, and uses statistics provided by YouTube. The awareness of the channel is the number of subscribers, and the video recognition per channel is confirmed by the number of views, likes, and comments. Since the number of subscribers and the number of comments are fixed, they can be displayed as a bar graph. The reason why the number of comments in a video is classified as a fixed value is because the comment does not need to consider the deviation for each video fairly. Since the number of comments is a measure of how much viewers are interested in the channel, we consider only fixed values equally. On the other hand, the number of views and likes are taken into account for distribution and the deviation is taken into account by video.

4.1.3 Qualitative data analysis

In this study, the comment data is analyzed at the same time as the statistical data provided by YouTube. Likes, in addition to the number of subscribers, we can rate those channels and videos with the feedback from people who actually watched the video. It is difficult to judge that the number of views is high because it can be climbed even if the user clicks the video once even if the viewer does not watch the video to the end. On the contrary, it is possible to determine whether the video is good or not by checking whether the user has stayed in the video for a longer time, that is, whether the video has been watched until the end. Comments on video, except spam, are mainly left after watching video, mainly video related content. The higher the ratio of the result, the comment and the video content match, the more the commenter will see the video. Therefore, the comment analysis can be used to determine whether the video is suitable for ranking highly. To understand the correlation between video and comment, we invoke video script and comment file and refine data. Sort videos and comment data classified by corpus by frequency. Then, the comment data is compared with the video data, and the matching word is denoted by 1, and the non-matching word is denoted by 0. Scoring function is used to score differently for each frequency, divided by the total number of corpus and expressed as a ratio.

That is, the proposed scheme used Term Frequency (TF) to measure the frequency of each video based on script and comments. If the comment data matches the script, a list of the words is generated. The more words and duplicates in scripts and comments, the more the subject and content match. As the number of words in the list increases, it means that the viewer has a high degree of understanding and understanding of the video. Therefore, the video is recommendable to other users with the increasing recommendation reliability by weighting the degree of correspondence between video and comment. The response of the viewer, that is, the content of the comment, becomes the criteria.

The proposed scheme also consider Inverse Document Frequency (IDF) for TF-IDF (Term Frequency-Inverse Document Frequency). The TF-IDF (Term Frequency-Inverse Document Frequency) is often used for keyword extraction and similarity between documents. The higher the value of the TF indicating the appearance frequency of a word, the higher the importance of the word is, but it is not an absolute measurement method. It is more likely that the word is often used in other documents, and the frequency and importance are inversely proportional. Thus, in many document clusters, we multiply the frequency of occurrence of the word IDF with TF to assign weights to the only frequently appearing words in a particular document. Therefore, we also considered TF-IDF per each channel video for the proposed scheme.

4.1.4 Normalization

Since quantitative data and qualitative data analysis can not be accessed from the same point of view, we use a normalization function. As shown in figure 3, we use the normalization function to integrate the quantitative and qualitative data analysis of each channel to provide the final channel ranking. As shown in figure 3, the reasons for putting the weight on the 20th word list are as follows. As a result of checking the list of words based on the experimental data, word matching ratios up to 20th were distributed on average regardless of the total number of words, and other words showed the same or subtle differences. Therefore, based on the TF-IDF, weights are assigned to the words from the first to the 20th.

Function 1 Scoring

```

1: if Words in MatchingList >=20
2:   for (i in 1:3)
3:     MatchingList[i] = 1.8
4:   for (i in 4:10)
5:     MatchingList[i] = 1.5
6:   for (i in 11:20)
7:     MatchingList[i] = 1.2
8: else
9:   for (i in 1:3)
10:    MatchingList[i] = 1.8
    
```

Figure 3: Normalization scoring function to integrate the quantitative and qualitative data analysis of each channel

The detailed rules for weighting criteria are as follows. The numbers 1 and 0 are assigned to the words that match each other. Since we place weight on words with a high percentage of match between video and comment content, they should be basically higher than the number 1 already granted. Therefore, based on various experiments as shown in figure 4, we have weighed the combinations of various numbers from 1.1 to 2 and confirmed the number that best matches the existing match ratio.

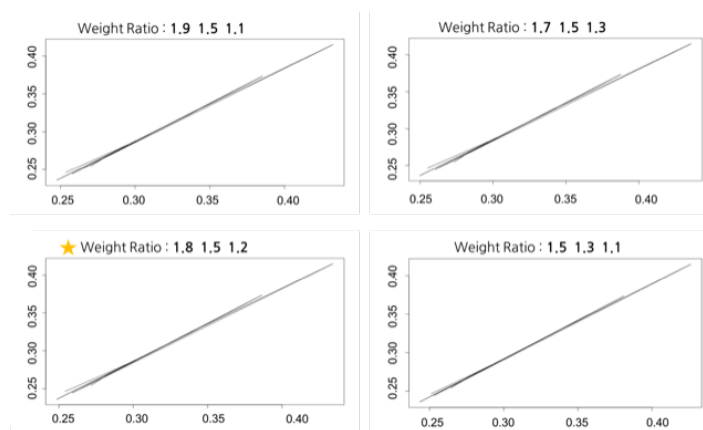


Figure 4: Weight ratio

4.2 Experiment Data

All the performance evaluation codes were written in the R environment suitable for data analysis, and the influencer channels with the subject of English learning were selected as the experimental subject. Four English language channels (English Coach, Interactive English, JForrest English, and Real English with Real Teachers) were selected based on the ratings of social blades that provide social rankings. In order to experiment with the channels that can be compared, we chose channels that can be compared with each other considering the channel information such as the total number of views, the number of subscribers, etc., except for the old channel. Quantitative data and qualitative data were analyzed for each channel. First, quantitative data analysis results are shown in figures figure 5–8.

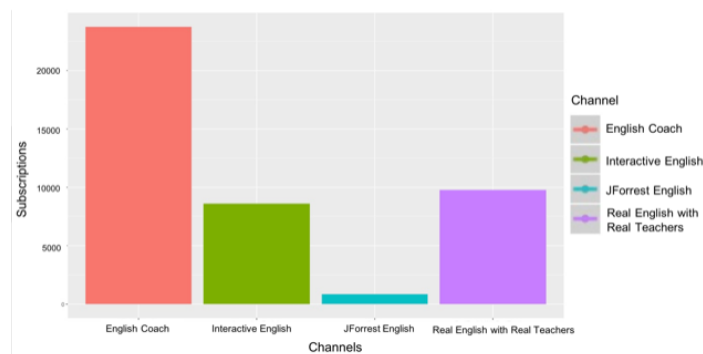


Figure 5: # of subscriber per channel

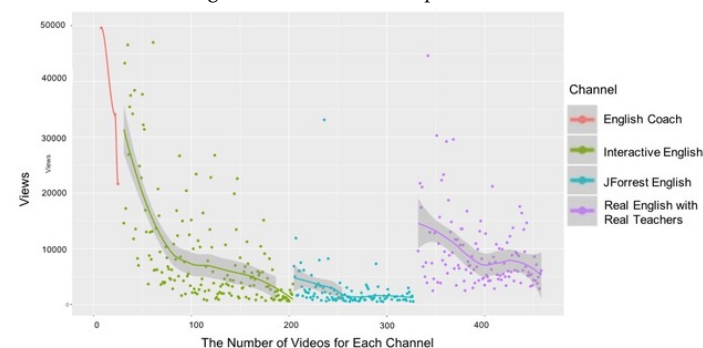


Figure 6: # of video views per channel

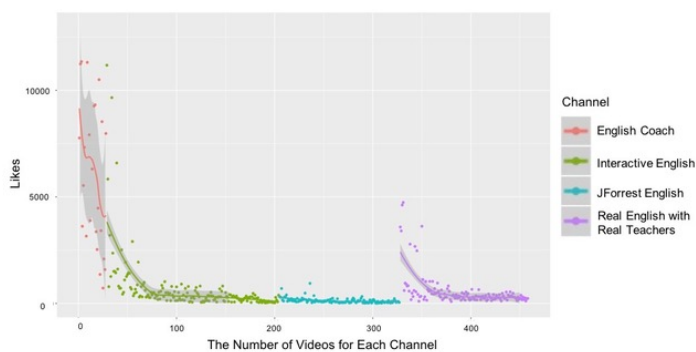


Figure 7: # of video likes per channel

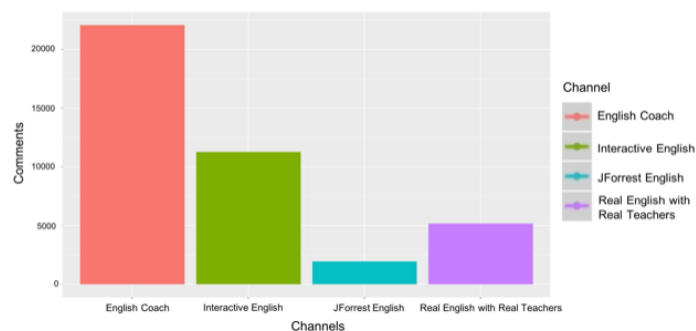


Figure 8: # of video comments per channel

Figure 9 and 10 show additional result graphs when considering different video data sets on the same channel.

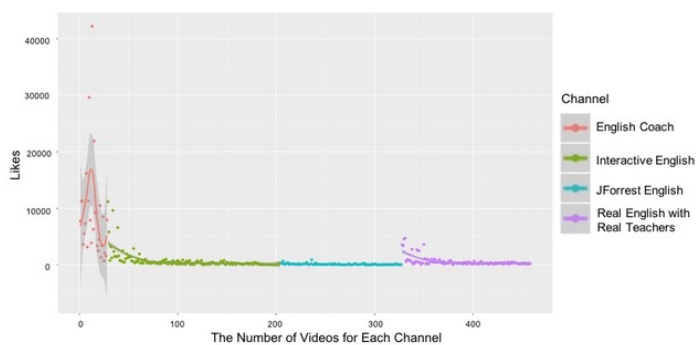


Figure 9: # of video likes per channel

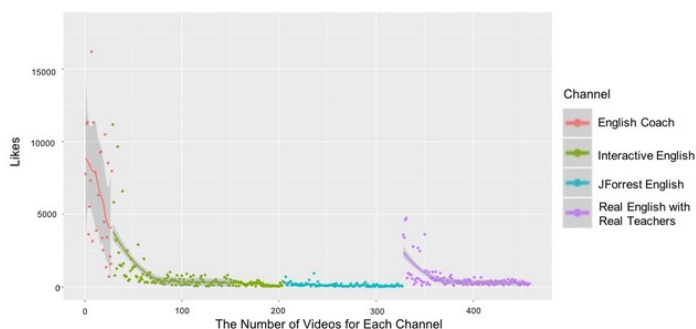


Figure 10: # of video likes per channel

Qualitative data analysis is shown in figure 11. The correlation between videos and comments is compared and scores are given.

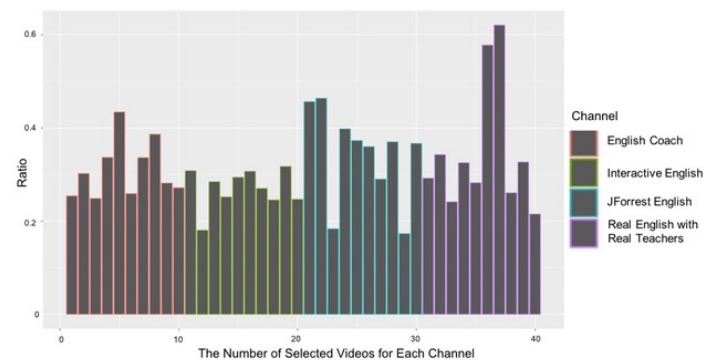


Figure 11: Correlation between video and comments per channel (i.e., Graph Analysis)

The above analyzes are different from each other of x coordinates because the fixed value graph and the distribution graph are mixed. To compare each graph, the analysis standard should be unified. As a result, all analysis results were adjusted through the normalization formula to integrate quantitative and qualitative data.

Figures 12, 13, 14 and 15 show cases where the quantitative data is normalized and re-expressed. Finally, considering both quantitative and qualitative information, it can be expressed as shown in figure 16. As the graph of quantitative and qualitative integrated normalization can be seen, satisfaction with other users can be increased at recommendation (ranking) when video is recommended considering qualitative data at the same time than when considering only quantitative data. Since the user actually watches the video for a long time and has a high probability of making a comment based on the contents of the video. In other words, the proposed scheme is more meaningful than the previous studies, the explicit analysis using the social network data alone, because it does not know the recognition of the video implicitly.

In addition, we found that the recommended videos of the proposed scheme were tracked for a certain period of time based on the same criteria. As a result, the amount of quantitative information such as the number of likes, comments, likes, and subscribers were increases and the quality correlation between video contents and comments was much higher, the performance was better than the existing methods.

In aspects of the business operators, their marketing strategies based on influencer YouTube data analysis were more successful than traditional approaches. Since the number of users and consistency degree between the contents and comments on top of big data analysis quantitatively and qualitatively were more higher with the trace analysis regardless of the time and space.

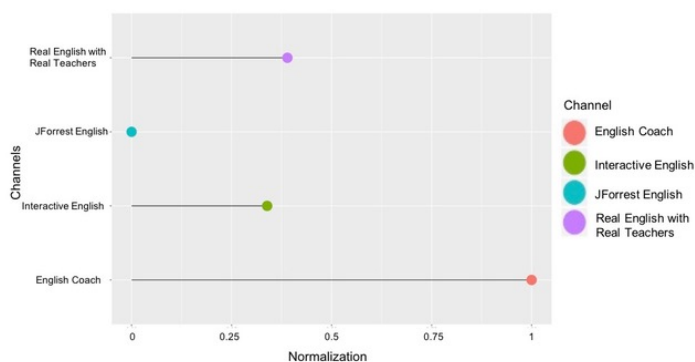


Figure 12: (Normalization) # of subscriber per channel

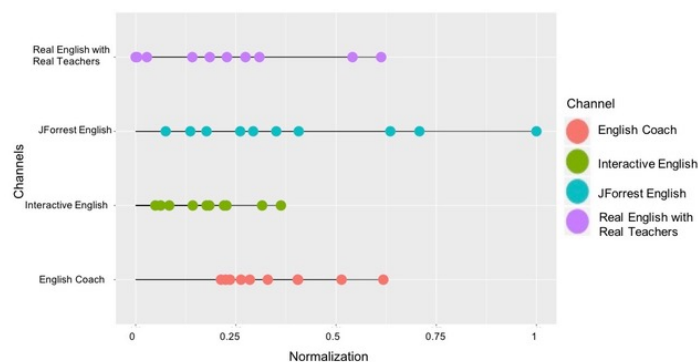


Figure 16: (Normalization) Correlation between video and comments per channel

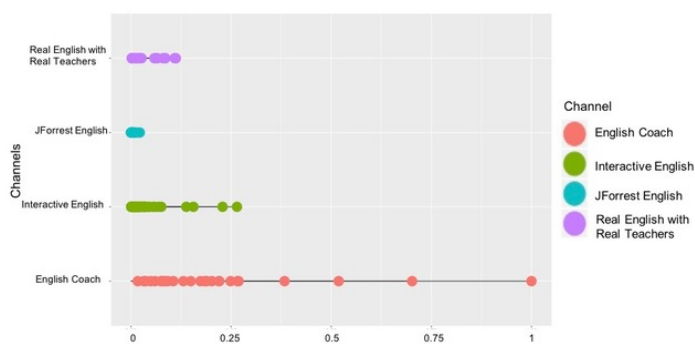


Figure 13: (Normalization) # of video likes per channel

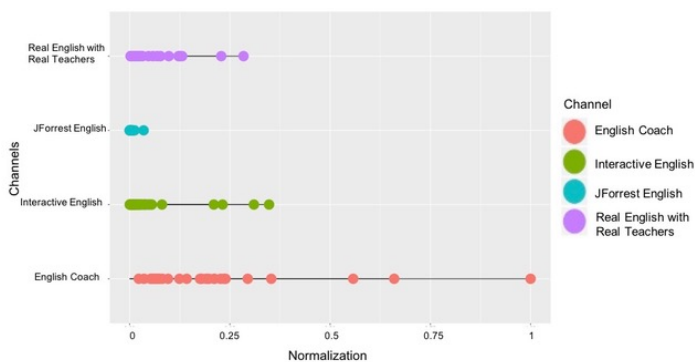


Figure 14: (Normalization) # of video views per channel

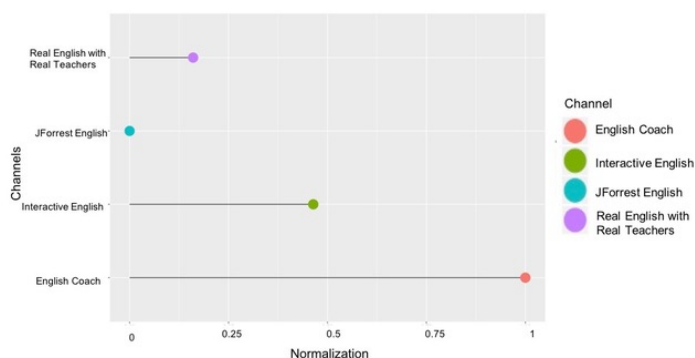


Figure 15: (Normalization) # of video comments per channel

5 Conclusion

With the development of social networks and wired and wireless networks, global users are constantly using YouTube, a huge platform from multiple angles. Although it provides a basic personalized ranking system in YouTube, it is based on simple statistical information. Therefore, it does not support sophisticated ranking and recommendation system by utilizing hidden secret information qualitatively at the same time. In this study, we utilize two factors at the same time, and in particular, we prove that not only highly visible channels but videos are visible. This study is very meaningful because it can recommend the personalized recommendation system and the customized learning channel to the user in the future, and it can lay the cornerstone to lead to the application field that maximizes the flipped learning effect regardless of time and space as well as novel marketing strategy to the business operator.

Conflict of Interest The authors declare no conflict of interest.

Acknowledgment This research was supported by the MIST(Ministry of Science and ICT), Korea, under the National Program for Excellence in SW supervised by the IITP(Institute for Information & communications Technology Promotion)“(20150009080031001), Basic Science Research Program through the National Research Foundation of Korea(NRF) funded by the Ministry of Education(2017R1D1A1B03035557) and Ajou University.

References

- [1] E. Çano, M. Morisio, “Hybrid Recommender Systems: A Systematic Literature Review” *Intelligent Data Analysis*, vol. 21, no. 6, pp. 1487-1524, 2017. <https://arxiv.org/abs/1901.03888>
- [2] A. M. Elkahky, Y. Song, and X. He, “A multi-view deep learning approach for cross domain user modeling in recommendation systems” In *Proceedings of the 24th International Conference on World Wide Web*, New York, NY, USA, 2015. ACM. <https://doi.org/10.1145/2736277.2741667>

- [3] K.J. Oh, W.J. Lee, C.G. Lim, H.J. Choi, "Personalized news recommendation using classified keywords to capture user preference" 16th International Conference on Advanced Communication Technology. <https://doi.org/10.1109/ICACT.2014.6779166>
- [4] P. Chiliguano, G. Fazekas, "Hybrid music recommender using content-based and social information" 2016 IEEE International Conference on Acoustics, Speech and Signal Processing (ICASSP). <https://doi.org/10.1109/ICASSP.2016.7472151>
- [5] I. Munemasa, Y. Tomomatsu, K. Hayashi, T. Takagi, "Deep reinforcement learning for recommender systems" 2018 International Conference on Information and Communications Technology (ICOIACT). <https://doi.org/10.1109/ICOIACT.2018.8350761>
- [6] X. Amatriain, L. Gatos, "Building industrial-scale real-world recommender systems" RecSys '12 Proceedings of the sixth ACM conference on Recommender systems. <https://doi.org/10.1145/2365952.2365958>
- [7] J. Carbonell and J. Goldstein. "Diversity-based Reranking for Reordering Documents and Producing Summaries" In Conference on Research and Development in Information Retrieval (SIGIR), 1998. <http://doi.acm.org/10.1145/290941.291025>
- [8] L. Chen, G. Zhang, and H. Zhou. "Improving the Diversity of Top-N Recommendation via Determinantal Point Process" In Large Scale Recommendation Systems Workshop at the Conference on Recommender Systems (RecSys), 2017. <http://arxiv.org/abs/1709.05135>
- [9] Y. Koren, R. Bell, and C. Volinsky. "Matrix Factorization Techniques for Recommender Systems" *Computer* 42, 8 (2009), 30–37. <http://dx.doi.org/10.1109/MC.2009.263>
- [10] N. Lathia, S. Hailes, L. Capra, and X. "Temporal Diversity in Recommender Systems" In Conference on Research and Development in Information Retrieval (SIGIR), 2010. <http://doi.acm.org/10.1145/1835449.1835486>
- [11] Young Il Chang, Jung You-Soo, "A Study on YouTube Product Review Channel Subscribers' Product Attitude Formation Process," *e-business research*, 20(2), 78, 2019.
- [12] James Davidson, Benjamin Liebald, Junning Liu, Palash Nandy and Taylor Van Vleet, "The YouTube Video Recommendation System" in Proceedings of the fourth ACM conference on Recommender systems Pages 293-296, 2010.
- [13] Minwoo Kim, JeongRyeon Park, Jiwon Park and Hayoung Oh, "Channel Attribute Analysis Scheme for Trustworthy Youtube Influencer Detection", in Proceeding of The 29th Joint Conference on Communications and Information on Big Data and Social Network, 2019.
- [14] Minwoo Kim, JeongRyeon Park, Jiwon Park and Hayoung Oh, "Influencer Attribute Decision-Making based on Principal Component Analysis" in Proceeding of KIPS Conference on Web Science, Korea, pp 672-674, 2019.
- [15] Ji-Won Park, Min-Woo Kim, Jeong-Ryeon Park and Hayoung Oh, "Stable Influencer Selection Criteria Scheme through Youtube Analysis of Hourly Comments" " in Proceeding of Korea Institute of Next Generation Coputing, 2019.
- [16] JeongRyeon Park, Minwoo Kim, Jiwon Park, Hayoung Oh "Influencer Identification based on TF-IDF and association rule analysis" in Proceeding of KIPS Conference on information system, Korea, pp 293-295, 2019.
- [17] Peter Schultes, Verena Dorner, and Franz Lehner, "Leave a Comment! An In-Depth Analysis of User Comments on YouTube" in Proceeding Wirtschaftsinformatik Proceedings 2013. 42, pp659-673, 2013.
- [18] Andres Bejarano, Agrima Jindal, Bharat Bhargava "Measuring user's influence in the Yelp recommender system" in Poceeding of PSU Reasearch review, Vol. 1 No. 2, pp. 91-104, 2017.

A Proposal of TCP Fairness Control Method for Two-Host Concurrent Communications in Elastic WLAN System Using Raspberry Pi Access-Point

Rahardhita Widyatra Sudibyo¹, Nobuo Funabiki^{* 1}, Minoru Kuribayashi¹, Kwenga Ismael Munene¹, Md. Manowarul Islam¹, Wen-Chung Kao²

¹Department of Electrical and Communication Engineering, Okayama University, Okayama, Japan.

²Department of Electrical Engineering, National Taiwan Normal University, Taipei, Taiwan.

ARTICLE INFO

Article history:

Received: 26 July, 2019

Accepted: 30 September, 2019

Online: 20 November, 2019

Keywords:

WLAN

TCP throughput fairness

Raspberry Pi

PI controller

Test-bed

Dynamic hosts

ABSTRACT

The IEEE802.11n based Wireless Local Area Networks (WLANs) have been extensively deployed due to the flexible coverage, the easy installation, and the lower cost. To reduce the energy consumption while increasing the performance, the elastic WLAN system has been studied, such that it can dynamically change the network configuration according to traffic demands. As well, the test-bed has been implemented and for the access point (AP), Raspberry Pi is used as a portable, energy conservation, and powerful computing device. Our test-bed measurements with a single AP of two concurrently communicating hosts found the unfairness throughput results, due to the TCP windows size became different among them. To overcome this drawback, in this paper, we propose the TCP fairness control method for two concurrently communicating hosts in the elastic WLAN system. By controlling the delay at the packet transmission, the slower host will obtain more transmission opportunities than a faster host. The delay is firstly calculated by the received signal strength (RSS) from every host. After that, the delay is controlled by the PI controller to balance the both throughputs. For evaluations, we execute the proposal in the elastic WLAN system test-bed and carry out extensive measurements, where the TCP throughput fairness is achieved.

1 Introduction

The IEEE802.11n based *Wireless Local Area Networks (WLANs)* have been widely adopted around the world due to the characteristics of the flexible coverage, the simple installation, and the low cost [2]. WLAN provides the Internet access by wireless medium and offers a lot of benefits such as mobility, reliability, and portability. Hence the popularity of WLAN is increasing in government offices, private companies, organizations for accessing the internet.

In WLAN, hosts are mostly non-uniformly located [3], and communicating hosts or traffics tends to fluctuate unpredictably [4, 5] according to the period time and in a week. Furthermore, conditions of network devices and communication links may be influenced by certain factors, such as device failures, power shortages, weather changes, or bandwidth controlled by their authorities [6].

Under such circumstances, we have examined the *elastic WLAN system* that dynamically optimizes the network configuration based on demands in a network, to reduce the energy consumption during

the time to improve the performance [7, 8]. In addition, we have developed the *elastic WLAN system test-bed* using *Raspberry Pi AP*. *Raspberry Pi* is a card-size, single-board computer that can solve a variety of practical problems requiring computation or networking abilities [9], additionally, it is equipped with the built-in wireless network interface (NIC) supporting IEEE802.11n.

In WLAN, the *fairness* of the throughput quality among the hosts is necessary to ensure the fair *quality of services (QoS)* for the users [10]. Hence, fairness problems in WLAN have been explored extensively [11]-[14]. Since a large number of network applications in the Internet adopt the *transmission control protocol (TCP)*, the TCP fairness is exceedingly critical.

Nevertheless, our preliminary measurements using the elastic WLAN system test-bed have revealed that the TCP throughput is not superior among the two concurrently communicating hosts associated with the same AP when they are located at different positions from the AP. It is assumed that this unfairness was caused by differences in the *TCP window size* and the *modulation and coding*

*Corresponding Author: Nobuo Funabiki, Dep. of Electrical and Communication Engineering, Okayama University, Okayama, Japan, Email: funabiki@okayama-u.ac.jp
This paper is an extension of work originally presented in 2nd International Conference on Communication Engineering and Technology (ICCET 2019) [1].

scheme (MCS) among them. Therefore, the packet transmission interval of the farthest host hereafter becomes longer, and the interval for the nearest host becomes shorter.

In this paper, we propose the *TCP fairness control method* for two concurrently communicating hosts in the elastic WLAN system. The *transmission delay* is implemented at the AP in the packet transmission to the nearer host. After that, it can be predicted that the nearer host will decrease the throughput, and the farther host will enhance it by obtaining more transmission opportunities. This delay is firstly calculated by the *received signal strength (RSS)* from hosts. After that, it is dynamically controlled using the *PI controller* [15] to achieve the desired throughput fairness.

For performance evaluations, the proposal is implemented in *Raspberry Pi* AP and conduct experiments to verify the effectiveness using the test-bed with static and dynamic hosts in different network fields.

The remainder of this paper is structured as follows: Section 2 shows the preliminaries of the works. Section 3 demonstrates the TCP fairness control method. Section 4 and 5 evaluates the proposal through test-bed experiments. Section 6 discusses the observation result. Finally, Section 7 concludes this paper with future works.

2 Preliminaries

In this section, we introduce our preliminary work to relate this paper.

2.1 Elastic WLAN System

The *elastic WLAN system* has been designed and developed to control and manage the number of active APs in the network field according to the traffic demand. Figure 1 shows the test-bed topology of the system.

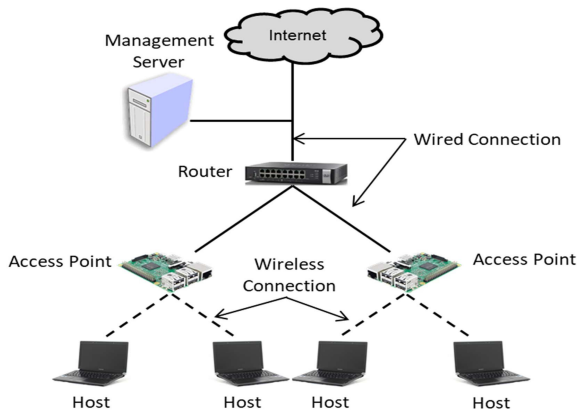


Figure 1: Elastic WLAN system topology.

The server has the administrative access to all the network devices including the APs, so that it can control them by executing the *active AP configuration algorithm* by the following procedure:

- The server examines the network devices and collects the necessary information for the active AP configuration algorithm.

- Then, it executes the active AP configuration algorithm and the output of the algorithm contains the minimum number of APs, the AP-host associations, and the allocated channels.
- Finally, it implements the output of the previous step by deactivating or activating the selected APs, changing the requisite host associations, and allocating the channels.

2.2 Software AP Configuration

In this paper, we adopt *Raspberry Pi 3*, that uses *Raspbian OS, Broadcom BCM2837 SOC, LPDDR2-900MHz 1GB SDRAM, 10/100Mbps Ethernet, IEEE 802.11b/g/n wireless NIC, Bluetooth 4.1 classics/low energy, and 400MHz video core IV GPU* [9]. The procedure to configure the *Raspberry Pi 3* device to function as a Wi-Fi AP is as follows:

- First, *hostapd* is installed by the command as follows:


```
#apt-get install hostapd
```
- Then, the */etc/hostapd/hostapdraspi.conf* configuration file is modified with the SSID and PASSWORD. An example of the configuration file is provided as follows:

```
interface=wlan0
ssid=RaspberryAP
wpa_passphrase=raspberry
channel=13
```

- Next, the absolute path is set to run *hostapd* while booting the system using the following command:

```
DAEMON_CONF="/etc/hostapd/hostapdraspi.conf"
```

- The static IP address in the *em wlan0* interface is assigned by modifying file */etc/network/interfaces* as follows:

```
auto wlan0
iface wlan0 inet static
address 172.24.2.10
netmask 255.255.255.0
network 172.24.2.0
```

- Finally, install the DHCP server for assigning the dynamic IP addresses to the hosts.

2.3 Jain's Fairness Index

There are various definitions have been proposed for the fairness index. Among them, *Jain's fairness index* [16] is the representative one for the TCP fairness:

$$F(n) = \frac{\left(\sum_{i=1}^k x_i\right)^2}{k \times \sum_{i=1}^k x_i^2} \quad (1)$$

Here k represents the total number of connections and x_i does the throughput for the i -th connection. When all the connections receive

the same throughput, this fairness index becomes 1, which means that all the connections are 100% fair. As the disparity increases, the fairness will decrease.

2.4 Unfairness Problem in Concurrent Communication

We initially measured the TCP fairness among concurrently communicating multiple links with a single AP using the elastic WLAN system test-bed with the various distances between host. We conducted the experiments in *Asahi Riverbed* as an outdoor environment. By using *Homedale* [17], it is confirmed that all interfering signals have been removed from this environment.



Figure 2: Outdoor measurement field.

Figure 2 indicates the locations of the AP and two hosts in the measurements. The position of the host *H2* is changed from 0m to 30m with the 5m step while the position of *H1* is fixed at the 0m distance from the AP. Then, the throughput and RSS are measured at both *H1* and *H2*. For each measurement, *iperf software* [18] is used to generate the traffic from both hosts at the same time to the AP.

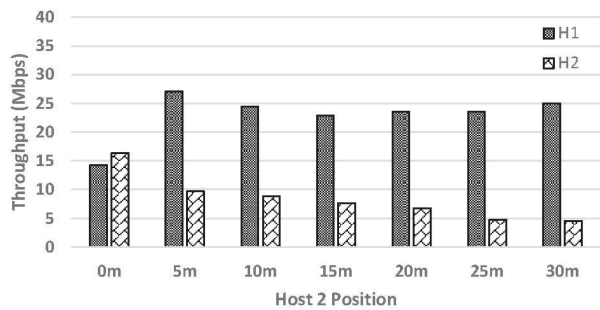


Figure 3: Throughput at different locations for *H2*.

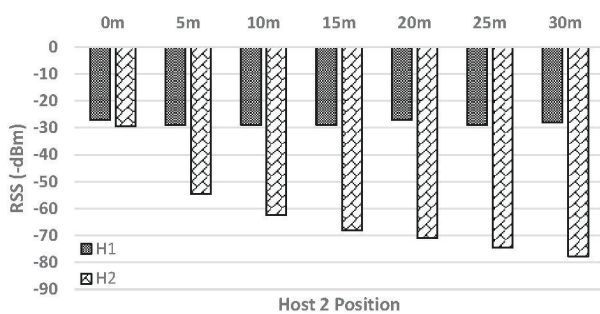


Figure 4: RSS at different locations for *H2*.

Figure 3 indicates throughput measurement results, which are similar at both hosts when the *H2* distance from the AP is 0m. However, as the *H2* distance increases, the throughput difference will

increase accordingly. The throughput of *H2* decrease due to the smaller RSS (receiving signal strength). Nevertheless, the throughput of *H1* will increase, although RSS at *H1* is constant as shown in Figure 4. This is considered as an inspiring result, that is to say, it seems that the nearer host to the AP will take higher transmission opportunities than the further host, which leads to the unfairness of the TCP throughput performance among them.

3 Proposal of TCP Fairness Control Method

In the section, we describe the proposal of the TCP fairness control method in the concurrent TCP communications of two hosts with a single AP.

3.1 Overview

Our test-bed experiments results unfold that the two-host concurrently communicating with a single AP causes the unfairness in the throughput performance, due to the different packet transmission intervals among them. Figure 5a demonstrates the packet transmission intervals between the near and far hosts. The throughput unfairness happens by the differences in the MCS and TCP window size. For the near host, the TCP windows size will be larger because of faster MCS compare to the far host. Then, it will occupy the far larger bandwidth during the communications compare to the other host, thus the packet transmission interval between them increases.

To overcome the issue, the *transmission delay* is intentionally introduced in the packet transmission of the AP to the near host. By minimizing the transmission bandwidth of the link with the near host, it will give more transmission bandwidth to the link to the far host. To achieve the throughput fairness, this delay should be controlled such that the intervals of packet transmission become equal, as shown in Figure 5b.

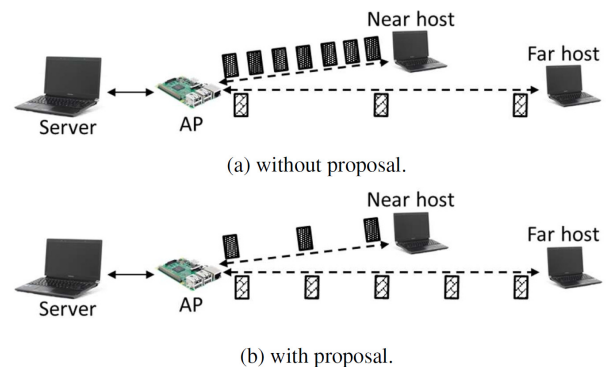


Figure 5: Background of TCP fairness control method.

The transmission delay is initially calculated by collecting the RSS at the AP from the near host and from the far host, because the measured RSS influences the MCS. After that, the transmission delay is controlled dynamically by the PI control during communications to attain the fairness accurately in the network.

3.2 Initial Delay Calculation

The initial transmission delay $D(0)$ is computed from the difference of the measured RSS between the two hosts:

$$D(0) = \frac{RSS_{near}}{-a} \left(\frac{RSS_{near}}{RSS_{min}} \right)^2 e^{b(RSS_{near} - RSS_{far})} \quad (2)$$

The parameter values are obtained from our experimental results in [19]. Where, $RSS_{min} = -88dBm$ from [20] is considered as the minimum RSS that a host can receive packets successfully from a *Raspberry Pi* AP, RSS_{near} does the measured RSS at the AP from the near host, RSS_{far} does the measured RSS from the far host, and the constant parameter a and b are needed to be set depending on the environment. Here, $a = 8$, $b = 0.15$ for the outdoor field, and $a = 9$, $b = 0.17$ for the indoor field are used, respectively. If the RSS is smaller than RSS_{min} , the host cannot receive any packet successfully.

3.3 Dynamic Delay Optimization by PI Controller

In this stage, to achieve the target fairness index, the delay is dynamically controlled by the *PI controller* [15]. The delay is optimized dynamically as follows:

$$D(n) = K_P \times (F_{tar} - F(n)) + K_I \times \sum_{i=0}^n (F_{tar} - F(i)) \quad (3)$$

Here, $D(n)$ represents the delay, $F(n)$ does the measured fairness index at the n -th time-step, and K_P and K_I does the gain for the P control and for the I control, respectively. Where, $F_{tar} = 0.97$, $K_P = 3$, and $K_I = 0.8$ are used. It is noted that the PI controller periodically changes the delay with the *20sec* time-step. In the system implementation, the equation in (3) is modified as follows:

$$D(n) = D(n-1) + K_P \times (F(n-1) - F(n)) + K_I \times (F_{tar} - F(n)) \quad (4)$$

The measured fairness index $F(n)$ is calculated by:

$$F(n) = \frac{(x_{far}(n) + x_{near}(n))^2}{2 \times (x_{far}(n)^2 + x_{near}(n)^2)} \quad (5)$$

where $x_{far}(n)$ and $x_{near}(n)$ represent the measured throughput of the far host and that of the near host at the n -th time-step, respectively.

3.4 Test-bed Implementation

Here, we show the implementation of our proposal in the elastic WLAN system test-bed.

3.4.1 RSS Measurement

We collect the measured RSS of every host by using the command as follows at the AP:

```
$ sudo iw dev wlan0 station dump |
  egrep "Station|signal:"
```

where the AP does not require to access to the host. Since the RSS continually fluctuates, RSS is measured for 30 seconds, and their average is used in Eq. (2).

3.4.2 Transmission Delay Application

Next, the transmission delay is applied to the packet transmission from the AP to the nearest host by the following procedure:

- Remove any delay previously assigned at the interface *wlan0*:

```
$ sudo tc qdisc del root dev wlan0
```

- Assign each delay at the packet transmission from the AP to every host, namely *d1* and *d2*:

```
$ sudo tc qdisc add dev wlan0 root
  handle 1: prio bands 3
$ sudo tc qdisc replace dev wlan0
  parent 1:1 netem delay $d1
$ sudo tc qdisc replace dev wlan0
  parent 1:2 netem delay $d2
```

- Enforce every delay to the packet transmission to the nearest host and the far host that is specified by the IP address:

```
$ sudo tc filter add dev wlan0
  protocol ip parent 1: u32 match
  ip dst $IPaddressofnearhost
  flowid 1:1
$ sudo tc filter add dev wlan0
  protocol ip parent 1: u32 match
  ip dst $IPaddressoffarhost
  flowid 1:2
```

Here, the IP address of each host is automatically set by the following program:

```
Linux commands for near host detection
#!/bin/bash
# for check total connected hosts
01: sudo hostapd_cli all_sta |
  grep "dot11RSNAStatsSTAAddress="
while [ "$i" -le "$totalConnectedHost" ]
do
# for collecting the IP address
02: arp -a | grep $mac
# merge MACAddress, IP Address and RSS
03: echo $mac " " $ip " " $rss >> data.tmp
done
# sort descending data.tmp by rss value
04: sudo sort -nrk 3 data.tmp > sort.tmp
# 1st line in sort.tmp is the nearest host
```

3.4.3 Dynamic Delay Optimization

Firstly, the initial delay is obtained to the nearest host from the server by the following step:

- Explore the IP and MAC addresses of the connected hosts.
- Request the AP to measure the RSS of the hosts for 30sec and send back to the server.
- Find the average of the measured RSS.
- Compute $D(0)$ by Eq. (2).
- Assign $D(0)$ as the transmission delay to the nearest host.

Then, the delay is optimized dynamically by the following steps at every 20sec:

- Measure the throughput of the hosts for 20sec using *iperf*.
- Compute $F(n)$ by Eq. (5).
- Update $D(n)$ by Eq. (4).
- Set $D(n)$ as the transmission delay to the faster host at the AP.

4 Evaluations with Static Hosts

In this section, we evaluate the proposal through experiments when all the hosts are stationary.

4.1 Experiment Setup

In our experiments, we generate TCP traffic from two concurrently communicating hosts to the server to measure the throughput. Figure 6 illustrates the network setup of the server, the AP, and the hosts. The server is connected with a 100Mbps wired connection to the AP, and the host is connected to the AP through the IEEE802.11n 2.4Ghz wireless link. The traffic is generated from the host to the server using *iperf*. The buffer size and the TCP window size are set to 8KB and 477KB, respectively.

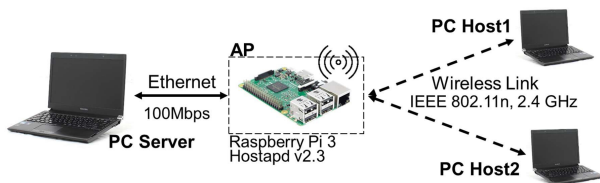


Figure 6: TCP link configuration.

Table 1 reveals software and hardware specifications for our experiments. Three laptop PCs are used for the two client hosts and the one server, and one *Raspberry Pi* is configured for the AP operating on channel 13.

Table 1: Hardware and software specifications.

server and hosts	
type	R731/B, Toshiba Dynabook
operating system	Linux (Ubuntu 14)
RAM	4GB DDR3-1333MHz
processor	Intel Core i5-2520M, 2.5Ghz
software	Iperf 2.0.5
access point	
type	Raspberry Pi 3
operating system	Linux (Raspbian)
RAM	LPDDR2 900MHz 1GB
processor	BCM2837 1.2Ghz, Broadcom ,
NIC	BCM43438, Broadcom
software	hostapd

4.2 Experiments in Outdoor Field

First, the experimental results are provided in the outdoor field.



Figure 7: Outdoor field.

4.2.1 Experiment Field

As the outdoor field, experiments are conducted in *Asahi Riverbed* shown in Figure 7. There is no interfering signal, which is confirmed by using *Homedale*. The height of the AP and the hosts are 135cm and 70cm, respectively. During experiments, the distance of $H1$ from the AP is set 0m, 5m, 10m, and 15m. Then, for each $H1$ distance, $H2$ is located at 0m, 5m, 10m, 15m, 20m, 25m, and 30m from the AP. Finally, the throughput experiments are carried out in three methods: 1) *without proposal*, 2) *initial delay only*, and 3) *proposal*.

4.2.2 Throughput Results

Figure 8 illustrates the throughput results of the two hosts for 1) *without proposal*, where the unfairness appears between $H1$ and $H2$. Figure 9 shows the results for 2) *initial delay only*, where the fairness of each host is improved. Figure 10 shows the results for 3) *proposal*, where the fairness is achieved at any position by implementing our proposal. Figure 11 shows the overall throughput comparison at each $H1$ location. Nevertheless, with the proposal, the overall throughput has been reduced by 2.78% on average.

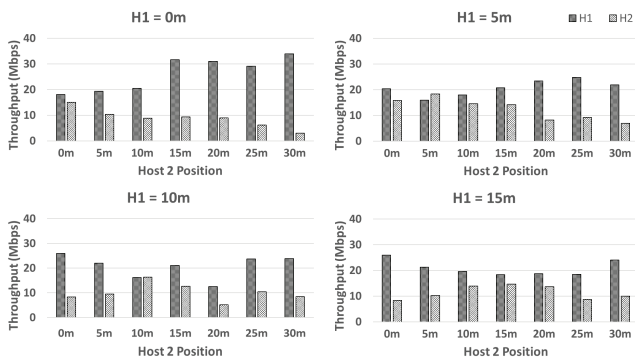


Figure 8: Results of throughput in outdoor field for 1) without proposal.

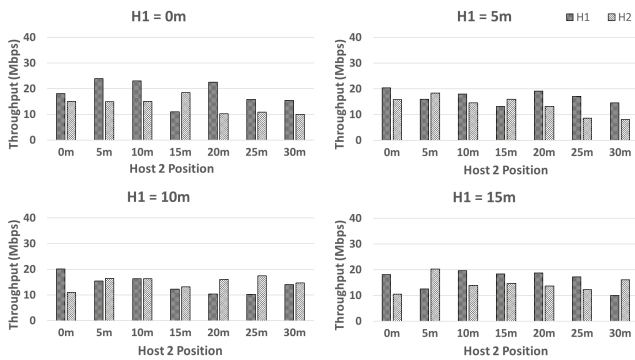


Figure 9: Results of throughput in outdoor field for 2) initial delay only.

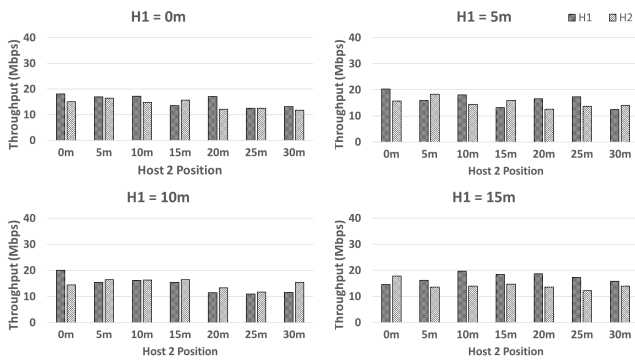


Figure 10: Results of throughput in outdoor field for 3) proposal.

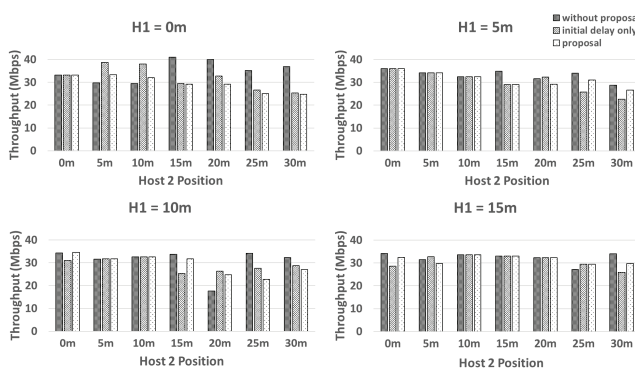


Figure 11: Results of overall throughput in outdoor field.

4.2.3 Fairness Index Results

Figure 12 demonstrates the *Jain's fairness index* result. From the Eq. (1) known 1 is the finest fairness index. For 1) without proposal, any result appears to be lower than 1. Nevertheless, for 3) proposal, the fairness index will generally become close to 1. It is found that the proposal presents better achievement in the fairness index than the comparisons.

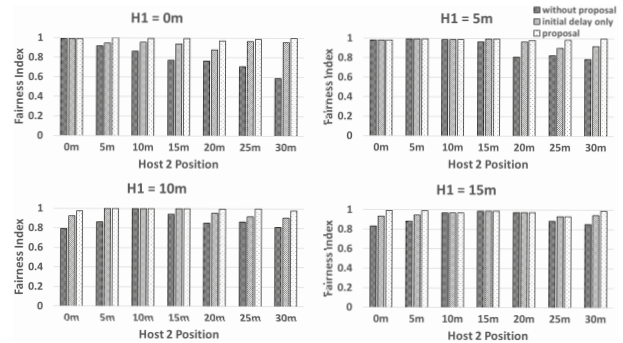


Figure 12: Observed TCP fairness index in outdoor field.

4.3 Experiments in Indoor Field

Second, experimental results in the indoor field are provided.

4.3.1 Experiments in Two-room Case

The two rooms in the 3rd floor of Engineering Building #2 at Okayama University are used in the experiment. Figure 13 illustrates the layout of this field.

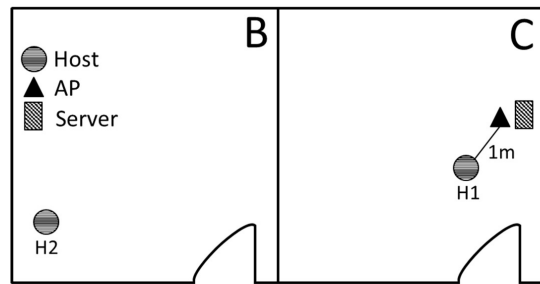


Figure 13: Experiment field for two-room case.

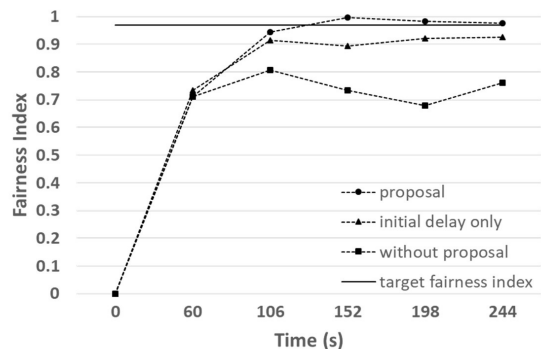


Figure 14: TCP fairness index results in indoor field for two-room case.

Figure 14 shows the fairness index results. The system collected the RSS and other necessary data during the first 60sec to measure the throughput. Next, it was observed that the fairness index for each method is about 0.7. Then after 130sec, fairness is achieved for 3) *proposal*. Conversely, 1) *without proposal* and 2) *initial delay only* could not achieve it.

4.3.2 Experiments in Four-room Case

Then, the four rooms on the same floor are used in the experiment. Figure 15 illustrates the layout of this building that has a complex structure of multiple rooms and walls. This figure shows the position of the AP (triangle), the server (square), and the possible position of the hosts (circle). Here, the AP and the host are configured similarly to the outdoor field. *H1* is located at A1 and B2 in the indoor field. Then, for each *H1* position, *H2* is moved from A1 to D4, respectively.

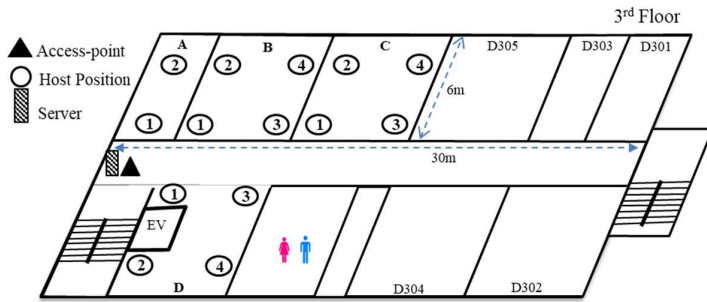


Figure 15: Indoor field.

Figure 16 illustrates the throughput results of the two hosts for 1) *without proposal*. The unfairness appears between *H1* and *H2*. Figure 17 shows the results for 2) *initial delay only*, where the fairness is slightly improved. Figure 18 shows the results for 3) *proposal*, where the fairness is achieved by the proposal. Figure 19 shows the overall throughput comparison at each *H1* location. However, by applying the proposal, the overall throughput has diminished by 14.83% on average.

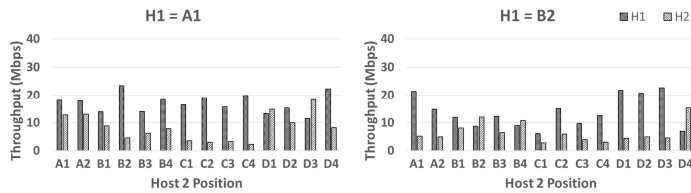


Figure 16: Results of throughput in indoor field for 1) *without proposal*.

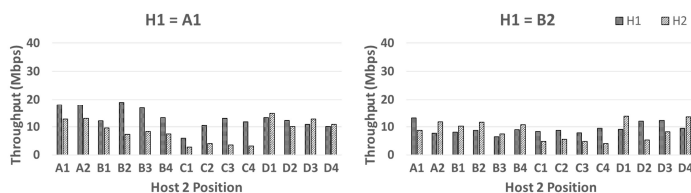


Figure 17: Results of throughput in indoor field for 2) *initial delay only*.

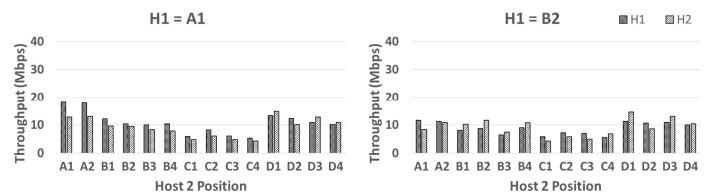


Figure 18: Results of throughput in indoor field for 3) *proposal*.

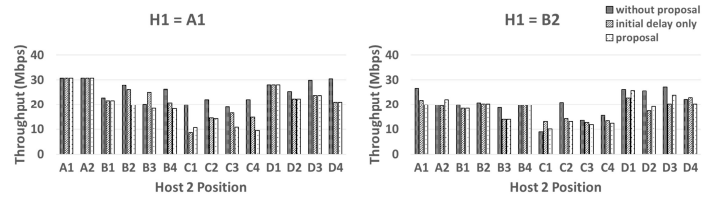


Figure 19: Results of overall throughput in indoor field.

Figure 20 shows the fairness index result of the four-room case. For 1) *without proposal*, the fairness index appears to be smaller than 1. Nevertheless, for 2) *initial delay only*, it increases significantly. Furthermore, for 3) *proposal*, it is going to be nearly 1. Thus, the effectiveness of the dynamic delay optimization using the PI controller is confirmed.

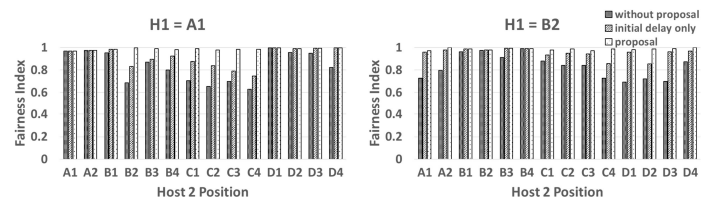


Figure 20: TCP fairness index results in indoor field for four-room case.

5 Evaluations with Dynamic Hosts

Next, we evaluate the TCP fairness control method through experiments when one host is dynamically connected and disconnected to the AP.

5.1 Experiment Setup

The topology in Figure 13 and the devices/software in Table 1 are used in this experiment. Figure 21 indicates the 20min scenario of dynamically connecting and disconnecting one host. Initially, *H1* is connected to the AP. At 0min, *iperf* TCP traffics are generated for 5min. At 5min, *H2* is connected to the AP, and the proposed method is started to run manually. Then, the server will collect the RSS and measure the throughput at *H1* and *H2*. Afterward, at 10min, *H2* is disconnected from the AP, and the server measures the throughput of *H1*. Lastly, at 15min, both *H1* and *H2* are connected.

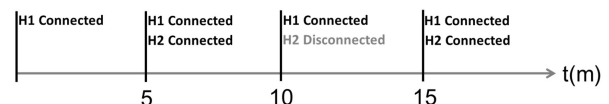
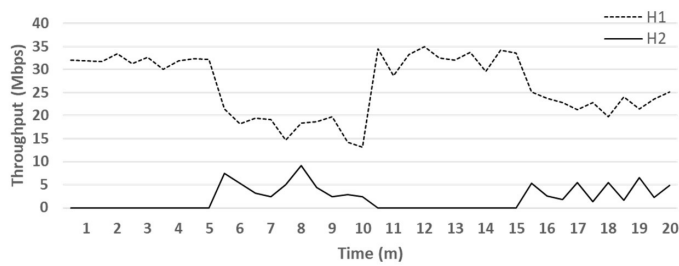
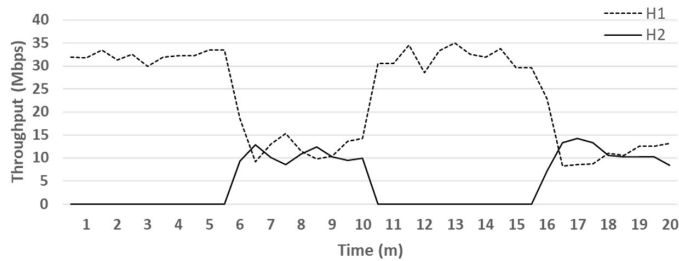


Figure 21: Time scenario for dynamically connecting/disconnecting host.



(a) Results of throughput without proposal.



(b) Results of throughput with proposal.

Figure 22: Individual throughput of $H1$ and $H2$ with dynamic hosts.

5.2 Results

Figure 22 shows the individual throughput for $H1$ and $H2$. At $0min$, where only $H1$ is connected to the AP, the individual throughput is about $33Mbps$. Next, at $5min$, where both hosts are connected, the individual throughput of $H1$ decreases due to the concurrent communication. Here, *with proposal* can achieve the throughput fairness between two hosts, where it is around $12Mbps$ for each host. On the other hand, *without proposal* cannot achieve it. Thus, our proposal has proved to reach the throughput fairness between two concurrently communicating hosts with a single AP, even if a host is continually connected and disconnected to the AP.

6 Discussions

In this section, we discuss the summaries of experiment results in the previous sections and future works.

The TCP fairness control method is proposed in this paper so that any host communicating with the same AP can enjoy the similar throughput regardless of the relative position from the AP. This service fairness is important in designing and managing a local-area network, including the wired and wireless LANs. To verify the effectiveness of the proposal, evaluations with static and dynamic hosts are conducted using real devices.

First, the experiment results with static hosts in Section 4 show the improvement of the fairness index from 0.85 to 0.98 on average by the proposal, whereas the average overall throughput is dropped by 2.78% in outdoor fields and by 14.83% in indoor fields on average. Since the possible throughput of WLAN is increasing rapidly due to the advancements of wireless communication technologies, these drops of the overall throughput are acceptable.

Second, the experiment results with dynamic hosts in Section 5 show that the fairness index is improved from 0.69 to 0.97 on

average by the proposal, whereas the average overall throughput is dropped by 3.21% on average. This small drop of the overall throughput is acceptable.

From these results, it is confirmed that the TCP fairness control method is practical and useful in achieving the throughput fairness among the two concurrently communicating hosts with the AP.

The weakness of the proposal is the use of the throughput measurement software (*iperf* in this paper). Every host in WLAN must install the client software, which can be an obstacle for practical use. In future works, we will investigate a method of estimating the throughput without installing this software at a host.

Besides, the proposed method is based on empirical works with a lot of experiments using real devices. The theoretical analysis of two-host concurrent communications and the model formulation for simulations will be also in future works. This model should accurately estimate the throughput for a given transmission delay at the packet transmission from the AP to a host when two hosts are concurrently communicating with the single AP.

7 Conclusion

This paper proposed the *TCP fairness control method* for two concurrently communicating hosts in the elastic WLAN system where the delay is implemented in the packet transmission of the faster host. Initially, the delay is estimated by collecting the RSS of the hosts at the AP. Then, it is dynamically controlled using the PI controller to achieve throughput fairness between the hosts. Extensive experiments with static and dynamic hosts confirmed the effectiveness of the proposal. In future works, the proposal will be extended to three or more concurrently communicating hosts and carry out experiments in different topologies and network fields.

Acknowledgments

This work is partially supported by JSPS KAKENHI (16K00127).

References

- [1] R. W. Sudibyo, N. Funabiki, M. Kuribayashi, K. I. Munene, M. M. Islam, and W.-C. Kao, "A TCP fairness control method for two-host concurrent communications in elastic WLAN system using Raspberry Pi access-point," in Proc. 2nd Int. Conf. Commun. Eng. Tech. (ICCET 2019), pp. 76-80, 2019.
- [2] B. P. Crow, I. Widjaja, J. G. Kim, and P. T. Sakai, "IEEE 802.11 wireless local area networks," IEEE Commun. Mag., vol. 35, no. 9, pp. 116-126, Sept. 1997.
- [3] K. Mittal, E. M. Belding, and S. Suri, "A game-theoretic analysis of wireless access point selection by mobile users," Comput. Commun., vol. 31, no. 10, pp. 2049-2062, Jan. 2008.
- [4] M. Balazinska and P. Castro, "Characterizing mobility and network usage in a corporate wireless local-area network," in Proc. Int. Conf. Mob. Syst. Appl. Ser., pp. 303-316, 2003.
- [5] D. Kotz and K. Essien, "Analysis of a campus-wide wireless network," Wirel. Netw., vol. 11, no. 1-2, pp. 115-133, Jan. 2005.
- [6] F. Nadeem, E. Leitgeb, M. S. Awan, and S. Chessa, "Comparing the life time of terrestrial wireless sensor networks by employing hybrid FSO/RF and only RF access networks," in Proc. Int. Conf. Wirel. Mob. Commun., pp. 134-139, 2009.

- [7] M. S. A. Mamun, M. E. Islam, N. Funabiki, M. Kuribayashi, and I-W. Lai, "An active access-point configuration algorithm for elastic wireless local-area network system using heterogeneous devices," *Int. J. Network. Comput.*, vol. 6, no. 2, pp. 395-419, July 2016.
- [8] M. S. A. Mamun, N. Funabiki, M. E. Islam, and W.-C. Kao, "A channel assignment extension of active access-point configuration algorithm for elastic WLAN system and its implementation using Raspberry Pi," *Int. J. Network. Comput.*, vol. 7, no. 2, pp. 248-270, July 2017.
- [9] Raspberry Pi, "The official website of the Raspberry Pi project," <http://raspberrypi.org>. Accessed 19 Feb., 2019.
- [10] S. Pilosof, R. Ramjee, D. Raz, Y. Shavitt, and P. Sinha, "Understanding TCP fairness over wireless LAN," in *Proc. IEEE INFOCOM*, April 2003.
- [11] T. Nandagopal, T. Kim, X. Gao, and V. Bharghavan, "Achieving MAC layer fairness in wireless packet networks," in *Proc. ACM Mobicom*, Aug. 2000.
- [12] N. Blefari-melazzi, A. Detti, A. Ordine, and S. Salsano, "A mechanism to enforce TCP fairness in 802.11 wireless LANs and its performance evaluation in a real test-bed," in *Proc. World. Wirel. Mob. Multi. Net.*, pp. 1-7, 2007.
- [13] B. A. H. S. Abeysekera, T. Matsuda, and T. Takine, "Dynamic contention window control mechanism to achieve fairness between uplink and downlink flows in IEEE 802.11 wireless LANs," *IEEE Trans. Wirel. Commun.*, vol. 7, no. 9, pp. 3517-3525, 2008.
- [14] E. Park, D. Kim, H. Kim, and C. Choi, "A cross-layer approach for per-station fairness in TCP over WLANs," *IEEE Trans. Mob. Comput.* vol. 7, no. 7, pp. 898-911, 2008.
- [15] K. Astrom and T. Hagglund, "PID controller: theory, design, and tuning, 2nd Ed.", Inst. Socie. America, 1995.
- [16] R. Jain, D. Chiu, and W. Hawe, "A quantitative measure of fairness and discrimination for resource allocation in shared computer system," *East. Res. Lab. (DEC)*, vol. 38, 1984.
- [17] Software Verzeichnis development, Homedale WLAN Monitor, <http://www.the-sz.com/products/homedale>. Accessed 19 Feb., 2019.
- [18] Iperf, The ultimate speed test tool for TCP, UDP and SCTP, <https://iperf.fr/>. Accessed 27 Feb., 2019.
- [19] R. W. Sudibyo, N. Funabiki, M. Kuribayashi, K. I. Munene, M. M. Islam, and W.-C. Kao, "A TCP fairness control method for concurrent communications in elastic WLAN system using Raspberry Pi access-point," *IEICE Tech. Rep., NS2018-175*, pp. 96-100, Dec. 2018.
- [20] Cypress, "CYW43438, Single-Chip IEEE 802.11 b/g/n MAC/Baseband/Radio with Integrated Bluetooth 4.2," 2016.

An ML-optimized dRRM Solution for IEEE 802.11 Enterprise Wlan Networks

Mehdi Guessous^{*}, Lahbib Zenkour

Department of Electrical Engineering, Mohammadia School of Engineers, Mohammed V University In Rabat, Morocco

ARTICLE INFO

Article history:

Received: 09 October, 2019

Accepted: 02 November, 2019

Online: 20 November, 2019

Keywords:

Machine learning

Radio coverage

Radio resources management

Wireless local area networks

ABSTRACT

In an enterprise Wifi network, indoor and dense, co-channel interference is a major issue. Wifi controllers help tackle this problem thanks to radio resource management (RRM). RRM is a fundamental building block of any controller functional architecture. One aim of RRM is to process the radio plan such as to maximize the overall network transmit opportunity. In this work, we present our dynamic RRM (dRRM), WLCx, solution in contrast to other research and vendors' solutions. We build our solution model on a novel per-beam coverage representation approach. The idea of WLCx is to allow more control over the architecture design aspects and recommendations. This dynamization of RRM comes at a price in terms of time and resources consumption. To improve the scalability of our solution, we have introduced a Machine Learning (ML)-based optimization. Our ML-optimized dRRM solution, M-WLCx, achieves almost 79.77% time reduction in comparison with the basic WLCx solution.

1 Introduction

In an enterprise Wlan network, the controller is the central component of the network architecture. The controller manages all the Wifi access points (APs) and provides their radio configuration: channel and transmit power. The controller plays another important role in Wlan integration to other parts of the enterprise network: Local Area Network (LAN), Wide Area Network (WAN), internet, and Datacenter Network (DCN), where application servers reside.

Processing the radio plan is the task of RRM functional architecture block of the controller. It helps minimize co-channel interference and efficient use by APs of the spectrum, thus, optimizing the latter transmit opportunity. Then, how does RRM decide on what channel an access point should use, and at what transmit power?

To build an efficient radio plan that maximizes the network capacity, the controller needs data from APs, Wifi clients or devices (WDs), wired network devices, and servers. This data is what pertains to the quality of the radio interface and client overall experience when accessing the services. However, this information is not sufficient to hint on the whole coverage quality such as the interference at any point in the coverage area. It is only limited to some coverage points, APs

and WDs, that are able to monitor the radio interface and report real radio measurements.

To overcome this limitation, either we place sensors everywhere, which is not feasible in an enterprise network (economically and technologically), or model the coverage area. The modelization effort could be done in a laboratory context, by vendors for example, to provide strict recommendations that customers may follow to build their networks. This approach works in common situations. But it requires a lot of engineering effort and monitoring to maintain the network at an optimal condition. In some situations, it may just not work or false the transmit opportunity estimation. For the rest of this work, this approach is referred to as static RRM (sRRM). The third alternative is to allow the controller to do more complex real-time processing without any or very few preconfigured settings and find out the suitable RRM configuration to apply. This approach is the focus of this study and will be referenced as dynamic RRM, or dRRM.

A controller, that supports dRRM, does not rely on preconfigured settings in hardware or software to decide on how to modify the radio plan to meet the utility function. In dRRM, even the system parameters are processed to optimize the network capacity, which is different from sRRM. However, the advantage of dRRM comes at a high price in terms of time,

^{*}Corresponding Author: Mehdi Guessous, Address: Mohammadia School of Engineers, Avenue Ibn Sina, B.P 765, Agdal Rabat 10090, Morocco, Contact No: +212 5377-71905 & Email: mehdiguessous@research.emi.ac.ma

system resources consumption to process the whole network coverage and, adaptation to frequent changes. In this work, we present our dRRM optimization solution that builds on concepts from the Machine Learning (ML) field. Our solution is built on a novel and realistic per-Beam coverage representation approach that is different from related-work encountered research approaches that we discuss later.

In Section 2, we present how related work, research and vendors, process RRM. In Section 3, we present our dRRM solution (that is not sRRM) and compare it to the vendor solution in processing the radio coverage. Before we state the problem in Section 5, and the presentation of our solution in Section 6, we introduce in Section 4, some important facts about Wlan network design, coverage representation models and important machine learning concepts. Section 7 is dedicated to the evaluation of our optimization, before we conclude.

This paper is an extension of the work originally presented in the 2018 15th International Conference on Electrical Engineering, Computer Science and Informatics [1].

2 RRM Related Work

In this section, we discuss RRM approaches from research and vendors of the Wifi market such as Cisco, Aruba-HPE, etc. as they pertain to enterprise Wlan networks. We are interested in algorithms that operate the APs transmit power to maximize the network capacity or optimize radio resource usage. An algorithm is different from another when the used variables are different.

For simplification, we discuss a mono channel condition. This work could then, be easily extended to a multi-channel condition.

2.1 In Research

The first category of approaches concentrate on lower-layer constraints: co-channel interference, physical interface and MAC performance.

The authors in these works [2, 3, 4], modeled the coverage area per-range: transmit, interference, and not-talk ranges, using a circular or disk pattern. The way this model represents the coverage is common but may not hint on some opportunities to transmit as discussed in this work [5].

The author in this work [6], focused instead on the interaction that an AP may have with its neighboring AP. The result is a per-zone, Voronoi zone, negotiated coverage pattern. This model is difficult to put into practice technologically and economically as it was discussed in [5] and [7]. Both models: per-zone and per-range, do not consider upper layer constraints.

Another set of similar works tackle the issue from a power saving perspective. The authors in [8] build their on-demand Wlan approach on the observation of idle APs that have no clients associated. The Wlan controller manages the activation or not of an AP.

The second category of approaches tackles the issue from an upper-layer perspective for applications such as FTP, HTTP. This work [9], as an example, presented an interesting idea to find out a suitable power, or RRM, scheme, that may optimize the application performance. It is a per-experience approach that requires a huge amount of data, to be put into practice. In addition, it is very dependent on the coexistent individual application's behavior. Another challenge is to be able to determine when the physical layer is responsible for the observed performance rather than the application one. Works like [10] use concepts from the Game theory, a powerful tool, to model the interactions between APs. These concepts are applied to the user perception of the QoS it receives. The same limitation of the previously cited work applies to this one also.

The third category tackles the problem from an inter-protocol cooperation point of view like in this example [11]. Making the protocols aware of each other is a good strategy to find an optimum inter-protocol negotiated power scheme that optimizes the performance of each of them individually. It is an idealistic scheme, difficult to put into practice technologically and economically, concerning vendors offering. Let us imagine the integration of a Wifi and a Bluetooth network. The impact of a Wifi AP on a Bluetooth piconet is very important but not the opposite. Then, as an example, it is necessary to find out a way to provide the network controller (for both Wifi and Bluetooth) with the necessary feedbacks so it can adjust the Wifi network power plan to allow a Bluetooth network optimum operation. This would require important data transfers (and power consumption) from the Bluetooth network to the controller, which is very difficult to implement, by design of the Bluetooth devices..

2.2 Vendor Solutions

The approach or theoretical background, behind the vendors' implementations, is hidden in general for commercial purposes; they only provide the settings (recommendations).

Cisco Transmit Power Control (TPC) algorithm, that is a part of Cisco RRM, processes, at each AP, the desired transmit power hysteresis, $Tx_{Hysteresis,Current}$, that is equal to the sum of the current transmit power (initially at maximum), $Tx_{Current}$, and the difference between the power threshold, Tx_{Thresh} , and RSSI^{3rd}, the third neighbor reported RSSI. If the difference between the processed power and the current one, $Tx_{HysteresisThresh}$, is at least $6dBm$, then the current power must be reduced by $3db$ (by half). We should then wait for 10 minutes before re-attempting another calculation. Details about this implementation are given in [12].

Aruba-HPE adopts another strategy. The Adaptive Radio Management (ARM) algorithm maintains two measures for every channel: a coverage index, cov_{idx} , and an interference index, $ifer_{idx}$. The decision of increasing or decreasing the transmit power level on a given channel is based on the processed coverage index as compared to the "ideal" coverage index, noted $cov_{idx,ideal}$, and "acceptable" coverage index, $cov_{idx,acceptable}$, for instance. As a general rule, the current

coverage index should be greater than $cov_{idx,acceptable}$ and equivalent to $cov_{idx,ideal}$. Coverage index, cov_{idx} , corresponds to the sum of two variables : x and y . x is the weighted average of all other APs SNR as being measured by the current AP. y is the weighted average of the processed x variables by other APs from the same vendor and on the same channel. The same thing applies to $ifer_{idx}$ processing. Details of this calculation are in [13].

Fortinet Auto Power that is a part of ARRP, *Automatic Radio Resource Provisioning*, solution, works by reducing automatically the transmit power if the transmit channel is not clear. From the corresponding documentation [14], it is an alternative to manually limiting the number of neighbors per channel (less than 20) by adjusting the transmit power level.

3 Our Dynamic RRM Solution

Our WLCx dynamic RRM solution is based on the per-Beam coverage representation we discuss in the upcoming section. Our solution is "dynamic" because even the parameters' values change: the optimum number of the supported directions per AP, in the case of the WLC2 variant of our solution, as an example. The workflow in Figure 1, describes how our solution works.

Our solution runs three algorithms: TDD (Discovery), TDM (Map) and TDO (Opportunity). After initialization, TDD optimizes the number of supported directions per AP by reducing the power level and doubling the initial number of directions until all neighbors are discovered and at almost one neighbor is discovered per AP direction. Based on information from TDD, TDM categorizes the coverage area points into categories that hints on how these points appear on APs directions. Each category is assigned a cost to hint on its probability to get a fair transmit opportunity. The TDO processes each coverage point opportunity to transmit, taking into account data from TDM and SLA (upper-layer input).

We simulate, using Matlab 2019a, two variants of our WLCx solution: WLC1 and WLC2. In WLC1, all APs share the same optimal number of supported directions and transmit at the same power level. In WLC2, the APs process the same optimal number of the supported directions but may use different transmit power levels per AP. In the same simulation, we compare both WLCx variants to vendor implementation: Cisco. We evaluate models based on their performance at processing the coverage and time this processing takes.

The coverage processing performance, $Pr()$, of a given model, m , is calculated in (1). $I()$, $H()$ and $O()$ are the model processed interference, number of coverage holes and transmit opportunity, respectively.

$$Pr(m) = K_1 \frac{\Sigma I}{I(m) + 1} + K_2 \frac{\Sigma H}{H(m) + 1} + K_3 \frac{O(m)}{\Sigma O} \quad (1)$$

The performance calculation in (1), is the weighted sum of relative interference, opportunity and coverage holes in each model. The weights K_1 , K_2 and K_3 , hints on how important is the processing of interference, opportunity or holes, to

the performance of a given model. For the rest of our study, we consider that all variables are of equal importance then, $K_1 = K_2 = K_3 = 1$.

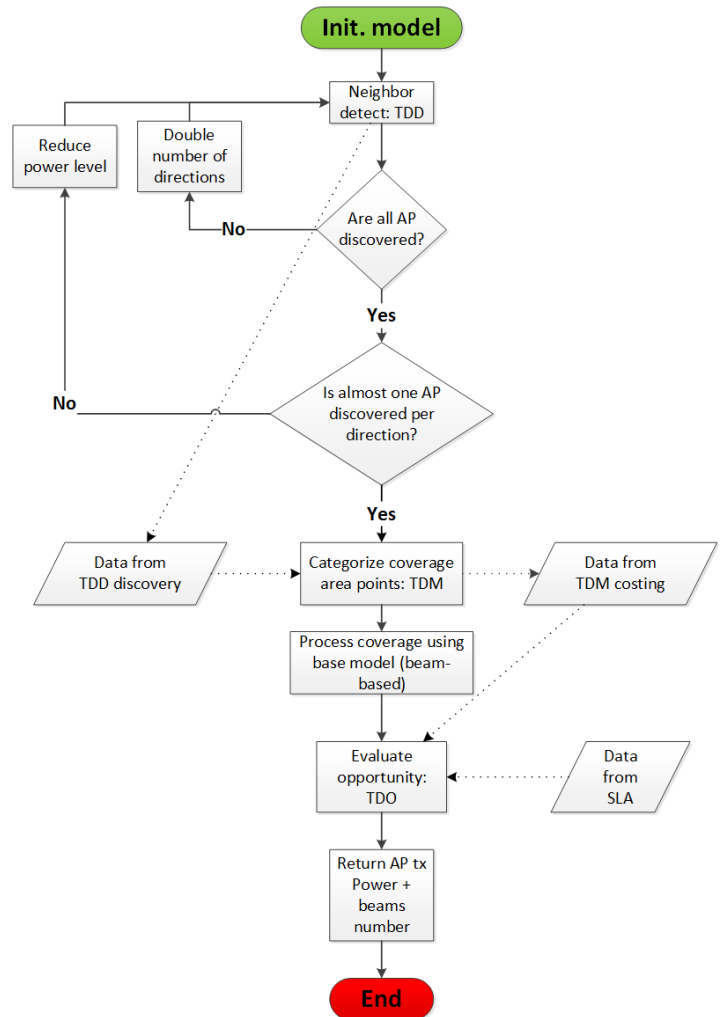


Figure 1: Our WLC dRRM solution workflow

The diagram in Figure 2, shows the performance of models after 10 iterations of the same simulation. Each simulation corresponds to a random distribution of a set of 30 APs and 100 WDs. We check that our WLC2 solution variant performs better than Cisco and WLC1. The Cisco model performance is comparable to WLC1. The processing time of models is represented in Figure 3. The models have a comparable processing time for a large number of the same simulation iterations.

In work [5], we discuss our WLC2 dRRM solution. For further details about our solution, refer to [7] work that is an extension of the previous one.

4 Theoretical Background

Before we dive into the description of the problem, let us recall some facts about Wlan enterprise network architecture design, the importance of coverage representation for

radio planning, and NURBS surfaces concepts that are the foundation of our NURBS optimized WLCx dRRM solution.

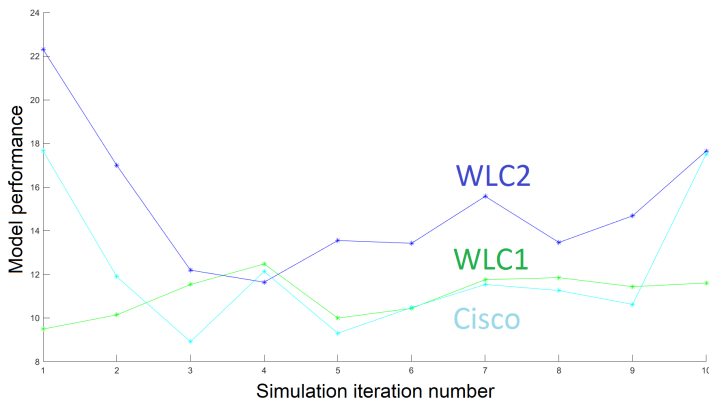


Figure 2: Performance of models after 10 simulations of the network of 30 APs and 100 WDs.

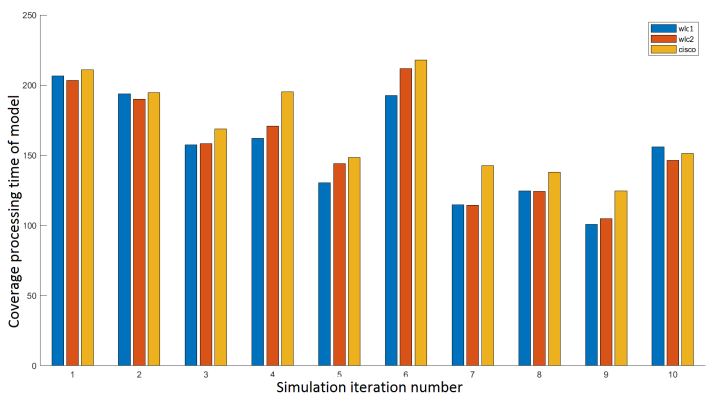


Figure 3: Processing time of models after 10 simulations of the network of 30 APs and 100 WDs.

4.1 Wifi Unified Architecture

In a standalone AP-based Wifi architecture, the network capacity does not scale with dense and frequently changing radio environments. To optimize the network capacity, some kind of coordination and control, distributed or centralized, is needed. In UWA, *Unified Wifi Architecture*, a WLC, *Wireless LAN Controller*, acts as a repository of APs intelligence, runs routines to plan radio usage, provides an interface to wired network, etc. and guarantees conformance to policies: QoS and Security, domain-wide, including LAN, MAN, WAN, and DCN, network parts. A typical enterprise Wlan architecture is given in Figure 4. Two market-leading implementations of such WLCs are the Cisco 8540 Wireless Controller and the Aruba 7280 Mobility Controller. The rest of our study focuses on Cisco implementation.

In Figure 4, the APs are located nearest to Wifi clients, WDs. All APs are connected to the LAN and are associated, via Virtual Private Networks (VPN), or tunnels, to the controller, WLC, located at the Datacenter, in a Hub and Spoke architecture. Depending on the network size and requirements, the controller may be located at the same location as

the APs. To build an association, an AP should be able to join the controller, via MAN, WAN or internet. After the AP’s successful association to the controller, the WDs start their association process that includes authentication, to the corresponding Wlan. Then the WDs access the network resources behind the controller or in some configurations, behind the APs (in FlexConnect or Local Switched mode).

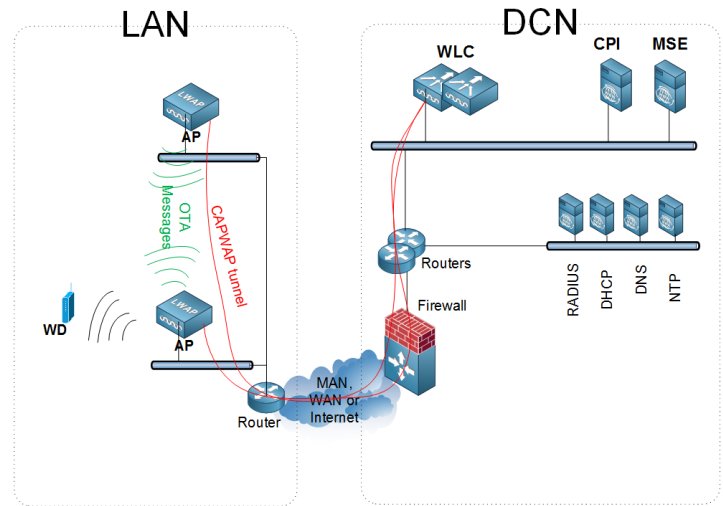


Figure 4: A Wifi unified architecture example topology

WLC receives information about the network from three sources: the wired path toward the datacenter, the radio interface counters of each associated AP, and OTA, *Over-The-Air*, AP-to-AP wireless messages over a dedicated low speed radio. In the case of Cisco, two protocols are available for exchanging data between APs, and between APs and WLC:

- Control and Provisioning of Wireless Access Points (CAPWAP) protocol is used by the APs to build associations to the RF group leader WLC and for control information and data exchange.
- Neighbor Discovery Protocol (NDP) allows the APs to exchange Over-The-Air (OTA) messages that carry standard, per-vendor proprietary control, and management information.

In addition to these protocols, Cisco APs have on-chip features such as CLIENTLINK and CLEANAIR. CLEANAIR enables the APs to measure real-time radio characteristics and send them to the controller via the already established CAPWAP tunnels. Cisco appliances such as Cisco Prime Infrastructure (CPI) and Mobility Services Engine (MSE), shown in Figure 4, extend the capability of this feature to process analytics on Wifi client presence, interfering devices management and heatmaps processing. CLIENTLINK version 4.0, is the Cisco at AP-level implementation of MU-MIMO IEEE 802.11ac beamforming. It works independently of CLEANAIR after the assessment of the quality of the channel. In this scheme, an AP sends a special sounding signal to all its associated WDs, which report, back to this AP, their signal

measurement. Based on these feedbacks, the AP, and not the controller, decides on how much steering toward a specific WD is needed to optimize the energy radiation.

4.2 Radio Coverage Representation Models

We categorize the related-work coverage representation models into three categories: Range-based, Zone-based and Beam-based. In the upcoming subsections, we describe each of them and discuss their limitations.

In the Range-based category of models, it is common to represent an AP's wireless coverage such as: a transmission, interference or no-talk range. These ranges processing is based on the estimation of the distance between the AP and a receiving point P (AP or WD). Further, this category of coverage representation models, consider that an AP's coverage pattern is omnidirectional, with the geometric shape of a circle or a disk, centered at the AP, like in Figure 5. In this scheme, the interference, for example, at any given point is approximated by the weighted intersection of all interfering devices patterns at this point.

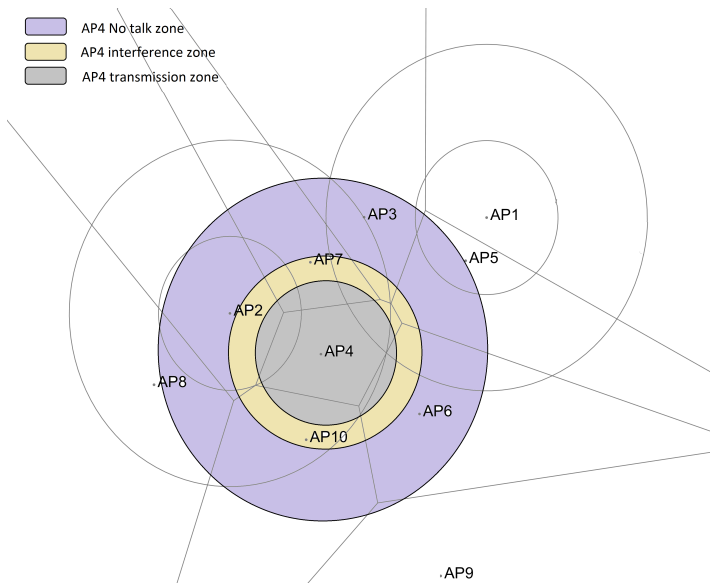


Figure 5: A range-based coverage representation example

In the Zone-based category of models, an AP coverage is a function of its transmission characteristics: channel, power level, etc., but depends also on the neighboring APs. The result of this is that the transmission shape is no more a solid circle but a convex polygon with straight sides. Each straight side defines a borderline that separates two neighboring APs' transmission ranges. The more an AP transmit power is strong, the more the borderline with its neighboring APs is far. Further, it is important to note that a point in a transmission zone of one AP could not be in another AP's transmission zone. An example of Zone-based AP's wireless coverage is represented in Figure 6. In this scheme, the interference caused by the transmission ranges in the previous model, is completely canceled. Only the interference

caused by the other ranges: interference, and no-talk ranges, is present.

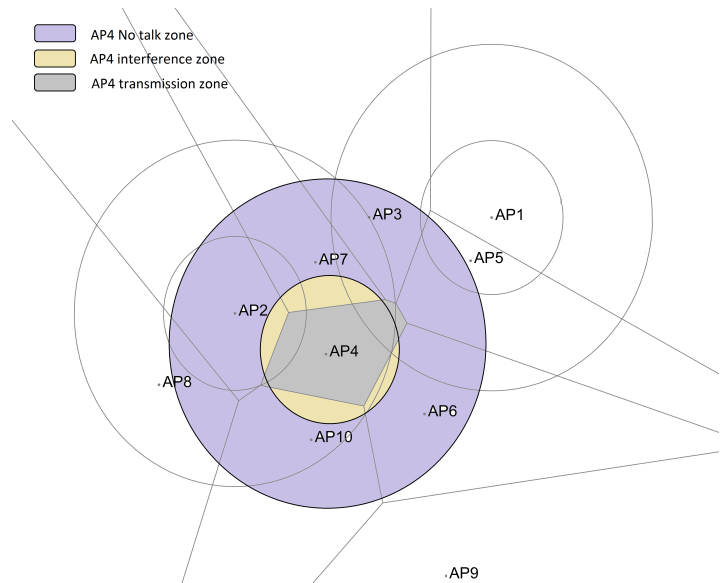


Figure 6: A zone-based coverage representation example

The previous two models: Range and Zone-based, come with these limitations:

- both models are limited to consider that the strength of interference is only inversely proportional to the distance (or quadratic) of an AP from interfering neighbors,
- both models would interpret an increase in a transmission power level as an expanded reach in all directions: uniformly in case of Range-based models but depending on neighboring APs in the case of Zone-based ones,
- a point could not be in two transmission ranges of two different APs at the same time in Zone-based models,
- both models would interpret falsely obstacles to the signal propagation, as a weaker signal from an AP in the context of indoor Wlans does not mean necessarily that this AP is out of reach,
- alternatively, a stronger signal from an AP does not mean necessarily that this AP is at reach: it may be guided or boosted under some conditions.

The consequences of these limitations, the adoption of a Range or Zone-based like representation model of coverage, and regardless of the RRM solution that is built upon, is to false our transmit opportunity processing and misinterpret some phenomena encountered in the specific context of indoor enterprise Wlans.

To overcome the limitations of the previous models, our Beam-based coverage representation, defines for each AP a number of directions over which it may transmit. Depending on the number of directions, their order and transmit power

levels, an AP may be able to mimic a Range or Zone-based scheme. The Figure 7, shows a per-Beam coverage pattern example. In this pattern, the APs have an equal number of directions, equal to eight, that are uniformly distributed and of equivalent transmit power. In works [5, 7], we discussed in detail how per-Zone and per-Range representation models are generalized to per-Beam representation and how our representation model could solve previous models limitations such as : per direction transmit power control, hole coverage reduction, obstacle detection, client localization and transmit opportunities maximization.

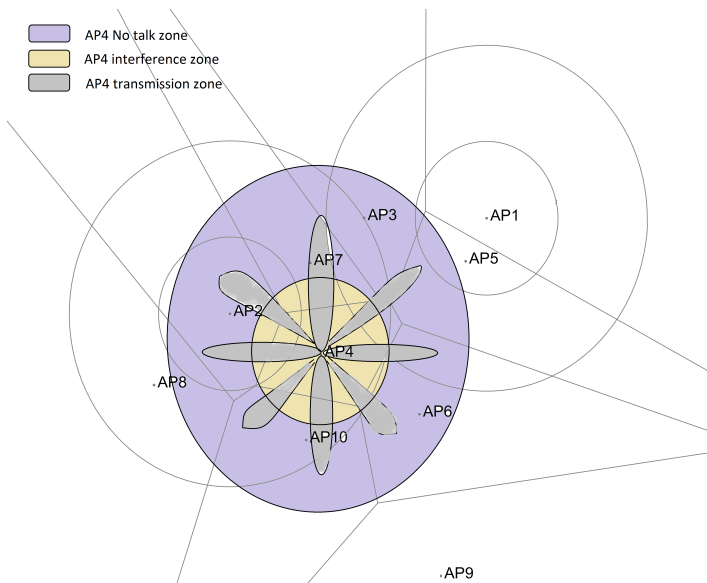


Figure 7: A beam-based coverage representation example

4.3 Machine Learning Regression Models

In his book [15], Tom Mitchell describes a machine, computer program, etc. process of learning when from an experience "E" with respect to some task "T" and some performance measure "P" of this task, its performance on "T", as measured by "P", improves with experience "E".

A simple form of this learning, focus of this work, is described as "supervised" learning. In this learning, the right answers to some input or training data, are provided in advance. Based on this training data, the inputs and corresponding outputs or "truth", the learning algorithm model parameters are processed such as to minimize the error between the predicted outputs and the observed "truth" on the training set.

This "trained" learning, also called hypothesis, is indeed a function that is built using the previously optimized model parameters. This function maps the input variables or features to a predicted outcome.

Supervised learning algorithms could be further classified by the nature of the outcome they work on. If the outcome is continuous, then "regression" models are more suitable. For categorical or discrete outcome values, "classification" algorithms are more suitable.

In our study, we work on outcomes that are continuous, and then we focus solely on regression models. Many types of regression models exist including: linear regression models (LR), regression trees (RT), Gaussian process regression models (GPR), support vector machines (SVM), and ensembles of regression decision trees (BDT).

To choose between models, we compare their Root Mean Square Error (RMSE) validation score. In all the simulations of our work, we observe that Coarse Gaussian SVM and BDT score the best RMSE scores. For the rest of our study, we focus solely on these two models.

Furthermore, SVM and BDT methods represent two distinct algorithm general approaches. In the following subsections, we introduce the important differences in these two approaches.

4.3.1 Support Vector Machines

In SVM, the samples are separated into categories. The idea of this algorithm is to find the maximum gap between these categories. The samples that help find this separation are called support vectors. Each support vector is seen as a dimensional data and the goal of the algorithm is to find the best hyperplane in terms of margin that separates these vectors.

In this work, we use SVM to resolve a linear regression problem. We use a variable that controls the trade-off between the classification errors and the size of the margin. This method corresponds to a soft-margin SVM.

4.3.2 Bagged Decision Trees

Bagging decision trees (BDT) is a meta-algorithm that builds on an ensemble of algorithms that run independently from each other. Each algorithm, called bootstrap, obtains a different result. The result of the meta-algorithm corresponds to the average of the bootstraps individual results. In our case, a bootstrap algorithm may correspond to a simple regression.

The initial training set has n elements. BDT generates, from this set, m new subsets of size n' less than the original set size. If n is equal to n' and n is very big, the probability that each subset has unique values from the initial set is almost 63.2%, the other values are duplicated.

An example of such meta-algorithm is Classification And Regression Trees (CART). The tree operates using a metric and by classifying at each stage, the initial set, the set we are predicting the outcome for. This metric is based on Gini impurity that is calculated from the probability of a certain classification. The classes, which are used in this classification, have been identified during the training phase. In the case of a regression, the algorithm introduces the notion of the variance reduction to build the classes and the corresponding metrics.

5 Problem Description

Coverage processing includes the calculation of interference, opportunity and coverage holes, as per our Beam-based representation model, that is a generalization of the previous work models such as Range or Zone-based representation models.

For the problem description, let us define:

- P_i — a coverage point.
- $L_{j,k}$ — AP_j , number k direction.
- C_i — the sensitivity of point P_i at reception.
- $C_{i,1}$ — AP to which P_i is associated, range of transmission.
- $C_{j,2}$ — AP_j , interference range.
- $C_{j,3}$ — AP_j , no-talk range.

We show in (2), the interference $I_B()$ that is calculated by WLC2, our WLCx dRRM solution variant, using Beam-based representation model. The processed interference by this model at a point P_i , corresponds to the sum of the intersections, $Sc()$, of all APs beam patterns with C_i and their interference and no-talk ranges with $C_{i,1}$ that is the transmission range of AP_i to which the point P_i is associated.

$$I_B(P_i(x, y)) = \alpha_1 \sum_j \sum_k \beta_{j,k} * Sc(L_{j,k}, C_i) + \sum_{k=2}^3 \alpha_k \sum_{j \neq i} \beta_j * Sc(C_{j,k}, C_{i,1}) \quad (2)$$

For the opportunity calculation, let us define:

- $s_{1,i}$ — passive survey result at a coverage point P_i .
- $s_{2,i}$ — active survey result at a coverage point P_i .

In (3), we give the opportunity calculated by WLC2 model, using our Beam-based representation model, $O_B()$. The opportunity is inversely proportional to the interference calculation and hints also, on the result of surveys on the active and passive network paths: $s_{1,i}$ and $s_{2,i}$. Passive surveys allow the controller to have statistics and metrics from the network devices and attached interfaces that are on the network path between the client and the server such as the number of transmit errors, number of lost packets, etc. and is generally available via protocols such: SNMP or *Simple Network Management Protocol*. Active surveys instead, construct traffic patterns and simulate actively the traffic between the client and the server, using protocols such as UDP or TCP, and report measurements such as delay, jitter, etc. to the controller.

$$O_B(P_i(x, y)) \sim \frac{s_{1,i} s_{2,i}}{I_B(P_i(x, y))} \quad (3)$$

The last element to include in the coverage processing, is the number of the detected coverage holes, that is given in (4). Coverage holes are evaluated at every coverage point P_i and correspond to points where the signal is insufficient to perform an accurate communication with their APs of association or the access network, if they are not already associated.

$holeThesh_i$ is another variable that is tight to the point P_i sensitivity at reception.

$$H_B(P_i) = |(P_i | \sum_j \sum_k * Sc(L_{j,k}, C_i) \leq holeThesh_i)| \quad (4)$$

The processing of the coverage, that is done in (2), (3) and (4), is a part of the general processing of our dRRM solution variants: WLC1 and WLC2 that is described in Figure 1 workflow. We give in (5) the necessary time to process the coverage and the changes to this coverage. In (5), we neglected, for simplification, the necessary time to process the optimal number of directions that are supported by the APs and the corresponding transmit power levels. M is the number of APs and any monitoring device. $T_{discovery}$ is the necessary time to run TDD and build a neighborhood map. N is the number of coverage points, where the coverage must be calculated. d is the optimum processed number of directions that are supported by APs. $T_{interference}$ corresponds to the necessary time to process coverage. We consider that $T_{interference}$, $T_{opportunity}$ and T_{holes} , times are equivalent.

$$T_{WLC2} = CONST + M * T_{discovery} + k(N - M) * M * d * T_{interference} \quad (5)$$

In Figure 8, we plot the processing time results of models with and without control: simplistic (Range-based), idealistic (Zone-based), WLC1, WLC2 (dRRM) and Cisco (sRRM). We notice that in general, the without-control models perform better than the with-control models due to the addition of the control part of processing. The processing times of the with-control models are equivalent but huge in comparison with the without-control models.

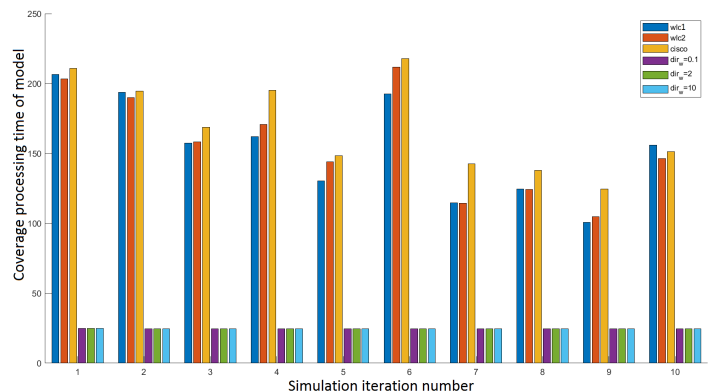


Figure 8: WLC2 time in comparison with idealistic and simplistic models.

The sRRM and dRRM solutions have advantages over each other and over the without-control models, approaches but they require important processing time and resources, which is not suitable in the context of indoor dense enterprise Wlans. In the next section, we propose an optimization solution to with-control RRM models, which is based on concepts from the Machine Learning (ML) field: SVM and BDT. To stick with the aim of this work, we apply this optimization to the example of our dRRM WLC2 solution, but it is easily applicable to the other approaches.

6 MLR-based Optimization Solution: M-WLC2

In this section, we present the details of our solution. We describe the general workflow of our solution, how the training set is chosen and the criteria that allows us to choose between models: RMSE validation score. At the end of this section, we present the new processing time of our solution.

6.1 Workflow

The workflow in Figure 9 describes how our solution processes the coverage. After the initialization, our solution model process a random AP distribution. In this work, we limit the dimension of the coverage plan to 128 coverage points in each dimension. The total number of the coverage points is equal to $128 * 128 = 16,384$ points. From the previous dataset, we build our Test dataset that corresponds to 30% of the total dataset. The Test set is then split into a Train dataset and a Validation dataset. Using the Train dataset, the model trains a number of machine learning models. The predicted data is then compared to the one available in the Validation dataset. Based on the RMSE validation score, the best algorithm is chosen to predict the remaining 70% of the overall dataset.

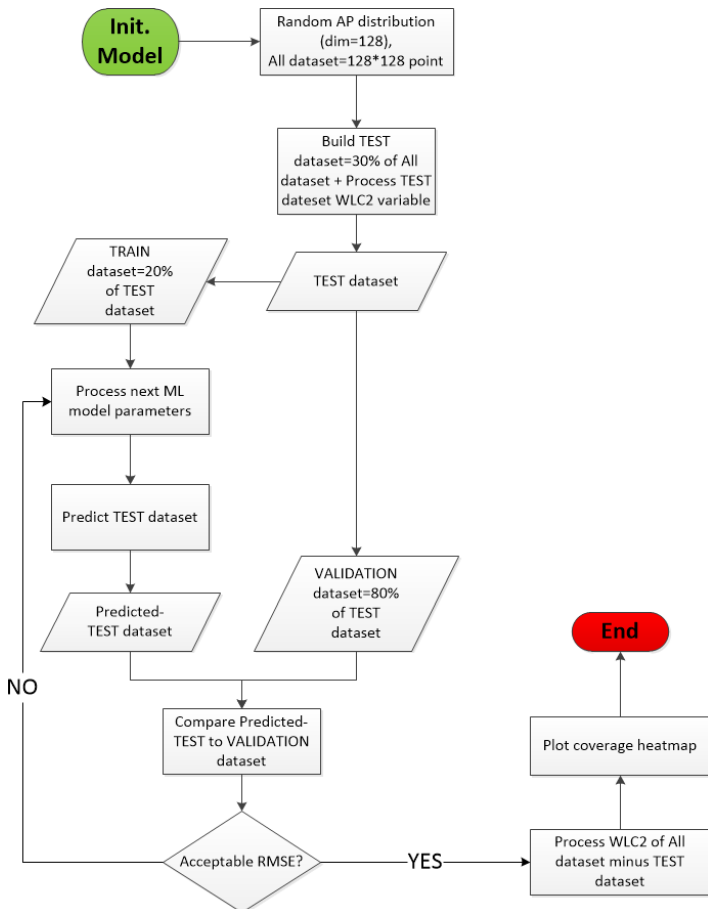


Figure 9: Our ML-WLC2 solution workflow

Our solution is written and simulated in Matlab programming language. Further work would consider the implementation of our solution on Linux-based APs and test its performance in a real laboratory setup. In Figure 10, the detailed description of the software architecture of our solution. The functionProcessML() module is responsible of processing the different data sets, training of the models and of the prediction of the outcomes.

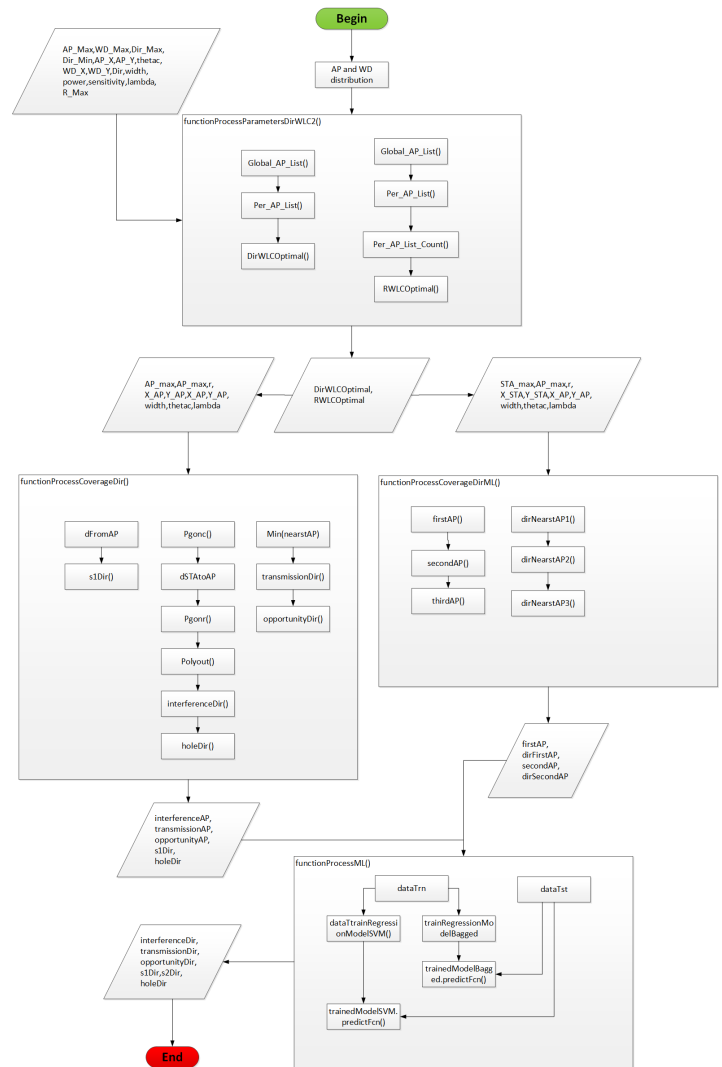


Figure 10: Our ML-WLC2 solution software architecture

6.2 Training Set

To overcome overfitting problems, the training set, Train dataset in the workflow of Figure 9, corresponds to 20% of the Test set. The Validation set is 80% of the the Test set. The Test set represents 30% of the overall available dataset (16,384 points).

For each point in the validation set (the training set is a subset of the validation dataset), we gather this information: the index of the WD or coverage point, the coordinates of this WD, the first AP of association, the corresponding direction of transmission, the transmit power level, the AP load, the

list of neighboring AP, the second AP of association, the corresponding direction of transmission, and so on. The list may be augmented by any relevant information or feature that may have an impact on the phenomenon under study (the interference, in our case).

6.3 RMSE Validation

RMSE stands for Root Mean Square Error. It measures the error between the predicted outcome using the trained model and the truth. The truth in our case is the real measures that were reported by the network APs, WDs, and sniffers.

An important number of tests, the same simulation of the previous networks, allowed us to choose SVM and BDT models. These models score an average of 16.03 and 14.75 points respectively.

Based on the historical results, we set the acceptable RMSE validation score for a model to be accepted in processing the remaining overall dataset points, as it was described in the workflow of Figure 9.

In addition to the RMSE validation score, we use statistical results and visual observations of the heatmap to validate the precision of the outcome.

6.4 Time

The total required processing time of our M-WLC2 solution is given in (6). The total time is the sum of the required time to train the model, T_{train} , and the time to process the validation set, $30\% * T_{WLC2}$, where T_{WLC2} is the total time required to process WLC2 solution model coverage. In case the training set points report the measurement in real-time, this time is very negligible.

$$T_{WLC2,ML} = CONST + 30\% * T_{WLC2} + T_{train} \quad (6)$$

7 Evaluation

In this section, we evaluate the predictions accuracy and the required processing time of the models with and without optimization: WLC2, SVM and BDT M-WLC2.

7.1 Simulation

We simulate a network of 30 APs that are distributed randomly in a 2D plan using the Matlab built-in `randperm()` function.

The coverage map has a dimension of 128 points in each direction. We process a total of $128 * 128 = 16,384$ coverage points. Each coverage point (in red) corresponds to a potential WD. The WDs are distributed uniformly on the plan.

In Figure 11, we show the distribution of the APs and WDs in the coverage area that corresponds to this simulation. AP1 and AP2 coverage is represented using their Beam-based coverage pattern. AP14 and AP15 coverage is represented by their Range-based coverage pattern.

7.2 Processing of Area Coverage Heatmap

Before we process the coverage of the optimized models, we process the coverage of the WLC2 without optimization. In Figure 12, we show the resultant heatmap of WLC2 processing that indicates the level of interference in the coverage area.

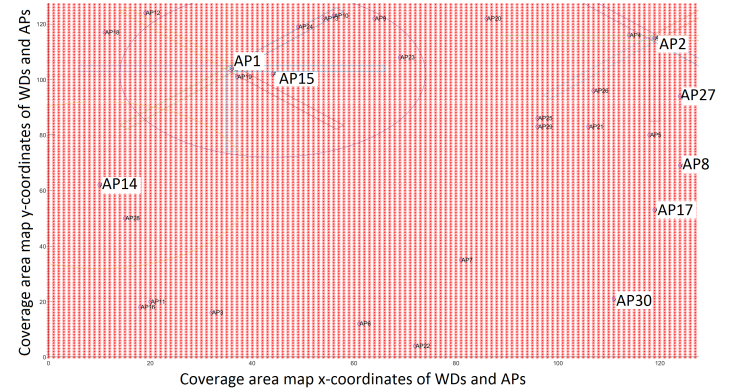


Figure 11: The distribution of APs and WDs in a simulated network

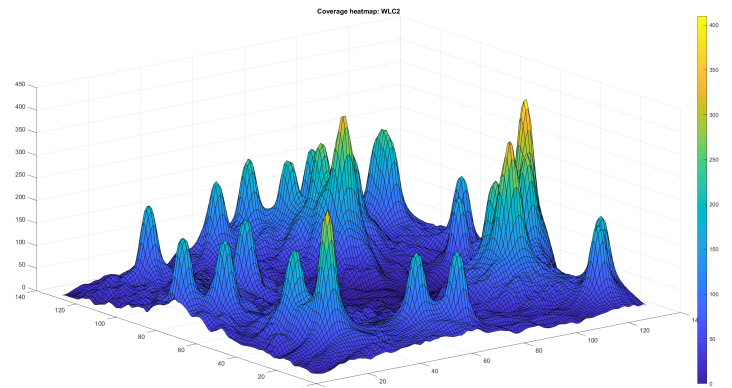


Figure 12: WLC2 area coverage resultant heatmap

In Figure 13 and Figure 14, we show the result of the BDT and SVM optimized WLC2 model coverage processing, respectively. Visually we observe a strong resemblance of the three patterns.

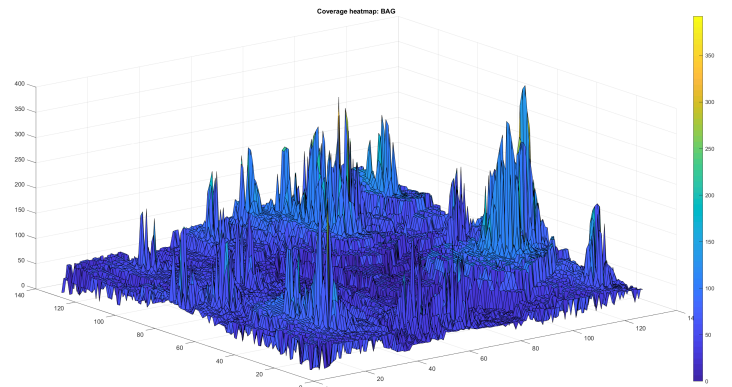


Figure 13: BDT ML-WLC2 area coverage resultant heatmap

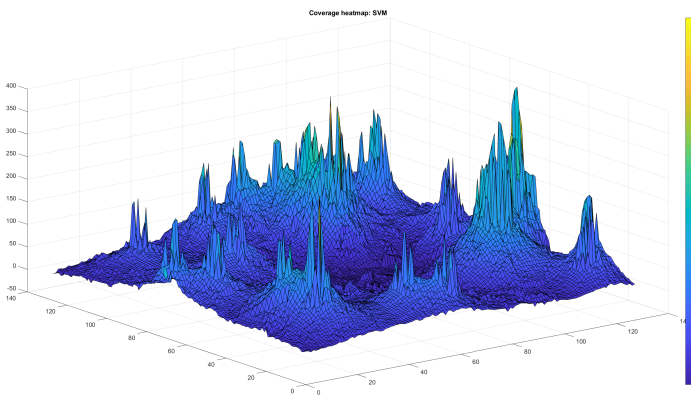


Figure 14: SVM ML-WLC2 area coverage resultant heatmap

In addition to the visual resemblance, the accuracy of the models' prediction is evaluated statistically and using the RMSE validation score. The statistical results hint on the mean, median, standard deviation in between the prediction and the WLC2 model calculated values. The performance of the models depends also on the required processing time.

7.3 Multiple Iterations of The Same Simulation

In this section, we present the results of multiple iterations of the same simulation (random distribution of APs at each iteration). In Figure 15, we draw the mean, median and standard deviation results for BDT and SVM models for 10 iterations of the same simulation.

In Figure 15, we observe that BDT presents a better mean around zero and a median slightly around five points in average. SVM shows a better median but a mean around three points in average. BDT standard deviation is twice greater in average than the SVM's, almost 40 points in the first simulations and 30 points in the last ones.

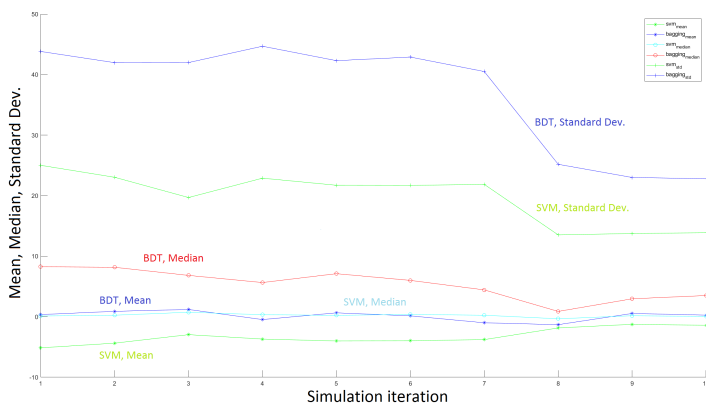


Figure 15: Statistical results of 10 iterations of BDT and SVM M-WLC2 simulation

For the same simulations, we show in Figure 16, the variation of the RMSE score. We observe that the BDT solution scores the best RMSE value, almost 45 points, against the SVM model, almost 25 points, in the first simulations. In the three last simulations, the RMSE score drops to almost 25 points for BDT model and only 15 points for the SVM model.

In Figure 17, we show the required processing time of models with and without optimization. In general, we observe that the optimized models: BDT and SVM times are comparable and very negligible in comparison with WLC2 time, almost 2.5 smaller.

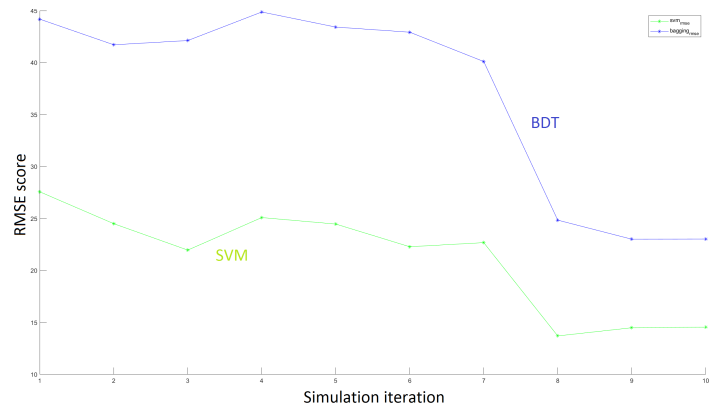


Figure 16: RMSE results of 10 iterations of BDT and SVM M-WLC2 simulation

7.4 The Effect of Modifying The Training Set Size

In this subsection, we propose to check the effect of modifying the training set size on the optimized models performance.

In Table 1, we show the results of modifying the size of the training set in this range: 10%, 20%, 30%, 50% and 90% of the total available data set. We notice no remarkable change in statistical results in terms of mean and median in between the models when the training set is 10%, 20% and 30%. For bigger training sets, these values are getting remarkably smaller. The SVM model standard deviation decreases with the increasing training set sizes. Concerning the BDT model, we observe the opposite; the standard deviation is at its highest value when the size of the training set is 90% of the total available data set.

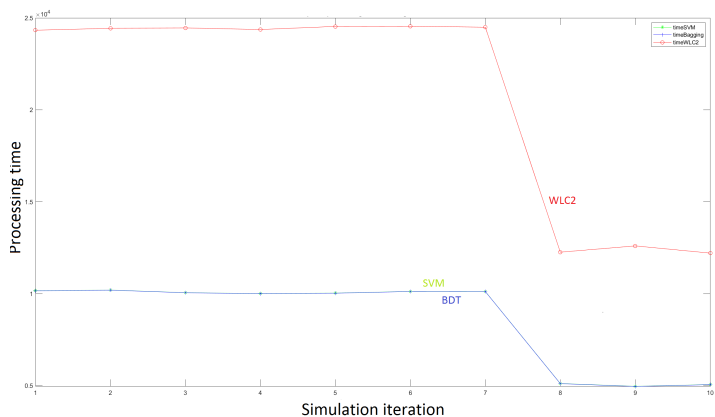


Figure 17: Required processing time of 10 iterations of BDT and SVM M-WLC2 simulation, training set 30% of total data set

Table 1: Effect of modifying the training set size on model performance

Var.	$trn_{set} = 10\%$	20%	30%	50%	90%
m_{svm}	-3,92	-3,23	-3,25	-2,39	-2,50
m_{bdt}	-0,27	0,18	0,11	-0,03	-0,05
med_{svm}	0,29	0,25	0,20	0,15	0,12
med_{bdt}	4,69	5,66	5,37	4,87	5,45
std_{svm}	23,76	20,55	19,69	16,50	16,40
std_{bdt}	34,93	34,75	36,90	35,90	38,91
$rmse_{svm}$	25,10	21,88	21,13	17,82	17,21
$rmse_{bdt}$	34,69	34,74	37,02	36,02	38,85
t_{svm}	2594,88	3776,93	5291,24	7602,12	1485,02
t_{bdt}	2594,19	3774,37	5286,25	7585,18	1479,40
t_{wlc2}	1209,41	1202,43	1280,81	1229,02	1469,01

In general, BDT scores better RMSE values than SVM. SVM's RMSE score is better when the size of the training set is the smallest, 10% of the total available data set. Differently from SVM, the BDT model scores the best RMSE value when the training set is 90% of the total data set.

The optimized models processing time is comparable. For a training set equal to 10% of the total available data set, this time is enhanced by almost 78.54% relatively to the WLC2 model.

7.5 Modifying The Dimension Size of The Coverage Area

In this subsection, we present the results of modifying the size of the coverage area or dimension on the performance of the optimized models. The training set is set to 10% of the total available data set.

In Table 2, we observe that the required time to process a 256 dimension coverage area is almost 842 times higher than processing a 16 dimension map. In the first case, our optimized models enhance the required time by almost 79.77%.

The visual aspect of the coverage is presented in Figure 18. The pattern is comparable between both optimized models and representative of WLC2 result. We notice though that SVM result is more precise than BDT if we focus on the lowest coverage values.

The BDT model scores the best RMSE score in comparison with the SVM models for the high dimensions. The opposite happens for the low dimension values.

In terms of the statistical results, the SVM model results in less standard deviation from the mean. The SVM median is around zero whereas the BDT model median is at almost 5 points for high dimensions.

Table 2: Modifying the dimension of heatmap effect on ML heatmap processing

Var.	$dim = 256$	128	64	32	16
m_{svm}	-2,15	-4,16	-1,87	-0,93	0,04
m_{bdt}	-0,15	-0,11	0,09	0,34	0,64
med_{svm}	0,15	0,36	0,32	0,19	0,69
med_{bdt}	4,15	5,56	1,59	-0,73	-0,67
std_{svm}	15,82	24,8	19,83	23,76	23,29
std_{bdt}	25	37,6	23,72	20,21	17,47
$rmse_{svm}$	16,04	26,7	20,94	24,08	25,63
$rmse_{bdt}$	24,75	37,63	23,29	21,02	18,2
t_{svm}	1297,54	2744,41	450,09	130,53	58,9
t_{bdt}	1295,84	2743,7	450,12	130,65	58,99
t_{wlc2}	6406,31	1280,94	1836,07	304,17	76,58

8 Conclusion

In this work, we have introduced our WLC2 dRRM solution in contrast with literature approaches: Zone or Voronoi diagram-based (idealistic) and Range-based (simplistic), and vendor sRRM category of models: Cisco especially. We have shown that our solution performs better than the vendor sRRM solution in a simulated controller-based Wifi environment.

Further, in this work, we have shown that the basic variant of our dRRM solution, WLC2, comes with some limitations: the important system resources consumption and the required processing time. The M-WLC2 optimization solution, which is based on important machine learning concepts, allowed us to achieve an average of 79.99% relative time reduction by processing only 10% of the total available data set. The accuracy of the results was evaluated visually and statistically.

Our M-WLC2 optimization solution does not depend on the Beam-based coverage representation model approach we adopted for the simulation of the coverage area. It relies only on the environmental variables, which influence the phenomena, to build a prediction model rather than on an analytical calculus of the physical phenomena itself. Besides, our optimization solution is not limited to only our dRRM solution but could be easily extended to optimize sRRM models too.

It is to mention that the optimization process of our dRRM solution, presented in this work, could be accomplished in different ways. The first approach is to describe analytically the physical phenomena under study like in our solution N-WLCx discussed in this work [16]. The second approach is to work deeply on the performance of the actual machine learning algorithms as it may be suggested by works such as [17]. The idea here is to adapt the standard machine learning algorithms to our specific need.

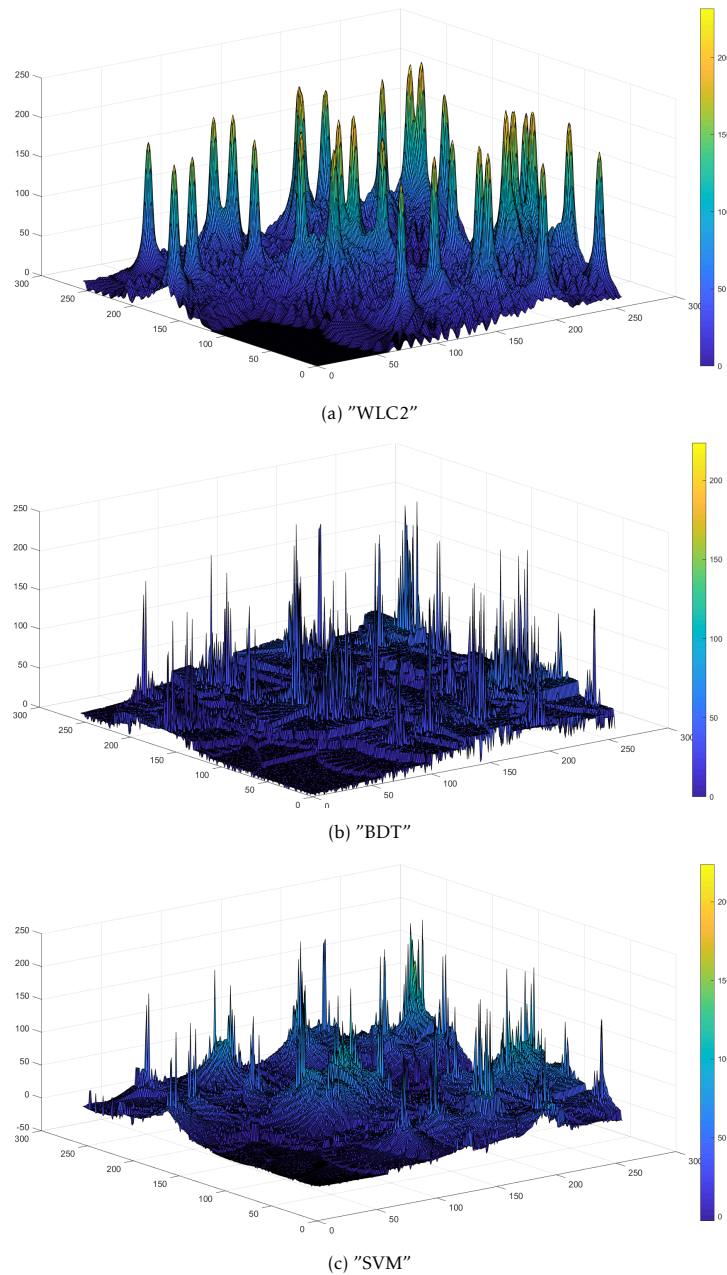


Figure 18: Visual aspect of ML optimized WLC2 coverage when $dim = 256$

Conflict of Interest The authors declare no conflict of interest.

Acknowledgment We would thank colleagues : researchers, engineers, and reviewers for sharing their precious comments and on-field experience that improved the quality of this paper.

References

- [1] M. Guessous and L. Zenkour. "ML-Optimized Beam-based Radio Coverage Processing in IEEE 802.11 WLAN Networks". In: *2018 5th International Conference on Electrical Engineering, Computer Science and Informatics (EECSI)*. Oct. 2018, pp. 564–570. doi: 10.1109/EECSI.2018.8752874.
- [2] Rafiza Ruslan and Tat-Chee Wan. "Cognitive radio-based power adjustment for Wi-Fi". In: *TENCON 2009-2009 IEEE Region 10 Conference*. IEEE. 2009, pp. 1–5. doi: 10.1109/TENCON.2009.5396078.
- [3] Daji Qiao et al. "Adaptive transmit power control in IEEE 802.11 a wireless LANs". In: *The 57th IEEE Semiannual Vehicular Technology Conference, 2003. VTC 2003-Spring*. Vol. 1. IEEE. 2003, pp. 433–437. doi: 10.1109/VETECS.2003.1207577.
- [4] Nabeel Ahmed and Srinivasan Keshav. "A successive refinement approach to wireless infrastructure network deploy-

- ment". In: *IEEE Wireless Communications and Networking Conference, 2006. WCNC 2006*. Vol. 1. IEEE. 2006, pp. 511–519.
- [5] Mehdi Guessous and Lahbib Zenkour. "Cognitive directional cost-based transmit power control in IEEE 802.11 WLAN". In: *2017 International Conference on Information Networking (ICOIN)*. IEEE. 2017, pp. 281–287. doi: 10.1109/ICOIN.2017.7899520.
- [6] Prateek R Kapadia and Om P Damani. "Interference-constrained wireless coverage in a protocol model". In: *Proceedings of the 9th ACM international symposium on Modeling analysis and simulation of wireless and mobile systems*. ACM. 2006, pp. 207–211. doi: 10.1145/1164717.1164754.
- [7] Mehdi Guessous and Lahbib Zenkour. "A novel beamforming based model of coverage and transmission costing in IEEE 802.11 WLAN networks". In: *Adv. Sci. Technol. Eng. Syst. J.* 2.6 (2017), pp. 28–39. doi: 10.25046/aj020604.
- [8] Amit P Jardosh et al. "Green WLANs: on-demand WLAN infrastructures". In: *Mobile Networks and Applications* 14.6 (2009), pp. 798–814. doi: 10.1007/s11036-008-0123-8.
- [9] Aditya Akella et al. "Self-management in chaotic wireless deployments". In: *Wireless Networks* 13.6 (2007), pp. 737–755. doi: 10.1007/s11276-006-9852-4.
- [10] Cem U Saraydar, Narayan B Mandayam, David J Goodman, et al. "Efficient power control via pricing in wireless data networks". In: *IEEE transactions on Communications* 50.2 (2002), pp. 291–303. doi: 10.1109/26.983324.
- [11] Dipankar Raychaudhuri and Xiangpeng Jing. "A spectrum etiquette protocol for efficient coordination of radio devices in unlicensed bands". In: *14th IEEE Proceedings on Personal, Indoor and Mobile Radio Communications, 2003. PIMRC 2003*. Vol. 1. IEEE. 2003, pp. 172–176. doi: 10.1109/PIMRC.2003.1264255.
- [12] *Radio Resource Management White Paper - Transmit Power Control (TPC) Algorithm [Cisco 5500 Series Wireless Controllers]*. en. June 2016. URL: https://www.cisco.com/c/en/us/td/docs/wireless/controller/technotes/8-3/b_RRM_White_Paper/b_RRM_White_Paper_chapter_0101.html (visited on 05/14/2019).
- [13] *ARM Coverage and Interference Metrics*. URL: https://www.arubanetworks.com/techdocs/ArubaOS_64x_WebHelp/Content/ArubaFrameStyles/ARM/ARM_Metrics.htm (visited on 05/17/2019).
- [14] *Lowering the power level to reduce RF interference*. URL: https://help.fortinet.com/fo50hlp/52data/Content/FortiOS/fortigate-best-practices-52/Wireless/Lowering_Power_Level.htm (visited on 05/17/2019).
- [15] Thomas M. Mitchell. *Machine Learning*. 1st ed. New York, NY, USA: McGraw-Hill, Inc., 1997. ISBN: 0070428077, 9780070428072.
- [16] Mehdi Guessous and Lahbib Zenkour. "A nurbs based technique for an optimized transmit opportunity map processing in wlan networks". In: *International Conference on Wired/Wireless Internet Communication*. Springer. 2017, pp. 143–154. doi: 10.1007/978-3-319-61382-6_12.
- [17] Alireza Babaei. "Longitudinal vibration responses of axially functionally graded optimized MEMS gyroscope using Rayleigh–Ritz method, determination of discernible patterns and chaotic regimes". In: *SN Applied Sciences* 1.8 (2019), p. 831. doi: 10.1007/s42452-019-0867-8.

Monitoring System Using GPS for Logistic's Key Performance Indicator

Abba Suganda Girsang*, Triadi Prabowo

Computer Science Department, BINUS Graduate Program-Master of Computer Science, Bina Nusantara University, 11480 Jakarta, Indonesia

ARTICLE INFO

Article history:

Received: 24 July, 2019

Accepted: 22 October, 2019

Online: 22 November, 2019

Keywords:

Kpi

Logistic

Gps

Tracking

Transporter

ABSTRACT

Transportation vendors are important for distribution companies to deliver goods or products. Operational problems of logistic process in transportation vendors' activities are difficult to track and monitor directly in the field, such as driver's position, the delivery, and so forth. These problems result in the difficulty to measure the performance of vendors' activities. The aim of this research is to develop a system which covers monitoring and tracking of their logistic process operation problems. The system is built based on Android integrated with GPS and GSM. This system is also equipped with the ability to recapitulate the performance of transportation vendors in running activities of logistic operation. The performance is measured from some important components in logistic process. They are task assessment, on-time delivery, completed administration and availability. The result of this system is capable to show the vendor transportation's key performance indicator (KPI) and minimize bureaucratic problems.

1. Introduction

The rapid growth of information technology has brought many changes to various business aspects, including logistics. Modern technologies such as GPS (Global Positioning System) and RFID (Radio Frequency Identification) can be used to change semi-manual process to systematic process [1]-[3]. Implementation of these technologies in logistic business sector enhances the performance of logistic process operation [4]. A survey shows that logistic company needs transparency in logistic process operation and more security [5]. GPS (Global Positioning System) is currently the most promising technology for acquiring position information in a field [6]-[9].

Manufacturers that process raw materials into ready-to-use product need logistic to transport their goods to other factories or their suppliers. Then, logistic operations provide transportation service of goods to desired locations (customer included) or warehousing. There are companies which keep their logistic function is part of the companies operation/business process and others keep their logistic function by using vendor transporters (outsourcing logistic) [10]-[12]. Both of them have advantages and disadvantages. Outsourcing logistic function has a high risk of loss competencies which may lead to high cost [13], [14] and hard to monitor their operation and management. Many researches look

into logistic function outsource issues but few addressed so far about in-house logistic provider issues [10], [15], [16]-

KPI (key performance indicator) in logistic business sector is mainly used to measure and show gaps between fundamental logistic process while delivering goods and the expected performance proposed by the company [17], [18]. Real-time data play a crucial part in this case, because obtaining information and giving feedback to correspondents can be done more quickly (between operators and courier). Implementation of websocket may help achieve that, because its behavior provides full-duplex, communication channel that operates through a single connection which builds scalable and real-time application [19].

We found empirical findings based on some cases in company. However, in this paper, a cement company, PT. XYZ, is used as a reference. This company uses outsourcing logistic function (vendor transporter). It is facing some issues, such as the incapability of the to complete given assignments, goods not delivered on time, incomplete documents, and availability of fleet difficult to maintain and ready to use. This study proposes a new approach to implementing fleet-management and vendor performance evaluation (KPI). Monitoring application based on node.js platform and android as its client is implemented in this case. It is expected to minimize the risk of outsourcing its logistic provider such as monitoring transporter movement and recording the whole trip data, which is later used to evaluate the transporter's

*Abba Suganda Girsang, Email: gandagirsang@yahoo.com

performance in doing logistic functions, and capable to evaluate vendor transporter KPI.

The study provides a system of performance for companies which use logistic transporters based on tour records of their drivers. This system is built based on four indicators obtained from the activities of the drivers.

2. Proposed Method

The proposed method is mainly aimed to identify the criteria which should be considered in vendor transporter work performance (KPI) evaluation aspect. We include relevant KPI aspects such as task assignment, manageable delivery time, completed administration and fleet availability management and its system design to achieve related aspects.

2.1. System design

Many technique designs are proposed to develop the system. Figure 1 indicates the scheme of our framework to implement monitoring logistic operation system, which is integrated with GPS (global positioning system) to monitor fleet movement in an on-going delivery process. By using device (smartphone) on each transporter, a real-time communication between transporter and head officer (HO) can be done. It look like using emitting data transaction through websocket [20]. It is to achieve full-duplex communication between client and server.

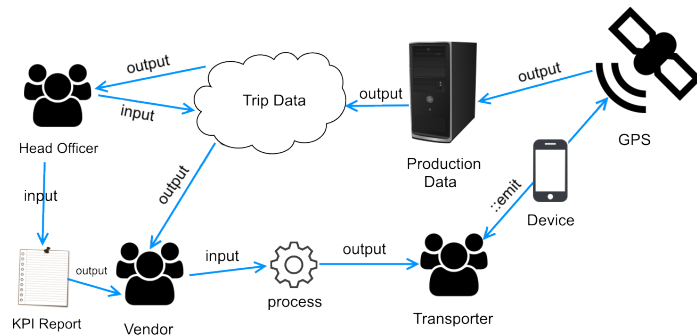


Figure 1: Proposed framework scheme

Three main actors in logistic function operation, which are HO (head officer), vendor transporter, and transporter (driver), are involved in the evaluation of vendor transporter KPI. Internal staff as head officer handles all data transactions between headquarter (HQ) and client (in this case vendor transporter and driver). The design steps can be described as follows. First, head officer input the required trip data (task assignment) which will be assigned to selected vendor. Then, it is processed by vendor and given to transporter (driver). All activities recorded in application device is bundled into one production data including the history of transporter position using GPS emitted from the device. It becomes an output to trip data history. Then, the trip data will be processed by head officer to assess or evaluate KPI of vendor transporter within each evaluation period time.

There are some steps to develop real-time monitoring and tracking system.

Business Requirement Analysis. This phase gathers information regarding business process from process business by interview with related job description required to obtain the requirements.

User Requirement Analysis. This phase is to obtain information from process owner regarding the new proposed model.

Evaluation analysis. Based on requirements analysis, the best method is chosen and transformed into suitable aspects evaluation.

Prototyping. This step is conducted in the architectural design and development of products or services. In this case, the requirements are transformed into an application to understand the system method or concepts.

Implementation. In this phase, the new proposed method is implemented which is customized based on existing business model and solving the current problem.

Reporting (Documentation). Reporting or documentation is taken to track which parts of model is proven to be successful or failed as the solution of the problems.

2.2. The Interview

One of the techniques to obtain information and data in this research is using interview [21]. The discussion of process logistic and performance is done with all stakeholders related to the KPI. Some questions used are listed below.

1. What is the SOP (standard operational procedure) of logistic function in your company?
2. What issues are faced by your company with the current SOP?
3. How can the master data be obtained?
4. What is going to happen if customers reject the delivery?
5. What is going to happen if fleets or vehicles get trouble on delivery?
6. Can vendor reject delivery orders?
7. Can transporter vendor track their driver on their own or only based on your company's monitoring function?
8. What is the expectation of this proposed system?
9. What is the KPI aspect you want to evaluate?

Table 1: KPI aspect evaluation

Aspects	Description	Grade
Task assignment (TA)	Vendor capable to complete given DO	25%
On-Time Delivery (OTD)	Vendor capable to deliver goods on-time	25%
Completed Administration (CA)	Vendor capable to submit required document	25%
Availability (A)	Vendor capable to make fleet ready in use (delivery order given)	25%
Total		100%

2.3. KPI Evaluation

The proposed system is developed based on vendor transporter's KPI assessment. This KPI evaluation is important for PT. XYZ to make decisions whether to continue outsourcing the

logistic with selected vendor or terminate the vendor and replace with a new one. The discussions and interviews were conducted by the authors with relevant parties to formulate KPI. As the results, there are four aspects as shown in Table 1. These aspects are formulated to evaluate KPI based on user requirements and the issues of outsourcing logistic functions. The four aspects have the same percentage because they are considered as having the same importance.

The four aspects on Table 1 are built based on the variables as shown in Eq (1), Eq. (2), Eq. (3) and Eq.(4).

Task Assignment (TA). Variable TA is derived from assignment (delivery order) completed by vendor divided by total assignment given per evaluation period as shown Eq. (1).

$$TA = \frac{\text{Completed assignment (per evaluation period)}}{\text{Total assignment (per evaluation period)}} \times 100 \quad (1)$$

On-Time Delivery Target (OTD). Variable OTD is derived from completed delivery expectation (by customer) divided by total assignment given per evaluation period as shown Eq. (2).

$$OTD = \frac{\text{Completed delivery expectation (per evaluation period)}}{\text{Total assignment (per evaluation period)}} \times 100 \quad (2)$$

Completed Administration (CA). Variable CA is derived from vendor capability to submit required document or return document to PT. XYZ as shown Eq. (3).

$$CA = \frac{\text{Returned administration (per evaluation period)}}{\text{Total assignment (per evaluation period)}} \times 100 \quad (3)$$

Availability (A). Variable A is derived from total accepted assignment or delivery order given by internal staff of PT. XYZ, and vendor must provide fleet based on contract while outsourcing permission as shown Eq. (4).

$$A = \frac{\text{Total accepted assignment (per evaluation period)}}{\text{Total contracted unit (per evaluation period)}} \times 100 \quad (4)$$

3. Results and Discussion

In the requirement analysis phase, user is able to set up fleet profile, fleet type, license number, and owner of the fleet. He / she can set up feature of transporter data registered under the vendor. Some features can be developed such as the capability to monitor and track location which allows user to use navigation to the destination place noted in delivery note document with Google Maps, delivery order allocation which allows user to set up delivery order dynamically and specifically, the function of Auto-Grab which allows user to grab delivery order along the way in specific radius near loading plant point, the function of Auto-Rejected when the transporter gets limit to order capacity per day,

and emergency feature which allows transporter and operator (head officer) to communicate through application message system real-time (using websocket).

Figure 2 shows the proposed business process in logistic operation. The process starts with creating delivery order, then HO determines maps of transporter routes. After mapping transporter routes, driver will confirm the given task to accept or reject delivery order (DO). If transporter accepts the DO, he / she gets delivery number (usually called delivery note). After the transporter has the route, then it will be sent to customer. Once customer accepts the order, then customer will sign receipt document. However, if the customer rejects, the document will be returned back to HO.

Figure 3 shows the flow of the proposed system that can be adjusted dynamically to the defined KPI aspects. It is based on empirical findings in manufacture or company which outsources their logistic provider. There are four main data characteristics flow as: User request report, in which users will request through HTTP to get the report; in this case, the calculation is done in four aspects of KPI previously mentioned. Next is collect data, which is the data source from the delivery process or operational logistics processes that have been running. Data is stored on a local database that is directly integrated with the system and the database residing on the ERP system. The next is data processing, in which data obtained either through the ERP or local database provisioned in the development of this application is processed through back-end. This request will end to the user in the form of report. After getting the result, reports that have been processed will be displayed on the application interface to be viewed by the user who performs data request to be used as consideration or decision making from the user. Figure 4, Figure 5, Figure 6, Figure 7, and figure 8 show the KPI result report based on selected aspect and period. The proposed KPI calculates the overall KPI grade or score based on recorded activity data done in evaluation period time which include task assignment, on-time delivery target, completed administration and availability. The formula of the overall KPI is shown in Eq. (5).

$$KPI = \frac{TA+OTD+CA+A}{4} \quad (5)$$

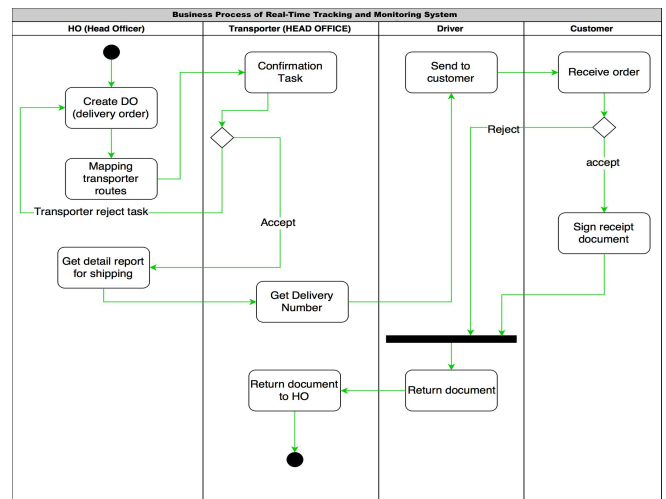


Figure 2: Proposed business process in manufacturer

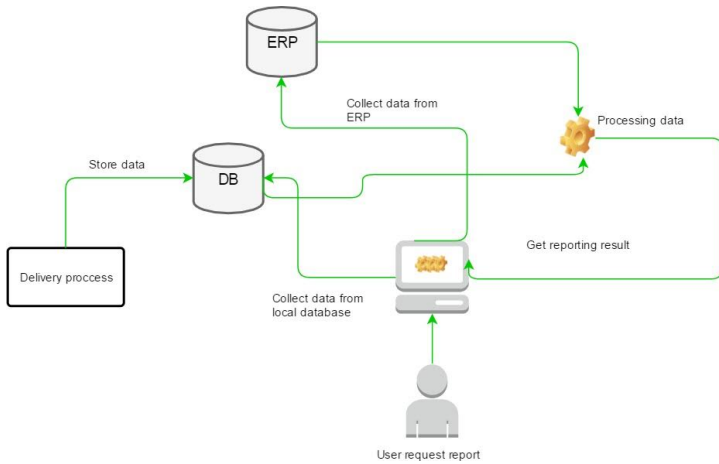


Figure 3: Flow system to evaluate KPI based on defined aspects

The Eq. (5) is calculated is based on Eq. (1), Eq.(2), Eq.(3) and Eq.(4). The result of Eq. (1) is be shown in Figure.4

nama_vendor	total_assignment	completed_assignment	TA
ANDALAN NUSA PR	43	38	88.37
BHANDA CILEGON	33	27	81.82
LINTAS JAWAMAS	19	12	63.16
MAGA NIAGA	22	15	68.18
SINAR PUTRA	15	9	60.00
LIVINA MULYA ABADI	7	6	85.71
TRI KUSUMA JAYA PERKASA, PT	27	25	92.59
TRANSINDO TRANSPORTASI BAHARI, PT	3	3	100.00

Figure 4 the sample data of task assignment

nama_vendor	total_assignment	on_time_delivery	OTD
ANDALAN NUSA PR	43	10	23.26
BHANDA CILEGON	33	5	15.15
LINTAS JAWAMAS	19	8	42.11
MAGA NIAGA	22	4	18.18
SINAR PUTRA	15	7	46.67
LIVINA MULYA ABADI	7	0	0.00
TRI KUSUMA JAYA PERKASA, PT	27	17	62.96
TRANSINDO TRANSPORTASI BAHARI, PT	3	0	0.00

Figure 5 the sample data of On-Time Delivery Target.

The result of Eq. (3) can be shown on Figure 6

nama_vendor	total_assignment	return_dn	CA
ANDALAN NUSA PR	43	26	60
BHANDA CILEGON	33	18	55
LINTAS JAWAMAS	19	6	32
MAGA NIAGA	22	7	32
SINAR PUTRA	15	3	20
LIVINA MULYA ABADI	7	0	0
TRI KUSUMA JAYA PERKASA, PT	27	16	59
TRANSINDO TRANSPORTASI BAHARI, PT	3	1	33

Figure 6 the sample data of completed administration

The result of Eq. (4) can be shown on Figure 7

nama_vendor	total_assignment	avail unit	AVG_unit_per_day	A
ANDALAN NUSA PR	43	50	1	98.00
BHANDA CILEGON	33	20	1	95.00
LINTAS JAWAMAS	19	10	1	90.00
MAGA NIAGA	22	10	1	90.00
SINAR PUTRA	15	10	1	90.00
LIVINA MULYA ABADI	7	5	0	100.00
TRI KUSUMA JAYA PERKASA, PT	27	20	1	95.00
TRANSINDO TRANSPORTASI BAHARI, PT	3	5	0	100.00

Figure 7 the sample data of availability.

Superuser > Vendor KPI

KPI Aspect: Task Assignment, May

Vendor ID	Nama Vendor	Completed Assignment	Total Assignment (Period)	Grade	Action
LG727317	ANDALAN NUSA PR	10	10	100	Detail
LG472742	MITRA TRANSPORTASI PR	15	20	75	Detail
LG123123	JAYA PR	12	15	80	Detail
LG554575	KARINDO MITRA BERSAUDARA PR	10	10	100	Detail
LG887422	HARMONI JAYA PR	8	17	47	Detail

Figure.8: KPI result report

Device ID	UUID	Timestamp	Created at	Lat	Lng	Accuracy	Activity	Battery
125c663531f37f55	67bd3ad48e70	09/14, 14:20:35.1	09/14, 14:20:42.0	45.519408	-73.6168163	13	still (100%)	-
125c663531f37f55	d7801330e1e6	09/14, 14:18:37.3	09/14, 14:20:41.8	45.5192516	-73.6168692	15	on_foot (62%)	96%
125c663531f37f55	07ad5111b499	09/14, 14:18:06.4	09/14, 14:20:41.8	45.5195434	-73.6163816	10	on_foot (100%)	96%
125c663531f37f55	e725aa24facc	09/14, 14:17:36.4	09/14, 14:20:41.8	45.5199382	-73.6159686	8	on_foot (100%)	96%
125c663531f37f55	c93c52ebd10	09/14, 14:17:01.4	09/14, 14:20:41.8	45.5203738	-73.6156441	6	on_foot (85%)	96%
125c663531f37f55	8c9dfc3943e5	09/14, 14:15:26.1	09/14, 14:20:41.8	45.5203233	-73.6149459	4	on_foot (85%)	96%
125c663531f37f55	c2845c8a8c4d	09/14, 14:14:56.1	09/14, 14:20:41.8	45.5201631	-73.6143485	4	on_foot (92%)	96%
125c663531f37f55	433cf408e55c	09/14, 14:14:26.1	09/14, 14:20:41.8	45.5198925	-73.6137712	5	on_foot (100%)	96%
125c663531f37f55	8ba00060edf3	09/14, 14:13:56.1	09/14, 14:20:41.8	45.5195956	-73.6131462	5	on_foot (92%)	96%
125c663531f37f55	000b7ea0eb48	09/14, 14:13:21.4	09/14, 14:20:41.8	45.5193214	-73.6125308	4	on_foot (100%)	96%
125c663531f37f55	bf32ceec0875f	09/14, 14:12:51.4	09/14, 14:20:41.8	45.5190425	-73.6119658	4	on_foot (85%)	96%
125c663531f37f55	8925a0ae53f0	09/14, 14:12:26.1	09/14, 14:20:41.8	45.5188121	-73.6113978	4	on_foot (100%)	96%
125c663531f37f55	4c4822d1a3ba	09/14, 14:11:41.0	09/14, 14:20:41.8	45.5184887	-73.6105816	6	on_foot (69%)	96%
125c663531f37f55	b2035ad5f139	09/14, 14:11:16.0	09/14, 14:20:41.7	45.5182135	-73.6100563	8	on_foot (100%)	96%
125c663531f37f55	a08cb6538951	09/14, 14:10:46.0	09/14, 14:20:41.8	45.5179428	-73.6095	4	on_foot (85%)	97%
125c663531f37f55	6f0d4e04e47e	09/14, 14:10:16.0	09/14, 14:20:41.7	45.517664	-73.6088969	4	on_foot (100%)	97%
125c663531f37f55	29e654415bd7	09/14, 14:09:41.0	09/14, 14:20:44.4	45.5173972	-73.6082512	5	on_foot (100%)	97%
125c663531f37f55	8a775a52c79e	09/14, 14:09:11.0	09/14, 14:20:44.4	45.517105	-73.6077112	6	on_foot (69%)	97%
125c663531f37f55	9ca51efce82f	09/14, 14:08:31.0	09/14, 14:20:44.4	45.516966	-73.6070105	10	on_foot (100%)	97%
125c663531f37f55	d52e50b493e0	09/14, 14:08:01.0	09/14, 14:20:44.3	45.5173395	-73.6066499	4	on_foot (100%)	97%
125c663531f37f55	e2922ccbd3fe	09/14, 14:07:24.5	09/14, 14:20:44.4	45.5177335	-73.6061499	20	on_foot (92%)	97%
125c663531f37f55	92e704c3c2b0	09/14, 14:06:44.4	09/14, 14:20:44.3	45.518188	-73.6057685	16	on_foot (100%)	97%

Figure 9: Monitoring data sample

This system uses the plugin cordova background geolocation to monitor and track module for implementing the system as shown in Figure 9 [22]. It logs all the required data to monitor transporter movements, such as device id, uuid, timestamp, latitude, longitude, accuracy, and activity (on_foot or stay still). Figure 10 shows the GPS (global positioning system) or GNSS (Global navigation satellite system) which allows users to

determine location (geo positioning) from satellite signal reception [23]. As table 2 indicates, the authors performed the trial using the proposed system in transporter while doing delivery. Trial done on Oct 2019 shows fleet movement with registered trip ID and recorded date of trial This system has a unique system which makes the process efficient and transparent. This system is also very useful for company PT XYZ for monitoring the drivers' activities. It can also sort the transportation vendor. This system is able to evaluate the KPI of transportation vendor at PT. XYZ, which is influential in decision-making for contract extension between transportation vendors and PT. XYZ.

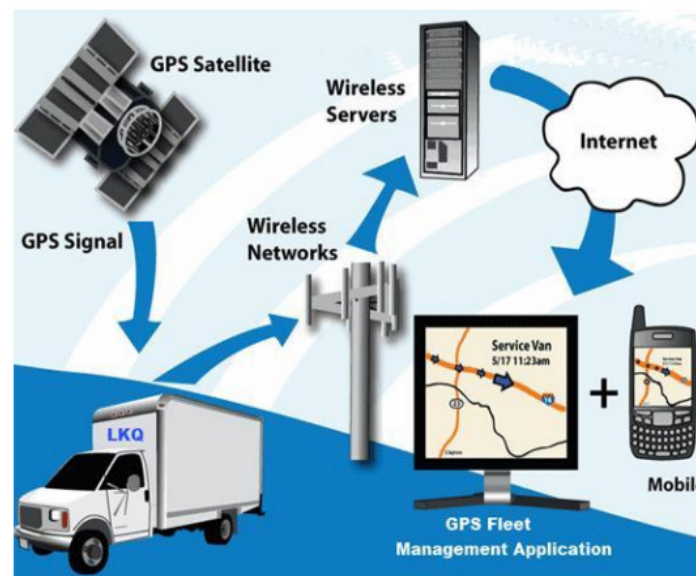


Figure 10: Monitoring process of logistic function

Table 2: Data sample result using monitoring system on transporter fleet

ID	ID Trip	LatLong	Date
SS998710-1570547100000	J21023	51.219243, 4.416459	10/9/2019 19:44
SS998710-1570547555000	J21023	51.218571, 4.422290	10/9/2019 19:49
SS998710-1570547865000	J21023	51.218100, 4.425086	10/9/2019 19:55
SS998710-1570548235000	J21023	51.215775, 4.431201	10/9/2019 20:01
SS998710-1570548502000	J21023	51.213819, 4.441723	10/9/2019 20:07
SS998710-1570548851000	J21023	51.213522, 4.445634	10/9/2019 19:44
SS998710-1570633500000	J21023	51.218243, 4.414238	10/10/2019 17:05
SS998710-1570633955000	J21023	51.219722, 4.415869	10/10/2019 17:12
SS998710-1570634265000	J21023	51.220797, 4.418186	10/10/2019 17:17
SS998710-1570634635000	J21023	51.224990, 4.417028	10/10/2019 17:23
SS998710-1570634902000	J21023	51.226182, 4.417764	10/10/2019 17:28
SS998710-1570635251000	J21023	51.229251, 4.420281	10/10/2019 17:34
SS998710-1570636124000	J21023	51.230112, 4.422311	10/10/2019 17:48
SS998710-1570636415000	J21023	51.230079, 4.426176	10/10/2019 17:53
SS998710-1570636696000	J21023	51.230818, 4.430296	10/10/2019 17:58
SS998710-1570826559118	J243354	51.230991, 4.429542	10/11/2019 08:24
SS998710-1570826561121	J243354	51.229908, 4.429128	10/11/2019 08:32
SS998710-1570826562122	J243354	51.229641, 4.426468	10/11/2019 08:37
SS998710-1570826563120	J243354	51.230152, 4.424990	10/11/2019 08:45
SS998710-1570826564121	J243354	51.229244, 4.424197	10/11/2019 08:50
SS998710-1570826565121	J243354	51.228151, 4.423330	10/11/2019 09:02
SS998710-1570826566118	J243354	51.228791, 4.421419	10/11/2019 09:07
SS998710-1570826567121	J243354	51.229881, 4.420538	10/11/2019 09:12

4. Conclusion

This paper has presented a new approach based on empirical findings and trial in a cement manufacturer outsourcing logistic service. KPI evaluation based on real-time data monitoring is important to determine transporter performance and solution to the issues by outsourcing logistic process function.

This approach will be applied to studies of t logistic business process resulting in KPI evaluation.

References

- [1] K. R. Trivedi and P. M. Dhiren, "Integration of GPS and GSM for the Weather Monitoring System," *Bulletin of Electrical Engineering and Informatics*, vol. 1, no. 3, pp. 209-212, 2012.
- [2] D. Liu, X. Cao, X. Zhou, and M. Zhang, "Cold Chain Logistics Information Monitoring Platform Based on Internet of Vehicles," in *2019 International Conference on Intelligent Transportation, Big Data & Smart City (ICITBS)*, 2019, pp. 348-351.
- [3] S. Fazel and J. Javad, "A Highly Efficient and Linear Class AB Power Amplifier for RFID Application," *Bulletin of Electrical Engineering and Informatics*, vol. 4, no. 2, pp. 147-154, 2015.
- [4] M. R. Kaloop, E. Elbeltagi, J. W. Hu, and A. Elrefai, "Recent advances of structures monitoring and evaluation using GPS-time series monitoring systems: A review," *ISPRS Int. J. Geo-Information*, vol. 6, no. 12, p. 382, 2017.
- [5] C. Kandel, M. Klumpp and T. Keusgen, "GPS based Track and Trace for Transparent and Sustainable Global Supply Chains," in *17th International Conference on Concurrent Enterprising*, Aachen, Germany, 2011.
- [6] K. R. Prasanna and M. Hemalatha, "RFID GPS and GSM based logistics vehicle load balancing and tracking mechanism," *Procedia Engineering*, vol. 30, pp. 726-729, 2012.
- [7] M. Bottero, C. B. Dalla and F. P. Deflorio, "Wireless sensor networks for traffic monitoring in a logistic centre," *transportation Research Part C: Emerging Technologies*, vol. 26, pp. 99-124, 2013.
- [8] X. M. Guo, L. S. Chen, M. Chen and C. L. Peng, "Design of real-time ECG monitoring system based on smart-phone," *Application Research of Computers*, vol. 6, p. 55, 2010.
- [9] Y. Yan, X. Hao and W. Wang, "Location-Based Services and Privacy Protection under Mobile Cloud Computing," *Bulletin of Electrical Engineering and Informatics*, vol. 4, no. 4, pp. 345-354, 2015.
- [10] R. Wilding and R. Juriado, "Customer perceptions on logistics outsourcing in the European consumer goods industry," *International Journal of Physical Distribution & Logistics Management*, vol. 34, no. 8, pp. 628-644, 2004.
- [11] M. Kiliç, A. Günsel, and H. G. Çekmecelioglu, "The Effects of Outsourcing in Logistics Services to Competitive Advantage," *Eur. J. Multidiscip. Stud.*, vol. 1, no. 4, pp. 233-242, 2016.
- [12] S. Zailani, M. R. Shahrudin, K. Razmi, and M. Iranmanesh, "Influential factors and performance of logistics outsourcing practices: an evidence of Malaysian companies," *Rev. Manag. Sci.*, vol. 11, no. 1, pp. 53-93, 2017.
- [13] B. Quelin and F. Duhamel, "Bringing together strategic outsourcing and corporate strategy: Outsourcing motives and risks," *European management journal*, vol. 21, no. 5, pp. 647-661, 2003.
- [14] M. Abdur Razzaque and S. C. Chang, "Outsourcing of logistics functions: a literature survey," *International Journal of Physical Distribution & Logistics Management*, vol. 2, pp. 89-107, 1998.
- [15] D. Pyza, R. Jachimowski, I. Jacyna-Golda, and K. Lewczuk, "Performance of equipment and means of internal transport and efficiency of implementation of warehouse processes," *Procedia Eng.*, vol. 187, pp. 706-711, 2017.
- [16] K. Moons, G. Waeyenbergh, and L. Pintelon, "Measuring the logistics performance of internal hospital supply chains—a literature study," *Omega*, vol. 82, pp. 205-217, 2019.
- [17] D. Radović and Ž. Stević, "Evaluation and selection of KPI in transport using SWARA method," *Int. J. Transp. Logist.*, vol. 18, no. 44, pp. 60-68, 2018.
- [18] A. Weber and R. Thomas, "Key performance indicators," *Measuring and Managing the Maintenance Function*, 2005.
- [19] Y.-H. Zhao, "Evaluation model of third-party logistics customer service quality based on KPI," *Logistics Sci-Tech*, 2009.
- [20] V. Pimentel and B. G. Nickerson, "Communicating and Displaying Real-Time Data with WebSocket," *IEEE Internet Computing*, vol. 16, no. 4, pp. 45-53, 2012.
- [21] R. Opdenakker, "Advantages and disadvantages of four interview techniques in qualitative research," *Forum Qualitative Sozialforschung/Forum: Qualitative Social Research*, vol. 7, no. 4, 2006.

- [22] T. Software, "The most sophisticated background location-tracking &," 2015. [Online]. Available: <https://github.com/transistorsoft/cordova-background-geolocation-lt>.
- [23] D. Abha, H. Shah, K. Shah and M. Vala, "Global Positioning System for Object Tracking," *International Journal of Computer Applications*, vol. 109, no. 8, pp. 40-45, 2015.

Optimization of Power Balance Transaction Based on Renewable Energy Sources Using Artificial Salmon Tracking Algorithm for Modeling the Interconnected Grid Development

Arif Nur Afandi^{*,1,2,3}, Aripriharta^{1,3}, Yuni Rahmawati¹

¹Electrical Engineering, Universitas Negeri Malang, Malang 65145, Indonesia

²Smart Power and Advanced Energy Systems Research Center, Batu 65317, Indonesia

³Center for Advanced Material for Renewable Energy, Malang 65145, Indonesia

ARTICLE INFO

Article history:

Received: 21 August, 2019

Accepted: 09 October, 2019

Online: 22 November, 2019

Keywords:

Artificial salmon

Energy mix

Solar energy

Unit commitment

Wind energy

ABSTRACT

Since environmental requirements penetrate engineering processes to keep global warming and to reduce pollutant emissions, the system operation should be designed based on environmentally approach friendly. Operationally, the system processes are supported by energy suppliers to meet continuously energy transaction while clean and green energies are also targeted to keep the environmental conditions. In other word, the renewable energy source becomes an opportunity integration of a potential natural source inclusion into conventional energy producers. Technically, the energy balance is also important to optimize to get an optimal power portion during the operating period. These works are prioritized to search the balanced combination of the integrated energy mix composition. The works also present the novel computational intelligence to find out the energy portion using Artificial Salmon Tracking Algorithm. By considering technical requirements and tested on the integrated renewable energy plants, this algorithm is applied to optimize the economic power production. The works show dynamically the total power for feeding the energy consumption through local loads. The power production is also balanced in various combination portions of energy sources in accordance with the power demand as similar as discharged pollutants. Moreover, the computation has been obtained clearly for optimal solutions within 24 hours using a proposed algorithm.

1. Introduction

Electricity is one of the energy types which is used to be an important factor to support many technical processes. This energy has been affecting various activities caused by an easy conversion to other types for supplying many appliances [1], [2]. It uses not only industries but also in daily activities. Moreover, stable energy producers are needed to cover continuously an energy dispatching quota (EDQ) where energy users are located far away from the potential supplier [1], [3], [4]. In addition, this condition should be also supported by the reliable infrastructure to transmit and distribute the produced power to wide spreading loads at different locations. To cover the EDQ, the energy producers should consist of all activated power plants [5], [6]. Technically, the EDQ is also faced with the load demand changes in the period of time operation related to scheduled loads. Operationally, the EDQ is also used to

divide each contribution in the integrated energy mix composition (IEMC) through a scheduling power output of energy plants associated with technical limitations, which is frequently operated based on an economic strategy [5], [7], [8]. In general, this strategy is supposed to the financial consideration based on the reducing fuel procurement fee and environmental compensation as the impact of the emission. Practically, this way concern in an integrated structure for the IEMC deal with generating sites for the generation systems, transmission systems, and distribution systems [4], [9], [10]. These conditions are associated with an energy stock to meet the total load and scheduled power outputs for the EDQ. Recently, a dynamic problem also becomes one of the main problems caused by demand changes within 24 hours considered reasonable composition energy sources for determining economically the operating cost and measuring energy producer contributions [7], [11].

* Arif Nur Afandi, Email: an.afandi@um.ac.id

Since global warming becomes an important aspect of the system operation, the application of air and environmental quality standards has increased, and pollution restrictions have also increased. Therefore, the operation of the system is increasingly fixed in implementing restrictions on pollution emissions due to the burning process of fossil fuels at energy production sites [12], [13]. Furthermore, to maintain the allowable emission limit, dynamically, the operation of the system is also increasingly considering releasing emissions as part of efforts to reduce its emission effects. Thus, the operation of the power plant must modify to find a more economical operating strategy by reducing pollutants, and reducing the cost of operating the electricity process. [5], [14]. The fossil fuel firing has contributed to the air quality condition through the disposal of contaminants. In other words, these combustions at thermal plants have also contributed to producing emissions, for example, CO, CO₂, SO_x, and NO_x [5]. Moreover, the pollutant emission quota (PEQ) is also presented as a dynamic problem to meet hourly demand changes whereas the IEMC is subjected to the optimal composition for energy producers. To avoid complexity problems of both dispatching types, the EDQ and PEQ are determined together at the same time throughout single quota objective function (SQOF) to cover EDQ and PEQ problems [7], [15], [16]. Moreover, the SQOF becomes the main objective of the optimization problem under various technical constraints.

At present, to overcome these problems many ways are applied to obtain optimal conditions through optimization problems and by means of approaches that include mathematical programming and optimization techniques [10], [17]. In detail, these methods belong to traditional and evolutionary approaches. Nowadays, the optimization problem under various technical constraints becomes complex and huge models with excluding non-affecting small parameters for the system. To cover this condition, classical approaches have suffered to find out the solution where smart ways have been widely applied and are increasingly in demand as a way of calculating to solve various problems [18]. These approaches have an opportunity to wide implementations on numerical targets. Moreover, computational intelligence has many types associated with its procedures and inspirations to get the optimal solution. Furthermore, in its development, evolutionary computation is increasingly being developed and algorithms are arranged by imitating the behavior and mechanisms of flocks in nature. This was presented using optimization principles in accordance with natural mechanisms and structures to improve the performance of the classical approach [16], [19]. This paper presents a novel computational intelligence, artificial salmon tracking algorithm (ASTA), for determining the optimal solution of the SQOF based on the EDQ and PEQ problems. Technical limitations and environmental requirements are also applied to the conventional and hybrid energy systems to locate suitable solutions on hourly desired portions for the IEMC. In these works, the IEMC also covers an integrated renewable energy source (IRES) presented in a wind energy source (WES) and solar energy source (SES) for the 24 hours operating period. Both potential sources are installed at selected buses of the system to present the infrastructure development of the conventional system connection.

2. Energy Mixed Approach

Dynamically, the energy production due to all possible combinations of the hybrid system based on conventional energy sources (CES) and the IRES [20]–[23]. The hybrid system is commonly constructed using many types of generating units and it also uses the various voltage level systems to cover installed power plants depending on the CES and the IRES. Technically, this condition steers up to maintain a power output combination from joined energy producers based on the CES and the IRES which is decided to cover the total hourly demand. Moreover, this operation faces decreasing an emission and the operating fee. To integrate two dynamic problems with different targets for reducing pollutant discharge and decreasing running charge of the CES, a penalty factor is one of the important variables [5], [14]. Many previous studies reported that the emission has corresponded to fossil fuel-based power plants to meet the given load [7]. In these studies, the integration of the PEQ into the EDQ problem is not combined using an ascending order method of the penalty factor but it is approached using a new technique as given in a dynamic penalty factor (DPF) approach associated with the allowed emission discharge (AED), the total produced emission (TPE), and the over rate emission coefficient (OREC) [6], [7]. This method is an alternative approach for the penalty factor based on a dynamic computation in the processes. Mathematically, the DPF and OREC is discussed clearly in [24] as presented in Equations (1) to Equation (3).

$$OREC_z = \frac{\sum TPE_{zs} - \sum TAE_{zs}}{nG_z \cdot \sum TPE_{zs}}, \quad (1)$$

$$h_z = \{hG_{zs}\}, \quad (2)$$

$$dh_z = OREC_z \cdot rh_z, \quad (3)$$

where OREC_z is the over rate emission coefficient of the zth iteration, TPE_{zs} is the total produced emission of the sth generating unit of the zth iteration (kg/h), TAE_{zs} is the total allowed emission of the sth generating unit of the zth iteration (kg/h), nG_z is the number of generating units of the zth iteration exceeded the allowed emission, h_z is a penalty factor set of the zth iteration (\$/kg), hG_{zs} is the individual penalty factor of the sth generating unit exceeded the allowed emission of the zth iteration step (\$/kg), dh_z is the dominant penalty factor of the zth iteration (\$/kg), and rh_z is the selected hG_{zs} of the zth iteration for the highest TPE_{zs}.

In particular, the penalty factor covers environmental effects from the conventional system operation using fossil fuel-based. Recently, the energy system operation (ESO) is developed using interconnected structures for connecting the CES and the SES which is located at different sites of the IRES [20], [25]. The ESO is also used to deliver power outputs at generation sites to the energy usages at faraway locations using interconnected topologies of the transmission and distribution systems. Operationally, the ESO is operated within 24 hours to provide a highly reliable electric energy based on the optimal energy dispatching [3], [26]. In general, the system operation is carried out within 24 hours, and this period considers the power output scheduled for 24 hours to meet energy consumption where the consumption changes load demand from this hour to the next according to technical and environmental requirements. In detail, this relation covers all possible combinations of suitable energy producers associated with reasonable power production [27], [28], which is presented as given in Equation (4) to Equation (6).

$$\sum_{i=1}^{ng} PP_i^t = \sum_{i=1}^{ng} PCES_i^t + \sum_{i=1}^{ng} PWES_i^t + \sum_{i=1}^{ng} PSES_i^t, \quad (4)$$

$$\sum_{i=1}^{ng} PP_i^t = TD_i^t + TLoss_i^t, \quad (5)$$

$$\sum_{i=1}^{ng} EP_i^t = \sum_{i=1}^{ng} PP_i^t \times \Delta T_i^t \quad (6)$$

where t is period intervals of time (t=1, 2, 3, ..., e), e is the total period, ng is the iterating number, PP is a power production, PCES is a power production of the CES, PWES is the power production of the WES, PSES is the power production of the SES, TD is the total demand, TLoss is the total loss, EP is the energy production, and ΔT is a duration of present and past hours.

Moreover, to obtain the optimal solution, the SQOF is operated by entering several constraints as technical criteria during operation, including power balance, power load flow with shrinkage losses for lines, power capacity limits, fluctuating voltages, power transfer capability limits, ramp limits, and emission standards. The ESO covers the CES, WES, and SES which is optimized together to reach the optimal portion of the power producer combination

3. Optimizing Procedure

In this section, ASTA is compiled using its procedures based on the exploring and surviving steps. Algorithm procedures and parameters are very important to present computational abilities while searching the optimal solution [29], [30]. This algorithm is inspired by migration of Salmon fish. In general, the salmon migrating history is illustrated in Figure 1 in terms of spawning fish in freshwater, migrating to the ocean, and returning home from the ocean. During these phases, the Salmon will face many predators and obstacles. By considering Salmon’s behavior, ASTA is constructed as given in Figure 2.

Computationally, these steps are illustrated in Figure 3 covered a transformation of the SQOF into programming sequences of the hybrid system. Moreover, the system is also evaluated using the Newton Raphson method for determining balanced energy performances as referred to in [31]. Furthermore, Figure 3 is also used to guide the procedures and hierarchies for optimizing the SQOF. This figure consists of two parts as given in the left and right sides. The left side is used to transform the mathematical model of the problem into a programming procedure as the sequencing processed flowchart. One other is used to optimize the problem based on the sequencing algorithm to search for the best solution. As illustrated in Figure 3, ASTA is programmed using pseudo-codes for searching the best solution using parameters.

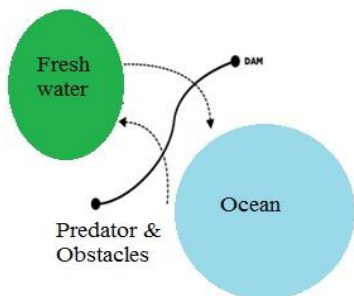


Figure 1: Salmon migrating path

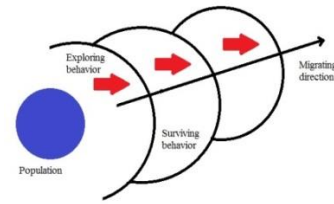


Figure 2: Salmon migrating approach model

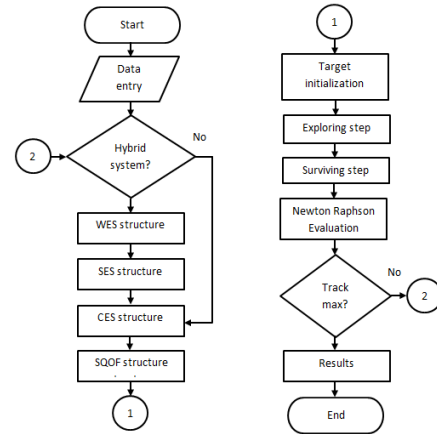


Figure 3: Computational sequences of ASTA

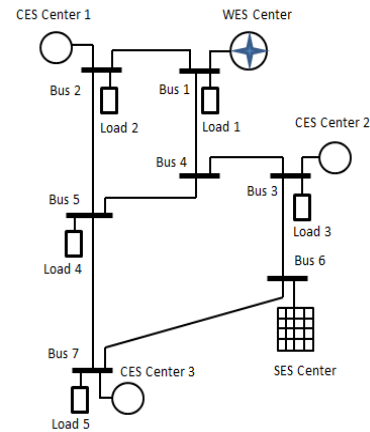


Figure 4: Hybrid energy system model

Table 1: Designed Hourly Demands

Hours	MW	Hours	MW
01.00	272.50	13.00	786.95
02.00	278.81	14.00	818.13
03.00	302.29	15.00	753.83
04.00	435.45	16.00	401.49
05.00	532.67	17.00	440.37
06.00	569.59	18.00	603.54
07.00	574.16	19.00	646.96
08.00	617.78	20.00	573.33
09.00	617.93	21.00	557.76
10.00	668.49	22.00	478.80
11.00	808.82	23.00	300.52
12.00	767.71	24.00	280.54
Total			13,088.42

In particular, Figure 4 shows the energy system model for applying ASTA and for optimizing the SQOF. The developed and standard models are very helpful to meet the problem caused by completed data of the real system and difficulty data collection on the existing operation [22], [32]. In these studies, the system consists of the CES, WES, and SES centers installed at different locations. In detail, the system covers five loads which are connected to Bus 1, Bus 2, Bus 3, Bus 4, and Bus 5. Moreover, conventional energy sources are installed at Bus 1, Bus 2, and Bus 3 whereas the WES is centered at Bus 1 and the SES is integrated to Bus 6. By considering this model and conditions, the system is optimized based on demand changes for 24 hours as provided in Table 1 with the period time operation is 24 hours. These demands also cover for the day and night peak loads.

Table 2: Individual Power Productions

Time	Conventional Generating Unit (MW)				
	CES C1		CES C2		CES C3
	Unit 1	Unit 2	Unit 1	Unit 2	Unit 1
	G1	G2	G3	G4	G5
01.00	65.75	22.34	21.77	24.40	26.98
02.00	58.06	28.74	25.00	27.78	26.49
03.00	64.27	37.72	37.43	22.63	29.06
04.00	89.87	89.72	84.27	38.33	37.21
05.00	127.16	85.70	71.48	85.07	73.56
06.00	133.42	75.05	79.94	75.32	75.02
07.00	133.74	72.76	76.86	77.47	87.10
08.00	149.42	79.68	85.00	63.75	93.10
09.00	137.76	73.57	89.19	71.75	77.55
10.00	220.36	70.42	72.17	67.85	72.31
11.00	257.25	98.50	97.34	98.83	98.90
12.00	254.38	84.62	94.91	82.94	86.13
13.00	259.31	91.36	91.23	84.94	92.13
14.00	268.31	94.62	98.92	95.84	97.28
15.00	239.49	82.72	96.54	88.84	83.35
16.00	100.16	49.21	46.27	42.02	23.58
17.00	103.99	59.12	80.98	35.00	24.62
18.00	187.57	74.37	74.37	78.78	65.11
19.00	187.56	81.73	84.41	87.17	83.90
20.00	187.51	78.21	77.96	67.25	72.88
21.00	166.58	73.98	75.74	73.14	73.78
22.00	125.94	68.77	61.35	61.14	64.78
23.00	62.52	31.52	32.29	33.54	31.24
24.00	53.65	35.52	25.00	28.10	27.87
Total	3634.03	1639.95	1680.42	1511.88	1523.93

4. Result

In this section, the IEMC is presented dynamically within 24 hours and it is optimized using ASTA. The 24 hours operation common approaches for the existing operation is based on all integrated energy producers [7], [27]. By considering ASTA’s parameters detailed in Section 3, the energy mixed producer is determined optimally as given in Table 2 for the optimal power production. Technically, this table shows the individual power commitment of the energy sources of the CES while the WES and SES are considered free for the natural energy sources as given in Table 3. From this table, it is known that this table informs the scheduled power production for 24 hours determined totally in 9,990.21 MW with the power fluctuation and contribution are illustrated in Figure 5 and Figure 6. These aspects are inlined with many previous works that the system has been delivered in www.astesj.com

variable portions associated with demand changes at the energy consumers [33].

According to Table 2 and Table 3, it is also known that all conventional generations have produced power outputs in different capacities. These different capacities show the generated participation in the system for supporting the provided energy for the load demand as reported in [14], [15]. The energy contributors cover all centers as detailed in both tables. In total, Center 1 takes a role in the highest power production of around 5,273.98 MW. Furthermore, the lowest contributor is supported by the CES Center 3 in 1,523.93 MW. By considering the IRES, Table 3 presents all penetrations within 24 hours for the SES and the WES. This penetration is very important to measure a renewable energy inclusion into the existing system with a certain portion of the participants to control the total energy production [10]. These penetrations cover hourly operations, totally, the system is penetrated in 1,450.00 MW of the SES and 2,522.93 MW of the WES. In detail, the system provides around 13,870.21 MW with the discharged pollutant of the CES is listed in Table 4 for all operating times. This emission is categorized in the produced emission, permitted emission, and over emission. As given in Table 4, the total emission is produced in 19,662.34 kg where the pollution is allowed around 8,491.65 kg based on standard emission. In addition, the system has 11,170.69 kg of the over emission during existing energy sources. It means that the system should be maintained to keep the emission level.

Table 3: Effective Balanced Power Contributions

Hour	CES (MW)	SES (MW)	WES (MW)	Total (MW)
01.00	161.24	50.00	75.00	286.24
02.00	166.07	50.00	75.00	291.07
03.00	191.11	50.00	75.00	316.11
04.00	339.40	50.00	75.00	464.40
05.00	442.97	50.00	75.00	567.97
06.00	438.75	50.00	112.50	601.25
07.00	447.93	50.00	112.50	610.43
08.00	470.95	75.00	112.50	658.45
09.00	449.82	75.00	127.50	652.32
10.00	503.11	75.00	127.50	705.61
11.00	650.82	85.00	127.50	863.32
12.00	602.98	85.00	127.50	815.48
13.00	618.97	85.00	127.50	831.47
14.00	654.97	85.00	127.50	867.47
15.00	590.94	85.00	127.50	803.44
16.00	261.24	50.00	112.50	423.74
17.00	303.71	50.00	112.50	466.21
18.00	480.20	50.00	112.50	642.70
19.00	524.77	50.00	121.05	695.82
20.00	483.81	50.00	116.76	650.57
21.00	463.22	50.00	134.36	647.58
22.00	381.98	50.00	100.48	532.46
23.00	191.11	50.00	63.91	305.02
24.00	170.14	50.00	43.87	264.01
Total	9,990.21	1,450.00	2,522.93	13,963.14

In particular, an energy balance is one of the important parameters in the system operation while the energy should be used in the final users at various types of appliances based on the power capacities [11]. In this case, the energy consumption has corresponded to individual power productions. This aspect is also

used to present individual contributors to the power unit commitment. In these works, individual performances of the energy producer unit are presented in Figure 7 and Figure 8 covered hourly power production changes and hourly power fluctuations. In total, the IEMC produces 9,990.21 MW with the power produced performances as given in Figure 7 and Figure 8. Figure 7 shows the fluctuation of power productions for the CES from the present to the next hours associated with the own scheduled power production. The detailed contributor to the power plants is presented in Figure 7. This figure informs that the highest contributor comes from G1 of the CES Center 1. Moreover, the IEMC also emits the total over emission of around 19,662.34 kg whereas the IRES penetrates are given in Figure 8. This figure illustrates the hourly penetration to the system covered in 24 hours for the WES and the SES. In addition, the CES is performed in Figure 7 for the hourly power production during an existing system to supply the load center.

Table 4: Emission Discharge of the CES

Hour	Production (kg)	Permission (kg)	Over Emission (kg)
01.00	164.08	137.05	27.03
02.00	174.84	141.16	33.68
03.00	206.05	162.44	43.61
04.00	551.79	288.49	263.3
05.00	829.62	376.52	453.1
06.00	805.44	372.94	432.5
07.00	852.91	380.74	472.17
08.00	922.52	400.31	522.21
09.00	849.31	382.35	466.96
10.00	1,009.86	427.64	582.22
11.00	1,680.31	553.2	1127.11
12.00	1,450.49	512.53	937.96
13.00	1,522.32	526.12	996.2
14.00	1,709.01	556.72	1152.29
15.00	1,392.26	502.3	889.96
16.00	307.68	222.05	85.63
17.00	438.46	258.15	180.31
18.00	915.03	408.17	506.86
19.00	1,101.78	446.05	655.73
20.00	923	411.24	511.76
21.00	858.86	393.74	465.12
22.00	603.34	324.68	278.66
23.00	209.17	162.44	46.73
24.00	184.21	144.62	39.59
Total	19,662.34	8,491.65	11,170.69

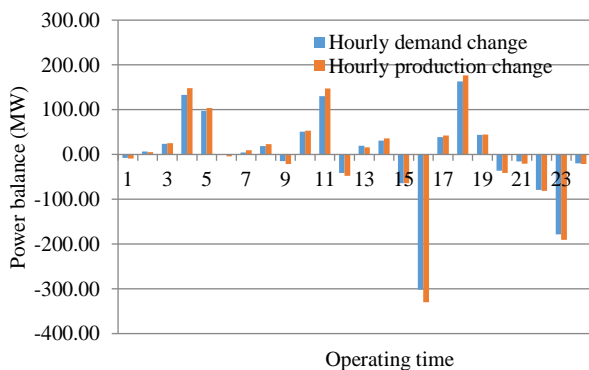


Figure 5: Hourly power fluctuation

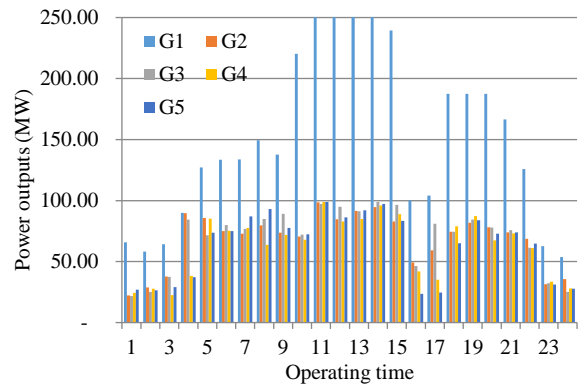


Figure 6: Hourly individual power production

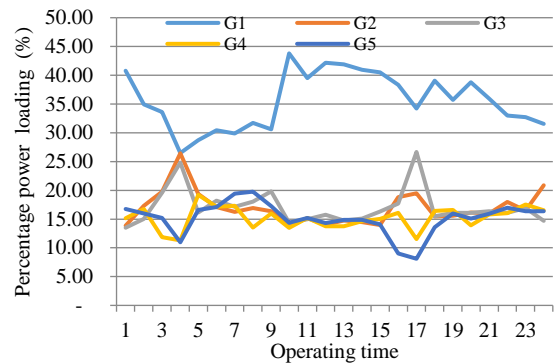


Figure 7: Hourly power production of the CES

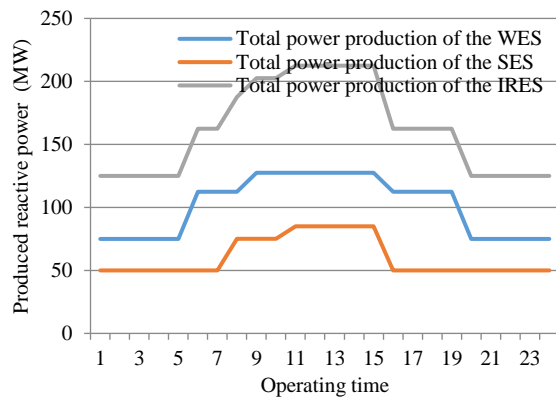


Figure 8: Hourly power penetration of the IRES

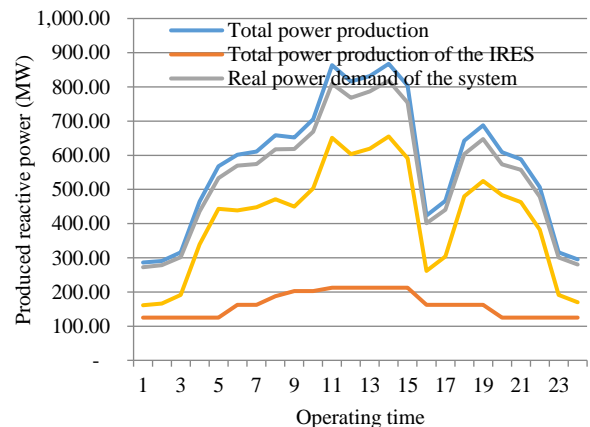


Figure 9: Hourly power balance performance

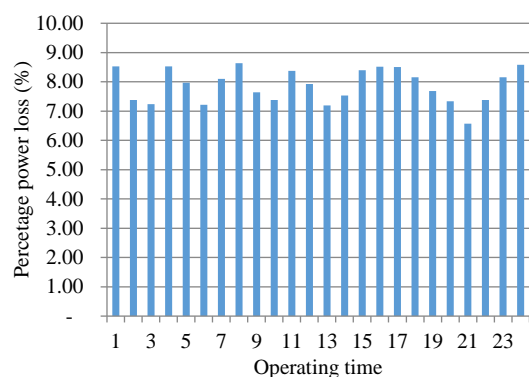


Figure 10: Total reactive power loss performances

By considering the 24 hours operation, the power balance is detailed in Figure 9. This figure shows all participation of the energy producers balanced to the total hourly demand. It is also known that the main power producers are covered in conventional energy producers. In addition, the IRES is operated to support this optimal condition which is linked to the hourly composition. In these works, another problem is given in the power loss as depicted in Figure 10 designed for the 24 hours operation. The system has fluctuated power losses for the 24 hours operation associated with day and night loads.

5. Conclusion

As stated earlier, the composition of the energy mix is integrated by considering integrated renewable energy sources and various technical requirements, as well as environmental constraints. The formula is outlined in a computational problem that is searched using the Artificial Salmon Tracking Algorithm to get the optimal composition for 24 hours. The calculation results show that dynamically the part of the energy produced is affected by IRES as given in solar and wind energy sources for 24-hour operations. In addition, ongoing conventional energy producers contribute with different capacities to support individual commitments to the production of power units. Furthermore, from these works, the implementation of real algorithms for large systems is suggested for future work in line with the placement of distributed renewable energy.

Acknowledgment

The authors gratefully acknowledge the support of the DRPM Research Grant 2019, Ministry of Research, Technology and Higher Education, Indonesia.

References

- [1] M. Malekidelarestaqi, A. Mansouri, and S. F. Chini, "Electrokinetic energy conversion in a finite length superhydrophobic microchannel," *Chem. Phys. Lett.*, vol. 703, pp. 72–79, Jul. 2018.
- [2] Z. Dimitrova and F. Maréchal, "Energy integration on multi-periods and multi-usages for hybrid electric and thermal powertrains," *Energy*, vol. 83, pp. 539–550, Apr. 2015.
- [3] X. Zhang, Z. Wang, H. Shen, and Q. J. Wang, "Dynamic contact in multiferroic energy conversion," *Int. J. Solids Struct.*, vol. 143, pp. 84–102, Jun. 2018.
- [4] P. Cuffe and A. Keane, "Visualizing the Electrical Structure of Power Systems," *IEEE Syst. J.*, vol. 11, no. 3, pp. 1810–1821, Sep. 2017.
- [5] M. Bhoje, M. H. Pandya, S. Valvi, I. N. Trivedi, P. Jangir, and S. A. Parmar, "An emission constraint Economic Load Dispatch problem solution with

Microgrid using JAYA algorithm," in *2016 International Conference on Energy Efficient Technologies for Sustainability (ICEETS)*, 2016, pp. 497–502.

- [6] A. Rabiee, B. Mohammadi-Ivatloo, and M. Moradi-Dalvand, "Fast Dynamic Economic Power Dispatch Problems Solution Via Optimality Condition Decomposition," *IEEE Trans. Power Syst.*, vol. 29, no. 2, pp. 982–983, Mar. 2014.
- [7] Y. Shang, S. Lu, J. Gong, R. Liu, X. Li, and Q. Fan, "Improved genetic algorithm for economic load dispatch in hydropower plants and comprehensive performance comparison with dynamic programming method," *J. Hydrol.*, vol. 554, no. Supplement C, pp. 306–316, Nov. 2017.
- [8] M. El-Shimy, M. A. Attia, N. Mostafa, and A. N. Afandi, "Performance of grid-connected wind power plants as affected by load models: A comparative study," in *2017 5th International Conference on Electrical, Electronics and Information Engineering (ICEEIE)*, 2017, pp. 1–8.
- [9] L. Wang, W. Liu, D. Malcolm, and Y. F. Liu, "An Integrated Power Module Based on Power-system-in-inductor Structure," *IEEE Trans. Power Electron.*, vol. PP, no. 99, pp. 1–1, 2017.
- [10] Y. Li, S. Miao, X. Luo, and J. Wang, "Optimization model for the power system scheduling with wind generation and compressed air energy storage combination," in *2016 22nd International Conference on Automation and Computing (ICAC)*, 2016, pp. 300–305.
- [11] L. Labib, M. Billah, G. M. S. M. Rana, M. N. Sadat, M. G. Kibria, and M. R. Islam, "Design and implementation of low-cost universal smart energy meter with demand side load management," *Transm. Distrib. IET Gener.*, vol. 11, no. 16, pp. 3938–3945, 2017.
- [12] T. J. Hammons, "Europe: transmission system developments, interconnections, electricity exchanges, deregulation, and implementing technology in power generation with respect to the Kyoto protocol," in *39th International Universities Power Engineering Conference, 2004. UPEC 2004.*, 2004, vol. 3, pp. 1251–1257 vol. 2.
- [13] S. Walker, K. W. Hipel, and T. Inohara, "Strategic analysis of the Kyoto Protocol," in *2007 IEEE International Conference on Systems, Man and Cybernetics*, 2007, pp. 1806–1811.
- [14] N. Ghorbani, E. Babaei, and F. Sadikoglu, "Exchange market algorithm for multi-objective economic emission dispatch and reliability," *Procedia Comput. Sci.*, vol. 120, pp. 633–640, 2017.
- [15] Y. Di, M. Fei, L. Wang, and W. Wu, "Multi-objective Optimization for Economic Emission Dispatch Using an Improved Multi-objective Binary Differential Evolution Algorithm," *Energy Procedia*, vol. 61, no. Supplement C, pp. 2016–2021, Jan. 2014.
- [16] L. T. Al Bahrani and J. C. Patra, "Orthogonal PSO algorithm for economic dispatch of thermal generating units under various power constraints in smart power grid," *Appl. Soft Comput.*, vol. 58, no. Supplement C, pp. 401–426, Sep. 2017.
- [17] P. Boonserm and S. Sitjongsataporn, "A robust and efficient algorithm for numerical optimization problem: DEPSO-Scout: A new hybrid algorithm based on DEPSO and ABC," in *2017 International Electrical Engineering Congress (iEECON)*, 2017, pp. 1–4.
- [18] A. Shenfield, D. Day, and A. Ayesh, "Intelligent intrusion detection systems using artificial neural networks," *ICT Express*, May 2018.
- [19] B. Chowdhury and G. Garai, "A review on multiple sequence alignment from the perspective of genetic algorithm," *Genomics*, vol. 109, no. 5, pp. 419–431, Oct. 2017.
- [20] C. L. Bottasso, S. Cacciola, and J. Schreiber, "Local wind speed estimation, with application to wake impingement detection," *Renew. Energy*, vol. 116, pp. 155–168, Feb. 2018.
- [21] G. Cervone, L. Clemente-Harding, S. Alessandrini, and L. Delle Monache, "Short-term photovoltaic power forecasting using Artificial Neural Networks and an Analog Ensemble," *Renew. Energy*, vol. 108, pp. 274–286, Aug. 2017.
- [22] K. B. Debnath and M. Mourshed, "Forecasting methods in energy planning models," *Renew. Sustain. Energy Rev.*, vol. 88, pp. 297–325, May 2018.
- [23] N. Tutkun, O. Can, and A. N. Afandi, "Low cost operation of an off-grid wind-PV system electrifying residential homes through combinatorial optimization by the RCGA," in *2017 5th International Conference on Electrical, Electronics and Information Engineering (ICEEIE)*, 2017, pp. 38–42.
- [24] A. N. Afandi, I. Fadlika, and Y. Sulistyorini, "Solution of dynamic economic dispatch considered dynamic penalty factor," in *2016 3rd Conference on Power Engineering and Renewable Energy (ICPERE)*, 2016, pp. 241–246.
- [25] F. P. Mahdi, P. Vasant, V. Kallimani, J. Watada, P. Y. S. Fai, and M. Abdullah-Al-Wadud, "A holistic review on optimization strategies for combined economic emission dispatch problem," *Renew. Sustain. Energy Rev.*, vol. 81, no. Part 2, pp. 3006–3020, Jan. 2018.

- [26] A. N. Afandi, "Weighting Factor Scenarios for Assessing the Financial Balance of Pollutant Productions and Fuel Consumptions on the Power System Operation," *Wseas Trans. Bus. Econ.*, vol. 14, 2017.
- [27] A. N. Afandi, Y. Sulistyorini, G. Fujita, N. P. Khai, and N. Tutkun, "Renewable energy inclusion on economic power optimization using thunderstorm algorithm," in *2017 4th International Conference on Electrical Engineering, Computer Science and Informatics (EECSI)*, 2017, pp. 1–6.
- [28] A. N. Afandi et al., "Designed Operating Approach of Economic Dispatch for Java Bali Power Grid Areas Considered Wind Energy and Pollutant Emission Optimized Using Thunderstorm Algorithm Based on Forward Cloud Charge Mechanism," *Int. Rev. Electr. Eng. IREE*, vol. 13, no. 1, pp. 59–68, Feb. 2018.
- [29] C. C. Columbus and S. P. Simon, "A parallel ABC for security constrained economic dispatch using shared memory model," in *Controls and Computation 2012 International Conference on Power, Signals*, 2012, pp. 1–6.
- [30] Denglijun, Zipeng, Anning, Shaoguanghui, Xuxingwei, and Houkaiyuan, "Empirical analysis on model and parameters of grid-connected Direct-driven Wind Turbine Generators in transient stability computation," in *2014 China International Conference on Electricity Distribution (CICED)*, 2014, pp. 1184–1189.
- [31] S. Chatterjee and S. Mandal, "A novel comparison of gauss-seidel and newton-raphson methods for load flow analysis," in *2017 International Conference on Power and Embedded Drive Control (ICPEDC)*, 2017, pp. 1–7.
- [32] L. Jodar, J. R. Torregrosa, J. C. Cortés, and R. Criado, "Mathematical modeling and computational methods," *J. Comput. Appl. Math.*, vol. 330, pp. 661–665, Mar. 2018.
- [33] M. EL-Shimy, N. Mostafa, A. N. Afandi, A. M. Sharaf, and M. A. Attia, "Impact of load models on the static and dynamic performances of grid-connected wind power plants: A comparative analysis," *Math. Comput. Simul.*, Feb. 2018.

The Relationship of Coalition on Employee Spiritual Engagement: Interplay of Organisational Politics

Isaac Onyeyirichukwu Chukwuma¹, Emmanuel Kalu Agbaeze^{*1}, Nkiru Peace Nwakoby², Gertrude Chinelo Ugwuja¹, Fidelis Odinakachukwu Alaefule¹, Ifeanyi Leo Madu³

¹University of Nigeria, Department of Management, Nigeria

²Nnamdi Azikiwe University, Department of Entrepreneurship Studies, Nigeria

³Gregory University, Department of Business Administration, Nigeria

ARTICLE INFO

Article history:

Received: 28 August, 2019

Accepted: 04 October, 2019

Online: 22 November, 2019

Keywords:

Coalition

Employee spiritual engagement

Organizational politics

ABSTRACT

The objective of the study was to establish the relationship between coalition and employee spiritual engagement. The research was quantitative, and data was administered and retrieved from employees at the selected private radio firms. Content validity was utilised to ascertain the validity of the instrument, and the reliability of the instrument was established using Cronbach's alpha coefficient. Kendall's tau τ_b correlation was used to show the result of the bivariate relationship between coalition and employee spiritual engagement ($p > 0.05$); hence, we accepted the null hypothesis. To know how much variance in employee spiritual engagement can be clarified by coalition, a simple linear regression was performed; with a result of 0.1 (percent), it was evidenced that coalition had no effect on employee spiritual engagement. The finding of the study showed that there is no statistical relationship between coalition and employee spiritual engagement. The result of this study also bears practical implications; executives should understand that organisations cannot achieve a zero-level coalition activity. Although this behaviour via the results does not possess a statistical relationship, executives should articulate its optimized use within acceptable terms.

1. Introduction

Politics has existed for centuries; however, the logical investigation of politics in organisation merely started taking shape about thirty years ago [1]. [2] posits that the purpose behind the paucity of study on organisational politics is likened to the focused study of politics in the regions of sociology, social psychology, and political science. During the late 1970s and mid-1980s, milestone works emerged that made way for the contemporary investigation of organisational politics [1, 3-5]; though the presence of politics inside organizations is known, the quest for a superior comprehension of how it affects employee engagement is developing as a significant challenge for executives in the 21st century.

Organisational politics from a global perspective create irresolute reactions since employees take a juxtapose stand on the

concept; contingent upon the specific point of view they have, and it is critical to state that the level of organisational politics varies amongst organizations. The fact remains that organisations have elements of micro and macro political activities that influence their activities [6, 7].

Organisational politics is perceived as either a symptom of social influence processes intentionally executed to achieve short-term or long-term advantages for the organisation or a self-serving activity that conflicts with the organisational objectives [8, 9]. Organisational politics is also seen as the management of influence to achieve goals not authorised by the organisation or to achieve authorised goals through non-authorised influence; via controlling information channels, managing impression, and forming a coalition [1, 10, 9]. [11] observes that organisational politics are significant since it gives a comprehension of the informal procedures of conflicts and co-operation in organisations, and their impact on the employees' engagement.

* Corresponding Author: Emmanuel Kalu Agbaeze, University of Nigeria, emmanuel.agbaeze@unn.edu.ng

In Nigeria, the presence of organisational politics highlights that employees are exceptionally sensitive to behaviours in their workplace, and their perspectives and discernments are influenced by the prevailing culture in the organisation. Organisational politics is overwhelming in Nigeria because the macro environment thrives with political interests; hence, organisational politics rule, characterize and restructure the state of organisational choices and activities in Nigeria [12].

Lately, there is a developing focus on the complexities of organisational politics. Extant literature has examined organisational politics behaviour (i.e., controlling information, creating obligation) primarily on the premise that such behaviour hinders optimal organisational goals and work-place related variables [13, 14], while this may be validated with their findings, other scholars; [15, 16] found contrary and positive results. While these studies have evaluated organisational politics behaviour at individual levels (i.e., impression management, creating obligation) in the organisation, which have produced equivocalness, the current study questions and examines the interplay of organisational politics at the group level (i.e., coalition) and its relationship on employee spiritual engagement. More so, extant studies have generally been focused with the results of employee performance [17-20], as opposed to the conditions or the unique situation (i.e., employee spiritual engagement) that propels performance, this study addresses that. Finally, the relationship between creating coalition and employee spiritual engagement has not been extensively examined in empirical studies, and the Nigerian context, hence the need for this study.

Coalition in this study context consists of persons within an organisation that influence goals via informal structure [21]. The forming of coalitions in organisations is mostly activated via conflicting goals. At the group level (i.e., coalition), the expressed objectives of the organisation are not the absolute organisational objective [22, 23]; denoting that implicit objective of the employees who sustain informal authority structure in the organisation via forming a coalition, compliment or undermine stated goals. Hence, the complimenting or undermining of stated goals is contingent on the level of dominance possessed by the coalition, which may influence employee spiritual engagement via perceived goal complexity.

The necessity for a spiritual connection has become significant to employees, mainly because of recurrent changes in organisational structure (i.e., political activities; coalition), which may result in feelings of insecurity for one's place in the organisation [24]. Employee spirituality engagement has gained a global corporate focus. It features a global development in which the focus has moved to the perspective that work ought to be significant and meaningful. This focus is presently on a spiritual paradigm; as a recent developing paradigm in which much advancement with regard to the understanding of the employee spiritual engagement are evolving [25]. Studies reveal that employees find it hard to disconnect their spiritual lives from their workplace environment [26]. They acknowledge that blending spirituality in the work environment will provide them significant and purposeful life. This also possesses a ripple effect in that the

organization experiences improved profits, increased morale and performance, and reduced absenteeism [27].

To remain relevant in this contemporary dynamic business environment, organisations are constantly seeking for engaged employees. In this context, engagement denotes employees' holistic commitment to their work via the application of discretionary effort [28]. This emerging concept has birthed terms, such as Faith at Work, Workplace Spirituality, Employee Spiritual Engagement [29]. The factor of employee spirituality encapsulates the notion that all employees have their internal inspirations, facts, and desires to be explored in professional activities that provide significant meaning to life. Hence, when employees are spiritually engaged, "work" connotes an important experience and encounter; when it is acknowledged as a calling, a consecrated obligation, a service opportunity or a higher purpose [30, 31].

As private radio broadcasting firms contribute significantly towards the economic, socio-cultural, and political development and sustenance, continued studies within this industry are critical. It is also significant that employees realise that the pressure to remain useful and relevant in a capitalist economy (i.e., Nigeria) that is highly dynamic has majorly influenced organisational political activities (i.e., coalition). In making sense of this dynamics and continuing to maintain productively, employees develop a mindset of wholeness, values, and discovering purpose and significance at work; which are the parameters of spiritual engagement [32]. Hence, when coalitions create or fail to create an atmosphere that value perspectives such as significant and fulfilling work, a consciousness of life, connectedness, and compassion, what effect or nature of relation exist?

There is presently paucity of information and studies on the relationship between coalition and employee spiritual engagement. The present research is an empirical attempt to explore the relationship of coalition on employee spiritual engagement within the context of private radio broadcasting firms in Southeast Nigeria. The research hypothesis for this study is:

- H₀:** there is no relationship between coalition and employee spiritual engagement.
- H₁:** there is a relationship between coalition and employee spiritual engagement.

The underlying hypothesis of this research is that the axiomatic conclusion that coalition affects employee spiritual engagement may not be true. The research is an empirical study of employees experience in private radio broadcasting firms in Southeast Nigeria.

This research is significant in several ways: First, it highlights the statistical relationship between coalition and employee spiritual employee within their work context. Secondly, it examines the construct with the potency of the social exchange theory. Thirdly, the study states the practical implication of the result which will help firms in achieving sustainable advantage. The study is expected to influence policy restructuring in handling coalition activities.

The remaining section of this study will be under these major sections; literature review, methodology, results, discussion, conclusion, recommendation, limitations and directions for further research, references, and appendices.

2. Literature Review

2.1. Coalition

Over time, the concept of coalition has remained ambiguous with respect to relevance and meaning within organisation theory. From the work of [33] who acknowledged coalition between but not within organisations, to the work of [34] who coined the term “dominant coalition” and “inner circle,” to the phase of the adoption of political science and social psychology method to organisational behaviour [35, 36]. And most recently its relevance to the political arena, where coalition influences all sectors of a nations’ sustenance. Notwithstanding the extant literature on coalition, it has still not produced a new perspective to understanding organisational behaviour [37].

Organisational power originates from numerous sources; a significant source is who you know and how accessible are information within your organisation; hence, forming a coalition are blueprints of relationships between employees [38].

Coalition has over time become one of the most widely recognized and famous element of every organisation’s workforce, which fulfill the following psychological functions of; character and confidence, defense mechanism, risk elimination, affiliation needs, social reality, information need, political maneuvering [39, 40]. It is thus viewed as a principal device and instrument utilized by employees in organisations to understand as well as to influence management decisions that are misaligned to their goals.

Coalition formation though evidently present is not always officially recognized by organisation, such coalition are sometimes the unofficial determinants of the activities of such organisations as they represent, serve, and affect organisational activities; playing different roles such as been the initiators (those who request that certain things be done, users (they utilize the things obtained), influencers (they influence decision making), approvers (they approve things to be done in organisations), deciders (they select those that will carry out the desired task), and gatekeepers (they control the inflow of information) [41].

Much of the work that gets done in organisations is influenced through the activities of the coalition. Forming coalition serves three significant roles. First, they convey privileged information. Also, they enable employees to access assorted skill sets. Finally, they can create, control, or influence authority [38]. Forming coalition amongst other things ensures employee gain greater bargaining power, minimize discrimination, heighten sense of security, disseminate information, and safeguards members ambition; hence motivating employee to discharge their responsible with an assurance of comrades, oneness and unity, which ultimately advance organisational sustainability, nonetheless, the same assurance gives them a platform to resist employers activities that are unfavourable to their interest [38, 42].

Notwithstanding the ambiguity to the definition of coalition, recurrent terms in diverse definition have acknowledged that coalitions are clusters of persons who temporarily collaborate to achieve a target aim via informal structure [43, 44, 45]. Coalitions are valuable for achieving a wide scope of objectives that span past the limit of any individual member in the organisation. These objectives range from knowledge sharing to facilitation of services, from sensitization and training to advocacy for policy (regulatory) changes [46]. Whatever definition of coalitions is utilised, understanding coalitions give understanding to employees’ behaviour in organisational structures.

Coalitions play an integral role in organisations operations; a dominant coalition can influence the goals of an organisation [47]; this is mostly achieved via informal, rather than formal channels. By forming a coalition, employees have the opportunity to affect organisational policies, decisions, and compensation structures. Coalition seeks relatively broad and strategic support of their objectives. It occurs more frequently in organisations with routine and standardized task and resource interdependencies.

Effective coalition building addresses an unpredictable cluster of challenges, which includes optimising the communication measures; strategically, communication is a major trigger for diverse levels of employee engagement. Optimal communication activities range from coordinating networks among like-minded employees; encouraging dialogue and building support among diverse interest [48]. Convincing employees to join a coalition requires subtlety, and strategically creating messages that aligns with the mission (shared purpose and anticipated rewards) of the prospective employee [49]. While coalitions seek to increase the scope and influence of their activities, the building of trust and members access to relevant resources and policy network is of paramount. Arguably, coalition members are more likely to access resources denied to non-members, as the formation of coalition mostly alters the distribution of resources, and modus-operandi of the organisation, which may influence employee’s spiritual engagement. Although studies have been executed with respect to the activities of coalition in organisations setting [41, 23], there is paucity or no studies on the relationship of coalition on employee spiritual engagement.

2.2. Employee spiritual engagement

Scholarly endeavours to incorporate spirituality into an organisational setting with the contention that spirituality not only impacts employees but also significantly influences organisational and managerial fields, prompted the development of the new field of inquiry called workplace spirituality [50]. However, it is important to stress that employee spiritual engagement is not restricted to religious tradition, employee spiritual engagement is not about getting employees into a particular arrangement of religious convictions [51], rather it focuses on individual and organisational values and practices; it is about helping employees explore their core values and work towards objectives that are personally meaningful, it denotes empowering employees to connect their inner lives and individual interests with their everyday work [52].

Numerous researchers contend that the major reasons for increased focus on employee spiritual engagement are the changing work and lifestyle, the rise of self-exploration, and a developing pattern to examine life importance and values by organisation scholars [50]. [53] asserts that life's demand stretches out beyond the materialistic aspects, and it is necessary to address the spiritual dimension of employees to accomplish better outcomes in an organisational setting.

In [54], the asserts that employee spiritual engagement possesses the following four dimensions; (a) Compassion (denotes empathy or care for the travail of others, often including a craving to help. [54] defines this dimension of employee spiritual engagement as a profound awareness of and compassion towards others and a craving to relieve their travailing; that leads to responsibility for others who are less fortunate or travailing). (b) Mindfulness (this dimension of employee spiritual engagement is characterised as a condition of inward awareness in which one is conscious of one's thoughts and actions. It is about an employee's mind being present, not meandering with past, future thoughts or distractions [54]. (c) Meaningful work, [54] characterises meaningful work as one's experience in which work is a significant and meaningful part to his/her life, this meaning is beyond the tangible rewards and creates a sense of energy and joy at work). (d) Transcendence (A significant component of employee spiritual engagement connotes whether employees can translate their work practices and their organisations' tasks in sacred terms [55].

In [56], the authors posits that employees have adapted and possess the required cognitive mechanisms for observing, evaluating, and regulating the suitable pattern of response to coalitions. These adaptations allow an employee to recalibrate their level of spiritual engagement as coalitions grow, function, and influence organisations goals and activities.

In today's world, an increasing number of employees are seeking more than just a monetary reward. Reward in the form of purposeful, motivational, impactful, and meaningful work is the optimal goal [57]. [58, 59] posit that employee spirituality is not about theoretical and religious construct. Rather, it is focused on employees who find strength, purpose, meaning, and completeness in their work [60, 61]. It also encircles employees sharing and encountering connection, attraction, and comradeship with persons within their work environment.

Notwithstanding the acknowledged equivocalness in the definition of employee spirituality [62] a recurrent theme has consistently occurred in the attempted definition, namely the meaningfulness and purpose in the workplace and employees' life, a feeling of interconnectedness and of belonging to the workforce, and personal joy and fulfilment [60, 61, 59].

Studies reveal that a work environment that encourages employees spiritual engagement can provide advantages in the areas of process improvement, creativity, customer service, satisfaction, team performance, honesty and trust, personal fulfillment, and commitment, which may result in optimised organisational performance [63, 27]. [64] posits that employee spirituality is focused on recognizing that employees attend to

their task at work with more than their bodies and minds; they possess individual talents and uniqueness, which ensures optimal performance when properly engaged.

2.3. Coalition and employee spiritual engagement

Notwithstanding the ambiguity to the definition of a coalition, recurrent terms in the diverse description have acknowledged that coalitions are clusters of persons who temporarily collaborate to achieve a target aim via informal structure [44, 45]. Coalition formation though evidently present is not always officially recognized by an organisation; such coalition is sometimes the unofficial determinants of the activities of such organizations as they represent, serve, and affect organizational activities and may influence employee spiritual engagement.

Employees have over time, evolved in developing an effective cognitive mechanism for identifying, examining, evaluating, and regulating the appropriate level of spiritual engagement to coalition activities [56]. This adaptability helps employees to regularly recalibrate their spiritual engagement level as coalitions grow, function, and influence organizations objectives and activities. Having acknowledged employee spiritual engagement as a topical construct, there is an increasing focus amongst researchers to empirically explore the relationship between employee spiritual engagement and different organizational actions (i.e., coalition) [65-69, 52, 70, 71]. Nonetheless, there is paucity in the literature concerning the relationship between coalition and employee spiritual engagement.

Employees are continually seeking a work environment whose objectives align with their values in other to fully encounter significance, and meaning in their task. While this is possible, the relationship in social interactions process and the interplay of organizational politics (i.e., coalition) in the work environment requires empirical credence to ascertain its influence on employee spiritual engagement.

2.4. A social exchange theory perspective of coalition and employee spiritual engagement

Social exchange theory (SET) is a crucial conceptual model for articulating workplace behaviour, SET views social activities (e.g., coalition) as a series of exchange which are interdependent; the behavior (e.g., level spiritual engagement) of one party (e.g., employee) is contingent on the actions (e.g., coalition activity) of another [72, 14]. Hence, a perceived alignment in values via actions executed generates an obligation (e.g., target level spiritual engagement) to reciprocate in kind; this also denotes a high level of unpredictability in employee spiritual engagement as the perception and interpretation of an aligned values or meaningfulness varies amongst employees in an organisations [73, 74]. Hence, the operationalised and covert structure of coalition activities and its ambiguous value to employees makes it difficult to predict employees level of spiritual engagement in a coalition work context [75, 76].

Employee spiritual engagement and social exchange perspectives share similar logic; specifically, both perspectives

acknowledge that perception to activities of workplace coalition is connected with employee subjectivity [14]. We propose that coalition have a direct effect on employee spiritual engagement. Nonetheless, the employee spiritual engagement level is intentionally exercised via the prerogative of employees' discretionary effort.

3. Methodology

The population of this study was employees of private radio broadcasting firms in Southeast (i.e., Abia, Anambra, Enugu, and Imo state) Nigeria. Twelve (12) private radio broadcasting firms in Southeast were selected for this study based on their popularity within their locality. By focusing on the private radio broadcasting sector, we avoided the possibility for unobserved differences that mark the government broadcasting industry. The population of the full-time staff in the selected private radio firms was 383; hence a census technique was applied, with questionnaires distributed to a population of 383 employees, and 359 complete responses were retrieved, denoting a response rate of 94% (approximate). Inferential statistical analysis was conducted using Kendall's tau_b correlation, and linear regression analysis was used to establish the relationship, and the degree to which the variance in employee spiritual engagement can be attributed to coalition, using SPSS. The participants were assured of complete confidentiality. These steps reduced the possibility of their responses been subjected to social desirability or acquiescence biases [77].

4. Results

4.1. Validity and reliability of the questionnaire

The validity of the instrument was established using content validity. The reliability of the instrument was assessed using Cronbach's alpha coefficient. The reliability results are indicated in Table 1. Coalition was measured with five items adopted from previous research viz [78]; the Cronbach's alpha coefficient for coalition is regarded as good (0.728). Employee spiritual engagement was measured with five items adopted from previous research viz [79, 28]; the Cronbach's alpha coefficient for employee spiritual engagement is also good (0.792); this implies that the instruments are reliable and valid for this study.

Table 1: Reliability assessment.

Variable	Cronbach's Alpha
Coalition	0.728
Employee spiritual engagement	0.792

4.2. Correlation between coalition and employee spiritual engagement

Table 2 reflects Kendall's tau_b correlation between coalition and employee spiritual engagement. Table 2 shows the result of the bivariate relationship between coalition and employee spiritual engagement via Kendall's tau_b correlation. Table 2 shows that there is no significant relationship ($p > 0.05$) between coalition and employee spiritual engagement, and the strength of the association between forming coalition and

employee spiritual engagement is very weak ($r = .046$). Since, $p (0.238) > 0.05$, we accept the null hypothesis and conclude that there is no relationship between coalition, and employee spiritual engagement.

Table 2: Kendalls' tau_b correlation results for coalition, and employee spiritual engagement ($n = 359$).

Construct	Category	Coalition	Employee spiritual engagement
Coalition	Kendalls' tau_b	1	0.046
	Sig. (2 tailed)	-	0.238
	N	359	359
Employee spiritual engagement	Kendalls' tau_b	0.046	1
	Sig. (2 tailed)	0.238	-
	N	359	359

4.3. Linear regression analysis

A simple linear regression analysis was conducted to predict the influence of coalition on employee spiritual engagement (see Table 3). To know how much variance in employee spiritual engagement can be clarified by coalition, a simple linear regression was performed. As can be seen from Table 3, coalition contributes 0.1(percent) to the variance in employee spiritual engagement, also the $p (0.503) > 0.05$. Hence, coalition has no relationship with employee spiritual engagement.

Table 3: Linear regression analysis results, where coalition is the independent variable, and employee spiritual engagement is the dependent variable.

Variable	Coalition					
	R	R ²	F	β	T	P
Employee spiritual engagement	0.035	0.001	0.449	0.037	0.670	0.503

R, R-value; R², R-squared value; F, F-value; β, beta-value; P, significance.

5. Discussion

Significant emphasis has been placed on the need to understand the dimensions of organisational political activities (i.e., coalition) [19, 20]. The research objective was to determine the relationship between coalition and employee spiritual engagement. This study reveals interesting findings; first, our finding linked coalition with employee spiritual engagement, and found no relationship, indicating that coalition has no statistical relationship with employee spiritual engagement. This finding also contradicts the axiom that coalition inhibits employee spiritual engagement, and should be avoided at all cost. In general, employees' spiritual engagement may be filtered through discretionary effort in responding to coalition activities. Nonetheless, employees been human coupled with the dynamic nature of the work environment might, in rare occasion exercise or fail to exercise discretionary effort in response to coalition behaviour and still create a neutral or zero relationships.

Beyond the fundamental bivariate relationship, our finding also contradicts the core of the social exchange theory [64, 63] connoting that employees spiritual engagement level is mostly influenced by their interpretation and perception of the benefits offered in a coalition activity; while this may be factual to an extent, employees ability to exercise discretionary effort may not be influenced by such interpretation and perception.

The result of this study also bears practical implications; executives should understand that organisations cannot achieve a zero-level coalition activity and that this behaviour via the results does not possess a statistical relationship. Hence executives should articulate its optimized use within acceptable ethical terms.

6. Conclusion

The research contributes to the paucity of empirical knowledge on the relationship between coalition and employee spiritual engagement. Specifically, the study found no relationship between coalition and employee spiritual engagement. From a practical viewpoint, the result of the study holds implication for private radio firms, which should be considered.

7. Recommendation

The researchers recommend that private radio broadcasting firms should adopt a culture of transparency and predictability in the process of resource allocation, in addition to a peer review authorization process. This will aid in down-playing the emergence of a dominant coalition that may deter optimal achievement of the organizational goals.

8. Limitation and Direction for Future Research

The study has acknowledged the following limitations; firstly, the scope of the study with respect to the geographic area and industry may compromise the external validity and applicability of its result; therefore, there is need to be careful in generalizing the findings to other geography and industry. Also, a common-method variance may influence the results, due to the census technique utilized and the self-administration of the questionnaire. Despite the acknowledged limitations, the study holds significant implications for radio firms that desire sustainable posterity. Also, there is a need to explore this relationship in other countries and industry, which will aid in an extensive comparative study, as well as meta-analysis; this will further the theoretical and practical relevance of the construct under study.

Conflict of Interest

The authors declare no conflict of interest.

References

- [1] T. Mayes, W. Allen, "Toward a definition of organizational politics" *Academy of Management Review*, 2(4), 672-678, 1977.
- [2] P. Block, "The empowered manager: positive political skills at work" San Francisco: Jossey-Bass, 1988.
- [3] B. Bacharach, J. Lawler, "Power and politics in organizations" San Francisco: Jossey-Bass, 1980.
- [4] H. Mintzberg, "The organization as political arena" *Journal of Management Studies*, 22(2), 133-154, 1985.

- [5] J. Pfeffer, "Managing with Power" Boston: Harvard Business School Press, 1992.
- [6] O. Bernard, N. Augustina, "The influence of power and politics in organizations" *International Journal of Academic Research in Business and Social Sciences*, 4(7), 164-183, 2014.
- [7] E. Mutambara, C. Botha, C. Bisshoff, "Perception of organizational politics at a national electricity provider in Southern African Development Community (SADC)" *Journal of Economics*, 6(3), 291-301, 2015.
- [8] P. Block, "The empowered manager: positive political skills at work" San Francisco: Jossey-Bass, 1988.
- [9] G. Gotsis, Z. Kortezi, "Ethical considerations in organizational politics: expanding the perspective" *Journal of Business Ethics*, 93, 497-517, 2010.
- [10] Drory, E. Vigoda-Gadot, "Organizational politics and human resource management: A typology and the Israeli experience" *Human Resource Management Review*, 20, 194-202, 2010.
- [11] E. Vigoda-Gadot, A. Drory, "Handbook of organizational politics" Cheltenham: Edward Elgar, 2006.
- [12] E. Ben, M. Ik, "The scope and patterns of organisational politics in Nigeria" *International Journal of Business Administration*, 3(3), 41-49, 2012.
- [13] E. Vigoda-Gadot, I. Talmund, "Organizational politics and job outcomes: the moderating effect of trust and social support" *Journal Applied and Social Psychology*, 40(11), 2829-2861, 2010.
- [14] Ying-Ni, Y. Chih-Long, L. Hung, "Transformational leadership and job involvement: The moderation of emotional contagion" *Military Psychology*, 24(4), 382-396, 2012.
- [15] C. Treadway, A. Hochwarter, R. Ferris, J. Kacmar, C. Douglas, P. Ammeter, R. Buckley, "Leader political skill and employee reactions" *Leadership Quarterly*, 15, 493-513, 2004.
- [16] D. Fedor, J. Maslyn, S. Farmer, K. Bettenhausen, "Perceptions of positive organizational politics and their impact on organizational outcomes" *Journal of Applied Social Psychology*, 38, 76-96, 2008.
- [17] R. Cropanzano, C. Howes, A. Grandey, P. Toth, "The relationship of organizational politics and support to work behaviors, attitudes, and stress" *Journal of Organizational Behavior*, 18, 159-180, 1997.
- [18] A. Witt, "Enhancing organizational goal congruence: a solution to organizational politics" *Journal of Applied Psychology*, 83, 666-674, 1998.
- [19] Witt, C. Andrews, M. Kacmar, "The role of participation in decision-making in the organizational politics-job satisfaction relationship" *Human Relations*, 53, 341-358, 2000.
- [20] E. Vigoda-Gadot, "Internal politics in public administration systems: An empirical examination of its relationship with job congruence, organizational citizenship behavior, and in-role performance" *Public Personnel Management*, 29, 185-210, 2000.
- [21] P. Timothy, K. James, L. Robyn, C. Darren, "The implications of coalition forms for work role innovation, resource reallocation, and performance" In: *Research in Personnel and Human Resources Management*. Emerald Group Publishing Limited, pp. 65-97, 2014.
- [22] C. Perrow, "Complex organizations: A critical essay" 3rd ed. New York: McGraw Hill, pp. 1-307, 1993.
- [23] M. Bowler, "Organizational Goals versus the dominant coalition: a critical view of the value of organizational citizenship behavior" *Institute of Behavioral and Applied Management*, 258-273, 2006.
- [24] P. Heaton, J. Schmidt-Wilk, F. Travis, "Constructs, methods, and measures for researching spirituality in organizations" *Journal of Organizational Change Management*, 17(1), 62-82, 2004.
- [25] M. Fourie, "Spirituality in the workplace: an introductory overview" *In die Skriflig*, 48(1), 1-8, 2014.
- [26] E. Zimmerman, "The many delicate issues of spirituality in the office" *New York times*, 2004. Available at: <https://www.nytimes.com/2004/08/15/jobs/the-many-delicate-issues-of-spirituality-in-the-office.html> [Accessed 23 May 2019].
- [27] C. Litzsey, "Spirituality in the workplace and the implications for employees and organizations" M.Sc. Dissertation, Graduate School: Southern Illinois University, 2006.
- [28] H. Macey, B. Schneider, "The meaning of employee engagement" *Industrial and Organizational Psychology*, 1(1), 3-30, 2008.
- [29] D. Miller, "God at work: the history and promise of the faith at work movement" Oxford University Press, pp. 1-232, 2006.
- [30] F. Paloutzian, A. Emmons, G. Keortge, "Spiritual well-being, spiritual intelligence, and healthy workplace policy. In: Giacalone, R., Jurkiewicz, C. (Eds.), *Handbook of workplace spirituality and organizational performance*. M.E. Sharpe: New York, 2003.
- [31] L. Reave, "Spiritual values and practices related to leadership effectiveness. *The Leadership Quarterly*, 16(5), 655-687, 2005.

- [32] J. Weinberg, B. Locander, "Advancing workplace spiritual development: a dyadic mentoring approach" *The Leadership Quarterly*, 25(2), 391-408, 2014.
- [33] G. March, A. Simon, "Organizations" New York: Wiley, 1958.
- [34] D. Thompson, "Organizations in action: social science bases of administrative theory" New York: McGraw-Hill, 1967.
- [35] J. Pfeffer, "New directions for organization theory: problems and prospects" New York: Oxford University Press, pp. 1-276, 1997.
- [36] M. Roberts, "Alliances, coalitions and partnerships: building collaborative organizations" St. Paul, MN: New Society Publishers, pp. 1-176, 2004.
- [37] S. William, P. Jone, P. Lyman, "The concept of coalition in organization theory and research. *Academy of Management Review*, 256-268, 1985.
- [38] B. Talya, E. Berrin, "Organizational behavior" Irvington, NY: Flat World Knowledge, 2010.
- [39] K. Baker, "Tapping into the power of informal groups" *Supervisory Management*, 26(2), 18-25, 1981.
- [40] E. Han, "The informal organization you've got to live ith" *Supervisory Management*, 28(10), 25-28, 1983.
- [41] O. Michael, "Industrial marketing management, principles, perspectives and practices" First Fountain Printing and Publishers Co. Awka- Nigeria, p. 62, 2010.
- [42] S. Bishal, "The effect of trade unionism on workers; a case study on PAM" A Project Report at University of Applied Sciences, 2012.
- [43] L. Hemphill, S. McGreal, J. Berry, S. Watson, "Leadership, power and multisector urban regeneration partnerships" *Urban Studies*, 43(1), 59-80, 2006.
- [44] M. Le-Ber, O. Branzei, "Towards a critical theory of value creation in cross-sector partnerships" *Organization*, 17(5), 599-629, 2010.
- [45] M. Shumate, A. O'Connor, The symbiotic sustainability model: conceptualizing ngo-corporate alliance communication" *Journal of Communication*, 60(3), 577-609, 2010.
- [46] L. Cohen, N. Baer, P. Satterwhite, "Developing effective coalitions: an eight step guide" In: Wurzbach, M. (Eds.), *Community health education and promotion: A Guide to Program Design and Evaluation*. Gaithersburg, Md: Aspen Publishers Inc., pp. 144-161, 2002.
- [47] M. Cyert, G. March, "A behavioral theory of the firm" Englewood Cliffs, NJ: Prentice-Hall, 1963.
- [48] J. Rosner, "Communicating difficult reforms: eight lessons from Slovakia" In: Odugbemi, S., Jacobson, T. (Eds.): *Governance reform under real-world conditions: citizens, stakeholder, and voice*. Washington, D.C.: The International Bank for Reconstruction and Development / The World Bank, pp. 395-396, 2008.
- [49] K. Bert, "Collective political action" In: Sears, D., Huddy, L., & Jervis, R. (Eds.), *Oxford Handbook of political psychology*, pp. 670-709, 2003.
- [50] C. Sheng, M. Chen, "Workplace spirituality scale design: the view of oriental culture" *Business and Management Research*, 1(4), 46-62, 2012.
- [51] N. Fagley, M. Adler, "Appreciation: a spiritual path to finding value and meaning in the workplace" *Journal of Management, Spirituality and Religion*, 9(2), 167-186, 2012.
- [52] S. Lee, K. Lovelace, C. Manz, "Serving with spirit: an integrative model of workplace spirituality within service organizations" *Journal of Management, Spirituality and Religion*, 11(1), 45-64, 2014.
- [53] B. Thaker, "Approaches to implement spirituality in business" *Journal of Human Values*, 15(2), 185-198, 2009.
- [54] P. Petchsawang, D. Duchon, "Measuring workplace spirituality in an Asian context" *Human Resource Development International*, 12(4), 459-468, 2009.
- [55] D. Grant, K. O'Neil, L. Stephens, "Spirituality in the workplace: new empirical directions in the study of the sacred" *Sociology of Religion*, 63(5), 265-283, 2004.
- [56] J. Tooby, L. Cosmides, "Evolutionary psychology and the generation of culture" *Ethology and Sociobiology*, 10, 29-49, 1989.
- [57] P. Bloch, "Complexity, chaos, and nonlinear dynamics: a new perspective on career development theory" *The Career Development Quarterly*, 53, 194-207, 2005.
- [58] J. Harrington, C. Preziosi, J. Gooden, "Perceptions of workplace spirituality among professionals and executives" *Employee Responsibilities and Rights Journal*, 13(30), 155-163, 2001.
- [59] S. Dhiman, J. Marques, "The role and need of offering workshops and courses on workplace spirituality" *Journal of Management Development*, 30(9), 816-836, 2011.
- [60] A. Giacalone, L. Jurkiewicz, "Toward a science of workplace spirituality" In: Giacalone, R., Jurkiewicz, C. (Eds.), *Handbook of workplace spirituality and organizational performance*. M.E. Sharpe Inc.: New York, pp. 3-28, 2003.
- [61] M. Kinjerski, J. Skrypnek, "Defining spirit at work: finding common ground" *Journal of Organizational Change Management*, 17(1), 26-42, 2004.
- [62] A. Hicks, "Religion and the workplace: pluralism, spirituality, leadership" University Press: Cambridge.
- [63] J. East, "A grounded study on how spirituality impacts a person's job satisfaction" Minneapolis: Capella, niversity.
- [64] P. Leigh, "The new spirit at work" *Training and Development*, 51(3), 26-34, 1997.
- [65] A. Faro, C. Campos, M. Dias, A. Brito, "Primary health care services: workplace spirituality and organizational performance" *Journal of Organizational Change Management*, 27(1), 59-82, 2014.
- [66] S. Indartono, Z. Wulandari, "Moderation effect of gender on workplace spirituality and commitment relationship: Case of Indonesian ethics" *Asian Journal of Business Ethics*, 3(1), 65-81, 2014.
- [67] A. Shrestha, "Workplace spirituality and employee attitudes: moderating role of organizational politics" *Journal of Business and Management Research*, 1(2), 33-51, 2017.
- [68] L. Daniel, "Workplace spirituality and stress: Evidence from Mexico and US" *Management Research Review*, 38(1), 29-43, 2015.
- [69] J. Byrne, M. Morton, J. Dahling, "Spirituality, religion, and emotional labor in the workplace" *Journal of Management, Spirituality & Religion*, 8(4), 299-315, 2011.
- [70] M. Saks, "Workplace spirituality and employee engagement" *Journal of Management, Spirituality & Religion*, 8(4), 317-340, 2011.
- [71] J. Word, "Engaging work as a calling: Examining the link between spirituality and job involvement" *Journal of Management, Spirituality & Religion*, 9(2), 147-166, 2012.
- [72] R. Cropanzano, M. Mitchell, "Social exchange theory: An interdisciplinary review" *Journal of Management*, 31(6), 874-900, 2005.
- [73] T. Hall, A. Hochwarter, R. Ferris, G. Bowen, "The dark side of politics in organizations" In: Griffin, W. O'Leary-Kelly, M. (Eds.), *The dark side of organizational behavior*, San Francisco: Jossey-Bass, pp. 237-261, 2004.
- [74] C. Russell, S. Marie, "Social exchange theory: An interdisciplinary review" *Journal of Management*, 31(6), 874-900, 2005.
- [75] L. Shore, L. Tetrick, P. Lynch, K. Barksdale, "Social and economic exchange: construct development and validation" *Journal of Applied Social Psychology*, 36(4), 837-867, 2006.
- [76] E. Eyvind, A. Knut, T. Are, "Social exchange theory as an explanation of organizational citizenship behaviour among teachers" *International Journal of Leadership in Education*, 14(4), 405-421, 2011.
- [77] P. Spector, "Method variance in organizational research: truth or urban legend?" *Organizational Research Methods*, 9, 221-232, 2006.
- [78] L. Brown, M. Feinberg, M. Greenberg, "Measuring coalition function: refining constructs through factor analysis" *Health Education and Behavior*, 39(4), 486-497, 2012.
- [79] J. Loehr, T. Schwartz, "The power of full engagement: managing energy, not time, is the key to high performance and personal renewal" New York: Free Press, 2003.

Appendices

Table A: Coalition scale

Instructions: Please tick on the response that best describes your observation.

Statement	Strongly Agree	Agree	Neither Agree nor Disagree	Disagree	Strongly Disagree
1. Organisational leadership are influenced by informal authority					
2. Informal authority determines the focus and direction of task in an organization					
3. Informal authority influence interpersonal relationships in organisation					
4. Coalition members are personally rewarded for the coalition involvement					
5. Organisational operations are influenced by informal authority					

Table B: Employee spiritual engagement scale

Instructions: Please tick on the response that best describes your observation.

Statement	Strongly Agree	Agree	Neither Agree nor Disagree	Disagree	Strongly Disagree
1. There is a good fit between my values and the organisation's values					
2. I feel like my work is meaningful and important to this organization					
3. I feel like I significantly contribute to the success of this organization					
4. I understand my purpose in helping my team, and the organisation be successful					
5. Overall, I get a real sense of achievement working for this organization					

Creating a Digital Twin: Simulation of a Business Model Design Tool

Kira Rambow-Hoeschele*, Nick Giani Rambow, Matthias Michael Hampel, David Keith Harrison, Bruce MacLeod Wood

School of Computing, Engineering and Built Environment, Glasgow Caledonian University, Glasgow, UK

ARTICLE INFO

Article history:

Received: 03 December, 2018

Accepted: 02 November, 2019

Online: 22 November, 2019

Keywords:

Business model development

Digital twin

Simulation tool

ABSTRACT

Digitization forces industry players to adapt to transforming market situations and buyer behavior. Technological advances, buyer power, and sharpened competitive intensity imply that businesses are confronted with the menace of commoditization. For companies to perform successfully in the market, outdated business models ought to be rethought and new business models should be created. Unique selling propositions and differentiation through research, innovation, and holistic stakeholder involvement help industry players to master the change. A tool was built to support businesses facing the consequences of digital transformation: the Business Model Builder. This research paper explores the steps of creating a software version of the analog Business Model Builder. The digital twin enables firms to simulate the iterative adaptation of business models to permanently changing market circumstances and customer demands on an ongoing basis. The user of the tool can edit single variables, understand interrelations, and see the effect on the outcome of the business case, e.g., earnings before interest and taxes or economic value added. Accordingly, the simulation offers the opportunity to have a dynamic view of the business model where any variances of input parameters are reflected in the business case. Thus, profitability, feasibility, and functionality of a business model can be validated, tested, and reviewed in the digital simulation tool.

1. Introduction

Digitization has an impact on most industries, value-creating architectures, and business models based upon them. The impact depends on the market and can – in several cases will – make current business models outdated.

Digitally connecting devices – TVs, household appliances, watches, etc. –, the Internet of Things creates chances for new business models in B2C commerce. Nevertheless, they need to be created and implemented as a first step. Furthermore, the Internet of Things substitutes business models in the B2B segment [1].

To adjust current business models to the transforming market situations, or to come up with new business models, the Business Model Builder was developed within the cooperative research project “low-carbon city” [2] – a project, state subsidized by the German Federal Ministry of Education and Research from August 2016 to December 2018 (references 02K12A150 and 02K12A151). The Business Model Builder represents a digital tool

that depicts the modules, drivers, and interrelations vital for the development or modification of business models.

2. Methodology

The creation of the digital twin simulating a business model design tool follows three major steps: conceptualization and design of the analog Business Model Builder, identification of interdependencies within the tool, and coding of the software-supported version to create the digital twin.

3. Digitization Process of the Tool

To customize single elements of a business model during its development, and to reveal consequences of changes on the other elements, the Business Model Builder is designed using application software. This software builds a digital twin of the business model. A digital twin stands for to a digital replica of a business model [3, 4].

This digital duplicate of the business model simulates adaptations or improvements of e.g., a product involved in the

* Kira Rambow-Hoeschele, Email: kira.rambow-hoeschele@t-online.de

business model. This includes testing the effects on function, handling, visual appearance, etc.

Internal links and databases in the background of the application enable to digitally show how adjustments of individual elements impact other ones. Additionally, the business case is calculated in the tool.

Not merely does the digital version of the Business Model Builder provide an iterative and efficient creation of business models, it also provides real-time information. Through the real-time depiction, transformations of business models can be reviewed in a convenient way.

4. Reference to Existing Work and Theories

Over time, the term “business model” has changed and has been defined in various ways. In order to fully comprehend the concept, it is therefore necessary to look at the past definitions as well as future requirements that business models need to fulfill. Business models illustrate a business idea as well as the ways and means by which the idea can be successfully implemented [5]. A business is defined as a product or service that owns a market presence and creates market- and resource-based synergies through collaboration with other entities [6].

Other researchers define the term “business model” as the synthesis of how a company selects its customers, how it defines and differentiates its products, how it structures its internal and external activities, how it uses its resources, how it enters the market, how it creates customer value, and how it earns profits [7]. A business model represents the complete system of how customer value is created and how it is monetized [8]. For several researchers, the elements of value propositions as well as customer segments are of high importance. Moreover, key resources and key activities that are necessary to create customer value as well as revenue streams are considered vital.

According to Timmers, a business model is “an architecture for the product, service and information flows, including a description of the various business actors and their roles and a description of potential benefits for the various business actors and a description of the sources of revenues” [9].

Business models can also be seen as planning and analysis tools. Companies dominating their markets therefore constantly adapt, refine, and develop current or new business models in order to remain competitive [10].

With the new economy boom at the beginning of the current century, the term “business model” was transferred to the business world, as competition was no longer defined as produces and services competing against each other but rather as a clash among various business models [11].

This led to changes in thinking about how to conduct business and where to best allocate resources in order to maximize competitiveness and value creation, since companies no longer possessed competitive advantages due to a superior product or service but rather through the design of complex and advanced business models. Instead of producing a good and simply selling it to the market, the business model needs to tell a reasonable story that is applicable to today’s accelerated and more volatile business environment [12].

Moreover, a business model can be defined as a business concept that is applied in the real world. A business concept identifies what value the business is providing to its stakeholders. Also, a business concept is an architecture that should describe how value is generated for customers and business partners. This architecture should include the different steps of value creation. Moreover, it should show how the business model will be able to generate revenues and profits to enable decision makers to identify the value of business ideas and the sustainability of their long-term success [13].

Most researchers see the term “business model” as a simplified depiction of business activities. However, the understanding of the importance of certain aspects of the business model varies [14–17].

Osterwalder and Pigneur define a business model as “nothing else than the value a company offers to one or several segments of customers and the architecture of the firm and its network of partners for creating, marketing, and delivering this value and relationship capital, in order to generate profitable and sustainable revenue streams” [18].

To visualize and to test the realization of business models, they developed the so-called “Business Model Canvas.” This is a tool for business model development that can also be used as a checklist to provide an overview of the tasks and requirements that need to be accomplished in order to turn the idea into a real-life business. It is especially helpful to create a common basis for all stakeholders that are involved in the business development process [19].

The concept consists of nine different components that should depict the model in regard to all important parts: customer segments, value proposition, channels, customer relationship, revenue streams, key resources, key activities, key partnerships, and cost structure.

The customer segments component includes consumers as well as businesses. This building block enables a clearer understanding of who the different parties are that are being served by the business. It provides clarity about whom value should be created for and how important those parties are for the business. The different customer segments can be structured according to their needs, their behavior, their specific characteristics, their financial buying power, and their preferred channels.

The value proposition consists of products or services that create value for specific customer segments. This value provided can differ with regard to its nature. It might include performance optimization, branding, work simplification, or entirely new products or services.

The customer relationships component describes how the business interacts with its customers to showcase how it can gain and retain customers. It shows how the relationship between the customer and the company is formed and what kind of relationship they have when conducting business.

The channels component includes all sorts of customer touchpoints as well as the different channels that are used to communicate with the customer and that are needed to distribute and sell the product or service.

Key activities include all important activities that are necessary for the entity in order to conduct business. This includes the processes that are needed to create and provide the value proposition to the customer, that are necessary to build and retain customer relationships, and that are used to reach all markets that are relevant for the business idea.

Key resources include all kinds of resources of physical, financial, human, or intellectual natures. This component gives an overview of all resources that are necessary to conduct the business.

In the key partnerships component, the network of all partners and suppliers that are needed for the business idea is described. This might include strategic alliances, joint ventures, and buyer-seller relationships.

Moreover, in the cost section of the business model canvas, all kinds of key fixed and variable costs are displayed in order to identify the biggest cost drivers that will affect the profitability of the business.

One of the most pivotal components of this model, however, is the revenue part. This section, in which the actual revenue streams are explained, will ultimately provide guidance on whether the business will be successful or not. This might include revenues from sales, rental services, leasing contracts, advertisements, commissions, or subscription fees.

In the following section, several innovative business model ideas are described. Some have existed for a long time in the business world, while others are comparably new, being enabled through technological developments such as e-commerce.

5. Innovative Business Model Approaches

One business model example is the sale of products or services with optional add-on features. This model enables the customer to buy a basic product at a lower price and then be charged a higher amount for additional options. Examples of such business practices can be seen in a variety of businesses such as the airline industry, the automotive industry, or the software industry [20].

A relatively new business model is revenue generation through affiliate links. Through the usage of such links, companies receive a commission based on the generation of sales of products or services through those links. Such business practices are used in e-commerce businesses, e.g., through review or price comparison websites generating additional sales channels for producers [21].

Another prominent business model, especially in the e-commerce sector, is based on auctions. This model enables customers to set the price, leading to higher ambiguity for the seller. Whereas the seller might be able to achieve higher returns in comparison to a traditional sales approach, the business risk increases as the predictability of revenues decreases [22].

Moreover, some companies use a barter approach to acquire new customers by providing free samples of their product. This is often found in the area of consumable products, where potential customers receive a small sample to convince them to convert to paying customers who buy the real product [22].

Bundling and cross-selling approaches capture customers through ecosystems of products and services that, once a customer

is acquired, make it rather difficult for them to leave the ecosystem again. Often, technology firms provide a software and hardware ecosystem that enables the customer to synchronize devices and use services on a variety of devices [23, 24].

Another innovative business approach is crowdfunding. This enables companies to make investments they would not have been able to make without the financial support of a broad variety of sponsors [25].

Crowdsourcing business models can be found in a variety of industries. Some companies only try to focus on their specific area of expertise and follow a crowdsourcing approach instead of a vertical integration approach, leading to potential cost savings and more flexibility [26].

Moreover, some companies base their business model on customer loyalty. Many of those companies earn revenues through the collection and analysis of data that is gained from customers who profit from customer loyalty programs, paying with their data [27].

An additional business model that has been developing over the past decades with the rise of digital technology is digitalization. Many businesses have been successful in providing digitized content to customers instead of more resource-intensive and less flexible physical content [28].

Furthermore, the development of the internet created higher market transparency for customers as well as companies and established new ways for producers to earn revenues through direct selling. By leaving out intermediaries, businesses can turn profitable and establish new market opportunities that had not existed before [29].

E-commerce business models are currently transforming the retail business and a variety of industries in ways that have not been seen before. Through lower costs, targeted advertising, broader product offerings, and further advantages, these businesses threaten many well-established companies [30].

Other businesses use flat-rate business models that require users to pay a specific amount in order to use a product or service to an unlimited extent. This has been visible in the online media world, e.g., for music or movie streaming [31].

Additionally, companies use franchising models that enable large scaling effects. After a concept has been developed and a brand established, e.g., in the food industry, local business owners pay for the usage of and supply from the brand [32].

A business model that is frequently visible in the web services industry is the freemium model. This allows customers to use a product in a basic form or for a limited time and offers a premium version that must be paid for [33].

An alternative business model that is often used in the web services industry is hidden revenues. Through the display of advertisements or promotions of complementary products, companies are able to generate revenues [31].

Also, many companies track, analyze, and sell customer data collected through a variety of channels in order to earn revenue. This model is especially used by social media platforms [34].

Intellectual property that might have not been commercialized in the past can be monetized through licensing. Many software firms base their business models on this architecture [33].

Furthermore, through easier accessibility and lower costs due to digitization, long-tail business models have been created that offer products and services that include not only mass products but also niche products that have now become profitable due to economies of scale and lower barriers of entry into a market [35].

Another business model, which became attractive to companies over the past decade, is mass customization, allowing customers to buy products that are mass-produced but customized for them. This has been enabled through technological developments in production, e.g., 3D printing, as well as automation of processes and further technologies. Exemplary industries are the automotive sector as well as the technology hardware sector [36].

Moreover, through lean startup approaches and the reduction of certain product features, no-frills business models have enabled market entry for lower-cost products. A variety of consumable product companies have been established that focus on specific, highly demanded features of a product while leaving out less important features in order to reduce price and increase product attractiveness as well as market attractiveness [37].

Other companies might use open source business models that allow external parties to improve the product. This is a commonly used approach in the software industry, where developers use certain tools that are more adaptable than standard software [38].

An approach that creates flexibility in regard to pricing is the “pay what you want” business model. This architecture can be found in, for example, the cultural sector or the web application sector [39].

With an increased usage of data analytics, pay-per-use business models have become more viable over the past years. Mobility services providers have been using this business model extensively [31].

The razor and razor blade business model architecture is also seen quite frequently in today’s consumables industry. Oftentimes, a basic product is provided at a low cost or even free. However, when a replacement of particular parts is needed, the purchase of those parts is more cost-intensive for the customer [33].

A very prominent business model, especially in the web-based industry, is a subscription architecture. This enables companies to earn recurring revenues that might lead to less price-sensitive customers who accept their current costs due to automatic payments. They thereby receive products or services periodically, such as consumables, media, or clothing [40].

Finally, everything-as-a-service (XaaS) business models have been seeing an increasing presence over the last years. In particular, in the software industry, product purchases have been transformed into consuming a service [41].

Those briefly introduced business models are only examples of currently existing business models and should not be seen as an exhaustive list. However, they give a good indication of the variety and complexity of business models that exist nowadays. The

forementioned business models are not only used exclusively but are often implemented as a combination of different models. Due to the potential complexity of business models, it is of high importance to use a development approach that is comprehensive, easy to understand, and flexible to changes.

6. Comparative Analysis of Business Model Definitions and Elements

The creation of a business model consists of multiple connected subcomponents, which build several components, which again join up to form modules. The business model building tool presents the individual elements of a business model and their underlying logic. The Business Model Builder is shown in low granularity in Figure 1.

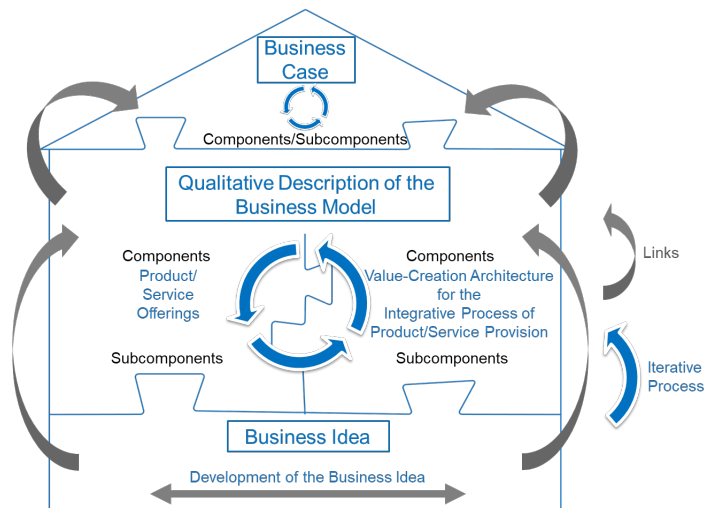


Figure 1: Business Model Builder Depicted in Low Granularity

The application of the Business Model Builder provides the user with business-specific yield numbers indicating the anticipated commercial performance of a business model. The application and field test of the analog Business Model Builder were a success [1].

There have been some former approaches for the creation of business models, e.g., from Gassmann et al. (2013) [42], Schallmo (2013) [43], Osterwalder and Pigneur (2011) [19], or Timmers (1998) [9]. These approaches often consist of diverse checklists, which are mainly grounded on theoretical concepts.

Including all important business model elements, a comparison and evaluation of established business model definitions took place (Figure 2) [7, 9, 10, 13, 15–18, 29, 40, 42–47].

Business models are built of several single elements with differing effect on the outcome of the business case. Various approaches for the creation of a business model can be chosen. For the digitization process of a business model creation tool, nonetheless, it is relevant to individually list all parts. This breakdown eases converting the impact and interrelationships of the single parts into a digital tool since precise relations can be assigned.

To comprehensively include all characteristics required for the development of the digital twin, the Business Model Builder was developed, originating from and enhancing former concepts.

As mentioned earlier, a checklist lacks some details for the complete development of a business model. Every business model requires a well-considered idea as its basis. Several checklists and related concepts still need to examine the soundness of a business idea and review the concept for its resistance. More than fifty percent of new business formations fail [48]. A key reason are unsustainable business ideas [49].

		Authors																
		Slywotzky (1995)	Timmers (1998)	Linder/Cantrell (2000)	Alf/Zimmermann (2001)	Amit/Zot (2001)	Schögel (2001)	Knyphausen-Aufseß/Meinhardt (2002)	Magretta (2002)	Stähler (2002)	Reinmeister/Klein (2003)	Shafer/Smith/Linder (2005)	Osterwalder/Pigneur (2002/2010)	Wirtz (2010)	Bieger/Reinhold (2011)	Gassemann (2013)	Schallmo (2013)	
Characteristics	Business case																1	
	Revenue and income																13	
	Business idea																2	
	Sales channels																3	
	Costs and expenses																2	
	Customers																8	
	Customer relationships																4	
	Value proposition																11	
	Market																3	
	Monitoring																1	
	Network																1	
	Products/services																5	
	Product life cycle																1	
	Processes																2	
	Legal aspects																1	
	Role of the stakeholders																3	
	Technologies																1	
	Transactions																1	
	Corporate activities																5	
	Business purpose																9	
Value creation																10		
Competitive environment																3		

Legend: ■ Characteristic is mentioned □ Characteristic is not mentioned

Figure 2: Comparative Analysis of Existing Business Model Theories

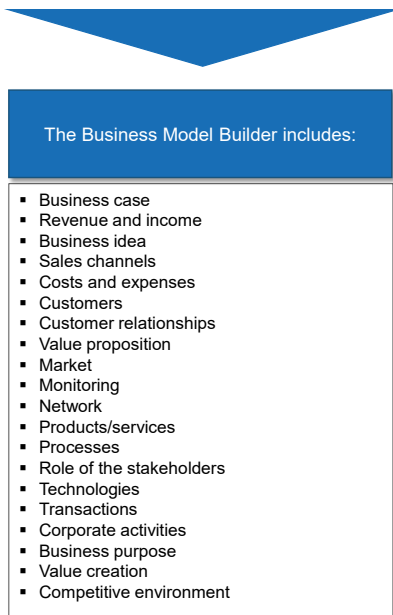


Figure 3: The Business Model Building Tool Extends the Existing State of Knowledge

Figure 3 shows that the Business Model Builder involves all characteristics that are vital for the success of a business model. The tool structures the elements to give a thought-out overview pursuing a distinct logical pattern. The goal of this tool is to enable effective creation of business models.

Compared to the concepts reviewed in Figure 2, the business model building tool follows an explicit architecture to allow for an adjustment of customer demands during and after the process of developing the business model. Pivotal advantages are that the application of this approach is both dynamic and iterative.

Some existing software-supported tools for the creation of business models offer the visualization of the business model elements. However, interrelated effects among the parts are not yet disclosed and precise figures, e.g., of the business case, are not yet calculated.

The software-based version of the business model building tool bridges this gap by paying attention on how individual parts impact each other. Also, business-specific earning numbers are calculated as a result. The digital tool of the Business Model Builder represents a self-contained, cohesive system.

7. Research and Innovation Approach

Within the state-subsidized project, various business ideas were created with the aid of the Business Model Builder for the loading of electric vehicles with self-produced electricity, generated by photovoltaic plants.

The single elements of the Business Model Builder are shown in Figure 4. The subcomponents of the tool form components, which sum up to condensed modules. These modules build on one another. Derived from the current state of research, the order of the subcomponents represents a recommendation on how to develop the business model step by step.

7.1. Module 1: Business Idea

The first module works as an idea filter for business ideas identified as fruitful. The value proposition is investigated from the customer’s point of view and reviewed with regard to an implementation in the market.

7.2. Module 2: Qualitative Description of the Business Model

This module comprises of the components product/service offerings as well as creation of offerings / value creating architecture, characterizing the business model under development or revision.

At the end of this process, a definite product/service offering is determined, including a rise in quantity and price on one side and a defined value creating architecture with respective quantities and specific costs on the other side

7.3. Module 3: Business Case

The core of this module is the measurement of how performant a business model will be. The success is quantified by key performance indicators, e.g., earnings before interest and taxes or economic value added. The basis, therefore, includes selling volume and price as well as production volume and costs from the second module. The business case – as a quantified business model – can also serve as the foundation for negotiations with investors, for instance.

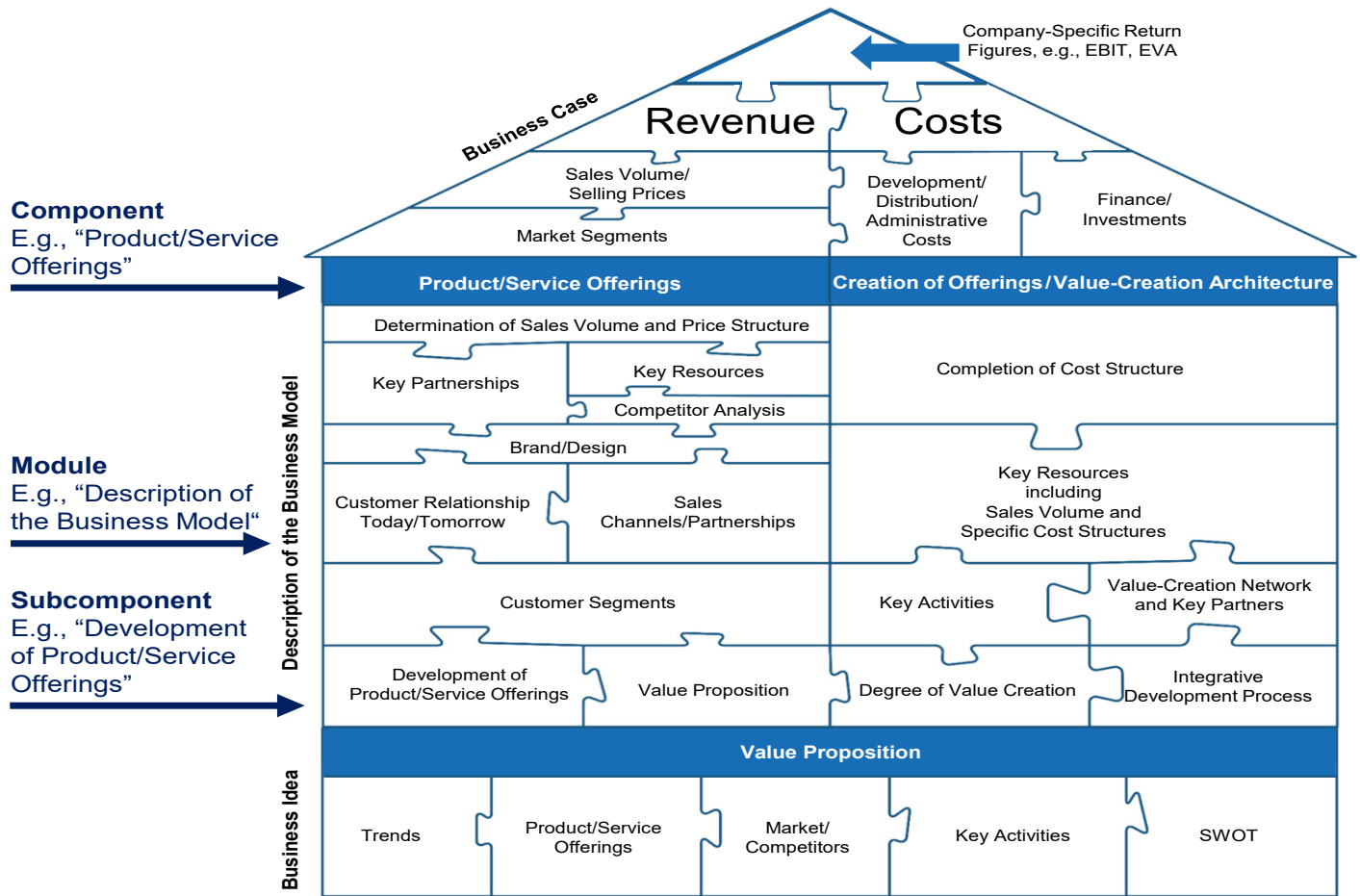


Figure 4: Business Model Builder Depicted in Fine Granularity

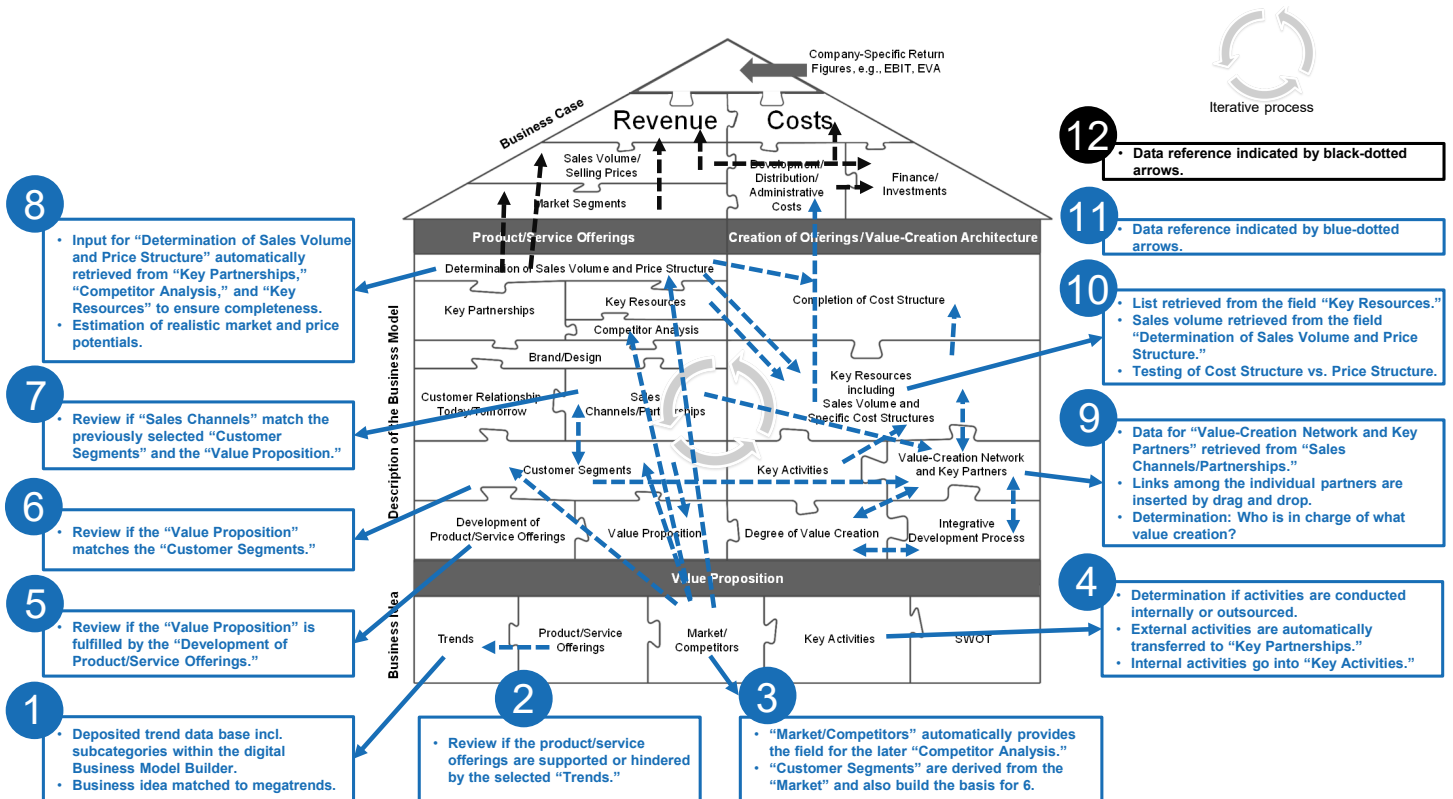


Figure 6: Interdependencies Within the Software-Supported Version of the Business Model Builder

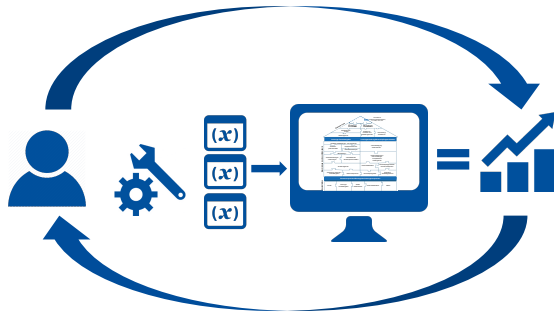
8. Conceptualization of the Tool and Its Digital Twin

The Business Model Builder is designed such that interrelated elements are linked and that effects from changes in one part on another part are revealed. Depending on the input variable, a change can also affect the business case.

The digitization of the Business Model Builder facilitates complex analyses. As multiple elements of the tool depend on other elements and are automatically updated through the links, impact on business results is easily uncovered and visualized.

Figure 5 depicts the schematic setup of the software-based tool. The user is responsible for the input of the elements. The elements automatically match as well as offset against each other. Hence, the operational results are automatically calculated.

Besides, the tool checks the user's input for plausibility and impact on other business model elements. In case of a mismatch, the user is given an error warning, and they are asked to reassess and correct the data entry.



9. Digitization Process of the Tool and Elaboration of Interrelations Among Elements

To digitize the business model building tool, it is pivotal to define which elements are freely definable, which import data from deposited databases, and which are the result of interrelated elements. The details of the interdependencies are shown in Figure 6. For the creation of this tool, all elements are studied for their impact on other elements involved. After the definition of these links, the attendant effects are programmed within the application software. This automizes the steps for the iterative business model development.

Providing an example, the first subcomponent in the tool is the trends. The trends are drawn from an external database. Thus, the user assigns their business idea to a megatrend at first. Subsequently, the idea is assigned to the macro trends related to the megatrend. Later, the trends chosen are collated with the subcomponent “product/service offerings” to check the content of these subcomponents is consistent.

In addition to the yield numbers, the software-based version of the tool generates a digital twin of the business model. This offers convenient further editing of the business model. For instance, if the figures of the business case calculation lead to a “no go” decision, the subcomponents of the business model can be edited so that yield numbers finally result in a “go” decision. The digital Business Model Builder offers users to gradually adapt and improve the digital twin over the total lifetime.

10. Findings

Digitizing the Business Model Builder, an instrument is developed enabling users to create new, or innovate current business models in a convenient and structured manner with the desired granularity. In the software-based version of the business model building tool, the elements are automatically interconnected. Hence, business models can be modified, and results can be simulated. The tool can holistically depict the complete lifecycle of business models. Thus, various scenarios can be simulated with little expenditure of human labor and time.

11. Limitations

At this phase of the research project, the coding of the digital twin is taking place. As a next step, pilot testing will be implemented to test the application under real-world conditions, collect feedback, and potentially revise and adjust the tool. Only after the rollout will it be possible to see the impact of how the digitized Business Model Builder enhances effectiveness and efficiency of businesses.

12. Conclusion

Digitization pushes businesses aiming for sustainable commercial success to adapt business models to new market situations or create new business models when the former ones become obsolete through technological change. The Business Model Builder was developed to serve this demand. As digital version, the tool enables the permanent iterative adaptation of business models to transforming market circumstances.

The software-based version of the tool allows firms to set up their current business models in a digital twin. In this way, firms have the possibility to conveniently simulate amendments to business models and review their profitability, functionality, and feasibility. Furthermore, new business models can be created, validated, and tested. The digital tool offers established businesses as well as start-ups the option to iteratively adapt their business models to continuously transforming market situations and customer demands over a lifecycle. The tool's mission is to support firms in growing sustainably, in generating and keeping unique selling propositions to stand their ground in the market, and in achieving durable success in the world's markets.

References

- [1] A. Nagl and K. Bozem, *Geschäftsmodelle 4.0 – Business Model Building mit Checklisten und Fallbeispielen*. Wiesbaden: Springer Gabler, 2018. ISBN 978-3-658-18841-2
- [2] Hochschule Aalen für Technik und Wirtschaft, “BMBF Cooperative Research Project CO₂-arme Stadt / Low-Carbon City.” Accessed: February 1, 2018. [Online]. Available: www.co2-arme-stadt.de
- [3] S. Boschert and R. Rosen, “Digital twin – the simulation aspect,” in *Mechatronic Futures*, P. Hehenberger and D. Bradley, Eds. Cham: Springer, 2016. DOI 10.1007/978-3-319-32156-1_5
- [4] M. Grieves and J. Vickers, “Digital twin: Mitigating unpredictable, undesirable emergent behavior in complex systems,” in *Transdisciplinary Perspectives on Complex Systems*, J. Kahlen, S. Flumerfelt, and A. Alves, Eds. Cham: Springer, 2017. DOI 10.1007/978-3-319-38756-7_4
- [5] A. Nagl, *Der Businessplan: Geschäftspläne erstellen – Mit Checklisten und Fallbeispielen*. Wiesbaden: Springer, 2015.
- [6] R. Grünig and R. Kühn, *Methodik der strategischen Planung: Ein prozessorientierter Ansatz für Strategieplanungsprojekte*. Bern: Haupt, 2000.

- [7] A. J. Slywotzky, *Value Migration: How to Think Several Moves Ahead of the Competition*. Boston: Harvard Business Press, 1995.
- [8] A. Zolnowski and T. Böhmman, "Grundlagen service-orientierter Geschäftsmodelle," in *Service-orientierte Geschäftsmodelle: Erfolgreich umsetzen*. T. Böhmman et al., Eds. Berlin: Springer, 2013, pp. 1–29.
- [9] P. Timmers, "Business models for electronic markets," *Electronic Markets*, vol. 8, no. 2, pp. 3–8, 1998.
- [10] J. Linder and S. Cantrell, *Changing Business Models: Surveying the Landscape*. Chicago: Institute for Strategic Change, Accenture, 2000. Accessed: April 12, 2016. [Online]. Available: businessmodels.eu/images/banners/Articles/Linder_Cantrell.pdf
- [11] G. Hamel, *Leading the Revolution*. Boston: Harvard Business School, 2000.
- [12] B. W. Wirtz, *Business Model Management: Design – Instrumente – Erfolgsfaktoren von Geschäftsmodellen*. Wiesbaden: Springer Gabler, 2010.
- [13] P. Stähler, *Geschäftsmodelle in der digitalen Ökonomie: Merkmale, Strategien und Auswirkungen*. Lohmar: Eul, 2002.
- [14] P. Stähler, *Merkmale von Geschäftsmodellen in der digitalen Ökonomie*. Köln: Eul, 2001.
- [15] D. Knyphausen-Aufseß and Y. Meinhardt, "Revisiting strategy: Ein ansatz zur systematisierung von geschäftsmodellen," in *Zukünftige Geschäftsmodelle*, T. Bieger et al., Eds. Berlin Heidelberg: Springer, 2002, pp. 63–89.
- [16] J. Rentmeister and S. Klein, "Geschäftsmodelle ein modebegriff auf der waagschale," *Zeitschrift für Betriebswirtschaft*, Ergänzungsheft 1, pp. 17-20, 2003.
- [17] S. M. Shafer, H. J. Smith, and J. C. Linder, "The power of business models," *Business Horizons*, vol. 48, no. 3, pp. 199–207, 2005.
- [18] A. Osterwalder and Y. Pigneur, "An e-business model ontology for modeling e-business," *Electronic Commerce Conf.*, Bled, 2002.
- [19] A. Osterwalder and Y. Pigneur, *Business Model Generation: Ein Handbuch für Visionäre, Spielveränderer und Herausforderer*. Frankfurt a. M.: Campus, 2011.
- [20] O. Gassmann, K. Frankenberger, and M. Csik, *The Business Model Navigator: 55 Models That Will Revolutionise Your Business*. Harlow: Pearson, 2014.
- [21] M. A. Rappa, "The utility business model and the future of computing services," *IBM Systems Journal*, vol. 43, no. 1, pp. 32–42, 2004.
- [22] M. Dubosson-Torbay, A. Osterwalder, and Y. Pigneur, "E-business model design, classification, and measurements," *Thunderbird International Business Review*, vol. 44, no. 1, pp. 5–23, 2002.
- [23] C. Zott and R. Amit, "Business model design: An activity system perspective," *Long Range Planning*, vol. 43, no. 2–3, pp. 216–226, 2010.
- [24] D. J. Teece, "Strategies for managing knowledge assets: the role of firm structure and industrial context," *Long Range Planning*, vol. 33, no. 1, pp. 35–54, 2000.
- [25] P. Belleflamme, T. Lambert, and A. Schwienbacher, "Crowdfunding: An industrial organization perspective," prepared for the workshop Digital Business Models: Understanding Strategies, Paris, June, 2010, pp. 25–26.
- [26] D. C. Brabham, "Crowdsourcing as a model for problem solving: An introduction and cases," *Convergence*, vol. 14, no. 1, pp. 75–90, 2008.
- [27] N. A. Morgan and L. L. Rego, "The value of different customer satisfaction and loyalty metrics in predicting business performance," *Marketing Science*, vol. 25, no. 5, pp. 426–439, 2006.
- [28] J. Gray and B. Rumpe, "Models for digitalization," *Software & Systems Modeling*, vol. 14, no. 4, pp. 1319–1320, 2015. DOI 10.1007/s10270-015-0494-9
- [29] J. Magretta, "Why business models matter," *Harvard Business Review*, vol. 80, no. 5, pp. 86–92, 2002.
- [30] K. C. Laudon and C. G. Traver, *E-commerce: Business, Technology, Society*. Harlow: Pearson, 2016.
- [31] E. Fleisch, M. Weinberger, and F. Wortmann, *Business Models and the Internet of Things: Interoperability and Open-Source Solutions for the Internet of Things*. Cham: Springer, pp. 6–10, 2015. DOI 10.1007/978-3-319-16546-2_2
- [32] W. Gillis and G. J. Castrogiovanni, "The franchising business model: An entrepreneurial growth alternative," *International Entrepreneurship and Management Journal*, vol. 8, no. 1, pp. 75–98, 2012.
- [33] D. J. Teece, "Business models, business strategy and innovation," *Long Range Planning*, vol. 43, no. 2–3, pp. 172–194, 2010.
- [34] R. Amit and C. Zott, "Creating value through business model innovation," *MIT Sloan Management Review*, vol. 53, no. 3, pp. 41–49, 2012.
- [35] C. Anderson, *The Long Tail: Why the Future of Business is Selling Less of More*. New York: Hachette Books, 2006.
- [36] F. Salvador, P. M. De Holan, and F. Piller, "Cracking the code of mass customization," *MIT Sloan Management Review*, vol. 50, no. 3, pp. 71–78, 2009.
- [37] M. W. Johnson, C. M. Christensen, and H. Kagermann, "Reinventing your business model," *Harvard Business Review*, vol. 86, no. 12, pp. 57–68, 2008.
- [38] H. W. Chesbrough, "Why companies should have open business models," *MIT Sloan Management Review*, vol. 48, no. 2, p. 22, 2007.
- [39] J. Y. Kim, M. Natter, and M. Spann, "Pay what you want: A new participative pricing mechanism," *Journal of Marketing*, vol. 73, no. 1, pp. 44–58, 2009.
- [40] A. Osterwalder and Y. Pigneur, *Business Model Generation: A Handbook for Visionaries, Game Changers, and Challengers*. New Jersey: Wiley, 2010.
- [41] P. Banerjee et al., "Everything as a service: Powering the new information economy," *Computer*, vol. 44, no. 3, pp. 36–43, 2011. DOI 10.1109/mc.2011.67
- [42] O. Gassmann, K. Frankenberger, and M. Csik, *Geschäftsmodelle entwickeln: 55 innovative Konzepte mit dem St. Galler Business Model Navigator*. München: Hanser, 2013.
- [43] D. Schallmo, *Geschäftsmodell-Innovation: Grundlagen, bestehende Ansätze, methodisches Vorgehen und B2B-Geschäftsmodelle*. Wiesbaden: Gabler, 2013.
- [44] R. Alt and H.-D. Zimmermann, "Introduction to special section: Business models," *Electronic Markets*, vol. 11, no. 1, pp. 3–9, 2001.
- [45] R. Amit and C. Zott, "Value creation in e-business," *Strategic Management Journal*, vol. 22., pp. 493–520, 2001.
- [46] K. Schoegel, *Geschäftsmodelle: Konstrukt-Bezugsrahmen-Management*. München: FGM, 2001.
- [47] T. Bieger and S. Reinhold, "Das wertbasierte Geschäftsmodell: Ein aktualisierter Strukturansatz," in *Innovative Geschäftsmodelle*, T. Bieger et al., Eds. Berlin Heidelberg: Springer, 2011, pp. 11–70.
- [48] C. Triebel and C. Schikora, "Scheitern bei Unternehmensgründungen," in *Failure Management*, S. Kunert, Ed. Berlin Heidelberg: Springer, 2016, pp. 235–248.
- [49] J. Egel, U. Falk, D. Heger, D. Höwer, and G. Metzger, *Ursachen für das Scheitern junger Unternehmen in den ersten fünf Jahren ihres Bestehens*. Mannheim Neuss: Zentrum für Europäische Wirtschaftsforschung, 2010.

Fast Determination of Tsunami Source Parameters

Mikhail Lavrentiev^{*1,2}, Dmitry Kuzakov^{1,2}, Andrey Marchuk^{1,3}

¹*Institute of Automation and Electrometry SB RAS, 630090, Russia*

²*Novosibirsk State University, 630090, Russia*

³*Institute of Computational Mathematics and Mathematical Geophysics SB RAS, 630090, Russia*

ARTICLE INFO

Article history:

Received: 31 May, 2019

Accepted: 23 September, 2019

Online: 22 November, 2019

Keywords:

Tsunami wave source

Sea surface displacement

Orthogonal decomposition

ABSTRACT

Source parameters of tsunami waves are an essential part of any modern tsunami warning system. Recalculation of a measured time series (wave profile obtained by a seabed-based pressure sensor) in terms of initial sea surface displacement at tsunami source is among the most (or) one of the promising approaches to be applied in a warning center. The “orthogonal decomposition”, that was proposed and studied earlier by the authors, is numerically studied here. Realistic shape of sea surface displacement and digital bathymetry of the southern part of Japan are used. To study functionality of the proposed approach, wave profiles are obtained by the sensors of DONET – Dense Oceanfloor Network system for Earthquakes and Tsunamis – pressure gauge network of Japan. We stress on the quality of tsunami source parameters reconstruction as well as on time required. As observed, just a part of the first wave period is enough for robust determination of such source parameters as amplitude and total volume of water. Results of numerical tests are summarized in tables and then discussed.

1. Introduction

This paper is an extension of work originally presented in OCEANS'18 MTS/IEEE Kobe/Techno-Oceans 2018, May 28-31, Kobe Japan [1].

Typical tsunami warning system includes the following parts: wave generation, propagation over the water area under study, and inundation of a dry land. Aiming to achieve real time tsunami danger prediction, we address the question of fast determination of tsunami source parameters. Having such information, there are several software packages for numerical simulation of wave propagation and inundation mapping. Here we refer the reader to MOST (Method of Splitting Tsunami – official tool of the NOAA UnS tsunami warning centers), see [2-4], and TUNAMI, see [5,6].

In any case numerical simulation of wave propagation requires the initial data, say initial sea bed displacement at tsunami source. In this paper we address the question of rather fast reconstruction of the sea surface displacement at tsunami source. As an input data we use direct measurements of the wave profile (time series), obtained at any sensor system. As is well known, a number of deep-water pressure recorders are located all around Pacific

Ocean, they measure and send such data via satellite channels. Among these systems we would like to mention the USA DART (Deep-ocean Assessment and Reporting of Tsunami) buoys (<https://nctr.pmel.noaa.gov/Dart/>), and DONET (Dense Oceanfloor Network system for Earthquakes and Tsunamis) pressure gauge network system, which is under construction in Japan (<https://www.jamstec.go.jp/donet/e/>).

Our goal is to recalculate these direct measurements of the water column over a single sensor (which is nothing but a curve of the wave profile) in terms of 2D function of initial sea surface displacement at tsunami source. In general mathematical statement it is not possible to solve this problem. So, we use the so-called “Calculation in Advance” inversion strategy [7]. It has been proposed to cover the subduction zone (area of possible tsunami sources) with the system of 100x50 km rectangles (typical size of the seabed displacement zone for tsunamigenic 7.5 M earthquake). In case of Alaska-Aleutian subduction zone there are 50 of such Unit Sources (UnSs), composed in two alongshore lines. Then a typical (for this region) shape of the initial sea-bed displacement, normalized with an amplitude of 0.57 m, is used at each UnSs as tsunami wave source. Propagation of such wave from all the UnSs were numerically calculated (in advance) over the entire Pacific

*Mikhail Lavrentiev & mmlavrentiev@gmail.com

www.astesj.com

<https://dx.doi.org/10.25046/aj040608>

Ocean according to the approximation of shallow water system. As a result, a database of the calculated tsunami wave profiles, generated by the source of the same initial shape at all UnSs, is available for all grid points of the Pacific Ocean.

Now, having the measured (real) wave profile at certain sensor location, one can approximate this curve with the help of linear combination of calculated wave profiles from a number of UnSs, picking up at the same point of sensor location. In other words, the problem is to determine the amplification coefficients for the UnSs such that the corresponding linear combination of UnSs (say, a Composed Source – CS) provides a good approximation of the initial sea-bed displacement.

The similar approach named SIFT – Short-term Inundation Forecasting for Tsunamis (https://nctr.pmel.noaa.gov/Pdf/SIFT_3_2_2_Overview.pdf) is used by NOAA (USA) for wave height assessment in grid points of computational domain. As well as in the method presented here, on the basis of “computations in advance” of the tsunami height distribution from the set of Unit Sources the authors [7] reconstruct the CS. Unlike the method presented here, by search of set of coefficients in linear combination of UnSs, the SIFT system uses the combinatory search of values of coefficients giving a discrepancy minimum between real and calculated tsunami wave series in several tsunami detectors. Such approach requires a lot of processor time if CS consists from more, than 5 UnSs. There is no such shortcoming of the approach here proposed, where CS restoration time practically does not depend on quantity of UnSs involved. By the way, authors of this article also took part in development of an algorithm for source inversion in the SIFT forecasting system.

This approach has been many times tested against the field observations after near field and trans-oceanic events. Amazing agreement has been observed by comparison of computed wave, generated by a calculated CS, and measurements taken at various gauge stations. Nowadays, all subduction zones around Pacific, Atlantic, and Indian Oceans were covered with such systems of UnSs unit sources (<https://nctr.pmel.noaa.gov/propagation-database.html>); synthetic marigrams at every grid point from every source have been saved in a specialized database. One of the problems is to choose the aforementioned amplification coefficients in an automated mode. The orthogonal decomposition approach to handle this was proposed in [8] and then tested in [1,9]. It happens that even a part of the first wave period is enough to determine the CS – the set of amplification coefficients. In this paper we continue to study the problem of robust determination of sea surface displacement at tsunami source by a part of the wave profile.

The paper is arranged as follows. We first describe the proposed orthogonal decomposition algorithm and provide the mathematical ground behind it. In the numerical section we briefly describe digital bathymetry in use and the parameters of realistic CS, which has a feature of the reconstructed source of historical event of 1707 [10]. Then we provide the obtained numerical results in the form of a table. Finally, numerical results are discussed.

2. Orthogonal decomposition algorithm

2.1. Mathematical ground of algorithm

Here we provide the brief explanation of the algorithm for reconstruction of the CS. More detailed description one can find in [8].

Let $f(t)$ be the marigram – time series, obtained at any particular sensor (DART buoy, bottom cable sensor of DONET, or other). We will use notations $f_k(t), (k = 1, \dots, N)$ for simulated wave profiles, calculated (according to the linear or nonlinear shallow water approximation) at the same point of sensor location, by direct numerical modeling of the tsunami wave propagation. It is understood, that the subindex k refers to a tsunami wave initiated by the normalized sea surface initial profile of a given shape from the k -th UnSs. We assume that all these functions, $f_k(t)$, are linearly independent. We are looking for coefficients, b_k , for the linear combination of these functions, which provide the best approximation of the function $f(t)$ in L_2 norm:

$$\int_0^T \left(\sum_{k=1}^N b_k f_k(t) - f(t) \right)^2 dt \rightarrow \min \quad (1)$$

So, we consider the problem of optimal approximation of a given function, $f(t)$, by the linear combination of the finite subset of functions from the system $\{f_k(t)\}$. Suppose that the system is orthogonal and normalized according to:

$$(f_i(t), f_j(t)) = \int_{t_0}^T f_i(t) f_j(t) dt = 0, \text{ if } i \neq j \quad (2)$$

$$(f_i(t), f_i(t)) = 1. \quad (3)$$

Here t_0 stands for the time moment when the wave approaches the closest receiver, T is the time of the latest (of all receivers) full period on marigram which is concerned as the end of the second phase of tsunami. For sensors which are more distant off the coast than a source, the second phase of tsunami is positive, and for those which are closer to the shore, it is negative.

As is well known in the Fourier series theory, the coefficients of such optimal approximation are nothing but the Fourier coefficients of expansion of $f(t)$ in a series with respect to $\{f_k(t)\}$ (see, for example, [11]).

2.2 Algorithm description

Based on the statement above, the following algorithm was proposed in [8] and tested in [1,9] for searching the coefficients of the linear combination allowing optimal approximation of the given function. It includes three steps.

- (a) The calculated set of “marigrams”, $\{f_k(t)\}$, from the unit sources should be orthogonalized and normalized, according to equations (2)-(3).
- (b) The measured marigram, $f(t)$, should be expanded to the Fourier series with respect to obtained orthonormal system of functions.
- (c) The so-determined Fourier coefficients should be recalculated in terms of initial functions $\{f_k(t)\}$.

Let us transform the given system $\{f_k\}$ to the corresponding ortho-normal system, $\{e_k\}$, with respect to the scalar product (2). Let

$$e_1 = f_1 \quad (4)$$

Suppose that pairwise orthogonal nontrivial functions e_1, e_2, \dots, e_{k-1} are already constructed. We will look for the function e_k in the form:

$$e_k = f_k + l_{k,1} e_1 + \dots + l_{k,k-1} e_{k-1} \quad (5)$$

i.e. we obtain the next function, e_k , as the linear combination of the new function, f_k , and the already constructed ortho-normal ones, e_1, e_2, \dots, e_{k-1} . The coefficients, $l_{k,1}, l_{k,2}, \dots, l_{k,k-1}$, in formula (5) should be found from the conditions that the new function, $e_k = f_k + l_{k,1}e_1 + \dots + l_{k,k-1}e_{k-1}$, is orthogonal with all the previous ones, e_1, e_2, \dots, e_{k-1} , and normalized. Thus, the coefficients in (5) are calculated according to:

$$l_{k,i} = - \frac{(f_k, e_i)}{(e_i, e_i)}, \quad (i = 1, \dots, k - 1) \quad (6)$$

As is well known in calculus, the optimal L_2 approximation, according to criteria (1), of a given function f by the linear combination of orthogonal and normalized functions, e_k

$$f_{appr} = \sum_{i=1}^k a_i e_i \quad (7)$$

is achieved at the Fourier coefficients, a_i , of the function $f(t)$, decomposition with respect to the system e_k :

$$a_i = \frac{\int_{t_0}^T f(t) e_i(t) dt}{\int_{t_0}^T e_i^2(t) dt} \quad (8)$$

So, to solve the original problem (1), we only need to provide the coefficients (8) in terms of the original basis functions f_k .

It is just an algebraic exercise to conclude that the desired coefficients, b_k , in expression (1), are calculated through the given coefficients, a_k , from the formula (8), as follows:

$$\begin{cases} b_k = a_k, \\ b_{k-1} = a_{k-1} + a_k F(L', k, k-1) \\ b_{k-2} = a_{k-2} + a_{k-1} F(L', k-1, k-2) + a_k F(L', k, k-2) \\ b_i = a_i + \sum_{j=i+1}^k a_j F(L', j, i) \end{cases}$$

$$F(L', j, i) = \begin{cases} 0, & \text{if } j = i, \\ l_{j,i}, & \text{if } j = i + 1, \\ l_{j,i} + \sum_{k=i+1}^{j-1} l_{j,k} F(L', k, i), & \text{if } j \neq i, j \neq i + 1. \end{cases}$$

So, the proposed algorithm to approximate the given marigram, $f(t)$, by the linear combination of synthetic marigrams, $\{f_k(t)\}$, $k=1, \dots, N$, in order to achieve minimal L_2 difference (1), is as follows.

We first transform the system $\{f_k(t)\}$ to the orthogonal system, $e_k(t)$, and normalize it according to formulae (4) – (8).

Then the recorded marigram, $f(t)$, is decomposed to the part of Fourier series with respect to obtained orthogonal and normalized (see (1), (2)) basis, $e_k(t)$, by the formula (8).

Finally, the obtained Fourier coefficients, a_i , are recalculated in terms of coefficients, b_i , of the original linear combination (1), by means of (9).

3. Numerical experiments

Numerical experiments were arranged in the area around the south-east coast of Japan (eastern Kyushu, Shikoku islands and Kii peninsula). Geography, bathymetry and location of UnSs and CSs in this region are shown in Figure 1.

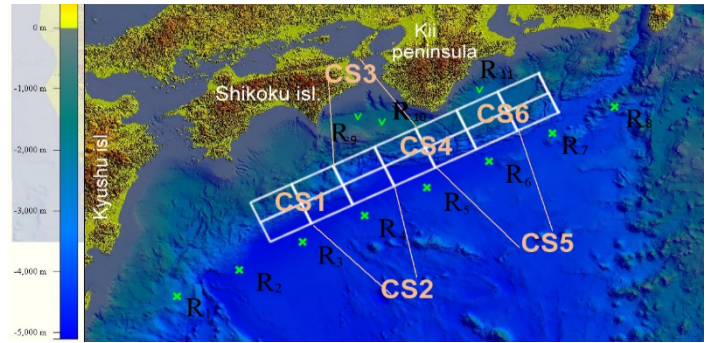


Fig. 1. Digital bathymetry of the water area under study. White rectangles show positions of model tsunami sources. Green crosses (R1-R8) indicate locations of artificial sensors. Green check marks (R9-R11) show the selected sensors of DONET.

3.1. Digital bathymetry

Numerical experiments were arranged at the gridded bathymetry around Eastern Kyushu, Shikoku Island and Kii Peninsula (southern part of Japan), built on the basis of Japanese bathymetric data produced by the Japan Oceanographic Data Center (JODC), presented in Figure 1. This digital gridded bathymetry has the following characteristics:

Size of array is 3000 x 2496 nodes;

Grid steps are 0.003 and 0.002 degrees (which means 280.6 and 223 meters, respectively);

Domain covers the area approximately between 131° E and 140° E, 30° N and 35° N.

3.2. Composition of tsunami source

In the course of numerical calculations model tsunami sources were formed of UnSs of 100x50 km in size located in two rows along the coast (Figure 1). Each of the six composed sources (CS), having the sizes of 200x100 km, is presented as the linear combination of four UnSs with given amplification coefficients (1.4; 1; 1.5; 1.1). For this set of coefficients, the maximum surface elevation in the source area is equal approximately to 3 m, and minimum water level there is estimated as -1.5 m (Figure 2). Bigger coefficients correspond to UnSs more distantly located off the coast. Numbering of CSs begins with UnSs which are at the western edge the source area (Figure 1). Two of them (the first and the last) are indicated in Figure 1. The ocean bottom displacement in the CS used for computations is shown in Figure 2.

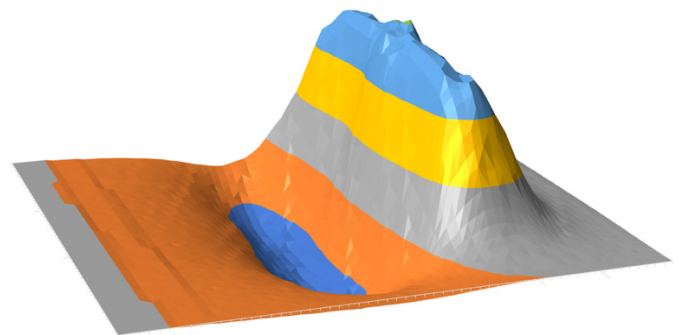


Fig. 2. Shape of the initial surface displacement at the Composite Source used for numerical experiments.

We assume precision of 10% as the value of reasonable accuracy of the tsunami height estimation. This value allows to determine parameters of the wave near the shore with the same precision, which is enough for the rapid tsunami hazard evaluation. It means that maximum difference between the initial and calculated surface displacement is less than 10 cm for a typical initial displacement height of 1 m. Accordingly, the deviation of 1 m is considered acceptable in case the wave height is 10 m.

As a rule, a part of the wave profile from the beginning to the zero level after the highest amplitude point (see Figure 2) is sufficient to reconstruct the amplification coefficients with a particular precision. So, we tried to determine how smaller could be a part of wave profile to keep the error in reconstructed ISSD amplitude within 0.1 discretization. The location of the model tsunami source centers for numerical calculations are chosen according to estimation of the source of the major tsunami, expected, according to [10], in the near future in the Nankai subduction zone (Figure 3 is taken from [10]). The size of the model sources corresponds to a tsunamigenic earthquake of magnitude 8.0.

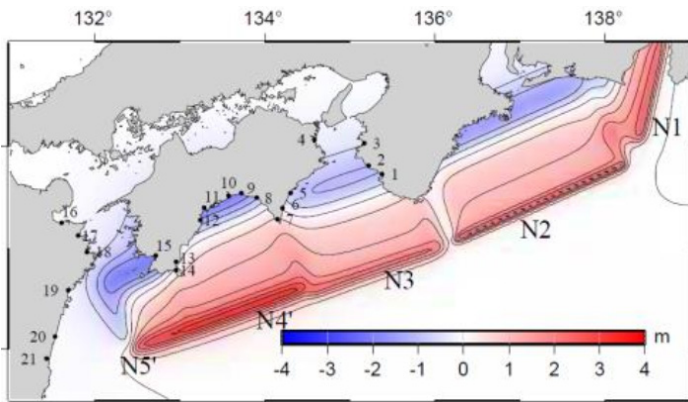


Fig. 3. The expected distribution of the initial water surface displacement in the tsunami source at the Nankai subduction zone, [10].

3.3. Positions of sources and sensor network

The virtual sensors network consists of one row of virtual deep-water wave detectors, installed along the Nankai Trough (R₁-R₈, indicated by green crosses in Figure 1). In addition, 3 sensors of DONET were also included to observation network system for source restoration in our numerical experiments. These sensors are indicated in Figure 4 as black squares, R₉, R₁₀ and R₁₁. Reconstruction of a source means determination of coefficients in the linear sum of UnSs composing CS.

3.4. Numerical experiments

As a result of numerical experiments, the tsunami wave signal from each of the six locations of CS (see Figure 1) was recorded by 11 detectors, R1-R11, given in Figures 1 and 4. By means of the described method, the minimum length of a wave signal, sufficient for determination of coefficients in the linear sum of UnSs (Necessary Part of Wave Profile – NPWP) have been determined with the required accuracy. These lengths as a percentage to length of the full wave period which means complete first two phases (positive and negative) of a wave are summarized in Table 1. The first column shows receiver’s number (1-11). In

the second column one can find the Composed Source number (1-6). In the third and the fourth columns the length in seconds of NPWP and the full wave period are presented, respectively. Column number 5 gives the length of NPWP in percentage of the full tsunami period. The last two columns present the NPWP ending time instance and the wave arrival time to a shore.

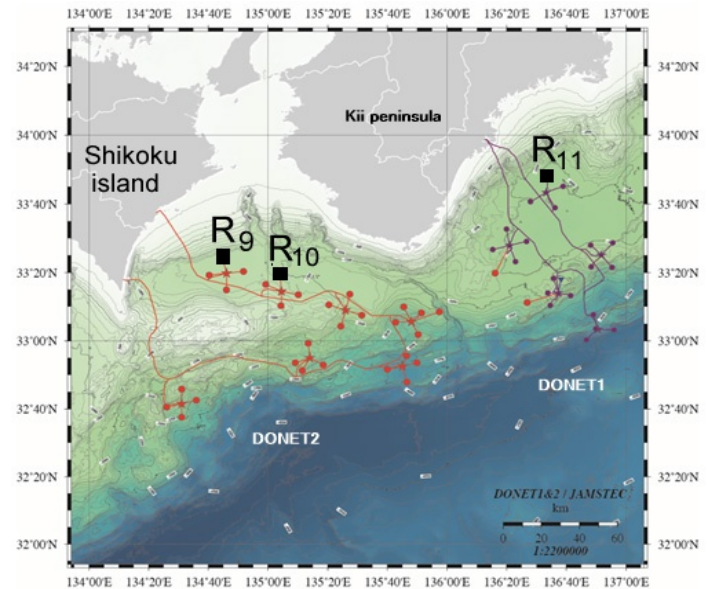


Fig. 4. Configuration of DONET-1 and DONET-2 system at the south-east of Japan (<https://www.jamstec.go.jp/donet/e/>). The existing sensors are in violet and sensors under construction are indicated in red. Black squares show three sensors, which positions were used for artificial sensors.

The duration of NPWP counted from the moment of wave arrival at receiver. More important for us is the end of NPWP on the record (column 6 in the Table 1). This record starts simultaneously with the initial ocean surface displacement. It is the same moment as regarded as zero in tsunami travel time. So, if NPWP (on record) is less than the tsunami travel time to the coast, then we have some time for reconstruction of CS and for estimation of the expected wave height near a shore.

Table 1: Numerical tests Parts of the entire wave profile (in percents), enough to determine the source parameters

Receiver	CS	NPWP, sec	Period, sec	NPWP, % of full wave period	Time required for accuracy to be achieved (from the generation moment), sec	Wave arrival time to a shore, sec
1	1	1511	1736	87.0	1511	837
2	1	224	1561	14.3	224	837
3	1	730	2553	28.6	998	837
4	1	442	1422	31.1	1731	837
5	1	419	1262	33.2	2313	837
6	1	1365	1608	84.9	3575	837
7	1	121	3867	3.1	2565	837
8	1	141	2949	4.8	3178	837
9	1	530	1257	42.2	698	837
10	1	496	1260	39.4	519	837
11	1	223	981	22.7	223	837

1	2	409	1311	31.2	409	876
2	2	223	1070	20.8	223	876
3	2	1724	2614	66.0	1724	876
4	2	474	2640	18.0	1327	876
5	2	679	1056	64.3	2057	876
6	2	542	2509	21.6	2469	876
7	2	247	3837	6.4	2369	876
8	2	328	2875	11.4	3040	876
9	2	219	1116	19.6	223	876
10	2	261	1031	25.3	261	876
11	2	293	1080	27.1	293	876
1	3	480	1359	35.3	480	525
2	3	223	1149	19.4	223	525
3	3	2043	2489	82.1	2043	525
4	3	728	1803	40.4	1012	525
5	3	922	1859	49.6	1786	525
6	3	1226	1594	76.9	2617	525
7	3	632	3844	16.4	2450	525
8	3	428	2769	15.5	2827	525
9	3	221	1003	22.0	223	525
10	3	311	904	34.4	311	525
11	3	380	1282	29.6	475	525
1	4	811	1322	61.3	1075	465
2	4	223	1134	19.7	223	465
3	4	419	2479	16.9	419	465
4	4	698	3203	21.8	698	465
5	4	868	1735	50.0	1183	465
6	4	1595	2767	57.6	2489	465
7	4	340	1503	22.6	1776	465
8	4	377	2808	13.4	2483	465
9	4	221	1359	16.3	223	465
10	4	223	1274	17.5	223	465
11	4	503	1482	33.9	928	465
1	5	596	1572	37.9	1405	510
2	5	988	2057	48.0	1090	510
3	5	1442	2585	55.8	1442	510
4	5	1450	1470	98.6	1450	510
5	5	1065	1882	56.6	1065	510
6	5	925	2183	42.4	1215	510
7	5	406	1895	21.4	1411	510
8	5	447	3062	14.6	2080	510
9	5	294	1484	19.8	301	510
10	5	350	1437	24.4	403	510
11	5	598	1746	34.2	1280	510
1	6	515	1138	45.3	1690	630
2	6	735	1201	61.2	1355	630
3	6	825	2457	33.6	1243	630
4	6	223	1497	14.9	223	630
5	6	568	1552	36.6	568	630
6	6	654	2124	30.8	654	630
7	6	630	2226	28.3	1093	630
8	6	460	3260	14.1	1625	630
9	6	389	1418	27.4	662	630
10	6	476	1361	35.0	851	630
11	6	539	1424	37.9	1523	630

Numerical experiments showed that in most cases use of even a wave record only from one sensor allows to restore the source (coefficients in the linear sum of UnSs) with the required accuracy, using only a part of a wave signal (less than a half of its full period). From the results presented in Table 1 it is visible that for each CS there are several sensors, processing of a wave signal from which allows to restore the source with the required accuracy even before arrival of a wave to the nearest coast. In particular, for CS1 those are detectors R1, R2, R9, R10 and R11. For CS2 those will be sensors R1, R2, R3, R9, R10 and R11. And so on.

4. Discussion

The fact that among such sensors there is always a tsunami detector which is included to observation system DONET (Figures 1 and 4) is important. In these sensors (R9-R11) the first phase of tsunami on the wave record is negative (surface inundation), and then the surface elevation is coming. Finally, we can conclude that with the help of observation network described the tsunami warning system is able to estimate expected wave heights along the coast before its arrival there.

By results of the numerical experiments given in table 1 one can notice that the length of NPWP for restoration of some CSs by records of some sensors exceed 80% of the full period of a wave. Though, in most cases duration NPWP does not exceed 50 percent of the tsunami period. In particular, more than 80 percent of the full wave period is required for sufficient-quality restoration of CS having number 1 by means of sensors R1 and R6. The CS3 by means of sensors R3 and R6. And, at last, CS5 on the basis of measurements by sensor R4. For the last case the length of NWDP reaches 98.6 percent of wavelength. From Figure 1 it is visible that in all these cases the sensor is located in the direction of a long axis of CS (a rectangle 200 x 100 km) or near it. It means that such relative positioning of the CS and the tsunami detector negatively affects speed and quality of restoration of coefficients in a linear combination of UnSs composing the source. CSs are most successfully restored using wave records taken from the detectors which are located in the direction of a short axis of the source.

5. Conclusion

The numerical method which was used for calculating the direct initial value problem on propagation of tsunami generated by a UnSs have been many times tested on exact solutions and on real tsunami data. So, correlation between initial surface displacement at the UnSs and synthetic marigrams in receivers seems to be reliable. According to the mathematical model the increase in height of Unit Source by N times causes the proportional growth of wave height in all grid-points of computational domain.

As a result of this research it is shown that at the reasonable relative location of the area of the possible tsunami sources and deep-water tsunami detectors for correct restoration of the composed source it is enough only a part of the recorded wave signal. At the same time, a part of a wave signal, necessary for restoration, can be used by the restoration algorithm even before arrival of a wave to the coast. It gives the chance for quick solution of a direct problem of the tsunami propagation from the initial water surface displacement to estimate the expected wave height along the entire coast. Besides the carried-out numerical

experiments will allow find optimal positions for installation of the new deep-ocean tsunami detectors capable to restore the composite tsunami sources more quickly.

Acknowledgment

The research was supported by the Russian Federal Targeted Program Grant 14.574.21.0145. Unique project ID - RFMEFI57417X0145.

References

- [1] D. Kuzakov, M. Lavrentiev, An. Marchuk, "Determination of Initial Sea Surface Displacement at Tsunami Source by a Part of Wave Profile" in Proc. OCEANS'18 MTS/IEEE Kobe, Japan, May 28-31, 2018.
- [2] V. Titov, "Numerical modeling of tsunami propagation by using variable grid" in Proc. IUGG/IOC International Tsunami Symposium, 46-51, 1989.
- [3] V. Titov, C. Synolakis, "Numerical modeling of tidal wave runup" J. Waterway, Port, Coastal and Ocean Engineering, **124**(4), 157-171, 1998.
- [4] J. Borrero, S. Cho, J. Moore, H. Richardson, C. Synolakis, "Could it happen here" Civil Engineering, **75**(4), 55-67, 2005.
- [5] N. Shuto, C. Goto, F. Imamura, "Numerical simulation as a means of warning for near field tsunamis" Coastal Engineering in Japan, **33**(2), 173-193, 1990.
- [6] A. Yalciner, B. Alpar, Y. Altinok, I. Ozbay, F. Imamura, "Tsunamis in the Sea of Marmara: Historical Documents for the Past, Models for Future" Marine Geology, **190**, 445-463, 2002.
- [7] E. Gica, M. Spillane, V. Titov, C. Chamberlin, J. Newman, "Development of the Forecast Propagation Database for NOAA's Short-Term Inundation Forecast for Tsunamis (SIFT)", NOAA Technical Memorandum, 2008. <http://www.ndbc.noaa.gov/dart.shtml>
- [8] A. Romanenko, P. Tatarintsev, "Algorithm for reconstruction of the initial surface disturbance at the tsunami epicenter", NSU J. of Information Technologies, **11**(1), 113-123, 2013.
- [9] M. Lavrentiev, D. Kuzakov, A. Romanenko, A. Vazhenin, "Determination of Initial Tsunami Wave Shape at Sea Surface", OCEANS 2017-Aberdeen, IEEE, 1-7, 2017.
- [10] M. Hyodo, T. Hori, K. Ando, T. Baba, "The possibility of deeper or shallower extent of the source area of Nankai Trough earthquakes based on the 1707 Hoei tsunami heights along the Pacific and Seto Inland Sea coasts, southwest Japan", Earth, Planets and Space, **66**(123), 2014. <http://www.earth-planet-space.com/content/66/1/123>.
- [11] D.R. Kincaid, E.W. Cheney, Numerical analysis: mathematics of scientific computing, **2**, American Mathematical Soc., 2002.

Multi Biometric Thermal Face Recognition Using FWT and LDA Feature Extraction Methods with RBM DBN and FFNN Classifier Algorithms

Evan Hurwitz, Chigozie Orji*

The University of Johannesburg, Department of Electrical and Electronic Engineering Science, Johannesburg, South Africa

ARTICLE INFO

Article history:

Received: 12 September, 2019

Accepted: 14 November, 2019

Online: 22 November, 2019

Keywords:

Thermal imaging

Soft-biometrics

an ensemble of classifiers

Fast Wavelet Transform

Linear Discriminant Analysis

Restricted Boltzmann Machines

Deep Belief Networks

Feed Forward Neural

Networks

Sensing

Imaging

Security

ABSTRACT

Person recognition using thermal imaging, multi-biometric traits, with groups of feature filters and classifiers, is the subject of this paper. These were used to tackle the problems of biometric systems, such as a change in illumination and spoof attacks. Using a combination of, hard and soft-biometric, attributes in thermal facial images. The hard-biometric trait, of the shape of a head, was combined with soft-biometric traits such as the face wearing glasses, face wearing a cap/headgear, face with facial hairs, plain face, female face, and male face. These were experimented with, using images from Carl's database and Terravic Facial Infrared Database, and used to train clusters of neural network algorithms for each biometric trait. These comprised Restricted Boltzmann Machines (RBM), Deep Belief Networks (DBN), and Feed Forward Neural Networks (FFNN). After feature extraction, using Fast Wavelet Transform (FWT), and Linear Discriminant Analysis (LDA). A classification error of 0.02887, 0.038695, 0.02381, 0.024629, 0.0268, 0.02369 and 0.03 was achieved for each biometric trait, respectively. Showing that they had each been learned, and could be used through a fusion method, to improve recognition. This was demonstrated using a test image, as the user, having four of the character traits (countenance, glasses, facial hair, and gender). Then attempting to recognize each trait, one after the other, using a cross-verification method. The algorithm was seen to return test values, close to those received during the training test, for each biometric trait.

1. Introduction

Thermal imaging is a preferable choice for facial biometrics because inconsistencies due to change in illumination are not present. The human body is luminous at frequencies, such as microwave, millimeter-wave and infrared. This makes it possible for thermal sensors to passively capture images of a consistent nature at these frequencies. Which are useful for biometric system applications such as person recognition [1]. Other frequencies, which are beyond Ultraviolet, are not suitable for such applications due to health-related issues such as genetic mutation and skin cancer, arising from their prolonged exposure [2]. Figure 1 shows these frequency bands, highlighting the millimeter-wave band and that of visible light [3].

1.1. Person recognition

Person recognition has been an ever-growing work area, in visual sensor based biometrics. A field within which scientists and

engineers are continually improving existing algorithms and developing new ones. These are useful in systems which detect, recognize and differentiate one type of person from the other. The following applications use biometrics with computer vision:

- Personal entertainment and assistance - Comprising video games, virtual reality, human-computer interaction, avatars, and robotics applications.
- Public enrolment and security - Some of which are driver's license, passport, voting, registration and enlistment programs. Along with welfare, identity document, passport, and voter forgery identification systems.
- Device access and authentication - Consisting of TV child proof locks, desktop access, personal device sign-in (mobile device and tablets), network and database authentication. Also, internet access, online record and portal access (medical and law enforcement) with removable storage device access.

* Chigozie Orji & Email: chris.sardius@gmail.com

- Remote monitoring and surveillance - Such as advanced video surveillance and CCTV Control in airports (drug trafficking), malls and departmental stores (shoplifting). Also conference centers, cinemas, private premises, office buildings, and convenient stores.

This paper is an extension of the research work done by Evan, Ali and Chigozie [4]. It focuses on the appraisal of biometric system security and the proposal of a protection method, using thermal imaging and multi-biometric [5] traits to harden a biometric system through fusion [6]. Galbally, Marcel and Fierrez [7] discussed ways of fooling a biometric system into, passing an improper user as a legitimate one. By presenting a counterfeit crafted version of the genuine biometric trait to the sensor. Such as, 2D face spoofing using fake fingerprints, irises, photos, videos. Also 3D face spoofing using masks made of paper, plastic or silicone. Such spoofing methods, have been used to, compromise secure systems and reduce the confidence people have in biometrics. According to Hong, Jain and Pankanti [8] the integration of additional pieces of evidence, makes a biometric system more reliable and, increases verification accuracy. Various approaches are possible, such as the integration of semblance and fingerprint, semblance and iris, and appearance and voice. For this research, additional evidence was created, using thermal images of *soft biometric* attributes, along with the *hard biometrics* of the human face. A technique which doesn't require, the use of, multiple sensor input devices to increase robustness.

The weaknesses that can exist in a recognition system arise from a hacker's awareness of the biometric information required for user authentication and his ability to falsify them. The use of hidden, authentication, evidence improves a system's robustness and hardens it against such attacks. All possible combinations, of biometric attributes, have not been exhausted. That is why the work in this research is focused on, multi-biometric person recognition, using soft and *hard biometric* traits in thermal facial images. Using a matching score and fusion approach, to combine biometric evidence and altogether boost security.

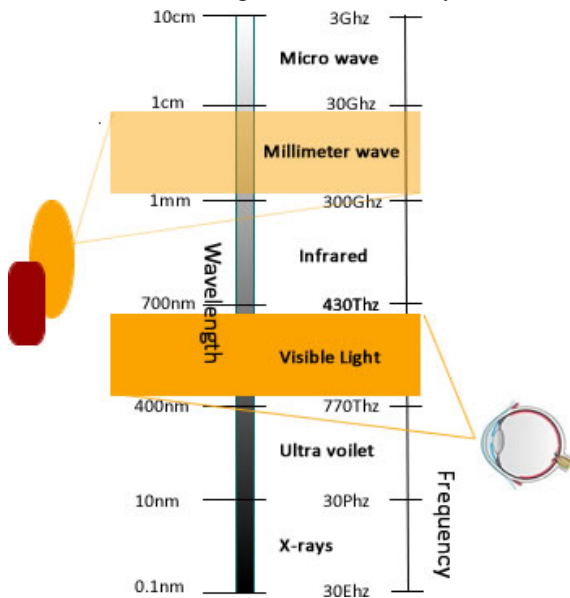


Figure 1: Imaging beyond the visible spectrum, showing the optical eye, using visible light frequencies, and thermal sensor device, using millimeter-wave frequencies

1.2. Data sets

The availability of datasets helped to further motivate the research initiative. These comprised images of different types of people captured under diverse conditions such as poses, lighting, dressing, and makeup. From these samples, for training and testing the anti-spoof algorithm to achieve reduced vulnerability, were derived. The Object Tracking and Classification Beyond the Visible Spectrum (OTCBVS) benchmark dataset collection [9], and Carl's databases [10], have provided a dataset of images, captured under diverse conditions, using thermal imaging. Which can help research work in the area of person recognition. The facial category, within the OTCBVS benchmark dataset collection: Terravic Facial IR Database, provides thermal facial images with good variability. These comprise real-life shots having diverse behavioral characteristics. While Carl's database consists of real-life facial images, captured simultaneously, using visible and invisible frequencies. They have gender variation and good behavioral attributes. Both datasets, comprise ideal thermal facial human categories and, are suitable for measuring the working of a multi-biometric person recognition system.

2. Literature Review

Biometrics is the science of knowing a person's identity, using their physical or behavioral qualities, such as the semblance, fingerprints, voice, and iris [11]. The idea, that spurred biometrics as a science, was introduced within the field of law enforcement. When Alphonse Bertillon, police head of the criminal identification department in Paris, introduced a new way to identify criminals. Using using body measurements such as eye color, skin, hair, beard, fingers, shape, and size of the head, [12].

A classical biometric system can verify identity by:

- Capturing biometric information such as images, fingerprint and voice samples from people.
- Extract features from the information.
- Match the feature set against feature patterns in the database.
- Conclude an identity verification.

Aside from verification, information collected by a biometric algorithm can be used to ascertain additional peculiarities of the persons concerned. Traits such as hair, gender, gait, age, clothing, ethnicity, and body weight can be captured [13]. This additional data can help in bettering recognition verity in a biometric algorithm [14].

Biometrics also saw application in the field of legal work such as criminal identification and illegal migrant monitoring. It is also useful for security clearances among employees in sensitive occupations, forensics, the identification of prisoners among suspects and ex-convicts. In today's world the private sector, comprising of civilians, is beginning to add biometrics to alphanumeric methods, for person recognition [15].

2.1. Biometrics systems

A biometric system can be used for recognizing persons using the recognition of patterns in a feature vector. These can be derived from a particular corporal or behavioral attribute that the individual

possesses. Depending on the type of application a biometric system works either in *verification* or *identification mode* [16].

2.2. Biometric system errors

Multiple samples of similar biometric attribute, retrieved from one individual, are not always alike. Such as two exposures of a person's face, two prints of a person's left index finger and two voice samples from the same person. Effects such as changes in the user's physiology, caused by wounds, cuts, unusual dressing, moods, ambient lighting, weather, and age, can cause errors in a biometric system. The user's way of interacting with the sensor can have the same effect. As a result a matching score, in numerical terms, is used to describe the similitude between the input (captured biometric trait) and database template. Such that, the higher the score the more convinced the system is that, the two biometric data come from the same user. The system's decision is regulated by a threshold "s", for the matching score, such that the higher the "s" the more secure the system. A biometric verification system can make, two kinds of errors, a *false accept* (false match) or a false reject (false nonmatch) [17]

2.3. Hard and Soft biometrics

A person's image, normally, comprises both hard and *soft-biometric* characteristics [18]. Some hard-biometric characteristics are countenance, the shape of the head and gait. While *soft-biometric* characteristics are features such as glasses, hair, hat, clothes, gender and other occlusions that an individual may have on.

2.3.1. Hard-biometrics

Memory-based authentication methods, such as usernames and passwords, can easily be compromised if written down in plain text and such text files are copied. Such authentication systems can be hardened by capturing and verifying a *hard biometric* trait along with the alphanumeric information. *Hard biometric* methods are more dependable than alphanumeric authentication schemes. They also have several advantages that alphanumeric methods do not grant. *Hard biometric* authentication involves the establishment of a person's identity with, the use of physical characteristics. These are traits such as the face, iris, fingerprint, hand geometry, gait, voice, etc. Unlike alphanumeric tokens, *Hard biometric* traits cannot be copied, shared or distributed, they can also neither be lost or forgotten. *Hard biometrics* always requires that the person, being validated, be present at the time and place where access is being requested. *Hard biometric* traits are arduous to forge and a lot of money, time, access and experience, would be needed to forge them. For application-specific use each hard biometric trait has its advantages and disadvantages. The type of use, however, derives from the application requiring it. ATMs would use facial biometric traits, video surveillance: gait, while telebanking and telemarketing would use voice.

2.3.2. Soft-biometrics

Semantics, in the context of person recognition, are characteristics which people often use in describing those they meet but don't know personally. Such as stature, gender, skin color, hair color, body weight, age, race, facial features, mode of dressing and mannerisms [19]. Using such semantic data, with features from a biometric dataset, to further enhance the working of a

person recognition algorithm, is called "*soft-biometrics*". It bears with it all the advantages of the hard-biometric authentication schemes, over alphanumeric methods, and can be used to further harden hard-biometric methods against spoofing. Reid and Nixon [14] attribute this to the use of labels and measurements, which take the appearance of mere human depictions, that people can easily grasp. Samangoeei, Guo, Mark, and Nixon [20] define these as semantic annotations. Dantcheva, Velardo, D'Angelo and Dugelay [21] present a novel definition for soft-biometrics based on additional biometric traits. Some of which are: color of clothes, material accessories, body weight, physical and behavioral traits. Jain, Dass, and Nandakumar [22] describe soft-biometrics as being able to provide information about an individual but without the ability to create a full distinction between that individual and others [23].

3. Related Work

Taking a lead from a paper on thermal facial recognition [24] and other works which use *soft biometrics* to augment hard biometric methods [25], [14]. A contemporary approach, to person recognition, using thermal imaging is being proposed. With a focus on facial data, *hard* and *soft biometric* attributes [4]. Most person recognition systems, depending on the operating environment and scenario, have to choose sensor type. Also, based on the sensing setup and output, have to choose a prediction approach. Irrespective of these, the following steps are common to most systems:

- Detection.
- Feature extraction.
- Semantic analysis.
- Feature matching.
- Recognition result.

Most systems begin with detecting a biometric aspect required for recognition such as head, gait, face, finger, and iris. Then separating it from the rest of the image. This step, which is the detection (data acquisition and pre-processing) step, is an integral part of the sensor device setup. It requires a lot of accuracy and is not always discussed. As the performance of the subsequent steps and the system as a whole, depend on it. As a result of the technicalities involved in the first step, the focus of this research project would begin with the second step. Which is about feature extraction. This chapter attempts to present an overview, of the work that has been done in the field of person recognition over the past few years, focusing on the techniques and algorithms used.

3.1. Person Recognition Methods

Experiments were done by, Bhattacharjee, Seal, Ganguly, Nasipuri, and Basu, with the Terravic Facial IR Database. Using Haar wavelet transform and Local Binary Pattern (LBP) [24]. Martinez, Binefa, and Pantic propose recognition, in thermal images, using the detection of the eyes, nostrils and mouth. Also the subsequent decomposition into a feature vector with Haar wavelets, and classification using SVM and Gentle boost [26]. Herrmann, Müller, Willersinn, and Beyerer achieved an error rate reduction, of up to 80% on Long Wave Infrared (LWIR) images, using the AMROS and OTCBVS benchmark datasets. The achieved detection, using Maximally Stable Extremal Regions

(MSER), and classification with a Convolutional Neural Network (CNN) [27]. For deep learning Krizhevsky, Sutskever, and Hinton used non-saturating neurons and a GPU implementation of CNN to classify 1.2 million high-resolution images [28].

Shangfei et al. worked on a Natural Visible and thermal Infrared facial Expression database (NVIE). Using expression recognition and emotion inference for 100 subjects with and without glasses. They analyzed with Principle Component Analysis (PCA), Linear Discriminant Analysis (LDA), and the Active Appearance Model (AAM) [29]. Kelly, Stefanie, and Tom did a study on, alternate access methods using, infrared sensing, electromyography, oculography, and computer vision for individuals with severe motor impairments [30]. Bhowmik et al. researched the advantages, of thermal face over visible face, for recognition, using IRIS and the Terravic Facial IR Database. They isolated the various IR spectrums, showing the Long Wave Infrared (LWIR) band, as that with the highest emissions and suitability for face recognition. They compared this to Short Wave Infrared (SWIR) and Medium Wavelength Infrared (MWIR) [31]. Ayan, Suranjan, Debotosh, Mita and Dipak Kumar proposed the use of Thermal Minutiae Points (TMP), using blood perfusion data as a feature, for thermal face recognition. They experimented with PCA, LDA, and Equinox, for feature extraction and a multi-layer perceptron back propagation feed-forward neural network for feature classification and recognition of thermal infrared face images [32]. Siu-Yeung, Lingyu, and Wen proposed, using the Modified Hausdorff Distance, to measure the similarity between two feature vectors of thermal faces [33]. Ognjen, Riad and Roberto worked on, improving recognition in visible and, thermal images through the detection of prescription glasses [34].

3.1.1. Background subtraction

This person detection method assumes an image to be part of a continuous stream of pictures and attempts to predict the type of background using the frame sequence in the time domain. A comprehensive overview of the method has been done by Piccardi [35]. The method, however, has a problem with, shadow effects, sudden changes in illumination, occlusions and, scenes within which a person remains static for a long time. These problems can be ameliorated by, equipping cameras with, ground analysis capability [36], thermal imaging and stereo capabilities [37].

Here is a list of background subtraction methods:

- Running Gaussian average
- Temporal median filter
- Mixture of Gaussians
- Kernel density estimation (KDE)
- Sequential KD approximation
- Co-occurrence of image variations
- Eigen backgrounds

3.1.2. Silhouette

This method involves creating the silhouette of an image through binarization [25], using its edges and contours, and matching it with prior models in the persons' database [38]. This

method works well for detecting people, using facial images showing countenance, not wearing occlusions or having unique behavioral attributes [39]. The detection of partially occluded persons, was tackled by Wu and Nevatia, by breaking down the image into segments they called edgelets. Then the learning of the features, of each segment, by an AdaBoost algorithm. Then compiling prediction results, made for each segment, to ascertain overall detection accuracy [40].

3.1.3. Appearance, look and feel

This method models the image, based on its appearance and attempts to extract features from it, using the look and feel of the many surfaces that make it up. The features are used to train a classifier algorithm, which learns its various attributes and is able, to make predictions on new images based on the feature set. The method can be used, based on the whole image or, by using bits of the image and summing up the learned features.

3.2. The Whole Image Approach

A novel way of achieving this is, by using wavelets, to analyze the whole image, at a pixel level and computing the difference between the different areas. Some known wavelet transform methods are Continuous Wavelet Transform (CWT), Gabor Wavelet Transform (GWT), Discrete Wavelet Transform (DWT), Haar's Wavelet Transform (HWT) and Fast Wavelet Transform (FWT) [41]. The first known one was DWT invented by, a Hungarian mathematician, Alfréd Haar in 1909.

Fourier transform is also useful for this type of analysis. Its weakness is that it doesn't account for the spatial information only the frequency aspects. These approaches are good for, extracting features from, thermal facial images. Bhattacharjee, Seal, Ganguly, Nasipuri, and Basu used the HWT method, with a Local Binary Patterns (LBP) classifier, to process cropped thermal faces. Divided into frequency bands LL1, LH1, HL1, HH1, where LL1 corresponds to, the lowest frequency band and HH1, the highest frequency band [25]. Figure 5 shows a sketch map, of the wavelet bands from a thermal face, after quadratic wavelet decomposition.

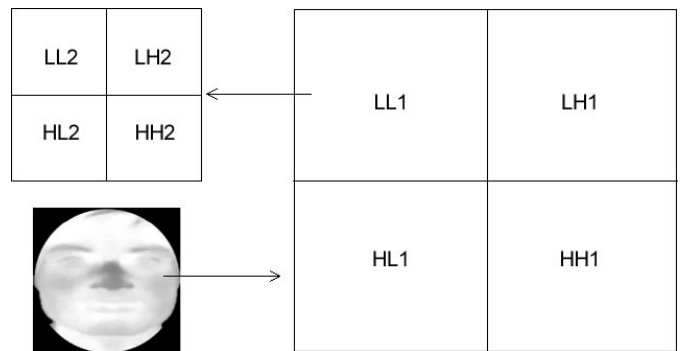


Figure 2: Sketch map of wavelet bands, after quadratic wavelet decomposition of a thermal facial image, showing low and high-frequency areas and sub-bands within the LL1 band [25].

Jones, Viola, and Snow used the wavelet technique, with motion and appearance information, to detect walking people, for outdoor surveillance. After which they classified, them, using a cascaded AdaBoost classifier [42]. For detecting walking people,

Zhu, Yeh, Cheng, and Avidan used the Histogram of Oriented Gradients (HOGs) technique. They applied a cascade of rejectors approach using a weak AdaBoost classifier. Using their method, they were able to reduce computation time [43].

3.3. The Part Image Approach

This approach processes images, by detecting their aspects for person recognition, and decides by combining the various classifications. For full-body images the head, hands, legs, and torso, are detected separately, processed, and classified. Mohan, Papageorgiou, and Poggio worked on detecting people, in cluttered scenes, using an Adaptive Combination of Classifiers (ACC). The method first uses a four-part, detector, separately trained, to detect four segments of the human body, namely: head, legs, right arm, and left arm. After the body parts have been detected, a subsequent classifier is used to classify the results of the four patterns, as a person or nonperson [44].

Wu and Nevatia worked on detecting, partially occluded, humans within video streams. They used part detectors, and weak classifiers, based on features they called edgelets [45]. Their method involved using face, eyes, nose, ears, and mouth separately, before processing and classifying. Trujillo, Olague, Hammoud, and Hernandez experimented with the IRIS data-set. They combined facial feature localization, with the holistic approach using clustering, Eigenface feature extraction and SVM for classification [46].

Martinez, Binefa, and Pantic focused on detecting, facial components (eyes, nostrils, and mouth) in thermal images, using Haar features with GentleBoost algorithm [47]. Al-Khalidi, Saatchi, Burke, and Elphick developed an approach, for tracking a Region of Interest (ROI) on the human face, using thermal video images. The ROI: tip of the nose was tracked using warm and cold facial points of the human face [48].

3.4. History of biometric recognition

Ever since the beginning people have used bodily attributes such as voice, hair, face, and gait, to recognize one another. The idea, that spurred biometrics as a science, was introduced within the field of law enforcement. Its inception was towards the end of the 19th century. When Alphonse Bertillon, police head of the criminal identification department in Paris, introduced the idea of using body measurements, such as skin, eye color, hair, beard, fingers, size, and shape of the head, to identify criminals [11]. This was followed by, a second finding within the same field of law enforcement. The discovery of how human fingerprints are distinct from each other. After which many law-enforcement bureaus began the practice of booking offenders by fingerprinting. The fingerprint data was stored in card files which were replaced by databases. In the hands of law enforcement this method was further improved for determining criminal identities. By using the ability to match fingerprint fragments, from crime scenes, with those in the criminal's database. Beyond law-enforcement biometrics also saw initial application in legal work. Such as in criminal identification, illegal migrant identification, security clearances among employees in sensitive occupations and forensics. Also the identification of ex-convicts, prisoners among suspects, paternal and maternal determinations and much more. In

today's world, the private sector, comprising civilians is beginning to include biometrics to alphanumeric methods for person recognition [49].

3.4.2. Verification mode

In *verification mode* a biometric scheme confirms an individual's identity, by comparing the received biometric characteristic, with the owner's biometric template captured in its database. Such systems work by using the assertion of one who is seeking access to perform a one to one comparison and return a true or false. This is done using a Personal Identification Number (PIN) code, an alphanumeric code, a bar code, a login name or smart card.

3.4.3. Identification mode

In *identification mode* the scheme recognizes, a person's identity, by searching the template database for a match. This is done with received biometric characteristic after comparing the input to many records in the database. The check either passes, when a match is found, or declines if the person is not enrolled in the system's database. The *Identification mode* is also used for negative recognition. This entails the system determining that a person is who he or she denies being. This is useful in a situation that a person attempts to use multiple or stolen identities. Negative recognition can however only be used with biometrics. Passwords, keys, tokens, and PINs, can only serve for positive recognition.

3.4.4. A false accept

A *false accept*, also known as a false match, is the confusion of biometric samples from two different users to be, from one person. For a biometric scheme it is represented numerically as the *False Match Rate (FMR)*.

3.4.5. A false reject

A *false reject*, also construed as a *false nonmatch*, is the mistaking of two biometric samples from the same user to be from two different individuals. For a system it is represented numerically as the *False Non-Match Rate (FNMR)*. Besides recognition error rates: *FMR* and *FNMR*, other parameters which help to sum up a biometric system's performance are the *Failure to Capture (FTC)* and *Failure to Enroll (FTE)* rates [50].

3.4.6. The Failure to Capture rate

FTC rate is the number of times, in percentage, the biometric device is unable to capture a sample when users present their biometric attribute.

3.4.7. The Failure to Enroll rate

FTE rate is the number of occasions, in percentage, users are unable to enlist in the recognition scheme. This could be because of a network issue, a system issue or an issue with the sensor, during biometric characteristic capturing.

3.5. Hard-biometrics

A person's image, normally, comprises both *hard* and *soft* biometric characteristics. The hard-biometric characteristics are -

face, iris, and gait. The *soft biometric* characteristics are - gender, hair, hat, clothes with other occlusions that the individual may have on [51].

3.5.1. Face

This is a commonly used and nonintrusive biometric trait. Its application ranges from authentication in a static fixed background, to one in a dynamic and changing environment. A method used in face recognition involves; 1) the identification of Regions of Interest (ROI) such as, eyes, eyebrows, nose, lips, and chin and the analysis of their spatial relationship; 2) another is total analysis, of all images that constitute a face, using a weighted aggregate of several model faces, to develop face space and the location of new images within face space. The challenge, with face recognition, is the capturing process.

A fixed and simple background, with known illumination type, is often assumed. However, it is not always the case. A *Facial Recognition System (FRS)* should be able to automatically; 1) Detect the presence of a face within captured images; 2) Locate the face; 3) Recognize the face [52]. The use of a thermal sensor, good feature extraction methods, with deep learning algorithms, would surmount the challenges and increase the capabilities of the system.

3.5.2. Iris

The Iris is the portion of the eye between the pupil and the white of the eye (sclera). Its complex patterns, carry distinct information per individual and, are useful for person recognition. The irises of all persons, even of identical twins, are expected to differ. Iris systems have low *False Accept Rate (FAR)* however their *False Reject Rate (FRR)* can be high [53].

3.5.3. Fingerprint

Fingerprints have been used, for decades, for personal identification. It dates back, to the origin of biometrics, as one of the first methods used for enrolling and documenting human beings. A fingerprint is peculiar for every person. It comprises a unique arrangement of ridges and valleys on the finger surface. For large scale identification, covering millions, an enrolment system comprising multiple fingerprints (all five fingers), from each person, would be more robust than one based on single fingers. However genetic factors, with aging and job-related issues (e.g., motor mechanics, farmers, bricklayers, and manual laborers), affect the general use of fingerprint for automatic identification.

3.5.4. Hand geometry

This recognition approach is based on dimensions of the human palm its length, width, shape, and size. Hand geometry is not affected by manual labor, work factors, or environmental factors, such as heat or humidity. It is however not very distinctive, and in a large population, more than one person could have the same hand geometry. Also factors such as physical impairment, lack of motor function, paralysis and arthritis, affect the universal use of hand geometry for automatic authentication.

3.5.5. Gait

Gait biometrics, is an appearance-based authentication method, which works well with video sequences. The ubiquity of video cameras has made this type of recognition popular. Gait biometrics, is quite distinctive and, can serve for automatic recognition among persons in a large population. It is very useful for recognition over distances, and under poor resolution conditions, but is affected by factors such as fast-changing backgrounds, occlusions, costumes and differences in lighting.

3.5.6. Voice

Voice recognition comprises both hard and soft biometrics. The *hard biometrics* being aspects such as, the mouth, vocal cavity, vocal tracts and lips. While the *soft biometrics* consist of emotional states such as age, health conditions, etc. Voice is not very distinguishing, and would not be useful for automatic recognition, among persons in a large population. A voice recognition scheme may be text-independent or text-dependent. The text-independent types, being more arduous to design than text-dependent ones and, offering better security. Voice is also affected by environmental influence such as noise and echo.

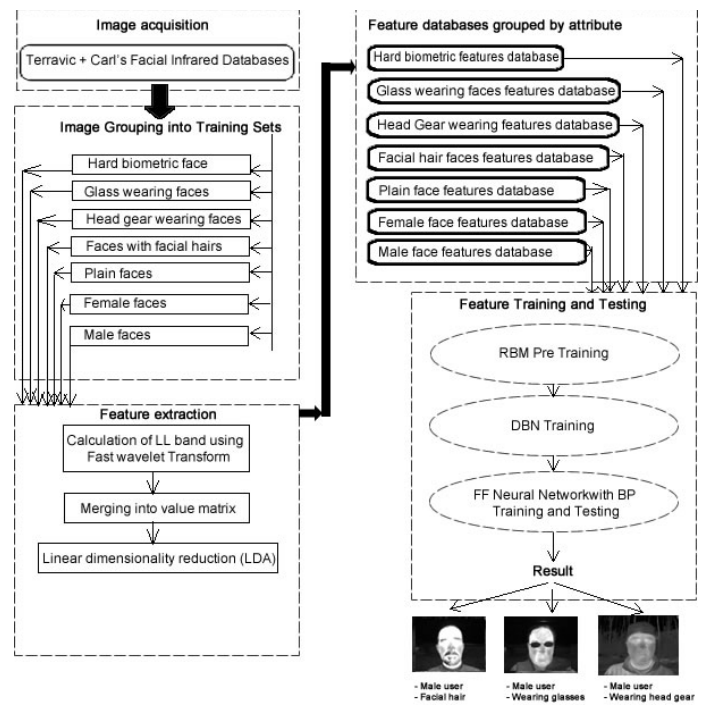


Figure 3: The proposed system, for multi-biometric thermal face recognition, using FWT image compression approach, LDA feature extractor, and RBM, DBN with FFNN classifiers.

3.6. Hybrid systems

These systems merge *soft biometric* data, with *hard biometric* information, to increase overall accuracy. Described by Jain, Dass, and Nandakumar, it suggests the complementing of primary biometric information gathered from fingerprint and face with *soft biometric* data, to achieve resistance to circumvention acceptability, collectability, permanence, universality and distinctiveness [54]. Scheirer, Kumar, Ricanek, Belhumeur and

Boult referred to this as, improving match scores from, face recognition attempts resulting from incomplete measurements done at match time. By using Bayesian Attributes Networks to combine descriptive attributes, such as *soft biometrics*, with primary biometric observations [55]. Also the use of multi-biometrics, comprising soft and hard biometrics, in a recognition system helps in hardening it against unwanted error rates and spoof attacks (such as fraudsters attempting to forge an identity). It also helps, in the case of insufficient population coverage, where little is known about most candidates monitored, using a recognition system [56].

4. The Proposed Method

The method was researched using thermal facial replicas from the Terravic Facial Infrared Database [9] and Carl's database [10]. These were processed using the Large Time-Frequency Analysis Toolbox (LTFAT) in Octave [57] for FWT and Byte fish face recognition toolbox [58] was used for facial image set importation tools. Rasmus Berg Palm's deep learning toolbox [59], was used for, Restricted Boltzmann Machines (RBM), Deep Belief Network (DBN) and Feed Forward Neural Network (FFNN) algorithms. Figure 3 shows a schematic of the proposed system's structure.

4.1. The Terravic Infrared Database

This is one of the two openly usable thermal face image databases. The other is IRIS (Imaging, Robotics and Intelligent System) Thermal/Visible Face Database. It is a subset of the OTCBVS benchmark and is good for experiments in the area of computer vision algorithms. Along with *hard* and *soft biometric* detection using thermal images. The data set comprises thermal sequences of 20 different people, each sequence having variations such as, right, left, front, outdoor, indoor, hat and glasses. All captured, with a Thermal-Eye 2000AS Raytheon L-3 sensor, with a focus on facial analysis for thermal imagery. The images have an 8-bit grayscale with, JPEG format, each one being 320 x 240 pixel in size [8]. Four independent training sets, having *soft biometric* attributes, were established from the dataset. Case study images from each one are presented in Figure 4, Figure 5, Figure 6 and Figure 7.

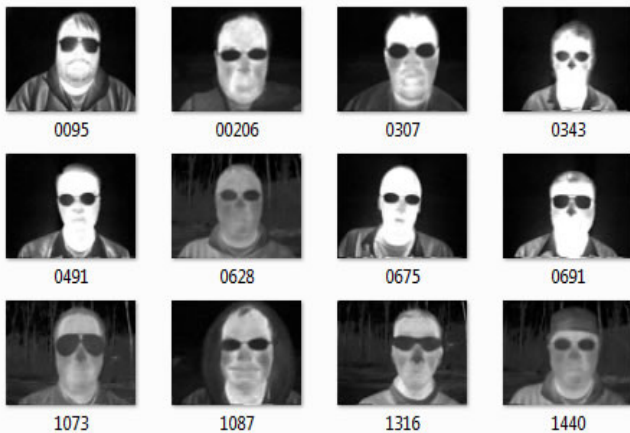


Figure 4: Case study images having glasses-wearing characteristic, from the Terravic Facial Infrared Database.

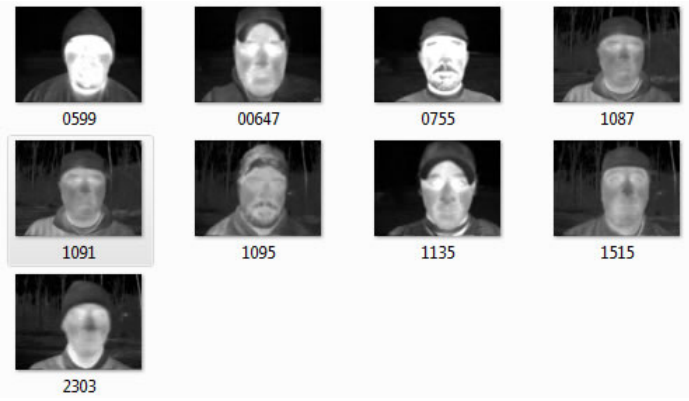


Figure 5: Case study images having headgear characteristic, from the Terravic Facial Infrared Database.

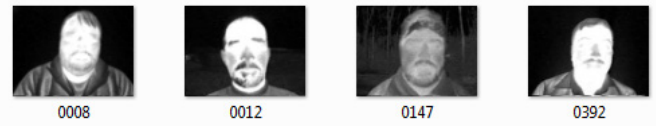


Figure 6: Case study images having facial hair characteristic, from the Terravic Facial Infrared Database.

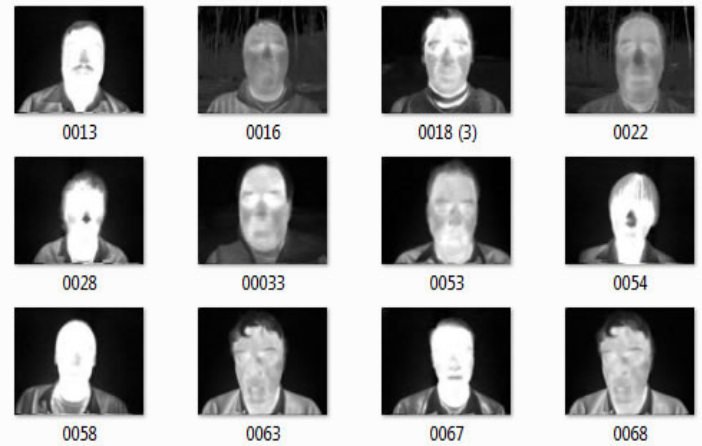


Figure 7: Case study images having plain face characteristic, from the Terravic Facial Infrared Database.

4.2. Fast Wavelet Transform (FWT)

Thermal images, which are a mixture of mixed and relevant detail, can be filtered using a wavelet transform technique. This breaks down the image into regions of high and low-frequency comprising frequency and spatial components, through a compression technique. Graphically these can be represented as sub-bands. Some common wavelet transform approaches are Fast Wavelet Transform, Discrete Wavelet Transform, Gabor Wavelet Transform and Continuous Wavelet Transform [60]. Fast Wavelet Transform (FWT) was used with Octave, in the experiments, because of its application to thermal facial imaging [61]. FWT is a constituent of the Large Time-Frequency Analysis Toolbox (LTFAT) [62].

4.3. Linear Discriminant Analysis (LDA)

LDA accomplishes the derivation of points of highest variance, from images in feature space. It does this by making sure the

within-class distance (S_w) is less, for images in the same class and between class distance (S_b) more, for images in separate classes. It advances the Principal Component Analysis (PCA) [63] method, through the way it derives the covariance matrices, applying linear discriminants [64].

$$AV = \lambda V \tag{1}$$

Where $A = Covariance$ matrix, $V = Eigen$ vector matrix,

$\lambda = Diagonal$ matrix of analogous Eigen values.

$$S_b V = \lambda S_w V \tag{2}$$

Where, $V = The$ eigenvector matrix, $\lambda = Eigen$ values.

4.4. Restricted Boltzmann Machines

Deep-belief networks are constituted using simple dual-layer neural networks called RBMs. Their layer design comprises both visible and hidden layers. Having same layer nodes restricted from communicating and different layer nodes allowed to communicate. Each node being a standalone center for data processing. Accepting its input and randomly choosing whether to transmit that input or not. Some applications of the RBM algorithm being regression, feature learning, classification, dimensionality reduction, topic modeling and collaborative filtering [65].

$$f((x * w) + b) = a \tag{3}$$

Where, $x = Input$, $w = Weights$, $b = Bias$, $f = Activation$ function, $a = Output$.

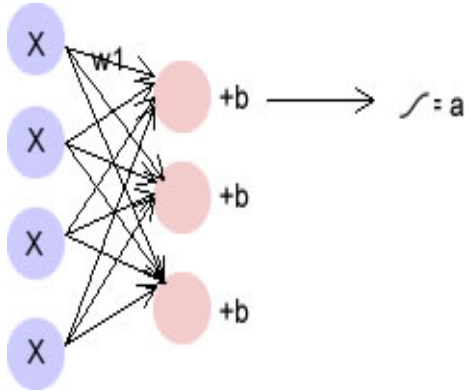


Figure 8: RBM network depicting inputs x , weight $w1$ for a connected node, bias for hidden layer and outputted activation function.

4.5. Deep Belief Networks (DBN)

When two RBM layers constitute a network, with many hidden layers, they become a Deep Belief Network (DBN). With this structure DBNs are able to learn highly structured data, such as thermal images. The irregular layer design of the RBM, makes its input to propagate through *Contrastive Divergence*, such that good classification is achieved irrespective of network depth. Using an unsupervised algorithm, the RBM is first pre-trained. After which the error received at the output, is sent to the input through

backpropagation. After which supervised learning begins, by adjusting the weights on the successive forward pass [66]. The expected outcome is to reconstruct a target vector, using a speculative approach, with as little inaccuracy as possible. This is done, after several forward and back passes. Tools from Rasmus Berg Palm's deep learning toolbox, for RBM and DBN, have been used [59]. The Deep Belief Net design comprises an RBM having 100 hidden layers and a DBN consisting of 100 by 100 RBM units. The RBM algorithm weights were used to commence the Deep Belief Network after pre-training with 10 epochs of 100 batches each. Using different start-up seeds, the DBN algorithm was trained many times, for each concourse. Running 100 batches per epoch, the DBN algorithm completed 10 epochs, for each *soft-biometric* class. After which the number of iterations was plotted against the average reconstruction error. An error of 0.026% was achieved for plain faces, 6.05% for glass faces, 0.026% for head gear faces, and 0.026% for facial hair faces. A feed-forward neural network classifier was initialized using the final DBN weights. Here is the DBN architecture.

Table 1: Deep Belief Network Architecture

Feature	Description
Activation function	Sigmoid
Input Layer	1
Output Layer	1
Momentum	0
Alpha	1
Batch scope	10
Epochs	100
RBM start-up weight	100 by 784 zero matrix
RBM unit scope	100 layers
DBN start-up weights	100 by 784 zero matrix
DBN scope	100 by 100 RBM units

4.6. Feed Forward Neural Network

A FFNN has been applied, as the secondary classifier, for the algorithm. After target vector reconstruction, the DBN, was spread out into a FFNN. This was trained by applying 10 epochs of 100 batches respectively and used to classify sample images from the *soft-biometric* groups.

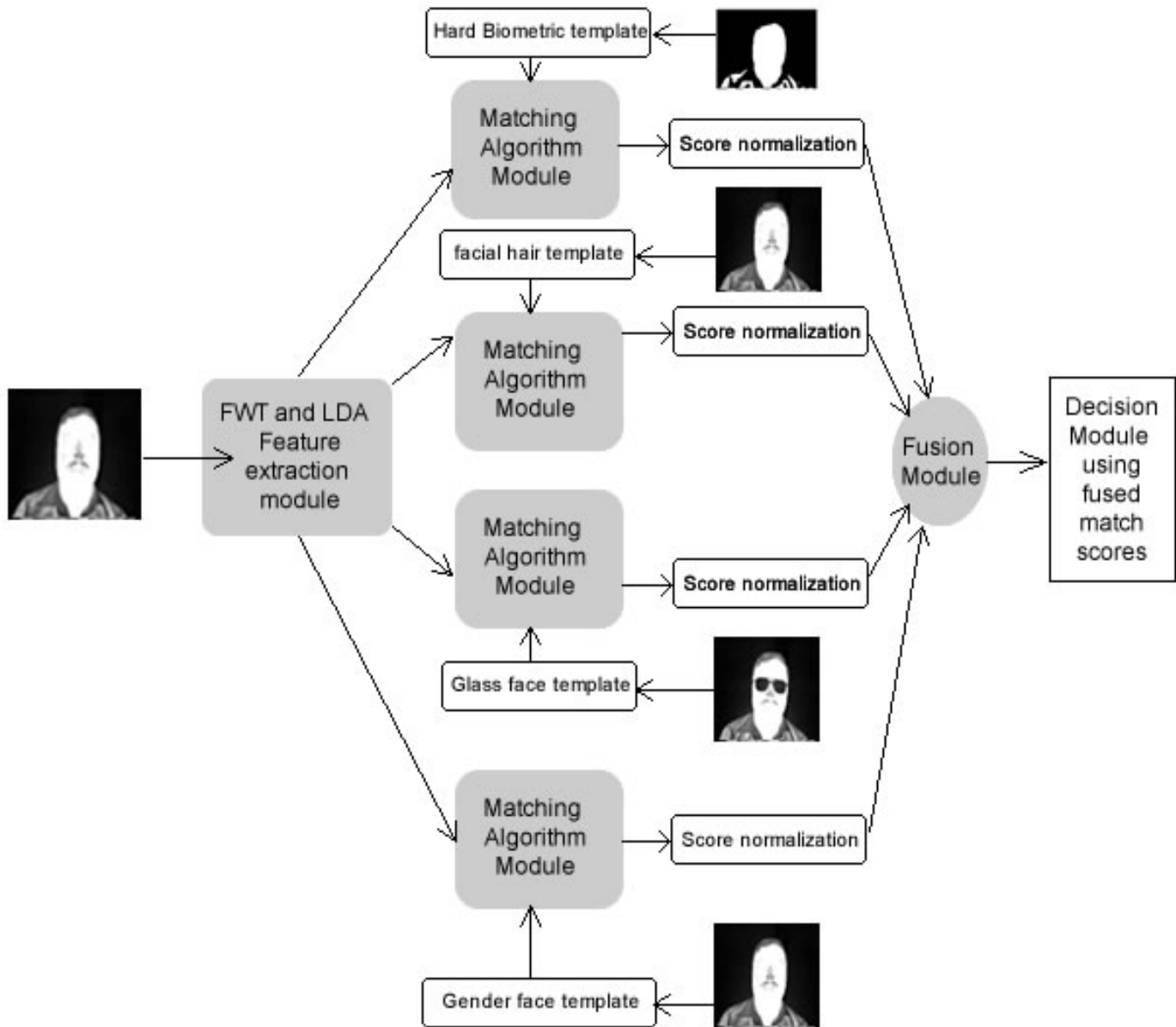


Figure 9: Proposed multi-biometric person recognition system, with single sensor thermal imaging, using a *parallel mode* of operation, with the score fusion approach, for soft and *hard biometric* traits; images from the Terravic Facial Infrared Database.

4.7. Training data acquisition

To design the biometric system, sample images were acquired using public and private thermal facial datasets, namely: the Terravic Facial Infrared Database [9] and Carl's database [10]. The former was used in learning soft and hard-biometric attributes, while the latter for gender attributes, of female and male.

4.8. Image pre-processing and feature extraction

The behavioral and physical attributes of persons, under low lighting conditions can be ascertained, using thermal imaging. Behavioral (outward) attributes such as cap, glasses, hat and facial hair with physical attributes such as head shape and size can be used to classify persons and afterwards recognize them. For thermal imaging a sturdy feature extraction method is requisite. Firstly, Fast Wavelet Transform (FWT), for filtering the noise

from the thermal images and secondly, Linear Discriminant Analysis (LDA), for extracting their principal components.

4.9. The multi-biometric recognition method

Using images from the Terravic Facial Infrared Database, the hard-biometric trait (shape of a head) along with *soft-biometric* traits (glasses, a cap, a mustache, beard or gender) will be detected from a single image. Using a single thermal sensor with matching algorithms trained to recognize each feature. After which the outcome of each match would be, fused and, used to make the final decision. This is illustrated in Figure 9.

4.9.1. Multi-biometric recognition modes

To implement multi-biometrics a system can function using any of these three diverse modes of operation, namely: 1) The

serial mode; 2) The parallel mode and; 3) The hierarchical mode [64].

4.9.1.1. The serial mode

Operating in the serial mode, the recognition result gathered from verifying the first trait, is used to reduce the scope of possible matches. The same is done, with subsequent traits, until a final trait is used, to complete the matching process.

4.9.1.2. Parallel

Operating in the parallel mode, recognition time is reduced by verifying all the traits concurrently, then using a fusion approach, to sum the matching scores from each search. After which, the result is measured against a threshold score “s” before, a final decision is made.

4.9.1.3. Hierarchical

In the hierarchical mode of operation, results from respective classifiers, for each biometric evidence, are combined using a staggered, trait by trait, approach with the decision made after a final fusion stage.

4.9.2. Types of multi-biometric fusion

In a multi-biometric recognition system’s evidence can be combined, before or after the matching process, using different schemes, some of which are: 1) A sensor level scheme; 2) A feature level scheme; 3) A match score level scheme and; 4) A decision level scheme [67]. Figure 9 shows a schematic of the proposed multi-biometric system, comprising several matching algorithms and a fusion module before decision, using the fused match scores.

4.9.2.1. The sensor level fusion scheme

This applies to a multi-sensor system. It works with fusion at the unprocessed data level, using the inputs from each sensor. The received traits are combined to form a single trait, from which features are extracted. An example, for face biometrics, is a system that combine inputs from visible, near-Infrared and thermal spectrum sensors [10].

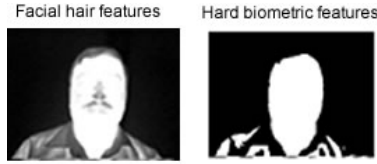


4.9.2.2. The feature level scheme

This method fuses processed features, from each biometric trait, into a final feature set with which the person is recognized. An example is the fusion of facial linear discriminants, from images of the shape of a user's head, with a soft-biometric trait such as gender [68]. To form a single feature set with which a user can be recognized.

4.9.2.3. The match level scheme

This method sums up, numerical, scores outputted from each classifier. The sum is used, to make the final decision, based on comparison to a threshold score s. An example is matching scores from verifying different soft-biometric traits such as, particular head shape, the presence of facial hair, glasses or male gender, as shown in Figure 9. Table 2 below illustrates the match level scheme with score fusion.

Table 2: Matching Algorithm With Score Fusion Method

Matching algorithm with the input image to the left	Score
 <p>Facial hair features Hard biometric features</p> <p>Test to confirm facial hair features belong to hard biometric user</p>	<p>Score 1, if the hard-biometric features in the input image belong to the authentic user (with facial hair).</p> <p>Score 0 if they do not.</p>
 <p>Facial hair features Glass face features</p> <p>Test to confirm facial hair features belong to glass face user</p>	<p>Score 1, if the glass wearing features in the input image belong to the authentic user (with facial hair).</p> <p>Score 0 if they do not.</p>
 <p>Facial hair features Male gender face features</p> <p>Test to confirm facial hair features belong to male gender user</p>	<p>Score 1 if the male gender features in the input image belong to the authentic user (with facial hair).</p> <p>Score 0 if they do not.</p>
Total score	3

4.9.2.4. The decision level scheme

This is a voting scheme in which each classifier makes its own decision after verifying the biometric trait presented to it. All the votes are presented at the output. A majority of positive votes indicate an identity as verified. While negative votes indicate an identity as unverified.

4.10. The approach

The single thermal imaging sensor approach, proposed here, will use the parallel mode of operation, as shown in Figure 9 with the matching classifier algorithms shown in Figure 3. It will

reduce biometric system errors, by working as a hybrid system in verification mode, using the whole image approach for face biometrics. By having each algorithmic cluster, verify a particular feature trait and, yield a matching score. Then use the *match level* scheme, to make its final decision, through score fusion, as shown in Table 2.

The matching algorithms will each comprise, Fast Wavelet Transform (FWT) and Linear Discriminant Analysis (LDA) for preprocessing, the removal of noise and retrieval of the spatial, time-frequency components. The isolation of the principal components of each image would be done using LDA. The pre-processed feature set will each be classified using, an ensemble of Restricted Boltzmann Machines (RBM) algorithms, Deep Belief Network (DBN) algorithms and Feed Forward Neural Network (FFNN) algorithms. For verifying, each feature trait, and yielding a matching score, for final decision making through *score fusion*.

5. Experiment One: Image Pre-processing and Feature Extraction.

These facial recognition experiments were conducted, for *hard* and *soft-biometric* thermal images, using FWT and Linear Discriminant Analysis (LDA) for feature extraction. FWT is part of the Large Time-Frequency Analysis Toolbox (LTFAT) and is available as a package in GNU Octave.



Figure10: Image from the Terravic Facial Infrared Database, before and after binarization.

5.1. Hard-biometrics

The image processing was first done to extract the hard-biometric traits from the facial images. This was achieved by

image binarization, using octave, to retrieve the shape of the head from each of the images.

5.1.1. Image binarization

This was done using a threshold technique, to determine the head size and shape. It was applied for extracting the hard-biometric attribute of the thermal images. The technique is a common pre-processor used in OCR (Optical Character Recognition), and is useful in pattern recognition, for exposing the uniqueness of an image.



Figure 11: Multiple exposures of the same person, from different angles, before binarization and LDA, images from the Terravic Facial Infrared Database.

5.1.2. Hard-biometric FWT Experiments

The hard biometric features from the thermal facial images, shown in Figure 11, after binarization were extracted using FWT. Figure 12 shows the wavelet sub-bands. The entire image set is a matrix of size 76800 by 144. This was processed to yield four sub-bands after FWT. The first band, is a matrix of size 9600 by 144, the second a matrix of size 19200 by 144, the third a matrix of size 19200 by 144, and the fourth a matrix of size 38400 by 144. The four sub-bands were merged to form a value matrix, rich in the spatial and frequency components, which served as input to the LDA stage.

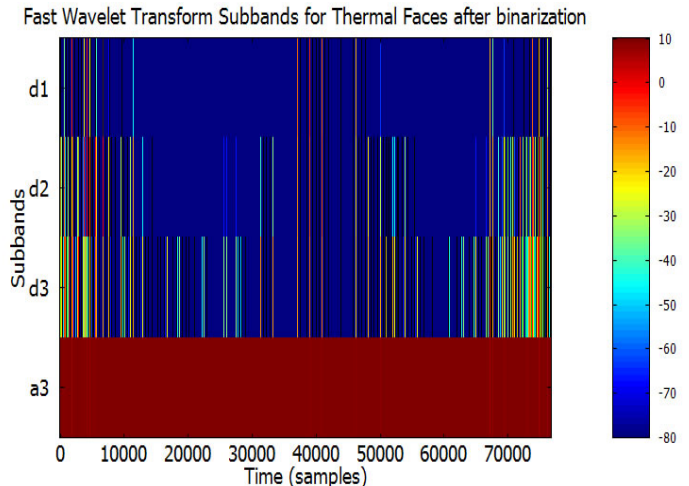


Figure 12: FWT of binarized images, of the same person in Figure 11

5.1.3. Hard-biometric LDA Experiments

LDA was performed on the spatial time-frequency features which formed the confidence matrix of wavelet sub-bands. To further extract points of highest variance. Figure 13 and 14 show a visualization of the time-frequency features, before and after Linear Discriminant Analysis, for the hard-biometric features.

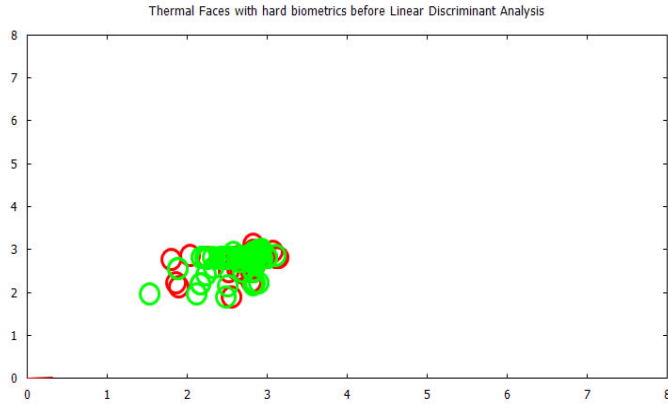


Figure 13: Graphical representation of spatial frequency components, of hard biometric features, for thermal faces shown in Figure 10, before LDA

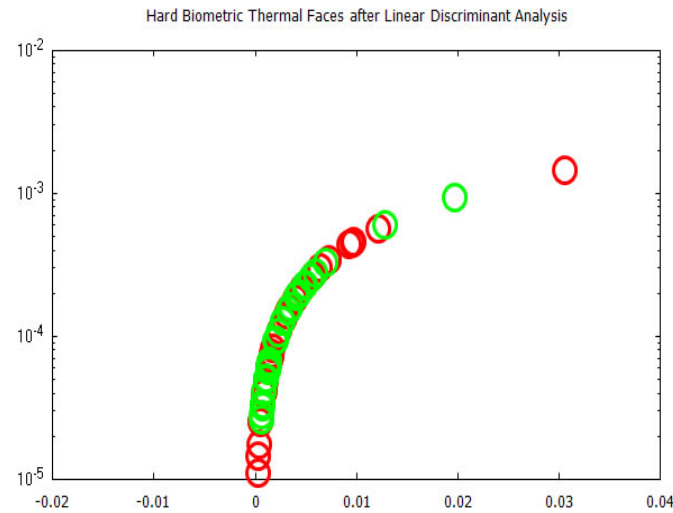


Figure 14: Graphical representation of spatial frequency components, of hard biometric features, for thermal faces shown in Figure 10, after LDA

5.2. Soft-biometrics

This part of the image processing was used for extracting time-frequency and principal components, from each *soft-biometric* attribute. This was achieved by grouping images from the datasets based on the *soft-biometric* attributes presented in Figure 4, Figure 5, Figure 6 and Figure 7.

5.2.1. Soft-biometric FWT Experiments

Figure 15, Figure 16, Figure 17, Figure 18, Figure 19, and Figure 20 show the wavelet sub-bands, for the *soft biometric* attributes after FWT, namely: face wearing glasses, face wearing headgear, face having facial hair, plain face, female face, and male face respectively.

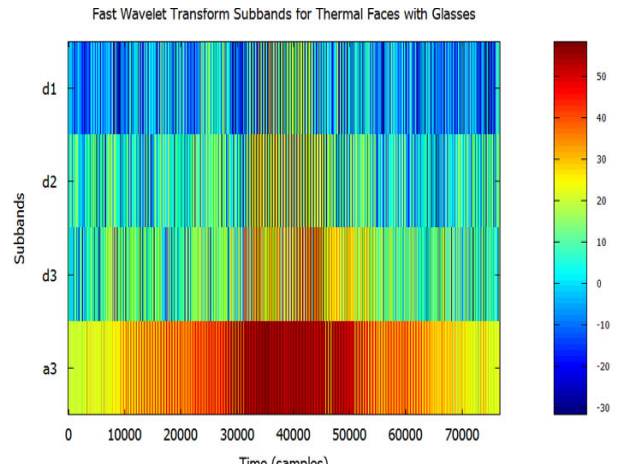


Figure 15: Visualized FWT of face images in glasses, from the Terravic Facial Infrared Database, depicting spatial and frequency information displayed using 4 sub-band

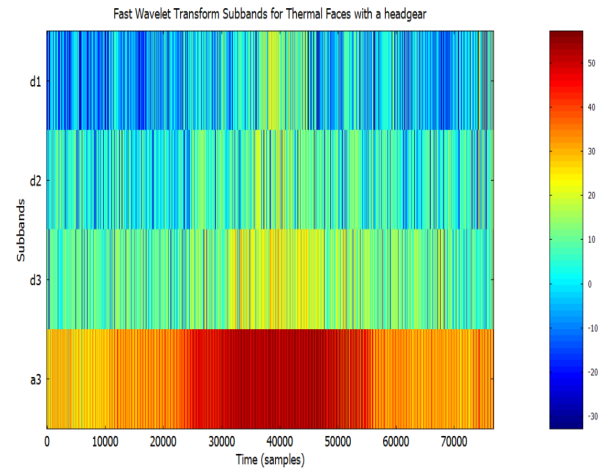


Figure 16: Visualized FWT of face images in headgear, from the Terravic Facial Infrared Database, depicting spatial and frequency information displayed using 4 sub-bands.

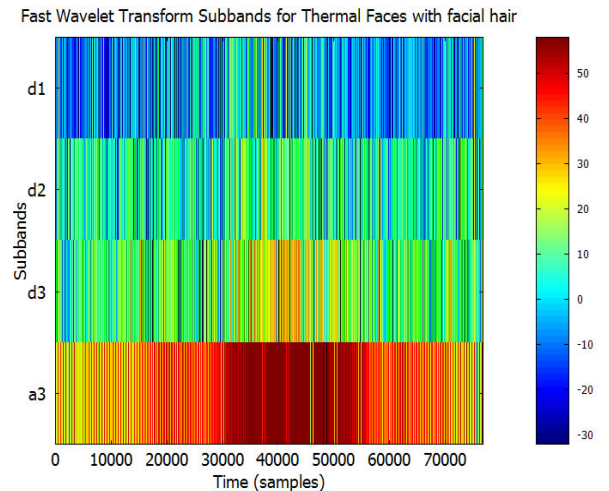


Figure 17: Visualized FWT of face images with facial hair, from the Terravic Facial Infrared Database, depicting spatial and frequency information displayed using 4 sub-bands.

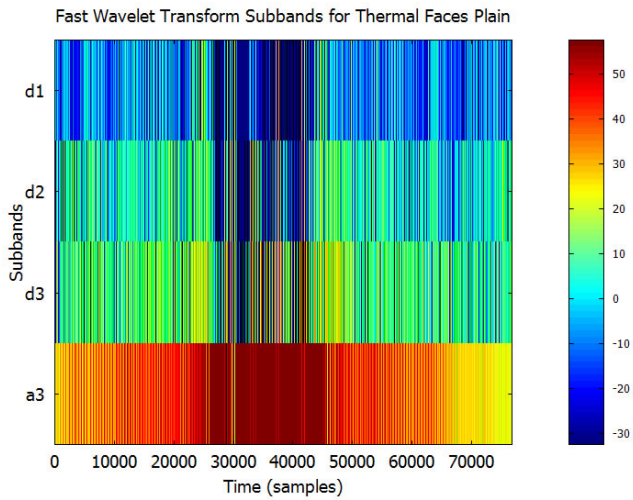


Figure 18: Visualized FWT of plain face images, from the Terravic Facial Infrared Database, depicting spatial and frequency information displayed using 4 sub-bands.

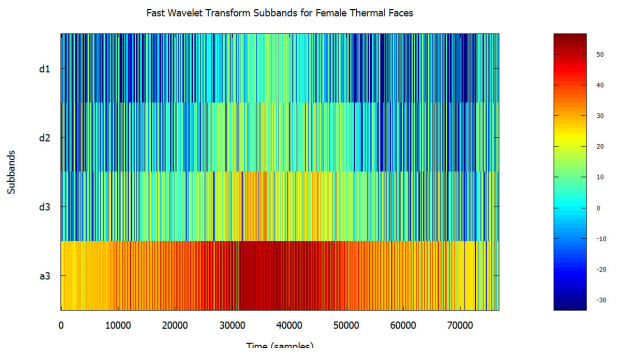


Figure 19: Visualized FWT of female facial images, from the Carl's Infrared Database, depicting time and frequency information displayed using 4 sub-bands.

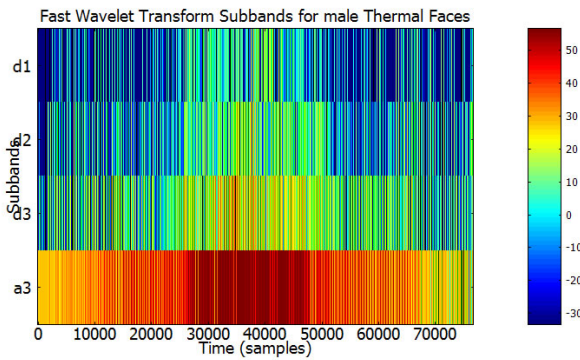


Figure 20: Visualized FWT of male facial images, from the Carl's Infrared Database, depicting time and frequency information displayed using 4 sub-bands.

5.2.2. Soft-biometric LDA experiments

After FWT, LDA was performed on the spatial time-frequency features, to derive points of most variance from the confidence matrix, for each *soft biometric* group. The following figures show a visualization of the spatial frequency features before and after Linear Discriminant Analysis, for face wearing glass, face, face wearing cap, face with hair, plain face, female face, and male face.

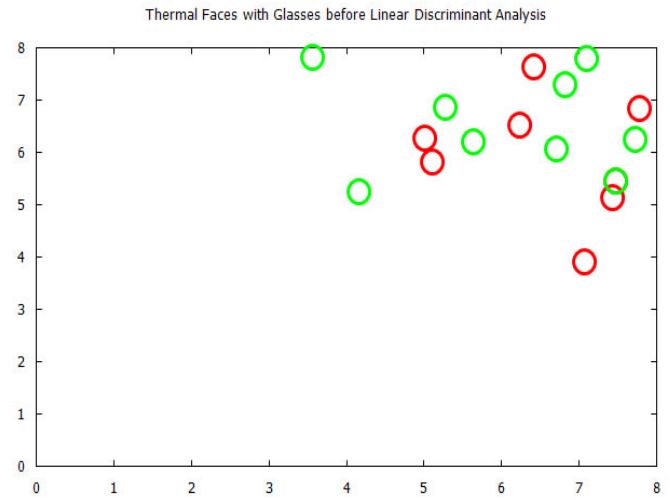


Figure 21: Visualized time-frequency (TF) features, before Linear Discriminant Analysis, for the Terravic Facial Infrared Database images, glass wearing faces

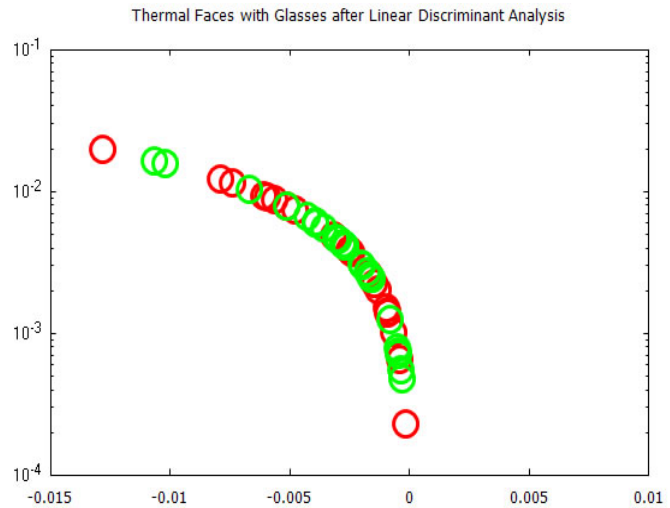


Figure 22: Visualized time-frequency (TF) features after Linear Discriminant Analysis, for images in the Terravic Facial Infrared Database, glass wearing faces

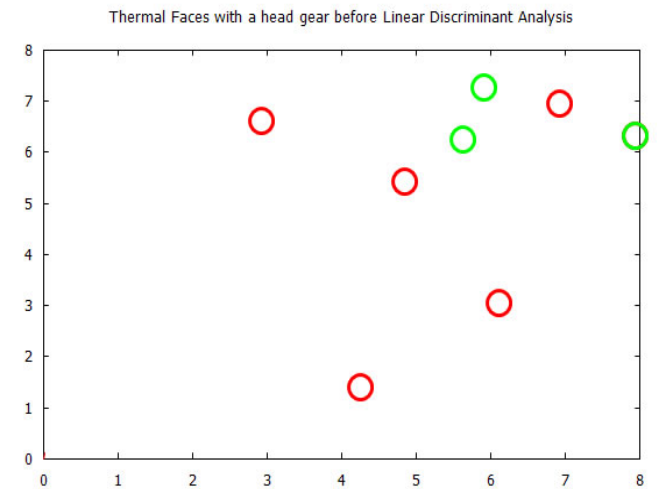


Figure 23. Visualized time-frequency (TF) features, before Linear Discriminant Analysis, for images in the Terravic Facial Infrared Database, cap wearing faces

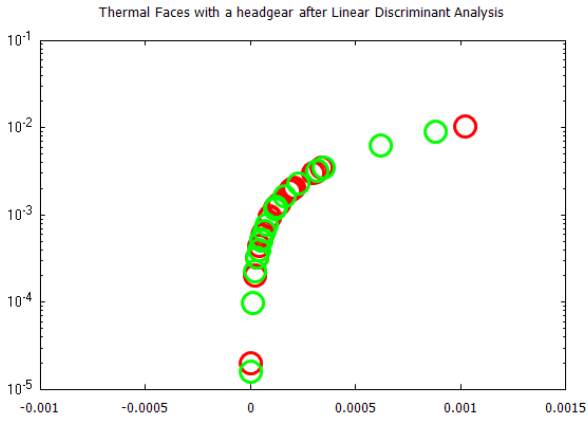


Figure 24: Visualized time-frequency (TF) features after Linear Discriminant Analysis, for the Terravic Facial Infrared Database images, cap wearing faces.

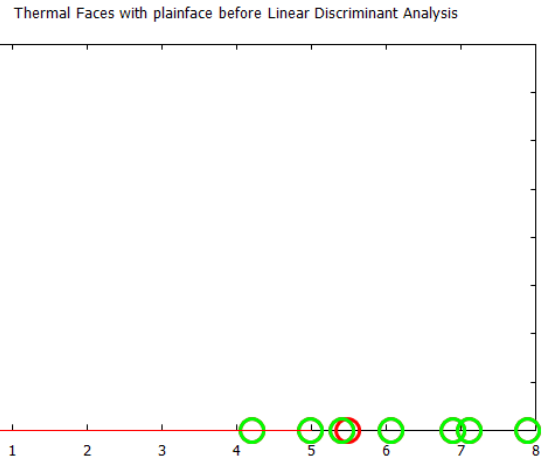


Figure 27: Visualized time-frequency (TF) features, before Linear Discriminant Analysis, for the Terravic Facial Infrared Database images, plain faces

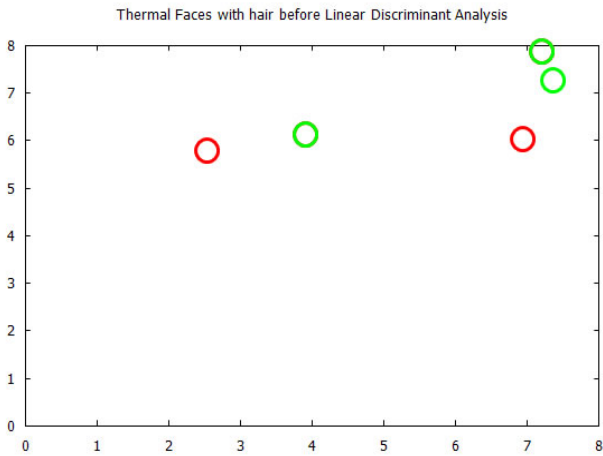


Figure 25: Visualized time-frequency (TF) features, before Linear Discriminant Analysis, for the Terravic Facial Infrared Database images, for faces with facial hair

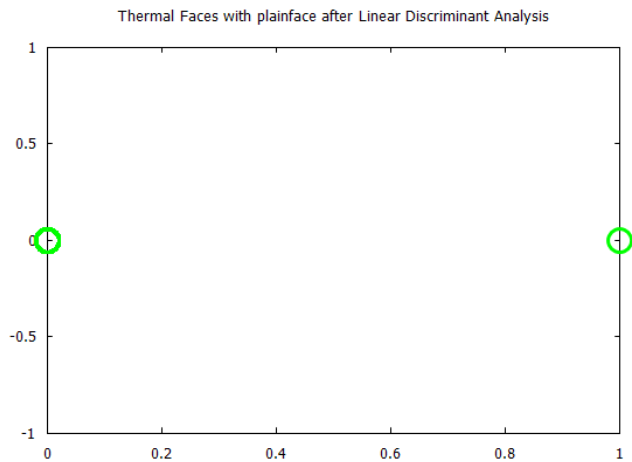


Figure 28: Visualized time-frequency (TF) features, after Linear Discriminant Analysis, for the Terravic Facial Infrared Database images, plain faces

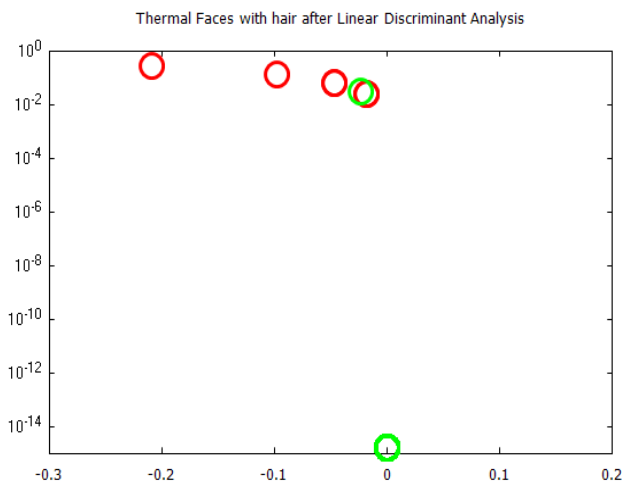


Figure 26: Visualized time-frequency (TF) features, after Linear Discriminant Analysis, for the Terravic Facial Infrared Database images, for faces with facial hair.

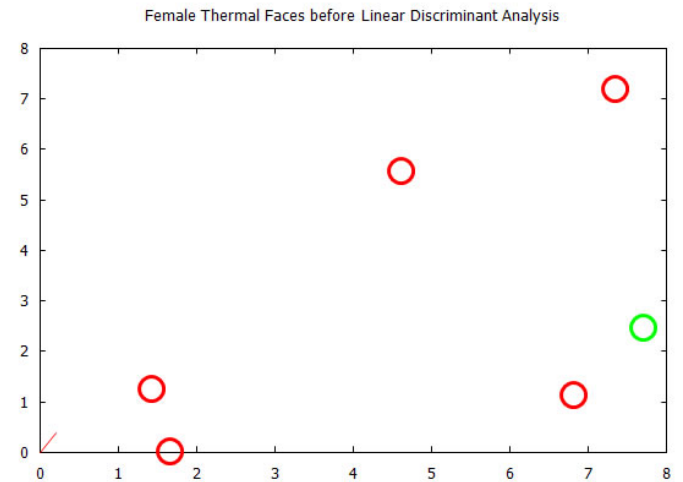


Figure 29: Visualized time-frequency (TF) features, before Linear Discriminant Analysis, for images in the Carl's Infrared Database, female faces.

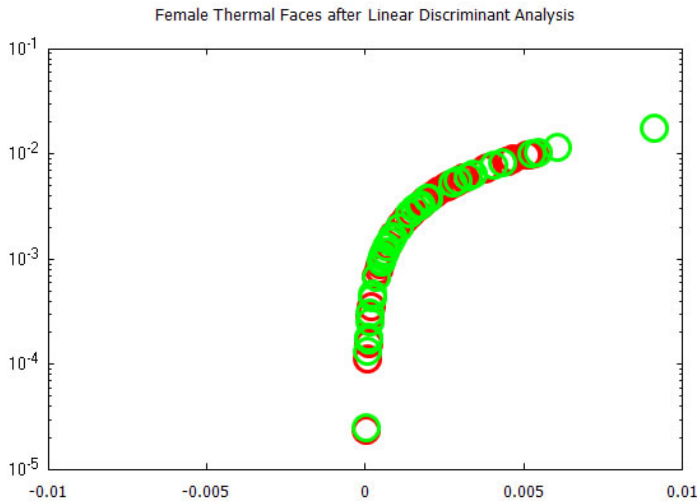


Figure 30: Visualized time-frequency (TF) features, after Linear Discriminant Analysis, for images in the Carl's Infrared Database, male faces.

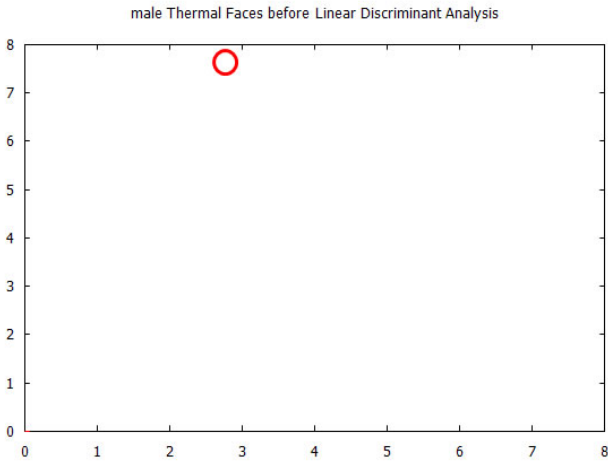


Figure 31: Visualized time-frequency (TF) features, before Linear Discriminant Analysis, for images in the Carl's Infrared Database, male faces

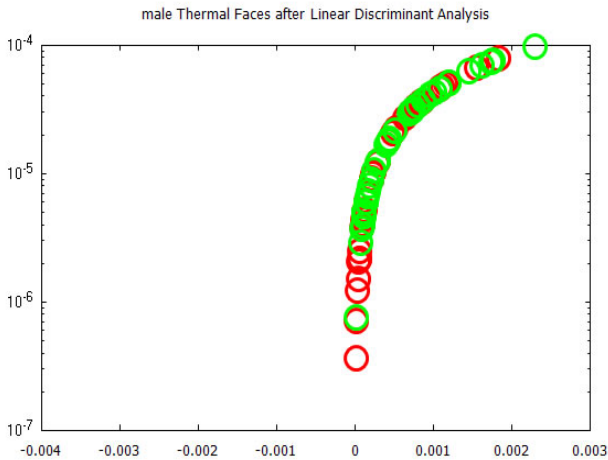


Figure 32: Visualized time-frequency (TF) features, after Linear Discriminant Analysis, for images in the Carl's Infrared Database, male faces

5.3. Summary

The outcome of the feature extraction experiments was stored in a data file using the Matlab format. This was done for both hard biometric and *soft biometric* feature sets. These data files, namely: *Linear Discriminants* for hard biometric features and *Linear Discriminants* for *soft biometric* features. The latter comprising, glass wearing faces, cap wearing face, faces with facial hair, plain faces female faces and male faces. With these the distinguishing features, which describe each of the biometric groups, were known. The objective being to train seven different neural networks, to learn each of the features, and subsequently validate a user's identity using at least two combined. Such that if a user appears, before a thermal sensor, seeking access, without any of the attributes, access would not be granted. But when he or she appears with facial hair, wearing glasses or wearing a cap, access would be granted.

6. Experiment Two: Deep Learning Neural Networks

These are a continuation of the pre-processing experiments reported. They were done, using Rasmus Berg Palm's deep learning toolbox, for RBM, DBN, and FFNN.

6.1. Classification

To achieve target vector reconstruction the *Linear Discriminants* realized from the first experiments were used for classification after training. After pre-training the DBN with RBM and further training and classifying with FFNN, a global minimum error was achieved on each training set group. These were: 0.02887 for hard biometric face, 0.038695 for glass wearing face, 0.02381 for headgear wearing face, 0.024629 for facial hair face, 0.0268 for plain face, 0.02369 for female face and 0.03 male face. Also introducing new test images randomly to the algorithm, while matching the FFNN global minimum error with these known values, demonstrated the *soft-biometric* person recognition approach. Making it possible to identify thermal facial images as: face in glasses, hairy face, plain face, face in a headgear. The following traces show the the full batch classification error, from the RBM, DBN, and FFNN algorithms, for each *soft-biometric* group.

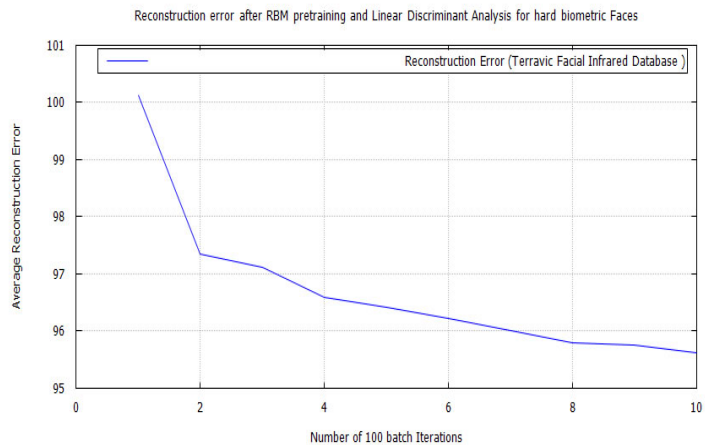


Figure 33: RBM classification error after LDA feature extraction applying the time-frequency features of images from the Terravic Facial Infrared Database, facial hard biometrics user.

6.2. Plots

The plots from each training session, for RBM, DBN, and FFNN, are graphically shown below for each of the seven semantic categories. In the following order: hard biometric face, faces wearing glasses, faces wearing a cap, faces having facial hair, faces plain, female faces, and male faces. Each one shows an improvement, in the algorithm's training error, up until the FFNN session. At which point the algorithm, fully learns the data and makes predictions on it, with little error.

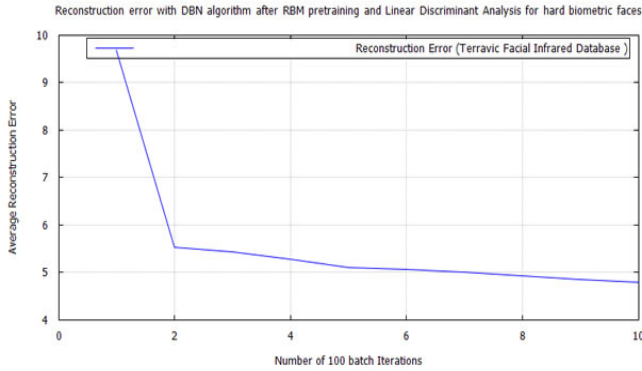


Figure 34: DBN classification error, after RBM pre-training for Terravic Facial Infrared Database images, user facial hard biometrics.



Figure 35: FFNN classification full batch error after DBN target vector reconstruction applying RBM pre-training and LDA feature extraction using the time-frequency features of Terravic Facial Infrared Database images, user facial hard biometric.

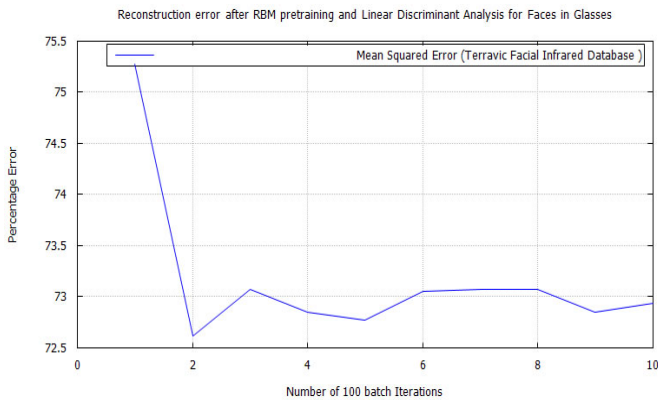


Figure 36: RBM classification error after LDA feature extraction applying the time-frequency features of Terravic Facial Infrared Database images, faces in glasses.

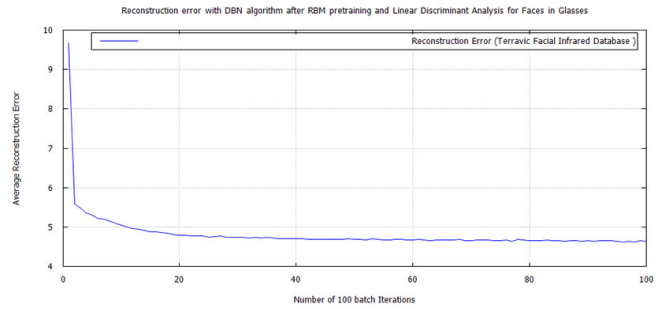


Figure 37: DBN classification error, after RBM pre-training for Terravic Facial Infrared Database images, glass wearing faces.

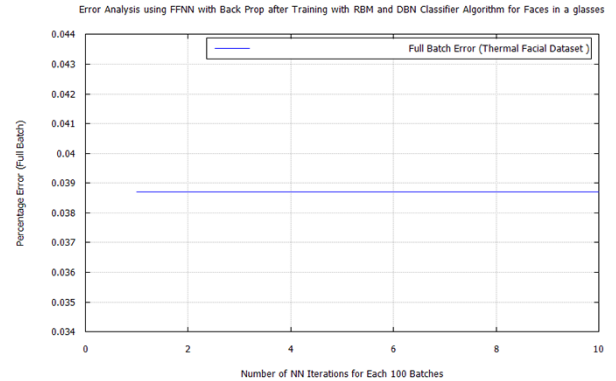


Figure 38: FFNN classification error after DBN target vector reconstruction with RBM pre-training and LDA feature extraction applying the time-frequency features of Terravic Facial Infrared Database images, glass wearing face group.

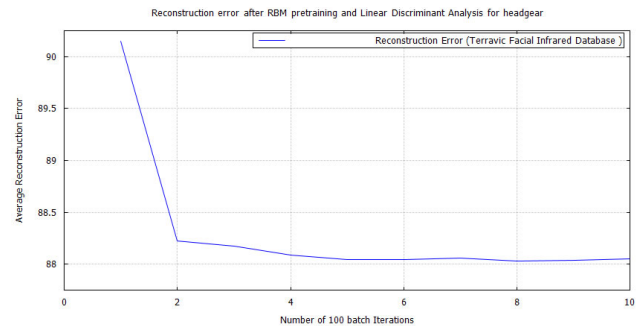


Figure 39: RBM classification error after LDA feature extraction applying the time-frequency features of Terravic Facial Infrared Database images, headgear faces.

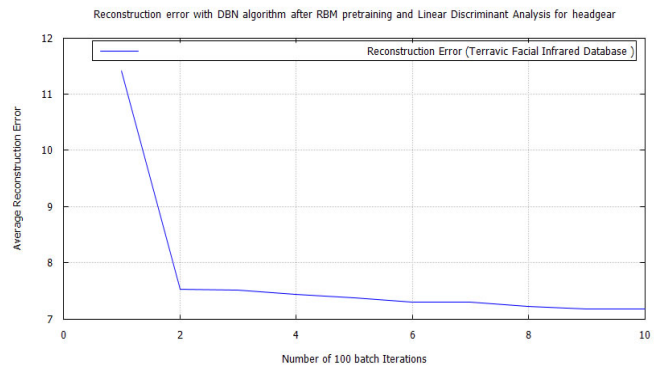


Figure 40: DBN classification error, after RBM pre-training for Terravic Facial Infrared Database images, headgear wearing faces.

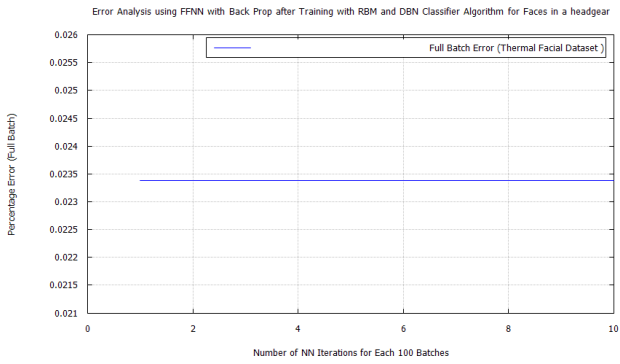


Figure 41: FFNN classification error after DBN target vector reconstruction with RBM pre-training and LDA feature extraction applying the time-frequency features of Terravic Facial Infrared Database images, headgear wearing group.

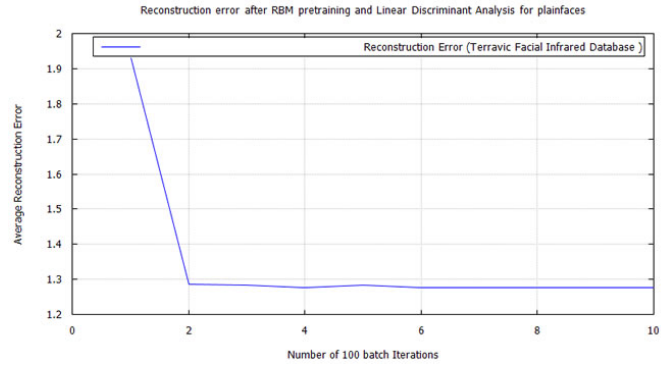


Figure 45: DBN classification error, after RBM pre-training for Terravic Facial Infrared Database images, plain faces.

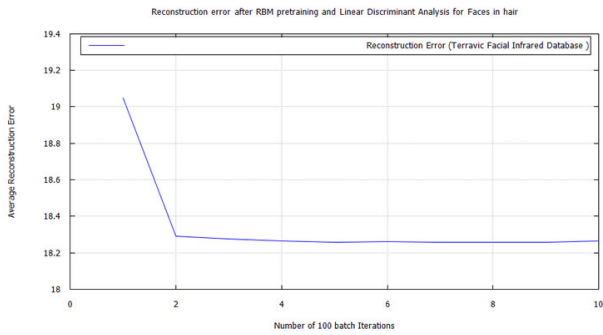


Figure 42: DBN classification error, after RBM pre-training for Terravic Facial Infrared Database images, faces having facial hair.

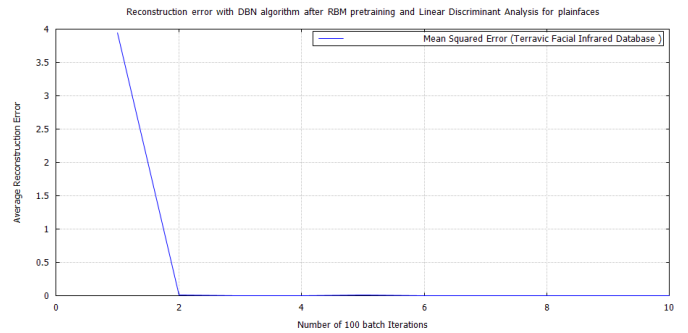


Figure 46: DBN classification error, after RBM pre-training for Terravic Facial Infrared Database images, plain faces.

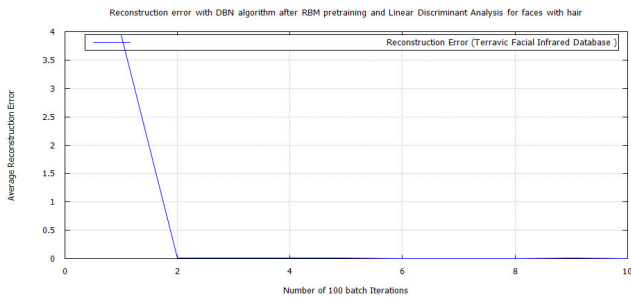


Figure 43: DBN classification error, after RBM pre-training for Terravic Facial Infrared Database images, faces having facial hair.

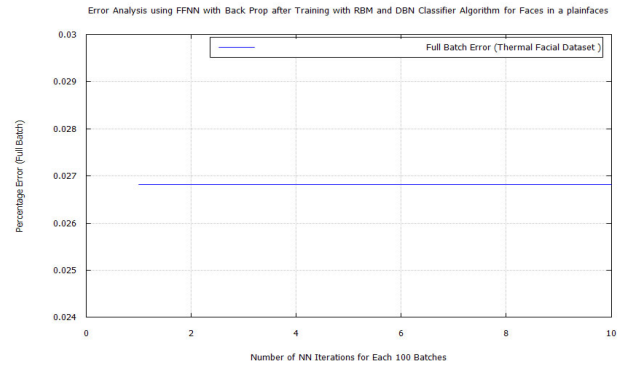


Figure 47: FFNN classification error after DBN target vector reconstruction with RBM pre-training and LDA feature extraction applying the time-frequency features of Terravic Facial Infrared Database images, plain face group.

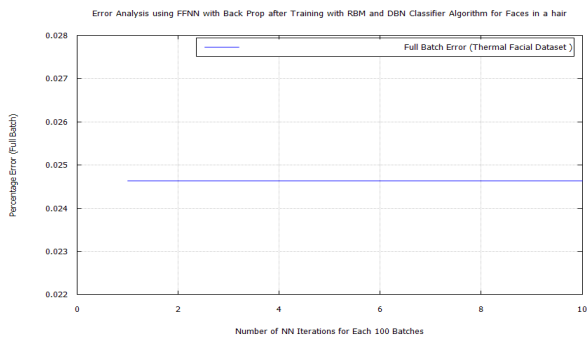


Figure 44: FFNN classification error after DBN target vector reconstruction with RBM pre-training and LDA feature extraction applying the time-frequency(TF) features of Terravic Facial Infrared Database images, hairy faces group.

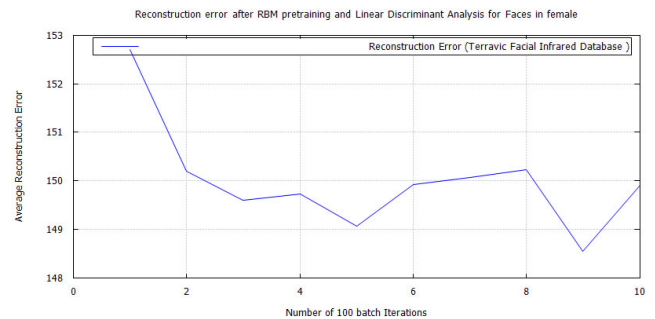


Figure 48: RBM classification error after LDA feature extraction applying the time-frequency features of Terravic Facial Infrared Database images, female faces.

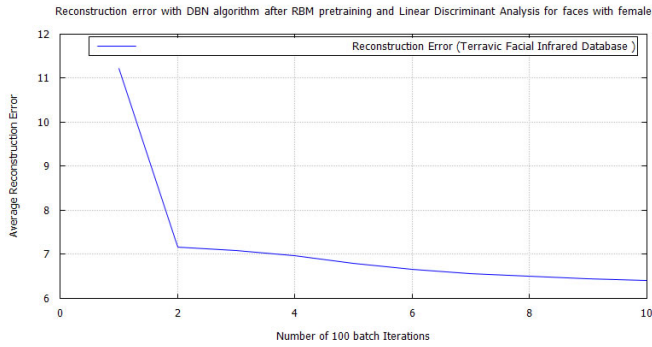


Figure 49: DBN classification error, after RBM pre-training for Terravic Facial Infrared Database images, female faces.

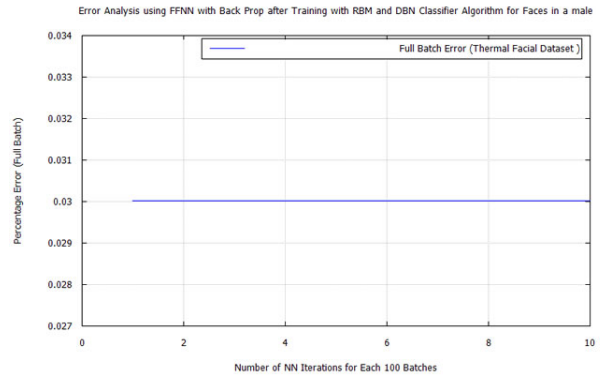


Figure 53: FFNN classification error after DBN target vector reconstruction with RBM pre-training and LDA feature extraction applying the time-frequency features of Terravic Facial Infrared Database images, male face.

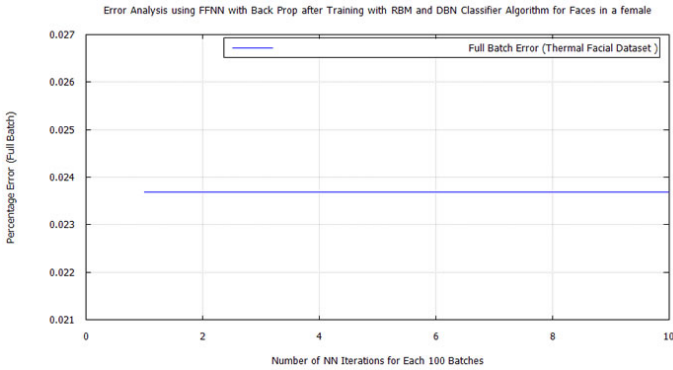


Figure 50: FFNN classification error after DBN target vector reconstruction with RBM pre-training and LDA feature extraction applying the time-frequency features of Terravic Facial Infrared Database images, female face.

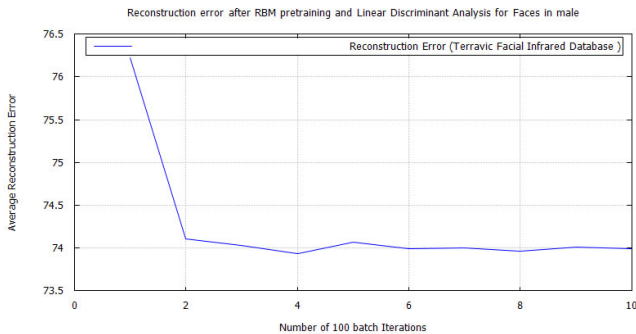


Figure 51: RBM classification error after LDA feature extraction applying the time-frequency features of Terravic Facial Infrared Database images, male faces.

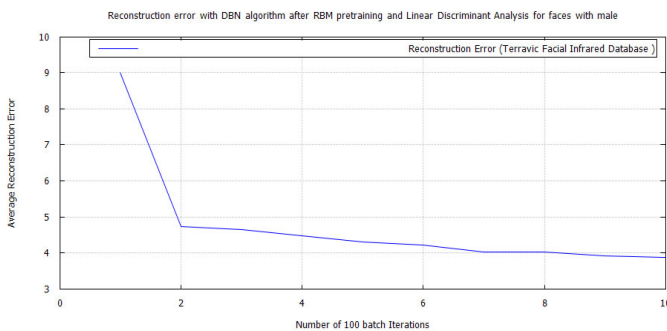


Figure 52: DBN classification error, after RBM pre-training for Terravic Facial Infrared Database images, male faces.

Table 3: RBM Test Error Results Per Semantics Attribute Group

Semantic Attribute	RBM error
hard biometric face	95.609
Faces in glasses	72.93
Faces wearing a cap/headgear	88.051
Faces with facial hair	18.265
Faces with a plain face	1.2756
Female faces	147.9
Male faces	73.98

Table 4: Test Error Results Per Semantic Attribute Group

Semantic Attribute	DBN error
hard biometric face	4.7895
Faces in glasses	4.6364
Faces wearing a cap/headgear	7.182
Faces with facial hair	0.026
Faces with a plain face	0.026
Female faces	6.406
Male faces	3.926

Table 5: Test Error Results Per Semantic Attribute Group

Semantic Attribute	FFNN error
hard biometric face	0.02887
Faces in glasses	0.038695
Faces wearing a cap/headgear	0.02381
Faces with facial hair	0.02462
Faces with a plain face	0.0268
Female faces	0.02369
Male faces	0.03

6.3. Result analysis

Applying the RBM pre-trained DBN, with FFNN classifier algorithm method, to the *Linear Discriminants* from the thermal facial images, it was observed that:

- Time-frequency (TF) components, gleaned from Fast Wavelet Transform, aided LDA in the facial thermal image investigation.
- On each of the biometric training sets a low reconstruction error was achieved, using DBN after pre-training with RBM,

through target vector reconstruction. This excepted faces wearing glasses, which needed to be trained using a bigger batch size of 100 to achieve a test error of 4.6364%. This value was further reduced to 0.038695% after additional training with the FFNN algorithm.

- The other biometric groups didn't require additional training and were trained using a batch size of 10.
- With the use of back propagation, DBN pre-trained with RBM algorithm successfully learned the features of the *soft-biometric* training sets. This was possible without lengthy training sessions.
- As in the case of glass wearing face including feature learning, and training with FFNN, aided the further reduction of the classification error.
- The reduced classification error realized, by applying FFNN with DBN pre-trained using RBM and LDA, showed that the algorithm would recognize each *soft biometric* trait and differentiate one from the other.

Table 6: FWT, LDA, RBM, DBN, and FFNN Multi-Biometric Experiment Results Per Semantic Attribute Group

Experiment	Result
Feature Extraction FWT	Numbers
FWT Sub-band one	9600 features
FWT Sub-band two	9600 features
FWT Sub-band three	19200 features
FWT Sub-band four	38400 features
FWT Sub-band four + LDA+RBM Hard-biometric features	4.7895 %
FWT Sub-band four + LDA+RBM Glass faces	4.6364%
FWT Sub-band four + LDA+RBM Head gear faces	0.026 %
FWT Sub-band four + LDA+RBM Facial hair faces	0.026 %
FWT Sub-band four + LDA+RBM Plain faces	0.026 %
FWT Sub-band four + LDA+RBM Female faces	6.406 %
FWT Sub-band four + LDA+RBM Male faces	3.926 %
FWT Sub-band four + LDA+RBM+DBN+FFNN Hard-biometric features	0.02887
FWT Sub-band four + LDA+RBM+DBN+FFNN glass wearing faces	0.038695 %
FWT Sub-band four + LDA+RBM+DBN+FFNN head gear wearing faces	0.02381 %
FWT Sub-band four + LDA+RBM+DBN+FFNN faces with facial hair	0.024629 %
FWT Sub-band four + LDA+RBM+DBN+FFNN plain faces	0.0268 %
FWT Sub-band four + LDA+RBM+DBN+FFNN Female faces	0.02369 %
FWT Sub-band four + LDA+RBM+DBN+FFNN Male faces	0.03 %

6.4. Observations

Classifying using FWT, LDA and RBM pre-trained DBN with FFNN algorithms, yielded less error of 0.038695% on the glass wearing semantic group. This was for the following reasons:

- The DBN classifier runs faster and uses fewer system resources because of the structure of its RBM unit. Thus it learns more about the problem within a short period.
- The DBN classifier uses back propagation during training for error reconstruction.
- The DBN classifier, is ensembled with a Feed-Forward Neural Network (FFNN) which further, learns the problem and reduces the classification errors.

Using images in the Terravic Facial Infrared and Carl's databases *Multi-biometric* person recognition in thermal images is demonstrated. This was done using FFNN classifiers, after feature extraction with FWT and LDA, and RBM pre-trained DBN for feature learning. *Hard biometric* features, coupled with outward attributes, such as face wearing glass, face wearing cap, face with facial hair, plain face, female face, and male face, of persons in the datasets, were learned for multi-biometric grouping. Trial images not in the training sets were afterwards recognized multi-biometrically, with both their hard biometric traits coupled with any of the six *soft biometric* traits, using the technique. Table 6 shows a tabulation of the experiment results.

6.5. Summary

The outcome, of the feature classification experiments are stored in a data file using the Matlab format. This is done for both, hard biometric and soft biometric, feature sets. These data files contain the error on the test set, for the prediction of the unknown variable (y) given the known variable (X) after training, for the hard biometric and *soft biometric* features. The latter comprising, faces wearing glass, faces wearing cap, face having facial hair, plain face, female face, and male faces. With these the extent to which the neural network knows each of the biometric, features are noted. Based on the low classification error on each of the test sets, as shown in Table 6, the system can recognize biometric features not in the training set, such as:

- Facial, hard biometric, features of the user used in training the algorithm, as shown in Figure 10.
- Faces of a user when in glasses, as shown in Figure 4.
- Faces of a user when wearing a cap, as shown in Figure 5.
- Faces of a user when having facial hair, as shown in Figure 6.
- Faces of a user when plain without facial hair, as shown in Figure 7.
- The face of a female user.
- The face of a male user.

With these biometric traits additional layers of security can be introduced into a person recognition system. Besides using a user's facial hard biometric features for authentication, two, three, four or five other biometric attributes can be used to make a system more difficult to fool. As a result of such complexity, a forger would find it hard to guess what traits the system would need for recognition to take place. Table 7 shows fifteen possible multi-biometric feature configurations, based on the traits used in this

research, along with their security levels. Each combination can work, using all traits or only one, before a person's identity is confirmed. In either mode, if a user appears before the sensor without at least one requisite *soft biometric* trait based on system requirements, the user's identity would not be verified.

The advantage of the system being that it can acquire all the needed biometric traits using a single sensor. Thus a hacker who watches while a user's identity is being verified, using this method, would be unable to know exactly what biometric attribute to forge.

Table 7: Multi Biometric Feature Configurations and Security Levels

	Biometric Features	Security Level
1	Countenance + Glasses	Robust
2	Countenance + Cap	Robust
3	Countenance + Facial hair	Robust
4	Countenance + Plain face	Robust
5	Countenance + Gender	Robust
6	Countenance + Glasses + Cap	More Robust
7	Countenance + Glasses + Facial hair	More Robust
8	Countenance + Glasses + Plain face	More Robust
9	Countenance + Glasses + Gender	More Robust
10	Countenance + Glasses + Cap + Facial hair	Much More Robust
11	Countenance + Glasses + Cap + Plain face	Much More Robust
12	Countenance + Glasses + Cap + Gender	Much More Robust
13	Countenance + Glasses + Facial hair + Gender	Much More Robust
14	Countenance + Glasses + Cap + Facial hair + Gender	Most Robust
15	Countenance + Glasses + Cap + Plain face + Gender	Most Robust

7. Experiment Three: Multi biometric person recognition

Using the trained algorithm cluster, with test results tabulated in Table 12. The system was tested in *verification mode* with the person in Figure 10 as a user. Working with a multi-biometric combinations of traits: Countenance + Glasses + Facial hair + Gender. Which are the user's hard-biometric features, glass wearing features, facial hair features and gender traits. The hard-biometric trait is taken as X (features to be learned) while the facial hair trait as the base for comparison y (unknown feature to be predicted y). Tests are done to confirm the other three soft-biometric characteristics and verify his identity.

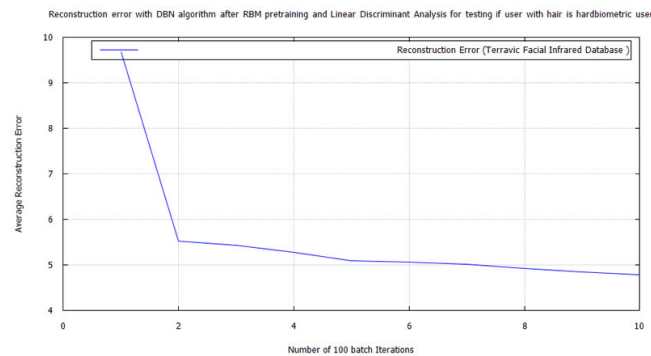


Figure 54: Error for facial hair algorithm testing hard biometric features for the presence of facial hair using RBM, LDA, and FWT for images from the Terravic Facial Infrared Database

7.1. Tests1 hard-biometric and facial hair algorithms

The first test is conducted to verify the hard-biometric features of the user for the presence of facial hair. By using the X variables after LDA, of the hard-biometric features, and the y variables after LDA, of the facial hair features. The RBM, DBN and FFNN tests were conducted to verify, that the user with the hard-biometric features (presented to the sensor), has facial hair as the authentic user. The FFNN result is shown, in comparison with those from the training test, in Table 8.

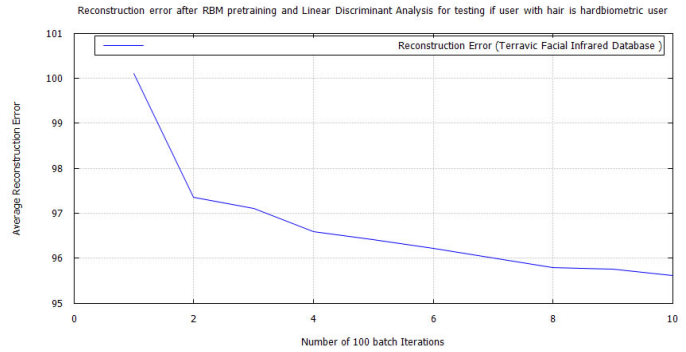


Figure 55: Error for facial hair algorithm testing hard biometric features for the presence of facial hair using RBM, LDA, and FWT for images from the Terravic Facial Infrared Database

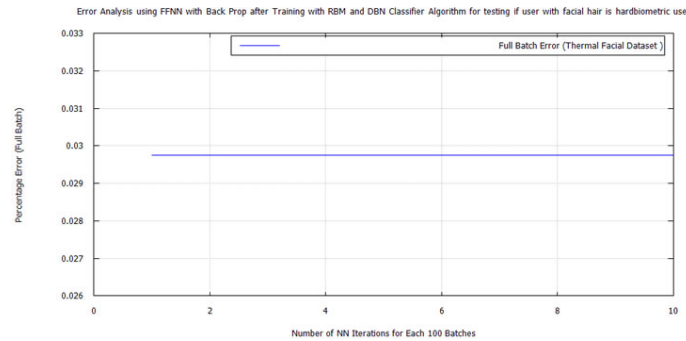


Figure 56: Error for facial hair algorithm testing if the hard biometric user is a user with facial hair using FFNN, DBN, RBM, LDA, and FWT for images from the Terravic Facial Infrared Database.

Table 8: FFNN Check for Facial Hair and Hard Biometric Traits

	Semantic Attribute	FFNN error
Training test	Hard-biometric face	0.02887
Training test	Faces with facial hair	0.02462
Verification test	Check if the user with hard-biometric features has facial hair as the main user does.	0.02975

7.2. Tests2 glass wearing and facial hair algorithms

The second test is conducted to verify that the user with facial hair, whose hard-biometric features have been confirmed, is putting on glasses. By using the X variables after LDA, of the glass wearing features for the user to be verified, and the y variables after LDA, of facial hair features. Based on facial hair attributes, the RBM, DBN, and FFNN tests were conducted to

verify that the user wearing glasses (presented to the sensor) is the authentic user. The FFNN result is shown, in comparison with those from the training test, in Table 9 below.

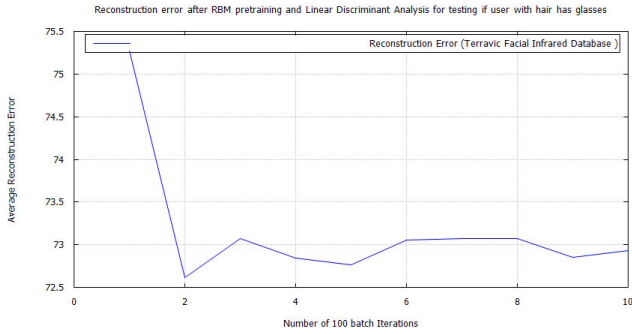


Figure 57: Error for facial hair algorithm testing glass wearing face for the presence of facial hair using RBM, LDA, and FWT for images from the Terravic Facial Infrared Database.

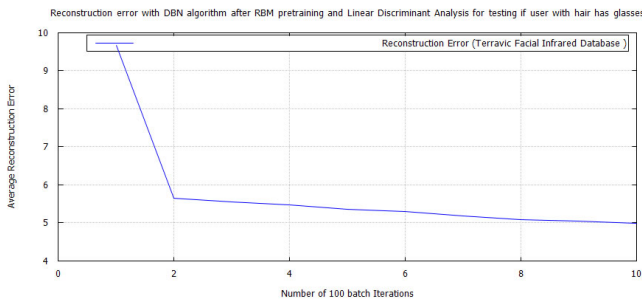


Figure 58: Error for facial hair algorithm testing glass wearing face for the presence of facial hair using DBN, RBM, LDA, and FWT for images from the Terravic Facial Infrared Database.

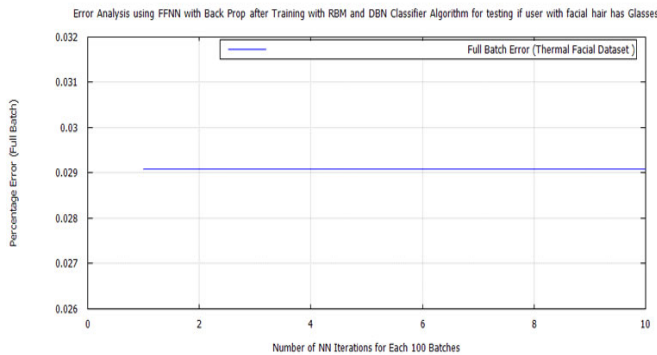


Figure 59: Error for facial hair algorithm testing glass wearing face for the presence of facial hair using FFNN, DBN, RBM, LDA, and FWT for images from the Terravic Facial Infrared Database

Table 9: FFNN Check for Facial Hair and Glass Wearing Face Traits

	Semantic Attribute	FFNN error
Training test	Faces with facial hair	0.02462
Training test	Faces in glasses	0.038695
Verification Test	Check if the user with facial hair has glasses	0.02908

7.3. Test 3, male gender and facial hair algorithms

The third test is conducted to verify that the user, with facial hair whose hard-biometric and glass wearing features have been confirmed, is masculine. By using the X variables after LDA, of the male gender features (from the sensor) of the user to be verified, and the Y variables after LDA of the facial hair features. RBM, DBN and FFNN tests are conducted to verify that the male, presented to the sensor, is the authentic user. The FFNN result is shown, in comparison with those from the training test, in Table 10.

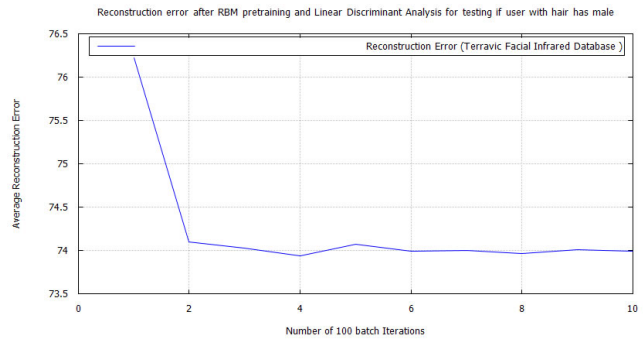


Figure 60: Error for facial hair algorithm testing male faces for the presence of facial hair using RBM, LDA, and FWT for images from the Terravic Facial Infrared Database

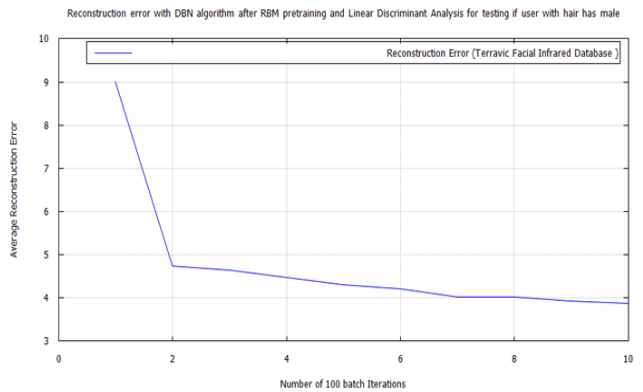


Figure 61: Error for facial hair algorithm testing male face for the presence of facial hair using DBN, RBM, LDA, and FWT for images from the Terravic Facial Infrared Database

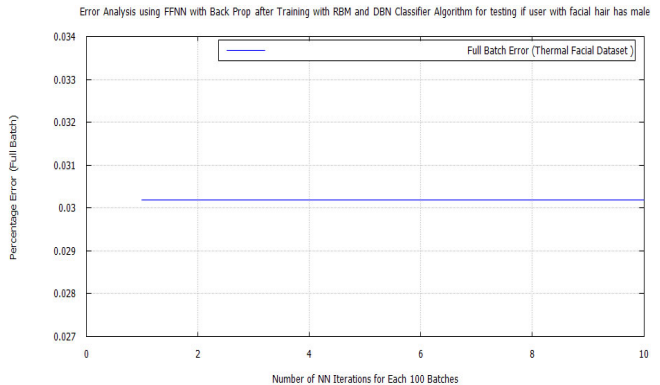


Figure 62: Error for male gender algorithm testing facial hair face for male gender using FFNN, DBN, RBM, LDA, and FWT for images from the Terravic Facial Infrared Database

Table 10: FFNN Check for Facial Hair and Male Gender Soft-Biometric Traits

	Semantic Attribute	FFNN error
Training test	Faces with facial hair	0.02462
Training test	Male faces	0.03
Verification Test	Check if a user with facial hair is male	0.03018

To ascertain that the person requesting verification is the authentic person. The results are summarized below.

7.4. Explanation

By comparing the FFNN error, from each of the cross-feature tests, to those from the algorithm. The trait check is seen to pass for each characteristic, based on comparison to the algorithm’s test results. This is explained for each test as shown below.

7.4.1. Tests1, hard-biometric and facial hair algorithms

The similarity of the FFNN verification test results to those of the hard-biometric features, from the training test, show that they belong to the original user. This also shows that the hard-biometric trait, used in training the algorithm, has a close similarity to those possessed by the user being verified.

7.4.2. Tests2, glass wearing, and facial hair algorithms

The similarity of the FFNN verification test results to those of the face in glasses biometric features, from the training test, show that they belong to the original user. Since they have a value that is between that outputted by the glass algorithm and the one belonging to facial hair, as these two *soft-biometric* traits are present, in the X and y test data. Showing that the biometric trait, used in training the algorithm, has a close similarity to those possessed by the user being verified.

7.4.3. Test 3, male gender and facial hair algorithms

The similarity of the FFNN verification test result to those of the male gender biometric features, from the training test, show that they belong to the original user. Since they have a value that is closer to that of the male gender algorithm than the one belonging to facial hair. This also shows that the male gender biometric trait, used in training the algorithm, has a close similarity to those possessed by the user being verified.

7.4.4 Summary

From the tests, the first assumption was that the person being verified has facial hair and this was used to verify the other three traits, one after the other. The approach adds redundancy into the system with each trait used, to verify the other, one after the other. Such that if facial hair is absent, glasses would be and if glasses and facial hair are absent, the masculine features would be. Thus increasing robustness and system performance. In *identification mode*, for a large population size of millions, the technique can help to achieve high distinctiveness, high persistence, better performance, high acceptability and low potential for spoofing.

Conclusion

Multi-biometric person recognition, using thermal images to improve biometric security, is established, with images from

Carl’s database and the Terravic Facial Infrared Database. This was done using FWT, LDA and RBM pre-trained DBN with FFNN classifiers. The hard biometric attribute, of shape of head, was combined with outward attributes, such as face in glasses, face in a cap/head gear, face with facial hairs, plain face, female face and male face, using persons in the thermal facial datasets. These were learned, used for multi-biometric classification and then multi-biometric person recognition. Using the parallel mode of operation, through score fusion, a test user possessing these traits was verified with the technique. Showing how biometric system security can be fortified through a combination of hard and soft-biometric traits.

Conflict of Interest

The authors declare no conflict of interest.

Acknowledgment

The financial assistance of the National Research Foundation (NRF) towards this research is hereby acknowledged. Opinions expressed and conclusions arrived at, are those of the author and are not necessarily to be attributed to the NRF.

References

- [1] Moreno-Moreno, M., Fierrez, J., and Ortega-Garcia, J., “Millimeter- and Submillimeter-Wave Imaging Technologies for Biometric Purposes,” in Proceedings of XXIV Simposium Nacional de Union Cientica Internacional de Radio, URSI, Spain, September 2009.
- [2] D.L. Narayanan, R.N. Saladi, J.L. Fox, "Ultraviolet radiation and skin cancer," Int. J. Dermatol., vol. 49, no. 9, pp. 978–986, Sep. 2010.
- [3] Moreno-Moreno, M., Fierrez, J., and Ortega-Garcia, J., “Biometrics Beyond the Visible Spectrum: Imaging Technologies and Applications,” in Proceedings of BioID-Multicomm, LNCS 5707, 154–161, Springer, September 2009.
- [4] E. Hurwitz, A. N. Hasan, and C. Orji, “Soft biometric thermal face recognition using FWT and LDA feature extraction method with RBM DBN and FFNN classifier algorithms,” ICIIP, 2017, pp. 1 – 6, doi: 10.1109/ICIIP.2017.8313796.
- [5] A.Meraoumia, S.Chitroub, A. Bouridane "Multimodal Biometric Person Recognition System based on Fingerprint & Finger-Knuckle-Print Using Correlation Filter Classifier", Communications (ICC), 2012 IEEE International Conference, Ottawa, Canada pages 820 - 824.
- [6] Galbally, J., Marcel, S., & Fierrez, J. (2014). Biometric Antispoofing Methods: A Survey in Face Recognition. IEEE Access, 2, 1530-1552
- [7] X. Geng, L. Wang, M. Li, Q. Wu, and K. Smith-Miles. Adaptive fusion of gait and face for human identification in video. In Applications of Computer Vision, 2008. WACV 2008. IEEE Workshop on, pages 1-6, Jan. 2008.
- [8] L.Hong, A.k.Jain, S. Pankanti, "Can multibiometrics improve performance ?", Proc. AutoID'99, pp. 59-64, 1999-Oct
- [9] IEEE OTCBVS WS Series Bench; Roland Miezianko, Terravic Research Infrared Database.
- [10] V. Espinosa-Dur o, M. Faundez-Zanuy, and J. Mekyska, “A new face database simultaneously acquired in visible, near-infrared and thermal spectrums," Cognitive Computation, vol. 5, no. 1, pp. 119–135, 2013
- [11] A. K. Jain, P. J. Flynn, and A. Ross. Handbook of Biometrics. Springer, 2007.
- [12] H.T.F. Rhodes. Alphonse Bertillon: Father of scientific detection. Pattern Recognition Letters, 1956.
- [13] L. Wen and G-D. Guo. A computational approach to body mass index prediction from face images. Image and Vision Computing, 31(5):392–400, 2013.
- [14] R. Zewail, A. Elsafi, M. Saeb, and N. Hamdy. Soft and hard biometrics fusion for improved identity verification. In Proc. of IEEE International Midwest Symposium on Circuits and Systems, volume 1, pages I – 225–8, 2004.

- [15] D. Reid and M. Nixon. Imputing human descriptions in semantic biometrics. In Proc. of ACM Workshop on Multimedia in Forensics, Security and Intelligence, 2010.
- [16] A. K. Jain, A. Ross, and S. Prabhakar, "An introduction to biometric recognition," IEEE Trans. Circuits Syst. Video Technology, Special Issue Image- and Video-Based Biomet., vol. 14, no. 1, pp. 4–20, Jan. 2004.
- [17] R.M. Bolle, S. Pankanti, and N.K. Ratha, "Evaluation Techniques for Biometrics-Based Authentication Systems (FRR)," Proc. 15th Int'l Conf. Pattern Recognition, vol. 2, pp. 831-837, Sept. 2000.
- [18] N. Kumar, A. C. Berg, P. N. Belhumeur, and S. K. Nayar. Attribute and simile classifiers for face verification. In Proc. of International Conference on Computer Vision, 2009.
- [19] S. Z. Li and A. K. Jain, Eds., Handbook of Face Recognition. New York: Springer Verlag, 2004.
- [20] D. Reid and M. Nixon. Using comparative human descriptions for soft biometrics. In Proc. of International Joint Conference on Biometrics, 2011.
- [21] S. Samangooei, B. Guo, and Mark S. Nixon. The use of semantic human description as a soft biometric. In Proc. of IEEE International Conference on Biometrics: Theory, Applications and Systems, 2008.
- [22] A.K. Jain, S.C. Dass, and K. Nandakumar. *Soft biometric* traits for personal recognition systems. In Proceedings of ICBA, pages 1–40. Springer, 2004.
- [23] A. Dantcheva, C. Velardo, A. D'Angelo, and J.-L. Dugelay. Bag of *soft biometrics* for person identification. New trends and challenges. Multimedia Tools and Applications, 51:739–777, 2011.
- [24] D. Bhattacharjee, A. Seal, S. Ganguly, M. Nasipuri, and D.K. Basu, "A Comparative Study of Human Thermal Face Recognition Based on Haar Wavelet Transform and Local Binary Pattern," Computational Intelligence and Neuroscience, vol. 2012, Article ID 261089, 12 pages, 2012. doi:10.1155/2012/261089
- [25] L. Hong, A. K. Jain, S. Pankanti, "Can multibiometrics improve performance?", Proc. AutoID'99, pp. 59-64, 1999-Oct
- [26] B. Martinez, X. Binefa, and M. Pantic. Facial component detection in thermal imagery. In Proc. IEEE Conference on Computer Vision and Pattern Recognition Workshops, pages 48–54, 2010
- [27] C. Herrmann, T. Müller, D. Willersinn, J. Beyerer, "Real-time person detection in low-resolution thermal infrared imagery with MSER and CNNs", in Proc. Electro-Optical and Infrared Systems, SPIE, 2016
- [28] A. Krizhevsky, I. Sutskever and G. Hinton. ImageNet Classification with Deep Convolutional Neural Networks. In Advances in Neural Information Processing Systems 25, pages 1106-1114, 2012
- [29] W. Shangfei, L. Zhilei, L. Siliang, L. Yanpeng, W. Guobing, P. Peng, C. Fei and W. Xufa, "A Natural Visible and Infrared Facial Expression Database for Expression Recognition and Emotion Inference", IEEE Transactions on Multimedia, vol.12, no.7, pp.682-691, Nov. 2010
- [30] K. Tai, S. Blain, and T. Chau, "A review of emerging access technologies for individuals with severe motor impairments," Assist. Technol., vol. 20, pp. 204–219, 2008
- [31] Bhowmik, M.K., Saha, K., Majumder, S., Majumder, G., Saha, A., Sarma, A.N., Bhattacharjee, D., Basu, D.K., Nasipuri, M., Corcoran, Peter M. "Thermal infrared face recognition – a biometric identification technique for robust security system". Reviews, Refinements and New Ideas in Face Recognition. 2011, 07, Zieglergase, Vienna, Austria, Europe: InTech Open Access Publisher, Vienna Office, ISBN: 978-953-307-368-2, (open access publisher of scientific books and journals)
- [32] A. Seal, S. Ganguly, D. Bhattacharjee, M. Nasipuri, D. K. Basu, "Minutiae Based Thermal Human Face Recognition using Label Connected Component Algorithm," Procedia Technology, In 2nd International Conference on Computer, Communication, Control and Information Technology (C3IT-2012), February 25 - 26, 2012. multilayer perceptron
- [33] S. Cho, L. Wang, and W. J. Ong. Thermal imprint feature analysis for face recognition. ISIE, pages 1875–1880, 2009.
- [34] O. Arandjelović, R. Hammoud, and R. Cipolla. On person authentication by fusing visual and thermal face biometrics. In Proc. IEEE Conference on Advanced Video and Singal Based Surveillance, pages 50–56, 2006.
- [35] M. Piccardi, "Background subtraction techniques: a review," in Proc. of the IEEE International Conference on Systems, Man and Cybernetics (SMC), vol. 4, pp. 3099-3104, IEEE, Oct. 2004.
- [36] S. Se and M. Brady, "Ground plane estimation, error analysis and applications," Robotics and Autonomous Systems, vol. 39, no. 2, pp. 59-71, 2002.
- [37] K. C. Sofiane Yous, Hamid Laga, "People detection and tracking with world-z map from a single stereo camera," in Proc. of the International Workshop on Visual Surveillance (VS) - (ECCV), (Marseille, France), October 2008.
- [38] A. Broggi, M. Bertozzi, A. Fascioli, and M. Sechi, "Shape-based pedestrian detection," in Proc. of the IEEE Intelligent Vehicles Symposium(IV), pp. 215-220, 2000.
- [39] D. Vaquero, R. Feris, D. Tran, L. Brown, A. Hampapur, and M. Turk. Attribute-based people search in surveillance environments. In Proc. of IEEE Workshop on Applications of Computer Vision, 2009.
- [40] B. Wu and R. Nevatia, "Detection of multiple, partially occluded humans in a single image by bayesian combination of edgelet part de-tectors," in Proc. of the International Conference on Computer Vision(ICCV), 2005.
- [41] G. Beylkin, R. Coifman, and V. Rokhlin. Fast wavelet transforms and numerical algorithms I. Communications on Pure and Applied Mathematics, 44 (2):141–183, March 1991
- [42] M. Jones, P. Viola, P. Viola, M. J. Jones, D. Snow, and D. Snow, "Detecting pedestrians using patterns of motion and appearance," in Proc. of the International Conference on Computer Vision(ICCV), pp. 734-741, 2003.
- [43] Q. Zhu, M.-C. Yeh, K.-T. Cheng, and S. Avidan, "Fast human de-tecton using a cascade of histograms of oriented gradients," in Proc. of the IEEE Conference on Computer Vision and Pattern Recognition(CVPR), (Washington, DC, USA), pp. 1491-1498, IEEE Computer Society, 2006.
- [44] A. Mohan, C. Papageorgiou, and T. Poggio, "Example based object detection in images by components," IEEE Transactions on Pattern Analysis and Machine Intelligence (PAMI), vol. 23, pp. 349-361, 2001.
- [45] B. Wu and R. Nevatia, "Detection and tracking of multiple, partially occluded humans by bayesian combination of edgelet based part de-tectors," International Journal of Computer Vision(IJCV), vol. 75, pp. 247-266, Nov. 2007
- [46] L. Trujillo, G. Olague, R. Hammoud and B. Hernandez. Automatic Feature Localization in Thermal Images for Facial Expression Recognition. Computer Vision and Pattern Recognition-Workshops, IEEE Computer Society Conference, p. 14, 2005.
- [47] Martinez B, Binefa X, Pantic M. Facial Component Detection in Thermal Imagery. Computer Vision and Pattern Recognition Workshops (CVPRW), IEEE Computer Society Conference, p. 48-54, 2010.
- [48] F.Q Al-Khalidi, R. Saatchi, D. Burke, H. Elphick. Tracking human face features in thermal images for respiration monitoring. Int Conf Computer Systems and Applications(AICCSA), p. 1-6, 2010.
- [49] S. Prabhakar, S. Pankanti, and A. K. Jain, "Biometric recognition: Security and privacy concerns," IEEE Security Privacy Mag., vol. 1, no. 2, pp. 33–42, 2003
- [50] R.M. Bolle, S. Pankanti, and N.K. Ratha, "Evaluation Techniques for Biometrics-Based Authentication Systems (FRR)," Proc. 15th Int'l Conf. Pattern Recognition, vol. 2, pp. 831-837, Sept. 2000.
- [51] Joshua C. Klontz and Anil K. Jain. A case study on unconstrained facial recognition using the boston marathon bombings suspects. Technical Report, (MSU-CSE-13-4), 2013
- [52] S. Z. Li and A. K. Jain, Eds., Handbook of Face Recognition. New York: Springer Verlag, 2004.
- [53] International Biometric Group, "Independent Testing of Iris RecognitionTechnology May 2005 [Online]. Available: http://www.biometricgroup.com/reports/public/reports/ITIRT_report.htm.
- [54] A.K. Jain, S. C. Dass, and K. Nandakumar. Can *soft biometric* traits assist user recognition? In Proceedings of SPIE, volume 5404, pages 561–572, 2004
- [55] W. J. Scheirer, N. Kumar, K. Ricanek, P. N. Belhumeur, and T. E. Boult. Fusing with context: a Bayesian approach to combining descriptive attributes. In Proc. of International Joint Conference on Biometrics, 2011
- [56] S. Denman, C. Fookes, A. Bialkowski, and S. Sridharan. Softbiometrics: Unconstrained authentication in a surveillance environment. In Proc. of International Conference on Digital Image Computing: Techniques and Applications, pages 196–203, 2009
- [57] N. Holighaus, Z. Pr'u'sa, C. Wiesmeyr, "Designing tight filter bank frames for nonlinear frequency scales, sampling Theory and Applications," 2015. [online]. Available: <http://lftat.github.io/notes/lftatnote039.pdf>.
- [58] P. Wagner, "Bytfish face recognition algorithms for MATLAB/GNU Octave and Python," 2015. [Online]. Available: <https://github.com/bytfish/facerec>.

- [59] R. B. Palm, "Prediction as a candidate for learning deep hierarchical models of data," 2012. [Online]. Available: http://www2.imm.dtu.dk/pubdb/views/publication_details.php?id=6284
- [60] G. Beylkin, R. Coifman, and V. Rokhlin. Fast wavelet transforms and numerical algorithms I. Communications on Pure and Applied Mathematics, 44(2):141–183, March 1991.
- [61] L. Sirovitch and M. Kirby, "Low-Dimensional Procedure for the Characterization of Human Faces," J. Optical Soc. of Am. A, vol. 2, pp. 519-524, 1987.
- [62] P.L. Søndergaard, B. Torrèsani, P.Balazs. The Linear Time-Frequency Analysis Toolbox. International Journal of Wavelets, Multiresolution Analysis and Information Processing, 10(4), 2012.
- [63] M. Turk and A. Pentland, "Eigenfaces for Recognition," J. Cognitive Neuroscience, vol. 3, no. 1, 1991.
- [64] R.A. Fisher, "The Use of Multiple Measures in Taxonomic Problems," Ann. Eugenics, vol. 7, pp. 179-188, 1936.
- [65] V. Nair and G. E. Hinton. Rectified linear units improve restricted boltzmann machines. In Proc. 27th International Conference on Machine Learning, 2010.
- [66] G. E. Hinton, S. Osindero, and Y. Teh, "A fast learning algorithm for deep belief nets," Neural computation, vol. 18, no. 7, pp. 1527–1554, 2006.
- [67] A. K. Jain, A. Ross, and S. Pankanti, "Biometrics: a tool for information security," IEEE Transactions on Information Forensics and Security, vol. 1, no. 2, pp. 125–143, 2006.
- [68] M. Madry-Pronobis. Automatic gender recognition based on audiovisual cues. Master Thesis, 2009.

The Influence of Adhesive on Roof Tiles Product from Water Hyacinth Fiber Residues

Arkorn Pasilo*, Umphisak Teeboonma

Department of Mechanical Engineering, Faculty of Engineering, Ubon Ratchathani University, Ubon Ratchathani, 34190, Thailand

ARTICLE INFO

Article history:

Received: 20 March, 2019

Accepted: 26 October, 2019

Online: 22 November, 2019

Keywords:

Adhesive

Roof tiles

Water hyacinth fiber

Mechanical properties

ABSTRACT

Problem statement: In general, the water hyacinth is a biennial aquatic plant for many seasons with propagated quickly to become serious weeds in general water sources. The water hyacinth is caused carbon dioxide in the atmosphere as a greenhouse effect, which leads to climate change, the environmental concerns of the world today. The agricultural residue materials are the most used manufactured material in the world through a lot of water hyacinth plant but a little is used efficiently. One approach to reduce agricultural waste and add value to them is to produce a fiber composite like roof tiles. Roof tiles are a product developed to replace natural fiber by mixing agricultural residues materials containing fiber such as rice straw, kenaf, corn cob, rice husk and palm fruit bunch. with adhesives, waterproof adhesives or other materials. **Approach:** This work is also aimed to investigate the influence of adhesive on roof tiles product from water hyacinth fiber. The urea-formaldehyde adhesive was added into the water hyacinth roof tile in 10%, 12%, and 14% weight ratios. It is then hot pressed and tested to determine physical, mechanical and thermal properties according to the industrial standard. Other factors are considered: temperature compression, the shape of roof tiles and distribution of moisture to roof tiles, heat transfer between sheets during compression, compression time, suitable compression and hardening before or after glueing of the adhesives. **Results:** The experimental observation revealed that the proportion obtained of 12% of the Urea-formaldehyde adhesive from the weight of the water hyacinth roof tile mixture, will absorb the adhesive better. **Conclusion:** With knowledge and technology, the roof tiles manufactured from water hyacinth can raise the quality of life as an innovative product for commercial utilization.

1. Introduction

The water hyacinth is a biennial aquatic plant for many seasons with propagated quickly to become serious weeds in general water sources, especially in Thailand and Southeast Asia. The weeding of water hyacinth plant residues causes carbon dioxide in the atmosphere as a greenhouse effect, which leads to climate change, the environmental concerns of the world today. The agricultural residue materials are the most used manufactured material in the world through a lot of water hyacinth plant but a little is used efficiently. One approach to reduce agricultural waste and add value to them is to produce a fiber composite like roof tiles.

Although water hyacinth is seen in many countries as a weed and is responsible for many of the problems outlined earlier in this fact sheet, many individuals, groups and institutions have been able to turn the problem around and find useful applications for plant.

The agricultural fiber residue materials are the most used manufactured material in the world through a lot of water hyacinth plant but a little is used efficiently. One approach to reduce

agricultural waste and add value to them is to produce a fiber composite like roof tiles. Roof tiles are a product developed to replace natural fiber by mixing agricultural residues materials containing fiber such as rice straw, kenaf, corn cob, rice husk and palm fruit bunch. With adhesives, waterproof adhesives or other materials.

The water hyacinth plant and adhesive are also contributed to higher heating bills. The increased density of the roof tiles will result in parts that are mixed with adhesive. If the roof tiles has low density, it will cause more rooms and make low thermal conductivity. On the other hand, if the extrusion roof tiles has higher density, it will get high thermal conductivity, while the heat resistance is low. However, the thermal conductivity of each materials also depends on the structure of the materials, in particular, crystalline shape and the temperature during the extrusion. As a result, the thermal conductivity differs from one material to others. [1]. The surface of building materials which expose directly to the outside air temperature and the sun light will absorb heat radiation. It makes this area get higher temperature than other surface areas. As a result, it causes the temperature differences between the outside air and the exposed surface of the exterior building materials. Thermal energy from

*Arkorn Pasilo, +668 3464 7155, arkom_pasilo@yahoo.com

this area is also transferred to some surface adjacent to a lower temperature by the amount of heat transferred in each direction based on the thermal resistance and the mass of the building. Agricultural fiber residues used as raw materials in the roof tiles product are rice straw, corn cobs, bagasse, pulp, kenaf, palm fruit bunch, and oil palm fiber [2-3].

This work is also aimed to investigate the influence of adhesive on roof tiles product from water hyacinth fiber. The roof tile containing different percentages 10%, 12%, and 14% of Urea-formaldehyde adhesive from the weight of the mixture as shown in Table 1. It is then hot pressed and tested to determine physical, mechanical and thermal properties according to the industrial standard. Other factors are considered: temperature compression, the shape of roof tiles and distribution of moisture to roof tiles, heat transfer between sheets during compression, compression time, suitable compression and hardening before or after glueing of the adhesives.

Table 1 : The specimens sample in this study

Specimens name	Adhesive : Fiber	Content (%)
A-1	Urea-formaldehyde	10
	Water hyacinth	90
A-2	Urea-formaldehyde	12
	Water hyacinth	88
A-3	Urea-formaldehyde	14
	Water hyacinth	86

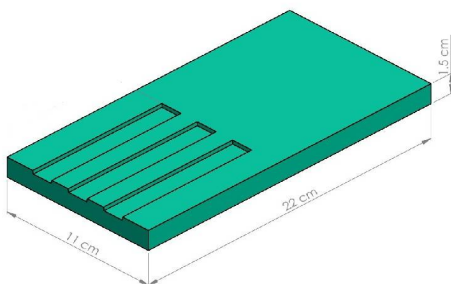


Figure 1. Illustrate the specimen size of roof tiles

2. Material and Methods

2.1 Materials

The water hyacinth fiber that using in this study

The illustrate of specimen size using of roof tiles in this study is 11 x 22 x 1.5 cm³, as shown in Figure 1.

The experiment was performed using the 100 TON universal testing machine as shown in Figure 2. The factors are considered:

- Water hyacinth fiber were cut into small size and moisture content of 2 - 5% after adhesive additions.
- 10%, 12% and 14% of Urea-formaldehyde adhesive content with 1% emulsion wax and 2% hardener chloride were thoroughly combined and sprayed onto the water hyacinth fiber mixture (Specimens name: A-1,A-2 and A-3). The adhesive coated water hyacinth fibers was spread evenly in the mold.
- The temperature compression at 150 °C, heat transfer between sheets during compression. The hot-pressed process under pressure of 180 kg/m². (12.41 bar), for 15 minutes.

- The shape of roof tiles, The weight of 533.7 grams and density of 600 kg/m³ were produced.
- The extrusion method is useful for the modelling and analysis of the problems which a response of interest is influenced by several variables and the objective is the optimization of yield. Which process of extrusion method follows in Figure 3.



Figure 2. The 100 TON universal testing machine

Summary Significance

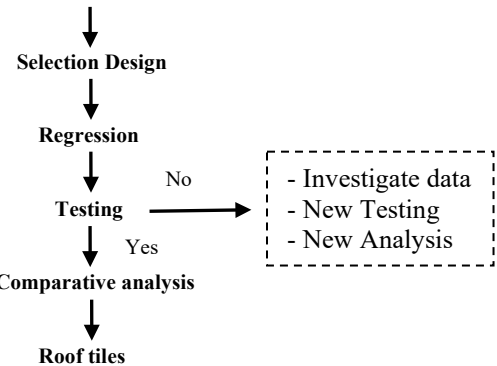


Figure 3. Process of extrusion method

2.2 Experimental procedure

The physical, mechanical and thermal properties were tested as follows. [4-5].

Physical properties testing: Density (D) was tested according to TIS 876-2547.

Mechanical properties testing: Modulus of Rupture (MOR) and Modulus of Elasticity (MOE) of roof tiles were according to TIS 535-2540.

Thermal properties testing: Thermal conductivity (K) was tested according to ASTM C 117- 2010.

And all the test was repeated on 3 specimens.

3. Results and Discussion

The presented laboratory results, the extrusion of roof tiles is according to the factors defined in all respects. Figure 3 shows the water hyacinth fiber residues deformation of roof tiles.

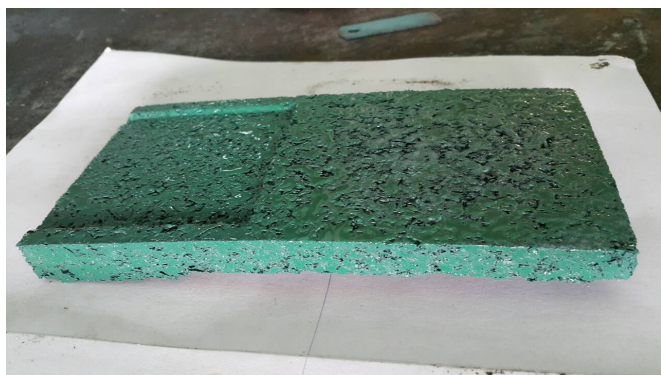


Figure 4. The deformation water hyacinth fiber of roof tiles

Table 2 : The summarizes of the roof tile containing the adhesive

Fiber	Adhesive Content (%)	D (kg/m ³)	MOR (MPa)	MOE (MPa)	K (W/m.K)
Water hyacinth	10	112.19	1.01	130	0.024
	12	581.31	225.75	44,500.10	0.098
	14	822.09	389.43	70,000	0.039

Table 2 summarizes the roof tile containing of 12% of Urea-formaldehyde adhesive from the weight of the mixture is best extrusion of roof tiles molded, with 10% being unable to be molded and 14% having too much density and strength. Due to the proportion obtained of 12% of the Urea-formaldehyde adhesive from the weight of the water hyacinth roof tile mixture, will absorb the adhesive better.

The results suggested that the roof tile containing different percentages 12% of Urea-formaldehyde adhesive is suitable ratio. This may be because the adhesive can hold with the water hyacinth fiber better than 14% and 10% respectively. In addition the roof tiles properties are suitable for the requirements such as density, strength and thermal conductivity. It is also found that the properties of the roof tiles according to the testing standards specification.

Table 3 : The results of roof tiles properties

Properties	Water hyacinth roof tiles (A-2)	Standard test
Density (D), kg/m ³	581.31	800
Modulus of Rupture (MOR), MPa	225.75	270
Modulus of Elasticity (MOE), MPa	44,500.10	68,000
Thermal conductivity (K), W/m.K	0.098	0.013

The results of properties were shown in Table 3. The physical, mechanical and thermal conductivity with water hyacinth fiber were investigated. It showed that the roof tiles of density do not pass the roof tiles specification. For the Modulus of Rupture (MOR) and Modulus of Elasticity (MOE) meet the requirements. However, Thermal conductivity (K) pass the standard. Anyhow, the roof tiles with increasing amount of water hyacinth fiber and adhesive have an issue of dissolving.

4. Conclusion

- The results are summarized as follows:
- The proportion obtained of 12% of the Urea-formaldehyde adhesive from the weight of the water hyacinth roof tile mixture, will absorb the adhesive better.

- Knowledge and technology, the roof tiles manufactured from water hyacinth fiber residues can raise the quality of life as an innovative product for commercial utilization.
- The potential further studies from the findings of this paper include the possibilities of using the roof tiles produced within the climatic characteristics and sustainability of the roof tiles produced [6].
- In the future, this is a roof tiles product to be benchmarked with industrial production process [7]. They are the economic analysis and the durability in exposing to sun light.

Acknowledgment

The authors would like to express their sincere thanks to Faculty of Engineering, Ubon Ratchathani University for financial support.

References

- [1] R.H. Myers and D.C. Montgomery, *Response Surface Methodology : Process and product optimization using designed experiments*, Forth ed, John Wiley & Sons Press, 2016.
- [2] Yan Li, Yiu-Wing Mai and Lin Ye, "Sisal Fibre and its composites: a review of recent developments" *Composites Science and Technology*, **60**, (2037-2055), 2000. [https://doi.org/10.1016/S0266-3538\(00\)00101-9](https://doi.org/10.1016/S0266-3538(00)00101-9)
- [3] Standard Test Method for Steady-State Heat Flux Measurements and Thermal Transmission Properties by Means of the Guarded-Heat-Flux Apparatus ASTM C177-10, *Annual Book of ASTM Standards*, 2010.
- [4] A. Pasilo, U. Teeboonma, "Development of roofing tiles manufactured from agricultural residues", 11th Conference on Energy Network of Thailand (E-NETT): 1142-1148, Chonburi, Thailand, 2015.
- [5] A. Pasilo, U. Teeboonma, "Investigation of the properties of roofing tiles manufactured from agricultural residues" in 2016, International Conference on Advanced Material Science and Mechanical Engineering, (AMSME -E140): Central Station Hotel, Bangkok, Thailand, 2016.
- [6] Ahmad Al Yacouby, Mohd Faris Khamidi, Muhd Fadhil Nuruddin. and Syed Ahmad Farhan. "Study on roof tile's colors in Malaysia for development of new anti-warming roof tiles with higher Solar Reflectance Index (SRI)", *Progress in ResearchGate*, September, 2011. <https://doi:10.1109/NatPC.2011.6136358>
- [7] Peter O. Akadiri, Ezekiel A. Chinyio and Paul O. Olomolaiye. "Design of A Sustainable Building: A Conceptual Framework for Implementing Sustainability in the Building Sector", *Buildings*, ISSN 2075-5309, **2**, (126-152), 2012. <https://doi:10.3390/buildings2020126>

Intelligent Wireless System for PV Supervision Based on The Raspberry Pi

Youssef Bikrat*, Khalid Salmi, Kamal Azghiou, Ahmad Benlghazi, Abdelhamid Benali, and Driss Moussaid

Electronics and Systems Laboratory, Faculty of Sciences, Mohamed First University, Oujda, Morocco

ARTICLE INFO

Article history:

Received: 31 March, 2019

Accepted: 04 October, 2019

Online: 22 November, 2019

Keywords:

Monitoring system

Photovoltaic

Raspberry Pi3

Wi-Fi

Bluetooth

Transfer

Processing

Acquisition

ABSTRACT

Photovoltaic systems and monitoring go hand in hand. There is no better way to check the health of your photovoltaic system than to utilize a remote monitoring system. Monitoring and tracking of photovoltaic systems are crucial for reliable functioning and optimal yield of any solar electric system. This paper aims to introduce a remote electronic monitoring system. The said system will allow us to retrieve, process and transfer, in real-time, the photovoltaic station data remotely. The main objective of this work is to build a robust system that could be said as a reliable and low-price system, which will allow the transfer of the installation state to the remote operator in real-time or store it on an online database. Our intelligent wireless system is contained two parts, the first part including a hardware system designed around a microcontroller card (the Raspberry pi3 card) and a second part including the software part, which is the installation and configuration of open source applications on the Raspberry card. On the other hand, the configuration of an online database is presented. The database will offer us the possibility to store and process the station's data remotely and in real-time. Moreover, we also developed an application that plays the role of an interface for our monitoring Raspberry Pi3 machine.

1. Introduction

Renewable energies (REs) are a set of means of generating energy from unlimited (on a human scale) sources or resources, available without time limits or recoverable more quickly than they are consumed. Renewable energies are often spoken of as opposed to fossil fuel energies, whose stocks are non-renewable and limited: coal, oil, natural gas. The renewable energies are unlimited which produced from many sources such as the wind and the ray of sun [1].

REs are often referred to as "clean energies" or "green energies". The environmental effect of their operations is very low which makes them a major element in companies' Corporate Social Responsibility (CSR) strategies in terms of sustainable development. The exploitation of renewable energies theoretically generates few pollutants: in particular, electricity of renewable origin emits very little CO₂ especially when compared to fossil fuels such as coal. For this reason, renewable energies are a particular vector of the fight against global warming. They are also considered as a factor of resilience because they allow decarbonized and decentralized productions.

There are different energy sources that produce several types of renewable energy. Maybe the most known is still the solar

energy. This type of energy comes directly from the capture of radiation coming from the sun. Specific sensors are used to absorb the energy of the solar radiation and rebroadcast it according to two main modes of operation:

- Solar photovoltaic (solar photovoltaic panels): solar energy is captured for the production of electricity.
- Thermal solar (solar water heater, heating, solar thermal panels): solar heat is captured and is redistributed, and more rarely used to produce electricity.

The global market stagnated last year, with around 98 GW deployed. For 2019, the experts expect stronger solar growth, PV Market Alliance warned its forecast for 2019 that global solar installations would grow by about 20% to as much as 120 GW, and volume of 180-200 GW by 2022 [1].

In the recent years, Morocco has engaged in a strategy of alternatives energies, all determined to move from a country importing all its oil and gas needs to major producer renewable energy (figure2), whereas it depended totally, and until a near past, of the outside for the energies needs.

Through its renewable energy development strategy, Morocco aims to ensure its relative energy independence, contribute to

* Youssef Bikrat, Email: y.bikrat@ump.ac.ma

reducing emissions and produce renewable energy that will shape the future of human consumption.

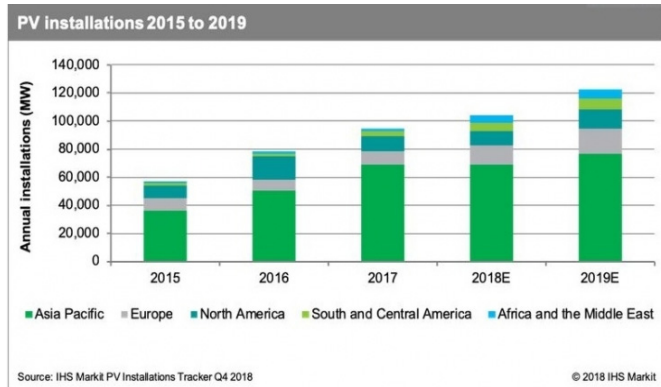


Figure 1: The global solar PV market will grow stronger than expected according to IHS Markit.

The kingdom has made tremendous progress in the field of green energy since 2009 and has set ambitious goals in the field of clean energy. The Moroccan strategy aims to increase the share of renewable energies to 42% by 2020 and 52% by 2030. In addition to the goal of reducing energy consumption to 12% by 2020 and 15% thanks to energy efficiency[2,3].

For this reason, the average power in next-generation installations is increasing day by day, with the need for systems capable of supervising and monitoring installations in a permanent form and interacting with all elements, thus ensuring a high level of optimal efficiency, from a technical as well as an economical point of view. At this point, it is essential to develop new infrastructures and technologies, to install remote monitoring system that allows a significant reduction in time response and keeps track on the PV energy production from a given PV plant[4].

The supervision, or monitoring, of isolated PV plants makes it possible to evaluate the quality of operation of the system and, conversely, to detect possible anomalies. It is generally composed of a data acquisition and storage system, a signal processing or analysis software, and a display. In some cases, the system is coupled with sunshine and temperature probes. Many PV inverter manufacturers offer their own monitoring connected to their inverter. Most often the data acquisition system is integrated into the inverter and its consultation is done by dedicated software. Sometimes, the supervision is composed of a datalogger which makes it possible to centralize the data of several inverters and possibly to make them accessible remotely via internet.

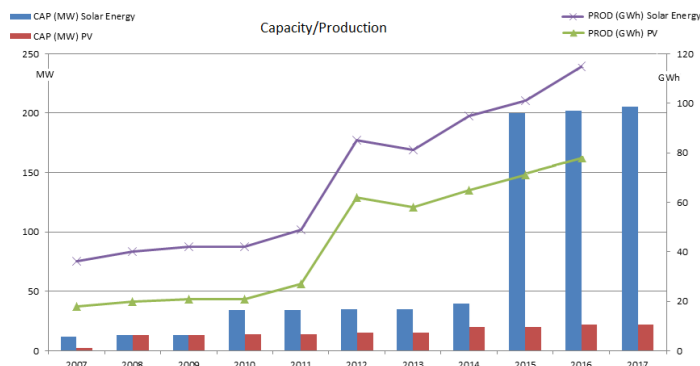


Figure 2: Photovoltaic energy development in Morocco.

Our objective in this article is to present the developed wireless monitoring system. The process is divided into two parts; the first part is the description of the used hardware mainly built around the Raspberry Pi3, the second part is the software development including the installation and the configuration of open source applications to settle the incompatibilities problem with open source systems. The proposed monitoring system will communicate with the inverter to retrieve, transfer and process data using a new open-source application in a completely remote and wireless way.

The paper is divided into three sections. We will start with a discussion on the encountered problematic and propose an adequate solution. The second section describes the choice of equipment for the designed system to meet the desired requirements. Finally, the last section presents our proposed wireless system for monitoring photovoltaic plants. The system is divided into three main parts: The data acquisition from the inverters via Bluetooth, the data processing in Raspberry Pi3[5] and the data transfer via Wi-Fi.

2. Problematic

There are different solutions to monitor the production and operation of an inverters or photovoltaic panels. The main selection criteria and questions to ask are:

- What information and settings will be saved and viewed?
- How will this information be saved and how will it be consulted?
- What will be the sources of the information: electricity meters, inverters, datalogger?
- What is the cost of the production tracking and monitoring system?

Nevertheless, the existing PV monitoring applications in the market are limited and incompatible with most of the operating systems. Moreover, the manufacturers of power plants tend to design systems that do not meet the desired constraints and contain some drawbacks [6].

2.1. The encountered situation

The situation we have is a PV installation composed of SMA electrical inverters [7] connected to six photovoltaic panels. The inverters allow the transformation of the generated direct current into an alternative current. In our photovoltaic system, these inverters are provided with a measurement and processing system, allowing the storage in real-time of data related to electricity generation.



Figure 3: The need of the operator presence in the field to retrieve data

The recovery of stored data can be provided in two ways; either via wireless Bluetooth or wired Ethernet. Practically, this monitoring system has a major issue: regardless of the used recovery method, there is always a need for an operator to be in close contact with the installation (figure 3). While the Bluetooth offers a wireless connection to the inverters, it does not allow real-time data recovery from distant locations.

2.2. Objectives

The main objective of this work is the development of a PV monitoring system to transfer data in real-time to a remote operator. To implement such a system, we should be ensuring the following points:

- A communication with the inverters via Bluetooth protocol.
- The data recovery in Bluetooth mode.
- The pre-treatment of data with SBF application.
- The wireless transfer of data to the server via WiFi.
- The data visualization by the operator in real-time via the Internet.
- The creation of a web interface for the storage and processing of retrieved data on the supervision machine.

The proposed system will provide us with a wireless communication to the inverters via the Bluetooth protocol. Once received, the data will be pretreated then transferred to the remote control machine through the network via Wi-Fi or directly stored in an online database (figure 4).

3. Equipment

3.1. Comparative study

The choice of equipment was constrained by some specifications.

The recommended equipment should:

- Have a reasonable price;
- Support the Bluetooth and the WiFi protocols;
- Have at least a 1 GHz CPU and a 1 Gb RAM;
- Card compatible with the most popular operating systems;
- Have a rich library and documentation.

There are multiple variants of nano-computer on the market that, relatively, encounter those conditions such as Orange PI, Odroid, Banana Pi M3, Raspberry Pi3 and Arduino. We chose the Raspberry Pi3 card after a comparative study, because it is the most appropriate among all the other cards[7].

Indeed, the Raspberry Pi is the undisputed heavyweight champion of the world. Beside it is most powerful, the most compact, and the cheapest; its devotees are legion, several developers use it in several projects, which means that its use is more convenient than others are.

3.2. Raspberry Pi

The main component on which our system is built is the Raspberry card.

The Raspberry Pi3 is a small integrated computer in the size of the hand, with a price not exceeding 40 \$ and most-lowest power consumption, less than 5 Watt. Designed at the University of Cambridge to help to teach programming, electronics and intelligent control systems at the same time. Its performance making this nano-computer astonishing success in both the educational and applied fields [5].

It works not only with numerous variants of Linux operating system but also with Microsoft Windows OS such as Windows 10 and phone operating systems.

Numerous versions of Raspberry Pi3 have been made from the time when the original Model B was created, each bringing either upgraded specifications or features specific to a particular use-case. All models feature a Broadcom on Chip (SoC) system and are compatible with a 700 MHz to 1.4 GHz compatible CPU and an integrated memory ranging from 256 MB to 4 Gb.

For our choice of equipment, our electronic and computer system is based on Raspberry Pi3 (figure 5), its performances are:

- 1.4 GHz processing CPU
- 1Gb RAM
- Wi-Fi 802.11n (150 Mbit/s) and Bluetooth 4.1 (24 Mbit/s)

3.3. Operating System

Like any computer system, the Raspberry Pi requires an operating system OS to work. Choosing an operating system is difficult task. The choice is based on the needs of the user but also on his tastes and preferences. It is thus difficult to say that such a system is the best. But for our case the adequate OS is Raspbian.

Raspbian is the reference OS for Raspberry Pi. It is based on Linux Debian and is updated very regularly. Optimized specifically for Raspberry Pi, it is a versatile distribution.

The greatest strength of Raspbian is not even the OS itself but its community and its reputation well-known by developers around the world [7].

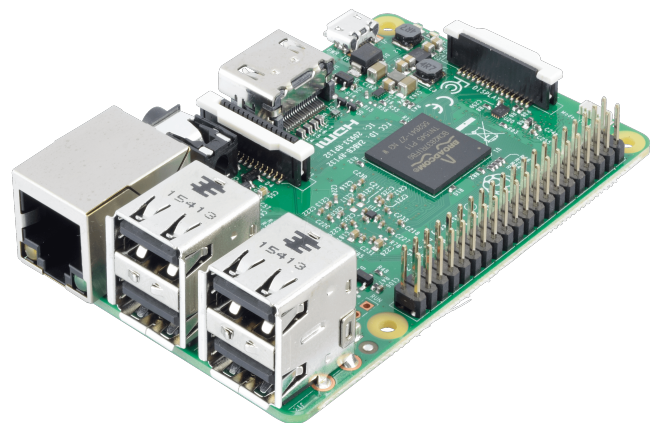


Figure 4: Raspberry Pi3

4. Overview of the proposed PV wireless monitoring system

Our proposed electronic and computer system (software and hardware) is constructed around six photovoltaic panels and their inverters. Each inverter is equipped with a Bluetooth module that will communicate with the Raspberry Pi3. This latter plays the main role of putting the link between the inverters and the servers in order to retrieve the data and store it directly in on line database (figure 6).

The installed wireless monitoring, give us the measurement of several quantities parameters by which we can qualify our panels performances. The quantities measured are Current, Voltage, and Energy as electrical parameters. Illumination and Temperature as metrological parameters.

Three parts are included in our proposed wireless monitoring system, which are:

- The data acquisition.
- The data processing.
- The data storage and transfer.

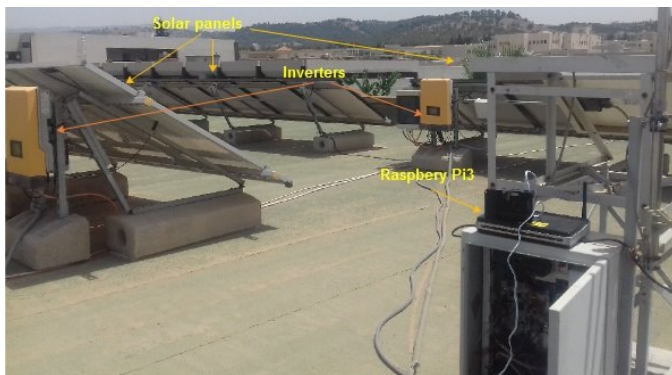


Figure 6: Prototype of our wireless PV monitoring system

4.1. Data acquisition

As stated in the second section, the inverters are associated to a system of storage of several parameters in real time. Our system will retrieve it remotely via Bluetooth Protocol.

Bluetooth is a radio communication; this type of technology does not require a large amount of energy. Bluetooth technology starts by generating radio waves. The value of frequency, when generated, is 2.45 GHz, a universally recognized value for industrial, scientific and medical devices. It is possible to establish several connections using Bluetooth in the same area; this will not affect them because there are different frequencies for each device at different times, called scattered frequency hopping. This technology allows the use of more than 79 frequencies randomly in a certain area. Note that the value of the frequency changes constantly, which means that the value of the frequency will be submitted 1600 times per second by a Bluetooth device, as result the radio spectrum will benefit a group of peripherals.

The Bluetooth is a protocol with Master/Slave architecture. Master has to connect with up to seven slave simultaneously, which call piconet. In the piconet there are up to 255 slaves in

parked mode. Thus, give us the chance to connect many inverters [8].

4.2. Data processing

For the data processing step we use the either Windows Sunny Explorer or SBFSpot [9].

The installation of the Sunny Explorer application is now possible after the launch of the Windows 10 operating system on the ARM platform of Raspberry PI3, which resolves our old compatibility problem between Windows applications and the ARM architecture.

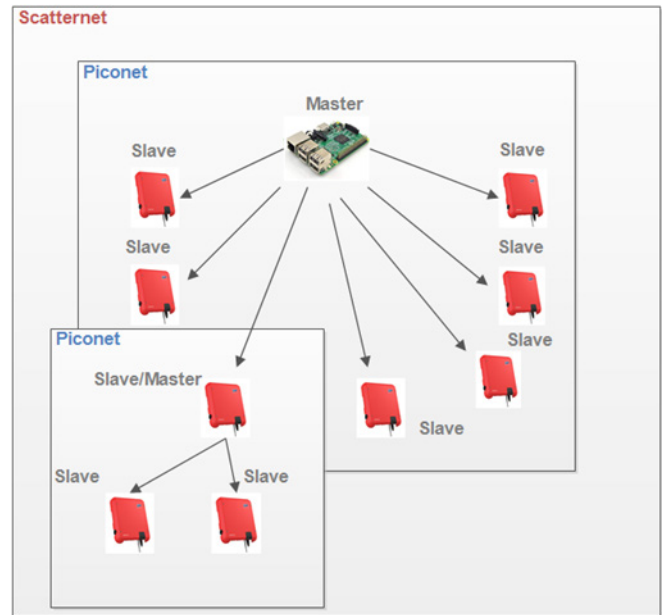


Figure 7: Organization of a Bluetooth network into scatternet and piconet

The proposed alternative is to use the SBFSpot application and the PVOutput [7] is an open source project to get actual and archive data out of the inverters over Bluetooth, it allows retrieving data from the inverters via Bluetooth, while the PVOutput stores the data and processing them into graphical figure. We also note that we developed our own interface application for the results visualization.

Finally, by those applications we are allowed to process the received data from our station (figure 8).

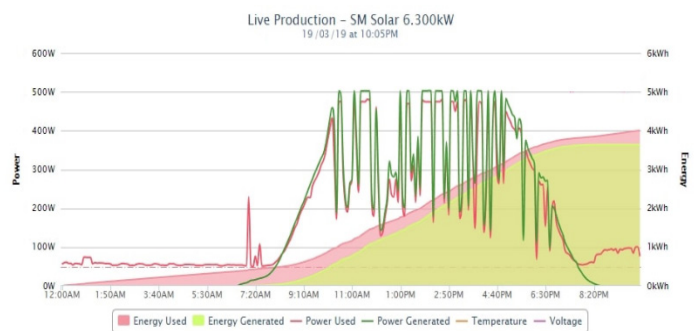


Figure 8: Different electrical parameters retrieved from the PV installation

4.3. Data transfer

The next phase is to transfer processed data to the control machine via Wi-Fi. We have two situations for control our power station. The control machine is either inside the institution or outside of it. For each situation, we used different secure method of transfer: SSH, secure and simple method of transfer. VNC virtual network computing, secure and complex graphical method.

Both methods require the installation of a server on the Raspberry PI3 card and a client on the control machine.

Data transfer via SSH

SSH [10], or Secure Socket Shell, is a network protocol that allows administrators to remotely access a computer in complete security. The Secure Shell protocol is a compensation of the previous protocol Telnet service where the transfer of information was open and vulnerable; allowing users of certain programs to spy on sensitive information such as username and password, while SSH is more powerful than its predecessor by encrypting the data transmitter between the user and server.

SSH is an open source application that allows you to open a terminal session on Raspberry PI3 from a command line on the host computer. By default, SSH is installed on the Raspberry PI3, but is disabled for security reasons. The first thing to do is to activate SSH on your Raspberry PI3. For that, you just have to connect the MicroSD card of Raspberry Pi on our computer, to go on the map, and to create a file named ssh in the boot partition, then install the SSH client on the control machine using the PuTTY emulator.

Data transfer via VNC

To control remotely in full desktop we use VNC [11].

VNC, or Virtual Network Computing, is a protocol that allows distant control of one computer by another. When using VNC, two different parts of the software are used.

The first part is the VNC server is installed on the Raspberry Pi3 side. The second part is the VNC client. It is installed on the control machine side, by which we will control and connect to the server to execute our requests remotely.

After installing and enabling VNC server by SSH command. Now we should simply put the address of our card in order to get remote graphic control of the raspberry desktop.

On the other hand, the choice of the machine address is related to the previous situations, either outside the institution and inside of it. If the control machine is inside so we used the RealVNC with a private IP address, , while if the machine is outside, we will need to use RealVNC with a pair containing a public IP address and a specified port assigned to the private address of the Raspberry card. In the case of a dynamic public address, use the dynamic No-IP DNS service.

5. Conclusion

In this article, we proposed the design and tests of a wireless monitoring system from a remote location based on three layers: the acquisition, the processing, and the storage and web service layers. The proposed system comes as a more compatible, flexible, and powerful system by solving the faults in our old system.

The main advantage of this supervision system is that it is a low-cost and low-power system with highly scalable software. The system is built around a nano-computer (the Raspberry PI3 card), a wireless protocol (Wi-Fi and Bluetooth) and an open-source application. Thus, providing us with a connection to the inverters and process the received data remotely and finally present them directly on our processing machine.

After some modifications and improvements, the proposed remote system, and the implementation of the application. Our system of monitoring has been validated and successfully tested by field trials.

Conflict of Interest

The authors declare no conflict of interest.

References

- [1] Y. Bikrat, K. Salmi, A. Benlghazi, A. Benali, and D. Moussaid, "A Photovoltaic Wireless Monitoring System," in *IEEE/2018 International Symposium on Advanced Electrical and Communication Technologies (ISAECT)*, 2018, pp. 1–5. <https://doi.org/10.1109/ISAECT.2018.8618825>
- [2] O. Ellabban, H. Abu-Rub, and F. Blaabjerg, "Renewable energy resources: Current status, future prospects and their enabling technology," *Renewable and Sustainable Energy Reviews*, vol. 39, pp. 748–764, 2014. <https://doi.org/10.1016/j.rser.2014.07.113>
- [3] A. Tazarine and H. El Omari, "Designing of a photovoltaic system for self-consumption at the faculty of technical sciences of Settat," in *Proceedings of 2016 International Renewable and Sustainable Energy Conference, IRSEC 2016*, 2017. <https://doi.org/10.1109/IRSEC.2016.7984025>
- [4] M. Hochberg, "Renewable Energy Growth in Morocco An Example for the Region Renewable Energy Growth in Morocco," 2016.
- [5] G. M. Tina and A. D. Grasso, "Remote monitoring system for stand-alone photovoltaic power plants: The case study of a PV-powered outdoor refrigerator," *Energy Convers. Manag.*, 2014. <https://doi.org/10.1016/j.enconman.2013.08.065>
- [6] Raspberry Pi Foundation, "Raspberry Pi 3 Model B," Datasheet, 2016.
- [7] Y. Bikrat, D. Moussaid, A. Benali, and A. Benlghazi, "Electronic and computer system for monitoring a photovoltaic station," in *IEEE/2018 International Conference on Intelligent Systems and Computer Vision (ISCV)* <https://doi.org/10.1109/ISACV.2018.8354018>
- [8] J. DeCuir, "Introducing Bluetooth Smart: Part 1: A look at both classic and new technologies," *IEEE Consum. Electron. Mag.*, vol. 3, no. 1, pp. 12–18, 2014. <https://doi.org/10.1109/MCE.2013.2284932>
- [9] R. Pi, "Changelog of SBFspot install on a Raspberry Pi Preparing the Raspberry Pi for SBFspot," 2014.
- [10] F. Bergsma, B. Dowling, F. Kohlar, J. Schwenk, and D. Stebila, "Multi-Ciphersuite Security of the Secure Shell (SSH) Protocol," in *Proceedings of the 2014 ACM SIGSAC Conference on Computer and Communications Security - CCS '14*, 2014, pp. 369–381 <https://doi.org/10.1145/2660267.2660286>
- [11] T. Tan-atchat and J. Pasquale, "VNC in high-latency environments and techniques for improvement," in *GLOBECOM - IEEE Global Telecommunications Conference*, 2010. <https://doi.org/10.1109/GLOCOM.2010.5683953>

A Word Spotting Method for Arabic Manuscripts Based on Speeded Up Robust Features Technique

Noureddine El Makhfi*

Faculty of Science and Technology, Department of Mathematics and Computer Science, PMIC Lab, 32003, Al-Hoceima, Morocco

ARTICLE INFO

Article history:

Received: 15 August, 2019

Accepted: 07 November, 2019

Online: 22 November, 2019

Keywords:

Arabic calligraphy

Arabic handwritten documents

Cultural heritage

Digital libraries

Features extraction

Text-Image format

Segmentation

Word matching

Word spotting

ABSTRACT

The diversity of manuscripts according to their contents, forms, organizations and presentations provides a data-rich structures. The aim is to disseminate this cultural heritage in the images format to the general public via digital libraries. However, handwriting is an obstacle to text recognition algorithms in images, especially cursive writing of Arabic calligraphy. Most current search engines used by digital libraries are based on metadata and structured data manually transcribed in Ascii format. In this article, we propose an original method of pattern recognition for searching the content of Arabic handwritten documents based on the Word Spotting technique. Our method is both effective and simple, it consists in extracting a set of features from the words we segment in the target images and comparing them with the features of the words in the requested images. The principle of the method is to characterize each word with the Speeded Up Robust Features algorithm whose goal is to find all occurrences of query words in the target image even in the case of low-resolution images. We tested our method on hundreds of pages of Arabic manuscripts from the National Library of Rabat and the Digital Library of Leipzig University. The results obtained are encouraging compared to other methods based on the same Word Spotting technique.

1. Introduction

This article is an extended version of an oral communication presented in 2019 at the 5th International Conference on Optimization and Applications (ICOA2019) [1].

Virtual libraries, developed by research institutions, are a means of preserving documentary heritage in the form of images. The old manuscripts preserved in these libraries are consulted by a minority of people because of the image content that is inaccessible by search engines. Some techniques used for indexing manuscript images include metadata, annotation and transcription.

Metadata provides a means of describing the content of manuscripts in image form. On the other hand, the transcription or annotation of manuscripts offers an alternative to partially deepen the search in the content of the images. However, these techniques are very limited in requiring a considerable effort to reproduce the content of images in text format (ASCII) and do not offer a thorough and complete search. We find that copiers use the same writing style in old manuscripts. Each word or element (letter, pseudo word, calligraphy, etc.) is repeated several times in the corpus of Arabic manuscripts. In the absence of photocopiers at

that time, most Arabic manuscripts are reproduced several times by the same copiers with the same styles of Arabic calligraphy (Naskh, Kufi, Diwani, Thuluth, Roqaa, etc.)

The idea is to reduce the number of elements to be transcribed manually when entering the content of images in Arabic manuscripts that use the same writing style. Our objective is to compare elements (content) of Arabic manuscripts based on a robust method. Comparing the content of manuscript images requires a multi-step process, each word or element being characterized by a unique signature. This signature must be invariable and must adapt to changes in scale, rotation, geometric variations and illumination. The extraction of the features of words or elements in the form of a signature, thus facilitates the automation of annotations or the complete transcription of Arabic manuscripts. Several research studies have been carried out in the field of access to the content of manuscripts in image form. However, most of this work is based on binary images, which results in a huge loss of information in the images. To overcome this problem, we used grayscale images to extract useful features in Arabic manuscript images. To this end, we have based ourselves on multi-scale theory using grayscale images to ensure maximum reliability when extracting all the features of the segmented words.

*Noureddine EL MAKHFI, Email: n.elmakhfi@gmail.com

In this paper, we present an original method for identifying the content of Arabic manuscript images. This method is based on the Word Spotting technique which allows the search for similar words in a target image to that of a query image. We used the Speeded Up Robust Features algorithm (SURF) [2]. This algorithm allows to extract the features of the images based on local invariant descriptors / detectors (at scale changes, rotation, luminosity variations, etc.). The SURF algorithm is known in an area of computer vision with its robustness and speed to detect and describe points of interest in 2D images. Arabic manuscripts presented in image form contain information that is repeated several times. The Word spotting technique we use allows us to search for similar words in the same manuscript in order to facilitate its identification, indexing or transcription.

2. Related Work

There are several recent projects, allowing the cataloguing and digitization of ancient manuscripts based on the metadata technique. We can mention the project called "Cultural Heritage" of the Digital Library of the Leipzig University [3]. This is a project aimed at the online dissemination of Arabic, Turkish and Persian Islamic manuscripts. The presentation of these manuscripts is in the form of high definition images, in different formats. Indexing and searching in the databases of this digital library are in Trilingual services (German, English, Arabic). Most of the current research work is focused on researching the content of manuscript images. Among the most commonly used methods, the Word Spotting technique which allows the identification of words in images. There are recent studies that address the problem of indexing manuscripts and the recognition of cursive writing, namely:

In several studies [4-9], the authors treat the Word Spotting technique as regions of interest composed of words in which each character follows its model. The indexing and recognition of words are done by a probability calculation of regions of interest formed by characters. Each candidate region of interest is classified using one of the following methods: Dynamic Time Warping (DTW) or Hidden Markov Models (HMM) [10]. Despite the possible changes in words caused by character models, the results are interesting. Another work [11] which concerns the search for words based on annotations in medieval manuscripts. The techniques used are the basis of the Neural Networks (NN) and Hidden Markov Models (HMM) methods. The major problem with this method is the manual aspect of the production of annotations or transcription.

Other works that deal with word search based on the measure of similarity. The words, images are characterized according to their shapes using generic descriptors [12]. Among the shape descriptors that is used for word detection we can mention Histogram of Oriented Gradients (HOG) [13]. This description provides a means to describe and detect characteristics of handwritten words in [14].

In recent works [15-19], word detection is based on the SIFT algorithm [20,21]. This SIFT descriptor uses points of interest to describe the shapes of the words to be detected. The main problem with this technique used for word detection is the execution time and the false matching of the interest points of the images. Despite the excellence of the method for characterizing image words, like

what is done in computer vision for the detection of 3D objects. The limitations of this method for word detection in 2D images can be improved by inserting other steps such as pre-processing.

In the general case, methods for detecting objects in images are represented by several research projects, particularly those in the field of image processing and computer vision. These methods are classified according to three approaches: contour, model-based and local extrema detection.

The first approach provides a means to detect storytellers based on the location of the shapes of the objects in the image. This approach exploits the geometric properties of objects in the image as corners to detect storyteller points. The second model-based approach provides a mapping of a theoretical model to points of interest in the intensity function. The latter approach provides a means to characterize and detect local extrema. Each extremum corresponds to points of strong intensity variations in the image.

2.1. Contour approach

The H. Moravec [22] detector is one of the older ones used for the interest points. This type of detector is highly dependent on containers and its major problem is its sensitivity to noise.

An advanced version of the H. Moravec detector by C. Harris and M. Stephen [23] is named the Harris detector. It's a corner detector. It is invariable to translation, to rotation. However, it does not provide good results in the case of change of illumination. Further improvements to the Harris detector were made by Mohr and Schmid [24]. P. Montesinos [25] has developed this detector to process even colour images. Other improvements were made by Y. Dufournaud [26] to make this detector invariable to changes in resolution. A highly advanced version of the Harris detector was developed by Mikolajczyk [27] to detect points of interest in scale space. This method consists of using Gaussian smoothing to get the points that have a local maximum in the scale space. A further improved version of the Harris detector that is invariable to affine transformations was developed by Harris-affine [28].

2.2. Theoretical signal model approach

The theoretical signal model approach was developed by Schmid [22]. It consists in bringing together shapes of objects in images with theoretical signal models to obtain more sub-pixellic precision. This approach allows to locate points in the shapes of complex objects and not only for corner detection. Rounded shapes such as circles and curves present an obstacle for corner detectors. Rohr [29, 30] developed a blur model based on the convolution of a Gaussian with a binary model to detect the junctions of lines. This model is based on several parameters for corner angles, namely the orientation of the symmetry axis and the opening. This model is also based on dot position, grayscale and blur. The adjustment of these parameters allows to obtain a theoretical signal approximating the observed signal in such a way as to obtain a result closer to the real. Corner detection is based on the least squares method in order to minimize parameters by offering a more precise model.

R. Deriche and T. Blaszk [31] optimized the processing time with the improvement of the Rohr method. The principle of their methods is based on the exponential function instead of using the Gaussian function. P. Brand and R. Mohr [32] improved

localization quality based on a theoretical model close to the signal by fine transformation. This reconciliation is performed with alignment tests, epipolar geometry calculation and 3D reconstruction. The authors announce that test results can achieve an accuracy of 0.1 pixels.

G. Giraudon and R. Deriche [31, 33, 34] proposed a theoretical corner model to increase detection accuracy. This model is used to track the behaviour of each detector. The authors demonstrated the relationship between responses in scale space and the position of the actual characteristic.

2.3. Approach based on local extrema

The approach based on local extrema allows to locate points of interest in the corresponding scale space. Several detectors have been processed in the literature and are widely used to locate local extrema. We quote some methods for detecting points of interest to characterize objects in the image:

T. Lindeberg [35] among the first who worked on scale space. The automatic scale detection method is used to characterize the points detected at the corresponding scale. The detected points are located at the maximum magnitude of the Laplacian. They correspond to the peak points of the scale characteristic of the associated local surface. This scale is determined in the main direction of dominant curvature.

The Scale Invariant Feature Transform (SIFT) method is presented by Lowe in [20, 21]. This method is based on the detection of points of interest corresponding to the local extrema. The principle of the method is based on the differences of the Gaussian DOG to detect invariable robust points in corresponding scales.

A study realised by Mikolajczyk and Schmid [36], proposed a method for the detection of invariable points of interest called Harris-Laplace. It is based on the former Harris detector, thus providing a localization of the local extrema. This method allows to keep only the local extrema at the neighbourhoods of the characteristic ladders in the form of invariable robust points of interest.

Another study realised by H. Bay et al [3], proposed a point of interest detection method based on the Speed Up Robust Features (SURF) algorithm. The method is also based on the location of local extrema as the other methods mentioned above: SIFT [21] by Lowe and Harris-Laplace [36] by Mikolajczyk. The authors of the SURF method have shown that their algorithm is more powerful, more robust. SURF's response time is largely optimized compared to the two SIFT and Harris-Laplace algorithms.

A recent study was developed by B. Bagasi et al. [37], It concerns the comparison between the SURF algorithm and the BRISK algorithm [38]. This is a study that deals with searching for images by content. It concerns the search for images by similarity in manuscript images without segmentation.

3. The Proposed Method

OCR optical character recognition software allows the conversion of characters in the image into the code (ASCII). These OCRs are only valid for printed text even though the recognition rate is not optimal for Arabic printed characters.

In this paper, we propose a method of searching the text in images of Arabic documents like that used in images of Latin manuscripts. In this context, due to the lack of methods for recognizing

manuscripts, it is difficult to access their content in image form. Annotation or transcription techniques require considerable effort when entering text equivalent to the content of manuscript images. For this reason, these techniques can be automated by adding the Word Spotting method. Our goal is to facilitate the identification of the words in each scanned manuscript in the form of images. It is a question of characterizing by a signature each handwritten element (word, pseudo-word, letter). This signature must be unique for words that are identical. The objective is to eliminate redundancies in repeating elements.

3.1. Principles of the proposed method

The method of identifying and searching for Arabic handwritten elements is illustrated in schematic form by a block diagram. We have an input target image containing one page of a manuscript and two types of input queries for which the proposed method uses the text query or image query containing the word to be searched. In the case, of the text entry that is common, we used a database in XML format containing the features of the words of each manuscript processed. In case the input is in the form of an image, we use the direct extraction of the features of the request image. In other words, our method is based on text-image matching for identification of the contents of the manuscripts. In the following we deal with the case of comparison of input query images with a target image.

After the feature comparison operations, the results are provided in a final step as an output, thus locating the detected words. The following figure shows a block diagram of the proposed Word spotting method:

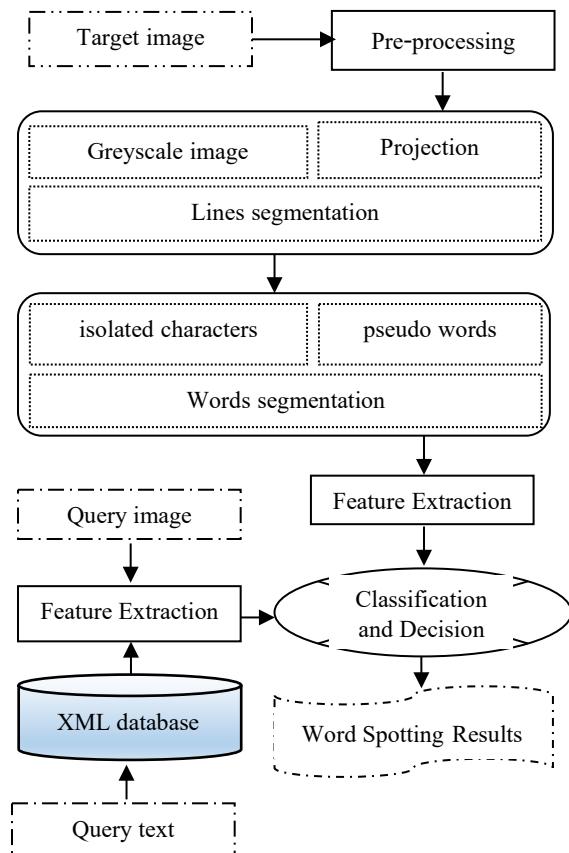


Figure 1: Synoptic diagram of the proposed Word Spotting method

• Acquisition and pre-processing

The first step is the acquisition of the manuscript in image form. Professional scanners make it possible to provide images with acceptable resolutions without damaging the manuscripts by the light emitted during scanning. Most often we obtain an image that contains two pages (left and right) in its raw state. We used as test images, manuscripts from the BNRM National Library in Rabat, Morocco. We also used images from a database of the Refaiya family [39] at the library of the University of Leipzig. The following figure shows the test image we used.



Figure 2: Original image [39]

After scanning, a series of pre-processing is required. Knowing that the scanned images are in their raw state in folders. Raw images take up a lot of space on storage disks. Image compression is necessary to reduce the storage capacity on the disk and speeds up processing time. Most of the professional scanners dedicated to manuscripts contain software and image processing algorithms. Other pre-processing must be applied to manuscript images such as: straightening, curvature correction, level spreading, contrast enhancement or detail enhancement, etc.



Figure 3: Left and right pages after pre-processing

In this article, we used the image on the right-hand side of the page. In most cases, Arabic manuscripts are written in different colours. We see in this example, that we have the colours of the red and black writing. The purpose of extracting text from the physical medium without losing important information. Colour segmentation of the image is an effective solution. It consists in selecting the pixel ranges in different colour layers. The most appropriate solution for our case is to segment each layer of the image separately and to assemble these layers with threshold values used. The HSV (Hue, Saturation, Value) space offers a simple way to detect thresholds. It allows easily distinguish intensity, saturation and hue.



Figure 4: Colour segmentation

• Line segmentation

The Word Spotting method requires a line segmentation [40] and subsequently a word segmentation to be able to locate the words to be searched in the image. In the first step, we will convert the colour image to a grayscale image whose purpose is to have a 1D signal. The projection algorithm [41] provides an effective way to facilitate line detection despite its sensitivity to noise. In this case, we use grayscale images instead of binary images because the projection of binary images [42] is very sensitive to line overlaps. It is widely used in the case of printed text because of the remarkable spacing between the lines. For our case, the projection of the grayscale image is represented by summing the intensity I at the coordinates of the image (x,y) to have the function of $f(y)$ according to the following relation:

$$f(y) = \sum_{x=0}^w I(x, y)$$

The function $f(y)$ represents the projected profile of image I . The calculation of the sum of pixels x along the y -axis is shown in Figure 5. Smoothing is essential to remove additional noise from the $f(y)$ function. The convolution of a Gaussian with this function allows to filter the high frequency noise as in [41].

$$p(y) = f(y) * g(y, \sigma)$$

$$g(y, \sigma) = \frac{1}{\sigma\sqrt{2\pi}} e^{-\frac{y^2}{2\sigma^2}}$$

The grayscale image projection profile provides several useful information about the text in the image. It allows to illustrate the various characteristics like the basic lines (minima), the heights of the lines and the background of the image (maxima). In this case,

the texture effect is not considered because we have added a pre-processing step as a colour segmentation. The maxima noted on the curve represent the spacing between the lines. The maxima (local) can be calculated by applying the derivative of the p(y) function.

$$\frac{dp(y)}{dy} = 0$$

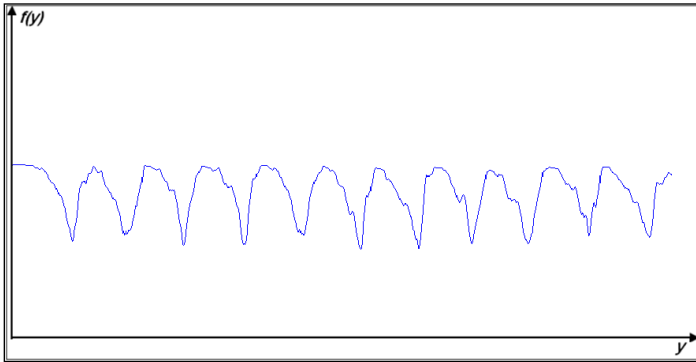


Figure 5: Line projection profile

The detection of local extrema facilitates the localization of the beginning and the end of lines. The following image shows the segmentation of the lines:



Figure 6: lines segmentation

• **Word segmentation**

The image in Figure 4, which is segmented in colour. It will be made binary by applying a global thresholding method. Among the thresholding methods, there is that of optimal Otsu thresholding [43] which we can apply thanks to the bimodal nature of the

histogram of this type of image. As an effect, the resulting image is affected by binary noise. As a solution, binary morphological filtering reduces the effect of this generated noise. We have already identified the text lines in the previous step of line segmentation. Dilation by applying a morphological filter of the binary image along each line allows the merging of pseudo-words and characters. The projection technique at the level of each line provides words. Overlapping characters prevent segmentation by this projection technique. The application of labelling of related components at the level of each line of the binary images makes it possible to locate isolated characters, pseudo-words and words. This method is also sensitive to noise, but it is effective. Additional noise from small areas is not considered by our algorithms. The following figure shows an example of segmentation of handwritten elements by applying labelling of related components (words, pseudo-words and characters).



Figure 7: Words and elements segmentation results

• **Feature extraction**

Arabic calligraphy has undergone several evolutions. It is considered an art of millennial history. The forms of Arabic letters follow refined rules. They change shape according to their position in the words (initial letter, median letter, final letter or isolated letter). Vowels can be designated by diacritical signs on words. Filtering of these diacritical signs is necessary to increase the quality of segmentation and recognition of words.

In most Arabic manuscripts, the writings follow uniform patterns according to the rules of the calligraphers. In many cases, these models are only the best-known fonts such as (Kufi, Andalus, Thuluth, Naskh, etc.). Words in manuscript images can be repeated several times with the same writing styles. The idea is to search for similar words in the same manuscript or in a collection of a calligrapher whose purpose is to use the occurrences of these words by our method.

Our objective is to choose such a method to extract the characteristics of words to be searched in manuscript images. We note that such a choice must be justified according to several constraints. In the literature, several approaches deal with recognition of forms. We opted for the use of invariable local detectors and descriptors to identify the forms of word writing. We justify the choice of these detectors by their acceptable response times and by their efficiency. On the other hand, we tested other methods, and could not obtain good results such as the theoretical signal model approach or the contour approach. We have the same character of the Arabic manuscript text that changes shape which makes the storyteller unstable. We opted for the approach based on local extrema because it uses points of interest recognized by their efficiency and by their optimised calculation times. In the literature, several approaches based on local extrema such as SURF descriptors offer a means of detecting these interest points.

In our case, the detection of words in images of Arabic manuscripts must take into consideration the styles of scripture. The approach using local extrema detection is based on variations in light intensity. However, in the case of small variations in light intensity, especially in manuscripts with almost identical intensities, the detection of word characteristics will be low. Another parameter to consider is the algorithmic cost and detector reliability. For example, the SIFT detector offers the interest points, with a higher computation time than the SURF detectors. That's why we use SURF's interest points to characterize the words in our Word Spotting method.

- **Classification and matching**

The degree of similarity of two words concerns the comparison of the characteristics of these two words. In our case, the characteristics of the words are based on SURF interest points. Comparison between points of interest requires a choice of the appropriate method to optimize processing time. Interest points of are characterized by their properties and their associated descriptor vectors. We compare these interest points in two stages: The first is to compare the trace sign of the Hessian matrix. This sign is from the Laplacian. It provides information on the meaning of blobs. Subsequently, two interest points to compare should have the same sign, if not different points.

The second is to compare the descriptor vectors of two interest points. Among the methods that can be used, the Euclidean distance or the Mahalanobis distance. The comparison is based on the calculation of distance and the correlation between these vectors.

4. Results and Discussion

Among the methods that are based on the Word Spotting technique we can mention the HADARA80P method [44] which

uses a dataset of 80 pages available on the internet [45] including images in Tiff format at high resolution. The documents handled are 9th century Arabic manuscripts. The authors of this method use three types of requests: by string, by polygon and by image which includes 25 test requests. Compared to the HADARA80P results, our proposed method provides satisfactory results even for low resolution images. However, the HADARA80P method requires high-quality images of about 300 dpi, especially when it comes to keyword images. In this case, images exceeding 50MB capacity can make their broadcasts difficult on the internet.

In our case, we used a microcomputer whose features is: CPU i5 Quad Core with a frequency of 2.4 GHz, 3 MB cache, 4 GB RAM and operating system Windows10 64-bit. We did tests on hundreds of pages and as well as on the dataset of HADARA80P. With twenty images request, we have achieved 95.27%-word matching accuracy with a run time of up to 910 ms for high memory capacity images.

Our method is to characterize the Arabic manuscripts. It identifies handwritten elements such as words, pseudo-words, isolated characters. The manuscripts we process are in the form of 2D images. The physical medium used in most manuscripts has a uniform texture and produces small variations in light intensity. However, ink generates large variations in light intensity. Indeed, the SURF points of interest used by our method characterise the text instead of the texture. Small variations in light intensity have a negligible effect on the detection of SURF interest points in manuscript images.

4.1. Word Matching

Word matching goes through several stages. These steps include extracting the features of words as interest points. Each word is represented by a set of interest points. These points are invariable to changes in scale, geometric variations, rotations and brightness variations. These invariances are shown by tests applied to the different words that are considered areas with a set of interest points. Regarding the effect of the texture of the physical medium was shown by the queries images 1, 2 and 4 on the table. In this case, we show as well that the texture allows to provide a negligible number of points. In addition, the accuracy of word matching depends on the number of interest points detected on each word. Many interest points allow to refine the description of each search word. To have high accuracy when matching words, it is necessary to use high quality images without increasing the execution time when searching for words.

The table shows the number of points detected on each query image. For this purpose, the interest points of the query images are located by small blue disks on these images. About the number of matching points between each query image and the target image is shown in the last column of the table.

The query images are compared with the target image with several of points detected in the target image equal to 773. We have a maximum of match points equal to 423 of the query image number 4 in the target image. However, the query image number 1 gives a minimum number of match points equal to 89.

The following figure shows all the query images used in the previous table. The target image is the one in the middle of the figure.

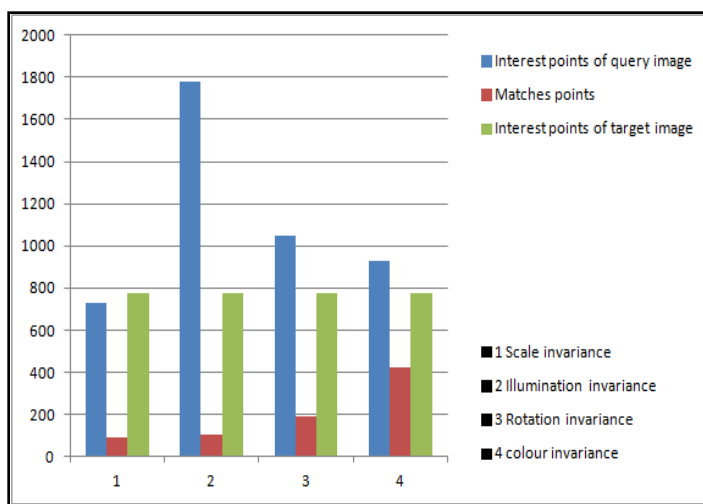


Figure 8: Histogram matching of interest points

Table 1: Experimental results of the matching points in query images with a target image

Query number	Invariance	Interest points	Query image	Matches points
1	Scale invariance	732		89
2	Illumination invariance	1782		107
3	Rotation invariance	1046		191
4	colour invariance	927		423

4.2. Application development

It is an application that is developed based on all the steps mentioned above (line segmentation, word and pseudo-word segmentation, feature extraction, classification). The extraction of the features is performed at the level of both query and target images. Word segmentation is an important tool to guide classification and identification. We used the SURF algorithm for the detection and description of features in the context of points of interest. This algorithm is known for its speed and robustness of its interest points in terms of invariance to scale changes, rotation, geometric variations and luminance. The following figure shows the interest points located in the target image and the query image on the left.

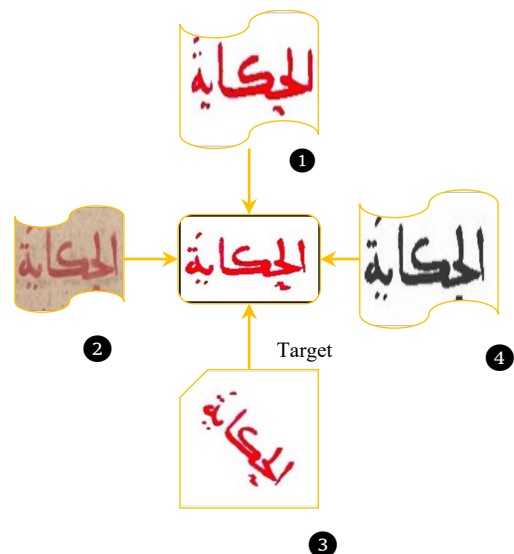


Figure 9: Four query images and the target image in the center

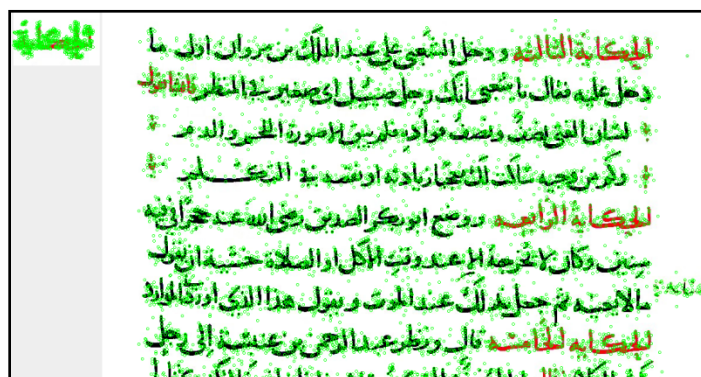


Figure 10: Interest points represented in the query images and in the target image

The objective is to develop a tool that allows access to the content of digitized Arabic manuscripts. The tools available for indexing handwritten documents in image form are very limited. In most cases, it is a search in databases describing the content of images with metadata. Our goal is to develop an application to identify text contained in images whose main interest is to integrate the Word Spotting technique for the search of occurrences of image word in handwritten documents. For this application, there are two possible cases:

- ✓ In a first case, the query image words are compared with those of the target image. Our method is based on interest points. However, an interest point belonging to a query image may belong to several words of the target image. Hence the need to segment the words of the target image and extract the features of each segmented word. Our interest is to search for all occurrences of a word image query in all pages of the same manuscript. The results of this research are acceptable despite some rejections due to segmentation problems in case of overlapping lines.
- ✓ In a second case, the query words can be text in ASCII format. This involves searching for the equivalent of text words in a database that stores the features of these words. Subsequently, the search for words in the target image is based on the features of the search words in the database.

The following figure shows the application we developed for the Word Spotting method. In the example, the comparison of the image query "history 'Al Hikayat' الحكياء" with a page image of an Arabic manuscript. The number of occurrences of this query image is equal to five times. As a perspective, we can expand this application to automate page annotations or help with transcription.

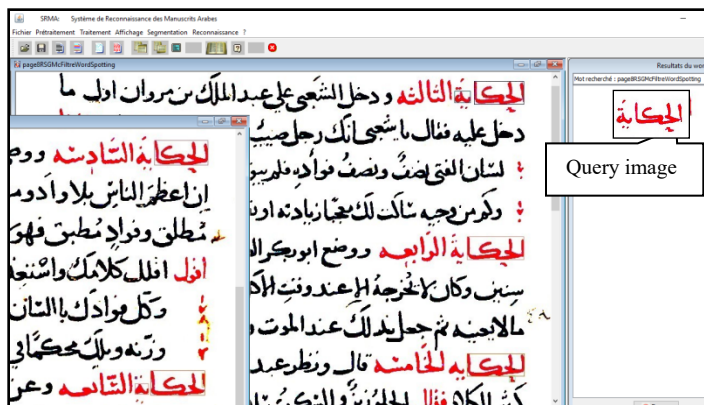


Figure 11: Word Spotting results

Conclusion

In this article, we have highlighted a method of searching for words in Arabic manuscripts. Most existing software (OCR) for Arabic text is only valid for printed text.

To this aim, we have proposed a word identification method based on the Word Spotting technique. The strength of this method lies in extracting the robust features of segmented words (or other elements: characters, pseudo-words). We use the invariant local detectors and descriptors of the SURF algorithm to extract the points of interest characterizing the words. The physical paper (or parchment) of the document has a negligible effect on the appearance of false points of interest belonging to the texture of the manuscript.

We have applied our method to hundreds of Arabic manuscripts from the National Library of Rabat and the Digital Library of Leipzig University. The test results of our method are excellent although some are very degraded. The limits of our method are in the case where the styles of writing and the fonts are varied, especially in the case the baldness of the lines where segregation is impossible.

Conflict of Interest

The authors declare no conflict of interest.

References

- [1] N. El makhfi, "Handwritten Arabic Word Spotting Using Speeded Up Robust Features Algorithm" in IEEE 5th International Conference on Optimization and Applications (ICOA), Kenitra, Morocco, 2019. <https://doi.org/10.1109/ICOA.2019.8727692>
- [2] Bay H., T. Tuytelaars, L.V. Gool, "SURF : Speeded Up Robust Features", in 9th European Conference on Computer Vision, Graz Austria, 404-417, 2006. <https://doi.org/10.1016/j.cviu.2007.09.014>
- [3] University of Leipzig. Project for the Cataloguing and Digitising of Islamic Manuscripts, www.islamic-manuscripts.net
- [4] R. Manmatha, C. Han, and E. M. Riseman, "Word spotting: A new approach to indexing handwriting", in Proceedings CVPR IEEE Computer Society Conference on Computer Vision and Pattern Recognition (CVPR), San Francisco, CA, USA, 1996. <https://doi.org/10.1109/CVPR.1996.517139>
- [5] T. Rath, R. Manmatha, and V. Lavrenko, "A search engine for historical manuscript images", in Proceedings of the 27th annual international ACM

- SIGIR conference on Research and development in information retrieval (SIGIR), Sheffield, United Kingdom, 2004. <https://doi.org/10.1145/1008992.1009056>
- [6] T. Rath and R. Manmatha, "Word spotting for historical documents", IJDAR, 9 (2), 13-152, 2007. <http://dx.doi.org/10.1007/s10032-006-0035-8>
- [7] I. Yalniz and R. Manmatha, "An efficient framework for searching text in noisy documents", in DAS, Gold Cost, QLD, Australia, 2012. <https://doi.org/10.1109/DAS.2012.18>
- [8] V. Frinken, A. Fischer, R. Manmatha, and H. Bunke, "A novel word spotting method based on recurrent neural networks", in IEEE Transactions on Pattern Analysis and Machine Intelligence (TPAMI), 34 (2), 211 – 224, 2012. <https://doi.org/10.1109/TPAMI.2011.113>
- [9] A. Fischer, A. Keller, V. Frinken, and H. Bunke, "HMM-based word spotting in handwritten documents using subword models", in ICPR, Istanbul, Turkey, 2010. <https://doi.org/10.1109/ICPR.2010.834>
- [10] F. Chen, L. Wilcox, and D. Bloomingberg. "Word spotting in scanned images using hidden markov models". In Acoustics, Speech, and Signal Processing, ICASSP-93., IEEE International Conference on, vol 5, 1-4, Minneapolis, MN, USA, 27-30 April 1993. <https://doi.org/10.1109/ICASSP.1993.319732>
- [11] A. Fischer, A. Keller, V. Frinken, and H. Bunke, "Lexicon-free handwritten word spotting using character hmms", Pattern Recognition Letters, vol. 33, no. 7, pp. 934-942, 2012. <https://doi.org/10.1016/j.patrec.2011.09.009>
- [12] D. Zhang and G. Lu, "Review of shape representation and description techniques", PR, 37(1), 1-19, 2004. <https://doi.org/10.1016/j.patcog.2003.07.008>
- [13] N. Dalal, B. Triggs, "Histograms of oriented gradients for human detection", CVPR, 2005. <https://doi.org/10.1109/CVPR.2005.177>
- [14] J. Almazan, A. Gordo, A. Fornes, and E. Valveny, "Efficient Exemplar Word Spotting", in BMVC, 2012. [Online]. Available: <http://www.bmvc.org/bmvc/2012/BMVC/paper067/paper067.pdf>
- [15] S. Sudholt and G. A. Fink, "A Modified Isomap Approach to Manifold Learning in Word Spotting", in 37th German Conference on Pattern Recognition, ser. Lecture Notes in Computer Science, Aachen, Germany, 2015. https://link.springer.com/chapter/10.1007/978-3-319-24947-6_44
- [16] J. Almazan, A. Gordo, A. Fornes, and E. Valveny, "Word Spotting and Recognition with Embedded Attributes" Transactions on Pattern Analysis and Machine Intelligence, 36 (12), pp. 2552-2566, 2014. <https://doi.org/10.1109/TPAMI.2014.2338414>
- [17] L. Rothacker and G. A. Fink, "Segmentation-free query-by-string word spotting with bag-of-features HMMs", in International Conference on Document Analysis and Recognition, Tunis, Tunisia, 2015. <https://doi.org/10.1109/ICDAR.2015.7333844>
- [18] M. Rusinol, D. Aldavert, R. Toledo, J. Lladós, "Efficient segmentation-free keyword spotting in historical document collections" Pattern Recognition, 48 (2), 545-555, 2015. <https://doi.org/10.1016/j.patcog.2014.08.021>
- [19] D. Aldavert, M. Rusinol, R. Toledo, and J. Lladós, "Integrating Visual and Textual Cues for Query-by-String Word Spotting", in International Conference on Document Analysis and Recognition, 511-515. Washington, DC, USA, 2013. <https://doi.org/10.1109/ICDAR.2013.108>
- [20] David. G. Lowe, "Distinctive Image Features from Scale-Invariant Keypoints". 60 (2), 91-110, 2004. [Online]. Available: <https://link.springer.com/article/10.1023/B:VISI.0000029664.99615.94>
- [21] David G. Lowe, "Object Recognition from Local Scale-Invariant Features". Proc. of the International Conference on Computer Vision, Kerkyra, Greece, 1999. <https://doi.org/10.1109/ICCV.1999.790410>
- [22] Cordelia SCHMID, "Pairing of images by local gray-scale invariants, Application to the indexing of a base of objects", Ph.D thesis, National Polytechnic Institute of Grenoble, France, 1996.
- [23] C. Harris and M. Stephens, "A combined corner and edge detector", Proceedings of the 4th Alvey Vision Conference. 147-151, 1988. [Online]. Available: <http://www.bmva.org/bmvc/1988/avc-88-023.pdf>
- [24] Schmid, & R. Mohr, "Local grayvalue invariants for image retrieval", IEEE Transactions on Pattern Analysis and Machine Intelligence. 19 (5), 530-534, 1997. <https://doi.org/10.1109/34.589215>
- [25] P. Montesinos, V. Gouet, and R. Deriche, "Differential invariants for color images", in IEEE 40th International Conference on Pattern Recognition, Brisbane, Queensland, Australia, 1998. <https://doi.org/10.1109/ICPR.1998.711280>
- [26] Y. Dufournaud, Cordelia Schmid, Radu Horaud, "Matching Images with Different Resolutions", in IEEE Conference on Computer Vision and Pattern Recognition (CVPR), Hilton Head Island, SC, USA, 2000. <https://doi.org/10.1109/CVPR.2000.855876>
- [27] K. Mikolajczyk, C. Schmid, "Indexing based on scale invariant interest points", in IEEE 8th International Conference on Computer Vision (ICCV), Vancouver, BC, Canada, 2001. <https://doi.org/10.1109/ICCV.2001.937561>
- [28] K. Mikolajczyk, "Detection of local features invariant to affine transformation", Ph.D thesis, institut national polytechnique, Grenoble, France, 2002.

- [29] K. Rohr, "Recognizing corners by fitting parametric". *International Journal of Computer Vision*, **9**(3): 213-230, 1992. [Online]. Available: <https://link.springer.com/article/10.1007/BF00133702>
- [30] k. Rohr, "Über die Modellierung und Identifikation charakteristischer Grauwertverläufe in Realweltbildern", In 12 DAGM-Symposium Mustererkennung, 217-224, 1990. [Online]. Available: https://link.springer.com/chapter/10.1007/978-3-642-84305-1_25
- [31] R. Deriche & T. Blaska, "Recovering and characterizing image feature using an efficient model based approach". In *Proceedings of IEEE Conference on Computer Vision and Pattern Recognition*, New York, NY, USA, 1993. <https://doi.org/10.1109/CVPR.1993.341079>
- [32] P. Brand & R. Mohr, "Accuracy in image measure". in *Proceedings of the SPIE Conference on Videometrics III*, **2350**, 218-228, Boston, MA, United States, 1994. <https://doi.org/10.1117/12.189134>
- [33] R. Deriche & G. Giraudon, "Accurate corner detection: an analytical study". In *Proceedings of the 3rd International Conference on Computer Vision*, Osaka, Japan, 1990. <https://doi.org/10.1109/ICCV.1990.139495>
- [34] R. Deriche & G. Giraudon, "A computational approach for corner and vertex detection". *International Journal of Computer Vision*, **10**(2): 101-124, 1993. [Online]. Available: <https://link.springer.com/article/10.1007/BF01420733>
- [35] T. lindeberg, "Feature detection with automatic scale selection", *International Journal of Computer Vision*, **30** (2), 79–116, 1998. [Online]. Available: <https://link.springer.com/article/10.1023/A:1008045108935>
- [36] K. Mikolajczyk, & C. Schmid, "A performance evaluation of local descriptors", *IEEE Transactions on Pattern Analysis and Machine Intelligence*, *PAMI*, **27** (10), 1615 – 1630, 2005. [Online]. Available: <https://doi.org/10.1109/TPAMI.2005.188>
- [37] B. Bagasi, L. A. Elrefaei, "Arabic Manuscript Content Based Image Retrieval: A Comparison between SURF and BRISK Local Features", *International Journal of Computing and Digital Systems* ISSN (2210-142X) *Int. J. Com. Dig. Sys.* **7** (6), 355-364, 2018. [Online]. Available: <http://dx.doi.org/10.12785/ijcds/070604>
- [38] S. Leutenegger, M. Chili, and RY. Siegwart, "BRISK: Binary Robust invariant scalable keypoints" in 2011 IEEE International Conference. *Computer Vision (ICCV)*, 2548-2555, 2011, Barcelona, Spain <https://doi.org/10.1109/ICCV.2011.6126542>
- [39] The Refaiya Family Library, Leipzig University Library. <https://www.refaiya.uni-leipzig.de/content/index.xml?lang=en>
- [40] N. El makhfi, O. El bannay. "SCALE-SPACE APPROACH FOR CHARACTER SEGMENTATION IN SCANNED IMAGES OF ARABIC DOCUMENTS". *Journal of Theoretical and Applied Information Technology*, **94** (1), 2016. [Online]. Available: <http://www.jatit.org/volumes/Vol94No2/19Vol94No2.pdf>
- [41] R. Manmatha, N. Srimal, "Scale space technique for word segmentation in handwritten manuscripts", In 2nd International Conference on Scale Space Theory in Computer Vision (Scale-Space 99). **1682** (2), 22-33, Corfu, GRECE, 1999. [Online]. Available: <http://ciir.cs.umass.edu/pubfiles/mm-27.pdf>
- [42] J. Ha, R. M. Haralick, and I. T. Phillips. "Document page decomposition by the bounding-box projection technique". In *Proceedings of the Third International Conference on Document Analysis and Recognition (ICDAR)*, pages 1119 1122, Montreal, Quebec, Canada, 1995. [Online]. Available: <https://pdfs.semanticscholar.org/e896/99bf5a1593490d6d93699ca17f3c75434178.pdf>
- [43] N. Otsu, "A threshold selection method from greyscale histogram", in *IEEE Transactions on Systems, Man, and Cybernetics*. on *SMC*, **9** (1), 62-66, 1979. <https://doi.org/10.1109/TSMC.1979.4310076>
- [44] W. Pantke, M. Dennhardt, D. Fecker, V. Möargner, T. Fingscheidt, "An Historical Handwritten Arabic Dataset for Segmentation-Free Word Spotting -HADARA80P", in *proceedings of the 14th International Conference on Frontiers in Handwriting Recognition (ICHFR)*, 15-20, Heraklion, Greece, 2014. <https://doi.org/10.1109/ICFHR.2014.11>
- [45] Technische Universität Braunschweig, HADARA80P Dataset. [Online]. Available: <https://www.ifn.ing.tu-bs.de/research/data/HADARA80P>

Discriminant Analysis of Diminished Attentiveness State Due to Mental Fatigue by Using P300

Kosuke Fujita¹, Kazuya Miyanaga², Fumiya Kinoshita^{*2}, Hideaki Touyama²

¹DENSO TECHNO Co., Ltd., Aichi 474-0025 Japan

²Department of Electrical and Computer Engineering, Faculty of Engineering, Toyama Prefectural University, Toyama 939-0398 Japan

ARTICLE INFO

Article history:

Received: 25 September, 2019

Accepted: 28 October, 2019

Online: 22 November, 2019

Keywords:

Mental fatigue

Electroencephalogram

P300

Linear discriminant analysis

ABSTRACT

Fatigue is broadly divided into two types depending on the content of a task: physical fatigue and mental fatigue. Mental fatigue is associated with human error. It is thus important to search for indicators that can easily evaluate mental fatigue. The aim of this study is to construct a system that can evaluate mental fatigue in a simple manner. To achieve this, we investigated the influence of the accuracy of linear discriminant analysis in two classes before and after the application of a mental load. In addition, we investigated whether the mental fatigue state can be estimated even when the number of trials for averaging is small, by combining the electroencephalogram power spectral density component and the P300 component. As a result, this combination of the power spectral density component with the P300 component resulted in measured waveforms that exhibited an accuracy of approximately 97%, even when the number of trials for averaging was as small as five trials.

1. Introduction

The technological development of wearable devices in recent years has made it easier to measure biological information. In addition to devices that can measure heart rate or activity level, wearable electroencephalogram (EEG) devices that can measure brain waves have emerged, and their use is becoming more widespread. In the past, expensive equipment was generally used to measure brain waves and it was difficult to continually take these measurements during a person's daily life. However, as wearable EEG devices have become more widespread, dry electrodes that do not require the application of conductive paste have emerged. This development is making it more and more feasible to collect big data in the field of neuroscience. However, the data obtained from wearable devices differ from biological information measured by medical devices. As such, these data need to be applied appropriately. This paper focuses on the use of EEG to evaluate mental fatigue as a method of applying measurement data obtained from wearable devices. This paper is an extension of work originally presented in IEEE International Conference on Systems, Man, and Cybernetics (SMC) 2018 [1].

Fatigue is broadly divided into two types depending on the content of a task: physical fatigue and mental fatigue. While the *in vivo* mechanisms and processes of physical fatigue have been

studied, particularly in fields like exercise physiology [2], there is no consensus regarding what mechanisms induce mental fatigue or how it should be measured, and even recent studies have taken a variety of different approaches to researching the subject [3, 4]. In the fields of ergonomics and occupational health, the flicker test is widely used to evaluate mental fatigue [5, 6]. The flicker test evaluates eye fatigue by measuring the frequency or flicker interval threshold, also known as the Critical Fusion Frequency (CFF), as the frequency of a flickering light is changed. However, the CFF is self-reported by subjects and the influence of subjective factors cannot be ruled out. Other than the flicker test, attempts have also been made to evaluate mental fatigue using salivary amylase [7, 8]. A rise in salivary amylase is generally thought to indicate an increase in sympathetic nervous activity. However, sympathetic nervous activity can arise because of negative emotions or mental stimulation. As such, evaluating mental fatigue using autonomic nervous activity indicators such as sympathetic nervous activity or vagal nervous activity often leads to difficulties with interpretation. Meanwhile, EEG waveforms contain both components for evaluating autonomic nervous activity and event-related potential components, which can both be used to evaluate cognitive function. This means that it may be possible to estimate the decreased attentiveness that accompanies mental fatigue by combining these EEG components. This paper focuses on brain waves as an indicator for evaluating mental fatigue.

* Fumiya Kinoshita, Email: f.kinoshita@pu-toyama.ac.jp

In previous studies, there are reports in which α -wave band power increases during mental fatigue [9, 10], there are also reports showing that it decreases as well [11, 12], and thus, there is no consistent trend. P300, an event-related potential, is the positive potential change produced 300 ms after exposure to external stimuli. Its amplitude is significant in that the amplitude is dependent on the amount of processing resources at the perceptual-central level assigned to the event that caused the positive potential change. Prolonged latency and lowered amplitude during mental fatigue have been reported [13, 14]. When calculating P300, the signal-averaging technique must be used in order to produce a clearer potential response to stimuli. Generally, it has been confirmed that about 20 trials are required for averaging to produce consistent results for P300 [15], but it is difficult to conduct 20 trials during the performance of actual tasks. As such, for the simple measurement of mental fatigue using P300, the evoked potential needs to be extracted with averaging over as few trials as possible.

This paper presents work that combined EEG frequency components and P300 components to perform linear discriminant analysis on EEG waveforms. Analysis was performed before and after a task that involved a mental load in order to study the number of trials required for averaging and the resulting discriminant accuracy. Furthermore, in order to confirm that the task had caused sufficient mental fatigue, subjective questionnaire surveys and studies of autonomic nervous activity indicators using electrocardiogram (EKG) analysis were also conducted at the same time.

2. Experimental method

The subjects were 10 young, healthy males (mean \pm standard deviation: 21.7 ± 0.9 years) with no history of nervous system disorders. The experiment was thoroughly explained to subjects beforehand and their consent to participate was obtained. The experiment was approved (4/2017) by the ethics committee of Toyama Prefectural University.

With subjects seated, the experiment measured mental fatigue with EEG, electrooculogram (EOG), and EKG analyses as well as a subjective questionnaire survey using the Visual Analogue Scale (VAS). The VAS evaluation axis in this study placed "optimal sensation with no fatigue at all" (0%) at the left end and "lowest level of sensation with so much fatigue that I cannot do anything at all" (100%) at the right end [16]. The distance from the point marked by the subject on the evaluation axis to the 0% point on the left end was measured with a ruler, and the value was expressed as a percentage. Biosignals were recorded with a g.USBamp system (g.tec Medical Engineering GmbH, Austria). The time resolution was set to 1 kHz for the EKG and 512 Hz for the EEG and EOG. Based on the extended 10–20 system, electrodes were positioned at Cz and Pz with the GND at AFz and the reference electrode on the left ear lobe. Additionally, EOG electrodes were positioned above and below the left eye, while EKG measurements were taken with lead III positioned between the left leg and left hand.

The experimental protocol was as follows: after applying a mental load for 15 minutes, all signals to be measured were recorded continuously for 10 minutes. One of these trials constituted one set, and a total of 8 sets were performed (Figure 1).

Below, results prior to measurements in the 1st set are labeled "Pre" and measurements in the 8th set are labeled "Post." In this experiment, mental load was created with mental arithmetic problems. In these mental arithmetic problems, a pair of two-digit integers was shown on a display placed 0.8 m in front of the subject's eye (Figure 2). The subject mentally calculated the sum of the first and second digit in each integer (in Figure 2, the results were 12 on the left and 8 on the right), then mentally calculated the units digit of the product of the two integers obtained in the previous step (in Figure 2, the answer was 6). The mental arithmetic problem involved the task of entering the resulting number with a keyboard, and this problem produced mental fatigue in the subject.

For bio signal recording, we conducted an oddball paradigm using visual stimuli and recorded EEG, EOG, and EKG data during that time. When the oddball paradigm in each set was complete, we also conducted a subjective questionnaire survey on fatigue using the VAS. In the oddball paradigms using visual stimuli, an "x" image was used as the infrequent stimulus and an "o" image as the frequent stimulus, with the images set to appear 30 times and 90 times, respectively. Both visual stimuli were displayed for 1 second at a time, and the display order was random. In experiments that use oddball paradigms, P300 detection accuracy is often increased by giving subjects prior instructions to calculate the number of times the infrequent stimulus appears. In this experiment, we instructed subjects to "Quickly press the Enter key when the infrequent stimulus is displayed". To synchronize biosignals with the presentation of stimuli during the oddball paradigm, we synchronized biosignals with trigger signals by installing a photoresistor circuit in the stimulus display and sending external inputs to a biological amplifier.

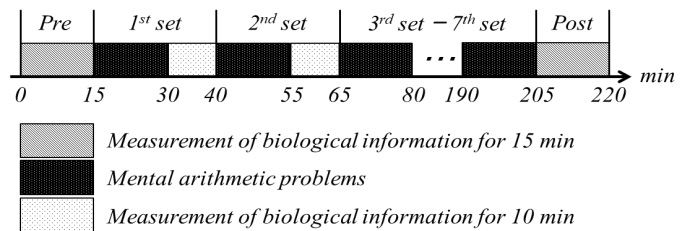


Figure 1: Experimental protocol.

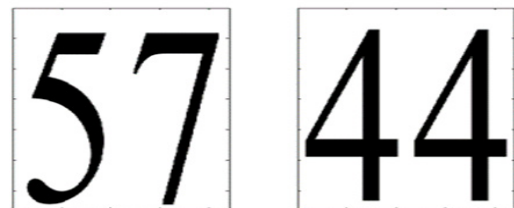


Figure 2: The typical content used in mental arithmetic problems

3. Analytical method

3.1. EKG analytical method

The R-R interval was extracted from the measured EKG time series data and an analysis was conducted using heart rate variability (HRV) [17]. With HRV, analyzing the R-R interval

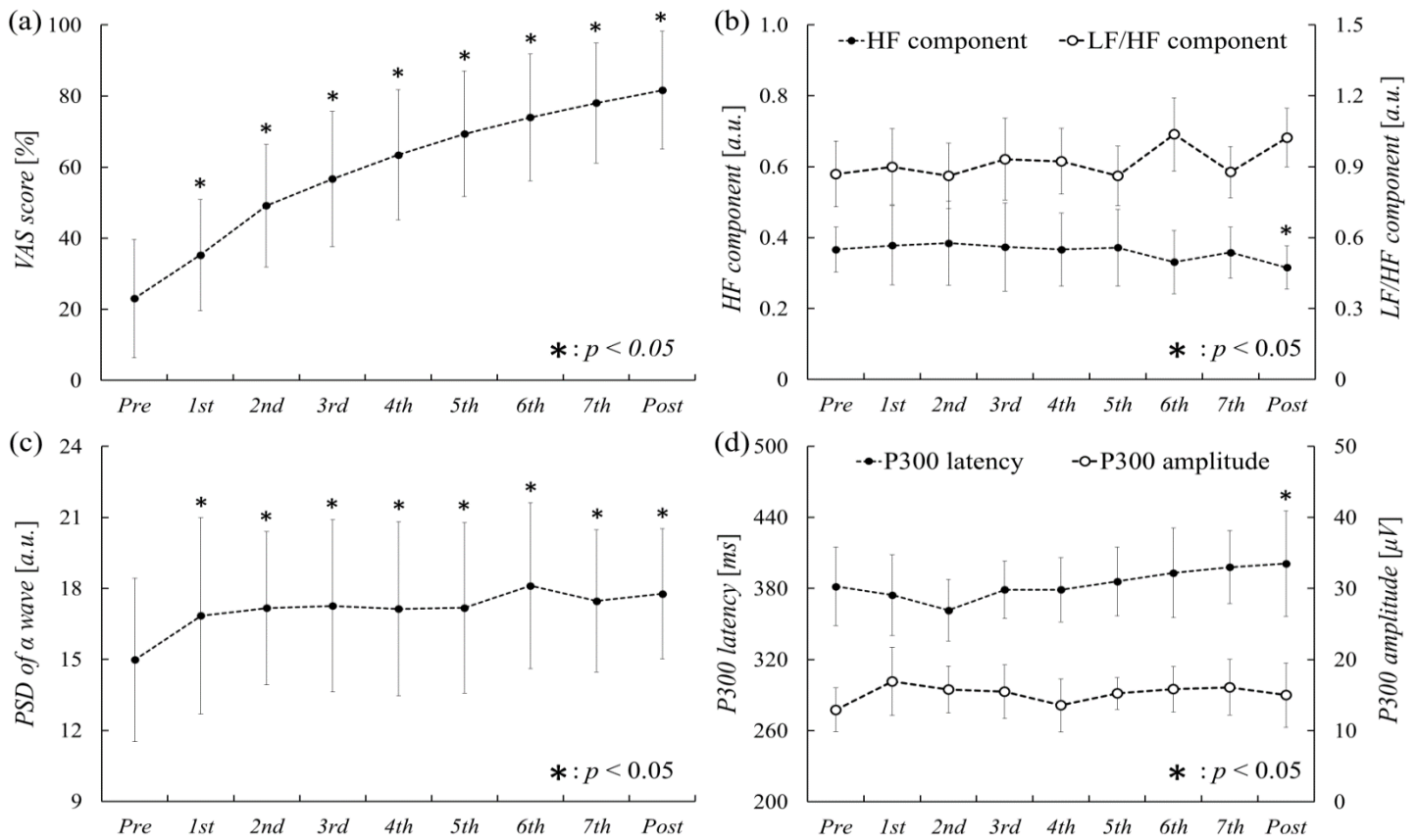


Figure 3: Results of measurement items (Average \pm SD)
 (a) VAS scores, (b) HF and LF/HF components, (c) PSD of the α wave, (d) The latency and amplitude of the P300 component.

(heart rate) from the time domain/frequency domain makes it possible to quantify sympathetic and parasympathetic nervous system indicators. The extracted R-R interval time series was resampled from a 256-point time series and a fast Fourier transform (FFT) was used to estimate the power spectral density (PSD). Using the PSDs of a low frequency component (LF) with a range of 0.04–0.15 Hz and a high-frequency component (HF) with a range of 0.15–0.4 Hz, this study calculated an LF/HF component and an HF component, which are considered indicators of sympathetic and vagal nervous activity, respectively.

3.2. EEG analytical method

Time series of 5 seconds before and after low-frequency stimulus presentation (a total of 10 seconds) were extracted from the measured EEG time series. After applying a 4–30 Hz bandpass filter to the extracted time series, eye blink artifacts were removed with the FastICA algorithm [18]. Then, data from 2.5 seconds before and after low-frequency stimulus presentation (a total of 5 seconds) were extracted from these time series and put through FFT processing. The PSD of the α bandwidth (8–13 Hz) in each time series and the average values from Cz and Pz were calculated to produce representative values for the sets.

Next, we will demonstrate how P300 was derived. Time series of 5 seconds before and after low-frequency stimulus presentation

(a total of 10 seconds) were extracted. After applying a 1–5 Hz bandpass to the extracted time series, eye blink artifacts were removed with the FastICA algorithm. P300 was derived by first correcting the baseline using the average value from 0.25 seconds before and after low-frequency stimulus presentation in the time series and then averaging the waveforms after low-frequency stimulus presentation in each subject. Additionally, this study identified the positive peak that appeared at 280–500 ms as P300 and calculated its latency and amplitude. The average values for P300 latency and amplitude were calculated from both Cz and Pz, and the results were used as the representative values of the sets.

3.3. Linear discriminant analysis

Linear discriminant analysis was performed using the frequency component of the α bandwidth before and after a mental load task and the P300 component of the time series [19]. For the frequency component and P300 component, principal component analysis was used to perform dimensionality reduction, and feature points were extracted [20]. To prevent overfitting, we calculated all levels of accuracy when the number of components in the principal component analysis was changed in the range of 1–15, and the accuracy level in the scenario that reached the local maximum was set as the final discriminant accuracy.

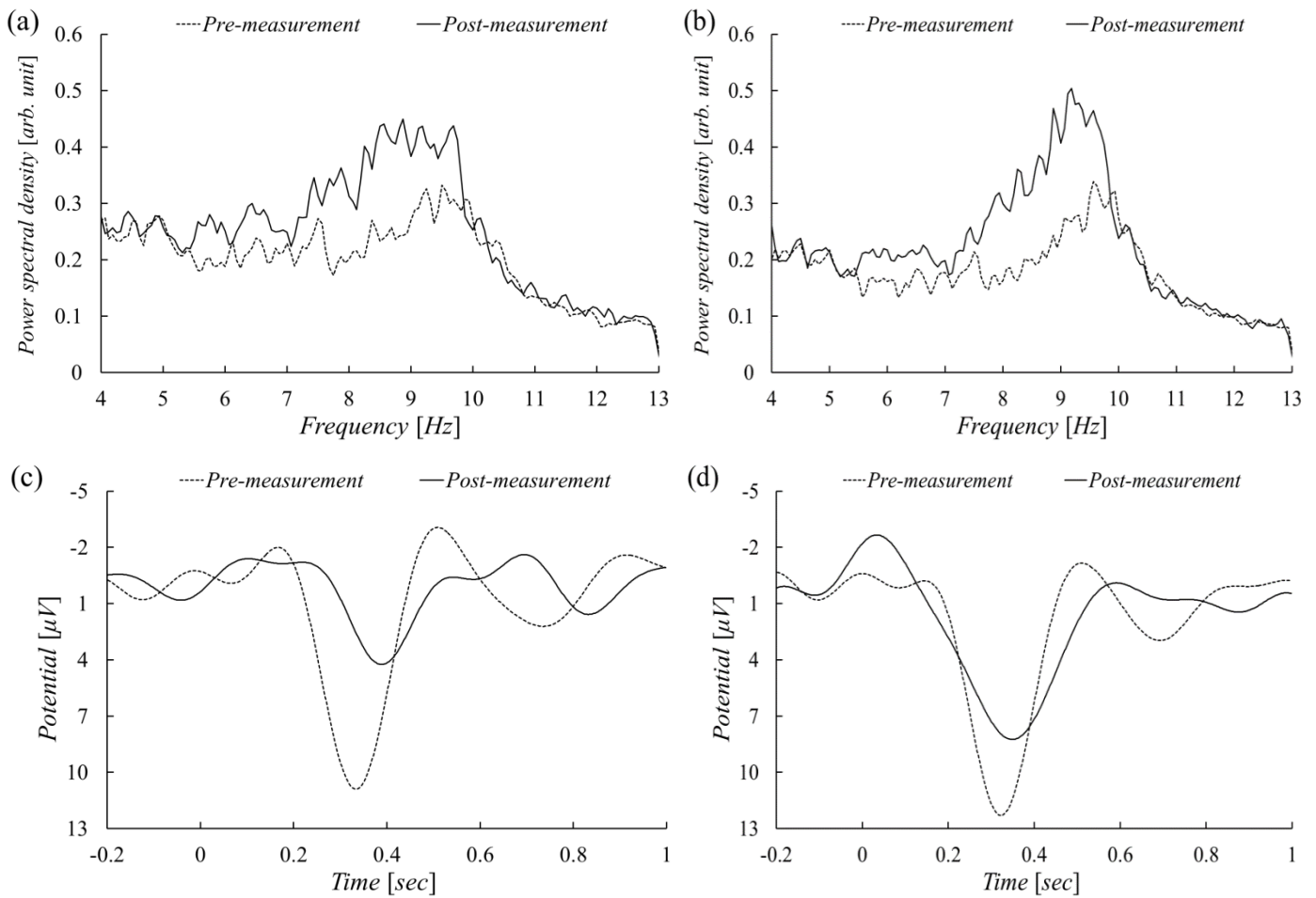


Table 1: Results of Linear Discriminant Analysis (F Value, Average \pm SD)

Averaging Times	Power spectrum component		P300 component		Power spectrum component and P300 component	
	Pre	Post	Pre	Post	Pre	Post
0 times	0.74 \pm 0.10	0.71 \pm 0.09	0.67 \pm 0.06	0.68 \pm 0.06	0.79 \pm 0.08	0.78 \pm 0.08
2 times	0.79 \pm 0.11	0.77 \pm 0.12	0.77 \pm 0.09	0.77 \pm 0.09	0.85 \pm 0.11	0.85 \pm 0.09
5 times	0.83 \pm 0.15	0.82 \pm 0.15	0.96 \pm 0.06	0.97 \pm 0.04	0.97 \pm 0.04	0.97 \pm 0.03

4. Results

Before performing a discriminant analysis using EEG time series, a subjective questionnaire survey and a study of autonomic

nervous analysis indicators using EKG analysis were also conducted in this experiment to confirm that enough mental fatigue had been produced. Figure 3 shows the changes over time in each measurement item. In the subjective questionnaire survey using the VAS, performing mental arithmetic increased the fatigue score (Figure 3a). As it was a subjective questionnaire survey, there was large variation in VAS scores between the subjects. While the average VAS score was about 20% in the Pre stage, it increased up to about 80% in the Post stage. The Pre results and subsequent measurement set results were compared using the Wilcoxon-signed rank sum test. The results showed that the average VAS score increased significantly in the subsequent measurement sets compared to the score in the Pre stage ($p < 0.05$).

For the HF component, which was extracted using heart rate variability and is considered an indicator of vagal nervous activity, the average score was about 0.4 in the Pre stage and about 0.3 in the Post stage (Figure 3b). The Pre results and subsequent measurement set results were compared using the Wilcoxon-signed rank sum test. The results showed that the average HF component score decreased significantly in the Post measurement set compared to the score in the Pre stage ($p < 0.05$). Furthermore, for the LF/HF component, which is considered an indicator of sympathetic nervous activity, the average score was about 0.9 in the Pre stage and about 1.1 in the Post stage (Figure 3b). The Pre results and subsequent measurement set results were compared using the Wilcoxon-signed rank sum test. Results showed no significant difference in LF/HF components between the measurement sets.

For the α bandwidth PDS, the average score was about 15 in the Pre stage and about 18 in the Post stage (Figure 3c). The Pre results and subsequent measurement set results were compared using the Wilcoxon-signed rank sum test. The results showed that the average α bandwidth PDS score increased significantly in the subsequent measurement sets compared to the score in the Pre stage ($p < 0.05$).

For P300 latency, the average score was about 380 ms in the Pre stage and about 400 ms in the Post stage (Figure 3d). The Pre results and subsequent measurement set results were compared using the Wilcoxon-signed rank sum test. The results showed that average P300 latency increased significantly in the Post stage compared to the Pre stage ($p < 0.05$). The average P300 amplitude was about 15 μV in both the Pre and Post stages (Figure 3d). The Pre results and subsequent measurement set results were compared using the Wilcoxon-signed rank sum test. Results showed no significant difference in P300 amplitude between any of the measurement sets.

The study presented in this paper performed linear discriminant analysis that combined the frequency component and P300 component to investigate whether mental fatigue can be estimated even when averaging is only performed over a small number of trials. Figure 4 shows a typical example of the frequency component and P300 component before and after a mental load task when averaging was performed over five trials. We observed that the frequency component on the α bandwidth tended to increase after mental fatigue compared to before mental fatigue (Figure 4a). Additionally, we observed that the P300 component

latency tended to lengthen after mental fatigue compared to before mental fatigue (Figure 4b).

Linear discriminant analysis was performed using the frequency component of the α bandwidth before (Pre) and after (Post) a mental load task and the P300 component of the time series. Table 1 shows the accuracy results when averaging was performed over 0, 2, and 5 trials. With linear discriminant analysis, combining the frequency component and the P300 component increased discriminant accuracy for all numbers of trials. When averaging was performed for two trials, the discriminant accuracy was about 78% for the frequency component alone and 77% for the P300 component alone, while combining the frequency component and P300 component increased the accuracy to 85%. Additionally, when averaging was performed over five trials, the discriminant accuracy was about 83% for the frequency component alone and 96% for the P300 component alone, while combining the frequency component and P300 component increased the accuracy to 97%.

5. Discussion

The EEG frequency bands recorded when waking are categorized in theta waves (4–7 Hz), alpha waves (8–13 Hz), beta waves (14–30 Hz) [22]. In addition, frequency drops in the α -wave band occur during states of decreased alertness elicited when falling asleep [23]. However, while there are reports in which α -wave band power increases during mental fatigue [9, 10], there are also reports showing that it decreases as well [11, 12], and thus, there is no consistent trend. While evaluating mental fatigue using autonomic nervous activity alone leads to difficulties with interpretation, adding the P300 component makes it possible to evaluate fatigue based on two indicators: cognitive function and autonomic nervous activity. This study performed linear discriminant analysis that combined the EEG frequency component and the P300 component, an event-related potential, to investigate whether mental fatigue can be estimated even when averaging is only performed over a small number of trials. The results showed that, when the P300 component was averaged for five trials, discrimination with 97% accuracy was possible before and after a mental load task. Furthermore, even when averaged over two trials, combining the frequency component and the P300 component produced a discriminant accuracy of 85%. We believe that the technique proposed by this paper makes it possible to estimate mental fatigue even when an event-related potential is averaged over a small number of trials.

In order to confirm that enough mental fatigue had been produced by the mental load when estimating fatigue, subjective questionnaire surveys and studies of autonomic nervous activity indicators using EKG analysis were also conducted in the work presented here. The results showed that subjects complained of fatigue, and subjective fatigue according to the VAS score also increased significantly. Heart rate variability showed a significant decrease in the HF component after a mental load task. There are reports that fluctuation in the HF component may reflect mental load, and the results of this experiment provide more supporting evidence that this is the case. Based on this result, we believe that, in this experiment, subjects were more affected by mental load than physical load. Additionally, this paper presents results that confirmed an increase in the α bandwidth power after a mental

load task, demonstrating the same patterns in changes to basic rhythms during mental fatigue caused by mental arithmetic that Trejo et al. reported [24]. In terms of P300, we confirmed prolonged latency after a mental load task, demonstrating the same trends in changes to P300 during mental fatigue caused by a driving simulation reported by Zhao et al. [25].

In this experiment, keys on the keyboard were only pressed for the low-frequency stimulus in an oddball paradigm where P300 was measured. As such, the possible influence of exercise-related potentials (for example, a decrease in the power of mu-rhythms around 10 Hz) should be investigated. Generally, C3 and C4 are considered the electrode positions most likely to detect exercise-related potentials due to hand motion. The electrode positions used in this experiment were Cz and Pz, and the key pressing was the same throughout all of the trials. Furthermore, we applied a 1–5 Hz bandpass filter during P300 signal processing, and we believe that hand motion had no effect on the results. However, P300 is a signal that tends to be drowned out by spontaneous brain waves. As spontaneous brain waves appear randomly, it has been proven that they will negate each other when averaged, allowing hidden P300 signals to appear. It has been confirmed that discriminant accuracy for P300 increases as the number of trials used for averaging is increased, meaning that the results in this paper are not accidental and can be reliably attributed to the appearance of P300. On the other hand, the linear discriminant analysis in this paper showed 97% accuracy of discriminant using only the P300 component with 5 times averaging process. This is a very high accuracy. However, in this experiment, it was a case of the accuracy where mental fatigue was given sufficiently, so in the future, we will examine the discrimination accuracy according to the degree of mental fatigue.

Lastly, the amplitude of P300 has been shown to depend on subjective probability and stimulus meaning in an additive manner, and the dimension of information transmission has a multiplicative effect on this [26]. As such, teaching data for machine learning needs to be recorded in advance, and it would take an enormous amount of time to reproduce mental fatigue in the manner discussed here. Transfer learning has been proposed as a method for shortening the process of securing the required teaching data [27]. Transfer learning is a technique in which training data from someone else is used for discriminating one's own data. In the future, to improve discriminant accuracy, we will propose a supervised spatial filter that uses training data from others by assuming a similar spatial distribution in the EEG waveforms of different subjects during mental fatigue using transfer learning.

6. Conclusion

Cognitive deficits brought on by mental fatigue include decreased alertness, difficulty solving problems, and lowered situational awareness. There are claims that human error is related to the cognitive deficits associated with mental fatigue, and it is important to search for indicators that can evaluate the decreased cognitive function associated with mental fatigue. This paper presents a study, which performed linear discriminant analysis that combined the EEG frequency component and the P300 component, an event-related potential, to investigate whether mental fatigue can be estimated even when averaging is only

performed over a small number of trials. Generally, it has been confirmed that about 20 trials are required to produce consistent results for P300, but the method proposed in this paper was able to achieve a discriminant accuracy of 97% before and after mental fatigue, even when P300 was only averaged over five trials. Moving forward, we will also investigate the detection of mental fatigue in real time during driving and actual tasks by using wearable EEG devices with dry electrodes that do not require the application of conductive paste.

References

- [1] K. Fujita, F. Kinoshita, H. Touyama, "Detection of Cognitive Decline Due to Mental Fatigue Using Electroencephalogram" in 2018 IEEE SMC: Passive BCIs, Miyazaki, Japan, 2018.
- [2] Japanese Society of Fatigue Science Clinical evaluation guidelines on designated health foods for physical fatigue in healthy people with no pathological fatigue, *Journal of Clinical and Experimental Medicine*, 228(6), pp.743-746, 2009.
- [3] S. Tajima, K. Yamaguchi, H. Kuratsune, Y. Watanabe, "Measuring fatigue with physiological biomarkers" *Adv. Anti. Aging. Med.*, 6(3), 329-334, 2010.
- [4] Y. Tanaka, S. Wakida, "Biomarkers of stress and fatigue" *J. Pharmacol. Sci.*, 137(4), 185-188, 2011.
- [5] K. Hashimoto, "The physiological meaning of flicker values and issues measuring them: flicker test theory and the reality" *Jpn. J. Ind. Health*, 5(9), 563-578, 1963.
- [6] K. Hashimoto, "Testing for mental fatigue" *The Japanese Journal of Ergonomics*, 17(3), 107-113, 1981.
- [7] M. Yamaguchi, T. Kanemori, M. Kanemaru, Y. Mizuno, H. Yoshida, "Can salivary amylase be an indicator for estimating stress?" *Japanese Journal of Medical Electronics and Biological Engineering*, 39(3), 234-239, 2001.
- [8] K. Nomura: The relationship between performance on mental arithmetic tasks and physiological stress responses, *Journal of Osaka University of Economics*, 68(5), p133-143, 2018.
- [9] M. Yamazaki, M. Matsuura, "Adult and elderly electroencephalograms", *Japanese Journal of Clinical Neurophysiology*, 42(6), 387-392, 2014.
- [10] The Japanese Society of Sleep Research Computer Committee, ed.: "PSG chart for learning: Interpretation method and explanation of sleep polygraph records," The Japanese Society of Sleep Research, 1999.
- [11] L. J. Trejo, K. Kubitz, R. Rosipal, R. L. Kochavi, L. D. Montgomery, "EEG-based estimation and classification of mental fatigue," *Psychology*, 6(5), 572-589, 2015.
- [12] M. Ishibashi, T. Yoshida, "The relationship between brain wave fluctuation and reaction times with the decrease in arousal level," *Ergonomics*, 36(5), 229-237, 2000.
- [13] N. Okamura, "How the event-related potential P300 is affected by mental fatigue caused by calculation tasks performed for a long period of time" *J. Occup. Health*, 49(5), 203-208, 2007.
- [14] T.W. Picton, S.A. Hillyard, "Human auditory evoked potentials. II. Effects of attention" *Electroen. Clin. Neuro.*, 36(2), 191-200, 1974.
- [15] J. H. Cohen, J. Polich, "On the number of trials needed for P300" *Int. J. Psychophysiol*, 25(3), 249-55, 1997.
- [16] M. E. Wewers, N. K. Lowe, "A critical review of visual analogue scales in the measurement of clinical phenomena" *Res. Nurs. Health*, 13(4), 227-236, 1990.
- [17] M. Malik, A.J. Camm, "Components of heart rate variability: what they really mean and what we really measure" *Am. J. Cardiol.*, 72(11), 821-822, 1993
- [18] A. Hyvarinen, "Fast and Robust Fied-Point Algorithms for Independent Component Analysis" *IEEE T. Neural Networ.*, 10(3), 626-634, 1999.
- [19] S. Mika, G. Rätsch, J. Weston, B. Schölkopf, K. Müller, "Fisher Discriminant Analysis With Kernels" *Neural Networks for Signal Processing IX: Proceedings of the 1999 IEEE Signal Processing Society Workshop*, 1999.
- [20] K. Fukui, "Past and Present of Subspace Method: Latest Technology Trend: Theoretical Extensions and their Applications" *Information Processing Society of Japan*, 49(6), 680-685, 2008.

- [21] V. N. Vapnik, *Statistical Learning Theory*, Wiley-Interscience, 1998.
- [22] H. Watanabe, Y. Koike, N. Sakurai, A. Takahashi, H. Iguchi, "Analysis of electroencephalogram fluctuations during mental work: mental arithmetic, inversion and association loading," *Japanese Journal of Electroencephalography and Electromyography*, **19**, 253–263, 1991.
- [23] M. Osaka, "Effects of mental work and alpha wave peak frequency-associated task difficulty," *Japanese Journal of Electroencephalography and Electromyography*, **11**, 248–254, 1983.
- [24] L. J. Trejo, K. Kubitz, R. Rosipal, R. L. Kochavi, L. D. Montgomery, "EEG-Based Estimation and Classification of Mental Fatigue" *Psychology*, **6**(5), 572–589, 2015.
- [25] C. Zhao, M. Zhao, J. Liu, C. Zheng, "Electroencephalogram and electrocardiograph assessment of mental fatigue in a driving simulator" *Accident Anal. Prev.*, **45**, 83–90, 2012.
- [26] H. Shinji, W. Yuki, F. Isato, "On the number of averaged electroencephalography epochs for correct detection with a new multiple probe protocol for P300-based concealed information tests" *Journal of the Faculty of Human Cultures and Sciences of Fukuyama University*, **14**, 99–106, 2014.
- [27] K. Simonyan, A. Zisserman, "Very Deep Convolutional Networks for Large-Scale Image Recognition" in *2015 ICLR: Computer Vision and Pattern Recognition*, 2015.

Learning Literary Style End-to-end with Artificial Neural Networks

Ivan P. Yamshchikov^{*1}, Alexey Tikhonov²

¹Max Planck Institute for Mathematics in the Sciences, Leipzig, Germany

²Yandex, Berlin, Germany

ARTICLE INFO

Article history:

Received: 20 June, 2019

Accepted: 26 October, 2019

Online: 28 November, 2019

Keywords:

Stylized text generation

Poetry generation

Artificial neural networks

ABSTRACT

This paper addresses the generation of stylized texts in a multilingual setup. A long short-term memory (LSTM) language model with extended phonetic and semantic embeddings is shown to capture poetic style when trained end-to-end without any expert knowledge. Phonetics seems to have a comparable contribution to the overall model performance as the information on the target author. The quality of the generated texts is estimated through bilingual evaluation understudy (BLEU), a new cross-entropy based metric, and a survey of human peers. When a style of target author is recognized by the humans, they do not seem to distinguish generated texts and originals.

1 Introduction

This paper is an extension of work presented initially in [1] enhanced with the reasoning and experiments described in [2] and [3].

Generation of authentic, stylistically expressive texts is still challenging despite numerous recent advancement in machine-generation of texts. The ability to generate texts that feel personal and expressive opens numerous possibilities for industrial and scientific applications, see [4] or [5]. For example, the generation of stylized texts could improve user experience in human-machine interfaces. When talking about interactions between a human and a machine, one tends to speak in terms of user experience or interface instead of communication. This is partly due to the fact that predictability in a narrow context was for many years (and still is) one of the main aspects of human-machine interfaces [6], [7]. Communication, on the other hand, naturally implies a certain degree of surprise and context shifts on the way [8]–[10]. We expect understandable and reproducible behavior when interacting with a machine, yet regularly allow other humans to be more versatile and obscure when communicating with us. Yet modern technologies that comply with these expectations tend to be perceived as flat and dull. Indeed, personal assistants such as Alexa or Siri have limited anthropomorphic features. However, they can not be tailored to the needs and preferences of every end-user. Other AI-powered solutions tend to have no anthropomor-

phism at all, yet humans voluntarily interact with them. One such example would be a game of advanced chess. In advanced chess, two players accompanied by two AIs play against one another. The concept of such a game was proposed in the 1970s [11], but the history of advanced chess started in 1998, just one year after the historic game between Garry Kasparov and Deep Blue. It represented a paradigm shift, from the twentieth-century 'humans against the machines' to the twenty-first-century 'humans with the machines.' Stylistically expressive text generation can facilitate and speed up this shift.

Modern generative models are typically trained on massive corpora of texts. These corpora consist of various texts created by different people in diverse genres and forms. Standard generative models do not incorporate the information on authorship in any manner and therefore learn to generate texts that are some sort of 'average' across the training dataset. Such texts could hardly be perceived as human-written. Indeed, there is an intuitive belief that each human has a recognizable writing style. This intuition, however, is not backed up by any quantitative definition of a literary style. Experts can have an extensive discussion on what distinguishes a text written by Edgar Allan Poe from a text written by Walt Whitman. However, as far as we are concerned, these expert opinions can rarely be quantified in the context of a rigorously defined natural language processing (NLP) task. That is the reason why this paper addresses the problem of author styl-

*Corresponding author: Ivan P. Yamshchikov, Inselstrasse 22, 04103, Leipzig, Germany, ivan@yamshchikov.info

ized text generation in an end-to-end setup. We propose a model that generates texts resembling the writing style of a particular author without any external information on stylistic aspects of the author's writing. We also restrict the scope of this paper to poetry rather than prose due to several reasons. First, the same machine learning model trained on a smaller dataset tends to show weaker performance. Naturally, for a given amount of authors, a poetic corpus would be inevitably smaller in terms of the number of available texts than a corpus that includes prose. This makes the problem more challenging. However, one can argue that if a proposed method manages to reproduce style when trained on a relatively small corpus of poems, it would be applicable to a bigger dataset as well. Second, poetry is often regarded as a more stylistically expressive form of literary art. This gives hope that even with relatively short chunks of generated texts, one could easily distinguish the style of a target author. One of the methods to estimate the performance of the generative model is to measure how often humans attribute the generated texts to the target authors. The expressive nature of poetry makes such assessment easier for the peers and, therefore, facilitates the experiments. Both these factors make poetry generation a more challenging and a more exciting task than the generation of prose. Nevertheless, we have every reason to believe that a model that successfully generates stylized poetry would also successfully mimic the style of a prosaic text.

This paper has four significant contributions: (1) formalization of stylized text generation framework; (2) a new sample cross-entropy metric that could be used to measure the quality of the stylization; (3) a long short-term memory artificial neural network with extended phonetic and semantic embeddings that generates stylized texts that are quantified both subjectively through a survey and objectively with sample cross-entropy and BLEU metrics; (4) the proposed approach is applicable to a multilingual setting. Most importantly, we show that modern generative neural networks can learn and mimic the author's style in an end-to-end manner without any external expert knowledge.

2 Related work

Almost a century ago, [12] suggested that computers can generate poetry algorithmically. In [13], one can find a detailed taxonomy of generative poetry techniques. However, to work with stylized poetry generation, one has to resolve the ambiguity of the literary style. In a rapidly developing field of textual style-transfer, one can see various definitions of literary style that often contradict one another [14]. Indeed, different aspects of literary style could include a sentiment of a text (see [15] or [16]), it's politeness [17] or a so-called style of the time (see [18]). The style of the time aspect is also addressed by [19] and by [20]. A paper by [21] generalizes these ideas and proposes to measure every stylistic aspect with a dedicated external classifier. Yet the problem of style transfer differs from the stylized text generation significantly: a human-written input could be used to control the saliency of the output [22].

This might improve the resulting quality of the texts that are generated. In the meantime, such input is not available for the generative model, and it has to generate stylized texts from scratch. This makes our problem setup, similar to [23]. This paper shows that modern artificial neural networks can learn the literary style of an author end-to-end without any predefined expert knowledge. This is a meaningful empirical result in itself since it serves as an initial proof-of-concept for further research of stylized text generation. In this paper, we focus on RNN-based generative models. Let us briefly mention several contributions in that area that are relevant for further discussion.

There are a few papers that decompose content and semantics of the input, see [24]–[29]. Yet none of them works with the literary style of the generated texts. In [30] the authors developed a persona-based model that was to be consistent in terms of response generation. There are works that specifically address Chinese classical poetry generation, for example [31]–[35]. However, the contributions in the area of generative poetry in languages other than Chinese or in a multilingual setting are relatively rare. In [36], an algorithm generates a poem in line with a topic given by the user, and in [37], the authors generate stylized rap lyrics with LSTM trained on a rap poetry corpus. These contributions are all based on the idea that when trained on a corpus of similar documents, an artificial neural network could infer certain properties of such text and reproduce them in generative mode. We suggest to make one step further and develop a model that could be trained on a broad dataset of various documents yet generate texts that resemble various subsets of the training dataset.

3 Generation of stylized texts

Consider a corpus $C = \{T_i\}_{i=0}^M$ of M texts written in a given language. Every text of length l is a sequence $T_i = (w_j)_{j=0}^l$ where words (denoted here as w_j) are drawn from a vocabulary set $V = \{w_j\}_{j=1}^L$, where L is the size of a given vocabulary. One can try to vary the length of T_i in training. For practical reasons we further assume that T_i are lines of poems. Since these are the text in natural language there is additional structure over the set V and certain principles according to which sequences T_i are formed. However, this information is only partially observable.

In a standard problem of text generation, a language model predicts the next word w_k using a conditional probability $P(w_k | (w_i)_{i=0}^{k-1})$. Neural networks are widely used for language modeling since [38], see also [39] and [40]. In particular, this family of algorithms allows to avoid the dimensionality curse of a classical language model. One typically would like to obtain a mapping $Y : (C, \mathbb{R}^m, F) \rightarrow \mathbb{R}^d$ and then train a model such that $G(C) : \mathbb{R}^d \rightarrow \{T_i^G\}$.

Usually one tries to use additional observable information in order to improve the general performance of the model, e.g. [41]. For example, if there is a performance metric D (such as BLEU, F1, etc.), one usually minimizes $D(\{T_i\}, \{T_i^G\})$, where $\{T_i\}$ is a randomized sample of C . Let us find a stylization

model $G(C|S)$ that takes into consideration a subset S of continuous and categorical variables out of (\mathbb{R}^m, F) and a metric D in such a way that

$$G(C|S): \begin{cases} (C, \mathbb{R}^m, F) \rightarrow \{T_i^G\} \\ \{T_i^G|S\} \sim \{T_i|S\} \text{ w.r.t. } D \end{cases} \quad (1)$$

A stark difference in our approach is that we train our model using all information available to us, i.e., (C, \mathbb{R}^m, F) . However, we do not measure its overall performance, but rather test it on a specific domain S . This core idea is, in some sense, similar to the principles of one-shot learning, see [42], and, generally, transfer learning, see [43], and author-attribution methods, see [44]. The model has access to information about a broader domain of data. This information happens to be exogenous to the problem in its narrow formulation. For a given domain S , it can seem irrelevant, yet it can significantly boost the results of the model. There are several advantages associated with this approach. First of all, such models naturally imply ample opportunities for customization. If one wants some additional control, the parameters of the model one can include them into S . The output $\{T_i^G|S\}$ will resemble original texts $\{T_i|S\}$ that satisfy S conditions. That property makes such methods applicable to personalized interfaces. At the same time, one would expect that due to the 'umbrella' structure in which $G(C|S)$ is trained on the whole corpus (C, \mathbb{R}^m, F) the model would outperform various smaller models trained on different subsamples of C . Artificial neural networks are known to generalize well. This allows to speculate that system he system that uses less information for training would show inferior performance when compared with a system that is trained on the whole corpus C .

Further we work with an artificial neural network that uses the name of an author as such condition S . Such models when trained on a sufficiently large dataset, generates lyrics similar to the text written by a target author. The quality of the stylization is assessed both subjectively (based on a survey of respondents) and objectively (in terms of BLEU and a sample cross-entropy that we define further). The model has been trained with English and Russian datasets. There are no obstacles to implement this model in other languages. Before we describe our model in detail, let us briefly address one of the issues of poetry generation that rarely gets enough attention from researchers, namely, the phonetics of the lyrics.

4 Importance of phonetics

The structure of the poem could be different across different languages. For example, Chinese poems have highly specific and distinct structures, see [35], whereas some American poetry of the twentieth century or so-called white poems in Russian hardly have any definite structure at all. The structure of poems can depend on various factors. These factors are primarily phonetic. In the broadest sense, a sequence of tones in a Chinese quatrain, a structure of a Persian ruba'i, rhymes in a classical western sonnet, or a structure within rap bars could be expressed as a set of phonetic rules based on a

particular understanding of expressiveness and euphony shared across a given culture. Some cultures and styles also have particular semantic limitations or 'standards,' for example, 'centrality' of specific topics in classical Japanese poetry, see [45]. We do not make attempts to address high-level semantic structure. However, one can add some pseudo-semantic rules to our model, say via some mechanism in line with [36] or [32]. Instead, we suggest focusing on syntax and phonetics.

The importance of phonetics in poetical texts was broadly discussed among Russian futurist poets, see [46]. Several Russian linguistic circles and art groups (particularly OPOJAZ) in the first quarter of 20th century were actively discussing the concept of the abstruse language, see [47], also stressing that the form of a poem, and especially its acoustic structure, is a number one priority for the future of literature. In their recent paper, [48] have challenged the broadly accepted idea that sound and meaning are not interdependent: unrelated languages very often use (or avoid) the same sounds for specific referents. [49] backs this idea up, showing that modern word embeddings capture such dependencies to a certain respect. In line with these ideas, one of the critical features of the model that we discuss below is its concatenated embedding that contains information on the phonetics of every word preprocessed by a bi-directional LSTM alongside with its vectorized semantic representation.

5 Model

Let us look at an LSTM-based language model that predicts the w_{n+1} word based on w_1, \dots, w_n previous inputs and other macro parameters of the sequence. Typically one passes the needed parameter to the network by writing it in its initial state. However, as the generated sequence gets longer, the network often 'forgets' the parameters of the document. We want to develop a model to address the problem given in (1). To do that, we support our model at every step with the embeddings of the document that is currently being analyzed (these are variables from the set S on which we want to condition our model during the generation process, such as the name of a document or its author). This idea makes our approach different from a classical word-based LSTM. It was used in [50] for stylized music generation. Figure 1 shows a schematic picture of the model; document information projections are highlighted with blue and white arrows.

We used an LSTM with 1152-dimensional input and 512-dimensional projection of a concatenated author and document embeddings. A concatenated word representation is shown schematically in Figure 2. At every step and use the word embeddings, which are generally used for a task of this type. However, we believe that word embeddings are not enough: the char-based information might allow for some useful grammar rules to be learned, and, as we discussed in the previous section, phonetics plays a crucial role in the euphony of the final output. To include this information, we suggest using two bidirectional LSTMs with a 128-dimensional vector as a final state. One of the LSTMs works with a char-representation of

the word whereas another uses phonemes of the International Phonetic Alphabet¹, employing heuristics to transcribe words into phonemes. Before training the model, we obtained a vocabulary V for the training dataset, then applied transcribing heuristics to it. The result was a phoneme-based vocabulary V_p . Then, in the training phase, the char-based bidirectional LSTM was reading words from the initial vocabulary $w_j \in V$, and the phoneme-based LSTM was reading words from the heuristically transcribed vocabulary $w'_j \in V_p$. [51] proposes a somewhat similar idea, but with convolutional neural networks rather than with LSTMs. The bidirectional LSTM approach is new to our knowledge.

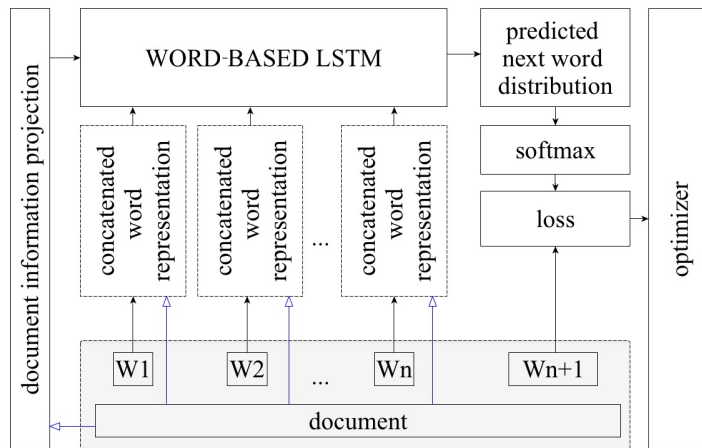


Figure 1: The scheme of the language model. Document information projections are highlighted with blue and white arrows. The projections on a state space of the corresponding dimension is achieved with simple matrix multiplication of document embeddings.

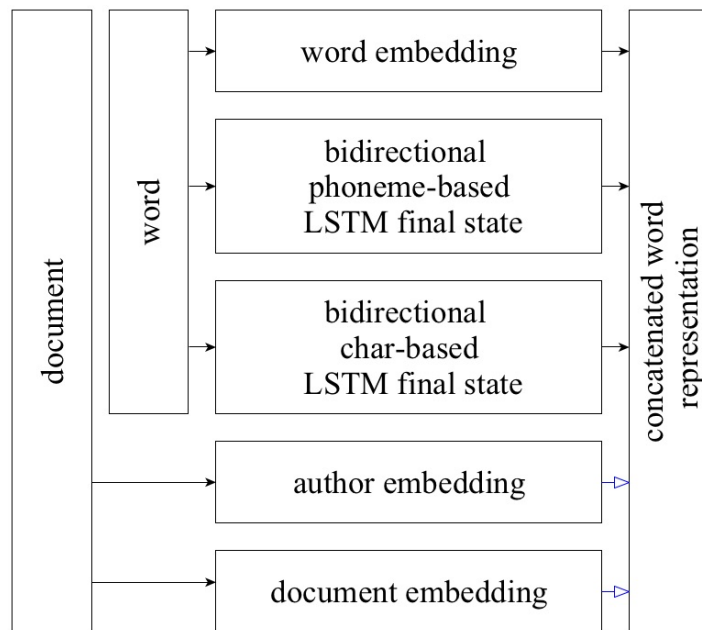


Figure 2: Concatenated word representation.

In Section 7, we describe a series of objective and subjective tests that we ran across a generated output $\{T_i|S\}$, but first, let us briefly describe the datasets used for training.

6 Datasets

Two proprietary datasets of English and Russian poetry were used for training. Every character was transferred to a lower case, and punctuation was deleted. No other preprocessing was made. The overview of the sizes of the datasets can be found in Table 1. This allowed having approximately 330 000 verses in train dataset and another 10 000 verses forming a test dataset for Russian poetry. For English poetry train data consisted of 360 000 verses with approximately 40 000 verses forming the test data.

Table 1: Parameters of the training datasets.

	N. of documents	Size of vocab.	N. of authors	Size
English	110000	165000	19000	150 Mb
Russian	330000	400000	1700	140 Mb

Table 2: Number of words in the training datasets for human-peer tested lyrics.

	N. of words		N. of words
Shakespeare	10 218	Pushkin	226 001
Carroll	19 632	Esenin	73 070
Marley	22 504	Letov	29 766
MUSE	7 031	Zemfira	23 099

During the training phase, the beginning and end of every text T_i were tokenized. In the generation phase, the network is conditioned on values of document parameters S and is initialized with a special 'start' token. As we stated previously, in the most general setup, the set of variables S on which we want to condition our generative model $G(S)$ can vary. Here we use only one categorical variable - the name of the author to test the proposed mechanism for the stylized text generation. We trained the model for Russian (Alexander Pushkin, Sergey Esenin, Joseph Brodsky, Egor Letov and Zemfira Ramazanova) and for English (running tests on lyrics of William Shakespeare, Edgar Allan Poe, Oscar Wilde, Lewis Carroll and Bob Marley as well as lyrics of the American band Nirvana and UK band Muse). Table 2 shows that there were far more authors in the dataset. For the experiments, we chose more prominent authors who are known for their poetic styles. A fluent speaker of the target language could easier identify these authors. The model produces results of comparable quality for both languages, so to make this paper shorter, we further address generative poems in English only and provide the experimental results for Russian in the Appendix. We do not see any difficulties that could prevent the implementation of the proposed model in other languages. As long as there

¹https://en.wikipedia.org/wiki/International_Phonetic_Alphabet

is a sufficiently large corpus C and a phonetically transcribed vocabulary V_p , one could use such a method.

The model produces results of comparable quality for both languages, so to make this paper shorter, we further address generative poems in English only and provide the experimental results for Russian in the Appendix.

Table 3 shows some examples of the generated stylized poetry. The model seems to capture the syntactic characteristics of the author (look at the double negation in the Neuro-Marley lyrics, for example). The vocabulary that is characteristic for a target author also seems to be captured. 'Darkness,' 'burden,' 'fears' could be subjectively associated with the gothic lyrics of Poe. At the same time, 'fun,' 'sunshine,' 'fighting every rule' could be associated with positive yet rebellious reggae music. Author-specific vocabulary can technically imply specific phonetics that characterizes a given author; however, this implication is not self-evident, and generally speaking, does not have to hold. As we demonstrate later, phonetics does, indeed, contribute to the author's stylization significantly.

7 Experiments and evaluation

There is a variety of metrics that could be used as D , for which we could estimate the quality of the generated texts. A standard approach for a comparison of two generative models is to measure cross-entropy loss at certain checkpoints. However, as [52] writes: "There can be significant differences in final performance across checkpoints with similar validation losses." In the case of the provided model, a cross-entropy does not seem to give any meaningful information. To quantitatively estimate the final model $G(C|S)$, we carried out an ablation experiment. We used a plain vanilla LSTM without word-by-word document information support that was only using classic word embeddings as a baseline. Another model to compare with included document information support but didn't have bidirectional LSTMs for phonemes and characters. All the models have shown comparable values of cross-entropy loss after an equal amount of epochs. It seems that the additional structures are not facilitating learning but are also not hindering it. Below we describe two automated metrics that are natural for the problems of such type, namely, the BLEU and the sample cross entropy. We demonstrate that the model captures styles of different authors and that instead of developing several different models $\{G(S_i)\}$ trained on corpora corresponding to different authors one can use one model $G|S$ and change S depending on the style that one wants to reproduce.

7.1 Sample cross entropy

Cross entropy seems to be one of the most natural theoretic-informational metrics to estimate the similarity of different discrete sequences. To distinguish it from the cross-entropy loss, we further call it the sample cross entropy. We calculate it as follows. One samples several subsets with the same

length (in words) from the original author texts. The sample is drawn so that there is a comparable number of unique texts for each author within the sample. Then one splits the texts of a given author A_i into two random groups and calculates the pairwise²cross-entropy between original texts of the author A_i and texts generated by the model $\{T_i^G|A_i\}$. The cross-entropy between the obtained sets of texts was calculated with MITML, see [53], as follows. For every sample written by the author, one built a standard 3-gram based language model with standard MITML smoothing. A shared vocabulary across all samples was calculated. Then the perplexity was computed by applying the language models based on the author-written texts to the original and generated texts. Though both values have a similar meaning, we suggest applying logarithm to the obtained value to get the cross-entropy instead of the perplexity. In Table 4 one can see the results of these calculations. Analogous results for Russian can be found in Appendix in Table 10. The model clearly captures the style of the time mentioned earlier alongside the individual styles. Generated texts stylized for the authors from a similar time period tend to demonstrate lower sample cross-entropy with human-written texts written close to that time.

The model captures the author's writing style better if the sample cross-entropy between the texts written by the given author and the texts generated by the model is lower. We also provide cross-entropy between random samples from the texts of the same author to demonstrate how self-similar are the human-written texts. The majority of texts in the training dataset were the texts from the 20th century. One can see that the model 'perceives' texts of Edgar Allan Poe or William Shakespeare to be closer to the lyrics of Oscar Wilde and Lewis Carrol than to the samples of the original texts. At the same time, Poe and Shakespeare are also reasonably well approximated by the model. To give a reference, we also provide cross-entropies between the texts sampled randomly out of the vocabulary as well as the texts obtained through a weighted average sampling and the human-written texts.

7.2 BLEU

BLEU is a metric estimating the correspondence between a human-written text and a machine's output. It is typically used to assess the quality of machine translation. We suggest to adopt it for the task of stylized text generation in the following way: a random starting line out of the human-written poems is used to initialize the generation. Generative model 'finishes' the poem generating three ending lines of the quatrain. Then one calculates BLEU between lines generated by the model and three actual lines that finished the human-written quatrain.

First of all, one can see that it makes sense to train the model on the whole dataset and then restrict it to the chosen author rather than train it on the target author exclusively. This is shown in Table 5.

²Hence 'sample' in the name of the metric.

Table 3: Examples of the generated stylized quatrains. The punctuation is omitted since it was omitted in the training dataset.

Neuro-Poe	Neuro-Marley
her beautiful eyes were bright	don t you know you ain t no fool
this day is a burden of tears	you r gonna make some fun
the darkness of the night	but she s fighting every rule
our dreams of hope and fears	ain t no sunshine when she s gone

Table 4: Sample cross entropy between generated texts $\{T_i^G|A_i\}$ and actual texts for different authors. The two smallest values in each row are marked with * and ** and a bold typeface. The sample cross entropy between random samples from the texts of the target author and randomly generated sequences of words (uniform and weighted respectively) as well as other samples written by the same author (denoted as SELF) are shown for reference.

Model $G(A_i)$ / author	Shakespeare	Poe	Carroll	Wilde	Marley	Nirvana	MUSE
Neuro-Shakespeare	19.0**	21.6	18.5*	19.9	21.8	22.0	22.4
Neuro-Poe	22.0	20.4**	21.2	19.0*	26.0	25.4	26.0
Neuro-Carroll	22.2	23.6	18.9*	22.5	22.4	21.8**	23.8
Neuro-Wilde	21.2	20.9	20.5**	18.4*	24.5	24.8	26.4
Neuro-Marley	24.1	26.5	22.0	27.0	15.5*	15.7**	16.0
Neuro-Nirvana	23.7	26.2	20.0	26.6	19.3	18.3*	19.1**
Neuro-MUSE	21.1	23.9	18.5	23.4	17.4	16.0**	14.6*
Uniform Random	103.1	103.0	103.0	103.0	103.5	103.3	103.6
Weighted Random	68.6	68.8	67.4	68.5	68.5	68.0	68.0
SELF	23.4	21.8	25.1	27.3	20.8	17.8	13.3

Table 5: BLEU for the full model trained on one particular author dataset, $G(S)$, and on the whole dataset, $G(C|S)$, calculated on the chosen author validation dataset and on the validation dataset that includes a variety of authors. The results may vary across authors depending on the relative sizes of S and C but the general picture does not change.

Model $G(A_i)$	Chosen author S	Validation dataset
$G(S)$	33.0%	19.0%
$G(C S)$	37.3%(+13%)	37.6%(+98%)

The model $G(S)$ is trained on texts of a particular domain S . In this case the domain corresponds to a particular author. One can see that $G(C|S)$ when tested on the lyrics of the chosen author outperforms $G(S)$. Moreover, $G(C|S)$ performs almost twice as good as $G(S)$ on the validation dataset comprised out of the texts of other authors.

Table 6 summarizes the results of the ablation experiments. One can see BLEU calculated on the validation dataset for the plain vanilla LSTM, LSTM extended with author information but without bidirectional LSTMs for phonemes and characters, and the full model. The uniform random and weighted random give baselines to compare the model.

Table 6: BLEU for uniform and weighted random random sampling, vanilla LSTM, LSTM with author embeddings but without phonetics, and for the full model. Phonetics is estimated to be almost as important for the task of stylization as the information on the target author.

Model $G(A_i)$	BLEU
Uniform Random	0.35%
Weighted Random	24.7%
Vanilla LSTM	29.0%
Author LSTM	29.3% (+1% to vanilla LSTM)
Full model	29.5% (+1.7% to vanilla LSTM)

Table 6 shows that extended phonetic embeddings play a significant role in the overall quality of the generated stylized output. It is essential to mention that phonetics is an inherent characteristic of an author and the training dataset. Humans do not have qualitative insights into phonetics of Wilde or Cobain, yet the information on it turns out to be necessary for the style attribution.

7.3 Survey data

For a survey we sampled quatrains from William Shakespeare, Lewis Carroll, Bob Marley, and MUSE band. Each sampled quatrain was accompanied by a quatrain generated by the model conditioned on the same author. One hundred and forty fluent English-speakers were asked to read all sixteen quatrains in a randomized order and choose one option out of five offered for each quatrain. They had to decide if the author of a given verse was William Shakespeare, Lewis Carroll, Bob Marley, MUSE, or an Artificial Neural Network. Table 7 shows the summary of the obtained results. For analogous results in Russian see in Table 11. A more detailed description of the methodology could be found in the Appendix. The generated texts were human-filtered for mistakes, such as demonstrated in Table 8. This stands to reason since clear mistakes would inevitably allow human peers to detect a generated text. The automated metrics provided above were estimated on the whole sample of generated texts without any human-filtering.

Table 7 shows that the model manages to stylize several given authors. The participants recognized Shakespeare more than 46% of the time (almost 2.5 times more often than compared with a random choice). They did slightly worse in recognizing Bob Marley (40% of cases) and MUSE (39% of

Table 7: Results of a survey with 140 respondents. Shares of each out of 5 different answers given by people when reading an exempt of a poetic text by the author stated in the first column. The two biggest values in each row are marked with * and ** and a bold typeface.

Model $G(A_i)$ or author	Shakespeare	Carroll	Marley	MUSE	LSTM
Neuro-Shakespeare	0.37*	0.04	0.05	0.14	0.3**
Shakespeare	0.46*	0.05	0.04	0.07	0.3**
Neuro-Carroll	0.02	0.07	0.26**	0.18	0.41*
Carroll	0.05	0.2**	0.14	0.11	0.32*
Neuro-Marley	0.02	0.01	0.47*	0.2	0.29**
Marley	0.15	0.05	0.4*	0.1	0.24**
Neuro-MUSE	0.09	0	0.12	0.34**	0.39*
MUSE	0.03	0.05	0.28**	0.39*	0.2

cases, 2 times higher than a random choice). It seems that the human-written quatrains were recognizable. The participants were also fluent enough in the target language to attribute given texts to the correct author. However, people believed that the generated text was actually written by a target author in 37% of cases for Neuro-Shakespeare, 47% for Neuro-Marley, and 34% for Neuro-MUSE, respectively. Lewis Carroll was less recognizable. His texts were only recognized in 20% of cases. The underperformance of the model can be explained with difficulty experienced by the participants in determining Carroll's authorship. If humans have a hard time recognizing the author's style, it is hard to expect an excellent performance of a model on such a target author. Combining the results in Table 6 with the results of the survey shown in Table 7, one could conclude that the phonetic structure of lyrics has an impact on the correct author attribution of the stylized content. This impact is usually not acknowledged by a human reader but is highlighted with the proposed experiment.

7.4 Discussion

Here we would like to share some of the insights into the nature of computational creativity. First, the stylized generation is thought-provoking since the model learns similarities between various authors in the dataset and extrapolates if there is a deficit of information. For example, one of the Nirvana-stylized lines ran:

a god who's always welcome to iraq

Kurt Cobain committed suicide long before the start of the Iraq campaign. However, since the model was trained on a massive corpus of poems (and not only on Nirvana ones), this line emerged among the generated lyrics. It also fits into the broader context of a song due to the correct rhythmic structure. When filtering the network's output, we found this line exceptionally interesting. It was meaningful to us because it resonated with our intuition that, if he were alive, Cobain would have spoken about the Iraq war in his lyrics. We also found it stylistically similar to Cobain lyrics and emotionally provocative. Formally speaking, all of these characteristics are human-attributed, and yet they can emerge out of explorative human-algorithm interactions. One could reason that the topic

of Iraq occurred in other songs by grange bans, and the model extrapolated the saliency of the topic to the Cobain lyrics.

Second, creativity is serendipitous and highly depends on the perception of the viewer. In the Appendix of this paper, we provide examples of typical mistakes. One such mistake that is characteristic for the state of the art artificial neural network is an abrupt end of a line. As we listed the examples of such behavior, we came across the following line:

at night i lay waiting for a

However, one of our colleagues pointed out that this line represents a perfect one-line poem; an abrupt ending only enhances the feeling of longing. We have decided to submit this poem among others into the journal of modern poetry, and it was published³. We find both these insights meaningful for further research on computational creativity.

Over the last several years, we have seen several attempts at employing AI as a tool for creators. Using the approach proposed in [54], some visual artists applied style transfer algorithms to various pictures, creating new and unique experiences. In a postmodern cultural context, style transfer can be a conceptual tool that is able to convey the thought of an artist in a more expressive and meaningful way, for example, see [55].

8 Conclusion

This paper addresses the problem of author-stylized text generation. We show that an extension of a language model supported by the document meta-information at every step is apt for such tasks. Large concatenated embeddings that consist of word embedding, a phoneme-based bidirectional LSTM final state, and a char-based bidirectional LSTM final state are shown to facilitate end-to-end learning of author poetic style. Moreover, extending word embeddings with phonetic information has a comparable impact on the BLEU of the generative model as the information on the authors of the text. A cross-entropy method to estimate the quality of stylization is proposed. This model is shown to perform in Russian and English, and there seem to be no obvious reasons for which one could not implement it in other languages. It was shown

³<https://nokturno.fi/poem/on-author-stylized-neural-network-poetry>

that the texts generated by the model tend to be closer to the texts of the target author than the text generated by a plain vanilla LSTM both in terms of the cross-sample entropy and BLEU. It was also shown that, when faced with an author with a recognizable style (an author who is recognized approximately two times more frequently than at random), humans mistakenly recognize the output of the proposed generative model for the target author as often as they correctly attribute original texts to the author in question.

References

- [1] Alexey Tikhonov and Ivan P. Yamshchikov. Guess who? multilingual approach for the automated generation of author-stylized poetry. In *IEEE Spoken Language Technology Workshop (SLT)*, pages 787–794, 2018.
- [2] Alexey Tikhonov and Ivan P. Yamshchikov. Sounds wilde. phonetically extended embeddings for author-stylized poetry generation. In *Proceedings of the Fifteenth Workshop on Computational Research in Phonetics, Phonology, and Morphology*, pages 117–124, 2018.
- [3] Ivan P. Yamshchikov and Alexey Tikhonov. I feel you: What makes algorithmic experience personal? In *Proceedings of EVA Copenhagen 2018 - Politics of the Machines - Art and After*, 2018.
- [4] Daniel Livingstone. Turing’s test and believable ai in games. *Computers in Entertainment*, 4(1):6, 2006.
- [5] Alan Dix. Human-like computing and human–computer interaction. In *Proceedings of the 30th International BCS Human Computer Interaction Conference: Fusion!*, page 52, 2016.
- [6] J. Weizenbaum. Eliza—a computer program for the study of natural language communication between man and machine. *Communications of the ACM*, 9(1):36–45, 1966.
- [7] S. K. Card, T.P Moran, and A. Newell. *The psychology of human-computer interaction*. CRC Press, 1983.
- [8] Y. Ohsawa. Modeling the process of chance discovery. *Chance discovery*, pages 2–15, 2003.
- [9] W. R. Saab, N. abd Joolingen and B. H. Hout-Wolters. Eliza—a computer program for the study of natural language communication between man and machine. *British Journal of Educational Psychology*, 75(4):603–621, 2005.
- [10] A. Abe. Curation and communication in chance discovery. In *Proceedings of the 6th International Workshop on Chance Discovery (IWCD6) in IJCAI*, 2011.
- [11] D. Michie. Programmer’s gambit. *New Scientist*, 17th of August:329–332, 1972.
- [12] Jon Wheatley. The computer as poet. *Journal of Mathematics and the Arts*, 72(1):105, 1965.
- [13] Carolyn Lamb, G. Brown, Daniel, and L. Clarke, Charles. A taxonomy of generative poetry techniques. *Journal of Mathematics and the Arts*, 11(3):159–179, 2017.
- [14] Alexey Tikhonov and P. Yamshchikov, Ivan. What is wrong with style transfer for texts? In *arXiv preprint*, 2018.
- [15] Tianxiao Shen, Tao Lei, Regina Barzilay, and Tommi Jaakkola. Style transfer from non-parallel text by cross-alignment. *31st Conference on Neural Information Processing Systems*, pages 6833–6844, 2017.
- [16] Juncen Li, Robin Jia, He He, and Percy Liang. Delete, retrieve, generate: A simple approach to sentiment and style transfer. In *Proceedings of the 2018 Conference of the North American Chapter of the Association for Computational Linguistics: Human Language Technologies*, volume 1, pages 1865–1874, 2018.
- [17] Rico Sennrich, Barry Haddow, and Alexandra Birch. Controlling politeness in neural machine translation via side constraints. In *Proceedings of the 2016 Conference of the North American Chapter of the Association for Computational Linguistics: Human Language Technologies*, pages 35–40, 2016.
- [18] James M. Hughes, Nicholas J. Foti, David C. Krakauer, and Daniel N. Rockmore. Quantitative patterns of stylistic influence in the evolution of literature. *Proceedings of the National Academy of Sciences*, 109(20):7682–7686, 2012.
- [19] Harsh Jhamtani, Varun Gangal, Eduard Hovy, and Eric Nyberg. Shakespearizing modern language using copy-enriched sequence-to-sequence models. In *Proceedings of the Workshop on Stylistic Variation*, pages 10 – 19, 2017.
- [20] Keith Carlson, Allen Riddell, and Daniel Rockmore. Zero-shot style transfer in text using recurrent neural networks. In *arXiv preprint*, 2017.
- [21] Zhenxin Fu, Xiaoye Tan, Nanyun Peng, Dongyan Zhao, and Rui Yan. Style transfer in text: Exploration and evaluation. In *arXiv preprint*, 2017.
- [22] Kelvin Guu, Tatsunori B. Hashimoto, Yonatan Oren, and Percy Liang. Generating sentences by editing prototypes. In *arXiv preprint:1709.08878*, 2017.
- [23] Jessica Fidler and Yoav Goldberg. Controlling linguistic style aspects in neural language generation. In *Proceedings of the Workshop on Stylistic Variation*, pages 94 – 104, 2017.
- [24] Remi Lebret, David Grangier, and Michael Auli. Neural text generation from structured data with application to the biography domain. In *Proceedings of the 2016 Conference on Empirical Methods in Natural Language Processing*, pages 1203–1213, 2016.
- [25] Alec Radford, Rafal Jozefowicz, and Ilya Sutskever. Learning to generate reviews and discovering sentiment. In *arXiv preprint*, 2017.
- [26] Jian Tang, Yifan Yang, Sam Carton, Ming Zhang, and Qiaozhu Mei. Context-aware natural language generation with recurrent neural networks. In *arXiv preprint*, 2016.
- [27] Zhiting Hu, Zichao Yang, Xiaodan Liang, Ruslan Salakhutdinov, and Eric P. Xing. Toward controlled generation of text. In *International Conference on Machine Learning*, pages 1587–1596, 2017.
- [28] Alexey Tikhonov, Viacheslav Shibaev, Aleksander Nagaev, Aigul Nugmanova, and Ivan P. Yamshchikov. Style transfer for texts: Retrain, report errors, compare with rewrites. In *arXiv preprint:1908.06809*, 2019.
- [29] Ivan P Yamshchikov, Viacheslav Shibaev, Aleksander Nagaev, Jürgen Jost, and Alexey Tikhonov. Decomposing textual information for style transfer. *arXiv preprint arXiv:1909.12928*, 2019.
- [30] Jiwei Li, Michel Galley, Chris Brockett, Georgios P. Spithourakis, Jianfeng Gao, and William B. Dolan. A persona-based neural conversation model. *CoRR*, abs/1603.06155, 2016.
- [31] Jing He, Ming Zhou, and Long Jiang. Generating chinese classical poems with statistical machine translation models. In *AAAI*, 2012.
- [32] Xiaoyuan Yi, Ruoyu Li, and Maosong Sun. Generating chinese classical poems with rnn encoder-decoder. In *Chinese Computational Linguistics and Natural Language Processing Based on Naturally Annotated Big Data*, pages 211–223, 2017.
- [33] Rui Yan. i, poet: Automatic poetry composition through recurrent neural networks with iterative polishing schema. In *Proceedings of the Twenty-Fifth International Joint Conference on Artificial Intelligence (IJCAI-16)*, pages 2238–2244, 2016.
- [34] Rui Yan, Cheng-Te Li, Xiaohua Hu, and Ming Zhang. Chinese couplet generation with neural network structures. In *Proceedings of the 54th Annual Meeting of the Association for Computational Linguistics*, pages 2347 – 2357, 2016.
- [35] Jiyuan Zhang, Yang Feng, Dong Wang, Yang Wang, Andrew Abel, Shiyue Zhang, and Andi Zhang. Flexible and creative chinese poetry generation using neural memory. In *Proceedings of the 55th Annual Meeting of the Association for Computational Linguistics*, volume 1, pages 1364–1373, 2017.
- [36] Marjan Ghazvininejad, Xing Shi, Yejin Choi, and Kevin Knight. Generating topical poetry. In *Proceedings of the 2016 Conference on Empirical Methods in Natural Language Processing*, pages 1183–1191. Association for Computational Linguistics, 2016.

- [37] Peter Potash, Alexey Romanov, and Anna Rumshisky. Ghostwriter: Using an lstm for automatic rap lyric generation. In Proceedings of the 2015 Conference on Empirical Methods in Natural Language Processing, pages 1919–1924. Association for Computational Linguistics, 2015.
- [38] Yoshua Bengio, Réjean Ducharme, Pascal Vincent, and Christian Jauvin. A neural probabilistic language model. *Journal of machine learning research*, 3(Feb):1137–1155, 2003.
- [39] Frederic Morin and Yoshua Bengio. Hierarchical probabilistic neural network language model. *Aistats*, pages 246–252, 2005.
- [40] Andriy Mnih and Geoffrey Hinton. A scalable hierarchical distributed language model. In *Advances in neural information processing systems*, pages 1081–1088, 2009.
- [41] Yangyang Shi. *Language Models with Meta-information*. PhD thesis, Technical University of Delft, 2014.
- [42] Li Fei-Fei, Rob Fergus, and Pietro Perona. One-shot learning of object categories. In *IEEE transactions on pattern analysis and machine intelligence*, pages 594 – 611, 2006.
- [43] Sebastian Thrun and Lorien Pratt. *Learning to learn*. Springer Science & Business Media, 2012.
- [44] Douglas Bagnall. Author identification using multi-headed recurrent neural networks. In *arXiv preprint*, 2015.
- [45] Senko K. Maynard. The centrality of thematic relations in japanese text. *Functions of language*, 1(2):229–260, 1994.
- [46] Aleksei Kruchenykh. *Phonetics of theater*. M.:41, Moscow, 1923.
- [47] Victor Shklovsky. *Poetics: on the theory of poetic language*. 18 State typography, Petrograd, 1919.
- [48] E Blasi, Damián, Søren Wichmann, Harald Hammarström, F. Stadler, Peter, and H. Christiansen, Morten. Sound – meaning association biases evidenced across thousands of languages. *Proceedings of the National Academy of Sciences*, 113(39):10818 – 10823, 2016.
- [49] Ivan Yamshchikov, Viacheslav Shibaev, and Alexey Tikhonov. Dyr bul shchyl. proxying sound symbolism with word embeddings. In *Proceedings of the 3rd Workshop on Evaluating Vector Space Representations for NLP*, pages 90–94, 2019.
- [50] Alexey Tikhonov and P. Yamshchikov, Ivan. Music generation with variational recurrent autoencoder supported by history. In *arXiv preprint*, 2017.
- [51] Rafal Jozefowicz, Oriol Vinyals, Mike Schuster, Noam Shazeer, and Yonghui Wu. Exploring the limits of language modeling. In *arXiv preprint*, 2016.
- [52] Ziang Xie. Neural text generation: A practical guide. In *arXiv preprint*, 2017.
- [53] Bo-June Hsu and James Glass. Iterative language model estimation: efficient data structure & algorithms. In *Ninth Annual Conference of the International Speech Communication Association*, 2008.
- [54] L.A. Gatys, A. S. Ecker, and M. Bethge. Image style transfer using convolutional neural networks. In *Proceedings of the IEEE Conference on Computer Vision and Pattern Recognition*, pages 2414 – 2423, 2016.
- [55] B. Joshi, K. Stewart, and D. Shapiro. Bringing impressionism to life with neural style transfer in come swim. In *arXiv preprint:1701.04928*, 2018.
- Since generation is done in a word-by-word manner, the model can deviate when sampling a low-frequency word;
 - Pronouns tend to cluster together, possibly due to the problem of anaphoras in the training dataset;
 - The line can end abruptly; this problem also seems to occur more frequently for the authors that are underrepresented in the training dataset.

Table 9 lists some subjectively cherry-picked, especially successful examples of the system outputs both for English and for the Russian language. Since the text is generated line by line, and verses are obtained through random rhyme or rhythm filtering, several types of serendipitous events occur. They can be broadly classified into four different types:

- Wording of the verse that fits into the style of the target author;
- Pseudo-plot that is perceived by the reader due to a coincidental cross-reference between two lines;
- Pseudo-metaphor that is perceived by the reader due to a coincidental cross-reference between two lines;
- Sentiment and emotional ambiance that corresponds to the subjective perception of the target author.

B Cross-entropy for texts in Russian

The cross-entropy between generated texts and samples of human-written texts was calculated as described in Section 7.1. The results are shown in Table 10

One can see that the model achieves the lowest level of cross-entropy when tested on the texts of the target author for all four authors.

C Survey design

The surveys were designed identically for English and Russian languages. We have recruited the respondents via social media; the only prerequisite was fluency in the target language. Respondents were asked to determine authorship for 16 different 4-line verses. The verses for human-written text were chosen randomly out of the data for the given author. The generated verses were obtained through line-by-line automated rhyme and rhythm heuristic filtering. Since LSTMs are not perfect in text generation and tend to have clear problems illustrated in Table 8, we additionally filtered generative texts leaving the verses that do not contain obvious mistakes described above. Each of the 16 questions consisted of a text (in lower case with stripped-off punctuation) and multiple-choice options listing five authors, namely, four human authors and an artificial neural network. Respondents were informed that they are to distinguish human- and machine-written texts. The correct answers were not shown to the respondents. Table 7 shows the results of the survey for English texts and Table 11 for Russian ones. Higher values in every row correspond to the options that were more popular among the respondents when they were presented with the text written by the author listed in the first column of the table.

A Examples of output

Table 8 lists some illustrative mistakes of the model both for English and for the Russian language. Reading the raw output, we could see several types of recurring characteristic errors that are typical for LSTM-based text generation. They can be broadly classified into several different types:

- If the target author is underrepresented in the training dataset, the model tends to make more mistakes, mostly, syntactic ones;

Table 8: Examples of several recurring types of mistakes that occur within generated lyrics.

Problem	English	Russain
broken syntax	<i>Neuro – MUSE :</i> every step inside on our faces that i would stop my self going crazy	<i>Neuro – Zemfira :</i> ты слышишь я слышу шаги мои в душу дрожи
'rare' word brakes the line	<i>Neuro – Shakespeare :</i> o ho de profundis she says i am on her	<i>Neuro – Letov :</i> иду гляжу в окно гляжу мне вслед на небо
pronouns 'entangle'	<i>Neuro – Shakespeare :</i> thou here shalt be and thine who will have to my grave	<i>Neuro – Zemfira :</i> тебе ли ты ль за
sentences don't end	<i>Neuro – Muse :</i> at night i lay waiting for a	<i>Neuro – Brodsky :</i> двух четырех десять лет за углом
nonsense	<i>Neuro – Shakespeare :</i> do many a fair honour best of make or lose	<i>Neuro – Lenov :</i> о о о о и о

Table 9: Cherry-picked examples of generated lyrics after either rhyme or rhythm filtering illustrating typical serendipities.

Serendipity	English	Russain
peculiar wording	<i>Neuro – Shakespeare :</i> a sense i may not comprehend of whom i had not to defend	<i>Neuro – Pushkin :</i> во славу вакха или тьмы мы гордо пировали
apophenic plot	<i>Neuro – Marley :</i> oh lord i know how long i d burn take it and push it it s your turn	<i>Neuro – Esenin :</i> ты под солнцем стоишь и в порфире как в шелку беззаботно горишь
apophenic metaphor	<i>Neuro – Carroll :</i> your laugh is bright with eyes that gleam that might have seen a sudden dream	<i>Neuro – Zemfira :</i> ветер в голове с красной тенью шепчется
peculiar sentiment	<i>Neuro – Muse :</i> i am the man of this universe i remember i still am a curse	<i>Neuro – Letov :</i> только в ушах отражается даль только белая смерть превращается в ад

Table 10: Sample cross entropy between generated texts $\{T_i^G|A_i\}$ and actual texts for different authors. The two smallest values in each row are marked with * and ** and a bold typeface. The sample cross entropy between random samples from the texts of the target author and randomly generated sequences of words (uniform and weighted respectively) as well as other samples written by the same author (denoted as SELF) are shown for reference.

Model $G(A_i)$ / author	Pushkin	Esenin	Brodsky	Letov	Zemfira
Neuro-Pushkin	17.9*	21.8**	23.4	27.0	30.8
Neuro-Esenin	20.4**	18.8*	21.0	22.7	26.0
Neuro-Brodsky	23.5	21.1**	17.2*	20.9	23.8
Neuro-Letov	22.2	20.0**	20.8	19.6*	23.6
Neuro-Zemfira	19.5	17.1**	18.1	18.2	16.6*
Uniform Random	103.0	103.1	103.0	103.0	103.8
Weighted Random	40.8	40.2	40.2	42.6	45.6
SELF	35.0	33.7	38.0	28.3	12.0

Table 11: Results of a survey with 178 respondents. Shares of each out of 5 different answers given by people when reading an exempt of a poetic text by the author stated in the first column. The two biggest values in each row are marked with * and ** and a bold typeface.

Model $G(A_i)$ or author	Pushkin	Esenin	Letov	Zemfira	LSTM
Neuro-Pushkin	0.31**	0.22	0.02	0.0	0.44*
Pushkin	0.62*	0.11	0.03	0.01	0.23**
Neuro-Esenin	0.02	0.61*	0.08	0.0	0.29**
Esenin	0.06	0.56*	0.07	0.02	0.29**
Neuro-Letov	0.0	0.02	0.40**	0.08	0.51*
Letov	0.0	0.01	0.61*	0.02	0.35**
Neuro-Zemfira	0.0	0.06	0.13	0.4**	0.41*
Zemfira	0.0	0.02	0.08	0.58*	0.31**

The Potential of Ocean Current as Electrical Power Sources Alternatives in Karimunjawa Islands Indonesia

Aris Ismanto^{1,2*}, Dwi Haryo Ismunarti¹, Denny Nugroho Sugianto^{1,2}, Siti Maisyarah¹, Petrus Subardjo¹, Agus Anugroho Dwi Suryoputro¹, Hendry Siagian¹

¹ Oceanography Department, Faculty of Fisheries and Marine Science, Diponegoro University, Semarang, Indonesia 50275

²PUI-CoREM (Center of Excellence for Science and Technology - Center for Coastal Disaster Mitigation and Rehabilitation Studies), Diponegoro University, Indonesia

ARTICLE INFO

Article history:

Received: 22 July, 2019

Accepted: 10 November, 2019

Online: 25 November, 2019

Keywords:

Renewable

Energy

Current

Model

Karimunjawa

ABSTRACT

Electrical energy shortage and expensive basic electricity costs are one of the problems that are occurred in Karimunjawa Island, Indonesia. The purpose of this research is to identify the potential of ocean currents energy as one of the alternatives to reduce the problem related to energy needs and to predict the electrical energy that can be obtained. The physical phenomena movement of ocean currents is made by using the 2-Dimensional hydrodynamic mathematical model. ADCP Multicell Argonaut-XR type is used to measure the speed of ocean currents to validate the model result. Tidal, wind, coordinate and bathymetry data are all the variables that are in the mathematical model of ocean current movement. The potential of electrical energy is determined by the value of power density which is calculated based on the speed ocean current model. The result of this research is the map of the potential distribution of ocean currents in Karimunjawa waters.

1. Introduction

Indonesia was a maritime country which is the largest archipelago with an area of 5,193,252 km², two-thirds of Indonesia's territory is an ocean, which is around 3,288,683 km² [1] and the whole island is about 17,508 islands [2]. Karimunjawa Islands situated on the Java Sea along of coordinate 5°40' - 5°57' SL and 110°4' - 10°40' EL. The area is around 111,625 ha, consisting of 7,033 ha of land and 104,592 ha of water. There are 5 inhabited islands out of 27 islands in Karimunjawa namely Karimunjawa, Kemujan, Parang, Nyamuk and Genting island [3]. One of the problems in the Karimunjawa islands is electricity. The occurrence of an electricity crisis in the form of service time duration is only lights up 6 hours each day and basic electricity cost are expensive [4]. Since the enactment of Government Regulation Number of 12, 2012 concerning retail cost and consumers of specific fuel users, diesel power plants sources (PLTD) in Karimunjawa must used industrial diesel at cost of IDR 14,700 each liter. The regional government spend money IDR 12 billion each year to welshed supply electricity [5].

According to [6,7], the sea potential being a course of energy is very high. The stored energies the potential of wave energy, tidal range, ocean currents, ocean thermal & salinity gradient energy, and subsea geothermal energy. According to the Indonesian Marine Energy Association (ASELI), the total of marine resources in Indonesia reaches 727,000 MW [8].

Research related to ocean currents as a potential source of electrical energy has been conducted since 2006 in East Nusa Tenggara, i.e. in Lombok Strait, Alas Strait, Nusa Penida Strait, Flores Strait, Pantar Strait [9] and Larantuka waters, East Flores [10]. The results of research in Larantuka waters show that ocean currents have great potential to be developed as an energy source of the power plant. The characteristics of ocean currents are generated by tidal currents. The morphological condition of the waters in the presence of Gonzales strait causes an optimum current speed. Forecast that 96% of ocean currents in Larantuka waters has the potential to be developed as a power plant. The average power density generated is 6271,75 watts [11].

Some countries have managed to harness ocean current and tidal energy as the source of power plants, from a generator's turbine prototype to the commercial-scale turbines with a capacity

*Ismanto, et al., Oceanography Department, Diponegoro University, +6285292419995. aris.ismanto@gmail.com

of 1.2 MW / turbine. Marine current energy plants have been built in Scotland, Sweden, France, Norway, England, Northern Ireland, Australia, Italy, South Korea, and the United States [12].

Ocean currents are horizontal motions of water masses so they have kinetic energy that can drive the rotor or turbine power plant as well as on wind power plants. An effort to explore a source of energy unconventional from the ocean currents begins with the mapping of the ocean currents and the potential energy. The movement of ocean currents that swept across the ocean currents in the water line data based observations and takes along time and is quite expensive in measuring data. An alternative approach mathematical models to study how the pattern of the current movement in the water line. The model is a prototype or imitation of real situation [13]. Over the past three decades the development of mathematical models has been rapidly driven by the development of numerical analysis, computer technology, and visualization techniques. The acceptance and confidence level of the mathematical model on hydrodynamics is currently very high, both in research, engineering and industry [14].

The Mathematical equation formulas that describe the physical phenomena of current movements include 2-D mathematical model in hydrodynamics. As for the force that can affect the movement of the current model is the tidal forces on the surface. Variables that will be used in the mathematical model of the movement of ocean currents conducted are tidal, wind coordinate and bathymetry data. Energy potential can be determined by the power density calculated based on the value of the current speed obtained from the ocean current model. Energy potential was presented in the map of potential energy distribution.

The purpose of this research are carried out in developing studies of renewable energy sources of ocean current in the Karimunjawa Islands. Ocean current energy is renewable energy that can be used as potential energy in the coastal areas, especially in small islands [15]. Ocean current pattern mapping is the first step to explore non-conventional energy sources of ocean currents. Information on current movement patterns can also be used for various purposes such as consideration in the construction of harbor docks, onshore and offshore structures (drilling rig and pipes to be installed on the seafloor), aquaculture and site selection most likely for development of current power generation [13].

2. Materials and Methods

2.1. The research area

Quantitative method as the main method used in this study, the resulting data includes quantitative data as the main and supporting data. quantitative data in the form of data figures that will be analyzed according to the method [16]. there are 2 types of data used in this study, namely primary and secondary data. Data including secondary data is wind data for 10 years (2004-2014) with hourly records obtained from BMKG Semarang. Data obtained from DISHIDROS are coordinate data and bathymetry data. Secondary data is used to build 2-D mathematical model of current speed and direction of the current. Water flow data throughout the year are generated from 2-D mathematical modeling.

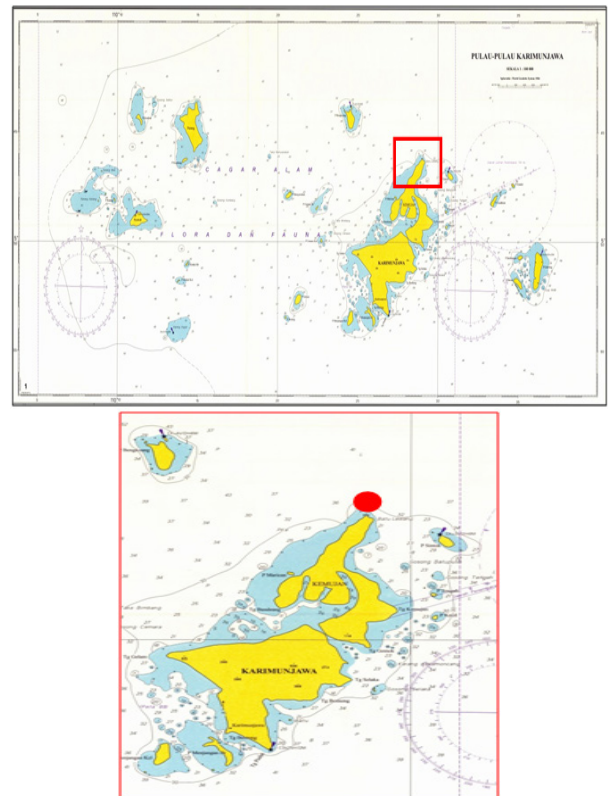


Figure 1. Study area and observation station [17].

Primary data measurement are tidal elevation and the current speed & direction data. Field data obtained are used to test the accuracy of the model. The current speed was measured using an ADCP Multi-Cell Argonaut-XR type device with wave length sensor beam 0.75 MHz and autonomous multi-cell system. Water depth is about 13 meters, while the total depth is 12 meters. Current speed is observed at eight points depth (d) or layers, i.e. at a depths of 1.5 meters, 3 meters, 4.5 meters, 6 meters, 7.5 meters, 9 meters, 10.5 meters, and 12 meters. Current speed measurements were carried out for 5 x 24 hours with measuring intervals at each layer and an average layer of 600 seconds. The obtained maximum current speed in the depths between 1.5 meters – 3 meters is 1.02 m/s. The measurement station point was determined based on the maximum current speed of the simulated numerical model at the same time as the field measurement [17].

2.2. Mathematical Model on Hydrodynamics

Ocean currents are the horizontal movement of seawater mass caused by the driving force acting on seawater. The main movement of water were caused by tides or the movements of sea levels due to the gravity [18-19], The current is also generated by the wind that blows on the surface of the water that transfers momentum and energy to the surface layer of water. Wind stress creates a tangential force which then moves the water in the direction of the wind.

The processes that occur in the fluid at sea are complex. The process described in a mathematical equations is called a mathematical model. Mathematical modeling on hydrodynamics to gain an understanding of ocean hydrodynamics. The goal is to study the mechanical variables of the fluid systems at sea. Utilization of models among others for tidal prediction, water level

elevation, current pattern, nutrient dispersion or pollutants, sedimentation and erosion.

The current movement patterns have vertical dimensions (depth) and horizontal dimensions. In general, the depth dimension is much smaller than the horizontal dimension so that the model that we used is a two-dimensional horizontal model (2DH). The mathematical equations that references the 2DH model is a continuity and momentum equation with simplicity: The mean value of depth is considered to represented parameters values that fluctuate along with the depth of flow. The speed and acceleration in the vertical direction are considered to be of small value, so they are ignored. the hydrostatic pressure distribution that applied together with the depth and the slope of base in both small horizontal directions.

The average value of the hydrodynamic variable at all depth is obtained by integrating it into the flow depth: $u = \frac{1}{h} \int_{z_0}^{z_t} u dz$. According to the study of Kowalik and Murty [20] the continuity and momentum equations for two DH current are:

The continuity equation :

$$\frac{\partial h}{\partial t} + \frac{\partial Uh}{\partial x} + \frac{\partial Vh}{\partial y} = 0 \quad (1)$$

The momentum equation in the X-axis direction:

$$\frac{\partial Uh}{\partial t} + \frac{\partial(U^2h + \frac{1}{2}gh^2)}{\partial x} + \frac{\partial UVh}{\partial y} = gh(S_{ox} - S_{fx}) + \frac{\partial}{\partial x}(\frac{h}{\rho}T_{xx}) + \frac{\partial}{\partial y}(\frac{h}{\rho}T_{yx}) \quad (2)$$

The momentum equation in the y-axis direction :

$$\frac{\partial Uh}{\partial t} + \frac{\partial UVh}{\partial x} + \frac{\partial(U^2h + \frac{1}{2}gh^2)}{\partial y} = gh(S_{oy} - S_{fy}) + \frac{\partial}{\partial x}(\frac{h}{\rho}T_{xy}) + \frac{\partial}{\partial y}(\frac{h}{\rho}T_{yy}) \quad (3)$$

Where:

x = distance in x-direction (direction of longitudinal flow), m

u = x-directional horizontal speed, m/s

y = distance in the y-direction (lateral flow direction), m

v = horizontal speed of the y-direction, m/s

t = time, s

h = water depth, m,

r = density, kg/m³

S_{ox} & S_{oy} is the basic slope of the x and y directions.

S_{fx} & S_{fy} is the slope of energy lines in the x and y-direction.

T_{ij} is the mean shear stress to depth

g = acceleration of gravity, m/s²

The slope of the energy line is calculated by the Manning or Chezy equation:

The Manning equation, i.e. $S_{fx} = \frac{n^2 U \sqrt{U^2 + V^2}}{h^3}$ and $S_{fy} = \frac{n^2 V \sqrt{U^2 + V^2}}{h^3}$ (4)

The Chezy equation, i.e. : $S_{fx} = \frac{U \sqrt{U^2 + V^2}}{C^2 h}$ and $S_{fy} = \frac{V \sqrt{U^2 + V^2}}{C^2 h}$ (5)

The basic friction coefficient is expressed by $\tau_x^b = \rho_w g \frac{U \sqrt{U^2 + V^2}}{C^2}$ (6)

The basic coarse coefficient is $C = \frac{1}{n} h^{\frac{1}{6}}$ (7)

2.3. Ocean Current Energy as A Power Plant

Utilization of ocean currents as a source of electrical energy has same principle as wind power. Kinetic energy from ocean currents is generated from water that moves through water turbines. Compared to wind turbines, currents turbine will produce greater energy at the same speed. This occurs because the density of seawater is much higher than the density of air [21].

Current-generated power plants almost do not produce pollution. Current power generation also has no impact on current flows or sediment transfers as it affects only the pattern of ocean currents at the site. Slow turbine blade speeds are harmless to marine organisms and do not produce underwater sound pollution compared to ship propellers so it will cause into the small ecology [22]. In addition, the current has a tendency phase along with the rise and fall of the tides so that the power generated is easy to predict [23].

The energy potential is assumed in terms of power density which is proportional to its speed. The power assemblies generated by ocean currents can be calculated using the following equation: $P = \frac{1}{2} \rho A V^3$, where ρ is the density of seawater (kg/m³); A is the area of turbine cross-section used (m²), and V is the speed of ocean currents (m/s) [24]. Seawater density is assumed to be homogeneous with a value of $\rho = 1.025$ kg/m³ [21].

- I. Zero to cut-in speed
- II. Cut-in speed to rated speed
- III. Greater than rated speed

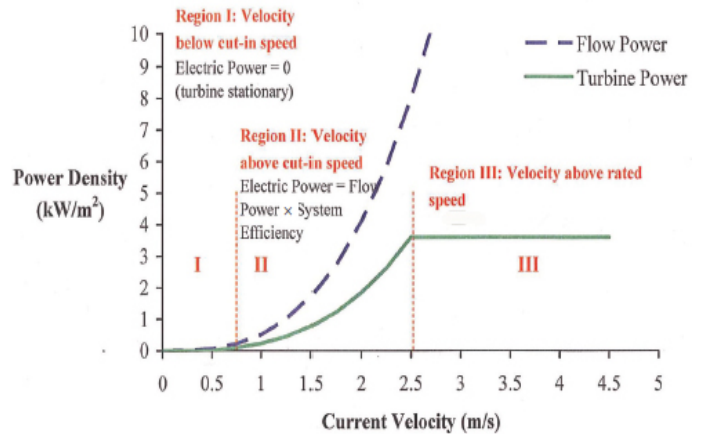


Figure 2. Relationship of power density and current speed; (I) Current speed less than cut-in speed; (II) Current speed between cut-in speed and rated speed; (III) Current speed above rated speed [21].

The statistical approach used is the potential probability analysis [25] Turbine boundary conditions used in the normal distribution are the Helix Gorlov turbine that is 0.5 m/s, while the normal distribution equation is [26] :

$$Z = \frac{\bar{x} - 0.5}{S_x} = \frac{\bar{x} - 0.5}{S/\sqrt{n}} \quad (8)$$

Turbine efficiency varies with current speed change. Cut-in speed is the minimum speed of current to be able to drive the turbine [27]. When the current speed is less than the cut-in speed, the kinetic energy to drive the turbine is insufficient and consequently, no power is produced. When the current speed is between the cut-in speed and rated speed, the power generated by the turbine can vary with the changes in current speed, which increases when the ocean current speed increases and decreases as the current speed decreases. Rated speed is the maximum speed that function as a barrier. Above that speed of the power generated by the turbine will be constant regardless of the current speed [23].

3. Results and Discussion

3.1. The validation of the result

The validation in this model used RMS (Root Mean Square) method [26], where RMS is a non-dimensional value to indicate a match two kinds of data. The set values of the model defined by b_1, b_2, \dots, b_n while the measurement define by a_1, a_2, \dots, a_n so we have:

$$X_{rms} = \left(\frac{\sqrt{\Delta x_1^2 + \Delta x_2^2 + \dots + \Delta x_n^2}}{n} \right) \text{ where } \Delta x_n = b_n - a_n \quad (9)$$

The results validate the model results with field results indicate that the water level modeling results are 0.06 m (Figure 3) where the tolerance is 0,1 m, which means that the model has very good criteria. Karimunjawa waters generally have a tidal type of single daily tidal waters with a Formzahl value of 4.16 ($F > 3$) [28]. sinusoidal which is equal to water level. High current speed occurs when tide elevations lead to low tide. The direction of the current shows the direction of the current which has 2 directions (bi-directional current). Changes in current direction occur following changes in water level, during high tide the current direction is receding dominated by the direction 270° to 315° (west-northwest). At low tide towards the tide direction that dominates the direction is 40° to 70° (northeast) [17].

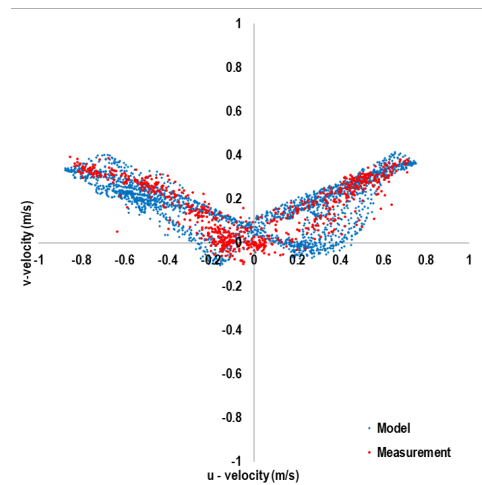
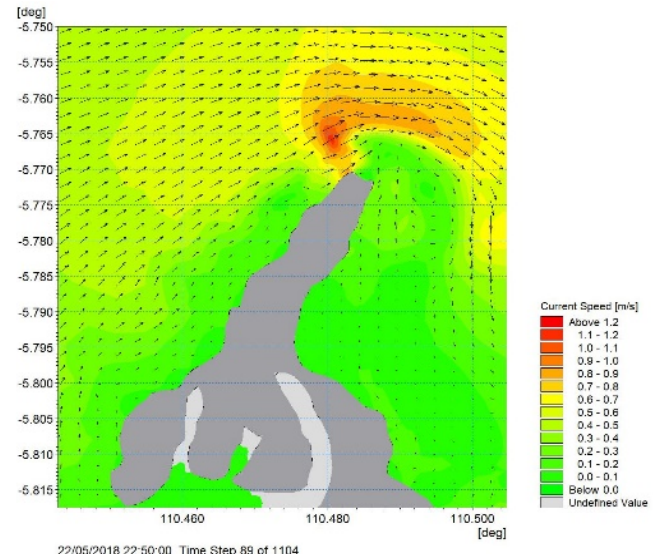
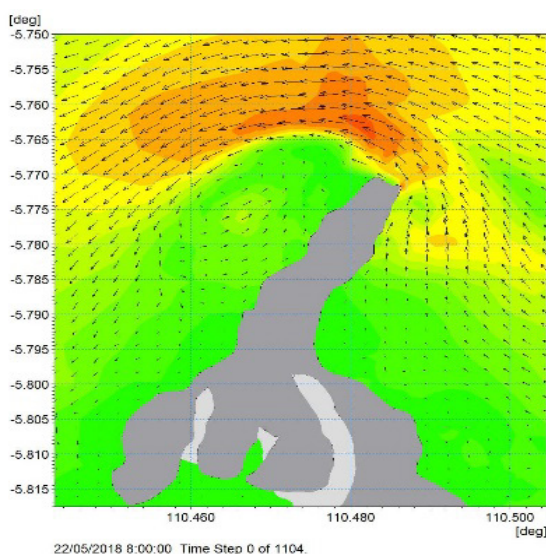


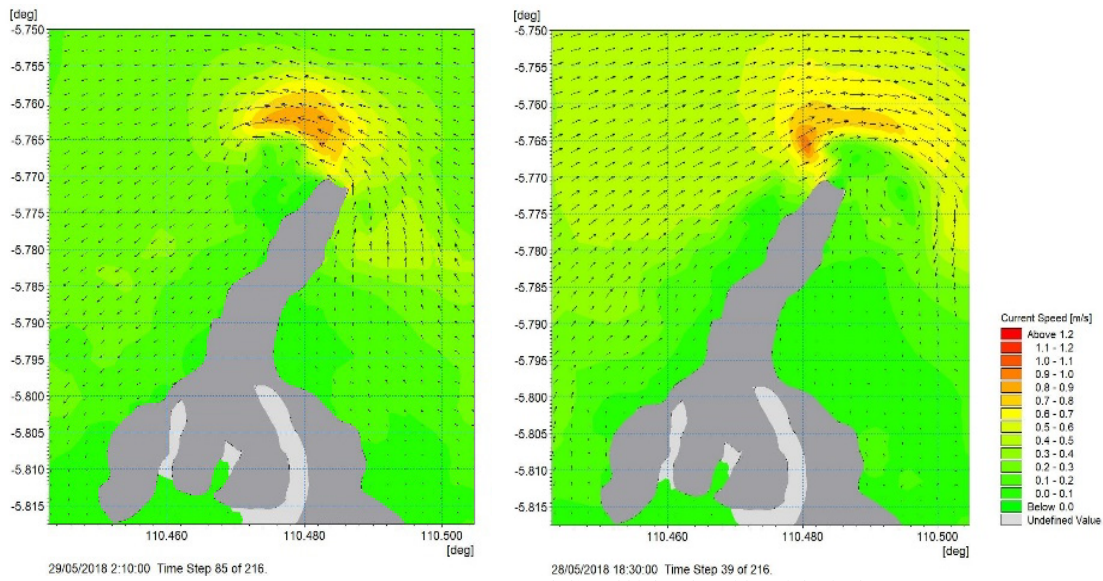
Figure 3. Validation result graphic between model and measurement vector velocity (Source: Data Processing, 2017)

Simulation of the ocean current numerical model in the depths between 1.5 meters – 3 meters was carried out in spring and neap tidal conditions. In this model tides is assumed has no influence of wind or basic friction. Full tides are formed due to the accumulation of lunar and sun attraction in a straight line. This statement is supported [29] who state that the earth's rotation and the relative position of the earth with respect to the moon and the sun affect the tides of the sea. The numerical simulation results are simplified by several complex parameters in the waters that are made into domains to facilitate the implementation of numerical simulations. Argues that to carry out simulations a system simplification is needed by maintaining the stability of the main components [30].

The model simulation is performed on high tides and low tides conditions (Figure 4 and 5). At the high to low tides shows that the ocean current moves from NorthEast to SouthWest, while in the low to high tides the ocean currents moves from southwest to northeast where the highest current speed is 1.2 m/s. This is consistent with the statement from [31] tidal currents have the nature of moving in opposite directions or bi-directional. The direction of current during tide is usually the opposite of the direction of current when receding.



left), high to low tides (right) in the spring season



left) and high to low tides (right) in the neap season.

According to [32], tidal currents will affect daily flow patterns. Tidal currents generally flow from the coast towards the Indian Ocean when the tide and vice versa will flow from the Ocean to the coast at low tide. This current dominates the waters of Karimunjawa.

3.2. Current speed Result

The current conditions from the numerical model simulation is shown in all season condition (west season, east season, the transition 1 and the transition 2 seasons). Presentation of current patterns spatially is the method of presentation in which data speed and current direction are displayed based on location or specific coordinates. The peak month of each season is represented by the conditions that are taken in. From this figure (Figure 6,7,8 and 9), we can see the highest speed is 1.1 m/s in the West and East Season, while the highest speed in the transition 1 and 2 Season is 0.9 m/s.

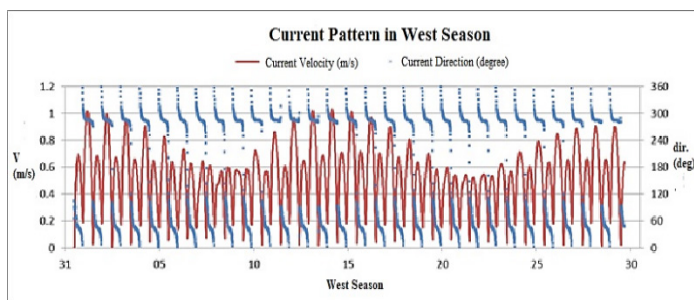


Figure 6 Current speed and direction graphic in west season

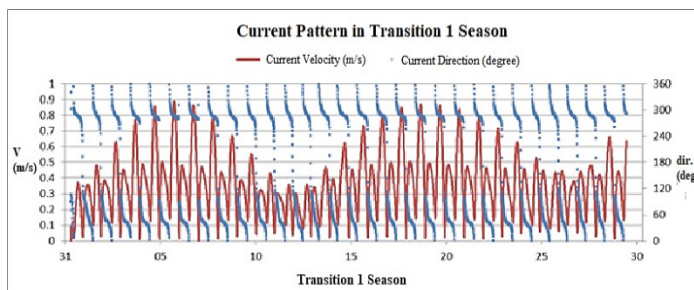


Figure 7. Current speed and direction graphic in the transition 1 season

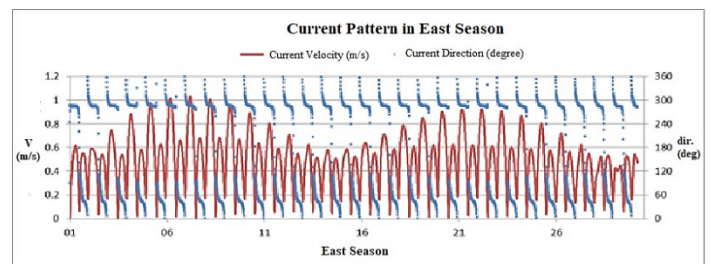


Figure 8. Current speed and direction graphic in east season

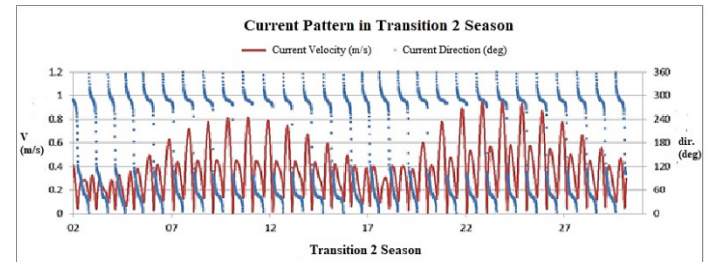


Figure 9. Current speed and direction graphic in transition 2 season

3.3. Analysis of Potential Energy

Overall current speed has a speed above the value of the turbine requirement limit (cut in speed) which is equal to 0.5 m / sec, in general, it can be seen that the current speed has the potential for ocean current energy in all seasons. The current speed from numerical model result is used to convert the estimation of electrical power calculations (watt) which is shown in all season conditions.

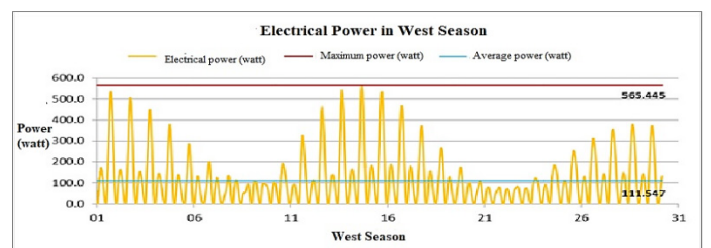


Figure 10. Potential power result (watts) in the west season

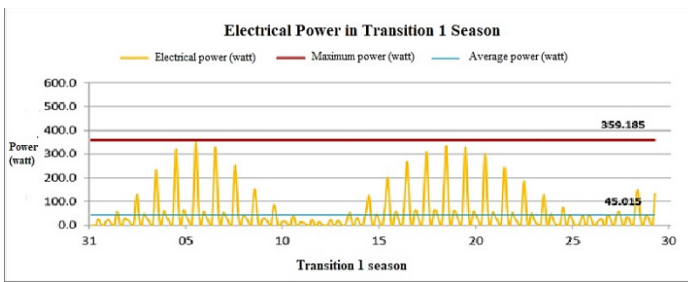


Figure 11. Potential power result (watts) in the transitional 1 season

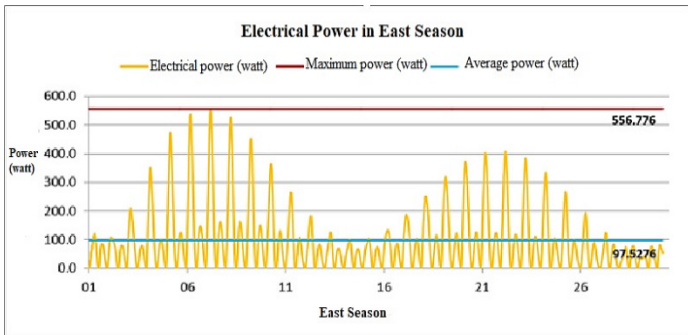


Figure 12. Potential power result (watts) in the east season

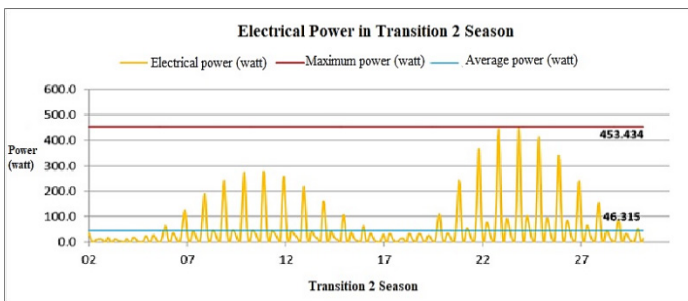


Figure 13. Potential power result (watts) in transitional 2 season

After we know the optimal potential of each season we can decide where will be the potential location of the ocean current power station. The highest potential Electrical Power in West season is 565.445 Watt, at the Transition 1 is 359.85 Watt, in the East Season is 556.76 Watt while in the transition 2 is 453.34 Watt. The analysis results are represented in Figures 10, 11, 12, and 13.

In the East Season the average of electrical power is 97.526 Watt and in the transition season is 46.315 Watt, while in the west season the highest average of electrical power obtained is 111.5 watts and the lowest average of electrical power is in the transition season 1 is 45.01 watts. We can see that the Electrical Power is really depended on the value of the ocean current speed (see Figure 10, 11, 12 and figure 13). The higher the speed value, the higher the electrical energy produced.

The current speed datum can then be calculated to show the estimated available power, where the higher the current speed, the greater the power produced. The location where the power meeting is the highest compared to other places. The area is then determined as the potential location. A high enough power density potential will occur when tide conditions lead from high to low tide and on the lowest tide condition. Whereas for the small amount of power density potential only appears when the tide is highest and when the tide is lowest.

3.4. Spatial Result of Power Density (watts) with Tidal Condition

From Figure 14 and 15 we can see the result of the current speed from the numerical simulation that has been converted into a spatial power density condition at each tidal condition. We can see that in the Northern area of the Karimun Jawa Island has the highest distribution of potential Electricity Power distributed with the average Electricity Power is 450 Watt.

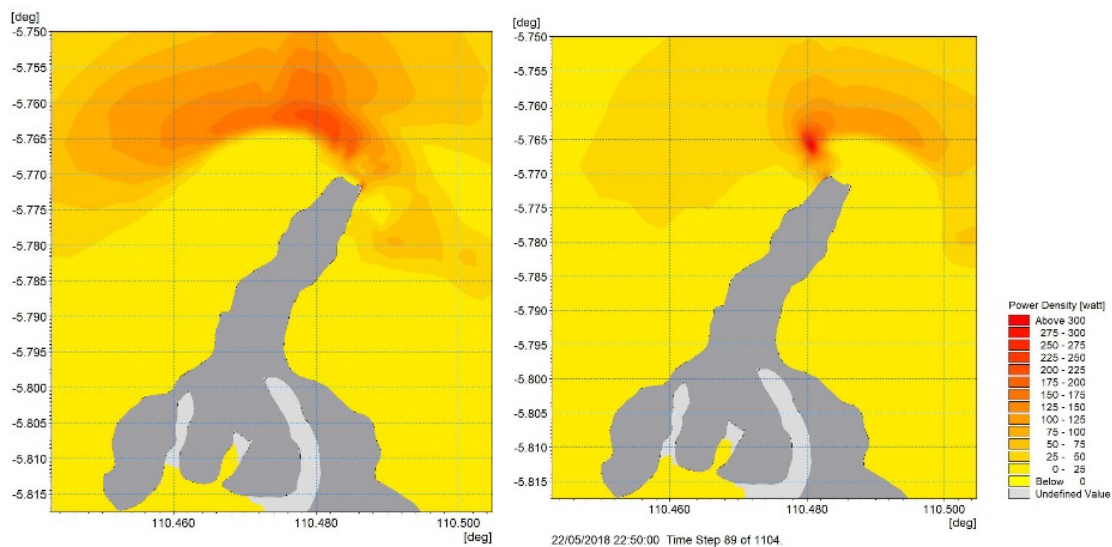


Figure 14. Spatial electrical power density result in low tides to high tides condition (left), high to low tides condition (right) in the spring season

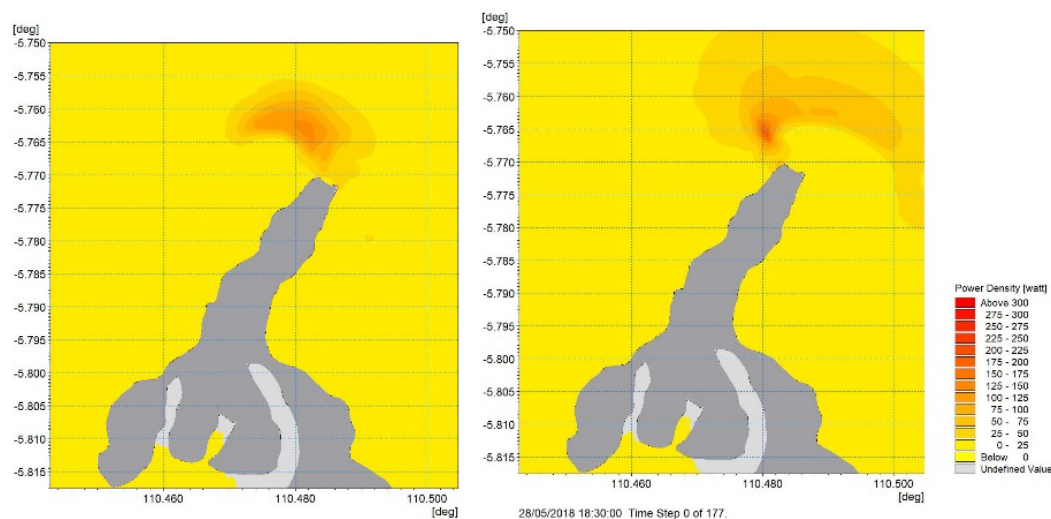


Figure 15. Spatial electrical power density result in low tides to high tides condition (left), high to low tides condition (right) in the neap season

4. Conclusion

potential in the West season is 565,445 Watt, and the lowest Electrical Power potential in Transition 1 season is 359.85 Watt. Based on the results of this study, it can be said that the Karimunjawa island which initially relied on PLTD for the fulfillment of its electricity powers, could have great potential to develop electricity from ocean currents, which is far more economical and environmentally friendly compared to fossil energy.

5. Acknowledgment

We would like to thanks to Ministry of Research, Technology and Higher Education which gave us funding from Fundamental Funding of Directorate of Research and Community Services, Directorate of General Research and Development, Ministry of Research, Technology and Higher Education as the agreement letter of Research Implementation assignment, with Research Number : 022 / SP2H / LT / DRPM / II / 2016 dated on 17th February 2016. Give thanks also to the students of the Oceanographic Department who involved in this research, i.e., Satrio Srijati, Albert Gunawan, Larosa Nurfikri, Muhammad Noerman and Radhitya Rega.

References

- [1]. Mulyanef, Marsal, Rizky Arman, K Sopian, "Sistem Distilasi Air Laut Tenaga Surya Menggunakan Kolektor Plat Datar Dengan Tipe Kaca Penutup Miring", Teknik Mesin Universitas Bung Hatta; Padang, 2006.
- [2]. Nurhayati, "Distribusi Vertikal Suhu, Salinitas dan Arus di Perairan Morotai, Maluku Utara, Oseanografi dan Limnologi di Indonesia", 2006.
- [3]. Departemen Kehutanan, Balai Taman Nasional Karimunjawa, "Penataan Zonasi Taman Nasional Karimunjawa Kabupaten Jepara Provinsi Jawa Tengah", 2004.
- [4]. Parwito, "Tiap Hari, Listrik di Pulau Karimunjawa Hanya Nyala 6 Jam", Merdeka.com, Thursday, 20th February, 2014.
- [5]. Humas Jateng, "Listrik Untuk Karimunjawa", Jatengprov.go.id, Accessed on Friday, 4th- April 2014, 3:31 pm, 2014.
- [6]. Bedard, R, "Technology characterization: Ocean wave and tidal energy", Global Marine Energy Conference, April, New York, 2008.

- [7]. Lopez, A, J.A. Somolinos, L.R. Nunez, and M. Santamaria, "Modeling and Simulation of Moored Devices for Ocean Currents Energy Harnessing", Journal of Maritime Research, VIII (1): 19 - 34, 2011.
- [8]. Asosiasi Energi Laut Indonesia (ASELI), "Potensi Sumber Daya Energi Laut di Indonesia", ASELI, Bandung, 14 pages, 2011.
- [9]. Lubis, S, "Pembangkit Listrik Tenaga Arus Laut bagi Desa Pesisir Tertinggal (Second Opinion) Ministry of Energy and Mineral Resources", 22nd April, 2014
- [10]. Yuningsih, A, and A. Masduki, "Potensi Energi Arus Laut untuk Pembangkit Tenaga Listrik di Kawasan Pesisir Flores Timur, NTT", Jurnal Ilmu dan Teknologi Kelautan Tropis, 3(1): 13-25, 2011.
- [11]. Siagian, Hendry Syahputra, I. B. Prasetyawan, D.H. Ismunarti, and R. B. Adhitya, "Study of the Potential of Ocean Current as an Energy Power Plant in the Larantuka Strait, East Flores, East Nusa Tenggara", Buletin Oseanografi Marina Januari 2014 Vol, 3(1): 1-8, 2014 <http://ejournal.undip.ac.id/index.php/buloma>
- [12]. Kementerian Energi dan Sumber Daya Mineral, "Peraturan Menteri Energi Dan Sumber Daya Mineral Republik Indonesia No. 13 Tahun 2015" Jakarta, 2015.
- [13]. Sugianto, D.N and D.S. Agus, "Studi Pola Sirkulasi Arus Laut di Perairan Pantai Provinsi Sumatera Barat". Jurnal ILMU KELAUTAN, June 2007, Vol, 12 (2): 79 – 92, 2007.
- [14]. Istiarto, "Model Hidrodinamika di Bidang Hidraulika Saluran Terbuka", <http://istiarto.staff.ugm.ac.id>. Accessed on 12 April, 2015.
- [15]. Erwandi, "Sumber Energi Arus: Alternatif Pengganti BBM, Ramah Lingkungan, dan Terbarukan", Laboratorium Hidro-dinamika Indonesia, BPP Teknologi, 2006.
- [16]. Priyono, "Metode Penelitian Kuantitatif", Revised Edt, Zifatama Publishing, Surabaya, ISBN : 978-602-6930-31-6. 206 pp, 2016.
- [17]. Ismunarti, Dwi. Haryo, Sugianto. D.N, Ismanto. A., "Kajian Karakteristik Arus Laut Di Kepulauan Karimunjawa Jepara", Prosiding Seminar Nasional Hasil-Hasil Penelitian Perikanan Dan Kelautan Ke-Vi Fakultas Perikanan Dan Ilmu Kelautan – Pusat Kajian Mitigasi Bencana Dan Rehabilitasi Pesisir, Undip, 254 263, 2017 .
- [18]. Pond, S. and G.L. Pickard, "Introductory Dynamic Oceanography Second Edition", Pergamon Press, Oxford, 329 p, 1983.
- [19]. Hadi, S. dan I.M. Radjawane, "Arus Laut", Institut Teknologi Bandung, Bandung, 88 pages, 2009.
- [20]. Kowalik and Murty, "Numerical Modeling of Ocean Dynamics", World Scientific, Volume 282, 10 January 1995, p. 407, 1993, <https://doi.org/10.1017/S0022112095240187>
- [21]. Hagerman, G., B. Polagye, R. Bedard, and M. Previsic., "Methodology for Estimating Tidal Current Energy Resources and Power Production by Tidal In-Stream Energy Conversion (TISEC) Devices", EPRI, Virginia, 52 p, 2006.
- [22]. Moreno, N., R. Sallent, A. Espi, D. Bao, and Y. Teillet., "Ocean Current's Energy: How to Produce Electrical Energy Thanks To The Marine Currents?", University of Gävle, Gävle, 23 p, 2008.

- [23]. Fraenkel, P.L., "Marine Current Turbines: Pioneering The Development of Marine Kinetic Energy Converters", Proc. Instn. Mech. Engrs., 221 (Part A) :159-169, 2007.
- [24]. Fraenkel, P.L., "Power From Marine Currents", Proc. Instn. Mech. Engrs., 216 (Part A):1-14, 2001.
- [25]. Thomson E.R. dan Emery J.W., Data Analysis Methods in Physical Oceanography, 1st ed. Pergamon. England, 1997.
- [26]. Gorlov, A.M., "Turbines with a twist", In: Kitzinger U and Frankel EG (eds) Macro Engineering and the Earth: World Projects for the Year 2000 and Beyond, pp, 1} 36, Chichester: Horwood Publishing, 1998.
- [27]. Giorgi, S. and J.V. Ringwood, "Can Tidal Current Energy Provide Base Load?", Journal of Energies, 6: 2840-2858, 2013.
- [28]. EVANS, G. P., "A Framework for Marine and Estuarine Model Specification in the UK", Foundation for Water Research, Report No FR0374, 1993.
- [29]. Trujilo, A.P., and H.V. Thurman, "Essentials of Oceanography 10th Edition", Prentice-Hall, Boston, 551pp, 2011.
- [30]. Cahyana, C, "Model Hidrodinamika Laut", BATAN, Jakarta, Buletin LIMBAH 9 (2) : 17-18 pp, 2005.
- [31]. Djunarsjah, E., dan Poerbandono, "Survei Hidrografi", PT. Refika Aditama, Bandung, 2005.
- [32]. Ongkosono, O.S.R, and Suyarso, "Pasang Surut", Pusat Pengembangan Oseanologi Lembaga Ilmu Pengetahuan Indonesia, Jakarta, 257 pp, 1989.

Spiral Curve for Revocable Touchless Fingerprint Template Securitisation

Tahirou Djara^{1,2,*}, Boris Sourou Zannou^{1,2}, Antoine Vianou^{1,2}

¹Laboratoire d'Electronique de Télécommunication et d'Informatique Appliquée (LETIA/EPAC), Université d'Abomey-Calavi (UAC), Cotonou, Bénin

²Institut d'Innovation Technologique (IITECH), Abomey-Calavi, Bénin

ARTICLE INFO

Article history:

Received: 03 August, 2019

Accepted: 07 November, 2019

Online: 25 November, 2019

Keywords:

Revocability

Secrecy

robustness

ABSTRACT

Fingerprint data is really protected by cancelable fingerprint template because it can be revoked when compromise and a new one can be reissued. We develop a touchless cancelable fingerprint template whose algorithm was published in our previous work. We implement here the algorithm and conducted several tests on several databases to confirm the stability of the model. To justify how specific keys are used, we used the Kolmogorv-Smirnov test (K-S) and the distribution histogram of legitimate / impostor scores. We compared two systems in which users register. This is the reason for the average value of K-S (0.7812) and similarity assessment (2.4703). These results improve sufficiently (6.1636 and 0.9934 for the successive separability and the K-S test) during the evaluation of the user keys through the second device. We have tested the diversity of curves that we generate. Our proposed non-contact revocable fingerprint model has demonstrated robustness against the security challenges that fingerprint authentication systems are exposed to. We evaluated it on our own database. The requirements of revocability, diversity and security are achieved with very good performance as evidenced by the FAR (False Acceptance rate) obtained on our database (0.0015).

1. Introduction

Biometry is the identification from human characteristic and traits. The most used feature in human authentication is the fingerprint. It performs well and is unique. Minutiae are the most used representation. Nevertheless, several researches have proved that one could reconstruct the original fingerprints from some characteristics. There are problems of correspondence and paring. It should be noted that during the matching phase, the model is exposed to several intrinsic security issues including the threat of privacy, attack record multiplicity (ARM) which are the most common. ARM remains the most formidable and continues to be the focus of intensive research. Therefore the issue of securing authentication with fingerprints comes out. We design a new model for data protection enhancement protection. Our vision is therefore to deal with them by taking into the paradigms of diversity, revocability, precision and invertibility.

In [1], Author identified three major classes of fingerprint-based protection models: feature transformation, biometric cryptosystem, and hybrid. Each of these methods present its own

limitation and advantages [2]. The principal requirement of a good protection template hasn't been achieved. Our interests focus on rigid transformations. Basically it will be a G transformation function with original characteristics by using a key b; the transformed template $G(a, b)$ is then stored in the database. We use that function to transform the characteristic test c, then the transformed characteristics $G(a, b)$ and $G(c, b)$ will be compared in order to know yes or no if the user is the right one. Entity transformation models are classified into two main classes, namely vector-based approach and point-of-interest approach (especially those based on minutiae). This depends on the representation model that is adopted.

This article proposes a new approach that is difficult to reverse, especially for systems using minutiae as model. This technic provides revocability, diversity and security while improving performance. It should be noted, however, that to ensure security through the bio-cryptosystem or transformation of characteristics, the fingerprint device observes a delay in the accuracy or during the inversion. Our device for strengthening the fingerprint authentication has the advantage of avoiding leash dragging during the image acquisition step. Our vision is to implement a non-invertible transformation that meets the requirements of

* Tahirou Djara, Email: csm.djara@gmail.com

performance, diversity, revocability and security. Thus, we use information provided by the minutiae obtained to generate contactless curves with respect to the center of mass. Section 1 presents the introduction, then in section 2 we present the security holes in contactless biometric systems. The section 3 present our revocable and secure contactless model. Section 4 presents the experimental results to finally give the conclusion in section 5.

2. Security holes in non-contact biometric systems

Biometric systems are exposed to many security vulnerabilities [3,4]. Malicious, for example, could attack the database and recover sensitive information. In order to secure the biometric systems of the most unimaginable attacks, intensive research efforts are conducted. Many techniques have been developed for the purpose of securing biometric data.

The basic idea of all these models is to generate revocable templates. By revocability it should be understood that in comparison to passwords that could be modified if they are damaged, the user model stored in the database could also be generated in a new (different from the previous) using the same biometric information. Diversity, security and performance are the characteristics that an ideal model of protection must have for security models. Diversity means that it is necessary to ensure that there is no correspondence between the compromised models and those newly generated in the case where a new model is generated to replace an old one. Security is the impossibility for a malicious person to recover the original data of a user who was used to build his model. Performance means keeping the authentication capacity of the biometric system intact, which should not be affected by data protection. In a biometric system, instead of storing biometric templates directly, the transformed templates are stored in the database for subsequent authentication. In this technique, the biometric characteristics are transformed into another domain [6] and only the transform (signature) is stored in such a way that the details of the original biometric data cannot be revealed to a malicious person. He gets the biometric pattern. The biometric characteristic elements are transformed into another model $G(a; b)$ which will be stored in a database for future authentication, the biometric information β of the user is transformed into $G(c, b)$ to allow a comparison with $G(a, b)$ to decide whether it is a malicious or an authentic one. The attacks essentially originate in the security vulnerabilities that can essentially be counted:

- Presentation attacks: fingerprint is presented at the inputs after having reproduced it;
- Hacking and using data from fingerprint after bypassing the sensor
- The usurped characteristics are substituted for the originals.
- Tripartouillage in the correspondence module to use the false features

In [1], Author have cited security loopholes through a fish skeleton.

3. Literature review

Given the security weaknesses listed above, it is necessary to look for sustainable solutions. It is within this framework that solutions approaches are born. We can mention revocable biometrics without alignment and biometrics based on pre-registration. These solutions are based on the local structures of the

minutiae or the taking of the minutiae in pairs or in a triangle because they do not vary with the rigid transformation. In the next paragraph we will go through the revocable models without alignment. In [5], Authors have proposed one of the most recent models by inserting two key factors. Their model focused on a self-alignment local structure based on textures as features. Their research was much more focused on the many possible attacks rather than dealing with algorithms managing the loss of models or two keys. Another recent technique in [5] evaluates the orientation of the minutiae in the surrounding area at each reference minutiae. All this is possible thanks to two functions allowing to evaluate the number of transformations around each minutiae of reference. The performance of this technique drops when it comes to poor quality images.

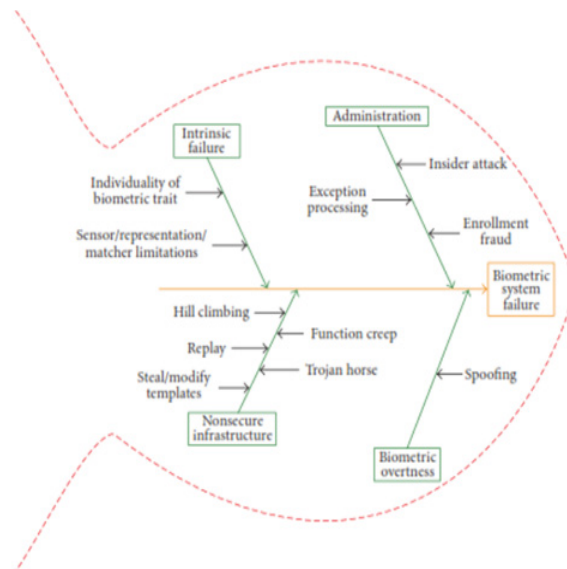


Figure 1: vulnerabilities in the form of fishbone [1]

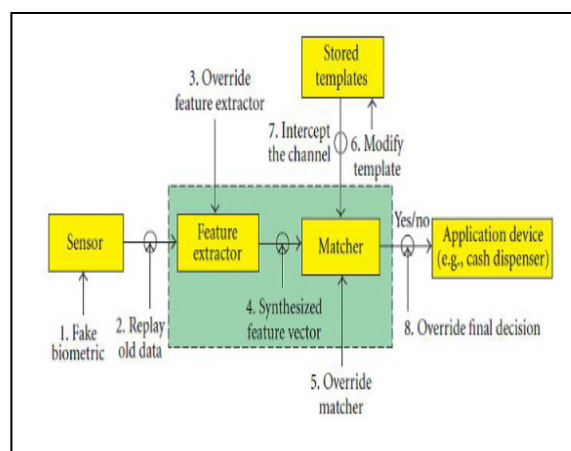


Figure 2: Attacks on Biometric System

In [6], author proposed a set of hash functions based on the position of the minutiae. These transformation function based on the position of the minutiae, takes into account the hazardous mobility points minutiae due to the sensor recording. This technique is well revocable and performs well with high complexity. The vicinity of the minutiae is a technique based on the dynamic random projection to secure the extracted features. It was developed by authors in [7]. The random projection matrix is dynamically assembled. The feature vector conditions the choice

of projection vectors. The test results on some databases are still insufficient to prelude because this approach would be applied to other databases. In [8], authors used a method based on the relative position between each reference minutiae. Another minutiae based template is built in a polar coordinate system whose faults reside in poor quality performance. In [9], authors developed an approach based on a characteristic vector based on a triangle. The template is formed by quantization and binarization. A descriptor based on a string of characters, allows to set up plates in the form of binary codes. This technique is called the multiline code (MLC) developed by authors in [10] and is based on the decomposition of neighborhood minutiae. Similarly, models referencing mapping in an infinite approach emerged with authors in [10]. They introduced the Hamming method based on graphs generating binary formats that can be revoked. Other not less powerful techniques such as reduced circular convolution [11], the partial transformation of Hadamard [12].

Despite of plethora of methods, fingerprint authentication systems have security vulnerabilities and are still vulnerable to ARMs (Multi-Object Attack) [1].

4. Touchless secured revocable template based on center of mass

Because of weaknesses of existant template we propose a spiral curve for securing contactless fingerprint template that use Zernike moment [13], Hausdorff distance modified [14, 15, 16] and the geometric moment [17]. In this section we will present our Touchless fingerprint revocable template based on center of mass. To strengthen fingerprint authentication, We plot the contactless curve using images obtained from our contactless sensors. Later we attach them to those previously stored. then we calculate the corresponding score to finally make a decision to accept or refuse.

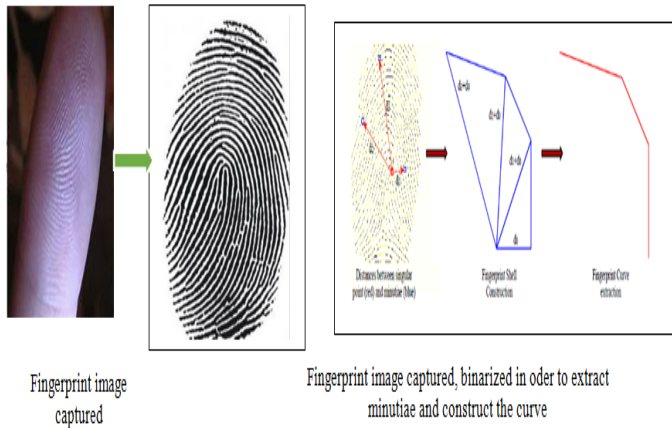


Figure 3: Building of the spiral curve

Our system is monomodal and is based on fingerprints. The rigid transformation [17] without modifying the extracted characteristics, protects the model stored there. Rigid transformation is a combination of translation and rotation expressed by:

$$\begin{pmatrix} u' - u_0 \\ v' - v_0 \\ 1 \end{pmatrix} = \begin{pmatrix} \cos \delta & -\sin \delta & 0 \\ \sin \delta & \cos \delta & 0 \\ 0 & 0 & 1 \end{pmatrix} \begin{pmatrix} 1 & 0 & b_x \\ 0 & 1 & b_y \\ 0 & 0 & 1 \end{pmatrix} \begin{pmatrix} u - u_0 \\ v - v_0 \\ 0 \end{pmatrix} \quad (1)$$

Where

$$\begin{pmatrix} u' \\ v' \\ 1 \end{pmatrix} = \begin{pmatrix} \alpha_0 & \alpha_1 & \alpha_2 \\ \beta_0 & \beta_1 & \beta_2 \\ 0 & 0 & 1 \end{pmatrix} \begin{pmatrix} u \\ v \\ 1 \end{pmatrix} \quad (2)$$

with

$$\alpha_0 = \cos \delta \quad \alpha_1 = -\sin \delta$$

$$\alpha_2 = (1 - \cos \delta)u_0 + v_0 \sin \delta + b_u \cos \delta - b_v \sin \delta \quad (3)$$

$$\beta_0 = \sin \delta \quad \beta_1 = -\cos \delta$$

$$\beta_2 = (1 - \cos \delta)v_0 + u_0 \sin \delta + b_u \sin \delta - b_v \cos \delta \quad (4)$$

Noted that $F_0 \begin{pmatrix} u_0 \\ v_0 \end{pmatrix}$ is the center of rotation, δ is the angle of rotation, $\begin{pmatrix} b_u \\ b_v \end{pmatrix}$ are the coordinate of translation vector and F' is the transformed point of F .

In order to eliminate all the above danger, we design a new method which is implement in [3].

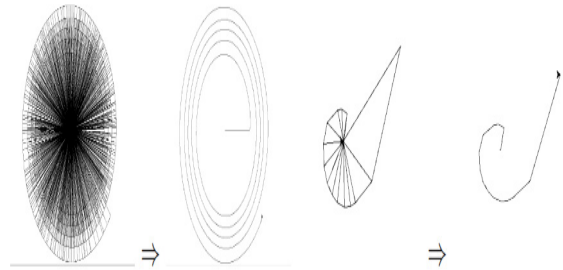


Figure 4: Different curves obtained according to the quality of the images and the number of minutiae present on these images

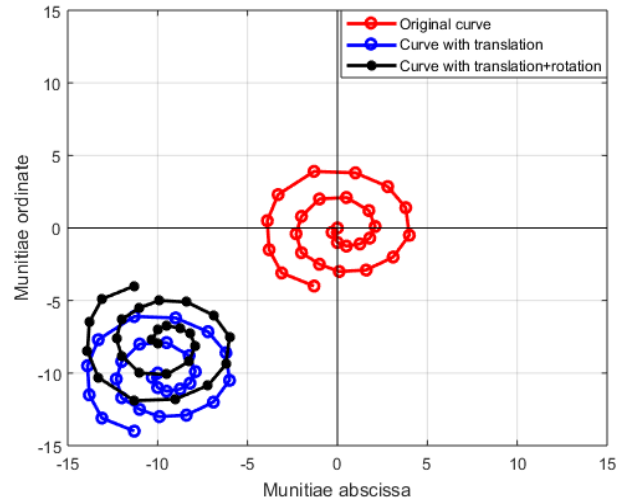


Figure 5: Construction of the secured touchless template

The requirements of revocability, diversity and security have been achieved with our new method. In reality the protection of a compromised model can go through the modification of C_0 . The mismatch of the most recent curve with the old one provides diversity (see Figure 4). In reality, it is impossible to find the

munities to walk a contactless curve but it is nevertheless necessary to look at the most extreme case. In this case, even if the thug gets the curve and knows how to leave the curve to recover the munities. In reality he could only recover distances that have infinite positioning. There exists only 360 positioning and 360n possible combinations with n corresponding to the number of munities. We therefore find that in the most extreme case our model remains stable and robust despite the complexity of the attacks perpetrated. Performance, Diversity and security will be further analyzed in the next subsection.

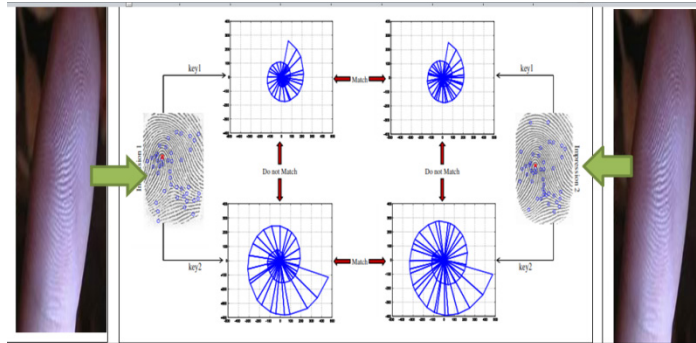


Figure 6: sample of two impressions of the same identity using two different keys to illustrate revocability/diversity

5. Experimental results and analysis

We tested the model by using our own fingerprints database. We describe the database in Table 1. We have a fingerprint database containing 1,512 fingerprints, obtained from 378 separate fingers. We take 4 impressions from each subject. Out of 378 people, the fingerprints of the four fingerprints could be automatically captured from 1512 people. Thus only 1250 fingerprints impressions were used in experiment. In fact, due to the lack of time and people from whom we can get fingerprint images, we import some images from existant database in order to reach the number we choose. It doesn't affect the result. We develop our own software for the fingerprint images treatment. To appreciate how our system performs, we use false acceptance rates and false rejection rates

Due to the fact that we use two keys, we notice the amelioration of the performance of template. Our c_0 allows us to have a significant improvement of the Equal Error Rate (EER) because of the specific way of it is compute and its only one occurrence [18]. The rigid transformation applied to the curves adds a high level of randomization. Because of the fact that the key value is specific to users, the use of rigid transformation help us to have the curve unable to be rebuilt. In Figure 6, We compare FAR obtained for the proposed technique with Fingerprint Shell [17, 18] for different thresholds.

We have modified the FVC evaluation protocol to avoid the zero effort scenarios, where the adversary knows and tries to bypass the system using his own fingerprints. Impostor scores is obtain from comparison of the first curve of one single finger and the first curve of the same finger in another system that we build with reference to the identic curve. We note that they must perform 8999 attacks before succeeding one time their attacks. We compare every single print of any finger with the remaining impression of same finger. We will have at least 2799 trying before succeeding one time. In addition, we select the key randomly belonging to the interval]0, 1001[. Figure 8 describe the scenario.

Table 2: Performance comparison: existing template versus proposed template following FVC

Various Techniques	Our collection	FVC2002 DB2(%)	FVC2002 DB1(%)
[12]	Not tested	1.2	2.1
[15]	Not tested	3.61	7.18
[2]	Not Tested	1.01	2.03
[18]	0.001	Not tested	Not tested
Our template	0.0015	0.96	1.54

The value of FRR remains the same comparatively to fingerprint shell because of the uniqueness of the key. Let us remarks that the rightness of the curve depends on the quality of the image. More there is minutiae better is the curve, and less there is minutiae, worst is the curve (figure 9). The propose template performs well. Our model presents good results and verifies the criteria of good protection systems. Our Solution is efficient against attacks without effort or even in case of usurpation of the user key. Although, as shown in Table it presents the values EER, FMR1000 and zeroFMR obtained. Performance is only maintained in the vicinity of ERR points (4.2705% for DB1 and 1.458% for DB2). Our template are no longer accurate for thresholds that are far from ERR threshold (figure 7). In any case, we retain that (in the FMR security applications of Table 3), the systems for securing which are based on the curves are efficient only if the threshold is close to the EER point in order to limit the passage in force of the effortless attacks.

Table 3: Verification of accuracy of our template in the zero effort attack:

	FVC 2004		FVC 2005	
	EER	FMR ₁₀₀	EER	FMR ₁₀₀
Our touchless Secure template	4,250	26,146	4,250	26,146

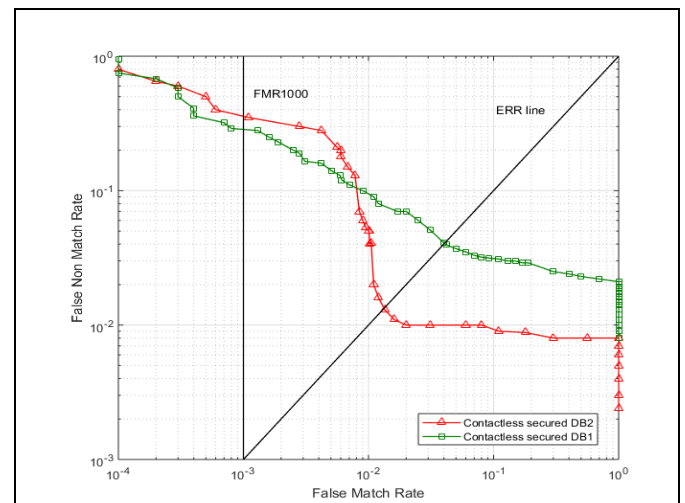


Figure 7: ROC curve in the presence of effortless attack

We remark that in high security applications based on their scheme, the systems should be operated only near the EER point to minimize the success of zero effort attacks.

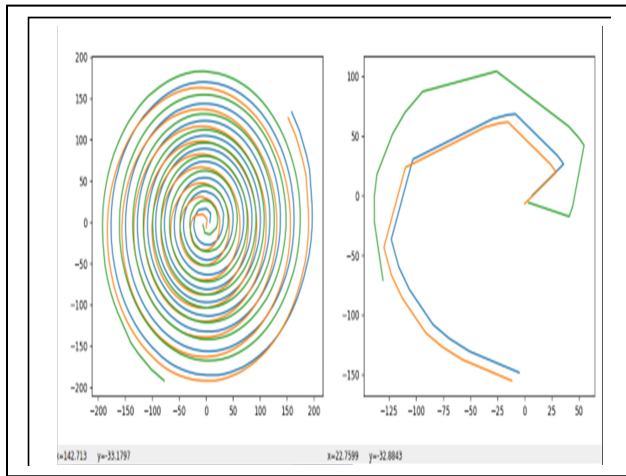


Figure 8: Sample of Template obtained from two kind of image: the first template is obtained from an image with many minutiae vs the second one is obtained from an image without enough minutiae.

Given the poor quality of some images, we observed 7 rejections for DB2 and 21 for DB1. Thus, we obtained $REJDB1 = 0.75\%$ and $REJDB2 = 0.25\%$. With the intention of testing the opportunity to make use of C_0 particular to each user, we calculate the separability.

To justify the way in which specific keys are used, we used the kolmogorv-Smirnov test and the distribution histogram of legitimate / impostor scores. We compared two systems in which users register. In the first, the registration is done without user key, while in the second, a user key is required (the keys are drawn randomly in the interval $[0; 1,5555]$). We have illustrated the results in Figure 9. We can notice a form of superposition between the two distributions. This is the reason for the average value of the K-S (0.7812) and the similarity evaluation (2.4703). these results improve sufficiently (6.1636 and 0.9934 for successively the separability and the K-S test) during the evaluation of the user keys through the second device (Figure 9-b). This is proof of the improvement of discredit. In conclusion, the rate of false acceptance improves when we assigns to each user a particular key C_0 . Thus, we improve the performance and accuracy of our device.

In a second step, we want to test the diversity of the curves that we generate. It will be a matter of reassuring oneself that the curve generated from one finger in one system does not coincide with another curve generated in other systems with the same finger. For this purpose, we have installed three devices that use loops. For randomly selected users in the ranges of $[0,1.5555]$, $[100,500]$ and $[1000,2000]$. The same finger is used to register in all three systems and then we look for pseudo-legitimate distribution. We conducted 6355 tests for each device, We did 6355 attempts at database DB1 and 6385 attempts for the database DB2. Figure 8 shows the results or we can clearly see that the real users and the malicious ones are well separated in the distribution of our first device. The closer they are to the distribution of the malfrats of the device 1 so the device 1 always considers the curves of the devices 2 and 3 as usurpers.

To summarize, we will say that revocability and diversity are taken into account by our device. The pseudo-distribution of the

device 3 is further from the distribution of the real users of the device 1 and 2, therefore the diversity of two devices that rely on our model increases when the choice intervals of the keys are distinct.

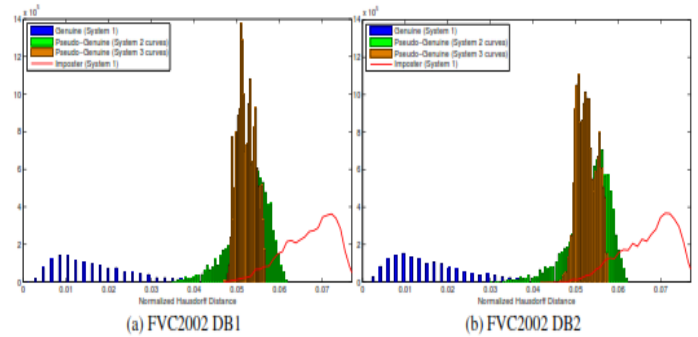


Figure 9: System Histogram 1 and pseudo-legitimate distributions using systems 2 and 3

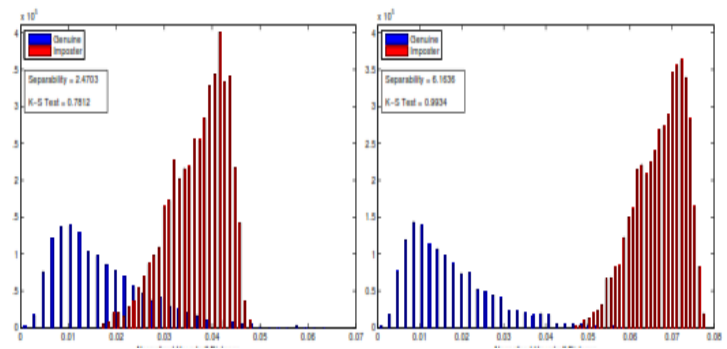


Figure 10: Histogram of Two Systems Protected by Fingerprint Shell Using FVC2002 DB1.

6. Conclusion

Our proposed contactless revocable fingerprint template has shown good robustness against the security challenges that fingerprint-based authentication systems are exposed to. It also bypasses the contagion hazards to which contact systems expose us. We evaluated it on FVC2002 DB1, DB2 and DB3 and FVC2994 DB2 and the results of the tests show that it performs very well compared to existing models in the literature review. the exigences of revocability, diversity, security are reached with very good performances. ARM issues will be better addressed with proposals for more stable models such as exploring a combination of DFTs and dynamic projection.

Conflict of Interest

The authors declare no conflict of interest.

References

- [1]. Jain, A. K., Nandakumar, K. and Nagar, A. 'Biometric Template Security', (January), pp. 1–20, 2008.
- [2]. Rathgeb, C., Uhl, A., A survey on biometric cryptosystems and cancelable biometrics. EURASIP Journal on Information Security 2011, 1–25, 2011
- [3]. S. B. ZANNOU, T. Djara, A. Vianou, "Secured revocable contactless fingerprint template based on center of mass", 2019 3rd International conference on Bio-engineering for Smart technologies (BioSMART), 2019.
- [4]. J. Breebaart, B. Yang, I. Buhan-Dulman and C. Busch. Biometric template protection. Datenschutz und Datensicherheit-DuD 33, 299–304, 2009.

- [5]. S. Chikkerur, N. Ratha, J. Connell, R. Bolle, Generating registration-free cancelable fingerprint templates, in: 2nd IEEE International Conference on Biometrics: Theory, Applications and Systems, pp. 1-6, 2008.
- [6]. W. Yang, J. Hu, S. Wang, J. Yang, Cancelable Fingerprint Templates with Delaunay Triangle-based Local Structures, *Cyberspace Safety and Security*, Lecture Notes in Computer Science. 8300 pp. 81-91, 2013.
- [7]. S. Tulyakov, F. Farooq, P. Mansukhani, V. Govindaraju, Symmetric hash functions for secure fingerprint biometric systems, *Pattern Recognition Letters*. 28 pp. 2427-2436, 2007.
- [8]. T. Ahmad, J. Hu, S. Wang, Pair-polar coordinate-based cancelable fingerprint templates, *Pattern Recognition*. 44 (10-11) pp. 2555-2564, 2011.
- [9]. P. Das, K. Karthik, B.C. Garai, A robust alignment-free fingerprint hashing algorithm based on minimum distance graphs, *Pattern Recognition*. 45 (9) pp. 3373-3388, 2012.
- [10]. W.J. Wong, A.B.J. Teoh, M.L.D. Wong, Y.H. Kho, Enhanced multi-line code for minutiae-based fingerprint template protection, *Pattern Recognition Letters*. 34 pp. 1221-1229, 2013.
- [11]. C. Li, J. Hu, Attacks via record multiplicity on cancelable biometrics templates, *Concurrency and Computation: Practice and Experience*. 26 (8) pp. 1593-1605, 2013.
- [12]. Song Wang, Wencheng Yang and Jiankun Hu, Design of Alignment-Free Cancelable Fingerprint Templates with Zoned Minutia Pairs *Pattern Recognition 2017*, <http://dx.doi.org/10.1017/j.patcog.2017.01.019>
- [13]. Djara, ASSOGBA, NAIT ALI and Vianou, 'Fingerprint Registration Using Zernike Moments: An Approach for a Supervised Contactless Biometric System', (9), pp. 254-271, 2009.
- [14]. Dubuisson, M. et al. DISTANCE Between Point Sets Research supported by a ', pp. 566-568, (1994).
- [15]. Syed Sadaf Ali, Surya Prakash, 3-Dimensional Secured Fingerprint Shell, *Pattern Recognition Letters*, 2018, doi:10.1018/j.patrec.2018.04.017
- [16]. A. A. Taha and A. Hanbury. An Efficient Algorithm for Calculating the Exact Hausdorff distance. *IEEE Trans. on PAMI* 37, 2153-2163, 2015.
- [17]. Moujahdi, C. et al. 'Fingerprint shell: Secure representation of fingerprint template', *Pattern Recognition Letters*, 45(1), pp. 189-196, 2014. doi: 10.1016/j.patrec.2014.04.001.
- [18]. Ali S. S. and Prakash, S. 'Enhanced fingerprint shell', 2nd International Conference on Signal Processing and Integrated Networks, SPIN 2015, pp. 801-805, 2015. doi: 10.1109/SPIN.2015.7095438.

A New Wire Optimization Approach for Power Reduction in Advanced Technology Nodes

Jalal Benallal¹, Lekbir Cherif^{*1,2}, Mohamed Chentouf², Mohammed Darmi¹, Rachid Elgouri³, Nabil Hmina¹

¹Laboratory of Systems Engineering, National School of Applied Sciences, Ibn Tofail University, B.P 241, Kenitra, Morocco

²ICDS Department, Mentor Graphics, Rabat, 11100, Morocco

³Laboratory of Electrical Engineering & Telecommunication Systems, National School of Applied Sciences, Ibn Tofail University, Kenitra, B.P 241, Morocco

ARTICLE INFO

Article history:

Received: 17 September, 2019

Accepted: 10 November, 2019

Online: 25 November, 2019

Keywords:

Integrated circuit conception

Physical design (EDA)

Physical implementation

Interconnect

Low power

Power optimization

Dynamic power

Total power

ABSTRACT

In advanced technologies nodes, starting from 28 nm to 7 nm and below, the power consumed of integrated circuits (ICs) becomes a big concern. Consequently, actual electronic design automation (EDA) tools are facing many challenges to have low power, reduced area and keep having required performance. To reach required success criteria, and because each picosecond and each picowatt counts, continuous development of new optimization technics is necessary. In this paper, we put to the experiment and analysis a new technic to reduce IC consumed power by optimizing its interconnections (nets). We propose an optimal algorithm and enhance it for a better compromise between having less consumed power and keep having a good design rout-ability. The new wire optimization technic based on an optimal choice of target nets for optimization: which is the list of nets consuming more than 80% of the total power in the interconnection without exceeding 30% of the total number of nets. Experiments on 14 test cases show an average total power saving of 5% on both dynamic and total power.

1. Introduction

Modern system on chip (SoC) and network on chip (NoC) circuits are known by the integration of complex interconnect IP which brings more difficulties for the timing closure especially with the 16 nm technology node (and below) [1]. In parallel with the circuit performance, new technology nodes allowed a very high transistors' integration to have more functionalities inside smaller die area [2], which brings many manufacturing challenges before having production circuits. On the other hand, modern designs are power-constrained (e.g., IoT, Automotive, Mobile) [3, 4]. Thus, electronic design automation (EDA) tools should have all necessary functionalities for a good compromise between required circuit performances, manufacturing, and power consumption.

In advanced technology nodes, wire capacitance has become a key challenge to design closure, and this problem only worsens with each successive manufacturing process mainly due to the minimum spacing between adjacent wires [5, 6]. Today, a physical

implementation flow for the digital circuit should be able to play with multiple scenarios during routing to find the best compromise between timing, power, and rout-ability. [7] Details the importance of interconnect optimization and how its optimization is playing a pillar role in chip performance. Also, [8, 9] Present more routing closure challenges.

Related to the power optimization, at the physical implementation, many technics are used targeting both leakage and dynamic power. [10, 11] Gives some technics to reduce power on the cells' element. [12, 13] present new technics for power optimization on the design network. [14, 15] focus more on the technology ways to decrease total consumed power in the design.

This work introduces a new technique for power optimization during the physical implementation of an IC by optimizing the wire capacitance of its power critical interconnections (nets). We then propose a new solution that directly improves upon the original solution [16] construction by proposing an enhancement of the procedure that gets target nets for optimization. The new solution helps for having good route congestion overflow while

*Corresponding Author: Lekbir Cherif, Technopolis, Building B0, Sala El Jadida, Morocco, +212611396180, Email Lekbir.cherif@gmail.com

keeping the same power reduction gain. The solution approach achieves improvement for both objectives, having a maximum power gain by simple nets re-routing, and reduce the overflow for better design rout-ability.

Experimental results on 14 test-cases made with most advanced technologies nodes (28, 20, 16&7 nm) demonstrate that this technique achieves an additional average of 5% on total power by targeting nets consuming more than 80% of the power.

This paper makes the following contributions:

- Starting with the final result from paper [16], in this paper, we propose an enhanced procedure that gets fewer data nets as a target for optimization.
- The enhanced solution helps on having acceptable routing congestion for better routing capability and, at the same time, keep having the same good power reduction gain of 5% in the average.
- Proves the benefit of this transform on power reduction on data nets by experimenting with the new flow on 14 real designs made with the most advanced technology nodes 28, 20, 16 and 7 nm.

The remainder of this paper is organized as follows. Section 2 presents the power trend on a modern integrated circuit and briefly, review the results achieved in paper [16]. Section 3 presents the enhanced solution that gets fewer targets for better routing congestion overflow as a wire promotion power-aware method. Section 4 reports our experimental results, and Section 5 concludes the paper.

2. Power in digital ICs at physical implementation stage

2.1. Power calculation and the trend in advanced technology nodes

Equations (1), (2) and (3) summaries how the IC power can be calculated: [17-19]

$$P_{dynamic} = P_{internal} + P_{switching} \quad (1)$$

$$P_{internal} = \frac{1}{2} \cdot toggle_rate \cdot (E_{rise} + E_{fall}) \quad (2)$$

$$P_{switching} = \frac{1}{2} \cdot toggle_rate \cdot (C_{load}) \cdot V^2 \quad (3)$$

Where:

E_{rise} and E_{fall} are rise and fall energy;

$toggle_rate$ is number of toggles per time-unit;

C_{load} is total wire capacitance;

V is the power supply voltage

During IC physical implementation, only a few parameters could be optimized; for example: reduce the wire capacitance C_{load} by making the interconnection wire-length shorter or by spreading. Swap cells with high internal or leakage power with lower cells' power.

In advanced nodes 28 nm and below, static power consumption represents less than 10%, on average, of the total power consumed by an IC. The dynamic circuit power is composed of the internal power that represents 20% to 30% and the switching power representing 70% to 80% of the overall consumption of a circuit [20, 21]. These numbers are proved in test-cases we are using for this paper: Table 1, shows a summary of their main characteristics. Figure 1, shows their average static and dynamic power repartition. Figure 2 shows the different average power components repartition. It is evident to see that by targeting all the "Data nets", we are targeting more than 50% of the total power for optimization.

Table 1: Design Specifications

Designs	Number of instances	Number of nets	Physical area (μm^2)	Technology (nm)
Design#1	535815	566853	407658	20
Design#2	557185	588503	470164	20
Design#3	905670	1268272	1072040	7
Design#4	137950	221084	46975.9	7
Design#5	477969	546368	236706	16
Design#6	3695650	8402104	5949560	28
Design#7	637450	642466	392697	16
Design#8	779966	777869	475353	16
Design#9	2780115	5315732	4468680	28
Design#10	2288833	3179391	2982620	28
Design#11	3362065	4974698	4752870	28
Design#12	885391	1162839	1608120	28
Design#13	798317	1042158	1916400	28
Design#14	587529	1286854	5309480	16

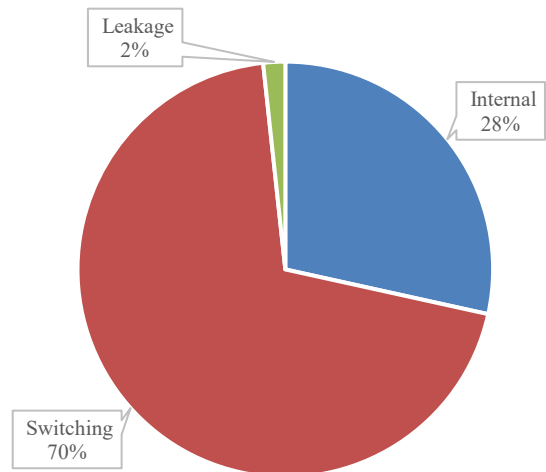


Figure 1: Static (Leakage) and dynamic (Internal + Switching) Power repartition

2.2. Wire optimization to reduce Net power

In our previous research [16], we presented a wire optimization technique for power saving on the interconnection at the physical implementation phase of an IC. At this stage, the circuit voltage and the TR are fixed by the circuit function, and we can't do anything to reduce them. The remaining parameter is the

interconnection capacitance. This represents an opportunity for significant power saving using routing transforms.

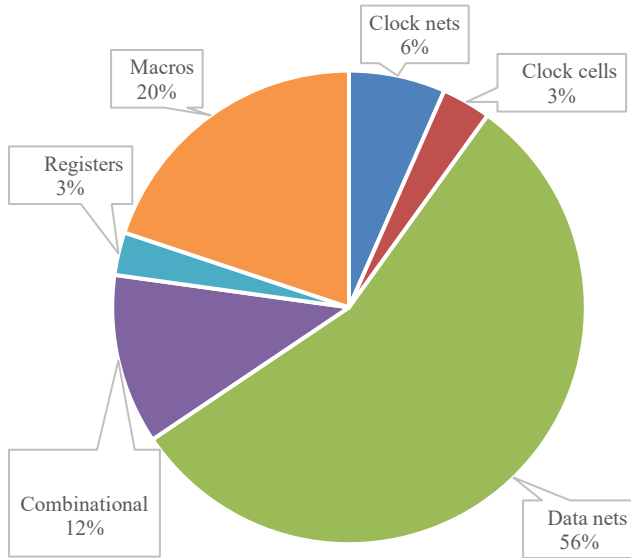


Figure 2: Multiple IC power components repartition

The complexity of capacitance variations makes it nearly impossible for the human mind to determine which combination of layers and via structures to use for a given net in order to obtain the less possible power consumption and keeping an acceptable timing and good routing. This can be achieved through layer promotion of power critical nets, coupled with a carefully set of double-spacing non-default rules (NDRs). Enabling the routing engines to efficiently trade-off timing quality of results (QoRs) and congestion.

We have used Mentor Graphics Nitro-SoC™ [22] tool and the correspondent place and route full flow [23, 24] to implement test-cases used during this study.

As a review of results achieved in our previous work, reference [16] proves the following results:

- 40% of data nets are consuming 92.6% of the total power as shown in Figure 3.
- Start having a signifying power reduction up to 20% on power consumed by data nets when the number of target nets exceeds 40% of the total number of data nets: Figure 4.
- Total power reduction percentage approaching 7 %: Figure 5.
- A good compromise between the power saving and the timing/congestion was achieved by taking the cases 40% and 30% of total data nets number as a target for power optimization.

3. Results and analysis

3.1. Algorithm enhancement for better congestion overflow

In the previous section, we have introduced our research by presenting a reminder of results achieved in previous work [16]. Experiment on one test-case shows an important total power saving gain exceeding 5% by targeting 30% of data nets for optimization.

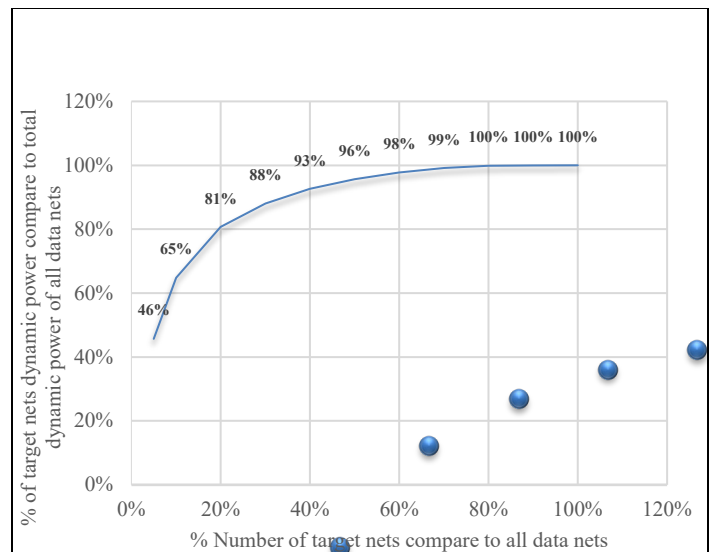


Figure 3: Data Nets power repartition

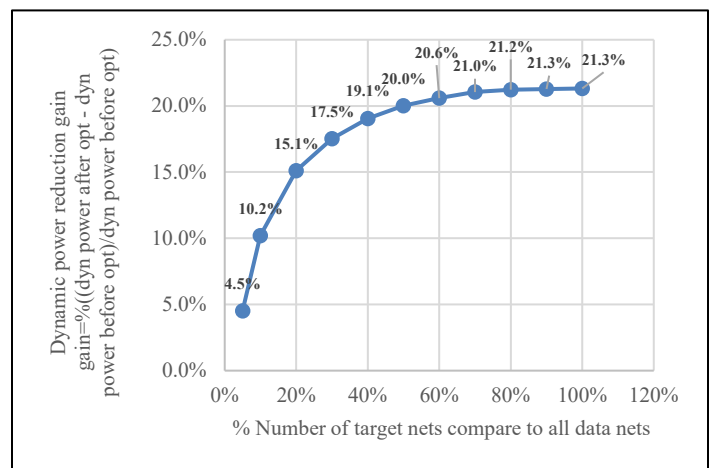


Figure 4: Dynamic power gain on data Nets

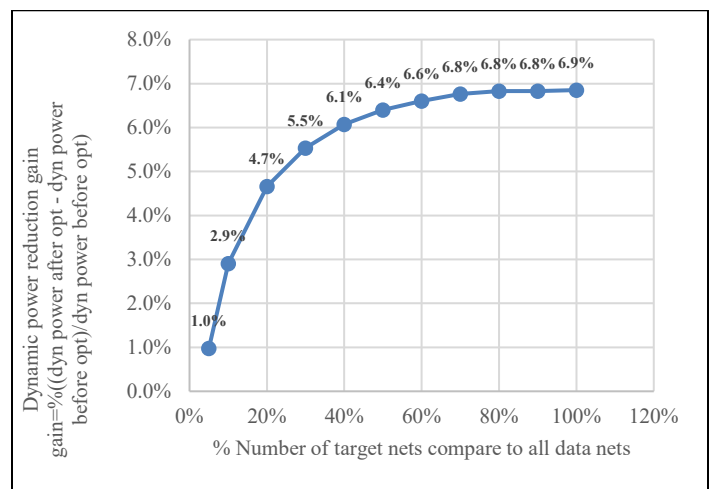


Figure 5: Total power gain on entire design

In this section, we will apply this optimal solution to multiple designs made with different technologies nodes. The goal is to see if this solution is robust enough for production usage.

For a good comparison, we are applying the wire optimization for power reduction on an optimized post-clock-tree-synthesis (post_CTS) database (db). The baseline run that produces initial post-CTS db is a full place and route flow power-driven [23, 24]. Thus, with our solution, we will be able to see the exact power gain after using existing power optimization transforms. Experiments are done on 14 test cases made with advanced technologies nodes 28 nm, 20 nm, 16 nm, and 7 nm. Their main characteristics are summarized in table 1:

Algorithm#2, shows the automatic incremental optimization flow for power reduction:

Algorithm # 2: Automatic incremental flow

1. *set designs_list = (Design#1, Design#2, Design#3, Design#4, Design#5, Design#6, Design#7, Design#8, Design#9, Design#10, Design#11, Design#12, Design#13, Design#14)*
2. **For design** (\$designs_list)
 - a. *Read baseline saved Post-CTS Database*
 - b. *Report & save Initial QoR (Timing, Power, and Congestion)*
 - c. *Create double spacing NDRs on all used layers for routing.*
 - d. *Get 30% of data nets with highest power consumption (see next section for more details: Procedure#1)*
 - e. *Apply NDRs on Target_Nets list*
 - f. *Run the native global route*
 - g. *Run one optimization pass for Timing recovery*
 - h. *Run the native global route*
 - i. *Report QoR (Timing, Power, and Congestion)*
3. **END for**

The section below describes the main procedure that gets target nets for optimization. Its objective is to get 30% of data nets having high dynamic power.

Procedure # 1: Get target nets: 30% of data nets with the highest power consumption

1. *Filter data nets from all nets (data_nets)*
2. **For each data_net** (\$data_nets)
 - a. *Get its dynamic power and save it in a table*
 - b. *Save the data_net and its dynamic power*
3. **END for**
4. *Rank nets in order of power consumption.*
5. *Return first 30% of data_nets*

For all trials, the target nets are 30% of data nets that have the highest power consumption, while in some test cases we see that by targeting only 20% of data nets we are targeting more than 80% of the total power consumed in the interconnection. This remark conducts us to an optimal solution by targeting a dynamic list of nets consuming more than 80% of the total power.

The new procedure that gets target nets for optimization is described below:

Procedure # 2: Get target nets: nets consuming > 80% of the total power in the interconnection

1. *Filter data nets from all nets (data_nets)*
2. *Get the total dynamic power of all \$data_nets (data_nets_power)*
3. **For each data_net** (\$data_nets)
 - a. *Get its dynamic power and save it in a table*
 - b. *Save the data_net and its dynamic power*
4. **END for**
5. *Rank nets in order of power consumption.*
6. *Return the first list of nets consuming >80% of total data_nets_power*

Table 2, shows a comparison between cases performed by using procedure#1 and procedure#2. We notice an important “Overflow” reduction in almost all test-cases.

The high overflow reduction is happening on designs having a low activity such as “Design#1, Design#2, Design#3 and Design#4”. The low overflow is coming especially from the important reduction of target nets from 30% to 2% for Design#1, 3% for Design#2, and 4% for Design#3. For these test-cases the low target nets percentage is sufficient to have good power reductions achieving -17.5%, -16.3%, -7.6% and -7.5% respectively.

For other designs, Design#5 to Design#13, by targeting 20% instead of 30% of data nets, we achieve almost the same power gain lower congestion overflow. Finally, one test-case “Design#14” ends with the same target nets percentage of 30% and a power gain of -19%.

3.2. Power gain on overall designs

In the previous section, we notice an important reduction of the number of target nets considered for optimization with proc#2 compare to proc#1. Fewer target nets number with almost the same or better power gain is helping for a fast run time accompanied by a better rout-ability. All of that conduct to an optimal solution, which is to target the number of nets consuming more than 80% of the total net's power with a maximum of 30% of the total nets number.

Table 3, presents the dynamic and total power gain for each design using the optimal solution. An average of 5% power reduction obtained in both dynamic and total power.

Table 2: Comparison between Procedure#1 and Procedure#2.

Target nets power gain = % (nets power after optimization- nets power before optimization)/ nets power before optimization

Designs		Total number of nets	Number of target nets	% of target nets (%)	Before Optimization			After Optimization		
					Total nets power (mW)	Target nets power (mW)	% power of target nets (%)	Overflow	Target nets power (mW)	Target nets power gain (%)
Design#1	Proc#1	483171	144951	30.0%	1.0423	1.0423	100.0%	3.41	0.8752	-16.0%
	Proc#2	483171	9663	2.0%	1.0423	0.8578	82.3%	1.10	0.7079	-17.5%
Design#2	Proc#1	501314	150394	30.0%	1.1548	1.1548	100.0%	3.80	0.9781	-15.3%
	Proc#2	501314	15039	3.0%	1.1548	0.9812	85.0%	1.69	0.8209	-16.3%
Design#3	Proc#1	878226	263468	30.0%	41.998	41.8647	99.7%	0.23	38.7659	-7.4%
	Proc#2	878226	35129	4.0%	41.998	34.7165	82.7%	0.15	32.0757	-7.6%
Design#4	Proc#1	147116	44135	30.0%	15.435581	15.435581	100.0%	0.40	14.312023	-7.3%
	Proc#2	147116	5885	4.0%	15.435581	15.435581	100.0%	0.05	14.270356	-7.5%
Design#5	Proc#1	433469	130041	30.0%	102.6567	96.0036	93.5%	4.46	70.924	-26.1%
	Proc#2	433469	86694	20.0%	102.6567	90.8166	88.5%	4.08	66.463	-26.8%
Design#6	Proc#1	3618017	1085405	30.0%	892.1152	821.1902	92.0%	7.56	712.3573	-13.3%
	Proc#2	3618017	723603	20.0%	892.1152	780.1937	87.5%	7.13	674.5511	-13.5%
Design#7	Proc#1	636971	191091	30.0%	53.3274	50.7283	95.1%	2.39	39.7819	-21.6%
	Proc#2	636971	127394	20.0%	53.3274	48.4197	90.8%	2.15	37.6407	-22.3%
Design#8	Proc#1	770303	231091	30.0%	57.9306	55.0936	95.1%	1.75	41.678	-24.4%
	Proc#2	770303	154061	20.0%	57.9306	52.2459	90.2%	1.49	39.1292	-25.1%
Design#9	Proc#1	2436751	731025	30.0%	939.3153	875.8495	93.2%	4.75	726.5736	-17.0%
	Proc#2	2436751	487350	20.0%	939.3153	831.0609	88.5%	4.50	688.0895	-17.2%
Design#10	Proc#1	2020267	606080	30.0%	1479.458	1377.5008	93.1%	8.69	1150.6352	-16.5%
	Proc#2	2020267	404053	20.0%	1479.458	1297.9898	87.7%	8.19	1082.2901	-16.6%
Design#11	Proc#1	3100457	930137	30.0%	2615.8898	2411.9914	92.2%	8.11	1991.3135	-17.4%
	Proc#2	3100457	620091	20.0%	2615.8898	2266.4228	86.6%	7.70	1865.8817	-17.7%
Design#12	Proc#1	822186	246656	30.0%	435.9402	411.998	94.5%	7.83	346.8801	-15.8%
	Proc#2	822186	164437	20.0%	435.9402	394.3237	90.5%	7.57	332.0825	-15.8%
Design#13	Proc#1	745762	223729	30.0%	378.2664	338.9859	89.6%	4.86	274.266	-19.1%
	Proc#2	745762	149152	20.0%	378.2664	313.018	82.8%	4.55	253.8826	-18.9%
Design#14	Proc#1	466631	139989	30.0%	903.8741	790.2763	87.4%	6.30	640.3705	-19.0%
	Proc#2	466631	139989	30.0%	903.8741	790.2763	87.4%	6.30	640.3705	-19.0%

Table 3: Dynamic and total power gain

power gain = %(power after optimization- power before optimization)/ power before optimization

Designs	Before Optimization		After Optimization		Dynamic power gain (%)	Total power gain (%)
	Dynamic Power (mW)	Total power (mW)	Dynamic Power (mW)	Total power (mW)		
Design#1	8.0476	8.0711	7.9125	7.9359	-2%	-2%
Design#2	8.7976	8.9791	8.6429	8.8298	-2%	-2%
Design#3	149.3188	152.1707	147.3411	150.1936	-1%	-1%
Design#4	113.042473	113.31836	111.774694	112.050549	-1%	-1%
Design#5	330.4627	330.8185	307.2876	307.6482	-7%	-7%
Design#6	2658.979	2659.736	2563.1845	2563.9415	-4%	-4%
Design#7	198.2466	198.3225	187.7011	187.7769	-5%	-5%
Design#8	218.2062	218.3048	205.2356	205.334	-6%	-6%
Design#9	2018.207	2126.9193	1872.6143	1981.4807	-7%	-7%
Design#10	2964.9741	3043.4681	2748.532	2830.5278	-7%	-7%
Design#11	4141.0681	4245.7608	3735.9251	3840.9783	-10%	-10%
Design#12	894.2836	894.3742	833.1615	833.2521	-7%	-7%
Design#13	702.7373	702.8631	643.1108	643.2364	-8%	-8%
Design#14	2693.7224	2694.3472	2595.0319	2595.6581	-4%	-4%
Average					-5.18%	-5.10%

4. Conclusion

In this paper, we present a new wire optimization technique for power reduction during IC physical implementation phase. The main outcome is the optimal choice of target nets for optimization, which is the list of power critical nets consuming more than 80% of total power in the interconnection without exceeding the number of nets of 30% of the total nets. Experiment on 14 test-cases made with advanced technologies nodes shows an important power reduction and, at the same time, keeps having good design routability.

The technique leads to an important dynamic power improvement through a simple critical Nets re-routing. The power on all data Nets reduced up to 20% and the average total power reduction in all test-cases by 5%.

Conflict of Interest

The authors declare no conflict of interest.

Acknowledgment

This research supported by Mentor Graphics Corporation. We thank Dr. Hazem El Tahawy (Mentor Graphics, Managing Director MENA Region) for initiating and supporting this work.

References

- [1] K. C. Janac, "Interconnect Physical Optimization," Proceedings of the 2018 International Symposium on Physical Design - ISPD 18, 2018.
- [2] D. J. Radack and J. C. Zolper, "A Future of Integrated Electronics: Moving Off the Roadmap," in Proceedings of the IEEE, vol. 96, no. 2, pp. 198-200, Feb. 2008. doi: 10.1109/JPROC.2007.911049.
- [3] D. Flynn, R. Aitken, A. Gibbons, K. Shi, Low power methodology manual: for system-on-chip design, 2ed. ed., Springer, 2007, p13.
- [4] I. Lee and K. Lee, "The Internet of Things (IoT): Applications, investments, and challenges for enterprises," Business Horizons, vol. 58, no. 4, pp. 431-440, 2015.
- [5] C. J. Alpert, W.-K. Chow, K. Han, A. B. Kahng, Z. Li, D. Liu, and S. Venkatesh, "Prim-Dijkstra Revisited," Proceedings of the 2018 International Symposium on Physical Design - ISPD 18, 2018.
- [6] ITRS 2015 Edition Report-Interconnect, https://www.semiconductors.org/wp-content/uploads/2018/06/6_2015-ITRS-2.0_Interconnect.pdf, 2015.
- [7] J. Hu, Y. Zhou, Y. Wei, S. Quay, L. Reddy, G. Tellez, and G.-J. Nam, "Interconnect Optimization Considering Multiple Critical Paths," Proceedings of the 2018 International Symposium on Physical Design - ISPD 18, 2018.
- [8] S. Mantik, G. Posser, W.-K. Chow, Y. Ding, and W.-H. Liu, "ISPD 2018 Initial Detailed Routing Contest and Benchmarks," Proceedings of the 2018 International Symposium on Physical Design - ISPD 18, 2018.
- [9] X. Qiu and M. Marek-Sadowska, "Routing Challenges for Designs With Super High Pin Density," IEEE Transactions on Computer-Aided Design of Integrated Circuits and Systems, vol. 32, no. 9, pp. 1357-1368, 2013.

- [10] L. Cherif, M. Chentouf, J. Benallal, M. Darmi, R. Elgouri and N. Hmina, "Usage and impact of multi-bit flip-flops low power methodology on physical implementation," 2018 4th International Conference on Optimization and Applications (ICOA), Mohammedia, Morocco, 2018, pp. 1-5. doi: 10.1109/ICOA.2018.8370498.
- [11] M. Rahman, R. Afonso, H. Tennakoon and C. Sechen, "Design automation tools and libraries for low power digital design," 2010 IEEE Dallas Circuits and Systems Workshop, Richardson, TX, 2010, pp. 1-4.
- [12] M. Chentouf, L. Cherif and Z. El Abidine Alaoui Ismaili, "Power-aware clock routing in 7nm designs," 2018 4th International Conference on Optimization and Applications (ICOA), Mohammedia, Morocco, 2018, pp. 1-6. doi: 10.1109/ICOA.2018.8370505.
- [13] L. Cherif, J. Benallal, M. Darmi, M. Chentouf, R. Elgouri, and N. Hmina, "ASIC Physical Design Flow: Power Saving Opportunities on Interconnection Components," Lecture Notes in Electrical Engineering Proceedings of the 1st International Conference on Electronic Engineering and Renewable Energy, pp. 258–265, Feb. 2018.
- [14] L. Cherif, M. Darmi, J. Benallal, R. Elgouri, and N. Hmina, "Last-Mile Post-Route Power Optimization in Integrated Circuit Conception," International Journal of Engineering & Technology, 7(4.16), 102-105. doi:http://dx.doi.org/10.14419/ijet.v7i4.16.21788.
- [15] G. J. Y. Lin, C. B. Hsu and J. B. Kuo, "Critical-path aware power consumption optimization methodology (CAPCOM) using mixed-VTH cells for low-power SOC designs," 2014 IEEE International Symposium on Circuits and Systems (ISCAS), Melbourne VIC, 2014, pp. 1740-1743.
- [16] L. Cherif, M. Chentouf, J. Benallal, M. Darmi, R. Elgouri and N. Hmina, "Layer Optimization for Power Reduction in Integrated Circuits," 2018 IEEE 5th International Congress on Information Science and Technology (CiSt), Marrakech, Morocco, 2018, pp. 625-629. doi: 10.1109/CIST.2018.8596605.
- [17] J. M. Rabaey, A. P. Chandrakasan, and B. Nikolic, Digital Integrated Circuits: A Design Perspective, 2nd ed., Prentice Hall Electronics and VLSI Series, Upper Saddle River, NJ: Pearson Education, 2003.
- [18] K. Y. Gary, Practical Low Power Digital Vlsi Design. Springer Verlag, 2012. doi:10.1007/978-1-4615-6065-4.
- [19] M. S. Elrabaa, I. S. Abu-Khater, and M. I. Elmasry, Advanced low-power digital circuit techniques. Boston: Kluwer Academic Publishers, 1997.
- [20] J-G. Cousin, D. Chillet and O. Sentieys, "Power Estimation and Optimisation for ASIPs", Submitted to 1997 International Symposium on Low-Power Design, Mont. CA, Aug. 1997.
- [21] E. Macii, "High Level Design and Optimization for Low Power", NATO Advance Study : Low Power in Deep Submicron Electronics, Aug 1996.
- [22] Nitro-SoC™ Software Version 2018.1, December 2018.
- [23] Nitro-SoC™ "User's Manual", Software Version 2018, December 2018.
- [24] Nitro-SoC™ "Advanced Design Flows Guide", Software Version 2018, December 2018.

Coordination between Heterogeneous Models Using a Meta-model Composition Approach

Naima Essadi*, Adil Anwar

SIWEB, E3S, EMI, Mohammed V University in Rabat, Rabat, Morocco

ARTICLE INFO

Article history:

Received: 17 September, 2019

Accepted: 26 October, 2019

Online: 25 November, 2019

Keywords:

Coordination

Transformation

Composition

DSML

Heterogeneity

Model

Meta-model

Offered Interface

Required Interface

Realization

Referencing

Relationship

Bridge Pattern

ABSTRACT

The technological advance as well as needs of human beings made that systems became more and more complex. In contrast, the use and creation of new modelling languages became simple and no more reserved for a handful of language experts. Consequently, many new practices of systems implementation emerged, among them, the use of different domain specific modelling languages (DSMLs) to represent the same system. Indeed, complex systems are composed by many components sometimes belonging to various domains. Thus, many teams of experts collaborate to develop such systems. Moreover, teams tend to use different DSMLs to design their concerns. This new practice generates an accidental heterogeneity due to production of various heterogeneous models representing a same system. However, those heterogeneous models need absolutely to be coordinated to facilitate communication between stakeholders and of course to ease implementation and validation of systems. This paper proposes a composition interface-based approach to coordinate and integrate heterogeneous DSMLs in order to coordinate their models. The proposed composition interface is defined according to Bridge Design Pattern. To illustrate this approach two DSMLs are used: An Indoor Service Transport Modelling Language and an Internet of Things Modelling Language.

1. Introduction

Model Driven Engineering (MDE) has as main goal a deep separation between business and technological concerns. It makes models in center of software and systems engineering. Hence, it provides concepts and tools assuring to bridge the gap between problem-level abstractions and implementation-level concepts.

However, the emergence complexity of nowadays systems raises numerous new conception and implementation challenges. Indeed, these systems involve many different domains. Consequently, many teams of experts contribute to implement a same system.

Moreover, the need and the large use of MDE as well as the popularization of software language engineering (SLE) induce the new practice of using specific hand maid modelling languages baptized Domain Specific Modelling Languages (DSMLs)

Recently, the use of DSMLs rather than Unified Modelling ones increases due to many reasons. Actually, Domain Specific Modeling languages are expressive and allow a concise and accurate specification in addition of a high level of abstraction [1, 2]. These highlights have a direct influence upon productivity and costs. Indeed, the use of domains vocabulary means less time and effort in modelling phase. It also means a high quality of communication between stakeholders thereby decreasing error rate and modelling iterations.

Actually, every domain has specific vocabulary, concepts and paradigm. This difference implies the use of a different DSML for every different domain involved in the same system.

Consequently, the use of multiple DSMLs to design systems induces an accidental heterogeneity. Actually, as result we get many heterogeneous models for a same system as illustrated by Figure 1. The diagram of Figure 2 summarises problematic causes and effect.

*Corresponding Author: Naima Essadi, SIWEB, E3S, EMI, Mohammed V University in Rabat, Rabat, Morocco, Email: naimaessadi@gmail.com

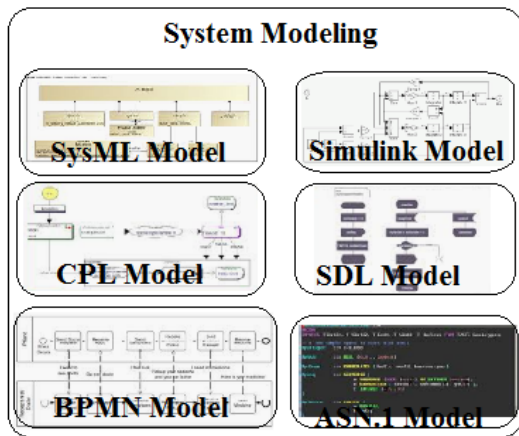


Figure 1: Heterogeneous Models for a same system

These models need inevitably to be coordinated and integrated to get a whole view of systems and, by the way to ease implementation and validation. Coordination between these models is also motivated by the need of getting relevant information scattered in different models as well as the concern to maintain the consistency of systems in case of evolution.

Many leads had been explored by current researches to resolve this issue [2, 3, 4, 5]. Specifically, this work fits in researches operating at meta-level [6, 7, 8, 9]. Actually, we choose to coordinate DSMLs used to elaborate heterogeneous models rather than coordinating models themselves. The need of a generic, reused and less error prone approach motivated this choice.

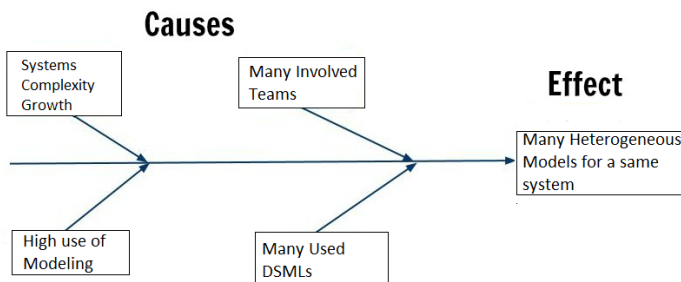


Figure 2: Causes effects diagram of current problematic

Adopting interface concept to coordinate the use of multiple DSMLs has been proposed by few interesting works [10, 11, 8, 12, 13]. Some of this works didn't give clear specification of how to define interfaces for languages, others didn't give any concrete process or tool to fulfil the proposed approach. Furthermore, those approaches didn't explain how to deal with pre-existent models.

Therefore, in this paper, we introduce a composition interface-based approach to coordinate heterogeneous DSMLs. This approach involves the application of a process in two steps: Coordination Meta-Model (CMM) elaboration and Models coordination. While, the first step aims to define interfaces for involved DSMLs and their composition to get a coordination meta-model (CMM), the second one involves the import of heterogeneous models in a model conforming to CMM. This import enables coordination between pre-elaborated heterogeneous models.

Our approach is in fact a structural interface-based composition of pre-elaborated models. It first gives a global view of system on hand and secondly affords the possibility to exchange important information between heterogeneous models as well as insuring their interoperability.

The remainder of this paper is organized as follows: we begin by giving an overview for DSMLs specification as well as heterogeneity in section 2. In Section 3, a motivating example is presented to advocate the need of resolution. Then, in following section, we introduce interface-oriented design basics for languages as well as Bridge Pattern Design. Section 5 illustrates the applicability of the approach using the motivating example where heterogeneous models are coordinated. Section 6 presents related works and finally, section 7 concludes this paper.

2. Heterogeneous DSMLs

2.1. DSMLs Overview

Domain Specific Modeling Languages aims to abstract problems and solution using domains vocabularies and concepts instead of generic and unified objects and shapes.

Contrary to a General-Purpose Modeling Language like UML, a DSML is tailored to a specific specialized domain. It allows stakeholders to contribute in modeling using notations close to their knowledge of respective domains [1]. DSMLs could be visual such as SDL, IFML, BPMN or textual like Data Modeling Languages: Abstract Syntax Notation (ASN.1) [14, 15], YANG [16, 17] and others.

DSMLs are first of all languages and consequently adhere to languages norms. Commonly, languages are specified using grammars with the famous Context-Free Grammars EBNF (extended Backus-Naur Form) [18]. Indeed, many other forms of specification exist [10] such as: Attribute Grammars [19], Graph Grammars [20], UML Profiles [21] and Meta-modeling [22]. Specifically, this work emphasizes meta-modeling specification.

2.2. DSMLs Specification

DSMLs are defined by two manners: white box specification and black box specification. The white box provides all necessary information about the language: the exhaustive list of including concepts with their allowed inter-relations as well as their concrete representation and optionally semantics giving the related meaning.

A white box classical specification reflects the language complexity. It is for example used to elaborate a compiler for the language or either to integrate languages to improve their expressiveness. Many recent researches use this specification to reuse existing DSMLs. Table 1 summarizes elements of white box specification.

However, a DSML black box specification is optional and aims to hide complexity and irrelevant information about a language. It could be defined by providing offered and required interfaces for a language. Table 2 describes offered and required interfaces.

Table 1: DSML White Box Specification

Parts	Relevance	Description
Abstract Syntax	Required	Provides concepts of a language with their exact rules of combinations [23].
Concrete Syntax	Required	Provides textual or graphical notation and symbols of language concepts [10]. A language could have one or more concrete syntax [23].
Semantics	Optional	Provides meaning and subjective understanding of a language expressions and concepts combination [10, 23]. Many types of semantics exist: Translational, Operational Semantic, Denotational and Extensional [23].
Semantics Mapping	Optional	Provides correspondences and relations between Semantic and Abstract syntax elements [23].
Syntactic Mapping	Optional	Assigns syntactic constructs to the abstract syntax [24]

The definition of interfaces for a DSML allows dealing with the language without knowing all detailed information and specification about it. The black box specification gives just restricted and needed elements. Actually, the definition of a DSML as a black box exposing specific interfaces allows language reuse in different contexts. Hence, a language could be substituted by another as long as it respects the same interface contract.

Table 2: DSML Black Box Specification

Parts	Relevance	Description
Offered Interface	Optional	Exposes elements to be used or referenced by other languages.
Required Interface	Optional	Represents elements and references needed by the language from other languages.

2.3. Heterogeneous DSMLs

We qualify, as heterogeneous, elements with different nature. In MDE, the heterogeneity of models is usual due to various domains, tools, concepts and paradigms of modelling. Many types of heterogeneity have been identified [2, 3, 25]. Nevertheless, we notice three levels of heterogeneity between models:

- Heterogeneity of points of views: includes models with different purposes and scopes. For example a model representing static point of view is considered as heterogeneous with a model describing a dynamic point of view or a requirements model.
- Heterogeneity of meta-model (language): means that models are elaborated with different DSMLs. We can also say that they are conform to different meta-models, e.g., language heterogeneity between a BPMN model and an SDL model.

- Heterogeneity of meta-meta-model means that models are elaborated with different DSMLs, and those DSMLs themselves are specified using different meta-models. An example of that form of heterogeneity could be a CPL model elaborated using CPL DSML conforming to GOPPRR [26] meta-meta-model, the second model could be an SDL model elaborated using SDL DSML which is specified with Ecore meta-model.

In this work we are concerned by heterogeneity of DSML which is the second level of heterogeneity. The first and third levels of heterogeneity are beyond the scope of this paper.

3. Motivating Example

In this paper we illustrate our approach using an Indoor Transport Service System (ITS). The ITS system is composed by Robots, Locations and Items as described by diagram in left of Figure 3. Robots execute tasks within a defined world [27]. It transports Items from source to target locations. This kind of systems is of course very useful and is more and more used for different purposes: In hospitals for providing patient rooms with medications and medical supplies, in restaurants to deliver ordered meals to customers, etc.

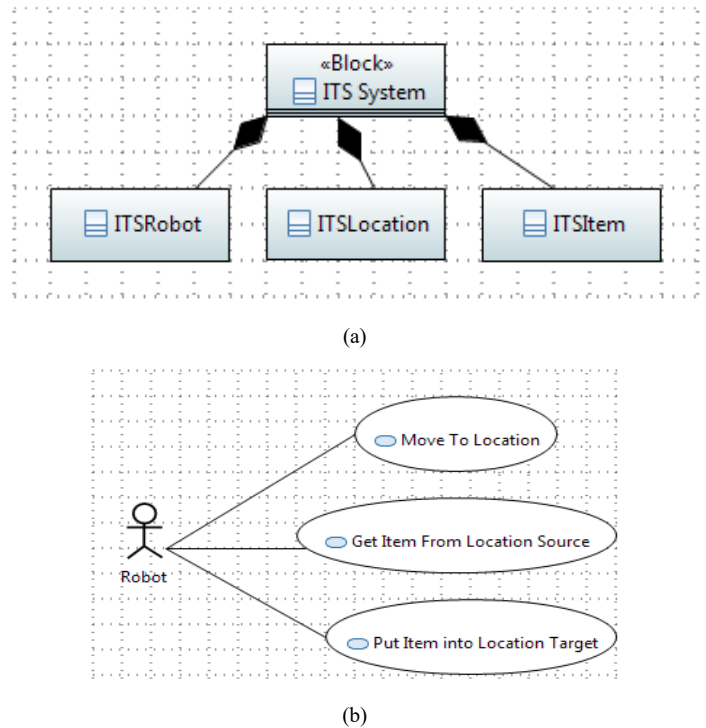


Figure 3: ITS System Main Elements and Features

However, the ITS system needs to be supervised. System users need to be informed about Robot’s location and activity while accomplishing their transportation service. They also need to get informed about item’s location in real time. A good solution for Robot and Items supervision is to consider them as connected objects.

This means that we need to compose our ITS system with an Internet of Things system.

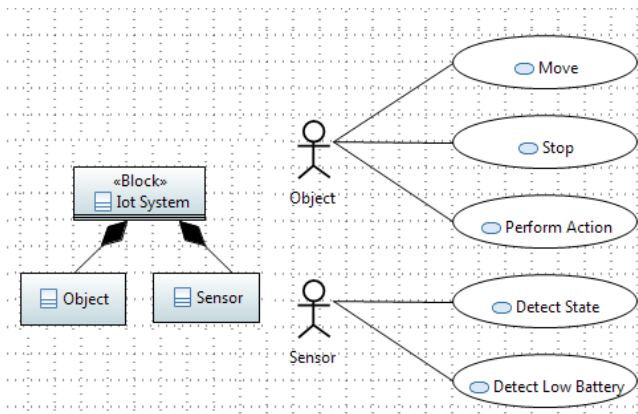


Figure 4: IoT System Main Elements and Main Features

An IoT system as described by left part of Figure 4 is composed by Object and Sensor. Many kinds of sensors exist: sensors to detect state change, location or battery thresholds. A sensor is related to an object to detect events over them. The right part of Figure 4 exposes object and sensor use cases. Sensor detects event over object that performs actions. Consequently, in this case study, we will deal with two heterogeneous domains: ITS domain and IoT Domain. Subsequently, the composition of these two systems will involve two experts' teams: ITS team and IoT team. Every team needs a dedicated DSML for modelling its concerns, ITS DSML and IoT DSML for instance.

3.1. ITS DSML

We have elaborated a specific DSML for the ITS System. This DSML uses domain vocabularies and concepts. In this section, we will give an excerpt of the white box specification of this language. The abstract syntax is illustrated in Figure 2 and described by semantics column of table 3. The graphical representation of DSML concepts and semantics are given in Table 3.

Table 3: ITS DSML Concrete Syntax and Semantics

Abstract Concepts	Graphical Representation	Description
ITSRobot		Concept responsible for indoor transportation.
ITSGoal		Concept describing a mission to be executed by robot. It includes an item as well as two locations source and target.
ITSTask		Concept regrouping a list of goals to be executed by a single robot.
ITSItem		Concept representing elements transported by robots.
ITSLocation		Concept representing site of departure and end points for robots missions.
Relation ITSTask-ITSRobot		Concept relating an ITSTask to an ITSRobot
Relation ITSGoal-Location		Concept relating a goal to Location concept.
Relation ITSGoal-Item		Concept relating a goal to Item concept

We have used Obeo Designer [28] to create and design a new DSML for ITS domain. Obeo Designer is an eclipse modeling tool that enables the creation of new DSMLs and their editors. It is based on the frameworks EMF, GEF [29] and GMF [30].

Figure 6 illustrates the elaborated ITS language editor. It illustrates also a model of this DSML produced using the graphical editor. In this model the instance "Hospital-Robot" of ITSRobot has the ITSTask "Hospital_Task" as mission to achieve. This task is composed by two ITSGoals: a goal "Source" to load ITSItem "oxygenBottle" from ITSLocation "Storage" and a second ITSGoal "Target" to transport "oxygenBottle" to "PatientRoom".

A second model of this DSML is given in Figure 7. This model concerns food delivery where an "FoodDeliveryRobot" has to accomplish the ITSTask "Pizza Delivery Task" of delivering ordered food "Pizza" to a specific ITSLocation "CustomerAddress".

3.2. IoT DSML

We have also elaborated a second DSML to cover internet of things domain [25]. This DSML introduces several basic concepts of IoT domain such as: Object, Sensor, Event and Action concepts. Sensors are associated to real word objects to detect events over them. Subsequently, actions are triggered according to detected events. The abstract syntax of IoT DSML is illustrated in Figure 8.

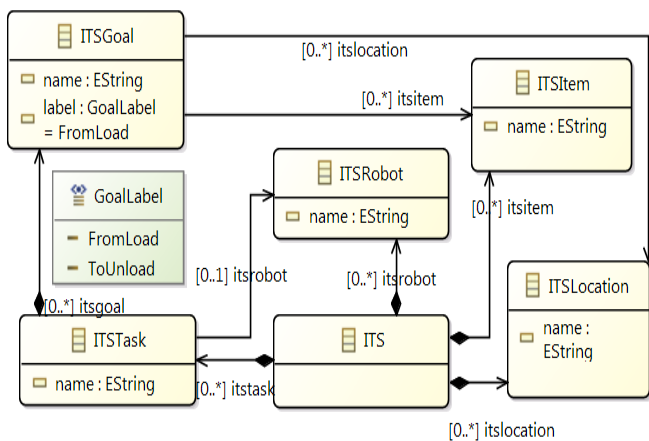


Figure 5: ITS DSML Abstract Syntax

As we can see in Figure 5, ITS DSML defines following new concepts: ITSRobot, ITSTask, ITSGoal, ITSItem and ITSLocation. ITSRobot has to achieve ITSTasks. Every ITSTask is composed by two ITSGoals: an ITSGoal to get an ITSItem from an ITSLocation source and an ITSGoal to put an ITSItem into an ITSLocation target.

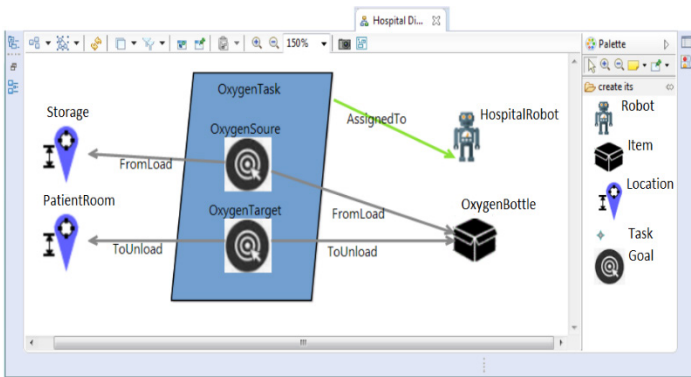


Figure 6: ITS Model for Hospital Use

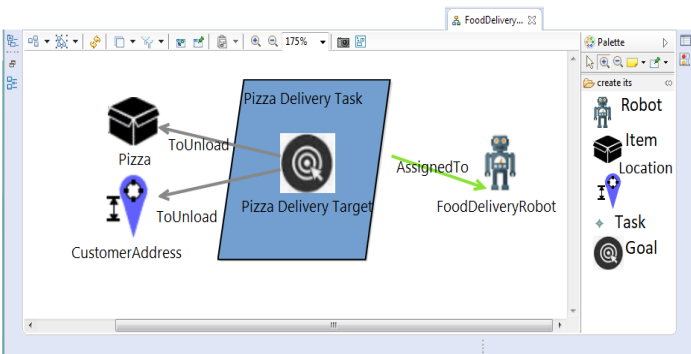


Figure 7: ITS Model for Food Delivery

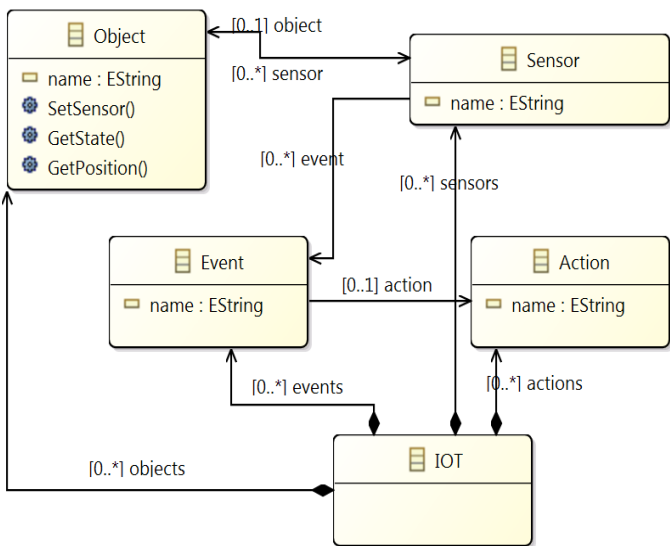


Figure 8: IoT DSML Abstract Syntax

The graphical representation and semantics of this DSML are described in Table 4.

An IoT model is illustrated in Figure 9. In this example, the instance of Object “Device” has two sensors “SpeedSensor” and “LocationSensor”. The “SpeedSensor” detects event “Moving” over “Device” which trigger the action “SendSms”. However, the sensor “BatterySensor” detects the event “LowBattery” and then triggers the action “SendSms”.

Table 4: IoT DSML Concrete Syntax and Semantics

Abstract Concepts	Graphical Representation	Description
Object		Concept representing connected objects.
Sensor		Concept sensor responsible of detecting events over connected objects.
Event		Concept event detected by sensors over objects.
Action		Concept describing action done when a sensor detects an event or an environment change.
Relation Event-Action		Concept relating an Event to a triggered Action.
Relation Sensor-Event		Concept relating a Sensor to detected Event.

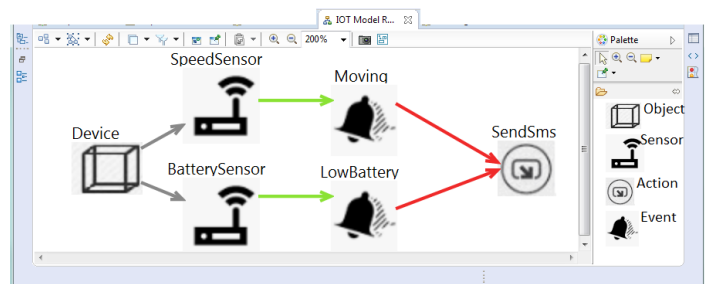


Figure 9: IoT DSML Model and Editor

A second model for IoT is given by Figure 10. The instance “Building” has “PositionSensor” as sensor. The action “SendSms” is triggered when the event “PositionChanged” is detected on “Building” Object.

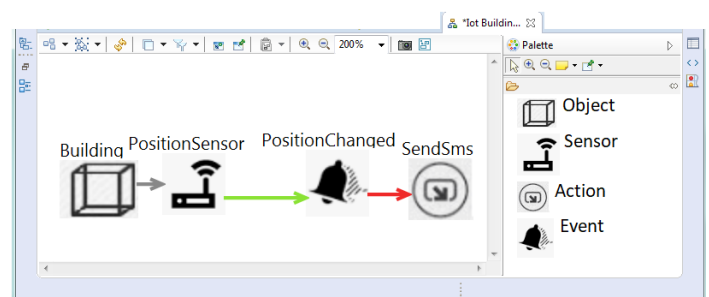


Figure 10: IoT DSML Second Model

3.3. ITS and IoT DSMLs Coordination Motivations

Both models given in Figure 6 and Figure 7 need to be related to model in Figure 9 for the following purposes: (i) To get activity and position information of “Hospital_Robot” and “FoodDeliveryRobot”. (ii) To get items’ position and situation of orders. However, coordinating ITS and IoT DSMLs is more

beneficial than coordinating their models. As, the coordination at language level holds to all its models [10]. It actually guarantees less elaboration time, less effort and less error prone. The coordination is done once instead of for every model.

Moreover, this operation is validated once for all which decreases bugs occurrences and coordination iterations. However, to achieve coordination we need to answer the following questions:

How can we coordinate the two DSMLs to get a global view of this system?

How can we coordinate the two DSMLs to achieve the whole system goals described by (i) and (ii)?

How can we represent and describe coordination between the two DSMLs?

4. DMLs Coordination

The recent design practices, for instance the use of different DSMLs to describe domains concerns, induce an accidental heterogeneity. Indeed, system designers from different teams produce heterogeneous models to describe a single system. These models are heterogeneous as they are expressed in different DSMLs. Consequently, coordination between involved DSMLs is needed to facilitate systems elaboration.

Actually, coordination could be seen as a combination between languages [10] to work together. It aims to join DSMLs's separate concepts to achieve a common goal. This join could however be structural to get hole static and global view of systems and either to get needed information and data among systems. On the other hand, the join could also be behavioral to achieve simulation to validate systems features and execution in early implementation stages.

Furthermore, coordination is considered as a less invasive form of integration [31]. It is done posteriori to get global analysis or global simulation of a system [32]. For some purposes, many interesting works [33, 6, 7] invoked instead globalization concept. This term is used as analogy with world globalization relationships between countries to regulate interchange, interaction and communication [6].

4.1. Interface-Based Coordination Approach

We propose to consider heterogeneous meta-models as component Figure 11. We relate them using interfaces considered as coordination points. Interfaces must be defined and related internally to their own meta-models and externally to other heterogeneous meta-models using coordination relationships.

4.2. Interface Description

DSMLs interfaces are part of black box modeling languages specification. It aims to define concepts exposing possible coordination join points and relationships to be established between languages.

Indeed, the use of an offered interface of a DSML1 by a DSML2 supposes that DSML1 exposes an offered interface and in the other side the DSML2 in its turn exposes a required interface.

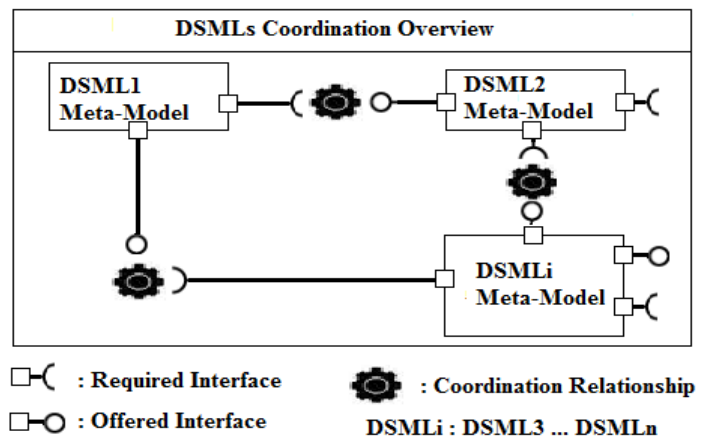


Figure 11: Heterogeneous DSMLs Coordination Overview

Our idea is described in Figure 11, where we define interfaces over DSMLs abstract syntax (meta-model). These interfaces are exposing concepts to other DSMLs and hiding details about exact structures and implementations.

In coordination, a DSML could be passive or active. The active DSML is the one exposing a required interface and thus uses interfaces offered by other DSMLs qualified as passive.

In this paper we consider external coordination between involved DSMLs. The external coordination has been defined in our previous work. It is done externally and is assured by a specific framework or workbench.

Many recent works [11, 8] discussed definition of DSMLs interfaces for various needs. However, they gave different proposition for defining it. In this work, we propose to create interfaces according to the Bridge Design Pattern [34].

4.3. Bridge Design Pattern Overview

Bridge Design Pattern has been first introduced by E.Gamma et al [34]. This design pattern aims to decouple an abstraction from its implementation so that the two can vary independently [34].

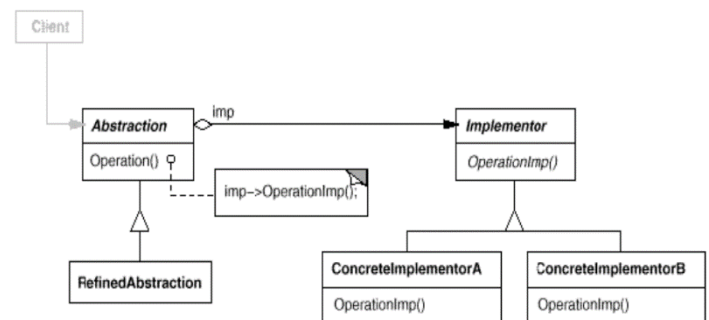
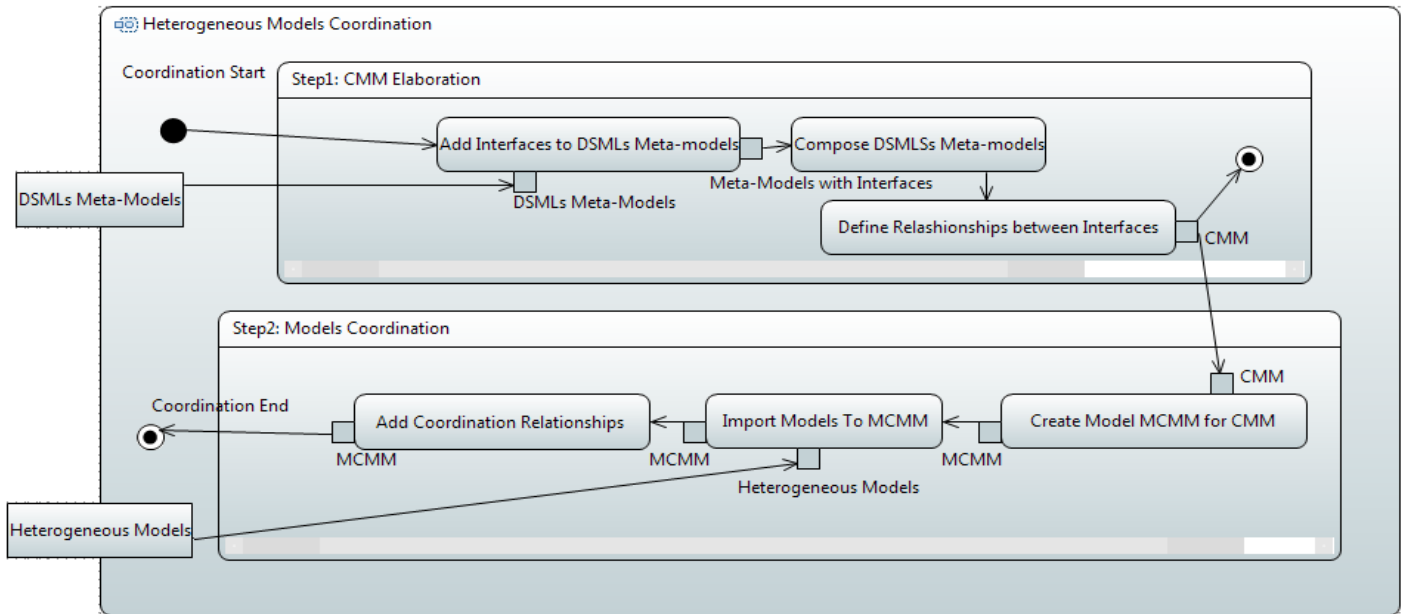


Figure 12: Bridge Design Pattern Concept [34]

The main idea of this design pattern illustrated in Figure 12 consists in the definition of an abstract class in the first part (“Abstraction” of Figure 12). This abstract class is inherited by the class requiring a specific implementation (“RefinedAbstraction” of Figure 12).



The defined Abstract class (“Abstraction”) references an interface defined in the other side (see “Implementor” in Figure 12) which is implemented by classes of this same side (see “ConcreteImplementorA”, “ConcreteImplementorB” in Figure 12). In case of DSMLs, we propose to define interfaces according to the Bridge Design Pattern.

Consequently, the abstraction part of the Bridge is the required interface and is defined by the first DSML while the second DSML defines the second part of the Bridge which is the interface to be referenced. This interface is exactly the offered interface of the second DSML. This means that an abstract meta-class must be defined in the first DSML. This meta-class is the super meta-class for meta-classes requiring coordination. While this meta-class represents a required interface for the first DSML, an interface is defined in the second DSML to represent its offered interface. This interface is implemented by elements of the second DSML.

The use of this pattern gives a generalized nature to coordination. Indeed, one of the two coordinated DSML could be easily replaced by another DSML as well as interfaces contracts are respected. In the proposed coordination process, a DSML could be coordinated to as many as needed DSMLs. It can be active or passive or the two at the same time.

4.4. Coordination Process Description

We introduced in Figure 11 a high-level overview of our approach. In this paragraph we propose to use this approach as a part of a coordination process composed by two main steps: CMM Elaboration and Models Coordination Figure 13.

“CMM Elaboration”, represented by Fig. 13 and Fig. 14, is done at DSML level. This step is done in three stages. We begin by adding interfaces to involved DSMLs’s meta-models and then we compose them to be able to define coordination relationships between their interfaces.

Interfaces are added using a transformation, while composition is done by creating a new element to be the root element of the CMM. The composition consists in including DSMLs’s meta-models root elements in this new element.

We assume that in a meta-model every meta-class must have at most a parent. At least one meta-class doesn’t have a parent. This meta-class is considered as the root element of a meta-model.

Subsequently, the result of this first step is coordination meta-model (CMM) that has a root element and coordinated meta-models as leaves

The second and final step is “Models coordination” illustrated by Figure 13 and Figure 15. The second step in this process enables us to achieve coordination.

We start by creating a new model MCMM conforms to CMM. The former will be composed by all input models and their mutual relationships. We first import input heterogeneous models then we relate input models interfaces using relationships defined in step 1.

The import operation is in fact a transformation that aims to transform input models to models that are conform to CMM. The result of this step is a model representing a global view of the whole system as well as its inter-relationships.

5. Application: Connected Indoor Transport Service System

To demonstrate the applicability of the proposed approach, we use the motivating example described in section 3. Actually, in this example we have two heterogeneous DSMLs to coordinate in order to get activity, position and battery threshold of ITSRobot. This coordination aims also to get position of Item and Room elements.

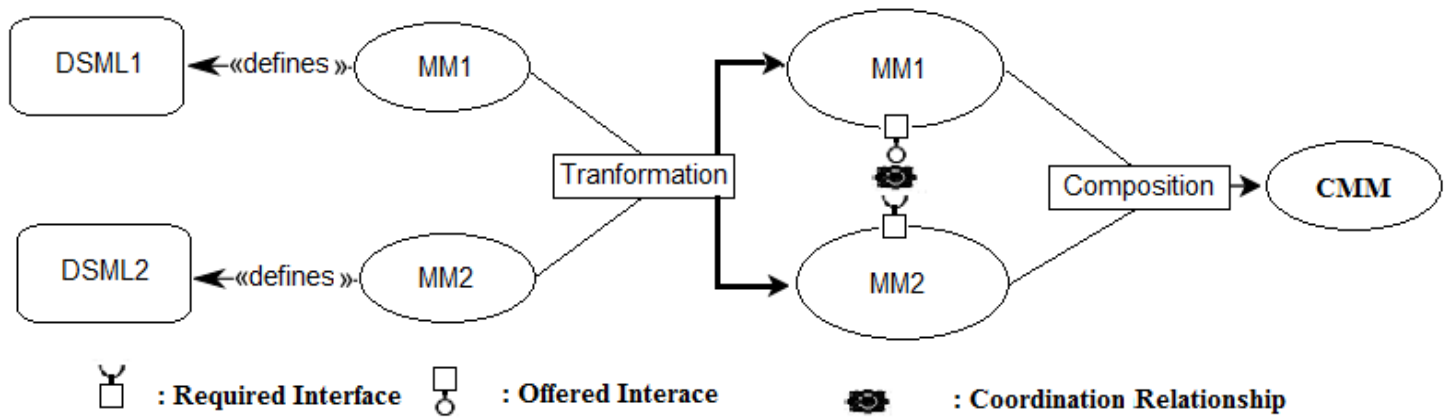


Figure 14: Step1: Coordination Meta-model (CMM) Elaboration

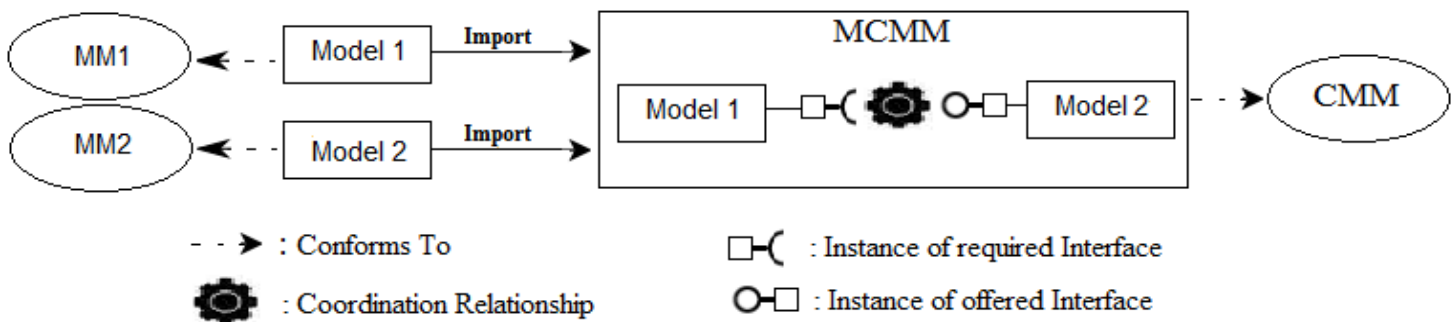


Figure 15: Step2: Models Coordination

5.1. ITS DSML Required Interface

The main feature of ITS DSML is the modeling of an Indoor Transport Service.

However, ITS team needs to get a real time activity of ITSRobot as well as position and battery thresholds. They also need to get location of Item and Room concepts. As said earlier, needs of a DSML are translated to required interface, for that we propose to define a required interface for ITS DSML. This interface is represented by the abstract meta-class named “ConnectedElement” see Figure 16.

According to Bridge Design Pattern, this meta-class is considered as super class of ITSRobot, Item and Room concepts. Moreover, this meta-class must use an element that provides its needs. The used element must be defined by another DSML offered interface. In the current example, the IoT DSML represents the other language.

5.2. IoT DSML Offered Interface

The IoT DSML offers connecting ability to objects by relating them to sensors able to detect events upon them. Subsequently and according to Bridge Pattern design, we propose to define the

interface “IObject” as offered interface see Figure 17. This interface is implemented by Object concept. Actually, referencing “IObject” enables connection to sensors.

5.3. CMM Elaboration

The coordination meta-model (CMM) of ITS and IoT DSMLs assures the composition of the two languages (Figure 18).

It has as root “ITS_IOT” element that contains involved languages root elements “ITS” and “IOT” for instance.

According to proposed approach, the coordination between the two languages must be done by defining coordination relationships between both required interface of ITS and offered interface of IoT, described in earlier paragraph. Subsequently, ‘ConnectableElement’ the super class of both ‘ITSRobot’, ‘Item’ and ‘Room’ must reference the interface ‘IObject’ of IoT DSML. This later is implemented by ‘Object’ meta-class belonging to IoT DSML.

While coordination elaborated between ITS and IoT DSMLs is qualified as external [25], we notice that relationship used between those languages interfaces is a composition relationship and more specifically a referencing relationship [25]: “ConnectedElement” references “Iobject”.

While coordination elaborated between ITS and IoT DSMLs is qualified as external [25], we notice that relationship used between those languages interfaces is a composition relationship

and more specifically a referencing relationship [25]: “ConnectedElement” references “Iobject”.

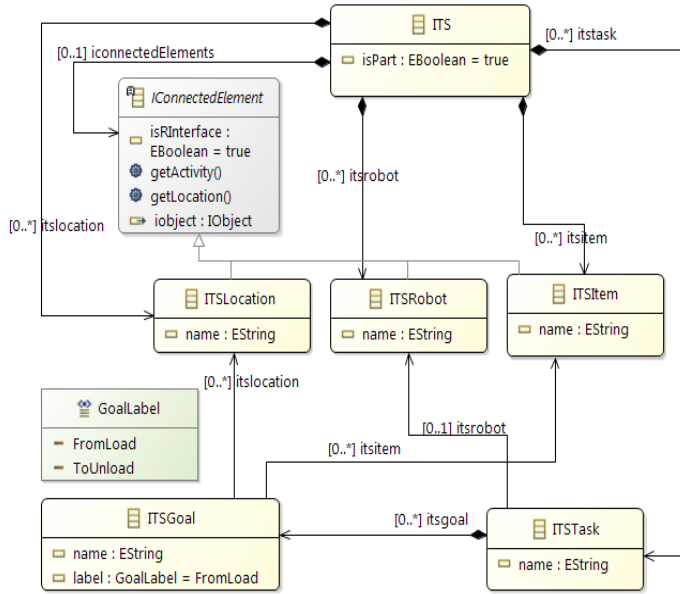


Figure 16: ITS Required Interface

The last step of the coordination process is the coordination between respective Models.

Figure 19 illustrates an ITS Model of a hospital robot transporting medical items from storage to patient rooms. This model has been linked to two IoT models.

The ‘Hospital-Robot’ has the ability to reference an Object due to the previous elaborated coordination. Hence, we associate it to a device Object having two sensors: Speed sensor to get activity and state of the ‘Hospital-Robot and the Battery sensor to monitor battery thresholds of the ‘Hospital-Robot.

On the other side, The ‘PatientRoom’ and ‘Storage’ have also the ability to be related to an Object element. Thereby, it has been associated to ‘Building’ object.

These associations provide connection to a Location sensor that gives information about Patient rooms and storage localization.

The coordination done at language level is also valuable for all conformed models. Thus, the same CMM could be used to coordinate models belonging to coordinated DSMLs. Consequently, to supervise elements of the second model illustrated in Figure 6 and Figure 7, we use the same CMM. Thereby, in Figure 20 ‘FoodDeliveryRobot’ and ‘CustomerAddress’ have both the possibility to reference an ‘Object’ element of IoT DSML.

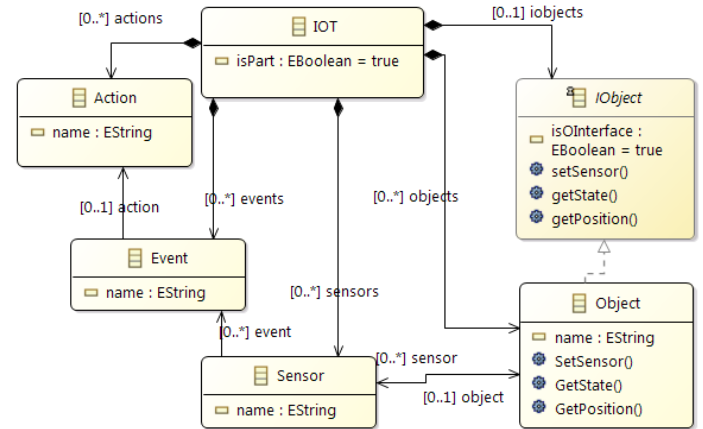


Figure 17: IoT Offered Interface

6. Related Works

Coordination between heterogeneous DSMLs is an active research topic. Although, many research papers discussed this subject, their objectives and motivations are different. Most of them emphasize reutilization and development of DSMLs.

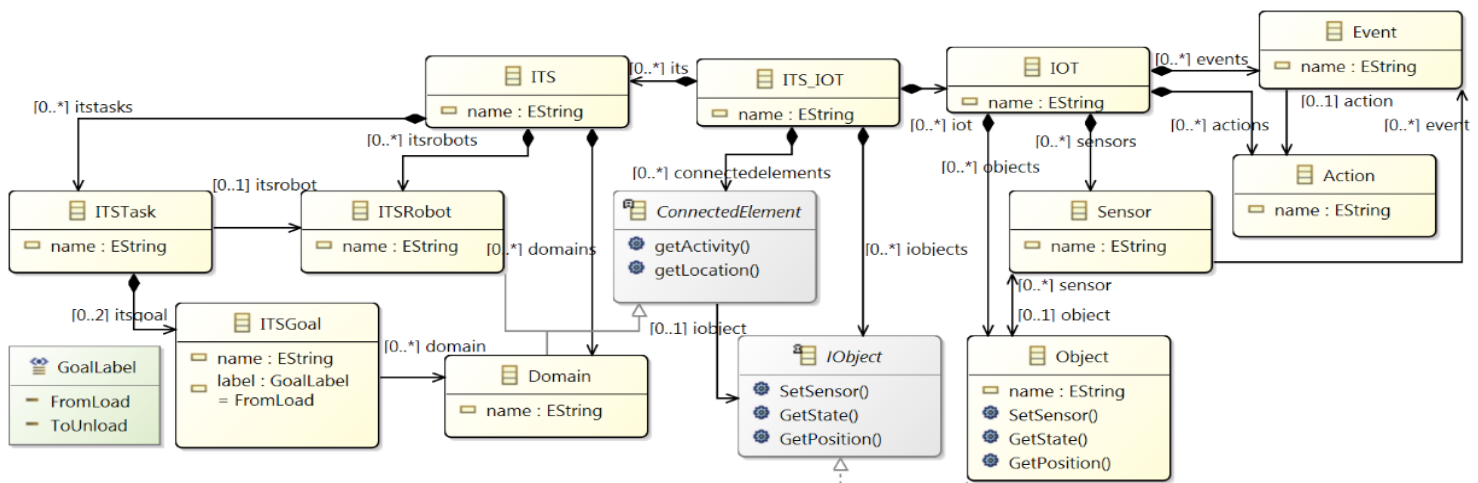


Figure 18: IoT Offered Interface

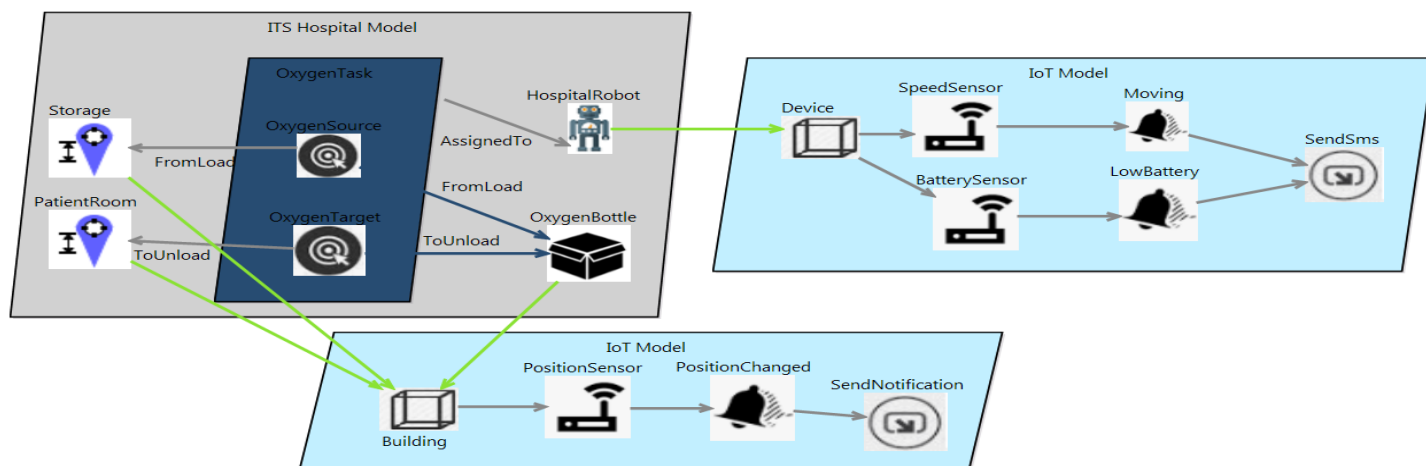


Figure 19: ITS and IoT Models Coordination

This coordination aims to help teams to cooperate with each other in different phases of systems implementation: specification, development, test, maintenance and evolution.

Modularization and interface-based techniques to compose and integrate DSMLs has been proposed by recent papers. A.Klepee [10] discussed the idea of language interfaces to combine languages and like this paper the author gave also a way to define a language interface using attributes and methods. However, our proposition is more explicit. Either, in [8] authors introduced an interface-based approach to define modular meta-models. The approach advises the use of a black-box meta-model definition based on interfaces and corresponding composition operators. This is done using an abstract meta-modeling language enabling the applicability of the approach for various meta-modeling languages. In the same line, our work proposes a composition technique based on offered and required interfaces.

In accordance with this work, Paper [11] advocates the definition of provided and required interfaces for languages as well as their syntactical and semantical composition operators to support DSLs modularity. However, author doesn't talk about how interfaces must be defined. In contrast, in [35] author proposes "Model Types" as example of DSLs interfaces defined on the abstract syntax of languages. Here, models are linked to Model Types using a typing relationship, while Model Types are related to each other with a subtyping relationship.

In [9], author proposes to coordinate heterogeneous behavioral models by specifying coordination patterns between languages. This is done using language behavioral interfaces as well as correspondence and coordination rules. Language behavioral interface in this approach is a set of Domain Specific Events (DSEs) defined in the context of language syntax meta-classes. DSEs are used as coordination points allowing both observation and control of models execution. Actually, coordination is enrolled using BCoool the coordination language. That language enables the definition of operators containing matching and coordination rules

over DSEs. This proposition is similar to ours as language interface is defined on top of language's abstract syntax even if author didn't give a precise design for interface specification.

In [36] Marco Di Natal et al. use a mapping language to integrate a functional language and a platform language. For that, a set of connectors are used to specify the mapping between the two languages. Once the mapping model is elaborated, communication code between functional model and platform model is generated. We can say that there are some similarities between this proposition and ours. Connectors and mapping model play respectively the same role of interface and coordination model in our proposition.

Finally, in [37] authors define composition interface for model fragments as a set of ports representing reference and variation points of a language. Reference points are root nodes for model fragments, where variation points are nodes that may be replaced during composition. Ports have unique names and map to one or more elements of the fragment. This work is interesting as we can consider model fragments as separate models that authors coordinate using ports.

7. Conclusion and Future Works

The use of divers DSMLs for modeling a same complex system becomes a common practice. Indeed, systems are more and more complex inciting experts to use their own specific modeling languages.

Albeit, while many language workbenches exist and allow an easy creation of DSMLs, the coordination and integration between them is not proposed or poorly provided.

Subsequently, many recent researches discussed this issue. In the same line, this paper introduces an approach based on both composition and interface concepts to coordinate heterogeneous DSMLs.

Actually, a detailed process composed by two main steps has been proposed. The first step consists in composing involved DSMLs and adds an interface layer to them. This layer is defined according to Bridge Pattern Design.

The proposed approach has been applied to a connected Indoor Transport Service system. The former involves two heterogeneous DSMLs.

For our future works, we plan to explore more relevant cases involving various coordination relationships. Hence, further case studies will help us to improve our coordination process. We also plan to provide a wizard enabling the use of proposed approach and assisting integrators to achieve coordination.

Conflict of Interest

The authors declare no conflict of interest.

Acknowledgment

Acknowledge your institute/ funder.

References

[1] M. Fowler, R. Parsons, Domain Specific Languages, Addison-Wesley Professional, 2010.

[2] C. Hardebolle, "Composition de modèles pour la modélisation multi-paradigme du comportement des systems," Ph.D Thesis, Université Paris-Sud XI Orsay, 2008.

[3] D. Simon-Zayas, "A framework for the management of heterogeneous models in Systems Engineering," Ph.D Thesis, Ecole Nationale Supérieure de Mécanique et d'Aérotechnique, 2012.

[4] M. El hamlaoui, "Mise en correspondance et gestion de la cohérence de modèles hétérogènes évolutifs," Ph.D Thesis, Université Toulouse-Jean-Jaurès, 2015.

[5] M. Chechik, S.Nejati, M.Sabetzadeh, "A Relationship-Based Approach to Model Integration" *Innovations in Systems and Software Engineering*, 8(1), 3-18, 2012. <https://doi.org/10.1007/s11334-011-0155-2>

[6] B. Combemale, J. Deantoni, B. Baudry, J. Jézéquel and J. Gray, "Globalizing Modelling Languages" *Computer* 47.6:68-71, 2014. <https://doi.org/10.1109/MC.2014.147>

[7] J. Deantoni, C. Brun, B. Caillaud, R.B. France, G. Karsai, O. Nierstrasz and E. Syriani, "Domain globalization: using languages to support technical and social coordination", *Globalizing Domain-Specific Languages* (pp. 70-87). Springer, Cham, 2015. https://doi.org/10.1007/978-3-319-26172-0_5

[8] S. Živković and D. Karagiannis, "Towards metamodelling-in-the-large: Interface-Based composition for modular metamodel development" in *Enterprise, Business-Process and Information Systems Modeling*. Springer, Cham, 2015. https://doi.org/10.1007/978-3-319-19237-6_26

[9] M.E.V Larsen, J. Deantoni, B. Combemale and F. Mallet, "A Behavioral Coordination Operator Language (BCOol)" in *Model Driven Engineering Languages and Systems (MODELS)*, ACM/IEEE 18th International Conference, 2015. <https://doi.org/10.1109/MODELS.2015.7338249>

[10] A. Klepee, *Software language engineering*, Addison-Wesley Professional, 2008.

[11] T. Degueule, "Towards Language Interfaces for DSLs Integration", 2015. <https://hal.inria.fr/hal-01138017>

[12] D. Strüber, G. Taentzer, S. Jurack & T. Schäfer. "Towards a distributed modeling process based on composite models" in *International Conference on Fundamental Approaches to Software Engineering*. Springer, Berlin, Heidelberg, 2013. https://doi.org/10.1007/978-3-642-37057-1_2

[13] D. Strüber, S. Jurack, T. Schäfer, S. Schulz & G. Taentzer. "Managing Model and Meta-Model Components with Export and Import Interfaces." in *Big-MDE Workshop on Scalability in Model Driven Engineering*. p. 31-36, 2016

[14] ITU-T Recommendation X.208, "Specification of Abstract Syntax Notation One (ASN.1)", 1988.

[15] ITU-T Recommendation X.209, "Specification of Basic Encoding Rules for Abstract Syntax Notation One (ASN.1)", 1988.

[16] M.Bjorklund, "YANG a data modeling language for the network configuration protocol (NETCONF)" (No. RFC 6020), 2010.

[17] M. Bjorklund, "The YANG 1.1 Data Modeling Language (No. RFC 7950)", 2016.

[18] ISO/IEC, "Standard EBNF Syntax Specification". Ebnf: Iso/iec 14977, 1996 (e). URL <http://www.cl.cam.ac.uk/mgk25/iso-14977.pdf>, 1996, vol. 70.

[19] J. Paakki. Attribute grammar paradigms—a high-level methodology in language implementation. *ACM Computing Surveys (CSUR)*, vol. 27, no 2, p. 196-255, 1995.

[20] G. Rozenberg. "Handbook of Graph Grammars and Comp", World scientific, 1997.

[21] L. Fuentes-Fernández & A. Vallecillo-Moreno, "An introduction to UML profiles". *UML and Model Engineering*, vol. 2, p. 6-13, 2004.

[22] T. Kühne, "Matters of (meta-) modeling". *Software & Systems Modeling*, vol. 5, no 4, p. 369-385, 2006. <https://doi.org/10.1007/s10270-006-0017-9>

[23] T. Clark, P. Sammut and J. Willans, *Applied metamodeling: a foundation for language driven development*, Middlesex University Research Repository, 2008.

[24] K. Chen, J. Sztipanovits and S. Neema, "Toward a semantic anchoring infrastructure for domain-specific modeling languages" in the 5th ACM international conference on Embedded software (pp. 35-43). 2005. <https://doi.org/10.1145/1086228.1086236>

[25] M. Klein, "Combining and relating ontologies: an analysis of problems and solutions". in *Workshop on Ontologies and Information Sharing, IJCAI, 2001*

[26] J. P. Tolvanen, R. Pohjonen & S.Kelly. "Advanced tooling for domain-specific modeling: MetaEdit+ " in the 7th OOPSLA Workshop on Domain-Specific Modeling, Finland, 2007. ISBN: 978-951-39-2915-2

[27] R. Heim, P.M.S Nazari, J.O. Ringert, B. Rumpe and A. Wortmann, "Modeling robot and world interfaces for reusable tasks" in *IEEE Intelligent Robots and Systems (IROS)*, IEEE/RSJ International Conference on (pp. 1793-1798), 2015. <https://doi.org/10.1109/IROS.2015.7353610>

[28] E. Juliot and J. Benois, *Viewpoints creation using oboe designer or how to build eclipse dsm without being an expert developer?*, Oboe, Tech. Rep., oboe designer whitepaper, 2010. <http://www.oboe.fr>

[29] Graphical Editing Framework (GEF), <http://www.eclipse.org/gef/>.

[30] Eclipse Community Forums: GMF (Graphical Modeling Framework): <http://www.eclipse.org/forums/eclipse.modeling.gmf>.

[31] K. Hölldobler, A. Roth, B. Rumpe and A. Wortmann, "Advances in modeling Language engineering" in *Proc of International Conference on Model and Data Engineering* (pp. 3-17), Springer, 2017. https://doi.org/10.1007/978-3-319-66854-3_1

[32] T. Degueule, "Composition and interoperability for external domain-specific language engineering", Ph.D Thesis, Rennes 1, 2016.

[33] T. Clark, M. Van den Brand, B. Combemale and B. Rumpe, "Conceptual model of the globalization for domain-specific languages" in *Globalizing Domain-Specific Languages*(pp.7-20). Springer, Cham, 2015. https://doi.org/10.1007/978-3-319-26172-0_2

[34] E. Gamma, R. Helm, R. Johnson, J. Vlissides, *Design patterns: Elements of Reusable Object-Oriented Software*, Pearson Education India ,1995.

[35] J. Steel, J.M Jézéquel, "On model typing" *Software & Systems Modeling* 6(4), 401-413, 2007. <https://doi.org/10.1007/s10270-006-0036-6>

[36] M. Di Natale, F. Chirico, A. Sindico and A. Sangiovanni- Vincentelli, "An MDA approach for the generation of communication adapters integrating SW and FW components from Simulink" in *International Conference on Model Driven Engineering Languages and Systems* (pp. 353-369), Springer, Cham, 2014. https://doi.org/10.1007/978-3-319-11653-2_22

[37] J. Johannes, R. Samlaus and M. Seifert, "Round-trip support for invasive software composition systems" in *July 2009 Springer, Berlin, Heidelberg, International Conference on Software Composition* (pp. 90-106), 2009. https://doi.org/10.1007/978-3-642-02655-3_8

Simulation and Reproduction of a Manipulator According to Classical Arm Representation and Trajectory Planning

Ahmad Yusairi Bani Hashim^{*1}, Silah Hayati Kamsani¹, Mahasan Mat Ali¹, Syamimi Shamsuddin¹, Ahmad Zaki Shukor²

¹Faculty of Manufacturing Engineering, Universiti Teknikal Malaysia Melaka, 76100, Malaysia

²Faculty of Electrical Engineering, Universiti Teknikal Malaysia Melaka, 76100, Malaysia

ARTICLE INFO

Article history:

Received: 16 July, 2019

Accepted: 13 October, 2019

Online: 25 November, 2019

Keywords:

Robot manipulator

Denevit-Hartenberg representation

Forward kinematics

Inverse kinematics

Trajectory planning

Technical and vocational education

Fused deposition modeling

ABSTRACT

The technical and vocational institutions are the key feeders for skilled human capital in the robotic revolution economy. It is essential to engage the students by creating new, affordable robotics at a fraction of the cost. This study presents the design and simulation of a six-axis robot manipulator specifically made for education and training. The robot was developed based on Chriss-Annin's configuration. The robot arm was printed using Fused Deposition Modelling technique using the acrylonitrile butadiene styrene filament. Before it was constructed, the arm parameters were assessed using Scilab as the tool and the traditional and fundamental methods: the Denevit-Hartenberg representation, the forward kinematics, the inverse kinematics, and the trajectory planning. The outcomes showed that the arm was working well on positioning and path planning. Therefore, the complete assembly of the robot should be able to assume a role in education and training. This work is an extension of the paper entitled "Lightweight Robot Manipulator for TVET Training using FDM Technique" published in 2018 Symposium on Electrical, Mechatronics and Applied Science 2018 (SEMA 2018).

1. Introduction

The world is embracing the Fourth Industrial Revolution (IR4.0), driven by nine pillars of technological advancement. They are; Autonomous Robot, Simulation, Horizontal and Vertical System Integration, The Industrial Internet of Things, Cybersecurity, The Cloud Computing, Additive Manufacturing, Augmented Reality, and Big Data and Analytics [1]. As one of the critical elements in IR4.0, robots have been widely used in various areas such as manufacturing, agriculture, retail, and services [2]. To date, there are 1.1 million working robots, and machines worldwide and 80% of the work in the manufacturing of a car is done by machines [3].

In Malaysia, technical and skill oriented educational institutions are one of the critical feeders for skilled and knowledgeable human capital in the area of robotics. The country has realized the importance of technical and vocational education and training (TVET) in spearheading the country's excellence in

economic and technological development [4]. Thus, it is essential to engage students in this field further by creating new, affordable robotics platforms through which they can involve themselves in current technologies at a fraction of the cost.

Most industrial robotics producers such as ABB, KUKA, MOTOMAN, and FANUC do provide robotic educational packages based on their smallest robot available. Nonetheless, due to their rigid structure, strict safety measures need to adhere to [5]. This will incur additional costs to the institution. Therefore, a small-scaled six-axis robot is seen as suitable for use in an educational setting. The robot system requires less damage and is safer when in contact with a human because it will generate less momentum when in motion compared to the metal structure.

One of the available techniques to construct a mechanical structure of a robotic arm manipulator is by using Fused Deposition Modelling (FDM). With this method, a polymer-based filament such as acrylonitrile butadiene styrene (ABS), Polylactic acid (PLA) or nylon is extruded in semi-liquid form through a heating process and deposited layer by layer until a 3D object is formed. It provides a trade-off between strength and cost. This is

* Ahmad Yusairi Bani Hashim, Faculty of Manufacturing Engineering, Universiti Teknikal Malaysia Melaka, 76100, Malaysia, +6062702665 & yusairi@utem.edu.my

vital in a lightweight robot configuration. Its ease of use and fast time from design to manufacturing also makes FDM printers prevalent in small manufacturing enterprises, design offices, and private residential [6, 7].

This study aims to design and develop a six-axis robot manipulator using FDM for educational purpose typically for TVET schools. This robot is small and compact compared to its vast industrial counterparts. Besides training, this robot can also be advertised to small and medium businesses who seek to increase their productivity through automation.

2. Methods

The methodology begins with studying existing designs of robot manipulators with the same payload and using open-access assembly drawing of a desktop-size robot by Chris-Annin [8], which is known as the AR2. Using SolidWorks 2018, a model was redrawn. This process considers the actuator sizing, the mechanism such as the belts, the gears, and the type of material for printing.

The tooth-belt transmission mechanism was selected for joint-1 to joint-5 because it is simple to integrate into CAD design. Joint 6 has the tool with a direct connection to the actuator. The drawings were fed to the FDM machine to produce the mechanical structure. All the joints apply the stepper motor with an encoder as the actuator. The controls would employ step input, and the encoder functions for feedback. The ABS was selected as it is a rigid material for a sturdy structure to mount the stepper motors. ABS is cost effective as compared to nylon and carbon fiber.

2.1. Classical Denevit-Hartenberg Representation

Before production, the CAD design requires parameter validation. As a start, the arm parameters have to be defined and later analyzed according to the standard Denevit-Hartenberg (stdDH) convention. Table 1 list the proposed AR2 arm parameter [9]. Each of the parameters determines the arm configuration and its outlook. Therefore, solid modeling using CAD is possible.

Table 1: The arm parameter for AR2. The *d* and the *α* parameters govern the arm's size.

Joint №	θ	α	<i>d</i> (mm)	<i>a</i> (mm)
1	θ_1	-90	169.77	64.20
2	θ_2	0°	0	30.50
3	θ_3	90°	0	0
4	θ_4	-90°	-222.63	0
5	θ_5	90°	0	0
6	θ_6	0°	-36.25	0

The kinematic chain seen in Figure 2 is built conforming with the stdDH. The orientation of the joint frame is significant because it allows the designer to decide how to assemble the actuator. It is usually that the actuator is attached along the z-axis. Using the tools found in the Robotic Toolbox module, the information is realized in the form seen in Figure 1.

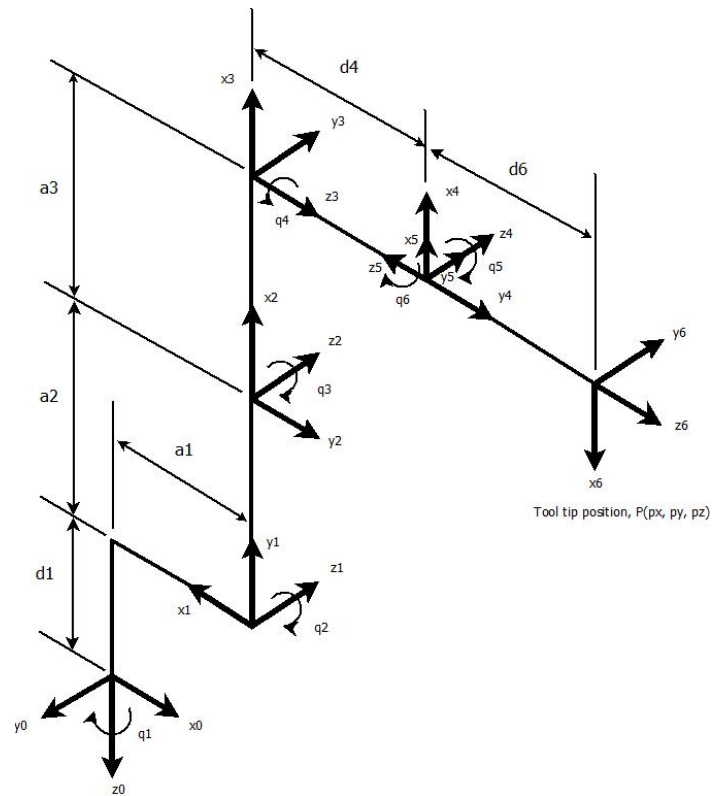


Figure 1: The kinematic chain that represents AR2. The configuration is unique. A correct configuration provides the descriptions that permit the designer to test for arm position and motion. If the setting is wrong, then the results from the analysis will be incorrect. By itself, the developed robot will not function as desired.

```
AR2 (6 axis, RRRRRR, stdDH)
-----+-----+-----+-----+-----+-----+
| J | alpha | a | theta | d |
-----+-----+-----+-----+-----+
| 1 | -1.5708 | 64.2000 | q1 | 169.7700 |
| 2 | 0.0000 | 305.0000 | q2 | 0.0000 |
| 3 | 1.5708 | 0.0000 | q3 | 0.0000 |
| 4 | -1.5708 | 0.0000 | q4 | -222.6300 |
| 5 | 1.5708 | 0.0000 | q5 | 0.0000 |
| 6 | 0.0000 | 0.0000 | q6 | -36.2500 |
-----+-----+-----+-----+-----+

grav = | 0.00 | base = | 1.00 0.00 0.00 0.00 | tool = | 1.00 0.00 0.00 0.00 |
        | 0.00 |         | 0.00 1.00 0.00 0.00 |         | 0.00 1.00 0.00 0.00 |
        | 9.81 |         | 0.00 0.00 1.00 0.00 |         | 0.00 0.00 1.00 0.00 |
        |         |         | 0.00 0.00 0.00 1.00 |         | 0.00 0.00 0.00 1.00 |
```

Figure 2: The simulated arm parameter runs onto Scilab. The outcome is the reproduction of the arm parameter seen in Table 1. Having the arm parameter configured correctly, the tools in Scilab let the robot to be evaluated with convincing results. The '6-axis' means that the robot has six joint where an actuator drives each joint, the 'RRRRRR' represent a revolute type of all the joint, the 'stdDH' depicts that the robot is specified according to the standard Denevit-Hartenberg convention.

2.2. Forward and Inverse Kinematics

Given the pose, and by analyzing the mechanisms, the relationship between the locations concerning the base, the serial chain can be derived. The device is dependent on the method of actuation typically for the forward kinematics problems where the tool pose can be found when the values of the joint variables of the actuated joints are given [10]. It is known that the inverse kinematics for the chain can have non-unique solutions, and so does the inverse kinematics.

The definition of the forward kinematic is given in (1) [11]. The vector in the last column except the last cell represents the tooltip position. In Figure 1, the said position is charted in frame 6. The remaining columns, up to row 3 define the tool orientation. If the joint angles are stated, then (1) can be evaluated. The results will be the tool's pose and orientation.

$${}^0_6T = \begin{pmatrix} n_x & s_x & a_x & p_x \\ n_y & s_y & a_y & p_y \\ n_z & s_z & a_z & p_z \\ 0 & 0 & 0 & 1 \end{pmatrix} \quad (1)$$

So, to test for the robot's plot, the joint angles need to be defined. Suppose the arm is positioned to vertical upright, the joint angle vector is then $[-90^\circ \ -90^\circ \ -90^\circ \ -90^\circ \ -90^\circ]^T$. Figure 3 shows the arm's position realized through Scilab. At this juncture, the forward kinematics is defined in (2) that has the tool tip position vector as $[-36.25 \ -64.20 \ 697.40]^T$.

$${}^0_6T = \begin{pmatrix} 6.12 \times 10^{-17} & 6.12 \times 10^{-17} & 1.00 & -36.25 \\ -1.00 & 1.23 \times 10^{-16} & 6.12 \times 10^{-17} & -64.20 \\ -1.23 \times 10^{-6} & -1.00 & 6.12 \times 10^{-17} & 697.40 \\ 0 & 0 & 0 & 1 \end{pmatrix} \quad (2)$$

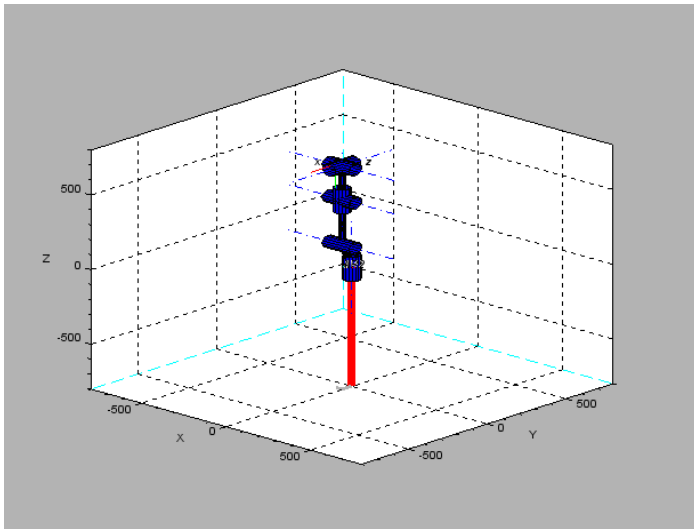


Figure 3: The arm is programmed to raise vertical upright. At this posture, the arm is assumed in the home position.

The inverse kinematics, however, does not define in a straightforward manner as the forward kinematics. A complicated derivation involves in determining each joint position. The general idea behind inverse kinematics is that given the desired tool position, the resulting joint angles may be obtained. Suppose the desired position vector is $[-36.25 \ -64.20 \ 697.40]^T$. Then the respective joint angle may be computed using the available tools in the Robotic Toolbox. The inverse kinematics results the required joint angles as $[-90^\circ \ -90^\circ \ -90^\circ \ -90^\circ \ -90^\circ]^T$, which exactly computed as the direct kinematics' inputs.

2.3. Trajectory Planning

The joint space trajectory is based on quintic polynomial with zero boundary condition for velocity and acceleration. The path of

each joint has to be planned so that the tooltip position reach a coordinate. For a quintic polynomial, (3a-3c) define the position trajectory, velocity trajectory, and the acceleration trajectory, respectively.

$$\theta_i(t) = a_{i0} + a_{i1}t + a_{i2}t^2 + a_{i3}t^3 + a_{i4}t^4 + a_{i5}t^5 \quad (3a)$$

$$\dot{\theta}_i(t) = a_{i1} + 2a_{i2}t + 3a_{i3}t^2 + 4a_{i4}t^3 + 5a_{i5}t^4 \quad (3b)$$

$$\ddot{\theta}_i(t) = 2a_{i2} + 6a_{i3}t + 12a_{i4}t^2 + 20a_{i5}t^3 \quad (3c)$$

In (3a-3c), the constant parameter a_i is not defined because the automatic derivation is made in the Scilab environment. Every incident of the joint trajectory is unique. It is, therefore, the value for the constant a_i dependent upon the incident of the joint trajectory as a function of the desired Δt . Because there are six joints, the index $i = 1, 2, \dots, 6$. At most, there are six functions for the position trajectory. Similarly, the velocity trajectory and the acceleration will each has six functions, tops. In total, there should be eighteen plottable functions as long as there is a position change for a joint.

3. Results

3.1. Assessment of Kinematics Solutions

Evaluation for the inverse kinematics solutions was done by assuming some desired positions. The answers were then compared with the inputs fed to the homogeneous transformation matrix defined in (1). Setting the Robotic Toolbox's *ikine* (inverse kinematics) function with *pinv* (pseudo-inverse), the inverse kinematic solutions are shown in Table 2, especially columns three and four. The respective joint positions were obtained using the desired positions mentioned in the preceding. For the computational purpose, seen in column three, the initial positions were adjusted very close to the earlier forward kinematics' joint angles.

Table 2: Evaluation of inverse kinematics solutions. Scilab's *ikine* function was used because the arm's wrist is not spherical. The answers were copied from Scilab's console. The 'D' notation is the power of ten.

Forw. kinem. inputs (θ_{fk})	Position Vector [P]	Initial joint angles (θ_0)	Inv. kinem. solutions (θ_{ik})	% error
-1.5707963		-1.4707963	-1.5707963	0.0000001
-1.5707963	-36.250000	-1.4707963	-1.5707963	0.0000005
-1.5707963	-64.200000	-1.4707963	-1.5707963	-0.0000012
-1.5707963	697.40000	-1.4707963	-1.5707963	6.542D-08
-1.5707963		-1.4707963	-1.5707963	-0.0000002
-1.5707963		-1.4707963	-1.5707963	0.0000007
-1.0471976		-0.9471976	-1.0471976	9.235D-09
-0.7853982		-0.6853982	-0.7853982	5.057D-08
-0.6283185	280.26218	-0.5283185	-0.6283185	-8.476D-08
-0.5235988	-466.5156	-0.4235988	-0.5235988	-8.089D-08
-0.4487990	358.95479	-0.3487990	-0.4487990	0.0000001
-0.3926990		-0.2926991	-0.3926991	0.0000001
-0.7853982		-0.6853982	-0.7853982	-7.513D-09
-0.6283185	384.6609	-0.5283185	-0.6283185	3.196D-08
-0.5235988	-393.17299	-0.4235988	-0.5235988	-0.0000001
-0.4487990	256.28879	-0.3487990	-0.4487990	-0.0000004
-0.3926991		-0.2926991	-0.3926991	7.452D-08
-0.3490659		-0.2490659	-0.3490658	0.0000004

The first column represents the forward kinematics solutions that yielded the position vectors. Based on the position vectors, the *ikine* function was executed. In the last column, it was obvious that the percent errors when compared between the forward kinematics

inputs and the inverse kinematics solutions were minimal. The overall solutions looked convincing. Therefore, the stdDH model applied was valid.

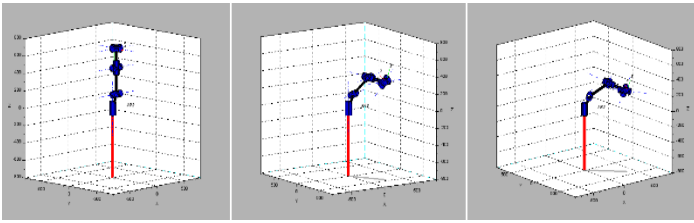


Figure 4: The arm's poses and positions. From left, the start pose and position. The stopover pose and position and lastly, the final pose and position. The snapshots when combined, would reveal a planned trajectory. They were three tool tip's positions that a straight line path was made possible.

The arm was made to move in the joint space trajectory. The respective joint positions would be determined according to the desired tool tip's position. A tool tip's path in the Cartesian space was planned that three positions were defined to complete the track. The position vectors in Table 2 were used as the coordinate of the point in the Cartesian space that the desired positions were $P_1(-36.25, -64.20, 697.40)$, $P_2(280.26, -466.52, 358.95)$, and $P_3(384.66, -393.17, 25.29)$ to achieve a straight line path. The first was the start position, the second was the stopover position, and the last was the final position where Figure 4 describes the incident.

3.2. Assessment of the Trajectory Planning

For the tooltip position that initiated from the start to the second point within five seconds, the results for the joint trajectories are shown in Figure 5. From the left is the position trajectories for all the joints. It follows for the velocity trajectories, and the acceleration trajectories, respectively.

Joint-6 represents the maximum velocity at about 2.5 seconds, the maximum acceleration at about one second and the minimum at about 4.0 seconds. Joint-1, however, makes the least positions, velocities, and accelerations. Similarly, Figure 6 exhibits the motion trajectories within 2.5 seconds, which is a one-half time range from the previous. The results show comparable patterns from the former. With less position change, the velocities and the accelerations were doubled.

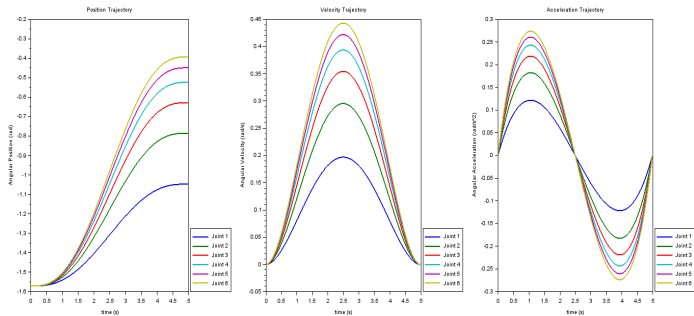


Figure 5: The joint trajectories for joint 1 to joint 6 that the tooltip moves from P_1 to P_2 . The curves were plotted because all joints experienced a position change. For the position trajectory, (3a) is the function where the time range was set for 5 seconds. The velocity trajectory was the derivative of the position trajectory, (3b) is the function. Similarly, the acceleration was the derivative of the velocity trajectory, (3c) is the function.

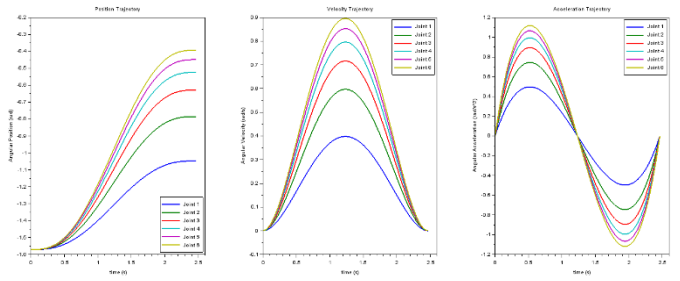


Figure 6: The joint trajectories for joint 1 to joint 6 that the tooltip moves from P_1 to P_2 . The time range was set for 2.5 seconds.

For the tooltip position that moved from the second point to the final point within five seconds, the results for the joint trajectories are shown in Figure 7. From the left is the position trajectories for all the joints. It follows for the velocity trajectories, and the acceleration trajectories, respectively. Joint-6 represents the least velocities, accelerations but the most for the position trajectories. In contrary, joint-1 made the least position trajectories but the most for the velocities and accelerations. The results show comparable patterns from the previous. With fewer position change, the velocities and the accelerations were amplified.

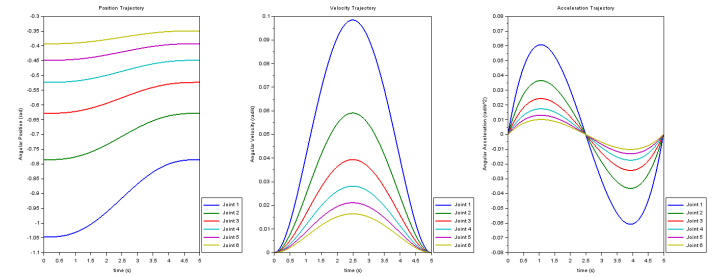


Figure 7: The joint trajectories for joint 1 to joint 6 that the tooltip moves from P_2 to P_3 . The time range was set at 5 seconds.

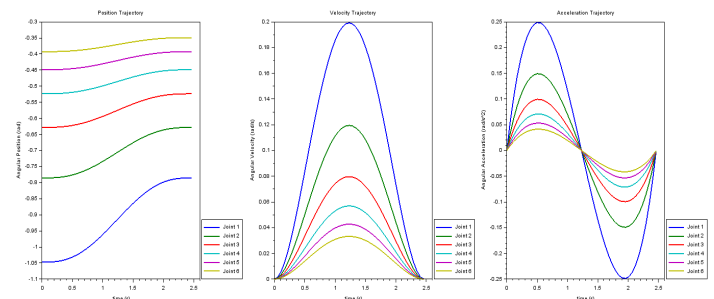


Figure 8: The joint trajectories for joint 1 to joint 6 that the tooltip moves from P_2 to P_3 . The time range was set at 2.5 seconds.

3.3. Fabrication of the Arm Structure

Figure 9 shows the constructed robot structure. It was produced using ABS filament. Due to the ABS material color, some of the parts are red, while others are white. From computation, it was estimated that the weight of the arm structure alone is 5.5 kg. With the stepper motors weight, the total weight of the manipulator is about 8.4 kg.

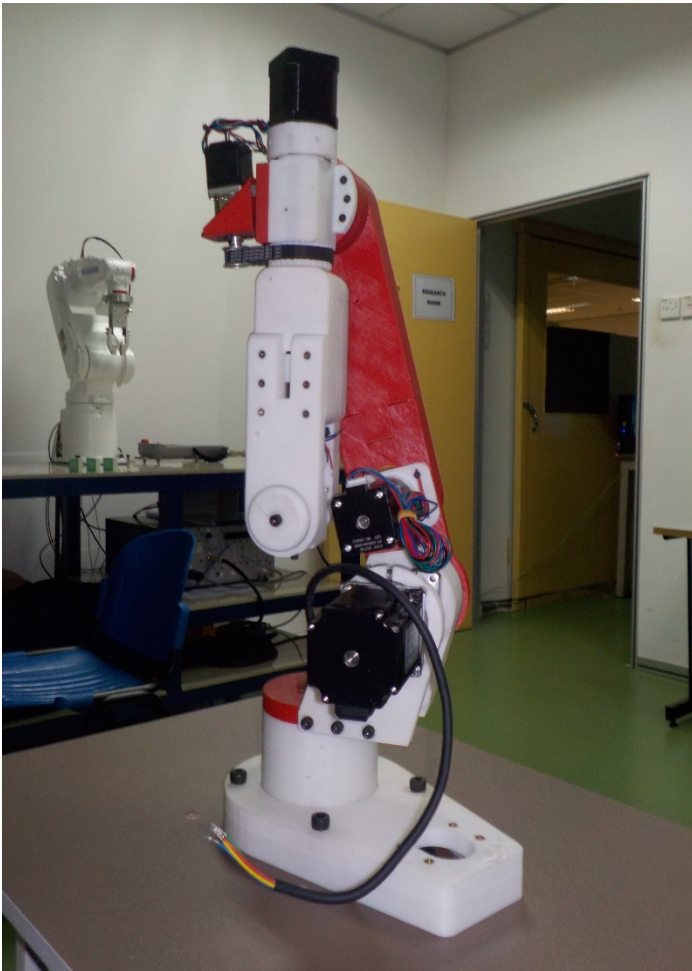


Figure 9: The fabricated manipulator is on the foreground. The project is on progress where at this stage, the controller module has not been assembled. As such, there are loose wires and connectors seen on the structure.

4. Conclusions

This paper shows the preliminary design works of a six-axis robotic arm for TVET education purposes. The arm should be capable of lifting load not more than one kilogram. The overall weight of the arm was acceptable for a training type robot and is comparable to others in the market. Before it was constructed, the arm parameters were assessed using Scilab as the tool and the traditional and fundamental methods: the Denevit-Hartenberg representation, the forward kinematics, the inverse kinematics, and the trajectory planning. The outcomes showed that the arm was working well on positioning and path planning. Therefore, the complete assembly of the robot should be able to assume a role in education and training.

Conflict of Interest

The authors declare no conflict of interest.

Acknowledgment

The authors would like to thank Universiti Teknikal Malaysia Melaka for financial support through PJP/2018/FKP (10C)/S01636 research grant, Nick Mathews A. Samuel for the arm fabrication and assembly.

References

- [1] M. Rübmann, M. Lorenz, P. Gerbert, M. Waldner, J. Justus, P. Engel, et al., "Industry 4.0: The future of productivity and growth in manufacturing industries," Boston Consulting Group, vol. 9, 2015.
- [2] K. Schwab, *The fourth industrial revolution*: Crown Business, 2017.
- [3] W. Knight, "This robot could transform manufacturing," MIT Technology Review, 2012.
- [4] M. Sandhya, "TVET to meet industry needs," in *The Star*, ed, 2017.
- [5] V. Gopinath, F. Ore, S. Grahn, and K. Johansen, "Safety-Focussed Design of Collaborative Assembly Station with Large Industrial Robots," *Procedia Manufacturing*, vol. 25, pp. 503-510, 2018. <https://doi.org/10.1016/j.promfg.2018.06.124>.
- [6] Q. Zhang, G. Sharma, J. P. Wong, A. Y. Davis, M. S. Black, P. Biswas, et al., "Investigating particle emissions and aerosol dynamics from a consumer fused deposition modeling 3D printer with a lognormal moment aerosol model," *Aerosol Science and Technology*, pp. 1-13, 2018. <https://doi.org/10.1080/02786826.2018.1464115>.
- [7] D. Owen, J. Hickey, A. Cusson, O. I. Ayeni, J. Rhoades, Y. Deng, et al., "3D printing of ceramic components using a customized 3D ceramic printer," *Progress in Additive Manufacturing*, pp. 1-7, 2018. <https://doi.org/10.1007/s40964-018-0037-3>.
- [8] Chriss-Annin. (2018). AR2. Available: <https://github.com/chris-annin/ar2>.
- [9] P. I. Corke, "A simple and systematic approach to assigning Denavit-Hartenberg parameters," *IEEE transactions on robotics*, vol. 23, pp. 590-594, 2007.
- [10] R. C. Gonzalez and R. E. Woods, *Digital Image Processing 2nd ed*. Upper Saddle River, New York: Prentice Hall Press, 2002.
- [11] J. J. Craig, *Introduction to robotics: mechanics and control vol. 3*: Pearson/Prentice Hall Upper Saddle River, NJ, USA., 2005.

Evaluation of Classroom Furniture Design for Ecuadorian University Students: An Anthropometry-Based Approach

Pablo Pérez-Gosende^{1,2,*}

¹Grupo de Investigación Interdisciplinar en Matemática Aplicada (GIIMA), Universidad Politécnica Salesiana, 090109, Ecuador

²Centro de Investigación en Gestión e Ingeniería de Producción (CIGIP), Universitat Politècnica de València, Alcoy, 03801, Spain

ARTICLE INFO

Article history:

Received: 07 August, 2019

Accepted: 22 October, 2019

Online: 25 November, 2019

Keywords:

Anthropometry

Ergonomic design

Design evaluation

Musculoskeletal disorders

Classroom furniture

ABSTRACT

It is widely known that students' exposure to poor postures due to inappropriate classroom furniture design may contribute to the increase of the prevalence of musculoskeletal disorders symptoms that if not identified on time could lead to severe health issues. In this context, due to the unavailability of scientific studies related to this topic in Ecuador, the aim of this research is twofold. The first aim was to define the classroom furniture design parameters' dimensions for university students according to relevant anthropometric information. The second aim is to conduct a preliminary diagnostic of the appropriateness of classroom furniture currently used in Ecuadorian universities to students' anthropometric characteristics. The obtained results are particularly relevant as the ten design parameters here proposed could be the starting point to the creation of a specific Ecuadorian standard to regulate classroom furniture design for university students. That would ensure domestic and foreign manufacturers could offer furniture more secure and adequate to the anthropometric characteristics of the university population of Ecuador. On the other hand, the preliminary study found evidence that all the examined classroom furniture presented mismatches in at least five design parameters, and students exposed to them over the past twelve months had a high prevalence of symptoms of musculoskeletal disorders in the hips, back, thighs, and neck.

1. Introduction

Anthropometry is the sub-branch of physical anthropology that studies the measurements of the human body in terms of the dimensions of bone, muscle and adipose tissue [1]. These measurements are vital for proper workstations design to prevent musculoskeletal disorders in the workforce [2,3] and at the same time, to facilitate the performance of labor activities with higher productivity [4,5].

Consideration of anthropometric information in classroom furniture design allows students to acquire higher levels of comfort [6], to reduce the presence of musculoskeletal disorders [7–11] and to facilitate the understanding of the knowledge imparted [12,14].

From the ergonomic point of view, three principles of design are known for the application of anthropometric information: the design for the average individual, for extreme individuals, and for an adjustable interval [15]. The latter has been the most suggested

by researchers in the design of school furniture [16–18], however, it is the least feasible from an economic point of view. From a technical perspective, the first one mentioned is the least recommended design principle as it guarantees comfort only for 50% of the population.

In general, the design principle for extreme individuals has been the most used in classroom furniture design [17]. It is based mainly on the idea that if the most relevant dimension of the design is suitable for extreme cases (5th or 95th percentile of the corresponding anthropometric measure), then it will guarantee comfort to the majority of the population.

Under this last principle of design, numerous international studies have identified discrepancies between the dimensions of classroom furniture and the anthropometric measures of its target audience: students of basic education [17,19–21], upper secondary education (between 15 and 18 years) [22, 23]; and university students (between 18 and 30 years) [24].

The few Ecuadorian studies that analyze ergonomic or anthropometric principles for school furniture design, do so for

*Corresponding Author: Pablo Pérez-Gosende, pperezg@ups.edu.ec

boys and girls in preschool education [25] or students at the levels of Basic Education [26]. In the latter case, work for children with motor impairment [27,28] stands out. In national scientific literature, studies that address this subject for university students are even scarcer.

The use of inappropriate classroom furniture is one of the causes that favor students in adopting poor postures while performing intraclass academic activities [14–16]. Some studies have concluded that when these postures are sustained over a long period of time, it is considered a risk factor in the development of musculoskeletal disorders [7,22,23].

Musculoskeletal disorders comprise a wide variety of degenerative and inflammatory diseases in the locomotor apparatus [29]. They are characterized by concomitant and non-concomitant symptoms that comprise pain caused by inflammation, paresthesia, strength loss, fatigue, and difficulty or incapacity to perform certain movements [30,31]. This group of injuries occurs more frequently in works that require important physical activity, weight carrying, repetitive movements, application of forces and as a consequence of bad postures sustained over long periods of time [32].

In order to detect the prevalence of musculoskeletal disorders symptoms (MDS), the Nordic Musculoskeletal Questionnaire (NMQ) designed and validated by Kuorinka [33], has been an instrument of extended use in the context of ergonomic or occupational health studies [29,30,32,34–36]. It allows the identification of initial symptoms, which have not yet triggered diseases or have not yet led the affected patients to consult the doctor. Consequently, its value lies in providing information that makes it possible to proactively estimate the level of risks and avoid exposure to them through corrective measures.

The unavailability of anthropometric databases in Ecuador for adults could imply that the classroom furniture currently in use by students in universities may not be in accordance with their anthropometric characteristics. According to this, their exposure to classroom furnishings for a long period of time could increase the prevalence of MDS, which could lead to serious musculoskeletal disorders and its irreversible consequences if not detected on time.

In this context, this paper aims to define standards for the design parameters of classroom furniture for university students in Ecuador, in accordance with relevant anthropometric information. Based on these standards, classroom furniture used in a sample of universities in Guayaquil is evaluated. In addition, MDS prevalence is measured in students who use such furniture in their daily academic activities and also possible risk factors are inquired.

2. Methods

For school furniture design, the anthropometric measurements considered relevant in this study are presented in Figure 1.

2.1. Anthropometric information

There are no official anthropometric databases in Ecuador. However, Lema-Barrera [37] made precise estimates of anthropometric measures selected for the 5, 50 and 95 percentiles of the adult Ecuadorian population of both sexes and self-

identified according to three ethnic origins: afro-Ecuadorians, indigenous and mestizos. This secondary information was used as the basis of calculation in this research. The mean and standard deviation values of these measures are presented in Table 1.

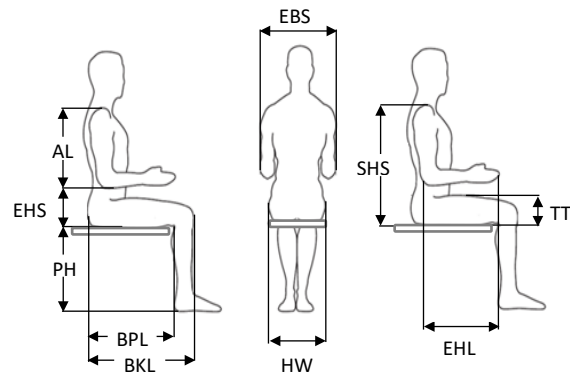


Figure 1: Relevant anthropometric dimensions for school furniture design: Arm length (AL); Elbow height sitting (EHS); Popliteal height (PH); Buttock-knee length (BKL); Buttock popliteal length (BPL); Elbow breadth sitting (EBS); Hip width (HW); Shoulder height sitting (SHS); Elbow-hand length (EHL); Thigh thickness (TT).

Table 1: Population mean and standard deviation (mm) of selected anthropometric measures for Ecuadorian men and women per ethnic group

Parameters	Mestizos		Indigenous		Afro-Ecuadorians	
	M	F	M	F	M	F
AL	363 (17.0)	347 (27.5)	371 (34.6)	330 (23.4)	390 (25.9)	341 (26.5)
EHS	232 (29.6)	235 (27.9)	220 (66.2)	231 (25.6)	209 (19.7)	225 (20.7)
PH	415 (30.4)	386 (30.2)	415 (34.5)	396 (41.6)	486 (27.9)	404 (28.5)
BKL	571 (36.0)	541 (31.6)	552 (31.7)	527 (34.2)	584 (26.8)	531 (27.3)
BPL	464 (38.6)	437 (27.4)	461 (15.6)	433 (33.7)	493 (24.8)	429 (29.5)
EBS	447 (40.6)	400 (40.3)	448 (62.8)	456 (30.7)	499 (21.4)	388 (34.6)
HW	356 (25.1)	356 (26.3)	379 (30.2)	391 (32.0)	406 (18.9)	361 (25.7)
EHL	503 (23.9)	466 (30.6)	503 (32.3)	448 (30.4)	524 (28.0)	476 (23.2)
TT	132 (19.7)	124 (17.4)	131 (20.5)	123 (19.6)	153 (12.8)	122 (09.7)

Note: Mean (standard deviation). Source: Adapted from [38].

Anthropometric measurement values of the Ecuadorian population are very heterogeneous [37]. According to this, it is important to define an approach strategy to guarantee comfort to 95% of people who could use school furniture. For this reason, this study will consider the measures of the biggest ethnic group in Ecuador. In this respect, according to the results of the 2001 and 2010 national censuses [38,39], mestizos represent the largest percentage of the population in Ecuador as shown in Figure 2.

To estimate extreme values for each relevant anthropometric measurement, the 5th percentile of the sex with the lowest

dimension and the 95th percentile of sex with the highest were taken among the mestizo population.

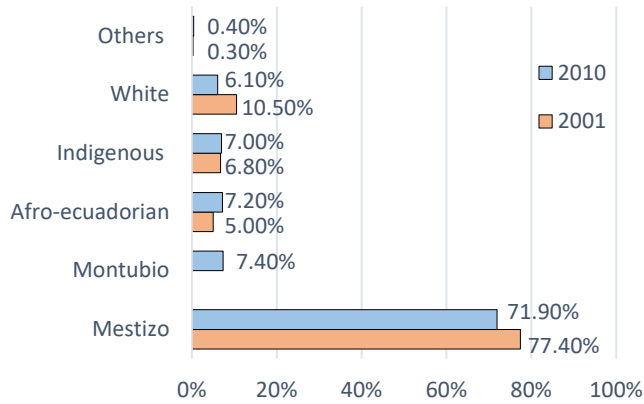


Figure 2: Ethnic self-identification in Ecuador according to 2001 and 2010 national censuses

2.2. School furniture design parameters

This section presents the mathematical formulae to estimate the design parameters of classroom furniture considering the casuistically relevant anthropometric measures and the biomechanics of the individual in a sitting position.

As an example, Figure 3 shows the design parameters of school furniture composed of a table and a chair. However, in Ecuadorian universities, it is also common to find chairs with mounted desktop.

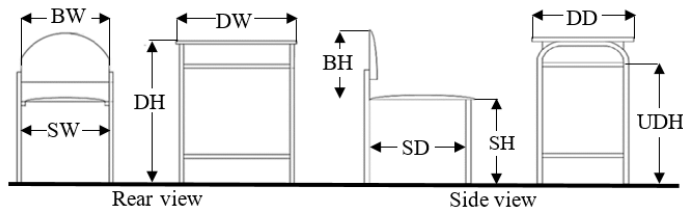


Figure 3: Representation of classroom furniture design parameters: Backrest width (BW), Seat width (SW), Seat height (SH), Backrest height (BH), Seat depth (SD), Desk height (DH), Desk width (DW), Desk depth (DD) and Under-desk height (UDH).

Traditionally seat height (SH) has been related to popliteal height (PH), which is measured from the ground to the popliteal fossa of the person sited with erected trunk [40]. The human being, when sitting, does it on the ischial tuberosities, which are bony structures that morphologically do not allow to maintain the balance of the body in this position [41]. To achieve such a balance, support is required in the back and feet. The seat height, on the other hand, must be shorter than popliteal height so that legs can lean forward between 5° and 30° regarding the vertical axis of the body [22]. These biomechanical considerations are considered in (1), where CC is a footwear correction.

$$(PH + CC) \cos 30^\circ \leq SH \leq (PH + CC) \cos 5^\circ \quad (1)$$

This equation has been widely used in research aiming to find an eventual mismatch between classroom furniture and the anthropometric characteristics of students who regularly use them

[4,11,17,19,21,22]. In this study the 5th PH percentile for mestizo women was used and a CC value equivalent to 20 mm.

According to ISO 9241-5: 1998, the seat width (SW) should be longer than the hips width (HW) of the person while seated to facilitate the adaptation of the chair to the changing needs of the individual [42]. In this regard, (2) has been regularly used in analogous researches [4,22] and implies that the appropriate seat width should vary between 10% and 30% of HW. Specifically, in this study, the 95th percentile of the hip width of mestizo women was used.

$$1,1HW \leq SW \leq 1,3HW \quad (2)$$

ISO 9241-5: 1998 establishes that the adequacy of seat depth (SD) is achieved when it is shorter than the user's popliteal-buttocks length (BPL) [42]. This relays on the idea that the popliteal fossa should be free to ease blood supply to the legs. Consequently, some researchers have agreed that the appropriate dimension for SD should lie within the interval of 80% to 95% of BPL [5,11,20-22] as shown in (3). In this study, the 5th percentile of mestizo women's BPL was employed.

$$0,80 BPL \leq SD \leq 0,95 BPL \quad (3)$$

Some authors suggest that upper backrest height (BH) should measure between 60% to 80% shoulder height (SHS) to ease mobility in the upper trunk [11,17,21,22]. The secondary anthropometric information available does not include data from this measure. However, since the SHS matches the sum of the arm length (AL) and the elbow height of the person in a seated position (EHS) according to [41], an equivalent form of calculation is presented in (4). There, EHS represents the 5th percentile of men and AL the 5th percentile of women.

$$0,6(EHS + AL) \leq BH \leq 0,8(EHS + AL) \quad (4)$$

The seatback width (BW) has not been widely discussed in the literature as noted in [17]. However, some authors have come to the agreement that for BW the width of the hips (HW) can be considered the relevant anthropometric measure [16,18]. In this regard, we decided BW be longer than the 95th percentile of HW for mestizo women, as shown in (5).

$$BW \geq HW \quad (5)$$

The under-desk height (UDH) must allow the sliding of the user seated towards the interior of the table. Thus, the ideal measurement should include seat height, seated thigh thickness (TT) and clearance (20 mm) to facilitate the change of posture of the legs in this position. These considerations are included in (6). Here, TT corresponds to the 95th percentile for men and PH to the 5th percentile for women.

$$(PH + CC) \cos 30^\circ + TT + 20 \leq UDH \leq (PH + CC) \cos 5^\circ + TT + 20 \quad (6)$$

For desk height (DH) estimation, previous research has taken into account the biomechanics of the shoulder and have

considered acceptable flexion angles from 0° to 25° and abduction angles between 0° and 20° for this joint [4,5,11,21]. Such authors have used (7). However, in the absence of SHS measurements and considering it equivalent to the sum of EHS and AL, the above expression can conveniently be converted to (8), which was used in this research to determine the match standard for DH. In this case, PH and AL correspond to the 5th percentile for women, while EHS corresponds to the 5th percentile for men.

$$EHS + [(PH + CC)\cos30^\circ] \leq DH \leq [(PH + CC)\cos5^\circ] + 0,8517EHS + 0,1483SHS \quad (7)$$

$$EHS + [(PH + CC)\cos30^\circ] \leq DH \leq [(PH + CC)\cos5^\circ] + EHS + 0,1483AL \quad (8)$$

According to [19], the design of the table depth (DD) and the table width (DW) have been sparsely discussed in the literature. Table depth is important to provide enough space for the user to change the posture of the lower part of the body. Thus, we consider that this dimension should exceed the 95th percentile of men knee-to-back length (BKL). This assumption is also true for the tablet length (TL) in chairs with mounted desktops. Consequently, the lower limit of these two design parameters will be estimated through (9).

$$DD \geq BKL \quad (9)$$

The width of the table (DW), on the other hand, should allow the users to rest their two forearms on the surface at the same time, whether they are upright or abducted in a relaxed posture. In this case, some authors have considered theoretical reference positions with a shoulder abduction angle between 0° and 20° [5,20,21]. Thus, in this study it was considered that the minimum acceptable table width should include: the length from elbow to elbow of the person while seated (EBS) corresponding to the 95th percentile of men, the distance that produces the abduction of the shoulders on the plane (equivalent to 2ALsen20°) considering the 95th percentile of AL for women and a 20 mm slack on each side as in (10).

$$DW \geq EBS + (0,684AL) + 40 \quad (10)$$

In addition to individual tables and chairs, Ecuadorian higher education institutions usually tend to purchase chairs with side-mounted desktop as classroom furniture. However, despite being so common, scarce attention has been given in the scientific literature to the ergonomics of its design [16]. All chair design parameters mentioned in this section are equivalent to those used in side-mounted desktop chairs (SH, SW, SD, BW, and BH). Similarly, the anthropometric criteria considered above for the design of the desk height (DH) and its depth (DD) correspond to those required for the design of tablet height for side-mounted desktop chairs (TH) and its length (TL), respectively. It is only necessary to specify a design criterion for tablet width (TW).

In this study, the minimum width of the tablet in chairs with side-mounted desktop should include half of EBS, plus the distance that implies the maximum acceptable abduction of the

elbow at 20° as suggested in [4,5,11,21] and 20mm of slack. However, TW should not exceed the 95th percentile of elbow-hand length (EHL, which is measured from the elbow to the tip of the middle finger in a seated position), since it would make it difficult for the student to access and leave the seat. All these considerations are presented in (11).

$$0,5EBS + (0,342AL) + 20 \leq TW \leq EHL \quad (11)$$

2.3. Data collection

Having secondary dataset on relevant anthropometric measurements of the adult population in Ecuador at hand, the sampling strategy focused on measuring, on the one hand, the main parameters of school furniture design in Guayaquil universities, and on the other hand, the prevalence of possible musculoskeletal disorders symptoms (MDS) in students who use such furniture on a daily basis.

The sample size was calculated considering an infinite population with a confidence level of 95% and a margin of error of 4%. The resulting value was 601 individuals taking into account a proportion of successes and failures of 50%. Among the 13 functional universities in Guayaquil, 5 were randomly selected. Then, in each institution, five classrooms were selected through a simple random sampling. For each identified furniture model, ten measurements were made of each of the ten design parameters considered relevant by the study authors (as shown in Figure 3). Such measurements were made with the use of a flexometer tape. The arithmetic mean was the measure of central tendency used to characterize every furniture design parameter dimension.

Next, the NMQ was used to identify MDS prevalence in students as a consequence of an eventual mismatch between the school furniture and their anthropometric characteristics. Its application was made in a self-administered way to those students who were willing to collaborate anonymously and who were not involved in work relations to any company in the last twelve months.

The questionnaire consisted of two general questions. The first one evaluated the presence of any MDS (pain, discomfort or numbness) over the last year in nine body parts (neck, shoulders, elbows, hands/wrists, upper back, lower back, hips/thighs/buttocks, knees, ankles/feet). The second question identified whether the presence of MDS within the last year would have prevented the user from doing any of their everyday domestic or entertainment activities. The questionnaire also recorded the age, height, weight, sex, ethnic self-identification, laterality, study time in Higher Education and the average number of hours per week that students spent seated.

The weight and height of the students were also measured using a Tanita UM-076 scale and a SECA 217 stadiometer, respectively. This information was used to determine the body mass index (BMI) of every polled individual. The data collection was carried out between October 2018 and April 2019.

2.4. Statistical analysis

The information collected was processed using the statistical

package IBM SPSS Statistics 22.0. The normal distribution of data for age, height, weight, study time, sitting hours per week, and students' body mass index was measured using the Kolmogorov-Smirnov test with correction of significance of Lilliefors to a significance level of $p < 0.05$. The characteristics of participants were presented as proportions or percentages in the case of categorical variables and the mean and standard deviation for normal continuous variables. MDS prevalence differences for the k identified furniture models were assessed using the chi-square test at a significance level of $p < 0.05$.

Associations between MDS prevalence and some variables suspected of being risk factors (gender, laterality, age, BMI, number of hours per week seated, years of higher education and type of furniture) were measured using the Odds Ratio (OR) with a confidence level of 95%.

3. Results

Using the formulae presented in the previous section, the compatibility ranges for the ten design parameters for university school furniture were calculated and are provided in Table 2. These ranges, theoretically assure the proper comfort to 95% of the university student population self-identified as mestizo.

Table 2: Match intervals of school furniture design parameters for university students in Ecuador

Parameter	Lower bound (mm)	Upper bound (mm)
Desk height (DH)	509	603
Under-desk height (UDH)	510	560
Desk width (DW)	822	-
Desk depth / Tablet length (DD/TL)	630	-
Seat height (SH)	326	375
Backrest height (BH)	291	388
Seat depth (SD)	313	372
Seat width (SW)	440	519
Backrest width (BW)	400	-
Tablet width (TW)	411	500

From the above, it is clear that the ideal area for the seat should be between 0.138 m^2 and 0.192 m^2 , the minimum surface area of the table should measure 0.518 m^2 and in the case of side-mounted desktop chairs, the minimum area recommended for the tablet is 0.259 m^2 .

The ten design parameters were measured in nine models of furniture that are used in five universities in the city of Guayaquil. Among these, two universities are public (identified as B and D), and the three remaining are co-financed by the Ecuadorian government (A, C and E). University A and D employ a single type of furniture composed of individual tables and chairs. These have been identified as M1 and M6 respectively. University B uses two models, a side-mounted desktop chair (M2) and an

individual table and chair station (M3). University C uses two different models of side-mounted desktop chairs (M4 and M5) and University E uses three of the same (M6, M7, and M8).

Table 3 shows the evaluation results of the nine types of furniture analyzed with respect to the computed compatibility ranges.

A second part of the study consisted of analyzing the prevalence of MDS in the student population that uses this furniture on a daily basis. For this, the NMQ was applied to a total sample of 672 students, however, only 628 questionnaires were valid, guaranteeing a real margin of error of 3.9%. The sample sizes according to the universities studied and the furniture models identified are presented in Table 4.

The majority of respondents identified themselves as mestizos (88.28%). 45.75% of the total were female and 54.25% male. 89.25% said they were right-handed and 10.75% were left-handed. The mean age was 21.45 years (SD=0.129 years). The mean height was 165.57 cm (SD=0.455 cm), the mean weight was 66.23 kg (SD=0.497 kg) and the mean BMI was 24.91 kg/cm² (SD=0.535kg/cm²). On average, these students sat in their school furniture 21.22 hours a week during the last year of school (SD=0.448 hours) and the average length of stay in Higher Education was 33.49 months (SD=0.669 months).

Table 5 shows MDS prevalence according to its anatomical classification, for the study population. As might be noted, the highest annual MDS prevalence occurred in the neck, along the entire spine (upper and lower back) and in the hips/thighs.

In general terms, between 86.28% and 91.24% of university students who used these nine furniture models on a daily basis over the last year, felt musculoskeletal discomfort in at least one place in their body. More specifically, it can be affirmed with 95% confidence that between 59.78% and 67.34% suffered some discomfort in the neck; between 53.41% and 61.19% felt such symptoms in the upper back and between 50.66% and 58.48% in the lower back. It is important to notice that the lowest MDS prevalence was located in elbows with 21.83% (95% CI: 0.186-0.251).

Problems along the spine appear to have had a greater impact on the health detriment and well-being of students. The upper back ailments prevented 34.35% of them (95% CI: 0.306-0.381) from performing their usual activities in the last year. On the other hand, those discomforts related to lower back made it impossible for 37.56% of them (95% CI: 0.338-0.414) to perform their daily non-academic activities.

In detail, Table 6 shows the annual MDS prevalence differences for the 9 samples of students according to the model of furniture used in their daily academic activities. As can be appreciated, such differences are significant ($p < 0.05$). This also shows that there is a relationship of dependence between the type of furniture and the presence of MDS in some parts of the body.

The neck-related annual MDS prevalence had a greater impact on students who used furniture model number eight (100% prevalence) and number five (88.24%), although this sort of prevalence was also relatively high for the remaining furniture models (greater than 50%) with the exception of the number nine. Particularly, those students who used furniture number five had a greater impact on their health. In fact, 48.53% of them were

Table 3: Match between school furniture and the ideal design parameters dimensions

Design parameters	A	B		C		D	E		
	M1	M2	M3	M4	M5	M6	M7	M8	M9
DH	730 ^b	660 ^b	720 ^b	660 ^b	760 ^b	721 ^b	671 ^b	721 ^b	761 ^b
UDH	590 ^b	640 ^b	670 ^b	631 ^b	731 ^b	670 ^b	650 ^b	700 ^b	740 ^b
DW	600 ^a		681 ^a			510 ^a			
DD/TL	320 ^a	450 ^a	391 ^a	300 ^a	300 ^a	360 ^a	300 ^a	350 ^a	300 ^a
SH	420 ^b	400 ^b	430 ^b	431 ^b	^b 450	430 ^b	430 ^b	430 ^b	500 ^b
BH	250 ^a	350	320	211 ^a	310	250 ^a	180 ^a	190 ^a	280 ^a
SD	420 ^b	510 ^b	430 ^b	351	350	400 ^b	390 ^b	390 ^b	440 ^b
SW	400 ^a	510	430 ^a	450	440	510	410 ^a	410 ^a	411 ^a
BW	400	510	400	431	430	430	410	410	410
TW		390 ^a		250 ^a	300 ^a		300 ^a	300 ^a	300 ^a

Note: Non-superscripted values denote the design parameters that match ideal measures, a represents low mismatch and b refers to high mismatch. Cells in blank represents the absence of the parameter in the furniture.

Table 4: Sample size

University	Furniture	Sample	Total
A	M1	137	137
B	M2	89	120
	M3	31	
C	M4	37	105
	M5	68	
D	M6	105	105
E	M7	64	161
	M8	43	
	M9	54	

Table 5: Estimation of annual MDS prevalence and proportion of students unable to perform regular activities as a consequence of this prevalence

Anatomical classification of MDS	MDS prevalence over the last year	Impediment to carry out daily activities over the last year
Neck	0.636 ± 0.038	0.291 ± 0.036
Shoulders	0.466 ± 0.039	0.199 ± 0.031
Elbows	0.218 ± 0.032	0.120 ± 0.026
Wrists/Hands	0.324 ± 0.037	0.246 ± 0.034
High back	0.573 ± 0.039	0.344 ± 0.037
Low back	0.546 ± 0.039	0.376 ± 0.038
Hips/Thighs	0.432 ± 0.039	0.302 ± 0.036
Knees	0.275 ± 0.035	0.183 ± 0.030
Ankles/Feet	0.268 ± 0.035	0.151 ± 0.028

Note: 95% confidence intervals estimation

prevented from carrying out their usual activities during the same period given the presence of neck-related MDS in the last year. Students who used furniture five also showed a high prevalence of MDS associated with the shoulders (63.24%), wrists and hands (75%), lower back (63.24%) and hips/thighs (64.71%). In addition, students exposed to furniture number eight also showed high MDS prevalence in the upper back (65.12%), lower back (67.44%), hips/thighs (66.32%) and ankles/feet (65.12%). A similar analysis can be done for each group of students according to the model of furniture used in their academic activities.

Table 7 shows the OR values and their respective 95% confidence intervals for those categories of selected variables that could be associated with MDS prevalence. When the OR value is greater than one and its confidence interval does not include the unit, then the association under study is considered statistically significant [43]. In other words, it is ruled out that the association between the analyzed variable categories and the presence of MDS in any part of the body is given by chance.

4. Discussion

In this study, 10 classroom furniture design parameters for university students were determined based on secondary anthropometric information corresponding to the mestizo adult population of Ecuador. Such ideal dimensions, expressed in compatibility ranges, could assure comfort to 95% of the university student population self-identified as mestizo since this ethnic group represents the majority of the population according to the last two population and housing censuses as shown in Figure 1.

These results are particularly relevant in the context of the few academic or scientific studies on school furniture design for Ecuadorian university students according to anthropometric principles. Actually, to the author's knowledge, there is only one study related to this subject [44]. However, in that work, the use of anthropometric measures included in DIN 33402 standards [45]

Table 6: Annual MDS prevalence and annual MDS prevalence differences among students according to furniture models

	Model	Neck	Shoulders	Elbows	Wrists/ Hands	High back	Low back	Hips/ Thighs	Knees	Ankles/ Feet
MDS prevalence over the last year	M1	56.20	42.34	16.79	29.20	58.39	62.77	37.96	25.55	18.25
	M2	55.06	38.20	29.21	33.71	62.92	38.20	22.47	24.72	23.60
	M3	69.23	46.15	11.54	23.08	57.69	38.46	50.00	30.77	30.77
	M4	78.38	56.76	35.14	45.95	64.86	62.16	48.65	27.03	18.92
	M5	88.24	63.24	38.24	75.00	38.24	63.24	64.71	50.00	51.47
	M6	56.19	44.76	7.62	22.86	55.24	60.00	37.14	22.86	17.14
	M7	67.19	59.38	26.56	15.63	78.13	62.50	53.13	7.81	23.44
	M8	100.00	48.84	32.56	32.56	65.12	67.44	66.32	48.84	65.12
	M9	33.33	29.63	11.11	18.52	37.04	22.22	37.04	22.22	18.52
	Total	63.56	46.55	21.83	32.42	57.30	54.57	43.18	27.45	26.81
		$\chi^2=76.51$ p=0.000*	$\chi^2=23.30$ p=0.003*	$\chi^2=40.86$ p=0.000*	$\chi^2=78.50$ p=0.000*	$\chi^2=33.85$ p=0.000*	$\chi^2=47.52$ p=0.000*	$\chi^2=46.15$ p=0.000*	$\chi^2=42.22$ p=0.000*	$\chi^2=67.47$ p=0.000*
Impediment to carry out daily activities over the last year	M1	24.09	16.79	5.84	12.41	31.39	36.50	21.17	11.68	10.95
	M2	24.72	15.73	15.73	33.71	19.10	24.72	33.71	15.73	8.99
	M3	26.92	19.23	0.00	15.38	19.23	15.38	19.23	11.54	11.54
	M4	37.84	21.62	10.81	27.03	40.54	37.84	21.62	10.81	16.22
	M5	48.53	11.76	36.76	63.24	50.00	63.24	50.00	63.24	25.00
	M6	19.05	12.38	0.00	17.14	30.48	26.67	16.19	13.33	7.62
	M7	31.25	25.00	25.00	25.00	51.56	43.75	40.63	10.94	7.81
	M8	32.56	48.84	0.00	16.28	48.84	65.24	64.15	16.28	65.12
	M9	33.33	29.63	14.81	14.81	25.93	29.63	18.52	11.11	7.41
	Total	29.05	19.90	12.04	24.56	34.35	37.56	30.18	18.30	15.09
		$\chi^2=22.39$ p=0.004*	$\chi^2=35.26$ p=0.000*	$\chi^2=79.79$ p=0.000*	$\chi^2=78.62$ p=0.000*	$\chi^2=35.17$ p=0.000*	$\chi^2=55.07$ p=0.000*	$\chi^2=66.14$ p=0.000*	$\chi^2=104.47$ p=0.000*	$\chi^2=103.6$ p=0.000*

Note: Prevalence is represented in percentages. The asterisk represents significant differences at a 95% confidence level between the MDS prevalence for each furniture model.

diminishes their furniture design proposal validity, given the outstanding anthropometric differences between the German and the Ecuadorian population.

The Ecuadorian technical standard NTE INEN 2583: 2011 [46] establishes the requirements for tables and chairs for students between the second year of primary education until the third year of upper secondary school, as well as the quality tests to which they must fulfill so as to prove their suitability for use. These standard does not include specific measures for the furniture of Higher Education students. In this context, the dimensions of the design parameters for tables, chairs and side-mounted desktop chairs proposed in this study, could be the starting point for the creation of a specific standard that regulates the design of school furniture for university students.

In general, every analyzed study station composed of tables and chairs in the 5 examined universities presented high discrepancy in seat height and seat depth, and also in desk height and under-desk height. Likewise, all of them presented a low mismatch in the table width and the table depth. On the other hand, every chair with side-mounted desktop analyzed showed a high mismatch in the inner and upper tablet height, as well as in seat height. The length and width of the tablet also presented a low mismatch.

This study also demonstrated a dependence between the presence of MDS in university students and the type of school furniture used during the last twelve months. Although the nine analyzed models have at least five mismatches in their design parameters, there is insufficient evidence to affirm that these

incompatibilities are the only cause of MDS. Therefore, providing students with furniture that is fully compatible with their anthropometric characteristics will not necessarily guarantee the total absence of MDS.

It is recommended that future researches deepen the identification of such causes, as the prevalence levels identified in this research are quite high considering that 88.76% of the students felt MDS in at least one part of their body during the last year (95% CI: 0.863-0.912). It is also important to note that among the latter, 62.92% (95% CI: 0.591-0.667) reported having been prevented from performing other usual daily activities.

The results show that women who use the furniture models assessed are more likely than men to feel MDS associated with neck, shoulders, upper back, lower back and hips/thighs. Individuals with a BMI greater than 25kg/m² (considered by the World Health Organization as being overweight/obese [47]) are at increased risk of having MDS along the entire spine and hips/thighs. Sitting longer than 20 hours a week poses a risk for the presence of MDS in the neck, lower back, and knees.

Upper-level students (third, fourth, and fifth year of study) are at increased risk of having MDS in the neck, lower back and hips/thighs. Students who use a side-mounted desktop chair on a day-to-day basis may be more likely to develop MDS in the neck, wrists/hands, and ankles/feet than students using a table and chair. The latter, are more likely to have problems in the lower back. The results also demonstrate that being left-handed and over 25 years of age are not risk factors for the presence of MDS in

Table 7: Risk factors related to annual MDS prevalence in university students

Characteristics	Neck	Shoulders	Wrists/ Hands	High back	Low back	Hips/ Thighs	Knees	Ankles/ Feet
Female gender	2.431 ^a (1.73-3.42)	2.837 ^a (2.05-3.93)	1.214 (0.86-1.69)	1.737 ^a (1.25-2.40)	1.759 ^a (1.27-2.42)	1.649 ^a (1.19-2.27)	0.816 (0.57-1.16)	1.283 (0.90-1.83)
Left-handed	0.516 (0.30-0.85)	0.450 (0.26-0.78)	0.291 (0.14-0.60)	0.216 (0.12-0.38)	0.524 (0.31-0.87)	0.375 (0.20-0.67)	0.326 (0.15-0.69)	0.628 (0.33-1.18)
Over 25 years old	1.062 (0.52-2.12)	0.974 (0.50-1.89)	0.557 (0.25-1.24)	1.239 (0.62-2.45)	0.692 (0.35-1.34)	0.891 (0.45-1.75)	0.977 (0.46-2.06)	1.166 (0.56-2.41)
BMI higher than 25 Kg/m ²	0.694 (0.49-0.98)	0.758 (0.54-1.06)	0.758 (0.53-1.09)	3.151 ^a (2.00-4.95)	4.331 ^a (2.23-8.40)	2.581 ^a (1.83-3.63)	0.906 (0.62-1.32)	0.884 (0.61-1.29)
To be seated more than 20 hours a week	1.968 ^a (1.17-3.29)	0.721 (0.52-0.98)	1.064 (0.76-1.48)	0.575 (0.41-0.79)	2.387 ^a (1.60-3.55)	0.839 (0.61-1.15)	1.590 ^a (1.11-2.27)	0.843 (0.59-1.20)
More than 2 years studying	1.766 ^a (1.02-3.03)	0.949 (0.67-1.34)	1.449 (0.99-2.13)	1.195 (0.84-1.69)	1.492 ^a (1.05-2.11)	1.648 ^a (1.15-2.36)	2.850 (1.80-4.52)	1.278 (0.85-1.91)
Use of side-mounted desktop chair	1.585 ^a (1.14-2.20)	1.227 (0.89-1.69)	1.674 ^a (1.18-2.37)	1.015 (0.74-1.40)	0.713 (0.52-0.98)	1.369 (0.99-1.89)	1.243 (0.87-1.78)	2.065 ^a (1.42-3.01)
Use of table/chair	0.631 (0.45-0.88)	0.815 (0.59-1.12)	0.597 (0.42-0.85)	0.985 (0.72-1.36)	1.402 ^a (1.02-1.93)	0.730 (0.53-1.01)	0.804 (0.56-1.15)	0.484 (0.33-0.71)

Note: Values correspond to OR. Ranges in parentheses stand for 95% OR confidence intervals. Superscript represents the OR is significant at a 95% confidence level.

university students.

In considering the presence of MDS in the nine parts of the body as nominal variables, the statistical techniques that could be applied were limited. In this regard, in addition to the presence of MDS it is recommended to study the intensity of pain perceived by students, this would increase the spectrum of statistical tools that could be used to delve into the problem.

The imminent solution to avoid the high prevalence of MDS in the students of the analyzed universities would be to change all school furniture in the short term, however, such corrective measure is impractical due to the high amount of the initial investment. A more economical alternative would be to adopt the policy of taking five minutes of active pauses between each hour of work in the classroom so that students can stretch their limbs and reduce exposure to bad postures that can produce pain, swelling, paresthesia, or any other musculoskeletal disorder symptom.

The human body is not designed to remain seated for long periods of time. Intervertebral discs do not have an independent blood supply and depend on the pressure changes that result from the body movement to receive nutrients and to discard their metabolic wastes [41]. The rigidity of the posture also reduces blood flow to the muscles and induces muscle fatigue and cramps [41].

In the same way, it would be advisable for higher education institutions to carry out campaigns to promote awareness in students about the importance to adopt the right postures when performing academic activities in a seated position.

5. Conclusions

This research determined ten design parameters for classroom furniture design for Ecuadorian university students based on relevant anthropometric information. Classroom furniture here examined were composed of tables with its correspondent chairs, and also side-mounted desktop chairs. These results are particularly relevant as they could stand as a starting point to the creation of a specific Ecuadorian standard to regulate classroom furniture design for university students. That would ensure domestic and foreign manufacturers could offer furniture more secure and adequate to the anthropometric characteristics of the university population of Ecuador.

Taking the above-mentioned measures as a reference, a sample of 9 school furniture models that were used in 5 universities of the city of Guayaquil was evaluated based on the computed match intervals and it was found that 100% does not fit, in at least five design parameters, to the anthropometric characteristics of its target population. Only the width of the chair backrest was within the matching range.

A high prevalence of musculoskeletal disorders symptoms (MDS) was found in students over the last year, mainly in the neck, along the whole spine and in the hips or thighs. Also, the percentage of students who reported having perceived these symptoms and thereby prevented other usual non-academic activities were significantly different for each model of furniture. This demonstrated that there is a relationship of dependence between the type of furniture and the presence of MDS in some parts of the body.

This study also showed evidence that female students who

spend more than 20 hours per week sitting at a side-mounted desktop chair are at greater risk of having MDS in the neck than men. Also, women who are overweight or obese (BMI over 25 kg/m²) are at higher risk of having MDS in the upper back and hips or thighs, and those that have studied more than two years in higher education institutions and spend more than 20 weekly hours using desk and chair study stations have a greater risk of having MDS in the lower back.

All of the above-mentioned findings support the need to extend the research immediately to a national level to identify the real prevalence of MDS in the Ecuadorian university students, provide the required medical rehabilitation if necessary, and establish a strategy that allows the gradual acquisition of safer and appropriate classroom furniture that matches students' anthropometric characteristics.

Conflict of Interest

The author declares no conflict of interest with any individual or organization.

Acknowledgment

The author would like to thank Universidad Politécnica Salesiana for funding this research. Also, a special acknowledge is dedicated to all the industrial engineering students who helped to collect relevant data.

References

- [1] Centers for Disease Control and Prevention, "National health and nutrition examination survey (NHANES) anthropometry procedures manual," USA, 2016.
- [2] I. Dianat, M. Kord, P. Yahyazade, M. A. Karimi, A. W. Stedmon, "Association of individual and work-related risk factors with musculoskeletal symptoms among Iranian sewing machine operators," *Appl. Ergon.*, 51, 2015, <https://doi.org/10.1016/j.apergo.2015.04.017>.
- [3] M. M. Robertson, Y. H. Huang, J. Lee, "Improvements in musculoskeletal health and computing behaviors: Effects of a macroergonomics office workplace and training intervention," *Appl. Ergon.*, 62, 182–196, 2017, <https://doi.org/10.1016/j.apergo.2017.02.017>.
- [4] M. K. Gouvali and K. Boudolos, "Match between school furniture dimensions and children's anthropometry," *Appl. Ergon.*, 37, no. 6, 2006, <https://doi.org/10.1016/j.apergo.2017.02.017>.
- [5] Z. Z. Afzan, S. A. Hadi, B. T. Shamsul, H. Zailina, I. Nada, A. R. S. Rahmah, "Mismatch between school furniture and anthropometric measures among primary school children in Mersing, Johor, Malaysia," in 2012 Southeast Asian Network of Ergonomics Societies Conference: Ergonomics Innovations Leveraging User Experience and Sustainability (SEANES), Langkawi, Malaysia, 2012.
- [6] G. Adu, S. Adu, B. Effah, K. Frimpong-Mensah, N. A. Darkwa, "Office Furniture Design–Correlation of Worker and Chair Dimensions," *Int. J. Sci. Res.*, 3, no. 3, 709–715, 2014.
- [7] I. T. G. Souza, C. R. B. Buski, E. C. Batiz, A. L. B. Hurtado, "Ergonomic Analysis of a Clothing Design Station," *Procedia Manuf.*, 3, 4362–4369, 2015, <https://doi.org/10.1016/j.promfg.2015.07.432>.
- [8] M. Azuan, H. Zailina, B. M. T. Shamsul, N. Asyiqin, M. N. Azhar, I. S. Aizat, "Neck, upper back and lower back pain and associated risk factors among primary school children," *J. Appl. Sci.*, 10(5), 431–435, 2010, <https://doi.org/10.3923/jas.2010.431.435>.
- [9] G. A. Mirka, C. Shivers, C. Smith, J. Taylor, "Ergonomic interventions for the furniture manufacturing industry. Part II—Handtools," *Int. J. Ind. Ergon.*, 29(5), 275–287, 2002, [https://doi.org/10.1016/S0169-8141\(01\)00068-3](https://doi.org/10.1016/S0169-8141(01)00068-3).
- [10] Y. Zakeri, M. Gheibizadeh, S. Baraz, D. B. Nejad, S. M. Latifi, "The relationship between features of desks and chairs and prevalence of skeletal

- disorders in primary school students in Abadan, South West of Iran," *Int. J. Pediatr.*, 4 (11), 3949–3956, 2016, <https://doi.org/10.22038/ijp.2016.7656>.
- [11] S. R. Agha, "School furniture match to students' anthropometry in the Gaza Strip," *Ergonomics*, 53(3), 344–354, 2010, <https://doi.org/10.1080/00140130903398366>.
- [12] M. Mokdad and M. Al-Ansari, "Anthropometrics for the design of Bahraini school furniture," *Int. J. Ind. Ergon.*, 39(5), 728–735, 2009, <https://doi.org/10.1016/j.ergon.2009.02.006>.
- [13] A. I. Musa, "Anthropometric evaluations and assessment of school furniture design in Nigeria: A case study of secondary schools in rural area of Odeda, Nigeria," *Int. J. Ind. Eng. Comput.*, 2(3), 499–508, 2011, <https://doi.org/10.5267/j.ijiec.2011.03.006>.
- [14] I. W. Taifa and D. A. Desai, "Anthropometric measurements for ergonomic design of students' furniture in India," *Eng. Sci. Technol. an Int. J.*, 1–8, 2016, <https://doi.org/10.1016/j.jestch.2016.08.004>.
- [15] B. W. Niebel and A. Freivalds, *Ingeniería industrial: métodos, estándares y diseño del trabajo*, 13th ed. Ciudad de México, México: McGraw-Hill, 2014.
- [16] M. G. Mohamed Thariq, H. P. Munasinghe, J. D. Abeyssekara, "Designing chairs with mounted desktop for university students: Ergonomics and comfort," *Int. J. Ind. Ergon.*, 40(1), 8–18, 2010, <https://doi.org/10.1016/j.ergon.2009.10.003>.
- [17] H. I. Castellucci, P. M. Arezes, J. F. M. Molenbroek, "Equations for defining the mismatch between students and school furniture: A systematic review," *Int. J. Ind. Ergon.*, 48, 117–126, 2015, <https://doi.org/10.1016/j.ergon.2015.05.002>.
- [18] I. W. Taifa and D. A. Desai, "Anthropometric measurements for ergonomic design of students' furniture in India," *Eng. Sci. Technol. an Int. J.*, 20(1), 232–239, 2017, <https://doi.org/10.1016/j.jestch.2016.08.004>.
- [19] H. I. Castellucci, P. M. Arezes, J. F. M. Molenbroek, "Applying different equations to evaluate the level of mismatch between students and school furniture," *Appl. Ergon.*, 45(4), 1123–1132, 2014, <https://doi.org/10.1016/j.apergo.2014.01.012>.
- [20] H. I. Castellucci, P. M. Arezes, J. F. M. Molenbroek, "Analysis of the most relevant anthropometric dimensions for school furniture selection based on a study with students from one Chilean region," *Appl. Ergon.*, 46, 201–211, 2015, <https://doi.org/10.1016/j.apergo.2014.08.005>.
- [21] A. Altaboli, M. Belkhear, A. Bosenina, N. Elfsej, "Anthropometric Evaluation of the Design of the Classroom Desk for the Fourth and Fifth Grades of Benghazi Primary Schools," *Procedia Manuf.*, 3, 5655–5662, 2015, <https://doi.org/10.1016/j.promfg.2015.07.778>.
- [22] I. Dianat, M. A. Karimi, A. Asl Hashemi, S. Bahrapour, "Classroom furniture and anthropometric characteristics of Iranian high school students: Proposed dimensions based on anthropometric data," *Appl. Ergon.*, 44(1), 101–108, 2013, <https://doi.org/10.1016/j.apergo.2012.05.004>.
- [23] H. I. Castellucci, M. Catalán, P. M. Arezes, J. F. M. Molenbroek, "Evidence for the need to update the Chilean standard for school furniture dimension specifications," *Int. J. Ind. Ergon.*, 56, 181–188, 2016, <https://doi.org/10.1016/j.ergon.2015.09.019>.
- [24] J. M. Mahoney, N. A. Kurczewski, E. W. Froede, "Design method for multi-user workstations utilizing anthropometry and preference data," *Appl. Ergon.*, 46, 60–66, 2015, <https://doi.org/10.1016/j.apergo.2014.07.003>.
- [25] F. W. Cayo-Chiluisa, "El diseño de estaciones de trabajo escolar y su incidencia en el proceso de enseñanza aprendizaje en niños y niñas de 3 a 5 años del Centro de desarrollo infantil y estimulación temprana pequeños traviesos de la Ciudad de Latacunga," Universidad Técnica de Ambato, 2014.
- [26] A. C. Viera-Meléndez, "Análisis ergonómico del mobiliario escolar en relación a las medidas antropométricas y evaluación postural de los niños del 6to año de educación básica de la escuela 'Quintiliano Sánchez,'" Quito, Pontificia Universidad Católica del Ecuador, 2012.
- [27] M. del R. Pomboza-Fioril and V. A. Cloquell-Ballester, "Determinación antropométrica para mobiliario escolar destinado a niños con discapacidad motriz en Ecuador," *Cienc. Trab.*, 17(53), 154–158, 2015.
- [28] J. L. Alarcón-Escobar, "Diseño de mobiliario escolar para niños y niñas con paraparesia espástica del instituto fiscal de discapacidad motriz," Pontificia Universidad Católica del Ecuador, 2016.
- [29] P. Romo-Cardoso and T. del Campo-Balsa, "Trastornos musculoesqueléticos en trabajadores sanitarios y su valoración mediante cuestionarios de discapacidad y dolor," *Med. del Trab.*, 20(1), 27–33, 2011.
- [30] A. Genç, T. Kahraman, E. Göz, "The prevalence differences of

musculoskeletal problems and related physical workload among hospital staff,” *J. Back Musculoskelet. Rehabil.*, 29(3), 541–547, 2016, <https://doi.org/10.3233/BMR-160655>.

- [31] M. Mendiñeta-Martínez and Y. H. Herazo-Beltrán, “Perception musculoskeletal discomfort and postural risk among employees of a higher education institution,” *Salud Uninorte*, 30(2), 170–179, 2014.
- [32] R. M. Rosario Amézquita and T. I. Amézquita Rosario, “Prevalencia de trastornos músculo-esqueléticos en el personal de esterilización en tres hospitales públicos,” *Med. Secur. Trab.*, 60(234), 24–43, 2014, <https://doi.org/10.4321/S0465-546X2014000100004>.
- [33] I. Kuorinka, B. Jonsson, A. Kilbom, H. Vinterberg, F. Biering-Sørensen, G. Andersson, K. Jørgensen, “Standardised Nordic questionnaires for the analysis of musculoskeletal symptoms,” *Appl. Ergon.*, 18(3), 233–237, 1987.
- [34] A. Tezel, “Musculoskeletal complaints among a group of Turkish nurses,” *Int. J. Neurosci.*, 115(6), 871–880, 2005, <https://doi.org/10.1080/00207450590897941>.
- [35] M. Mendiñeta, Y. Herazo, Y. Pinillos, “Factores asociados a la percepción de dolor lumbar en trabajadores de una empresa de transporte terrestre,” *Salud Uninorte*, 30(2), 192–199, 2014.
- [36] T. Kahraman, A. Genç, E. Göz, “The Nordic Musculoskeletal Questionnaire: cross-cultural adaptation into Turkish assessing its psychometric properties,” *Disabil. Rehabil.*, 38(21), 2153–2160, 2016, <https://doi.org/10.3109/09638288.2015.1114034>.
- [37] D. V. Lema-Barrera, “Comparación estadística de medidas antropométricas entre mestizos, indígenas y afro ecuatorianos de la Región Sierra del Ecuador,” MSc Thesis, Universidad San Francisco de Quito, 2013.
- [38] Instituto Nacional de Estadística y Censos (INEC), Base de datos Censo de población y viviendas 2001, 2001. Available: <http://www.ecuadorencifras.gob.ec/base-de-datos-censo-de-poblacion-y-vivienda-2001>.
- [39] Instituto Nacional de Estadística y Censos (INEC), Base de datos Censo de población y viviendas 2010, 2010. Available: <http://www.ecuadorencifras.gob.ec/base-de-datos-censo-de-poblacion-y-vivienda-2010>.
- [40] ISO, Basic human body measurements for technological design—Part 1: Body measurement definitions and landmarks (ISO 7250-1:2008), 2008.
- [41] C. Parcells, M. Stommel, R. P. Hubbard, “Mismatch of classroom furniture and student body dimensions,” *J. Adolesc. Heal.*, 24(4), 265–273, 1999, [https://doi.org/10.1016/S1054-139X\(98\)00113-X](https://doi.org/10.1016/S1054-139X(98)00113-X).
- [42] ISO, “Ergonomic requirements for office work with visual display terminals (VDTs). Part 5: Workstation layout and postural requirements (ISO 9241-5:1998), 1998.
- [43] J. Cerda, C. Vera, G. Rada, “Odds ratio: aspectos teóricos y prácticos,” *Rev. Med. Chil.*, 141(10), 1329–1335, 2013, <https://doi.org/10.4067/S0034-98872013001000014>.
- [44] P. S. Espinosa-Tabango, “Diseño de una estación de trabajo para los estudiantes de la Universidad Central del Ecuador,” Eng Thesis, Universidad Central del Ecuador, 2013.
- [45] Deutsches Institut für Normung. DIN 33402-2 Ergonomie - Körpermaße des Menschen – Teil 2, Berlín, 1981.
- [46] Instituto ecuatoriano de normalización (INEN), NTE INEN 2583: 2011 Muebles escolares. Pupitre con silla para alumnos. Requisitos e inspección. Quito, Ecuador, 2011.
- [47] OMS, “Obesity: preventing and managing the global epidemic,” Geneva, Switzerland, 2000.

Quranic Reciter Recognition: A Machine Learning Approach

Rehan Ullah Khan^{*1,3}, Ali Mustafa Qamar², Mohammed Hadwan^{1,3}

¹Department of Information Technology, College of Computer, Qassim University, Saudi Arabia

²Department of Computer Science, College of Computer, Qassim University, Saudi Arabia

³Intelligent Analytics Group (IAG), College of Computer, Qassim University, Saudi Arabia

ARTICLE INFO

Article history:

Received: 09 October, 2019

Accepted: 16 November, 2019

Online: 25 November, 2019

Keywords:

Audio analysis

Quran analysis

MFCC

Machine learning

ABSTRACT

Recitation and listening of the Holy Quran with Tajweed is an essential activity as a Muslim and is a part of the faith. In this article, we use a machine learning approach for the Quran Reciter recognition. We use the database of Twelve Qari who recites the last Ten Surah of Quran. The twelve Qari thus represents the 12-class problem. Two approaches are used for audio representation, firstly, the audio is analyzed in the frequency domain, and secondly, the audio is treated as images through Spectrogram. The Mel Frequency Cepstral Coefficients (MFCC) and Pitch are used as the features for model learning in the first case. In the second case of audio as images, Auto-correlograms are used to extract features. In both cases, the features are learned with the classical machine learning which includes the Naïve Bayes, J48, and the Random Forest. These classifiers are selected due to their overall good performance in the state-of-the-art. It is observed that classifiers can efficiently learn the separation between classes, when the audio is represented by the MFCC, and the Pitch features. In such a case, we get 88% recognition accuracy with the Naïve Bayes and the Random Forest showing that Qari can be effectively recognized from the recitation of the Quranic verses.

1. Introduction

Quranic audio analytics lacks thorough research and understanding from machine learning perspectives. Out of many Qari tilawat recitations available offline and online, an automated system could help in the selection of specific voice of Qari, depending upon the person's mood and choice. This drives the motivation for our work. Altalmas et al. [1] processed the Spectrogram features for the Qalqalah letters, describing the process of Qalqalah correctly. However, in [1], there is no recognition part. In [1], the authors declare classification and recognition as future work. The work of [2] develops an autonomous delimiter that performs the extraction of Quranic verses from the tilawat by using the Sphinx framework. [2] only uses Surah "Al-Ikhlâss" for analysis. There are many limitations in [2], not only because of the sample but also due to the usage of the Hidden Markov Model (HMM). The [3] analyzes the recitation of many Surah of the Quran. It is found that there is 21.39% of voiced speech in Quranic recitations, which is 3 times higher than audiobooks. Therefore, a linear predictor component can be used

for efficiently representing the Quranic signals. The authors in [4] propose an online speech recognition technique for verification of the Quranic verses. According to Kamarudin et al. [5], the rules of the Quran verse are prone to additive noise. Therefore, they can affect the classification of Quranic results. The authors propose an Affine Projection approach as the optimized solution for echo cancellation. Elobaid et al. [6] develop "Noor Al-Quran" for handheld devices for Non-Arabic speakers for correct recitation learning. Khurram and Alginahi [7] discuss the concerns and the challenges of digitizing and making the Quran available to the masses. The authors in [8] focus on user acceptance of the speech recognition capabilities of mobile devices. Another article [9] represents blind and disabled people to use education-related services for Quran. The [10] demonstrates the Computer-Aided Pronunciation Learning module (CAPL) to detect Quranic recitation errors.

In this article, we analyze the recitation of the Twelve Qari, reciting the last ten Surah of the Quran, thus representing a 12-class problem. For this setup, the audio is analyzed in the frequency domain, and as images through Spectrogram. The Mel

*Rehan Ullah Khan, re.khan@qu.edu.sa

www.astesj.com

<https://dx.doi.org/10.25046/aj040621>

Frequency Cepstral Coefficients (MFCC) and Pitch are used as the features for model learning. In the scenario of audio as images, the Auto-correlograms are used to extract features. The features are learned with the Naïve Bayes, J48, and the Random Forest, being selected due to their over-all excellent performance in the state-of-the-art. The experimental analysis shows that the classifiers can efficiently detect the reciter of the Quran if the audio is represented by the MFCC and Pitch features. In such a case, we get 88% recognition accuracy with the Naïve Bayes and the Random Forest showing that the Qari class can be effectively recognized from the recitation of the Quranic verses.

2. Recognition Models and Features

In this section, we discuss the classifiers and feature extraction, which are used in experimentation and analysis.

2.1. Naïve Bayes

Naïve Bayes classifiers are a family of probability-based classifiers with the use of strong (naïve) assumptions about the independence in Bayes' theorems [11]. Naïve Bayes assign class labels to classes of a certain problem, where feature label consists of a specific set of class labels. Not only the algorithm for designing such classifiers but the family of algorithms is based on the general principle: all naïve Bayes classifiers assume that the value of a particular attribute does not depend on the value of any other attribute of the data in question.

2.2. J48

J48 is the implementation of the Open Source Quinlan C4.5 decision tree algorithm [12]. Decision tree algorithms start with a series of questions and examples and create tree data structures that can be used to classify new tasks. Each case is described by the attributes (or properties). Each training case has a class label associated with it. Each node within the decision tree is included in the test, which results in which branch to choose from.

2.3. Random Forest

Recently, Decision tree classifiers have gained considerable popularity. This popularity is due to the intuitive nature and overall easy learning paradigm. The classification trees, however, suffer from low classification accuracy and generalization. The accuracy of classification and generalization cannot be increased simultaneously. For this purpose, Breiman [13] introduced Random Forest. It uses a combination of several trees from one data set. A random forest creates a forest of trees, so each tree is generated based on a random grain plus data. For classification stages, the input vector is applied to every tree in the forest. Each tree decides about the class of the vector. These decisions are then summed up for the final classification.

2.4. Mel Frequency Cepstral Coefficients (MFCC)

The first step in any automated speech processing is to extract the functions, that is, the properties of the phonetic features that are effective at identifying words, and all other components containing information such as background sounds, thoughts, etc. [14]. The sound emitted by humans is filtered through the structure of the tongue, teeth, and so on. This structure determines which sounds come out. If we can learn exactly what that looks like, it should

give us a true representation of the phoneme produced. The vocal structure is presented in the envelope of the short-time spectrum of power, and the function of the MFCCs is to represent this envelope accurately. MFCCs are widely used features in automatic speech recognition.

2.5. Pitch and Frequency

The pitch is an audio sensation for which the subject assigns music tones to the relative position on the music-based scale on the perception of the vibrational frequency [15]. The pitch is strongly related to the frequency but they are not similar. Frequency is an objective and scientific quality that can be measured. Pitch has a personal perception of the sound wave for each person, which cannot be measured directly. However, it does not mean that most people will not agree on which audio/music notes are lower and higher. Pitch can be quantified as frequencies in Hertz or cycle per second by a comparative analysis of the subjective sound signals with the ones with standard pure tones having aperiodic, sinusoidal wave structure. This approach is mostly used to assign a pitch value to the complex and aperiodic sound signals.

3. Experimental Evaluation

In this section, we discuss the dataset and the experimental evaluation performed for different parameters.

The dataset consists of 120 Quranic recitations performed by the 12 Reciters. The dataset is downloaded and collected from [16]. The 10 Surahs recited by 12 Qaris are as follows:

- Al-Fil
- Quraysh
- Al-Ma'un
- Al-Kawthar
- Al-Kafirun
- An-Nasr
- Al-Masad
- Al-Ikhlâs
- Al-Falaq
- An-Nas

For experimental evaluation, we select Naïve Bayes, J48, and the Random Forest. These are selected based on their good overall performance in the state-of-the-art audio classification based on MFCC and Pitch.

Two types of features are extracted. In the first scenario, the features are extracted based on the MFCC and Pitch of the recitation audio. The second is based on the image domain. The Tilawat (recitation) is first converted to image representation. For the conversion, we use the spectrogram approach.

The spectrogram approach works on the principle of Fourier transform. The key elements are then represented as frequency response coefficients. These are then combined as a time-domain structure. This time-domain structure is represented as an image signal. After an image is obtained, image-based feature extraction

can be applied. We adopt the Auto-Correlogram approach [17] for feature extraction. The Auto-Correlogram approach takes into consideration not only the pixel values but also the distance of a particular color from the next similar color. These features have shown excellent performance in state-of-the-art [17].

3.1. Performance analysis based on audio features

Two methods are used to extract features from the audio. In the first case, the features are extracted based on the MFCC and Pitch of the recitation audio. The details of MFCC and Pitch are given in the previous section.

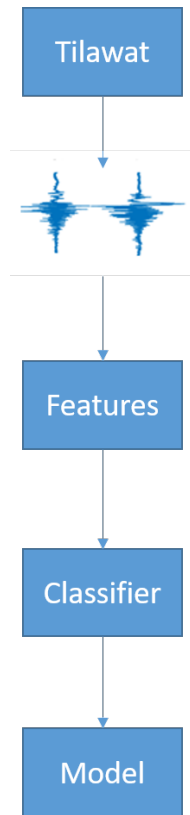


Figure 1. The classification model for Qari recognition

Figure 1 shows the flow of the recognition model. The recitation is converted to the MFCC and Pitch features. The features are then learned by the classifier. The output of classifier learning is generally called the model. The model is then used to test other recitation audios. We use the 10-folds cross-validation scheme. In this scheme, 90% of data is used for training the model, and 10% is used for testing. This procedure is repeated 10 times.

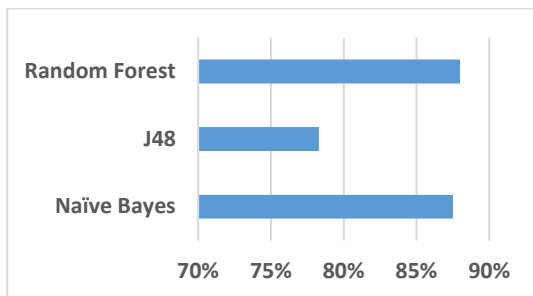


Figure 2. Accuracy of MFCC and Pitch with the three classifiers

Table 1: Performance analysis of the MFCC and Pitch features

Classifier	Accuracy
Naïve Bayes	88%
J48	78%
Random Forest	88%

Figure 2 shows the performance of the classification paradigm for the three classifiers, namely Random forest, J48, and the Naïve Bayes using the features of the MFCC and the Pitch. Table 1 shows similar performance in the form of accuracy values.

Figure 2 shows the accuracy of the models. We select the accuracy parameter because the data is almost balanced with reference to classes. In Figure 2 and Table 1, it can be noted that Random Forest and the Naïve Bayes have the highest accuracy. We represent the accuracy as the percentage. This means that the Random forest accuracy of 88% is linked to the recognition of the Qari. As such, Random Forest can recognize the Qari with 88% accuracy. The total error the Random forest will make in identifying the Qari will be only 12%.

Similarly, the accuracy of Naïve Bayes is also 88%. This is coinciding with the Random Forest. Therefore, the Naïve Bayes classifiers learn the Qari with a good recognition model like that of the Random Forest. In Figure 2, and Table 1, the lower performance is exhibited by the J48. The performance of the J48 is 78%. This means that the J48 classifier model has a 22% chance of not recognizing the Qari correctly. This is higher compared to the Random forest and the Naïve Bayes, which is only 12%. This low performance could be due to the sensitivity of the decision trees (J48) to the noise in the data.

3.2. Performance analysis based on image features

For the conversion of the audio recitation to the image representation, the Fourier transform approach is used. After Fourier transformation, the frequency response coefficients are combined as a time-domain structure. This time-domain structure is represented as an image signal. The image-based feature extraction of the Auto-Correlogram approach [17] for feature extraction is used. These features have shown very good performance in state-of-the-art [17].

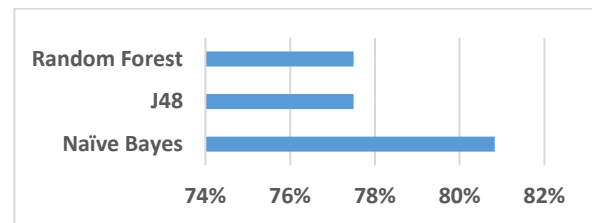


Figure 3. Accuracy of the spectrogram-based recognition models

Table 2: Performance analysis of the Spectrogram features

Classifier	Accuracy
Naïve Bayes	81%
J48	78%
Random Forest	78%

Figure 3 and Table 2 show the performance analysis of the image-based representation of the Quran recitation audio.

In Figure 3 and Table 2, the Naïve Bayesian algorithm has the highest accuracy. The performance parameter is Accuracy, which is used for balanced classes. Similar to Figure 2, the accuracy is represented as the percentage. The Naïve Bayes classifier's accuracy of 81% means that Naïve Bayes is capable of recognizing the Qari with an 81% accurate model. The chance of the error being made by the Naïve Bayes in identifying the Qari is 19%. This error can be explained as such that out of 100 recitations performed by different Qari, only 81 recitations are correctly identified and mapped to the corresponding Qari of the recitation. The accuracy of the Random Forest is 78%. This means that 22 samples out of 100 samples of recitations will be wrongly identified and mapped to a different Qari. Interestingly, the accuracy of J48 is also 78%. The general trend, however, is that Random Forest normally has a higher classification accuracy than J48 in state-of-the-art.

The same detection performance for both the Random Forest and the J48 is an exciting result. Since both of the algorithms work on the same principle of decision trees, similar results in special cases make sense. Moreover, the Naïve Bayes classifier learns the Qari with a good recognition model like that of Figure 2. However, the Naïve Bayes performance in Figure 2 and Figure 3 is not consistent, though higher than other models, especially, in Figure 3. As such, the Naïve Bayes' higher performance in both the cases of audio features and image features is motivating for further analysis and practical applications.

4. Conclusion

By using 120 total recitations, we analyzed the recitations of 12 Qari. We used two approaches to process the audio recitations. The first one being the MFCC and Pitch, and the second one as the Spectrogram-based images. Auto-correlograms are used to extract features in case of image representation. The features are learned with the Naïve Bayes, J48, and the Random Forest, being selected due to their over-all good performance in the state-of-the-art. The experimental analysis shows that the classifiers can efficiently learn the reciter of the Quran if the MFCC and the Pitch features represent the audio. In such a case, we get 88% recognition accuracy with the Naïve Bayes and the Random Forest showing that the Qari class can be effectively recognized from the recitation of the Quranic verses.

Conflict of Interest

The authors declare no conflict of interest.

Acknowledgment

The work in this article is funded in its entirety by the Deanship of Scientific Research (SRD), Project number: **3600-coc-2018-1-14-S** at the Qassim University, Kingdom of Saudi Arabia.

We also gratefully acknowledge the support of NVIDIA Corporation with the donation of the Titan Xp GPU which is used for relevant research.

References

[1] T. Altalmas, S. Ahmad, W. Sediono, and S. S. Hassan, "Quranic letter pronunciation analysis based on spectrogram technique: Case study on qalqalah letters," in *CEUR Workshop Proceedings*, vol. 1539, pp. 14–22, 2015.

[2] H. Tabbal, W. El Falou, and B. Monla, "Analysis and implementation of a Quranic verses delimitation system in audio files using speech recognition techniques," in *2nd International Conference on Information and Communication Technologies: From Theory to Applications, ICTTA, Damascus, Syria*, vol. 2, pp. 2979–2984, 2006. <https://doi.org/10.1109/ICTTA.2006.1684889>

[3] T. S. Gunawan and M. Kartiwi, "On the characteristics of various Quranic recitation for lossless audio coding application," in *6th International Conference on Computer and Communication Engineering: Innovative Technologies to Serve Humanity, ICCCE, Kuala Lumpur, Malaysia*, pp. 121–125, 2016. <https://doi.org/10.1109/ICCCE.2016.37>

[4] A. Mohammed and M. S. Sunar, "Verification of Quranic Verses in Audio Files using Speech Recognition Techniques," in *Int. Conf. Recent Trends Inf. Commun. Technol.*, 2014.

[5] N. Kamarudin, S. A. R. Al-Haddad, M. A. M. Abushariah, S. J. Hashim, and A. R. Bin Hassan, "Acoustic echo cancellation using adaptive filtering algorithms for Quranic accents (Qiraat) identification," *Int. J. Speech Technol.*, 19(2), pp. 393–405, 2016. <https://doi.org/10.1007/s10772-015-9319-z>

[6] M. Elobaid, K. Hameed, and M. E. Y. Eldow, "Toward designing and modeling of Quran learning applications for android devices," *Life Sci. J.*, 11(1), pp. 160–171, 2014.

[7] M. K. Khan and Y. M. Alginahi, "The holy Quran digitization: challenges and concerns," *Life Sci. J.*, 10(2), pp. 156–164, 2013.

[8] N. Kamarudin, S. A. R. Al-Haddad, A. R. B. Hassan, and M. A. M. Abushariah, "Al-Quran learning using mobile speech recognition: An overview," in *International Conference on Computer and Information Sciences (ICCOINS), Kuala Lumpur, Malaysia* 2014. <https://doi.org/10.1109/ICCOINS.2014.6868401>

[9] S. A. E. Mohamed, A. S. Hassanin, and M. T. B. Othman, "Educational system for the holy Quran and its sciences for blind and handicapped people based on Google speech API," *JSEA*, 7(3), pp. 150–161, 2014. <http://dx.doi.org/10.4236/jsea.2014.73017>

[10] S. M. Abdou and M. Rashwan, "A Computer Aided Pronunciation Learning system for teaching the holy quran Recitation rules," in *IEEE/ACS International Conference on Computer Systems and Applications (AICCSA), Doha, Qatar*, pp. 543–550, 2014. <http://dx.doi.org/10.1109/AICCSA.2014.7073246>

[11] D. Zhang, "Bayesian Classification," 2019, pp. 161–178.

[12] S. L. Salzberg, "C4.5: Programs for Machine Learning by J. Ross Quinlan. Morgan Kaufmann Publishers, Inc., 1993," *Mach. Learn.*, 16(3), pp. 235–240, Sep. 1994. <https://doi.org/10.1007/BF00993309>

[13] L. Breiman, "Random Forests," *Mach. Learn.*, 45(1), pp. 5–32, 2001. <https://doi.org/10.1023/A:1010933404324>

[14] X. Huang, A. Acero, and H.-W. Hon, *Spoken Language Processing: A Guide to Theory, Algorithm & System Development*, 2001. 2001.

[15] P. A. Cariani and B. Delgutte, "Neural correlates of the pitch of complex tones. I. Pitch and pitch salience," *J. Neurophysiol.*, 76(3), 1996. <https://doi.org/10.1152/jn.1996.76.3.1698>

[16] "A2Youth.com - The Youth's Islamic Resource." [Online]. Available: <https://www.a2youth.com/>. [Accessed: 06-Oct-2019].

[17] J. Huang, S. R. Kumar, M. Mitra, W.-J. Zhu, and R. Zabih, "Image Indexing using Color Correlograms," in *IEEE Computer Society Conference on Computer Vision and Pattern Recognition, San Juan, Puerto Rico, USA, USA*, pp. 762–768, 1994.

Data Dashboard for Decision Support Systems for Intrapreneurship in A Company

Evaristus Didik Madyatmadja*, Evaristus Didik Madyatmadja, Alvi Sasqia Putri, Siti Sabilul Hiqna, Wigna Pratita

Information Systems Department, School of Information Systems, Bina Nusantara University, 11480, Indonesia

ARTICLE INFO

Article history:

Received: 03 October, 2019

Accepted: 14 November, 2019

Online: 25 November, 2019

Keywords:

Intrapreneurship

Innovation Management

Data Visualization

Dashboard

ABSTRACT

Nowadays, as the Information and Technology rapidly growing all across the world, Indonesia as one of many developed countries always tries to keep up relating to this trend. Regarding to this situation, the use of Information and Technology in various fields are greatly enhanced, and not to mention businesses. There are a lot of businesses using technology, building a start-up is one of the common ways to combine technology with innovation. Intrapreneurship is a media to develop new venture within an organization and to exploit new opportunities. To help the continuity of entrepreneurship, there must be an Innovation Management that serves help to develop ideas from the internal employees and always find the best solution to help the intrapreneurs grows in the best environment. To make a better decision making, management need some tools to monitor and evaluate the Intrapreneurs. Data Dashboard aims to help the decision maker to see the Intrapreneurs' performance and at once feel their pain and gain. With those insights that can be obtained from the dashboard, hopefully, management can get enough information to make the best decision regarding the continuity status of each Intrapreneurs. This research will provide the dashboard with some algorithm to show the recommendation data about the status of Intrapreneurs.

1. Introduction

Entrepreneurship by contrast is the act of developing a new venture outside an existing organization [1]. Intrapreneurship can be very advantageous for a company because intrapreneurs explore the concealed opportunity, use the creativity and innovate a new idea that leads to company's better performance. In order for intrapreneurs to run and managed well, there must be an Innovation Management manages intrapreneur's environment with the aim of making it grand and supportive of their outgrowth that intrapreneur has the best opportunity to grow fast and unleash their maximum potential, compared to other growth environment. Because of the large number of intrapreneurs that needs to be taken care of, Innovation Management has many sources of data coming from each intrapreneur, the data is mainly the representative of their performances throughout monitoring and evaluation process.

Intrapreneur is very valuable in corporate let alone, in State-Owned Enterprises in Indonesia. It's not just making a small community to make money, but also to raise awareness about the importance of innovation and how innovation builds the culture. The impact from having intrapreneur in corporate, already proven

in one of the State-Owned Enterprise in Indonesia that runs in telecommunication sector, that building innovation lab helps the corporate to find the right culture that can be implemented in the whole corporation and gain more money because they treat the intrapreneur in a right way.

Based on study in Industrial Management & Data System by Emerald about Information technology -enabled intrapreneurship culture and firm performance, they said that the results indicate that intrapreneurship culture is a valuable capability that leads to firm performance and that two types of IT resources (technological IT and managerial IT resources) lead to the development of an intrapreneurship culture. Moreover, the results indicate that the investment in both technological IT resources and managerial IT resources influences competitive performance positively by means of intrapreneurship culture. The study also shows that IT-enabled intrapreneurship culture leads to significantly better firm performance. The findings are consistent with the perspective of IT-enabled organizational capabilities that perceives IT resources as impacting positively on firm performance by means of other higher-order process capabilities [2]

They found that the development of an intrapreneurship culture leads to higher sales growth, market share growth and

* Evaristus Didik Madyatmadja, Email: emadyatmadja@binus.edu

product and market development. It is possible that the current economic crisis, with some exacerbating factors in the Spanish entrepreneurial context, is changing the managerial perception of the business value of the innovation culture in commercial terms. Finally, this study responds to the call for empirical research on innovation-supportive culture, of which there has been little to date [2]

Another study that stated the effect of intrapreneurship on corporate performance is from Management Decision by Emerald. The study shows that intrapreneurship influences the performance of firms, contributing to a deeper understanding of the importance of intrapreneurship in the context of entrepreneurship and the resource-based view theories. The multidimensional structure of intrapreneurship is confirmed and it is influenced by the important role of proactivity and innovative action, associated with the challenge to the intrapreneurs in their propensity for risk. Within the framework of intrapreneurship, the autonomy granted to the entrepreneurs, their competitive energy and the risk of uncertainty associated with their initiative and capacity for innovation have a lower importance. This work highlights the importance of the factor growth and improvement, of a qualitative nature, to reflect the multidimensional effect of intrapreneurship. The proactivity and innovation action of entrepreneurs project the effects in the long term aiming to ensure the development of companies. [3]

Data is a material that needs to be processed in order to get complete and clear information. Data is a fact that strengthens the truth about the information. In computational systems data are the coded invariances. In human discourse data is that which is stated, for instance, by informants in an empirical study [4]. The data itself won't provide much benefit if there's no further action to make those data worth, one of the basic things that can be done as the starting point is setting the goal, which determine what and how the data will be processed for the management. The function of the management beside helping intrapreneur to have a supportive environment is to make an appropriate decision that can make a great impact, not just for the intrapreneur itself but also for The Company. In order to do so, management need some tools to help them to gain insights which supports on decision making.

As the information and technology has enhanced, decisions support tools have become more sophisticated. "Data management for decision support has moved through three generations, with the latest being real-time data warehousing" [5]. Today decision support system is used in various fields for a variety of purposes including real-time performance monitoring and strategic business intelligence queries. This system in its development, eventually can make the management to see the bigger picture. Managers can use the system that include historical data of Amoeba's performance to support many decision tasks. When the tasks are performed regularly then a computerized decision support system can potentially increase access to the data and help managers gain insights regarding the continuity of Amoeba's status in this program.

Decision support system in general have the concept of processing the data. One of many common methods to process the data is data mining. Data mining can be implemented to the data so the data can provide results based on the intentioned purpose. Data Mining is discipline that emerged at the meeting of several other disciplines, mainly driven by huge growth of databases.

What triggers data mining is the essential information that lays under the piles of inessential data which makes it hidden. Data mining is the way to extract the essential data so it can be processed and provides essential information [6]. There are some kind of data mining techniques, which are classification, clustering, association rules, regression, etc[7].

Decision support system can be visualized in various kinds of presentation, one of the visualization tools that are commonly used is dashboard. The content of dashboard can help the management read the data in the best possible way. Data visualization is the representation of data in a systematic form that can be the 'front end' of big data [8]. The results can be useful depending on the quality and the quantity of data itself. Dashboard is one of the ways to visualize the data.

Organization Dashboard as a relatively small collection of interconnected key performance metrics and underlying performance drivers that reflects both short- and long-term interests to be viewed in common throughout the organization [9]. Dashboard typically have 3 types of purposes: a) Strategic purposes, b) Analytical purposes, c) Operational purposes.

With having a large amount of data by combining the data mining and data visualization, hopefully it can dig underneath valuable information and present it in the simplest way. The decision maker can also use the visualization to see the progress of intrapreneurs and the result from data mining processes can be used to gain more insight to help make better decisions regarding the intrapreneur's growth. All of these purposes are become our motivation to make one dashboard to display all of the information needed so it can be more effective and efficient.

2. Definition of Intrapreneurs Dashboard

Dashboard is a representative of data which contain the visualization of many data combined resulting the summarization of interconnected key performance metrics to communicate some performances and achievements throughout the company. Dashboard are related to decision support system in a way that they can provide such an insight that can be viewed as a combination of individual decision support system [9].

There are three types of dashboard regarding to the purpose, they are: strategic purposes, analytical purposes, and operational purposes. Strategic purposes dashboard is common to be used in executive levels to monitor the long-term company strategy. It tracks the performance metrics while lining up with the company's goals. The data behind strategic purposes dashboard is updated periodically and less frequent than operational purposes dashboard. Analytical purposes dashboard is a dashboard that contains an up to date massive amount of data to be analyzed to provide support for executives. What we can do from analytical dashboard is to make an analysis like make a prediction or discover insights. The analysis is based on the historical data. Operational dashboard is a monitoring dashboard that has a timely updated data so that progress can be tracked on time. It is commonly used to monitor and manage operations [10].

The purposes of using dashboard as a tool to visualize the data are:

1. Dashboard can enforce consistency in measures and measurement procedures across departments and business units.

2. Dashboard can help management to monitor and evaluate performance in order to make better product development.

3. Dashboard can be used as a plan to make basic strategies and determine the goal for the future given.

4. Dashboard also may be used to share and communicate with stakeholders about particular data that can make the stakeholders understand easily and make a quick decision regarding the data given in the dashboard [9].

Intrapreneur dashboard is an analytical dashboard that contains the visualization about the talent's data and intrapreneur's performance to help the management monitor and evaluate intrapreneur's progress in order to make the best decision regarding the continuity status of intrapreneur.

3. Development of Intrapreneur Dashboard

As shown in Figure 1, those are the steps to develop a Business Intelligence Systems:

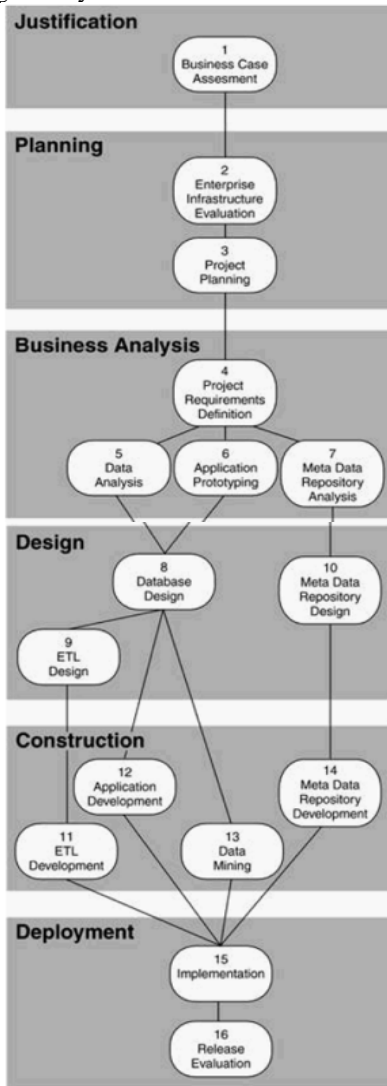


Figure 1: Business Intelligence Roadmap Lifecycle Diagram

1. Business Case Assessment

Business case assessment is the step of exploring the idea from the business side. It defines the obvious business reason to

develop the project. It also assesses the current system and compare it to the competitor's BI Application. After finding the problem, the BI solution can be proposed and be considered by doing some analysis like cost benefit analysis or do a risk assessment. Then the assessment report can be produced.

2. Enterprise Infrastructure Evaluation

Enterprise infrastructure evaluation is an activity of assessing the current platform, selecting the new product, write the report, and until installing and testing it.

3. Project Planning

Project planning is detailing the plan to develop the BI Application. We can do it by revising the cost estimates, risk assessment, determining the condition of source files, identifying critical success factor, preparing the high-level plan until start kicking off the project.

4. Project Requirement Definition

This step is generally defining requirement for many aspects like technical infrastructure enhancements, non-technical infrastructure enhancements, reporting, requirements for source data, review the project scope, expand the logical data model, define the preliminary service level agreement, and write the application requirements documents.

5. Data Analysis

In this step we do a more thorough analysis of data by analyzing the external data sources, refine the logical data model, analyze the source data quality, expand the logical enterprise data model, resolve data discrepancies, and write the data cleansing specification for the further step.

6. Application Prototyping

Application prototyping means planning a prototype starting from the requirement analysis, defining scope, develop it, and demonstrate the prototype.

7. Metadata Repository Analysis

This step is the first step in developing the metadata repository before designing and developing metadata repository. Here, things like analyzing requirements for metadata, analyzing the interface requirements for metadata repository, analyzing the access, create the logical meta model, and create the meta-data data is conducted.

8. Database Design

It starts from reviewing the data access requirements to know what are the things that the database needs. Then it continues to determining the aggregation and summarization requirements because data aggregation and summarization needs to be finalized first before committing to the final schema. The next steps are designing the BI target databases, designing the physical database structure, build the BI target databases, developing database maintenance structure, preparing to monitor and tune the database designs, preparing to monitor and tune the query designs.

9. ETL Design

This step is designing for ETL Process. The steps are: create the source-to-target mapping document, test the ETL tools functions, design the ETL process flow, design the ETL programs, and set up the ETL staging area.

10. Metadata Repository Design

After doing the analysis for developing a metadata repository, then process of designing is starting from design the metadata repository. It continues to install and test the metadata repository product, design the meta data migration process, and design the metadata application.

11. ETL Development

After the concept has been conceptualized the ETL development can be started. First build and unit test the ETL process. Then the integration or regression to test the ETL process, do performance test for ETL process, do quality assurance test, and acceptance test of the ETL process.

12. Application Development

In application development step, the application is being designed, build, until tested. Lastly, providing data access and analysis training.

13. Data Mining

Data mining is the process of finding useful information from a large size of data. To do data mining, the first thing to do is stating the business problem. Then collect the data, consolidate and cleanse the data, prepare the data, Build the analytical data model, interpret the data mining result, perform external validation of data mining results, and monitor the analytical data model overtime.

14. Metadata Repository Development

After being analyzed and designed, the development can be started. The steps need to be followed are: Build the metadata repository database, build and unit test the metadata migration process, build and unit test the metadata application, test the metadata repository programs or product functions, prepare the metadata repository for production, and provide metadata repository training.

15. Implementation

After all been installed then the implementation can be started. Planning the implementation is the first step needed, it sets the date and make sure everything needed is available. Then setting up the environment, install all the BI applications components, set up the production schedule, load the production databases, and prepare for ongoing support after the implementation.

16. Release Evaluation

After a period of time that have been agreed, release evaluation is needed to keep an eye to the implemented application so it can be tracked. Release evaluation may consist of some steps like prepare for the post implementation review, organize the post implementation review meeting, conduct the post implementation review meeting, and follow up the post implementation review [11].

4. Data Visualization

Having a massive number and complex types of data may seem very complicated for data owner, but the data is actually very profitable for the organization. The data can be analyzed by combining different variables and can give analytical views. This can be done by doing a visualization. Data visualization is the visualization of the information in graphs, charts or maps and it provides an easy way to understand the data [11]. By having the data visualized in some ways, it provides benefits such as improving decision making, better ad hoc data analysis, improve collaboration/information sharing, provide self-service capabilities to end users, increase return of investments (ROI), time savings, and reduced burden on IT [8].

Data visualization needs to pay attention on designing the visualization because the objective of visualizing the data is to make it easily understood but still give the important information. There are some ways to visualize the data:

1. Line graph

Gives information about relationship between items

2. Bar chart

Makes the comparison more visible

3. Scatter plot

Two-dimensional plot showing variations of two items

4. Pie chart

Compare parts of whole [12].

In its application, data visualization is very useful for helping the decision maker or executives to monitor the intrapreneurs regarding their progress, so the decision maker may be able to see it based on actual data that can be provided real time.

5. Data Mining

Data Mining as already mentioned, is the process of finding useful information from a large size of data. There are some techniques of data mining that can be use, classification, clustering, prediction, and association. In this research, using classification might be the best way to process the data. There are some methods like Decision Tree and Naïve Bayes that can be used to help make an insight for decision maker. Using those two methods can make a descriptive result to gain some insight. By using data mining, hopefully the decision maker makes better decisions that can make a great impact for the company.

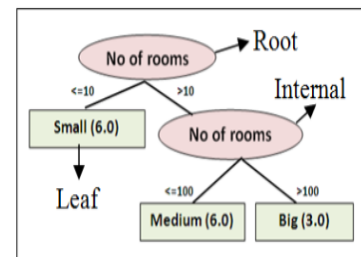


Figure 2: Decision Tree

6. Decision Tree

A decision tree is a decision support system that uses a tree-like graph decisions and their possible after-effect, including chance event results, resource costs, and utility. Decision Tree is one of the common classification methods that easy to interpret by human, and decision tree also known as a prediction method that using a tree structure or hierarchy structure. It's easy to classify the data using this method because the data will be classified into some groups which result a prediction.

There are some benefits that can be obtained of using decision tree:

1. Easy to understand
2. Can process various kind of data
3. Produce optimal result with less effort
4. Can be used in data mining packages over many kind of platforms

Figure 2.0 depicts the example of decision tree. It contains a root node, leaf nodes (classes), and internal nodes (test conditions applied on attributes). [13]

7. Naïve Bayes

The naïve Bayesian classifier is based on Bayes theorem and assumes that the effect of an attribute value on a given class is independent of the other attributes [14]. Naive Bayes is machine for probabilistic learning algorithm used to discriminate different

objects by many features. It can be used for wide classification task or high dimensional data. One of Naïve Bayes characteristic is a very strong assumption (naive) of independence from each condition / event.

Naïve Bayes classification algorithm also has several advantages such as easy to use and only requires one-time training data iteration but Naïve Bayes requires initial knowledge to be able to make decisions.

The Advantage of using this method is that it only requires slight of bunch data set to determine the estimated parameters that needed in the process of classification. Naive Bayes Classifier is considered to work very well compared to other classifier models, namely Naïve Bayes Classifier has a better level of accuracy than other classifier models.

8. Rule Based Reasoning

Rule Based Reasoning or RBR is one of important and complementary reasoning methodologies in artificial intelligent (AI) beside Case Based Reasoning. Rule Based Reasoning integration can manage to problem solving, in complex and real-world situation. Instead of predicting the outcomes, rule-based reasoning is more likely analyze the pattern of the data. This can be useful if the data that we have, has many different outcomes. RBR has the rule based by two major components: first, the knowledge based that consist of "IF... THEN..." to represent the knowledge. Second, the inference engine who contain some domain independence inference mechanisms.

The mechanism has two types which the forward chaining and backward chaining. In forward chaining, starting with data then look for rules which apply and often called data driven reasoning. For the backward chaining, it starts from the goals the look for the rules until the conclusion reached and sometimes called goal driven reasoning [15].

9. Problem Identification, Learning Objectives, Learning Significances

In the start of Intrapreneurship Program, all data that was obtained from the intrapreneurs, such as data about talent, ideas, and monitoring and evaluation, was collected, stored, and processed using Microsoft Excel. Microsoft Excel might be an adequate tool at first, because the data back then was probably not as much as it is now. As the data keeps growing, the management also need to obtain insights to help them make a good decision.

Every intrapreneur needs to get through a series of steps to be able to graduate from Intrapreneurship Programs and join the subsidiaries to adapt in their new environment to be able to scale up. In that process, Innovation Management needs to be keep informed about Intrapreneur's Performance in purposes of monitoring and evaluating the progress of Intrapreneur. At some point, in every monthly review, intrapreneurs will present their progress, and Innovation Management will make decisions regarding to Intrapreneur's performance whether they need to pass the intrapreneur team to the next stage or fail the intrapreneur team because they are proved to be not improving.

Up until now, management doesn't have the tool to monitor the Intrapreneur's progress or data clarity to support the decision making. With the Intrapreneur Dashboard, all the data will be

integrated and visualized in one place and the information will be easily accessed in real-time.

The implementation of Intrapreneur Dashboard for Innovation Management is expected to benefits Intrapreneurs itself. There are some problems obtained from the background:

1. Management doesn't have the tool to monitor the Intrapreneur's progress or data clarity to support the decision making

2. Management find it difficult to decide regarding the continuity status of Intrapreneur Team

Based on the identified problems, the objectives to be achieved from this learning are:

1. To help the decision maker (Innovation Manager) decide regarding continuity status of Intrapreneur based on data progress and data recommendation

2. To give the recommendation of which Intrapreneur that has the potential to pass the stage or not based on performance data

3. To help Innovation Management in monitoring performance of each Intrapreneur

4. To make visualization of information about Intrapreneur's progress and recommendation data in anytime that needed

The benefits expected from the objectives are:

1. Can monitor Intrapreneur with a dashboard that can provide information about the performance progress of each Intrapreneur Team and also recommendation data from the results of data processing using an algorithm

2. Overcome the problem of decision making regarding to Intrapreneur Team's continuity status

3. Overcoming the problem of data visualization to be more easily understood and can be seen at any time.

10. Conclusion

Having lots of data coming from many different sources can give some companies a distinct advantage, depends on how those companies collect and process those data. The data can be so worthwhile and give some insights if its properly processed. These insights can be obtained by using Decision Support System that can be useful to help decision makers making decisions based on data that can be considered.

Using data mining to process the data, evidently it makes the data more useful and gain more insights, such as giving the prediction and see the pattern of the data to give some information needed. After using data mining to process the data, we can visualize our data to make it more appealing and easier to understand.

People tend to see a visualization in order for them to understand what is the actual meaning of data. Data visualization can be displayed in different form depends on the data itself. Using a dashboard to visualize the data can be applied in order to present the data in the best way possible.

The research presented in this paper aims at improving the quality of dashboard for Innovation Management and using it for innovation manager to gain more insight, so they can make a firm decision regarding the continuity of Intrapreneur Team based on data. Also, by seeing the intrapreneur dashboard, it will be easier to monitor and track the progress of intrapreneurs.

Conflict of Interest

The authors declare no conflict of interest.

References

- [1]. Parker, Simon C. (2009) Intrapreneurship or entrepreneurship? *Journal of Business Venturing* 26 (2011) 19–34. doi:10.1016/j.jbusvent.2009.07.003
- [2]. Benitez-Amado, J., Llorens-Montes, F. J., & Nieves Perez-Arostegui, M. Information technology-enabled intrapreneurship culture and firm performance. *Industrial Management & Data Systems*, 110(4), 550–566. (2010) 561-562, doi:10.1108/02635571011039025
- [3]. Augusto Felicio, J., Rodrigues, R., & Caldeirinha, V. R. The effect of intrapreneurship on corporate performance. *Management Decision*, 50(10), 1717–1738. (2012) doi:10.1108/00251741211279567
- [4]. Zins, Chaim. (2007). Conceptual approaches for defining data, information, and knowledge. *JASIST*. 58. 479-493. 10.1002/asi.20508.
- [5]. Power, D. J. (2008). Understanding Data-Driven Decision Support Systems. *Information Systems Management*, 25(2), 149–154. doi:10.1080/10580530801941124
- [6]. Hand, D. J. (2013). *Data Mining*
- [7]. Chen, L.-D., Sakaguchi, T., & Frolick, M. N. (2000). Data Mining Methods, Applications, and Tools. *Information Systems Management*, 17(1), 65–70. doi:10.1201/1078/43190.17.1.20000101/31216.9
- [8]. Wang, L., Wang, G., & Alexander, C. A. (2015). Big Data and Visualization: Methods, Challenges and Technology Progress. *Digital Technologies*, 1(1), 33-38
- [9]. Pauwels, K., Ambler, T., Clark, B. H., LaPointe, P., Reibstein, D., Skiera, B., Wiesel, T. (2009). Dashboards as a Service. *Journal of Service Research*, 12(2), 175–189. doi:10.1177/1094670509344213
- [10]. Smith, V. S. (2013). Data Dashboard as Evaluation and Research Communication Tool. *New Directions for Evaluation*, 2013(140), 21–45. doi:10.1002/ev.20072
- [11]. *Business intelligence roadmap* 576 pages, Publisher: Addison-Wesley Professional; 1 edition (March 7, 2003), Language: English, ISBN-10: 0201784203, ISBN-13: 978-0201784206
- [12]. Sadiku, Matthew & Shadare, Adebawale & Musa, Sarhan & Akujuobi, Cajetan & Perry, Roy. (2016). DATA VISUALIZATION. *International Journal of Engineering Research and Advanced Technology (IJERAT)*. 12. 2454-6135.
- [13]. Mathuria, M., Bhargava, R., Sharma, G. B. N. (2013). Decision Tree Analysis on J48 Algorithm for Data Mining, 3(1). 1114-1119.
- [14]. NH Niloy, MAI Navid, Naïve Bayesian Classifier and Classification Trees for the Predictive Accuracy of Probability of Default Credit Card Clients, *American Journal of Data Mining and Knowledge Discovery*. Vol. 3, No. 1, 2018, pp. 1-12. doi: 10.11648/j.ajdmkd.20180301.11
- [15]. Dutta, S., & Bonissone, P. P. (1993). Integrating case- and rule-based reasoning. *International Journal of Approximate Reasoning*, 8(3), 163–203. doi:10.1016/0888-613x(93)90001-t

A Joint Source Channel Decoding for Image Transmission

Slim Chaoui^{*1,4}, Osama Ouda^{2,5}, Chafaa Hamrouni^{3,6}

¹College of Computer and Information Sciences, Dep. of Computer Engineering and Networks, Jouf University, Skaka, KSA.

²College of Computer and Information Sciences, Dep. of Computer Sciences, Jouf University, Skaka, KSA.

³Khurma University College, Dep. of Computer Sciences, Taif University, Khurma, KSA.

⁴Unit-Lab of Sciences of Electronics, Technologies of Information and Telecommunications, Sfax University, Sfax, Tunisia.

⁵Faculty of Computers and Information, Mansoura University, Mansoura, Egypt.

⁶REGIM-Lab, Sfax University, Sfax, Tunisia.

ARTICLE INFO

Article history:

Received: 23 August, 2019

Accepted: 24 October, 2019

Online: 09 December, 2019

Keywords:

Joint source-channel decoding

Arithmetic coding

Error resilience technique

Bit back-tracking

LDPC iterative decoding

ABSTRACT

In this paper, we present a joint source-channel decoding (JSCD) scheme for image transmission. The binary sequences, resulting from the compression of several number of image blocks using arithmetic coding (AC), are written line-wise in the so called read-matrix (RM). In succession, a systematic Low Density Parity Check (LDPC) encoding is applied to the sequence produced by the column-wise reading of the RM. The proposed approach to JSCD incorporates error-free AC-decoder information feedback and error-detection AC-decoder information feedback in each sub-sequence. An error resilience (ER) technique within AC provides whether the input sequence is correct or not and possibly identifies the corrupt segment. In case of error detection, the reliabilities of the bits in the AC decoder input stream are estimated involving the detection delay distribution of the erroneous symbols. This information is provided to the iterative LDPC decoder after a bit back-tracking stage. Experimental results show that the proposed JSCD scheme outperforms the separated source-channel model and reduces the number of decoding iterations.

1 Introduction

Joint source-channel coding and decoding are effective techniques to overcome the shortcomings of the separation theorem [1], and are emerging as a good choice to transmit digital data over wireless channels since the bandwidth limitations and the increased demands of multimedia transmission systems. Joint source-channel coding/decoding techniques are able to benefit from the residual redundancy of the source coding so as to improve the error resilience of the transmitted data.

Arithmetic coding [2] is widely adopted as entropy encoder in the latest compression standards such as JPEG2000, H.264/AVC, MPEG-4 and HEVC. Comparing to others, it achieves superior efficiency because non-integral number of bits can be allocated to each symbol [3, 4, 5] and adapts better

to adaptive data models. However, arithmetic codes are extremely vulnerable to any errors that occur if the transmitted symbols are affected by noise during transmission.

This issue has motivated standards such as JPEG2000 to include certain error resilience (ER) techniques and gave rise for the development of joint source-channel techniques dedicated for the AC-encoded data [6, 7]. ER techniques were applied to identify the corrupt segment of the AC code-stream. A common method for error detection in arithmetic coding was introduced in [8] where a non zero coding interval is reserved to a non coded symbol called forbidden symbol (FS). While decoding, if the FS is decoded, then an error in the received sequence is indicated. A study on the trade-off between the amount of added redundancy due to the FS and the amount of time required to detect an errors was proposed in [9]. In the works [10, 11], sequential decod-

*Slim Chaoui, College of Computer and Information Sciences, Department of Computer Engineering and Networks, Jouf University, Skaka, Kingdom of Saudi Arabia, +966538017567 & schaoui@ju.edu.sa

ing schemes were involved on binary trees and path pruning technique was applied relying on the FS error detection. In [11], Grangetto *et al.* have modeled arithmetic codes as state machines and a trellis representation for AC code with FS was used in conjunction with the maximum a-posteriori (MAP) decoding algorithm. The authors in [12] proposed a soft input soft output (SISO) arithmetic decoding where a FS-based ER technique was applied and a Chase-like algorithm was slightly modified to provide additional information on the reliability of the decoded bits. Practical implementations on the joint source-channel coding scheme with FS were studied in [13].

The iterative joint source-channel decoding (JSCD) was usually studied by making use of the channel observations and source information to improve the a-posteriori probabilities of each transmitted bit. This can be achieved through the repetitive update and adjustment of a-posteriori and extrinsic information on the one hand and source information on the other hand to achieve a better joint decoding error ratio. In [14], the extrinsic messages in the Turbo decoder are enlarged or reduced by means of the multiplication with a factor which depends on the channel conditions. In [15] channel adaptive plus or minus operations are made to modify the messages in LDPC decoder. Iterative JSCD based on bit flipping algorithms were proposed in [16, 12, 17] where a set of error patterns are generated by identifying the least reliable bits among the decoded sequence. Each test pattern is then checked for correctness by means of a verification code.

In this concern, we propose a JSCD algorithm that takes advantage of the error detection capability provided by the FS-based ER technique in the AC decoder to improve the error correction capability of the iterative message passing algorithm (MPA) used for Low Density Parity Check (LDPC) decoding. The iterative decoding procedure offers a convenient way to make use of the source information feedback provided by the ER technique.

In this study, the arithmetic coded sequences of a certain number of image blocks are written line-wise in the so-called read-matrix (RM). In succession, the RM is read column-wise to form the information input sequence of the LDPC encoder. It is worth to note that block partitioning is a common process in the image compression standards, such as in JPEG2000 and H264, and is justified by the average entropy decrease of the image especially when block transformation are employed. For instance discrete cosine transform is employed in JPEG-XR and HEVC and the discrete wavelet transformation in JPEG2000 and context-based compression algorithm, where the advantage of the correlation between neighboring image blocks is taken. With respect to error resilience, image partitioning is beneficial since error propagation may be prevented.

As a first contribution, the interplay between error detection position and bit reliabilities in the AC input code-stream is discussed and the error probability of each bit positioned before the detected error position is estimated. In this concern, a method for bit back-tracking is proposed which is of great importance in this work. It is worth to note that AC-

based error detection is performed in symbol-takt whereas channel decoding is processed in bit-takt, and hence, the feedback information from the AC decoder is transformed in bit-takt.

A second contribution is associated with the proposed approach to JSCD and consists on the way how to involve the estimated bits reliabilities from the AC decoder in the iterative LDPC decoder. The purpose of this approach is to increase the reliabilities of the error-free AC decoded segments and to reduce them in possibly corrupted segments. This is reached by the conditional update of the messages during the iterative process with respect to the AC decoding results. Experimental results have shown that the proposed JSCD scheme outperforms the Tandem decoding and bit-flipping based JSCD schemes in terms of peak signal-to-noise ratio (PSNR), as well as accelerates the iterative MPA process.

The rest of this paper is organized as follows. Section 2 presents the proposed source-channel encoding scheme. In section 3 an overview over the AC is given and the FS-based ER technique is analyzed in terms of bit error probability versus error detection delay. The proposed JSCD scheme is outlined in Section 4. Simulation results are reported in Section 5. Section 6 concludes this paper.

2 Proposed source-channel coding scheme and transmission model

The proposed encoding scheme at the transmitter is depicted in Figure 1. Applying AC over N_B equal size image blocks $\mathbf{S}_1, \dots, \mathbf{S}_{N_B}$ produces N_B compressed sequences $\mathbf{s}_1, \dots, \mathbf{s}_{N_B}$ which are written line-wise into the $K \times L$ matrix, the so-called read-matrix (RM). The number of image blocks invited to be written in the RM is variable and depends on the RM size, on the image block size and on the AC compression rate for each image block. In order to restrict the zero filling, the block sequences have to be chosen in such a way that the number of not occupied positions in the RM becomes as small as possible. Set partitioning method is applied for this purpose. The sequence resulting from the column-wise reading of the RM is fed into a LDPC systematic encoder. Let $\mathbf{c} = (c_1, \dots, c_{N_c})$ be the resulting LDPC codeword where N_c is the codeword length. The code bits of \mathbf{c} are mapped into modulated sequence \mathbf{x} . For simplicity, we consider a binary phase-shift keying (BPSK) modulation where the m^{th} modulated symbol in \mathbf{x} is given by $x_m = (1 - 2c_m)$, $1 \leq m \leq N_c$. The m^{th} symbol within the received sequence \mathbf{y} can be expressed as

$$y_m = \sqrt{P}x_m + n_m, \quad 1 \leq m \leq N_c, \quad (1)$$

where P is the received signal power at the receiver and n_m is the instantaneous additive noise which is modelled as zero-mean Gaussian random variable with variance σ_n^2 . In the sequel, we assume that P is unity. For a BPSK transmission the noise power is $E\{n^2\} = \sigma_n^2 = BN_0/2$, where B is the bandwidth of the passband signal and $N_0/2$ is the power spectral density per frequency unit of the white Gaussian noise. In

addition, we note that the zero forced bit may be not transmitted when assuming the knowledge of the AC coded sequences lengths at the receiver which may re-establishes the zeros at the non-transmitted positions.

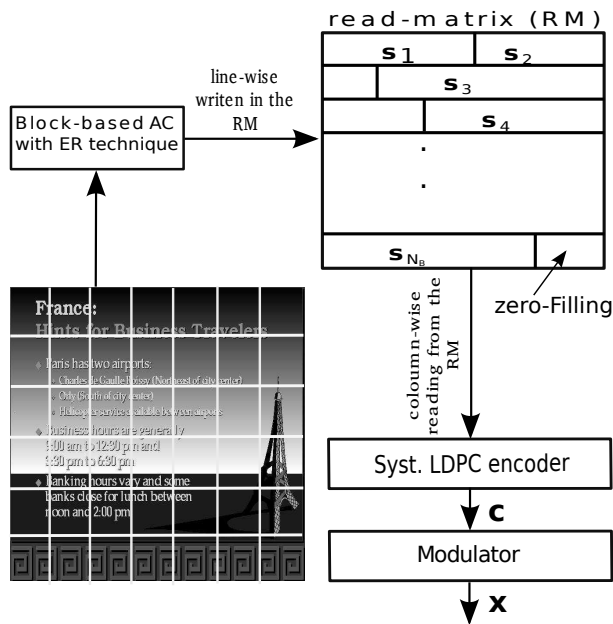


Figure 1: Proposed encoding scheme

For the purpose of the LDPC decoding, supplied by the MPA, the log-likelihood-ratio (LLR) of the m^{th} estimated code bit, $1 \leq m \leq N_c$, given the observation y_m at the destination is given by

$$\begin{aligned}
 L_m &= \log \frac{P(c_m = 0|y_m)}{P(c_m = 1|y_m)} \\
 &= \log \frac{P(y_m|c_m = 0)}{P(y_m|c_m = 1)} + \log \frac{P(c_m = 0)}{P(c_m = 1)} \\
 &= \frac{2y_m}{\sigma_n^2} + L_a(c_m),
 \end{aligned} \tag{2}$$

where $L_a(c_m)$ is the LLR corresponding to the *a-priori* information of the m^{th} estimated code bit.

3 Overview of AC and ER techniques

Let $\mathbf{S}_b = (S_{b,1}, \dots, S_{b,N_S})$ be the b^{th} image block sequence of N_S symbols from a finite alphabet $\mathcal{A} = \{a_1, \dots, a_{N_A}\}$ composed of N_A symbols. Arithmetic coding requires the probability distribution of the input sequence. The interval $[0,1)$ is divided into maximum N_A sub-intervals, each with length equal to the occurrence probability of the alphabet symbols in the sequence \mathbf{S}_b . The symbols $S_{b,1}, \dots, S_{b,N_S}$ are entered symbol by symbol to the arithmetic encoder. Let Low be the lower bound of the interval in which the symbol sequence so far is arranged and $Length$ be the interval length, which is the

product of the probabilities of all previous encoded symbols. Low and $Length$ are initialized to 0 and 1, respectively. To encode a symbol from the sequence \mathbf{S}_b , corresponding to the i^{th} symbol in \mathcal{A} , both Low and $Length$ must be updated. Low is refreshed by $Low + Length \sum_{j=1}^{i-1} f_{b,j}$ and $Length$ is replaced by

$Length f_{b,i}$, where $f_{b,j}$ is the probability of j^{th} symbol in the alphabet \mathcal{A} . After the entire sequence is arranged, it is uniquely specified by any value between Low and $High = Low + Length$. A number with the shortest binary representation in the interval will be transmitted. The most important advantage of AC is its optimality. AC is optimal in theory and is very nearly optimal in practice. In [18], it was shown that the required bit-size representing \mathbf{S}_b is upper bounded by:

$$\left\lceil -\log_2 \left(\prod_{s=1}^{N_S} f_{b,j(S_{b,s})} \right) \right\rceil + 2,$$

where $j(S_{b,s})$ corresponds to the position of the symbol $S_{b,s}$ in \mathcal{A} . The major drawback of such algorithm is that the encoding and decoding processes needs an infinite precision machine (values used for Low and $High$). This drawback was solved in [3], where the authors proposed the use of integer probabilities $F_{b,i} = N_S \cdot f_{b,i}$ and scaling techniques. The initial interval $[0,1)$ was substituted by $[0, W)$, where $W = 2^{Pr}$ and $Pr \geq 2$ is the bit precision of the initial interval.

In order to generate incremental output while encoding, the authors in [3] proposed the scaling method where the size of the interval $[Low, High)$ has to be doubled if one of the following conditions holds:

- $E_1 : 0 \leq High < W/2$:
 1. $Low \leftarrow 2 \cdot Low$
 2. $High \leftarrow 2 \cdot High + 1$
 3. $Output : 0$ followed by $Scale3$ ones
 4. $Scale3 \leftarrow 0$
- $E_2 : W/2 \leq Low < W$:
 1. $Low \leftarrow 2 \cdot (Low - W/2)$
 2. $High \leftarrow 2 \cdot (High - W/2) + 1$
 3. $Output : 1$ followed by $Scale3$ zeros
 4. $Scale3 \leftarrow 0$
- $E_3 : W/4 \leq Low < W/2 \leq High < 3W/4$:
 1. $Low \leftarrow 2 \cdot (Low - W/4)$
 2. $High \leftarrow 2 \cdot (High - W/4) + 1$
 3. $Output : no output$
 4. $Scale3 \leftarrow Scale3 + 1$

Note that $Scale3$ represents the number of the last E_3 scaling done and is initialized to 0.

3.1 Proposed bit back-tracking within AC decoding with ER technique

The concept of ER technique is usually deployed with AC for the purpose of error detection which can help to reconstruct the corrupted segments of a code-stream. As far as JSCD is concerned, the error propagation properties of AC with the deployed ER technique is worthy studying. An accurate location of the bit errors is generally unachievable when making use of a simple ER technique. AC-based error detection is accomplished in symbol-takt and channel decoding is processed in bit-takt, and hence, the feedback information from the AC decoder should be obviously transformed in bit-takt. This is referred to as bit back-tracking.

We note that the decoding process is similar to the encoding process, and hence the AC decoder will either decode no source symbol or it will decode one or more source symbols for each input bit as described in the encoding process. For the purpose of bit back-tracking, we first define the AC extended encoding/decoding step as follows:

Definition: The AC extended encoding/decoding step is the succession of concluded AC encoding/decoding steps producing at least one output symbol/one output bit with Scale3 is zero or reset to zero.

We note that a concluded AC decoding step is settled when the new subinterval is not entirely within one of the intervals $[0, 1/2)$, $[1/4, 3/4)$ or $[1/2, 1)$. At the t^{th} extended decoding step, the input bits located in the bit positions range ϕ_t produce output symbols located in the symbol positions range Φ_t . Up to now, let $\hat{\mathbf{u}}_{b,t}$ and $\hat{\mathbf{S}}_{b,t}$ denote the input bit sequence and the corresponding output symbol sequence at the t^{th} extended decoding step, respectively. The main idea in the following subsections is that if at least one bit in $\hat{\mathbf{u}}_{b,t}$ is erroneous, then at least one symbol in $\hat{\mathbf{S}}_{b,t}$ is erroneous. For implementation issue a stack can be accessed, where the t^{th} line contains the tuples $(\hat{\mathbf{u}}_{b,t}, \hat{\mathbf{S}}_{b,t})$. In order to elucidate the principle of AC extended encoding/decoding step and since encoding and decoding are similar, Table 1 illustrates an example of encoding a sequence $\mathbf{S} = \mathbf{abaac}$, where the symbols \mathbf{a} , \mathbf{b} and \mathbf{c} have the occurrence frequencies 20, 10 and 20, respectively, cumulative counts $\{\mathbf{a}, \mathbf{b}, \mathbf{c}\} = \{0, 20, 30, 50\}$ and $W = 256$. The first column is reserved for the extended encoding steps enumerator t .

For instance, at the third extended encoding step, \mathbf{aa} and $\mathbf{010}$ constitute the input symbol sequence and the corresponding output bit sequence, respectively.

3.2 Forbidden symbol technique and error detection delay distribution

Let ϵ be the probability of the FS in the interval $[0, 1)$ which is never encoded. The amount of generated redundancy due to the FS is $-\log_2(1 - \epsilon)$. Decoding the FS at the AC decoder is interpreted as an error detection.

Let $\psi_{b,p}$ be the event that the FS is first appeared at the p^{th} symbol position in the b^{th} AC-decoded sequence and let $\hat{S}_{b,p-d}$ be the decoded symbol at the $(p-d)^{th}$ symbol position, $1 \leq d \leq p$. The joint probability that the $(p-d)^{th}$ symbol is erroneous and the event $\psi_{b,p}$ occurs can be expressed by

$$P(\hat{S}_{b,p-d} \neq S_{b,p-d}, \psi_{b,p}) = A_p(1 - f_{b,S_{p-d}})(1 - \epsilon)^{d-1}\epsilon, \quad (3)$$

where S_{p-d} is the really transmitted symbol in the finite alphabet set and A_p is a normalization factor which depends on the position p . The probability given in (3) corresponds to the probability that a delay of d symbols is occurred before an error detection at the position p is performed. Thus, d is referred to as error detection delay.

Table 1: AC integer encoding of a sequence \mathbf{abaac} with cumulative counts $\{\mathbf{a}, \mathbf{b}, \mathbf{c}\} = \{0, 20, 30, 50\}$ and $W = 256$ showing the extended encoding steps.

t	\mathbf{S}_t	Low	High	\mathbf{u}_t	Scaling	Scale3
-	-	0	255	-	-	0
1	\mathbf{a}	0	101	$\mathbf{0}$	E_1	0
		0	203	-	-	0
2	\mathbf{b}	81	121	$\mathbf{0}$	E_1	0
		162	243	$\mathbf{1}$	E_2	0
		68	231	-	-	0
3	\mathbf{a}	68	132	-	E_3	1
		8	137	-	-	1
	\mathbf{a}	8	59	$\mathbf{01}$	E_1	0
		16	119	$\mathbf{0}$	E_1	0
		32	239	-	-	0
4	\mathbf{c}	156	239	$\mathbf{1}$	E_2	0
		56	223	-	-	0

For simplicity, we assume that the occurrence probabilities of the symbols in the alphabet set are near to the forbidden symbol probability. Hence, (3) can be approximately given by the following truncated geometric distribution:

$$P(\hat{S}_{b,p-d} \neq S_{b,p-d}, \psi_{b,p}) \approx A_p(1 - \epsilon)^d \epsilon, \quad (4)$$

where $A_p = 1 / \sum_{j=1}^p (1 - \epsilon)^j \epsilon$.

The error detection delay distribution in the presence of a FB-based ER technique is investigated. A single bit error is arbitrarily introduced at the input sequence. The number of decoded symbols before decoding the FS is recorded. The probability density functions (PDF) of the error detection delay for two FS probability values, namely $\epsilon = 0.1$ and $\epsilon = 0.2$, are plotted in Figure 2. The finding reveals that the geometric distributions with parameters $\epsilon = 0.1$ and $\epsilon = 0.2$ fit the measured PDFs of the error detection delay.

3.3 Bit error probability estimation from the FS-based ER technique in the AC decoder

In this subsection we intend to determine the error probability of the AC decoder input bits before detecting the FS. Let $\hat{\mathbf{S}}_{b,t}$ be the decoding result of the input bit sequence $\hat{\mathbf{u}}_{b,t}$ at the t^{th} extended decoding step and let ϕ_v and Φ_v be the

ranges of input bit positions and output symbol positions at the t^{th} extended decoding step, respectively. Within an extended decoding step, the AC encoding process is a one-to-one relationship between the input symbol sequence and the output bit sequence. Accordingly, if the decoded sequence $\hat{\mathbf{S}}_{b,t}$ is different from the correct one denoted by $\mathbf{S}_{b,t}$, then the input bit sequence $\hat{\mathbf{u}}_{b,\phi_t}$ is certainly erroneous. Hence, the joint probability that the input sequence $\hat{\mathbf{u}}_{b,t}$ is error prone and the event $\psi_{b,p}$ occurs can be given by

$$P(\hat{\mathbf{u}}_{b,t} \text{ is error prone}, \psi_{b,p}) = P(\hat{\mathbf{S}}_{b,t} \neq \mathbf{S}_{b,t}, \psi_{b,p}) \quad (5)$$

$$= \bigcup_{p-d \in \Phi_t} P(\hat{S}_{b,p-d} \neq S_{b,p-d}, \psi_{b,p}).$$

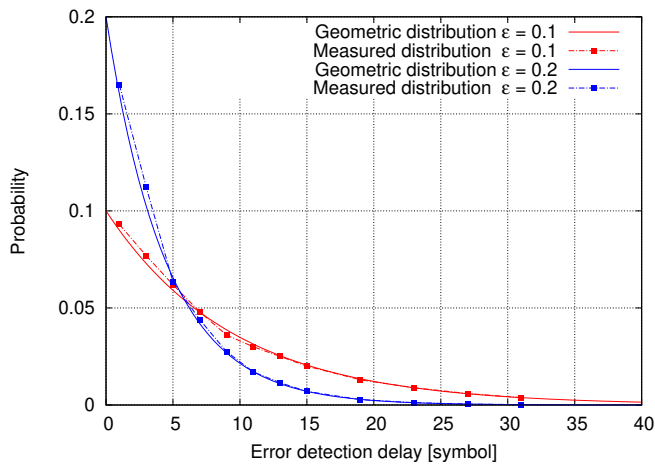


Figure 2: PDF of the error detection delay in the presence of a FS-based ER technique and comparison with the geometric distribution in (4) for $\epsilon = 0.1$ and $\epsilon = 0.2$.

Applying the approximation given in (4) and the pointcarré formula where all the multiplicative terms are neglected lead to the following approximation:

$$P(\hat{\mathbf{u}}_{b,t} \text{ is error prone}, \psi_{b,p}) \approx A_p \sum_{p-d \in \Phi_t} (1 - \epsilon)^d \epsilon. \quad (6)$$

Furthermore, the bit error probabilities in the bit range ϕ_t are assumed to be constant and denoted by $P_{e,t}$. This assumption reveals that the probability $P(\hat{\mathbf{u}}_{b,t} \text{ is error prone}, \psi_{b,p})$ can be approximately given the following expression:

$$P(\hat{\mathbf{u}}_{b,\psi_t} \text{ is error prone}, \psi_{b,p}) = \bigcup_{i \in \phi_t} P(\hat{u}_{b,i} \neq u_{b,i}, \psi_{b,p}) \approx |\phi_t| P_{e,t}. \quad (7)$$

where $|\phi_t|$ is the size of the bit range ϕ_t and $u_{b,i}$ is the correct bit at the input bit position i . From (6) and (7), the error probability of the bits in the input bit range ϕ_t can be approximately given by

$$P_{e,t} \approx \frac{1}{|\phi_t|} A_p \sum_{p-d \in \Phi_t} (1 - \epsilon)^d \epsilon \forall i \in \phi_t. \quad (8)$$

The bit error probability given in (8) is calculated within the AC decoding process so as to be involved in the JSCD as shown in the following section.

4 Iterative joint source-channel decoding

Error correction is usually done without taking into account any characteristics of the source data. This is attributable to the Shannon's well-known source and channel coding separation theory [19]. However, many works in the last decades have shown that considering these two parts jointly can help to enhance the error control performance of the whole system [20, 21].

In the proposed JSCD scheme the information from the ER-based AC decoder, in form of error probabilities of the bits within the corrupted segment, is involved in the decoding process. The main purpose of this strategy is to increase the bit-wise reliabilities of the error-free AC decoded segments and to reduce them in possibly corrupted bit segments. The JSCD scheme is illustrated in Figure 3. The systematic nodes in the Tanner graph correspond to the input bits of the different AC decoders. Let $q_{vr}^{(l)}$ denotes the message passing from the variable node v to the check node r at the l^{th} round and represents the probability of $c_v = 0$ given the channel observation y_v , messages from all check nodes linked to the message node v except the check node r ($r' \in C_v \setminus r$) and the check equation \mathcal{E}_v involving the variable node v .

The corresponding log-likelihood ratio can be expressed by the following expression:

$$L_{vr}^{(l)} = \log \frac{q_{vr}^{(l)}(0)}{q_{vr}^{(l)}(1)}$$

$$= \log \frac{P(c_v = 0 | y_v, L_{r'v}^{(l-1)} : r' \in C_v \setminus r, \mathcal{E}_v)}{P(c_v = 1 | y_v, L_{r'v}^{(l-1)} : r' \in C_v \setminus r, \mathcal{E}_v)}$$

$$= \begin{cases} L_v & \text{if } l = 0 \\ L_v + \sum_{r' \in C_v \setminus r} L_{r'v}^{(l-1)} & \text{if } l \geq 1 \end{cases}, \quad (9)$$

where L_v is the LLR of the estimated code bit \hat{c}_v conditioned on its observed value y_v , as given in equation (2), $L_{r'v}^{(l-1)}$ is the LLR message passed from the check node r' to the variable node v at the $(l-1)^{th}$ round that the check equation in r' is satisfied given the code bit c_v and the messages from all variable nodes linked to check node r' except the variable node v ($v' \in V_r \setminus v$). $L_{r'v}^{(l-1)}$ is defined as follows [22]:

$$L_{rv}^{(l-1)} = \log \frac{1 + \prod_{v' \in V_r \setminus v} \tanh(L_{v'r}^{(l-1)}/2)}{1 - \prod_{v' \in V_r \setminus v} \tanh(L_{v'r}^{(l-1)}/2)}. \quad (10)$$

The estimated hard code bit \hat{c}_v at the l^{th} round is given by

$$\hat{c}_v^l = \begin{cases} 0 & \text{if } L_v^{(l)} = L_v + \sum_{r' \in C_v} L_{r'v}^{(l-1)} \geq 0 \\ 1 & \text{if } L_v^{(l)} = L_v + \sum_{r' \in C_v} L_{r'v}^{(l-1)} \leq 0 \end{cases} \quad (11)$$

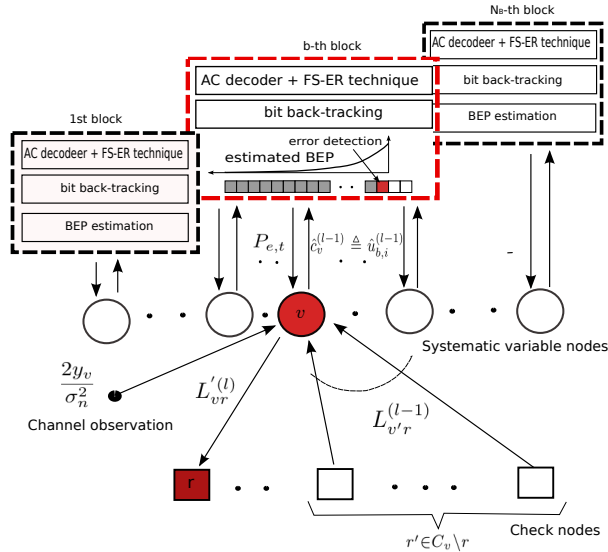


Figure 3: Joint Source-Channel Decoding scheme.

Let $\hat{c}_v^{(l-1)}$ corresponds to the i^{th} estimated information bit $\hat{u}_{b,i}^{(l-1)}$ in the b^{th} AC decoder input sequence $\hat{\mathbf{u}}_b^{(l)}$ at the $(l-1)^{th}$ iteration, in other words $\hat{c}_v^{(l-1)} \triangleq \hat{u}_{b,i}^{(l-1)}$. The correspondence between the code bit position v and the information bit position i in the b^{th} input sequence is ensured according to the read write process in the RM. The AC decoder in the b^{th} block performs error detection using the FS-based ER technique as described above. We distinguish two cases depending on the AC decoding results. The first case holds when AC error-free decoding is performed, in other words no FS is decoded. Let $\psi_{b,corr}^{(l-1)}$ be the event when no error is detected while AC decoding of the b^{th} input sequence at the $(l-1)^{th}$ round. For these bits, the message passing from the variable node v to the check node r is modified according to the following expression:

$$L'_{vr}{}^{(l)} = \log \frac{P(c_v = 0 | y_v, L_{r'v}^{(l-1)} : r' \in C_v \setminus r, \mathcal{E}_v, \psi_{b,corr}^{(l-1)})}{P(c_v = 1 | y_v, L_{r'v}^{(l-1)} : r' \in C_v \setminus r, \mathcal{E}_v, \psi_{b,corr}^{(l-1)})} \sim (1 - 2\hat{c}_v^{(l-1)})A, \quad (12)$$

where A is a large positive value. These bits in correct decoding passes are now disclosed to the channel decoder, and they can support decoding other undetermined bits involved in the same check equations.

The second case holds when a FS at the position p at the $(l-1)^{th}$ round is detected. Let $\psi_{b,p}^{(l-1)}$ denotes this event and let $\hat{E}_{b,p}$ denotes the estimated bit-end position corresponding

to the detected FS position. At this stage a bit back-tracking effort must be made to resolve the bit positions from the corresponding symbol position as described in subsection 3.1. The Bit error probability (BEP) of each information bit $u_{b,i}$, at the positions i before $\hat{E}_{b,p}$ is estimated according to (8) and is denoted by $P_{e,t}^{(l-1)}$, where t is the extended decoding step corresponding to the bit position i , in other words $i \in \phi_t$. No information about the input bits at positions after $\hat{E}_{b,p}$ is provided. The estimated $P_{e,t}^{(l-1)}$ corresponds to bit error probability of the systematic variable node c_v . The conventional message $L_{vr}^{(l)}$ passing from the variable node v to the check node r at the l^{th} iteration is given in (9). The updated message from the variable node v conditioned on the event $\psi_{b,p}^{(l-1)}$, which returns due to the independence between the AC decoder input bits to the conditioning on the estimated bit error probability $P_{e,t}^{(l-1)}$, is calculated as follows:

$$\begin{aligned} L'_{vr}{}^{(l)} &= \log \frac{P(c_v = 0 | y_v, L_{r'v}^{(l-1)} : r' \in C_v \setminus r, \mathcal{E}_v, \psi_{b,p}^{(l-1)})}{P(c_v = 1 | y_v, L_{r'v}^{(l-1)} : r' \in C_v \setminus r, \mathcal{E}_v, \psi_{b,p}^{(l-1)})} \\ &= \log \frac{q_{vr}^{(l)}(c_v = 0 | P_{e,t}^{(l-1)})}{q_{vr}^{(l)}(c_v = 1 | P_{e,t}^{(l-1)})} \\ &= \log \frac{q_{vr}^{(l)}(c_v = 0)(1 - P_{e,t}^{(l-1)}) + q_{vr}^{(l)}(c_v = 1)P_{e,t}^{(l-1)}}{q_{vr}^{(l)}(c_v = 0)P_{e,t}^{(l-1)} + q_{vr}^{(l)}(c_v = 1)(1 - P_{e,t}^{(l-1)})} \\ &= \log \frac{(1 - P_{e,t}^{(l-1)})e^{L_{vr}^{(l)}/2} + P_{e,t}^{(l-1)}e^{-L_{vr}^{(l)}/2}}{(1 - P_{e,t}^{(l-1)})e^{-L_{vr}^{(l)}/2} + P_{e,t}^{(l-1)}e^{L_{vr}^{(l)}/2}} \end{aligned} \quad (13)$$

Applying the aforementioned change to all bit prior the error detection position could lead to weakening strong bits. To cope with this, it is convenient to limit the reliability change to the most unreliable bits. For this purpose, let Q be the random variable which characterizes the rank of ascending reliabilities $L_v^{(l)}$ in (11) of erroneous bits. For example, $Q=5$ means that the fifth least reliable bit is erroneous. Figure 4 shows the distribution of Q for the signal to noise ratio (SNR) levels per source information bit $E_b/N_0 = 2, 3, 4$ and 5 , and emphasizes that the rank of the most unreliable bits where errors occur is limited by a specific value denoted by Q_L that is considered as a parameter in the decoding process so as to limit the set of modified messages and hence to preserve strong bits. The value of Q_L will be fixed experimentally.

5 Simulation results

In this section we demonstrate the performance of the proposed JSCD scheme. Simulation studies are performed using a LDPC code of length $N_c = 40000$ and rate $1/2$ with parameters $(3, 6)$. The outputs of the LDPC encoder are BPSK modulated and transmitted over the additive white Gaussian noise channel. We have tested our JSCD scheme using image block sizes of 16×16 and RM size of 200×100 . The

512 × 512 Washsat image, initially coded at 8 bit per pixel (bpp), compressed at 5.52 bit per pixel (bpp), is considered as test image. Mean-squared error (MSE) values of decoded image are averaged over 1000 independent image transmissions at desired signal to noise ratio level. The average MSE is then converted to PSNR. The absolute value A of the LLRs in (12), corresponding to the segment of bit-streams that do not cause error detection, should be set to arbitrarily high values. In this work the value of A is set to 10. As a consequence, these bits are recognized as very reliable during the subsequent LDPC iteration.

First of all, the aforementioned value Q_L is examined. Q_L is the number of the most unreliable bits where errors occur and is dependent on the received SNR level per source information bit E_b/N_0 since the absolute value of LLRs become an increasingly significant reliability indicator as SNR increases. Figure 5 shows the PSNR evolution of the proposed JSCD scheme for E_b/N_0 of 1, 2, 3 and 4 dB as a function of Q_L . The figure shows that the best PSNR performance is given for a certain Q_L value. For instance, for $E_b/N_0 = 3$ dB, the best Q_L value is 4. It is worth noting that the higher the SNR level is, the smaller Q_L is.

The performance of the proposed JSCD scheme is compared to that of the Tandem decoding scheme using soft input channel decoding and conventional arithmetic decoding. The PSNRs of the reconstructed images versus E_b/N_0 are illustrated for the two schemes in Figure 6.

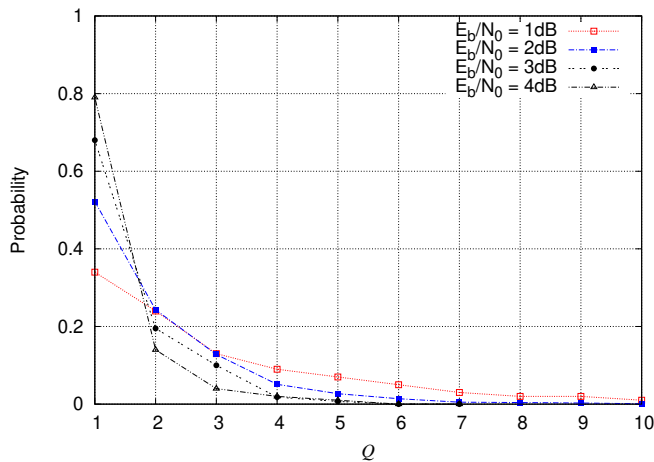


Figure 4: Distribution of the rank of ascending reliabilities' erroneous bits for $E_b/N_0 = 1, 2, 3$ and 4 dB, .

It is worthy to remark that gains are obtained in terms of average PSNR throughout the SNR per source information bit range. In fact the proposed JSCD scheme exhibits PSNR gains of ~ 4.5dB, ~ 8dB and 4.5 dB over the Tandem decoding scheme at the SNRs 2dB, 3dB and 4dB, respectively. The proposed method adds AC decoding operations to each iteration, this can lead to a decoding complexity increase, which is obvious by JSCD subjects. This complexity rise could be balanced out by the suppression of the iteration number. Figure 7 illustrates the mean number of iterations needed for the proposed JSCD scheme as well as for the separated model.

It is obvious that the proposed JSCD system requires less decoder iterations, which means that the required decoding time can be reduced. The decoding iteration number gain can be achieved by as much as 13.8% to 22.18% in the range of E_b/N_0 between 1 and 2 dB.

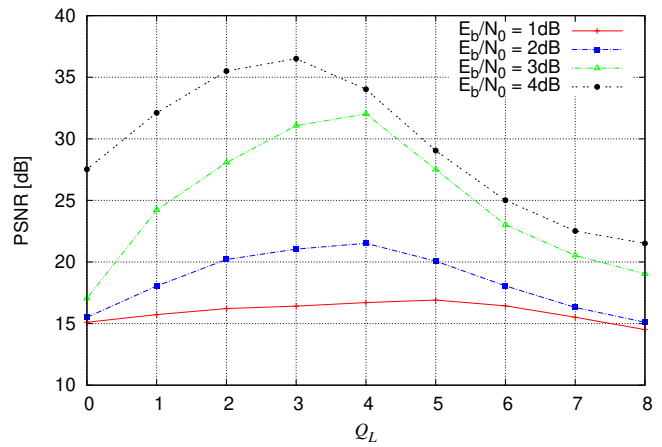


Figure 5: Average PSNR evolution versus Q_L for $E_b/N_0 = 1, 2, 3$ and 4 dB.

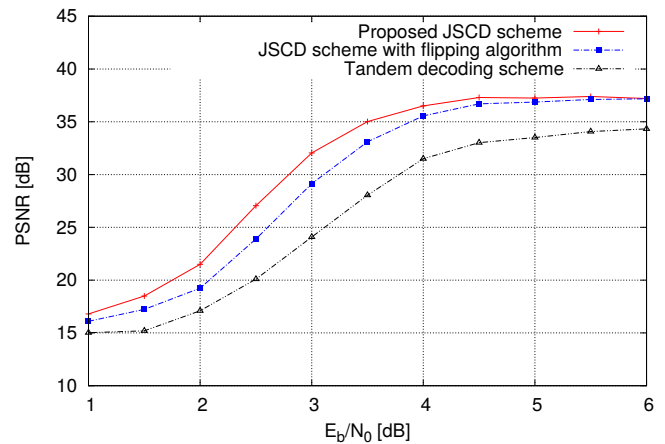


Figure 6: Average PSNR evolution versus E_b/N_0 of the proposed JSCD scheme with $\epsilon = 0.2$, Tandem decoding scheme and JSCD scheme with bit flipping algorithm.

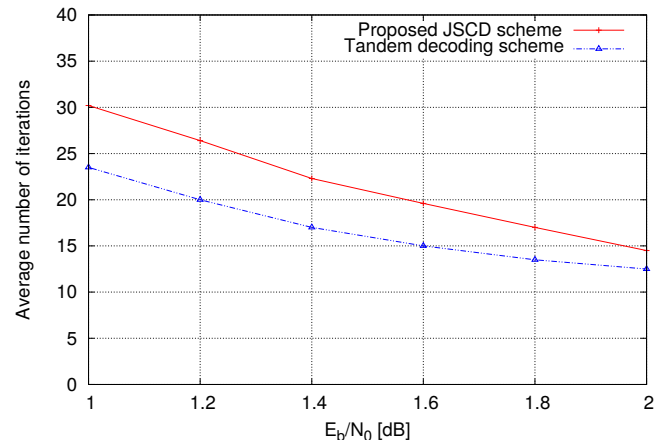


Figure 7: Average number of iterations of the proposed JSCD scheme and Tandem decoding scheme.

The results reported in the performed simulations show that the proposed JSCD outperforms standard separated scheme. On the other hand, the optimal choice of the system parameters remains an open issue; in fact, given a channel SNR, the error correction performance depends on the parameters such as FS probability ϵ , RM size, image block size. A large value of ϵ means more coding redundancy and assures a faster error detection. The value of ϵ is chosen as a trade-off between coding efficiency and error detection. One could look through simulations for a value achieving the best performance; since analytical performance bounds for the JSCD is very exhaustive. Figure 8 shows that the best JSCD performance is obtained with a value of $\epsilon = 0.2$. In fact, the increase of ϵ from 0 to 0.2 gives a PSNR gain of ~ 8 dB for $E_b/N_0 = 3$ dB. Furthermore, a suitable choice of the RM size could lead to a well distribution of the strong bits over the whole LDPC decoder input sequence. Strong bits could be detected from the correct AC-decoded segments.

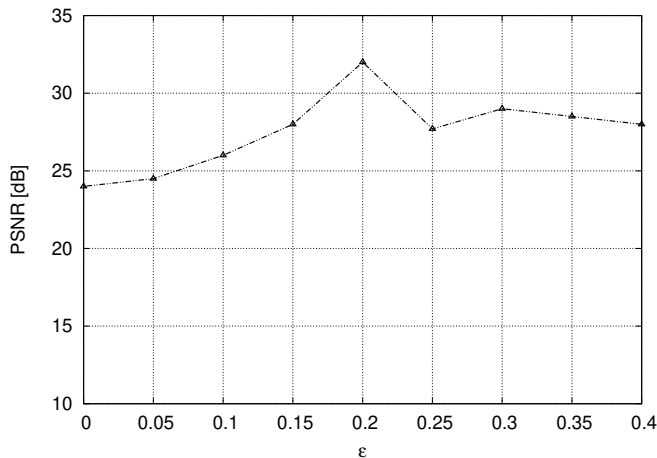


Figure 8: Average PSNR versus FS probability ϵ for $E_b/N_0 = 3$ dB.

As mentioned in the introduction, we compare the performance of the proposed JSCD scheme with that of the JSCD using the bit flipping algorithm. Such a bit-flipping idea has been used in various joint source-channel decoding approaches as in [16, 12, 17]. It consists on the flipping of the last Q unreliable bits. From these least reliable Q positions, one generate $2^Q - 1$ different error patterns. A candidate codeword is given by flipping the non-null bits in the error pattern. If no error detection is verified, the process stops. We note that no image partitioning is carried out during the bit flipping algorithm. A huge number of iterations could arise since 2^Q error patterns must be tested for each image block. To cop with this, a single AC encoding operation was performed on the source message. In this work Q is set to 4. The results reported in Figure 6 allow us to appreciate the gain offered up to a certain SNR.

6 Conclusion

In this paper, we proposed a JSCD scheme for image transmission. An error resilience technique was applied with AC and

the interaction between error detection position and bit reliabilities in the AC input code-stream was discussed. The proposed approach to JSCD incorporates error-free AC-decoder information feedback and error-detection AC-decoder information feedback. In case of corrupted segments, bit backtracking is performed and bits reliabilities are estimated depending on the symbol error position. We have shown how the reliabilities of the bits in the AC decoder input stream are involved in the iterative MPA algorithm. The results show that the proposed scheme at low-to-medium SNRs outperforms the separate source-channel model by approximately 4 to 8 dB with respect to PSNR and reduces the average number of iterations.

Acknowledgment The authors would like to thank the Deanship of Scientific Research at Jouf University for providing the financial support for publishing this work.

References

- [1] S. Vembu, S. Verdu and Y. Steinberg, "The source-channel separation theorem revisited" IEEE Transactions on Information Theory, **41**(1), 44-54, 1995. DOI: 10.1109/18.370119
- [2] J. Rissanen and G.G. Langdon, "Arithmetic coding" IBM Journal of research and development, **23**(2), 149-162, 1979. DOI: 10.1147/rd.232.0149
- [3] I.H. Witten, R.M. Neal and J.G. Cleary, "Arithmetic coding for data compression" Communications of the ACM, **30**(6), 520-540, 1987.
- [4] A. Moffat, R.M. Neal and I.H. Witten, "Arithmetic coding revisited" ACM Transactions on Information Systems (TOIS), **16**(3), 256-294, 1998. DOI: 10.1145/290159.290162
- [5] P.G. Howard and J.S. Vitter, Practical implementations of arithmetic coding In Image and text compression, Springer, Boston, MA, 1992.
- [6] I. Moccagatta, S. Soudagar, J. Liang and H. Chen, "Error-resilient coding in JPEG-2000 and MPEG-4" IEEE Journal on Selected Areas in Communications, **18**(6), 899-914, 2000. DOI: 10.1109/49.848245
- [7] K. Kamaras, JPEG2000 image compression and error resilience for transmission over wireless channels, NAVAL POSTGRADUATE SCHOOL MONTEREY CA, 2002.
- [8] C. Boyd, J.G. Cleary, S.A. Irvine, I. Rinsma-Melchert and I.H. Witten, "Integrating error detection into arithmetic coding" IEEE Transactions on Communications, **45**(1), 1-3, 2000. DOI: 10.1109/26.554275
- [9] J. Chou and K. Ramchandran, "Arithmetic coding-based continuous error detection for efficient ARQ-based image transmission" IEEE Journal on Selected Areas in Communications, **18**(6), 861-867, 2000. DOI: 10.1109/49.848240
- [10] B.D. Pettijohn, M.W. Hoffman and K. Sayood, "Joint source/channel coding using arithmetic codes" IEEE Transactions on Communications, **49**(5), 826-836, 2001. DOI: 10.1109/26.923806
- [11] M. Grangetto, P. Cosman and G. Olmo, "Joint source/channel coding and MAP decoding of arithmetic codes" IEEE Transactions on Communications, **53**(6), 1007-1016, 2005. DOI: 10.1109/TCOMM.2005.849690
- [12] S. Zaibi, A. Zribi, R. Pyndiah and N. Aloui, "Joint source/channel iterative arithmetic decoding with JPEG 2000 image transmission application" EURASIP Journal on Advances in Signal Processing, (1), 114, 2012. DOI: 10.1186/1687-6180-2012-114
- [13] W. Zhang, F. Cen and F. Zhu F, Research on practical implementation of binary arithmetic coding with forbidden symbol for error resilience, In Frontiers in Computer Education, Springer, Berlin, Heidelberg, 2012.
- [14] Z. Peng, Y.F. Huang and D.J. Costello, "Turbo codes for image transmission-a joint channel and source decoding approach" IEEE Journal on Selected Areas in Communications, **18**(6), 868-879, 2000. DOI: 10.1109/49.848241

- [15] W. Liu and DG. Daut, "Progressive image transmission based on joint source-channel decoding using adaptive sum-product algorithm" *Journal on Image and Video Processing*, (1), 18-18, 2007. DOI: 10.1155/2007/69805
- [16] B. Zheng and S. Gao, "A soft-output error control method for wireless video transmission" in 2016 8th IEEE International Conference on Communication Software and Networks (ICCSN), Jun 2016. DOI: 10.1109/ICCSN.2016.7586585
- [17] T. Tonnellier, C. Leroux, B. Le Gal, B. Gadat, C. Jégo C and N. Van Wambeke, "Lowering the error floor of turbo codes with CRC verification" *IEEE Wireless Communications Letters*, 5(4), 404-407, 2016. DOI: 10.1109/LWC.2016.2571283
- [18] PG. Howard and JS. Vitter, "Arithmetic coding for data compression" *Proceedings of the IEEE*, 82(6), 857-865, 1994. DOI: 10.1109/5.286189
- [19] CE. Shannon, "A mathematical theory of communication" *Bell system technical journal*, 27(3), 379-423, 1948. <https://doi.org/10.1002/j.1538-7305.1948.tb01338.x>
- [20] JL. Massey, Joint source and channel coding, MASSACHUSETTS INST OF TECH CAMBRIDGE ELECTRONIC SYSTEMS LAB, Sep 1977.
- [21] J. Hagenauer, "Source-controlled channel decoding" *IEEE Transactions on Communications*, 43(9), 2449-2457, 1995. DOI: 10.1109/26.412719
- [22] A. Shokrollahi, LDPC codes: An introduction Digital Fountain, Inc., Tech. Rep, 2003.

Integration of Third-Party Routing Stack to NetScaler CPX

Shreyas K K^{*1}, Abhishek H P¹, Sneha M¹, Shobha G¹, Deepak Kumar²

¹Department of CSE, R. V. College of Engineering, 560059, India

²Network Professional, Citrix Systems, Bangalore, 560059, India

ARTICLE INFO

Article history:

Received: 26 August, 2019

Accepted: 16 November, 2019

Online: 05 December, 2019

Keywords:

Application Delivery Controller

Quagga

Virtual IP

NetScaler CPX

Route Health Injection

Border Gateway Protocol

ABSTRACT

The Citrix NetScaler CPX, is one of the many Application Delivery Controllers (ADCs), which is used mainly for load balancing between the application servers in a datacenter network. ADCs are typically placed in the demilitarized zone in an organization's network, handling the connectivity of the external clients to the organization's servers. While performing load balancing between the servers, there is need for better routing between application servers. Route Health Injection (RHI) delegates the control of routing protocol announcement to a server based on the health of a service and the connectivity of the server to the network. This paper discusses on how the current version of NetScaler CPX is integrated with a third-party routing stack, Quagga, to enable the connectivity of the clients to the servers, with the additional feature of Route Health Injection (RHI) for better routing.

1. Introduction

Application delivery controllers (ADC) [1], which are widely deployed as a key fixture in the enterprise, help applications adapt to the networks and protocols that are in place today. ADCs can help ensure high availability of applications by providing seamless failover. This is done by balancing application workloads across a cluster of active servers in one or multiple sites.

One side of the ADC is the server farm capable of providing services and the other side is the Internet with clients and routers. A group of servers providing the similar service can be pooled and assigned a single Virtual Internet Protocol (VIP) address. This enables load balancing the incoming request among one of the servers in the pool.

NetScaler is available as a physical appliance or as software appliance. It supports a varied functionality including load balancing, SSL offloading, HTTP compression, content filtering, etc. NetScaler CPX [2] brings the power of advanced L4-7 application delivery services to containerized microservices infrastructures [3].

Route Health Injection (RHI)[4] allows a router to publish a host route to a globally distributed website. Normally, an IP address must exist on a single host in the Internet. However, with

global server load balancing, the same IP address can exist on multiple machines using the Virtual IPs. Thus, a VIP is an IP address that will associate to real servers attached to the load balancer.

In a normal configuration, a router may have multiple paths to the VIP corresponding to a server site. But the router chooses the path with minimum cost. The router's behavior works well when all the servers are available. In case of a failure of the service at a particular site, the VIP must no longer be visible to the rest of the network.

However, if the gateway routers advertise the network routes rather than host routes, then even if the VIP is down, the router still advertises the network to which the VIP belongs, thus leading a path to an unavailable server.

To avoid this problem, only the host route of the servers can be advertised instead of the network route. As a result, paths to the website those are no longer available ages out of the routing tables and only the paths to the available sites exists.

Figure 1 shows an example topology wherein there are two sites serving the same website. When the site at location 1 fails, then the request is routed to the VIP of servers at location 2.

An ADC must be able to take smart real time decisions based on the status/availability of the backend servers. It must effectively

* Shreyas K. K., Bangalore, Contact: 6360441200, shreyaskk97@gmail.com

divert traffic from any non-responsive backend server and continue to send that traffic to an alternate load balanced server that is available. The decision of advertising and removing a VIP to/from the downstream routers is made based on the availability of a VIP.

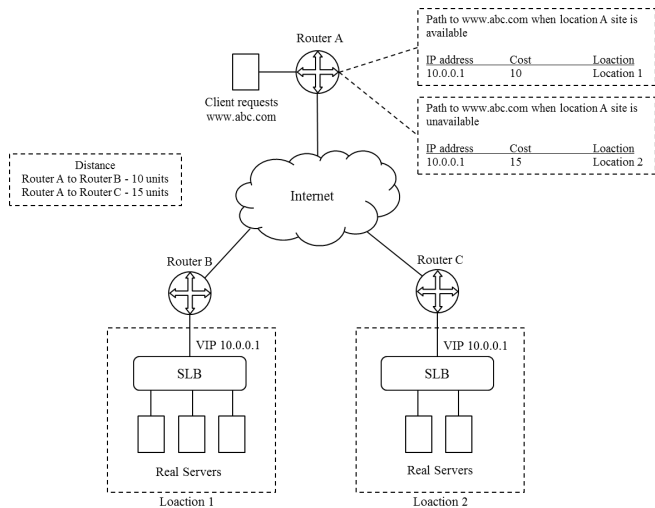


Figure 1: RHI example

To demonstrate the routing in our environment, we use a routing software package Quagga [5] that provides the features of TCP/IP based routing services. It supports routing protocols such as RIP, OSPF, BGP, IS-IS, etc. In addition to the IPv4 support, Quagga also provides support to the IPv6 routing protocols. Quagga is distributed under the GNU General Public License.

2. Existing System

Hogge, Jr. et al. [6] described the use of route health injection using the OSPF protocol. It explains the use of RHI in mobile SMS and MMS technology. SMS and MMS require the Short Message Service Center (SMSC). It explains the advantages of using redundant message servers. The primary message service center and the secondary message service center are typically distributed globally. When the primary service center faces a catastrophic failure, the secondary or the redundant service center is used to serve the SMS and MMS requests.

Naseh et al. [7] describes the technique of having active/standby data center to achieve high availability of applications. In normal conditions, the primary data center is functional and the secondary data center monitors the state of the primary data center. When the primary data center fails, the secondary data center injects the IP address to the Internet and makes the service. Now, any requests from the clients that arise are directed to the secondary data center. This illustration is an example of RHI used for availability in case of a disaster.

Clients request the VIP for a service. The request is then forwarded to one of the physical server based on a load balancing algorithm [8] that runs on the ADC (for example, the ADC might use Round Robin method of allocating user requests in a circular fashion). It is required to make an end to end connection from the client to the servers through the VIP. Thus, a routing stack has to be integrated in the NetScaler CPX, which makes this connection possible. Along with the integration of a routing stack, it will

obviously be an added benefit to implement the Route Health Injection (RHI) functionality, wherein, only the active VIPs are advertised to the downstream routers and the inactive ones are removed, hence increasing the overall response time.

The objective is to develop a web application which does the following: monitor the health of NetScaler CPX VIPs, and inject the route using open-source routing engine.

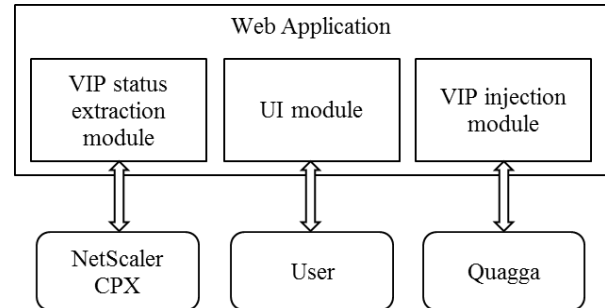


Figure 2: System block diagram

3. Proposed Methodology

To achieve the main objective of establishing an end to end connectivity of the clients to the VIP, the NetScaler CPX is integrated with a routing system as shown in Figure 2. The system is composed of the NetScaler CPX container, a routing engine called Quagga, and a web application. The web application is developed to communicate to NetScaler CPX on one side and the routing engine on the other. The VIP statuses are retrieved from the NetScaler through the VIP extraction module and are parsed to determine its state. The main function of active VIPs injection and inactive VIPs removal is handled next.

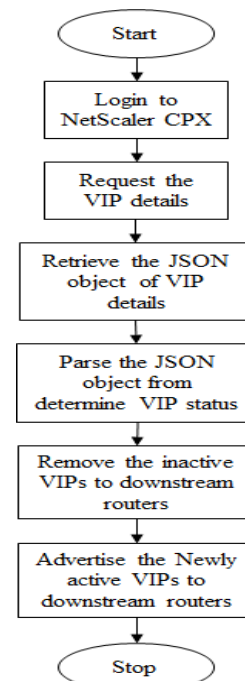


Figure 3: Flowchart of the system

The VIP injection module handles the task of advertising/removing VIPs to/from the local Quagga routing engine. The active VIPs are advertised as host routes to the routing

table if they aren't previously advertised. The inactive VIPs are removed from the routing table if they previously existed. The user can view the details of the active and inactive VIPs through the UI module.

The VIP details are to be retrieved from NetScaler CPX. A request from the web application is sent to NetScaler CPX asking for the VIP details. NetScaler CPX bundles the VIP details in an JSON object and delivers to the web application. The JSON object containing the VIP details are parsed to determine the VIP status. All the inactive VIPs are removed from the local routing table. All the recently active VIPs are advertised to the local routing table.

The BGP further handles the task of updating the routing tables of all neighboring routers and hence, assuring that only the active VIPs are visible throughout the network. The flow of the system is shown in Figure 3.

4. Experimental Analysis and Discussion of Results

The project is based on a system to make connectivity from the clients to the services. Hence, there is no specific evaluation metrics used. The only possible evaluation criteria used to verify the system is the connectivity of the client to the VIP. The system is checked with the existence of connectivity from the clients to the VIPs. It is also verified that only the active VIPs are visible and the inactive ones are not.

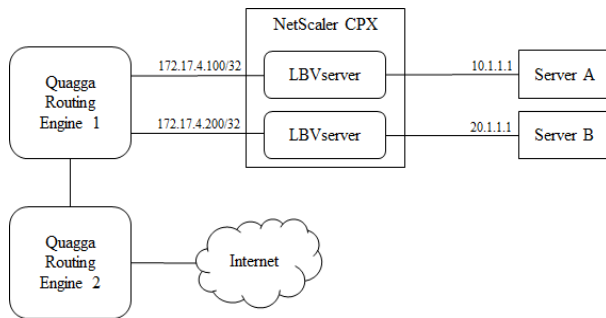


Figure 4: Sample Topology with NetScaler CPX

Consider a simple topology depicted in Figure 4 with NetScaler CPX connected to two servers.

The physical IP addresses of server A and server B are 10.1.1.1/24 and 20.1.1.1/24 respectively. The physical servers are logically grouped based on the service they provide. Hence, the clients have a logical view of the servers. In our case, server1 and server2 are the logical group of servers. The VIPs of server1 and server2 are 172.17.4.100/32 and 172.17.4.200/32 respectively.

Server Name	IP Address	State	Total packets sent	Packet received rate	Packet sent rate
server1	172.17.4.100	UP	0	0	0
server2	172.17.4.200	DOWN	0	0	0

Figure 5: Web Application – VIP Published

The Quagga routing engine 1 is local to the NetScaler CPX and Quagga routing engine 2 is used to verify the route publishing.

The following two cases illustrate the routing table contents of Quagga Routing Engine 2 which demonstrates the route advertising and removal.

If VIP is UP - VIP 172.17.4.100 is UP and it is published to all neighboring routers' routing table. Any request to the VIP will be reachable. The web application is shown in Figure 5 and the routing table in Figure 6.

```

bgpd> show ip bgp
BGP table version is 0, local router ID is 2.2.2.2
Status codes: s suppressed, d damped, h history, * valid, > best, = multipath,
               i internal, r RIB-failure, S Stale, R Removed
Origin codes: i - IGP, e - EGP, ? - incomplete

   Network        Next Hop        Metric LocPrf Weight Path
* > 0.0.0.0        10.1.1.1        600             0 100 ?
* > 172.17.15.254  172.17.15.254   600             0 100 ?
* > 10.1.1.0/24    10.1.1.1        0               0 32768 ?
* > 169.254.0.0    10.1.1.1        1000            0 100 ?
* > 172.17.0.0     10.1.1.1        1000            0 100 ?
* > 172.17.4.100/32 10.1.1.1        0               0 100 i
* > 172.18.0.0     10.1.1.1        0               0 100 ?
* > 192.168.43.0   10.1.1.1        0               0 100 ?

Total number of prefixes 7
bgpd>
    
```

Figure 6: Routing Table – VIP Published

If VIP is DOWN – VIP 172.17.4.100 is DOWN and will be removed from all neighboring routers' routing tables. The VIP is not accessible. The routing table is shown in Figure 7.

```

bgpd> show ip bgp
BGP table version is 0, local router ID is 2.2.2.2
Status codes: s suppressed, d damped, h history, * valid, > best, = multipath,
               i internal, r RIB-failure, S Stale, R Removed
Origin codes: i - IGP, e - EGP, ? - incomplete

   Network        Next Hop        Metric LocPrf Weight Path
* > 0.0.0.0        172.17.15.254   600             0 100 ?
* > 10.1.1.0/24    10.1.1.1        0               0 32768 ?
* > 169.254.0.0    10.1.1.1        1000            0 100 ?
* > 172.17.0.0     10.1.1.1        1000            0 100 ?
* > 172.18.0.0     10.1.1.1        0               0 32768 ?
* > 172.18.0.0     10.1.1.1        0               0 100 ?

Total number of prefixes 5
    
```

Figure 7: Routing Table – VIP Removed

5. Conclusion

The system is implemented to achieve the main objective of establishing an end to end connectivity of the clients to the VIP along with reducing the response time with RHI. The system, hence, integrated the third party routing stack to the NetScaler CPX. The NetScaler CPX is configured and the routing engine set up with the web application. The active VIPs are advertised while the inactive VIPs are removed from the routing tables.

However, the system is compatible only with NetScaler CPX deployed environment and in the Citrix enterprise network. It also is designed specifically to the Quagga routing engine. Thus, any necessity to work with different routing engines requires modification. The system also has limited configuration capability.

6. Future work

The future enhancements considered to the project tries to overcome the limitations. They are described as follows:

- Development of a Wrapper API to work with any kind of Routing Engine.
- Development of the system capable for many other configuration capabilities through the web interface.

Conflict of Interest

The authors declare no conflict of interest.

Acknowledgment

A number of personalities, in their own capacities have helped us in carrying out this project work. We would like to take this opportunity to thank them all. We would like to thank Head of Department, Computer Science & Engineering, and the Principal, R V College of Engineering, for their moral support towards completing our project work. We also thank the entire team of Citrix for providing us an opportunity to carry out the project and for their continuous support and guidance.

References

- [1] Citrix ADC data sheet, https://www.citrix.com/content/dam/citrix/en_us/documents/data-sheet/citrix-adc-data-sheet.pdf, Accessed Date: 01-12-2019
- [2] Citrix Networking CPX Datasheet, <https://www.citrix.com/en-in/products/citrix-adc/resources/netscaler-cpx-data-sheet.html>, Accessed Date: 01-12-2019
- [3] Wes Felter, Alexandre Ferreira, Ram Rajamony, Juan Rubio, "An Updated Performance Comparison of Virtual Machines and Linux Containers", IEEE, 978-1-4799-1957-4, 171-172, 2015
- [4] Netscaler - Dynamic routing and route health injection, <https://www.virtualdesktopdevops.com/netscaler/netscaler-dynamic-routing.html>, Accessed Date: 01-12-2019
- [5] Quagga Routing Suite, www.quagga.net, Accessed Date: 01-12-2019
- [6] Hogge, Jr., "OSPF Routing to Geographically Diverse Applications using OSPF and Route Health Injection", United States Patent, Patent No. US 7707308 B1
- [7] Naseh, "Disaster Recovery for Active Standby Data Center using Route Health and BGP", United States Patent, Patent No. US 7710865 B2
- [8] Sandeep Sharma, Sarabjit Singh, and Meenakshi Sharma, "Performance Analysis of Load Balancing Algorithms", World Academy of Science, Engineering and Technology, 38, 2008 pp. 269- 272.

The Correlation of the Specific and Global Performance of Teachers in UNTELS Engineering Schools

Omar Freddy Chamorro Atalaya^{1,*}, Dora Yvonne Arce Santillan¹, Jorge Isaac Castro Bedriñana², Yesica Pamela Leandro Chacón¹
Martin Díaz Choque¹

¹Faculty of Engineering and Management, Universidad Nacional Tecnológica de Lima Sur, Lima, Perú

²Faculty of Zootechnics, Universidad Nacional del Centro del Perú, Huancayo, Perú

ARTICLE INFO

Article history:

Received: 13 September, 2019

Accepted: 03 November, 2019

Online: 05 December, 2019

Keywords:

Teaching performance

Student appreciation

Professional schools

Specific Dimension

Global Dimension

University

School of Engineering

Course planning

Teaching strategies

Student communication

Administration of the class

ABSTRACT

This article presents an analysis on the existing correlation of the specific and global performance of teachers in UNTELS engineering schools, whose data collection was carried out during the development of the first academic semester of the year 2019, using the Survey technique; which presents indicators classified in two dimensions: "Specific Dimension of Teaching Performance" and "Global Dimension of Teaching Performance", the first dimension includes indicators such as course planning, teaching strategies, teaching communication, student communication, administration of the class, and personal and professional traits, that the teacher shows towards the student; Likewise, the global dimension is related to the student's appreciation, as to whether the teacher surveyed should continue with the development of the course. This research was carried out, due to the low percentage of satisfaction in the student survey, and the appreciations in some negative cases, of the students in the Professional Engineering Schools. For this, initially it was sought to identify the number of teachers by Professional School of Engineering, whose teaching performance is poor, resulting in 17 teachers, which represents 14.05% of the total number of teachers; with which it was determined the Specific Dimension that presents the lowest level of qualification, resulting in Dimension 2 (D2): Didactic strategies, with an average grade of 10.41; These results will allow decisions to be made by the University authorities, regarding the development of a pedagogical training plan focused on improving said dimension, thus benefiting teachers in improving their teaching methodology. According to the analysis made, the dimensions of the specific and global performance of teachers in UNTELS engineering schools show a high positive level of Pearson's correlation.

1. Introduction

University teaching is one of the primary functions of the university; The university teacher is one of the pillars on which educational quality is supported, so the evaluation of teacher performance is a practice that is taking more and more strength in higher education institutions, it is becoming the key element of efforts to improve the quality of education, and the idea that the success of an educational system depends essentially on the quality of the performance of its teachers is increasingly widespread. [1]

Within the framework of institutional evaluations, university teaching should be approached from the whole university work, containing the different teaching and learning functions. [2]

In the process of evaluating teacher performance, it is crucial to have clarity in the aims and objectives that are to be achieved; some researchers consider teaching as an institutional project aimed at raising the quality of education. [3] For higher education institutions it is vital to have a teacher evaluation system that responds to the needs of the educational process and the functions of the teaching staff and fosters a culture of evaluation in the institution. [4]

Thus, the evaluation of the student to the teaching performance translates to some extent, in the evaluation of the

*Omar Freddy Chamorro Atalaya, Jr. Los Damascos 986, Urb. Virgen de la Puerta, Los Olivos, Lima, Perú, 968053089 & omar_chamorro1@hotmail.com

same teaching, since the quality of the explanation of the knowledge is related to the quality of understanding on the part of the student. [5] University teaching does not admit the slightest contradiction between knowing a subject well and not knowing how to teach it, in order to achieve continuous training towards the development of the professional skills necessary to meet the challenges of education. [6]

The results of research on the evaluation of teaching based on student opinions have found that the use of this source of information has benefits. [7] Numerous studies have examined the validity of students' assessments of their teachers and have found that students are one of the most important sources of information on teacher performance. [8]

In September 2015, through Supreme Decree No. 016-2015-MINEDU, the Policy for Quality Assurance of Higher University Education in Peru was approved, as the main guiding document of the reform process, which allows universities provide a quality educational service, based on getting graduates from public universities with adequate skills for their professional performance. Thus, one of the aspects to be considered by universities in Peru is the strengthening of the teacher evaluation system based on student surveys. [9]

In this sense, the present article seeks, through a descriptive analysis, to identify the number of teachers per Professional School of Engineering, whose teaching performance is poor, and then determine the dimensions in which they present the lowest level of qualification; In addition, it is also intended to determine if there is a correlation between the specific dimensions of the teacher and the Global Dimension of teacher performance.

2. Methodology

2.1. Level of Research

The level of research addressed in this article is Descriptive / Correlational. Descriptive because it seeks to specify the properties and characteristics of a group of teachers whose performance is poor. That is, they only intend to measure or collect information independently or jointly. And it is correlational since it seeks to know the relationship or degree of association with the Global Dimension of teacher performance. [10].

In the search to achieve these results; the following specific objectives have been set: Identify the number of teachers by Professional School of Engineering, whose teaching performance is poor. Determine the Specific Dimension that has the lowest level of qualification.

2.2. Source of Data Collected

The source of data collected was generated by the 2228 students of the 2019-I academic semester of the Engineering degrees, which qualified the teaching performance of the National Technological University of South Lima.

For greater detail these teachers are distributed as follows: 23 belong to the School of Mechanical and Electrical Engineering, 35 to the School of Systems Engineering, 31 to the School of Environmental Engineering and 32 to the School of Electronic

Engineering and Telecommunications Being a total of 121 teachers.

2.3. Instrument used data collection

The instrument used in data collection is the "Survey", this instrument responds to what is established by the Ministry of Education within its policies of Quality Assurance of Higher University Education in Peru. The structure of the student assessment survey of teacher performance is approved with Resolution of the Organizing Committee RCO N ° 090-2018-UNTELS. [11]

Which is composed of five dimensions which make up the group of "Specific Dimensions of Teacher Performance" and one dimension which forms the "Global Dimension of Teacher Performance".

Table 1: Survey Dimensions

SURVEY DIMENSIONS	
<i>Specific Dimension of Teaching Performance</i>	<i>Global Dimension of Teaching Performance</i>
Planning (D1)	Global evaluation of Teaching performance (D6)
Teaching strategies (D2)	
Communication (D3)	
Class administration (D4)	
Professional and personal traits (D5)	

Source: Untels

The previous table shows the 6 dimensions of each survey; The following factors have intervened in each of them (See Table 2).

Next, in the following Table 3, the range of scores is detailed, which was used to rate the teaching performance, these averages classified the teachers as excellent, very good, good, regular and deficient.

Table 3: Averages that Classify Teachers

Description Value	Description Value
Excellent teaching performance	18 to 20
Very Good teaching performance	16 to 17
Good teaching performance	14 to 15
Regular teaching performance	12 to 13
Deficient teaching performance	Less than or equal to 11

Source: Untels

Table 2: Factors Intervening in each Dimension

Question	Dimensions	
Skill and effort of the teacher in the preparation and achievements of the course		
Do you present and explain the syllable on the first day of class?	D1	
Does the student communicate clearly and precisely the objective and activities to be developed in the class?		
Make known the bibliographic support material required to broaden the topic?		
Teacher effectiveness so that their students acquire relevant knowledge, skills and attitudes		
Do you apply appropriate teaching methods, procedures and techniques to the development of the subject?	D2	
Does it promote basic or applied research in the development of the subject?		
Is it motivating, dynamic, innovative and promotes student participation and teamwork in the development of the subject?		
Does it lead to problem solving and exemplify the topic discussed with practical or real-life applications?		
Does it reinforce learning with feedback activities?		
Does the evaluation form coincide with that indicated in the syllabus, is it fair and objective in its grades and returns the exams and qualified practices on the established dates, showing the solution of them?		
Do you practice and encourage positive attitudes and values (discipline, responsibility, punctuality, ethics) towards the profession during class development?	D3	
Teacher effectiveness in promoting a favorable learning environment		
Does it arouse interest and encourage student participation through opinions, questions, discussions, teamwork or other actions and answer questions and concerns accurately and in a good way?		
Do you use oral (syntax, tone, diction), written (clarity of the letter, syntax, spelling) and gestural languages?	D4	
Group management and achievement of objectives		
Does your class start and end at the scheduled times?		
Do you maintain discipline and comply with the activities scheduled at the beginning of the class and indicated in the syllabus?	D5	
Do you invest all the time in the class in academic and training activities, without addressing issues outside the class?		
Personality attributes, characteristics of the professional teacher and ability to interact positively with students		
Does it show solid mastery of the knowledge of the subject it teaches and relates it to professional practice?	D5	
Do you pour your academic and professional experiences in the development of the subject?		
Do you project positive attitudes towards the University, life and social responsibility?		
Do you always assume proactive attitudes that allow you to lead by example?	D6	
Perception		
Should the teacher continue again with the development of this course?	D6	

Source: Untels

It should be noted that the results in the survey are obtained from the tabulation of the six dimensions, considering a Likert scale, then in Table 4, the described is shown.

Table 4: Likert Scale Indexes

Alternative	Factor (Fi)
Strongly disagree	0
In disagreement	1
Neither agree nor disagree	2
Disagreement	3
Totally disagree	4

Source: Untels

3. Results

Being consistent with the purpose of the research proposed in this article, then we proceed to describe the results obtained as part of the processing of the data collected:

The Table 5, shows the number of teachers grouped by their performance status.

Table 5: Number of Teachers Grouped by Their Performance Condition

	Performance Condition				
	Poor	Fair	Good	Very Good	Excellent
Number of Teachers	17	32	60	12	0
Percentage	14.05%	26.45%	49.59%	9.92%	0.00%

Source: Untels

It is important to highlight that the concern is focused on analyzing the dimension of teacher performance, in which teachers with a “Poor” condition have a lower level of qualification, so that from this result the authorities can establish policies that improve the teacher performance condition. In this sense, Table 6 shows the distribution by Professional School of the number of teachers whose qualification status is poor:

Table 6: Number of Teachers with Deficient Condition Grouped by Professional Care

	Professional Schools			
	Mechanical and Electrical	Systems	Environmental	Electronics and Telecommunications
Number of Teachers	1	4	5	7
Percentage	5.88%	23.53%	29.41%	41.18%

Source: Untels

In relation to the distribution of teachers whose performance condition is “Poor”, the grades were determined on average in the 6 dimensions that make up the data collection instrument, by Professional School.

The average result by area (PA) has been determined by applying the following formulas:

$$PA = 5 \left(\frac{\sum x_i * f1_i}{\sum x_i} \right) \tag{1}$$

Where: Xi is the number of students who marked the alternative i.

The general average classification (PG) is obtained as:

$$PG = \frac{\text{Saveraging by area (PA)}}{6} \tag{2}$$

Shown the method with which the average was found, in relation to the distribution of teachers classified as deficient, in the following Fig. 1, the results obtained in relation to the Average of qualifications by dimension of the deficient teachers of the School of Electric engineering and telecommunications.

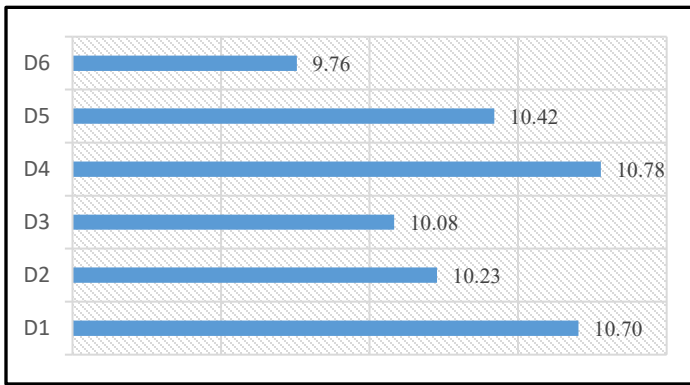


Figure 1. Average grades by size of poor teachers of the School of Electronic Engineering and Telecommunications (Source: Untels)

As seen in the previous figure, dimension D6, has the lowest grade point average, that is, the grade point average is 9.76, this is reflected in the students' disagreement regarding the permanence of teachers, in the dictation of the course.

In Fig. 2, the graphic representation of the results obtained in relation to the Average of grades by dimension of the poor teachers of the School of Environmental Engineering is shown.

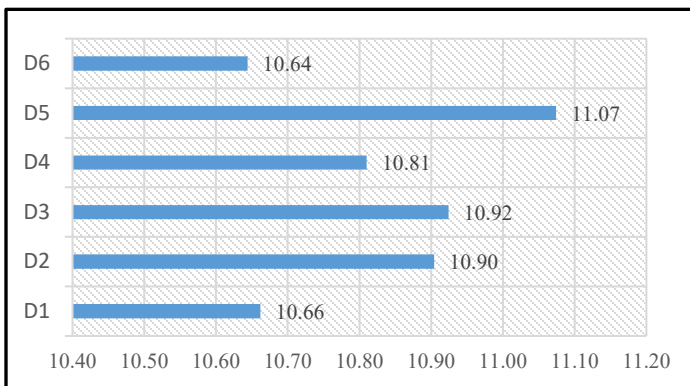


Figure 2. Average grades by area of poor teachers of the School of Environmental Engineering (Source: Untels)

In Fig. 3, the graphic representation of the results obtained in relation to the Average of grades by dimension of the poor teachers of the School of Systems Engineering is shown.

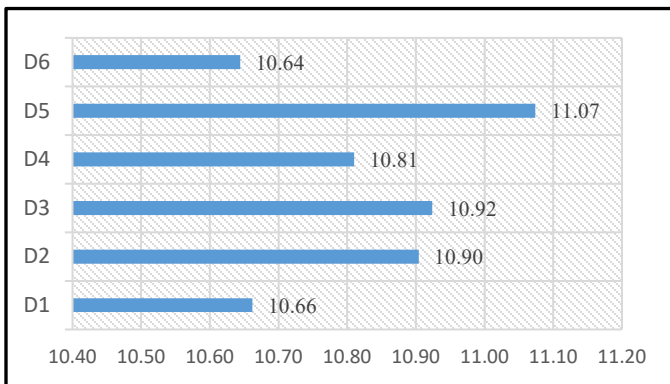


Figure 3. Average grades by area of poor teachers of the School of Systems Engineering (Source: Untels)

As can be seen in the previous figure, dimension D6 has the lowest grade point average of 10.64; also, dimension D1 follows with a 10.66, this is reflected in the students' disagreement in

relation to teacher planning; at these points the ability and effort of the teacher intervene in the preparation and achievements of the course.

In Fig. 4, the graphic representation of the results obtained in relation to the Average of grades by dimension of the poor teachers of the School of Mechanical and Electrical Engineering is shown.

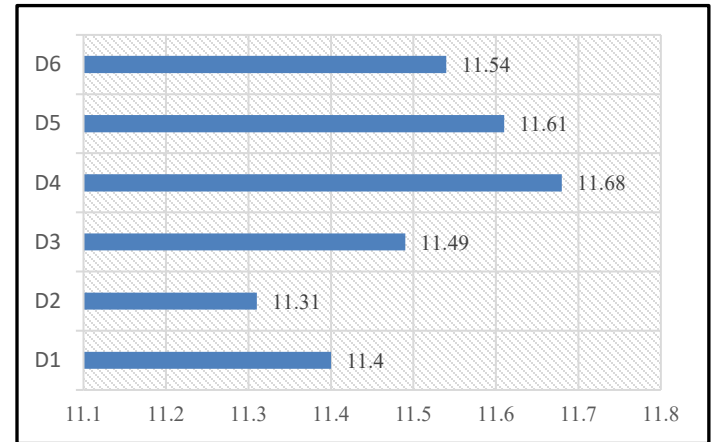


Figure 4. Average grades by area of poor teachers of the School of Mechanical and Electrical Engineering (Source: Untels)

As can be seen in the previous figure, dimension D2, has the lowest grade point average, this is reflected in the students' disagreement in relation to the teaching strategies of the teacher; at these points the effectiveness of the teacher intervenes so that their students acquire relevant knowledge, skills and attitudes.

From the Figures shown above you can determine the average of the dimension with the lowest qualification of teachers with "Deficient" performance, of all professional schools, these are shown in Fig. 5.

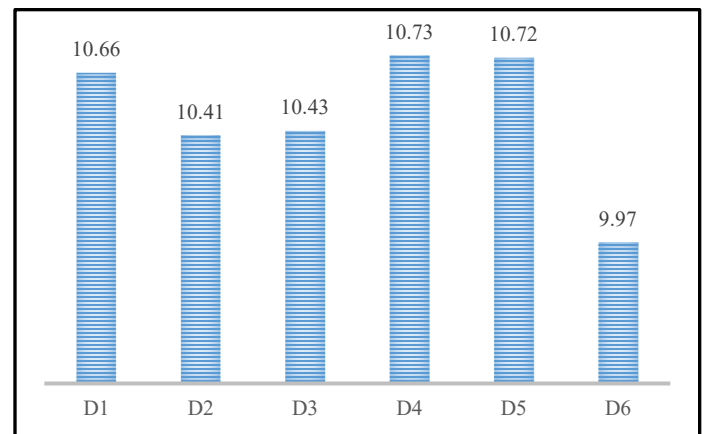


Figure 5. Average of grades grouped by dimensions of all Professional Schools of teachers with poor performance (Source: Untels)

From the last figure above, we can determine that the lowest qualification percentage of all the races is in dimension D2. "Teaching strategies of the teacher" (10.41); at these points the effectiveness of the teacher intervenes so that their students acquire relevant knowledge, skills and attitudes.

Now if we look at the rating of the overall dimension of teacher performance, we determine that the result is quite low (9.97), compared to the specific dimensions.

Thus, in order to identify if there is a relationship or degree of association between the Specific Dimensions and the Global Dimension of teacher performance, the Pearson Correlation Index was determined, using the statistical software SPSS V25.

In Table 7, Pearson's correlation between dimension D6 and dimension D5 is shown.

Table 7. Pearson Correlation Between D6 and D5

Pearson correlation between D6 and D3			
		D6 Global evaluation of Teaching performance	D3 Comunication
D6	Correlation Pearson	1	,978**
	Sig. (bilateral)		,000
	N	121	121
D3	Correlation Pearson	,978**	1
	Sig. (bilateral)	,000	
	N	121	121
**. The correlation is significant at the 0.01 level (bilateral).			

Source: SPSS

As the correlation of the global evaluation of teacher performance (D6) with professional and personal traits (D5) is shown, it is 0.982, this result reflects a high positive level of significance between the dimensions.

In Table 8, Pearson's correlation between dimension D6 and dimension D4 is shown.

Table 8. Pearson Correlation Between D6 and D4

Pearson correlation between D6 and D4			
		D6 Global evaluation of Teaching performance	D4 Class Administration
D6	Correlation Pearson	1	,952**
	Sig. (bilateral)		,000
	N	121	121
D4	Correlation Pearson	,952**	1
	Sig. (bilateral)	,000	
	N	121	121
**. The correlation is significant at the 0.01 level (bilateral).			

Source: SPSS

As the correlation of the global evaluation of teacher performance (D6) with the administration of the teacher's class

(D4) is shown, is 0.952, this result reflects a high positive level of significance between the dimensions.

In Table 9, Pearson's correlation between dimension D6 and dimension D3 is shown.

Table 9. Pearson Correlation Between D6 and D3

Pearson correlation between D6 and D5			
		D6 Global evaluation of Teaching performance	D5 Professional and personal traits
D6	Correlation Pearson	1	,982**
	Sig. (bilateral)		,000
	N	121	121
D5	Correlation Pearson	,982**	1
	Sig. (bilateral)	,000	
	N	121	121
**. The correlation is significant at the 0.01 level (bilateral).			

Source: SPSS

As the correlation of the global evaluation of teacher performance (D6) with the teacher's communication (D3) towards the student is shown, it is 0.978, this result reflects a high positive level of significance between the dimensions.

In Table 10, Pearson's correlation between dimension D6 and dimension D2 is shown.

Table 10. Pearson Correlation Between D6 and D2

Pearson correlation between D6 and D2			
		D6 Global evaluation of Teaching performance	D2 Teaching Strategies
D6	Correlation Pearson	1	,979**
	Sig. (bilateral)		,000
	N	121	121
D2	Correlation Pearson	,979**	1
	Sig. (bilateral)	,000	
	N	121	121
**. The correlation is significant at the 0.01 level (bilateral).			

Source: SPSS

As the correlation of the global evaluation of teacher performance (D6) with teaching strategies of the teacher (D2) towards the student is shown, it is 0.979, this result reflects a high positive level of significance between the dimensions.

In Table 11, Pearson's correlation between dimension D6 and dimension D1 is shown.

As the correlation of the overall evaluation of teacher performance (D6) with teacher planning (D1) towards the student is shown, it is 0.979, this result reflects a high positive level of significance between the dimensions.

It is important to specify that in all cases the correlation analysis is significant high; this allows us to establish that if there is an association between the Specific Dimensions and the Global Assessment of teaching performance.

Table 11. Pearson Correlation Between D6 and D1

Pearson correlation between D6 and D1			
		D6 Global evaluation of Teaching performance	D1 Planation
D6	Correlation Pearson	1	,979**
	Sig. (bilateral)		,000
	N	121	121
D1	Correlation Pearson	,979**	1
	Sig. (bilateral)	,000	
	N	121	121

** . The correlation is significant at the 0.01 level (bilateral).

Source: SPSS

Also, in order to determine the validity of the data collection instrument, the results of the Cronbach's alpha test are shown below:

Table 12. Reliability Statistics

Reliability Statistics	
Cronbach Alfa	Numero of elements
,995	44560

Source: SPSS

The value obtained for Cronbach's alpha is 0.995 which gives evidence of the reliability of the data collection instrument is reliable; The number of elements represents the number of students surveyed (2228) and the number of questions answered (20).

4. Discussion

In relation to the results obtained and the objectives set forth, the following discussions are required:

In relation to objective 1: Identify the number of teachers by Professional Engineering School that have poor classification

Regarding the percentage of teaching performance by Professional School of Engineering, which is deficient in 14.05%, it can be said that this result is consistent with that carried out in the article entitled, The evaluation of teaching performance in higher education, which states that 44.2% of students evaluate teacher performance as regular or deficient, so they recommend permanent training to improve their professional development and performance and thus improve the quality of learning management offered to students. [12]

In relation to objective 2: Determine the dimensions in which the lowest level of teacher qualifications is presented

Regarding the Specific Dimension that presents the lowest level of qualification, which is, Teaching Strategies, with a grade point average of 10.41; which is related to the effectiveness of the teacher so that their students acquire relevant knowledge, skills and attitudes; It can be said that these results are consistent with the study carried out in the Educational Institution No. 3089 "Los

Angeles" - Ventanilla, where they conclude that methodological strategies influence 37.1% in the planning of teaching work in Educational Institution No. 3089 "Los Angeles" - Window. Lima 2017, the generating satisfaction in students. [13]

5. Conclusions

It is concluded that the number of teachers was determined per Professional School of Engineering, whose teaching performance is poor, which turned out to be 17, which represents 14.05% of the total number of teachers, distributed per school in one of Electrical Mechanical Engineering, 4 of Systems Engineering, 5 of Environmental Engineering and 7 of Electronic and Telecommunications Engineering.

It is concluded that the Specific Dimension that has the lowest level of qualification was determined to be Dimension 2 (D2): Teacher's teaching strategies, with a grade point average of 10.41. It should be noted that comparing with the other dimensions corresponding to the Specific Dimensions, the difference between one and the other does not turn out to be much, which allows to conclude that as long as some type of training is intended, it should be given at the level of all indicators contained this dimension

It is concluded that there is a significantly high and positive correlation between each of the dimensions that are part of the Specific Dimensions, with the Global Dimension of Teaching performance.

6. Recommendations

It is recommended to develop pedagogical training plans, in order to improve the teaching methodology.

It is recommended to implement a mechanism for supervision and control of teachers in the classroom, since, currently, the university does not have a marking system for the beginning and end of class; It is also recommended to implement mechanisms for the supervision and control of school directors, since teachers currently do not carry out class plans, which should be consigned to a teaching portfolio.

It is recommended to implement tools related to the use of Information and Communication Technologies (ICT); it is also recommended to conduct training for the student and the teacher; in order to improve planning, academic management and research and dissemination of knowledge.

References

- [1] Jaik Dipp, A., Villanueva Gutiérrez, R., García Salas, M. E., & Tena Flores, J. A. (2017). Assessment of teacher performance and presence of Burnout in teachers of higher education. *Electronic Journal Educational Dialogues*, 11 (21), 71-87
- [2] Albarrán, D. & Alarcon, L. (2017). Evaluation of teaching performance in UAGro High School I. *Iberoamerican Magazine for research and educational development*.
- [3] León, L., Noriega, E. & Murillo, M. (2018). Impact of the organizational climate on the teacher's work performance. *Fides et Ratio - Journal of Cultural and Scientific Dissemination of La Salle University in Bolivia*, 16 (16), 15-32.
- [4] Guzman, F. (2018). The Teaching Evaluation Experience in Mexico: Critical Analysis of the Taxation of the Professional Teaching Service. *Iberoamerican Journal of Educational Evaluation*, 2018, 11 (1), 135-158
- [5] Cabero, J., Llorente, M., Morales, J. (2018). Evaluation of teaching performance in virtual training: ideas for the configuration of a model. *Iberoamerican Journal of Distance Education*, 21 (1), pp. 261-279.

- [6] Yáñez, S., Hernandez, H., Cheza, L., Valdiviezo, W., Méndez, J., Rivera, M., Vargas, C., (2018). Teaching performance in the training of the accompaniment to the complex exam. Scientific magazine domain of science. Vol. 4, no. 1, pp. 102-114
- [7] Gálvez, E., & Milla, R. (2018). Assessment of teacher performance: Preparation for student learning in the Framework of Good Teacher Performance. Purposes and Representations, 6 (2), 407-429.
- [8] Obreque, A., Hernández, C., Peña, S., Agredo, M., & Salvatierra, M. (2019). Evaluation of teacher performance in Chile: perception of poorly assessed teachers. Cadernos de Pesquisa, 49 (172), 144-163
- [9] MINEDU. (September 25, 2018). MINEDU Retrieved from <https://www.gob.pe/institucion/minedu/normas-legales/118310-016-2015-minedu>
- [10] Valenzuela, J. (2018). Fundamentals of educational research. Volume 2 and 3. Mexico: Monterrey Digital Technology Publishing
- [11] Sur, U. N. (s.f.). National Technological University of South Lima. Obtained from <http://www.untels.edu.pe/>
- [12] Pacheco, M., Ibarra, I., Iñiguez, M., García, H. & Sánchez, C. (2018). The evaluation of teaching performance in higher education. University digital magazine.
- [13] Vidal, O. (2018). Management Leadership Management and Teaching Performance in the Educational Institution No. 3089 "Los Angeles" - Ventanilla. Journal of scientific research igobernanza.

Comparative Analysis of Student Dissatisfaction of the Continuing Academic Semesters at UNTELS

Omar Freddy Chamorro Atalaya^{1*}, Dora Yvonne Arce Santillan¹, Jorge Isaac Castro Bedriñana², Teodoro Neri Díaz Leyva¹, Denisse Marie Barrientos Pichilingue¹

¹ Faculty of Engineering and Management, Universidad Nacional Tecnológica de Lima Sur, Lima, Perú

² Faculty of Zootechnics, Universidad Nacional del Centro del Perú, Huancayo, Perú

ARTICLE INFO

Article history:

Received: 17 September, 2019

Accepted: 07 November, 2019

Online: 05 December, 2019

Keywords:

Dissatisfaction

Students

Continuous Improvement

Academic Services

Administrative Services

ABSTRACT

Student dissatisfaction is of the utmost importance when it comes to establishing a process of continuous improvement in a University. Currently, at the National Technological University of Lima Sur (UNTELS) there is no information regarding the levels of student dissatisfaction with the services offered by UNTELS. In this context, the purpose of this research project is to collect information from the students of the Professional Careers of Systems Engineering, Environmental Engineering, Mechanical and Electrical Engineering, Electronic Engineering and Communications, and Business Administration of the academic semesters 2017-I, 2017-II and 2018-I. To assess student dissatisfaction, a physical questionnaire was applied; through which the indicator of the highest level of dissatisfaction was determined, being "Sufficient work tables or capacity", corresponding to the category of laboratory service, whose value of dissatisfaction is 65.61%, 47.23% and 52.11%; in the academic semesters 2017-I, 2017-II and 2018-I, respectively. Next, the indicators whose level of research is greater than 40% were determined, with three indexes of higher percentage of increase, these are; Registration and enrollment, Internet Service and the Efficiency of Administrative Personal Work; These results are intended to take relevant actions for the continuous improvement of the educational quality of UNTELS.

1. Introduction

In search of quality assurance of university higher education, the Peruvian State according to Supreme Decree No. 016-2015-MINEDU states that, "The general objective of the policy of quality assurance of university higher education is to identify that all Young people in the country have the opportunity to access a quality educational service, which offers comprehensive training and continuous improvement, focused on the achievement of competent professional performance. Under this policy it is essential to quantify the percentage of satisfaction and dissatisfaction of university students, both academic services and administrative services provided by the University. [1]

For this, it is important to evaluate perceptions so that relevant improvements can be made and maintain good for the level of satisfaction improved. It is appropriate to comment, that all this effort to improve the service should seek that the student is

prepared in a positive environment and with the appropriate tools for their development as a professional future reach the optimum possible. [2]

Dissatisfaction is made up of factors that have to do with the possibilities and opportunities that the university offers the student to start or continue his studies; taking into account the way in which its policies favor performance and permanence in the institution. It is also proven that these variables establish criteria for the decision of permanence and academic dropout, among which are: deficiency in physical, technological and human resources, disagreement with the university, lack of academic planning by teachers, discomfort with the university environment, inadequate treatment received at the university by professors and administrators, schedule programming, the institutional proposal is limited according to their expectations, and limited funding opportunities offered by the university. [3]

Also, dissatisfaction arises from not reaching expectations, which are reasonable and sustained possibilities of something happening, that is, it is not any hope or aspiration. It is constituted

*Omar Freddy Chamorro Atalaya, Jr. Los Damascos 986, Urb. Virgen de la Puerta, Los Olivos, Lima, Perú, 968053089 & omar_chamorro1@hotmail.com

from previous experiences, desires and attitudes. Some characteristics of the expectations are: they are generally expected to be fulfilled, they are based on past experiences that can be of success or failure, influence the context, can be positive or negative and are changing according to the experiences. [4]

It should be noted that hygienic factors or extrinsic factors are also factors that are related to dissatisfaction; other factors are the conditions surrounding the study situation, such as class schedules, physical environment, student services, transportation, security, class interruptions and the relationship with teachers. These elements cannot be regulated by students. When they are unfavorable they produce dissatisfaction and discomfort; manifesting itself in low academic performance, high levels of repetition and in the worst case, dropout. [5]

In this sense, the National Technological University of Lima Sur (UNTELS) has the responsibility of offering quality and excellence education, for which it is necessary to have relevant initial information on student dissatisfaction regarding professional competences, personal and social attitudes, teaching staff, university environments, library services, laboratory services, computer center, administrative service of the faculty and professional school and support services of the University, which leads the authorities to make relevant decisions in order to establish the assurance of the educational quality at UNTELS.

2. Methodology

2.1. Type and level of Research

This research is non-experimental and descriptive, since it presents a single variable, this being student satisfaction; It is descriptive since it seeks the characterization of a fact, phenomenon, individual or group, in order to establish its structure or behavior. [6]

2.2. Population and Sample

In student satisfaction surveys. It is clear that a source of information about the teaching and learning processes are the students themselves. [7]

In that sense, the study population is made up of 3,119 students, which is the result of adding the number of students surveyed belonging to the seventh, eighth, ninth and tenth cycle of the Academic semesters 2017-I, 2017-II and 2018-I, of all professional schools of the National Technological University of South Lima. In the present investigation, the entire population has been considered as a sample, since the survey was compulsory applied to all students.

2.3. Applied Techniques in the Collection of Information and Measuring Instruments

For the collection of information, a segmented survey instrument was used in specific indicators for its analysis, which consider the degree of satisfaction in relation to professional competences, personal and social attitudes, teaching staff, university environments, library services, library services laboratory, computer center, administrative service of the faculty and professional school and support services of the University; The proposed measuring instrument, prior to its application, was validated through expert judgment.

It should be noted that questionnaires were used to measure satisfaction, since they are simple, fast and moderately cost tools; and being the first time this research is carried out, the National Technological University of South Lima, opted for an easy to understand tool. In addition, the questionnaires are more suitable for use in quantitative data and have a wide scope.

Likewise, the method used to obtain objective views of the students for an authentic research study is that of Maxwell, this method suggests four components: [8]

1. The relationship established by the researcher with the study.
2. The sources of information and the selected sample.
3. Data collection.
4. The analysis of the results.

In the first component, the relationship of research with aspects related to educational programs is established.

In the second component, it is recommended that the groups include “people who have information about the phenomenon since they are experts in the area with the privilege of witnessing the facts”; This point is represented by the students of the seventh, eighth, ninth and tenth cycle of the Academic semester 2017-I, 2017-II and 2018-I, of the professional careers of Systems Engineering, Mechanical and Electrical Engineering, Environmental Engineering, Business Administration and Electronic Engineering and Telecommunications. [8]

In the third component, it anticipated the difficulties that might arise regarding the responsibility for participating in the survey; to do this, communications were prepared via email and communications in each classroom, to encourage student participation. The students' responses were recorded in the instrument, in addition, emotional reactions and body language were evaluated by a professional. These observations nurtured the validity of the survey.

Finally, in the fourth component, the results obtained were analyzed; it should be noted that quantitative research gives greater precision, to adequately explain the results and to make comparisons between them.

3. Results

Below are the results obtained from the application of the data collection instrument of the “Student Satisfaction Survey”, the same ones that were carried out via the web, during the academic semesters 2017-I, 2017-II and 2018- I.

The following Figure 1 shows the results of the indicators of greatest dissatisfaction of all categories in the academic semesters 2017-I, 2017-II and 2018-I.

As shown in Figure 1, the indicator that shows the highest percentage of dissatisfaction in the 2017 - I semester is Sufficient Work Tables or Capacity, this indicator is related to the category of Laboratory Services, then there is the Internet Service and the Recreation and Sports Areas, which belong to the categories of Computing Center and Environments of the University respectively. While in the 2017 - II semester, it is Sufficient Work Tables or Capacity, this indicator is related to the category of Laboratory Services, then there are Registries and Enrollments and the Number of Computers, which belong to the Support

Service categories from the University and Computer Center respectively.

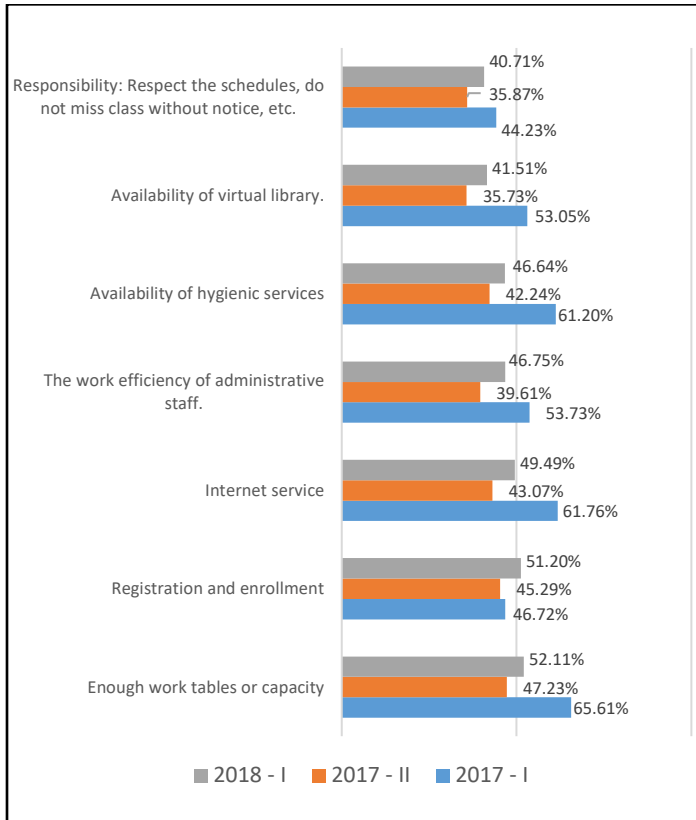


Figure 1: Comparison of the indicators of greater dissatisfaction of all categories of the academic semester 2017-I, 2017-II and 2018-I. (UNTELS)

Likewise, the indicator that shows the highest percentage of dissatisfaction in the semester 2018 - I, is Sufficient Work Tables or Capacity, this indicator is related to the category of Laboratory Services, then there are Registries and Enrollments and the work efficiency of administrative staff, which belong to the categories of University Support Service and Administrative Service of the Faculty and Professional School respectively.

Table 1: Indicators of greater increase in student dissatisfaction between all categories

Indicator	Levels of Dissatisfaction		
	Semester Academic 2017-I	Semester Academic 2017-II	Semester Academic 2018-I
Enough work tables or capacity	65.61%	47.23%	52.11%
Registration and enrollment	46.72%	45.29%	51.2%
Internet service	61.76%	43.07%	49.49%
The work efficiency of administrative staff.	53.73%	39.61%	46.75%
Availability of hygienic services	61.20%	42.24%	46.64%
Availability of virtual library	53.05%	35.73%	41.51%
Responsibility: Respect the schedules, do not miss class without notice, etc.	44.23%	35.87%	40.71%

Once the results of the comparison of the indicators of greatest dissatisfaction between all categories are obtained, the indicators whose level of dissatisfaction is greater than 40% are shown, in the academic semester 2018-I and that showed an increase in dissatisfaction compared to the academic semester 2017-II and 2017 - I.

With the results of the indicators with the greatest dissatisfaction, we will now determine in which professional career, there are the greatest number of dissatisfied students, for this, we use the results of table 1, and we will choose the 3 indicators that have the highest percentage of variation in relation to the previous semester, that is, the indicator for the 2017-II semester, which presents a greater increase compared to the 2018-I semester.

Table 2: Total of unsatisfied students by professional career of the indicator records and registration

Category: University Support Services	
Registration and enrollment	Total Unsatisfied Students
Electric engineering and telecommunications	104
Systems engineer	99
Mechanical and Electrical Engineering	77
Environmental engineering	90
Business Administration	77

Table 3: Total of unsatisfied students by professional career of the indicator internet service

Category: Computer Center	
Internet Service	Total Unsatisfied Students
Electric engineering and telecommunications	86
Systems engineer	87
Mechanical and Electrical Engineering	56
Environmental engineering	77
Business Administration	62

Table 4: Total of unsatisfied students by professional career of the indicator the efficiency of administrative personal work

Reliability statistics		
Semestre	Cronbach's Alpha	Number of elements
2017-I	,990	69
2017-II	,990	69
2018-I	,991	69

Table 5: Alfa de cronbach of the semester 2017-I, 2017-II and 2018-I

Administrative Service of the Faculty and Professional School	
<i>The Efficiency of Administrative Personal Work</i>	<i>Total Unsatisfied Students</i>
Electric engineering and telecommunications	98
Systems engineer	88
Mechanical and Electrical Engineering	79
Environmental engineering	84
Business Administration	72

As can be seen in Table 2, the professional career that shows the greatest dissatisfaction in relation to Registries and Enrollment, is the Electronic Engineering and Telecommunications career, also in Table 3, it is observed that the career that presents the highest level of dissatisfaction in In relation to the Internet Service, it is the Systems Engineering degree; finally, it is observed in Table 4, that the professional career of Electronic Engineering and Telecommunications is the career that presents the greatest degree of dissatisfaction in relation to the Efficiency of Administrative Personal Work of the Faculty and Professional School.

4. Discussion

Once the comparative analysis of student dissatisfaction of three continuous academic semesters has been carried out, at UNTELS, we will carry out the Cronbach Alpha test, using the reliability statistics of the SPSS program; Reliability has several concepts, although broadly it can be defined as the absence of measurement errors in a questionnaire, or as the accuracy of its measurement.

As a general criterion, George and Mallery (2003, p. 231) suggest the following recommendations to evaluate Cronbach's alpha coefficients. [9]

- Alpha coefficient > 0.9 is excellent
- Alpha coefficient > 0.8 is good
- Alpha coefficient > 0.7 is acceptable
- Alpha coefficient > 0.6 is questionable
- Alpha coefficient > 0.5 is poor
- Alpha coefficient < 0.5 is unacceptable

The results of the Cronbach Alpha test performed on the results obtained in the semester 2017 - I, 2017 - II and 2018 - I.

As observed in the results, Cronbach's Alpha is greater than 0.9, this value is classified as excellent; since, Cronbach's alpha coefficient ranges between 0 and 1 and the closer it is to 1, the more reliable the data.

Continuing with the statistical analysis we will perform the frequency test in order to determine the amount of the number of dissatisfactions, of the indicators that show the greatest increase in student dissatisfaction among all categories, for this we will use Table 1, where the comparative analysis performed; It should be noted that only the results of the last two semesters 2017-II and 2018-I have been taken; since, it is irrelevant to take the 2017-I semester as a reference; because there is already information on the academic semester 2018-I; and the concern is to address the indices of dissatisfaction that show a tendency to increase between the semesters 2017-II and 2018-I.

Table 6: Number of unsatisfied students

	<i>Unsatisfied Students</i>	
	2017 - II	2018 - I
Enough work tables or capacity	341	457
Registration and enrollment	327	449
Internet service	304	434
The work efficiency of administrative staff.	285	410
Availability of hygienic services	305	409
Availability of virtual library.	240	364
Responsibility: Respect the schedules, do not miss class without notice, etc.	305	409

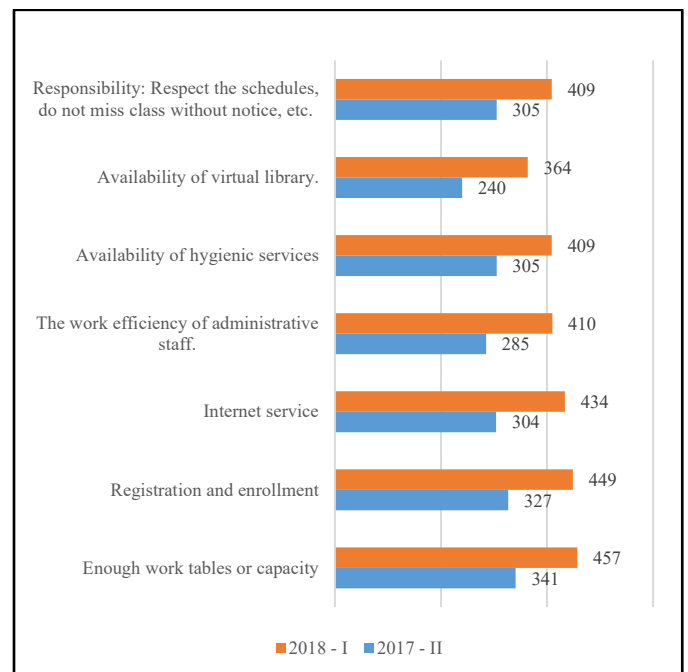


Figure 2: Number of unsatisfied students. (UNTELS)

The following shows the number of dissatisfied students per indicator whose level of dissatisfaction is greater than 40%. The following shows its graphic representation.

5. Discussion

In relation to the results of the present investigation, the following discussions are then carried out:

Regarding the “Registration and enrollment” indicator, it is evident that in the academic semester 2018-I a level of dissatisfaction of 51.20% was shown, compared to the semester 2017-II and 2017-I, which showed a level of dissatisfaction of 45.29 % and 46.72%, respectively; it is possible that this increase is reflected, due to the implementation of a new curriculum mesh; and in the rejection on the part of the students, in their understanding that this change of mesh was going to carry out the backward movement of their academic cycles; and in turn the registry and registration office was not in a position to carry out this process. According to Gómez (2016), 60% of students surveyed indicate that the enrollment process is not good and demand that the online system be prioritized, acquiring cutting-edge technology to improve the enrollment process. [10]

Regarding the “Internet Service” indicator, it is evident that a level of dissatisfaction of 49.49% in the academic semester 2018-I, although the value has decreased compared to the other semesters, it is still a necessary indicator to improve; it is possible that this dissatisfaction is due to the fact that there is no high network coverage, capable of covering the demand of the students; reason why resources are not used, such as the laboratory, library, and other University services. For Li (2008), the internet is the most requested and necessary service for the students of the San Martín de Porres University. [11]

Regarding the indicator “The efficiency in the work of administrative staff”, it is evident that in the academic semester 2018-I, a level of dissatisfaction of 46.75% was shown, this value has increased compared to the academic semester 2017-II, whose dissatisfaction It was 39.61%. This result is compared with that carried out by Li (2008), which indicates that, in most of the Peruvian Universities, 20% of students show dissatisfaction in the attention and work of the administrative staff, since there is no good treatment, nor a willingness to make student requests. [11]

6. Conclusions

It is concluded that the indicator of the highest level of dissatisfaction was determined, of all categories, being the indicator “Sufficient work tables or capacity”, belonging to the category Laboratory Services, whose value of dissatisfaction is 65.61%, 47.23% and 52.11 %; in the academic semesters 2017-I, 2017-II and 2018-I, respectively; This is due to the fact that laboratory equipment is not located in the most appropriate environment, that is, there is a bad dimensioning, so it is not possible to locate more work tables.

It is concluded that the Internet Service indicator, presented the greatest dissatisfaction increase in the 2018-I academic semester, compared to the 2017-I and 2017-II academics; this is because there is no high network coverage, able to meet the demand of the students; reason why resources are not used, such as the laboratory, library, and other University services.

It is concluded that the indicator “Efficiency in the work of administrative staff” is the one that shows the highest number of dissatisfied students; in the career of Electronic Engineering and Telecommunications; It is possible that this increase is due to the fact that there are no customer service training programs (students) for the personnel in charge of the different administrative offices.

References

- [1] PCM-Peru. (September 25, 2015). Coordination Secretary of the PCM. Obtained from the PCM Coordination Secretary: <http://sc.pcm.gob.pe/wp-content/uploads/files/politicas/Formatos/DS%200016-2015-MINEDU%20+%20Anex.pdf>
- [2] Cieza, J., Castillo, A., Garay, F., & Poma, J. (2018). Satisfaction of the students of a Peruvian medical school. Lima: Heredian Medical Magazine
- [3] Ariza, S. & Marín, D. (2009). Intervening factors in the school dropout of the Faculty of Psychology, Los Libertadores University Foundation. Psychological thesis Network of Scientific Journals of Latin America and the Caribbean, (4), 72-85.
- [4] Carrillo, A. & Ramírez, S. (2011). Academic and work expectations of students coming to graduate from a degree in Educational Psychology. (Bachelor thesis). Available at <http://digitalacademico.ajus.co.upn.mx:8080/thesis/handle/123456789/9257>
- [5] Tobón, M., Durán, M., & Áñez, A. (2016). Academic and professional satisfaction of university students. Venezuela: Electronic Journal of Humanities, Education and Social Communication
- [6] Rica, U. C. (04 of 09 of 2017). Univesia.net Obtained from Univesia.net: <http://noticias.univesia.cr/educacion/noticia/2017/09/04/1155475/types-research-descriptive-exploratori-a-e-xpliativa.html>
- [7] Malpica, F. (2013). 8 Key Ideas. Quality of educational practice. Barcelona: GRAÓ.
- [8] Rodríguez, C., & Rodríguez, M. (2016). Usefulness of Maxwell's methodology in research design. Bogota: University of the Andes.
- [9] George, D., & Mallery, P. (2003). SPSS for Windows step by step: A Simple Guide and Reference. Boston: Allyn & Bacon.
- [10] Gómez, N. (2016). Redesign of Processes to Improve Tuition at the Faculty of Administrative Sciences of the National University of San Marcos. Peru: Research Rev. of the Faculty of Administrative Sciences, UNMSM
- [11] Castañeda, R. (2013). Factors associated with dropping out of university students. (Postgraduate thesis). San Martín de Porres University. Lima

Eye Feature Extraction with Calibration Model using Viola-Jones and Neural Network Algorithms

Farah Nadia Ibrahim*, Zalhan Mohd Zin, Norazlin Ibrahim

Industrial Automation Section, University Kuala Lumpur Malaysia France Institute, 43650 Selangor, Malaysia

ARTICLE INFO

Article history:

Received: 14 June, 2019

Accepted: 28 August, 2019

Online: 05 December, 2019

Keywords:

Eye detection

Calibration

Viola-Jones

Neural network

ABSTRACT

This paper presents the setup of eye tracking calibration methodology and the preliminary test results of the training model from the eye tracking data. Eye tracking requires good accuracy from the calibration process of the human eyes feature extraction from facial region. Viola-Jones algorithm is applied for this purpose by using Haar Basic feature filters based on Adaboost algorithm which extract the facial region from an image. From the extracted region, the eyes feature is selected to find the center coordinate of the iris and be mapped with the calibration point coordinates to create the training model of the eye calibration process. Thus, this paper shows the performance and efficiency of three training functions in Neural Network algorithm to get the best training model with fewer error for more efficient eye tracking calibration process.

1. Introduction

Human features which are once a very selective parameter has been widely applied as the main input for various research of vision. Detection and tracking of human features can improve the performance of system specifically such as security, safety and also human monitoring. For eye tracking system, accurate detection of eyes feature extraction is important as it is the first information eye data and calibration process have to be done. Calibration is the process of measuring the eye gaze point calculation which recording the user's gaze before an eye tracking recording is started. For the calibration procedure to be achieved in good accuracy, good eye tracking method has to be applied. There are several types of the eye tracking such as electrography, scleral coil and the most popular method of video tracking. This paper is an extension of work originally presented in 2018 International Symposium on Agent, Multi-Agent Systems and Robotics (ISAMSR) conference [1].

Electrography is a method that uses electric potentials measured with electrodes placed around the eyes. N. Steinhausen, R. Prance, and H. Prance [2] applied three sensors of electrodes, P. Aqueveque and E. J. Pino [3] aims on developed a low cost electrography system while H. Manabe, M. Fukumoto, and T. Yagi [4] went into automatic drift calibration for electrography. This method requires only very low computational power but relatively poor gaze direction accuracy to locate where a subject is looking

*Farah Nadia Ibrahim, Putrajaya, Malaysia, +6014-8271947 & fnadiaibrahim@gmail.com

compared to a video tracking even though the time of eye movements can be determined.

For video-based eye tracking, calibration has been created by different approaches and presentations. There is an approach of calibration procedure where the user's gaze is being calculated and also an approach of calibration-free where the aims are towards removing the calibration process for a fully automatic system.

D. Model and M. Eizenman [5] proposed general method by extending the tracking range for the remote eye gaze tracking system. By using a stereo pair of cameras, the overlapping field of view is used to estimate the user eye parameters. While, J. Chen and Q. Ji [6] proposed general method by gaze estimation without personal calibration which is the 3D gaze estimation. There is also other research such as [7-9] that also applying the same concept of calibration-free and needed more added inputs while adjusting certain parameters. These research shows that calibration-free system is achievable but the need of calibration for measuring accuracy of user's gaze is still considered as the most important process that cannot be removed in eye tracking.

This paper aims to implement calibration process in order to achieve good accuracy and performance. In order to achieve these objectives, regression technique with good training function is needed. A research from K. Harezlak, P. Kasprowski, and M. Stasch [10] have focus on the process of calibration and analyses the possible steps with ways to simplify this process. The authors compared three regression methods of Classic Polynomial, Artificial Neural Networks (ANN) and Support Vector Regression

(SVR) to build the calibration models with presents different sets of calibration points.

Another approach used detection of the user attention by moving calibration target. This technique is presented by K. Pfeuffer, M. Vidal, J. Turner, A. Bulling and H. Gellersen [11] where the work is focused on smooth pursuit eye movement. This system collects sample of gaze points by displaying a smooth moving target to the user. Three realistic applications have been designed with different abilities in each such as Automated Teller Machine (ATM), stargazing and lastly is the waiting screen application. However, this study showed that too slow and too quick effects the accuracy of the system.

Facial region is divided into several features such as eyes including pupil, iris, eye corners, eyelid, nose and mouth. There is a method using template matching in facial image presents by Bhoi, N, & Mohanty, M. N. [12] which use the correlation of the eye template as the eye region and P. Viola and M. Jones [13] that used integral images from Haar Basic filters with Adaboost algorithm to create the region of interest around the area of face features.

After taking consideration of eye tracking types and regression method, this paper adapts the same methodology of [10] in building the calibration models with displaying set of calibration points by using video-based tracking and applied Neural Networks algorithm as the regression method with implementation of Viola-Jones algorithm as the eye feature extraction technique. The extracted eye feature information from Viola-Jones become the input data for training the calibration model. To achieve best training model, three training functions are compared for its performance and processing time.

2. Proposed Method

2.1. Displaying the calibration point as a dot

At the beginning of calibration process, stimuli of calibration point must be display to the user. Thus, we have set up two different calibration points, 4 points and 9 points calibration dots each locate at different position. This process is projected to the computer screen in front of the user to generate the raw data of eye detection. The size of the computer screen is 1920x1080 in pixels. The displayed stimuli are divided evenly on the screen as in Figure 1 and 2.

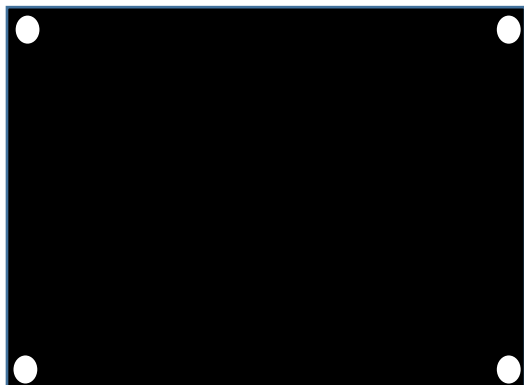


Figure 1: Screen display of 4 calibration points

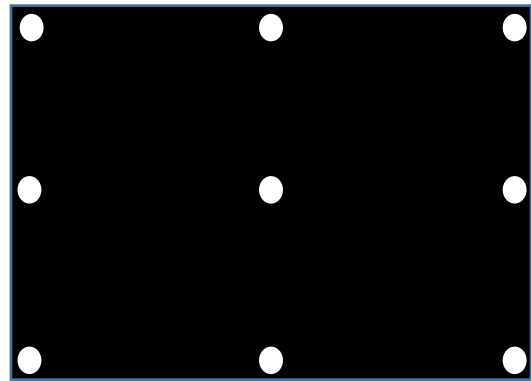


Figure 2: Screen display of 9 calibration points

From Figure 1 and Figure 2, the calibration points are being displayed to the user, one by one point. This process is being conducted by using a Logitech HD Pro Webcam C920 which is a full 1080p high definition. This webcam is equipped with the application of video, and photo capture, face tracking, and motion detection with the size of 640x480 in pixels. The setup of tracking the user's eye features and coordinates are as shown in Figure 3.

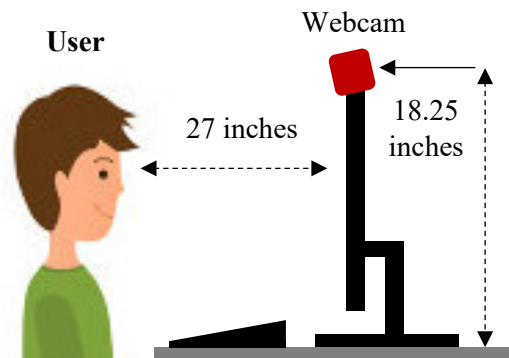


Figure 3: Setup of eye tracking

As seen in the figure above, the user's eye position is being recorded by the web camera. User looked at each point displayed for every 3 seconds at different locations of the calibration point that has been setup. The recorded process is saved in a video format. Thus, the images of user's interaction must be extracted frame-by-frame before the face and eye features detection being carried out. Figure 4 below shown the image of the user looking towards the displayed stimuli of calibration points of 4 points and 9 points on the computer screen.



Figure 4: Image of user looking towards computer screen

2.2. Face and eye features detection

A video recording is the first step on capturing the user’s eye images for the extraction of the eye center coordinates. As the next step of this research, the face and eye features detection are carried out by using a technique proposed by P. Viola and M. Jones [13], Viola-Jones algorithm. The input data for this algorithm is the image of the user as in Figure 4, that has been extracted frame-by-frame previously. Viola-Jones algorithm is widely known for its ability and performance in detecting the face feature.

P. Viola and M. Jones [13] proposed this method together by using the three main key attributions of integral images, AdaBoost classifier with more complex classifier in a cascade that has been proven to lessen the computational time with high level of detection accuracy. As per mentioned, this research has applied this algorithm which used the Haar-based features that involved the sums of image pixels within the face region in the rectangular areas as shown in Figure 5 and 6.

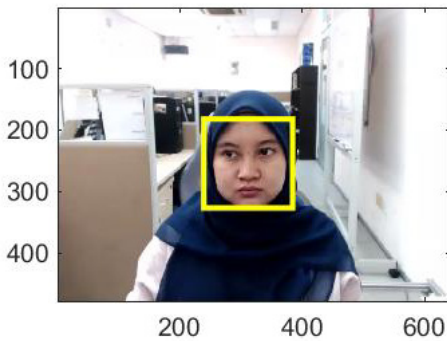


Figure 5: Face feature detection by Haar-like feature

From Figure 6, it shows the rectangular subset of the detection window that will determines whether it looks like a face. Two-rectangle features are shown in (A) and (B) while three-rectangle feature in (C) and (D) a four-rectangle feature. Two-rectangular feature is the different between the sum of pixels within two rectangular regions and both have the same size and shape with horizontally or vertically adjacent. As for three-rectangular feature is the different of the sum within two outside rectangles subtracted from the sum in a center rectangle. While the four-rectangle feature is the difference between the diagonal pairs of rectangles.

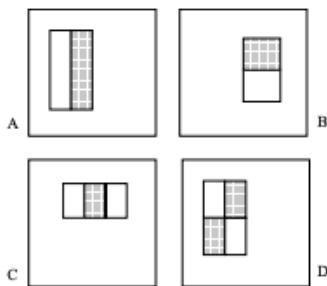


Figure 6: Example rectangle features shown relative to the enclosing detection window

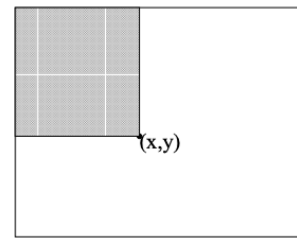


Figure 7: The value of integral image at point (x, y) is the sum of all the pixels above and to the left

Integral image is defined as the summation of all pixels in the image at point (x, y) above and to the left.

$$ii(x, y) = \sum_{x' \leq x, y' \leq y} i(x', y')$$

where $ii(x, y)$ is the integral image and $i(x, y)$ is the original image (Figure 7). By using pair of recurrences:

$$s(x, y) = s(x, y - 1) + i(x, y) \tag{2}$$

$$ii(x, y) = ii(x - 1, y) + s(x, y) \tag{3}$$

where $s(x, y)$ is the cumulative row sum, $s(x, -1) = 0$, and $ii(-1, y) = 0$, the integral image can be computed in one pass over the original image. By using integral image, any rectangular sum can be calculated in four array references as in Figure 8.

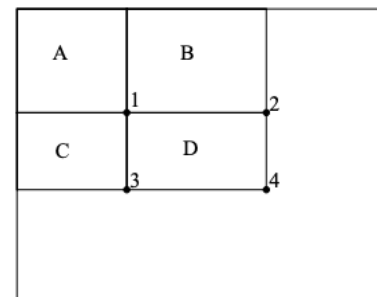


Figure 8: The sum of pixels within rectangle D can be calculate with four array references. The value of integral image at location 1 is the sum of pixels in rectangle A. The value at location 2 is A + B, at location 3 is A + C, and at location 4 is A + B + C + D. The sum within D can be computed as 4 + 1 - (2 + 3)

Haar feature used the image integral area to compute the value of a feature and its classifier multiply the weight of each rectangle by its area and the results are added together. Since the detection moved across the image of integral, face recognition filter is applied and when the filter gives a positive answer, it will return feedback as face detected in the current rectangle window.

Each face recognition filter contains a set of cascade-connected classifiers that looks at a rectangular subset of the detection window and determines if it looks like a face feature. The classifier will move to the next classifier until all classifiers and filter give a positive answer, the face feature is considered recognized. The Adaboost algorithm is applied to the training of the cascade classifier to minimize the computational time.

The process of feature extraction is continued by filter out the eye pair feature. After the eye pair is detected, the algorithm extracted only half of the eye pair from the user’s face feature image. The image of the eye feature is shown in Figure 9 below.

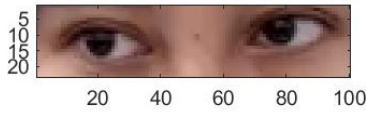


Figure 9: Eye pair feature

From the half of the eye pair feature, a circle detection algorithm is applied to extract the eye center coordinates. This circle detection is a feature extraction technique for detecting circles called Circle Hough Transform (CHT) where the parameters are containing the center of the circle and the radius. A circle can be described by:

$$(x - a)^2 + (y - b)^2 = r^2 \tag{4}$$

where (a, b) is the center of the circle, and r is the radius.

The coordinates will be used as the input data for training the calibration model. When the circle feature has been detected only then the eye center coordinates can be extracted and stored as the raw eye data. Figure 10 shown a circle that are being highlighted in the eye feature image.

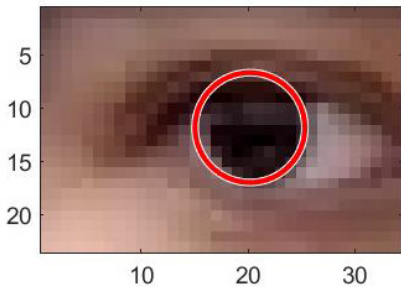


Figure 10: Circle detection on eye feature

2.3. Training the calibration model

After all processes of feature extraction has been done, the raw of eye center coordinates have been produced. These data must be normalized before training the data since the size of the user’s eye feature images extracted from the video and the computer screen are different in value.

The normalized eye center coordinates data is stored and be used by Neural Network algorithm for training the model. Neural network can learn and identify images that have been manually trained or labeled for the system to process. A few researches have been conducted using the neural network like [14,15] where they both used neural network for training and identify the parameters of calibration, and input images. Thus, this paper used the

approach of neural network to train the calibration model by using the normalized eye center coordinates data from previous process.

There are two sets of calibration points which are 4 points and 9 points that have been distributed at each specific location on the display screen. Thus, two neural networks are been trained for this paper. The type of neural network used is feed-forward back propagation algorithm.

Feed-forward is known for its simplicity of single layer perceptron network which consist of single layer of output nodes where the inputs are fed directly to the outputs via a series of weights. Back propagation is applied with the feed-forward neural network as it is a renowned representative from all iterative gradient descent algorithms that used for supervised learning. This method helps to calculate the gradient descent to looks for the minimum value of the error function in weight space as in Figure 11.

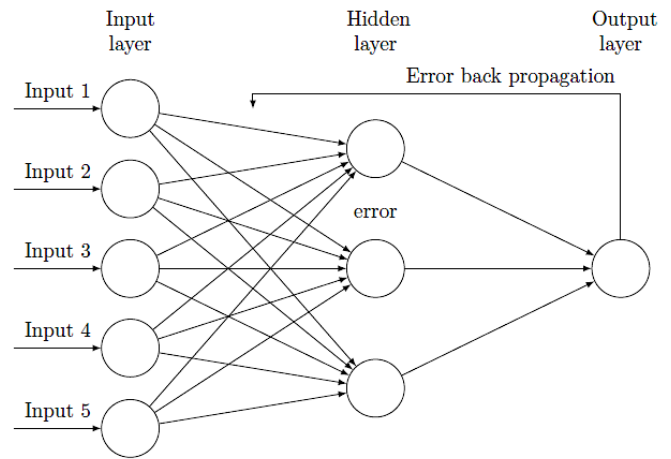


Figure 11: Neural Network architecture with back propagation

As shown in Figure 11, the input given is modeled by using real weights that are usually randomly selected. The output is computed for every neuron from the input layer, to the hidden layer, and to the outer layer. Error is then computed in the output by calculated the differences of the actual output with the desired output. This value will travel back from the output layer to the hidden layer to adjust the weights such that the error is decreased. This process is repeated until the desired output is achieved.

As for the training function, this paper compared the performance and computational time between 3 types of function which are Levenberg-Marquardt known for its fastest, Bayesian Regularization for its efficiency in difficult, small, or noisy datasets, and Scale Conjugate Gradient that requires less memory.

Levenberg-Marquardt (LM) is widely used optimization algorithm for it is outperform simple gradient descent and other conjugate methods. This algorithm provides the nonlinear least squares minimization. Basically, it consists in solving the equation:

$$(J^T J + \lambda I) \delta = J^T E \tag{5}$$

where J is the Jacobian matrix for the system, λ is the Levenberg’s damping factor, δ is the weight update vector that we want to find, and E is the error vector contained the output errors for each input vector used for training the network. The Levenberg-Marquardt is very sensitive to the initial network weights and does not consider outliers in the data that can lead to overfitting noise. For this situation, we will compare the performance with another technique known as Bayesian Regularization.

Bayesian Regularization can overcome the problem in interpolating noisy data which allows it to estimate the effective number of parameters that actually used by the model such as the number of network weights. It expands the cost function to search for minimal error while using the minimal weights. This function works by introducing two Bayesian hyperparameters, α and β , to tell which way the learning process must seek. The cost function is as follows:

$$C(k) = \beta^* E_d + \alpha^* E_w, \tag{6}$$

where E_d is the sum of squared error, and E_w is the sum of squared weights. By using Bayesian Regularization, cross validation can be avoided and can reduce the need for testing different number of hidden neurons. However, this technique may be failed to produce robust iterates if there is not much of a training data.

As for Scale Conjugate Gradient, developed by Moller [16], was designed to avoid time-consuming line search. The basic of this algorithm is to combine the model-trust region approach used in Levenberg-Marquardt with the conjugate gradient approach. It requires the network response to all training inputs to be compute several times for each search.

For achieving fast and efficient training model for calibration process, the best training function has to be selected. Thus, the three training functions consists of Levenberg-Marquardt, Bayesian Regularization, and Scale Conjugate Gradient are computed and analyzed the total iterations it takes for achieved minimal error, the processing time and the performance of the algorithm.

The training of 4 points calibration is being carried out first with the total number of neurons for hidden layer of 10, the input data of 200 and the output layer is 150. For each point of the input data, 50 values have been selected. The comparison of those 3 functions are as Table 1 below.

Table 1: Comparison of three training function for 4 points

Training Function	Iterations	Time	Performance
Levenberg-Marquardt	20 Epochs	1m 47sec	1.88e-09 mse
Bayesian Regularization	37 Epochs	5m 29sec	5.39e-08 mse
Scale Conjugate Gradient	76 Epochs	0sec	6.69e-07 mse

From Table 1, Levenberg-Marquardt achieved the minimal training with only 20 epochs of iterations, following with Bayesian Regularization of 37 epochs and lastly with the highest number of iterations of 76 epochs, Scale Conjugate Gradient. For the fastest function, Scale Conjugate Gradient achieved the best computational time with 0 seconds following with Levenberg-Marquardt and Bayesian Regularization. As for the best performance, Levenberg-Marquardt achieved it with only 1.88e-09 mean squared error that is nearest to zero values.

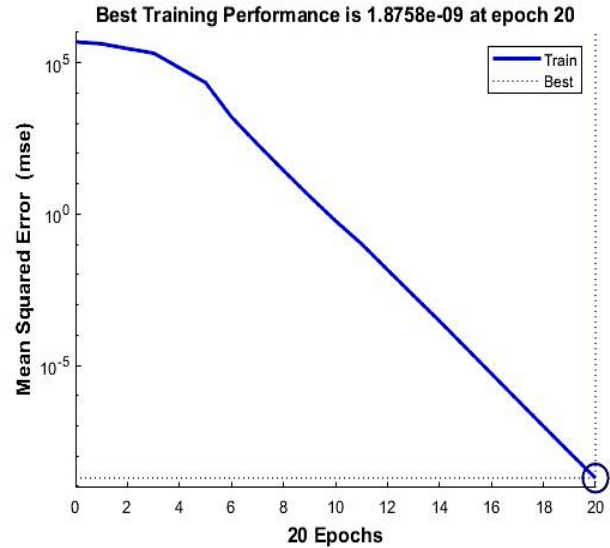


Figure 12: Performance of Levenberg-Marquardt for 4 points calibration model

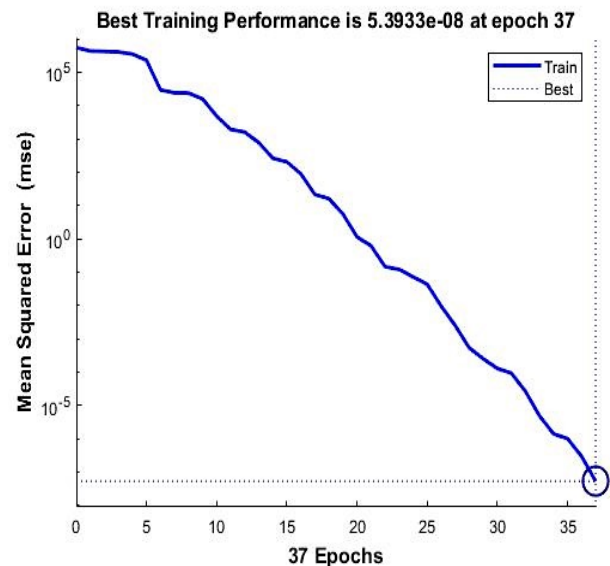


Figure 13: Performance of Bayesian Regularization for 4 points calibration model

From Figure 12,13 and 14, it is shown that the best training performance are from the training function of Levenberg-Marquardt, followed by Bayesian Regularization and Scale Conjugate Gradient. As for the regression values which measure the correlation between outputs and targets data, all three training functions achieved a close relationship with R value of 1 as shown in Figure 15.

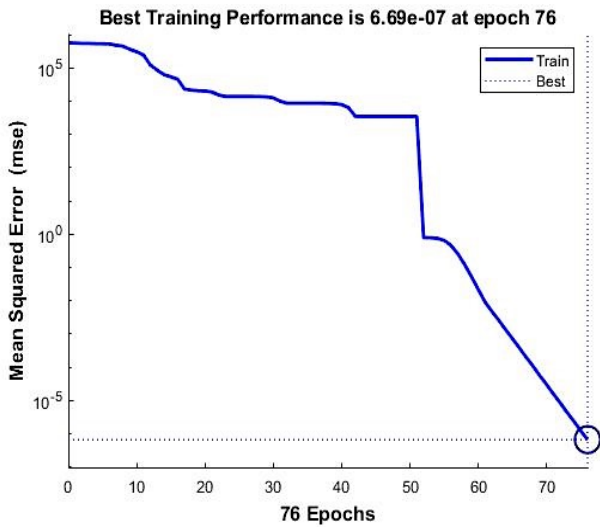


Figure 14: Performance of Scale Conjugate Gradient for 4 points calibration model

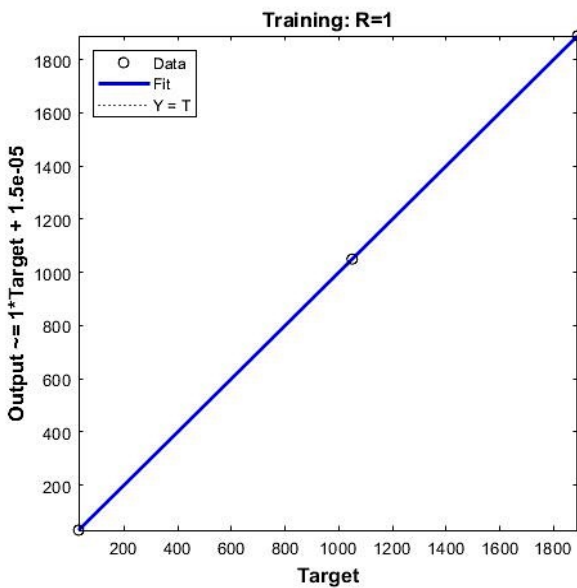


Figure 15: Regression values of all three-training function for 4 points calibration

For the training of 9 points calibration, the total number of neurons for hidden layer is 10, the input data of 455 and the output layer is 404. The total number of input data for each point are also 50 values which make the input data for neural network of 9 points calibration is 455. Table 2 shown the comparison of the three-training function for 9 points calibration.

Table 2: Comparison of three training function for 9 points

Training Function	Iterations	Time	Performance
Levenberg-Marquardt	20 Epochs	24m 55sec	1.97e-09 mse
Bayesian Regularization	43 Epochs	1h 25m 44sec	3.56e-08 mse
Scale Conjugate Gradient	446 Epochs	2sec	8.41e-07 mse

From Table 2, Levenberg-Marquardt achieved the minimum iterations of 20 compared to Scale Conjugate Gradient which achieved the highest iteration of 446 epochs. Even though Levenberg-Marquardt achieved the minimum iterations, it cannot be compared with Scale Conjugate Gradient for its computational time. This function required only 2 seconds to finish compared with the other two functions of Levenberg-Marquardt and Bayesian Regularization each takes around 24 minutes and 1 hour 25 minutes.

Since this modeling is from 9 points calibration which contains 455 inputs data, it's proven that Scale Conjugate Gradient are the fastest training function even by given many datasets. For the best performance of the training model, Levenberg-Marquardt outdone the other two functions by achieved mean squared error of 1.97e-09 as shown in Figure 16 below.

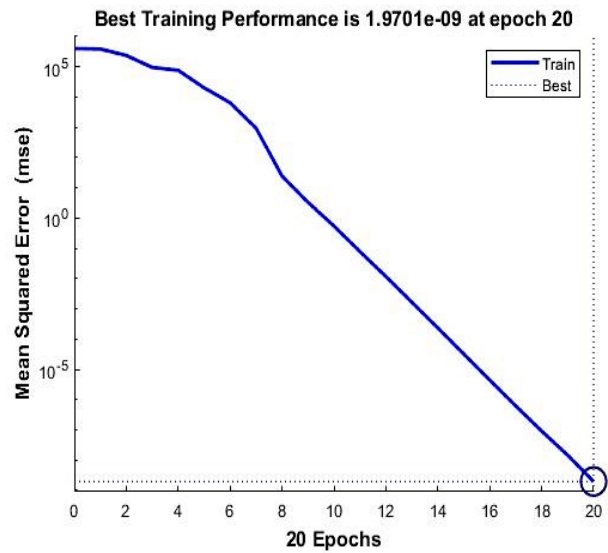


Figure 16: Performance of Levenberg-Marquardt for 9 points calibration model

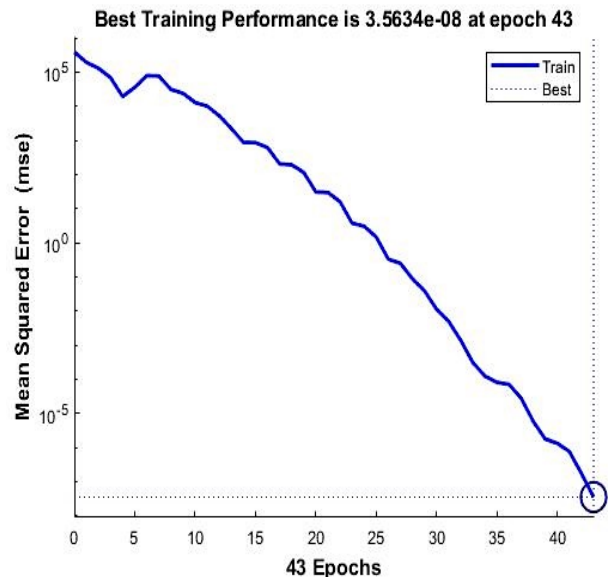


Figure 17: Performance of Bayesian Regularization for 9 points calibration model

Figure 17 and 18 are the performance achieved by Bayesian Regularization and Scale Conjugate Gradient for the 9 points calibration model. Bayesian Regularization achieved its best performance of 3.568-08 mse at the iterations of 43 while Scale Conjugate Gradient achieved its performance at 8.41e-07 mse at the iterations of 446.

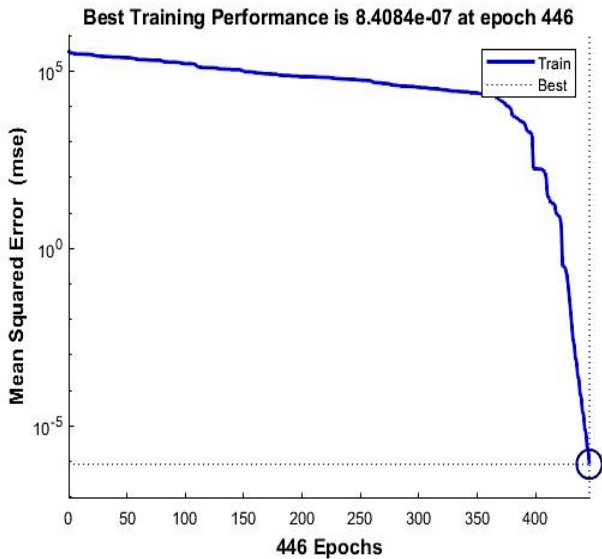


Figure 18: Performance of Scale Conjugate Gradient for 9 points calibration model

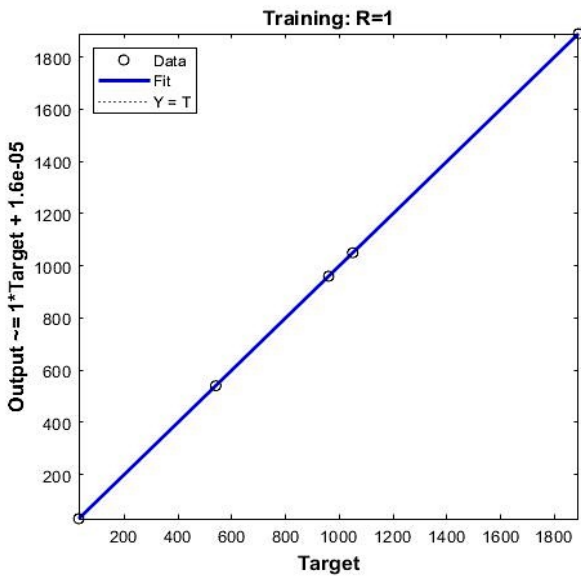


Figure 19: Regression values of all three-training function for 9 points calibration

As for the regression values, all the training functions have gained close relationship with R value of 1 as shown in Figure 19.

3. Discussion

The raw eye center coordinates data required normalization which are crucial process that can affect the performance of the data itself. Thus, this normalization can be improved or automated directly in the algorithm so that the process of the training data can

be simplified. As for training models, back propagation is proven to be fast, simple and does not need any special mention of the features of the function to be learned but can be quite sensitive to noisy data and the actual performance dependent on the input data given. From the training functions that we have used, taken from the results of their performance, the best training function is Levenberg-Marquardt that is proven the best for its efficiency and good performance while gaining minimum iterations of error with fast computational time even though Scale Conjugate Gradient is a lot faster, the iterations of the error is too high.

4. Conclusions

In this paper, the eye feature extraction and calibration model were conducted by applying Viola-Jones and Neural Network algorithms. Viola-Jones approach using the Haar-like features that involve sums of pixels with integral image by minimizing computational time with Adaboost algorithm and detected the feature of face. As for the Neural Network, the feed-forward back propagation algorithm is applied together and compared the performance and efficiency of three training functions; Levenberg-Marquardt, Bayesian Regularization, and Scale Conjugate Gradient. The overall result shown that these algorithms can be applied and improve the performance and lessen the computational time for eye data training for calibration model.

Conflict of Interest

The authors declare no conflict of interest.

References

- [1] F. N. Ibrahim, Z. M. Zin and N. Ibrahim, "Eye Center Detection Using Combined Viola-Jones and Neural Network Algorithms," 2018 International Symposium on Agent, Multi-Agent Systems and Robotics (ISAMSR), Putrajaya, 2018, pp. 1-6. doi: 10.1109/ISAMSR.2018.8540543.
- [2] N. Steinhausen, R. Prance, and H. Prance, "A three sensor eye tracking system based on electrooculography," IEEE SENSORS 2014 Proc., pp. 1084–1087, 2014.
- [3] P. Aqueveque and E. J. Pino, "Eye-Tracking Capabilities of Low-Cost EOG System," 36th Annu. Int. Conf. IEEE Eng. Med. Biol. Soc., pp. 610–613, 2014.
- [4] H. Manabe, M. Fukumoto, and T. Yagi, "Automatic drift calibration for EOG-based gaze input interface," Proc. Annu. Int. Conf. IEEE Eng. Med. Biol. Soc. EMBS, pp. 53–56, 2013.
- [5] D. Model and M. Eizenman, "User-calibration-free remote eye-gaze tracking system with extended tracking range," Can. Conf. Electr. Comput. Eng., pp. 001268–001271, 2011.
- [6] J. Chen and Q. Ji, "Probabilistic gaze estimation without active personal calibration," Proc. IEEE Comput. Soc. Conf. Comput. Vis. Pattern Recognit., pp. 609–616, 2011.
- [7] Y. Sugano, Y. Matsushita, and Y. Sato, "Calibration-free gaze sensing using saliency maps," Proc. IEEE Comput. Soc. Conf. Comput. Vis. Pattern Recognit., pp. 2667–2674, 2010.
- [8] F. Alnajar, T. Gevers, R. Valenti, and S. Ghebreab, "Calibration-Free Gaze Estimation Using Human Gaze Patterns," 2013 IEEE Int. Conf. Comput. Vis., pp. 137–144, 2013.
- [9] Y. Zhang, A. Bulling, and H. Gellersen, "Pupil-canthen-ratio: a calibration-free method for tracking horizontal gaze direction," Proc. AVI, pp. 129–132, 2014.
- [10] K. Harezlak, P. Kasprowski, and M. Stasch, "Towards accurate eye tracker calibration – methods and procedures," Procedia - Procedia Comput. Sci., vol. 35, pp. 1073–1081, 2014.

- [11] K. Pfeuffer, M. Vidal, and J. Turner, "Pursuit calibration: making gaze calibration less tedious and more flexible," Proc. 26th ..., pp. 261–269, 2013.
- [12] Bhoi, N., & Mohanty, M. N., "Template Matching based Eye Detection in Facial Image," *International Journal of Computer Applications*, 12(5), pp. 15-18, 2010 doi:10.5120/1676-2262.
- [13] P. Viola and M. Jones, "Rapid object detection using a boosted cascade of simple features," Proceedings of the 2001 IEEE Computer Society Conference on Computer Vision and Pattern Recognition. CVPR 2001, Kauai, HI, USA, 2001, pp. I-I. doi: 10.1109/CVPR.2001.990517
- [14] M. Wang, Y. Maeda, K. Naruki, and Y. Takahashi, "Attention prediction system based on eye tracking and saliency map by fuzzy neural network," 2014 Jt. 7th Int. Conf. Soft Comput. Intell. Syst. 15th Int. Symp. Adv. Intell. Syst., pp. 339–342, 2014.
- [15] E. Demjén, V. Aboši, and Z. Tomori, "Eye tracking using artificial neural networks for human computer interaction.," *Physiol. Res.*, vol. 60, no. 5, pp. 841–4, 2011.
- [16] Møller, M. F., "A scaled conjugate gradient algorithm for fast supervised learning," *Neural Networks*, 6(4), pp. 525-533, 1993 doi:10.1016/s0893-6080(05)80056-5.

Development of Evaluation Metrics for Learners in Unplugged Activity

Woochun Jun*

Seoul National University of Education, Department of Computer Education, 06639, Korea

ARTICLE INFO

Article history:

Received: 14 July, 2019

Accepted: 04 November, 2019

Online: 05 December, 2019

Keywords:

Unplugged Activity

Unplugged Computing

Evaluation Metrics

ABSTRACT

As well as physical computing, unplugged activity is important in ICT (Information and Communication Technology) education, that uses information and communications technology to support, enhance, and optimize the delivery of information, and software education. In order to achieve educational objectives in unplugged activity, evaluation metrics of learners are necessary. However, there is little work on evaluation metrics in unplugged activity. In this paper, evaluation metrics of learners are proposed and developed using based on the general design principles and opinions of experts.

1. Introduction

This paper is an extension of work originally presented in ICTC2018[1].

Unplugged activity is a teaching method that literally learns about a computer without using a computer. In the origin, Professor Tim Bell of New Zealand suggested a new way of teaching students to learn the principles of computer science by learning the principles of computer operation and creative ideas that invented and developed computers through specific manipulation activities. Through the unplugged method, play learning materials in the form of specific manipulations were developed and applied to understand the principles of operation of algorithms and computers, such as expression, alignment, search, algorithm, routing, and deadlock of data without using the computer.

Unplugged learning is a new method of education for elementary and middle school computer education, so students can learn the principles of computer science easily and interestingly. Unplugged learning was initially a teaching method for elementary school students, but it can be easily used and applied to anyone who wants to learn the principles of computer science. Learning in the form of play related to specific experiences and real life has led to a change in the concept of computer science as an easier and more interesting subject. And it gave teachers a new direction in

computer education to effectively teach logical computer science subjects without the need for computer and programming.

Unplugged activity has a big advantage. That is, it is to let students not to feel busy, feel fun and good. It also emphasizes cooperative thinking rather than competition from individuals, and uses computers to help people think in abundance. Unplugged activity can be said to be a new computer education created between ideas and activities for learners, and it has given teachers a new direction in computer education in that they can effectively teach logical computer science subjects without the need for computer and programming learning [2,3].

For the successful fulfillment of unplugged activity in ICT education, it is necessary to establish certain and secure evaluation standards or metrics for learners. That is, according to proper evaluation metrics, learners must be evaluated and education contents or teaching-learning method can be updated or modified depending on result of evaluation metrics.

However, in the literature, there is little research work on evaluation of learners in unplugged activity. The purpose of this paper is to develop evaluation metrics of learners in unplugged activity. For this purpose, in this work, overall categories are proposed and detailed evaluation metrics items are proposed depending on each category.

The rest of this paper is organized as follows. In Chapter 2, related works for unplugged activity is introduced. In Chapter3, evaluation metrics of learners are proposed. Finally, in Chapter 4, conclusions and further research issues are discussed.

*Corresponding Author: Woochun Jun, Seocho Dong, Seocho Gu, Seoul, Korea, wocjun@snu.ac.kr

2. Related Works

2.1. Principles of Unplugged Activity

In the literature [4], there are 10 principles of unplugged activity. That is, 10 class activity design principles are suggested. Those principles are also main characteristics of unplugged activity. The followings are those principles.

- No Computers Required

The first principle implies that a computer is not used at all. It means that the main objective of unplugged activity is not to use computers while students are learning the principles and concepts of computer science.

- Real Computer Science

Unplugged activity can have students to know basic principles of computer science such as database, software engineering, computer architecture, computer graphics, communication network, operating systems, and programming languages through a variety of unplugged activities. That is, the purpose of unplugged activity is to let students understand the various concepts of computer science. It means that unplugged activity must include the main principles of computer science in their activities.

- Learning by doing

"Learning by doing" is accompanied by the emphasis of progressive education. It provides solutions based on the constructivism that students can learn new concepts by participating in active activities voluntarily with a purpose. That is, students can learn the concepts of computer science through discovery learning on their own. That is, rather than providing what learners need to know from the beginning, such as the discovery learning principle presented by Bruner, the learning can proceed in a situation that requires the learner to organize the final form or content on his or her own. In other words, the logic is that students can understand their learning more deeply by participating in the discovery process of knowledge. Therefore, it does not conform to the basic concepts of unplugged activities to present and understand concepts, principles and ideas immediately.

- Fun

Unplugged activity should keep the rules and principles by learning the concepts of computer science through play and activity, gain fun through play, and make learners feel a sense of achievement in your activities. This is because if students are not given enough fun in the course of "Learning by doing," they can turn into activities that the teacher understands and forces them to understand rather than acquire them. Therefore, teachers present some rules along with basic data, and students solve tasks according to the rules presented by the teachers. The caveat in unplugged activities should be that the activities give students challenges and competitive psychology, as well as fully reflecting the interesting points in the process of problem solving. The activities should also be organized so that students can be fully satisfied with the sense of achievement they achieve in the process.

- No special equipment

www.astesj.com

The materials available for use in unplugged activities can be various objects used in our lives. That is, we do not use computers, and we use things that are readily available around us to organize activities that include the concepts of computer science. For instance, various materials can be used, such as cards, threads, chalk, cups, balls, pencils, and colored paper.

- Variation encouraged

Unplugged activity recommends that computer scientists from all over the world participate together through the Creative Commons License (CCL). It also respects open thinking so that changes, adaptations and extensions can be made to previously developed activities.

- For Everyone

Unplugged activity can be applied to any age group. If you are a beginner who first comes across the principles of computer science, you can use them extensively, from elementary school students to the elderly, regardless of age. It can also be used in various ways, not dependent on a particular country, culture or society.

- Co-operative

One of unplugged activity's main goals is cooperation. In other words, rather than solving a problem on the learner's own, he or she solves the problem through various collaborative work with his colleagues, and discovers the principles of computer science contained in it. That is, it emphasizes collaborative learning, which is the main philosophy of the theory of constructivism of learning. It is suitable for team activities rather than individuals, and is applicable in competitive situations.

- Stand-alone activities

The main objective of unplugged activities is to acquire the concepts of computer science embedded in the content of the activities, while carrying out activities that include the basic concepts or principles of computer science. Therefore, individual activity should not be dependent each other and can present a single computer principle in one activity. In other words, if multiple concepts or principles are included in an activity, it is difficult to exclude the possibility of a misconception.

- Resilient

Since unplugged activity is focused on activities that can learn the concepts or principles of computer science and also does not focus on understanding or memorization, it is difficult to present the principles or all very difficult steps precisely. Therefore, even if there is the possibility of small mistakes or misconceptions, it should be able to demonstrate the flexibility to implement them, unless they are a major obstacle to understanding the principles of computer science.

2.2. Literature Review

In [5], unplugged activities for information protection education applicable to primary and secondary schools are proposed. Unplugged activities developed in this study were designed using Lickona's integrated morality model and unplugged activity design pattern, and developed after expert review and pilot testing for elementary school students. The developed activities were applied to 21 middle school students and their usefulness was assessed.

In [1], an evaluation standard of unplugged activity is proposed. The following table 1 shows the whole standard.

Table 1: Evaluation Standard

Number	Standards	Description
1	Computer	Is any computer (including notebook, tablet PC, or other electronic devices) necessary?
2	Fun	Does the activity give fun to students?
3	Computer Science Principle	Does the activity deliver any idea or principle of computer science theory?
4	Student Participation	Does the activity require active participation of all students?
5	Independent Activity	Does the activity represent any independent computer science theory?
6	Learning by Doing	Does student learn by doing?
7	For everyone	Can everyone participate the activity?
8	Background	Does the activity require any academic background or preliminary course?
9	Safety	Is the activity is safe?
10	Report	Does the activity let student submit activity report?

3. Development of Evaluation Metrics for Learners

In this chapter, evaluation metrics for learners in unplugged activity are proposed. The proposed metric is developed based on the previous research works and experts from ICT education such as professors and teachers.

3.1 Design Principles

The proposed evaluation metrics are developed as following principles. First, they are based on 10 design principles of unplugged activity in previous chapter. It means that the metrics are in accordance with 10 design principles. Second, the proposed metrics are developed to test students' participation and interest in unplugged activity. Third, metrics are developed to test how much learners understand the overall idea or principle in computer science theory.

3.2 Evaluation Metrics

The following table 2 shows the overall evaluation metrics of unplugged activity.

Table 2: Evaluation Metrics

Number	Metrics	Description
1	Understanding	Do learners understand the whole idea or principle of computer science theory?
2	Fun	Do learners have fun or feel fun during unplugged activity?
3	Participation	Do learners participate in activity actively or positively?
4	Interest	Do learners have interests on unplugged activity?
5	Safety	Do learners feel safe during unplugged activity?
6	Cooperation	Are learners engaged well in unplugged activity?
7	Assistance	Do learners have chance for assistance from teacher or friends?
8	Communication	Do learners have chance to communicate each other during unplugged activity?
9	Expandability	Can learners expand the unplugged activity with more member?
10	Applicability	Can learners apply the unplugged activity for other similar activity?

4 Conclusions and Further Research Issues

Currently informatics education becomes popular in the forms of software education and ICT education, etc. Informatics education is important in raising human resource in artificial intelligence areas [6,7]. Informatics education also becomes mandatory education in primary and secondary schools in many countries.

Unplugged activity becomes popular in ICT education and software education since it does not require any special equipment including computer. It means that unplugged activity can be done any place any time. The main purpose of unplugged activity is to let learners' study computer science theory or

principles with play activity.

In order for unplugged activity to be successful, the correct and general evaluation metrics for learners are necessary. It is very important to check how learners understand the overall principle or theory. However, in the literature, there is little research work on evaluation metrics for learners. In this paper, evaluation metrics are developed. The metrics are developed in accordance with design principles of unplugged activity and the general education purpose of ICT education.

The further research issues are as follows. First, it is necessary to refine the proposed evaluation metrics further. That is, more detailed metrics are necessary depending on various unplugged activities. Second, it is also necessary to test the validity of the proposed metrics. For this purpose, the extensive survey work and analysis work are essential.

Conflict of Interest

The authors declare no conflict of interest.

References

- [1] W. C. Jun, "A Study on Development of Evaluation Standards for Unplugged Activity" in 2018 International Conference on Information and Communication Technology Convergence, Jeju Island, Korea, 2018. <http://10.1109/ICTC.2018.8539505>
- [2] J. R. Kim, "A Study on Systematic Review of Unplugged Activity" *Journal of the Korean Society of Information Education*, 22(1), 103-111, 2018. <http://dx.doi.org/10.14352/jkaie.2018.22.1.103>
- [3] Y. H. Bae, C. S. Na, "Effectiveness of Unplugged Activity in Korean Education: A Meta-Analysis" *The Journal of Educational Information and Media*, 25(1), 121-150, 2019. <http://dx.doi.org/10.15833/KAFEIAM.25.1.121>
- [4] W. K. Lee and J. M. Kim, "Research Report on Unplugged Activity", Research Report, The Korean Society of Computer Education, 2015.
- [5] Y. J. Jang, D. H. Kim, H. S. Kim, W. K. Lee, H. C. Kim, "Development of Unplugged Activity and its Evaluation of Usability for Information Security Education" *The Journal of Korean Association of Computer Education*, 14(1), 55-67, 2011.
- [6] C. Gokul, P. Sakthivel and P. R. Karthikeyan, "Minimization of Test Time in System-on-Chip using Artificial Intelligence based Test Scheduling Techniques, Neural Computing & Applications, 2019. <https://doi.org/10.1007/s00521-019-04039-6>.
- [7] C. Gokul, P. Sakthivel and P. R. Karthikeyan, "Test scheduling for system on chip using modified firefly and modified ABC algorithms, *SN Applied Sciences*. 1(9), 1079, 2019. <https://doi.org/10.1007/s42452-019-1116-x>.

SCMS: Tool for Assessing a Novel Taxonomy of Complexity Metrics for any Java Project at the Class and Method Levels based on Statement Level Metrics

Issar Arab^{1,2,*}, Bouchaib Falah³, Kenneth Magel⁴

¹Department of Informatics, Technical University of Munich, 80333, Germany

²Faculty of Pharmacy and Pharmaceutical Sciences, University of Alberta, 8613, Canada

³School of Science and Engineering, Al Akhawayn University in Ifrane, 53000, Morocco

⁴Faculty of Computer Science, North Dakota State University, ND 58108-6050, USA

ARTICLE INFO

Article history:

Received: 20 September, 2019

Accepted: 14 November, 2019

Online: 05 December, 2019

Keywords:

Software Testing

Complexity Metrics

Software Metrics Tool

Effectiveness

Data Flow

Data Usage

Taxonomy

JAVA

ABSTRACT

Software is the primary and indispensable entity in our technologically driven world. Therefore, quality assurance, and in particular software testing, represents a vital component in the software development cycle. Throughout the years, many tools have been developed to collect metrics of software that had been implemented. These tools have some differences but continue to play an important role in improving the quality of software products. This paper introduces a newly developed tool, named Spectra Complexity Metrics System (SCMS), which compiles a novel taxonomy of complexity metrics of any given software written in the Java programming language. Our suggested metrics have been invented to identify and evaluate the characteristics of Java computer programs. They aim at increasing the efficiency of the testing process by significantly reducing the number of test cases without having a significant drop in test effectiveness. We assess our proposed taxonomy of different complexity metrics based on the product levels (statement, method, and class) and their characteristics. For further evaluation, our software metrics coverage is compared to other existing software metric tools. The results show the novelty of our taxonomy of complexity metrics and the capability of our tool to compute these measurements based on all three of the product level categories. We have published our tool at <https://github.com/issararab/SCMS> under an open-source license.

1. Introduction

Over the current decade, concerns over present and future software quality have grown, as have the range and complexity of software and its applications. Increasingly, developers, researchers, and users are dissatisfied with the quality of available software. Hence, we have seen a growing focus on software testing, where the engineers' main job is to assess and quantify the quality of a given product. The key challenge in this field is to reduce costs and maximize benefits. Those challenges have motivated software engineers to develop metrics or rules for quantifying given characteristics and attributes of software entities. For good quality software, these characteristics should be understandable and measurable [1]. These metrics aim to validate and verify the quality and the assurance of software. As it is

extremely time-consuming and requires a great deal of time and effort, the overall testing process needs to be automated for testing practices [2].

This article is an extension of a paper previously presented in the International Conference on Software Engineering Research and Practice (SERP 2015), in Las Vegas, NV, USA [3]. Our contribution in this paper consists of explaining the theory behind our suggested taxonomy and presenting the first tool, SCMS, that compiles this introduced set of metrics. Furthermore, we are benchmarking the software metrics coverage against state-of-the-art tools. Our SCMS tool will be used to evaluate the complexity metrics, primarily following a static analysis, of any program written in Java language. The strength of this tool is that it is implemented to compute metrics at three different levels (statement, method, class). The tool outputs a CSV file of either

*Issar Arab & Email: issar.arab@gmail.com

www.astesj.com

<https://dx.doi.org/10.25046/aj040629>

the 20 metrics of all classes or the 9 metrics of all methods of a given Java project, based on statement level metrics. The set of metrics is discussed in later sections.

2. Related Work

Numerous tools have been implemented to compute metrics from a program's source code. These tools are very important factors in the reliability of the metrics, as their rules are well defined formulas producing after each run the same value on a similar input. There are numerous commercial, non-commercial and open source metric tools that are available for measuring code complexity.

One commonly used metric tool is an Eclipse plug-in for Java programming language maintained by IBM, which calculates numerous metrics for the source code during build cycles and warns the tester, via the problem view of 'range violations' for each metric [4]. These violations are derived from rules built in the tool which can be modified to fit local conditions. This allows the user to stay continuously aware of the program's source code's health. One of the advantages of using this Eclipse plug-in tool is the possibility of exporting the metrics in HTML, CSV or XML format.

VizzAnalyzer Framework [5] is another software tool that measures the quality of a Java implemented software system. In the VizzAnalyzer implementation, Welf et al. [5] rely on the RECODER meta-programming library [6], providing a compiler front-end for Java programs and an API for accessing AST and semantic analysis results. The software computes a set of metrics that are well established in the literature, such as metrics from the C&K metric suite as well as newly developed metrics including Data Abstraction Coupling (DAC), Package Data Abstract Coupling (PDAC), Edge Size, Tight Class Cohesion (TCC), Tight Package Cohesion (TPC), and Lack of Documentation (LOD) [5].

In what concerns other programming languages, Pymetrics is a famous open source complexity metrics measurement tool implemented by Charney [7]. It is a tool that compiles metrics for Python source code only. Metrics include McCabe's Cyclomatic Complexity [1, 8], LOC, etc. One of the main features of this tool is the output format. It allows users to customize their own reports as well as the option to output either to stdout, SQL files, or CSV files.

According to the article in [9], test tools can be divided into seven groups: design, implementation, evaluation, load, performance, GUI, dynamic and static analysis. In our study, we focus only on the last category, that deals with static and dynamic complexity metric tools. In this category, the most famous and widely used assessment metrics by far are the LOC (lines of code) and Cyclomatic Complexity [1, 8, 3]. However, the use of Object-Oriented (OO) languages has pushed researchers to come up with novel taxonomies of complexity metrics to evaluate OO solutions. The metrics introduced in [10] are very popular in dealing with Object-Oriented design and are used in the coding phase. The approach presented is based on mathematical formula that describe the relationships between the different variables. Moreover, the metrics proposed are designed to determine quantitative measures by studying the operators and operands used in the code. These metrics are referred to as 'Software Science' and are used in the

development stage in order to assess the code. Another set of metrics is presented by Chidamber et al. in [11]. These metrics deal with many principles related to Object-Oriented development for the sake of enhancing software maintenance.

Numerous metrics have been introduced, discussed, scrutinized, and published. Those measurements were implemented in multiple commercial and open source tools, which raises one important question: do these metric tools produce the same values for the same metrics on the same input? This has been investigated by Lincke et al. in [12]. The authors conducted an experiment with ten commercial and free metrics tools. Using these tools, a set of nine complexity metrics were computed on the same software systems. Their investigation showed that, given the same input, metrics tools deliver different results. One reason for the disparity is the looseness of the definition of most metrics. Different tools may interpret even a simple metric such as LOC differently (e.g. are blank lines counted or not).

3. Novel Taxonomy of Complexity Metrics

In general, a metric is defined as a measurement and any measurement can be a useful metric. Software engineers use measurement throughout the entire development cycle by measuring the characteristics of software to get some notion of whether the software fulfills the requirements consistently and completely. Additionally, metrics measure the design quality and whether the software is ready for testing. Project Managers measure attributes of the product to be able to tell when the software will be ready for delivery and whether the budget will be exceeded. Customers measure aspects of the final product to determine if it meets their requirements and if its quality is sufficient. Finally, maintainers must be able to assess and evaluate the product to see what should be upgraded and improved [3].

Software metrics can be clustered into four main categories [1]:

- Product
- Process
- People
- Value of the Customer

In this paper, our focus was on the product metrics as being the main selectors for test cases. As opposed to the previous work done in the domain, we focus on the development of a comprehensive taxonomy based on two main criteria:

1. Which product level is the metric applied on?
2. And which feature does the metric measures at a given product complexity level?

The suggested taxonomy of metrics can be projected into a 2-dimensional space where each axis represents one criterion as shown in Figure 1 [3]. Each datapoint in the graph represents the metric computed by SCMS tool given its coordinates, where x-axis (kind) represents the type of metrics measured and the y-axis (scope) represents the product level at which the metric is applied. The grouping of data points in the graph visualizes the number of metrics under a similar type compiled at a given product level. For instance, the top right cluster of points shows that 4 metrics under data usage type are computed at the class level.

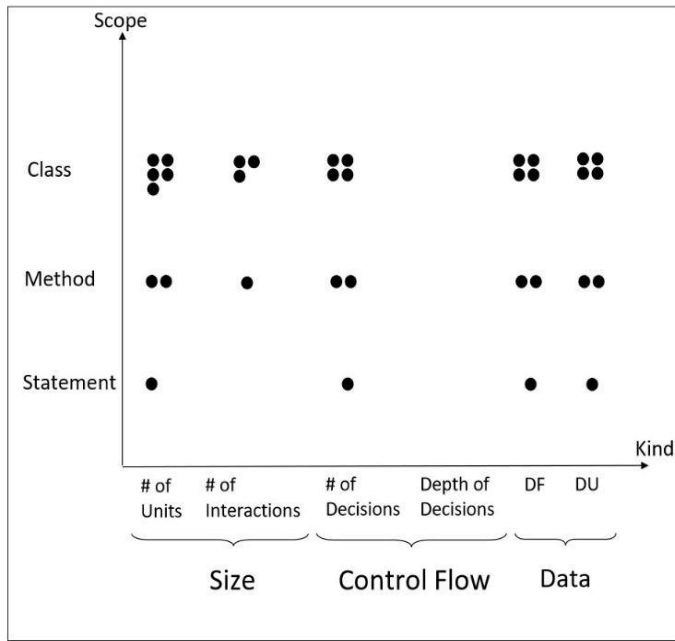


Figure 1: Our suggested taxonomy dimensions compiled by SCMS tool where y-axis (scope) represents the product level at which the metric is applied and the x-axis (kind) represents the type of metrics measured. The small clusters of datapoints in the graph shows the number of metrics under a similar type compiled at a given product level

4. Metrics at Statement Level

4.1. Data Complexity

Data complexity metrics are studied in our work by two different means, data flow and data usage. Data flow measures how the data behaves taking into consideration its interactions within the system [3, 13, 14]. It is defined as the number of ‘formal parameters of activities and the mappings between activities’ data. It tracks the flow of the data through the system in order to detect errors related to the usage and interactions of variables between each other. Data flow has been the choice of many testers due to its close relationship with the Object-Oriented principle of cohesion. On the other hand, data usage for a statement is defined to be the number of variable values used in that statement plus one if the computed equation is being assigned to a variable in that statement. It is based on the number of data defined in the unit being considered or the number of data related to that unit. From a software testing point of view, the data usage metric is simply the sum of uses (p-uses and c-uses) plus definition variables in a given statement.

4.2. Control Flow Complexity

McCabe’s Cyclomatic complexity metric [a, h, c] is a widely and well-established measurement in the literature used in this category. It has been implemented by many software complexity tools for different programming languages and especially for Object-Oriented ones. Basically, the idea behind Thomas McCabe’s metric is that software complexity increases with the number of control paths generated by its code [8]. A control path is determined by the existence of a control block, also named scope, that includes predicates as a condition to fork a flow in a

path. From these observations, we chose the scope level metric of a given statement as the measurement of choice for this category. This method requires counting how many control constructs (do-while, if-else, while, for, etc.) are present in the source code [15].

4.3. Size Complexity

Size Complexity is one of the oldest measures in software engineering to quantify the length, functionality, and complexity of software [16]. One of the most widely used and easiest to compute measures in this category is the number of Lines of Code (LOC). However, many other size metrics are based on Halstead Software Science Definition [10]. It is a traditional measurement of complexity metrics tackling the issue from one single view, which is the number of operators.

Halstead measure counts all the types of operators including traditional operators (ex. +, /, and ||) and punctuations (ex. ; and ()), where one opening and closing pair of parenthesis is counted as one. From our point of view, the most important metric to identify the complexity of a statement is just the number of traditional operators. While, you can blow up Halstead metric by adding as many parentheses as one wants without altering the complexity of the system. Hence, for simplicity, we suggest using a subset of Halstead measurement dealing only with traditional operators, by counting the number of operators used in each statement.

4.4. Statement Level Metrics Summary

Table 1 represents the four metrics compiled by SCMS tool at the statement level of a Java code.

Table 1: Statement level spectrum of metrics computed by SCMS tool

Metric Short Name	Short Description
NumOp	Number of Operators
NumLev	Number of Levels
DF	Data Flow
DU	Data Usage

5. Metrics at Method Level

A method consists of a set of statements performing a specific functionality. Therefore, metrics at this granularity can be derived from previously computed statement metrics. For method level measurements, we suggest two strategies: the first is to calculate the sum of the same precomputed measurement of all statements in the method, and the second is to compute the maximum value of the same metric among all statements constructing the method [3, 17, 18]. This adds up to eight metrics at the method level derived from the statement level metrics. Additionally, we added a 9th metric, InMetCall, which counts the number of methods within the same class calling the method being studied.

Table 2 represents and defines the nine metrics compiled by SCMS tool at the method level of a Java code. The output is in CSV format including the class path to the method as well as its type.

Table 2: Method level spectrum of metrics computed by SCMS tool

Metric Short Name	Short Description
MaxOp	Maximum number of operators of each statement in the method. Metric based on the statements results
TotOp	Total number of operators of each statement in the method. Metric based on the statements results
MaxLev	Maximum number levels at each statement in the method. Metric based on the statements results
TotLev	Total number of levels at each statement in the method. Metric based on the statements results
MaxDF	Maximum number of data flow of each statement in the method. Metric based on the statements results
TotDF	Total number of data flow of each statement in the method. Metric based on the statements results
MaxDU	Maximum number of data usage of each statement in the method. Metric based on the statements results
TotDU	Total number of data usage of each statement in the method. Metric based on the statements results
InMetCall	Number of within class method calls of the method in question

Table 3: Class level spectrum of metrics computed by SCMS tool

Metric Short Name	Short Description
Tot2Op	Counts the total number of operators. (method output based)
TotMaxOp	Counts the total of the max operators. (method output based)
Max2Op	Counts the max of max operators. (method output based)
MaxTotOp	Counts the max of the total number of operators. (method output based)
Tot2Lev	Counts the total number of levels in the whole class code. (method output based)
TotMaxLev	Counts the sum of the maximum level in each method.
MaxTotLev	Counts the max of the total number of levels in each method.
Max2Lev	Counts the max level in the whole class, i.e. the deepest branch. (method output based)
Tot2DU	Counts the total number of data usage in the class. (method output based)
TotMaxDU	Counts the total number of the max data usage in the class. (method output based)
MaxTotDU	Counts the max of the total number of data usage in each method. (method output based)
Max2DU	Counts the max of max data usage. (method output based)
Tot2DF	Counts the total number of data flows in a class. (method output based)
TotMaxDF	Counts the total of the max data flows in each method of the class. (method output based)
Max2DF	Counts the max of max data flows in each method of the class. (method output based)
MaxTotDF	Counts the max of the total data flows in each method of the class. (method output based)
TotInMetCall	Counts the total number of within class method calls. (method output based)
MaxInMetCall	Counts the max number of within class method calls. (method output based)
inOutDeg	Counts the number of in class call of external methods. Similar to out degrees of a dynamic call graph.
pubMembers	Counts the number of members in a class.

6. Metrics at Class Level

The main entity in Object-Oriented design is the class. A class is a combination of attributes and methods. From this definition, we can derive the class level metrics given precomputed measurements at method level. Following the same approach applied to compute method level metrics, we again compute the total and the maximum of each measurement of the methods in a class [3, 17, 18].

We then add two additional metrics: the in-out degree of that class, which is the number of methods outside of that class that are called by at least one method in that class, and the number of public members within the class, i.e. attributes and methods in a class [c]. The public members within a class are defined as the public fields and the public methods declared in that class. Table 3 and Figure 2 depict the 20 metrics compiled by SCMS tool at the class level of a Java program as outputted in the CSV file by SCMS tool. Figure 2 shows how the 18 class level metrics, blue, are derived from the 9 method level ones, green, adding on top the In-Out Degree and the Number of Public Members.

7. Spectra Complexity Metric System (SCMS)

Spectra Complexity Metric System (SCMS), is a software that allows any Java software engineer to assess the complexity of a Java program using the above described metrics.

The tool is implemented using the Java 1.8 and Maven 3 framework. It makes use of the ASTParser pre-built Java library that allows you to convert a given Java class into an Abstract Syntax Tree for evaluation.

Figure 3 shows the UML class diagram of our tool, where CMSRunner class represents the main entry point of the software. The main class uses FileUtils functionalities to extract all the java files in the project to be assessed; then, it translates each file into an abstract syntax tree via the class Parser. This parse tree is then traversed, using AstClassExplorer and AstStatementExplorer, to retrieve the relevant information to our suggested taxonomy in

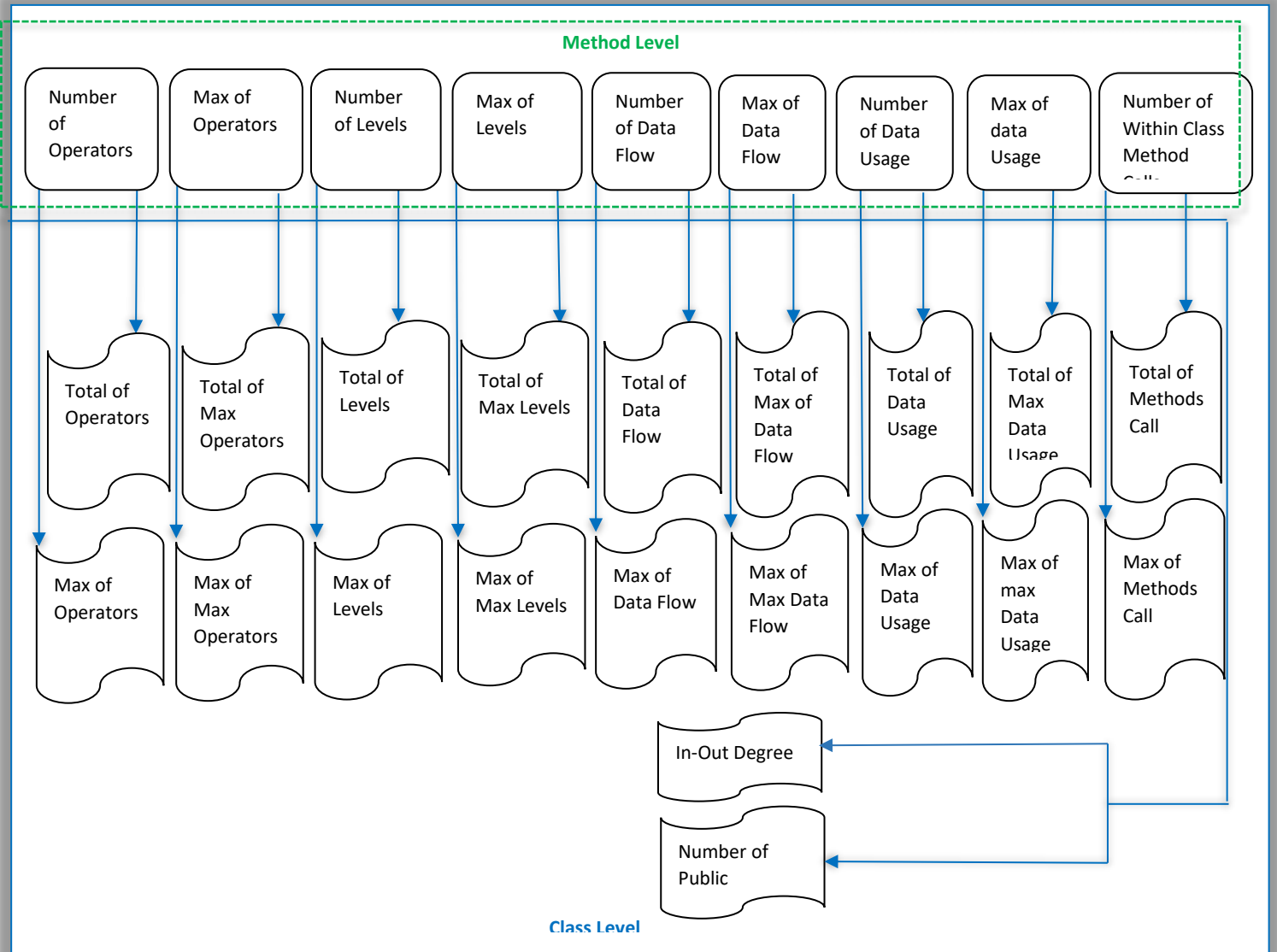


Figure 2: Taxonomy of class level complexity metrics derived from the method level ones as they are compiled by SCMS tool

order to populate the metrics fields. The metrics are organized by Scope (product level) as fields in the classes Statement, Method, and Class shown in the UML diagram.

8. SCMS Tool Evaluation and Benchmarking

In this evaluation, we focus on the product metrics category to compare existing software tools with our suggested taxonomy. As a first step, we want to showcase the importance of automated tools to calculate complexity metrics. Then provide a detailed description of the selected tools in order to make the comparison with our software. And finally, we compared our SCMS tool with the different tools based on three main levels, namely statement, method, and class level.

8.1. Manual vs. Automated Metric Evaluation

Software quality assessment has been researched by engineers and pioneers in the field to express quality attributes of a software. Therefore, solid numbers and measures should be

generated for a program to better assess its complexity. Many tools have been developed to collect metrics from a system that has been implemented. Moreover, these tools have differences in myriad aspects.

The two questions that might be asked here are: why do we need tools? And why can't we measure the complexity of a program manually or only by reading through the program's code? The answer to these questions is that the complexity of a software has increased tremendously [16]. A system now may contain thousands of lines of code which makes measuring its complexity manually not viable.

Therefore, there is a need for tools that analyze files and components of a system rapidly and generate reports. The results will then be used to optimize the process of test case generation. These measurements can give a software developer a deep view of the different non-functional requirements such as maintainability and performance. Furthermore, a tool follows repeatable and consistent calculation procedures in assessing a

program. Therefore, compiled information can be easily interpreted and analyzed via graphical and data visualization techniques. On the other hand, calculating metrics manually adds an overhead to the software testers, which may lengthen the testing phase, usually taking much more time than the development period. The manual process is very tedious, especially when it comes to complex software that contains a very large number of units [16]. Therefore, complexity metrics tools are essential in assessing the quality of a program.

The tool is described mainly as a static code analysis tool since it takes as input the program code to compute metrics. The computed metrics are based on several aspects ranging from relationships between components, volume, and complexity. The JHawk tool delivers both the process and the product quality metrics. We retrieved only the list of product metrics. JHawk calculates complexity metrics on all levels. The system level is the container or the upper layer as it wraps all the remaining levels which are method, class, and package level. Table 4 shows a sample set of metrics calculated by the JHawk tool at the method and class levels [19].

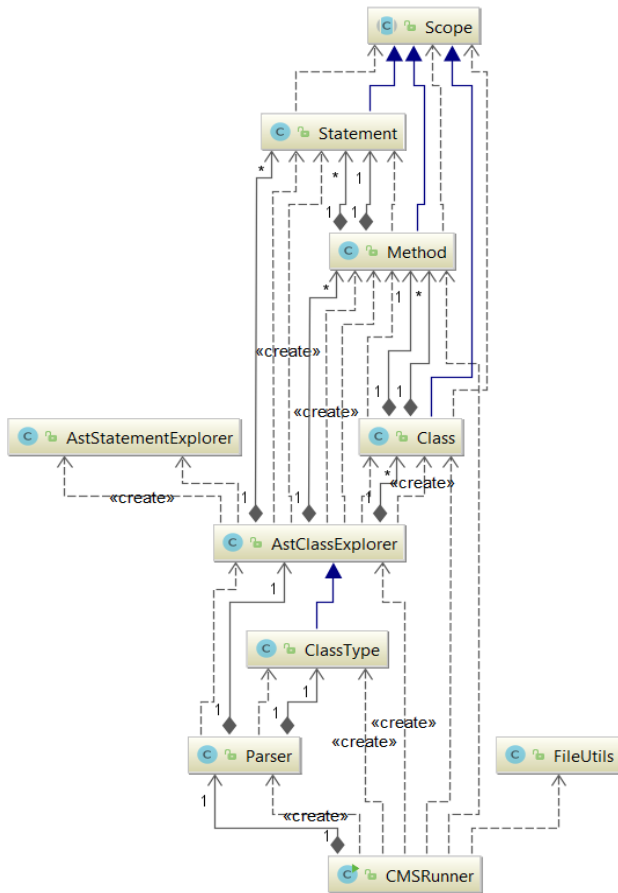


Figure 3: Simplified UML class diagram of SCMS tool

8.2. Selection Process of Tools

An investigation through the available tools online showed that most of the tools provide process and product quality attributes. In order to make a reliable benchmarking of our software, we only picked tools computing product quality metrics based on three criteria. The first criterion was to select tools that have a large set of product metrics. Second, the focus was only on tools calculating complexity metrics for object-oriented programming languages. Third, the selection was based on the ease and regularity of how tools are deployed and used. Usability of the tools was a key selection criterion in our study.

8.3. Selected Tools Summary

8.3.1 JHawk Tool

The first software tool we examined is called JHawk. JHawk was developed to compute complexity metrics for Java programs.

Table 4: Class and method level metrics measured by JHawk

Level	Metric Name	Metric Description
Method	Number of Arguments	The number of arguments per method
	Variable Declaration	The number of variables declared in the method
	Number of Statements	The number of statements in the method
	Number of Loops	The number of loops (for, while...) in the method
	Number of Operators	The total number of operators in the method
	Number of Operands	The total number of operands in the method
Class	Number of Statements	The number of statements in the class
	External Method Calls	The external methods called by the class and methods in the class
	Lines of Code	The number of lines of code in the class and its methods
	Modifiers	The modifiers (public, protected, etc) applied to the declaration of the class
	Local Methods Calls	The local methods called by the class and by methods in the class that are defined in the hierarchy of the class
	Instance variable	The instance variables defined by the class

8.3.2 Analyst4J

Analyst4J was developed both as a plugin for Eclipse Integrated Development Environment, and as an application that can be installed and executed independently [12]. Analyst4J was designed to provide several functionalities of a Java program including:

- Computing metrics
- Analysing source code
- Generating reports containing information about a Java program

Analyst4j V1.5.0 version supports regression testing by analyzing code before and after being changed. It provides an easy to read report about the design and maintainability of the system to be used. Moreover, code quality can be easily analyzed by the tool. Analyst4J can be integrated with bug finding tools in order to maintain Java programs. It also provides several complexity metrics for java programs including complex classes and methods.

8.3.3 CCCC Tool

CCCC is a software tool designed mainly to measure Cyclomatic Complexity of code in a program. It is generally used for two main programming languages which are C and C++. The generated output from this tool is a web page containing detailed information of all the program source code. This tool is freely available for download and use [20].

CCCC generates the following information about a given program:

- The number of lines for each module in a program
- McCabe Cyclomatic Complexity metric
- Coupling between different components
- Object-oriented metrics as depth of inheritance tree
- Chidamber and Kemerer complexity suite

8.3.4 JMetric Tool

This tool was created by Cain and Vasa [21] for a project at COTAR in Australia. It calculates object-oriented metrics for the Java code. JMetric was installed to retrieve the product metrics it calculates. This tool computes complexity metrics at five different levels: project, package, class, method, and variable level. Table 5 shows a sample set of the computed metrics by JMetric at the method and class levels relevant to our product measurements comparison study.

Table 5: Class and method level metrics measured by JMetric

Level	Metric Name	Metric Description
Method	Number of Statements	The number of statements in the method
	Collaboration	Collaboration with other methods or units
	Cyclomatic Complexity	Cyclomatic complexity of the method
	Lines of Code	The total number of lines of code in the method
Class	Number of Statements	The number of statements in the class
	Number of Methods	The number of methods in the class
	Lines of Code	The number of lines of code in the class and its methods
	Public Methods	Count the number of public methods in the class
	Local Methods Calls	The local methods called by the class and by methods in the class that are defined in the hierarchy of the class
	Instance variable	The instance variables defined by the class

8.3.5 NDepend Tool

NDepend was designed to analyze code developed in .NET technology. This tool has a large support for code metrics since it analyzes the program code at six different levels:

- Metrics on application
- Metrics on assemblies

- Metrics on namespaces
- Metrics on types
- Metrics on methods
- And metrics on fields

Table 6 shows a partial list of metrics calculated by the NDepend tool [22].

Table 6: Sample of complexity metrics computed by NDepend

Level	Metric Name	Metric Description
Application	NbLinesOfCode	Computing the number of logical lines of code of the application
	NbLinesOf Comment	Number of lines of comment that can be found in the application
	NbMethods	Number of methods for the whole application/program
	NbFields	The number of fields. The field can be either regular, enumeration value, or other types.
Method	NbLinesOfCode	Number of lines of code inside a method
	NbOverloads	The number of overloads of a method
	NbLinesOf Comment	Number of comments within a method
	NbParameters,	Number of methods inside a method
	NbVariables	Number of variables in a method
Field	Size of Instance	The size in bytes of instances
	Afferent coupling at field level (FieldCa)	The number of methods that directly use a field

8.3.6 Chidamber and Kemerer Java Metrics (CKJM) Tool

The Chidamber and Kemerer metrics were among the first introduced metrics in the history of software metrics.

CK metrics objectives are [23]:

- To measure unique aspects of OO approach
- To measure complexity of the design
- To improve the development of the software

Diomidis Spinellis developed a tool named CKJM [24] to compute the Chidamber and Kemerer suite of metrics. This tool measures these metrics by processing the bytecode of compiled Java files. Java files are compiled prior to be given as input to the CKJM. For each class of the program or project, CKJM provides as output the six well known metrics of Chidamber and Kemerer. The six metrics that are calculated by the CKJM are:

- WMC: Weighted methods per class
- DIT: Depth of Inheritance Tree
- NOC: Number of Children
- CBO: Coupling between object classes
- RFC: Response for a Class
- LCOM: Lack of cohesion in methods

8.4. Comparison to SCMS tool

In our benchmarking, we considered only similar metrics to our presented novel taxonomy computed by CSMS and discarded the rest. The four stated metrics at the level of a statement will be used as the basis to derive other high-level complexity metrics, namely for the method and class level.

Table 7: Statement level comparison

Tools	Metrics				
	Name	Level Number	Data Flow	Data Usage	Number of Operators
SCMS		x	x	x	x
Analyst4j			x		
JMetric			x		
CCCC			x		
CKJM			x		
JHawk			x		
NDepend			x		

Table 8: Method level comparison

Tools	Metrics									
	Name	Total # of levels	Max # of levels	Total # of operators	Max # of operators	Total # of DF	Max # of DF	Tot # of DU	Max # of DU	# In Method Calls
SCMS		x	x	x	x	x	x	x	x	x
NDepend		x	x	x		x	x			
Analyst4j		x		x	x	x	x			
JMetric				x	x	x	x			
CCCC				x		x	x			
CKJM				x		x	x			
JHawk				x		x	x			

As illustrated in Table 7, the only metric that is measured at the statement level by all the selected tools is the data flow (DF) metric. This shows the uniqueness and the added value of our tool. Likewise, at the method level in Table 8, we see that the closest tools to our software are NDepend and Analyst4j with a coverage of 55% of our suggested taxonomy. Also, three metrics in our suggested set is covered by all of the selected tools. Those are the total number of operators, the total number of DF and the maximum DF. Furthermore, since the class level metrics are derived from the method level ones by computing the sum and the maximum, we can conclude that only six metrics from a total of 18 metrics are covered at the class level by all those selected tools. Therefore, we show the novelty and the added value of our suggested taxonomy and Spectra Complexity Metric System.

9. Conclusion and Future Work

This paper presents a tool, SCMS, which evaluates and assesses a novel comprehensive taxonomy of complexity metrics, following a bottom-up approach, of any given software written in Java language. These measurements can then be used to optimize

the process of test case generation by targeting the complex units in the system. The taxonomy tackles the issue from two dimensions. The first being the scope/product dimension and it covers the metrics at three granularity levels: statement, method, and class level. The second being the type of evaluation, which covers three types of metrics measurements: the size focusing on the number of units/operators, the control flow focusing on the number of decisions, and the data type focusing on both the data flow and the data usage. Those metrics have as a goal to increase the efficiency of the testing process by significantly reducing the number of test cases without having a significant drop in test effectiveness. The paper also covers the design and technology used to implement SCMS tool by providing a UML class diagram of the software which can offer insights for a starting point of any future development of new complexity metric tools. Finally, we have compared our tool with the major existing Java related tools that cover a large set of product level metrics in the market. We showed the novelty of our taxonomy of complexity metrics and the capability of our tool to compute these measurements based on the three different product categories. The tool is available as an open source at <https://github.com/issararab/SCMS>.

In the future, we will investigate the usability of this tool as well as other tools with their potential in software diagnosability and fault detection. Our aim is to gather a large set of features/metrics and combining them with machine learning algorithms to artificially predict the faulty units in a software. Our unit level of interest as of now is the class level.

Conflict of Interest

The authors declare no conflict of interest.

Acknowledgment

The authors would like to thank reviewers for their exceptionally constructive reviews to improve this work and inspire future work. The authors would like also to thank their sponsor, Al Akhawayn University in Ifrane, for funding this project.

References

- [1] T. J. McCabe, C. W. Butler, "Design complexity measurement and testing", in 1989 ACM 32, 12, 1415-1425. DOI: <http://dx.doi.org/10.1145/76380.76382>
- [2] I. Arab, S. Bourhnane, Reducing the cost of mutation operators through a novel taxonomy: application on scripting languages, in 2018 Proceedings of the International Conference on Geoinformatics and Data Analysis (ICGDA '18). ACM, New York, NY, USA, 47-56. DOI: <https://doi.org/10.1145/3220228.3220264>
- [3] F. Bouchaib and K. Magel. (2015). "Taxonomy Dimensions of Complexity Metrics" Int'l Conf. Software Eng. Research and Practice , pp. 96-102: Las Vegas, Nevada, USA. Available: https://www.researchgate.net/publication/281858313_Taxonomy_Dimensions_of_Complexity_Metrics
- [4] <https://marketplace.eclipse.org/content/eclipse-metrics> (accessed on May 2019)
- [5] L. Welf, E. Morgan, L. Jonas, P. Thomas, P. Niklas, VizzAnalyzer- A Software Comprehension Framework, 2003 Available: https://www.researchgate.net/publication/241753972_VizzAnalyzer-A_Software_Comprehension_Framework
- [6] A. Ludwig, RECODER Homepage, <http://recoder.sf.net>, 2001.
- [7] R. Charney, Programming Tools: Code Complexity Metrics, Jan 2005, Available: <https://www.linuxjournal.com/article/8035>

- [8] T. J. McCabe, "A Complexity Measure", in July 1976 IEEE Trans. Softw. Eng. 2, 4, 308-320. DOI: <https://doi.org/10.1109/TSE.1976.233837>
- [9] P. Pohjolainen, Software Testing Tools, Department of Computer Science and Applied Mathematics, 2002. Available: <http://cs.uef.fi/uku/tutkimus/Teho/SoftwareTestingTools.pdf>
- [10] M. H. Halstead. "Elements of Software Science (Operating and Programming Systems Series)". Elsevier Science Inc., New York, NY, USA, 1977
- [11] S. R. Chidamber, C. F. Kemerer, "A Metrics Suite for Object Oriented Design". in June 1994 IEEE Trans. Softw. Eng. 20, 6, 476-493. DOI=<http://dx.doi.org/10.1109/32.295895>
- [12] R. Lincke, J. Lundberg, W. Löwe, "Comparing software metrics tools". in 2008 In Proceedings of the 2008 international symposium on Software testing and analysis (ISSTA '08). ACM, New York, NY, USA, 131-142. DOI: <https://doi.org/10.1145/1390630.1390648>
- [13] J. Cardoso, "Control-Flow Complexity Measurement of Processes and Weyuker's Properties," Word Academy of Science, Engineering and Technology, August 2005.
- [14] J. Cardoso, "Control-flow Complexity Measurement of Processes and Weyuker's Properties." in 2007 International Journal of Mathematical and Computational Sciences Vol:1, No:8, 2007. doi.org/10.5281/zenodo.1076476
- [15] J. Cardoso, How to Measure the Control-flow Complexity of Web processes and Workflows, Workflow Handbook, Future Strategies Inc., pp.199-212, 2005
- [16] A. Arenas, J. Duch, A. Fernandez, S. Gomez, "Size Reduction of Complex Networks Preserving Modularity", in 2007 New Journal of Physics 9, P. 176, iopscience.iop.org/article/10.1088/1367-2630/9/6/176
- [17] Y. Shin, A. Meneely, L. Williams, J. A. Osborne, "Evaluating complexity code churn and developer activity metrics as indicators of software vulnerabilities", in 2011 IEEE Transactions on Software Engineering, vol. 37, no. 6, pp. 772-787
- [18] B. Falah, K. Magel. (2013) "Test Case Selection Based on a Spectrum of Complexity Metrics". Proceedings of 2012 on International Conference on Information Technology and Software Engineering (ITSE), Lecture Notes in Electrical Engineering, Volume 212, pp. 223-235, DOI: 10.1007/978-3-642-34531-9_24
- [19] Virtual Machinery, "Download JHawk Trial Version", Virtual Machinery, 2017. [on ligne]. Available: <http://www.virtualmachinery.com/jhdownload.htm>
- [20] B. Wicht, (August 2011) "How to Compute Metrics of C++ project using CCCC". [on ligne]. Available: <https://baptiste-wicht.com/posts/2011/08/compute-metrics-of-c-project-using-cccc.html>
- [21] A. Cain, R. Vasa, and D. Franek, Source Forge.(accessed. 20.05.2019) Available: <https://sourceforge.net/p/jmetric/wiki/Home/>
- [22] P. Smacchia, "Partitioning Your Code Base Through .NET Assemblies and Visual Studio Projects," Redgate Hub, accessed. 10.06.2019 Available: <https://www.red-gate.com/simple-talk/dotnet/net-framework/partitioning-your-code-base-through-net-assemblies-and-visual-studio-projects/>.
- [23] S. R. Chidamber and C. F. Kemerer , "Towards a Metrics Suite for Object Oriented Design", in October 1991 C onference proceedings on Object-oriented programming systems, languages, and applications (OOPSLA '91), Andreas Paepcke (Ed.). ACM, New York, NY, USA, 197-211. DOI=<http://dx.doi.org/10.1145/117954.117970>
- [24] Diomidis Spinellis. Tool writing: A forgotten art? IEEE Software, 22(4):9-11, July/August 2005. (doi:10.1109/MS.2005.111).

Attacks classification and security mechanisms in Wireless Sensor Networks

Amine Kardi^{1*}, Rachid Zagrouba²

¹Faculty of Mathematical, Physical and Natural Sciences of Tunis, University of Tunis El Manar, 2092 El Manar, Tunisia

²College of Computer Science and Information Technology, Imam Abdulrahman Bin Faisal University, P.O. Box 1982, Dammam 31441, Saudi Arabia

ARTICLE INFO

Article history:

Received: 12 September, 2019

Accepted: 16 November, 2019

Online: 05 December, 2019

Keywords:

Wireless Sensor Networks

Routing attacks

Cryptography

Security

NS3 simulator

ABSTRACT

This paper proposes a new classification model distinguishing four classes of attacks in Wireless Sensor Networks (WSNs) namely: attacks based on the protocol stack, on the capability of the attacker, on the attack impacts and on the attack target. Then, it presents and classifies the most known attacks in WSNs based the proposed model. Simulations implemented under the NS3 simulator prove that the network lifetime can decrease by more than 45% in the presence of attacks. Afterwards, it discusses the main security methods and protocols of management and distribution of encryption keys used to ward off different types of attacks. Obtained results confirm that these security methods must be adapted to the specific characteristics of WSNs to achieve the intended objectives.

1. Introduction

With the widespread use of WSNs [1][2], composed of a small and low-powered communicating devices usually deployed in hostile environments, and due to their resources constraints, security factors become crucial and challenging with the appearance of a variety of attacks targeting these networks [3][4][5]. The main contribution of this paper is to provide a survey of these attacks and of the security techniques which will facilitate the design of WSNs for researchers and routing protocol programmers.

The rest of the paper is organized as follows: Security requirements for WSNs are discussed in Section 2. Section 3 introduces our proposed taxonomy and discusses each category of attacks. Section 4 presents the main attacks in WSNs and analyzes them using NS3 simulator. The basic security mechanisms in WSNs are presented in Section 5 then followed by the analysis and findings in section 6. Lastly; we conclude the paper and highlight our future work in section 7.

2. Security requirements for WSNs

Due to the lack of a wired communication medium, the limited resources of sensors and the properties of the deployment [6][7], WSNs, deployed mostly in hostile environments with mission-critical tasks, have several security challenges which are more

complex than with other types of networks. As an ad hoc network, security requirements for WSNs include the standard security metrics known as CIAA (Confidentiality, Integrity, Authentication and Availability) in addition to the security requirements specific to this type of network which aim to protect the information and resources from attacks and misbehavior. In the following we discuss the security properties and requirements we would like to achieve in order to establish a reliable communication in WSNs and to provide secure services [8].

2.1. Standard security requirements

As with other types of networks, standard security requirements are needed in WSNs such as:

- **Confidentiality:** This is the most important issue in network security which guards data from eavesdroppers. It ensures that a given message remains hidden and cannot be used by anyone other than the desired receiver. It protects packets from undertaking traffic analysis, passive attackers and modification. The standard approach for achieving this requires use of encryption techniques [9].
- **Integrity:** Data integrity is needed to ensure the reliability of data packets. In fact, sent packets must be protected from modification (adding, altering, deleting, damaging or losing) by malicious intermediate nodes or by wireless channel disturbance during the transmission [10].

*Amine Kardi, Tunis, (+216.96.27.90.33), Email : amine.kardi@fst.utm.tn

- **Authentication:** all applications require data authentication which ensures the reliability of the message by giving the ability of each communication host to identify its origin and to verify the other's identity to counter to packet injection or spoofing and to all malicious routing information. Critical characteristics of sensor nodes and the wireless nature of the communication medium in WSNs make extremely challenging to ensure authentication in these networks [11].
- **Availability:** Availability affects several sides in the sensor network. In fact, it determines whether a node can use the resources if needed, whether data and services are available for on-demand use and whether the network is always available to ensure communication even in the presence of malicious attacks. A loss of availability may have serious impacts and threat the entire network, e.g. it may open a backdoor for malicious invasion in some cases and sensed information may become useless or of lower value, but also providing availability can hurt the network lifetime especially with limited energy resources [12].

2.2. Specific security requirements

Node characteristics and deployment environments make WSNs vulnerable to special attacks and subsequently several security requirements specific to this type of networks are needed such as:

- **Authorization:** ensures that only authorized nodes can manipulate data (provide, update...) in the network and prevents unauthorized access to resources [13].
- **Nonrepudiation:** it prevents a node from denying sending a message it has previously sent through the network [14].
- **Data freshness:** implies that used data are recent and valuable and cannot be replayed by a malicious actor, under any circumstances, after abandonment to prevent, i.e. overloading the network by sending previously captured packets. Timestamps and time-related counters can be used to ensure data freshness [15].
- **Transparency:** after leaving the network a sensor node should not be able to replay old packets or to read any future messages in the same way as a joining node should not be able to reload or to read any previously transmitted message in order to protect the network from malicious injected nodes [16].
- **Self-Organization:** In the absence of an overall network management infrastructure, sensor nodes which have the ability of self- organization may encounter several hazards and risks threatening the safety and operation of the entire network [17].

Time Synchronization: due to its limited energy resources, sensor nodes may be turned off for periods of time in the form of a smart sleep in order to conserve energy and, in some application, the end-to-end delay of some packets is of a great extent that is why collaborative sensor nodes require a synchronization system which must be ensured by a secure synchronization protocol to deal with attacks that attempt to affect proper synchronization between nodes [18].

- **Secure Localization:** In several applications, sensor networks are designed to locate faults. Consequently, the network must be able to accurately and automatically locate each sensor node that is why location information must be handled in a secure manner to avoid attacks taking advantage of the security weaknesses of this information [19].
- **Anonymity:** malicious actors do not have to decrypt the source node of a packet in order to secure nodes and the sensing area which can be affected by erroneous data [20].
- **Survivability:** Network services and functionalities must be maintained even with the low levels required in the case of failures, attacks and compromised or destroyed nodes [21].

According to these security requirements, it's obvious that attacks in WSNs can be of different types and can affect the entire network system such as nodes, packets, data, paths, routing etc. The following section presents our proposed taxonomy.

3. Taxonomy of attacks in WSNs

Because of its specific characteristics, WSNs are vulnerable to various types of attacks. These attacks are of different mechanisms, techniques and goals which makes necessary to find and adopt a well-defined taxonomy in order to facilitate design and development of WSNs for researchers and protocol programmers.

According to the security requirements mentioned above, and taking into account the mechanisms and parameters of attacks; we propose a new taxonomy which divides attacks in WSNs into four major classes namely: **attacks based on the protocol stack, based on the capability of the attacker, based on the attack impacts and based on the attack target** as shown in figure 1.

A detail overview of each security attack class is discussed in the rest of this section.

3.1. Attacks based on protocol stack

The protocol stack used by nodes in a wireless sensor network consists of the Physical Layer, Data Link Layer, Network Layer, Transport Layer, Application Layer, power management plane, mobility management plane and task management plane as shown in figure 2. It ensures the energy efficiency in the network, manages the use of the wireless medium with the routing task and facilitates synchronization and cooperative efforts between sensor nodes.

Each level on the protocol stack takes on a set of tasks and guarantees a set of services. Therefore, it will be targeted by several attacks.

- Physical Layer:

This layer ensures the data transmission services which encompass the selection of access channels, radiofrequency regulation and deflection, signal processing and data encryption to increase the communications reliability. The importance of this layer exposes it to a variety of attacks targeting data privacy, resource depletion, signal and communications interruption, and so on [22].

- Data Link Layer:

This layer is responsible of physical addressing, error detection and/or correction, data streams multiplexing, medium access and

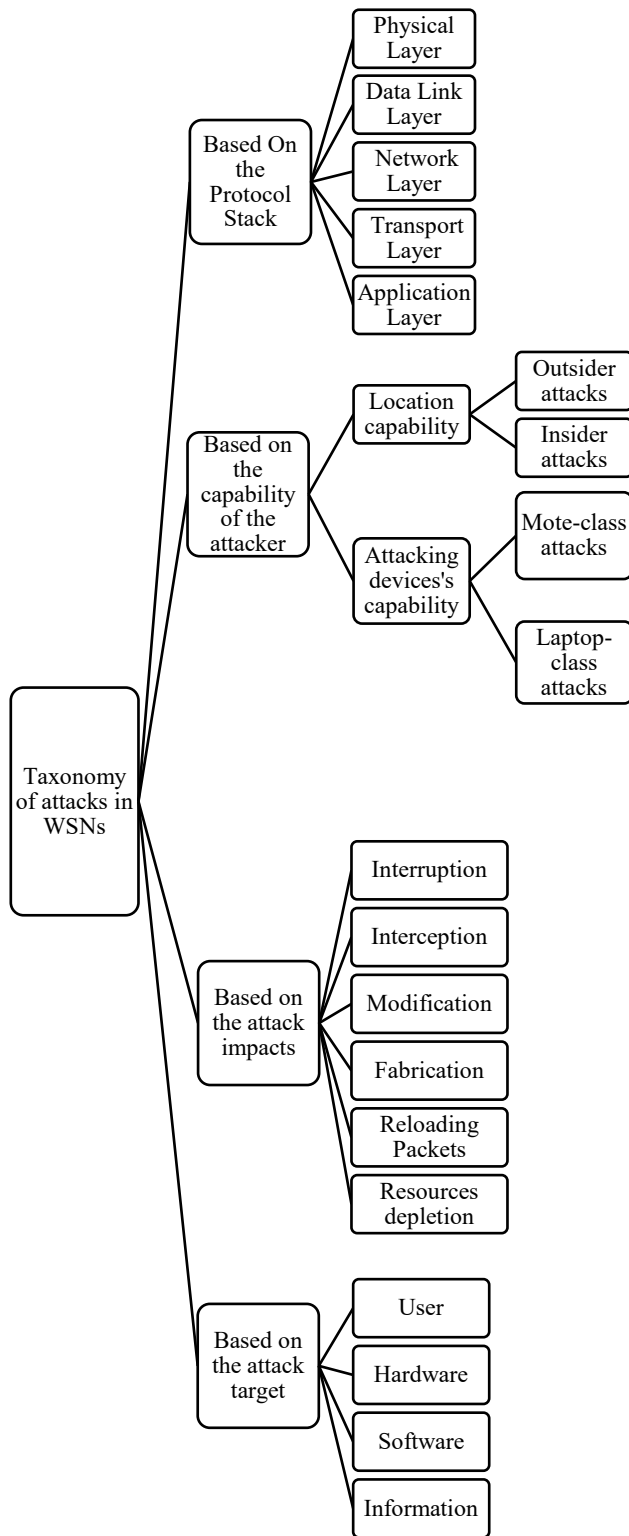


Figure 1: Security attacks in WSNs: A taxonomy

flow control as well as ensuring reliable point-to-point and point-to-multipoint connections in the network. The medium access control (MAC) protocol must support mobility and be able to handle collisions and to achieve energy efficiency in the network. The importance of this layer makes it vulnerable to several types of attacks sources of collisions, resource exhaustion, and network destruction [23].

- Network Layer:

This layer is in charge of routing the data supplied by its upper layer. It is very important task encompasses packets routing and forwarding, addresses assignment and energy management. These axial and fundamental tasks attract several attacks aimed at absorbing the network traffic, disrupting communication, exhausting resources, intercepting paths and injecting malicious packets [24].

- Transport Layer:

The transport layer ensures the management of end-to-end reliable delivery of packets connections and the establishment of end-to-end connection in addition to flow and congestion control. It is especially needed when the system is planned to communicate with external networks. Several attacks target this layer in order to reduce the network's availability, to degrade or even prevent data exchange and to waste energy [25].

- Application Layer:

This layer contains user applications which oversee the sensing tasks. It manipulates user data with a set of application protocols, and it is a target of attacks aiming at affecting the synchronization of communications and data confidentiality.

The power management plane and the mobility management plane are responsible, respectively, for the management of energy resources and the mobility of nodes in order to achieve maximum energy efficiency and stability of communications. The task management plane manages the sensing tasks and ensures synchronization between sensor nodes [26].

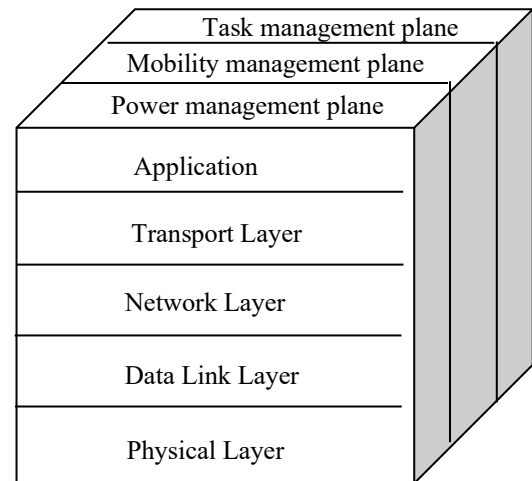


Figure 2: The protocol stack of sensor networks

3.2. Attacks based on the capability of the attacker

Based on the capability of the attacker, attacks in WSNs can be subdivided into two classes: Location capability and Attacking

device's capability. Each of these classes is further divided into two broad subclasses according to the relative capabilities of the attacker which are respectively: Outsider/ Insider attacks and Mote-class/ Laptop-class attacks. In the following we detail each of these subclasses.

- Outsider/ insider attacks

Based on the location capability of attackers, attacks in WSNs can be classified into Insider and Outsider attacks. We are talking about insider attacks when a legitimate nodes belonging to the network and which are actually part of it are compromised and participates in unintended and/or unauthorized ways in the attack contrary to outsider attacks which are launched only from outside the networks application environment and performed by external nodes which do not belong to the WSN. Insider attacks are more severe when compared with outside attacks since compromised nodes contains secret information and may not be detected due to the possesses privileged access rights they had. These attacks target the entire network and affect the resources, data, communications and even the existence of the network. Some papers refer to internal and external attacks [27].

- Mote-class/ laptop-class attacks

Based on the Attacking device's capability, attacks in WSNs can be classified into Mote-class and laptop-class attacks. In mote-class attacks, attackers use malicious nodes with similar techniques capabilities and hardware proprieties to the network nodes in order to execute malicious codes aiming to affect the network functionalities (data, routing, paths, energy management...). Contrariwise, attackers use more powerful devices with great transmission range, processing power, and energy supply than the network's sensor nodes in laptop-class attacks e.g., a laptop which results in launching more serious attacks and consequently lead to more serious damage to the target network [28].

3.3. Attacks based on the attack impacts

Based on the attack impacts, attacks in WSNs can be subdivided into six classes: Interruption, Interception, Modification, Fabrication, Reloading Packets and Resources depletion. In the following we detail each of these four classes.

- Interruption

The attacker aims, through some techniques, to interrupt the network's functionalities. These attacks are varied and can target nodes, sinks, paths, routing task, resources depletion etc. which threaten services availability. Even in the presence of an attack, the network must be capable of maintaining its functionalities without interruption [29].

- Interception

These attacks are used when the attacker intended to eavesdrop on the network information. This threatens message confidentiality, network services availability and may result in the depletion of resources [30].

- Modification

These attacks threaten data integrity. Attackers intend to eavesdrop to information and to tamper with it in various ways: Injection, removal, modification etc. in order to disrupt the network functionalities and threaten the accuracy of services and treatments [31].

www.astesj.com

- Fabrication

These attacks are manifested by the injection of erroneous data into the WSN. Attacker aims to threaten message authenticity and network availability through the depletion of the energy resources of the network especially with wireless communications which are very energy intensive [32].

- Reloading Packets

In some cases, the attacker seeks to reload and read previously transmitted packets from a compromised node or from buffers of active nodes which threatens data confidentiality and packets transparency. These packets can be injected back into the network, which threatens messages freshness and wastes energy [33].

- Resources depletion

In a WSN, resources depletion leads to the complete collapse of the network. Attackers aim to waste limited energy resources of nodes using various processing and transmission tasks [34].

3.4. Attacks based on the attack target

Attacks in a WSN can target different actors and components of the network which are users, hardware, software and information [35]. In the following we detail each of these targets.

- User

Various users of a WSN like humans, robots etc. can be targeted by malicious attacks aiming to have an authorized access to the network system through legitimate compromised identifiers. These attacks seek to take control of the network, to use it for personal tasks, to use information or to destroy it.

- Hardware

Attacks targeting hardware in WSNs tend to compromise nodes for malicious intent, waste limited energy resources or destroy equipment. A compromised node may contain secret information and may be used for unauthorized access to the network.

- Software

Attacks targeting software in WSNs aim to eavesdrop information, control the network and disrupt the services and functionalities.

- Information

Attacks targeting information in WSNs are various e.g. the attacker can falsify the data supposed to be sensed in the sensing area, in other cases, sensed data can be targeted by attacks, packets in transit, authentication parameters etc. Attackers aim at affecting the network functionalities, services availability and data confidentiality.

Each of these classes helps to analyze and study attacks in WSNs from different perspectives. We detail, in the following section, the most known attacks and countermeasures to counter their effects.

4. Attacks in WSNs

Generally, attacks under these four classes, can be either active or passive. A passive attack is an attack that aims to gets exchanged

data in the network without interrupting the communication to remain hidden and not be discovered. Passive attackers listen and collect data that can be used later to start other types of attacks. While active attacks involve some modifications in the data stream. In fact, it seeks to modify, fabricate, inject a false stream or intercept the data or the communication to disrupt the normal functionality of the network. In the active mode the attacker is more aggressive and aims to damage the entire network [36].

4.1. The most known attacks:

Among the most known attacks in WSNs we find:

- Jamming:

Jamming attack [37] takes advantages of the sensitivity of the wireless medium to interferences and results in a denial of service in the network. Attacker identifies the radio frequencies used by the targeted WSN and tries to disrupt or block communications by emitting signals (unnecessary information) in the same frequencies that inhibit communication (messages transmission and/or reception) between nodes. This interference may be temporary, intermittent or permanent and can affect all or part of the network depending on the radio range of the jamming source which can have the same characteristics as the network nodes as it can be more powerful. Jamming can be of different types: it can be constant if it targets and corrupts data packets in transit, deceptive when sending a constant data stream in the network, random when injected data streams are dispersed over time and reactive if the jamming source sends a jam signal following the detection of traffic. Jamming can target different layers: It can interfere with radio frequency signals at the physical layer, as it can take advantages of the medium access control protocol causing malicious collisions at the link layer as it can target the network layer by injecting malicious packets. Defense techniques [38][39][40] against Jamming attack involve spread-spectrum techniques for radio communication such as frequency hopping to switch between many frequency channels, authentication mechanisms to detect malicious and replayed packets, the use of secure medium access control protocols etc.

- Tampering or destruction [41]:

WSNs are highly vulnerable to physical attacks as they are often deployed in unprotected areas. A Tampering attack will be triggered after physically capturing the node and aims to retrieve cryptographic material as encryption keys and the program code stored within a node which can be used later to trigger other types of attacks such as modifying routing information, creating duplicate data packets, tampering routing services etc. or to manipulate the captured node by installing a new code causing an abnormal behavior of the compromised sensor, controlled by the attacker, in order to disrupt the network. Destruction attack consists of removing the sensor from the network by destroying it resulting in isolated areas and even the destruction of the entire network. Defense techniques against this attack are based on the principle of considering the situation in which sensor nodes are compromised such as tamper-proofing the physical package of nodes.

- Continuous Channel Access (Exhaustion):

Exhaustion [42] belongs to DoS attacks. It aims to exhaust the batteries of the nodes in order to reduce the network lifetime. It

consists to disrupt the Media Access Control protocol, by continuously injecting unnecessary packets in the network and requesting or transmitting data over the channel entail the waste of node energy in unnecessary retransmissions. A possible solution to this attack is the Rate Limiting at the MAC admission control which allows ignoring corrupted packets and excessive malicious requests [43] [44].

- Collision:

Collision attack [45], similar to the continuous channel attack, can be caused by malicious nodes by transmitting packets in the network in order to block / delay the communication between nodes which results, in addition to the throughput, in a waste of energy and a loss of data. It is difficult to detect Collision attack in WSNs because it is a short time attack using malicious packets which are similar to legitimate packets. Researches, such as [46], proposed several Collision detection techniques such as error-correcting codes.

- Unfairness:

Unfairness attack [47] is a partial or a weak form of DOS attack that can result in marginal performance degradation. Based on other attacks such as collision and exhaustion, collision attack decreases significantly the utility and efficiency of services. In fact, attackers request continuously to access to the channel which results in undermining communication and limiting channel capacity. One of the countermeasures to such an attack is time-division multiplexing [48] allowing each node to transmit only in a specific time slot.

- Interrogation [49]:

To soften the problem of frame collisions introduced by the hidden node problem, several MAC protocols use the RTS/CTS handshake [50]. Attackers take advantages of this synchronization mechanism by repeatedly sending RTS packets leading to CTS responses from neighboring nodes. To counter this type of attack, nodes can use several mechanisms such as anti-replay protection and link layer authentication [51].

- Sybil Attack [52]:

As shown in figure 3 Sybil Attacks allow malicious nodes to have multiple identities by using the identities of the nodes targeted by the attack in order to participate in distributed algorithms such as election to take advantage of legitimate nodes to endorse the creation of several routes passing through the malicious node. This attack is located between the link and the network layers and it aims to degrade the integrity of data, the security level of and the use of resources. Among these attacks we can find Data Aggregation attacks aiming to falsify the aggregated message and Voting attacks affecting routing path and node selection. Several researches, such as [53] [54], sought to counter this attack using different mechanism such as public key cryptography and digital signatures.

- Sinkhole:

Sinkhole attack [55] belongs to DoS attacks in WSNs. As shown in figure 4, the attacker (malicious node) must appear to other nodes as being very attractive by presenting optimal routes in order to attract packets as much as possible to control most of

the data circulating in the network. Consequently, malicious node acts as a base station by attracting data packets and preventing them from continuing their path creating a kind of well or black hole in the network. The attacker, having a strategic routing location in the network, manipulates packets as desired, causing the suspension of the network routing service and the depletion of critical resources of nodes. Geo-routing protocols, using localized information and routing traffic through the physical location of nodes, are resistant to sinkhole attacks.

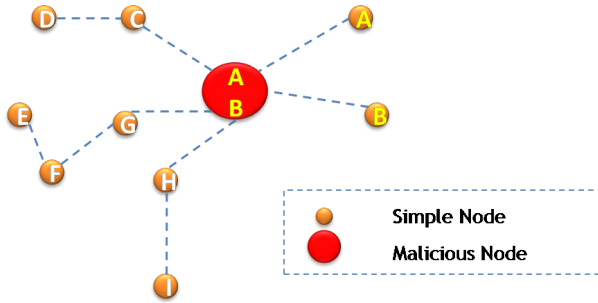


Figure 3: Sybil Attack

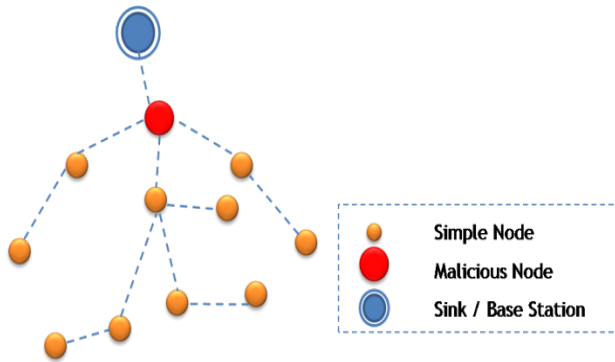


Figure 4: Sinkhole attack

- Hello Flood [56]:

The presence of laptop-class attackers and the limited transmission range of sensors led to the appearance of the Hello flood attacks. This attack takes advantages of the powerful signal of the attacking device to broadcast the information of an optimal route to all the nodes which will update their local tables. When a targeted node wants to communicate, it will not be able to use this route because the attacker, which is the imaginary neighbor, is out of range which results in the waste of energy from the sensors which leads to a malfunction of the network. Security mechanisms such as cryptography and source authentication, used to verify the bidirectionality of a path before taking action received over it, are used to counter this type of attacks.

- Node Capture:

In most applications, sensor nodes are highly vulnerable to physical attacks as they are often deployed in open areas easily accessible to attackers which raise the possibility of node capture to be used in tampering attacks. Researches such as [57] show that even a single node capture led to take over the entire network by attackers which makes the resilience against node capture attacks one of the most challenging issues in WSNs [58].

- Selective Forwarding:

Routing protocols assume that nodes will faithfully relay the packets that pass through them. We talk about Selective Forwarding attack when attacker may create malicious nodes and can violate this rule by removing all or some of these incoming packets randomly (neglectful node) or by giving high priority to its own messages (greedy node). Multipath routing, braided paths and random selection of paths to destination are a possible defense against this type of attack [59] [60].

- Black Hole Attack:

This attack can be considered as a form of selective forwarding attack dropping all incoming packets, it consists of inserting a new node or compromising a network node which falsifies the routing information to broadcast itself as the shortest path to oblige a maximum of neighbors to modify their routing tables in order to force the data to pass through it. This information will be destroyed which makes the malicious node as a well or black hole in the network. When attacker is placed on a strategic routing location in the network such as sinks or base stations the attack cause a network partition, packets loss, resource exhaustion and even the suspension of the routing services of the entire network. Black hole attack often targets hierarchical architectures and more specifically aggregator nodes. Multiple paths routing presents a defense against black hole attack [61] [62].

- Wormhole Attacks [63]:

Also known as tunneling, it is one of the most severe attacks. As shown in Figure 5, it requires at least two malicious nodes linked by a powerful radio link or by a wire link. In a wormhole attack, information received by a malicious node in one side of the network are encapsulated and relayed to be reintroduced by another malicious node on the other side of the network, revealing that the message originates from a close node. Encapsulation can be done in two ways: "Multi-hop encapsulation" aiming to hide intermediate nodes located between the two attackers to make the paths through the malicious node appear shorter which facilitates the creation of sinkholes with protocols using the number of hops as main metric of paths selection and "direct communication" in which paths going through the attackers are faster because they are composed of a single hop and can be used against protocols using the first discovered path and those based on paths latency. This type of attacks can considerably disrupt a location system by introducing erroneous reference points. It can be further divided into three classes: Half Open Wormhole, Closed Wormhole, and Open Wormhole. Several mechanisms for detecting and defending against wormhole attacks are presented such as WRHT [64].

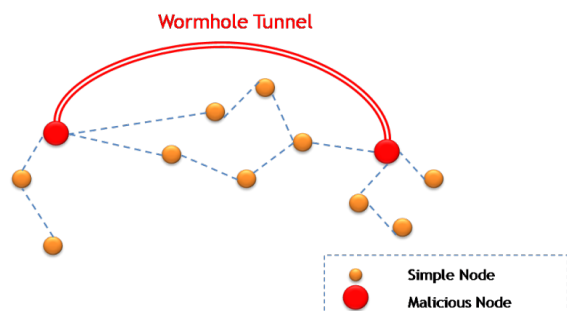


Figure 5: Wormhole attack

- Spoofed, Altered, or Replayed Routing Information [65]:

routing information in transit are targeted by several attacks, they can be spoofed, altered, or replayed. Malicious nodes can attract or repel the network traffic, inject false and misleading packets, overflow routing tables and create routing loops which result in disrupting the network traffic, partitioning the communication system and even destruction on the entire network. Several researches, such as [66], aim to counter these attacks using counters, timestamps, encryption and various authentication techniques.

- Misdirection [67]:

This active attack consists in misdirecting the data packets. In fact, instead of sending the packets in a correct direction, malicious nodes redirect them in a wrong direction through which the right destination is unreachable. Targeted node, flooded without any useful information, suffers from a waste of resources. Some security mechanisms [68] such as smart sleep [69] avoids this attack.

- Homing [70]:

This attack aims to locate critical nodes in the network providing essential services such as cluster heads and key managers by monitoring and analyzing the network traffic and nodes activities in order to eavesdrop their activities, take control of the network and extract sensitive data. To prevent homing attacks, protocols designers use different types of cryptographic schemes, algorithms and hide management messages [71] [72].

- Flooding [73]:

This attack aims to provoke a denial of service in order to decreases network lifetime. Indeed, one or several malicious nodes propagate many connection requests and carry out a regular massive sending to a strong emission power until exhausting the resources required the connection or reaching a maximum limit in order to saturate the network and prevent legitimate nodes from establishing communications which exhaust the resources (memory and energy) and reduce availability. One proposed solution to this attack is to demonstrate the commitment to this connection or to put a limit on the number of connections from a particular node [74] [75].

- De-synchronization Attacks [76]:

It is a part of the resource depletion attacks. The attacker causes missed frames by distorting, changing or increasing the sequence number of exchanged packets between end points. By receiving the modified packets, the destination deduces that the packets have been lost and requests the forwarding of these packets to the senders which disrupts the synchronization of communications and led to a considerable waste of energy of legitimate sensors by attempting to recover from errors which never really existed. Packets authentication is one of the main solutions to counter this attack [77] [78].

- Overwhelm attack [79]:

It is a part of QoS attacks. It consumes network bandwidth causing resource depletion by forwarding large amounts of data packets due to an exaggerated stimulation of sensors. A good

adjustment of sensors and stimulation parameters, rate-limiting and efficient data-aggregation algorithms help to counter this attack [80].

- Path-based DOS attack [81]:

In this attack malicious nodes inject spurious or replayed packets in the network which waste energy resources and bandwidth on the path to the base station. Hence, legitimate nodes are prevented from sending packets to the base station. Authentication techniques and anti-replay protection counter this attack [82].

- Deluge (reprogram) attack [83]:

This attack uses one or more compromised nodes that the attacker reprograms them and then reinsert them on the network as malicious nodes working in his service. Deluge attack aims to disrupt the network and the application by causing an abnormal behavior of nodes. Indeed, these nodes run malicious codes in order to steal secret or sensitive information, attempt to disrupt the normal operation of the entire system and take control of large portions of a network. Several researches such as [84], introduce various techniques to counter this type of attacks.

Table 1 classifies the previously detailed routing attacks on WSNs according to our taxonomy proposed in the previous section.

4.2. Simulation results

4.2.1. Network model

To show the effect of these attacks on WSNs, we used the NS3 simulator to simulate the effect of Jamming and Hello Flood attacks on a WSN using LEACH protocol [85].

As indicated in Table2, the adopted network model consists of 100 nodes randomly deployed in 100m * 100m area with unlimited power sink centered in the field as shown in Figure 6.

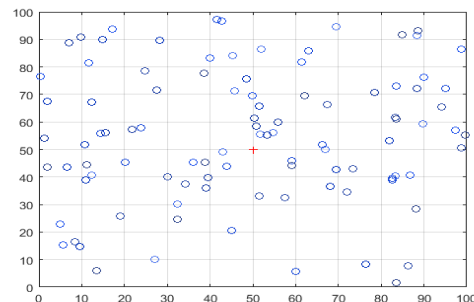


Figure 7: Nodes distribution

4.2.2. Results and discussion

In this section, the following metrics are used to evaluate the effect of Jamming and Hello Flood attacks:

- Network lifetime (Alive nodes Versus Rounds + Dead nodes Versus Rounds)
- Stability /instability periods
- Remaining energy Versus Rounds

We start with the evaluation of the network lifetime.

Table1: Comparison table of routing attacks in WSNs

Types Attacks	Based On Protocol Stack					Based on the capability of the attacker				Based on the attack impact					Based on the attack target			Pas sive /acti ve	
	P	D	N	T	A	LC	DC	I	I	M	F	R	R	U	H	S	I	P	A
	L	L	L	L	L														
Jamming	*	*	*			*	*	*	*	*				*	*				*
Tampering or destruction	*						*	*		*	*				*	*	*		*
Continuous Channel Access (Exhaustion)		*				*	*	*	*					*	*				*
Collision		*				*	*	*	*	*		*	*	*	*				*
Unfairness		*				*	*	*	*	*		*	*	*	*				*
Interrogation		*				*	*	*	*				*	*					*
Sybil Attack		*	*			*	*		*	*	*	*	*	*	*		*		*
Sinkhole			*			*	*		*	*	*	*	*	*	*		*	*	*
Hello Flood			*			*			*	*	*	*	*	*	*		*	*	*
Node Capture			*			*	*		*	*	*	*	*	*	*	*	*	*	*
Selective Forwarding			*			*	*		*	*	*	*	*	*	*		*	*	*
Black Hole Attack			*			*	*	*	*	*			*	*	*	*	*	*	*
Wormhole Attacks			*			*			*	*	*	*	*	*	*	*	*	*	*
Spoofed, Altered, or Replayed Routing Information			*			*	*	*	*	*	*	*	*	*	*	*	*	*	*
Misdirection			*			*	*	*	*	*			*	*	*	*	*	*	*
Homing			*			*			*	*						*	*	*	
Flooding			*			*	*	*	*	*	*	*	*	*	*	*	*	*	*
De-synchronization Attacks			*			*	*	*	*	*	*	*	*	*	*	*	*	*	*
Overwhelm attack					*	*		*			*	*	*	*	*	*	*	*	*
Path-based DOS attack					*	*	*	*		*	*	*	*	*	*	*	*	*	*
Deluge (reprogram) attack					*	*	*	*	*	*	*	*	*	*	*	*	*	*	*

- PL: Physical Layer
- DLL: Data Link Layer
- NL: Network Layer
- TL: Transport Layer
- AL: Application Layer
- LC: Location Capability
- O: Outsider
- I: Insider
- DC: Device Capability
- M: Mote Class
- L: Laptop Class
- IRP: Interruption
- ITC: Interception
- M: Modification
- F: Fabrication
- RP: Reloading Packets
- RD: Resources Depletion
- U: Users
- H: Hardware
- S: Software
- I: Information
- P: Passive
- A: Active

Table 2: Network parameters

Parameters	Values
Network size	100m * 100m
Number of nodes	100
Sink location	50,50
Packet size	4000 bits
Initial energy	0.5 J
Energy Dissipation (Efs)	10 pJ/bit/m ²
Energy for transmission (ETx)	50 nJ
Energy for reception (ERx)	50 nJ
Data Aggregation	5 nJ/bit/report
Number of rounds	2000

• Network lifetime

The network lifetime is one of the main metrics to be considered to evaluate the efficiency of the network. It is the period between the beginning of the network and the death of last node. The two complementary Figures 8.a) and 8.b) respectively show the evolution of the number of alive and dead nodes in the network using LEACH protocol with and without the presence of attacks.

As shown in Figure 8, the network lifetime using LEACH protocol without undergoing attacks is about 1560 rounds, while it does not exceed 1080 rounds in the presence of Hello Flood attack and 820 rounds with Jamming attack. Using a powerful signal, Hello flood attack broadcast the information of an optimal imaginary route according to which the sensors update their local

tables. This technique led to a waste of energy and to a malfunction of the network. As explained earlier in this survey, deceptive Jamming attack, used in this simulation, consist in sending a constant data stream in the network which leads to overloading the antennas of the sensors and therefore to a great loss of energy and the disappearance of the network in a short time.

all nodes in the network. Figure 9 shows the stability and instability periods of the network using LEACH protocol with and without the presence of attacks.

As shown in Figure 9, the stability period almost reached 790 rounds without attacks, but it does not exceed 320 rounds in the presence of Hello flood attack and 255 rounds with Jamming attack. In the same way, the instability period is about 773 rounds in the absence of attacks but does not surpass 760 rounds with Hello flood attack and 565 rounds in the presence of Jamming attack. This is obviously explained by the effect of the attacks on the consumption of energy.

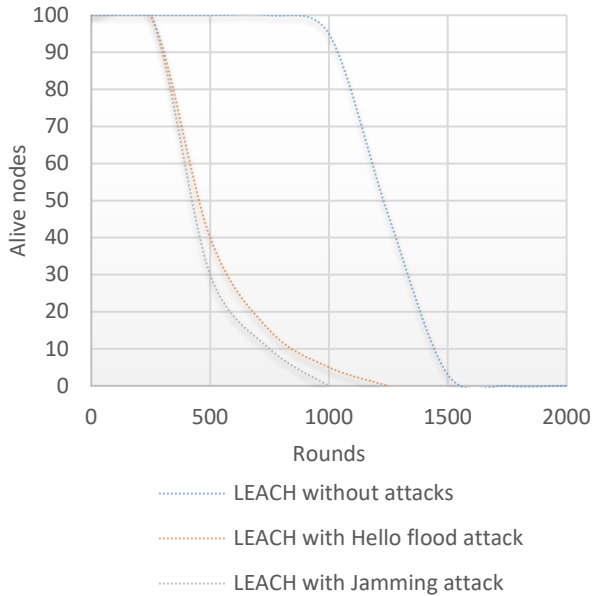


Figure 8-a: Alive nodes VS. rounds

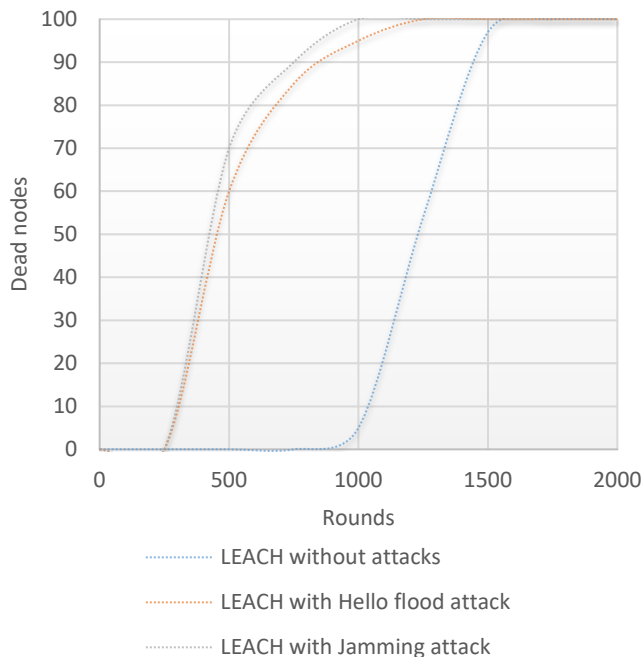


Figure 8-b: Dead nodes VS. rounds

Figure 8: Network lifetime

- Stability / instability period

A stability period triggers with the beginning of the network until the death of the first node which declares the beginning of an instability period. This instability period extends until the death of

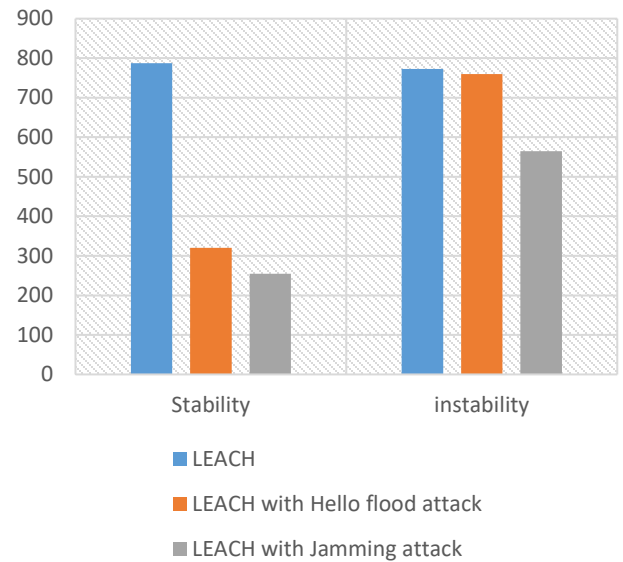


Figure 9: Stability and instability periods

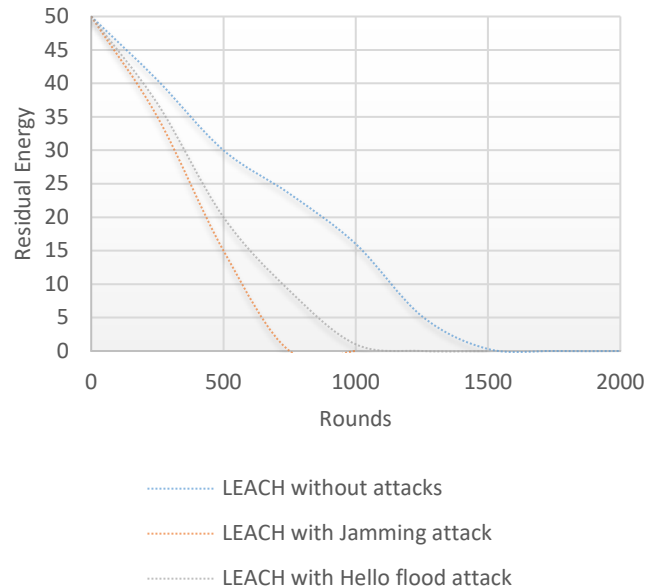


Figure 10: Residual Energy VS. Time

- Remaining energy

The residual energy, shown in Figure 10, results from the evolution of the number of nodes in the network. The curves show

the acute effect of the attacks on the residual energy of the network where half of the energy is consumed before reaching 500 rounds in the presence of attacks. The evolution of energy in this way leads to the formation of several isolated areas and subsequently affects the efficiency of the network.

In the following section, we present the main security mechanisms used to counter these attacks.

5. Basic security mechanisms in WSNs

In the absence of strong security architecture, WSNs are targets of several attacks that we presented previously in this paper. Most of these attacks take advantage of cryptographic system failures to derive the initial data (clear) or to find the used keys. We are talking here about cryptanalysis. In this section, we talk about cryptography and the cryptographic systems used to secure the WSNs [86] [87].

Indeed, the cryptanalysis targets the encryption keys which are based on cryptographic systems. These systems, that can be either symmetric, asymmetric or hybrid, take care of the management and distribution of the encryption keys [88] [89]. In the following, we detail each of these classes.

5.1. Symmetric Cryptography in WSNs

Symmetric cryptography, shown in Figure 11, is the oldest form of encryption where the same key is used between two communicating nodes to encrypt and decrypt the data using a symmetric encryption algorithm. In modern security techniques, even symmetric encryption algorithms can be public. The major disadvantage of this solution is that the pre-loaded key in the nodes could lead to compromise the entire network through compromised nodes. One of the proposed solutions to overcome this limit is to establish symmetric encryption schemes based on pair-wise keys rather than a single global key [90] [91].

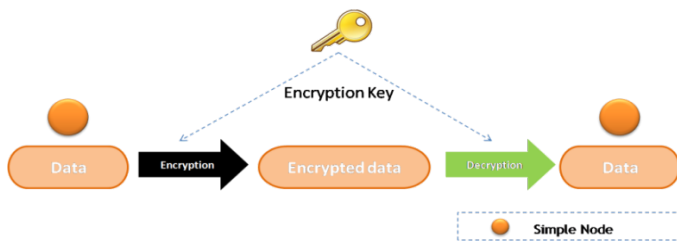


Figure 11: Symmetric cryptography

5.2. Asymmetric Cryptography in WSNs

Contrary to symmetric cryptography, asymmetric cryptography, also known as public-key cryptography, too heavy used in WSNs, uses a pair of keys instead of one (public and private). Asymmetric keys are generated in pairs. The message encrypted by the public key will be decrypted by the private key. Indeed, the public key of a node B, published between two communicating nodes is used by the node A to encrypt a message that will be decrypted by the node B through its secret private key as shown in Figure 12 and vice versa. This encryption mechanism allows not only the encryption of information but also the guarantee the authentication of the nodes by using the signatures and digital certificates. Slowness and resources consumption are the major drawbacks of this encryption mechanism [92].



Figure 12: Asymmetric cryptography

5.3. Hybrid Cryptography in WSNs

Hybrid cryptography is a cryptographic system that combines and benefits from the two cryptographic systems: asymmetric and symmetric. Generally, asymmetric encryption, greedy in time and resources, is used only to exchange a secret key in order to use symmetric encryption afterwards.

5.4. Elliptic curve cryptography in WSNs

Elliptic Curve Cryptography (ECC) is becoming increasingly popular as a security solution for WSNs. This technique is an approach of public-key cryptography, it is based on elliptic curve theory to create faster, smaller and more efficient encryption keys with quite less key size and very low computational overhead. In fact, the ECC generates keys through the properties of the elliptic curve equation and the discrete logarithm of an elliptic curve must be calculated for the decryption process which is much more difficult than factoring.

5.5. Comparison of symmetric and asymmetric cryptographic systems

Encryption algorithms can be evaluated in different parameters. Table 3, provided by National Institute of Standards and Technology NIST compares the encryption key size for RSA, ECC (asymmetric) and AES (symmetric) shows the development of key size compared to the security of an 80-bit symmetric key [93].

Table 3: Comparison of key length (bits) of the well-known symmetric and asymmetric techniques [NIST]

Symmetric (AES)	RSA	ECC
80	1024	160
112	2048(x 2)	224(x 1.4)
128	3072(x 3)	256(x 1.6)
192	7680(x 7.5)	384(x 2.4)
256	15360(x 15)	521(x 3.2)

Researchers agree that symmetric methods are faster and require small keys e.g. a key size of 3072 bits with RSA, which is equivalent to 256 bits with ECC, offers the same level of security as a key of only 128 bits with AES. However, for a network of N nodes, N-1 symmetric keys must be stored in each node, which exceeds the memory capacity of sensors in networks that can contain thousands of nodes as well as the key distribution problem.

Figure 13, developed from experiments done using MATLAB R2015a [92] compares the energy consumed by RSA-1024 and ECC-160 for signatures generation and verification, and the energy cost of key exchanges excluding authentication and certificate verification. It shows that RSA is characterized by a very expensive signature operation and a small verification cost contrary to ECDSA signatures which are significantly cheaper than RSA. In the same way, key exchanging costs are significantly cheaper with ECDSA than with RSA.

As a result, the ECC has emerged as it offers keys that can be much smaller than those required by the RSA algorithm, and at the same time of size close to symmetrical solutions. These characteristics make this technique more suitable for WSNs and IoT applications but not optimal in its general form [94] [95].

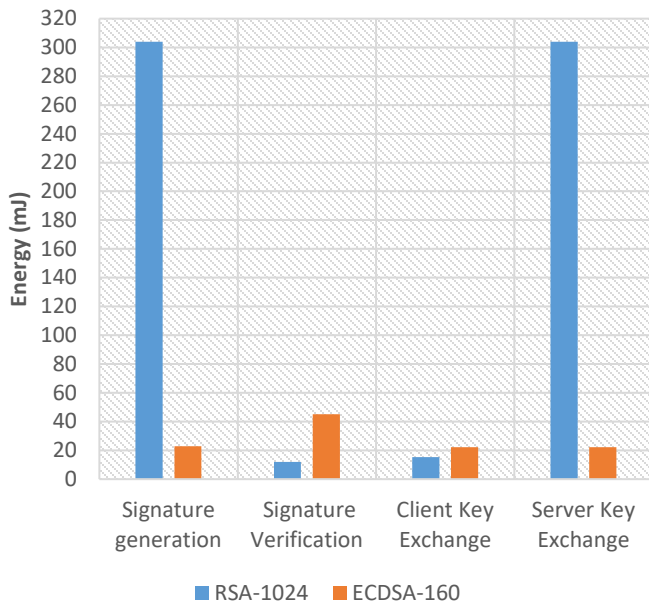


Figure 13: Energy cost of digital signature and key exchange using RSA-1024 and ECDSA-160

symmetric, asymmetric or hybrid-based method. This task includes the generation, distribution, verification and storage of encryption keys so that each node will be equipped with a set of secret keys or private/public pair of keys according to the adopted system in a secure, private and safe manner.

Several management classifications and key distribution have been proposed in the literature based on various technical and functional criteria [96]. We propose in this work a new classification based on the three previously proposed encryption methods (symmetric, asymmetric and hybrid) as shown in Figure 14. In the following we detail each of these key distribution methods.

5.7. Management of encryption key in symmetric patterns

The establishment of a common key between nodes in a WSNs to securely communicate in a symmetric cryptographic-based model is as follows: Before the nodes are deployed, the memory of each node is initially equipped with several keys in a Key Pre-distribution phase then it is the routing protocol that deals with the common key management between the nodes after the deployment in a key discovery process which makes it possible to constitute secure paths between nodes. The pre-distribution of these keys can be random or through an intermediary trust element of the network.

5.7.1. Random keys

The random pre-distribution of keys can be guaranteed by probabilistic, deterministic or hybrid methods. In the following we detail each of these methods

5.7.1.1. Deterministic methods

Deterministic methods require a large storage capacity because several encryption keys deterministically generated are stored in the memory of each node. They allow each node to establish a unique key known as “pair-wise key” with any other node of the network to establish a secure communication. Among the proposed mechanisms we quote the deterministic method proposed by Liu et al. [97] which is based on virtual spaces (logical grids) containing the identifiers of the nodes. Thus, many groups of sensor nodes are formed based on the positions of the nodes. The pre-distribution of two encryption keys is thus necessary: “in-group pre-distribution” making it possible to establish a unique shared key (pair-wise key) between two nodes of the same group and “cross-group pre-distribution” to establish a unique shared key between two different groups.

5.7.1.2. Probabilistic methods

In probabilistic methods, each node in the network is equipped with several encryption keys randomly chosen by the network administrator before being deployed. Common keys are thus installed in the memories of the nodes with a certain probability. In [98], Jones et al. propose a secure probabilistic architecture based on a probabilistic key distribution method. Indeed, each sensor is loaded with a set of “m” encryption keys, randomly selected from a set of “k” keys with a probability of matching “p” between nodes. After deployment, the BS splits the network into independent sectors and secret keys are distributed by the BS to ensure secure communication.

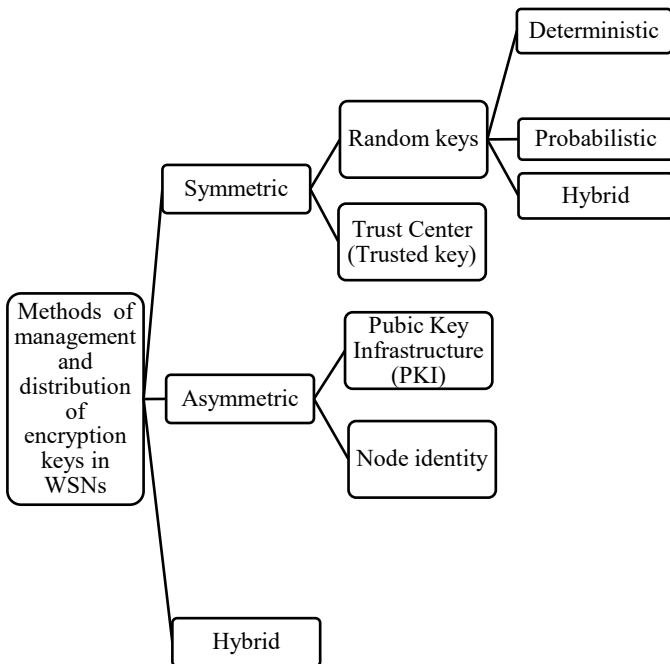


Figure 14: Methods of management and distribution of encryption keys in WSNs

5.6. Management of encryption keys in WSNs

Key management in WSNs is one of the most difficult aspects when configuring a security cryptographic system whether in a

5.7.1.3. Hybrid methods

Hybrid pre-distribution methods combined and benefits from the two previous methods, depending on the application to increase connectivity between nodes while ensuring secure communication.

5.7.2. Trust Center

In this key pre-distribution model, a Trust Center e.g. the BS is used either to store a copy of pre-loaded keys or to derive encryption keys from a trusted key pre-loaded into the nodes. In a Zigbee topology managed by the protocol stack known as ZigBee [99] based on the IEEE 802.15.4 standard, the nodes can play three roles: coordinator, routers, and sensors. The coordinator, placed in a particular position in the network, plays the role of a Trust Center (TC) and distributes keys that can be Link Key (LK), Network Key (NK) or Master Key (MK) shared by one node respectively with another node, with the entire network and for the establishment of the key LK.

5.8. Management of encryption key in asymmetric patterns

Another way to establish a common key between two nodes or a group of nodes in a WSN to secure communications is to use schemes based on asymmetric systems as already explained. In the following we detail the most know methods.

5.8.1. Public Key Infrastructure

Public Key Infrastructure (PKI) based specifically on cryptography, are a set of protocols and services aiming to secure communication in a network through various techniques such as authentication, digital certificates, digital signatures etc. The Micro Public Key Infrastructure (micro-PKI) method proposed by Munivel et al. [100] for WSNs is based on two keys: a public key loaded in each node before the deployment used to identify with the BS and a private key used by the BS to decrypt the data sent by the nodes. The PKI in this method ensures identification between the nodes as well as with the BS.

5.8.2. Node identity

These methods seek to provide the same cryptographic services as a PKI based solely on the node identity information in the creation and establishment of cryptographic keys shared between each pair of nodes in the network. These methods are known in cryptography as the Identity-Based Non-Interactive Key Distribution Scheme (ID-NIKDS) [101]. Among these methods we quote the method proposed by Oliveira et al. [102] where each node of the network has a unique identifier and a private key. A unique secret key shared with another node of the network is derived by knowing only its identifier.

5.9. Management of encryption key in hybrid patterns

Hybrid cryptography is a system that combines the symmetric and asymmetric cryptography. It benefits from their advantages to ensure a high level of security in particular situations as mentioned previously in this work. The Transport Layer Security (TLS) [103] combines the two cryptographic systems. Indeed, as asymmetric cryptographic operations are very expensive, it is only used in the key distribution then a symmetric algorithm is used for the bulk encryption of the data.

In the following section, we summarize and discuss the results obtained in this survey.

6. Analysis and Findings

The specific characteristics of WSNs, usually deployed in hostile environments make these networks targeted by various types of attacks which can target all components of the network such as nodes, routes, packets etc. Simulation results show that the network lifetime can decrease by more than 45% as in the presence of Jamming attack. These conditions lead us to discuss the existing security techniques which, despite their proven effectiveness with other types of networks, cannot be directly adapted to the limited resources of sensors and a new security mechanism taking advantage of existing solutions must be proposed.

7. Conclusion and future work

As an involving field, WSNs usually used in unattended environments and characterized by limited resources become vulnerable to several types of attacks targeting all network components such as nodes, packets and routing protocols etc. In this paper, we aim to facilitate the design and implementation of reliable and secure routing protocols for researchers. So, we summarize the security requirements for WSNs then we propose a new taxonomy distinguishing four possible categories of attacks namely: attacks based on the protocol stack, based on the capability of the attacker, based on the attack impacts and based on the attack target. Then, we classify and analyze the most known attacks based on the proposed model and using the NS3 simulator. Thereafter, we present and discuss the basic security methods and protocols of management and distribution of encryption keys in WSNs.

Security Mechanisms in WSNs, used to counter these attacks in order to keep the network running smoothly will be the objective of our future work aiming to propose a new security method which will be adapted to the specific properties of WSNs and able to counter the majority of these attacks.

References

- [1] YADAV, Devendra, SINGAM, Jayanthu, DAS, Santos, et al. A Critical Review on Slope Monitoring Systems with a Vision of Unifying WSN and IoT. IET Wireless Sensor Systems, 2019.
- [2] PRABHU, Boselin, BALAKUMAR, N., et ANTONY, A. Johnson. Wireless Sensor Network Based Smart Environment Applications. 2017.
- [3] SHAHZAD, Furrakh, PASHA, Maruf, et AHMAD, Arslan. A Survey of Active Attacks on Wireless Sensor Networks and their Countermeasures. arXiv preprint arXiv:1702.07136, 2017.
- [4] SENGAR, P. et BHARDWAJ, N. A Survey on Security and Various Attacks in Wireless Sensor Network. International Journal of Computer Sciences and Engineering, 2017, vol. 5, no 4, p. 78-84.
- [5] MITTAL, Vikas, GUPTA, Sunil, et CHOUDHURY, Tanupriya. Comparative Analysis of Authentication and Access Control Protocols Against Malicious Attacks in Wireless Sensor Networks. In : Smart Computing and Informatics. Springer, Singapore, 2018. p. 255-262.
- [6] BANA, Suman et BAGHLA, Silki. Wireless sensor network. International Journal of Engineering Science, 2016, vol. 1706.
- [7] Kardi, A., Zagrouba, R., & Alqhtani, M. (2018, May). Hierarchical Routing Techniques in Wireless Sensor Networks. In International Symposium on

- Web and Wireless Geographical Information Systems (pp. 77-84). Springer, Cham.
- [8] TOMIĆ, Ivana et MCCANN, Julie A. A Survey of Potential Security Issues in Existing Wireless Sensor Network Protocols. *IEEE Internet of Things Journal*, 2017, vol. 4, no 6, p. 1910-1923.
- [9] CUI, Jie, SHAO, Lili, ZHONG, Hong, et al. Data aggregation with end-to-end confidentiality and integrity for large-scale wireless sensor networks. *Peer-to-Peer Networking and Applications*, 2017, p. 1-16.
- [10] ORACEVIC, Alma, DILEK, Selma, et OZDEMIR, Suat. Security in internet of things: A survey. In : *Networks, Computers and Communications (ISNCC)*, 2017 International Symposium on. IEEE, 2017, p. 1-6.
- [11] DAS, Ashok Kumar. A secure and effective biometric-based user authentication scheme for wireless sensor networks using smart card and fuzzy extractor. *International Journal of Communication Systems*, 2017, vol. 30, no 1.
- [12] MENDEZ, Diego M., PAPAPANAGIOTOU, Ioannis, et YANG, Baijian. Internet of things: Survey on security and privacy. *arXiv preprint arXiv:1707.01879*, 2017.
- [13] PRITCHARD, Sean W., HANCKE, Gerhard P., et ABU-MAHFOUZ, Adnan M. Security in Software-Defined Wireless Sensor Networks: Threats, Challenges and Potential Solutions. In : *IEEE Int. Conf. of Ind. Informat.*, Emden, Germany, 2017.
- [14] SHAHZAD, Furrakh, PASHA, Maruf, et AHMAD, Arslan. A Survey of Active Attacks on Wireless Sensor Networks and their Countermeasures. *arXiv preprint arXiv:1702.07136*, 2017.
- [15] ZHU, Liehuang, ZHANG, Zijian, et XU, Chang. Secure data aggregation in wireless sensor networks. In : *Secure and Privacy-Preserving Data Communication in Internet of Things*. Springer, Singapore, 2017, p. 3-31.
- [16] MATHEW, Prabha Susy, PILLAI, Anitha S., et PALADE, Vasile. Applications of IoT in Healthcare. In : *Cognitive Computing for Big Data Systems Over IoT*. Springer, Cham, 2018, p. 263-288.
- [17] TOMIĆ, Ivana et MCCANN, Julie A. A Survey of Potential Security Issues in Existing Wireless Sensor Network Protocols. *IEEE Internet of Things Journal*, 2017, vol. 4, no 6, p. 1910-1923.
- [18] ZHANG, Anran et BAI, Fengshan. An energy efficient and dynamic time synchronization protocol for wireless sensor networks. In : *Seventh International Conference on Electronics and Information Engineering*. International Society for Optics and Photonics, 2017, p. 103221X.
- [19] LI, Peng, YU, Xiaotian, XU, He, et al. Research on secure localization model based on trust valuation in wireless sensor networks. *Security and Communication Networks*, 2017, vol. 2017.
- [20] LI, Xiong, NIU, Jianwei, KUMARI, Saru, et al. A three-factor anonymous authentication scheme for wireless sensor networks in internet of things environments. *Journal of Network and Computer Applications*, 2018, vol. 103, p. 194-204.
- [21] ALIBERTI, Giulio, DI PIETRO, Roberto, et GUARINO, Stefano. Epidemic data survivability in Unattended Wireless Sensor Networks: New models and results. *Journal of Network and Computer Applications*, 2017, vol. 99, p. 146-165.
- [22] ZHANG, Junqing, DUONG, Trung Q., WOODS, Roger, et al. Securing Wireless Communications of the Internet of Things from the Physical Layer, An Overview. *Entropy*, 2017, vol. 19, no 8, p. 420.
- [23] DENER, Murat et BAY, Omer Faruk. Practical Implementation of an Adaptive Detection-Defense Unit against Link Layer DoS Attacks for Wireless Sensor Networks. *Security and Communication Networks*, 2017, vol. 2017.
- [24] SAINI, Rakesh Kumar, RITIKA, Ritika, et VIJAY, Sandip. Data Flow in Wireless Sensor Network Protocol Stack by using Bellman-Ford Routing Algorithm. *Bulletin of Electrical Engineering and Informatics*, 2017, vol. 6, no 1, p. 81-87.
- [25] KIRAZ, Ayhan et ÇAKIROĞLU, Murat. ALORT: a transport layer protocol using adaptive loss recovery method for WSN. *Sādhanā*, 2017, vol. 42, no 7, p. 1091-1102.
- [26] LI, Xiaomin, LI, Di, WAN, Jiafu, et al. A review of industrial wireless networks in the context of industry 4.0. *Wireless networks*, 2017, vol. 23, no 1, p. 23-41.
- [27] CHOI, Jaewoo, BANG, Jihyun, KIM, LeeHyung, et al. Location-based key management strong against insider threats in wireless sensor networks. *IEEE Systems Journal*, 2017, vol. 11, no 2, p. 494-502.
- [28] TYAGI, Akshat, KUSHWAH, Juhi, et BHALLA, Monica. Threats to security of Wireless Sensor Networks. In : *Cloud Computing, Data Science & Engineering-Confluence*, 2017 7th International Conference on. IEEE, 2017, p. 402-405.
- [29] GRGIC, Kresimir, MENDELSKI, Vedran, et ZAGAR, Drago. Security framework for visual sensors and smart camera networks. In : *Telecommunications (ConTEL)*, 2017 14th International Conference on. IEEE, 2017, p. 131-138.
- [30] JAITLEY, Sunakshi, MALHOTRA, Harshit, et BHUSHAN, Bharat. Security vulnerabilities and countermeasures against jamming attacks in Wireless Sensor Networks: A survey. In : *Computer, Communications and Electronics (Comptelix)*, 2017 International Conference on. IEEE, 2017, p. 559-564.
- [31] SHAHZAD, Furrakh, PASHA, Maruf, et AHMAD, Arslan. A Survey of Active Attacks on Wireless Sensor Networks and their Countermeasures. *arXiv preprint arXiv:1702.07136*, 2017.
- [32] BHUSHAN, Bharat et SAHOO, Gadadhar. Recent Advances in Attacks, Technical Challenges, Vulnerabilities and Their Countermeasures in Wireless Sensor Networks. *Wireless Personal Communications*, 2017, p. 1-41.
- [33] SENNIAPPAN, Vijayalakshmi et SUBRAMANIAN, Jayashree. Threshold-based Energy Efficient Clustering Protocol for Corrosion Risk Monitoring of Reinforced Concrete. *International Journal of Computer Applications*, 2017, vol. 157, no 6.
- [34] RAMACHANDRAN, Shyamala et SHANMUGAM, Valli. Impact of DoS Attack in Software Defined Network for Virtual Network. *Wireless Personal Communications*, 2017, vol. 94, no 4, p. 2189-2202.
- [35] DESNITSKY, Vasily et KOTENKO, Igor. Modeling and Analysis of IoT Energy Resource Exhaustion Attacks. In : *International Symposium on Intelligent and Distributed Computing*. Springer, Cham, 2017, p. 263-270.
- [36] SHAHZAD, Furrakh, PASHA, Maruf, et AHMAD, Arslan. A Survey of Active Attacks on Wireless Sensor Networks and their Countermeasures. *arXiv preprint arXiv:1702.07136*, 2017.
- [37] VADLAMANI, Satish, EKSHIOGLU, Burak, MEDAL, Hugh, et al. Jamming attacks on wireless networks: A taxonomic survey. *International Journal of Production Economics*, 2016, vol. 172, p. 76-94.
- [38] SHABANA, Kalsoom, FIDA, Nigar, KHAN, Fazlullah, et al. Security issues and attacks in Wireless Sensor Networks. *International Journal of Advanced Research in Computer Science and Electronics Engineering (IJARCSEE)*, 2016, vol. 5, no 7, p. pp: 81-87.
- [39] ZHU, Jia, ZOU, Yulong, et ZHENG, Baoyu. Physical-Layer Security and Reliability Challenges for Industrial Wireless Sensor Networks. *IEEE Access*, 2017..
- [40] BHAVATHANKAR, Prasenjit, SARKAR, Subhadeep, et MISRA, Sudip. Optimal decision rule-based ex-ante frequency hopping for jamming avoidance in wireless sensor networks. *Computer Networks*, 2017.
- [41] DINKER, Aarti Gautam et SHARMA, Vidushi. Attacks and challenges in wireless sensor networks. In : *Computing for Sustainable Global Development (INDIACom)*, 2016 3rd International Conference on. IEEE, 2016, p. 3069-3074.
- [42] DINKER, Aarti Gautam et SHARMA, Vidushi. Attacks and challenges in wireless sensor networks. In : *Computing for Sustainable Global Development (INDIACom)*, 2016 3rd International Conference on. IEEE, 2016, p. 3069-3074.
- [43] DENER, Murat et BAY, Omer Faruk. Practical Implementation of an Adaptive Detection-Defense Unit against Link Layer DoS Attacks for Wireless Sensor Networks. *Security and Communication Networks*, 2017, vol. 2017.
- [44] MISHRA, Alekha Kumar. Security Threats in Wireless Sensor Networks. *Handbook of Research on Advanced Wireless Sensor Network Applications, Protocols, and Architectures*, 2016, p. 307.
- [45] JAN, Mian Ahmad et KHAN, Muhammad. Denial of Service Attacks and Their Countermeasures in WSN. *IRACST-International Journal of Computer Networks and Wireless Communications (IJCNCW)*, 2013, vol. 3.
- [46] REN, Ju, ZHANG, Yaoxue, ZHANG, Kuan, et al. Adaptive and channel-aware detection of selective forwarding attacks in wireless sensor networks. *IEEE Transactions on Wireless Communications*, 2016, vol. 15, no 5, p. 3718-3731.
- [47] MOHAMMADI, Shahriar et JADIDOLESLAMY, Hossein. A comparison of link layer attacks on wireless sensor networks. *arXiv preprint arXiv:1103.5589*, 2011.
- [48] NEWAZ, SH Shah, CUEVAS, Ángel, LEE, Gyu Myoung, et al. Improving energy saving in time-division multiplexing passive optical networks. *IEEE Internet Computing*, 2013, vol. 17, no 1, p. 23-31.
- [49] SINGLA, Aashima et SACHDEVA, Ratika. Review on security issues and attacks in wireless sensor networks. *International Journal of Advanced Research in Computer Science and Software Engineering*, 2013, vol. 3, no 4.
- [50] KAUR, Ramandeep et SHARMA, Reecha. An Analysis of RTS/CTS Mechanism for Data Transfer In Wireless Network: A Review. 2016.
- [51] GHEORGHE, Laura, RUGHINIS, Razvan, DEACONESCU, Razvan, et al. Authentication and anti-replay security protocol for wireless sensor networks. In : *Systems and Networks Communications (ICSNC)*, 2010 Fifth International Conference on. IEEE, 2010, p. 7-13.
- [52] LI, Xun, HAN, Guangjie, QIAN, Aihua, et al. Detecting Sybil attack based on state information in Underwater Wireless Sensor Networks. In : *Software, Telecommunications and Computer Networks (SoftCOM)*, 2013 21st International Conference on. IEEE, 2013, p. 1-5.

- [53] JAN, Mian Ahmad, NANDA, Priyadarsi, HE, Xiangjian, et al. A Sybil Attack Detection Scheme for a Centralized Clustering-based Hierarchical Network. In : Trustcom/BigDataSE/ISPA, 2015 IEEE. IEEE, 2015. p. 318-325.
- [54] JAN, Mian Ahmad, NANDA, Priyadarsi, HE, Xiangjian, et al. A sybil attack detection scheme for a forest wildfire monitoring application. Future Generation Computer Systems, 2016.
- [55] SHAFIEI, Hosein, KHONSARI, Ahmad, DERAKHSHI, H., et al. Detection and mitigation of sinkhole attacks in wireless sensor networks. Journal of Computer and System Sciences, 2014, vol. 80, no 3, p. 644-653.
- [56] SINGH, Virendra Pal, UKEY, Aishwarya S. Anand, et JAIN, Sweta. Signal strength based hello flood attack detection and prevention in wireless sensor networks. International Journal of Computer Applications, 2013, vol. 62, no 15.
- [57] LIN, Chi et WU, Guowei. Enhancing the attacking efficiency of the node capture attack in WSN: a matrix approach. The Journal of Supercomputing, 2013, vol. 66, no 2, p. 989-1007.
- [58] TAHIR, Ruhma et MCDONALD-MAIER, Klaus. Improving resilience against node capture attacks in wireless sensor networks using icmetrics. In : Emerging Security Technologies (EST), 2012 Third International Conference on. IEEE, 2012. p. 127-130.
- [59] REN, Ju, ZHANG, Yaoyue, ZHANG, Kuan, et al. Adaptive and channel-aware detection of selective forwarding attacks in wireless sensor networks. IEEE Transactions on Wireless Communications, 2016, vol. 15, no 5, p. 3718-3731.
- [60] SHAHZAD, Furrakh, PASHA, Maruf, et AHMAD, Arslan. A Survey of Active Attacks on Wireless Sensor Networks and their Countermeasures. arXiv preprint arXiv:1702.07136, 2017.
- [61] BASKAR, Radhika, RAJA, PC Kishore, JOSEPH, Christeena, et al. Sinkhole Attack in Wireless Sensor Networks-Performance Analysis and Detection Methods. Indian Journal of Science and Technology, 2017, vol. 10, no 12.
- [62] ALJUMAH, Abdullah et AHANGER, Tariq Ahamed. Futuristic Method to Detect and Prevent Blackhole Attack in Wireless Sensor Networks. International Journal of Computer Science and Network Security (IJCNS), 2017, vol. 17, no 2, p. 194.
- [63] SHAHZAD, Furrakh, PASHA, Maruf, et AHMAD, Arslan. A Survey of Active Attacks on Wireless Sensor Networks and their Countermeasures. arXiv preprint arXiv:1702.07136, 2017.
- [64] SINGH, Rupinder, SINGH, Jatinder, et SINGH, Ravinder. WRHT: A Hybrid Technique for Detection of Wormhole Attack in Wireless Sensor Networks. Mobile Information Systems, 2016, vol. 2016.
- [65] MULLA, Ms Raisa I. et PATIL, Rahul. Review of Attacks on Wireless Sensor Network and their Classification and Security. Imperial Journal of Interdisciplinary Research, 2016, vol. 2, no 7.
- [66] DINKER, Aarti Gautam et SHARMA, Vidushi. Attacks and challenges in wireless sensor networks. In : Computing for Sustainable Global Development (INDIACom), 2016 3rd International Conference on. IEEE, 2016. p. 3069-3074.
- [67] YOUNIS ABDULLAH, Maan, HUA, Gui Wei, et ALSHARABI, Naif. Wireless sensor networks misdirection attacker challenges and solutions. In : Information and Automation, 2008. ICIA 2008. International Conference on. IEEE, 2008. p. 369-373.
- [68] SAINI, Meenu, KUMAR, Rajan, et al. To Propose a Novel Technique for Detection and Isolation of Misdirection Attack in Wireless Sensor Network. Indian Journal of Science and Technology, 2016, vol. 9, no 28.
- [69] ABDALZAKER, Mohamed S., SEDDIK, Karim, ELSABROUTY, Maha, et al. Game Theory Meets Wireless Sensor Networks Security Requirements and Threats Mitigation: A Survey. Sensors, 2016, vol. 16, no 7, p. 1003.
- [70] KURBAH, Rangstone Paul et SHARMA, Bobby. Survey On Issues In Wireless Sensor Networks: Attacks and Countermeasures. International Journal of Computer Science and Information Security, 2016, vol. 14, no 4, p. 262.
- [71] AGRAWAL, Dharma Prakash. Authentication, Encryption, and Secured Communication. In : Embedded Sensor Systems. Springer Singapore, 2017. p. 393-413.
- [72] SARANYA, K., SATHYA, D., et KUMAR, P. Ganesh. A Survey On Intrusion Detection System In Wireless Sensor Networks. International Journal of Advance Research, Ideas and Innovations in Technology. 2017, vol. 3, no 1, p. 692-703
- [73] MANOHAR, Ram Pradheep et BABURAJ, E. Detection of Stealthy Denial of Service (S-DoS) Attacks in Wireless Sensor Networks. International Journal of Computer Science and Information Security, 2016, vol. 14, no 3, p. 343.
- [74] ACHARJYA, D. P. et AHMED, N. Syed Siraj. Recognizing Attacks in Wireless Sensor Network in View of Internet of Things. In : Internet of Things: Novel Advances and Envisioned Applications. Springer International Publishing, 2017. p. 149-172.
- [75] MANSOURI, Djamel, MOKDAD, Lynda, BEN-OTHTMAN, Jalel, et al. Dynamic and adaptive detection method for flooding in wireless sensor networks. International Journal of Communication Systems, 2017.
- [76] SHAHID, Jahanzeb, SALEEM, Shahzad, et QURESHI, Muhammad Nauman. DOS Attacks on WSN and Their Classifications With Countermeasures-A Survey. NUST Journal of Engineering Sciences, 2016, vol. 9, no 2.
- [77] CAPOSSELE, Angelo T., CERVO, Valerio, PETRIOLI, Chiara, et al. Counteracting Denial-of-Sleep Attacks in Wake-up-radio-based Sensing Systems. In : Sensing, Communication, and Networking (SECON), 2016 13th Annual IEEE International Conference on. IEEE, 2016. p. 1-9.
- [78] GOPE, Prosanta, LEE, Jemin, et QUEK, Tony QS. Resilience of DoS Attacks in Designing Anonymous User Authentication Protocol for Wireless Sensor Networks. IEEE Sensors Journal, 2016, vol. 17, no 2, p. 498-503.
- [79] GARCIA-FONT, Victor, GARRIGUES, Carles, et RIFA-POUS, Helena. Attack Classification Schema for Smart City WSNs. Sensors, 2017, vol. 17, no 4, p. 771.
- [80] DINKER, Aarti Gautam et SHARMA, Vidushi. Attacks and challenges in wireless sensor networks. In : Computing for Sustainable Global Development (INDIACom), 2016 3rd International Conference on. IEEE, 2016. p. 3069-3074.
- [81] DENG, Jing, HAN, Richard, et MISHRA, Shivakant. Defending against path-based DoS attacks in wireless sensor networks. In : Proceedings of the 3rd ACM workshop on Security of adhoc and sensor networks. ACM, 2005. p. 89-96.
- [82] DHAKNE, A. R. et CHATUR, P. N. Detailed Survey on Attacks in Wireless Sensor Network. In : Proceedings of the International Conference on Data Engineering and Communication Technology. Springer Singapore, 2017. p. 319-331.
- [83] SARANYA, K., SATHYA, D., et KUMAR, P. Ganesh. A Survey On Intrusion Detection System In Wireless Sensor Networks. In the proceeding of the 2nd International Conference on Engineering Technology, Science and Management Innovation (ICETSMI- 2017)- India, January 2017. P. 158-165
- [84] SAINI, Meenu, KUMAR, Rajan, et al. To Propose a Novel Technique for Detection and Isolation of Misdirection Attack in Wireless Sensor Network. Indian Journal of Science and Technology, 2016, vol. 9, no 28.
- [85] ZHENSHAN, Bao, BO, Xue, et WENBO, Zhang. HT-LEACH: An improved energy efficient algorithm based on LEACH. In : Mechatronic Sciences, Electric Engineering and Computer (MEC), Proceedings 2013 International Conference on. IEEE, 2013. p. 715-718.
- [86] RADHAPPA, Harish, PAN, Lei, XI ZHENG, James, et al. Practical overview of security issues in wireless sensor network applications. International Journal of Computers and Applications, 2017, p. 1-12.
- [87] HE, Daojing, CHAN, Sammy, et GUIZANI, Mohsen. Cyber Security Analysis and Protection of Wireless Sensor Networks for Smart Grid Monitoring. IEEE Wireless Communications, 2017, vol. 24, no 6, p. 98-103.
- [88] SINGH, Pooja et CHAUHAN, R. K. A Survey on Comparisons of Cryptographic Algorithms Using Certain Parameters in WSN. International Journal of Electrical and Computer Engineering, 2017, vol. 7, no 4, p. 2232.
- [89] ZHANG, Ping, WANG, Shaokai, GUO, Kehua, et al. A secure data collection scheme based on compressive sensing in wireless sensor networks. Adhoc Networks, 2018, vol. 70, p. 73-84.
- [90] CHELLI, Kahina. Security issues in wireless sensor networks: attacks and countermeasures. In : Proceedings of the World Congress on Engineering. 2015. p. 1-3.
- [91] LI, Juan. A Symmetric Cryptography Algorithm in Wireless Sensor Network Security. International Journal of Online Engineering (iJOE)
- [92] CHELLI, Kahina. Security issues in wireless sensor networks: attacks and countermeasures. In : Proceedings of the World Congress on Engineering. 2015. p. 1-3.
- [93] KARDI, Amine, ZAGROUBA, Rachid, et ALQAHTANI, Mohammed. Performance Evaluation of RSA and Elliptic Curve Cryptography in Wireless Sensor Networks. In : 2018 21st Saudi Computer Society National Computer Conference (NCC). IEEE, 2018. p. 1-6.
- [94] LI, Xiong, NIU, Jianwei, BHUIYAN, Md ZakirulAlam, et al. A robust ECC-based provable secure authentication protocol with privacy preserving for industrial internet of things. IEEE Transactions on Industrial Informatics, 2018, vol. 14, no 8, p. 3599-3609.
- [95] IQBAL, Ummer et SHAFI, Saima. A Provable and Secure Key Exchange Protocol Based on the Elliptical Curve Diffie-Hellman for WSN. In : Advances in Big Data and Cloud Computing. Springer, Singapore, 2019. p. 363-372.
- [96] BOJANOVA, Irena, BLACK, Paul E., et YESHA, Yaacov. Cryptography classes in bugs framework (BF): Encryption bugs (ENC), verification bugs (VRF), and key management bugs (KMN). In : Software Technology Conference (STC), 2017 IEEE 28th Annual. IEEE, 2017. p. 1-8.

- [97] LIU, Donggang, NING, Peng, et DU, Wenliang. Group-based key predistribution for wireless sensor networks. *ACM Transactions on Sensor Networks (TOSN)*, 2008, vol. 4, no 2, p. 11.
- [98] JONES, K., WADAA, Ashraf, OLARIU, Stephan, et al. Towards a new paradigm for securing wireless sensor networks. In : *Proceedings of the 2003 workshop on New security paradigms*. ACM, 2003. p. 115-121.
- [99] <http://www.zigbee.org/>.
- [100] MUNIVEL, E. et AJIT, G. M. Efficient public key infrastructure implementation in wireless sensor networks. In : *Wireless Communication and Sensor Computing, 2010. ICWCSC 2010. International Conference on*. IEEE, 2010. p. 1-6.
- [101] MALEH, Yassine et EZZATI, Abdellah. An advanced Study on Cryptography Mechanisms for Wireless Sensor Networks. arXiv preprint arXiv:1609.05323, 2016.
- [102] OLIVEIRA, Leonardo B., ARANHA, Diego F., GOUVÊA, Conrado PL, et al. TinyPBC: Pairings for authenticated identity-based non-interactive key distribution in sensor networks. *Computer Communications*, 2011, vol. 34, no 3, p. 485-493.
- [103] DIERKS, Tim. The transport layer security (TLS) protocol version 1.2. IETF RFC 5246, August 2008.

Current Trends and Challenges in Link Prediction Methods in Dynamic Social Networks: A Literature Review

Elfadil Abdalla Mohamed^{*1}, Nazar Zaki², Mohammad Marjan²

¹College of Engineering and Information Technology, Ajman University, Ajman, UAE

²Dep. of Comp. Science and SW Eng., College of Info. Technology, UAEU, Al Ain, UAE

ARTICLE INFO

Article history:

Received: 29 September, 2019

Accepted: 15 November, 2019

Online: 05 December, 2019

Keywords:

Link inference

Link prediction

Dynamic social networks

ABSTRACT

In more recent times, researchers have turned their attention to link prediction and the role link inference can play in better understanding the evolutionary nature of social networking sites. The objective of this paper is to present an in-depth review, analysis, and discussion of the cutting-edge link prediction methods that can be applied to better understand the development of social networks. The findings of the literature review reveal that there has been a steady increase in the number of published articles that present novel link prediction models that are designed to enhance the efficiency and accuracy of link prediction. In this paper, this most recent techniques to be proposed in this regard are compared and categorized, and features and evaluation metrics are presented for each approach. The results of the evaluation reveal that there are no complete or definitive methods available that can accurately and reliably be applied within different dynamic social networks to predict missing, emerging, and broken links within the network. The paper concludes by presenting potential future directions and recommendations for further studies

1. Introduction

This paper is an extension of work originally presented at the International IEEE Congress on Information Science and Technology [1].

Starting from the beginning of this century, social networks have significantly evolved, and the progression of social media platforms (Facebook, Twitter, LinkedIn, etc.) has been well documented in a significant number of publications. In the contemporary era of connectivity, the majority of organizations complement their traditional marketing strategies with digital campaigns that rely heavily on social media channels. Due to its increase in popularity, social media has become integral to organizations' advertising and marketing campaigns, representing a cost-effective and efficient channel through which companies target and communicate with members of a given audience.

Since their inception in the late 90s, the value of social networks (SNs) has dramatically increased to reach billions of dollars. As such, they represent an attractive investment proposition, especially in the marketing sector. Their rise in popularity and social and economic implications has also attracted

significant research attention. One area of interest particularly notable in recent times is the prediction of missing links [2, 3].

1.1. Predicting Links in SN

By using graph theory concepts, SN can be represented as a graph of vertices and edges: $G(V, E)$. The vertex V represents a user while the edge E represents a link. Figure 1 shows a simple representation of a social network.

The issue of predicting links in SN is concerned with the forecasting of possible connections and interactions that can be observed between various members within a certain network. As explained in [4], considering an SN, G , at a certain time, t , the objective of link prediction here is to predict possible new links or the breaking of existing ones at a later time, t' . Several researchers have expressed an interest in predicting existing, expected, and missing links by developing a range of different methods. Despite the fact that several methods have been proposed, however, [5] indicate that none of them are reliable in effectively predicting the missing links.

An important feature of link prediction in SN is concerned with identifying missing links. Having the ability to predict missing links would provide us with clues of how SN evolves within a

* Elfadil Abdalla Mohamed, Email : elfadil.abdalla@ajman.ac.ae

range of settings. Predicting missing links has important connotations, for example, in the academic world, where doing so would help to identify possible academic collaboration in certain fields of interest [6, 7].

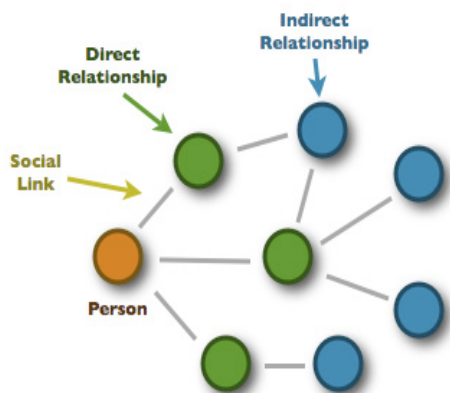


Figure 1: Simplified representation of SN

A further area where social link prediction could be of use is within criminal investigation; for example, similarity-based link-prediction methods are viable for identifying links between members of criminal networks. Identifying possible missing links in criminal networks can be achieved by exploiting node similarity in noisy or incomplete situations [8]. Predicting broken links is also of paramount importance within commercial settings, as marketing, customer service, and customer experience strategies based on link prediction can maintain customer loyalty. In bioinformatics, biology, and healthcare, the prediction of missing links can assist organizations in locating the relevant specialists who are able to receive future referrals, while within gene expression networks [9] they can be employed to better understand protein-protein interactions. Elsewhere, as explained in [2, 10], within security-related networks, link prediction can be used to detect suspected communications that countries are more likely to find harmful.

Social networks contain significant amounts of data; as such, it is not possible to collect all the information connected to a user's relationships. Link prediction, therefore, represents a viable means by which it is possible to apply an understanding of known relationships between users to estimate unknown relationships.

The existing literature highlights a continual increase that has occurred in the number of link-prediction methods that are capable of predicting SN links. This vast rise in the number of such methods is exponential to a large number of publications in renowned journals or conference proceedings that either propose a new method of predicting links or else to improve the accuracy and efficiency of an existing approach. Figure 2 depicts the number of articles published in Scopus indexed journals or conference proceedings. As the graph reveals, there has been a steady rise in the number of articles published that have focused on link prediction practices. Subsequently, many solutions have been introduced to handle the problem of accurately and efficiently predicting the missing links.

A link-prediction method that exploits the information diffusion feature was discussed in [11]. This study demonstrated the correlation between information diffusion processes and the

creation of new links. The proposed method managed to enhance the accuracy of link prediction by virtue of information diffusion and was tested on a Sina Weibo dataset. The experimental data revealed that the proposed method outperformed approaches that rely on topological features alone.

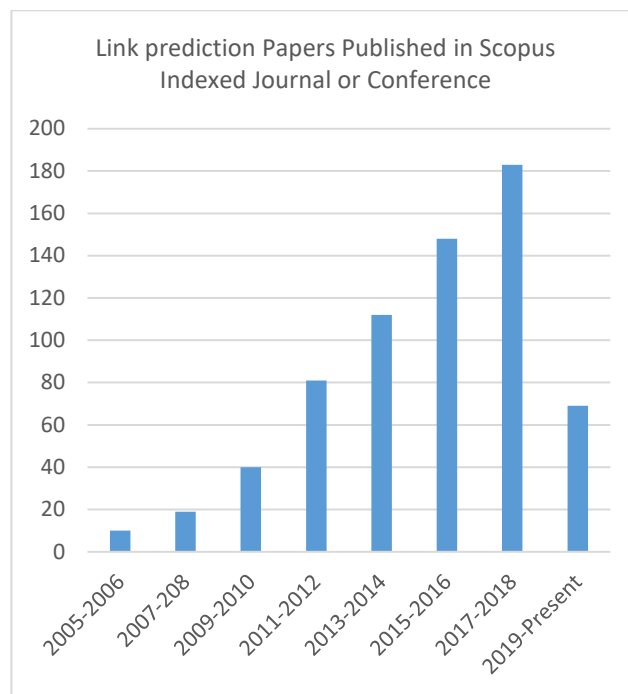


Figure 2: Papers related to link prediction published in Scopus-indexed journals or conference proceedings

Several link prediction approaches that are based on a deep belief network were presented in [12]. The results obtained from the experiments on datasets collected from different sources revealed that the methods effectively predicted link values and exhibited a remarkable generalization capability among the studied datasets.

Due to the vast amount of data in social networks, achieving efficiency within link-prediction methods represents a significant challenge. To address this problem, [13] proposed two algorithms for link prediction. The proposed algorithms solved the efficiency problem by adopting low-rank factorization models, while also proving very efficient compared to other methods. As such, the study represents a significant step forward in the challenge of developing an efficient link-prediction model.

Another important problem that needs to be addressed concerns the accuracy of link prediction approaches. [14] developed an innovative link-prediction method that aimed to improve the accuracy of link predictions. The experimental findings revealed that the proposed approach outperformed many other methods in terms of accuracy and scalability and the associated runtime was significantly less than that observed in previous studies. However, although the proposed approach did enhance link prediction accuracy, it remains untested on large network data, which may see its efficiency become undermined.

Improving the accuracy of link prediction can also be achieved using methods that predict links in uncertain frameworks. [15] proposed a new approach for addressing the problems of link

prediction in the context of an uncertain framework based on the theory of belief functions. Results obtained from the experimental work of [15] outperformed traditional approaches.

Another problem related to link prediction in signed SNs concerns the sparsity of data. To alleviate this problem, [16] proposed an innovative approach that is capable of exploring the personality of the user using social media. The experimental results obtained indicated that a complementary relationship exists between the signed link prediction problem and personality information.

An interesting state-of-the-art method for facilitating link prediction is the use of the temporal regularity in interpersonal communication as a means of prioritizing weighted edges in network graphs [17]. Compared with other methods, this method predicts links even if there is a scarcity in the number of edges needed for analysis.

A contrasting similarity-based link-prediction method, based on fuzzy link importance, was presented in [18]. The method performed well, using two strategies to achieve its objectives. Firstly, for the selection of the neighbor, the distance between nodes was used. Secondly, to find the relevant link, the fuzzy link importance was employed. By using these strategies, the method has obtained sound results.

An approach aiming to solve the problem of link prediction problems in large complex networks was proposed by [19] following two steps. In the first step, the complex network is transformed into a different simple network, before the second step uses probability to predict the possible links. The experimental test results indicate that the method achieved promising results.

Methods for predicting temporal links in temporal networks have been introduced. For example, [20] proposed an innovative approach based on a semi-supervised learning network with the aim of predicting current and future links. The approach was tested using real data. The results obtained from the experimental test demonstrated that the approach was very effective and highly scalable.

A myriad of similarity-based methods has been introduced to address link prediction problems. However, methods of this nature require substantial data to work effectively. Recent methods have been introduced to alleviate such problems, and approaches based on similarity indices have accomplished considerable efficiency. For example, [21] proposed a method that uses a clustering coefficient index found to outperform many existing approaches. The improvements the approach exhibited were attributed to the use of an index of clustering.

Within the context of multiple networks, the link prediction problem was discussed in [22]. In terms of accuracy, the supervised learning method achieved 92.5%, which is very promising. The unsupervised method achieved a resounding accuracy result of 97% using normalized discounted cumulative gain.

Another interesting method proposed as a means of addressing the problems of similarity-based link prediction approaches was put forward by [23], which successfully managed to address the issue of lack of efficiency. The experimental results revealed that

the LDR index enhanced the prediction performance in undirected networks. However, the researchers highlighted a need to investigate the method's application further within directed and signed networks.

Many researchers have achieved remarkable improvements in link prediction within the context of social networks. However, studies that address trusted link prediction are very few. Recently, [24] proposed a method that sought to forecast links by using the user's most important features. The experimental results revealed that the method outperformed many existing approaches in terms of effectiveness. Moreover, the quality of community detection was improved.

In the past, research that investigates issues related to link prediction in signed networks has been very scarce. Only recently have we witnessed an increase in the number of studies that discuss issues related to link prediction in signed networks. For example, [25] proposed a fresh approach with experimental results that show a high quality in terms of the accuracy and efficiency of link predictions.

Many further new methods have been introduced with the aim of improving link prediction accuracy, for example, [26] has proposed a method that achieves good accuracy using associated degrees.

A more interesting method for link prediction was proposed by [27], which employed the level-2 node clustering coefficient. As previously described, most link-prediction methods suffer from either lack of efficiency or accuracy. Plus, increased efficiency can lead to a reduction in accuracy. [27] suggested a method that was tested experimentally over 11 real-world datasets. The obtained results indicated that the method outperformed many of the state-of-the-art existing methods in terms of accuracy.

In dynamic SNs, categories of users exert social influence on other members within the social network. These individuals are commonly referred to as influencers. Influential users play a fundamental role in digital marketing [28]. As such, predicting links to and from influential users is of paramount importance for many organizations. [29] introduced a method aiming to predict influential links. The approach was tested experimentally and the test's findings revealed that the proposed approach outperformed comparable link prediction metrics. Moreover, the link prediction performance was improved in comparison to that associated with classical topological metrics.

Low link prediction accuracy remains a major challenge that requires attention. A myriad of methods and algorithms has been introduced by many research field scholars. A current approach that aims to address the problem of low link prediction accuracy, which is based on matrix factorization, is proposed by [30]. The experimental results of the method indicate that it achieves a higher prediction accuracy than existing methods.

Despite the fact that matrix-factorization-based methods have achieved good security, such methods suffer from the problem of having to build the adjacent-matrix. [31] has developed a technique to address the problem of matrix-factorization-based methods by fusing the adjacent matrix and some key topological metrics in a unified probability matrix. The [31] models were experimentally tested with real data, with the results of the

experiment revealing that the proposed models achieved an impressive link prediction performance.

Another important and interesting method that has achieved great link prediction accuracy was put forward by [32], which used H-index and the influence of degree. The method achieved remarkable link prediction accuracy by utilizing information about the endpoint node.

Among the methods that have been developed to utilize real node influence and improve link prediction accuracy is that of node ranking [33]. This method uses the concept of node ranking to improve link prediction accuracy.

Even though there are some problems inherent in similarity-based methods, they have achieved considerable results in terms of accuracy and efficiency. However, further such improvements will be required. A method that is based on the kernel graph, which utilizes the structural information extracted from a signed social network, was proposed in [34]. This method involves initially generating a set of subgraphs with different strengths of social relations for each user. Having been tested with real data, the experimental test results revealed that the method achieved considerable link prediction performance on the two types of positive and negative links. Moreover, the accuracy and F1-Score exceeded that of existing methods, indicating that there is room to improve accuracy.

More methods that use a similarity index for link prediction have recently been introduced. A method that took the attribute similarity between the node pair into consideration, named attribute proximity, was discussed in [13]. The experimental test results showed that it achieved higher accuracy than approaches that didn't take node attribution into account.

1.2. Link Prediction in Dynamic SNs

Dynamic networks can be used to describe members that exhibit varying dynamics over time [1]. In such a network, a new member joins, existing members may leave the network, and members create or break relationships [46]. As a consequence of this phenomenon, the network can expand or shrink. For this reason, there is a compelling need to take dynamic changes into consideration when developing approaches that can accurately predict new, current, or missing links. Link prediction in temporal SNs is more challenging due to the continuous network changes. The dynamic changing nature of temporal SNs will result in the emergence of different types of sub-graph. Many applications have attempted to exploit this nature of networks, for example, countries seeking to beef up their security can use such features to predict criminal links, and online recommendations [4]. Biological networks can also utilize temporal networks, with a vast number of applications having been proposed that do so, [57] developing innovative methods for detecting protein complexes. The method proposed by [57] exploited the dynamic nature of protein, while [35] has developed a model that detects the progress of a community over time by utilizing the temporal nature of SNs. [36] discussed an interesting method that predicted links in a dynamic SN based on three metrics. The proposed method was experimentally tested on DBLP data and the results obtained indicate that the method achieved superior results to alternative approaches. The predicting of future links in social networks using

the proximity of node is discussed in [37]. In this approach, future interaction can be obtained from network topology alone.

The structure of social networks is rapidly evolving. To leverage this evolving structure, [38] proposed a method that exploited characteristics calculated by a known time prediction of measures computed using a pair of nodes. The method was tested using real data. The experimental results obtained revealed that the approach achieved high accuracy.

The influx of methods that are capable of predicting future relationships in dynamic SNs continues to increase. For example, [39] introduced a method that utilizes learning automata for link prediction. In the same direction another new method proposed by [40] uses learning automata to predict links in stochastic SNs. The method was tested using data collected from social networks and has achieved sound link prediction accuracy. One of the interesting features of this is that it deals with online stochastic SNs that can encounter complex online variations.

Clustering, one of the prominent data-mining techniques, has also been employed for predicting future links in dynamic SNs. An interesting method that uses the clustering approach for predicting future links is proposed by [41], while another method is discussed in [42]. These two methods have obtained sound results in comparison with existing methods.

Deep learning is one of the data-mining techniques that has received more interest from researchers working in the field of data mining and machine learning. The nature of this technique makes it suitable for use in dynamic SNs. [1] discussed a number of techniques that predict links using deep learning. Also, a viable approach that successfully managed to predict links using machine learning is discussed in [43].

Some link-prediction methods suffer from a lack of precision. However, some researchers have attempted to alleviate such a problem by proposing different types of techniques. For example, [44] proposed an approach that utilizes community information to improve prediction accuracy. Taking the same approach, [45] introduced a technique that exploited the structure of community information to predict new edges and hence improve link prediction precision.

One of the most important features of online SNs is their rapid change over time [46]. Currently, most of the methods used for predicting links depend on structural SNs. There is a compelling need for methods that are capable of predicting links in dynamic SNs. Moreover, the required methods should also possess high link prediction accuracy and efficiency. Organizations intend to exploit online SNs for a number of applications and require information on state-of-the-art methods that can be used to predict possible links. The main objective of this paper is to discuss and analyze the most prominent link-prediction methods that are able to accurately and efficiently predict links in dynamic SNs.

This paper is organized as follows. Section 2 discusses the problems of link prediction. The next section discusses the strategies used by link-prediction methods to solve the problem of link prediction. This is followed by discussing and analyzing existing work. The paper wraps up with conclusions and future work.

2. Problems of Link Prediction

A simple question and answer summarizes the problem of link prediction. As discussed in [47], if we have SN at a certain time, t_1 , after a period of time, t_2 , can we predict a possible link between members of the SN? Many methods have been introduced that use structural SNs but, in real life, SNs are dynamic. In this section, we try to provide an overview of the problems of link prediction in dynamic SNs.

2.1. Link Prediction in a Temporal Network

A temporal network is a network that evolves over time. For predicting the emergence of links in such a type of a network, time factors are crucial [48]. Details on how links can be predicted using a temporal network can be found in [49]. The main problems and challenges of predicting links in a temporal network that require addressing are related to the changing nature of the network over time. Many methods and techniques have been proposed to address this problem. For example, [48] introduced a technique to exploit the general network structure and managed to successfully predict links in the process. [5] proposed a technique using graph theory to predict links, and [50] used community structure information to do so. An efficient method proposed by [51] produced far better results than many contemporary temporal link-prediction methods.

In [52], the authors explored methods of inferring links in a special type of network; ego-networks – where there is a scarcity of information about neighbors. The proposed methods introduced numerous approaches to retrieve information about communities. In doing so, they have improved the prediction of links compared with other methods that use structural SNs. An interesting method that determines the edge weight based on a calculation of the scores using spectral analysis is given in [17]. The method achieved good prediction results.

An effective and scalable method for predicting links within a real-world temporal social network was presented in [20]. [53] proposed a method that takes into consideration the time features of the network. The method captured the importance of timestamps in the interaction between network nodes and the experimental results showed significant improvement of link prediction. In the context of a temporal network, [54] proposed a method that predicts links by using a cross-temporal concept, which involves inferring the nodes at different time intervals. The method was tested experimentally using real-world data and the results showed sound improvements in the link prediction accuracy.

2.2. Link Prediction in Heterogeneous Networks

In SNs, there are two major types of networks: homogeneous networks and heterogeneous networks. The homogeneous networks assume that all the nodes and edges are of the same type while, in heterogeneous networks, there is variation in the nodes and the links between them. The majority of the existing link-prediction methods deal with homogeneous SNs. In the real world, the majority of SNs are heterogeneous with different types of nodes and edges that pose many challenges requiring intervention. For addressing such problems, many new link-prediction methods have been introduced. For example, the work of [55, 56, 5, 57] and recently [58].

2.3. Link Prediction with Active/Inactive Links

Interactivity in SNs is generally represented by sending e-mails, receiving phone calls, commenting on messages, etc.

Historical information related to interactivity between nodes in the networks, such as the timestamp, is likely to improve the accuracy of link prediction. Using the temporal features of dynamic SNs has been proven to improve accuracy too [4].

2.4. Link Prediction Scalability

The era of big data has emphasized the importance of efficiency for link prediction algorithms. The link prediction algorithm scalability remains questionable unless the algorithm is tested and evaluated with a huge amount of data. However, most of the current existing link-prediction methods have been tested and evaluated using limited datasets, which make it harder to ensure their scalability. The issue of algorithm scalability remains one of the challenges that need to be addressed. Attempts were made by [59] to develop a scalable link prediction algorithm. The developed algorithm managed to predict links using features of endpoints and neighborhood, adopting the locality-sensitive hashing algorithm to enhance the scalability so that the proposed approach could effectively predict links in large networks spanning long-term sequences.

3. Link Prediction Strategies

This section discusses the strategies used for link prediction, which include similarity-based methods, maximum likelihood methods, clustering-based methods, probabilistic models, fuzzy link methods, and matrix factorization-based link-prediction methods.

3.1. Similarity-based Strategies

Similarity-based link-prediction methods are among the first and simplest methods used in link prediction. The idea behind this class of methods is that each node pair – say n_1 and n_2 – is given a score that reflects the similarity between n_1 and n_2 . The algorithm then ranks the pair of nodes based on their score, and the node pair with the highest score is most likely to have a link between them [60]. Nodes show more similarities if they have shared neighbors.

There are some problems and challenges associated with the link-prediction methods that use a similarity score. As discussed in [18], predicting the link is based on computing the rating and the selection of the neighbors by using similarities between the pairs. If the algorithm fails to find enough information on the ratings, there will be problems with computing the similarity. Moreover, the accuracy of link prediction will be negatively impacted by the number of neighbors.

Similarity-based link-prediction methods are not confined to structural SNs. In dynamic SNs, a number of methods have also been introduced. For example, [4] and [50] proposed an interesting method that employs similarity indices in dynamic SNs. The model proposed in [4] is based on the Covariance Matrix Adaptation Evolution Strategy. Plus, a modified similarity-based link-prediction method was discussed in [61]. The approach was experimentally tested and evaluated using real-world data. The results obtained indicate that the method outperformed existing similarity-based link-prediction methods in terms of accuracy. Two improved algorithms, based on the similarity method that applies the network topology sufficiently, were presented in [62]. The experimental results of the two improved algorithms reveal that the prediction performance was far better than the existing traditional one.

Some efficiency improvements have been made to the similarity-based strategy. For example, [23] proposed an algorithm that improved computation efficiency. The improvements were made by the algorithm with the virtue of using linear computation. Further improvements in terms of effectiveness, efficiency, reliability, and strength were achieved using the method introduced by [24]. This approach made use of several user features to predict trusted links. Additional improvements in terms of the accuracy of link prediction were achieved by [26]. Their method used strategies that depend on the depth of the path passing from the source to destination nodes and the associated degree.

Accuracy, which is consistently used to evaluate link-prediction methods, represents an important consideration when developing and implementing any method that can be used for predicting links. A modified similarity-based method employing graph theory was proposed by [34]. Their method achieved significant improvements in the accuracy of predicting links compared with existing methods, thereby demonstrating that similarity-based methods continue to play a significant role in link prediction. The accuracy of similarity-based link-prediction methods was further improved by [63]. Their method achieved a remarkably high prediction accuracy by using a similarity index called attribute proximity. The authors concluded that the higher the similarity between the topological neighborhoods of two nodes, the more likely that a link will emerge.

3.2. Maximum Likelihood Algorithms

Maximum likelihood algorithms for link prediction is a concept applied to determine the parameter distribution of the network structure. In link prediction, the assumption made here is to organize the network structure and then maximize the likelihood of the observed structure. Based on this concept, a number of methods have been developed. For example, [55] employed the concept of maximum likelihood to predict links in SNs. With limited datasets, the method obtained good results.

Link-prediction methods based on maximum likelihood face practical applications related to the time taken by the algorithm to converge, especially if the dataset is very large, implying that the algorithms are not scalable.

3.3. Probabilistic Models

An interesting class of methods used to predict SN links is based on a probabilistic concept. This approach can be applied to both static and dynamic SNs. In dynamic SNs, [64] employed a probabilistic concept to deal with the complexity of a non-linear dynamic created by the data features. The model managed to predict links with good accuracy. Additional methods were proposed using this concept to predict links such as [55, 56, 5]. Some methods combined the features of graph theory and probabilistic concept to predict links in SNs [65]. This hybrid method is very scalable due to the innovative approach used to approximate the probability of links.

In [66], the authors proposed an algorithm framework that combines probability with the Hamiltonian structure to predict links in SNs. The algorithm was tested and evaluated experimentally using numerical simulation data. The results obtained from testing the algorithm showed that it achieved a very high accuracy compared with the best available link-prediction methods. The algorithm also successfully managed to identify and uncover the missing links.

Despite the fact that link-prediction methods based on probabilistic features have achieved sound results in predicting links in SNs, the main problems of these methods center around efficiency. The computational time needed by the method is very high, so there is a need for reducing this reliance.

3.4. Clustering-Based Link-Prediction Methods

Clustering-based link prediction approaches have played a considerable role in enhancing the efficiency and accuracy of links inferencing. These methods have been discussed in several studies, for example, [11, 67, 21, 27].

In [11], the method achieved better improvements in the accuracy of links forecasting as the number of clusters grew, whereas [67] proposed a cluster-based method that used clustering information to predict the missing links. Their method was tested on three large-scale networks, with the experimental results revealing that it outperformed other approaches and, more interestingly, that information about link clustering has improved the accuracy of link prediction. [21] used an index that took into consideration more information related to the structures provided for link forecasting to enhance its accuracy in comparison to alternative indices. The accuracy of the method proposed by [21] was compared with twelve representative link-prediction methods, and the findings revealed that it exceeded their performance.

The approach proposed by [27] first involved extracting similar neighbors and grouping them into clusters, then computing the coefficients of the cluster up to two common levels. Their method exceeded the performance of all the alternative baseline methods. The only method that outperformed theirs is Node2vec, albeit with medium accuracy.

3.5. Fuzzy Link-based Methods

Link prediction based on the fuzzy concept has only recently been applied. For example, [18] proposed a model based on this concept with the proposed model, when tested and evaluated on real data, achieving considerable accuracy improvements. [68] proposed two methods that employ the concept of fuzzy-link prediction. The first approach used the concept of a fuzzy soft set, while the second employed the Markov model concept to improve the efficiency of link-prediction methods. They claimed that their models achieved better prediction than the existing approaches.

3.6. Matrix Factorization Methods

The simple idea behind matrix factorization is to decompose a complex matrix into a simpler one to make it possible to compute more complex operations. Numerous link-prediction methods based on matrix factorizations were proposed that have effectively improved performance in terms of the accuracy and efficiency of link prediction. For example, [31] propose a framework that can be used for link prediction incorporating the matrix factorization concept. [69] discussed an interesting link-prediction method that uses the concept of matrix factorization. The proposed method produced better results in terms of link prediction accuracy when compared with other methods. A recent study based on matrix factorization was discussed in [30]. Although the method of [30] achieved high prediction accuracy, the data was relatively limited as it was confined to sales datasets. As such, further evaluation involving more complex datasets is required to confirm its level of prediction accuracy.

4. Analysis and Discussion of Existing Methods

In the previous sections, we have discussed the challenges and problems of predicting the emergence of new links using a special type of SN; namely, dynamic SNs. Furthermore, we have also discussed the different types of link-prediction methods proposed by many scholars working in the SN field. This section discusses the most current solutions introduced by researchers in the field of predicting links in SNs. The main topics to be discussed in this section start with the summary of the proposed solutions for addressing links prediction problems, followed by datasets used, the main features of link prediction, the techniques used in link prediction, and concluding with the evaluation and accuracy measures. A summary of the solution’s evaluation results is depicted in Table 2.

4.1. Summary

Once online SNs had become an important platform for the exchange of a huge amount of data between users, their existence attracted a significant number of scholars intending to study how these networks evolve over time. The emergence and deletion of links help researchers to understand the dynamic nature of SNs [2].

In the past two decades, many link-prediction methods have been introduced, implying that the problem is not new. However, the new and most challenging SN-related task concerns the forecasting of links in dynamic SNs, which are characterized by growing or shrinking networks. The majority of the work that has been performed in the area of dynamic SNs to date has been conducted with the acknowledgment of the importance of a dynamic nature within the network. Many scholars have taken into consideration the changing time features of the SN by using past information related to the node transactions, while others used the temporal feature of community structure [50]. These approaches forecast the future importance of a node based on eigenvector centrality. Subsequently, this view of future importance is used to predict links.

Some researchers have tried to develop new techniques for predicting future links using historical data. Their main objective is to improve the efficiency and accuracy of the methods applied. A model for link prediction in dynamic SNs using deep learning is discussed in [1]. Another model for link prediction based on a triad transition matrix, using statistical data, is given in [56].

The model discussed in [55] predicts future links by using the Euclidian latent distance. Nodes that exhibit closeness in the Euclidian distance are more likely to emerge as links. [4] proposed a model depending on the local information of nodes to predict future links in the dynamic SNs, while [5] introduced a model that uses graph theory to predict links by including temporal features.

In [17], it is introduced a method for link prediction based on graph theory. The method used the spectral analysis technique to calculate the score for each edge in the network graph. Based on this score, the edge weight will be determined. The method was tested and evaluated using real-world data, with the obtained results indicating that the method has enhanced the prediction of links. More interesting, however, is that the edges used in the analysis were very limited.

4.2 Datasets Issues

Most of the research conducted for the sake of developing link-prediction methods involves the use of some form of data that is

either artificial or real world, as with [64] and [55]. The major problem concerning the datasets used for testing and evaluating the link-prediction methods is the absence of standardization [2]. Researchers have used numerous SNs of various sorts and sizes according to their proposed model and there are several dataset types available for researchers to use. The majority of networks used in the existing literature include collaboration networks, online SNs, generated datasets, and friends and family e-mails. [55, 56, 5] have used collaboration SN datasets. [64] employed two biological SNs. Most of the datasets used are small in size, with the exception here being [4] who employed a moderately large size of the online SN (Twitter) for the development of their method. For testing and evaluating their method, [50] used five email SNs. [56] employed a merging of two datasets; namely, scientific collaboration networks and email. Table 1 shows a summary of the datasets used by various researchers surveyed in this paper.

Table 1: Datasets used by researchers [1]

Datasets	No. of nodes	No. of links
Irvine Msg	896	2,201
Enron	200	714
News Words	503	15,638
Manufacturing Emails	167	3,250
Robot	352	1,611
Twitter (RRNs)	5.71*10 ⁶	49*10 ⁶
DBLP	437,515	1,359,471
astro-ph	55,233	644,496
Friends and Family Emails	1,130	1,344
Math	24,818	506,550
Ask	159,316	964,437
Super	194,085	1,443,339
Stack	2,601,977	63,497,050

From the literature that we surveyed, we found that the choice of suitable dataset depends on the judgment of the researchers who want to develop the link-prediction method and evaluate its performance using the collected data. Furthermore, the datasets used in many applications are synthetic, artificial or generated [64] [55] which might raise some concerns about the results obtained using such a type of dataset. Moreover, the size of the data used in testing the performance of the methods is not large. Another problem regarding the data is the nature of the datasets which, in many cases, is static and needs to be used to test the method based on the dynamic network. Some researchers have attempted to address this problem by including features of a temporal network [64, 55, 56, 5]. As most SNs grow and shrink over time, indicating that these networks are dynamic, it will prove more interesting for link-prediction methods to be applied in these dynamic SNs rather than structured ones. To judge the practicality of such methods, the datasets used should be real and applicable for link predictions. As many studies indicate that the datasets used for evaluating the developed methods are either static, artificial, or with a sample size, these issues represent great challenges that need to be addressed. These challenges point to the important need for setting database standards that will be used for evaluating the performance of all these methods.

4.3. Features Used in the Link Prediction Process

The two main features used to predict links in dynamic SNs are node attributes information and network topology. Both features

have been used by numerous studies to predict links in dynamic SNs. For example, [55] developed a model that employed the latent space concept and used the local topologies feature. The model predicts links based on past information, assuming that if there are two nodes, n_1 and n_2 , which have links in the time, $t-1$, then mostly likely they will be gaining a link at a time, t .

The model proposed by [4] employed the two predominant features used to predict future links in dynamic SNs; namely, the network topology and node attributes. A test of this model using a vast amount of data indicates a high convergence with astonishing precision. Unlike the majority of the techniques proposed to detect dynamic community, [4] proposed a model named Hierarchical and Overlapping Community Tracker (HOCTracker) that is capable of detecting the progression of an overlapping community in dynamic SNs. The results obtained from the experimental test of the model indicate that the community structure detected is far better than the best available methods.

The model proposed by [56] uses the concept of a triad transition matrix to discover the dynamic pattern of networks. The main feature used is a local topology network and observations of the recorded network history. The model merges statistical characteristics with the topology of the network. This merger resulted in a method with the strength to perform better in detecting the evolution of a network. The model introduced by [5] incorporated the available past information about links on the current SN state. The model shows that including a timestamp of the historical interaction improves the accuracy of predicting new links. The technique used by the model to predict links is a joining of the graph with the temporal information included in the evolving SNs.

4.4. Techniques Used in Link Prediction

Link-prediction methods employ a variety of approaches and strategies in the form of a cluster-based, similarity-based, or fuzzy link, etc. The most appropriate prediction technique is selected on the basis of the features used in the link-prediction method. In similarity-based models, the method predicts the links among nodes based on a similarity score computed among the pair of nodes. A pair of vertices with high similarity value is most likely to foster a relationship or link in the future. Methods based on maximum likelihood predict future links between two nodes by identifying a centric node. If the likelihood that the two nodes fall in the radius of that centric node is high, then there is a possibility that a link might emerge between them. Methods based on a probabilistic approach use probability to predict the future links between two nodes in the dynamic SNs. The methods predict the links by calculating the probability of the edge weights of the two nodes and the probability of the neighboring nodes. The clustering-based link-prediction methods use a node clustering coefficient to predict the link. The technique first computes the clustering coefficient then uses it to predict the future link [27].

The research of [4] is focused on a node's local feature, for which they use the similarity index to predict the emerging link. The work of [55] used an approach that ranks the likelihood of two vertices expected to be linked based on the frequency of joining in the test set.

The model proposed by [56], which is based on the Triad Transition Matrix, relied on the probabilistic approach in that it contained triad transition probabilities in the network. The local probabilistic model was extended by [5] to predict links using the

timestamp feature and demonstrating the incorporation of link weight into the prominent link prediction approaches. [50] model integrated various kinds of information into the SNs, such as node centrality and temporal information.

Another model that relied on the probabilistic approach uses Conditional Temporal Restricted Boltzmann Machine (CTRBM), described by [64], to forecast emerging links on individual transition variance and the influences of local neighbors.

4.5. Methods Evaluation

This section discusses the diverse evaluation measures and metrics employed by the different types of methods proposed by various researchers. The evaluation in terms of method accuracy and efficiency represents an important factor for its applicability and acceptability. To date, there are no common metrics and measures that can be employed to evaluate these methods. This lack of common evaluation metrics and measures, coupled with the absence of standardized datasets, entails that it is very hard to assess each solution and, as such, we cannot present a reliable and valid conclusion as to which is the best in terms of link forecasting in dynamic SNs.

The methods explored in this study can be evaluated either by two machine-learning measures; namely, receiver operating characteristics (ROC) [70] and the area under ROC (AUC) or other measures. The interpretation of the values of these measures depends on the method, as each method has features that are different from the others.

For example, when evaluating two models that have an AUC score close to each other, it will be very hard to determine which one is the best to select. As such, [64] employed a measure that computes the sum of the absolute difference to distinguish between various types of models. The methods discussed in [4, 55, 15, 17] employed ROC and AUC for evaluation.

Researchers in [56] employed another means for evaluating their methods in terms of efficiency. They have used two evaluation techniques, with the first one being known as average normalized rank (ANR), and the second known as discounted cumulative gain (DCG), which is employed for node ranking. ANR was employed to directly pinpoint the location of the important item in the ranking. In comparison, [20] used two measures, F1Score and Kendall's Tau Coefficient (KTC), to evaluate their methods.

From the surveyed and discussed methods, we found that each researcher has typically selected the evaluation metric and measure that best suits their model. As a result of this, while every researcher claims to have developed a model that offers superior performance to the alternative methods, this performance was measured in a testing environment directly tailored to the method being assessed.

This variation in the method evaluation indicates that it is very hard to tell which model is superior to the others.

5. Conclusion and Future Recommendations

Link prediction within the context of social networks is by no means a novel research topic. However, the greatest challenge associated with predicting new or missing links in dynamic SNs characterized by ongoing evolution is yet to be adequately addressed.

Table 2: Summary of Famous Link Prediction Methods

No.	LP Strategy	Dataset	Proposed Model (Method)	Features Used	Evaluation and Accuracy Measures	Remarks
[64]	Probabilistic	Synthetic data A and B (10,000 nodes each) Robot.Net (2,483,776 nodes) Two biological datasets (Control and Exposure 13,483,584 nodes each) from Stevenson	Deep learning framework (ctRBM) + can quickly learn	Node attributes and network topology	ROC and AUC curves Sum of Absolute Differences (SumD)	Reliable for handling uncleaned data
[4]	Similarity-based	51 million tweets Twitter reciprocal reply networks over 81 days	Covariance Matrix Adaptation Evolution Strategy (CMA-ES)	Node-specific features and network topological similarities	ROC and AUC	Does not require parametric thresholds. The linearity of the model is one of its weaknesses. Can handle different types of network
[50]	Similarity	Irvine Message Enron Email Infectious SocioPatterns News words Nodobo	Integrated Time Series Model (ITM) that combines topological (community and centrality) and temporal information	Network topology, community structure, and node centrality feature	AUC	More realistic for dynamic networks
[56]	Probabilistic	Two email social network datasets Enron dataset Wroclaw University of Technology	Triad Transition Matrix (TTM) comprising the probabilities of transitions between triads found in the network	Network Local topology observations of the recorded network past information	Compared to preferential attachment (PA) and common neighbors (CN) predictor	Data was pre-processed
[55]	Maximum likelihood and probabilistic	NIPS co-publication data + synthetic data generated by a model	DSNL model handle change of friendship	Local topologies (represent each entity with a location p in the latent space)	AUC & ROC	Little data with only around 11,000 nodes. Cannot handle large data
[5]	Probabilistic	DBLP and astro-ph of ArXiv.	Graph-based link prediction techniques based on the local probabilistic model	Time-based edge weights derived from temporal aspects	Discounted Cumulative Gain (DCG) and Average Normalized Rank (ANR)	Cannot handle many types of networks
[17]	Temporal Method	Enron E-mail, Irvine SNS, Friends and Family SMS	Temporal regularity in interpersonal communication	Node-pair records extraction and time-domain signal generation	Area Under the Curve (AUC)	There is a need to take into consideration the directions of interpersonal communication
[18]	Fuzzy Link	100,000 ratings and 1,300 tag applications	Distance between two different objects	Links among items, fuzzy link importance	MAE and RMSE	There are limitations on the procedure used for evaluating the method
[20]	Temporal Network	Data obtained from (SNAP) Math, Ask, Super, Stack	(Cox PHM), Game theory	Topological features	Average F1Score, Kendall's Tau Coefficient (KTC)	The first method achieved good accuracy

This paper examines the most current and innovative methods for predicting links in dynamic SNs. Each method explored and discussed in this paper exhibited some sort of good performance, such as accuracy, efficiency, or scalability, in respect of one SN type. A variety of models were explored in this paper. For each explored model, the paper discussed the prediction strategy, the datasets used, the type of features, and the evaluation measures used.

One vital feature of dynamicity concerns the temporal aspects of SNs, which is something that many researchers have considered. Some emerging methods have made great strides in terms of link prediction accuracy and efficiency, including the novel methods that have used different topology and harnessed both supervised and unsupervised techniques. Some methods, such as temporal-based methods, are highly scalable in terms of their ability to predict links [20].

This rigorous analysis of the emerging solutions indicates that there is no one complete method available that predicts emerging or lost links in dynamic social networks to a high degree of accuracy, efficiency, and scalability. Continuous efforts are needed to develop an innovative model that is capable of handling different types of SNs.

Despite the influx of research that aims to predict links in dynamic SNs, we still believe that there is a need for further research to address the problem of the absence of complete research that exhibits high accuracy, high efficiency, and is very scalable as well. Further improvements in accuracy, efficiency, and scalability are very important due to the huge data generated from dynamic SNs.

Conflict of Interest

The authors declare no conflict of interest.

Acknowledgment

The authors would like to acknowledge the assistance and support provided by Ajman university library and United Arab Emirates University library for procuring most of the papers and the books used in this article.

References

- [1] Mohammad Marjan, Nazar Zaki, and Elfadil A. Mohamed (2018). "Link Prediction in Dynamic Social Networks: A Literature Review." IEEE CiS'18 5th Edition International IEEE Congress on Information Science and Technology, Marrakech, Morocco, October 21 - 27, 2018.
- [2] Wang, P., Xu, B., Wu, Y. and Zhou, X. (2014). Link prediction in social networks: the state-of-the-art. *arXiv preprint arXiv:1411.5118*.
- [3] Al Hasan, M. and Zaki, M. J. (2011). A survey of link prediction in social networks. In *Social network data analytics* (pp. 243–275). Springer US.
- [4] Bliss, C. A., Frank, M. R., Danforth, C. M. and Dodds, P. S. (2014). An evolutionary algorithm approach to link prediction in dynamic social networks. *Journal of Computational Science*, 5(5), 750–764.
- [5] Tylenda, T., Angelova, R. and Bedathur, S. (2009, June). Towards time-aware link prediction in evolving social networks. In *Proceedings of the 3rd workshop on social network mining and analysis* (p. 9). ACM.
- [6] Mori J, Kajikawa Y, Kashima H, et al. Machine learning approach for finding business partners and building reciprocal relationships. *Expert Systems with Applications*, 2012, 39: 10,402–10,407.
- [7] Wu S., Sun J., Tang J. Patent partner recommendation in enterprise social networks. In: *Proceedings of the 6th ACM International Conference on Web Search and Data Mining (WSDM'13)*, Rome, Italy, 2013. 43–52.
- [8] Berlusconi G., Calderoni F., Parolini N., Verani M., Piccardi C. (2016). "Link Prediction in Criminal Networks: A Tool for Criminal Intelligence Analysis." *PLOS ONE*, DOI:10.1371/journal.pone.0154244, April 22, 2016.

- [9] Almansoori W., Gao S., Jarada T. N., et al. Link prediction and classification in social networks and its application in healthcare and systems biology. *Network Modeling Analysis Health Informatics Bioinformatics*, 2012, 1: 27–36.
- [10] Huang Z., Lin D. K. J. The time-series link prediction problem with applications in communication surveillance. *INFORMS Journal on Computing*, 2009, 21: 286–303.
- [11] Li D., Zhang Y., Xu Z., Chu D. and Li S. (2016). "Exploiting Information Diffusion Feature for Link Prediction in Sina Weibo." *Scientific Reports* vol(6), article number: 20058(2016).
- [12] Liu F., Liu B., Sun C., Liu M., and Wang X. (2015). "Deep Belief Network-Based Approaches for Link Prediction in Signed Social Networks." *Entropy*, Vol(2015), No(17), PP. 2140-2169; doi:10.3390/e17042140.
- [13] Zhang H., Wu G. and Ling Q. (2019). "Distributed Stochastic Gradient Descent for Link Prediction in Signed Social Networks." *Journal on Advances in Signal Processing*, (2019) 2019:3. <https://doi.org/10.1186/s13634-019-0601-0>.
- [14] Bastami E., Mahabadi A., and Taghizadeh E. (2019). "A gravitation-based link prediction approach in social networks." *Swarm and Evolutionary Computation*, 44 (2019), PP. 176–186.
- [15] Mallek S., Boukhris I., Elouedi Z., and Lefevre E. (2018). "Evidential link prediction in social networks based on structural and social information." *Journal of Computational Science*, 30 (2019), PP. 98–107.
- [16] Ghazaleh Beigi, Suhas Ranganath, and Huan Liu. (2019). "Signed Link Prediction with Sparse Data: The Role of Personality Information." In *Companion Proceedings of the 2019 World Wide Web Conference (WWW '19 Companion)*, May 13–17, 2019, San Francisco, CA, USA. ACM, New York, NY, USA. <https://doi.org/10.1145/3308560.3316469>.
- [17] Shinkuma R., Yuki Sugimoto Y., and Inagaki Y. (2019). "Weighted network graph for interpersonal communication with temporal regularity." *Soft Computing*, (2019) 23, PP. 3037–3051.
- [18] Ai J., Su Z., Li Y. (2019). "Link prediction based on a spatial distribution model with fuzzy link importance." *Physica A*, 527 (2019) 121155.
- [19] Aslan S., Kaya B., and Kaya M. (2019). "Predicting potential links by using strengthened projections in evolving bipartite networks." *Physica A*, 525 (2019), PP. 998–1011.
- [20] Bu Z., Wang Y., Li H., Jiang J., Wu Z., and Cao J. (2019). "Link prediction in temporal networks: Integrating survival analysis and game theory." *Information Sciences*, 498 (2019), PP. 41–61.
- [21] Dharavath R. and Arora N. S. (2019). "Spark's GraphX-based link prediction for social communication using triangle counting." *Social Network Analysis and Mining* (2019) 9:28.
- [22] Eberhard L., Trattner C., and Atzmueller M. (2018). "Predicting trading interactions in an online marketplace through location-based and online social networks." *Information Retrieval Journal*, (2018), <https://doi.org/10.1007/s10791-018-9336-z>.
- [23] Gao H., Huang J., Cheng Q., Sun H., Wang B., and Li H. (2019). "Link prediction based on linear dynamical response." *Physica A*, 527 (2019), 121397.
- [24] Golzardi E., Sheikahmadi A., and Abdollahpouri A. (2019). "Detection of trust links on social networks using dynamic features." *Physica A*, 527 (2019), 121269.
- [25] Gu S., Chen L., Li B., Liu W., Chen B. (2019). "Link prediction on signed social networks based on latent space mapping." *Applied Intelligence*, 2019, <https://doi.org/10.1007/s10489-018-1284-1>.
- [26] Jibouni, A., Lotfi, D., EL Marraki, M., Hammouch, A. (2018). "A novel parameter free approach for link prediction." *Proceedings - 2018 International Conference on Wireless Networks and Mobile Communications, WINCOM, Marrakesh, Morocco; 16 October 2018 through 19 October 2018*.
- [27] Kumar, A., Singh, S.S., Singh, K., Biswas, B. (2019). "Level-2 node clustering coefficient-based link prediction." *Applied Intelligence*, Volume 49, Issue 7, 15 July 2019, Pages 2762-2779.
- [28] Dinh, T.N., Nguyen, D.T., and Thai, M.T. (2012) "Cheap, Easy, and Massively Effective Viral Marketing in Social Networks: Truth or Fiction?," *Proceedings of the 23rd ACM Conference on Hypertext and Social Media*, June, 2012, pp. 165-174.
- [29] Monteserin A. and Armentano M. G. (2019). "Influence me! Predicting links to influential users." *Information Retrieval Journal*, Volume 22, Issue 1-2, 15 April 2019, Pages 32-54.
- [30] Mutinda F. W., Nakashima A., Takeuchi K., and Sasaki Y. (2019). "Time Series Link Prediction Using NMF." *2019 IEEE International Conference on Big Data and Smart Computing, BigComp 2019 - Proceedings* April 2019, Article number 86795022019 *IEEE International Conference on Big Data and Smart Computing, BigComp 2019; Kyoto; Japan; 27 February*

- 2019 through 2 March 2019; Category numberCFP1940X-ART; Code 146803.
- [31] Wang Z., Liang J., and Li R. (2018). "A fusion probability matrix factorization framework for link prediction." *Knowledge-Based Systems*, 159 (2018), PP. 72–85.
- [32] Wang Z., Wang Y., Ma J., Li W., Chen N., and Zhu X. (2019). "Link prediction based on weighted synthetical influence of degree and H-index on complex networks." *Physica A: Statistical Mechanics and its Applications*, Volume 527, 1 August 2019, Article number 121184.
- [33] Wu J., Shen J., Zhou B., Zhang X., and Huang B. (2019). "General link prediction with influential node identification." *Physica A: Statistical Mechanics and its Applications*, Volume 523, 1 June 2019, Pages 996-1007.
- [34] Yuan, W., He, K., Guan, D., Zhou, L., Li, C. (2019). "Graph kernel based link prediction for signed social networks." *Information Fusion*, Volume 46, March 2019, PP. 1-10.
- [35] Greene, D., Doyle, D. and Cunningham, P. (2010, August). Tracking the evolution of communities in dynamic social networks. In *Advances in social networks analysis and mining (ASONAM), 2010 International Conference* (pp. 176–183). IEEE.
- [36] Yao L., Wang L., Pan L., and Yao K. (2016). "Link Prediction Based on Common-Neighbors for Dynamic Social Network." *Procedia Computer Science*, Vol (83), 2016, PP. 82 – 89.
- [37] Liben-Nowell, D. and Kleinberg, J. (2007). The link-prediction problem for social networks. *Journal of the Association for Information Science and Technology*, 58(7), 1,019–1,031.
- [38] Rossetti G., Guidotti R., Miliou I., Pedreschi D., and Giannotti F. (2016). "A supervised approach for intra-/inter-community interaction prediction in dynamic social networks." *Soc. Netw. Anal. Min.* (2016) 6:86, DOI 10.1007/s13278-016-0397-y.
- [39] Moradabadi, B. and Meybodi, M. R. (2018). Link prediction in weighted social networks using learning automata. *Engineering Applications of Artificial Intelligence Journal*, 2018, 70: 16–24.
- [40] Moradabadi, B. and Meybodi, M. R. (2018). Link prediction in stochastic social networks: Learning automata approach. *Journal of Computational Science*, 2018, 24: 313–328.
- [41] Wu, Z., Lin, Y., Zhao, Y., Yan, H. (2018). Improving local clustering based top-L link prediction methods via asymmetric link clustering information. *Physica A: Statistical Mechanics and its Applications Journal*, 2018, 492: 1,859–1,874.
- [42] Fu, C., Zhao, M., Fan, L., Chen, X., Chen, J., Wu, Z., Xia, Y., Xuan, Q. (2018). Link Weight Prediction Using Supervised Learning Methods and Its Application to Yelp Layered Network. *IEEE Transactions on Knowledge and Data Engineering Journal*, 2018, 99.
- [43] Julian, K., & Lu, W. (2016). Application of Machine Learning to Link Prediction.
- [44] Mohan, A., Venkatesan, R., Pramod, K. V. (2017). A scalable method for link prediction in large real-world networks. *Journal of Parallel and Distributed Computing*, 2017, 109: 89–101.
- [45] Caiyan, D., Chen, L., Li, B. (2107). Link prediction in complex network based on modularity. *Journal of Soft Computing*, 2017, 21(15): 4,197–4,214.
- [46] Bhat, S. Y. and Abulaish, M. (2015). HOCTracker: Tracking the evolution of hierarchical and overlapping communities in dynamic social networks. *IEEE Transactions on Knowledge and Data Engineering*, 27(4), 1,019–1,013.
- [47] Liben-Nowell, D. and Kleinberg, J. (2007). The link-prediction problem for social networks. *Journal of the Association for Information Science and Technology*, 58(7), 1,019–1,031.
- [48] Gao, S., Denoyer, L. and Gallinari, P. (2011, October). Temporal link prediction by integrating content and structure information. In *Proceedings of the 20th ACM International Conference on Information and Knowledge Management* (pp. 1,169–1,174). ACM.
- [49] Dunlavy, D. M., Kolda, T. G. and Acar, E. (2011). Temporal link prediction using matrix and tensor factorizations. *ACM Transactions on Knowledge Discovery from Data (TKDD)*, 5(2), 10.
- [50] Ibrahim, N. M. A. and Chen, L. (2015). Link prediction in dynamic social networks by integrating different types of information. *Applied Intelligence*, 42(4), 738–750.
- [51] Niladri S., Saptarshi B., Sukumar N., Sanasam R. S. (2018). Temporal link prediction in multi-relational network. *World Wide Web Journal*, 2018, 21(2): 395–419.
- [52] Tabourier L., Libert A-S., and Lambiotte R. (2016). "Predicting links in ego-networks using temporal information." *EPJ Data Science*, (2016) 5:1, DOI 10.1140/epjds/s13688-015-0062-0.
- [53] Munasinghe L. and Ichise R. (2012). "Time score: A new feature for link Prediction in Social Networks." *IEICE Trans. Inf. & Syst.*, Vol(E95-D), No. 3, March 2012, PP. 821-828.
- [54] Oyama S., Hayashi K., and Kashima H. (2012). "Link Prediction Across Time via Cross-Temporal Locality Preserving Projection." *IEICE Trans. Inf. & Syst.*, Vol(E95-D), No. 11, November 2012, PP. 2664-2674.
- [55] Sarkar, P. and Moore, A. W. (2006). Dynamic social network analysis using latent space models. In *Advances in Neural Information Processing Systems* (pp. 1,145–1,152).
- [56] Juszczyszyn, K., Musial, K. and Budka, M. (2011, October). Link prediction based on subgraph evolution in dynamic social networks. In *Privacy, Security, Risk and Trust (PASSAT) and 2011 IEEE Third International Conference on Social Computing (SocialCom), 2011 IEEE Third International Conference on* (pp. 27–34). IEEE.
- [57] Zaki et al.: Protein complex detection using interaction reliability assessment and weighted clustering coefficient. *BMC Bioinformatics* 2013 14:163.
- [58] Chen G., Xu C., Wang J., Feng J., Feng J. (2020). "Robust non-negative matrix factorization for link prediction in complex networks using manifold regularization and sparse learning." *Physica A* 539 (2020) 122882.
- [59] Sarkar, P., Chakrabarti, D. and Jordan, M. (2012). Nonparametric link prediction in dynamic networks. *arXiv preprint arXiv:1206.6394*.
- [60] Lü, L. and Zhou, T. (2011). Link prediction in complex networks: A survey. *Physica A: statistical mechanics and its applications*, 390(6), 1,150–1,170.
- [61] Virinchi S., Mitra P. (2013). "Link Prediction Using Power Law Clique Distribution and Common Edges Distribution." In: Maji P., Ghosh A., Murty M.N., Ghosh K., Pal S.K. (eds) *Pattern Recognition and Machine Intelligence, PReMI 2013. Lecture Notes in Computer Science*, vol 8251. Springer, Berlin, Heidelberg.
- [62] Dong, L., Li Y., Yin H., Le H., and Rui M. (2013). "The Algorithm of Link Prediction on Social Network." *Mathematical Problems in Engineering*, Vol(2013), Article ID 125123, 7 pages, <http://dx.doi.org/10.1155/2013/125123>.
- [63] Zhang Y., Shen S., and Wu Z. (2018). "Improve Link Prediction Accuracy with Node Attribute Similarities." *International Conference on Computer Engineering and Networks CENet2018 2018: The 8th International Conference on Computer Engineering and Networks (CENet2018)*, PP. 376-384.
- [64] M. T. Riaz, Y. Fan, J. Ahmad, M. A. Khan, and E. M. Ahmed, "Research on the Protection of Hybrid HVDC System," in 2018 International Conference on Power Generation Systems and Renewable Energy Technologies (PGSRET), 2018, pp. 1–6.
- [65] Li, X., Du, N., Li, H., Li, K., Gao, J. and Zhang, A. (2014, April). A deep learning approach to link prediction in dynamic networks. In *Proceedings of the 2014 SIAM International Conference on Data Mining* (pp. 289–297). Society for Industrial and Applied Mathematics.
- [66] Pan L., Zhou T., Lü L., and Hu C-K. (2016). "Predicting missing links and identifying spurious links via likelihood analysis." *Scientific Reports*, Vol(6:22955), DOI: 10.1038/srep22955.
- [67] Wu Z., Lin Y., Wan H. and Jamil W. (2016). "Predicting top-L missing links with node and link clustering information in large-scale networks." *Journal of Statistical Mechanics: Theory and Experiment*, (2016) 083202.
- [68] Bhawsar Y. and Thakur G.S. (2016). "Performance Evaluation of Link Prediction Techniques Based on Fuzzy Soft Set and Markov Model.", *Fuzzy Information and Engineering*, 8:1, 113-126, DOI: 10.1016/j.fiae.2016.03.007.
- [69] Menon A.K., Elkan C. (2011) Link Prediction via Matrix Factorization. In: Gunopulos D., Hofmann T., Malerba D., Vazirgiannis M. (eds) *Machine Learning and Knowledge Discovery in Databases. ECML PKDD 2011. Lecture Notes in Computer Science*, vol 6912. Springer, Berlin, Heidelberg.
- [70] Han J., M. Kamber, and J. Pei. 2012. *Data Mining Concepts and Techniques*. Morgan Kaufmann: Waltham, MA 02451, USA, 2012.

Optimization of the Electrical Discharge Machining of Powdered Metallurgical High-Speed Steel Alloy using Genetic Algorithms

Mohd Razif Idris¹, Imad Mokhtar Mosrati^{2,*}

¹Malaysia Italy Design Institute (MIDI), Universiti Kuala Lumpur, 56100, Malaysia.

²Mechanical Engineering Department, Faculty of Engineering, Azzaytuna University, 21218, Libya.

ARTICLE INFO

Article history:

Received: 04 October, 2019

Accepted: 10 November, 2019

Online: 05 December, 2019

Keywords:

EDM machine

Genetic algorithm optimization

Tool wear rate

Micro-crack size

Silver-Tungsten electrode

ABSTRACT

Through the Electrical Discharge Machining, the temperature is very high, which can lead to the material phase's transformation and affects material properties, which can lead to failure of the products in the industry. This study aims to investigate the effect of a new input parameter (pulse cycle time T_c), with other parameters on the EDM responses, prediction models are developed. 3D Laser Microscope is used to measure the surface defects. And to assess the effect of using a silver-tungsten electrode on improving EDM performance during machining of powdered metallurgical high-speed steel which is a very important material in the industry, such as aerospace, automotive, and electrical power industries, it is used in structural components and heat exchangers. An integrated approach combines Response surface design and Genetic Algorithm optimization methodology for modeling and optimizing the process responses is utilized. Two software's Minitab software and Matlab software were used for this purpose. The experimental results demonstrated comparative findings when the silver-tungsten electrode was used, and the optimization percentage was increased when the Genetic Algorithms method was used. Optimized values of the responses were as following: Micro-crack size was $0.965 \mu\text{m}$, the optimization percentage is 20.64%. Tool Wear Rate was 0.0020 g/min , the optimization percentage is 13.04 %.

1. Introduction

The product quality relies on the manufacturing process, optimization tools play a key role in enhancing product quality. Therefore the interest of this study to optimize the parameters and responses during the Electrical Discharge Machining EDM process of the material Powdered metallurgical high-speed steel. EDM is a nonconventional manufacturing process, utilized for very high hardness material, which can not be machined with traditional processes like turning or milling. It is a thermoelectrical process in which there is spark generation between the electrode and the workpiece. Response surface design methodology (Box Behnken) and genetic algorithm (GA) were integrated to optimize the input parameters and process responses. Genetic Algorithm (GA) Optimization Methodology is an artificial intelligence prediction tool, it has been getting

interested to solve problems that are hardly solved by the use of conventional methods.

A review of the literature undertaken found that most researches likely used the same ideas for optimization of process responses, like Taguchi, and study the same input parameters. Here is a review of the literature on the EDM process optimization based on the publishing year of the researches. In [1], the researcher improved process performance such as metal removal rate, surface roughness and overcut based on Grey Taguchi technique for EDMing of Ti-6Al-4V Titanium alloy. The process parameters selected in this study are current, T-on, voltage, T-off,

and duty factor. The optimized process parameters result in a lower wear ratio of the electrode, higher MRR, and better SR, the study shows an improved TWR of 15%, the MRR of 12% and SR of 19%. In [2], the authors established an analytical study for investigating the impact of input parameters on the MRR, SR, and RLT. The copper electrode is utilized, the other inputs are current and T-on. The best selection of input parameters and EDM

* Imad Mokhtar M., Email: imadmokhtar@yahoo.com

machining conditions is performed. Study [3] used the Taguchi design methodology and Grey Relational Analysis tool to improve the outputs like MRR, TWR, and SR of mild steel IS 2026 during the EDM process. It is found the optimal pulse current at 26A, pulse on time at 55 μ s and pulses off time at 5 μ s.

The impact of operating parameters like voltage, pulse on-time, pulse of-time and current on outputs such as MRR and SR of AISI D2 workpiece EDM, a copper electrode is investigated [4], the experiment design was made using L9 OA and using response surface methodology to improve the outputs, it was discovered that the current is the most significant parameter influencing the MRR and the SR. Another study [5], authors researched the impact of wire EDM on aerospace material fracture toughness, Grade 5 titanium (Ti6Al4V), fracture toughness is widely used for damage tolerance analysis of aerospace components in which critical crack sizes are computed for given loading conditions to arrive at safe inspection and maintenance intervals. The compact tension was used to evaluate the fracture toughness. Obtained results indicate a slight decrease in fracture toughness compared to those reported in the literature.

In [6] the authors studied electrical discharge machining (EDM) of insulating ceramic materials, such as diamond, using the assisting electrode method. This study investigated the dependence of the machining properties on amounts of additives, three types of insulating Si₃N₄ ceramics were machined by sinking EDM and by wire EDM. The MRR and the SR were estimated for the EDMed material. Different dependencies on the amounts of added Al₂O₃ were observed, and the MRR depended on the size of the electrode. In [7], the researcher introduced a micro-EDM electrothermal system to simulate the crater forming. This model integrates machining conditions such as heat flux, temperature-dependent thermal properties, and plasma radius, the heat transfer equation and its calculations of the produced crater are used to assess the fraction of energy distribution to the electrodes, results show a good agreement with experimental results. The parameters that affect the performance output (MRR) of the workpiece, parameters were chosen for optimization are a T-on, T-off followed by the current to examine the impact of the process inputs on the MRR. For AISI D2 die steel, brass is the used electrode material [8].

In [9], authors implemented an approach to assess the MRR in the EDM process. In this study, a finite element model was used to simulate and investigate the process parameters and their impact on outputs such as MRR of die steel. The optimal process inputs combination at the machining of alumina using the electrochemical machining process is investigated [10], the main input parameters are electrolyte concentration, voltage and feed rate, machining performance are MRR and TWR, graphite was used as electrode material.

In [11], authors presented a study to investigate the overcut and taper angles in the machining of stainless steel 304, parameters were current, T-on and T-off. The experimentation is performed using the RSM method, the current was found to be the most significant factor affecting the overcut and the taper angle followed by T-on and T-off, as the current and T-on increase, the overcut and taper angle is increased, so as T-off increases, the two

responses decrease, the optimized parameters that give the minimum overcut and taper angle response are 9 A current, 30 μ s Pulse on time and 35 μ s Pulse off time which gives 0.010 mm overcut and 0.244° taper angle. Grey relational analysis for Dry Electrical Discharge Machining is used in [12], to investigate and optimize the process parameters T-on, T-off, current, and voltage on the SR using the deionized water and air as a dielectric liquid for workpiece EN-8. ANOVA was performed to find the significant parameters on responses, found that current and T-on were the most significant input parameters.

It is clear from previous studies, manufacturers and researches relied on the use of non-traditional manufacturing methods like (EDM) instead of traditional methods like turning and milling when manufacturing the metals and alloys with high hardness such as the study task material, that could not be machined in traditional ways because the hardness of the workpiece is higher than the hardness and rigidity of the machine and cutting tool.

The main contribution of this study introducing an integrated approach combines both the Box-Behnken design and modeling method and the Genetic Algorithm as an optimization methodology that can be an effective design and optimization tool. And to investigate the influence of electrode materials (Silver-Tungsten) and pulse cycle time as a new input parameter on the EDM responses during machining of powdered metallurgical high-speed steel alloy.

2. Materials, Experimental Procedure and Data Setup

This part consists of the experimental setup, selection of workpiece, equipment and tool materials, design and optimization experimental methodologies.

2.1 Machine

All experiments were carried out on the EDM machine model (CHARMILLES Roboform 40). The machine is complete with programming. It features a PC-based CNC control with an LCD screen for faster data processing and servo control. Figure 1 shows the used EDM machine.



Figure 1: EDM machine

2.2 Workpiece Material

The task material in this study is Powdered Metallurgical High-Speed Steel Alloy, the nearest equivalent material is (AISI

M3-2). It is a very important material in the industry; it has not been investigated in the previous literature. Table 1 displays chemical compositions of the material [16], figure 3 shows a sample of material applications.

The chemical compositions as following:

Table 1: Chemical composition of the workpiece material

C	Cr	Mo	W	V
1.30	4.00	5.00	6.50	3.00

Material Properties: Hardness (187.6 HV), Density (0.008166 g/mm³). The shape of the workpiece is a plate, its width 40 mm, length of 60 mm and depth 10mm, required to machine a hole with 20mm diameter, and with 2mm depth. Figure 2 shows the shape and dimensions of the workpiece.

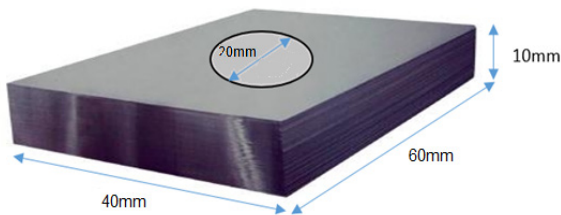


Figure 2: Dimensions of workpiece Material

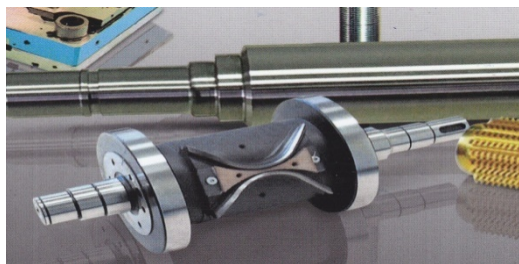


Figure 3: Sample of the workpiece material

2.3 Electrodes

The electrode material used is silver-tungsten, had 100 mm long, diameter 20.70mm. Silver tungsten is strong, capable of penetrating the toughest materials, and machinable. Silver has great conductivity at high temperatures and pressures. Figure 4 shows the electrode shape. Table 2 shows the Physical and Mechanical Properties of Silver - Tungsten electrode [17].



Figure 4: Shape of the electrodes

Table 2: Physical and mechanical properties of silver-tungsten electrode material

Nominal Composition (% Weight)	Density (g/cm ³)	Electrical Resistivity (20°C, μΩ•cm) ≤	Electrical Conductivity (IACS%, ≥)	Hardness (HB, ≥) Kgf/mm ²	Bending Strength (MPa)
25 Silver 75Tungsten	15.40	4.2	41	165	686

2.4 The 3D Laser Microscope Instrument

The 3D Laser Scanning Microscope was utilized for measuring Micro-Cracks size and taking the topography images. The magnification used in this inspection was 1000X. Figure 5 shows the 3D Measuring Laser Microscope. Due to huge temperature in the EDM process, and rapid heating and quenching, surface defects are created on the workpiece such as cracks, recast layer, surface roughness, and craters, in this study Micro- Cracks Size will be investigated. 3D Laser Microscope was used to measure the surface response in units of a micrometer, with a magnification of 1000.

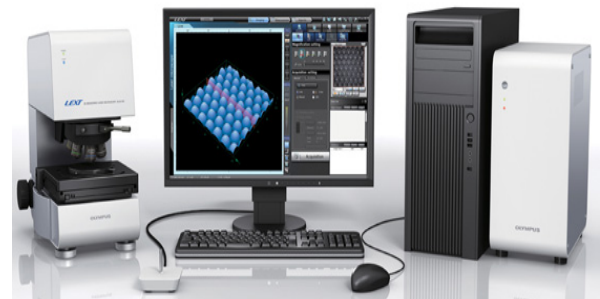


Figure 5: The 3D Laser Microscope device

2.5 EDM Process Responses and surface responses

Industries like automotive and aerospace have used the EDM process to produce products. "The aerospace industry used the EDM process to manufacture some aircraft parts because of the intricate shapes, tough alloys, and very tight tolerances involved, but it also recognized the dangers of the damaged surfaces and product defects resulting from the process" [13]. The process responses will be investigated and optimize in this research were: Tool Wear Rate and Micro-Crack Size.

Tool Wear Rate (TWR):

The wear rate of the electrode was determined using the formula:

$$TWR \text{ (g /min)} = \frac{Eb - Ea \text{ (g)}}{MT \text{ (min)}} \quad (1)$$

Where (Eb) and (Ea) are the weights of electrode material before and after machining, respectively, and MT is the machining time.

2.6 Experimental Setup

In this study Box-Behnken Experimental design Methodology was used to design the EDM process for Powdered

Metallurgical High-Speed Steel Alloy, L30 Orthogonal Array (OA) is designed, with (3) center points. Machining parameters are three continuous factors: Pulses cycle time (Tc), also it is called (U) as shown in Figure 6 [14]. Dielectric Fluid Flushing Pressure (P), and Voltage (V), one category factor: (the type of electrode material). Table 3 displays the input parameters and their values.

Fixed parameters: current 6A, Pulse width 200 μs, the polarity of the electrode is positive. Dielectric hydrocarbon fluid with a density of 0,783 g / ml and a flashpoint of 125 °C is used. Flushing method: the dielectric fluid was injected through side pipe novels providing adequate flushing to remove the eroded particles away from the working gap.

Table 3: Machining parameters and their levels

Parameters	Symbol	Levels			Unit
		1	2	3	
Period of machining (Pulses cycle time)	Tc	0.1	6.4	12.8	Sec
Dielectric fluid Flushing pressure	P	5	15	25	Psi
Machining voltage	V	120	160	200	V
Electrode material	Ag-W Silver-Tungsten				

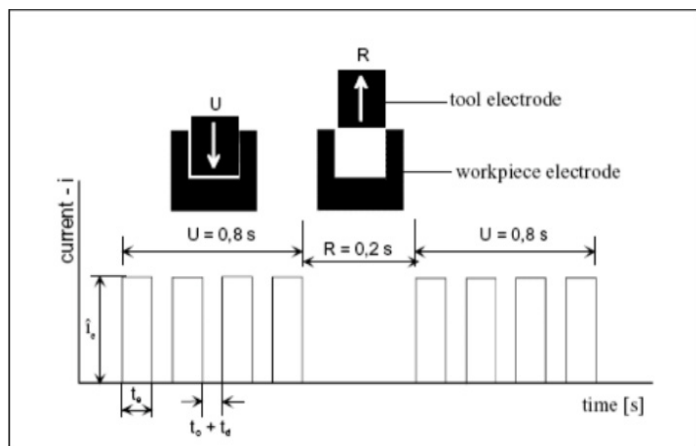


Figure 6: Series of pulses cycle time Tc, (U)

2.7 Genetic Algorithms Optimization Tool (GA)

“Genetic Algorithms, GA contains a chromosome, set of population, fitness function, mutation and selection, it begins with a set of solutions represented by chromosomes, called population, solutions from one population are taken and used to form a new population, which is motivated by the possibility that the new population will be better than the old one, further, solutions are selected according to their fitness to form new solutions, this process is repeated until some condition is satisfied. Algorithmically, the basic of GA is contains the following actions, start, fitness, new population, replace, test, and loop” [15].

Figure 7 shows the flowchart of the Genetic Algorithm optimization methodology.

In this research the models developed by (Box – Behnken) design methodology will be used as an objective function, the upper and lower bounds of parameters are identified in the GA optimization technique as below. The aim was to minimize the Response value.

Minimize $f(x) = \text{Response}$

Responses to be as minimum as better

Subjected to,

$120 \leq V \leq 200$;

$0.1 \leq Tc \leq 12.8$;

$5 \leq P \leq 25$.

GA Toolbox of MATLAB software is used. All the previous steps of the Genetic Algorithm will be done using Matlab software, after achieving and building the models of all the responses from the (Box – Behnken) optimization methodology to be used as objective function equations, all results obtained from the runs are presented in the following chapters.

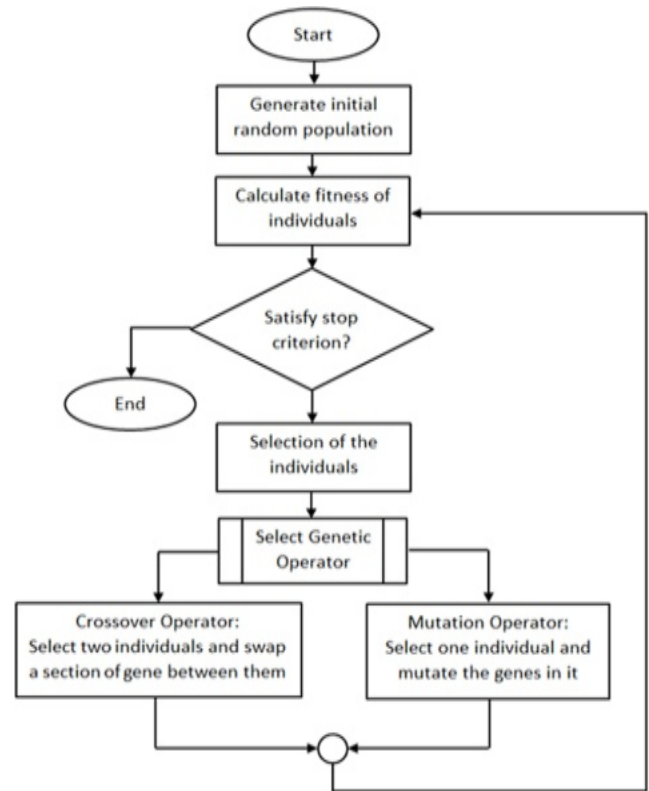


Figure 7: Flowchart diagram of Genetic Algorithm optimization methodology

3. Results and Analysis

In this section, the results obtained from the running of Minitab design software and Matlab GA optimization software are discussed for each response variable, tool wear, micro crack size. Then a regression analysis was conducted to find the best-fit models. The main effects and interaction effects were discussed. Table 4 shows the Experimental results.

Table 4: Experimental Results

Run Order	V Volt	Tc Sec	P	TWR g/min	Micro-crack size μm
1	160	0.10	5	0.0059	1.344
2	120	6.45	25	0.0071	2.363
3	120	6.45	5	0.0088	1.688
4	160	6.45	15	0.0091	1.905
5	160	12.8	25	0.0142	2.026
6	160	12.8	5	0.0087	1.608
7	160	6.45	15	0.0090	1.817
8	160	0.10	25	0.0023	1.350
9	120	12.8	15	0.0093	1.721
10	200	6.45	5	0.0083	2.001
11	200	12.8	15	0.0175	2.157
12	120	0.10	15	0.0033	1.905
13	200	0.10	15	0.0047	1.216
14	160	6.45	15	0.0085	1.616
15	200	6.45	25	0.0122	1.794

The Minitab17 software package was used to estimate the models of the data obtained from the experiments. Figures 8-23 Show the 2D plots, to analyze the main effect and the mutual interactions between the input machining parameters (V, Tc, P, and electrode material) on the responses. The ANOVA analysis is shown in tables 5 - 6. In this analysis, all parameters with a p-value of less than 0.05 are significant.

Table 5: Analysis of Variance of TWR

Source	DF	Adj SS	Adj MS	F-Value	P-Value
Model	6	0.000208	0.000035	29.40	0.000
Linear	3	0.000168	0.000056	47.44	0.000
V	1	0.000025	0.000025	21.41	0.002
Tc	1	0.000140	0.000140	119.14	0.000
P	1	0.000002	0.000002	1.78	0.218
2-Way Interaction	3	0.000040	0.000013	11.35	0.003
V*Tc	1	0.000012	0.000012	9.82	0.014
V*P	1	0.000008	0.000008	6.66	0.033
Tc*P	1	0.000021	0.000021	17.58	0.003
Error	8	0.000009	0.000001		
Lack-of-Fit	6	0.000009	0.000002	14.86	0.064
Pure Error	2	0.000000	0.000000		
Total	14	0.000217			
S	R-sq	R-sq(adj)	R-sq(pred)		
0.0010851	95.66%	92.41%	77.72%		

3.1 Effect of Process Parameters on Tool Wear Rate TWR

Statistical inferences:

1. The model is significant, as seen p-value is 0.000, that is meant the model is significant and adequate.
2. Lack of Fit is 0.064, it is not significant.
3. The "R-Squared" of 95.66%, "Pred R-Squared" of 77.72 %, the "Adj R-Squared" of 92.41%, indicates an adequate signal.
4. Values of "Prob. less than 0.05" indicate model terms are significant. In this case, V, Tc, (Tc*P), (V*P), and (V*Tc) are significant model terms.

Equation model of TWR:

$$TWR = 0.01524 - 0.000051 V - 0.000949 Tc - 0.000740 P + 0.000007 V*Tc + 0.000004 V*P + 0.000036 Tc*P$$

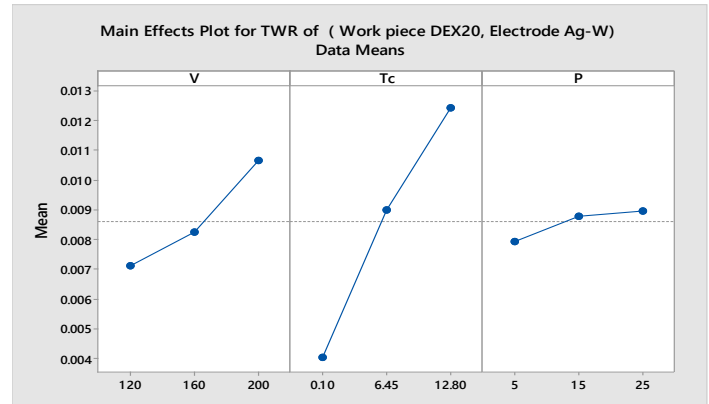


Figure 8: Main effects plot for TWR

The main effects: Figure 8 displays the main effects plot for TWR. As the voltage increased as TWR increased. Increasing pulse cycle time resulted in increasing of TWR, the minimum value in TWR was at 0.10s. Dielectric liquid pressure is increased as TWR stays almost no change, no significant effect.

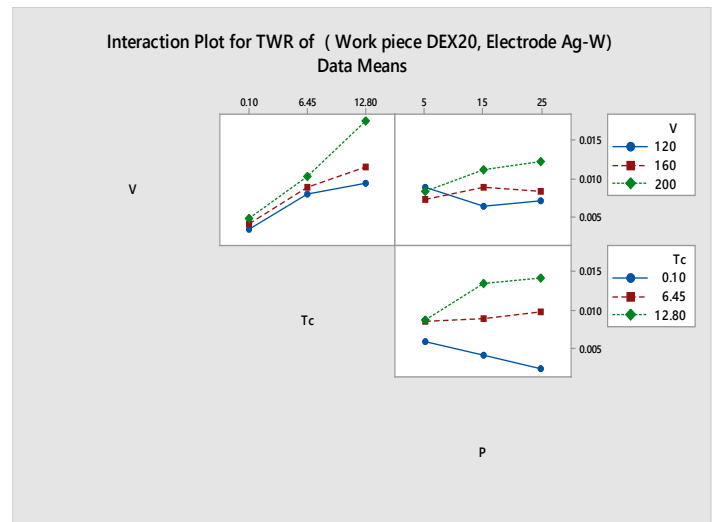


Figure 9: Interaction effects plot for TWR

The interaction effect: Figure 9 displays the interaction effects plots for TWR. Based on the ANOVA table, the p-value of all interactions (Tc*P), (V*P), (V*Tc) was less than 0.05. Therefore, the interaction effects were significant.

3.2 Effect of process parameters on Micro-crack Size

Statistical inferences:

1. P-value of the model is 0.004, so it is significant and adequate.
2. The "R-Squared" of 90.22%, "Pred R-Squared" of 87.74 %, the "Adj R-Squared" of 96.51%. This model can be used to navigate the design space and indicates an adequate signal.
3. Tc, P, (V*V), (Tc*Tc), (V*Tc), and (V*P) are significant terms.

Regression Equation of Micro-C racks:

$$\begin{aligned} \text{M-Crack Size} = & 4.232 - 0.0355 V - 0.1027 Tc + 0.0867 P \\ & + 0.000109 V*V - 0.00507 Tc*Tc + 0.000072 P*P \\ & + 0.001107 V*Tc - 0.000551 V*P + 0.001622 Tc*P \end{aligned}$$

Table 6: Analysis of variance for Micro-crack size

Source	DF	Adj SS	Adj MS	F-Value	P-Value
Model	9	1.33501	0.148334	15.35	0.004
Linear	3	0.49182	0.163940	16.96	0.005
V	1	0.03239	0.032385	3.35	0.127
Tc	1	0.35998	0.359976	37.25	0.002
P	1	0.09946	0.099458	10.29	0.024
Square	3	0.28987	0.096622	10.00	0.015
V*V	1	0.11302	0.113023	11.70	0.019
Tc*Tc	1	0.15448	0.154476	15.99	0.010
P*P	1	0.00019	0.000192	0.02	0.893
2-Way Interaction	3	0.55332	0.184441	19.09	0.004
V*Tc	1	0.31641	0.316406	32.74	0.002
V*P	1	0.19448	0.194481	20.13	0.006
Tc*P	1	0.04244	0.042436	4.39	0.090
Error	5	0.04832	0.009664		
Lack-of-Fit	3	0.00443	0.001476	0.07	0.972
Pure Error	2	0.04389	0.021944		
Total	14	1.38333			
S	R-sq	R-sq(adj)	R-sq(pred)		
0.0983035	96.51%	90.22%	87.74%		

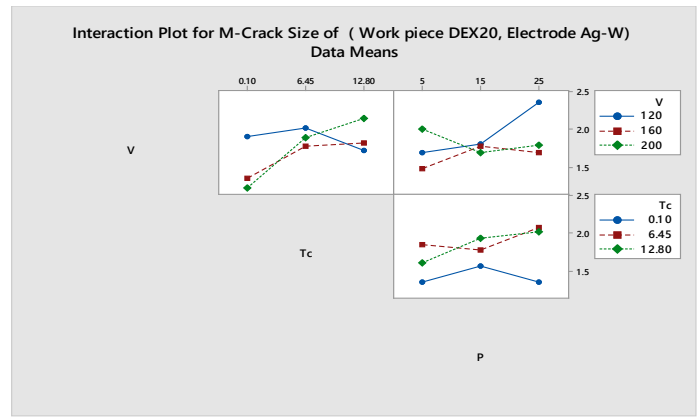


Figure 11: Interaction effects plot for Micro-Crack Size,

3.3 Topography Images using 3D Laser Microscope

The following image depicted how surface responses changed by the process parameters and electrode types. Figure 12 shows the best results for the surface defects got from performing experiments. The micrograph of EDMed surfaces with the high magnification (1000×), for the machining parameter combination V/Tc/P of 200v/0.1s/15psi is shown in figure 12. These machining combinations produced minimum Micro-crack width 1.216µm.

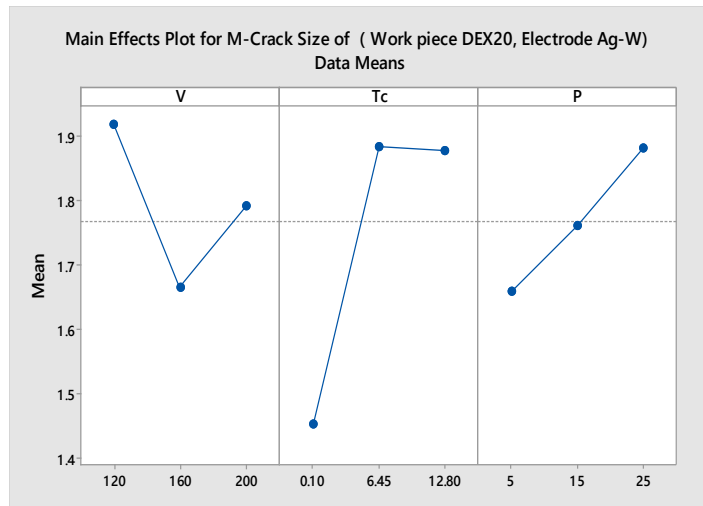


Figure 10: Main effects plot for Micro-Crack Size

The main effects: based on the plot in figure 10, the Micro-crack size decreased when the voltage increased until 160v then it increases. And at the pulse cycle time increasing resulted in increasing of Micro-crack size until 6.45s then it decreases slightly. Dielectric liquid pressure increased as the Micro-crack size increased. The minimum value was at P 5psi, Tc 12.8s, and V 160v.

The significant interaction effect was only between voltage and pulse cycle time (V*Tc), and between voltage and liquid pressure (V*P), from the analysis table, the p-value of this interaction effect was less than 0.05 Therefore, this interaction effect was significant.

www.astesj.com

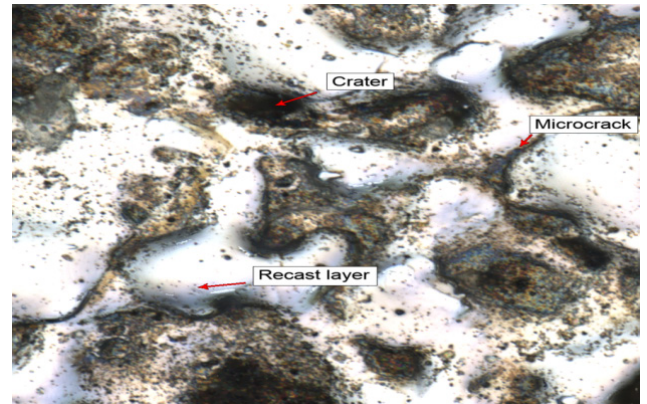


Figure 12: Minimum Micro-crack size 1.216µm, at V=200v, Tc=0.1Sec, P= 15psi

4. Responses Optimization using Genetic Algorithm methodology

The equations developed from the Response surface design in the last section will be used as objective functions in the Genetic Algorithm optimization, the target of these responses will be minimized.

Subjected to,
 $120 \leq V \leq 200;$
 $0.1 \leq Tc \leq 12.8;$
 $5 \leq P \leq 25;$
 Tool Material = Ag-W.

The equation variables and the input parameters are changed to the coding system that accepted in the Genetic Algorithm Tool.
 Response = f(x)

V=X1, Tc=X2, P=X3, Responses=f(x), Maximum and minimum boundary conditions are [120, 0.1, 5] and [200, 12.8, 25]. Tables 7-8 and Figures 13-14 show the optimization results.

4.1 Optimization of Tool Wear Rate TWR using Genetic Algorithm

Response surface equation:

$$TWR = 0.01524 - 0.000051 V - 0.000949 Tc - 0.000740 P + 0.000007 V*Tc + 0.000004 V*P + 0.000036 Tc*P$$

Coding equation (minimization):

$$f(x) = 0.01524 - 0.000051*x(1) - 0.000949*x(2) - 0.000740*x(3) + 0.000007*(x(1)*x(2)) + 0.000004*(x(1)*x(3)) + 0.000036*(x(2)*x(3));$$

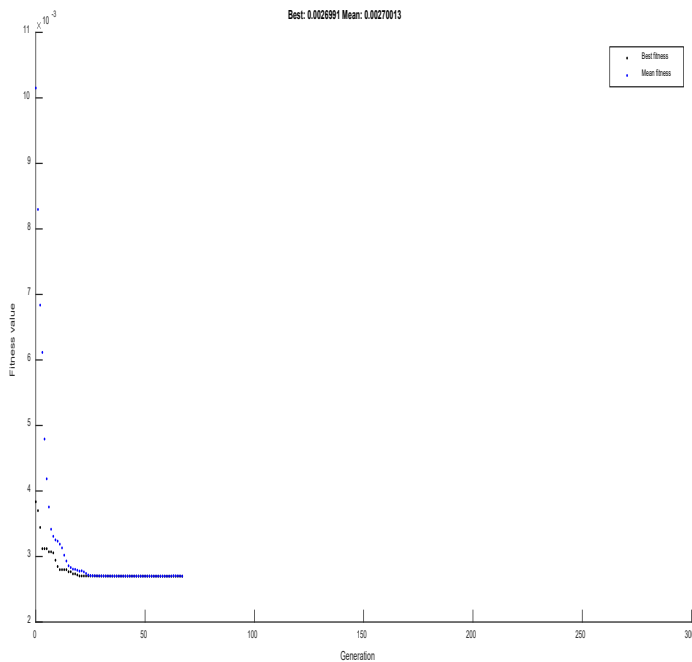


Figure 13: Plots of fitness value with the number of generations of TWR

Table 7: The optimum values of process parameters and optimized value of Tool Wear Rate

Response	Optimize the value of input parameters			Value g/mm	Iteration Number
	V	Tc	P		
TWR	120	0.1	25	Objective function value: 0.002699	67

4.2 Optimization of Micro-Crack Size using Genetic Algorithm

Response surface equation:

$$M\text{-Crack Size} = 4.232 - 0.0355 V - 0.1027 Tc + 0.0867 P + 0.000109 V*V - 0.00507 Tc*Tc + 0.000072 P*P + 0.001107 V*Tc - 0.000551 V*P + 0.001622 Tc*P$$

Coding equation (minimization):

$$f(x) = 4.232 - 0.0355*x(1) - 0.1027*x(2) + 0.0867*x(3) + 0.000109*(x(1)^2) - 0.00507*(x(2)^2) + 0.000072*(x(3)^2) + 0.001107*(x(1)*x(2)) - 0.000551*(x(1)*x(3)) + 0.001622*(x(2)*x(3));$$

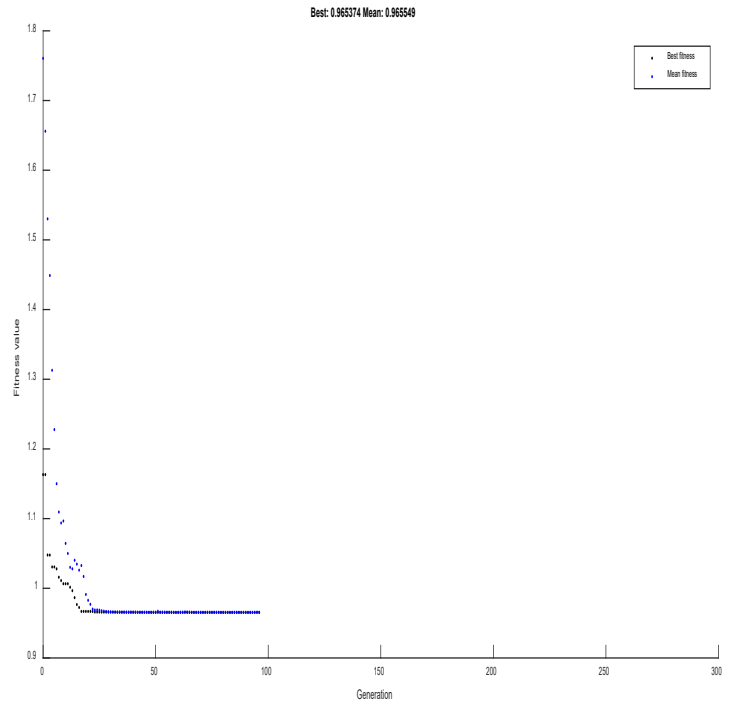


Figure 14: Plots of fitness value with the number of generations of Micro-Crack Size

Table 8: The optimum values of process parameters and the optimized value of Micro-Crack

Response	Optimize the value of input parameters			Value μm	Iteration Number
	V	Tc	P		
M-Crack Width	200	0.1	25	Objective function value: 0.965	96

5. Conclusion

This research demonstrated very good results of the modeling and optimization of TWR, and Micro Crack size for the material Powdered Metallurgical High-Speed Steel Alloy during the EDM process using Box Behnken Design Method with Genetic Algorithm optimization methodology to increase the optimization percentage. The results of using Silver – Tungsten electrode were very good and showed that it has an important impact on the output values, this leads to thinking about not relying on the use of copper electrode only as is clear from the previous studies. This research contributed to highlighting the importance of using genetic algorithms as a method to improve the outputs of the EDM process. Also contributed to study and investigate a new input parameter called Pulses Cycles Time Tc, that it has not been studied previously, results demonstrated it has an effective effect on improving the outputs of the manufacturing process

The summary of optimal results of TWR and Micro Crack Size for EDMing of the material Powdered Metallurgical High-Speed Steel Alloy using Silver-Tungsten electrode to be as follows:

- For Tool Wear Rate TWR: Tc and V are significant parameters. P is not significant. The model is significant, where is R², 95.66% and Lack of Fit 0.064. Minimum Value of TWR as predicted from experiments was 0.0023 g/min. Optimized value using Genetic Algorithm is 0.0020 g/min, if the applied machining conditions are: V=120v, Tc=0.1s, P= 25psi, optimization percentage using GA is 13.04 %.
- For Micro-crack size: Tc is the most significant parameter by then P. V is not significant, the model is significant where R² 96.51% and Lack of Fit 0.972. The minimum Value of Micro-crack size as predicted from experiments was 1.216 μm. Optimized value using Genetic Algorithms was 0.965 μm when the applied machining conditions are: V=200v, Tc=0.1s, P= 25psi, optimization percentage using GA is 20.64%.

These findings will enable EDM researchers and manufacturing engineers to select the correct parameters for Powdered Metallurgical High-Speed Steel material EDMing. The models and the data in this work are expected to become a powerful tool in the hands of EDM researchers to extend the system understanding, and also to improve the process performance.

Conflicts of Interest

The authors declare no conflict of interest.

References

- [1] J. Y. Kao, C. C. Tsao, S. S. Wang, and C. Y. Hsu. Optimization of the EDM parameters on machining Ti-6Al-4V with multiple quality characteristics. *Int. J. Adv. Manuf. Technol.*, 2010.
- [2] M. Gostimirovic, P. Kovac, M. Sekulic, and B. Skoric. Influence of discharge energy on machining characteristics in EDM. *J. Mech. Sci. Technol.*, 2012.
- [3] S. Raghuraman, K. Thirupathi, T. Panneerselvam, and S. Santosh. Optimization of Edm Parameters Using Taguchi Method and Grey Relational Analysis for Mild Steel Is 2026. *Int. J. Innov. Res. Sci. Eng. Technol.*, 2(7): 3095–3104, 2013.
- [4] S. B. Chikalthankar, V. M. Nandedkar, and S. V Borde. Experimental Investigations of EDM Parameters, 7(5): 31–34, 2013.
- [5] D. M. Madyira and E. T. Akinlabi. Effects of Wire Electrical Discharge Machining on Fracture Toughness of Grade 5 Titanium Alloy. *Int. J. Mech. Prod. Engineering*, 2: 1–5, 2014.
- [6] D. Hanaoka, Y. Fukuzawa, Y. Kaneko, and T. Harada. Discharge Machining of Insulating Si₃N₄ Ceramics with added Al₂O₃. *Int. J. Electr. Mach.* 19: 45–50, 2014.
- [7] B. Shao and K. P. Rajurkar. Modeling of the crater formation in micro-EDM. In *Procedia CIRP*, 2015.
- [8] J. Jeykrishnan, B. Vijaya Ramnath, A. Jude Felix, C. Rupan Pernesh, and S. Kalaiyaran. Parameter optimization of electro-discharge machining (EDM) in AISI d2 die steel using Taguchi technique. *Indian J. Sci. Technol.*, 9(4), 2016.
- [9] A. Gosavi and A. B. Gaikwad. Predicting Optimized EDM Machining Parameter through Thermo Mechanical Analysis. *IOSR J. Mech. Civ. Eng.*, 13(3): 2320–334, 2016.
- [10] M. Goud, A. K. Sharma, and S. Zafar. A Taguchi approach to optimize electrochemical discharge machining of alumina, 2016.
- [11] E. A. H. Hanash. Investigation of the Effect of Edm Parameters on Dimensional Accuracy of Drilled Holes of 304 Stainless Steel Using Rsm Method By International Islamic University. *Int. Islam. Univ. MALAYSIA*, 2017.
- [12] N. Singh Khundrakpam, G. Singh Brar, and D. Deepak. Grey-Taguchi Optimization of Near Dry EDM Process Parameters on the Surface Roughness. In *Materials Today: Proceedings*, 5(2): 4445–4451, 2018.
- [13] Aerospace Manufacturing, EDM for Aerospace, Aerospace Production, Radical Departures. Retrieved from <https://www.radical-departures.net/articles/advances-in-edm-for-aerospace>, 2019.
- [14] I. A. Amorim, F.L.; Schäfer, G.; Stedile, L.J.; Bassani. On the Behavior of Parameters and Copper -Tungsten Electrode Edge Radius Wear When Finishing Sinking EDM of Tool, 35, 2010.
- [15] M. N. Ab Wahab, S. Nefti-Meziani, and A. Atyabi. A comprehensive review of swarm optimization algorithms. *PLoS One*, 10(5): 1–36, 2015.
- [16] Special steel and Alliance. Retrieved from <http://www.specialsteel.com.my/page.php?page=powder>, (2019)
- [17] Stanford Materials Corporation. Retrieved from: <http://www.stanfordmaterials.com/Tungsten-copper.html>, (2019)

Prediction of Demersal Fishing Ground Associated with Coral Reefs in the Coastal Jepara Regency, Central Java, Indonesia Based on Sentinel 2a Imagery

Kunarso^{*1,2}, Muhammad Zainuri^{1,2}, Denny Nugroho Sugianto^{1,2}, Jarot Marwoto¹, Hariyadi¹, Muslim¹

¹*Department of Oceanography, Faculty of Fisheries and Marine Science, Diponegoro University, Semarang, Indonesia, Prof. Soedarto, SH Street, Tembalang Phn./Fax. (021) 7474698 Semarang 50275*

²*Center for Coastal Rehabilitation and Disaster Mitigation Studies (CoREM), Diponegoro University, Center of Excellence Science and Technology (PUI), Indonesia*

ARTICLE INFO

Article history:

Received: 11 September, 2019

Accepted: 22 November, 2019

Online: 05 December, 2019

Keywords:

Fishing Ground

Demersal

Sentinel 2a

Jepara

ABSTRACT

Map of prediction of fishing ground that already exists in Indonesia issued by the Bali Marine Research and Observation Center (BPOL) and the National Aeronautics and Space Agency (LAPAN) of Jakarta, there are still many weaknesses including the spatial aspect of the point of forecasting far from the coast and the unclear type of fish predicted. The lack of understanding of the type of fish predicted, the risk of fishermen carrying the wrong fishing gear so that when reaching the forecasting location, fishermen can not catch fish that are abundant. The method of determining fishing ground for demersal fisheries is carried out in three stages, first step, environmental tabulation of demersal fisheries, the second stage of mapping corals area and its supporting parameters, the third stage of mapping the demersal fishing ground. The results of the study obtained several statements, namely demersal fishing ground can be made based on an understanding of childhood fish habitat, adulthood, substrate base habitat, an optimum depth of catchment area. Sentinel 2A satellite imagery can be used to help determine the fishing ground of demersal fish species, but for the coastal waters of Jepara Regency, there are still obstacles related to spatial resolution and water turbidity. Field data is still needed to help determine the demersal fishing ground. Based on the fishing ground mapping, there are four economical types of fishery resources that live in the coral reef environment, namely Lobster, Red Snappers, Blue Line Seabass and Leopard Coral Grouper. The demersal fishing ground associated with corals in the Coastal Jepara Regency Waters which is seven segments apparently only four segments have the potential to become demersal fishing ground associated with coral reefs, namely the second to fourth segments, including the coastal waters of Jepara, Mlonggo, Bangsri, and Kembang. District and the most potential is the coastal waters of the Mlonggo District.

1. Introduction

Catching systems in Coastal Jepara District are generally still traditional because without the help of high technology, only based on experience or feeling alone. Although the fishing gear used is quite advanced, but the departure to the sea has a very high gambling rate and tends to remain like the catchment area of the previous year. The increasing number of boats, making a fishing ground congested with fishing effort so that the results catch per

boat tends to fall from year to year [1]. Fishermen's lack of understanding the temporally and spatially changing of fishing ground due to changes in oceanographic conditions makes fishing more difficult, time and costly-consuming, but the results are less than optimal.

In Indonesia, there are already institutions that make fishing ground predictions, namely BPOL (Research and Marine Observation Center) in Perancak Bali and LAPAN (National Aeronautics and Space Institute), but their utilization of fishing ground prediction is not optimal, because there are still many

*Kunarso, et al., Oceanography Department, Diponegoro University, +6285875762162 . kunarsojpr@yahoo.com

weaknesses that need to be fixed. These weaknesses include locations plotted as potential catchment areas generally in offshore areas so that small fishermen cannot take advantage, forecasting in the form of spots so they do not represent the area, besides that there is no specification of fish species, whether for demersal or pelagic fish species. Different types of fish require different habitat locations and different fishing technologies. Another weakness is the basic data used for forecasting is especially based on two parameters, namely chlorophyll-a (fertility indicator) and sea surface temperature from MODIS imagery, this is certainly not suitable if for forecasting demersal fish [1]

Demersal fisheries types from fishes, crustaceans or mollusks are generally associated with vital habitats in the form of corals, seagrasses and mangroves [2]. Types of demersal fisheries that are associated with coral on the coast of Jepara, for example, lobsters, red snapper, coral grouper and tiger grouper [3]. A good understanding of the location of coral reefs can help identify the demersal fishing ground associated with coral. Sentinel 2 satellite imagery has proven to be very satisfying to be used to identify and monitor coral reefs in coastal waters [4,5] The purpose of this research is to make an innovation in determining the fishing ground for demersal fisheries associated with coral reefs on the coast based on data from sentinel 2 satellite imagery, corals field data, and bathymetry data. Research Location in the coastal waters of Jepara Regency, Central Java Indonesia (Figure 1).

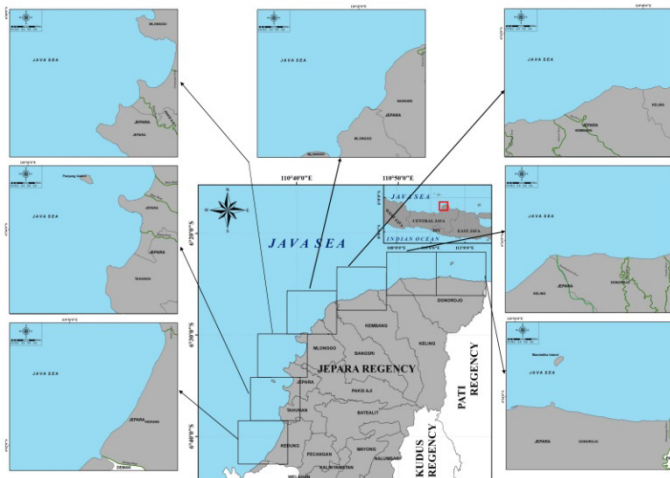


Figure 1: Research Location in the Coastal of Jepara Regency Waters

2. Materials and Methods

2.1. Research Material

The material used in this study includes main data and supporting data. The main data used consists of vital habitat distribution data, namely the distribution of coral reefs, estuarine locations, besides oceanographic parameter data, including bathymetry, total suspended solids (TSS), and bottom substrate. Supporting data include Jepara Regency marine environment map data and demersal fish bioecology data. The data of corals and TSS

(Total Suspended Solid) were obtained from sentinel-2 satellite image data processing. The coral's distribution data supplemented with field survey data. Bathymetry data from the Navy Hydro-oceanography Center (PUSHIDROSAL).

2.2. Research Methods

The method used in this study is a descriptive method that seeks to describe the coral's distribution and oceanographic conditions especially TSS that support the life of demersal fish. Furthermore, describe the optimum bioecological factors for demersal fish. The corals, TSS, and the estuary locations are used for delineation (determination) of demersal fish potential prediction in the waters of Jepara Regency.

- *Method of Collecting Data*

The Distribution data of coral reefs from Sentinel-2 Imagery, besides corals data, TSS data were also obtained from Sentinel 2 this has been done by researchers [6,7], corals data from field also be surveyed by acoustic check, and estuarine location information used in this study. The Sentinel satellite data was obtained from the web site www.earthexplorer.usgs.gov. The spacial resolution of sentinel image data of 10 m. The water depth data obtaining from earthexplorer.usgs.gov

- *Data analysis and Processing*

- a. Sentinel-2 Satellite Image Data

The Sentinel-2 image processing is carried out in several stages, including image correction and processing and using the lyzenga algorithm to determine the extent of corals. The image used in this study is sentinel-2 which has a cloud cover of less than 10% so that the sea and land look well. Sentinel-2 imagery has 12 bands, in which there are green, blue and NIR channels with various spatial resolutions (10m, 20m, 60m). The required channel in the lyzenga algorithm has been fulfilled.

The first stage of sentinel image processing is geometry correction, this correction is done in the global mapper software and aims to bring up coordinates in the image. The second step is radiometry correction, this correction is done in software mapper and aims to eliminate disturbances when recording images. The third stage is determining the extent of corals using the lyzenga algorithm.

The lyzenga algorithm used [8, 5]

$$Y = \ln(L_i) - \left[\left(\frac{k_i}{k_j} \right) x \ln(L_j) \right] \quad (1)$$

Where:

L_i = blue channel reflectant value

L_j = the reflectance value of the green channel

k_i/k_j = ratio of attenuation coefficients of blue and green channels

Equation (1) is used for the extraction of water bottom information (Y). That requires two image spectral channels and k_i / k_j ratio which is the attenuation coefficient ratio between the two channels, in this case, the blue channel and the green channel. This algorithm calculation is influenced by channel pairs i (blue channel) and j (green channel) used. The wavelength of the channel used will affect how deep the channel can detect the

bottom of the water. Blue canals and green canals have the best penetration wavelengths among other channels [5].

The attenuation coefficient (k_i / k_j) is calculated by the equation:

$$\frac{k_i}{k_j} = a + \sqrt{a^2 + 1} \quad (2)$$

The value of a is determined by the equation:

$$a = \frac{\sigma_{ii} + \sigma_{jj}}{2\sigma_{ij}} \quad (3)$$

Where: σ_{ii} = channel variety or variant i
 σ_{jj} = channel variety or variant

b. Sentinel-2 Satellite Diagram of Method for Determination of Demersal Fishing Ground

The innovations to create a potential area for demersal fishing ground, carried out with the stages described in three flow diagrams.

- The first stage

The first stage is the environmental tabulation of demersal fisheries. This stage is carried out with reference studies and collecting catch data from the Jepara Regency area which will be predicted for its fishing ground area. This stage is carried out with a reference study from the Department of Maritime Affairs and Fisheries of Jepara Regency and a survey to the Fish Auction Site (TPI) in Jobokuto Jepara, about the types and amount of demersal fish catches. Then conducted to reference study about the bioecology of demersal fish available from various books and websites. The results of this reference study and survey are tabulated in the environmental table for demersal fisheries.

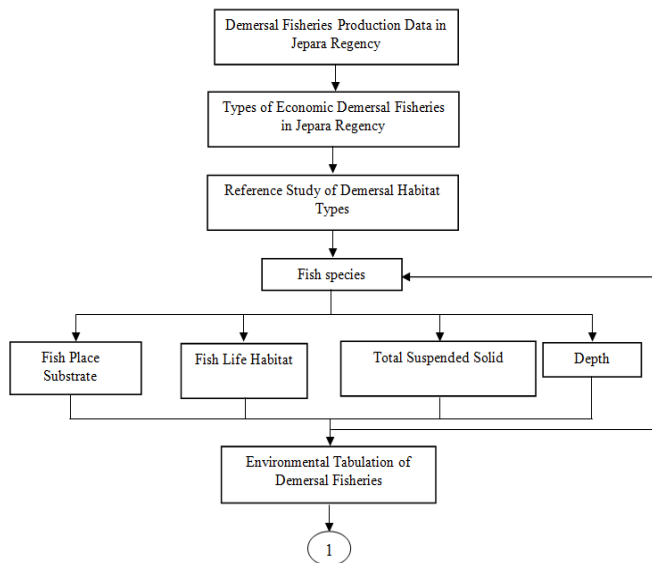


Figure 2: Flow chart of demersal fish environmental tabulation in Jepara Regency

- The second stage

The second stage is the mapping of vital habitat (coral reefs) and its supporting parameters. The second phase is done by downloading Sentinel-2 and bathymetry data, be supported by soft file data of the Jepara Regency environmental map. All data is processed to display the distribution of corals, water depth, TSS and location of river mouths.

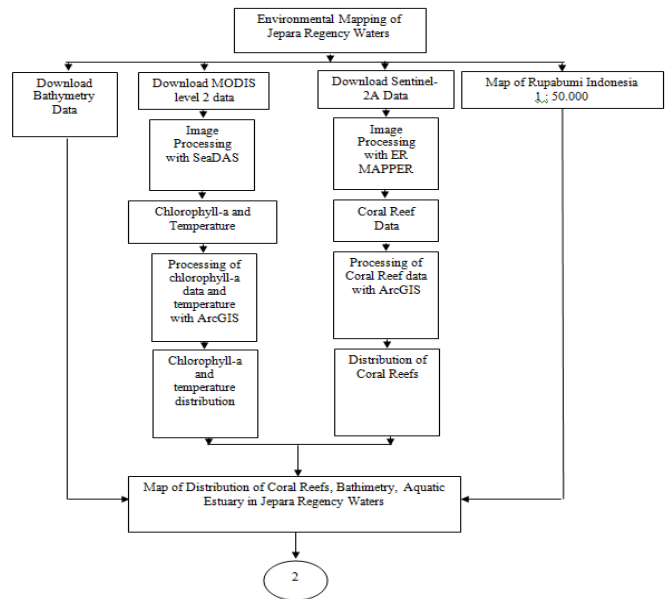


Figure 3: Flow chart of the distribution of vital habitat (coral, estuarine) and environmental conditions on the coast of Jepara Regency

- The third stage

The third stage is mapping the potential area of demersal fish. The third step is verification of field corals data and note the local name of the corals. All data both image data and field data are overlaid so formed maps of corals habitat distribution data and oceanographic factors, including bathymetry and TSS. Subsequently, an analysis was conducted to plot the potential catchment area of demersal fisheries (red snapper, coral grouper, sunu grouper, stingray, and lobster). Plotting of fish potential area based on the environmental

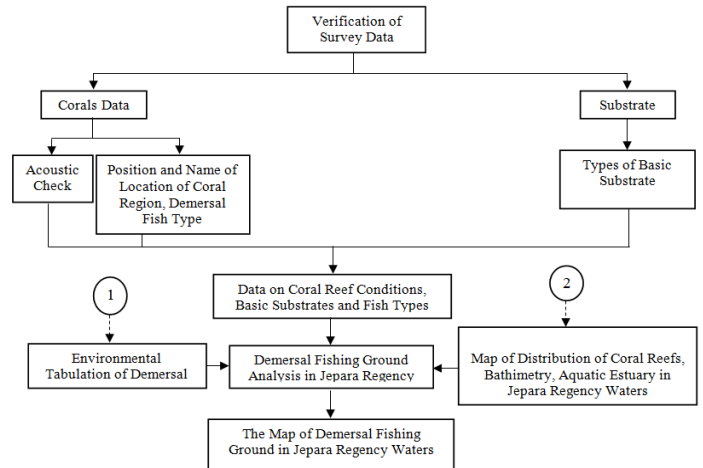


Figure 4: Flow chart prediction of demersal fishing ground mapping on the coast of Jepara Regency

3. Result and Discussion

3.1. The Economic Demersal Fish Species Associated with Corals in Jepara Coastal Waters

Based on the reference study and a survey at a fishing landing port in Jepara there are 10 economical demersal fish from Jepara Beach were found, namely Sea Catfishes, Red Snappers, Blue Line Seabass , Leopard Coral Grouper, Hairtails, Rays,

Lobster, White Shrimp, Rainbow Shrimp and Swimming Crabs (Figure 5). Based on the data there are only 4 types of economic demersal fisheries associated with corals were obtained from Jepara coastal waters, namely: Lobster, Red Snappers, Blue Line Seabass and Leopard Coral Grouper. Based on the environmental types of potential demersal fisheries in Jepara Regency Waters shown in Table 1, Lobster from childhood to adulthood live in a coral environment, a childhood in the bottom of sandy waters and an adult verada in the sidelines or hole of a coral [9]. Red Snappers and, Blue Line Seabass of his childhood life in beaches and river estuaries, but when it has begun to mature migrate to the rocky area [10]. Leopard Coral Grouper in childhood spawn and develop in seagrass areas, but when they mature they migrate to coral reef areas [10]. Demersal fisheries consisting of fish and crustaceans associated with corals are mature and foraging in coral areas. They are caught with fishing gear and traps in the coral reef area. However, when approaching spawning the corals fish migrate to the seagrass, muddy or sandy coastal areas.

Table 1: Environmental Conditions of Economical Demersal Fisheries Fish in Jepara Regency Table

N u m	Type of Habitat/ Associated fish types						
	Corralling Beach/ Rocky	Seagrass Beach	Mangrove Beach	Estuarine	Offshore	Substrate	Depth/ Optimum (meters)
1	Lobster (larvae-adults)					Corals-sand / mud- sand	<100/7-15
2			Sea Catfishes (larvae - young)	Sea Catfishes (adult)		mud	<100
3	Red Snappers (adult)			Red Snappers (larvae - young)		Mud mixed with coral fragments	<100/40-70
4	Blue Line Seabass (adult)			Blue Line Seabass (larvae - young)			<40
5	Leopard Coral Grouper (adult)	Leopard Coral Grouper (larvae-young)					<40/7-9
6				Hairtails (larvae)	Hairtails (adult)	mud	<2000/ 1-250
7	Rays			Rays		Sand-mud	<90/ <40

3.2. Prediction of Demersal Fishing Ground Associated with Corals in the Coastal Jepara Regency

Determination of demersal fishing ground is different from determining pelagic fishing ground. The fishing ground for demersal fish is closely related to the condition of its vital habitat, namely the location of corals, seagrasses, mangroves, and river mouths. Another limiting factor is the base substrate and the depth of the water. The dependence on these factors makes demersal

fishing groundfish such as Red Snapper, Blue Line Seabass, Leopard Coral Grouper, and Lobster likely to remain location. So that our understanding of the habitat location of the demersal fisheries, makes it easier to determine the prediction of its fishing ground.

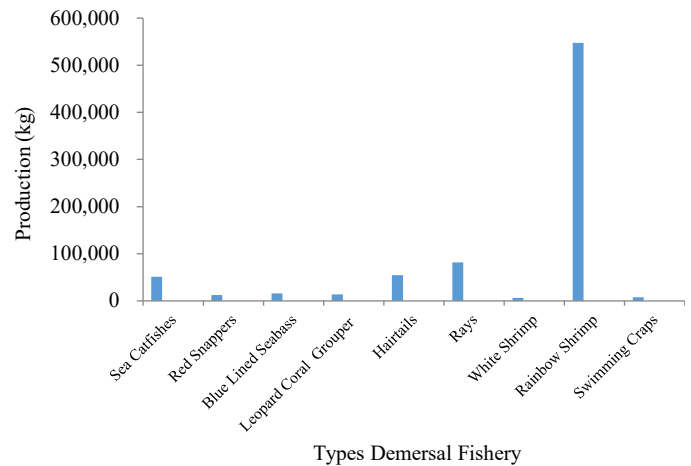


Figure 5. Demersal fisheries production in Jepara Regency (DKP Jepara, 2017)

Based on the results of the Sentinel-2 satellite image data processing and field survey, the Jepara Regency Coastal Area from West to East was divided into 7 segments (Figure 1), apparently only 4 segments contained coral reef habitats. The four segments are segment 2 namely the coastal waters of Tahunan and Jepara Districts (Figure 5), segment 3 namely the waters of the Districts of Jepara and Mlonggo (Figure 6), segment 4 namely the coastal waters of the Districts of Mlonggo and Bangri (Figure 7), and segment 5 which is the waters coast of Kembang and Keling Districts (Figure 8).

Three segments were not found coral reefs, that is in segment 1 namely Kedung District Coastal waters, segment 6 namely Keling and Donorojo District Coastal waters and segment 7 in the Donorojo District Coastal waters (Figure 1). Based on the field survey, the three segments that were not found in the coral reef had a substrate dominant with mud.

• Prediction of Demersal Fishing Ground in Segment 2

Segment 2, which covers the waters of the Tahunan District up to part of Jepara District based on Sentinel-2 satellite imagery and a field survey found 8 groups of coral reefs, with the local name and approximate area of Bokor Reef (5 ha), Teluk Awur Reef (12 ha), Tegal Sambi Reef (3 ha), Dalem Reef (3 ha), Pemandian Reef and Pulau Reef (66.4 ha), Panjang Island Reef (8 ha) and Sekumbu Reef (17.5 ha). Based on Sentinel-2 imagery, all clusters of reefs can be identified in terms of area and position, except for Bokor Reef only identified with field survey by snorkeling.

Seven other coral reef visible from Sentinel imagery are predicted as demersal fishing ground, especially type of fish Red Snappers, Blue Line Seabass and Leopard Coral Grouper, in green clusters (Figure 5). The highest potential demersal fishing ground

in terms of the extent of coral reef is predicted to be in the east coast region of Jepara District, which is along the location between Pemandian Reef and Sekumbu Reef.

and approximate area of Prawean Reef (17.5 ha), Kuniran Reef (38 ha), Dogo Reef (10 ha), Ujung Tumpuk Reef (14 ha), Sependok Reef (20 ha), Gunung Panas Reef (9 ha), Ujung Piring Reef (39 ha) and Prenitan Reef (9 ha) (Figure 6).

Six coral reef visible from Sentinel imagery are predicted as demersal fishing ground, especially type of Red Snappers, Blue Line Seabass and Leopard Coral Grouper, and lobster in green clusters (Figure 6). The Six coral reef are Prawean Reef, Kuniran Reef, Dogo Reef, Sependok Reef, Ujung Piring Reef, and Prenitan Reef. The highest potential demersal fishing ground in terms of the extent of coral reef is predicted to be in the coast region of Mlonggo District, which is along the location between Ujung Piring Reef than followed Prawean Reef.

• Prediction of Demersal Fishing Ground in Segment 4

Segment 4, which covers the waters of the Mlonggo District up to part of Bangsri District based on Sentinel-2 satellite imagery and a field survey found 9 groups of coral reefs, with the local name and approximate area of Semayit Reef (2 ha), Sejongkok Reef (5 ha), Purancak Reef (5 ha), Kemangi Reef (5 ha), Ombo Reef (19.6 ha), Pandan Reef (2 ha), Lasak Reef (9 ha) and Ngelo Utara Reef (dead) dan Selaran Reef (dead) (Figure 7).

Four coral reefs visible from Sentinel imagery are predicted as demersal fishing ground, especially type of Red Snappers, Blue Line Seabass and Leopard Coral Grouper, and lobster in green clusters (Figure 7). The Four coral reef are Sejengkok Reef, Purancak Reef, Ombo Reef, and Lasak Reef. The highest potential demersal fishing ground in terms of the extent of coral reef is predicted to be in the coast region of Ombo District, which is in offshore depth 10 m than followed Lasak Reef.

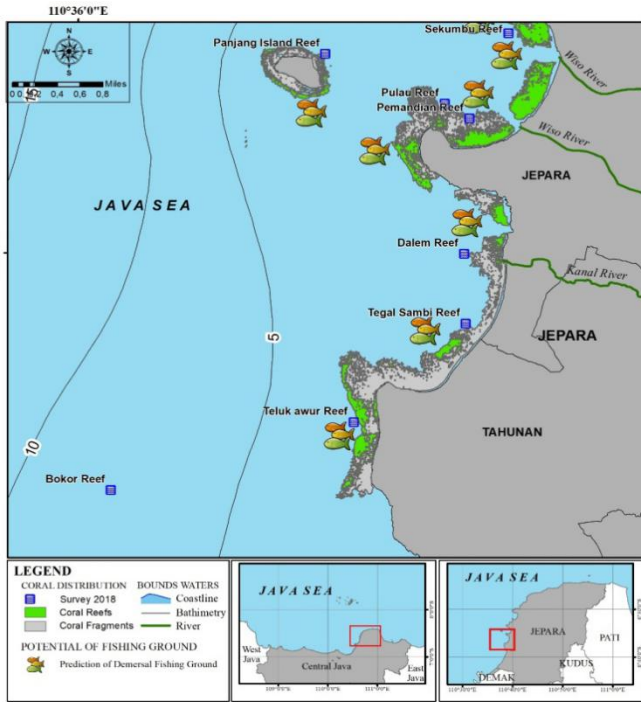


Figure 5. Predictions of potential fishing ground associated with corals in Coastal of Jepara segment 2 (Tahunan and Jepara Districts)

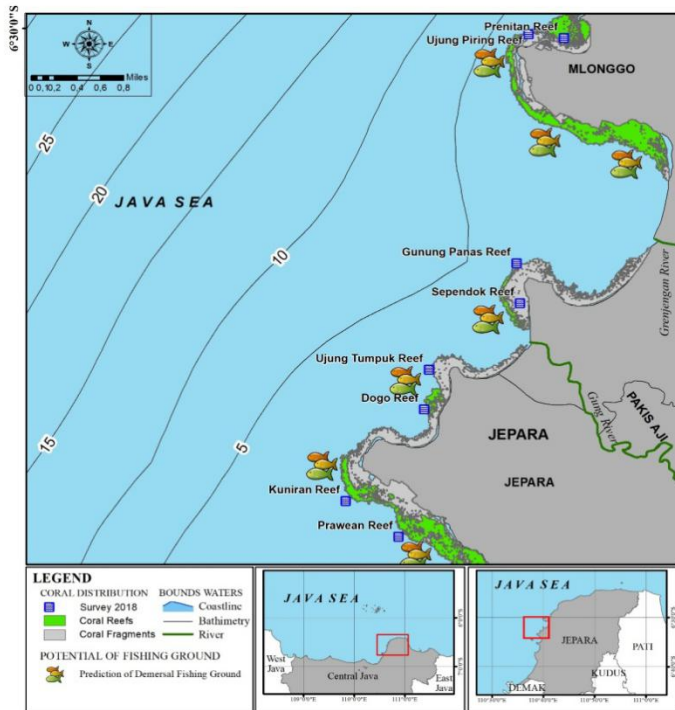


Figure 6. Predictions of potential fishing ground associated with corals in Coastal of Jepara segment 3 (Jepara and Mlonggo Districts)

• Prediction of Demersal Fishing Ground in Segment 3

Segment 3, which covers the waters of the Jepara District up to part of Mlonggo District based on Sentinel-2 satellite imagery and a field survey found 8 groups of coral reefs, with the local name

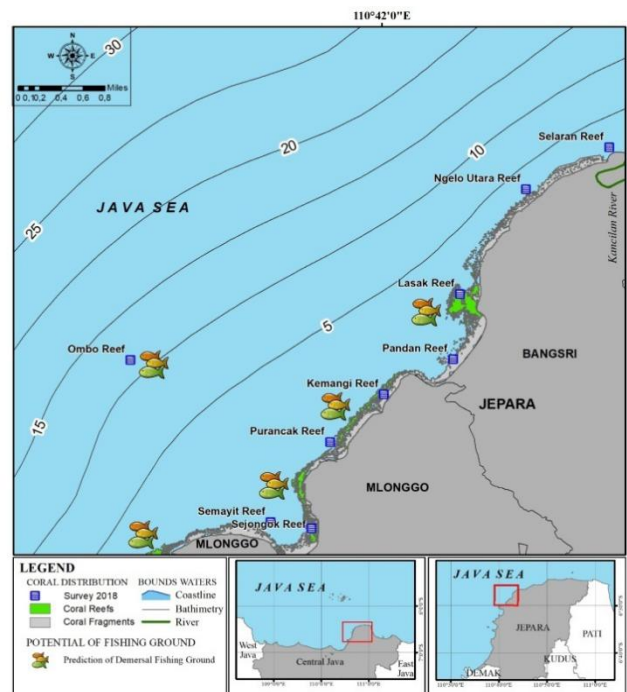


Figure 7. Predictions of potential fishing ground associated with corals in Coastal of Jepara segment 4 (Mlonggo and Bangsri Districts)

• Prediction of Demersal Fishing Ground in Segment 5

Segment 5, which covers the waters of the Kembang District up to part of Keling District based on Sentinel-2 satellite imagery and a field survey found only one group of coral reefs, with the local name and approximate area is Segedek Reef (10 ha) (Figure 8). Segedek Coral reef is about 4 m under surface waters, it's location in the Coastal of Keling District. That coral reefs are found by field survey predicted as demersal fishing ground, especially the type of Red Snappers, Blue Line Seabass and Leopard Coral Grouper, and lobster (Figure 8).

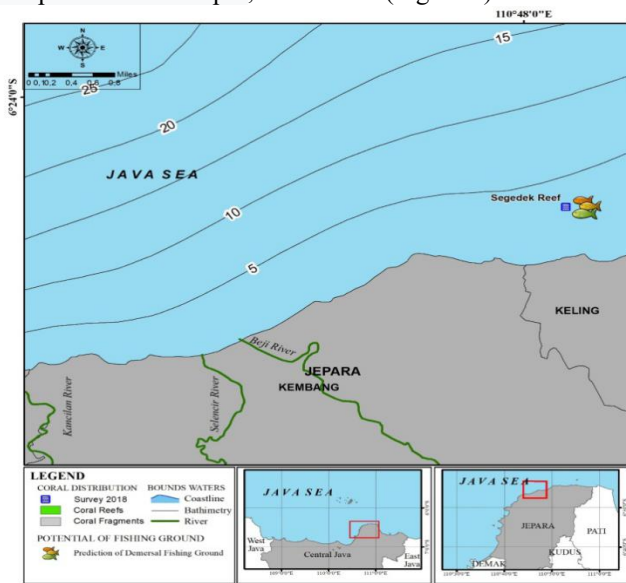


Figure 8. Predictions of potential fishing ground associated with corals in Coastal of Jepara segment 5 (Kembang and Keling Districts)

• Limitations on the use of Sentinel-2 Satellite Imagery to be applied to Corals

The use of Sentinel-2 satellite imagery to analyze the distribution of coral reefs in the coastal area of Jepara Regency turned out to be a problem so that some areas were not visible. Two things that are suspected as the main cause are spatial resolution and water turbidity.

3.3. Spatial Resolution

The sentinel image is used sentinel 2A, with a spatial resolution of 10 m. This pixel is influenced by the environment inside the pixel itself and outside the pixel. If the pixel is dominated by sand with only a few corals, then the coral will be invisible. Likewise, the environment around the pixel also affects, if around the pixel it turns out to be dominated by sand, while appears is sand. So that one pixel of coral can be seen the coral then there is a minimum of 3 x 3 pixels covered by coral. This is in accordance with what explained, which states that pixels outside the sample area need to be considered, and related to the size of the object (too small) will be a difficulty. So for the use of sentinel 2A imagery, the minimum coral cover that can be identified is 30 m². Examples of corals in Jepara that are present but not visible in the image are Karang Bokor on the

west coast of Teluk Awur, Karang Ombo, Karang Mandalika and Karang Beteng (Figures 5, 7 and 9).

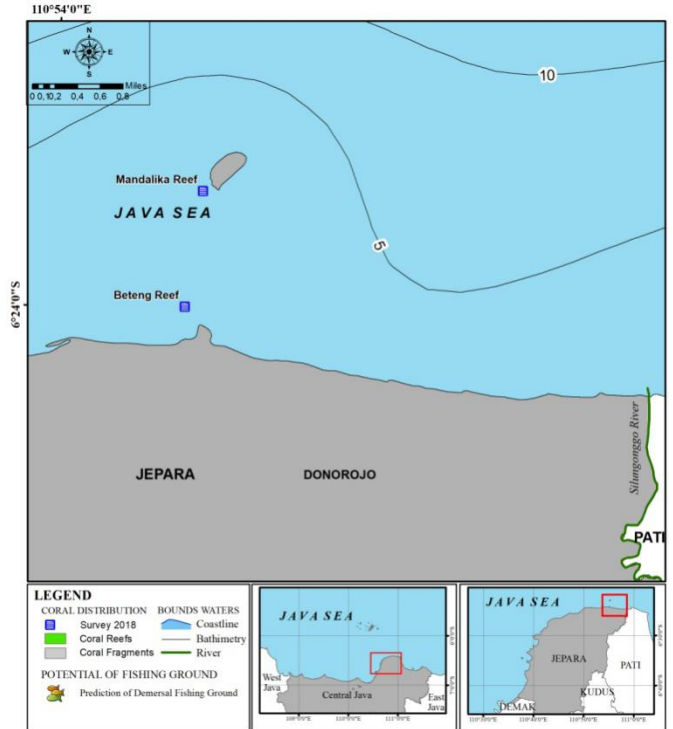


Figure 9. Beteng Reef and Mandalika Reef based on field surveys found its location in the northern waters of the Donorojo Regency, but from Sentinel Citra-2 it was not seen.

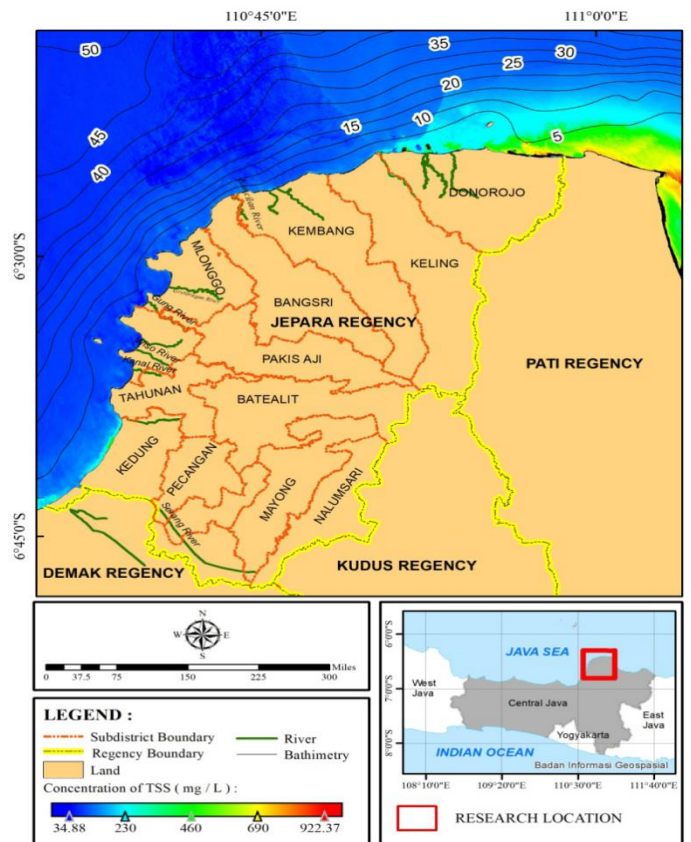


Figure 10. The Coastal Waters Northern Donorojo District and Western Kedung District contain high turbidity because high TSS (in the red squares)

3.4. Water Turbidity

Water turbidity is a serious obstacle. Coral reefs habitats in the northern coastal region, starting from Keling, Kembang, Donorojo District Waters with identification using Sentinel 2A images, did not show any coral. This is thought to be related to the high turbidity value, which is caused by the flow of rivers carrying mud from the Pati District area. Water masses carrying high Total Suspended Solids (TSS) values with range concentration 250-690 mg/L (Figure 10) are carried by ocean currents entering the Jepara region (Figure 10). This high TSS mass makes the sun's electromagnetic energy unable to penetrate the water so that the coral objects are not visible. Presumably, the reflection of the suspended solids, makes the sea surface closed, and looks like sand (Figure 10).

4. Conclusion

Innovation of demersal fishing ground prediction can be done in three stages, first tabulating demersal fisheries environmental conditions, second mapping of vital habitat (coral reefs) and its supporting parameters, third mapping prediction of the potential area of demersal fish. Namely, demersal fishing ground can be made based on an understanding of childhood fish habitat, adulthood, substrate base habitat, an optimum depth of catchment area. Sentinel satellite imagery can be used to help determine the fishing ground of demersal fish species, but for the coastal waters of Jepara Regency, there are still obstacles related to spatial resolution and water turbidity. Field data is still needed to help determine the demersal fishing ground. Based on the fishing ground mapping, there are four economical types of fish that live in the coral reef environment, namely lobster, red snapper, coral grouper, and tiger grouper. The demersal fishing ground associated with corals in the Coastal Jepara Regency Waters which is seven segments apparently only four segments have the potential to become demersal fishing ground associated with corals, that are the second to fourth segments, including the coastal waters of Jepara, Mlonggo, Bangsri and Kembang District and the most potential is the coastal waters of Mlonggo District.

Acknowledgment

We thank the Diponegoro University for receipt of research funds with contract number 1501-33 / UN7.5.10 / LT / 2018 and Head of the Oceanography Department, Dr. Denny Nugroho S, ST., M.Sc, for the support of easy research administration. We also thank two of my assistants namely Mr. Bayu Munandar and Mr. Dika Ahmad Rojikin for their help so far.

References

[1] Kunarso, "Opportunities for Improvement of Fish Potential Location Forecast Models (Development of New Models for Increasing the Accuracy and Coverage of Fishing Area)", Paper of Focus Group Discussion in Topics "Maximizing Fish Potential Information for Fishermen" in the forum ICCTF (Indonesian Climate Change Trust Fund) and National Planning Agency of the Republic of Indonesia (BAPENAS), Jakarta June 30th 2014, 16 pages, 2014.

[2] Lalli, C.M. and Parson, T.R., "Biological Oceanography: An introduction", Pergamon, BPC Wheatons Ltd, British.1994

[3] DKP Jepara (Jepara Regency Fisheries Service), "Profile Book of Fisheries Sector in Jepara Regency", Fisheries Service, Jepara Regency Government-Indonesia, 51 pages, 2017.

[4] Hedley, J.D., Roelfsemab, C., Brandoc, V., Giardinoc, C., Kutserd, T., Phinnb, S., Mumby, P.J., Barrilerof, O., Laporteg, J., Koetzh, B., "Coral reef applications of Sentinel-2: Coverage, characteristics, bathymetry and benthic mapping with comparison to Landsat 8", *Remote Sensing of Environment*. Vol. 216: 598-614 pp, 2018. <https://doi.org/10.1016/j.rse.2018.07.014>

[5] Jaelani L M, Laili N, and Marini. Y, "Pengaruh Algoritma Lyzenga dalam Pemetaan Terumbu Karang Menggunakan Worldview-2, Studi Kasus: Perairan PLTU Paiton Probolinggo". Research Report: Institusi Teknologi Sepuluh Nopember, Surabaya Indonesia, 2015.

[6] Gernez, P., Lafon, V., Lerouxel A., Curti C., Lubac, B., Cerisier, S., Barile', L., "Toward Sentinel-2 High Resolution Remote Sensing of Suspended Particulate Matter in Very Turbid Waters: SPOT4 (Take5), Experiment in the Laore and Geronde Estuaries", *Remote Sensing*, 7, 9507-9528, 2015. DOI: 10.3390/rs 70809507.

[7] Bioresita F., Pribadi, C.B., Firdaus, H.S., Hariyanto, T., Puissant, A., "The Use of Sentinel-2 Imagery to Total Suspended Solids (TSS) Estimation in Porong River", *Sidoarjo, Elipsoida* Vol. 01, No 01, 2018.

[8] Green, E., Edwards, A. and Mumby, P., "Mapping bathymetry" In A.J. Edwards (Ed.), *Remote sensing handbook for tropical coastal management* (pp.219-234). Paris: UNESCO, 2000.

[9] Holthuis, L.B., "FAO Species Catalogue. Vol. 13. Marine Lobsters of the World", An annotated and illustrated catalog of species of interest to fisheries known to date, *FAO Fisheries Synopsis*, No. 125, Vol. 13. Rome, FAO. 1991. 292 p, 1991.

[10] Habibi, A., Sugianta, Yusuf, C., "Groupers and Snappers Fish- Guidelines for Catching and Handling", *World Wildlife Fund (WWF) Indonesia*, 34 pages, 2011.

Multiscale Texture Analysis and Color Coherence Vector Based Feature Descriptor for Multispectral Image Retrieval

Devulapalli Sudheer, Rajakumar Krishnan*

School of Computer Science and Engineering, Vellore Institute of Technology, 632014, india

ARTICLE INFO

Article history:

Received: 07 September, 2019

Accepted: 28 November, 2019

Online: 16 December, 2019

Keywords:

CBIR

Texture

Feature Extraction

Remote Sensing

Curvelet

CCV

ABSTRACT

Content Based Image Retrieval (CBIR) for remote sensing image data is a tedious process due to high resolution and complexity of image interpretation. Development of feature extraction technique is a major portion to represent the image content in an optimal way. In this paper, we propose a feature descriptor which combines the color coherent pixel information and GLCM texture features in multi scale domain. Curvelet transform is used to decompose the image into coarse and detail coefficients. Then Gabor magnitude is computed for each coefficient to improve the directional information. GLCM texture features are extracted from the Gabor magnitude response. The novel feature set by combining the CCV and GLCM using curvelet and Gabor filter is developed. Mahalanobis distance measure is used to find the similarity between query and feature database. Average Normalized Modified Retrieval Rate (ANMRR) is computed to evaluate the performance with the state of art methods.

1 Introduction

Texture represent the pattern arrangement of the pixels in the image. It is an inherent property of any image. Especially in remote sensing applications, images represent the surface reflectance of the earth. Various sensors are used to capture the earth surface like Multi/Hyperspectral, RADAR and LiDAR [1]. Texture extraction in spatial domain using Local Binary Patterns (LBP) and Gray Level Co-Occurrence Matrix has been explained in [2, 3, 4]. Other local texture pattern features like Local Derivative Patterns (LDP), Local Tetra Patterns (LTrp) are reviewed by [5, 6]. Recent advancements in texture features have been developed using multi-scale GLCM windows [7] and Local Contourlet Tetra Patterns [8]. Texture analysis in multi-scale and multi resolution analysis is very useful to extract more precise features. In proposed work, Curvelet transform has been used to analyze the input image in multi scale domain. Curvelet is directionally more efficient than other existing multi resolution transforms. It can preserve the tiny non linear edge information due to its anisotropic nature. Coarse and detail scale coefficients of curvelet are used to compute the Gabor magnitudes. Total four Gabor magnitude responses are be used to extract the GLCM properties. Applying the Gabor magnitudes on each scale of curvelet gives more directional features of the non

linear edges. Texture information extracted from these coefficients can perform retrieval applications efficiently. To carry the spatial domain information, color coherent pixels are computed and merged to the texture feature descriptor. The proposed feature descriptor outperforms the state of art retrieval methods. It has been tested on the public remote sensing image retrieval dataset namely UCmerced. The paper has been organized as follows: Section 2 Related work, Section 3 Methodology, Section 4 Results & Evaluation and Section 5 Conclusion.

2 Related Work

2.1 Importance of Texture Feature in Remote Sensing

In recent years, many texture-based feature descriptors have been developed for the purpose of CBIR in remote sensing. This section explains comprehensive review of texture feature extraction in remote sensing image data. The importance of spatial information retrieval in theoretical perspective for model fit and model selection techniques has been explained by Mihai Datcu, et.al, in (1998) [9]. Seisuke Fukuda, et.al (1999) have developed a wavelet-based texture feature set for the polarimetric SAR image data, Where Downsampling of

*Corresponding Author: Rajakumar Krishnan, Vellore Institute of Technology, Vellore, +91 9894079434 & rajakumar.krishnan@vit.ac.in

wavelet coefficients are omitted. The energy of the wavelet coefficients is considered as texture descriptor [10]. M. Chica-Olmo, et.al (2000) have proposed univariate and multivariate texture features by using spatial variability based variogram measures [11]. It will refine the spatial and spectral structure of the image. A multiband image will be given as an output to quantify the local spatial variability of radiometric data. Jean-Luc Starck, et.al (2002) have improved the curvilinear feature extraction in multiscale domain by using curvelet transform to overcome the wavelet drawbacks [12]. Second and higher order statistical measures have been applied to get the texture information in multiscale and multi resolution domains. Andrey V. Bogdanov, et.al (2005) have applied neural network based classification on GLCM features for the classification of the sea ice in multi-sensor data [13]. F. Kayitakire (2006), et.al, have derived Forest variables from the high spatial resolution data by using GLCM [14]. Interactive retrieval system is proposed by Marin Ferecatu, et.al (2007), using relevance feedback method to improve the accuracy [15].

Feature level fusion also improves classification accuracy. Vijaya V, et.al (2009) had developed a system for texture feature classification by fusing statistical and wavelet-based texture features [16]. Changren Zhu, et.al (2010) have proposed shape and texture based feature set for detecting the ship in spaceborne optical images. Compactness, Convexness, Rectangularity, and Eccentricity are used for the shape based feature set and Mean, Standard variance and Entropy are used for analyzing the statistical features. Local Multiple Patterns are used as local texture features [17]. Shufu Xie, et.al (2010) had developed a Local Gabor Xor Patterns (LGXP) for facial recognition [18]. Multi-resolution based feature extraction has succeeded in extracting robust features. Gholamreza Akbarizadeh, et.al (2012) have proposed Kurtosis wavelet energy feature for the texture recognition in SAR images [19]. 3D DWT is suitable for extracting structure and texture information from the Hyperspectral data. Hyperspectral image consists of continuous spectral bands that provide more accurate information. Yuntao Qian, et.al (2012) has proposed a 3D wavelet-based texture feature extraction and classified it using sparse linear regression [20]. Simple statistics, Gabor filter bank and color histogram has been used as feature descriptors for efficient image retrieval by Yi Yang, et.al (2012) [21]. Local spectral histogram features are generated by merging the local histograms. Jiangye Yuan, et.al, (2014) have computed local spectral histograms and Gabor filter based texture features to segment the image regions [22]. Morphological texture features based on structuring elements have also shown good results in CBIR techniques. Erosion, Dilation, Open, Close operations by structuring elements will improve the feature extraction efficiency. Erchan Aptoula (2014) have developed a morphological texture descriptor based on Circular Covariance Histogram (CCH) and Rotation Invariant Triplet (RIT) for Land Cover image retrieval [23]. Alaa Al-Hammami and Hisham Al-Rashdan (2010) have proposed an enhancement to the Color Coherence Vector (CCV) based on modification of the distance and angle [24]. Zhen-

feng Shao, et.al have extracted Gabor filter based texture and color features for retrieval application. Unichrome feature of each channel of the image data using Gabor filter with orientation (u, v) and opponent feature with (u, v') are used as color features respectively [25]. GLCM is the best features to extract texture information of mono channel image data. For Multichannel or Hyperspectral image, Data clustering and sparse representation based GLCM has been proposed by Xin Huang, et. al (2014) [26]. Local Binary Patterns (LBP), Local Ternary Patterns (LTP), Local Terra Patterns (LTrP) and Local Derivative Patterns (LDP) are most popular texture extraction methods evaluated by [27, 28, 29]. Color and Texture descriptor based image retrieval system has been developed by using Block Difference Inverse Probability (BDIP) and Block Variation of Local Correlation Coefficients (BVLC) by Chandan Singh, et.al (2016) [30]. Spectral end members and texture features based on GLCM has been developed for hyperspectral image retrieval by Jing Zhang, et.al (2017) [31].

2.2 Efficiency of Curvelet Transform

The wavelet-based approach have failed to preserve nonlinear singularities due to the directional limitation. Anisotropic nature of curvelet transform helps in extracting curved singularities. It is a multiscale and multi-resolution transform which can process an image in several orientations at each scale. Curvelet-based SAR image classification has been performed by using the Histogram of Curvelet (HOC) [32]. The curvelet transform has been developed by Emmanuel J. Candès, David L. Donoho, et al. (2002) in order to overcome the drawbacks of wavelet [33]. Lindsay Semler et al. (2006) highlighted the curvelet-based texture descriptors over CT scan images. Energy, entropy, mean, standard deviation has been calculated by using the effective curvelet-based texture descriptors. The results have been compared with similar algorithms based on wavelet and ridgelet descriptors [34]. Tobias Gebaek et al. (2009) have explained that when the number of coefficients that are required to represent the edge to a specified accuracy is regarded, curvelets dispense an almost ideal representation of C^2 edges. Decomposition of the image f into J feature levels have been furnished by the discrete curvelet transforms, with L_j directions on each level, and $K_{j,l,1} \times K_{j,l,2}$ spatial shifts for each of these directions. [35]. Jianwei ma and Gerlindplonka (2010) have described that the compression based on a wavelet, removal of noise or structure extraction have become computationally inefficient for geometric features with line and surface singularities. The first-generation curvelets have been used for image denoising. The first-generation curvelets are also been used to intensify image contrast, render astronomical images and integrate satellite images. After introduction of the second-generation curvelets in 2004, the applications of curvelets escalated in several fields. Hybrid methods are more popular that are pertaining to discrete curvelet transform, which is formulated by incorporating curvelets with another technique for image processing [36]. F. Gomez et al. (2011) have mapped the image to the curvelet space thus data diffusion is approached by

statistical parametric model for each of the sub-bands. Their proposed descriptor (Rotation invariant texture characterization using a curvelet-based descriptor) have been calculated by using the statistical patterns of the curvelet coefficients. Kullback-Leibler distance have been used to find the distance between statistical features. Curvelet is efficient in multiscale decomposition to improve the limits in wavelets for representation of geometrical information [37]. Yungang Zhang et al. (2011) had described that the idea of Discrete Curvelet Transform (DCT) is easy to choose acceptable sampling at the range of scales, position, and orientation. The prevalence space is decomposed into dyadic rectangular coronae. These dyadic spaces are further divided into wedges. The number of wedges increases two times at each level. [38]. NourElDin Laban et al. (2012) have made use of two dissimilar types of features, viz. Color Histograms (CH) and textures in wavelet domain for every band of the multispectral image. The quantization method is use to extract the color histograms from satellite images. Daubechies wavelets are used to extract texture features. The above authors proposed a technique to improve the procedure of satellite image retrieval using two stages: Candidate selection stage and Refinement stage. The refinement stage depends on the outcomes of the candidate selection stage that comprises the adjoining regions in which non-uniform polygon shapes that cover the semantic type area are utilized. They have evaluated the potentiality of their system using a wide area of satellite images and then analyzed in terms of precision and recall rates [39]. ErkanUslu et al. (2014) have stated that the curvelet becomes finer and smaller in the spatial domain and shows more reactivity to curved edges when the resolution level increases. This allows to capture the curves in an image efficiently. As a result, a few coefficients can estimate curved singularities. The energy feature is computed in both discrete curvelet transform and wavelet transform[40]. Benoit Beguet et al. (2014) have developed a global framework of forest variable retrieval methodology by using Haralick Texture Features. The panchromatic and multispectral bands are used to create test frames which are made up of image samples. Then the texture features which have several parameterizations are computed on test frames. Using these test frames, linear regression based feature selection is performed for retrieving the best texture features pertaining to each forest variable. Both single and multiple linear regressions are processed. Multi-scale texture descriptors are formed by choosing the best image texture features through statistical modeling. Five common forest structure variables have been modeled efficiently [41]. Wen-Chyi Lin et al. (2015) described that the curvelet transform for curved singularities in images is particularly attractive for multiscale analysis of microscopic tissue images where cellular structural information exhibits abundant curved singularities. Mean, energy, variance, and entropy vales are calculated as texture features in each sub-band. SVM classifier is used to classify the results of [42]. Wen-Chyi Lin et al. (2016) have explained that higher-order statistical moments of fine-scale curvelet coefficients are selected as critical features. To incorporate the skewness and kurtosis of curvelet coefficients at a

specified scale as texture features. The above authors added the third and fourth order moments to variance, energy, and entropy, so that a better discriminative capability is provided to them. The curvelet coefficients are chosen as discriminative features because they are used to implicitly capture the nucleus and glandular boundary [43]. Sudheer Devulapalli and Rajakumar Krishnan (2019) have developed a image fusion application for multi sensor image data using curvelet coefficients and adaptive neuro fuzzy inference system [44]. Du-Ming Tsai et al. (2017) states that a structural texture is depicted in the satellite image by planting pattern of coffee trees. To extricate the structural features in the spectral domain for image segmentation, a technique based on Fourier transform is proposed. Unidirectional frequency components with high energy are produced by row planted coffee fields, whereas the frequency components are produced in different directions in the spectral domain image by naturally growing plants. The experimental outcome shows that row-planted coffee field can be sectioned in a satellite image with the conjunction of structural and density features. The yield of coffee production can be determined from the data on physical area and density, which is provided by these features. [45].

3 Methodology

Remote sensing benchmark multispectral dataset UC Merced is considered for the experiment in the proposed work. The dataset is consisting of 21 classes of land use data for research purpose [46]. The images are subsampled from USGS National Map urban area image collection. Each image consists of 256 x 256 pixels. The resolution of each pixel is 1 foot. The input image bands will be separated to apply the 2D Fast Discrete Curvelet Transform in Unequally Spaced Fast Fourier Transform (USFFT). Curvelet transform will decompose the image into three coefficients which are coarse, detail, and fine scale coefficients. The detail scale coefficients again consist of multiple orientations at each resolution [47]. Figure. 1 shows the process of retrieval system.

3.1 Feature Extraction

3.1.1 Probabilistic Principle Component Analysis (PPCA)

PCA is a popular method for dimensionality reduction. It will increase the variance of the projected space. The high dimensional strongly correlated data $\{D_p\}_{p \in P}$ will be converted into low dimensional uncorrelated data $\{D_l\}_{l \in L}$ removing low variance data. This may lead to some data loss due to reducing the dimension to (P-L) Eigen subspace. PPCA is a method of finding principal axes by the probabilistic way [48]. Each variable of this model is calibrated by a specific probability density function (pdf). The uncorrelated input variable z with some additive noise e is represented by the equation form $x=A.z+e$. Where A is model parameter. If some probability densities are set to the generative input variable then it can be called as probabilistic model. PPCA is used to find the maximum likelihood parameter set $\Theta \equiv A, \lambda$. Where $A \in \mathbb{R}^{(p \times L)}$ is

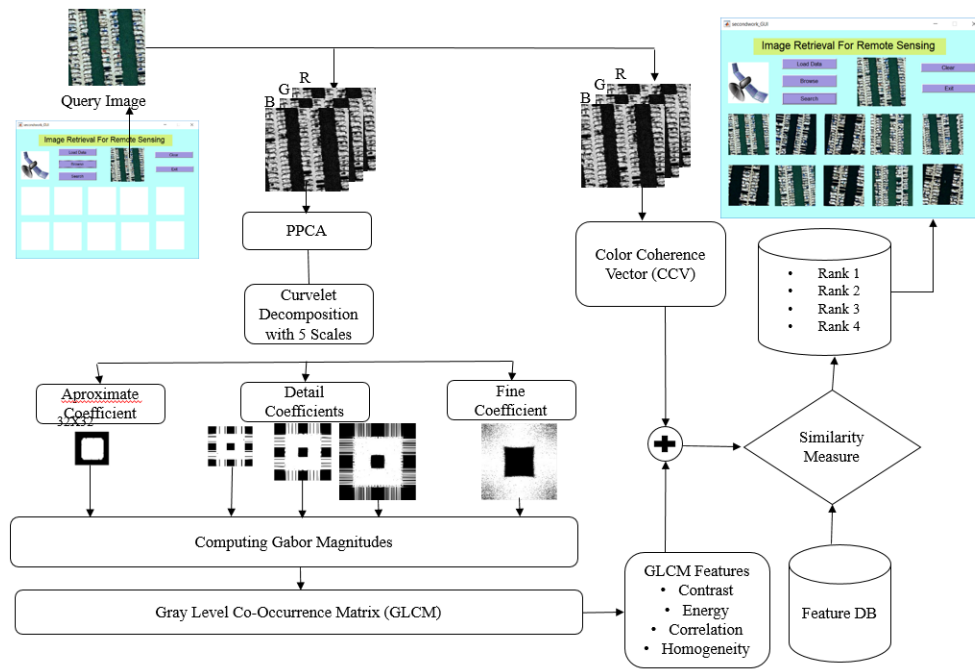


Figure 1: Architecture of the proposed system

the loading the matrix, z is pdf of latent variable and e is pdf of additive noise variable. The parameter Θ can be measured by Expectation and Maximization (EM) algorithm [49]. PPCA assumes that $p(z) = \mathcal{N}(z : 0, I)$ and $p(e) = \mathcal{N}(e : 0, \lambda.I)$. Gaussian pdf is similar to linear operations so that the linear transformation of the Gaussian will produce the new Gaussian distribution.

3.1.2 Curvelet Decomposition

The directionality and anisotropic natures are the main features of the curvelet transform which can help to extract more information from the image data. The curvelet transform decomposes the image into three components like coarse, detail and fine scale coefficients [50]. The input image I will be decomposed with the help of low pass and bandpass filters l_0, Δ_s respectively. $\Delta_s = \{\Delta_1 I, \Delta_2 I, \Delta_3 I \dots \Delta_s I\}$ where Δ_s contains the 2^{-2s} width. The Discrete Fourier Transform (DFT) will be applied to the input image to apply the filters at different scales. Mathematical derivation of the DFT is as follows

$$f(n_1, n_2) = \sum_{p=0}^{M-1} \sum_{q=0}^{N-1} f(p, q) e^{-i2\pi(\frac{n_1 p}{M}, \frac{n_2 q}{N})} \quad (1)$$

The default number of scales will be $\log 2(n) - 3$. Where n is length of the image. Curvelet coefficients are denoted as $c\{j\}\{l\}\{k\} = \langle f, \varphi_{j,l,k} \rangle$. Where j represents scale, l represents orientation and k represents the position (k_1, k_2) . The curvelet coefficients can be stored in a cell matrix $C_{j,l}$. Here scale j is from coarse to finest and orientation l is starts from top left corner and rotates in clockwise[51]. The rotation angles $\theta_{j,l}$ will be equidistant and sequence can be

represented as $\theta_{j,l} := \frac{\pi l_2^{-[j/2]}}{2}$ with $l = 0, 1, \dots, 4.2^{[j/2]} - 1$. For the value of $j=4$ rotation angle $\theta_{j,l} = \pi l/8, l = 0, 1, 2, \dots, 15$ and eight translations with different grids will be considered. The grid sizes will be $1/2^{-j} \times 1/2^{-j/2}$. So the anisotropic scaling principle of the curvelet will be width = length². Each subband is partitioned into squares of proper scales as, $\Delta_s I \rightarrow (W_Q \Delta_s I)_{Q \in Q_s}$. Where W_Q is smooth window. Assume that window W_Q (n_1, n_2) is supported within the sheared rectangle $p_j = \{(n_1, n_2) : 0 \leq n_1 - n_0 < L(j), -L_j/2 \leq n_2 < L_j/2\}$ The localized dyadic squares $Q = \left[\frac{k_1}{2^s}, \frac{(k_1+1)}{2^s} \right] \times \left[\frac{k_2}{2^s}, \frac{(k_2+1)}{2^s} \right]$. By multiplying the function with corresponding window function will give the localized result near Q . Let $(T_Q I)$ denotes the operator which can transport and renormalizes I so the part of the input supported near Q will become the part of the output supported near to $[0, 1]^2$. $T_Q I(n_1, n_2) = 2^s I(2^s n_1 - k_1, 2^s n_2 - k_2)$. The outcomes of dyadic squares are renormalized into single scale. $g_Q = (T_Q)^l - 1(W_Q \Delta_s I)_{Q \in Q_s}$. Each standardized dyadic square will be analyzed by ridgelet transform. It has basis element ρ_λ that make an orthonormal basis for $l^2(R^2)$. $\alpha_\mu = (g_Q, \rho_\lambda)$ where $\mu = (Q, \lambda)$.

3.1.3 Color Coherence Vector

Color histograms are the most popular features to extract color descriptors for CBIR. But the spatial information will not cover by the color histogram features. To consider the color and spatial information of the image Color Coherence Vector (CCV) [53, 52] descriptor has been used. The first stage to compute the CCV is blurring the image with Gaussian filter. Then the discretization of the color space will be applied to divide into n distinct colors of the image. The input image has

3 channels, discretization function will find unique colors in each channel to form V unique values of each channel. Table. ?? shows the pseudo code for computing CCV feature vector.

3.1.4 Gabor Magnitude

Magnitude response of image will be calculated by applying Gabor transform for an input image in multiple scales and different orientations [54]. Bandlimited filters can be used to represent optimal localization in both spatial and frequency domain. If the amplitude of the frequency spectrum goes to zero which exceeds the threshold frequency value. The Gabor transform can also be defined as a Short Time Fourier Transform (STFT) with a Gaussian kernel. The 2D Gabor filter can be mathematically defined as

$$\psi_{x,y}(u, v) = \frac{f_x^2}{\pi\gamma\eta} e^{-\left(\frac{f_x^2}{\gamma^2}u'^2 + \frac{f_y^2}{\eta^2}v'^2\right)} \quad (2)$$

where $u' = u\cos\theta_y + v\sin\theta_y$, $v' = -u\cos\theta_y + v\sin\theta_y$, $f_x = \frac{f_{max}}{2(x/2)}$, $\theta_y = \gamma\pi/8$. f_x and θ_y Parameters are the center frequency and orientation of the plane wave for the Gaussian kernel. The variables γ is the ratio of the center frequency and η is the sharpness constant. If the γ and η values are fixed then the center frequency f_u will define the scale of the Gabor filter. Gabor filters are complex type, which is a combination of sine and cosine functions. Gabor filter is applied to the input gray image with wavelength 4 and 90-degree orientation. Wavelength denotes the sinusoidal carrier in pixels per cycle. Orientation defines the direction of the plane wave range in 0 to 360 degree. Convolution of the Gabor filter and input image will produce the resultant image in the time-frequency domain. It can be decomposed into real and imaginary parts [55]. The mathematical representations of the convolution and decomposition as follows

$$T_{x,y}(u, v) = I(u, v) * \psi_{x,y}(u, v). \quad (3)$$

$$E_{x,y}(u, v) = Re[T_{x,y}(u, v)] \quad (4)$$

$$O_{x,y}(u, v) = Im[T_{x,y}(u, v)] \quad (5)$$

where $Re[T_{x,y}(u, v)] = \cos(2\pi(x_0u + y_0v) + P)$ and $Im[T_{x,y}(u, v)] = \sin(2\pi(x_0u + y_0v) + P)$. $T_{x,y}(u, v)$ is the transformed image obtained after convoluting with Gabor filter $\psi_{x,y}(u, v)$. u, v are the spatial coordinates of the image. Where I is the input image. $E_{x,y}(u, v)$ and $O_{x,y}(u, v)$ are the even and odd functions for the sin and cosine functions and P is the phase response of the sinusoid carrier. From the decomposed sine and cosine functions of the Gabor filter, Magnitude and Phase responses will be calculated as follows

$$M(x, y)(u, v) = \sqrt{(E_{x,y}^2(u, v) + O_{x,y}^2(u, v))} \quad (6)$$

$$\phi_{x,y}(u, v) = ArcTan(O_{x,y}^2(u, v)/E_{x,y}^2(u, v)) \quad (7)$$

The magnitude responses for the curvelet coefficients are considered for the extraction of Haralick texture features. The adjoint transform of the curvelet coefficients will be computed for each scale j and orientation l by applying 2D Inverse Fast Fourier Transform (IFFT).

$$g_{j,l}[n_1, n_2] = F(C_{j,l,k}) \quad (8)$$

$$g[t_1, t_2] = IFFT\left(\sum_{j=1}^J \sum_{l=0}^L g_{j,l}[n_1, n_2] * U_j[n_1, n_2]\right) \quad (9)$$

The adjoint transform will be computed for coarse, detail and fine scale coefficients separately. Gabor transform will be applied on the resultant image at each scale to compute the magnitude response. The surface view of the magnitude response at each scale has shown in Figure. 2.

3.1.5 Texture Analysis

To identify local or global pixel patterns, texture features are very important. GLCM plays a vital role in texture analysis. Haralick, et.al, (1973) derived statistical texture features based on GLCM. GLCM matrix consists value i with a sum of the frequency of the pixel value at a pixel value u with a pixel value y in a specific spatial orientation at v . Mathematically it can be represented as follows

$$G_{u,v} = Freq(F(x, y) = u \& F(x + 1, y + 1) = v) \quad (10)$$

The texture is an inherent property for all kind of surfaces. It can give important information about the pixel arrangement structure of each surface and spatial relationship. The smallest differences in texture for large image databases is very difficult. GLCM properties will be helpful to detect the texture features in local and global areas. Some of the GLCM properties derived by Haralick [4] are considered for the experiment.

$$Energy = \sum_{u=0}^{n-1} \sum_{v=0}^{n-1} GLCM(u, v)^2 \quad (11)$$

$$Correlation = \sum_{u=0}^{n-1} \sum_{v=0}^{n-1} \frac{GLCM(u, v)(u - \mu_x)(v - \mu_y)}{\sigma_x \sigma_y} \quad (12)$$

$$Contrast = \sum_{u=0}^{n-1} \sum_{v=0}^{n-1} GLCM(u, v)(u - v)^2 \quad (13)$$

$$Homogeneity = \sum_{u=0}^{n-1} \sum_{v=0}^{n-1} \frac{GLCM(u, v)}{1 + (u - v)^2} \quad (14)$$

3.2 Similarity Measure

In this work, the Mahalanobis distance measure is used as a distance metric. Suppose if there are two groups G_1 and G_2 with some characteristics. these characteristics are considered as the feature vectors representing the objects of each group

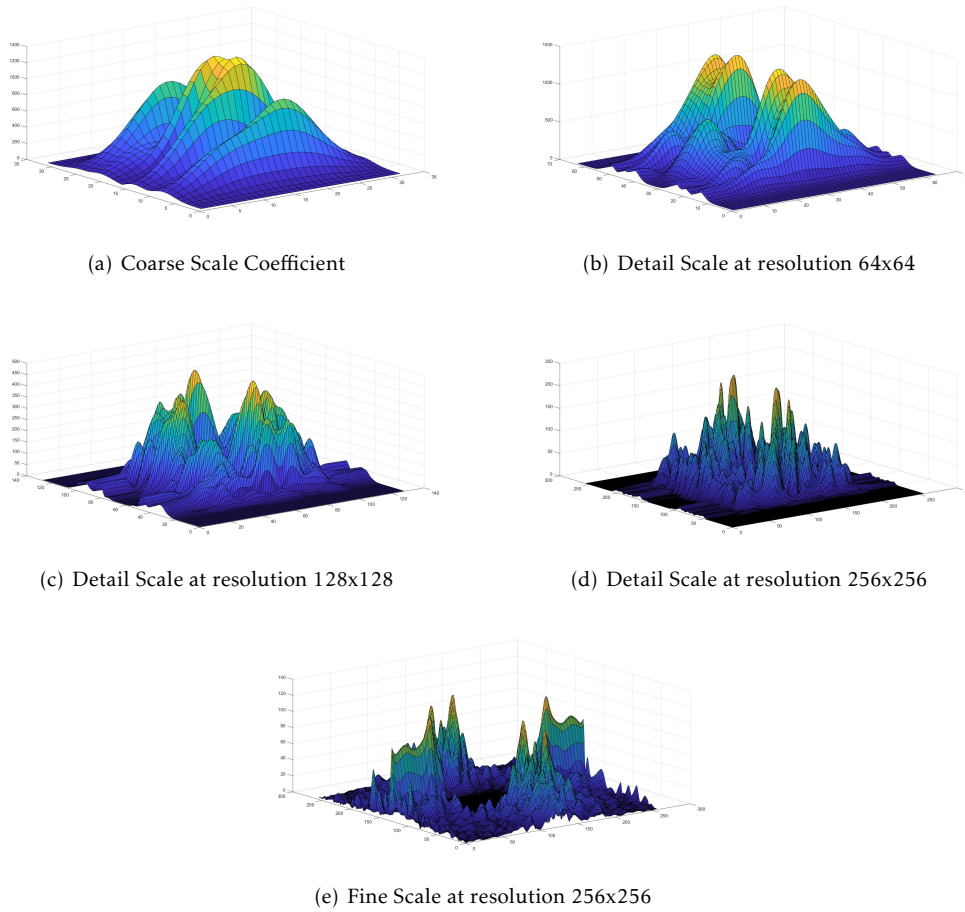


Figure 2: Gabor Magnitude Responses of the Curvelet Coefficients

[56]. the feature vector x with dimension p have the same variation about its mean within either group. The mathematical representation of Mahalanobis distance is as follows

$$Dist = (\mu_1 - \mu_2)^T S^{-1} (\mu_1 - \mu_2) \quad (15)$$

where μ_1 and μ_2 are the mean of two vectors S is covariance matrix.

4 Results and Evaluation

The features have been extracted using the process explained in the section 2. The experiment has been conducted on UC Merced Land use dataset which contains 21 classes with 50 samples of each class. Each image has 256×256 pixels. The spatial resolution of the data is 0.3m. The feature descriptor size for each image is 1×24 . color coherence vector feature length is 1×8 because in this experiment only coherent pixel information is considered as a feature. The color coherence vector feature is computed for the multispectral image directly. Further feature extraction process the input image will be reduced to a single band by applying PPCA. The resulting of PPCA image will be decomposed into coarse and detail coefficients using curvelet transform. The coarse coefficient

in one scale and detail coefficients at three different scales are used to extract the texture information. Obtained Gabor magnitude response of each coefficient to compute the GLCM properties. Contrast, Correlation, Energy and Homogeneity features have been extracted from each coefficient. The feature length of texture features is 1×16 . The color and texture features will be combined together to form a single feature descriptor of an image. Feature descriptor of each image in the database will be computed and stored as a feature base. While the query image submitted to the retrieval system the same features will be extracted to describe the content of the image and matched with the feature base using Mahalanobis similarity metric. The feature obtained lower distance is considered as the most relevant image to the query. In this experiment, top 10 relevant images are shown as a result. Figure. 3 shows the retrieval results of four different classes in the dataset.

The performance metrics are very much important to compare the system accuracy with other systems. The most important performance measures are precision and Recall. Precision can be described as a number of relevant images retrieved over a total number of images retrieved. Recall can be defined as number of relevant images retrieved over the total number of relevant images in the database. These traditional mea-

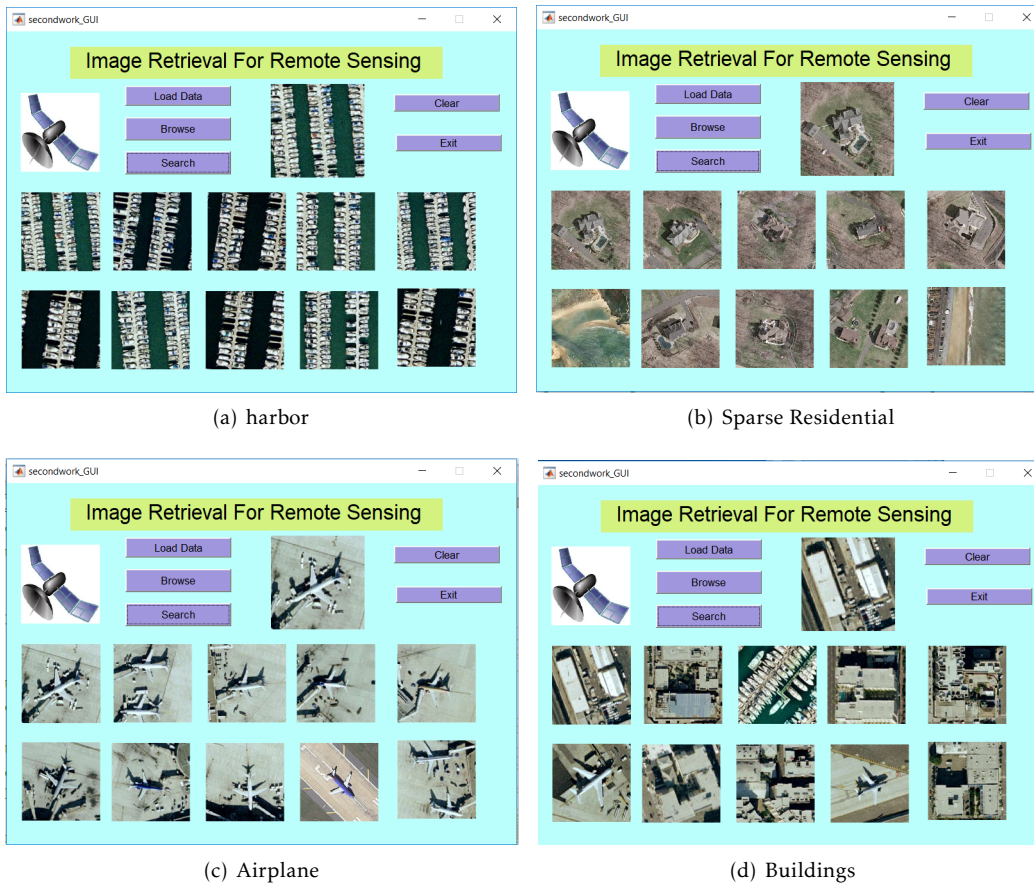


Figure 3: Retrieval Results of the System

asures will not considered the position of the relevant image appears among the top retrieved results. The retrieval system performance is evaluated by using Average Normalized Modified Retrieval Rate (ANMRR) metric [57, 58]. ANMRR The performance metric ANMRR as shown below

$$R(I) = \begin{cases} R(I) & \text{if } R(I) \leq I(q) \\ 1.25 * I(q) & \text{if } R(I) > I(q) \end{cases} \quad (16)$$

where $R(I)$ is position of relevant image I retrieved, $I(q)$ is retrieved images for query q . $I(q) = \min\{4.TG(q), 2.\max[TG(q), \forall q]\}$ Average Rank will be calculated as follows

$$Average_R(q) = \frac{1}{TG(q)} \sum_{I=1}^{TG(q)} R(I) \quad (17)$$

where $TG(q)$ is the total ground truth images in the database to the query q . $TG(q)$ is influencing the average rank in the above equation. to reduce this factor Modified Retrieval rate (MRR) is computed as $Average_R(q) - 0.5.[1 + TG(q)]$. Normalization will be applied to make the value exist between 0 and 1.

$$NMRR(q) = \frac{MRR(q)}{1.25 * I(q) - 0.5 * [1 + TG(q)]} \quad (18)$$

Finally the ANMRR is derived for the Total number of queries TQ is follows

$$ANMRR(q) = \frac{1}{TQ} \sum_{q=1}^{NQ} NMRR(q) \quad (19)$$

Table 2 shows the ANMRR values for the sample retrieval results with ten queries from each class. we have tested for the four classes in the database. Retrieval performance was compared with the five existing popular texture feature extraction methods. The proposed method is developed by combining the CCV and texture features using GLCM from the Gabor magnitude of the curvelet sub-bands in different scales. Extracting Gabor magnitude from the curvelet sub-bands in multiple scales will improve the directional features of the input image. Curvelet is capable of extracting anisotropic edge information in various orientations at different scales. The resultant of the curvelet decomposed image will have one coarse and three detail coefficients as explained in the section 3. The comparison of the proposed method with existing literature has been shown in Figure 4.

5 Conclusion

This paper develops a feature extraction method which is a combination of color coherent pixel information and multi

	Harbor	Sparse Residential	Airplane	Buildings
LBP	0.2405	0.2633	0.2367	0.2304
LDP	0.2329	0.2633	0.2418	0.2304
LSP	0.2291	0.2658	0.245	0.2430
LTrp	0.2456	0.2646	0.2278	0.2253
Gabor [25]	0.2370	0.2642	0.2378	0.2322
CCV [24]	0.231	0.262	0.231	0.243
GLCM [26]	0.241	0.236	0.223	0.234
Proposed	0.2096	0.215	0.2096	0.2215

Table 2: ANMRR Performance Results

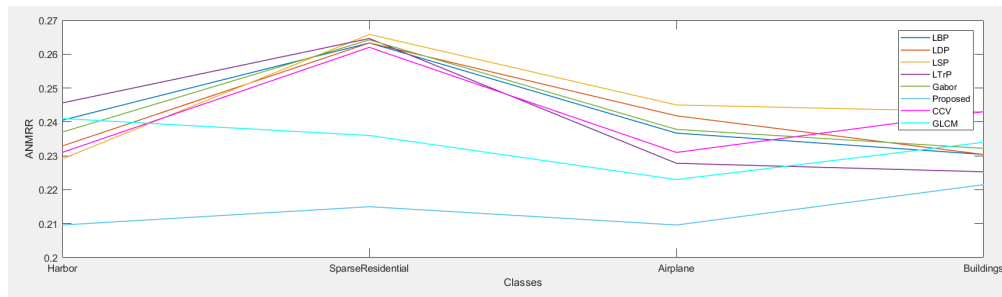


Figure 4: Performance Graph for state of art methods

scale texture features. The proposed feature descriptor is extracted using Haralick texture features from curvelet coefficients. To extract the robust directional information, Gabor magnitude responses are computed from the curvelet coefficients. Haralick texture features extracted from the resultant gabor magnitude responses are shown best retrieval rate than other state of art feature extraction techniques. It improves the retrieval accuracy of the CBIR search engines. Retrieval system was tested on various classes of remote sensing image data. ANMRR performance metric gives the best average retrieval rate for a set of queries from various classes. Four classes have been tested in the dataset. This work will be enhanced by adopting machine learning techniques for the target classification for high resolution imagery data.

References

- [1] Melesse, Assefa, et al. "Remote sensing sensors and applications in environmental resources mapping and modelling." *Sensors* 7.12 (2007): 3209-3241.
- [2] He, Dong-Chen, and Li Wang. "Texture unit, texture spectrum, and texture analysis." *IEEE transactions on Geoscience and Remote Sensing* 28.4 (1990): 509-512. DOI:10.1109/TGRS.1990.572934.
- [3] Guo, Zhenhua, Lei Zhang, and David Zhang. "A completed modeling of local binary pattern operator for texture classification." *IEEE transactions on image processing* 19.6 (2010): 1657-1663. DOI: 10.1109/TIP.2010.2044957.
- [4] Haralick, Robert M., and Karthikeyan Shanmugam. "Textural features for image classification." *IEEE Transactions on systems, man, and cybernetics* 6 (1973): 610-621.
- [5] Juneja, Komal, et al. "A survey on recent image indexing and retrieval techniques for low-level feature extraction in CBIR systems." 2015 IEEE International Conference on Computational Intelligence & Communication Technology. IEEE, 2015. DOI:10.1109/CICCT.2015.92
- [6] Yadav, Susheel Kumar, Dharendra Pratap Singh, and Jaytrilok Choudhary. "A Survey: Comparative Analysis of Different Variants of Local Binary Pattern." 2018 Second International Conference on Inventive Communication and Computational Technologies (ICICCT). IEEE, 2018. DOI:10.1109/ICICCT.2018.8473220.
- [7] Lan, Zeying, and Yang Liu. "Study on multi-scale window determination for GLCM texture description in high-resolution remote sensing image geo-analysis supported by GIS and domain knowledge." *ISPRS International Journal of Geo-Information* 7.5 (2018): 175. DOI:10.3390/ijgi7050175.
- [8] Kumar, TG Subash, and V. Nagarajan. "Local contourlet tetra pattern for image retrieval." *Signal, Image and Video Processing* 12.3 (2018): 591-598. DOI:10.1007/s11760-017-1197-1.
- [9] Datcu, Mihai, Klaus Seidel, and Marc Walessa. "Spatial information retrieval from remote-sensing images. I. Information theoretical perspective." *IEEE transactions on geoscience and remote sensing* 36.5 (1998): 1431-1445. DOI:10.1109/36.718847.
- [10] Fukuda, Seisuke, and Haruto Hirotsawa. "A wavelet-based texture feature set applied to classification of multifrequency polarimetric SAR images." *IEEE Transactions on Geoscience and Remote Sensing* 37.5 (1999): 2282-2286. DOI:10.1109/36.789624.
- [11] Chica-Olmo, M., and F. Abarca-Hernandez. "Computing geostatistical image texture for remotely sensed data classification." *Computers & Geosciences* 26.4 (2000): 373-383. DOI:10.1016/S0098-3004(99)00118-1.
- [12] Starck, Jean-Luc, Emmanuel J. Candès, and David L. Donoho. "The curvelet transform for image denoising." *IEEE Transactions on image processing* 11.6 (2002): 670-684. DOI: 10.1109/TIP.2002.1014998.
- [13] Bogdanov, Andrey V., et al. "Multisensor approach to automated classification of sea ice image data." *IEEE Transactions on geoscience and remote sensing* 43.7 (2005): 1648-1664. DOI: 10.1201/9781420003130.ch25.

- [14] Kayitakire, François, C. Hamel, and Pierre Defourny. "Retrieving forest structure variables based on image texture analysis and IKONOS-2 imagery." *Remote sensing of environment* 102.3-4 (2006): 390-401. DOI:10.1016/j.rse.2006.02.022.
- [15] Ferecatu, Marin, and Nozha Boujemaa. "Interactive remote-sensing image retrieval using active relevance feedback." *IEEE Transactions on Geoscience and Remote Sensing* 45.4 (2007): 818-826. DOI:10.1109/TGRS.2007.892007.
- [16] Chamundeewari, Vijaya V., Dharmendra Singh, and Kuldip Singh. "An analysis of texture measures in PCA-based unsupervised classification of SAR images." *IEEE Geoscience and Remote Sensing Letters* 6.2 (2009): 214-218. DOI:10.1109/LGRS.2008.2009954.
- [17] Zhu, Changren, et al. "A novel hierarchical method of ship detection from spaceborne optical image based on shape and texture features." *IEEE Transactions on geoscience and remote sensing* 48.9 (2010): 3446-3456. DOI:10.1109/TGRS.2010.2046330.
- [18] Xie, Shufu, et al. "Fusing local patterns of gabor magnitude and phase for face recognition." *IEEE transactions on image processing* 19.5 (2010): 1349-1361. DOI:10.1109/tip.2010.2041397.
- [19] Akbarizadeh, Gholamreza. "A new statistical-based kurtosis wavelet energy feature for texture recognition of SAR images." *IEEE Transactions on Geoscience and Remote Sensing* 50.11 (2012): 4358-4368. DOI:10.1109/TGRS.2012.2194787.
- [20] Qian, Yuntao, Minchao Ye, and Jun Zhou. "Hyperspectral image classification based on structured sparse logistic regression and three-dimensional wavelet texture features." *IEEE Transactions on Geoscience and Remote Sensing* 51.4 (2012): 2276-2291. DOI:10.1109/TGRS.2012.2209657.
- [21] Yang, Yi, and Shawn Newsam. "Geographic image retrieval using local invariant features." *IEEE Transactions on Geoscience and Remote Sensing* 51.2 (2012): 818-832. DOI:10.1109/TGRS.2012.2205158.
- [22] Yuan, Jiangye, DeLiang Wang, and Rongxing Li. "Remote sensing image segmentation by combining spectral and texture features." *IEEE Transactions on geoscience and remote sensing* 52.1 (2013): 16-24. DOI:10.1109/TGRS.2012.2234755.
- [23] Aptoula, Erchan. "Remote sensing image retrieval with global morphological texture descriptors." *IEEE transactions on geoscience and remote sensing* 52.5 (2013): 3023-3034. DOI:10.1109/TGRS.2013.2268736.
- [24] Al-Hamami, Alaa, and Hisham Al-Rashdan. "Improving the Effectiveness of the Color Coherence Vector." *Int. Arab J. Inf. Technol.* 7.3 (2010): 324-332.
- [25] Shao, Z., Zhou, W., Zhang, L., & Hou, J. "Improved color texture descriptors for remote sensing image retrieval." *Journal of applied remote sensing* 8.1 (2014): 083584. DOI:10.1117/1.
- [26] Huang, Xin, Xiaobo Liu, and Liangpei Zhang. "A multichannel gray level co-occurrence matrix for multi/hyperspectral image texture representation." *remote sensing* 6.9 (2014): 8424-8445. DOI:10.3390/rs6098424.
- [27] Fadaei, Sadegh, Rassoul Amirfattahi, and Mohammad Reza Ahmadzadeh. "Local derivative radial patterns: A new texture descriptor for content-based image retrieval." *Signal Processing* 137 (2017): 274-286. DOI: 10.1016/j.sigpro.2017.02.013.
- [28] Tiwari, Ashwani Kumar, Vivek Kanhangad, and Ram Bilas Panchori. "Histogram refinement for texture descriptor based image retrieval." *Signal Processing: Image Communication* 53 (2017): 73-85. DOI:10.1016/j.image.2017.01.010.
- [29] Jenitta, A., and R. Samson Ravindran. "Content Based Geographic Image Retrieval using Local Vector Pattern." *Brazilian Archives of Biology and Technology* 61 (2018). DOI:10.1590/1678-4324-2016160717.
- [30] Singh, Chandan, and Kanwal Preet Kaur. "A fast and efficient image retrieval system based on color and texture features." *Journal of Visual Communication and Image Representation* 41 (2016): 225-238. DOI:10.1016/j.jvcir.2016.10.002.
- [31] Zhang, Jing, et al. "Hyperspectral remote sensing image retrieval system using spectral and texture features." *Applied optics* 56.16 (2017): 4785-4796. DOI:10.1364/AO.56.004785.
- [32] Uslu, Erkan, and Songul Albayrak. "Curvelet-based synthetic aperture radar image classification." *IEEE Geoscience and Remote Sensing Letters* 11.6 (2013):1071-1075. DOI:10.1109/LGRS.2013.2286089.
- [33] Candès, Emmanuel J., and David L. Donoho. "New tight frames of curvelets and optimal representations of objects with piecewise C^2 singularities." *Communications on Pure and Applied Mathematics: A Journal Issued by the Courant Institute of Mathematical Sciences* 57.2 (2004): 219-266. DOI:10.1002/cpa.10116.
- [34] Semler, Lindsay, and Lucia Dettori. "Curvelet-based texture classification of tissues in computed tomography." 2006 International Conference on Image Processing. IEEE, 2006. DOI:10.1109/ICIP.2006.312873.
- [35] Gebäck, Tobias, and Petros Koumoutsakos. "Edge detection in microscopy images using curvelets." *BMC bioinformatics* 10.1 (2009): 75. DOI:10.1186/1471-2105-10-75.
- [36] Ma, Jianwei, and Gerlind Plonka. "A review of curvelets and recent applications." *IEEE Signal Processing Magazine* 27.2 (2010): 118-133.
- [37] Gómez, F., and E. Romero. "Rotation invariant texture characterization using a curvelet based descriptor." *Pattern Recognition Letters* 32.16 (2011): 2178-2186. DOI:10.1016/j.patrec.2011.09.029.
- [38] Zhang, Yungang, Wei Gao, and Jun Liu. "Integrating Color Vector Quantization and Curvelet Transform for Image Retrieval." *International Journal of Design, Analysis and Tools for Integrated Circuits and Systems* 2.2 (2011): 99.
- [39] Laban, NourElDin, et al. "System refinement for content based satellite image retrieval." *The Egyptian Journal of Remote Sensing and Space Science* 15.1 (2012): 91-97. DOI:10.1016/j.ejrs.2012.05.001.
- [40] Uslu, Erkan, and Songul Albayrak. "Curvelet-based synthetic aperture radar image classification." *IEEE Geoscience and Remote Sensing Letters* 11.6 (2013): 1071-1075. DOI:10.1109/LGRS.2013.2286089.
- [41] Beguet, Benoit, et al. "Automated retrieval of forest structure variables based on multi-scale texture analysis of VHR satellite imagery." *ISPRS journal of photogrammetry and remote sensing* 96 (2014): 164-178. DOI:10.1016/j.isprsjprs.2014.07.008.
- [42] Lin, Wen-Chyi, et al. "Curvelet-based classification of prostate cancer histological images of critical gleason scores." 2015 IEEE 12th International Symposium on Biomedical Imaging (ISBI). IEEE, 2015. DOI:10.1109/ISBI.2015.7164044.
- [43] Lin, Wen-Chyi, et al. "Curvelet-based texture classification of critical Gleason patterns of prostate histological images." 2016 IEEE 6th International Conference on Computational Advances in Bio and Medical Sciences (ICCABS). IEEE, 2016. DOI:10.1109/ICCABS.2016.7802768.
- [44] Sudheer Devulapalli, Rajakumar Krishnan, "Synthesized pansharpening using curvelet transform and adaptive neuro-fuzzy inference system," *J. Appl. Remote Sens.* 13(3), 034519 (2019), doi: 10.1117/1.JRS.13.034519.
- [45] Tsai, Du-Ming, and Wan-Ling Chen. "Coffee plantation area recognition in satellite images using Fourier transform." *Computers and electronics in agriculture* 135 (2017): 115-127. DOI:10.1016/j.compag.2016.12.020.
- [46] Yang, Yi, and Shawn Newsam. "Bag-of-visual-words and spatial extensions for land-use classification." *Proceedings of the 18th SIGSPATIAL international conference on advances in geographic information systems.* ACM, 2010. DOI:10.1145/1869790.1869829.

- [47] Luo, Jing, et al. "Fingerprint classification combining curvelet transform and gray-level cooccurrence matrix." *Mathematical Problems in Engineering* 2014 (2014). DOI:10.1155/2014/592928.
- [48] Tipping, Michael E., and Christopher M. Bishop. "Probabilistic principal component analysis." *Journal of the Royal Statistical Society: Series B (Statistical Methodology)* 61.3 (1999): 611-622. DOI:10.1111/1467-9868.00196.
- [49] Ju, Fujiao, et al. "Image outlier detection and feature extraction via L1-norm-based 2D probabilistic PCA." *IEEE Transactions on Image Processing* 24.12 (2015): 4834-4846. DOI:10.1109/TIP.2015.2469136.
- [50] Ma, Jianwei, and Gerlind Plonka. "The curvelet transform." *IEEE signal processing magazine* 27.2 (2010): 118-133. DOI:10.1109/MSP.2009.935453.
- [51] Donoho, David L., and Mark R. Duncan. "Digital curvelet transform: strategy, implementation, and experiments." *Wavelet applications VII*. Vol. 4056. International Society for Optics and Photonics, 2000. DOI:10.1117/12.381679.
- [52] Roy, Kalyan, and Joydeep Mukherjee. "Image similarity measure using color histogram, color coherence vector, and sobel method." *International Journal of Science and Research (IJSR)* 2.1 (2013): 538-543.
- [53] Pass, Greg, Ramin Zabih, and Justin Miller. "Comparing Images Using Color Coherence Vectors." *ACM multimedia*. Vol. 96. 1996. DOI:10.1.1.29.9596.
- [54] Lee, Jen-Chun. "Copy-move image forgery detection based on Gabor magnitude." *Journal of Visual Communication and Image Representation* 31 (2015): 320-334.
- [55] Struc, Vitomir, and Nikola Pavesic. "From Gabor magnitude to gabor phase features: tackling the problem of face recognition under severe illumination changes." *Face Recognition*. IntechOpen, 2010.
- [56] De Maesschalck, Roy, Delphine Jouan-Rimbaud, and Désiré L. Massart. "The mahalanobis distance." *Chemometrics and intelligent laboratory systems* 50.1 (2000): 1-18. DOI:10.1016/S0169-7439(99)00047-7.
- [57] Zier, Detlef, and Jens-Rainer Ohm. "Common datasets and queries in MPEG-7 color core experiments." *ISO/IEC JTC1/SC29/WG11 MPEG99 M 5060* (1999).
- [58] Cieplinski, Leszek. "MPEG-7 color descriptors and their applications." *International Conference on Computer Analysis of Images and Patterns*. Springer, Berlin, Heidelberg, 2001. DOI:10.1007/3-540-44692-3_3.

Smart Ambulance: Speed Clearance in the Internet of Things paradigm using Voice Chat

Noor A.Hussein*, Mohamed Ibrahim Shujaa

Electrical Engineering Technical College Middle Technical University & Baghdad, Iraq

ARTICLE INFO

Article history:

Received: 21 August, 2019

Accepted: 23 November, 2019

Online: 12 December, 2019

Keywords:

Voice command

Smart Ambulance

Socket Programming

Speech Recognition

MQTT Protocol

Internet of things

Vehicle network

Raspberry pi

ABSTRACT

In recent years, researchers have focused on the development of many applications of information and communication which could lead to enhance human life. The congestion and road traffic are one of the most problems facing the ambulance transportation to provide fast healthcare services for patients. In this work, a tracking and data transfer system has been introduced such that a central monitoring and tracking unit can observe ambulance using MQTT protocol where each vehicle is occupied with the embedded system unit. When an ambulance being on the road it will communicate with other cars by means of socket communication whenever the ambulance enters a new region of the city. Chat between drivers has been designed using speech recognition library-based Google API. The proposed system has been designed and implemented using a python source network programming.

1. Introduction

IoT is the next step of the evolution of the internet, which merge heterogeneous ubiquitous devices by means of network connectivity to improve the entire system. The devices could be home appliances, environmental, vehicle or buildings. Smart city is one of IoT applications, where the final goal is to improve life quality of people [1]. Some problems such as accident, traffic congestion, emergency vehicle, and large number of cars transportation are one of the most yet problems in large cities. The idea of smart city has been introduced the objective to find solutions for such problems. The traffic light control system is not fully adapted to different traffic situations that can found in the course of a day. According to street situation, it is needed that traffic flow being controlled and managed according to the current situation under the control of an on-site traffic officer, where the traffic lights can be controlled dynamically [2].

Different from other IoT applications, the internet of vehicle (IoV) has dynamic characteristics and frequently changing network topologies along with many existing communications that expose nodes of IoV. When vehicles are capable of transfer information between the vehicular ad-hoc networks (VANETS) are formed. Mobility is an essential characteristic in VANETS, but unlike MANETS fixed mobility patterns are followed in vehicular scenarios. Normally, there are two types of communications can

be found which are: Vehicle to Vehicle communications (V2V) that as many vehicles formed a VANETS and Vehicle to Infrastructure communication (V2I) that is hybrid VANETS with both fixed and mobile nodes. The fixed infrastructure can be easily connected to the internet acting as an access point for the VANETS or MANETS [3, 4].

Traffic jam on the road is one of the most issues that ambulance, fire brigades, and police are faced. They may get stuck in this status, which could threat patients' lives. Also, currently, these vehicles use the siren to inform other road user to clear the path which is annoying approach same times. In this work, we developed a voice chat system such that each car would have an embedded card (Raspberry pi3) with sound system (Mike and speakers) to encounter the proposed problem. The developed system is fully auto smarted and hand free.

The rest of this paper is organized as follows; section two provides a survey of the most related work. Section three provide the require preliminaries in this work such as IoT protocol, socket programming, and speech recognition. Section four discussed the proposed system design. Results and discussion are introduced in section five and finally section six the conclusion.

2. Related Work

In [5] introduce an IoT scenario to clear the traffic light by sending a command such that the ambulance would have a clear path without any delay. They used an embedded system to

*Noor A.Hussein, Email: noor.alaa.hussein@gmail.com

control traffic lights. In [6] proposed smart home system with multi-function where voice command is used to control the home appliances. The proposed system can recognize user voice independent of the accent with a dedicated hardware module. In [7] proved speech recognition transcription system for healthcare application. The proposed system can be used by counselor to record the speech of patient and convert it to text in data base systems.

In [8] proposed a central monitoring and control system using the internet for a traffic management system for smart city controlled by traffic using a smartphone. In [9] proposed a wireless detection, and monitoring system for vehicle speed. An intelligent wireless monitoring is designed to identify speed of the vehicle with a protocol laboratory environment which produces random data on vehicle speed. The proposed system has been designed based Java script socket programming for vehicle monitoring using server computer. In [10] Provides image processing algorithm to track vehicles such that the location of the vehicle and any malicious activity could be discovered. They proposed a smartphone application which mail image of the interior and exterior environment of the vehicle along with its GPS location to the CIS.

In [11] discussed the connected car concept for car maintenance they use the MQTT Protocol to implement the predictive system by sharing different types of data with backend application. In [12] implemented a wifi based road sign to improve car driver awareness by using Qduino provides Arduino API where real time multithread event handling are presented. In [13] discusses in the client server application using socket programming in a distributed.

In this work, ambulance tracking with data transfer system has been design and implemented such that a control and emergency monitoring and tracking CEMT can observe ambulance using MQTT protocol. Where each vehicle is provided with an embedded system (Raspberry pi3) unit. When an ambulance is being in the road it will communication with other vehicles or road traffic by means of socket communication. Chat between drivers has been designed and implemented using speech recognition library based Google API. The voice chat has been designed and implemented experimentally. The proposed system design is combination different work discussed previously like [5, 8, 9, 12].

3. Preliminaries

3.1. MQTT Protocol

The message Queuing Telemetry Transport (MQTT) protocol is a machine to machine M2M protocol, which runs over TCP/IP. It uses a Publish/subscribes model between IoT nodes. A broker cloud server (Eclipse cloud server) is the station where the publisher nodes send their messages in a specific topic, where the client node checks these topics. Nodes may subscribe in some topics and not in another. Also, other nodes can publish in a specific topic. If for an instant, a node publishes in a topic, then each node subscribes in that topic would receive the message while other nodes whose not subscriber in that topic would not receive the message [14]. In this work, all messages which are transferred between IoT nodes have been encrypted in the publisher and decrypted in the subscriber side using One Time

Pad (OTP) technique and DNA computing. Figure 1. Shows a schematic diagram at MQTT protocol.

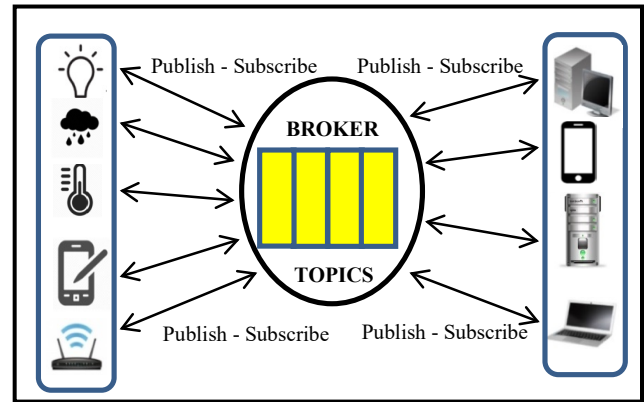


Figure 1: Schematic diagram at MQTT protocol.

3.2. Socket Programming and Interface

The Socket is communication channel between computers based internet protocol. Socket programming is the using of application socket programming to establish the communication link. In terms of server client schemes, the client is an application program that sends a request to the server and waits for response by the server. Socket interface could be programmed by many high level languages; in this work, python network programming has been used which provides many modules such as socket (), bind (), listen (), accept (), connect (), send (), recv (). Figure 2. shows the structured programming of socket on both sides where the ambulance is considered as a server computer while the other cars in the road are a client. [15, 16].

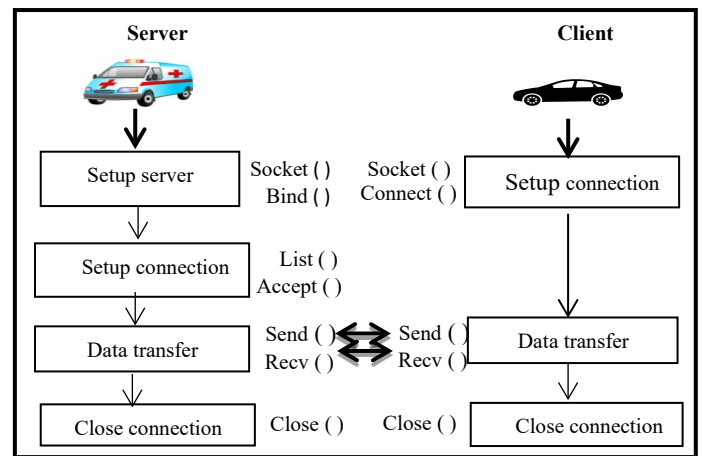


Figure 2: Structure and Flow Chart Socket Programming

3.3. Speech Recognition

The final goal of this work is to implement a hand free personal assistance for car's a driver which uses speech recognition to convert speech into text and in the other side (other cars) convert the text into speech. By doing so, the proposed system will not effect on the drivers focus on the road. The proposed system is achieved by using different libraries based python such as: speech recognition, Pyaudio and espeak. The speech recognizer has been designed by using Google's speech recognition application

interface (API) [17, 18]. Figure 3. Shows the proposal voice to text and text to the voice system design of an ambulance and cars.

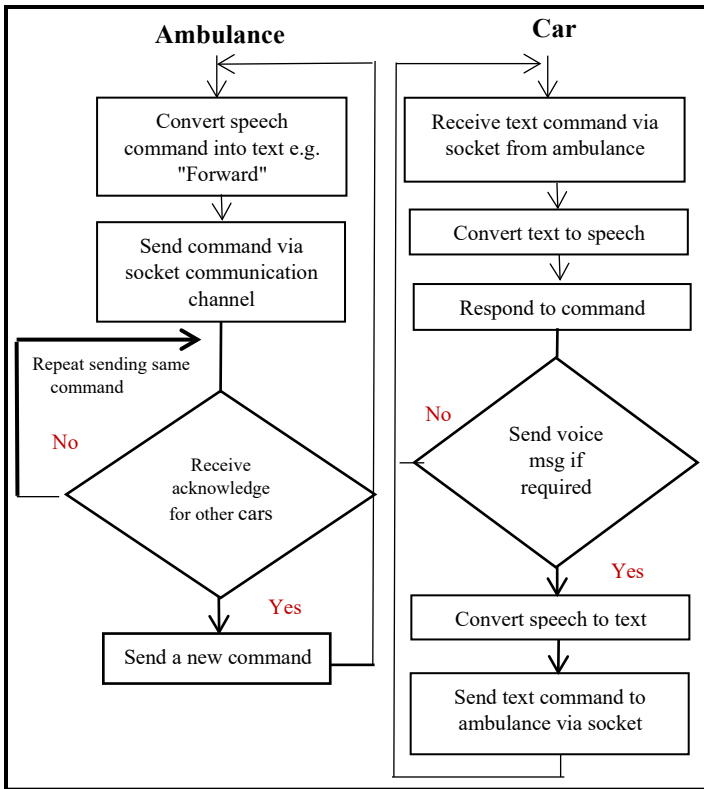


Figure 3: Proposed Voice to Text and Text to Voice System Design of an Ambulance and Cars.

4. Proposed System Description

Figure 4. Shows system design; it consists of a control and emergency monitoring and tracking CEMT which monitor and communicate with ambulance by using MQTT protocol. The CMET is located in the hospital, its responsibility is to send command and arrange the work of ambulance if there any emergency case. Also, it tracks the ambulance when moving in the city. Each ambulance vehicle can communicate with other cars on the road as a (V2V) by means of voice to text and text to voice; this has been done by using socket programming along with MQTT protocol. The proposed system works as follows:

- When an emergency case is happened for a patient. The CMET send a message to ambulance in the hospital via MQTT. The message structure is shown in Figure 5. Which include task such as the location of the patient and his status, etc.
- When an ambulance moves to the patient location, it will send its latitude and longitude to the CMET which will convert it to a location in the maps. For this, a google maps has been used and a python library "geopy" is used.
- When ambulance responded to that order. It will send its locations to the CEMT each time it enters a new region.
- The ambulance will broadcast its IP address and list of ports for socket communication using MQTT such that each car in that region will receive the IP and ports of the ambulance.

- The driver of the ambulance can start conversation with neighboring cars by sending voice message which would be converted into a text that is sent to other cars.
- Cars receive text message and convert it into a voice message and respond to the required command.

In these works four commands have been proposed, namely: **Forward, Right, Left, and Kill**. If the ambulance drivers want to speed up forward and there is a car in front of the ambulance. Then the driver can send a voice command message **"Forward"** this voice message is converted into a text message and sent using a socket interface. When the front car receives a text message it will convert it into a voice message again. By doing so, the process will not disturbed the drivers. The same is done with the other commands left and right. The **"kill"** command will close any connection between the ambulance and other cars preparing to enter a new region where the process is repeated again.

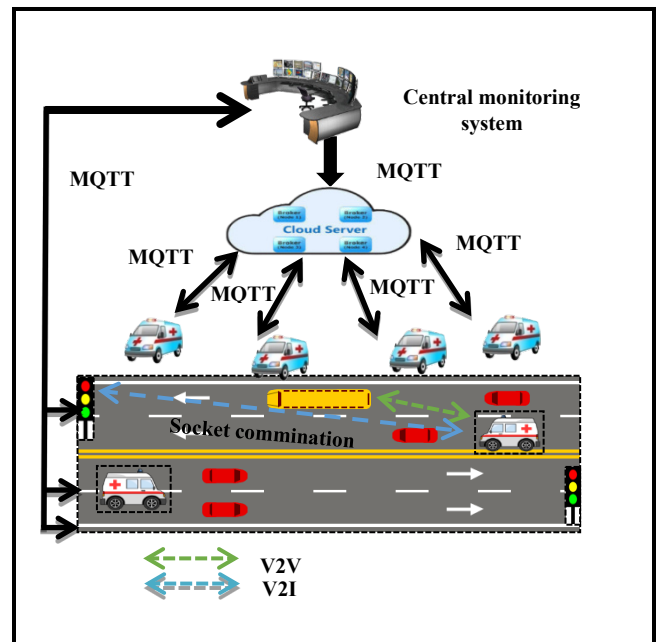


Figure 4: Propose System Design.

Name contact	: Noor alaa
Task No.	: BG096002
Location Patient	: Saydia
Proposed path	: Emergency Event
Patient (Gender, Name, Age)	: Male, Ali, 55
Status Patient	: Dangerous
Accident Type	: Car Accident

Figure 5: Standard Messages for Car Ambulance.

5. Result and Discussion

A monitoring and tracking system of ambulance has been designed which uses two techniques MQTT as an IoT protocol and socket programming. MQTT is used when the ambulance and vehicle are away from the central units which give the required commands to ambulance. While socket communication is used to transfer immediate and direct commands between ambulance and another vehicle to clear the path for the ambulance and hence decrease time for the patient to reach the hospital. Fig. 6 (A) and (B) shows a sample of speech recognition and commands. The proposed system has been designed and implemented experimentally and tested by using an embedded system represented by a raspberrypi3 which is the main device used in this work, it has a 1.4 GHZ, quad core process 1G SDRAM, HDMI, USB ports, DSI display port and other features provide fast processing and internet connectivity. Google speech recognition API has been used which is not quite accurate for any accent and take same times to recognize the speech depends on the connection speed of the internet. The proposed system is a promising technique which will enhance healthcare services provided by health organization to improve the life of people.

```

pi@raspberrypi: ~/Desktop/final
File Edit Tabs Help

pi@raspberrypi:~/Desktop/final $ python publish_socket.py
192.168.0.102

Socket created.
Socket bind complete.
Connected to: 192.168.0.108: 48748
Say a command :left, right, forward, or kill: left
OK,
OK, Left Road is clear
Data has been sent!
Say a command :left, right, forward, or kill: forward
OK,
OK, Forward Road is clear
Data has been sent!
Say a command :left, right, forward, or kill: kill
pi@raspberrypi:~/Desktop/final $
    
```

(a)

```

pi@ali: ~/Desktop/final
File Edit Tabs Help

uealsa.device'
ALSA lib conf.c:4528:(snd_config_evaluate) function snd_func_refer returned error: No such file or directory
ALSA lib conf.c:4996:(snd_config_expand) Args evaluate error: No such file or directory
ALSA lib pcm.c:2495:(snd_pcm_open_noupdate) Unknown PCM bluealsa
ALSA lib pcm_hw.c:1713:(snd_pcm_hw_open) Invalid value for card
ALSA lib pcm_hw.c:1713:(snd_pcm_hw_open) Invalid value for card
ALSA lib pcm_hw.c:1713:(snd_pcm_hw_open) Invalid value for card
ALSA lib pcm_hw.c:1713:(snd_pcm_hw_open) Invalid value for card
Cannot connect to server socket err = No such file or directory
Cannot connect to server request channel
jack server is not running or cannot be started
JackShmReadWritePtr::~JackShmReadWritePtr - Init not done for -1, skipping unlock
JackShmReadWritePtr::~JackShmReadWritePtr - Init not done for -1, skipping unlock
left command received and respond
forward command received and respond
connection closed
    
```

(b)

Figure 6: Practical Implementation of Ambulance Voice Chat Based Socket Programming.

Conclusion

In this work, a CMET control the operation of the ambulance through MQTT protocol. Also, socket communication is implemented for voice chat between ambulance and other cars in the roads. The speech commands are converted into a text by using Google API. The speech recognition is not accurate enough, because the process depends a speech accent, also, ambient could affect the accuracy of recognition. Multi experimental and different accent has been used to reach a good accuracy finally.

References

- [1] A., Salahuddin, M.A., Hussini, S.J., Khreishah, A., Khalil, I., Guizani, M. and Al-Fuqaha, "A Smart cities: A survey on data management, security, and enabling technologies" in IEEE Communications Surveys & Tutorials, vol. 19, pp. 2456-2501, 2017.
- [2] Tammishetty, S., Ragunathan, T., Battula, S.K., Rani, B.V., RaviBabu, P., Nagireddy, R., Jorika, V. and Reddy, V.M, "IOT-based traffic signal control technique for helping emergency vehicles" in Proceedings of the First International Conference on Computational Intelligence and Informatics, pp. 433-440. Springer, Singapore, 2017.
- [3] Wang, S., Wang, J., & Yu, Z, "Privacy-Preserving Authentication in Wireless IoT: Applications, Approaches, and Challenges" in IEEE Wireless Communications, vol. 25, pp. 60-67, 2018.
- [4] Chatrpathi, C., M. Newlin Rajkumar, and V. Venkatesakumar, "VANET based integrated framework for smart accident management system" in: International Conference on Soft-Computing and Networks Security (ICSNS), pp. 1-7, 2015.
- [5] Venkatesh, H., Perur, S.D. and Jagadish, M.C, "An approach to make way for intelligent ambulance using IoT" in International Journal of Electrical and Electronics Research, vol.3, 2015.
- [6] Mittal, Y., Toshiwal, P., Sharma, S., Singhal, D., Gupta, R. and Mittal, V.K, "A voice-controlled multi-functional smart home automation system" in Annual IEEE India Conference (INDICON), pp. 1-6, 2015.
- [7] Lakdawala, B., Khan, F., Khan, A., Tomar, Y., Gupta, R. and Shaikh, A, "Voice to Text transcription using CMU Sphinx a mobile application for healthcare organization" in Second International Conference on Inventive Communication and Computational Technologies (ICICCT), pp. 749-753, 2018.
- [8] Misbahuddin, S., Zubairi, J.A., Saggaf, A., Basuni, J., Sulaiman, A. and Al-Sofi, "A.: IoT based dynamic road traffic management for smart cities" in: 12th International Conference on High-capacity Optical Networks and Enabling/Emerging Technologies (HONET), pp. 1-5, 2015.
- [9] Ahsan, M., Haider, J., McManis, J. and Hashmi, M.S.J, "Developing intelligent software interface for wireless monitoring of vehicle speed and management of associated data" IET Wireless Sensor Systems, vol. 6, pp. 90-99, 2016.
- [10] Leelavathi T C, Dr. Shivalcelavathi B G, Shubha B, "IoT for Smart Car using Raspberry PI" International Research Journal of Engineering and Technology (IRJET), vol. 3, pp. 2395-0056, 2016.
- [11] Dhall, R. and Solanki, V, "An IoT Based Predictive Connected Car Maintenance", International Journal of Interactive Multimedia & Artificial Intelligence, vol. 4, 2017.
- [12] Bhawiyuga, A., Sabriansyah, R.A., Yahya, W. and Putra, R.E, "A Wi-Fi based electronic road sign for enhancing the awareness of vehicle driver", Journal of Physics: Conference Series, Vol. 801, pp. 012085. IOP Publishing, 2017.
- [13] Maata, R.L.R., Cordova, R., Sudramurthy, B. and Halibas, "A Design and Implementation of Client Server Based Application using Socket Programming in a Distributed Computing Environment" in IEEE International Conference on Computational Intelligence and Computing Research (ICICR), pp. 1-4, 2017.
- [14] Hejazi, H., Rajab, H., Cinkler, T. and Lengyel, L, "Survey of platforms for massive IoT" in IEEE International Conference on Future IoT Technologies (Future IoT), pp. 1-8, 2018.
- [15] Zulkefli, M.A.M., Mukherjee, P., Sun, Z., Zheng, J., Liu, H.X. and Huang, P, "Hardware-in-the-loop test bed for evaluating connected vehicle applications" Transportation Research Part C: Emerging Technologies, vol. 78, pp. 50-62, 2017.

- [16] Barbon, G., Margolis, M., Palumbo, F., Raimondi, F. and Weldin, N, "Taking Arduino to the Internet of Things: the ASIP programming model". *Computer Communications*, pp. 128-140, 2016.
- [17] Mehrabani, M., Bangalore, S. and Stern, B, "Personalized speech recognition for Internet of Things" in *IEEE 2nd World Forum on Internet of Things (WF-IoT)*, pp. 369-374, 2015.
- [18] Gharaibeh Chayapathy, V., Anitha, G.S. and Sharath, B, " IOT based home automation by using personal assistant" in *International Conference on Smart Technologies for Smart Nation (Smart Tech Con)*, pp. 385-389,2017.

Designing and Using a MySQL Database for Human Resource Management

Evaristus Didik Madyatmadja*, Chelsea Adora

Information Systems Department, School of Information Systems, Bina Nusantara University, 11480, Indonesia

ARTICLE INFO

Article history:

Received: 04 October, 2019

Accepted: 26 November, 2019

Online: 12 December, 2019

Keywords:

Database Design

Relational Database

HRIS

ABSTRACT

In this paper, we would like to discuss the methods and ideologies used to create a database to be used for Human Resource purposes. Because we want this database to be accessible anywhere at any time, it is safe to conclude that an internet-based (web-based) database would work best, therefore we chose MySQL as the database management system. Before diving deep into the making of the database itself, it is important to understand certain basics of database design and the phases of the database life cycle itself. This paper will conclude on a few of the basic things to understand before designing a database for Human Resource Management on MySQL.

1. Introduction

Every company in the world has more than one person working for its purpose. These people involved in a company are what we know as employees, human resources to a company that drives the company closer to its goal and purpose. As a company grows, it will need more employees to expand its wings [1], and to some Human Resource Managers, it is a pain to organize and keep tabs on all the human resource data. The bigger the company, the harder the Human Resource Managers will have to work to keep the data accurate and tidy.

At the end of 2018, the Economist Intelligence Unit reports that 82% of companies in the world (taking samples) plan to start using or increasing the use of a human resource database. These companies also realize the importance of good management of human resource data by implementing an employee database.

Not that doing all the human resource management work manually is painful and tiring for the Human Resource Managers and administrators, it may also cause the company and owner some great loss. Imagine having a construction company with hundreds of workers working different shifts and all their attendance data must be recorded manually using paper and pen without supervision. The workers might put in false data on their attendance record resulting in a big loss for the company where the company pays a big amount of money for salaries and wages while the construction project itself has not progressed much.

Another problem is that by doing every human resource process manually, it will take longer for the Human Resource

Manager or administrator to work on the employees' payroll calculation. Not to mention, there is a possibility that there may be an error in the payroll calculation due to the manual work of reading and counting the attendance data on a calculator to produce a paycheck.

All the problems stated above may be solved by having a database that covers human resource management, from employee personal data, employee attendance data, to their payroll data. Even in Hong Kong, industries have confirmed that one of the best things they gained by having a human resource computer system in assisting their human resource activities is the seamless flow of data [1]. By having all human resource data recorded in an organized database, the accuracy of data is definite, resulting in accurate budgeting for human resources (salaries & wages). This also means that the Human Resource Managers can work faster with the human resource database working alongside as an assistant [2].

When making a database for a specific concern, like human resources perhaps, assessment of the needs of the company is needed. For more universal use, a free, open-source database will be discussed further, along with its web-based benefit. Because MySQL is web-based and the fact that it works on a server [3], the human resource database will be accessible anywhere and at any time if there is an internet connection, that is if the company decides to use it as an internet-based system. Either way, by using the localhost or the internet, MySQL has a more general purpose and can serve both needs.

According to a company in Indonesia that has yet to use a human resource database, employee data storage, especially those related to attendance, still has many shortcomings because

*Evaristus Didik Madyatmadja, Jl KH Syahdan No. 9, Palmerah, Jakarta, Indonesia, Contact No: +62811254952, Email: emadyatmadja@binus.edu

attendance data collection (including overtime calculations) is still done manually. Because attendance data collection is still done manually using paper and pens, fraud often occurs in filling attendance and overtime information. This fraud resulted in huge losses for this company because the nominal salary paid to employees of this company is not in accordance with the development of the project. In addition, there were also errors in entering data from paper into digital form (Microsoft Excel). As a result of these errors is the administrator must check the data that has been entered a few times and correct errors that exist to ensure that the data entered is correct. For this reason, this company requires a database system that can record employee attendance factually to reduce these losses and facilitate the work of the human resource department or commonly known as HRD.

2. Definition of Human Resource Information System

Human Resource Information System (HRIS) is a software that keeps all data regarding human resource management activities, from the employee master data, employee attendance data, payroll data, even their performance (for more advanced measures) in a centralized manner. Improvement in performance levels is very much possible when using a proper Human Resource Information System, and thus allows consultation activities to take place, such as discussion and coaching or mentoring [4]. Using HRIS also gives us data that are more accurate and consistent, therefore resulting in accurate processed data [5]. Human resource information systems (HRIS) are "combinations of databases, computer applications, and hardware also software needed to collect / record, store, manage, send, present, and manipulate data for human resources", as stated in [6].

Not using an automated Human Resource System may lead to fraud and data inconsistencies. Using an automated Human Resource System on the other hand, helps an organization in strategically organizing human resource data, as well as help top-level management in human resource related decision making [7]. An automated Human Resource System has been proven to bring benefits such as effectiveness and efficiency in the Human Resource Department, as there may be a downsizing in the HR staff [8].

3. Development of Human Resource Information Systems

Human Resource Information Systems may seem like a senior technology to some, but for companies in developing countries, HRIS may seem relatively new. Technology has brought different results in terms of effectiveness in helping manage human resources. This depends on the abilities of the user in using the technology itself [9].

The size of the company impacts what gains and losses will be received by the implementor of the HRIS. Larger companies which already possess technological properties will most definitely feel more benefits as they can retrieve important staff data in a flash. Small businesses may not have the resources and technical competence to do such things.

A simple and good alternative to creating a customized HRIS is to use a pre-packaged HRIS software instead. To buy the most suitable package for a company, it is necessary to contact the supplier or vendor and compare all of the candidate products to

find the HRIS product that best suits the requirements of the business.

Most HRIS implementations fail due to the lack of commitment from senior managers. Without having the support of senior managers, the implementation of the HRIS will most likely not be prioritized and the resources needed will not be provided to be used [10]. One of the most important resources that can be provided by senior managers are financial resources, which plays a critical role in an HRIS implementation in an organization [11]. Senior managers need to understand exactly why an HRIS in managing the organization's human resource activities is important, and the business values they will gain after implementing an HRIS [12]. By understanding such matters, senior managers may support the implementation by providing a bigger budget. This money provided by senior managers will not only play a role in the implementation, but also operation and maintenance. More promotional efforts and action plans are needed to show the specific benefits of using HRIS if senior management knows the benefits that can be achieved by implementing HRIS.

4. Research Methodology

This research regarding a Human Resource Database System uses the Literature Review Methodology. A literature review is a compilation of theories, findings, and research results used as references in a research to get a better understanding on a problem and its proposed solution.

A Literature Review is more or less analysis in the form of criticism (construction or fall) of the research being done on a specific topic or question in a part of science. The literature review is a scientific history of a particular problem.

Materials for the literature review may be found from trusted sources on the internet, books, articles, newspapers, or other sources that are confirmed as press. A good review of the literature should be relevant, current and adequate. The theoretical basis, the theoretical review and the literature review are several ways of conducting the literature review.

- Formulating the problem. Choose a topic that matches your topic and interest. The problem must be written completely and accurately.
- Literary search. Look for relevant literature for research. Get an overview of research topics. When looking for related materials from previous studies, it is important to make sure that the source of these materials is trusted press, offline or online.
- Evaluating the data. Not only literature, but data can also be obtained from previous studies. These data, qualitative or quantitative, need to be analyzed according to the problem statement of the research.
- Analyzing and interpreting. Discuss and find and summarize the literature. After gathering all the materials and data, start analyzing everything gathered from the point of view of the problem. Summarize all the materials and propose a solution based on all the trusted materials.

5. Introduction to Database

According to [13], A database is an integrated collection of data that is stored, managed and centrally controlled. Databases usually store information about entities in large numbers (tens, hundreds, to thousands of entities). Information stored in the database is the entity's attributes (for example, name, price, and account balance) and the relationship of an entity with other entities (for example, which orders belong to which customers). The database also stores descriptive information about the data, such as field names, allowable value restrictions, and controls access to sensitive data items.

The database has its own language called query. There are several kinds of languages in the query where the explanation is as follows:

- Data Definition Language (DDL), which is a language that governs the making of structures from a database. DDL is not related to data that fills in the database structure. Some examples of DDL are CREATE, DROP, and ALTER.
- Data Manipulation Language (DML), which is a language that governs changes to database contents. Some examples of DML are INSERT, UPDATE, DELETE, and SELECT.
- Data Control Language (DCL), which a language that regulates anyone who can access a part of the database designed. Some examples of DCL are GRANT and REVOKE.

6. Database Management System

According to [14], a Database Management System (DBMS) is a software system that is created specifically to facilitate the management of databases. A Database Management System is a software that allows users to create, access and manage a database. In the database approach, each file in each department is stored on a database server with a new designation, namely the table. Each program can then access parts of the database as necessary.

At the moment there are many database management systems available to meet the business needs of every company. Each database management system has advantages and disadvantages of each, where the decision to choose the right candidate is certainly based on the scale, budget, and needs of the company itself. According to a survey conducted by DB-Engines in May 2019, the most commonly used database management system is Oracle, MySQL, and Microsoft SQL Server.

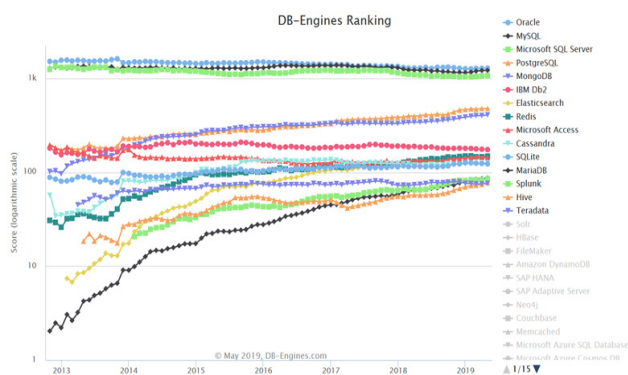


Figure 1: DBMS Ranks by DB-Engines

In accordance with the needs and business scale of the organization, MySQL is one of the best candidates to become a database management system from an employee database that will be built and implemented. That's because MySQL is not too complex and sufficient for the business scale of the organization which consists of hundreds of employees, unlike Oracle which is very complex and is more aimed at companies with a much larger scale. Because the application to be built is also web-based, so a database that is suitable for use and in accordance with the scale of the company the organization is MySQL. In addition to these factors, MySQL is very affordable compared to Oracle, where MySQL is a Database Management System (DBMS) that is free to use and is licensed by the GNU General Public License, while Oracle is a paid DBMS (Express version can be accessed free of charge, but features -The DBMS features are limited and only recommended for educational and testing use).

MySQL is a database management system that is used through the web where MySQL operates on a server [3]. This provides a good opportunity for writers to develop prototypes related applications using a web base. Our desire to build a prototype of a web-based application is supported by the Information Services Group's statement in 2018, namely that 48% of professional workers in the field of Human Resources want to switch to internet-based Human Resource applications, or familiarly known as the cloud.

7. Database Life Cycle

In order to design a database that is usable in the long run, there are a few steps that should be followed. One of the most general and common guidelines used is the Database Life Cycle. The steps of the Database Life Cycle are as follows.

7.1. Database Planning

Database Planning include management activities that enable the Database Life Cycle's success in effective and efficient implementation. This step involves defining the mission statement dan mission objective. The Mission Statement defines the main purpose of the database application, the purpose of this database design project, and clarifies the flow of making a database application so that the design can be carried out effectively and efficiently. Examples of mission statements are "The purpose of creating a database for XYZ Inc. is to facilitate all the activities of XYZ Inc. clients who use their services and also their daily staff so that the business processes carried out can run efficiently with the availability of information that is complete in real-time. ". Mission Objectives are written as a list that contains further details of the mission statement. These further details can be in the form of general features that will be developed in the new database system. One example of a mission objective is "To maintain (insert, update, delete) data on the hotels, rooms, guests, and bookings".

7.2. System Definition

System Definition is the process of determining and elaborating the boundaries and scope of the database system development project and the main user view of the database system. What is meant by the user view here is the access rights of a role (such as manager or supervisor) or department (such as

marketing or human resources) to data entities in the database to be developed.

7.3. Requirements Collection and Analysis

Requirements Collection and Analysis is the process of gathering the needs of users or companies so that the database system is designed right on target and in accordance with company needs [14]. These company needs are documented in the requirements specifications. A few approaches that may be used here are the Centralized Approach, View Integration Approach, or both of them combined. Some of the techniques said before can be carried out in accordance with the scope of the project and the company, as well as the conditions of the project itself, such as the availability of time and resources that support research. All techniques can be used for a project, but a project can only use one or two because the scope is too large or resources are not available, and time is limited.

7.4. Database Design

Database Design is basically the designing of the database from the conceptual, logical, and physical model. There are a few approaches to this step which are Bottom-up, Top-down, Inside-out, and Mixed [14]. The Bottom-up Approach is an approach where data modeling starts from the properties or attributes, then a larger entity is identified. The bottom-up approach starts from the initial attributes (entities and relationships) that are analyzed by the relationship between attributes, then relationships are formed that represent the types of entities and relationships between entities. This approach is suitable for simple database designs with relatively fewer attributes. The Top-down Approach is an approach where data modeling starts from large entities first, then attributes are identified. The top-down approach starts with developing a data model that consists of several or many entities and relationships, then identifies low-level entities, relationships, and associations between attributes. This approach is explained by the Entity Relationship Diagram, which starts with the identification of entities and the relationships between entities. The Inside-out is an approach where the modeling of data starts from a larger cup first, then a smaller cup. This approach is related to the bottom-up approach, but it is slightly different from the initial identification of the main entity which then spreads to the entities, relationships, and other attributes that were first identified. The Mixed Approach is a combination of the Top-Down and Bottom-Up approach where both are used for different aspects and then a merging of the results of the data model from both.

7.5. DBMS Selection

DBMS Selection is a stage in the Database System Development Life Cycle where there will be a comparison between outstanding DBMS products and the selection of DBMS that is deemed most suitable for database design projects. This DBMS selection can also be done before the Database Design stage to ensure the physical database design of the database is designed in more detail and in accordance with the technical needs of the selected DBMS. Several aspects of the company must be taken into consideration when choosing a DBMS to be the foundation of the database to be built, such as the scale of the company's business and the company's budget for the database design project itself. The selection of the DBMS must also

consider the needs and requirements of the company that have been collected at the requirements collection stage. Each DBMS has its own features, strengths, and weaknesses, so the chosen DBMS must be truly in accordance with the needs of the company. The main steps for selecting a DBMS are defining reference study terminology, registering two or three products, product evaluating, and choosing one that best fits the needs and create product reports for senior management.

7.6. Application Design

Application design is a process in which the user interface and features of a database application are described in detail. It is very important to make the application as user-friendly as possible to ensure the database will be used in the future [15-16]. In the application design process, there are two main processes that are key to the application design, the transaction design and the user interface design. The Transaction Design is a transaction flow in which there are actions that can access or change the contents of the database. In other words, transaction design is the entire business process in the context of a company that can access or change the contents of the company database. In general, transaction design can be done by creating a Use Case Diagram, and sometimes an Activity Diagram to describe the flow of the overall process. User Interface Design in the other hand is the process of designing the final appearance of a database system that will be seen by end-users. The main purpose of the user interface design activity is to produce a display design that is easy to use by users or more familiarly referred to as user-friendly.

7.7. Prototyping

Prototyping is an activity of making a prototype of the system as a whole. A Prototype itself is a working model or model that serves to display some features or functionality of the entire database system that is built [14]. A prototype is a tangible artifact, not something abstract. In general, there are two types of prototypes, namely Offline or paper prototype and Online or prototype software. The purpose of making a prototype is to ensure that all the needs and expectations of the end-user are met before making a real application. There are several techniques that can be used to make prototypes, some of which are as follows:

- **Representation:** Representation is a representative of a database system that as a whole is quite large. The representation can be in the form of a simple drawing or paper sketch or computer simulation.
- **Precision:** Precision means that the prototype that is designed must be determined whether it will be made in detail, or made in outline only to introduce some key features to the end-user.
- **Interactivity:** Interactivity refers to the interaction that occurs between the user and the prototype, whether only watch-only or whether the prototype is fully interactive. Interactivity is closely related to Representation.
- **Evolution:** Evolution refers to the use of the prototype itself. There are two types of prototypes in this evolutionary context, throwaway and iterative. Throwaway means that the prototype is made only as presentation material that will not be used again after the

presentation to the user. Iterative: Iterative means that the prototype that is made will continue to be developed until it becomes an application that will actually be used operationally by the company.

7.8. Implementation

Implementation is the physical realization of database design and software design. At this stage, the realization of the database is achieved by using Data Definition Language (DDL) from the selected DBMS. Apart from the database side, the creation of Graphical User Interface (GUI) is also done as a form of implementation in terms of its application.

7.9. Data Conversion and Loading

Data Conversion and Loading is an activity to fill tables that have been made before with real company data [14]. Data Conversion and Loading is a mandatory activity so that the database system can be used operationally by the company. Conversion here can mean changing the data format from one format to another so that it can be used in a new database system. Company data itself can be retrieved from legacy systems or even paper-based manual records. Including real data is somewhat important, even if it is still in the early stages of the process. Not having them included from the start may cause the developers to modify everything they have built just to make it compatible with the data [17].

7.10. Testing

Testing is an activity to run a database system that is designed with the aim of finding errors or errors that exist. With testing, the designer prevents errors when the system has been used operationally which results in hampered the company's daily activities. In testing, the designer not only directs attention to the coding of the system but also the environment and ambiance of the system. Before carrying out testing, the person responsible for testing must understand the quality standards of what the test intends to do in order to achieve the appropriate testing results.

7.11. Operational Maintenance

Operational Maintenance is the activity of monitoring activities done within the system in order to maintain the performance of the system while the business runs, as usual, using a database system that has been developed. In addition to maintaining the performance of the database system, it is also necessary to collect the requirements for the next Database System Development Life Cycle.

Sadly, developing a database most likely requires knowledge on database technology and how it works, as well as its syntax and other information that is quite exclusive to the technological world [18-21]. But fortunately, as technology develops, studies and experts have come up with approaches that allow even people who are unfamiliar with database programming to create web applications and their databases easily. A few examples of the approaches said are model-driven [19, 21] and goal-driven approaches [22, 23].

8. Discussion

After analyzing the ongoing business processes, there are several problems that can be corrected to reduce the losses experienced by the company. Some of these problems are:

- Payroll costs are inflated because of fraud in recording attendance using only paper and pens without close supervision.
- The cost of paying overtime wages that are inflated due to fraud in recording overtime duration.
- The results of work that are not in accordance with the cost of salaries and overtime wages incurred (the progress of the project undertaken is not comparable with statements of overtime and work from employees).
- Frequent redundancy and inconsistencies in employee data, especially if there are changes in employee personal data or revisions to employee attendance data.
- HRD employees have difficulty finding data that has long been due to manual archive storage without the existence of a database that is a centralized company data storage.

Analysis of business processes that run at the company has exposed the needs of the company which is a database system for the management of the company's workforce. From the database system to be designed, the expectation of the organization is that the database system can fulfill the following:

- The database system can be the actual data storage regarding employee attendance (with the help of attendance machines). This means that the database system can read data in the extension format produced by the attendance machine.
- The database system can help HRD employees in data searching so that data search can be done quickly and accurately. This means that the database system must be able to display the data needed by HRD employees when HRD employees need them.
- To accelerate the manual recording transition to database system usage, the user interface of the database application that is designed is expected to be user-friendly so that it is easy for HRD employees to use to input and pull data output.
- The database system can store data without duplication, redundancy, and inconsistency, so the data drawn by HRD employees is the actual or most recent data.

Based on the problems and needs of the database system that has been described above, the author can suggest a solution which is making a database system for the management of the organization's human resource with the following explanation:

- Creating a database for the organization which will be a centralized data repository for all HRD operational activities of the organization such as employee personal data collection, employee attendance records, also the calculation of salaries received by employees.
- Making a prototype of a web-based application that will be a bridge for users (HRD employees of the organization) to input data into the database, process data, and also receive output information needed.

By adopting the solution, the organization can feel some business values that can be beneficial for the organization, some of them are as follows:

- Can access the right data quickly, without inconsistencies and redundancy.
- Can reduce the burden of excessive salary and overtime pay that is not in accordance with the progress of the project being carried out because recording absences is difficult to commit fraud.
- HRD employees can process salaries faster and easier, without having to count them manually using a calculator every month.

9. Conclusion

Having an HR database is a necessity in a company, whether it is a global company or even a company with a smaller scope. Business processes that were running before the database system implementation brought many losses for the organization. This is because the manual recording that is easily done by employees who are absent. Employees who are absent can be easily recorded as attending. Employees who are not overtime can be recorded as overtime due to records that use paper and pens. This resulted in a very large expenditure on the part of employee salaries, which is not comparable with the progress of the organization. This can be avoided if the organization uses an absent engine and database system that can ensure employee attendance data is accurate to the real situation. Without a proper HR database working as an HRIS, it would be a pain for the HR Manager to work on the employee data manually and produce the paycheck for each employee. Having an HRIS will ensure the data consistency and accuracy, thus resulting in accurate payroll calculation. For a more global approach, the DBMS used for this HRIS will be MySQL since it runs on a server and is web-based, allowing both interests to fit in, whether it is using localhost or the internet. This MySQL database will be accessed through a web-based application, which is another plus since now the human resource database can be accessed anywhere at any time, if the user has internet access and a device that can access websites through browsers. HR databases have been proven to be of help for a long time, however, to design an HR database for specific needs, there are several things that should be understood. These things are what databases are, what DBMS are and why we are choosing the DBMS we have chosen (in this case, MySQL), the Database Life Cycle which will be the overall guideline of the process.

Conflict of Interest

The authors declare no conflict of interest.

Acknowledgment

We thank Prof. Dr. Ir. Harjanto Prabowo, MM, as the Rector of Bina Nusantara University, Dr. Yohannes Kurniawan, S.Kom., S.E., M.MSI, as the Dean of Information Systems Faculty and Head of Information Systems Department, and Dr. Tanty Oktavia, S.Kom., MM, as the Head of Information Systems Study Program for all the support in the making and submission of this paper.

References

- [1] E.W.T. Ngai F.K.T. Wat, "Human resource information systems: a review and empirical analysis. *Personnel Review*, Vol. 35 Iss 3, 297 – 314, 2006. doi: 10.1108/00483480610656702

- [2] Z. Hussain, J. Wallace, N. E. Cornelius, "The use and impact of human resource information systems on human resource management professionals", *Information & Management*, Vol. 44 Iss 1 pp. 74-89, 2007. doi: 10.1016/j.im.2006.10.006
- [3] B. Schwartz, P. Zaitsev, V. Tkachenko, *High-Performance MySQL*, Third Edition, O'Reilly Media, Inc., 2012.
- [4] S. Strohmeier, "Concepts of e-HRM consequences: a categorization, review and suggestion", *The International Journal of Human Resource Management*, 20:3, 528-543, 2009. doi: 10.1080/09585190802707292
- [5] David Grant, Sue Newell, "Realizing the strategic potential of e-HRM", *The Journal of Strategic Information Systems*, 22:3, 187-192, 2013. doi: 10.1016/j.jsis.2013.07.001
- [6] Beckers, A.M., Bsat, M.Z., "A DSS classification model for research in human resource information systems", *Information Systems Management*, Vol. 19 No. 3, 41-50, 2002. doi: 10.1201/1078/43201.19.3.20020601/37169.6
- [7] Marler, J. H., Parry, E., "Human resource management, strategic involvement and e-HRM technology", *The International Journal of Human Resource Management*, 27(19), 2233-2253, 2015. doi: 10.1080/09585192.2015.1091980
- [8] Strohmeier, S., "Research in e-HRM: Review and implications", *Human Resource Management Review*, 17(1), 19-37, 2007. doi: 10.1016/j.hrmr.2006.11.002
- [9] Stone, D. L., Deadrick, D. L., Lukaszewski, K. M., Johnson, R., "The influence of technology on the future of human resource management", *Human Resource Management Review*, 25(2), 216-231, 2015. doi: 10.1016/j.hrmr.2015.01.002
- [10] Kovach, K.A., Hughes, A.A., Fagan, P., Maggitti, P.G., "Administrative and strategic advantages of HRIS", *Employment Relations Today*, Vol. 29 No. 2, 43-8, 2002. doi: 10.1002/ert.10039
- [11] Sadri, J., Chatterjee, V., "Building organizational character through HRIS", *International Journal of Human Resources Development and Management*, Vol. 3 No. 1, 84-98, 2003. doi: 10.1504/IJHRDM.2003.001048
- [12] Bondarouk, T., Schilling, D., Ruël, H., "eHRM adoption in emerging economies: The case of subsidiaries of multinational corporations in Indonesia", *Canadian Journal of Administrative Sciences / Revue Canadienne Des Sciences de l'Administration*, 33(2), 124-137, 2016. doi: 10.1002/cjas.1376
- [13] Satzinger, Jackson, Burd, *System Analysis and Design with the Unified Process*, Pearson, 2012.
- [14] Connolly, T., Begg, C., *Database System - A Practical Approach to Design, Implementation, and Management*, Pearson, 2015.
- [15] Haigh, I. D., Wadey, M. P., Gallop, S. L., Loehr, H., Nicholls, R. J., Horsburgh, K., Brown, J. M., Bradshaw, E., "A user-friendly database of coastal flooding in the United Kingdom from 1915-2014", *Sci Data* 2, 150021, 2015. doi: 10.1038/sdata.2015.21
- [16] Fan, J., Li, G., Zhou, L., "Interactive SQL query suggestion: Making database user-friendly", In *Proceedings of the 2011 IEEE 27th international conference on data engineering (ICDE '11)*, 351-362, Washington, DC, USA: IEEE Computer Society, 2011. doi: 10.1109/ICDE.2011.5767843
- [17] Cross SS, et al., "How to design and use a research database", *Diagnostic Histopathology*, 2017. doi: 10.1016/j.mpdhp.2017.09.005
- [18] Borges, C. R., Macias, J. A., "Feasible database querying using a visual end-user approach", In *Proceedings of the 2nd ACM SIGCHI symposium on Engineering interactive computing systems (EICS '10)*(pp. 187-192). New York, NY, USA: ACM, 2010. doi: 10.1145/1822018.1822047
- [19] Brdjanin, D., Maric, S., "Towards the automated business model-driven conceptual database design", *Advances in Databases and Information Systems Advances in Intelligent Systems and Computing*, 186, 31-43, 2013.
- [20] Deng, Y., Churcher, C., Abell, W., McCallum, J., "Designing a framework for end-user applications, end-user development", *Lecture Notes in Computer Science*, 6654, 67-75, 2011. doi: 10.1007/978-3-642-21530-8_7
- [21] Fraternali, P., Comai, S., Bozzon, A., Toffetti, C. G., "Engineering rich internet applications with a model-driven approach", *ACM Trans (p. 47)*, Web 4, 2, Article7, 2010. doi: 10.1145/1734200.1734204
- [22] P. Nicolaos, T. Katerina, "Diagnosing user perception and acceptance using eye tracking in web-based end-user development", *Computers in Human Behavior* 27, 23-37, 2017. doi: 10.1016/j.chb.2017.02.035
- [23] P. Nicolaos, T. Katerina, "Simple-talking database development: Let the end-user design a relational schema by using simple words", *Computers in Human Behavior* 48, 273-289, 2015. doi: 10.1016/j.chb.2015.02.002

Fuzzy Modelling using Firefly Algorithm for Phishing Detection

Noor Syahirah Nordin¹, Mohd Arfian Ismail^{1,*}, Vitaliy Mezhujev², Shahreen Kasim³, Mohd Saberi Mohamad^{4,5}, Ashraf Osman Ibrahim⁶

¹ Faculty of Computing, College of Computing and Applied Sciences, Universiti Malaysia Pahang, 26300, Malaysia.

² FH JOANNEUM University of Applied Sciences, Institute of Industrial Management, Austria.

³ Soft Computing and Data Mining Centre, Faculty of Computer Science and Information Technology, Universiti Tun Hussein Onn, Johor, Malaysia.

⁴ Institute for Artificial Intelligence and Big Data, Universiti Malaysia Kelantan, City Campus, Pengkalan Chepa, 16100 Kota Bharu, Kelantan, Malaysia.

⁵ Faculty of Bioengineering and Technology, Universiti Malaysia Kelantan, Jeli Campus, Lock Bag 100, 17600 Jeli, Kelantan, Malaysia.

⁶ Faculty of computer Science and Information Technology, Alzaiem Alazhari University, Khartoum North 13311, Sudan.

ARTICLE INFO

Article history:

Received: 30 August, 2019

Accepted: 16 November, 2019

Online: 12 December, 2019

Keywords:

Fuzzy modeling

Firefly algorithm

Phishing detection

ABSTRACT

A fuzzy system is a rule-based system that uses human experts' knowledge to make a particular decision, while fuzzy modeling refers to the identification process of the fuzzy parameters. To generate the fuzzy parameters automatically, an optimization method is needed. One of the suitable methods provides the Firefly Algorithm (FA). FA is a nature-inspired algorithm that uses fireflies' behavior to interpret data. This study explains in detail how fuzzy modeling works by using FA for detecting phishing. Phishing is an unsettled security problem that occurs in the world of internet connected computers. In order to experiment with the proposed method for the security threats, a database of phishing websites and SMS from different sources were used. As a result, the average accuracy for the phishing websites dataset achieved 98.86%, while the average value for the SMS dataset is 97.49%. In conclusion, both datasets show the best result in terms of the accuracy value for fuzzy modeling by using FA.

1. Introduction

Phishing is a cyber-attack criminal activity that is intended to steal sensitive information such as credit card information or account login credential from users by using bogus websites [1], [2]. There are three components in phishing techniques; medium of phishing, vector to transmit the attack, and technical approaches used during the attack. The first component, the medium of phishing is the base means of conveying the phishing attacks to the victims which involve three bases; internet, voice, and short messaging service (SMS). The second component, the vector that defines the vehicle in place for launching the attack such as Email, eFax, websites, and social networks that are accessible through the

Internet. The last component is the technical approaches which are used to improve the phishing effectiveness during an attack.

Nowadays, many approaches are being used by the phishers to steal personal information such as browser vulnerabilities, mobile phone or man-in-the-middle. A phishing attack is the simplest kind of security threat, but at the same time is the most effective and dangerous violence. This is due to the fact that attackers use malware to remotely control a victim's device for their particular intention such as spying or stealing personal information. While not many people are aware that they may be a victim of a phishing attack, it is poses a major threat in network security. Therefore, many researchers are focused on the methods to detect phishing efficiently and produce better results than the previous methods.

*Corresponding Author: Mohd Arfian Ismail, arfian@ump.edu.my

One way to improve the efficiency to detect the phishing attack is by using the fuzzy techniques. With the fuzzy system, people can make an intelligent decision that works based on the combination of several factors. However, this method is a time consuming and does not guarantee an optimum solution because a fuzzy system requires the identification of the fuzzy parameters; fuzzy rules and the membership function. Hence, the optimization method needs to be applied in the system in order to tune the parameters of the fuzzy system automatically. This paper proposes a novel method by application of the Firefly Algorithm (FA). FA can be considered as a recent optimization method that is being used in artificial intelligence [3].

2. Materials and Methods

2.1. Related Works

There are many existing phishing detection techniques proposed in recent years. Researchers [4] proposed a software named anti-phishing simulator that collects phishing and spam messages where the users can examine the link addresses in the mail. It prescribes whether the messages can be classified as a phishing attack by using the Bayesian classification algorithm. Authors [5] have given a phishing site detection approach via URL analyses. Their work uses a URL detection method to discover phishing websites using a random forest algorithm. They have limited the feature set of URL detection to eight out of thirty-one features. The parameters considered to measure the accuracy level include f-measure, ROC Curve, precision, and sensitivity for analysis purposes. As a result, the accuracy level of this method was 95% [5]. By using the machine learning, researchers [6] proposes a hybrid solution that combines three approaches; blacklist and whitelist, heuristics, and visual similarity. The hybrid solution will be fed to the machine learning algorithm to calculate the accuracy results. By using different approaches, it will produce better accuracy and provide more efficient protection system [6]. According to [7], PhishBox is a new approach for phishing validation and detection that collects phishing data in real-time. The modules in this method include extract-transform-load, modelling, voting, monitoring, and visualization. The results [7] show that the proposed method has achieved high performance compared to the other works. Authors [8] used the C4.5 decision tree algorithm to analyse phishing sites. The data contain URL heuristics and the sites ranked to decide on a phishing attack. The proposed method extracts URL features and calculates their heuristic value. Then, the C4.5 decision tree algorithm was used to generate rules and identify the probability of phishing. There are 9 features of the URL used in the proposed method to detect phishing sites. The results showed that the method is more robust and precise compared to previous methods. Researchers [9] proposed a secured methodology for anti-phishing. The algorithm and techniques used were balanced block replacement, advanced encryption standard, and code generation. There are two phases in the proposed techniques which are user registration phase and user login phase. The method [9] is not flexible to accommodate the increasing number of consumers, therefore it will be difficult to provide a unique code to each user. Authors [10] proposed phishing emails detection using Cuckoo Search SVM (CS-SVM). Cuckoo Search algorithm was used for parameter selection. It extracts 23 features that are used to construct the hybrid classifier. This method uses the measures of a true positive rate, a false

positive rate, and an accuracy as evaluation metric to evaluate the performance. CS-SVM shows a 91 percent higher result in terms of phishing email detection accuracy at different training sets when compared with traditional SVM classifier [10].

Overall, a lot of methods have been proposed by other researchers and have their advantages and disadvantages in producing the results. For detecting phishing in real-time, the researchers create new software that uses specific tools and algorithms to collect phishing data. On the other hand, the machine learning approach was recognised by researchers as the most effective method.

2.2. Fuzzy System

The fuzzy system is a rule-based system which works by using the fuzzy logic to reason data. Most of the fuzzy concepts come from the human language. It is an approach based on the "degrees of truth" and it imitates the way humans make decisions that involve the possibilities between YES and NO.

To ensure that the fuzzy system works properly, fuzzy parameters are needed. The parameters are the fuzzy rules and membership functions [11]. Fuzzy rules were originally obtained from human experts through the knowledge engineering processes. However, this approach cannot be applied when there are no human experts or if the data are too complex. Besides, membership function is a function that defines the degree to which a given input belongs, where the output is between 0 and 1. To implement a fuzzy logic technique, four elements are required which are fuzzification, fuzzy inference engine, fuzzy rule base, and defuzzification. The elements of the fuzzy system are shown in Figure 1 while the list and description of the components in a fuzzy system are described in Table 1.

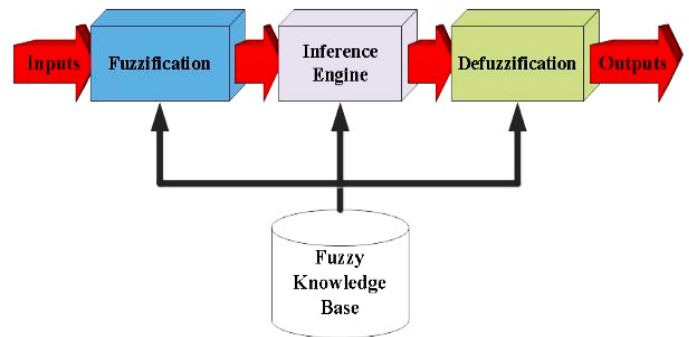


Figure 1: Elements of the fuzzy system

Table 1: Description of the fuzzy system elements

Component	Description
Fuzzy knowledge base	It contains a set of fuzzy sets and fuzzy rules
Fuzzification	Convert crisp data into the membership function
Inference Engine	Perform fuzzy operation by combining membership functions with the fuzzy rules to obtain the fuzzy output
Defuzzification	Convert fuzzy output into crisp data

Meanwhile, fuzzy modelling is a task of finding or identifying the fuzzy parameters to achieve the desired behaviour. An effective method should be used to generate the fuzzy parameters automatically from data. Regarding that, using an optimization method is the best choice by automatically generating the fuzzy parameters from available data [12].

2.3. Representation of Fuzzy Parameter

In the study, the fuzzy rule is defined by using numerical form where it is responsible for representing the fuzzy sets in the model. The fuzzy rules use the IF-THEN form as shown in Figure 2.

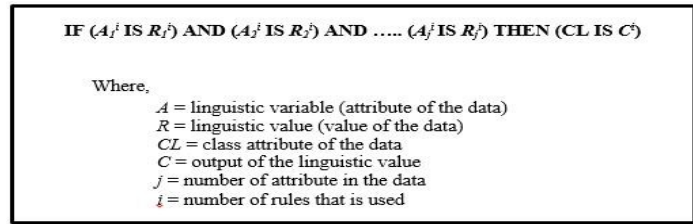


Figure 2: IF-THEN rule form description

The A in the IF-THEN form represents the input of the linguistic value while the output is the value of C for the class variable. The value of the attribute (A) is set in a range of 0 until 3, where the values of 1 and 2 are represented as phishing and legitimate respectively while the values of 0 and 3 do not apply. It gives meaning where if the fuzzy rule produces the value of 0 or 3 in the attribute's value, the attribute will not be included as the fuzzy set. Meanwhile, the value of class (CL) is set to 0 and 1, where it represents the result of the attribute.

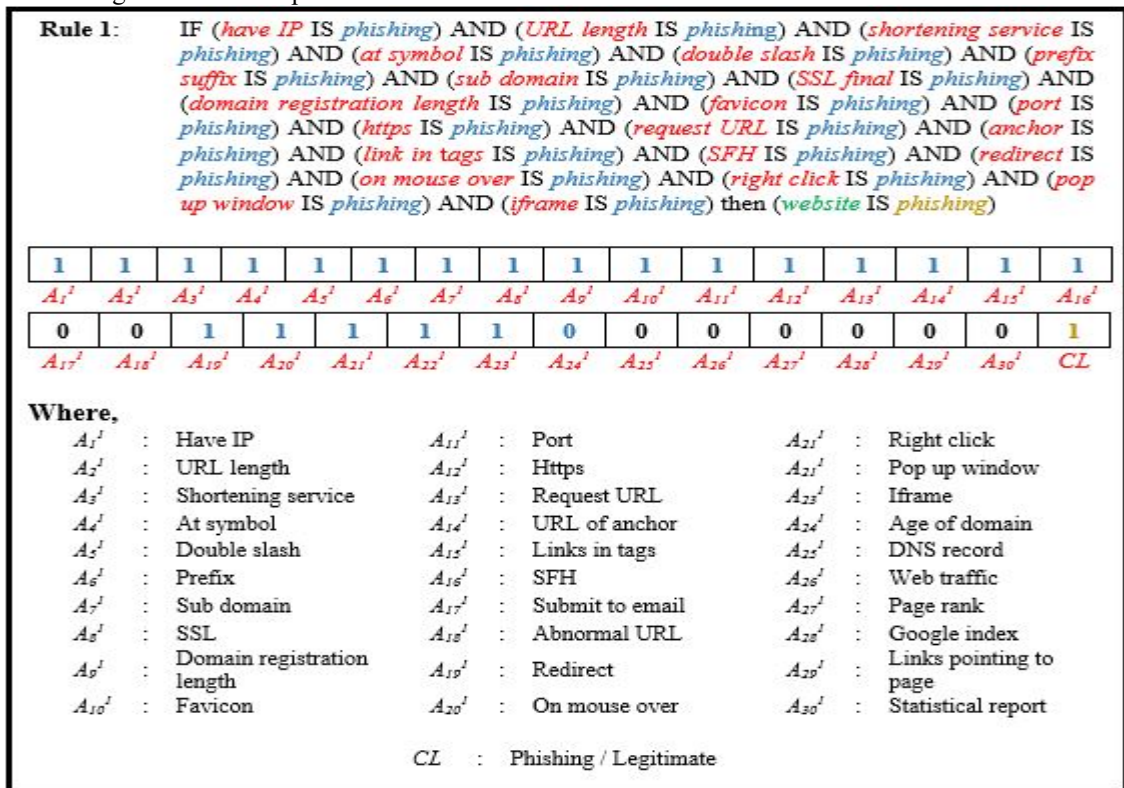
The example of the process of encoding the fuzzy rules in the case study shown in Figure 3. The sample was taken from the

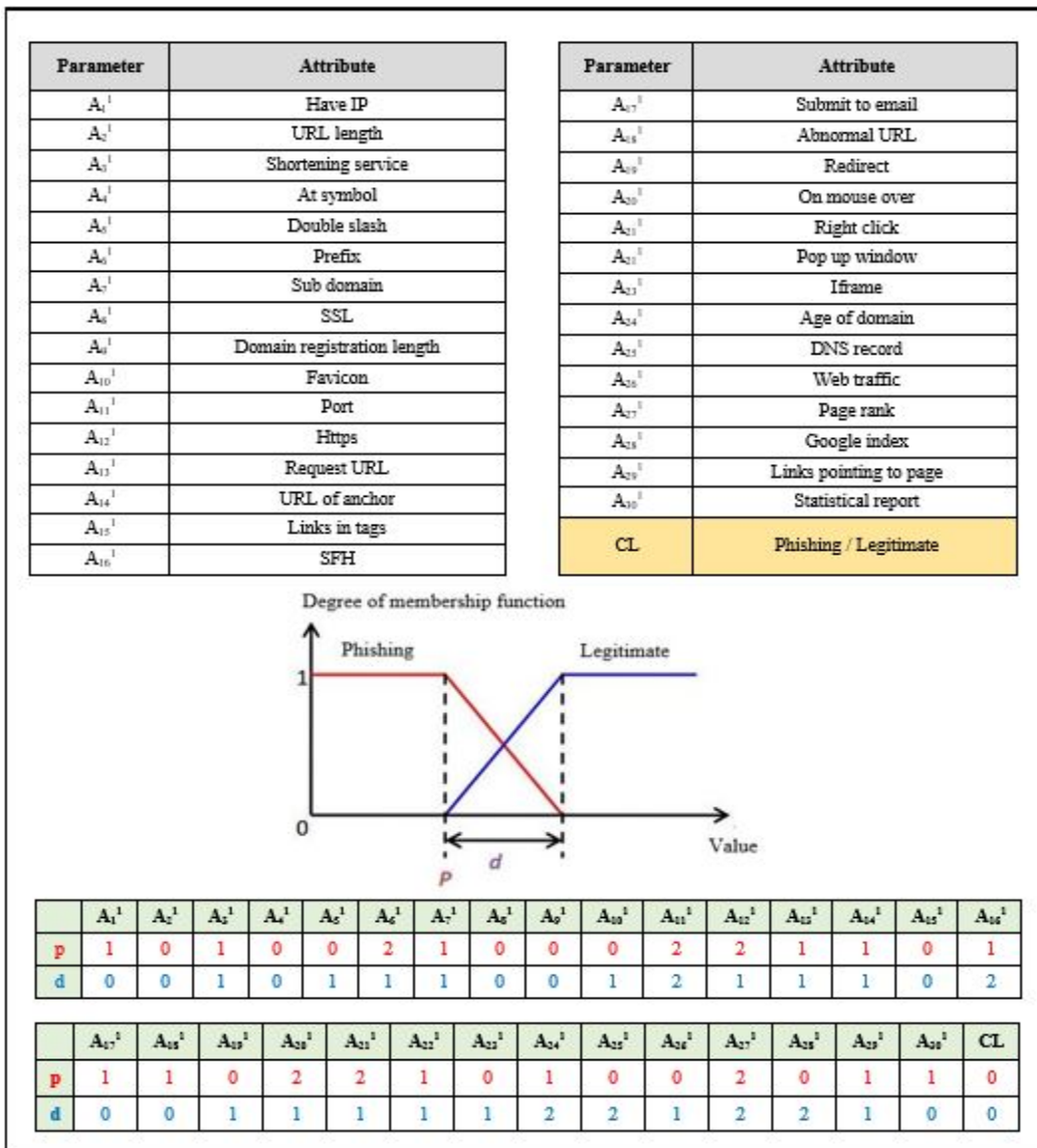
Phishing Websites Dataset. In this example, almost all 30 attributes were included in the fuzzy rule in which 8 produced the value of 0, which is not included in the fuzzy sets. This is because the attribute has a value of 1; "phishing". If the fuzzy set stated "legitimate", the value will be 2. At the end of the fuzzy rules that represent a membership function, the results will be shown.

The schematic shape of the membership function used in this study is trapezoidal. The encoding process of the membership function is demonstrated in Figure 4, where it applied on the first dataset (the phishing websites dataset). The value of every parameter represented the starting point of the overlap in the membership functions. Since the number of attributes in the dataset is 31, the length of the membership function is equal to 31 as well.

2.4. Firefly Algorithm

The FA is an algorithm that was developed by Xin-She Yang at Cambridge University in 2007 [13]. The FA is a swarm intelligence-based metaheuristic approach inspired by the behaviour of fireflies. The flashing light of fireflies acts as a signal system or communication to attract other fireflies. It can also function as a protective warning mechanism. The flashing characteristics of the fireflies are as follows: i) All fireflies are unisex, therefore they become attracted to other fireflies without being concerned about their sex; ii) The less bright fireflies will move to the other fireflies who has the brighter flash as the attractiveness is proportional to their brightness. The attractiveness and brightness of the firefly are reduced as the distance increase. If no firefly is brighter than them, the fireflies will move randomly without the right direction; iii) The brightness of a firefly is determined by the setting of the objective function to be optimized.





The work of FA is started by initializing the objective function, followed by generating the initial population of fireflies. Then continued with determining the light intensity and ranking the fireflies before updating the fireflies' position in the population. Figure 5 shows the flowchart of the FA.

2.5. Model and Experimental Data

In order to test the efficiency of the proposed method in detecting phishing, two benchmarks datasets were used. The first dataset is taken from the University of California, Irvine (UCI) machine learning repository. This database is the trusted and most widely used dataset for detecting phishing attacks, which can be accessed at <http://archive.ics.uci.edu/ml/>. The dataset involved is a phishing website dataset that contains 2456 instances and 30 attributes. The dataset collected is mainly from trusted sources; PhishTank archive, MillerSmiles archive, Google searching operators.

Meanwhile, the second dataset that was used contains SMS messages that were obtained from the Unicamp website at www.astesj.com

<http://www.dt.fee.unicamp.br/~tiago/smsspamcollection/>. The dataset contains 5574 instances and 2 attributes that were collected from various sources such as Grumbletext Web, NUS SMS Corpus, and SMS Spam Corpus v.0.1 Big.

The experiments were conducted by using 10-fold cross-validation for both datasets. The cross-validation was performed by partitioning the data into 10 partitions where every partition consists of equal number of data in it. The process was then repeated 10 times. In evaluating these experiments, the results were measured by their fitness value which is equivalent to the accuracy of the model. There are three categories considered in the model, which are the best solution, worst solution, and average value. The best solution is the highest accuracy in each experiment amongst the 10-fold cross-validation in a single run while the worst solution indicates the lowest accuracy value in a single run. The purpose of determining the best and worst result in every experiment is to show the potential of fuzzy modelling by using FA. Meanwhile, the average solution is the mean value of all the fitness value results in the experiments.

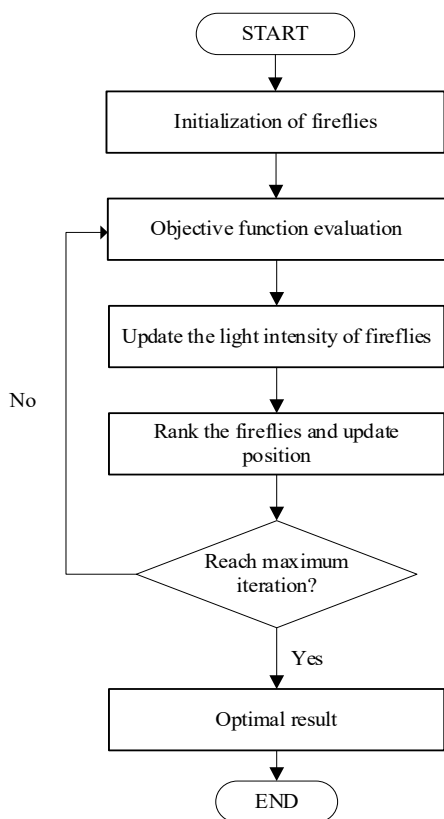


Figure 5: Flowchart of the Firefly Algorithm

In this study, the fuzzy system is used to generate fuzzy rule and membership function by using the FA. For the classification process, the fuzzy engine used was Sazonov Fuzzy Engine. It is a freely available fuzzy engine which is fully implemented in Java. It can be downloaded at <http://people.clarkson.edu/~esazonov/>.

3. Experimental Results

This section presents the analysis of the results obtained. Fuzzy modelling by using FA was tested with many parameters affecting the performance of the system. The effects of five parameter's performance which are population size, gamma probability, alpha0 probability, alphan probability, and the number of generations are shown in Table 2.

Table 2: Parameters setting

Parameter	Value
Population size	[10,40]
Gamma probability	[0.5,2.0]
Alpha0 probability	[0.1,0.4]
Alphan probability	[0.001,0.004]
Number of generations	[50,200]

As mentioned in most of the research papers, FA needs a small number of populations e.g. from 10 to 40 [14]. This is to make sure that the solution can be gained in a short time. For the gamma probability value, the current study stated that the ideal value for the gamma is 1.0 [15]. Next, the papers stated that 0.2 is the ideal value for the alpha0 parameter and 0.001 is the ideal value to be used for alphan probability [15]. Meanwhile, the number of generations tested was in a range of 50 to 100.

Table 3: The best parameters setting

Parameter	Value
Population size	20
Gamma probability	1.0
Alpha0 probability	0.2
Alphan probability	0.001
Number of generations	100

After the sensitivity analysis of every parameter in the algorithm has been performed, the best parameter setting can be found. The best parameter generated can be used to find the highest fitness value and is able to produce higher interpretability of the fuzzy model. Table 3 shows the best results for every parameter setting when being applied to both datasets.

Lastly, the accuracy of the results for every dataset was recorded and analyzed. The results were obtained after applying the best parameter value shown in Table 3. The first dataset shows that the highest accuracy, which is the best result, manages to reach up to 100% accuracy while the worst value is 97.72% and the average accuracy is 98.86%. Meanwhile, the second dataset indicates the value of 99.46% as the best accuracy value, 95.52% as the worst value, and 97.49% as average accuracy. To access the performance of the proposed study, the accuracy results for both datasets obtained were compared with other works. Table 4 gives the comparison of dataset 1 while Table 5 compared the results of dataset 2 with other works. Table 4 and Table 5 clearly show that the proposed method produces the best results compare to others.

Table 4: The comparison of results with other works for dataset 1

Work By	Result
Kaytan and Hanbay [16]	95.05%
Ubung et al.[17]	92.5%
Vrbančič, Fister, and Podgorelec [18]	94.4%
Mohd Foozy [19]	95.53%
This study	98.86%

Table 5: The comparison of results with other works for second dataset

Work By	Result
Mathew and Issac [20]	98.22%
Kawade[21]	98.34%
Raj et al. [22]	96.17%
Safie et al. [23]	97.13%
This study	99.46%

4. Conclusion

In this study, an improved method for fuzzy modelling was proposed and presented in detail. The method used FA for generating the fuzzy rule and membership function automatically for identifying the fuzzy parameter. To test the performance of the proposed method, two benchmark datasets were used. The results of the implementation of the method have been analyzed and it showed that the proposed method performed well compared to other works in terms of accuracy. To conclude, the implementation of FA for fuzzy modelling was able to produce good results.

Conflict of Interest

There is no conflict of interest declared by the authors.

Acknowledgment

Special appreciation to Universiti Malaysia Pahang for the sponsorship of this study by approve the Ministry of Higher Education (MOHE) for Fundamental Research Grant Scheme (FRGS) with Vot No. RDU190113.

References

- [1] K. Leng, C. Lin, K. Wong, K. S. C. Yong, and W. King, "A new hybrid ensemble feature selection framework for machine learning-based phishing detection system," *Inf. Sci. (Nijl.)*, vol. 484, pp. 153–166, 2019. <https://doi.org/10.1016/j.ins.2019.01.064>
- [2] M. M. Moreno-Fernández, F. Blanco, P. Garaizar, and H. Matute, "Fishing for phishers. Improving Internet users' sensitivity to visual deception cues to prevent electronic fraud," *Comput. Human Behav.*, vol. 69, pp. 421–436, Apr. 2017. https://doi.org/10.1007/978-3-319-09129-7_17
- [3] R. B. Francisco, M. F. P. Costa, and A. M. A. C. Rocha, "Experiments with Firefly Algorithm," in *Computational Science and Its Applications -- ICCSA 2014*, 2014, pp. 227–236. https://doi.org/10.1007/978-3-319-09129-7_17
- [4] M. Baykara and Z. Z. Gurel, "Detection of phishing attacks," in *2018 6th International Symposium on Digital Forensic and Security (ISDFS)*, 2018, pp. 1–5. <https://doi.org/10.1109/ISDFS.2018.8355389>
- [5] S. Parekh, D. Parikh, S. Kotak, and S. Sankhe, "A New Method for Detection of Phishing Websites: URL Detection," in *Proceedings of the International Conference on Inventive Communication and Computational Technologies, ICICCT 2018*, 2018, no. Icicct, pp. 949–952. <https://doi.org/10.1109/ICICCT.2018.8473085>
- [6] V. Patil, P. Thakkar, C. Shah, T. Bhat, and S. P. Godse, "Detection and Prevention of Phishing Websites Using Machine Learning Approach," in *Proceedings - 2018 4th International Conference on Computing, Communication Control and Automation, ICCUBEA 2018*, 2019, pp. 1–5. <https://doi.org/10.1109/ICCUBEA.2018.8697412>
- [7] J. H. Li and S. De Wang, "PhishBox: An approach for phishing validation and detection," in *Proceedings - 2017 IEEE 15th International Conference on Dependable, Autonomic and Secure Computing, 2017 IEEE 15th International Conference on Pervasive Intelligence and Computing, 2017 IEEE 3rd International Conference on Big Data Intelligence and Compu*, 2018, vol. 2018-Janua, pp. 557–564. <https://doi.org/10.1109/DASC-PICom-DataCom-CyberSciTec.2017.10>
- [8] L. MacHado and J. Gadge, "Phishing Sites Detection Based on C4.5 Decision Tree Algorithm," in *2017 International Conference on Computing, Communication, Control and Automation, ICCUBEA 2017*, 2018, pp. 1–5. <https://doi.org/10.1109/ICCUBEA.2017.8463818>
- [9] T. Churi, P. Sawardekar, A. Pardeshi, and P. Vartak, "A Secured Methodology for Anti-Phishing," in *International Conference on Innovations in Information, Embedded and Communication Systems*, 2017, pp. 1–4. <https://doi.org/10.1109/ICIECS.2017.8276081>
- [10] W. Niu, X. Zhang, G. Yang, Z. Ma, and Z. Zhuo, "Phishing emails detection using CS-SVM," in *Proceedings - 15th IEEE International Symposium on Parallel and Distributed Processing with Applications and 16th IEEE International Conference on Ubiquitous Computing and Communications, ISPA/IUCC 2017*, 2018, pp. 1054–1059.
- [11] L. S. Riza, C. Bergmeir, F. Herrera, and J. M. Benítez, "frbs : Fuzzy Rule-Based Systems for Classification and Regression in R," *J. Stat. Softw.*, vol. 65, no. 6, pp. 1–30, Jun. 2015. <https://doi.org/10.18637/jss.v065.i06>
- [12] S. K. Rawat, "A Review on Spam Classification of Twitter Data Using Text Mining and Content Filtering," *Int. J. Adv. Res. Comput. Sci. Softw. Eng.*, vol. 5, no. 6, pp. 485–488, 2015.
- [13] A. J. Umbarkar, U. T. Balande, and P. D. Seth, "Performance evaluation of firefly algorithm with variation in sorting for non-linear benchmark problems," in *AIP Conference Proceedings*, 2017, vol. 1836. <https://doi.org/10.1063/1.4981972>
- [14] X.-S. Yang, "Firefly algorithms for multimodal optimization," in *Stochastic Algorithms: Foundations And Applications*, 2009, p. 178. https://doi.org/10.1007/978-3-642-04944-6_14
- [15] J. Kwiecień and B. Filipowicz, "Firefly algorithm in optimization of queueing systems," *Bull. Polish Acad. Sci. Tech. Sci.*, vol. 60, no. 2, pp. 363–368, 2012. <https://doi.org/10.2478/v10175-012-0049-y>
- [16] M. Kaytan and D. Hanbay, "Effective Classification of Phishing Web Pages Based on New Rules by Using Extreme Learning Machines," *Anatol. J. Comput. Sci.*, vol. 2, no. 1, pp. 15–36, 2017.
- [17] A. A. Ubung, S. Kamilia, A. Abdullah, N. Jhanjhi, and M. Supramaniam, "Phishing Website Detection: An Improved Accuracy through Feature Selection and Ensemble Learning," *Int. J. Adv. Comput. Sci. Appl.*, vol. 10, no. 1, pp. 252–257, 2019. <http://dx.doi.org/10.14569/IJACSA.2019.0100133>
- [18] G. Vrbančić, I. Fister, and V. Podgorelec, "Swarm Intelligence Approaches for Parameter Setting of Deep Learning Neural Network," in *Proceedings of the 8th International Conference on Web Intelligence, Mining and Semantics - WIMS '18*, 2018, pp. 1–8. <http://doi.acm.org/10.1145/3227609.3227655>
- [19] C. F. Mohd Foozy, R. Ahmad, M. A. Faizal Abdollah, and C. C. Wen, "A Comparative Study with RapidMiner and WEKA Tools over some Classification Techniques for SMS Spam," *IOP Conf. Ser. Mater. Sci. Eng.*, vol. 226, no. 1, 2017. <https://doi.org/10.1088%2F1757-899x%2F226%2F1%2F012100>
- [20] K. Mathew and B. Issac, "Intelligent spam classification for mobile text message," *Proc. 2011 Int. Conf. Comput. Sci. Netw. Technol. ICCSNT 2011*, vol. 1, no. December, pp. 101–105, 2011.
- [21] D. R. Kawade, "SMS Spam Classification using WEKA," *Int. J. Electron. Commun. Comput. Technol.*, vol. 5, no. ICICC, pp. 43–47, 2015. <https://doi.org/10.1109/ICCSNT.2011.6181918>
- [22] H. Raj, Y. Weihong, S. K. Banbhani, and S. P. Dino, "LSTM Based Short Message Service (SMS) Modeling for Spam Classification," in *Proceedings of the 2018 International Conference on Machine Learning Technologies*, 2018, pp. 76–80. <http://doi.acm.org/10.1145/3231884.3231895>
- [23] W. N. H. W. Safie, N. N. A. Sjarif, N. F. M. Azmi, S. S. Yuhani, R. C. M. Yusof, and S. Yaacob, "SMS spam classification using Vector Space Model and Artificial Neural Network," *Int. J. Adv. Soft Comput. its Appl.*, vol. 10, no. 3, pp. 130–142, 2018.

BPMN4 Collaboration: An Extension for collaborative Business Process

Leila Amdah*, Adil Anwar

Mohammed V University in rabat, Siweb Team Research, EMI, Morocco

ARTICLE INFO

Article history:

Received: 15 September, 2019

Accepted: 07 November, 2019

Online: 12 December, 2019

Keywords:

Business Process modeling
Collaborative business process
BPMN2 Modeler
BPMN Extension Mechanism
BPMN4Collaboration Meta-model

ABSTRACT

Nowadays the collaboration of organizations, systems or services becomes more and more answered in practice. Indeed, organizations try to expand their service, other to satisfy the needs of their customers. Thus, the need to work collaboratively with other partners whether internally or externally becomes trivial. However, process modeling in a collaborative environment becomes heavy because of the diversity of information exchanged and the complexity of shared task. Certainly, the BPMN is the most answered standard for the modeling of business processes, moreover it offers a collaborative diagram that allows to model collaborative processes, but later we will see that its capabilities are very limited. For that, we try in this work to create a collaborative business process modeling language that allows to better model these types of processes and respects some aspects of a collaborative environment. We used the BPMN extension mechanism to create our own language that we named «BPMN4Collaboration».

1. Introduction

The ability to collaborate has always been of vital importance to businesses to businesses. Combining the resources and talents of a group of people together is the best way to solve complex problems and tasks. Collaborative work is the work done jointly by several people who pool their knowledge and skills, organize and coordinate their actions to achieve a result for which they are collectively responsible. Of course, the collective work is not decreed overnight in a company. It is the result of a common desire gradually implemented around a common project. The success factors of this approach are: the benevolence of the various stakeholders, the clarity in the collaboration and the application of the principle give and take. Collaborative work is one of the major challenges of project management. Until now, designers use many languages to model collaborative business process (CBP), such us: XPDL, BPMN, WS-CDL, BPDM, WSFL, XLANG, BPSS, ebXML, WPDL etc.

Business processes are by nature collaborative processes. The modeling of collaborative systems is at the center of current management's concerns and therefore constitutes the main issue of modeling efforts.

Collaboration is viewed as set of exchange between a collection of participants and their processes. We can say that there are two types of collaboration: (1) Integrated Collaboration, which

means that business and application logic are integrated into a single monolithic system used by all participants; (2) External Collaboration that takes place between two or more autonomous systems. Practically, collaborative process modeling are very used [1, 2] and software engineering results have shown that collaboration can increase quality and efficiency significantly.

The main goal of a collaborative process is to define the choreography of the interactions between the partners involved in this collaboration. So it's a process that occurs between two or more collaborators and consists of two parts: a public interface and several private interfaces corresponding to each partner figure 1.

- Private process: it's composed of confidential information and is developed internally.
- Public process: it is a partial image of a private process. It consists of all the activities that can be viewed by the other partners.
- Collaborative Process: consists of activities shared among participants during a collaboration.

During a collaboration collaborative process can represent inter-organizational process (between two internal services of the organization) or extra-organizational process (with an external partner). There are several independent identities that represent several decision makers which means autonomy of collaborators; several collaborative activities which means sharing resources and

*Amdah Leila, Morocco, leila.amdah@gmail.com

communication between actors; sharing of responsibility and decisions; finally, a confidentiality and security of resources and data. We can say that all these requirements are essential for a successful collaboration.

concepts. Section 6 is an illustration to our approach to better understand the benefit of the extension. Finally, we concluded the paper in section 7.

2. Business process modeling

Business Process Modeling is a method of representing the activity of an organization to respond more quickly to customer demand and corporate goals. Thus, it is an organizational management that systematizes the daily tasks of the organization and allows a process to be better understood by the different partners, be it manager, process owner or IT engineering who will implement the system. Business process modeling languages are a great help to model these processes, they are designed for several purposes so it is very difficult to categorize them into one dimension. However, we can distinguish four major scientific traditions of language [4]: the traditional process modeling languages that are typically non-formal, the workflow modeling languages that describe a workflow, they are formal and executable, the integration languages processes and object-oriented languages.

2.1. Business Process Model and Notation (BPMN)

Indeed, BPMN (Business Process Modeling Notation) as Business Process Modeling Language [5] is an important OMG standard that meets the requirements of standardization. Among other popular standards [6, 7, 8], only the BPMN has been widely accepted by the professional world. Thus BPMN is qualified a leader in the field of business process modeling.

The first version of BPMN1.0 was released in 2004 with the purpose of providing a graphical notation to business processes. The last version of BPMN2.0 was published in 2011, this version has brought more elements to the standard and new diagrams (Choreography and collaboration diagram). BPMN 2.0.2, released in December 2013, included only minor modifications in terms of typo corrections. The main advantages of BPMN is:

- Provide a graphical notation understandable by all types of users. Whether it is the business analysts who define the processes or the developers responsible for the implementation, or the employers responsible for the deployment of these processes.
- The possibility of giving life to these processes thanks to BPEL [9] (also known as WS-BPEL) which allows their execution
- Provide an extension mechanism [10] that allows to integrate domain-specific concepts by ensuring the validity of the basic elements of BPMN.

Based in the previous information, BPMN is a base for the representation of business processes. BPMN graphical elements are divided into five basic categories: Flow Objects, Data, Connection Objects, Swimlanes, and Artefacts. Moreover, the BPMN modeling environment consists of three diagrams:

- Processes (Orchestration): These process are called generally workflow or BPMN process, they can be private or public.
- Choreographies: Represent a procedural contract between interacting Participants. Thus, choreography

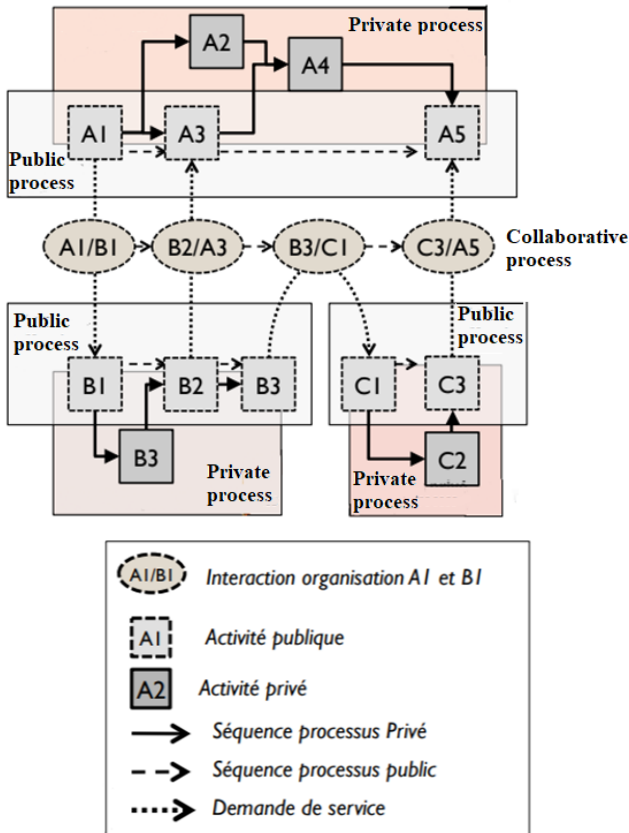


Figure 1: Collaborative Process: Private, public and collaborative process [3]

In fact, BPMN is a business process modeling method that is based on graphical notation and can be used to model collaborative processes. So, we directly think about using BPMN for modeling our collaborative processes. Nevertheless, it still represents some restrictions on the description of the data exchanged between the participants and specification of the roles of the collaborators.

To address the lack of a clear and comprehensive vision of CBP. First we try to define a set of collaborative concepts that are primordial to in collaborative environment namely: confidentiality, traceability, communication, decision making and task monitoring, as present in section 4. Second, we developed a collaborative modeling language with a rich graphic notation corresponding to these concepts of collaboration. Our language named BPMN4Collaboration is an extension of BPMN which is clearly defined because it respect the graphical syntax of the BPMN and finally, offer new concepts for collaborative environment. Our language not only add new notation useful for CBP but also help in the evolution and updating of these processes.

The remainder of this paper is structured as follows: section 2 present background on business process model and notation (BPMN) also the shortcoming of this standard. Section 3 is a related work on BPMN extensions. Section 4 presents an overview on collaborative business process and the central concepts that describe this environment. Section 5 describe the proposed approach which is extending BPMN 2.0 with new collaborative

exists between Pools or participants. It's similar to a process because it consists of activities, Gateways and Events (Figure 2). However, it's different in that the Activities are interactions that represent a set of Message exchanges.

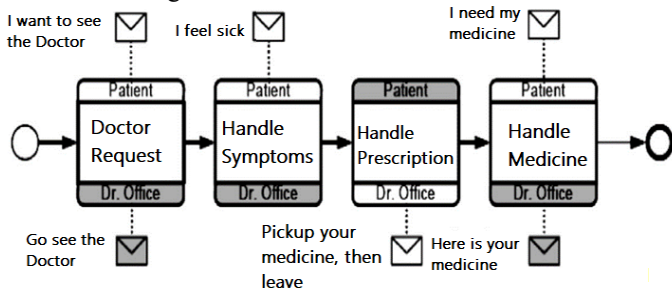


Figure 2: Example of choreographic [11]

- Collaborations: Can include Processes and/or Choreographies: it models the existing interactions between two or more organizations. It contains the pools that represent each participant as well as the message flows. These latter connect the pools (Figure 3). Choreography elements may be shown “in between” the Pools as they bisect the Message Flows between the Pools.

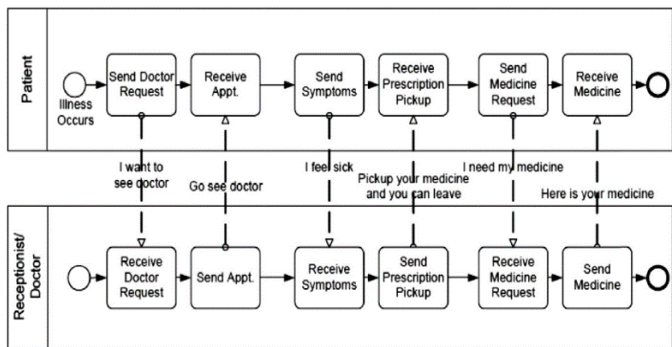


Figure 3: Example of collaboration [11]

2.2. BPMN shortcoming

- Insufficient support for the process state concept. In fact the BPMN does not understand the concept of task progress knowing that this concept is very important to follow the progress of the tasks by collaborators.
- The concept of confidentiality is not taken into account by the BPMN. Confidentiality of information is essential for successful collaboration. The shared information should not be distributed outside or even inside the organization with non-affected persons.
- In PBMN individual participants are represented by Pools so all the activities into this one belong to the same participant. However, a collaboration consist of several participant how can made the same activity. So we need to know if one participant is involved or if there can be potentially many participants involved.
- Of course BPMN represents the exchange of data between several processes. However, this representation

remains very limited compared to the need for collaboration. Indeed, in a collaborative environment, the artefact exchange representation is a key point for the success of the collaboration. We must distinguish between the types of these artifacts their level of importance, their version etc .Data objects are represented simply by a symbol; their internal structure is not defined and their main purpose is not specified. However the exchange of data is a very sensitive point when it comes to collaborative work. The type of data and their purpose must be specified to add value to the collaborative process.

3. Related works

Several works benefit from the mechanism of extension of the BPMN to adapt it to their needs. We will present therefore some work that has developed BPMN extension in different ways: in the field of knowledge dimension and sensitive business process model, [12] developed an extension (named BPMN4KM) that link different types of knowledge, information and data to the BPMN model. Other work [13] focuses on the field of clinical pathways and develops an extension (named BPMN4CP) which allows to integrate the concepts of this domain into BPMN model.

Concerning collaborative environments, [14] is interested in the life cycle of the data objects and the information exchanged between the processes during a collaboration. Thus, it develops an extension to model artifact-centric processes by taking inspiration from the existing graphical notations and best modeling practices. As for [15], he is interested in highly collaborative processes by adding new notations to model tasks that are common in this type of process. In [16] the author treats on complex collaborative processes. He presents the limitations of the BPMN concerning the modeling of complex choreographies. So he develops an extension to remedy this problem by adding new concepts, then he validates his work by using Service Interaction Patterns.

In other field the author introduce BPMN4TOSCA[17]. He expands the BPMN to model portable management plans for a standard called TOSCA. In fact, this standard captures cloud application topologies. So the author, defined four extension namely: topology management task, node management task, script task and finally data object specific to TOSCA. Zor and al. [18] propose a BPMN extension for the manufacturing domain to explicitly handle products and resources. [19] Used the BPMN extensibility mechanism to model specific tailoring relationships such as: deletion, local contribution, and local replacement. In addition, the author tries to ensure the consistency of the BPMN models when using tailoring relationships by creating some specific rule. Some works are interested to include the security aspect into BPMN. For example in [20] the author include access control or intrusion detection through a set of new annotations. To introduce security concepts in process models, [21] extend the BPMN by modeling elements such as access control or separation of duty, binding of duty. It names its extension SecureBPMN dedicated to secure business process.

Extension mechanisms tend to develop new concepts for a specific use from a general modeling language, or to enrich already existing elements with new information. The technical structuring of BPMN is based on the concept of expandable layers around a simple element core that provides this extension mechanism. As

you can see, each approach represents a new BPMN extension for a specific domain. While there are some who have approached the collaborative process, none of them has specified an extension that covers the different aspects of collaborative processes. Inspired by some work, we try to extend BPMN with graphic elements that:

- Represent concept of CBP
- Respect the shape of the standard
- Appear the extension as natural as possible

4. Collaborative business process

4.1. Overview

The concept of collaboration is derived from the Latin *collaborare* meaning “to work together” and can be seen as a process of shared creation. It can be defined as a process in which partners share information, resources and responsibilities to jointly evaluate a program of activities to achieve a common goal. Thus it's a process by which one group of entities enhances the capabilities of the each other. Collaboration involves mutual engagement of participants which implies mutual trust, sharing risks, responsibilities, and rewards. A collaborative process occurs, for instance, when a team of experts jointly develops a new product or improve an internal service to satisfy their customers. Such collaboration concerns the association between different organizations by connecting their business processes and exchanging data, messages or resources between their different departments. Thus the development of such collaborative systems becomes a challenge because it requires the linking of several heterogeneous elements of each organization of course by creating a coherent overall system and keeping the internal workings of each organization intact. In addition, this must be done in accordance with the organization's policies, industry guidelines, applicable legislation, technical capabilities and limitations.

Furthermore, organizations must be able to model their requirements so that: its internal processes describe its private activities; its public processes describe how it can interact with others; and its partner's public process describes what it expects from its partner. These requirements can be diverse, ranging from sequencing activities to sharing resources, defining security objectives, etc. On the basis of these requirements, organizations must then have the means to establish a clear, well-defined collaborative process that respects these requirements and the consistency of private and public behavior of partners.

To this end, there is strong interest from organizations in utilizing collaborative modelling concepts to be able to specify the different requirements applicable to their collaboration. On the basis of the resulting collaborative model, companies must then be

able to evolve their internal processes or rectify specific requirements of the collaboration contract without affecting the proper functioning of the overall collaborative process as well as partner's process. Finally, the sketched development allows the modeling of the resources exchanged between the partners as well as the flow of relevant activities. To describe and model collaborative business processes, several companies have come up with their own specification languages, such as Microsoft, IBM, SAP, etc.

4.2. Concept of collaboration unit

Previously we have seen that the BPMN is limited with respect to collaboration. In fact, collaboration is not just about sharing resource and exchanging messages between collaborators but it is a very complex operation that requires a lot of effort from participants. Collaborative business process are difficult and their success depend on some requirements:

- Traceability: Sharing implies sharing responsibility of participation and sharing responsibility of results. Indeed, a successful collaboration depends on a job with traceable tasks that allow the smooth running of the process.
- Confidentiality: Confidentiality of information is essential for successful collaboration. The shared information should not be distributed outside or even inside the organization with non-affected persons.
- Communication and sharing of resources is a great challenge, whether it is resources exchanged by collaborators or resources acquired during a meeting in order to fulfill the task.
- Decision-making: any decision made must be shared with collaborators
- Task monitoring and the progress of work: these two points are of a great importance in collaboration work. When sharing resources, it is necessary to assess their stat of progress.

To develop rich collaborative business process modeling. We try to exploit as much as possible the requirements we have mentioned before thus we propose a conceptualization for specifying collaborative business process in the form of a generic BPMN Meta-model for Collaboration (BPMN4Collaboration). Our work is based on the principle of extending the basic concepts of BPMN namely Activity, DataObject, SequenceFlow etc. The extension of the concepts of collaboration on these artifacts is detailed in Figure 4.

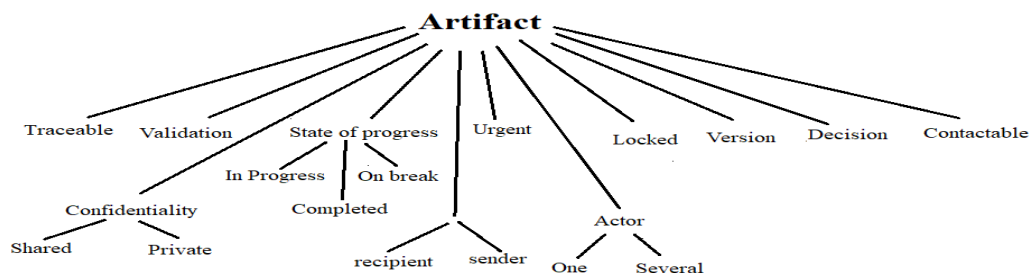
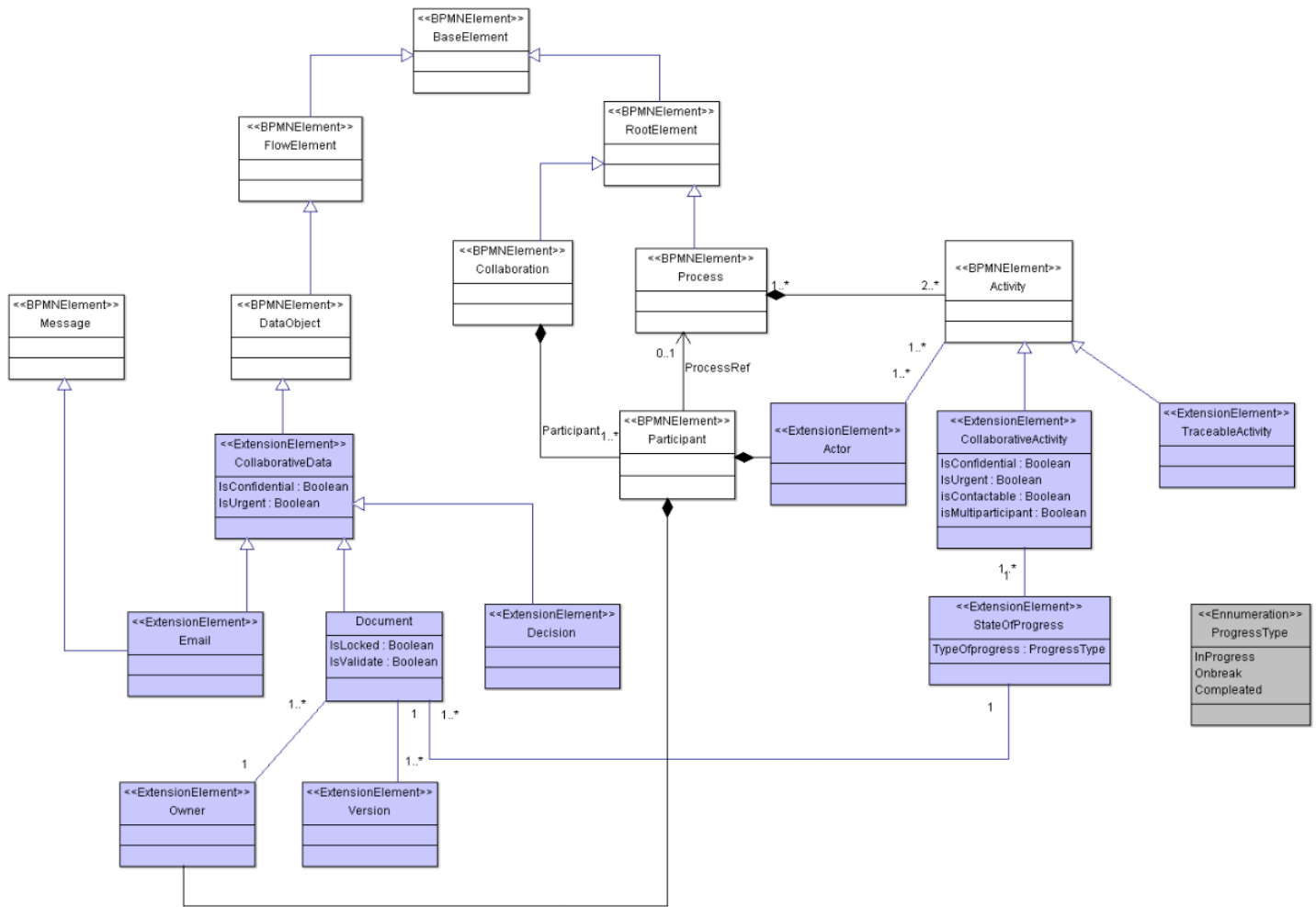


Figure 4: Extension of the concept of collaboration on BPMN artefacts



The concepts discussed in this section will help us later to build a modeling language that better describes business processes in a collaborative environment.

5. BPMN4Collaboration: A BPMN extension including collaboration concepts

5.1. Extended BPMN4Collaboration Meta-model

The metamodel of our extension called BPMN4Collaboration is shown in Figure 5. We try to represent in detail the stereotypes that describe the new concepts of collaboration

CollaborativeActivity: We add the property of privacy, urgency, the mode contactable and multiparticipant by creating this stereotype which is an extension of BPMN Activity. The attribute isConfidential show that Activity can be private or shared. Private activity can be seen only by the participant to which it belongs. Otherwise, shared activity is seen by all participants. The attribute isUrgent specifie that the attribute isContactable specifies that we can contact this activity before the end of the execution of the process. The attribute isMultiParticipantTask specifies if activity is made by several participants. A collaborative activity has also a state of progress.

TraceableActivity: this stereotype add the option of traceability. We can trace the execution status of the activity

Actor: this metaclass specifies that activity has an actor so that it can be on or several actors.

CollaborativeData: extends BPMN Data Object. It has also the attribute isConfidential and isUrgent. A collaborative data can be in the form of: Email, Decision or Document

Decision: this metaclass is a type of collaborative data, it must be an output of an activity. It's always connected with an activity and a Message Notification event. A decision must be notified to all participants before the end of the process.

Document: this metaclass is a type of collaborative data, it has two attributes: isLocked to specify that document cannot be modified or updated. isValidDate to specify that the manager or responsible of this document has validated it. A Document has also an owner and version and state of progress.

Owner: a document has always an owner which describes the initial state of the document for example decide if the document is locked or not, if it's confidential, etc.

Version: this metaclass specifies the version of the document. A document has inevitably at least a first version and a final version if it's completed.










stateOfProgress: this metaclass is linked to the stereotype CollaborativeData and CollaborativeActivity to shown the state of

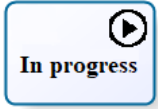

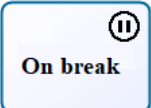








progress of artifact. It has three states: in progress, on break and completed.

5.2. Graphical Concrete Syntax

We propose an advanced graphical syntax which defines the elements of the new concepts of BPMN4Collaboration in Table 1 below:

Table 1: Extended element of BPMN

Abstract syntax	Graphical concept	Description
Multi participant Activity		Activity made by many participants
Contactable Activity		This activity can be contacted at any time by an external partner to be able to make changes before the end of the process
Traceable Activity		A task is said trackable to an external organization, if that organization is allowed to trace the execution status of the task
Private Artifact	 	This element is used to specify that the artifact is confidential and cannot be shared with a third party
Shared Artifact	 	Artifact shared between partners
Urgent Artifact	 	the artifact is urgent so its treatment must be immediate

State of Progress of an Artifact	 	The artifact is in progress
	 	The treatment of the artifact is on break
	 	The artifact is completed
Validate Data		Data validate by the responsible of the data
Locked Data		The exchanged data is locked, so it cannot be modified or updated.
Decision Data		Set of decision made by the partners before the end of the process that must be sent to the relevant stakeholders.
Data Rules		Data Rules which are mandatory before performing the task
Version of Data		Specifies that Data has a version « X »

5.3. Discussion

Through this modeling, we have been able to achieve an extension that satisfies the collaboration concepts mentioned in section 4. Indeed:

- Traceability is modeled by "traceable activity"
- confidentiality lies in defining « private artefacts », « public artefacts » and « locked data »
- Communication and exchange of resources is a trivial point that is represented by all of these new elements and specially « contactable Activity ».

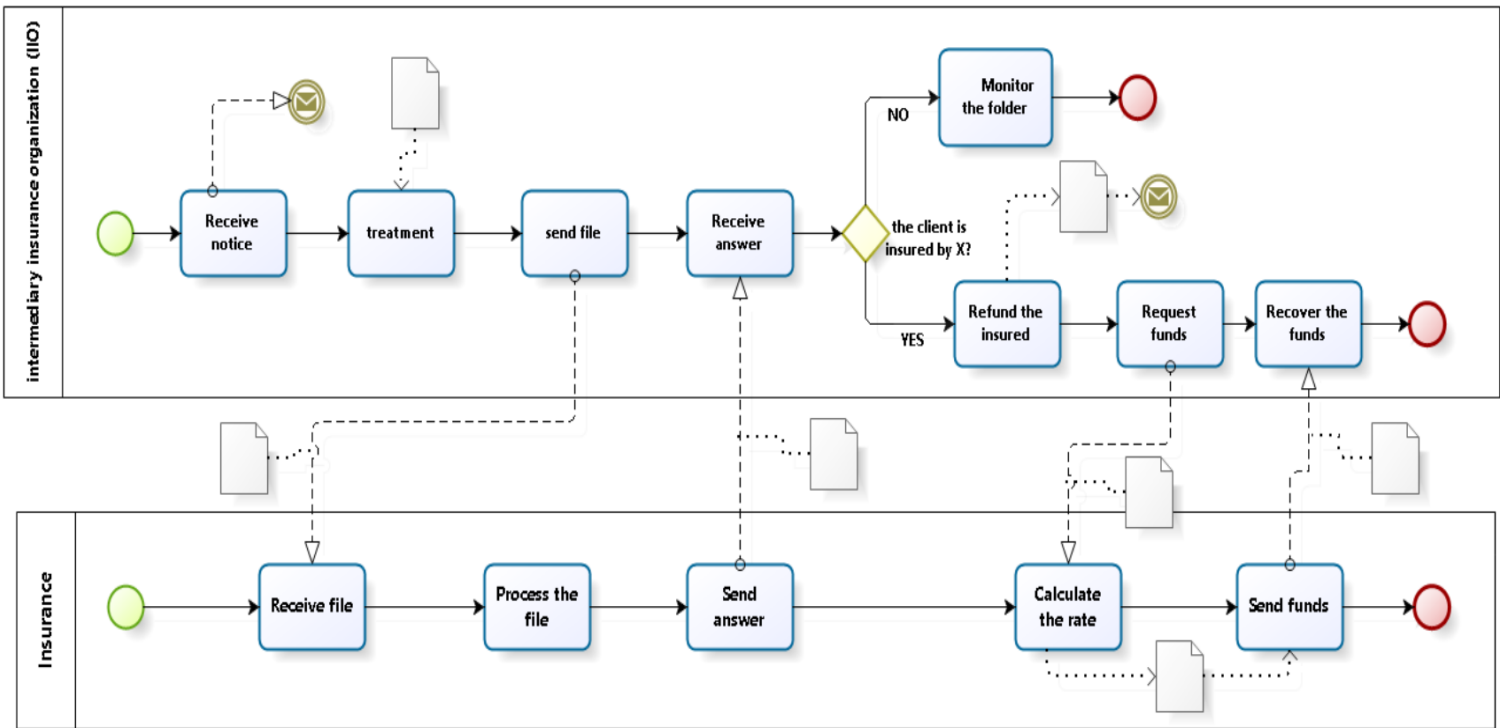


Figure 6 : Example of collaborative BPMN within an insurance

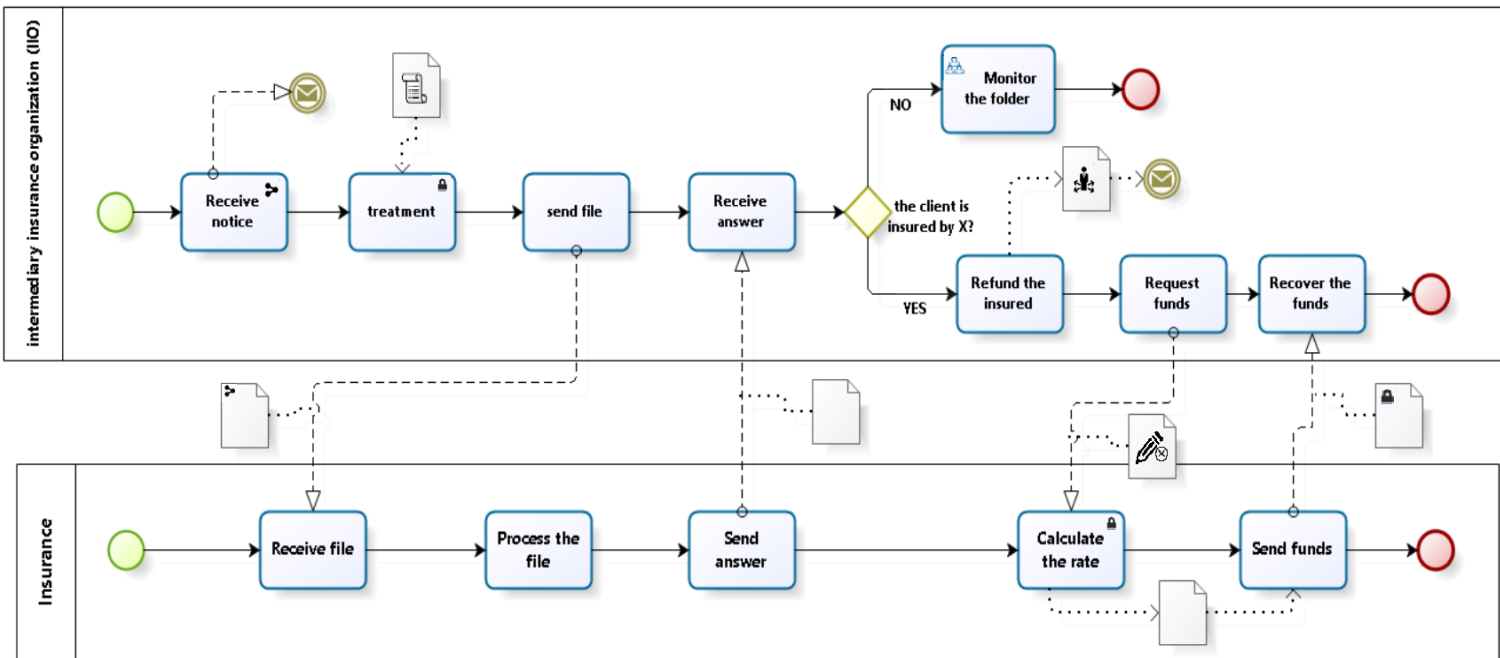


Figure 7: Example of collaborative BPMN conform to collaborative business process language

- Decision-making is ensured by « Decision Data » and « Data Rules ».
- Task monitoring and progress of work are provided by the elements « state of progress artefact », « urgent artefact » and « validate data ».
- Finally, the collaboration is more precise by "multi-participant Activity". The latter allows to emphasize the fact that task can be performed by several

participants and not by the actor specified by the model BPMN.

6. Demonstration

6.1. Illustrative example

Our example illustrates a collaboration between several organizations in the insurance field. Indeed, the collaboration is between the IIO and several insurances;

- Intermediate Insurance Organism (IIO): It is an organization that mediates between national and international insurance.
- Insurance: In our example we call our insurance "insurance X" as the IIO collaborates with several insurance at the same time.
- Description of the scenario: A person having an accident in a foreign country, the IIO will receive his notice of damage then will contact his insurance on his country to take charge of the material and corporal damage.

The process begins at the IIO as seen in Figure 6. As soon as the IIO organization receives a notification of damage from his client (the victim). It notifies the concerned insurance (named in this example X) by sending a notification message. Before the

We notice that this modeling is not precise since a quantity of information is not specified on the model.

Figure 7 demonstrate the evolved BPMN extension by presenting the new concepts of collaboration: Shared activity like "receive notice" is a public activity shared between client and IIO. Private activity like "calculate rate" is private, it's done inside the insurance and can't be seen by other participant. To supervise the progress of the treatment of the file, the IIO must keep in touch with this task. Then, the activity "process the file" done inside the insurance is traceable by the IIO. "Monitor the folder" is an activity made not only by the IIO, but by the insurance and the client, so it's a multi-participant task.

Concerning the exchange of data, in our extend model, data Objet are more clear. For example we can distinguish the private

process of the file some rules of collaborations must be checked by collaborators (these rules specifies that insurance X is in agreement with the organism). The file is then sent to the corresponding insurance which deals with it in turn and sends an answer to the organism. The process continues, if the client is not covered by insurance X, the IIO supervise the filed, then, the process ends. Otherwise, if the victim is insured by the insurance X the IIO reimburse the client. Of course this decision is sent to all collaborators. The IIO requests the funds from the insurance company, the latter makes its calculations and sends them to the organism, thus, the process of insurance X ends. Finally, the process of the organism ends after having received funds. In this process, there are several actors, namely: the client (or the victim), the intermediary organization (IIO) and the insurances that collaborates with the IIO. The exchange of data between these participants is done either by sending documents by email or post.

data (which keep the confidentiality of data). Rules date are input for the activity "treatment", in fact, this activity can't be performed if these rules are not satisfied. The integrity of data is clearly defined in the model (editable and locked data). And finely the decision data, when the IIO decide to refund the insured, all the participant (client, insurance) must be informed by a notification message .

6.2. Tool demonstration

For our demonstration we use Eclipse BPMN2 modeler which is built on the Eclipse Plug-in Architecture. This graphical modeling tools provide extension points that help to customize and edit the appearance of editor by using the extension mechanism of BPMN2.0.

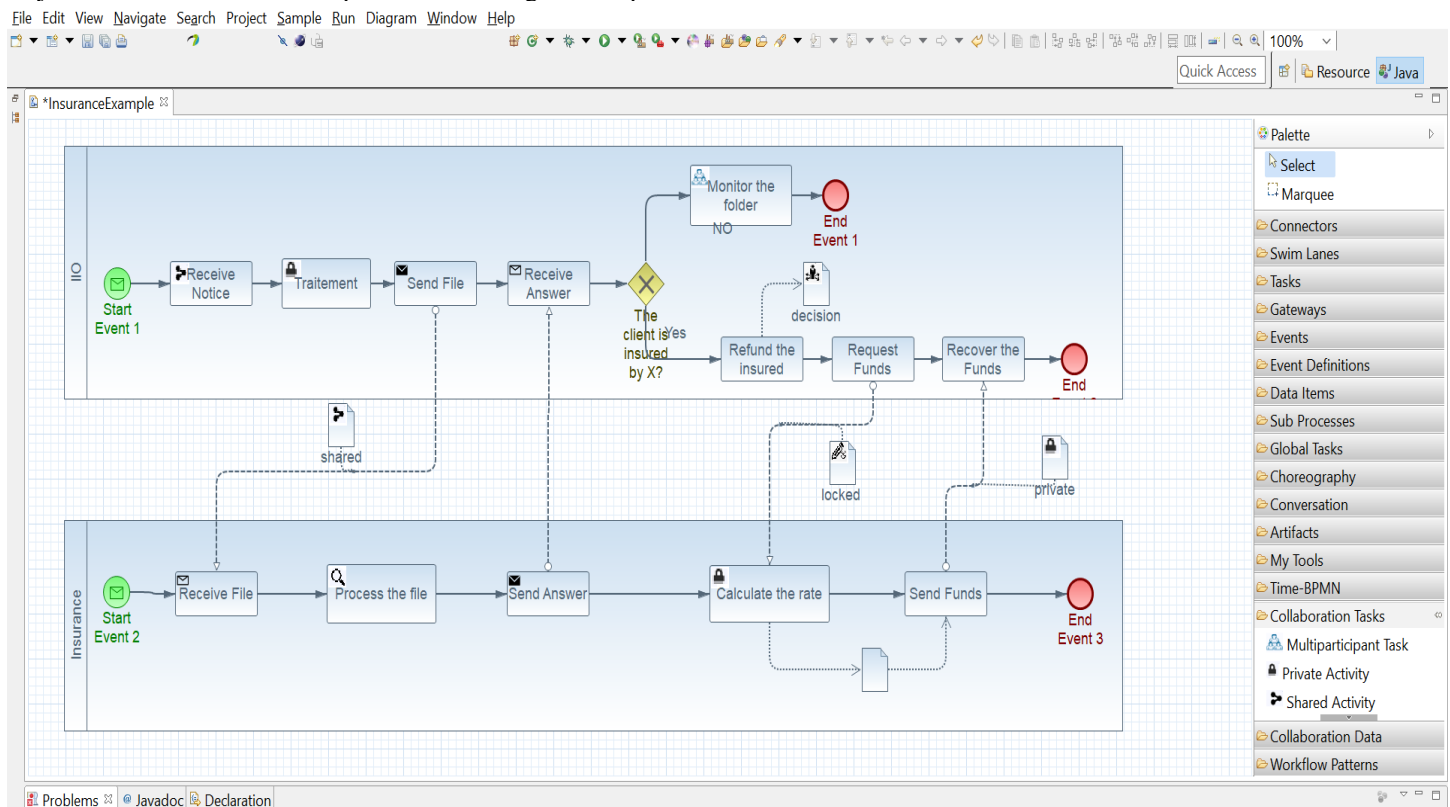


Figure 8: Screenshot from Eclipse that present Extension for Eclipse BPMN2 Palette

We developed a specific plug-in that represent the aspects of collaboration which are treated by our approach. As we have explained is an extension of the Eclipse BPMN2 Modeler plug-in [22]. It allows us to integrate new attributes, properties and new graphic elements adapted to our needs.

As we have extended in our work BPMN Activities and Data Objects. Now the BPMN2 palette include this new graphical element.

An example of a BPMN4Collaboration diagram and our proposed extension is depicted in Figure 8. We can see two tabs added in the palette "Collaboration Task" and "Collaboration Data". They contain the new graphical collaboration syntaxes explained by our approach.

7. Conclusion and future work

The modeling of collaborative processes is handled by several works and languages, namely the BPMN which is the standard most used by collaboration tools and companies. However, even the BPMN recognizes limitations in modeling collaborative processes and especially the modeling of data exchange that are presented in a general and unclear way. We have exploited the capacity of BPMN 2.0 extension mechanism which is specially designed to represent extensions of its standard elements to create an extension for collaborative environments [23]. We tried to add new concepts useful for BPMN modeling and we gave more attention to the representation of the data exchanged between the collaborators. To create this extension we began by collecting some aspects useful in modeling collaborative process, after we create our proper metamodel by extending BPMN metaclasses and adding new stereotypes. Then, we gave a graphical syntax to this new elements, also we have defined a textual semantic for the new extended element. We can say that our extension is a useful for modeling collaborative processes by providing more precision on the shared elements between partners.

Collaborative business processes are very complex and our extension only allows to treat a small part of this complexity. For that we will try in our next work: to enrich our extension even more by adding other aspects like security which is primordial in a collaboration environment. We will define a complete collaborative business process modeling language by adding semantics to our language. As we know, BPMN can be mapped to many executable languages to be implemented, so we will explain exactly how to implement our new elements, and how they can be implemented for example in existing BPMN tools such as JBoss Jbpm [24] or BonitaSoft [25] or others. And finally, the execution of these elements will be treated.

References

[1] Rittgen, P.: Collaborative Modeling – A Design Science Approach. In: Proc. HICSS '09. (2009) 1–10
 [2] J.Mending, J.C.Recker,, Wolf, J.: Collaboration features in current bpm tools. EMISA Forum 32 (2012) 48–65
 [3] Cours Angnès Front «Systèmes d'Information Conception et Processus»
 [4] H. Mili, G. B. Jaoude, É. Lefebvre, G. Tremblay, and A. Petrenko, « Business Process Modeling Languages: Sorting Through the Alphabet Soup », p. 54.
 [5] Business Process Modeling Notation Specification, OMG Final Adopted Specification, February 2006, dtc/06-02-01 (http://www.bpmn.org/Documents/OMG_Final_Adopted_BPMN_1-0_Spec_06-02-01.pdf).
 [6] Mayer, R.J., Menzel, C.P., Painter, M.K., deWitte, P.S., Blinn, T., Perakath, B.: IDEF3 Process Description Capture Method Report, Knowledge Based Systems, Inc., 1997.

[7] Eriksson, H.E., Penker, M. Business Modeling with UML: Business Patterns at Work, Wiley, 2000, ISBN 978-0-471-29551-8.
 [8] Scheer, A. W: Architecture of Integrated Information Systems: Principles of Enterprise Modeling. Berlin et al.. (1992).
 [9] Web Services Business Process Execution Language Specification. <<http://docs.oasis-open.org/wsbpel/2.0/OS/wsbpel-v2.0-OS.pdf>>
 [10] Stroppi, L.J.R., Chiotti, O., Villarreal, P.D.: Extending BPMN 2.0: Method and Tool Support. Business Process Model and Notation, 59- 73 (2011)
 [11] M. von Rosing, S. White, F. Cummins, and H. de Man, « Business Process Model and Notation—BPMN », in *The Complete Business Process Handbook*, Elsevier, 2015, p. 433-457.
 [12] M. Ben Hassen, M. Turki, and F. Gargouri, « A BPMN Extension for Integrating Knowledge Dimension in Sensitive Business Process Models », in *Information Systems*, vol. 299, M. Themistocleous and V. Morabito, Éd. Cham: Springer International Publishing, 2017, p. 559 578.
 [13] R. Braun, H. Schlieter, M. Burwitz, and W. Esswein, « BPMN4CP: Design and implementation of a BPMN extension for clinical pathways », 2014, p. 9 16.
 [14] N. Lohmann and M. Nyolt, « Artifact-Centric Modeling Using BPMN », in *Service-Oriented Computing - ICSOC 2011 Workshops*, vol. 7221, G. Pallis, M. Jmaiel, A. Charfi, S. Graupner, Y. Karabulut, S. Guinea, F. Rosenberg, Q. Z. Sheng, C. Pautasso, et S. Ben Mokhtar, Éd. Berlin, Heidelberg: Springer Berlin Heidelberg, 2012, p. 54 65.
 [15] Pedro Antunes and Al. « Modeling highly collaborative process » 2013
 [16] G. Decker and F. Puhlmann, « Extending BPMN for Modeling Complex Choreographies », in *On the Move to Meaningful Internet Systems 2007: CoopIS, DOA, ODBASE, GADA, and IS*, vol. 4803, R. Meersman et Z. Tari, Éd. Berlin, Heidelberg: Springer Berlin Heidelberg, 2007, p. 24-40.
 [17] O.Kopp, T.Binz, U.Breitenbucher, and F.Leymann « BPMN4TOSCA: A Domain-Specific Language to Model Management Plans for Composite Applications »
 [18] Zor, S., Leymann, F., Schumm, D.: A Proposal of BPMN Extensions for the Manufacturing Domain. In: Proceedings of the 44th CIRP Conference on Manufacturing Systems. (2011)
 [19] Raquel M.Pillat, Toacy C.Oliveira, Paulo S.C.Alencar, Donald D.Cowan «BPMN: A BPMN extension for specifying software process tailoring » *Information and Software Technology Volume 57*, January 2015, Pages 95-115
 [20] Rodriguez, A., Fern´andez-Medina, E., Piattini, M.: A BPMN Extension for the Modeling of Security Requirements in Business Processes. *IEICE Transactions on Information and Systems* 90(4) (2007) 745–752
 [21] Brucker, A.D., Hang, I., L'uckemeyer, G., Ruparel, R.: SecureBPMN: Modeling and Enforcing Access Control Requirements in Business Processes. In: *ACM Symposium on Access Control Models and Technologies*. (2012)
 [22] BPMN2 Modeler. <http://www.eclipse.org/bpmn2-modeler/>
 [23] L.Amdah and A.Anwar : BPMN Profile for Collaborative Business Process . The 5th International IEEE CiSt Congress on Information Sciences and Technology (Cist'18) .Marrakech, Morocco, October 21 – 24 ,2018
 [24] BonitaSoft Home page.< <http://www.bonitasoft.com/>>
 [25] JBoss jBPM Home page. < <http://www.jboss.org/jbpm>>

A Comparative Study of Safety Leading and Lagging Indicators Measuring Project Safety Performance

Sevar Dilkhaz Salahaddin Neamat*

Department of Mechanical Engineering, University of Zakho, 42002, Zakho, Kurdistan Region - Iraq

ARTICLE INFO

Article history:

Received: 30 August, 2019

Accepted: 18 November, 2019

Online: 12 December, 2019

Keywords:

Construction safety injuries

Leading indicators

Safety measures

Lagging indicators

ABSTRACT

The safety management system is recognized by safety leading and lagging indicators, and their correlation with injury rates. The background on this specific subject is vague in definition, labelling, and indicators measurement. The comparativeness between leading and lagging indicators have been introduced in the constructing safety performance projects evaluation. Safety performance leading indicators are the metrics of the safety method in constructing work. While the lagging indicators associated with safety results. Many suggestions have been considered during the usage and selection of the effective leading indicators. Also, the research results outlined that the leading indicators can be used to discriminate the variances in the safety performance of projects. In this specified research, leading and lagging indicators have been reviewed and investigated. Eighteen papers have been investigated from the period of 2010 to 2019 in order to recognize the common leading and lagging indicators. In addition, this review will recognize the gaps in leading and lagging research in order to concentrate on extra studies in that field. Four papers mentioned the correlation between lagging and leading indicators. A scoping review is focusing on the points and the significant ideas associated with the research area in accordance with the history time.

1. Introduction

In construction projects, fatality and disable injuries are larger than industry average by three times (Center for Construction Research and Training 2008). According to [1]–[3] the proactive safety management system have an effective and positive influence on the performance. In the past research many effective and proposed cause have been investigated. An examples of designing for safety management [3]–[5] and schedule-based safety management are mentioned [6], [7]. Nevertheless, during the construction work the safety proactive strategies should occur in order to catch the world-class performance. For example, pre-task preparation, stop work authority, and hazard acknowledgement programs used to control and recognize possible hazards which previously resulted in injuries [1], [2], [8]–[10].

To recognize the main reasons around site results of incidents and injuries, the leading indicators are identified. In addition, they have unrestrained hazards and administrative policies together with practices, agendas, and applies that monitor, control, and remove these hazards. The leading indicators are obtainable in

daily work of construction organization and have a better role in measuring the safety performance in the workplace.

In this study, a wide range of various leading indicators been investigated, including Alcohol / Drug Testing, Attitudes and Safety Climate, Fall Protection... until, Training and Job Safety Talks Worker.

The introduction of the comparison between using leading indicators of the safety performance correlatively with lagging indicators been proposed. Within the constructing projects the term of leading indicators used to assess the safety process, meanwhile lagging indicators describe the safety outcomes. This study investigates the most common list of leading and lagging factors associated with the selected articles. An example of lagging indicators, Behavior first aid and Reported Incidents. The research contains detailed overview of safety leading and lagging indicators and suggests a dissimilarity between leading indicators and lagging indicators of safety expectation. Researchers can use the results to explain and mark resource expenditures by means of universal scientific indication. Some other studies such as [10]–[14] used different technologies and others used web technology tools as in [15]–[20] to perform investigations.

* Sevar Dilkhaz Salahaddin Neamat, Email: sevar.dilkhaz@uoz.edu.krd

These positive approaches are seldom officially dignified or checked to recruit positive replies when results are not seen. Investigation was wanted to improved apprehend the strategies that might help as forecasters of safety performance and how they can monitor, and control safety risk. This study aims in determining what relationships are found when contractor administrative data is used to measure safety performance.

18 recent articles had been reviewed and analyzed to make a confident conclusion about the leading and lagging indicators to distinguish the positive and negative impacts between them and how they correlate to each other's. Only four paper discuss the interrelation between leading and lagging indicators. Ten leading indicators and two lagging indicators had been resulted after the analyzing of the 19 indicator to be further investigated in the future works.

2. Methodology of the Literature Review

In the beginning, it is a compulsion to cultivate a list of factors in order to choose which administrative data must be selected. To develop a widespread list of leading with lagging safety indicators that have been used in construction projects, a scoping review was accomplished. Additionally, to add a wide-ranging list of indicators, this study sums up the relationship between leading and lagging indicators in previous researches. In order to choose the suitable indicators for the review study, the contents of the earlier studies have been depended. Appropriate lessons were chosen using the electronic database such as PubMed, Scopus and Web of Science. The information coverage is from both medical and engineering research fields, very crucial in safety construction subjects.

Fifty papers were chosen by means of the search plan. Afterward the duplicate articles were omitted, 48 researches were reread for enclosure depended on the following criteria: 1) Construction fields association; 2) safety factors; 3) recognizing leading and lagging indicators; and 4) academic journals studies.

After that, 38 of the 48 articles remained with 10 exclusions due to duplications and not related to the desirable subject. Later on, 20 articles underwent further examination. Only articles that assessed the safety indicators at a construction project class were included. A total of 2 papers were unenclosed. Finally, the articles that have a direct relation to construction and safety indicators were involved. The remaining articles that have been depended in this study were 18 articles. We prepared some excel sheets to track the researchers, publication years, research types, and the goals together with the indicators that have been used with leading and lagging group. The steps for searching process are in shown figure 1.

Largely, the papers embrace case studies, pilot studies, and literature reviews. Additionally, only a few researchers participated in the research. Table 1 summarizes the type and goal of the reviewed researches.

As it can clearly be seen from the Table 1, the research goals of the final eighteen articles are wide-ranging. Leading indicators used in constructing work should firstly been developed. Secondly, tested in a construction project setting [1]. Numerous of these papers were focused on the first step – development of indicators. This includes defining [21], [22], developing [23]–[25], or measuring the indicators [26], [29].

The followed articles focused on progressing the indicators such as [21]–[27]. Only a few articles concentrated on the second step which is the testing on construction projects through completion of validation testing of the leading on the lagging indicators [1], [28].

The articles in this review paper were depended on the classified collection of safety indicators. The study categorized the indicators to either leading or lagging indicators. So, fifteen leading and four lagging indicators were comprised. By taking in consideration that not all authors used the same vocabularies for the similar indicators were grouped together for the purpose of this

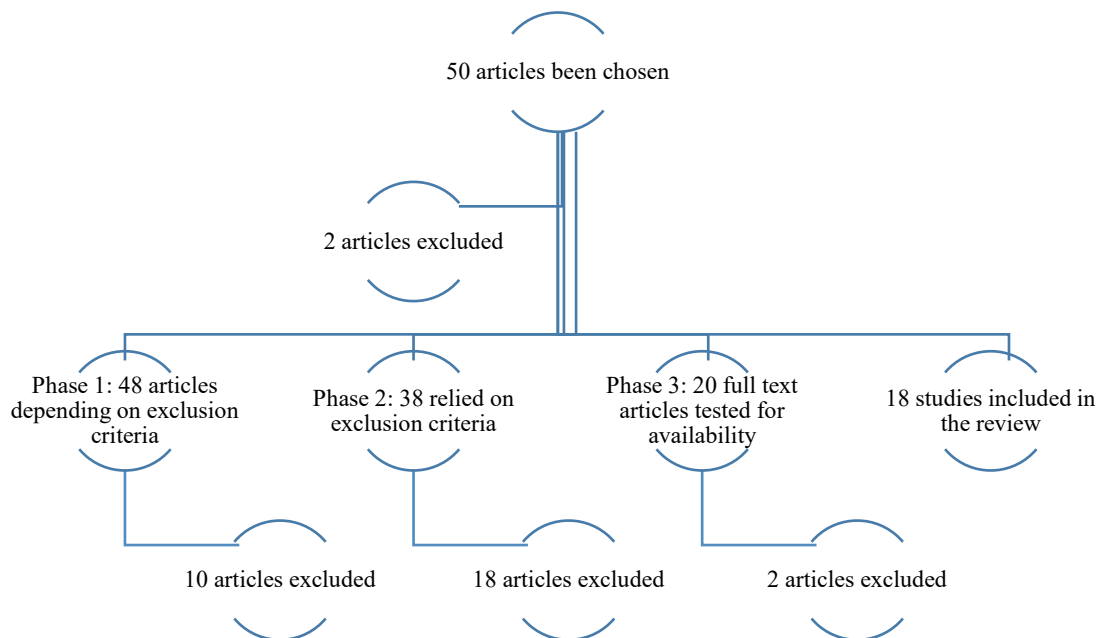


Figure. 1. The searching steps.

Table 1: Summary of Research Types and its Goals

Research	Year	Research Type and Goal
[26][27]	2010	Case Study: to measure the impact of a 5-S assessment tool and safety leading indicators on project safety
[23][24]	2011	Case Study: a once-a-month weighted safety key score and safety climate review were used to assess the safety performance on a construction project
[27][28]	2012	Case Study: analysis of use of a 5-S assessment tool on one construction project to observe how safety leading indicators were reported over the course of the project
[29][30]	2012	Academic framework for using safety performance pointers in safety-critical societies had been presented. It combines 3 sorts of safety performance indicators – outcome, monitor and drive indicators
[30][31]	2013	Review Article: Discusses the difference between passive and active leading indicators within construction safety performance
[31][32]	2013	Case Study: Analysis of leading and lagging indicators of one project to estimate leading indicators below real project circumstances
[32][33]	2014	Review Article: The paper emerged several articles, models utilized in designing of meters, object of study, objectives of interpretation, terms of implementation and revision, actors impacted by the product, and expressions to certify the scientific application and working feasibility
[33][34]	2015	Pilot Study: This research developed a leading indicator-based incentive program for construction projects
[24][25]	2015	Theoretical Article: This article works to create a conceptual framework for developing safety leading indicators for use within the construction industry
[22][23]	2016	Review Article: Discusses the literature on the leading indicator, safety climate, including on a project level.
[28][29]	2017	Case Study: Analysis of the temporal relationships of leading indicators within one five-year construction project.
[25][26]	2017	Focus Groups: This research works to develop indicators that influence site safety that can be measured using safety climate tools

[34][35]	2018	The paper displays a ML method in improving leading indicators that categorize places in accordance to their safety risk in construction projects.
[35][36]	2018	It would be necessary to improve compound key connecting the main features of safety containing the cultural and climatic issues to add a further illustrative picture of platforms' safety performance
[36][37]	2018	Quasi-experimental longitudinal investigation design will be used within 2 Ontario critical clinics. The first stage of the investigation will be based on evaluating the existing OHSMSs consuming the leading indicators. 2 nd will pilot test and assess the tailored intervention
[37][38]	2019	In a cross-sectional analysis of CSAP (Contractor safety assessment program) database, several organizational leading safety indicators have been identified, that are associated with safety performance in the construction industry
[38][39]	2019	This research symbolizes safety prequalification reviews presently in usage in the construction industry to recognize methods that contain leading indicators of employee safety performance
[39][40]	2019	This study contains a comprehensive review of safety leading pointer research, suggests a dissimilarity between leading indicators and other approaches of safety prediction, and describes a clear method for distinctive between active and passive indicators.

scoping review. The furthest communal pointers that were classified as leading indicators were, attitudes and safety climate, site inspections/audits, training and safety talks, and worker safety behavior.

The most popular factors among lagging groups were first aid injuries and lost time injuries. More information can be noticed in Table 2.

Only the indicators that been used in two or more than two studies have been selected in the results. Some indicators were only used by [26], [27]. Though, these writers did not express their indicators or categorize what was measured, beyond a wide classification, such as fall protection. Consequently, some usable indicators by these researches were not further explained. Including, fall protection, ladders and stairs, Personal Protection Equipment (PPE), and railings and covers.

2.1. Results of Comprehensive Literature Review

Ten leading indicators and four lagging indicators were identified over a scoping review. Also, they have been used in researches that concentrated on contractor project data. The lagging and leading indicators will be more clarified below.

2.1.1. Summary of Leading Indicators

In this section, the leading indicators are widely discussed and proposed than lagging indicators. These studies appeared to be concentrated more on the attitude and behavior of the leading indicators such as safety climate, in comparison to avoidance indicators such as site inspections. The familiar leading indicators are proposed below:

Attitudes and Safety Climate: Numerous articles largely premeditated the attitude of employees or managers in the place of work. One specific measure is safety climate. Safety climate is largely well-defined as the employee insights of safety in the job site, specifically as it related to manager opinions [22], [40].

Housekeeping: Housekeeping is considered a physical hazard indicator in the workplace [25]. Housekeeping is a comprehensive phrase restricting the cleanliness of a site. It comprises features such as waste removal, and material and equipment storage (Construction Projects, 1991).

Near Miss: Is deliberated a close call incident. It may cause injuries or totally damaged, but no damage was caused [1] as the navigation of how to manage and control the hazards and avoid it is occurrence in the workplace. Through using PPE, change in the task sequence and controlling of guards [49].

Safety Corrections: In the [26], [27] Safety Corrections are measured as safety correction frequencies prepared by workers on an ad hoc basis. Conversely, [23], measured non-compliance measurements during the site inspections.

Site Inspections: Site inspections, and their similar coordinate, site examining, are tests that evaluate the hazards number on the workplace. In [1] used a scoring system where opinions were subtracted depended on the number of safety violations that happened on the site. Site checks are checklists prepared by some familiar individuals such as a supervisor or safety representative [28].

Subcontractor Safety: Subcontractor safety can be noticed at various levels. [24] Focused on the subcontractor managing of safety as an indicator in the advance safety condition. Also, in project construction until now they did not offer a measurement methodology. In [33] the calculated subcontractor safety performance system depended on the subjective calculation which investigates safe and unsafe work comments to add a single score. [30] Added examples on how subcontractor safety system can be worked and restrained subcontractor safety score not from job work actions Prior to subcontractor award relied on subcontractor safety history, safety policy and their site-specific safety program and pre-task safety plan [24].

Table 2: Leading and Lagging Indicators

Research	Year	Leading Indicators														Lagging Indicators				
		Alcohol / Drug Testing	Attitudes and Safety Climate	Fall Protection	Housekeeping	Ladders and Stairs	Near Miss	Pre-Task Safety Plans	Personal Protection Equipment	Railings and Covers	Safety Corrections	Safety Positive Reinforcement	Site Inspections / Audits	Subcontractor Safety	Training / Job Safety Talks	Worker Safety Behavior	First Aid Injuries	Lost Time Injuries	Members of the Public Injured	Reported Incidents
[26][27]	2010			✓	✓	✓			✓	✓	✓									
[23][24]	2011		✓							✓		✓		✓	✓	✓	✓	✓		
[41][42]	2012			✓	✓	✓			✓	✓	✓									
[29][30]	2012		✓				✓	✓		✓	✓	✓	✓			✓	✓			
[30][31]	2013		✓				✓				✓	✓	✓	✓						
[1]	2013						✓	✓				✓			✓	✓	✓			✓
[32][33]	2014	✓	✓	✓	✓				✓		✓								✓	
[24][25]	2015		✓		✓			✓						✓	✓	✓	✓			✓
[33][34]	2015												✓	✓	✓					
[22][23]	2016		✓												✓					
[28][29]	2017	✓						✓				✓		✓				✓		
[25][26]	2017		✓											✓	✓					
[34][35]	2018		✓				✓							✓					✓	✓
[36][37]	2018														✓	✓	✓	✓	✓	✓
[35][36]	2018		✓																	
[37][38]	2019	✓		✓	✓	✓	✓		✓			✓				✓	✓			
[38][39]	2019						✓					✓	✓	✓	✓					

[39][40]	2019		✓				✓			✓		✓	✓			✓
----------	------	--	---	--	--	--	---	--	--	---	--	---	---	--	--	---

Training/Job Safety Talks: [24] point out safety discussions, safety instruction, and safety training for supervisors to edit safety conditions considered as safety practices. Training has often measured a side of safety climate [22], [25]. Toolbox talks, or job safety talks, used to change the conversation between the management and workers on a steady base and can be seen as a type of safety communication [28].

Worker Safety Behavior: Worker safety behavior was dignified in lots of studies. It includes measures such as worker participation in safety [22], employee safety inspiration, and worker safety capability [24]. [1] depended on using checklists instead of safety professional evaluation to evaluate workers' safety behavior.

As shown by the leading indicators explained above, the leading indicators focused on hazard identification or correction such as site inspections or training, as well as attitudes and behaviors such as safety climate. All indicators were related to behaviors or attitudes that promote accident prevention rather than negative safety outcome.

2.1.2. *Summary of Lagging Indicators*

Lagging indicators, have been researched within a longer time than leading, are typically easily accessible and well documented. Yet, lagging indicators were less commonly used in the studies of this specified review. Lagging indicators are generally accessible as they are reporting measures that are required by various health and safety authorities. It used to track company performance and to monitor injury trends (OHSa, 1990). It makes the research on lagging indicators convenient. Yet, despite the convenience, there seems to be a shift towards leading indicators in the current research. This shift leaves common lagging indicators such as first aid injuries and lost time injuries, less used in research.

There are many reasons as to why lagging indicators are less commonly researched. One is the focus on injury prevention in research and in occupational health and safety practice. Researchers and practitioners have chosen to focus on indicators that can lead to injury prevention, such as site inspections, instead of indicators that document safety outcomes, such as injuries. The thought is that leading indicators allow for research to be more proactive, rather than retroactive with lagging indicators

First Aid Injuries: First aid injuries include any injury that can be treated with minimal first aid and require no further medical treatment [1]. First aid injuries are recorded on site as part of the reporting requirements in the OHSa (1990). This reporting requirement is similar across many jurisdictions. This measure was included by [23] as well.

Lost Time Injuries: Lost Time Injuries or Total Recordable Injury Rate is the ratio used by the United States Occupational Safety and Health Administration (OSHA) including any injuries that require medical treatment beyond first aid [1].

A subset of the Total Recordable Injury Rate is the Lost Time Injuries, where workers miss work leading to loss of earnings (Ontario Health and Safety Act, 1990). The documentation of lagging indicators is related to safety authority documentation www.astesj.com

requirements. The type of indicators used, whether total recordable injury rate or lost time injuries, is often based on the safety authority in the research area. Lost time injury is the more commonly used metric, as it is used by the Workplace Safety and Insurance Board (WSIB) under the reporting requirements of the OHSa (Ontario Health and Safety Act, 1990).

As it can be seen through the factors recognized in this study, the lagging indicators were correlated to undesirable safety results and precisely varying levels of injuries. Lagging indicators are willingly obtainable depended on government recording requirements, but are not widely used in the investigation in favors of leading indicators.

2.1.3. *Interaction of Leading and Lagging Indicators*

The scoping review concentrated on how leading and lagging indicators are correlated to one another during construction projects. To the best of our knowledge, only four studies were found investigating such studies. Therefore, this interaction became the main part of the project discussion. Unfortunately, although these four studies added some research into leading and lagging indicators in construction projects, the existence of limited articles being obtainable, presented the necessity for more research in this field.

Research [28] had been accomplished the analyses of leading indicators temporally. The researchers are not insured if the leading indicators are really leading, and how time-consuming until the implementation of leading indicators resulted in the improvements of the lagging indicators. They planned 11 leading indicators counting safety talks, hazards testified and safety inspections. These academics used frequency data gathered by sub-contractors and workers on a huge, five-year construction project in Australia.

This incidence data experienced numerous stages of pre-processing such as modification for man hours previous to being involved in results. This research found that the 'leading' feature of leading indicators is really energetic in nature. Leading indicators did not develop the lagging indicator, precisely the full recordable injury rate is estimated in the foreseeable technique.

This led the researchers to consider that the safety leading indicators is complicated. Additionally, they suggest that there is a two-directional correlation between leading and lagging meters. Similar, this paper was not supporting the considerable temporal feature of leading indicators. They resulted through the searching that leading indicators both led and lagged. For instance, toolbox talks caused to minimize in injuries for the first 4 months then damages led toolbox talks for the next 2 months. Herein matter, toolbox talks and injuries considered as a leading and lagging indicator, and were consequently bidirectional. This demonstrates that theory that forms the basis leading and lagging indicators is very simple in relation to the nature of construction complexity. These writers recommend concentrating fewer on leading and lagging categories, and somewhat tag indicators as positive and negative. Whereas the research almost provided the research on leading and lagging indicators, they are unsuccessful in verifying in what way the importance of their research effects management

and construction companies. In spite of that, they pay attention to the significance of this paper on other research. Such that, if the use of leading and lagging expressions possibly will outcome with struggles in the research setting, would it not also cause complications in management interference? This specific question and many still in vague.

The authors of [49] evaluated the active and passive leading indicators relationship in the safety construction projects by using meta-analysis technique. Depending on [42] and [43], the analyzing been prepared. The meta-analysis process consisted of four stages, literature reviewing, coding studies, normalizing effect sizes, computing the combined effect size. The researchers used the followed search engines to collect the papers ASCE, Web of Science, Scopus, Engineering Village, and Google Scholar. Moreover, many different keywords been used to search such as, safety management system, safety program, construction safety practices, safety performance, safety strategies, safety leading indicators, and proactive indicators. 114 papers had been selected to take apart in the study. Some conditions must be present in the studies that participate in the meta-analysis procedure, if they: 1) examined the association between either active or passive safety leading indicators and accidents or injury; 2) re-counted the effect size (e.g., correlation values) or sufficient info to compute the effect size; 3) tested data from the construction industry; and 4) were peer studied.

As a result, the analyzing software found that the effect sizes of correlation of leading and lagging are extensively different, nine construction safety leading indicators participated in this analysis. The effect sizes of the relationships among safety inspection and observation and injury ($r = 0.51$; 95%CI = 0.30–0.67) and between pre-task safety meeting and injury were very large ($r = 0.45$; 95%CI = 0.32–0.57). For the nine passive leading indicators, eight were significant ($p < 0.05$), the relationship between injury rate and safety record ($r = 0.56$; 95%CI = 0.20–0.79) and safety resources ($r = 0.48$; 95% CI = 0.28 to 0.65) had large effect sizes. Staffing for safety ($r = 0.44$; 95%CI = 0.12–0.68), owner involvement ($r = 0.45$; 95%CI = 0.16–0.67), training and orientation ($r = 0.42$; 95%CI = 0.10–0.66), personal protective equipment ($r = 0.40$; 95%CI = 0.17–0.58), and incentives programs ($r = 0.30$; 95%CI = 0.15–0.43) were all moderate. Finally, the effect size of safety inspections and observation was low ($r = 0.27$; 95%CI = 0.12–0.41), and that of pre-task meetings was not significant ($p = 0.103$). Finally, the results ensured that the pre-task safety meetings considered an important forecaster for future performance measurement. If dignified and preserved as an active leading indicator. However, considering pre-task safety meetings as a passive pointer is not prognostic.

In [34], the research demonstrates a method in order to improve the leading indicators that categorize the location according to construction work safety risk. The key forms of statistics involved is the safety examination accounts, accident cases and project-related data. The data achieved from a big contractor company in Singapore and collected from 2010 till 2016. From 33 independent variables, 13 input variables had been chosen by a connection of Boruta feature collection technique and decision tree. Six of 13 input variables are project-related (type of project, project possession, contract amount, percent finished, level of postponement and plan manpower) and 7 of them are matters in

the contractor's safety inspection checklists (crane/lifting operations, scaffold, mechanical-elevated working platform, falling hazards/openings, environmental management, good practices and weighted safety inspection score). The author used 5 common machine learning algorithms to run models for the forecast of accident existence and harshness. Throughout predicting the validity, random forest (RF) added the greatest forecast performance with an accurateness of 0.78 and has attained a considerable power of arrangement with Weighted-Kappa Statistics of 0.70. Associating with parallel studies, this outcome is talented. The forecast (i.e. the output variable) added by the RF model can be used as a safety leading pointer of the risk level of a place. It is suggested that the prognostic RF model be organized in construction administrations, particularly large public and private creators, contractors and industry relations, to offer a monthly prediction of project safety performance so that preventive examinations and involvements can be fulfilled in a further directed manner.

In [1] the author gathered both leading and lagging indicators for a single constructing project in order to reveal any relation between the indicators of leading and lagging. The three leading indicators recycled were pre-task plan review, worker safe behavior remark mark, and site safety audit score. After that, they have been investigated to show a correlation between the four lagging indicators: first aid or emergency treatment, near-miss incidents, OSHA recordable incidents, and all project incidents. This info was gathered for 37 weeks by safety professionals. The researchers found the associations between pre-task plan review and total incidents ($r = -0.507$), pre-task plan review and first aid (emergency treatment) ($r = -0.573$), worker safe behavior observations and whole incidents ($r = -0.588$), worker safe behavior observations and first aid ($r = -0.635$). Although the relationships observed were talented, the statistical significance for the correlation coefficients were not added. Additionally, the research based on optimistic results to clarify that out of 12 only 4 only correlations sustained the research hypothesis. The writer added little dialogue of the undesirable results or afford results that did not support their 19 hypotheses. Meanwhile, this research paper started the conversation on leading and lagging indicators on construction projects, an additional vigorous investigation should be done.

The four studied that discussed above added the information in leading and lagging during a construction job. The pilot/case study type of study delivered the vision into the actual relations of these indicators, but superior examples want to be recycled in extra research. Moreover, the results showed that the leading and lagging are not easily correlated and are complex in construction work. While there is a lack of info on the correlation between leading and lagging, some decisions must be done depending on the articles examined. Lagging indicators based on injuries and incidents. All lagging pointers had negative results, corresponding the description of lagging indicators. Further hand, leading indicators can be classified into categories: attitudes and avoidance actions. Instances of leading indicators that evaluate outlooks contain the safety climate and manager attitude towards safety. Illustrations of leading indicators concentrated on the protective measures such as, employee safe behaviors, site safety inspections and pre-task safety plans. Leading indicators depended on the popular attitudes, this result is because the avoidance leading

indicators measurement not always negatively related to lagging indicators such as pre-task plan review and site inspections, shown by researches [1] and [23].

3. Conclusion

In conclusion, the sample size of 18 recent articles have been reviewed and analyzed to make a confident conclusion about the leading and lagging indicators in construction. The research is made in order to distinguish the positive and negative impacts between leading and lagging indicators and how they correlate to each other's. Only four papers discuss the interrelation between leading and lagging indicators. Ten leading indicators and two lagging indicators have been resulted after analyzing 19 indicators to be further investigated in the future works, which focused on contractor project data. This review paper will be very benefit to be a start point in the deeply future research.

References

- [1] J. Wanberg, C. Harper, M. R. Hallowell, and S. Rajendran, "Relationship between construction safety and quality performance," *J. Constr. Eng. Manag.*, **139**(10), p. 04013003, 2013.
- [2] M. R. Hallowell and J. A. Gambatese, "Construction safety risk mitigation," *J. Constr. Eng. Manag.*, **135**(12), 1316–1323, 2009.
- [3] S. Neamat, "Factors Affecting Project Performance in Kurdistan Region of Iraq," *Int. J. Adv. Eng. Res. Sci.*, **4**(5).
- [4] J. A. Gambatese, J. W. Hinze, and C. T. Haas, "Tool to design for construction worker safety," *J. Archit. Eng.*, **3**(1), 32–41, 1997.
- [5] T. M. Toole, "Construction site safety roles," *J. Constr. Eng. Manag.*, **128**(3), 203–210, 2002.
- [6] N. A. Kartam, "Integrating safety and health performance into construction CPM," *J. Constr. Eng. Manag.*, **123**(2), 121–126, 1997.
- [7] J. Hinze, J. Nelson, and R. Evans, "Software integration of safety in construction schedules," presented at the Proceedings of the 4th Triennial International Conference, Rethinking and Revitalizing Construction Safety, Health, Environment and Quality, Port Elizabeth, South, Africa, 2005, 16–17.
- [8] P. X. Zou, "Fostering a strong construction safety culture," *Leadersh. Manag. Eng.*, **11**(1), 11–22, 2010.
- [9] K. Jacksi, "Database Teaching in Different Universities: A Phenomenographic Research," *Int. J. Emerg. Technol. Comput. Appl. Sci.*, **2**(12), 96–100, May 2015.
- [10] S. Neamat and I. Yitmen, "Factors Affecting the Innovation and Competitiveness in Kurdistan Region of Iraq Construction Industry," *Int. J. Adv. Eng. Res. Sci. IJAERS*, **4**(2), 157–162, 2017.
- [11] S. Neamat, "The Development Of Management Control Systems Framework In Public-Private Partnerships," *Int. J. Sci. Technol. Res.*, **8** (10), 299–305, 2019.
- [12] S. Neamat, "A Developed Framework for Energy Technology Sustainability Assessment," *Int. J. Innov. Technol. Explor. Eng. IJITEE*, **9** (1), 832–838, 2019.
- [13] S. Neamat, "Models Developed for Creep of High Strength Concrete," *Infogain Publ*, **3** (3), 174–80, 2017.
- [14] S. D. Salahaddin, "Factors Affecting the Competitiveness and Innovation in Northern Iraq Construction Industry," 2016.
- [15] K. Jacksi and S. M. Abass, "Development History of the World Wide Web." 2016.
- [16] K. Jacksi, "Design and Implementation of E-Campus Ontology with a Hybrid Software Engineering Methodology." 2016.
- [17] K. Jacksi, S. R. M. Zeebaree, and N. Dimililer, "LOD Explorer: Presenting the Web of Data," *Int. J. Adv. Comput. Sci. Appl. IJACSA*, **9** (1), 2018.
- [18] M. A. Sadeeq, S. R. Zeebaree, R. Qashi, S. H. Ahmed, and K. Jacksi, "Internet of Things Security: A Survey," presented at the 2018 International Conference on Advanced Science and Engineering (ICOASE), 2018, 162–166.
- [19] K. Jacksi, N. Dimililer, and S. R. M. Zeebaree, "A Survey of Exploratory Search Systems Based on LOD Resources," in PROCEEDINGS OF THE 5TH INTERNATIONAL CONFERENCE ON COMPUTING & INFORMATICS, COLL ARTS & SCI, INFOR TECHNOL BLDG, SINTOK, KEDAH 06010, MALAYSIA, 2015, 501–509.
- [20] K. Jacksi, N. Dimililer, and S. R. Zeebaree, "State of the Art Exploration Systems for Linked Data: A Review," *Int. J. Adv. Comput. Sci. Appl. IJACSA*, **7**(11), 155–164, 2016.
- [21] J. Hinze, S. Thurman, and A. Wehle, "Leading indicators of construction safety performance," *Saf. Sci.*, **51**(1), 23–28, 2013.
- [22] N. V. Schwatka, S. Hecker, and L. M. Goldenhar, "Defining and measuring safety climate: a review of the construction industry literature," *Ann. Occup. Hyg.*, **60** (5), 537–550, 2016.
- [23] H. Lingard, R. Wakefield, and P. Cashin, "The development and testing of a hierarchical measure of project OHS performance," *Eng. Constr. Archit. Manag.*, **18** (1), 30–49, 2011.
- [24] B. H. Guo and T. W. Yiu, "Developing leading indicators to monitor the safety conditions of construction projects," *J. Manag. Eng.*, **32**(1), p. 04015016, 2015.
- [25] M. Niu, R. M. Leicht, and S. Rowlinson, "Developing safety climate indicators in a construction working environment," *Pract. Period. Struct. Des. Constr.*, **22**(4), p. 04017019, 2017.
- [26] K. Ng, A. Laurlund, G. Howell, and G. Lancos, "An experiment with leading indicators for safety," presented at the Proceedings Annual International Group for Lean Construction Conference, 2010, 253–262.
- [27] K. Ng, A. Laurlund, G. Howell, and G. Lancos, "lean safety: using leading indicators of safety Incidents to improve construction safety," presented at the Proceedings for the 20th Annual Conference of the International Group for Lean Construction: are We Near a Tipping Point, 2012, p. 173.
- [28] H. Lingard, M. Hallowell, R. Salas, and P. Pirzadeh, "Leading or lagging? Temporal analysis of safety indicators on a large infrastructure construction project," *Saf. Sci.*, **91**, 206–220, 2017.
- [29] T. Reiman and E. Pietikäinen, "Leading indicators of system safety—monitoring and driving the organizational safety potential," *Saf. Sci.*, vol. **50**(10), 1993–2000, 2012.
- [30] J. Hinze, S. Thurman, and A. Wehle, "Leading indicators of construction safety performance," *Saf. Sci.*, **51**(1), 23–28, 2013.
- [31] S. Rajendran, "Enhancing construction worker safety performance using leading indicators," *Pract. Period. Struct. Des. Constr.*, **18**(1), 45–51, 2012.
- [32] G. Delatour, P. Laclémence, D. Calcei, and C. Mazri, "Safety performance indicators: a questioning diversity," presented at the 6. International Conference on Safety & Environment in Process & Power Industry (CISAP-6), 2014, **36**, 55–60.
- [33] E. H. Sparer, R. F. Herrick, and J. T. Dennerlein, "Development of a safety communication and recognition program for construction," *New Solut. J. Environ. Occup. Health Policy*, **25**(1), 42–58, 2015.
- [34] C. Q. Poh, C. U. Ubeynarayana, and Y. M. Goh, "Safety leading indicators for construction sites: A machine learning approach," *Autom. Constr.*, **93**, 375–386, 2018.
- [35] K. H. D. Tang, S. Z. M. Dawal, and E. U. Olugu, "A review of the offshore oil and gas safety indices," *Saf. Sci.*, **109**, 344–352, 2018.
- [36] J. M. Almost et al., "A study of leading indicators for occupational health and safety management systems in healthcare," *BMC Health Serv. Res.*, **18**(1), p. 296, 2018.
- [37] J. Manjourides and J. T. Dennerlein, "Testing the associations between leading and lagging indicators in a contractor safety pre-qualification database," *Am. J. Ind. Med.*, **62**(4), 317–324, 2019.
- [38] K.-H. Liu, J. Tessler, L. A. Murphy, C.-C. Chang, and J. T. Dennerlein, "The gap between tools and best practice: an analysis of safety prequalification surveys in the construction industry," *NEW Solut. J. Environ. Occup. Health Policy*, **28**(4), 683–703, 2019.
- [39] W. M. Alruqi and M. R. Hallowell, "Critical Success Factors for Construction Safety: Review and Meta-Analysis of Safety Leading Indicators," *J. Constr. Eng. Manag.*, **145**(3), p. 04019005, 2019.
- [40] S. Neamat, "Risk Assessment for Uzun Construction and Real Estate Company in TRNC," *Sch. J. Econ. Bus. Manag.*, **5**(3), 332–343, 2018.
- [41] K. Ng, A. Laurlund, G. Howell, and G. Lancos, "lean safety: using leading indicators of safety Incidents to improve construction safety," presented at the Proceedings for the 20th Annual Conference of the International Group for Lean Construction: are We Near a Tipping Point, 2012, p. 173.
- [42] N. A. Card, "Applied meta-analysis for social science research: Methodology in the social sciences," N. Y. Guilford, 2011.
- [43] J. Tenboer et al., "Time-resolved serial crystallography captures high-resolution intermediates of photoactive yellow protein," *Science*, vol. **346**(6214), 1242–1246, 2014.

Fabrication of Glaze Material from Recycled Bottle Glass and Kaolin

Agus Dwi Anggono*, Elkana Bilak Lopo, Joko Sedyono, Tri Widodo Besar Riyadi

Department of Mechanical Engineering, Universitas Muhammadiyah Surakarta, Jl.Ahmad Yani, PO.BOX 1 Pabelan, Surakarta 57162, Indonesia

ARTICLE INFO

Article history:

Received: 24 October, 2019

Accepted: 22 November, 2019

Online: 12 December, 2019

Keywords:

Glaze

Recycle Glass Bottle

Kaolin

Vickers Hardness

ABSTRACT

This research aimed at developing a method of glaze material making from used glass bottle waste combined with kaolin. Then, the microstructure and hardness level of glaze products were characterized. Furnace heaters were used in research to heat glaze material by varying the holding time of 30, 45 and 60 minutes. The composition of glaze material was varied with the ratio between glass and kaolin of 70:30, 80:20 and 90:10. The results revealed that the process of glaze material making was successfully carried out. The results of the hardness test showed that at the 30 minutes holding time, the hardness was 82.53 VHN. The hardness value increased when the holding time was 45 minutes with an average hardness value of 85.03 VHN. The highest average hardness obtained when the variation of 60 minutes holding time was 87.6 VHN. The difference in hardness value in variation possibly occurred because of the differences in the distribution of amorphous solids, porosity, and pinhole which was influenced by the differences in glass and kaolin composition.

1. Introduction

Ceramic glass products are widely known for their unusual combination properties which have exotic combinations of material properties that produce a variety of high-tech products according to the market needs [1]. S.D Stookey introduced the term “pyroceram” for ceramic glass (glass code 9606) in which pyroceram is an original ceramic glass material developed and licensed by Corning Glass in the 1957s. Prior to the development of pyroceram, Stookey worked in controlled crystallization in glasses that were sensitive to radiation (glass code 8603) and was named photosensitive opal glass. But in 1959, Stookey adopted and used the term “ceramic glass” for two types of material, not depend on the type of nucleation agent used (Cu, Ag, Au or TiO₂) [2].

The term ceramic glass indicates a material that contains a significant crystal volume fraction of > 50%. The volume fraction of ceramic glass crystals is significantly lower than that which has been developed over the past 60 years. Therefore, problems that limit the number of crystalline phases or the composition of ceramic glass have been removed. Aluminasilikat system is widely used as an object of research and has been commercialized as ceramic glass materials. The importance of new features in the

development of ceramic glass production is the need for evolution control in various types of crystals simultaneously or independently grow in large numbers or on the surface of the sample [3][4].

Ceramic products have been widely applied in engineering, especially in machineries such as cutting tools, nozzles, valves, turbines, and ball bearing [5]. The advantages of ceramics, in general, are a high melting point, high-temperature resistance, friction resistance, corrosion resistance, low heat conductivity, relatively low density and low thermal expansion coefficient [6]. Currently, ceramic materials have been developed into modern products with very varied advantages. Ceramic base material in the market is usually made from clay which has passed the process of molding, heating, and finishing. Clay is one of the basic ingredients of ceramic which is plastic, easy to print, stiff after being dried and glassy after being heated at a certain temperature. The use of clay as a base for ceramics is largely determined by the nature of the mineral of the clay compilers. The nature of clay minerals is determined by several factors such as chemical composition and mineral types, physical and chemical properties, and the structure of clay minerals so that clay quality test as a ceramic raw material can not only be determined by chemical composition testing, but also must be tested through the test for the types, mineral structures and physical properties. The clay is most commonly used as ceramic materials such as red brick, tile,

*Corresponding Author: Agus Dwi Anggono, Email: ada126@ums.ac.id

earthenware, and others. Generally, the tile is made of clay, but it has some weaknesses such as cracking, breaking and selling price is too expensive. So, it is necessary to increase mechanical and physical properties through experimental studies of the material coating.

The data from the Ministry of Environment and the Ministry of Public Works of the Republic of Indonesia in 2017 showed that the total waste in Indonesia reaches 187.2 million tons/ year, where the composition of glass waste reached 17% of 187.2 million tons. Waste is the material that is thrown, will be thrown or no longer used according to its purpose in which a material considered waste if no longer used or it is essentially a kind of waste such as liquid waste. From the data, it can be seen that if the waste cannot be reduced, it will harm the environment and nature. Quoted from ristekdikti.go.id about "how to manage urban waste" written by Agus Puji Prasetyono, it is said that the priority of the city or capital to waste becomes "Apiori" in which apiori is existing knowledge before having experience. The term is used to explain that someone can think and have assumptions about everything before having experience and finally draw conclusions. By this, talk about rubbish means to talk about "how". Therefore this becomes a guideline or motivation in selecting the research topic. It should be noted that glass waste takes 10-1000 years for the glass to completely decompose. Based on this, concrete steps must be taken to reduce glass waste so that the amount of glass waste does not increase. Several steps to reduce glass waste are implementing the 3R method involving Reuse, Reduce and Recycle. This method has been carried out by several industries, non-governmental organizations, and individuals who care about the environment and want to help to reduce the impact of glass waste on the environment. From those three steps, the quite effective step in reducing the impact of glass waste is recycle stage. Recycle method is the process of turning a used material into a new material to prevent waste. By applying the recycling process, it is expected that glass waste can be utilized as reusable materials and can reduce waste at a certain limit, can save natural resources and reduce dependence on certain raw materials.

The research reported by Celik [7] on ceramics making using mineralogy method and chemical analysis method which is a sample of raw soil was carried out using X-ray diffraction (XRD) techniques to obtain clearer soil patterns. Clay minerals can be expanded and then heated to 550°C for 3 hours to differentiate chlorite and kaolinite. The XRD pattern is obtained from Rigaku Rint-2200 diffractometer that operates at a tube voltage and current of 40kV and 30mA. Related to "Thermal analysis (DTA-TGA)", Netzsch STA 409 differential calorimeter tool under atmospheric air is used to analyze thermal termogravimetri (DTA-TGA). The temperature is raised from room temperature to 1200° C at a speed of 10° C per minute and maintained at this maximum temperature for 10 minutes. In "Dilatometry test", raw clay is heated to 1200° C at a heating rate of 50° C per minute to 1100° C, and 30° C per minute for temperatures between 1100° C and 1200° C is maintained at a maximum temperature of 10 minutes. Samples that are dried overnight at 105° C were then heated in a Misura dilatometer of 3.32 (ODHT-HSM) in which 1600/80 changes are recorded every minute during heating. From the research, it is concluded that clay from Afyon Istanbul is characterized using chemical, mineral and thermal analysis. Afyon clay has the

qualities needed to make ceramic tiles and is an alternative ceramic raw material for developing Turkish ceramic tiles.

In [8], the authors reveal that alumina-oriented ceramics with fraction textures ranging from 9.6% to 93.6% are prepared by templated grain growth (TGG) of nanoscale matrices, the fraction texture can be controlled directly on ceramic density, and absorption of grain texture can be observed at $\geq 58.4\%$. The research used the X-ray diffraction (XRD) method, morphological features can be observed by scanning electron microscopy (SEM), to measure the density using the Archimedes method, the characteristics of mechanical properties are measured by three bends in universal testing, while hardness testing uses Vickers indenter (HVS-5). By this, it is concluded that the microstructure, mechanical properties, and the development period of alumina ceramic textures occur the compaction in the sample. Anisometric granules attachment occurs when orientation of $\geq 58.4\%$, cracked deflection between surfaces originating from oppressed grains because energy fractures is lower than the surface, in which further enhancements result in longer cracking deflection distances, texture characteristics of 93.6% alumina ceramics substantially increase $K_c = 4.6 \text{ MPa}\cdot\text{m}^{1/2}$ and $\sigma_f = 589 \text{ MPa}$, and therefore the luck occurs when the crack deflection.

In [9], the researchers report that the implementation of innovative materials for energy-saving focusing on the building sector is a very interesting topic throughout the world. In this case, aerogel is indicated as a promising material because it has increased in recent years in which aerogel has very low thermal conductivity around 0.01-0.02 W/(m.k). In his paper, he explained that the development of a dual glass panel system is with monolithic silica aerogel. It is mentioned that the results of the multi-disciplinary analysis include thermal and lighting tests. From the results, it is concluded that research carried out in different climates, the aerogel window can be used as a solution to reduce energy demand and even the demand in winter by reducing the increase in solar heat in buildings. It is important to state that when the internal burden on school buildings and office buildings is high, climate adjustment tends to be considered. And moreover, the use of aerogel glass on the window allows a lot of light during the day enters the room which affects on activity and prosperity. The window glass in this study is applied in real life, especially at the risk of condensation and heat changes.

In [10], the authors pinpointed that the characteristics of glaze sanitary physical properties are controlled and improved by changing the chemical composition of raw materials. Glaze industry from ten raw materials has different compositions, by spraying traditional ceramic substrates, then thermally treated and processed at 1250°C. The glaze characteristics obtained are diffracted with X-rays to reveal the mineralogical composition and are confirmed by the FTIR spectrum and observed through images to see the electron distribution to study the microstructure and then, it is found that micro characteristics are obtained in white from the colorimeter data. From the results, it is concluded that the 10% difference in calculations and experiments is derived from the coefficient of thermal expansion and white color increase reaches 87.5%, the maximum zircon content is 14.5wt%, the lowest ZnO content is 2.5wt% and the flexural strength is 47.61 MPa.

The same research has also been reported by Martinez et. al [11] about the development of glaze material with glass and calcite-based material (CaCO_3). In this research, variations in holding time are carried out including 15 minutes, 30 minutes and 45 minutes with a combustion temperature of 1000°C using a furnace machine and also the hardness test (Vickers) is carried out. Then, it is concluded that the micro photo showed that at 15 minutes holding time, there is cracking on the ceramic glaze layer, 30 minutes holding time has also cracking but there is a pinhole in the glaze layer, while at the 45 minutes holding time, the pinhole and cracking decreases. In the hardness test, the 15 minutes holding time is 452,761 VHN, the 30 minutes holding time is 479,914 VHN, the 45 minutes holding time is 391,695 VHN. This is done successfully and it obtained the highest results at a holding time of 30 minutes.

According to Demidenko [12], the characterization of calcium silicate ceramics using scanning electron microscopy (SEM) techniques sintered at temperatures of 850°C to 1100°C reveals that the microstructure of calcium silicate ceramics is going better at sintering temperatures of 1100°C with a density of 2.32 g/cm^3 , and porosity of 27.5%.

In [13], the authors examine the zircon corrosion behavior of glazed ceramic glass against strong acid solutions. It showed that the composition of the glass phase is determined by its glaze resistance. When ZrO_2 is involved in the glassy phase, very poor resistance is obtained through the formation of soluble Zr-containing compounds. Enhancing SiO_2 content is enhanced the resistance of the glass phase and dissolution of the observed grain or grain boundary phases. The coalescing of ZrO_2 into the glass phase must be avoided to increase the chemical resistance of zircon containing glaze. When ZrO_2 is in the grains, good chemical resistance can be obtained.

Additionally, In [14], the authors concluded that the mixture chosen from waste and low-cost mineral initial materials can be converted into glass ceramic components either by vitrification and subsequent crystallization or by direct sintering. The sintered-crystallization approach leads to strong glass ceramics, under the simple conditions (pressing fine powder and sintering at 950°C for only 30 minutes). The porosity of the glass-ceramic body surface from direct sintering can be sealed by ceramic glaze which resulted from the same initial mixture of waste and minerals. The characteristics of the waste ceramic glaze can be adjusted by the addition of secondary components (glass panels from disassembled CRT and zircons). Because of their specific strength characteristics, coated ceramic glass can be applied in the building industry as lightweight tiles.

In [15], the authors reported that the milling method used is a technological scheme for the synthesis of ceramic materials using waste material from oil refineries containing heavy metals. This study experimented with the SEM test and revealed that pigments calcined in experiments using temperature of 700, 900, has a morphology that is very agglomerated, while, at a temperature of 1100, agglomerates that have formed undergo structural decomposition. For compositions containing almost all metal iron (92%) turned to magnesium chromium at temperatures of 1000. It is concluded that the proposed alternative technology scheme could provide economical production of ceramic pigments with

exceptional compositional stability at relatively low temperatures from calcination.

In [16], the authors reported that glass powders are used as an alternative material to replace cement. In this study, glass powders are as an additive to cement because it depends on the chemical elements present in glass and also in cement, namely silica (SiO_2). In this study, it is compared using four mixed compositions, among others 0%, 10%, 20%, 30% with a total of seven specimens each with a 28-day treatment period based on SNI 03-0349-1989 standards. The results indicated that the use of glass powder on bricks with a mixture composition of 10%, 20%, 30% has met the requirements for the water absorption of solid concrete brick quality level I according to the provisions of SNI 03-0349-1989, bricks with a composition of 0% are included in quality level III according to the provisions standard of SNI 03-0349-1989 with an average compressive strength of 58.16 kg/cm^2 , while bricks with a composition of 10%, 20%, 30% are included in quality level II with an average compressive strength of 74.41 kg/cm^2 . So, it can be concluded that the most optimum mixture is bricks with a mixture composition of 20%.

In [17], the authors explained that the heat treatment process is an effort to increase the strength and hardness of steel by heating the steel to achieve austenite temperature that is followed by quench so that the martensite phase arises. In principle, the surface treatment of the material is almost the same but only done on the surface of the material in which the main goal is to get a hard surface of the component but the inside of the component remains resilient. From that condition, the method used is induction heating. Principally, it uses heating obtained from Eddy currents caused by flux magnetic originating from the coil of alternating electric current. Furthermore, it is tested using induction heaters for the heat treatment process on the surface of ST 37 steel specimens with the room temperature controlled by thermodigital, while, the specimens are quenched using a water cooling medium.

The manufacture of quality hardflek products from plastic waste and rice husks. The method of processing plastic waste and rice husk into hardflek products as a substitute for wood raw materials in furniture products has a high creative value in which quality and productivity is much better. Furthermore, the economic value of a furniture product is largely determined by the design or shape and appearance offered by the raw material. Plastic waste material combined with rice husk waste provides a very attractive aesthetic nature with interesting color because the coloring has been integrated in the material so that it cannot fade or be degraded by time. Processing methods of products made from polyethylene terephthalate (PET) plastic waste is reinforced with rice husk waste. The method applied can use the system hand lay-up (pouring). The test results showed that the addition of rice husk ash at a volume fraction of 93% plastic waste and 7% rice husk ash has a lower impact strength value than that of the initial specimen (without rice husk) from $0.0024 \text{ joules/mm}^2$ to $0.0015 \text{ joules/mm}^2$. The hardness testing of the Vickers method showed that the addition of rice husk ash in a volume fraction of 93% plastic waste and 7% of rice husk ash has increased from the initial specimen which is about 35% (10.6 HV to 13.5 HV), so there is a need for research development with SEM (scanning electron microscopy) method to know the composition and properties of the material contained in the product [18].

All things considered, it was necessary to conduct research that utilizes used bottle waste to be used as a more useful material in the form of glaze material. The purpose of this research was to develop glaze material by utilizing glass waste from used bottles combined with kaolin. To find out the characteristics and structure of glaze material, it was conducted the micro photo testing and hardness level analyzing of the glaze material using the Vickers hardness test.

2. Research Methodology

2.1. Materials

This study used bottle waste as the main material to coat the surface of the tile and also kaolin as an additional material in the coating process in which the combustion process used a furnace machine. Three types of time variations used were 30 minutes, 45 minutes and 60 minutes, besides, variations comparison of material composition between glass and kaolin were also used by the comparisons of 90:10, 80:20 and 70:30. This experiment began with the preparation of tile material since the tile material will be coated, followed by cutting the tile with a length of 2 cm, width 2 cm, and thickness 0.8 cm. This process used tile material that had not been burned. Figure 1 showed the tile material that had been cut and sanded using sandpaper ranging from 800, 1000, 1500, 2000 to 5000 grits.

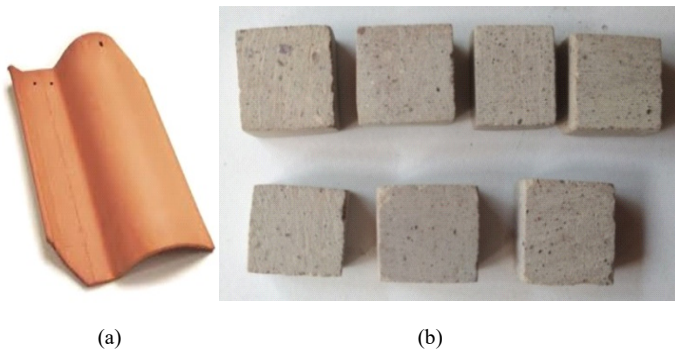


Figure 1: Clay tile specimens: (a) before being cut, (b) after being cut and mashed

Glass pounding machine was used to refine glass from used bottles into powder with a size of 200 meshing. To refine the used bottle glass used a glass pounding machine in an existing glass pulverizer at the Metallurgy Laboratory. Then it was meshed using size 200 mesh. Figure 2 shows the glass powder that had not been meshed and after meshing.

Kaolin (clay) is a clay mineral containing several layers of aluminum silicate. Kaolin is a kind of clay that is smooth, soft and white resulted from weathering granite rocks which is then used as material to make porcelain or to make a mixture of woven fabric (paper, rubber, and medicine, etc.), commonly called Chinese clay. Furnace machine is an equipment used to heat materials and change their shape (eg rolling, forging) or changing its properties (heat treatment). It is commonly referred to as an oven. Energy transfer in the furnace occurred during the heat energy by generation steps through element heater whose energy was supplied from electrical energy. In this study, a furnace machine was used to heat glass powder on a tile.

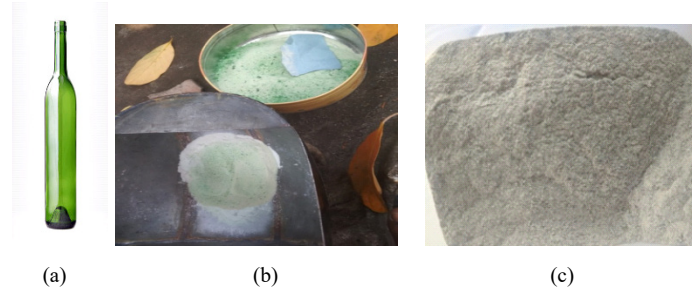


Figure 2: Recycle bottle glass (a), Glass powder before meshing (b) and after meshing 200 mesh (c).

The coating process is done manually with a thickness of 1mm. It is done by giving the liquid mixture of glass powder, kaolin, and water on the tile. This to mix glass and kaolin powder so that it can stick on the surface of the tile. The drying process is carried out so that the coating adheres firmly to the specimen. This process is done at room temperature and allowed to stand for a day. The combustion process uses ceramic tile specimens that have been coated with glass powder and kaolin. This process is carried out using a furnace engine involving necessary steps which are when the furnace engine is turned on, set the temperature on the screen with 1000°C, wait for the furnace machine to show the temperature of 1000°C on the screen in front. When the temperature already reaches 1000°C, set the time with a stopwatch for 30, 45, and 60 minutes. When the stopwatch shows the desired time, turn off the furnace machine and leave the specimen in the furnace machine until the temperature drops using room temperature. After the furnace machine reaches room temperature, then take a specimen from the furnace machine, then leave it for a day to proceed to testing.

2.2. Experiments

In the research, to investigate the influence of kaolin contents and holding time to the glaze hardness the micro hardness test was conducted. The experiment is carried out based on the ASTM E384 standard. The force was 0.5 kgf and 10 s of holding time.

Micro-photograph analysis testing was conducted to determine the microstructure of the results of the coating glass process on the tile. The observation is done by obtaining an image that shows the distribution of ceramic material with a zoom of 200 times, and also by arranging the lighting. From this picture, it finds out the properties and characteristics of ceramic materials.

3. Results and Discussion

3.1. Photo Micro

To facilitate reading comprehension in this test analysis, the glaze coating carried out using a variety of composition compared to glass powder and kaolin consisted of (A) 90% : 10%, (B) 80% : 20%, and (C) 70% : 30. There was also a variation of the time ratio performed including 30 minutes, 45 minutes, and 60 minutes, with the same temperature of 1000°C. This was to find out which one is better for use after the rain process.

Figure 3 shows the results of micro-photographs on the surface of the glaze material. Figure 3 is the results of micro-photographs with the variations in the composition of the glaze material with a comparison between glass and kaolin.

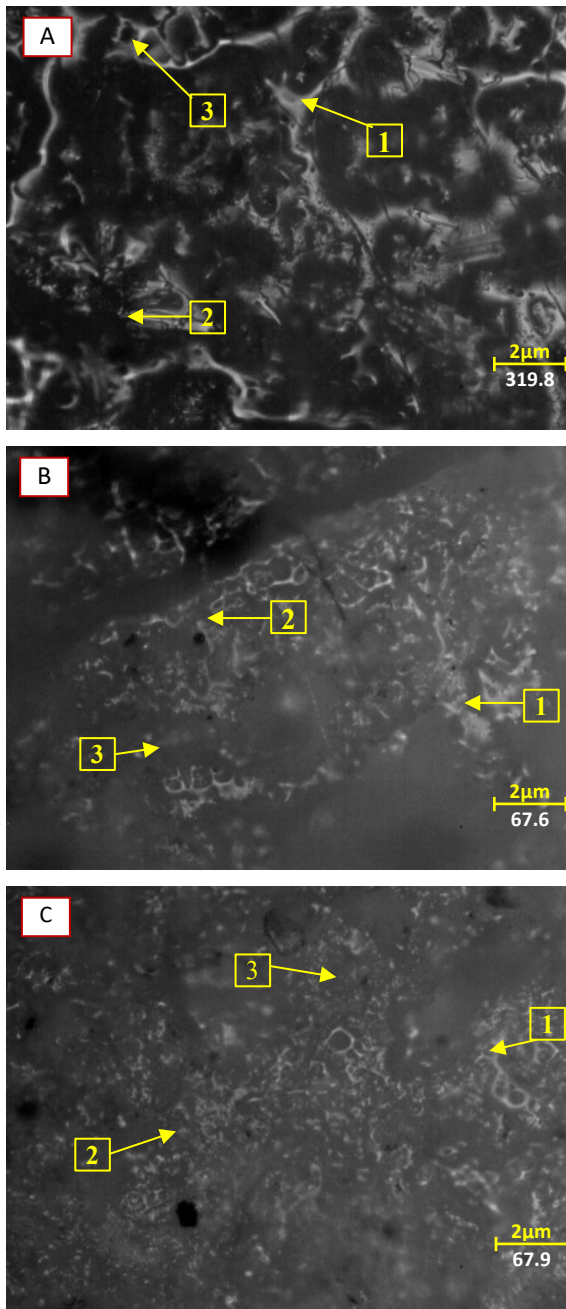


Figure 3: The results of micro-photographs on the glaze material holding time 30 minutes

From the observation results of micro-photographs tests conducted in Figure 3 (A), number 1 is shown in the form of longitudinal lines like fibers and marked in white. It is the melted glass material and has formed on the glaze layer on the surface of the tile or commonly called amorphous solids. While the black one shown in number 2 is porosity. It can possibly occur when kaolin as a binding material glaze is burning to ash and trapped on the surface of the glaze layer. Then, number 3 shows that the existence of pinholes that are possible to occur due to the release of oxygen during combustion and inside the material contains flammable materials at low temperatures. The oxygen arises in the combustion process because the room in the furnace is not in a vacuum condition, so the materials are combusted first and form holes on the surface of the layer. The same process is also shown

in the figure B and figure C in which number 1 shown as the shape of a long line that looks like a fiber and marked white is a glass material that has melted but is somewhat less than what is shown in figure A. It is possible occurs because it affects the material composition, whereas porosity that occurs in figure B and C looks more possible occurs because it has more kaolin. The pinholes shown in figure B and C shows that those are in glaze layer and have a smaller size with a greater amount than in figure A. Figure 3 analysis shows that the use of temperatures of 1000°C during the combustion process successfully melt the glass.

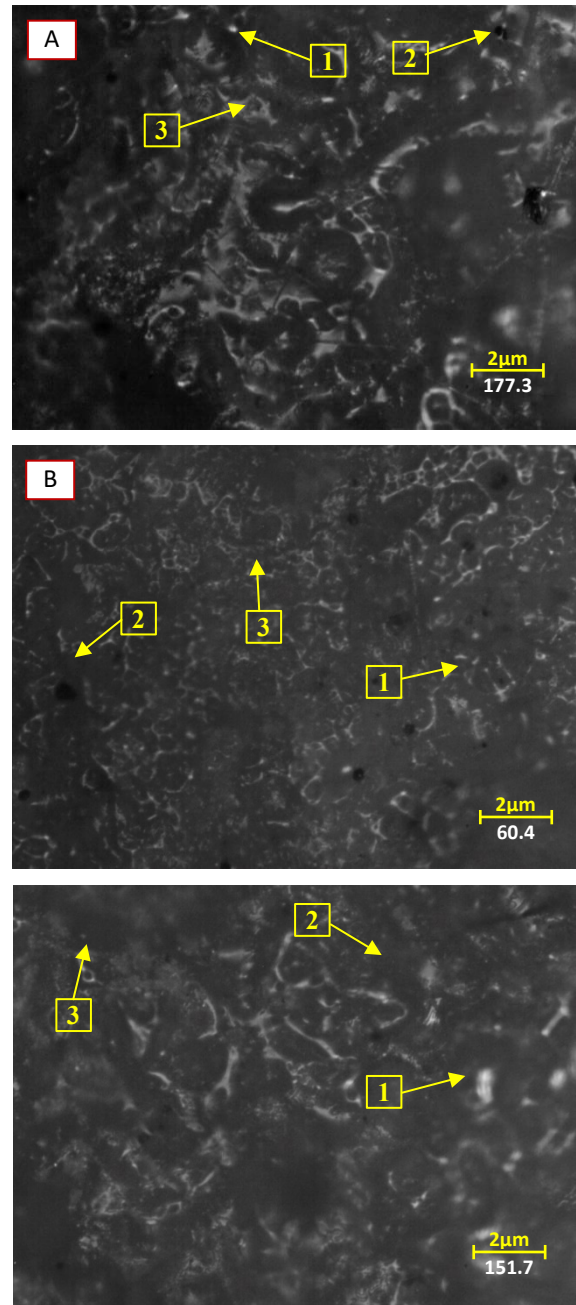


Figure 4: The results of micro-photographs on the glaze material holding time 45 minutes.

Figure 4 shows the results of micro-photographs on the surface of the glaze material. Figure 4 is the result of micro photographs with composition variation of the glaze material with a comparison between glass and kaolin. The longitudinal lines like fibers that are

marked in white are melted glass materials or commonly called amorphous solids. It forms a glaze layer on the tile surface, but it can be seen that the melting rate of glass material is not evenly distributed well. Equally, it happens in figure B and C. It can be seen that the melting rate of glass material that occurs in figure B shows that the melting rate of glass material looks more evenly distributed if compared to the figure A and C. This is possible due to differences in the composition of glass and kaolin. Figure A number 2 shows porosity in which it occurs in smaller and fewer sizes. Porosity also occurs in figure B and C, but in figure C the porosity looks less if compared to figure A and figure B. Pinholes that occur in the observation can be seen in number 3, but in part B, it looks smaller pinhole. This possibly happens because it depends on the length of time to hold the combustion and composition comparison.

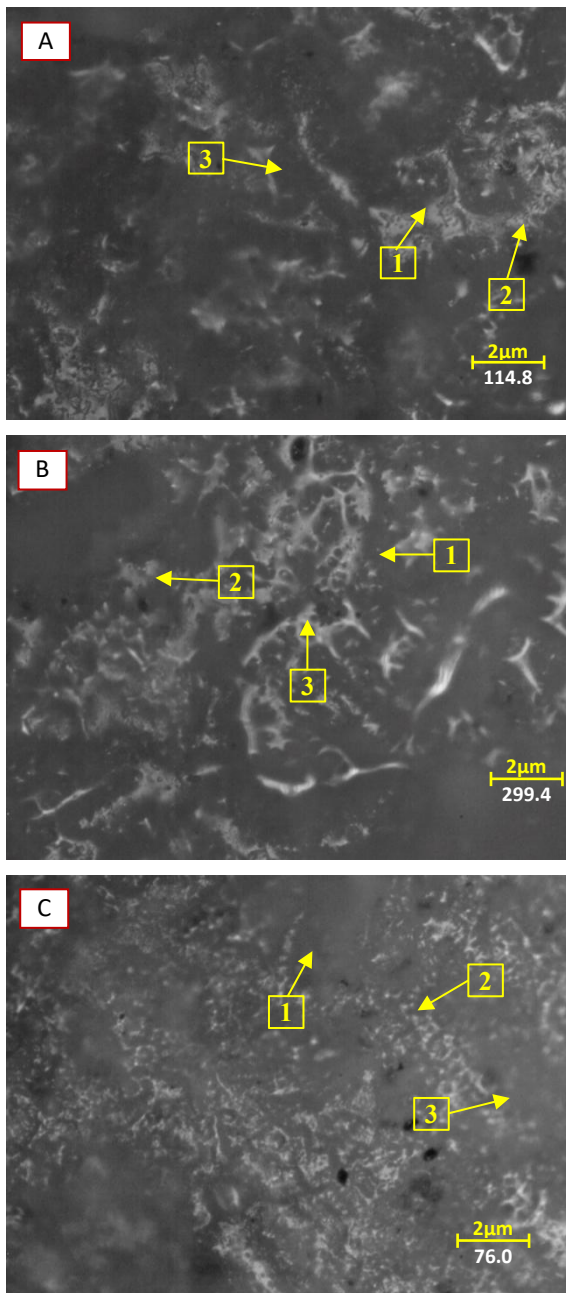


Figure 5: The result of micro-photographs on the glaze material holding time 60 minutes

Figure 5 shows the results of micro-photographs on the surface of the glaze material. Figure 5 is the result of micro-photographs with variations in the composition of the glaze material with a comparison between glass and kaolin. The observation results of micro-photographs tests conducted in figure A, number 1 is shown in the long lines like fibers and marked in white. It is the melted glass material and has formed on the glaze layer on the surface of the tile or commonly called amorphous solids. But it can be seen that the melting rate of glass material is not evenly distributed properly. Identically, it happens in figure B and C. But it can be seen that the melting rate of glass material that occurs in figure C shows that the melting rate of glass material looks more evenly if compared to figure A and B. This is possible because of differences in the glass and kaolin composition. The observations can be strengthened by other studies [19][2]. Number 2 shown in figure A, B and C shows the porosity, but the porosity seemed less is found in figure C compared to figure A and B. This possibly happens because it affects the composition variation [2]. Pinholes are shown in number 3 of figure A, B and C. In figure A, there is no pinhole compared to figure B and C. This may occur due to differences in composition in figure A and the length of combustion duration.

From the analysis results of micro-photographs on glaze material with a holding time of 30 minutes, 45 minutes and 60 minutes, as well as the variations of material composition comparison between kaolin and glass powder with a ratio of 90:10, 80:20, 70:30, figure 5 part C that has a variation of 70:30 and a holding time of 60 minutes shows the results of a dense glaze layer compared to other variations. It is because the glaze materials have different compositions and holding times.

3.2. Micro Hardness

Figure 6 is the result of the photos of glass material that has been coated and has been through the heating process with the furnace. Then, it will conduct the process of specimen testing of finished material using a hardness test tool.

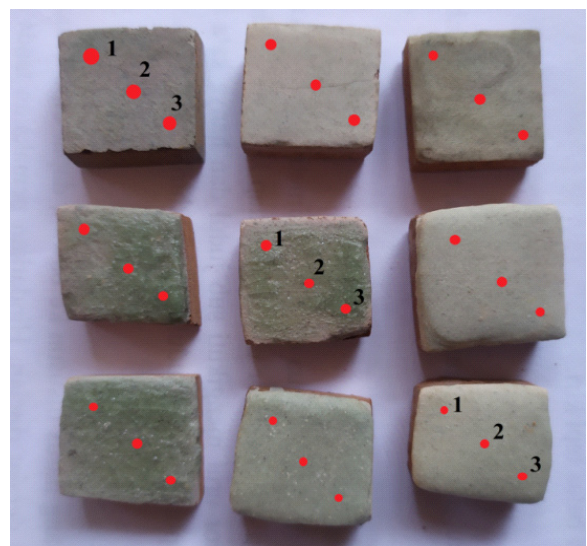


Figure 6: Location of the indenter point on micro Vickers hardness testing

Specimens used in this test were tile materials that had been coated with glass powder and kaolin with variation composition after being heated at 1000° C. The combustion aims at increasing

the hardness on coated material and the surface a thin layer was formed. After completing the combustion process, a hardness test (Vickers) is conducted to find out the hardness value on the surface of each material. The rectangular diamond pyramid indenter is used in the hardness test with 0.5 kgf and a time of 10 seconds is set as the loading test. The results of the hardness test that have been carried out can be seen in figure 7.

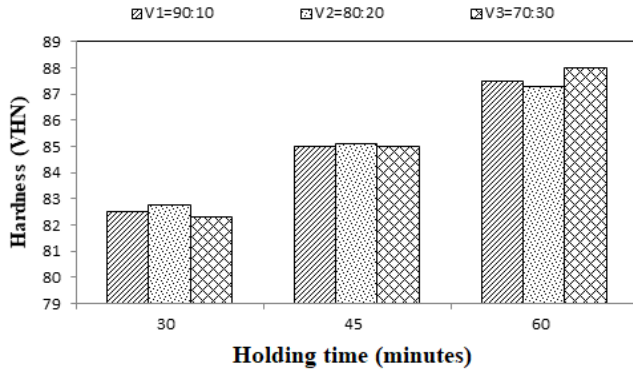


Figure 7: Comparison of glaze hardness values with composition variations

The overall results of the hardness test figure 7 analysis is a variation of the glaze composition between glass and kaolin, and different variations of the holding time. It has been proven by test results in figure 7. It can be stated that the process of a hard layer forming on the surface of tile material that is on the highest Vickers hardness testing occurs at a holding time of 60 minutes and composition variation of 70: 30% with an average hardness value of 88.1 VHN. While the lowest hardness is at a time variation of 30 minutes with an average hardness value of 81.9. The difference in the hardness value in each variation is possible because the characteristics of microstructure formed are also different. This is evidenced in section 4.1 which discusses the results of micro-photographs testing in which the less of the diminishing product defects in the form of pinhole and porosity, the higher the hardness.

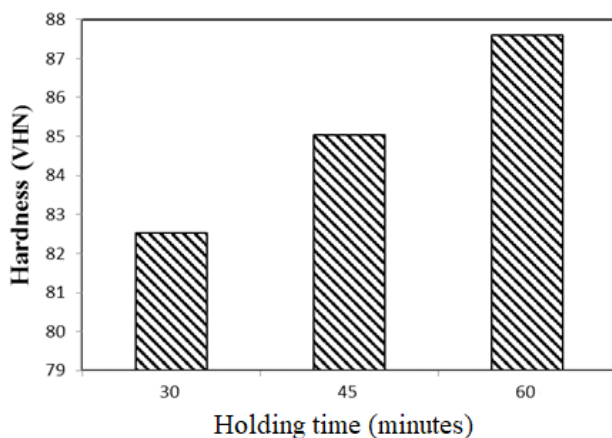


Figure 8: Comparison between the average hardness value (Vickers) with time variations.

4. Conclusion

From the results of the analysis and discussion regarding the coating of glaze material using glass and kaolin based materials, it can be concluded that the time variation is very influential on the results of micro-photographs analysis and hardness test. So, the

longer the holding time given, the more the melting rate of the glass evenly distributed and the hardness test has also increased. The results of micro-photographs analysis on glaze material samples using glass and kaolin base materials are combusted at a temperature of 1000°C with different variations of holding time of 30 minutes, 45 minutes, and 60 minutes. It can be concluded that the holding time of 30 minutes indicates the glass melt at the holding time of 30 minutes maximum melting at this temperature, and there are still pinholes and porosity in the analysis. At the 45 minutes holding time, it shows that the glass melt has not been evenly distributed since there are some pinholes and porosity but it looks less and smaller than the 30 minutes holding time. At the 60 minutes holding time, the glass melt is still visible but looks smaller and less, porosity and pinhole are still visible but look smaller and less than the holding time of 30 minutes and 45 minutes. The results of hardness test (Vickers) analysis revealed that the hardness value increases in each composition variation carried out. At a holding time of 30 minutes, 45 minutes and 60 minutes, it shows the increase average hardness value of 82.53 VHN, 85.03 VHN, 87.6 VHN.

Conflict of Interest

The authors certify that they have NO affiliations with or involvement in any organization or entity with any financial interest or non-financial interest in the subject matter or materials discussed in this manuscript.

Acknowledgment

Authors would like to thanks to Universitas Muhammadiyah Surakarta, and Master Program of Mechanical Engineering for supporting the research.

References

- [1] M. J. Davis and E. D. Zanotto, "Glass-ceramics and realization of the unobtainable: Property combinations that push the envelope," *MRS Bull.*, vol. 42, no. 3, pp. 195–199, 2017. <https://doi.org/10.1557/mrs.2017.27>
- [2] J. Deubener, M. Allix, M.J Davis, A. Duran, T.Hoche, T. Komatsu, S. Kruger, I. Mitra, R. Muller, S. Nakane, M.J. Pascual, J.W.P. Schmelzer, E.D. Zanotto, S. Zhou., "Updated definition of glass ceramics," *J. Non. Cryst. Solids*, vol. 501, no. January, pp. 3–10, 2018. <https://doi.org/10.1016/j.jnoncrystol.2018.01.033>
- [3] M. Rampf, M. Dittmer, C. Ritzberger, and W. Höland, "Controlled parallel crystallization of lithium disilicate and diopside using a combination of internal and surface nucleation," *Front. Mater.*, vol. 3, no. October, pp. 1–9, 2016. <https://doi.org/10.3389/fmats.2016.00047>
- [4] A. Halliyal, A. Safari, A. S. Bhalla, R. E. Newnham, And L. E. Cross, "Grain-Oriented Glass-Ceramics for Piezoelectric Devices," *J. Am. Ceram. Soc.*, vol. 67, no. 5, pp. 331–335, 1984. <https://doi.org/10.1111/j.1151-2916.1984.tb19532.x>
- [5] V. Luntz-Leybman, R. K. Freund, and A. C. Collins, "5A-Pregnan-3A-Ol-20-One Blocks Nicotine-Induced Seizures and Enhances Paired-Pulse Inhibition," *Eur. J. Pharmacol.*, vol. 185, no. 2–3, pp. 239–242, 1990. [https://doi.org/10.1016/0014-2999\(90\)90648-P](https://doi.org/10.1016/0014-2999(90)90648-P)
- [6] Yasin Erdoğan, "Physicochemical Properties of Handere Clays and Their Use as a Building Material", *Journal of Chemistry*, Volume 2015. <http://dx.doi.org/10.1155/2015/374245>
- [7] H. Celik, "Technological characterization and industrial application of two Turkish clays for the ceramic industry," *Appl. Clay Sci.*, vol. 50, no. 2, pp. 245–254, 2010. <https://doi.org/10.1016/j.clay.2010.08.005>
- [8] M. Zhang, Y. Chang, R. Bermejo, G. Jiang, Y. Sun, J. Wu, B. Yang, W. Cao., "Improved fracture behavior and mechanical properties of alumina textured ceramics," *Mater. Lett.*, vol. 221, pp. 252–255, 2018. <https://doi.org/10.1016/j.matlet.2018.03.123>

- [9] U. Berardi, "The development of a monolithic aerogel glazed window for an energy retrofit project," *Appl. Energy*, vol. 154, pp. 603–615, 2015. <https://doi.org/10.1016/j.apenergy.2015.05.059>
- [10] K. Boudeghdegh, V. Diella, A. Bernasconi, A. Roula, and Y. Amirouche, "Composition effects on the whiteness and physical-mechanical properties of traditional sanitary-ware glaze," *J. Eur. Ceram. Soc.*, vol. 35, no. 13, pp. 3735–3741, 2015. <https://doi.org/10.1016/j.jeurceramsoc.2015.05.003>
- [11] Juan Daniel Martínez, Santiago Betancourt-Parra, Ivonne Carvajal-arín, Mariluz Betancur-Vélez, "Ceramic light-weight aggregates production from petrochemical wastes and carbonates (NaHCO₃ and CaCO₃) as expansion agents," *Construction and Building Materials*, Volume 180, 2018, Pages 124-133, <https://doi.org/10.1016/j.conbuildmat.2018.05.281>.
- [12] N. I. Demidenko and G. B. Tel'nova, "Microstructure and properties of a material based on natural wollastonite," *Glas. Ceram. (English Transl. Steklo i Keramika)*, vol. 61, no. 5–6, pp. 183–186, 2004. DOI: 10.1023/B:GLAC.0000043088.65135.11
- [13] G. Topateş, B. Tarhan, and M. Tarhan, "Chemical durability of zircon containing glass-ceramic glazes," *Ceram. Int.*, vol. 43, no. 15, pp. 12333–12337, 2017. <https://doi.org/10.1016/j.ceramint.2017.06.097>
- [14] M. A. Binhussain, M. Marangoni, E. Bernardo, and P. Colombo, "Sintered and glazed glass-ceramics from natural and waste raw materials," *Ceram. Int.*, vol. 40, no. 2, pp. 3543–3551, 2014. <https://doi.org/10.1016/j.ceramint.2013.09.074>
- [15] M. Doynov, T. Dimitrov, and S. Kozhukharov, "Alternative technological approach for synthesis of ceramic pigments by waste materials recycling," *Bol. la Soc. Esp. Ceram. y Vidr.*, vol. 55, no. 2, pp. 63–70, 2016. <https://doi.org/10.1016/j.bsecv.2016.01.002>
- [16] Fernanda Andreola, Luisa Barbieri, Isabella Lancellotti, Cristina Leonelli, Tiziano Manfredini, "Recycling of industrial wastes in ceramic manufacturing: State of art and glass case studies", *Ceramics International*, Volume 42, Issue 12, 2016, Pages 13333-13338. <https://doi.org/10.1016/j.ceramint.2016.05.205>.
- [17] Anggono, A. D., Muttaqiem, Z., Darmawan, A. S., Besar Riyadi, T. W., Yulianto, A., Sugito, B., Abdullah, E. M. (2019). Mechanical Properties of Concrete Block Reinforced with Recycle HDPE and Coal Bottom Ash. *Materials Science Forum*, 961, 51–56. <https://doi.org/10.4028/www.scientific.net/msf.961.51>
- [18]. A. D. Anggono, B. Sugito, A. Hariyanto and Suranto, "Investigation on mechanical properties of friction stir welding of 2 mm thick aluminium alloy sheet," 7th Brunei International Conference on Engineering and Technology 2018 (BICET 2018), Bandar Seri Begawan, Brunei, 2018, pp. 1-4. doi: 10.1049/cp.2018.1519
- [19] X. Lu, J. Yang, X. an Ning, K. Shih, and F. Wang, "Crystallization pathways in glass-ceramics by sintering cathode ray tube (CRT) glass with kaolin-based precursors," *J. Eur. Ceram. Soc.*, vol. 38, no. 15, pp. 5184–5191, 2018. <https://doi.org/10.1016/j.jeurceramsoc.2018.06.047>

MIMO Fractional Order Control of a Water Tank Plant

Arturo Rojas–Moreno*, Juan Hernandez–Garagatti

Universidad de Ingenieria y Tecnologia - UTEC, Electronic Engineering Department, Lima 15063, Peru

ARTICLE INFO

Article history:
 Received: 13 October, 2019
 Accepted: 22 November, 2019
 Online: 23 December, 2019

Keywords:
 Fractional order controller
 Integer order controller
 Water tank plant
 Centralized control

ABSTRACT

This work implements a MIMO (Multiple Input Multiple Output) FO (Fractional Order) control system for controlling the level and temperature of the water inside a tank by means of two inflow rates: cold and hot water, which are mixed to produce an outflow rate. Such a process exhibits coupling between inputs and outputs. A linear model of the plant is obtained experimentally. Such a model, the transfer matrix function of the plant, is used to design a centralized MIMO IO (Integer Order) controller that permits to achieve complete decoupling between the set points of level and temperature and the corresponding controlled outputs: level and temperature in the tank. The MIMO FO controller is obtained making fractional all de transfer functions of the MIMO IO controller. Experimental results demonstrate that the MIMO FO control system improves the control performance of the plant outputs: level and temperature of the water in the tank.

1 Introduction

In the literature, few studies have been performed for modelling a MIMO tank water plant having interaction (coupling) between its inputs: cold and hot water flow rates, and its outputs: level and temperature of the water into the tank. For instance, in [1], the level and temperature inside the tank are controlled by means of cold and hot water flow rates using two control configurations. The first configuration, called coupled control, employs two PID controllers, while the second, called decoupled control, uses two PID controllers and two decoupler devices. Figure 1 shows the controlled level and temperature using a coupled control configuration.

In [2], a water tank plant is modelled and controlled using two PID (Proportional Integral Derivative) controllers. The work in [3] employs a decoupled model of the water tank plant, which is controlled by means of two PID controllers and four decoupling devices, while in the work published in [4], the water tank plant is controlled by a MIMO PID controller using as control inputs the cold water flow rate and the electric current supplied to a heating resistance. The simulation work in [5] employs a fuzzy logic controller to control the temperature and water Level in a boiler. At the present, no work that employs a MIMO fractional order controller has been published.

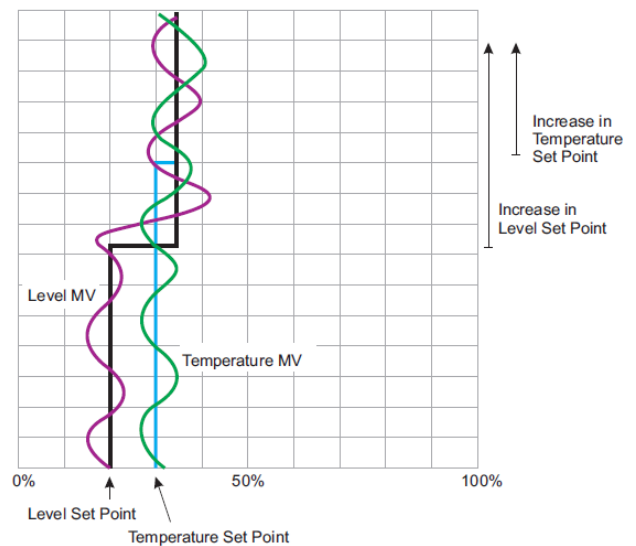


Figure 1: Controlled level and temperature using a decoupled control configuration. MV stands for Manipulated Variable. Taken from [1].

This work is organized as follows. Section 2 describes the multipurpose plant and the supervision module used in this work to implement the MIMO feedback control systems. Section 3 deals with the experimental modelling of the water tank plant. The design and implementation of a MIMO IO as well as a MIMO FO control systems are the topics of Sections

* Arturo Rojas–Moreno, Jr. Monte Algarrobo 518, Lima 15063, Peru, Phone (51) 948699637, Email: arojas@utec.edu.pe

4 and 5, respectively. Section 6 presents some concluding remarks derived from this work.

2 Plant Description

Figure 2 shows the multipurpose plant, patented by UTEC (Universidad de Ingeniería y Tecnología) [6] used in this work, while Figure 3 depicts the corresponding supervision module patented by UTEC [7]. Such equipment is located in the Process Automation Lab of UTEC.



Figure 2: The multipurpose plant



Figure 3: The supervision module

Figure 4 depicts the P&ID (Piping and Instrument Diagram) of the multipurpose plant. In Figure 4, T-10 is the water tank plant. Observe that a flow rate q_C of cold water and a flow rate q_H of hot water are entering into T-10. A warm water flow rate q_D is exiting from T-10. Such a tank possesses a water overflow pipe not shown in Figure 4. The on-off valve DV-10 allows the passage of q_C . The control valve FV-10 is used to regulate q_C , while the flow transmitter FT-10 measures q_C .

The hot water flow rate of q_H is regulated by the control valve FV-11 and measured by the flow transmitter FT-11. In-

side the tank T-10 there is a temperature transmitter TT-10 and a pressure transmitter PT-10, which is used as a level transmitter. In the tank T-10, there exists an electric heating resistance, whose electric current is controlled by the power controller PW-10 located in the supervision module. Both devices are not used in this paper. This work employs the tank T-20 to produce the required hot water flow rate q_H at a temperature of 50°C. The water flow rate q_D exits T-10 through the on-off valve DV-30.

Observe in Figure 4, that the on-off valve DV-20 permits the entering of the flow rate q_C to the tank T-20. This tank possesses a low level switch (LL-20) and a high level switch (HL-20) to indicate if the tank is either empty or filled with water, respectively. The water into the tank T-20 is heated electrically. The temperature into this tank is measured by the temperature transmitter TT-20 and controlled by means of the power controller PW-20 located in the supervision module. A flow rate q_H with a temperature of about 50°C is pumped to the tank T-10 by using the pump P-20. The pressure into the pipe that connects tanks T-10 and T-20 is measured by the pressure transmitter PT-20. The speed of the pump is kept constant by means of a speed controller (a variable frequency drive) located in the supervision module.

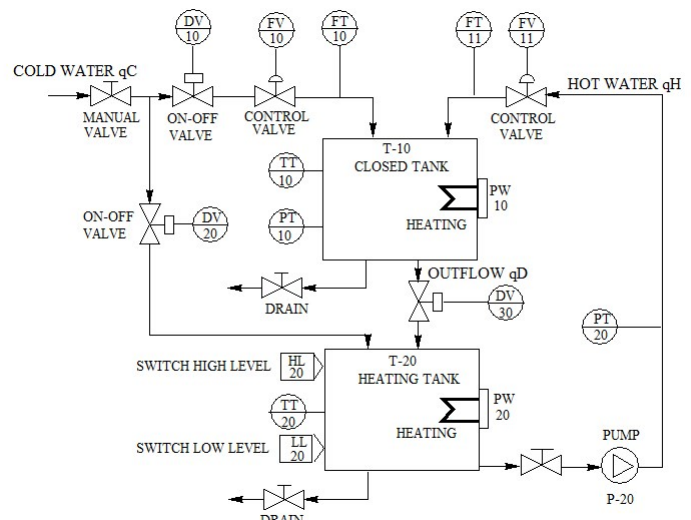


Figure 4: P&ID of of the multipurpose plant

Figure 3 shows the supervision module that is equipped with breakers, power sources, a PanelView front, two powerful PAC (Programmable Automation Controller), a PLC (Programmable Logic Controller), and a Flex I/O (Input/Output) switch among others. The latter device permits Ethernet communication between the PACs and the PLC of the supervision module with the valves and transmitters of the multipurpose plant. For such a purpose, input and output connectors available on the front panel of the supervisory module (Figure 3) permit to wire the PACs an PLC with the field instrumentation.

The software Studio 5000 from Rockwell Automation is used to elaborate the HMI (Human Machine Interface) and to

implement the control algorithms written in structured text language. This work employs the ControlLogic 5000 PAC. Table 1 shows the valued parameters and variables used in this paper.

Table 1: Parameters and variables employed in this work

Symbol	Description	Value
A	Tank rectangular section	0.12 m ²
A_o	Output pipe section	5.06×10 ⁻⁴ m ²
$\bar{h} = \bar{y}_1$	Steady state of h	0.2 m
$\bar{q}_C = \bar{u}_1$	Steady state of q_C	6.66×10 ⁻⁵ m ³ /s
$\bar{q}_H = \bar{u}_2$	Steady state of q_H	7.66×10 ⁻⁵ m ³ /s
\bar{q}_D	Steady state of q_D	12×10 ⁻⁵ m ³ /s
g	Earth's gravity	9.81 m/s ²
θ_C	Temperature of q_C	289 K
θ_H	Temperature of q_H	321 K
$\bar{\theta} = \bar{y}_2$	Steady state of θ	304 K
ρ_C	Water density in q_C	998 kg/m ³
ρ_H	Water density in q_H	988 kg/m ³
ρ_D	Water density in q_D	995 kg/m ³
C_p	Heat specific capacity	4186.8 J/(kg·K)
C_d	Discharge coefficient	0.16
α	Discharge factor	3.586 m ^{2.5} /s

The outflow rate q_D shown in Table 1 can be computed from

$$q_D = C_d \sqrt{2gh} D_d \frac{\pi}{4} = \alpha \sqrt{h} \quad \alpha = C_d \sqrt{2g} D_d \quad (1)$$

In (1), C_d is the dimensionless discharge coefficient, g is the gravitational acceleration, and D_d is the diameter of the pipe for the outflow q_D . Knowing the steady state values \bar{h} and \bar{q}_D of h and q_D , respectively, C_d and α can be calculated from

$$C_d = \frac{\bar{q}_D}{\sqrt{2g\bar{h}} D_d}; \quad \alpha = C_d \sqrt{2g} D_d \quad (2)$$

Three experiments are performed to determine the discharge coefficient C_d shown in Table 1. For each experiment, the valve FV-10 is opened in a certain percentage to allow the flow rate q_C enter the tank T-10. At the same time, the flow rate q_D is regulated by means of the manual valve until the level h into the tank remains unchanged. At that point, the output flow rate of magnitude \bar{q}_D equals the input flow rate of magnitude \bar{q}_C . Then, the discharge coefficient C_d can be computed from (2). Table 2 shows the results of the experiments. The selected value for C_d is 0.16.

Table 2: Experiment results to obtain C_d

\bar{q}_C (m ³ /s)	\bar{h} (m)	C_d	α (m ^{2.5} /s)
1.45× 10 ⁻⁴	0.162	0.160	3.586
1.95× 10 ⁻⁴	0.307	0.157	3.518
9.72× 10 ⁻⁵	0.092	0.142	3.182

3 Experimental Plant Modelling

Figure 5 depicts the block diagram of the MIMO LTI (Linear Time Invariant) control system, where s is the Laplace operator, $G_p(s)$, $G_c(s)$, $G(s)$, and $G_T(s)$ are transfer matrix functions of the plant, the controller, the open-loop system, and the closed-loop system, respectively. Also, r , e , u , and y are the reference, system error, control, and output vectors, respectively.

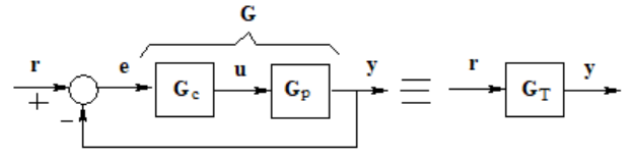


Figure 5: Block diagram of the MIMO feedback control system.

From Figure 5: $y(s) = G_p(s)u(s)$, which can be expressed as

$$\begin{bmatrix} y_1(s) \\ y_2(s) \end{bmatrix} = \begin{bmatrix} G_{p11}(s) & G_{p12}(s) \\ G_{p21}(s) & G_{p22}(s) \end{bmatrix} \begin{bmatrix} u_1(s) \\ u_2(s) \end{bmatrix} \quad (3)$$

The four transfer functions of (3) can be obtained experimentally from

$$\begin{aligned} G_{p11} &= \left. \frac{y_1}{u_1} \right|_{y_2=0, u_2=0} & G_{p12} &= \left. \frac{y_1}{u_2} \right|_{y_2=0, u_1=0} \\ G_{p21} &= \left. \frac{y_2}{u_1} \right|_{y_1=0, u_2=0} & G_{p22} &= \left. \frac{y_2}{u_2} \right|_{y_1=0, u_1=0} \end{aligned} \quad (4)$$

In the figures shown hereinafter, the water level and temperature in the tank are expressed in cm and °C, respectively. Let us consider a level transmitter span from 0 cm (0% of the span) to 40 cm (100% of the span). To determine G_{p11} , the valve FV-10 (Figure 4), which regulates the flow rate of cold water u_1 , is opened from 30 to 50%, making y_1 (the water level into the T-10 tank) to change from 10 cm (25% of the span) to 19.5 cm (48.75% of the span) as seen in Figure 6. Using the tangent method in Figure 6, the transfer function G_{p11} with gain K_{p11} and time constant T_{p11} is found to be

$$\begin{aligned} G_{p11} &= \left. \frac{y_1}{u_1} \right|_{y_2=0, u_2=0} = \frac{K_{p11}}{T_{p11}s + 1} = \frac{1.1875}{180s + 1} \quad (5) \\ K_{p11} &= \frac{(48.75 - 25)}{(50 - 30)} = 1.1875 \end{aligned}$$

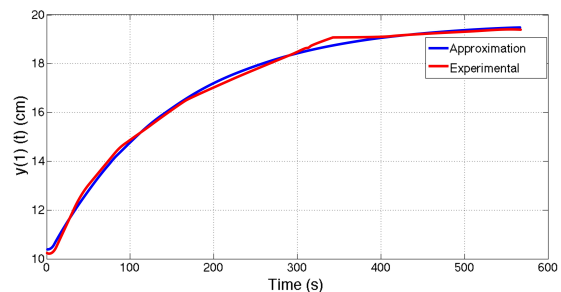


Figure 6: Experimental reaction curve for the G_{p11} transfer function.

To compute G_{p12} , the valve FV–11 (Figure 4), which regulates the flow rate of hot water u_2 , is opened from 40 to 60%, making y_1 to vary from 10 cm (25% of the span) to 19.5 cm (48.75% of the span) as seen in Figure 7. Using the tangent method in Figure 7, the transfer function G_{p12} with gain K_{p12} and time constant T_{p12} is computed as

$$G_{p12} = \left[\frac{y_1}{u_2} \right]_{y_2=0, u_1=0} = \frac{K_{p12}}{T_{p12}s + 1} = \frac{1.1875}{180s + 1} \quad (6)$$

$$K_{p12} = \frac{(48.75 - 25)}{(60 - 40)} = 1.1875$$

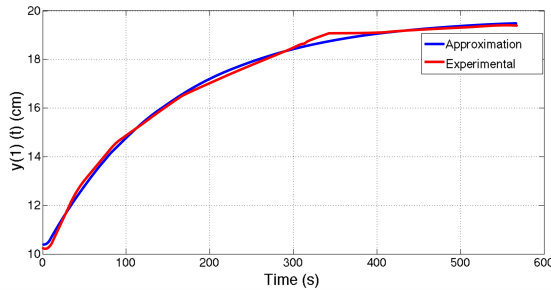


Figure 7: Experimental reaction curve for the G_{p12} transfer function.

Now, let us consider a temperature transmitter span from 16 °C (0% of the span) to 50 °C (100% of the span). To find G_{p21} , the valve FV–10, which regulates the flow rate of cold water u_1 is opened from 30 to 50%, making to drop the temperature y_2 from 32 °C (47% of the temperature span) to 24 °C (23.5%) as seen in Figure 8. From such a reaction curve, the transfer function G_{p21} with gain K_{p21} and time constant T_{p21} is calculated as

$$G_{p21} = \left[\frac{y_2}{u_1} \right]_{y_1=0, u_2=0} = \frac{-K_{p21}}{T_{p21}s + 1} = \frac{-1.175}{180s + 1} \quad (7)$$

$$K_{p21} = \frac{(47 - 23.5)}{(50 - 30)} = 1.175$$

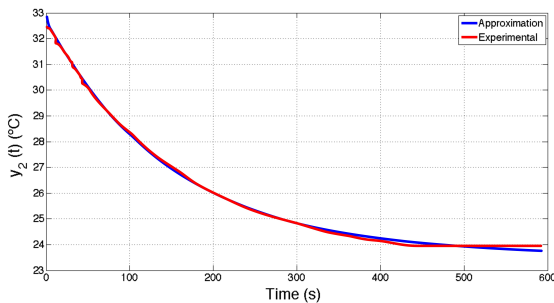


Figure 8: Experimental reaction curve for the G_{p21} transfer function.

To find G_{p22} , the valve FV–11 is opened from 40 to 60%, making to change y_2 from 33 °C (50% of the span) to 43 (79.4% of the span) as seen in Figure 9. From such a figure,

the transfer function G_{p22} with gain K_{p22} and time constant T_{p22} is found to be

$$G_{p22} = \left[\frac{y_2}{u_2} \right]_{y_1=0, u_1=0} = \frac{K_{p22}}{T_{p22}s + 1} = \frac{1.487}{180s + 1} \quad (8)$$

$$K_{p22} = \frac{(79.74 - 50)}{(60 - 40)} = 1.487$$

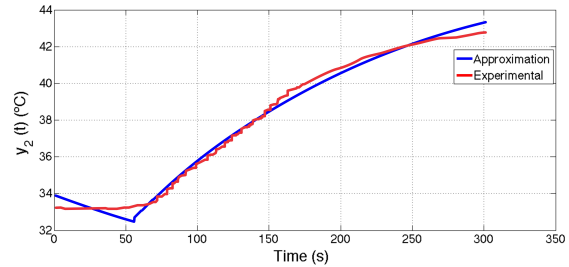


Figure 9: Experimental reaction curve for the G_{p22} transfer function.

4 Design of the the Multivariable IO Control System

From Figure 5

$$\mathbf{G}(s) = \mathbf{G}_p(s)\mathbf{G}_c(s) \quad (9)$$

$$\mathbf{G}_T(s) = [\mathbf{G}(s) - \mathbf{I}]^{-1}\mathbf{G}(s) \quad (10)$$

Consider the following diagonal closed-loop transfer matrix function to assure complete decoupling between the different p inputs.

$$\mathbf{G}_T(s) = \begin{bmatrix} G_{T11} & & \\ & \ddots & \\ & & G_{Tpp} \end{bmatrix} \quad (11)$$

From (10)

$$\mathbf{G}(s) = \mathbf{G}_T(s)[\mathbf{I} - \mathbf{G}_T(s)]^{-1} \quad (12)$$

Since \mathbf{G} is diagonal, $[\mathbf{I} - \mathbf{G}]$ and $[\mathbf{I} - \mathbf{G}]^{-1}$ are also diagonal matrices. Therefore, matrix \mathbf{G} takes on the diagonal form

$$\mathbf{G}(s) = \begin{bmatrix} \frac{G_{T11}}{1+G_{T11}} & & \\ & \ddots & \\ & & \frac{G_{Tpp}}{1+G_{Tpp}} \end{bmatrix} \quad (13)$$

The system error is given by

$$\mathbf{e}(s) = \mathbf{r}(s) - \mathbf{y}(s) = [\mathbf{I} - \mathbf{G}_T(s)]\mathbf{r}(s) \quad (14)$$

The necessary condition to obtain $\mathbf{e}(t) = \mathbf{0}$ is

$$\lim_{s \rightarrow 0} \mathbf{G}_T(s) = \mathbf{I} \quad (15)$$

For instance, the following $\mathbf{G}_T(s)$ transfer matrix meets the condition given by (15)

$$\mathbf{G}_T(s) = \begin{bmatrix} \frac{1}{T_{11}s+1} & & \\ & \ddots & \\ & & \frac{1}{T_{pp}s+1} \end{bmatrix} \quad (16)$$

In (16), T_{ii} for $ii = 11, \dots, pp$ are time constants. Introducing condition (15) into (10) results

$$\mathbf{I} + \mathbf{G}(0) = \mathbf{G}(0) \quad (17)$$

This requirement means that each element of the diagonal matrix \mathbf{G} must contain at least one integrator. Using (9) into (10), we obtain the following MIMO controller

$$\mathbf{G}_c(s) = [\mathbf{G}_p(s)]^{-1} \mathbf{G}_T(s) [\mathbf{I} - \mathbf{G}_T(s)]^{-1}$$

$$\mathbf{G}_c(s) = [\mathbf{G}_p(s)]^{-1} \begin{bmatrix} \frac{1}{T_{11}s} & & \\ & \ddots & \\ & & \frac{1}{T_{pp}s} \end{bmatrix} \quad (18)$$

Assuming that all parameters of \mathbf{G}_p and \mathbf{G}_T are known, then the following MIMO controller with known parameters takes on the form

$$\mathbf{G}_c(s) = \begin{bmatrix} K_{c11} + \frac{K_{i11}}{s} & -K_{c12} - \frac{K_{i12}}{s} \\ K_{c21} + \frac{K_{i21}}{s} & K_{c22} + \frac{K_{i22}}{s} \end{bmatrix} \quad (19)$$

Figure 10 depicts the simulation result of the MIMO IO control system using a sampling time of 0.1 s. Reference level and temperature signals were set to 20 cm and 33 °C.

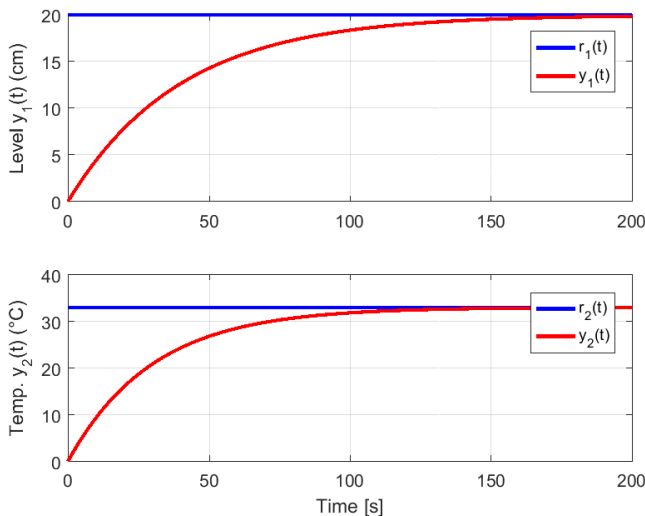


Figure 10: Simulated time-responses of the MIMO IO control system. Top graph: controlled level $y_1(t)$. Lower graph: controlled temperature $y_2(t)$.

Figure 11 depicts the experimental results of the MIMO IO control system employing most of the parameters obtained in the simulation phase. Some parameters required a real-time post-tuning to achieve the desired responses. Observe in Figure 11 that the controlled level $y_1(t)$ possesses a settling time of 225 s, null P.O. (Percent Overshoot), and about a null steady-state error. On the other hand, the controlled temperature $y_2(t)$ shows a settling time of 200 s, a P.O. of 25%, and around a null steady-state error.

It is worth to mention that the MIMO IO controller given by (19) constitutes the structure of the MIMO FO controller to be designed in the next Section.

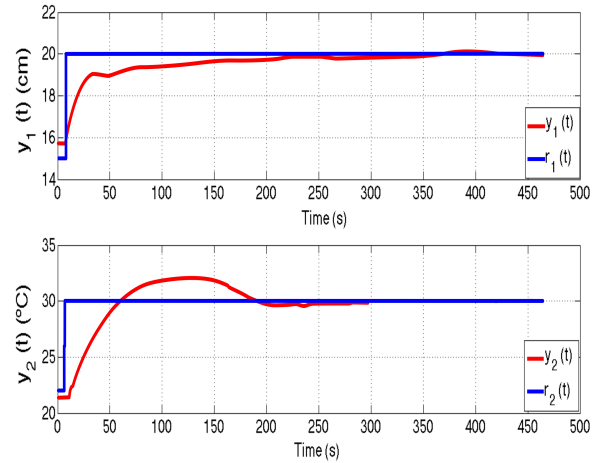


Figure 11: Experimental time-responses of the MIMO IO control system. Top graph: controlled level $y_1(t)$. Lower graph: controlled temperature $y_2(t)$.

5 Design of the MIMO FO Control System

The approach used in this section was employed in [9] to control two robot manipulators. The MIMO FO controllers is obtained making fractional the MIMO IO controller given by (19). That is, replacing in (19) all Laplace operators s by s^δ and s^λ , where δ and λ are fractional numbers between 0 and 1. Then, the MIMO FO controller takes on the form

$$\mathbf{G}_{cFO}(s) = \begin{bmatrix} K_{c11} + \frac{K_{i11}}{s^\delta} & -K_{c12} - \frac{K_{i12}}{s^\delta} \\ K_{c21} + \frac{K_{i21}}{s^\lambda} & K_{c22} + \frac{K_{i22}}{s^\lambda} \end{bmatrix} \quad (20)$$

The FO differentiators s^δ and s^λ given in (20) may be approximated by polynomials that depend on the Laplace operator s employing various formulas. For example, for the frequency range of operation $[\omega_b, \omega_h]$, s^δ and s^λ can be approximated by the following modified Oustaloup filter described in [10]

$$s^m \approx C \prod_{k=-N}^N \left(\frac{s + \omega'_k}{s + \omega_k} \right) \quad (21)$$

$$C = \left(\frac{d\omega_h}{b} \right)^m \left[\frac{ds^2 + b\omega_h}{d(1-m)s^2 + b\omega_h s + dm} \right]$$

$$\omega_u = \sqrt{\omega_h/\omega_b}$$

$$\omega'_k = \omega_b \omega_u^{(2k-1+m)/N} \quad \omega_k = \omega_b \omega_u^{(2k-1-m)/N}$$

According to [10], the Oustaloup filter produces a good approximation for $b = 10$ and $d = 9$. The frequency range of operation can be obtained from the Bode diagrams of transfer functions of the robot manipulator's transfer matrix function. However, such an approximation is not employed in this work because we will perform real-time implementation of recursive codes in the discrete-time domain.

There are various approximations for the FO differentiators s^δ and s^λ as a function of the shift operator z . This work employs the Muir’s recursion method [11], which establishes

$$s^\delta \approx \left(\frac{2}{T}\right)^\delta \frac{A_n(z^{-1}, \delta)}{A_n(z^{-1}, -\delta)} \quad (22)$$

In (22), T is the sample time and z is the shift operator. $A_n(z^{-1}, \delta)$ can be computed in recursive form as follows

$$\begin{aligned} A_n(z^{-1}, \delta) &= A_{n-1}(z^{-1}, \delta) - c_n z^{-n} A_{n-1}(z, \delta) \\ A_0(z^{-1}, \delta) &= 1 \\ c_n &= \begin{cases} \delta/n & \text{if } n \text{ is odd} \\ 1 & \text{if } n \text{ is even} \end{cases} \end{aligned} \quad (23)$$

This work uses $n = 3$ in (23). Therefore

$$\begin{aligned} s^\delta &\approx \left(\frac{2}{T}\right)^\delta \frac{A_3(z^{-1}, \delta)}{A_3(z^{-1}, -\delta)} \\ A_3(z^{-1}, \delta) &= -\frac{1}{3}\delta z^{-3} + \frac{1}{3}\delta^2 z^{-2} - \delta z^{-1} + 1 \\ A_3(z^{-1}, -\delta) &= \frac{1}{3}\delta z^{-3} + \frac{1}{3}\delta^2 z^{-2} + \delta z^{-1} + 1 \end{aligned} \quad (24)$$

A similar expression to (24) is obtained for λ as follows

$$s^\lambda \approx \left(\frac{2}{T}\right)^\lambda \frac{A_3(z^{-1}, \lambda)}{A_3(z^{-1}, -\lambda)} \quad (25)$$

Using (20), we formulate $\mathbf{u} = \mathbf{G}_{cFO}\mathbf{e}$. Hence, the control laws u_1 and u_2 are formulated as

$$\begin{aligned} u_1 &= \left(K_{c11} + \frac{K_{i11}}{s^\delta}\right)e_1 - \left(K_{c12} + \frac{K_{i12}}{s^\delta}\right)e_2 \\ u_2 &= \left(K_{c21} + \frac{K_{i21}}{s^\lambda}\right)e_1 + \left(K_{c22} + \frac{K_{i22}}{s^\lambda}\right)e_2 \end{aligned} \quad (26)$$

In (26), $e_1 = r_1 - y_1$ and $e_2 = r_2 - y_2$ are the system errors, and r_1 and r_2 are the set points. Replacing (24) and (25) in (26), we obtain two control laws of the form

$$\begin{aligned} u_1(k) &= -\sum_{i=1}^3 \alpha_i u_1(k-i) + \sum_{i=0}^3 \beta_i e_1(k-i) + \sum_{i=0}^3 \rho_i e_2(k-i) \\ u_2(k) &= -\sum_{i=1}^3 \eta_i u_1(k-i) + \sum_{i=0}^3 \tau_i e_1(k-i) + \sum_{i=0}^3 \sigma_i e_2(k-i) \end{aligned} \quad (27)$$

In (27), k is the discrete time. Note that parameters α_i , β_i , and ρ_i depend on δ , while parameters η_i , τ_i , and σ_i depend on λ . Recall that fractional numbers δ and λ depend on the sampling time T .

Figure 12 depicts the simulation result of the MIMO FO control system obtained with the following parameters: $T_{11} = 30$, $T_{22} = 40$, $K_{c11} = 1.012$, $K_{i11} = 0.005$, $K_{c12} = -2.334$, $K_{i12} = -0.013$, $K_{c21} = 0.0846$, $K_{i21} = 0.007$, $K_{c22} = 2.334$, $K_{i22} =$

0.013. Reference level and temperature signals were set to 20 cm and 33 °C. The simulation phase employed a sampling time of 0.1 s.

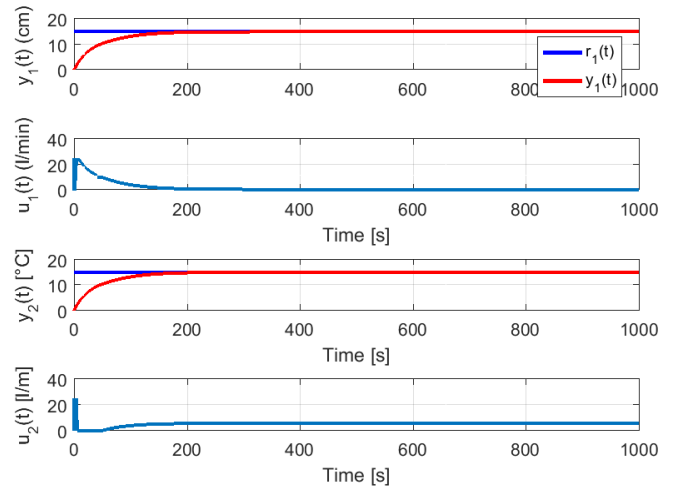


Figure 12: Simulation time–responses of the MIMO FO control system. Top graph: controlled level $y_1(t)$, second graph from the top: control force $u_1(t)$, third graph from the top: controlled temperature $y_2(t)$. Bottom graph: control force $u_2(t)$.

Figure 13 illustrates the experimental results of the MIMO FO control system using most of the parameters employed in the simulation phase. Some parameters needed a post-tuning to achieve the desired responses. Note in Figure 13 that the controlled level depicts a settling time of 70 s, null P.O., and null steady–state error. Also, the controlled temperature possesses a settling time of 125 s, null P.O., and null steady–state error.

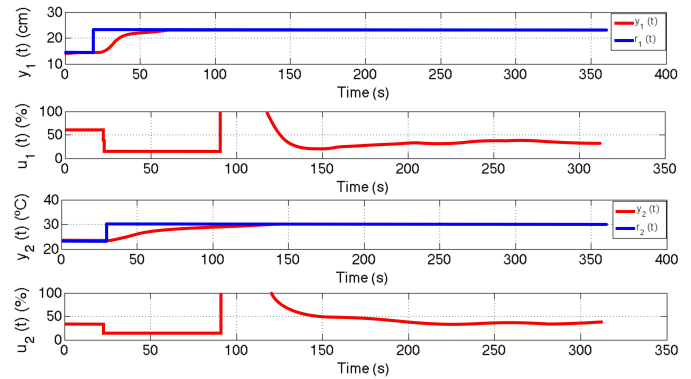


Figure 13: Experimental time–responses of the MIMO FO control system. Top graph: controlled level $y_1(t)$, second graph from the top: control force $u_1(t)$, third graph from the top: controlled temperature $y_2(t)$. Bottom graph: control force $u_2(t)$.

6 Concluding Remarks

A MIMO IO as well as a MIMO FO control systems were implemented for comparison purposes in this work. At the

present, no work that employs a MIMO fractional order controller has been published.

Experimental results demonstrate that the MIMO FO control system performs better because the settling time of the controlled level decreases from 225 s (Figure 11, top graph) to 70 s (Figure 13, top graph), while the settling time of the controlled temperature diminish from 200 s (Figure 11, lower graph) to 130 s (Figure 13, lower graph).

No P.O. (Percent Overshoot) shows the controlled level and temperature using a MIMO FO controller as seen in Figure 13. However, the controlled temperature using a MIMO IO controller depicts a P.O. of 20% as illustrated in the lower graph of Figure 11.

The main problem faced with the employed water tank plant was the supply of hot water in sufficient quantity to perform the experiments.

The simulation of the MIMO IO control systems is necessary to analyse the behaviour of the controlled plant and estimate the tuning parameters required for real–time implementation.

As seen in Figures 11 and 13, the controlled level and temperature do not present oscillations. However, using the decoupled control configuration developed in [1], the controlled level and temperature depicted in Figure 1 show strong oscillations.

Conflict of Interest The authors declare no conflict of interest.

Acknowledgment We are very grateful to the Electronic Engineering Department of the Universidad de Ingeniería y Tecnología (UTEC) for supporting this research work.

References

[1] TE37 Equipment Control and Instrumentation Study Station, User Guide, Tecquipment Ltd, UK, 2009.

- [2] V. Tzouanas, “Temperature and Level Control of a Multivariable Water Tank Process”, in 120th ASEE Annual Conference & Exposition, Atlanta, Georgia, Jun 23–26, 2013, pp. 1–11.
- [3] E. Cornieles, et al., “Modelling and Simulation of a Multivariable Process Control”, in IEEE ISIE, Montreal, Quebec, Canada, July 9–12, 2006, pp. 1–11. DOI: 10.1109/ISIE.2006.296039
- [4] A. Rojas–Moreno and A. Parra–Quispe, “Design and Implementation of a Water Tank Control System using a Multivariable PID Controller”, in 6th International Conference on Computing, Communications and Control Technologies (CCCT), Orlando, USA, June 2008. ISBN: 1934272442 9781934272442, Number OCLC: 552110236
- [5] C. Dinakaran, “Temperature and Water Level Control in Boiler by using Fuzzy Logic Controller”, International Journal of Electrical Power System and Technology, Vol. 1: Issue 1, pp. 27–37, 2015
- [6] A. Rojas–Moreno, et al., “Planta industrial multipropósito para control e instrumentación.” Resolution N° 001545–2019/DIN-INDECOPI, May 20, 2019, Lima, Peru
- [7] A. Rojas–Moreno, et al., “Planta industrial multipropósito para control y supervisión.” Resolution N° 001035–2019/DIN-INDECOPI, March 28, 2019, Lima, Peru.
- [8] A. Rojas–Moreno and J. Hernandez–Garagatti, “Modelling of a Multipurpose Water Tank Plant”, in IEEE XXIV International Conference on Electronics, Electrical Engineering and Computing (INTERCON), Cusco, Peru, Aug. 15–18, 2017, pp. 1–4. <https://doi.org/10.1109/intercon.2017.8079668>
- [9] A. Rojas–Moreno, “An Approach to Design MIMO FO Controllers for Unstable Nonlinear Plants,” IEEE/CAA Journal of Automatica Sinica, vol. 3, no. 3, July 2016, pp. 338–344. <https://doi.org/10.1109/jas.2016.7508810>
- [10] C. A. Monje et al., “Implementation of Fractional Order Controllers,” in Fractional–Order Systems and Control. Fundamentals and Applications, Springer–Verlag London Limited 2010, pp. 195–196.
- [11] B. Vinagre, et al., “Two direct Tustin discretization methods for fractional-order differentiator/integrator,” J. of the Franklin Institute, 340, pp. 349–362, 2003. <https://doi.org/10.1016/j.jfranklin.2003.08.001>

A Method for Mosaicking Aerial Images based on Flight Trajectory and the Calculation of Symmetric Transfer Error per Inlier

Daniel Arteaga^{*1}, Guillermo Kemper¹, Samuel G. Huamán Bustamante¹, Joel Telles¹, León Bendayán², José Sanjurjo²

¹Universidad Nacional de Ingeniería, Instituto Nacional de Investigación y Capacitación de Telecomunicaciones, Lima, 15021, Perú

²Instituto de Investigación de la Amazonía Peruana, Iquitos 16007, Perú

ARTICLE INFO

Article history:

Received: 16 October, 2019

Accepted: 30 November, 2019

Online: 23 December, 2019

Keywords:

Image Mosaicking

Random Sample Consensus

Georeferencing

Unmanned Aerial Vehicles

Forest Monitoring

ABSTRACT

In recent years, development of aerial autonomous systems and cameras have allowed increasing enormously the number of aerial images, and their applications in many research areas. One of the most common applications is the mosaicking of images to improve the analysis by getting representations of larger areas with high spatial resolution. This paper describes a simple method for mosaicking aerial images acquired by unmanned aerial vehicles during programmed flights. The images were acquired in two scenarios: a city and a forest in the Peruvian Amazon, for vegetation monitoring purposes. The proposed method is a modification of the automatic homography estimation method using the RANSAC algorithm. It is based on flight trajectory and the calculation of symmetric transfer error per inliers. This method was implemented in scientific language and the performance was compared with a commercial software with respect to two aspects: processing time and geolocation errors. We obtained similar results in both aspects with a simple method using images for natural resources monitoring. In the best case, the proposed method is 6 minutes 48 seconds faster than the compared software and, the root mean squared error of geolocation in X-axis and Y-axis obtained by proposed method are less than the obtained by the compared software in 0.5268 and 0.5598 meters respectively.

1 Introduction

During most of the twentieth century, the photogrammetry required a lot of monetary and time resources. After the technological development of electronic systems like the Global Positioning System (GPS) and the Inertial Measurement Unit (IMU), the design of autonomous vehicles, and the production of digital cameras, time and cost limitations have been steadily declining. Thus, the rise of the Unmanned Aerial Vehicles (UAVs) started. Nowadays, there is a wide range of UAVs with multiple sensors and digital cameras that are being used in many different areas such as photogrammetry, agriculture, management of natural resources, mapping and urban planning, rescue [1], assessment and mitigation of disasters, and other Remote Sensing applications [2].

One of the most important and common uses given to the aerial images acquired by UAVs, also known as drones, is the image mosaicking, which allows better visualization and assessment of an event or area of study. For instance, the usage of image mosaicking in agriculture [3] is beneficial not just because it generates an image that covers bigger areas of crops with high resolution, in fact, it also

allows control the temporal resolution and the periodical assessment of the fields to improve decision-making regarding the amounts of pesticides, irrigation, land usage, and other variables.

Image mosaicking is about the reconstruction of a scene in two dimensions (2D) by using individual images with overlapping areas. In order to perform this process, the estimation of geometric transformations between pairs of images is required to project them over the others and merge them together with the minimum possible error. These projective transformations, which are commonly known as 2D homographies, are estimated from matching points of two overlapping images.

Multiple mosaicking algorithms have been developed depending on the requirements of accuracy and time. There are high accuracy algorithms based on Structure from Motion technique that estimates the scene information in three dimensions, the orientation and the localization of the camera, and in this way, it calculates the homographies [4]; however, these algorithms imply high computational cost and are difficult to implement. Other algorithms utilize the information of the GPS and gyroscope of the UAV to obtain approximations of localization and orientation of the cameras during

*Daniel Arteaga, Lima, 15067, Peru, (+51) 995550108 & darteaga@inictel-uni.edu.pe

the flight [5] but matching images and gyroscope information by the acquisition time may not be accurate. In addition, it has been implemented algorithms that perform feature matching based on bag of words (BoW) and dictionaries [6, 7] to accelerate this step, for example, in [8] author compared processing times of different methods of feature matching. Moreover, other researchers have modified the Structure from Motion technique and have changed the Bundle Adjustment by other techniques of global adjustment [9, 10]; nevertheless, these algorithms are difficult to implement.

We present a simple method of mosaicking aerial images with geographical information acquired by UAV that obtains viable results for applications in natural resources monitoring, and competitive results in terms of processing time and geolocation error, in comparison with professional software. This method is based on the image mosaicking of aerial images acquired in the same line of flight, and the usage of symmetric transfer error per inlier as an indicator of acceptable estimation of the homography.

This work is organized as follow: Section 2 develops the proposed mosaicking algorithm and the implementation details. In section 3, the results are presented and compared with those of one professional software. Finally, in section 4, we present the conclusions and comment some limitations of the proposed algorithm.

2 Proposed Method

The proposed method is based on a modification of the Random Sample Consensus (RANSAC) method used to automatically estimate homographies. According to Figure 1, this method first creates a mosaic of all images acquired in the same line of flight and then obtains the final mosaic by merging properly the mosaics of flight lines. Given that our method is based on the flight trajectory, first, we mention some details related to the acquisition of images via UAV: the images must be composed of three channels (the most common case is RGB), and they should be geotagged (latitude and longitude) in order to obtain flight lines and to perform the georeferencing step. In this section, we describe and explain the implementation details regarding the steps of the proposed method.

2.1 Image Reading and Image Preprocessing

The first step is to read geotagged images and obtain the number, the names, the directory, the size and the geographical information of the images. Then the images are resized to a maximum resolution of 1500 x 1000 pixels and the geographical information is transformed to the Universal Transverse Mercator (UTM) coordinate system.

The preprocessing consists of the selection of images that belong to the same flight lines, which are almost straight lines as those of Figure 2. It is important to understand that the geolocation information of each image corresponds to the point located in the middle of the image. To determine which images belong to the same lines we propose an approach based on the distance between two adjacent images also known as shooting distance.

If the shooting distance between two images is inside a certain range of distances, the method will consider those images have been acquired in the same flight line. The range of distances is

established from the most common values of shooting distances and it is calculated as follow:

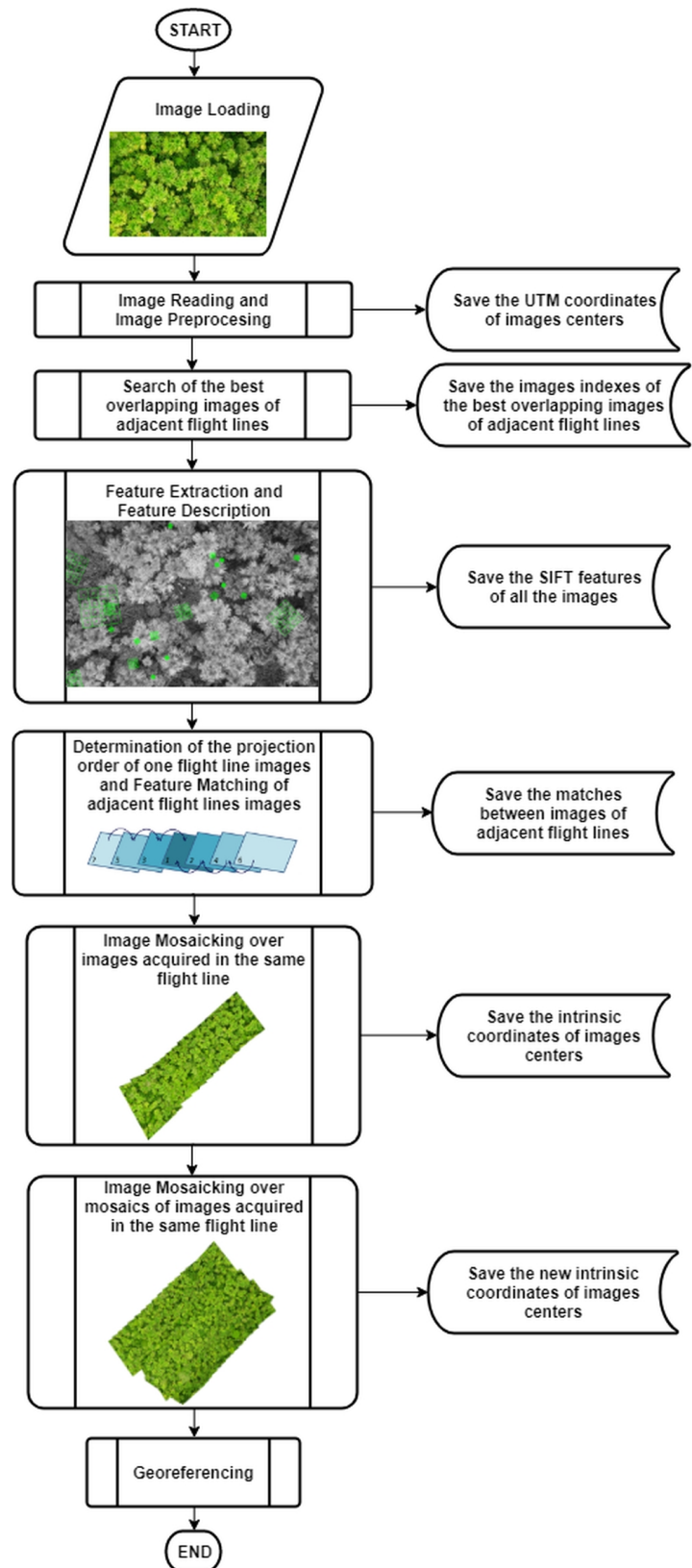


Figure 1: Flow Diagram of the proposed mosaicking method.

1. All the shooting distances $dist$ are used to generate a histogram with equally spaced intervals.
2. The most common shooting distance $dist_{mr}$ is calculated as the mean value of the interval with the larger number of observations or greater frequency.
3. We define the parameter w as the ninth part of the difference between the largest and shortest shooting distance, according to (1). After evaluating the shooting distance for all the geotagged images of different flights, we found that dividing the difference between the boundaries in nine parts performs a better selection of images pertaining to the same flight line.

$$w = \frac{\max(dist) - \min(dist)}{9} \quad (1)$$

4. The range of distances is fixed by (2). The minimum value of this range is the most common shooting distance $dist_{mr}$ minus two times the parameter w , while the maximum value is the most common shooting distance $dist_{mr}$ plus five times the parameter w . This is mainly because the majority of shooting distances that do not correspond to images of the same flight line, indicated in the histogram of Figure 3 as red bars, are smaller than $dist_{mr}$. The choices of the multiplicative factors 2 and 5 were given after evaluating all the available geotagged images of different flights.

$$Range_{dist} = [dist_{mr} - 2w; dist_{mr} + 5w] \quad (2)$$

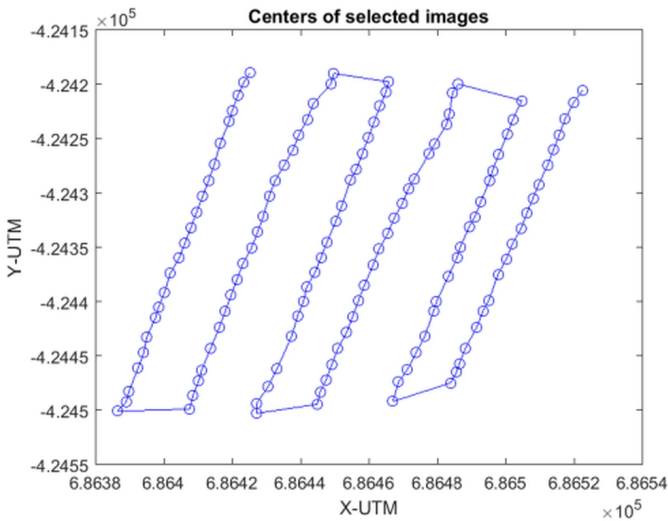


Figure 2: Plot of the geolocation of image centers selected for mosaicking.

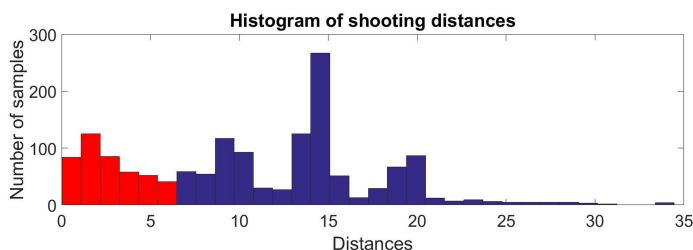


Figure 3: Histogram of shooting distances corresponding to six flights.

2.2 Search of the best overlapping images of adjacent flight lines

In order to perform the mosaicking of individual flight lines mosaics, it is required to compute image matching between images of adjacent lines. The optimal procedure is to search for the best overlapping images of adjacent lines rather than perform image matching for all the acquired images due to the time and computational cost. We utilize Delaunay Triangulation [11] and the UTM geographical coordinates of each image to search for pairs of images with enough overlap that belongs to adjacent flight lines. We applied the Delaunay Triangulation algorithm of Matlab that is basically an incremental implementation.

The fundamental property of Delaunay Triangulation can be explain based on the circles circumscribed to a triangle for the 2D case. Given four points V_1, V_2, V_3 and V_4 , Delaunay Triangulation is fulfilled when each circle circumscribed to the triangle drawn from three points contains no other point inside of it. The importance of this property is that the majority of the drawn triangles possess relatively large internal angles. Thus, those triangles are considered to be “well shaped” (more similar to an equilateral triangle than to an obtuse one) and for our application, the edges of those triangles connect points that represent two images with enough overlap because the larger edges are smaller than the larger edges of triangles in the non-Delaunay Triangulation.

By applying Delaunay Triangulation, the connections between images with enough overlap are obtained, and shown in Figure 4a; nevertheless, those connections between images of adjacent lines are required to be selected and the rest, to be filtered out. In addition, all the edges of triangles with any internal angle larger than 90 degrees should be deleted to ensure better overlap and therefore more accurate matching points or inliers. After this process, the connections between the images are depicted in Figure 4b.

2.3 Feature Extraction and Feature Description

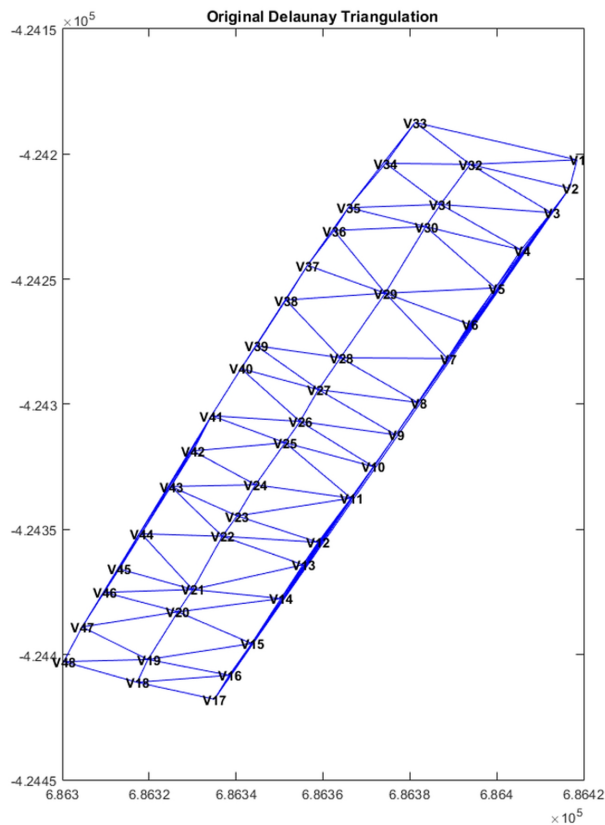
There are many feature extraction techniques in the literature but one of the best techniques used for mosaicking are the Scale Invariant Feature Transformation (SIFT) [12] because of the property to find corresponding points in different scale, rotated and translated images. Images in different scales are the result of convolution between an image $I(x, y)$ and 2D Gaussian filters $G(x, y, \sigma)$ with different values of standard deviations σ . Equation (3) describes how images in different scales $L(x, y, \sigma)$ are produced, while (4) describes the 2D Gaussian filter.

$$L(x, y, \sigma) = G(x, y, \sigma) * I(x, y) \quad (3)$$

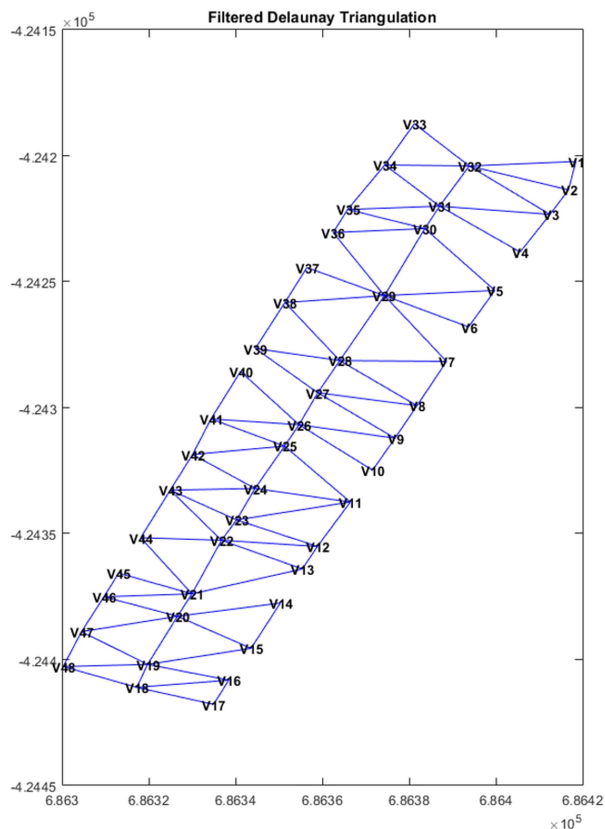
$$G(x, y, \sigma) = \frac{1}{2\pi\sigma^2} e^{-\left(\frac{x^2+y^2}{2\sigma^2}\right)} \quad (4)$$

SIFT features are located in the local maximum in a neighborhood of $3 \times 3 \times 3$ (X-axis, Y-axis and the scale) over the result of the convolution between an image and the difference of the Gaussians with scales k and $k\sigma$, as expressed in (5). In addition, the gradients and its orientations are calculated in the neighborhood of the feature.

$$D(x, y, \sigma) = (G(x, y, k\sigma) - G(x, y, \sigma)) * I(x, y) \quad (5)$$



(a)



(b)

Figure 4: Delaunay Triangulation used to search the best overlapping images of adjacent flight lines (a) Original Triangulation (b) Filtered Triangulation.

The first step is feature extraction, also known as feature detection. It computes the detection vector, which is composed of the location in the X-axis and Y-axis, the scale (represented by the standard deviation σ) and the resultant orientation of the gradients. Then, feature description computes the description vector, a 128-vector, from the gradients calculated in the neighborhood of the feature point.

Both feature extraction and description are computed by using the implementation of the SIFT algorithm in the open source library VLFeat [13]. Figure 5 shows some SIFT features computed over an aerial image acquired by an UAV over a swampy forest of the Peruvian Jungle in Iquitos, known as Aguajales [14-16].

2.4 Determination of the projection order of one set of flight line images and Feature Matching of sets of adjacent flight lines images

Performing image mosaicking over one set of flight line images requires certain implementation considerations because it implies the projection of images by the homographies, which estimation is not error free. Because of this, determining the projection order is a fundamental step that avoids generating mosaics with visual errors accumulated in certain direction of the image, as the one shown in Figure 6a.

The idea is to project all images over a projection plane aligned with the image located in the middle of the flight line. Therefore, the first image in the projection order is the image in the middle of the line. The next images in the projection order are those that are adjacent to the first one, and then it continues in the same manner but alternating between the two directions of the flight line. This criterion is depicted in Figure 6b.

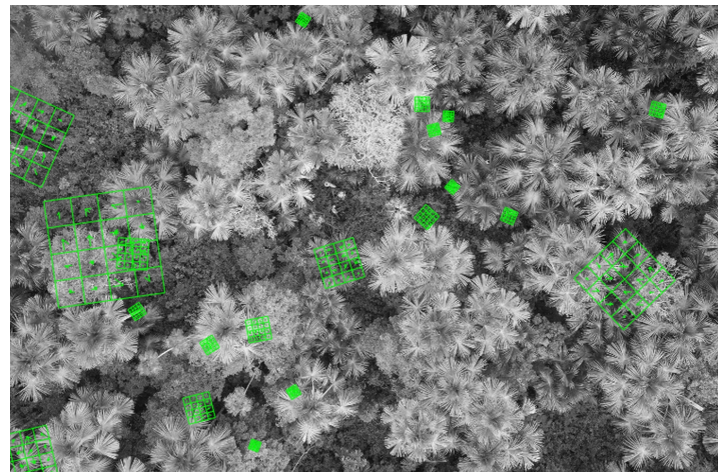


Figure 5: SIFT features computation over an aerial image acquired in a forest.

In this step of the proposed method, the feature matching is also performed, between images of adjacent flight lines that were selected in second step of this method. This operation finds two features, one per image, that possess similar SIFT descriptor vectors. We used the SIFT feature matching algorithm implemented in VLFeat and we obtained two results: the matches (pair of features) and the Euclidean distances between them.

The matches between two images are represented as a group of points X_c and X'_c ; each match is represented as the homogeneous vectors x_c and x'_c . These homogeneous vectors are 3-vectors composed by the position of the feature in the X-axis and the Y-axis, and the unity. It is important to mention that the X-axis of the image refers to the horizontal axis (columns) and the Y-axis refers to the vertical axis (rows).

To find the best matches between images of adjacent flight lines, we select the 50 matches with the lowest Euclidean distance for every pair of image established in the second step of the proposed method. By doing this, more than 500 matches can be computed, between images corresponding to two adjacent flight lines that will be used to perform the calculation of homographies between mosaics of flight lines. Any transformation that will be applied to an image during the generation of mosaics of flight lines should be also applied to the features of each image corresponding to the matches between images of adjacent lines because they represent positions over images that are being modified.

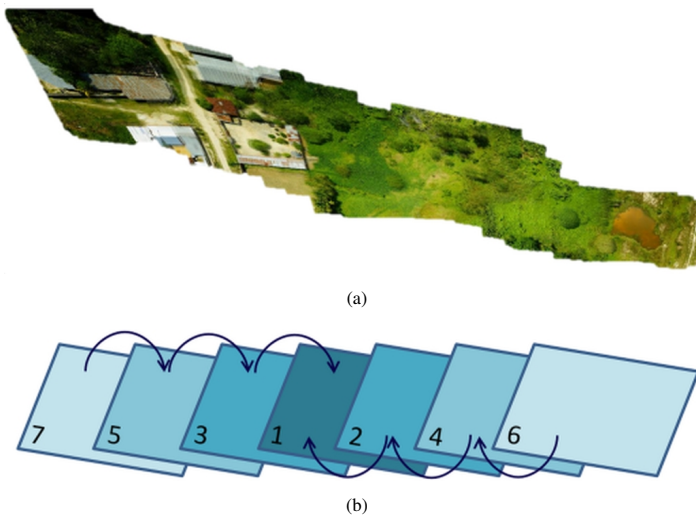


Figure 6: Projection order of images: (a) Mosaic generated after projecting the images respect to an image in the end or beginning of line (b) Projection order proposed for image mosaicking over images in a flight line.

After several homography estimation tests, we observed that 50 matches should be computed to reduce the processing time and, at the same time, to ensure that the number of wrong matches or outliers is very small in comparison with the inliers; thus, the probability p_o of choosing a sample free of outlier increases.

2.5 Image Mosaicking over images acquired in the same flight line

This is the most important step of the proposed method. Both the homography estimation and the projection of images are performed following the projection order computed in the previous step (step 4th). To perform homography estimation, the feature matching between images of the same flight line is required. In this case, we select the 150 matches with lowest Euclidean distance instead of 50 because these matches are used to estimate the homography between individual images rather than mosaic images (mosaic of images acquired in the same flight line).

The homography H is a 3×3 matrix that projects a set of points X_c belonging to the plane $P \in R^2$, as another set of points X'_c , belonging to another plane $P' \in R^2$. The projection of a point represented by a homogeneous vector x_c through the homography H is expressed in (6).

$$x'_c = Hx_c \tag{6}$$

One of the most common methods to perform homography estimation is based on the Random Sample Consensus or RANSAC method, and a posterior optimization which consists in minimizing a cost function depending on the homography and the inliers. This method is denoted as RANSAC-OPT in this work, for simplification purposes. RANSAC performs a robust estimation based on the calculations for a random sample by iteratively approximating a model. In each iteration, RANSAC computes not only the estimated model; in addition, it classifies all the matches. If a match adjusts to the estimated model with an error less than a threshold t , then it will be considered an inlier; otherwise, it will be considered an outlier.

We implemented RANSAC-OPT method for homography estimation and we observed that it gives good results with a tolerable error for images with an overlap of 60 percent or greater. Nevertheless, due to factors external to the flight planning, some images could be acquired with less overlap. In this situation, RANSAC-OPT can wrongly estimate the homography, producing deformations in mosaics, as those shown in Figure 7. Besides, this estimation can take more iterations to finish, thus increasing the processing time.

Because of these limitations of the RANSAC-OPT method, the proposed method verifies that the symmetric transfer error per inlier would be low, ensuring an acceptable homography estimation. The proposed algorithm of automatic homography estimation, depicted in Figure 8, is based on two modifications of the RANSAC algorithm followed by the optimization step. These two modifications are denoted RANSAC-1-OPT and RANSAC-2-OPT. The inputs of both modifications are the S matches between two images X_c y X'_c ; the outputs are the estimated homography H_e , the percentage of inliers p_{inl} , and the symmetric transfer error per inlier ste_{inl} . The steps of this method are indicated below.



Figure 7: Deformation during mosaicking produced by the wrong estimation through RANSAC for two images with low overlap.

1. RANSAC-1-OPT is performed. This is composed of the first modification of RANSAC (RANSAC-1) and the posterior optimization (OPT).

(a) RANSAC-1: The iteration counter cnt_1 is initialized with a value of zero, and the number of required iterations N with a value different from zero. The probability p_o of choosing a sample free of outlier is also initialized with a value of 0.99 as described in the original RANSAC method.

- i. $s = 4$ matched points are randomly selected, from the sample space of S matches, so that these s matches are as distant as possible. These s matches are used to perform the initial estimation of the homography through the Direct Linear Transformation (DLT) algorithm. This allows that the estimated homography can project appropriately any set of points dispersed in the whole image, rather than just points located in one portion of the image. In order to find the most distant matched points, the matches were randomly paired and then the two most distant pairs of matched points were chosen. The fact that $s = 4$ is because it is the number of matches needed to estimate the homography H_o by using the DLT method.
- ii. Given the S homogeneous vectors x_c and x'_c (representing the matches) and the estimated homography H_o , the solution of the minimization problem of (7) is a homography H_R that minimizes the symmetric transfer error for all the S matches. The cost function of this minimization problem is the sum of the symmetric transfer error per match ste_c . Equation (8) is used to calculate ste_c , where $d(\cdot)$ denotes the Euclidean distance between two points.

$$H_R = \min_{H_o} \sum_{i=1}^S ste_{c_i} \quad (7)$$

$$ste_{c_i} = d(x_{c_i}, H_o^{-1}x'_{c_i})^2 + d(x'_{c_i}, H_o x_{c_i})^2 \quad (8)$$

- iii. Using the homography H_R , the errors of each match with respect to the estimated model (the homography) are represented by the values of ste_c , so they are calculated by using (8). Then the standard deviation of those errors σ_c are computed.
- iv. The inliers of the model are represented by the homogeneous vectors x_{inl} and x'_{inl} , and they are those matches whose values of ste_c are less than the threshold t , computed according to (9). Once the inliers are identified, it is also computed the number of inliers n_{inl} , the sum of symmetric transfer errors of the inliers STE_{inl} , and the standard deviation of the symmetric transfer errors of the inliers σ_{inl} .

$$t = \sqrt{5.99}\sigma_c \quad (9)$$

- v. During the first iteration, the estimated homography H_R , the homogeneous vector of the inliers x_{inl} and x'_{inl} , the number of inliers n_{inl} , the sum of symmetric transfer errors of the inliers STE_{inl} , and the standard deviation σ_{inl} , are save as reference for

the following iterations. For the rest of iterations, the following instructions are performed:

- If the calculated STE_{inl} is less than or equal to 10 times its reference, the reference will be updated with the calculated STE_{inl} , and then it will proceed with the next item.
 - If the computed n_{inl} is greater than its reference, the reference for the values of H_R , n_{inl} , STE_{inl} , σ_{inl} , x_{inl} and x'_{inl} will be updated with the computed values. Otherwise, it will proceed with the next item.
 - If the computed n_{inl} is equal to its reference, the standard deviation σ_{inl} computed will be compared with the respective reference. If the calculated σ_{inl} is less than or equal to its reference, the reference values of H_R , n_{inl} , STE_{inl} , σ_{inl} , x_{inl} and x'_{inl} will be updated with the computed values. Otherwise, it will proceed with the step 1-(a)-vi.
- vi. The iteration finishes and the iteration counter cnt_1 increases in 1. Then the number of required iterations N is computed adaptively based on the number of inliers n_{inl} . Equation (10) is used to make this calculation. The probability of choosing an outlier ϵ is calculated using (11).

$$N = \frac{\log(1 - p_o)}{\log(1 - (1 - \epsilon^S))} \quad (10)$$

$$\epsilon = 1 - \frac{n_{inl}}{S} \quad (11)$$

- vii. When the iteration counter cnt_1 would be greater than or equal to N , RANSAC-1 finishes and its outputs are the reference values for H_R , n_{inl} , STE_{inl} , σ_{inl} , x_{inl} and x'_{inl} .

(b) OPT: The homography obtained after RANSAC-1 H_R is re-estimated utilizing just the n_{inl} homogeneous vectors representing the inliers x_{inl} and x'_{inl} . The output is the homography H_e , which solve the minimization problem of (12). The cost function is the sum of the symmetric transfer error of all the inliers, presented in (13).

$$H_e = \min_{H_R} \sum_{i=1}^{n_{inl}} ste_i \quad (12)$$

$$ste_i = d(x_{inl_i}, H_R^{-1}x'_{inl_i})^2 + d(x'_{inl_i}, H_R x_{inl_i})^2 \quad (13)$$

(c) Given the estimated homography H_e and the inliers, (14) is used to calculate the percentage of inliers p_{inl} , and (15) is employed to compute the symmetric transfer error per inlier ste_{inl} .

$$p_{inl} = \frac{n_{inl}}{S} \quad (14)$$

$$ste_{inl} = \frac{\sum_{i=1}^{n_{inl}} ste_i}{n_{inl}} \quad (15)$$

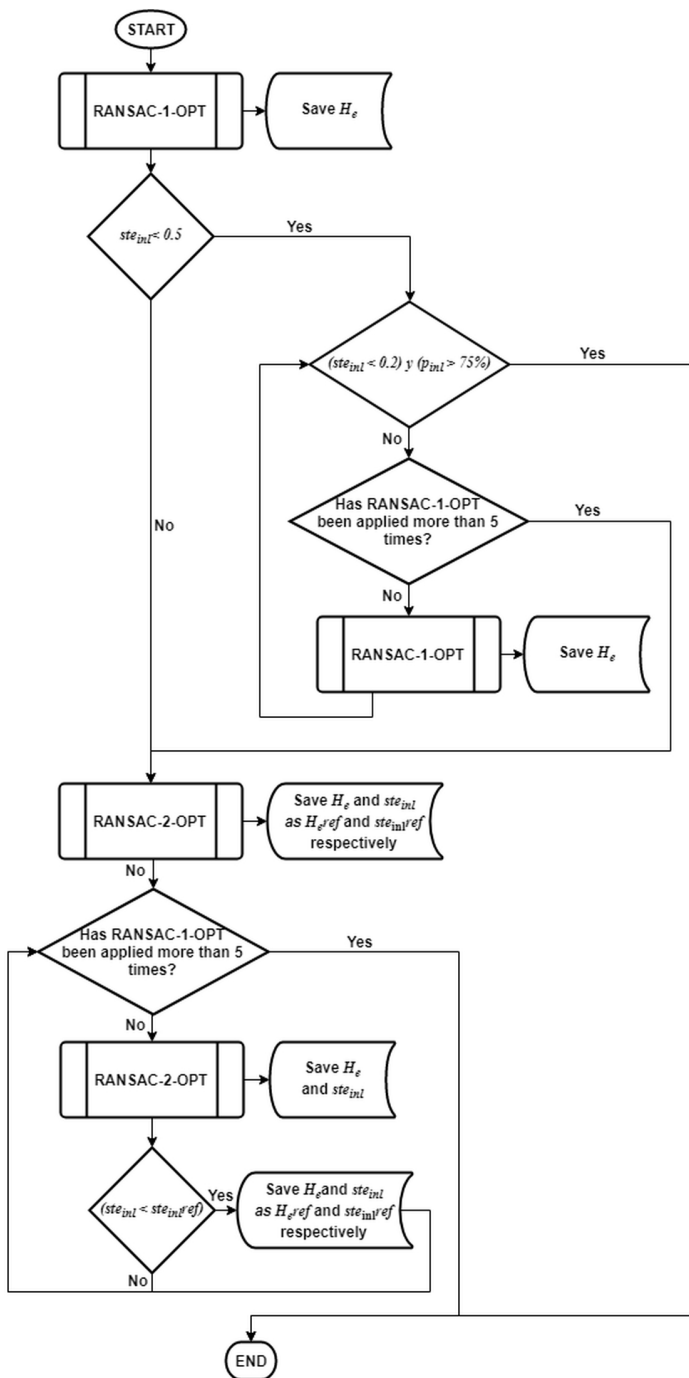


Figure 8: Proposed algorithm for the automatic estimation of homographies.

2. If the ste_{int} obtained in the step 1 is less than 0.5 pixels, it will proceed with the following item. It is important to mention that the value of 0.5 pixels was established after several tests of homography estimation between images with low overlap.

(a) If the ste_{int} is less than 0.2 and the p_{int} obtained in the step 1 is greater than 75%, the estimated homography H_e will be the solution and the proposed method for automatic estimation of homography will end. Otherwise, it will proceed with the next item. The threshold value for the percentage of inliers p_{int} was also established

empirically.

(b) RANSAC-1-OPT (described in the step 1) is applied again until the conditions of the previous item are satisfied, or until RANSAC-1-OPT has been applied 5 times in total. We applied continuously RANSAC-1-OPT several times and we found that the result of the homography estimation did not improve after 5 times, so we established this threshold. If the solution is not found after applying RANSAC-1-OPT 5 times, it will proceed with the step 3.

3. RANSAC-2-OPT is performed. This is composed of the second modification of RANSAC (RANSAC-2) and the posterior optimization (OPT).

(a) RANSAC-2: It initializes the same parameters of RANSAC-1 with the same values: the iteration counter cnt_2 , the number of required iterations N , and the probability p_o of choosing a sample free of outlier.

i. $s = 4$ matched points are randomly selected, from the sample space of S matches, to perform the initial estimation of the homography through the DLT algorithm. In this case, the matches are randomly selected without any other condition.

ii. Given the S homogeneous vectors x_c and x'_c and the estimated homography H_o , the symmetric transfer error per match ste_c is computed using (8). The standard deviation of those errors σ_c is also computed.

iii. In the same manner as for RANSAC-1, the homogeneous vectors of inliers x_{int} and x'_{int} , the number of inliers n_{int} , and the standard deviation of the symmetric transfer error of the inliers σ_{int} are calculated.

iv. During the first iteration, the estimated homography H_o , the homogeneous vector of the inliers x_{int} and x'_{int} , the number of inliers n_{int} , and the standard deviation σ_{int} , are saved as reference for the following iterations. For the rest of iterations, the following instructions are performed:

- If the computed n_{int} is greater than the reference value of n_{int} , the reference values of H_o , n_{int} , σ_{int} , x_{int} and x'_{int} will be updated. Otherwise, it will proceed with the next item.

- If the computed n_{int} is equal to its reference, the standard deviation σ_{int} computed will be compared with the respective reference. If the computed σ_{int} is less than or equal to its reference, the reference values of H_o , n_{int} , σ_{int} , x_{int} and x'_{int} will be updated with the computed values. Otherwise, it will proceed with the step 3-(a)-v.

v. The iteration finishes and the iteration counter cnt_2 increases in 1. Then the number of required iterations N is computed adaptively as it was done for RANSAC-1.

- vi. When the iteration counter cnt_2 would be greater than or equal to N , RANSAC-2 finishes and its outputs are the reference values for H_o , n_{inl} , σ_{inl} , x_{inl} and x'_{inl} .
 - (b) OPT: The homography obtained after RANSAC-2 H_o is re-estimated utilizing just the n_{inl} homogeneous vectors representing the inliers x_{inl} and x'_{inl} . This is performed in the same way as performed in the step 1-(b), and the result is the homography H_e .
 - (c) Given the estimated homography H_e and the inliers, the percentage of inliers p_{inl} and the symmetric transfer error per inlier ste_{inl} are computed as it was done in the step 1-(c).
4. The homography H_e and the symmetric transfer error per inlier ste_{inl} obtained in the step 3 are saved as references H_e^{ref} and ste_{inl}^{ref} . Then, RANSAC-2-OPT is applied again and the calculated ste_{inl} is compared with the reference ste_{inl}^{ref} . If the calculated value is less than the reference, then the references H_e^{ref} and ste_{inl}^{ref} will be updated. This procedure is repeated 4 times.

The H_e^{ref} obtained after the repetitions is the solution and the proposed algorithm for the automatic estimation of the homography finishes.

An important detail of the implementation of RANSAC-1 and RANSAC-2 is the normalization of the homogeneous vectors of the matches. Before using these vectors for the homography estimation, it is required to normalize them; at the same time, denormalization must be performed after the homography estimation in order to maintain the original scale. Both normalization and denormalization improve the results by avoiding high errors during homography estimation.

The algorithm to calculate adaptively the number of iterations, the DLT algorithm, the normalization algorithm, and the original RANSAC algorithm are well developed in [17].

Once the homographies between two adjacent images in the same flight line are computed, the homographies between any image of the line and the central image (first image in the projection order) can be computed by multiplying homographies according to the sequence established and depicted in Figure 6b.

The homographies allow the computation of the location of images over the mosaic images, and then, the intensities of pixels are interpolated for the new positions. Merging all the projected images implies to find the intensity of pixel over the mosaic by averaging (or applying another similar procedure) the intensity of the same pixel in the projected images.

The new position of the images centers, and the position of the matches points between images of adjacent flight lines should be computed for each projected images through the homographies.

2.6 Image Mosaicking over mosaics of images acquired in the same flight line

This step of the proposed mosaicking method performs the image mosaicking of the mosaics obtained from images acquired in the

same flight lines. The homographies between those individual mosaics are computed through the matches from images of adjacent lines. It proceeds as follows:

1. From the new positions of matches from images of adjacent lines, the matches from two adjacent mosaics X_m and X'_m are computed.
2. The sequence of projection is determined in the same manner that was done for the images belonging to same flight lines (step 4th) so the first image in the sequence is the mosaic image located in the middle.
3. The proposed algorithm for automatic estimation of homography (step 5th) is applied to compute the homography between mosaic images.
4. The positions of the mosaic images in the whole mosaic is calculated, and the pixels information is interpolated for the new positions. This procedure is the same performed for individual images in the previous step (step 5th).
5. The new positions of the images centers are computed by using the estimated homographies. Georeferencing requires the calculation of the new position of the images centers.

2.7 Georeferencing

In order to proceed with the georeferencing of the final mosaic, the position of the images centers as well as the UTM coordinates are required. The following steps detail this procedure:

1. The orientation of the Y-axis of the image is inverted to make possible align the image axes with the UTM coordinates axes through a rotation. Given the number of rows in the image M and the coordinates in Y-axis y , the new coordinates in the inverted Y-axis y' are calculated by (16).

$$y' = M + 1 - y \quad (16)$$

2. The angle between the image axes and the UTM coordinates axes α_{rot} , shown in Figure 9, is computed. Given the intrinsic coordinates (image coordinates) of the images centers belonging to the first two images in the projection order (Step 4th) of the central line (xc_1, yc'_1) , and (xc_2, yc'_2) , and the UTM coordinates of the same images $(xutm_1, yutm_1)$ and $(xutm_2, yutm_2)$; the angle between the line that connect the centers of these two images and the X-axis of the image α_{pix} is calculated using (17). Besides, the angle between the line that connect the centers of these two images and the X-axis of UTM coordinate system α_{UTM} is computed using (18). The angle α_{rot} is computed using (19).

$$\alpha_{pix} = \arctan\left(\frac{yc'_2 - yc'_1}{xc_2 - xc_1}\right) \quad (17)$$

$$\alpha_{UTM} = \arctan\left(\frac{yutm_2 - yutm'_1}{xutm_2 - xutm_1}\right) \quad (18)$$

$$\alpha_{rot} = \alpha_{pix} - \alpha_{UTM} \quad (19)$$

3. The image of the final mosaic is rotated $-\alpha_{rot}$ in the clockwise direction to align the axes of the image and the axes of the UTM coordinates.
4. After rotating the final mosaic image, the intrinsic coordinates of images centers will vary. Because of this, it is required to calculate these new rotated coordinates from the distances between centers of individual images and the center of the final mosaic, the rotated coordinates of the center of the final mosaic, and the rotated angle.
5. Linear regression is performed from the rotated coordinates of images centers and the UTM coordinates of the centers. Given the coordinates of images centers (xc, yc') , the UTM coordinates of the centers $(xutm, yutm)$ can be expressed based on the coefficients of the linear regression a_1, a_2, a_3, a_4, a_5 and a_6 according to (20) and (21).

$$xutm = a_1xc + a_2yc' + a_3 \tag{20}$$

$$yutm = a_4xc + a_5yc' + a_6 \tag{21}$$

6. The UTM coordinates of the four corners of the image are computed from (20), (21) and the coefficients a_1, a_2, a_3, a_4, a_5 and a_6 .

Structure from Motion to generate 3D points and then orthorectified the mosaic as explained in [18]. We compared the processing time and the geolocation errors obtained in the same computer: HP Z820 Workstation with two processors Intel Xeon E5-2690 2.9GHz and 96 GB RAM. It is important to mention that the software Pix4DMapper Pro also processed the images resized to a quarter of the original size.

The processing time required to obtained each mosaic image is shown in Table 1. Pix4DMapper Pro performs a preprocessing step to calibrate images and it uses just the calibrated images for the image mosaicking; therefore, the processing time for this process is not included in our analysis.

Table 1: Processing Time

Flight	Number of images	Pix4DMapper Pro	Proposed Method
1	73	10 min 29 s	10 min 36 s
2	145	24 min 44 s	21 min 37.2 s
3	148	24 min 20 s	24 min 15 s
4	168	30 min 06 s	23 min 18 s
5	168	28 min 46 s	27 min 13.5 s
6	138	20 min 46 s	27 min 46 s

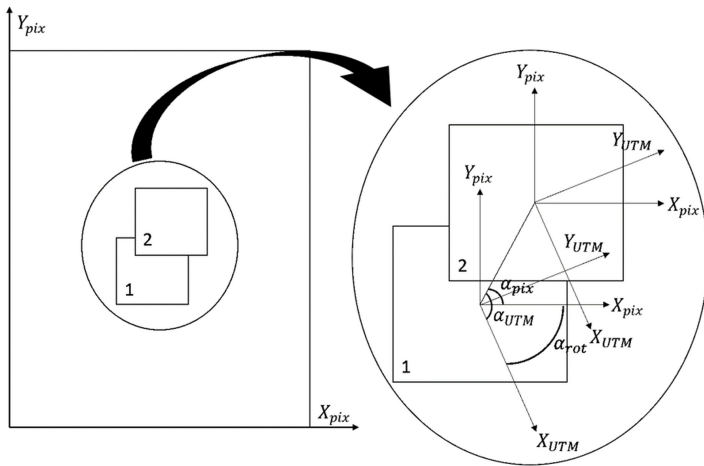


Figure 9: Angle between the image axes and the axes of the UTM coordinates.

3 Results and Discussion

We describe the results of applying the proposed method over 6 sets of images acquired in 6 different flights regarding two scenarios: a city and a forest in Peruvian Amazon. These images were acquired with the professional camera Sony NEX-7, which allows taking images of 24.3MP, at a height of 100 meters from the ground. Each image possesses a spatial resolution of 6000x4000 pixels; but their sizes are reduced to a quarter of the original size during the processing, as it was explained in the first step of the proposed method.

The proposed method was implemented in MATLAB R2016a, and for validation purposes, we utilized the professional software Pix4DMapper Pro version 3.2.10, whose algorithm is based on

In addition, the geolocation errors corresponding to the UTM X-axis and the UTM Y-axis have been computed. From those errors, we calculate the mean absolute error (MAE) and the root mean square error (RMS) which are shown in Table 2.

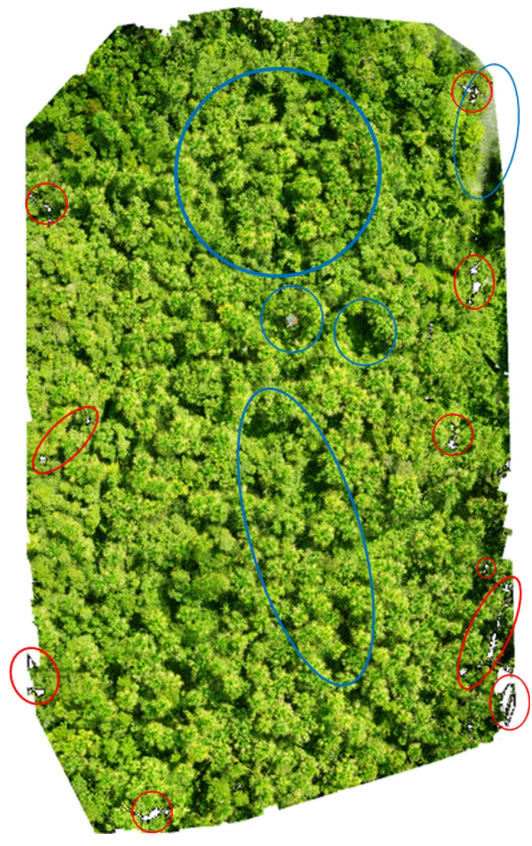
Table 2: Geolocation Errors

Flight	Axes	Pix4DMapper Pro		Proposed Method	
		MAE (m)	RMS (m)	MAE (m)	RMS (m)
1	X	0.9341	1.5209	1.2280	1.5942
	Y	3.7711	4.8955	3.4296	4.0248
2	X	1.9233	2.3048	2.5927	3.1386
	Y	4.3136	5.4267	4.0290	4.5155
3	X	2.2737	2.6818	3.4259	3.6941
	Y	4.6558	5.7388	8.1738	9.1930
4	X	4.2449	4.9988	3.9255	4.4720
	Y	3.7049	4.3406	3.1868	3.7808
5	X	3.6335	4.3212	4.4445	4.9658
	Y	3.8871	4.6748	2.8436	3.2852
6	X	0.8314	1.3360	1.7022	2.0033
	Y	4.6199	5.6286	3.7153	4.1984

From Table 1, we can observe that for flights 2, 3, 4 and 5 (corresponding to a forest in Peruvian Amazon), the proposed method was 6 minutes and 48 seconds faster in the best case, and just 5 seconds faster in the worst case. On the other side, for the flights 1 and 6, Pix4DMapper Pro was 7 minutes faster in the best case, and just 7 seconds faster in the worst case.



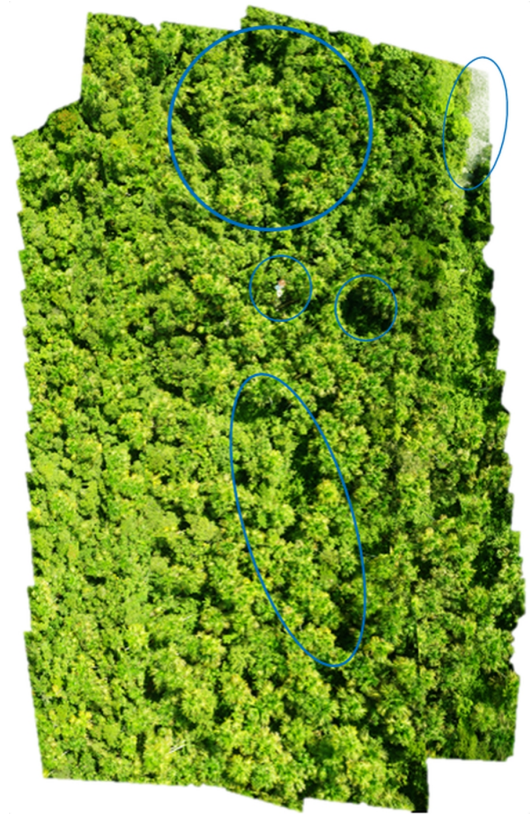
(a)



(a)



(b)



(b)

Figure 10: Image mosaics obtained for the flight 1: (a) Pix4DMapper Pro (b) Proposed Method.

Figure 11: Image mosaics obtained for the flight 6: (a) Pix4DMapper Pro (b) Proposed Method.

Regarding the MAE and RMS geolocation errors of the flights 1, 2, 5 and 6, the geolocation errors (both MAE and RMS) in X-axis computed with the proposed method were greater than those obtained by Pix4DMapper Pro; while, the geolocation errors in Y-axis computed with the proposed method were less than those obtained by Pix4DMapper Pro.

In the case of flight 3, MAE and RMS in both axes computed with our method were greater than those computed with Pix4DMapper Pro; but in flight 4, MAE and RMS in both axes computed with our method were less than those computed with Pix4DMapper Pro. For the majority of flights, the difference of both geolocation errors are low.

We observe that the geolocation errors computed with both methods in the Y-axis are always greater than the computed in the X-axis because of the employed GPS has that horizontal error distribution for all its measurements.

The highest differences in processing time and geolocation errors observed in Table 1 and Table 2 are because the inliers and the estimated homography for the same pair of images may produce different errors and different processing time. These differences are typical of the homography estimation step.

In Figure 10 and Figure 11, we compared the mosaic images obtained with Pix4DMapper Pro and our method for the flight 1 and 6 respectively. In the mosaic image of flight 1, regarding to a city, we can observe more clearly the differences between image mosaics. The image mosaic obtained by Pix4DMapper Pro presents some small holes in the boundaries of the image (indicated with red circles and ellipses). Besides, some trimmed edges and other differences caused by the enhancement of interpolated pixels information performed by Pix4DMapper Pro are encircled by blue ellipses. The mosaic image obtained with our method does not present holes and trimmed edges. For flight 6, the differences are not so clear as those of Figure 10 because it is difficult to see these differences in a scenario like a forest. Visible differences in Figure 11 are shown in the same way that was done for Figure 10.

4 Conclusions

The proposed method requires images acquired when the camera points the nadir, so an stabilization system or gimbal should be used. In this way, a mosaicking algorithm without any preprocessing (like the one performed in the algorithm of Pix4DMapper Pro) can be utilized to obtain good results. Otherwise, a more complicated algorithm should be used to perform the estimation of position and orientation of the cameras.

Finally, our mosaicking algorithm based on a simple process results being viable and reproducible to perform image mosaicking of aerial images for applications of natural resources monitoring because it obtains similar geolocation errors and processing time in comparison with a professional software based in Structure from Motion; moreover, our results do not present any holes or color incoherencies.

Conflict of Interest The authors declare no conflict of interest.

Acknowledgment We thank the National Innovation Program for Competitiveness and Productivity, Innóvate Perú, for the funds allocated to our project (393-PNICP-PIAP-2014).

References

- [1] A. Chaves, P. Cugnasca, J. Jose "Adaptive search control applied to Search and Rescue operations using Unmanned Aerial Vehicles (UAVs)" *IEEE Latin America Transactions*, **12**(7), 1278–1283, 2014. <https://doi.org/10.1109/TLA.2014.6948863>
- [2] J. Everaerts, "The use of Unmanned Aerial Vehicle (UAVS) for remote sensing and mapping" in 2008 XXI ISPRS Congress Technical Commission I: The International Archives of the Photogrammetry, Remote Sensing and Spatial Information Sciences. Vol. XXXVII Part B1, Beijing, China, 2008.
- [3] Z. Li, V. Isler, "Large Scale Image Mosaic Construction for Agricultural Applications" *IEEE Robotics and Automation Letters*, **1**(1), 295–302, 2016. <https://doi.org/10.1109/LRA.2016.2519946>
- [4] A. Iketani, T. Sato, S. Ikeda, M. Kanbara, N. Nakajima, N. Yokoya "Video mosaicing based on structure from motion for distortion-free document digitization" in 2007 Computer Vision ACCV 2007. Lecture Notes in Computer Science. Vol. 4844, Tokyo, Japan, 2007. https://doi.org/10.1007/978-3-540-76390-1_8
- [5] Y. Yang, G. Sun, D. Zhao, B. Peng "A Real Time Mosaic Method for Remote Sensing Video Images from UAV" *Journal of Signal and Information Processing*, **4**(3), 168–172, 2013. <https://doi.org/10.4236/JSIP.2013.43B030>
- [6] T. Botterill, S. Mills, R. Green "Real-time aerial image mosaicing" in 2010 25th International Conference of Image and Vision Computing New Zealand, Queenstown, New Zealand, 2010. <https://doi.org/10.1009/IVCNZ.2016.6148850>
- [7] E. Garcia-Fidalgo, A. Ortiz, F. Bonnin-Pascual, J. Company "Fast image mosaicing using incremental bags of binary words" in 2016 IEEE International Conference on Robotics and Automation (ICRA), Stockholm, Sweden, 2016. <https://doi.org/10.1109/ICRA.2016.7487247>
- [8] D. Brito, C. Nunes, F. Padua, A. Lacerda "Evaluation of Interest Point Matching Methods for Projective Reconstruction of 3D Scenes" *IEEE Latin America Transactions*, **14**(3), 1393–1400, 2016. <https://doi.org/10.1109/TLA.2016.7459626>
- [9] T. Kekcec, A. Yildirim, M. Unel "A new approach to real-time mosaicing of aerial images" *Robotics and Autonomous Systems*, **62**(12), 1755–1767, 2014. <https://doi.org/10.1016/j.robot.2014.07.010>
- [10] Y. Xu, J. Ou, H. He, X. Zhang, J. Mills "Mosaicing of Unmanned Aerial Vehicle Imagery in the Absence of Camera Poses" *Remote Sensing*, **8**(3), 204–219, 2016. <https://doi.org/10.3390/RS8030204>
- [11] A. Moussa, N. El-Sheimy, "A fast approach for stitching of aerial images" in 2016 XXIII ISPRS Congress, Commission III: The International Archives of the Photogrammetry, Remote Sensing and Spatial Information Sciences. Vol. XLI Part B3, Prague, Czech Republic, 2016. <https://doi.org/10.5194/isprsarchives-XLI-B3-769-2016>
- [12] D. Lowe "Distinctive image features from scale-invariant keypoints" *International Journal of Computer Vision*, **60**(2), 91–110, 2004. <https://doi.org/10.1023/B:VISI.0000029664.99615.94>
- [13] A. Vedaldi, B. Fulkerson "VLFeat: An open and portable library of computer vision algorithms" in Proc. 18th International Conference on Multimedia, Firenze, Italy, 2010. <https://doi.org/10.1145/1873951.1874249>
- [14] D. Del Castillo, E. Otárola, L. Freitas, Aguaje: the amazing palm tree of the Amazon, IIAP, Iquitos, Peru, 2006.
- [15] L. Freitas, M. Pinedo, C. Linares, D. Del Castillo, Descriptores para el Aguaje (*Mauritia flexuosa* L. f.), IIAP, Iquitos, Peru, 2006.
- [16] J. Levistre, J. Ruiz "El Aguajal: El bosque de la vida en la Amazonía Peruana" *Ciencia Amazónica (Iquitos)*, **1**(1), 31–40, 2011. <https://doi.org/10.22386/ca.v1i1.6>
- [17] R. Hartley, A. Zisserman, Multiple view geometry in computer vision, 2th edition, Cambridge University Press, 2003.
- [18] O. Küng, C. Strelca, A. Beyeler, J. Zufferey, D. Floreano, P. Fua, F. Gervais, "The accuracy of automatic photogrammetric techniques on ultra-light UAV imagery" in International Conference on Unmanned Aerial Vehicle in Geomatics (UAV-g): The International Archives of the Photogrammetry, Remote Sensing and Spatial Information Sciences. Vol. XXXVIII Part C22, Zurich, Switzerland, 2011. <https://doi.org/10.5194/isprsarchives-XXXVIII-1-C22-125-2011>

Study of $M^X/M/1$ Queueing System with Vacation, Two kinds of Repair facilities and Server Timeout

Naga Rama Devi Vedala^{1,*}, Yadla Saritha², Ankam Ankamma Rao², Gaddam Sridhar²

¹Department of Mathematics, GRIET, Hyderabad, Telanagana, 500049, India

²Department of Statistics, Acharya Nagarjuna University, Guntur, Andhra Pradesh, 522508, India

ARTICLE INFO

Article history:

Received: 18 June, 2019

Accepted: 16 November, 2019

Online: 16 December, 2019

Keywords:

Vacation queueing system

Two types of repair facilities

Server timeout

ABSTRACT

The present paper details a queueing model with two kinds of repair facilities and server timeout. Here the customer arrives in compound Poisson process into the system and the lifetime of the server follows exponential distribution. At the point when the system is vacant, the server waits for customers for a settled time 'c'. If nobody enters into the system amid this time, the server takes vacation otherwise the server commences the service to the arrived customers exhaustively. If the server fails, repair process will be initiated immediately. Here broken-down server is facilitated with two kinds of repair facilities. Type -I repair is done if the customer service is interrupted due to server failure and the customer stays back in the system with a probability of $1-q$ to receive the remaining service whereas Type-II repair is initiated if the customer whose service is interrupted due to server failure quits the service zone and joins head of the queue with a probability of q . Explicit expressions are derived for various constants of queueing System and also numerical results are illustrated with various batch size distributions.

1. Introduction

Queueing models are used to evaluate operational attributes of the service facility: service times, waiting times, number of customers including impatient customers in the system and more. Quite often, the service process includes delays.

The waiting time for service is one of the most key attributes of service process. Customer surveys in service systems demonstrate that holding up time is a key factor while assessing quality of service. Long waits may lead to feelings of anger and low customer satisfaction. Obviously, a balance must be brought between the number of servers that provide service and the factors like waiting times, cost etc.

In queues the situation where a server is unavailable for primary clients in occasional intervals of time is known as vacation. Queues with server vacations have been studied over long period and also being adapted in many areas such as manufacturing, computer communication network models. In vacation queueing model the server completely stops service when it is on vacation. Queueing system with server vacations has pulled in the consideration of numerous analysts.

*Corresponding author: Naga Rama Devi Vedala, Department of Mathematics, GRIET, Hyderabad, ramadevivr@gmail.com

The subject of queueing systems with server failures is a prominent subject which has gained lot of attention of many researchers in the last five decades. In many realistic situations, the server may face unforeseen failures. For example, in manufacturing systems the machine may suddenly fail which leads a span of unavailable time until it is restored. Understanding the nature of the unreliable server in terms of unforeseen failures is vital as it influence system's efficiency in terms of average Queue length and the customers' mean waiting time. Hence, queueing problems with server breakdowns are more realistic phenomena. Single server queue subjected to breakdown and repair has been studied by number of authors.

Optimum utilization of server is vital for any system to run optimally. In this context we have explained the Vacation with the concept of Timeout and Server Breakdown with two types of repair facilities for an $M^X/M/1$ queueing model and also derived expected system length. Further, numerical solutions for various parameters by using batch size distributions are also illustrated. did by the author [1] did numerous excellent surveys on the vacation concept and explained different kinds of vacation models. The paper [2] explained an $M/G/1$ Queueing System with interruption service and connection with the priority model. The paper [3] discusses queueing model with different types of server interruptions and also obtained the performance measures of the

queue and customer delay. The authors [4] presented Vacation bulk queueing Model with setup time and server timeout and derived the average waiting time of this system. The author [5] has proved that the M/G/1 retrial queueing system with server breakdowns has a unique non negative transient solution and also studied asymptotic behavior of it. was explained by The authors [6] explained a short survey on vacation models and also intends to provide a brief compact of the most recent trends in queueing systems with vacation in the previous 10 years. The paper [7] detailed M/G/1 type queue with Time-Homogeneous Breakdowns and Deterministic Repair times by using supplementary variable technique, The author [8] studied an M/G/1 queue in steady state with optional deterministic server vacation also designate the system as M/G/D/1 queueing system. The authors [9] were first studied vacation .They have shown the utilization of idle time of M/G/1 queue.

When the system is empty, the server will wait for settled time is known as server timeout; The paper [10] discussed the M/G/1 queue with vacation and timeout and elaborated the Average waiting time of the system and also developed for N-policy. The paper [11] detailed the analysis of optimization in single server queueing system with vacation and elicited the mean waiting time for single queue and also formulated for N-policy. The authors [12] studied M/M/1 Queue with vacation, server breakdown, Heterogeneous arrival as well as departure and also derived various constants of both system and queue in both un-operating modes i.e.; either empty or server breakdown.

The authors [13] explained an M^x/G/1 Vacation queueing model with Server Timeout and calculated expected system length for varying different bulk size distributions. The paper[14] detailed derivation of Queueing constants for an M/G/1 Vacation Queueing model with server breakdown, repair and Timeout. The authors [15] studied Optimal Strategy Analysis of N-Policy M/Ek/1 Vacation Queueing System with Server Start-Up and Time-Out and derived explicit expressions for the system length .

2. Model Description

Consider single server queue where arrival rates are of compound Poisson process with mean rate ‘λ’. The server commences service in FIFO discipline. Whenever the system becomes empty the server waits for certain time ‘c’, which is called server timeout. At this time if a customer arrive the server return to the system and do service. At the end of this timeout period if no customer arrive the server takes vacation. Service may be interrupted due to Server breakdowns. Here we consider two kinds of repair facilities. Type-I repair is done if the customer’s service is interrupted due to server failure and the customer stays back in the system with a probability of 1-q to receive the remaining service whereas Type-II repair is initiated if the customer whose service is interrupted due to server failure quits the service zone and joins head of the queue with a probability of q. Service is restored immediately upon the repair of server.

3. Analysis of the Model

The customer arrivals are assumed under Poisson process with parameter ‘λ’. The service rate is μ s per exponential law. The service time for a customer ‘X’ assumed to be General with cumulative distribution function $F_X(x)$ having mean E(x) and its

second moment E(X²). The Laplace stieltjes transform function of X is $M_X(s)$, which is taken as

$$M_X(s) = E(e^{-sX}) = \int_0^\infty e^{-sx} f_X(x) dx \quad (1)$$

‘V’ is the duration of a vacation assumed to follow general distribution with CDF $F_V(v)$ and Laplace stieltjes transform function of V is $M_V(s)$. The average value of V is E (V) and its second moment E (V²).

$$M_V(s) = \frac{\gamma}{s+\gamma} \quad (2)$$

X and V are independent variables.

The system may break down with a rate **a**, then system go for deterministic repair with rate **d**. After repair process completed then server start service to the customer.

Let $G_{L(M/G/1)}(z)$ is PGF the number in system is given by [Ref 8]

$$G_{L(M^x/M/1)}(z) = \frac{(1-\rho)(z-1)\mu(\beta+W_x(z))}{(\beta+W_x(z))[(z-1)\mu+zh_\alpha(W_x(z))]-z\alpha q\beta} \quad (3)$$

Let the number of customers in the system at the beginning of busy period is indicated as A. The probability distribution function of this variable A is $P_A(a) = P[A=a]$, and corresponding z-transformation $G_A(z)$ is given by

$$G_A(z) = E(Z^A) = \sum_{a=1}^\infty Z^a P_A(a) \quad (4)$$

Let B denotes the number of customers left by an arbitrary departing customer. The Probability distribution of B is $P_B(b)$ with the corresponding z-transform $G_B(z)$ as

$$G_B(Z) = \frac{1-G_A(z)}{(1-z)E(A)} \quad (5)$$

Let L be the number of customers in the system at an arbitrary point of time. The distribution of L is $P_L(l)$ and corresponding Z-transform is given by

$$G_L(z) = G_B(z) G_{L(M^x/M/1)}(z) \quad (6)$$

E (L) and E (L²) are the mean and second moments of L.

Specific batch size distributions

As the batch size ‘d’ may also varies and hence assumed as a random variable. In particular Deterministic, Geometric and Positive Poisson distributions are considered for it.

1.) If the batch size distribution is Deterministic, then the generating function equals to

$$D(z) = z^d$$

This gives mean $\bar{D} = D'(Z) = d$ and second moment $\bar{D}'' = D''(Z) = d^2 - d$, where d is the average batch size.

2.) The batch size distribution is Positive Poisson, then the generating function equals to

$$D(Z) = \frac{me^{-\alpha}(e^{\alpha z}-1)}{\alpha}, \text{ where } m = \frac{\alpha}{1-e^{-\alpha}}$$

This gives mean $\bar{D} = D'(Z) = m$ and second momen $\bar{D}'' = D''(Z) = \frac{\alpha^2}{1-e^{-\alpha}}$, where m is the average batch size.

3.) If the batch size distribution is Geometric, then the generating function equals

$$D(z) = p [z^{-1} - (1-p)]^{-1}$$

This gives mean $\bar{D} = \bar{a} = \frac{1}{p}$ and second moment $\bar{D}^2 = \bar{a}^2 = \frac{2(1-p)}{p^2}$

, where \bar{a} is the average batch size.

Let W_q denotes the waiting time in the system to determine system length. We get the mean of system length of the customer by using little's law as [Ref 9]

$$E(W_q) = \frac{1}{\lambda} * \left. \frac{dG_L(z)}{dz} \right|_{z=1} - E(X) \tag{7}$$

$$E(W_q) - E(X) = \frac{1}{\lambda} * \left. \frac{dG_L(z)}{dz} \right|_{z=1}$$

$$\lambda (E(W_q) - E(X)) = \left. \frac{dG_L(z)}{dz} \right|_{z=1} = E(L) \tag{7(a)}$$

We can obtain E(L) iff we know $G_A(z)$.

$$G_A(z) = ZP_2 + \frac{M_V(\lambda - \lambda Z) - M_V(\lambda)}{1 - M_V(\lambda)} P_3 \tag{8}$$

Where $P_2 = \frac{M_V(\lambda)(1 - e^{-\lambda c})}{1 - e^{-\lambda c} M_V(\lambda)}$ and

$$P_3 = \frac{(1 - M_V(\lambda))}{1 - e^{-\lambda c} M_V(\lambda)}$$

From this we get

$$E(A) = \frac{\gamma^2(1 - e^{-\lambda c}) - \lambda(\lambda + \gamma)}{((\lambda + \gamma) - e^{-\lambda c} \gamma)} \tag{9}$$

and

$$E(A^2) = \frac{2\lambda^2(\lambda + \gamma)}{((\lambda + \gamma) - e^{-\lambda c} \gamma)^2} \tag{10}$$

By assuming equation (2), we can derive

$$M_V(S) = \frac{\gamma}{s + \gamma} \Rightarrow M_V(\lambda) = \frac{\gamma}{\lambda + \gamma} \tag{11}$$

By substituting equation (3), (5) in equation (6), we get

$$G_L(z) = \frac{1 - G_A(z)}{(1 - z)E(A)} * \frac{(1 - \rho)(z - 1)\mu(\beta + W_x(z))}{(\beta + W_x(z))[(z - 1)\mu + zh_\alpha(W_x(z))] - z\alpha q\beta} \tag{12}$$

$$G_L(z) = \frac{1 - G_A(z)}{E(A)} * \frac{(1 - \rho)\mu(\beta + W_x(z))}{z\alpha q\beta - (\beta + W_x(z))[(z - 1)\mu + zh_\alpha(W_x(z))]} \tag{13}$$

Put $k = \frac{(1 - \rho)}{E(A)}$ in the above equation (13), we get

$$G_L(z) = \frac{(1 - G_A(z))\mu(\beta + W_x(z))}{z\alpha q\beta - (\beta + W_x(z))[(z - 1)\mu + zh_\alpha(W_x(z))]} \tag{14}$$

By differentiating the above equation (14) w.r.to z, we get

$$G_L'(z) = \frac{k.E(A)\alpha(\alpha + 1)M_x(\alpha)}{\alpha M_x(\alpha) - (1 - M_x(\alpha))(\lambda + \lambda\alpha d)} \tag{15}$$

Now substituting K value and put z=1 in equation (14) we get

$$G_L(1) = 1 \tag{16}$$

Again differentiating the above expression 14 w.r.to z we get

$$G_L'(1) = \frac{1}{2(\mu - \lambda(1 + \alpha d))} ((p_1 G_A''(1)(1 + \alpha)) + 2p_1 G_A'(1)\alpha + 2\lambda(1 + \alpha d) + \alpha(\lambda d)^2) \tag{17}$$

Now substituting equations (9), (10) and k value in above equation (17) we get

$$G_L'(1) = (1 - \rho)/E(A) (\{(\mu\alpha + \alpha^2)\mu(\beta + \lambda - \lambda X(1))\} + \{(\mu\alpha + \alpha^2)\alpha\beta q - (\alpha + \mu)(\alpha + \lambda - \lambda X(1))\} + \{\mu(\beta + \lambda - \lambda X(1))\}) / (\{\alpha(\beta q - \beta + \lambda - \lambda X(1)) - \beta(\lambda - \lambda X(1)) + \lambda^2(1 - 2X(1) - (X(1))^2)\} \tag{18}$$

Thus by above expression, we obtain expected system length.

Particular case: If system suffers no breakdowns and repairs facilities then letting $\beta=0, d=0, q=0$ and $\alpha=0$ in the above expression (in equation 18) then the resulting expression is a known for the M/G/1 vacation queuing model with server timeout(Ref (12)).

4. Numerical Illustrations

Thus by using equation (18) and varying different parameters, we get some numerical illustration in Table 1 is given below:

Table 1: Effect of Different Variables (d, λ, μ, c, α, q and γ) on expected system length for fixed values of d=2, λ=2, μ=50, c=1, α=4 and γ=0.25.

Parameter	Parameter Values	Deterministic Distribution of E(L)	Geometric Distribution of E(L)	Positive Distribution of E(L)
D	2	6.5515	6.8621	8.0512
	3	10.7012	9.8528	11.7669
	4	14.2671	10.6947	16.0318
	5	20.4660	11.9441	21.4815
	6	26.5421	23.8526	27.7996
λ	2	6.5515	6.8621	8.0512
	6	9.3980	9.7938	11.6209
	10	10.5412	11.9592	14.2696
	14	12.4641	13.4027	17.6098
	18	13.0614	15.6601	24.6651
μ	50	6.5515	6.8621	8.0512
	60	6.5345	6.8364	8.0277
	70	6.5205	5.8154	7.9902
	80	6.5088	5.7979	7.9613
	90	6.4989	5.7830	7.9479
C	1	6.5515	6.8621	8.0512
	2	6.5495	6.8582	8.0473
	3	6.5489	6.8571	8.0432
	4	6.5445	6.8494	8.0383
	5	6.5421	6.8475	8.0364
γ	0.25	6.5515	6.8621	8.0512
	0.75	3.3932	4.6704	5.0478
	1.5	1.2247	2.4775	3.6639
	2	0.9712	1.2177	1.3564
	2.5	0.8304	1.0865	1.0621
α	4	6.5515	6.8621	8.0512
	6	7.3980	8.3628	10.3239
	8	9.4412	11.2947	14.2496
	10	11.4641	11.8441	18.6098
	12	14.0614	23.8526	24.6651

As d , λ , and α were increasing then expected system length $E(L)$ is also increasing.

As μ , γ and c are increasing then expected system length $E(L)$ is decreasing.

5. Conclusion

In this model, we have derived an expression of expected system length for $M^X/M/1$ vacation queueing model with two varieties of repair facilities and server timeout. Sensitivity analysis is carried out on the system length.

Conflict of Interest

The authors declare no conflict of interest.

Acknowledgment

Uide Dr. Kotagiri Chandan and affiliated institutes for their continuous support

References

- [1] Doshi, B.T (1986), Queueing system with vacations. A survey on queueing system: Theory and Applications. 1(1), 29-66.
- [2] D. Gaver Jr. (1962), A Waiting line with interrupted service, including priorities. Journal of the Royal statistical Society, Vol.B24:73-90.
- [3] Dieter Fiems, Tom Maertens and Herwig Bruneel (2005), Queueing system with different types of service interruptions, SMACS Research Group, Department TELIN (IRO7), {df, tmaerten,hb}@telin.Ugent,Belgium.
- [4] E.Ramesh Kumar and Y. Praby Loit (2016), A Study on Vacation Bulk Queueing Model with setup time and server timeout. IJCMS, 5(12), 81-89.
- [5] Geni Gupur, (2010), Analysis of the M/G/1 retrial Queueing Model with server breakdowns. Oper. 1:313-340.
- [6] Jau-Chuan Ke, Chia-Huang Wu and Zhe George Zhang, (2010), Recent Developments in Vacation Queueing Models: A Short Survey. Operation Research Vol 7, No 4.3-8.
- [7] K.C. Madan, (2003), An M/G/1 type queue with Time-Homogeneous Breakdowns and Deterministic Repair Times, Soochow Journal of Mathematics Volume 29, No. 1, pp. 103-110, January 2003.
- [8] K.C. Madan, (1999), On a M/G/1 Queue with Optional deterministic Server vacations, MENTRON, LVII, 3-1, 83-95.
- [9] Levy.Y and Yechiali. U, (1975), Utilization of Idle Time in an M/G/1 QueueingSystem.ManagementScience,22,202-211.
<http://dx.doi.org/10.1287/mnsc.22.2.202>.
- [10] Oliver C. Ibe (2007) Analysis and optimization of M/G/1 Vacation Queueing Systems with Server Timeout, Electronic Modeling, V.29, no. 4, ISSN 0204-3572.
- [11] Oliver C. Ibe (2015), M/G/1 Vacation Queueing Systems with Server Timeout, American Journal, 5, 77-88, <http://www.scrip.org/journal/ajor>.
- [12] R.P.Ghimire and Sushil Ghimire, (2011), Heterogeneous Arrival and Departure M/M/1 Queue with vacation and service Breakdown. Management Sciences and Engineering, Vol. 5, No. 3, pp. 61-67.
- [13] Y.Saritha, K.Satish Kumar and K.Chandan (2017), M^s/G/1 Vacation Queueing System with Server Timeout.International Journal of Statistics and Applied Mathematics, 2(5): 131-135.
- [14] Y.Saritha, K.Satish Kumar,V.N.Rama Devi and K.Chandan (2018), M/G/1 Vacation Queueing System with breakdown, repair and Server Timeout. Journal of emerging Technologies and innovative Research(JETIR), Volume 5, issue 2 2349-5162.
- [15] K.Satish Kumar, K.Chandan and Y.Saritha. (2018), Optimal Strategy Analysis of N-Policy M/Ek/1 Vacation Queueing System with Server Start-Up and Time-Out.JETIR, Vol 5, Issue 10, 380-385

Multi-Stage Enhancement Approach for Image Dehazing

Madallah Alruwaili*

College of Computer and Information Sciences, Department of Computer Engineering and Networks, Jouf University, 42421, KSA

ARTICLE INFO

Article history:

Received: 06 September, 2019

Accepted: 01 December, 2019

Online: 16 December, 2019

Keywords:

Haze images

Wiener filter

Image restoration

Image enhancement

ABSTRACT

Over the past decades, huge efforts have been devoted for image enhancement under uncontrolled scene such as fog and haze. This work proposes Multi-stage de-hazing approach for improving the quality of hazy images. Four main stages are introduced, in our approach, to achieve an automated, efficient and robust de-hazy processing. The first two stages are utilized to diminish the blurring noise and enhance the contrast using Wiener filter and contrast scattering in the RGB color, respectively. In contrast, the last two stages are utilized for luminance and quality enhancement using luminance spreading and color correction. It is obvious from the experimental that the proposed approach significantly improves the prominence of the hazy images and outperforms the performance of conventional methods, such as multi-scale fusion and histogram equalization. In addition, it is also found that our approach exhibits low complexity compared to existing works.

1. Introduction

Nowadays, hazy weather appears more and more frequently in different areas of the world as a result of pollution. Under hazy weather conditions, suspended particles in atmosphere for example fog, murk, the mist, dust causes poor visibility image and distorts the colors of the scene. Images taken in such conditions represent a major issue for numerous outdoor applications of vision community including surveillance, object recognition, target tracking, which require high-quality images. Figure 1 shows an example of hazy and de-hazy images taken from [1].

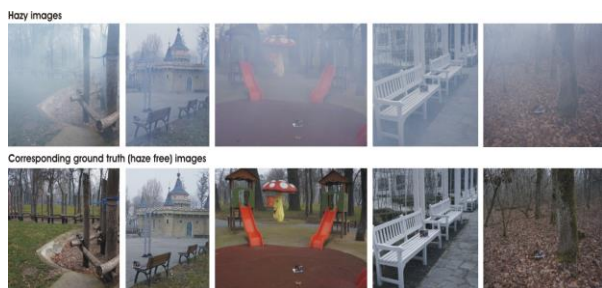


Figure 1: Sample Hazy and De-hazy Images

Images under hazy weather exhibit very poor quality and blurred even in a small dynamic range of color intensities [2]. The main

factors causing hazy images might be represented as the mixture of scene vivacity, air-light and communication [3,4]. The study of haze is related to the works on scattering of light in the atmosphere (see Figure 2). In imaging system, the radiance captured by the camera along the sightline is declined due to atmospheric light and it is replaced by scattered light that leading to lose contrast and colors in captured images.

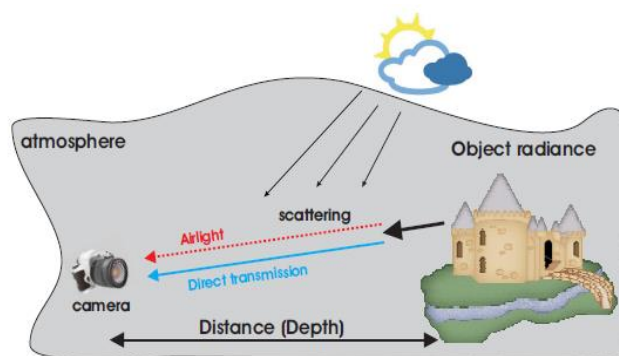


Figure 2: Optical model against diverse weather situations [5].

In general, the following equation has been widely employed to improve the quality of the haze images:

$$IM(x) = F(v)t(v) + L(1 - t(v)) \quad (1)$$

*Madallah Alruwaili, Email: madallah@ju.edu.sa

where F, L and I represent haze image, free scene in the haze image and the atmospheric light, respectively. In contrast, v is denoted as the location of the image component while t is denoted as the intermediate of broadcast to describe the percentage of the bright, which is not dispersed by the camera. The haze reduction aims to recuperate F, L, and t from IM.

2. Literature Review

In the recent years, different types of techniques have been proposed for de-hazing images, which further are classified into two main categories with respect to the amount of images utilized for de-hazing process [6,7]. The first category relies on multiple images taken from a hazy scene with different densities at the same point [8, 9, 10]. This category provided impressive results by assuming the scene depth can be estimated from multiple images. However, this requires specific inputs (fixed scene under different weather condition) making this type of method impractical for real-time applications.

To overcome the need of changed weather conditions [11], polarization based approach has been introduced to simulate changed weather conditions. This simulation is obtained by applying various filters on different images. However, this approach still is not appropriate for real-time applications as the static scenes cannot be considered unless the polarization filter based approaches are utilized.

The second category relies on a single image to achieve haze removal [12–13]. This type of methods is capable effectively to improve both the contrast and the visibility of hazy images. However, it may result in vanishing some detailed information and increasing the computational burden.

He et al. [14] developed a Dark Channel Prior (DCP) method based on the measurements about the haze-free images. The proposed method utilized dark pixels to estimate haze transmission map. These dark pixels are categorized through low intensity worth of as a minimum one-color parameter. Meng et al. [15] proposed an enhancement to dark channel prior through estimating transmission map. The prior map was estimated via enhancing intrinsic edge limit with biased L1 standard relative regularization. In contrast, Zhu et al [16] developed a color attenuation prior (CAP) that defines a undeviating model on local priors which aims to recover depth information. Some other works tried to optimize the dark channel by combining it with other methods. For example, Xie et al (2010) introduced a model that utilizing dark channel and Multi-Scale Retinex [17]. This technique implemented on the luminance element in YCbCr space. Wiener filtering also has been implemented with dark channel prior to have well enhancement [18]

Over the past decades, Retinex theory [19] has been considered a millstone in many image enhancement and de-hazy methods. This theory is basically based on lightness and color constancy and it has several advantages including dynamic range compression, color independence and color and lightness rendition. Therefore, Retinex theory has been extensively employed in image processing

tasks. For example, the center/surround Retinex method has gained a huge interest as it offers low computational cost and no calibration for scenes.

Based on the Retinex theory, this work proposes a novel Multi-stage de-hazing method for improving the superiority of hazy images. In the proposed approach, the first two stages are utilized to diminish the blurring noise and enhance the contrast, while the last two stages are utilized for luminance and quality enhancement. More details about the proposed approach is given in the next part.

3. Proposed Approach

This approach involves four stages to enhance the quality of hazy images. These stages as follows

- i. Wiener filter.
- ii. Contrast scattering
- iii. Luminance spreading
- iv. Color correcting.

The workflow of the proposed approach is described in Figure 3, in which every stage is explained in the next parts.

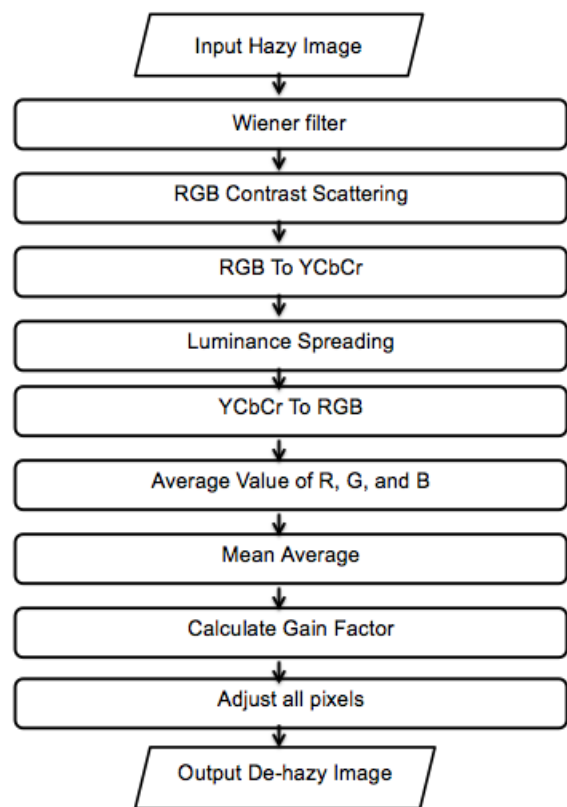


Figure 3: Workflow of the proposed approach.

3.1 Wiener filter

The exciting camera devices still have some problems specifically with images taken form haze environment. Haze environment greatly affects quality of image captured by the camera. As mention above a noise occurs in the captured image. To overcome this problem, the well-known method have been used to reduce blur in images due to linear motion is the Wiener filter. This filter

was proposed by Norbert Wiener during the 1940s and was published in 1949 [20]. It reduces the noise impact in frequency domain. The main goal of this filter is to obtain noisy image \hat{f} of the original image f and reduce mean square error e^2 between the two images [21]. The next formula is used to measure the error where E represents the expected value.

Following three conditions are assumed:

- The images have zero mean, i.e., the images will be noise free.
- Noise and the image are uncorrelated.
- Grey levels in the restored image are linear functions of the gray levels in the noisy image.

Using the above conditions, the best value of the error function in frequency domain is given by next formulas

$$\begin{aligned} \hat{F}(u,v) &= \left[\frac{H^*(u,v)S_f(u,v)}{S_f(u,v)|H(u,v)|^2 + S_\eta(u,v)} \right] G(u,v) \\ &= \left[\frac{H^*(u,v)}{|H(u,v)|^2 + S_\eta(u,v)/S_f(u,v)} \right] G(u,v) \\ &= \left[\frac{1}{|H(u,v)|^2 + S_\eta(u,v)/S_f(u,v)} \right] G(u,v) \end{aligned} \quad (2)$$

where

$H(u,v)$ = Degradation function

$H^*(u,v)$ = complex conjugate of $H(u,v)$ $|H(u,v)|^2 = H^*(u,v)H(u,v)$, $S_h(u,v)$ = Power spectrum of noise, $S_f(u,v)$ = Power spectrum of the un-degraded image.

In haze environment the original image is not typically available. Thus, the power spectrum ratio is substituted by a parameter K that is experimentally determined. Practically, the value of K is chosen to be 0.00025 in order for achieving the best visual result. The following formula is used to decrease noise from hazy images.

$$F^\wedge(u,v) = \left[\frac{1}{|H(u,v)|^2 + K} \right] G(u,v) \quad (3)$$

3.2 Contrast Scattering

In the second stage, the contrast scattering technique is used so as to improve the hazy images contrast. This technique selects smallest and highest values of the each RGB color model. Then, all the color parameter values are scattered among the smallest and highest values, as shown in Figure 4. Next formula is used for contrast scattering:

$$O_o = (O_i - sml) \frac{(\max - \min)}{(\text{lag} - sml)} + \min \quad (4)$$

where O_o is is denoted as the novel pixel value and O_i is denoted as the current pixel value. min , max, sml, and lag represent he minimum, maximum, least, and highest pixel value in each color parameter respectively.

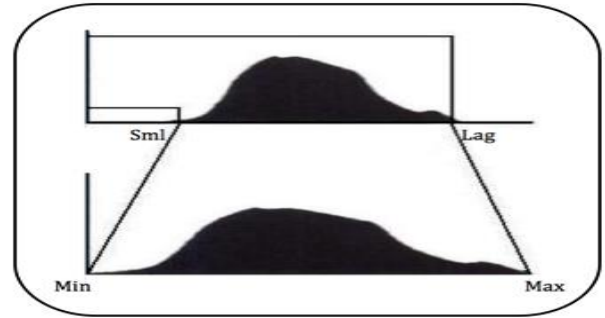


Figure 4: Contrast Scattering

3.3 Luminance Spreading

Subsequently, in order to achieve a true Luminance; an improvement method is applied. The Luminance in YCbCr plays a major role in image quality. The YCbCr color model is used to separate chrominance and luminance, in which, Y denotes the luminance parameter; while, Cb and Cr are respectively the chrominance parameters. On the other hand, RGB color model mutually make luminance. the following formulas are used to convert RGB color model to YCbCr color model:

$$Y = 0.587 * R + 0.114 * B + 0.299 * R \quad (5)$$

$$Cb = -0.299 * R - 0.587 * G + 0.886 * B = B - Y \quad (6)$$

$$Cr = 0.701 * R - 0.587 * G - 0.114 * B = R - Y \quad (7)$$

Consequently, the luminance parameter is adjusted to reach true colors and illumination. The proposed approach spans the luminance toward both directions 0 and 255 as shown in figure 5. The next formula is used for luminance spreading [22].

$$O_o = \frac{(O_i - \min) \times 255}{(\max - \min)} \quad (8)$$

where O_o and O_i are novel and current luminance value correspondingly. min denotes the minimum value, while max denotes the maximum value of luminance. Subsequently, following formulas are used to transfer image from the YCbCr to the RGB color model.

$$R = Cr + Y \quad (9)$$

$$G = Y - 0.194 * Cb - 0.509 * Cr \quad (10)$$

$$B = Cb + Y \quad (11)$$

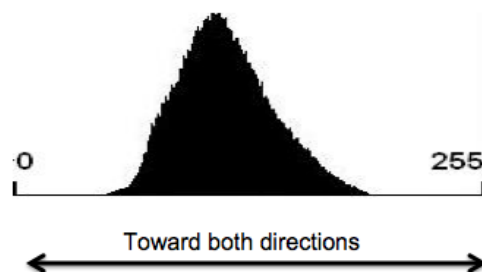


Figure 5: Luminance Spreading

3.4 Color Correcting

Color correcting method plays a major role to produce great quality images, which need balance number for pixels values. In this approach to get true colors, following formulas are used to calculate the average value [23]:

$$R_{avg} = \frac{1}{MN} \sum_{x=1}^M \sum_{y=1}^N I_{Red}(x, y) \quad (12)$$

$$G_{avg} = \frac{1}{MN} \sum_{x=1}^M \sum_{y=1}^N I_{Green}(x, y) \quad (13)$$

$$B_{avg} = \frac{1}{MN} \sum_{x=1}^M \sum_{y=1}^N I_{Blue}(x, y) \quad (14)$$

The proposed approach utilizes the mean average value of all colors. The mean average value is employed to increase the other values due to which the entire color is balanced. Mean value is used to overcome the over-saturation matter and keeps both the illumination and color at same levels [24]. This value is calculated for de-haze image using next formulas:

$$Avg = \frac{Red_{avg} + Green_{avg} + Blue_{avg}}{3} \quad (15)$$

$$Gain = \frac{Avg}{Blue_{avg}} \quad (16)$$

Then a diagonal model [25] is used to adjust all pixels values the image. Following formulas are utilized to recover the superiority of the hazy images.

$$R = Gain \times Red \quad (17)$$

$$G = Gain \times Green \quad (18)$$

$$B = Gain \times Blue \quad (19)$$

where Red, Green, and Blue are the values of the pixels in the hazy images respectively; while, R , G , and B denote the balanced values of the pixels.

4. Experimental Evaluation

The proposed methods were assessed based on detached techniques such as PSNR (peak signal to noise ratio), SSIM (structural similarity index), and RMSE (root mean square error). RMSE is well known method used for result evaluation. RMSE is an accumulative aligned fault among de-hazy image and a free haze image by using next formula:

$$RMSE = \sqrt{\frac{1}{IJ} \sum_{x=1}^I \sum_{y=1}^J [F(x, y) - H(x, y)]^2} \quad (20)$$

when RMSE is very small and close to zero that means a high quality de-haze image.

The second approach is PSNR. In order to get an excellent quality of de-haze image, the value of PSNR should be high. However, to find MSE among the new and de-haze images respectively.

Furthermore, we need to find the MSE between free haze and de-haze images in order to calculate PSNR. Next formulas were used to find MSE and PSNR

$$MSE = \frac{1}{IJ} \sum_{x=1}^I \sum_{y=1}^J [F(x, y) - H(x, y)]^2 \quad (21)$$

$$PSNR = 10 * \log_{10} \left(\frac{255^2}{MSE} \right) \quad (22)$$

The third approach is the SSIM (structural similarity index). SSIM measures the visual impact of brightness, dissimilarity and construction. The value of SSIM is among [0, 1] when free haze and de-haze images are almost identical; the SSIM is close to 1.

$$SSIM(z, v) = [L(z, v)]^\alpha \cdot [T(z, v)]^\beta \cdot [s(z, v)]^\gamma \quad (23)$$

where α , β and γ are factors to adjust the relative importance of the components[26]. Next formulas were used to compute SSIM

$$L(z, v) = \frac{2\mu_z\mu_v + T_1}{\mu_z^2 + \mu_v^2 + T_1} \quad (24)$$

$$T(z, v) = \frac{2\sigma_z\sigma_v + T_2}{\sigma_z^2 + \sigma_v^2 + T_2} \quad (25)$$

$$s(z, v) = \frac{\sigma_{zv} + T_3}{\sigma_z\sigma_v + T_3} \quad (26)$$

$$SSIM(z, v) = \frac{(2\mu_z\mu_v + T_1)(2\sigma_z\sigma_v + T_2)}{(\mu_z^2 + \mu_v^2 + T_1)(\sigma_z^2 + \sigma_v^2 + T_2)} \quad (27)$$

where μ_z , μ_v , σ_z , σ_v , and σ_{zv} are the mean, standard deviation, and covariance for images z , v . $T_1 = (0.01 * L)^2$, where L is 255.

$$T_2 = (0.03 * L)^2 \quad (28)$$

$$T_3 = T_2/2 \quad (29)$$

5. Experimental Setup

In this work, we employed two kinds of open-source datasets namely I-Haze [2], and generalized dataset for validating the proposed approach performance. All the datasets are explained below.

5.1 Used Datasets

In this study, we utilized two datasets to show the efficacy of the proposed approach. These datasets are defined as below.

Generalized Dataset: Hazy images were downloaded from different free websites such as personal web pages. The collected images served as inputs to the program and process in order to produce the enhanced images. The generalized dataset consisted of total of 50 images with different haze effect.

I-Haze Dataset: C. O. Ancuti et al have proposed I-Haze dataset, which includes 35 of hazy and conforming interior images of haze-free. Haze images have been produced under the same illumination conditions includes a MacBeth color checker.

5.2 Setup

To validate the effectiveness of defined method, the following set of experiments were executed using Matlab.

- The first experiment was conducted on generalized dataset to show the efficacy of the defined method on real hazy images against the state-of-the-art methods namely multi-scale fusion[13], Dark channel prior [14], Gray world, White patch and Histogram equalization.
- The second experiment was conducted on I-Haze dataset in order to show the performance of the proposed approach against the state-of-the-art methods. Here, RMSE, PSNR, and SSIM have been calculated to compare proposed results with state-of-the-art methods.
- Finally in the third experiment, a inclusive set of the comparisons was performed using two datasets. In the first experiment, the defined technique is matched against the well-known methods like multi-scale fusion [13], dark channel prior [14], gray world, white patch and histogram equalization. While, in the second set of experiment, the comparison has been performed against the latest methods such as RMSE, PSNR, and SSIM.

6. Results and Discussion

6.1 A First Set of Experiments

As described before, this experiment validates the efficacy of the defined approach on real dataset. A few sample images are shown in Figure 6. As observed from figure 6., images produced using the proposed approach have better clarity and no blur noise matched against latest methods.

6.2 Second Set of Experiments

As described before, the second experiment was conducted to show the importance of the defined method using I-Haze dataset. For this purpose, this study has used the most known methods for image enhancement and restoration. The unbiased valuations are described in Table 1. The proposed approach was able to provide smaller RMSE values and higher PSNR values. In addition, the values of SSIM are close to 1 compared to the result produced by latest methods. It is clear that the defined approach has provided better results s shown in Figure 6.

6.3 Third Set of Experiments

In the third set of experiments, a strong comparison has been performed under the two datasets. The comparison results are presented in Figures 7 – 11. It is obvious that the defined method showed significant performance than of the existing methods. The proposed approach can acquire the resulting image without color distortion. Nevertheless, the histogram equalization creates unwanted color and some artefacts in images. The. The results produced by Multi-scale fusion and dark channel prior were acceptable, but new colours were created in some images, which changed their appearances. Therefore, the proposed approach accurately and robustly enhance different kind of images degraded by haze.

7. Conclusions

De-hazing approach have become a need for many computer applications. This work has proposed a Multi-stage approach for image de-hazing. Four main stages have been utilized in our

approach. The first stage is defined to diminish the blurring noise using Wiener filter. The second stage is defined to enhance the luminance, where each RGB color pixel was spread among the least and highest values. IN the next stage, the luminance adjustments is achieved by transforming the resultant images from the RGB model to YCbCr model. Finally, the last stage is utilized to overcome colorcast by color correcting. The proposed approach has showed high superior performance under challenging conditions including distorting images, incomplete variety, and little contrast. The approach also keeps the properties and characteristics of the images through de-hazing the images. In addition, unlike other approaches, our approach exhibit low complexity makes applicable for online scenarios

Conflict of Interest

The authors declare no conflict of interest.

References

- [1] C. Ancuti, C. O. Ancuti, R. Timofte, L. Van Gool, L. Zhang, M.-H. Yang, et al. NTIRE 2018 challenge on image dehazing: Methods and results. In The IEEE Conference on Computer Vision and Pattern Recognition (CVPR) Workshops, June 2018.
- [2] C. O. Ancuti, C. Ancuti, R. Timofte, and C. De Vleeschouwer. I-HAZE: a dehazing benchmark with real hazy and haze-free indoor images. In arXiv, 2018.
- [3] He, Renjie; Wang, Zhiyong; Fan, Yangyu; Feng, David Dagan: 'Combined constraint for single image dehazing', *Electronics Letters*, 2015, 51, (22), p. 1776-1778, DOI: 10.1049/el.2015.07071ET Digital Library
- [4] Mahdi, Hussein & El abjadi, Nidhal & Mohammed, Hind.' Single image dehazing through improved dark channel prior and atmospheric light
- [5] Xu D.; Xiao C. and Yu J. COLOR-PRESERVING DEFOG METHOD FOR FOGGY OR HAZY SCENES. In *Proceedings of the Fourth International Conference on Computer Vision Theory and Applications VISAPP, 2009*
- [6] Mahdi, Hussein & El abjadi, Nidhal & Mohammed, Hind.' Single image dehazing through improved dark channel prior and atmospheric light estimation'. *Journal of Theoretical and Applied Information Technology*. 2017.
- [7] Wenfei Zhang, Jian Liang, Haijuan Ju, Liyong Ren, Enshi Qu, Zhaoxin Wu, Study of visibility enhancement of hazy images based on dark channel prior in polarimetric imaging, *Optik*, Volume 130, 2017, Pages 123-130.
- [8] Zhiyuan Xu. "Fog Removal from Video Sequences Using Contrast Limited Adaptive Histogram Equalization", *International Conference on Computational Intelligence and Software Engineering*, 2009.
- [9] Ancuti C.O., Ancuti C., Hermans C., Bekaert P. A Fast Semi-inverse Approach to Detect and Remove the Haze from a Single Image. In: Kimmel R., Klette R., Sugimoto A. (eds) *Computer Vision – ACCV 2010*. ACCV 2010. Lecture Notes in Computer Science, vol 6493. Springer, Berlin, Heidelberg
- [10] S. Narasimhan and S. Nayar, "Contrast Restoration of Weather Degraded Images" in *IEEE Transactions on Pattern Analysis & Machine Intelligence*, vol. 25, no. 06, pp. 713-724, 2003.
- [11] S. G. Narasimhan and S. K. Nayar, "Shedding light on the weather," 2003 IEEE Computer Society Conference on Computer Vision and Pattern Recognition, 2003. Proceedings., Madison, WI, USA, 2003, pp. 1-1.
- [12] Makkar, Divya & Malhotra, Mohinder. (Single Image Haze Removal Using Dark Channel Prior. *International Journal Of Engineering And Computer Science* 2016).
- [13] .O. Ancuti and C. Ancuti, "Single image dehazing by multiscale fusion," *IEEE Transactions on Image Processing*, vol. 22(8), pp. 3271–3282, 2013
- [14] K. He, J. Sun, and X. Tang, "Single image haze removal using dark channel prior," *IEEE Trans. Pattern Anal. Mach. Intell.*, vol. 33, no. 12, pp. 2341–2353, Dec. 2011.
- [15] G. Meng, Y. Wang, J. Duan, S. Xiang and C. Pan, "Efficient Image Dehazing with Boundary Constraint and Contextual Regularization," 2013 IEEE International Conference on Computer Vision, Sydney, NSW, 2013, pp. 617-624.

[16] Q. Zhu, J. Mai and L. Shao, "A Fast Single Image Haze Removal Algorithm Using Color Attenuation Prior," in *IEEE Transactions on Image Processing*, vol. 24, no. 11, pp. 3522-3533, Nov. 2015.

[17] Xie, Bin, Fan Guo, and Zixing Cai. "Improved single image dehazing using dark channel prior and multi-scale Retinex." *Intelligent System Design and Engineering Application (ISDEA), 2010 International Conference Vol.1.IEEE*, 2010

[18] Shuai, Yanjuan, Rui Liu, and Wenzhang He. "Image Haze Removal of Wiener Filtering Based on Dark Channel Prior." *Computational Intelligence and Security (CIS), 2012 Eighth International Conference on IEEE*, 2012

[19] E. H. Land and J. J. McCann, "Lightness and retinex theory," *Journal of the Optical Society of America A*, vol. 61, pp. 1–11, 1971.

[20] R. C. Gonzalez and R. E. Woods, "Digital Image Processing". New Jersey: PearsonPrentice Hall, 2008.

[21] Alruwaili, M., & Gupta, L. (2015). A statistical adaptive algorithm for dust image enhancement and restoration. *Proceedings of 2015 IEEE International Conference on Electro/Information Technology* (pp. 286–289).

[22] Fisher, R., Perkins, S., Walker, A. & Wolfart, E. Contrast stretching Retrieved 25th August 2019, from Web site: <http://homepages.inf.ed.ac.uk/rbf/HIPR2/stretch.htm>

[23] Barnard, K., Cardei, V. & Funt, B. A comparison of computational color constancy algorithms-part I: Experiments with image data, *IEEE Transactions on Image Processing*, Vol. 11, no. 9, 2002.

[24] G.D. Finlayson, S.D. Hordley, and P.M. Hubel, "Color by correlation: A simple, unifying framework for color constancy," *IEEE Transactions on Pattern Analysis and Machine Intelligence*, vol. 23, no. 11, pp. 1209–1221, November 2001.

[25] Fairchild, M.D. *Colour appearance models*, 2nd Edition. Wiley-IS&T, Chichester, UK, ISBN 0-470-01216-1, 2005.

[26] Z. Wang, A. C. Bovik, H. R. Sheikh and E. P. Simoncelli, "Image quality assessment: From error visibility to structural similarity," *IEEE Transactions on Image Processing*, vol. 13, no. 4, pp. 600-612, Apr. 2004.

Table 1: The average value of RMSE, PSNR, and SSIM of 30 images

30 Images Average value of	Proposed Approach	Multi-scale fusion	Dark channel prior	Gray World	White Patch	Histogram Equalization
RMSE	21.8	29.6	34.4	26.7	27.9	22.5
PSNR	21.9	18.9	17.7	20.1	20.7	21.5
SSIM	0.75	0.56	0.61	0.68	0.66	0.73



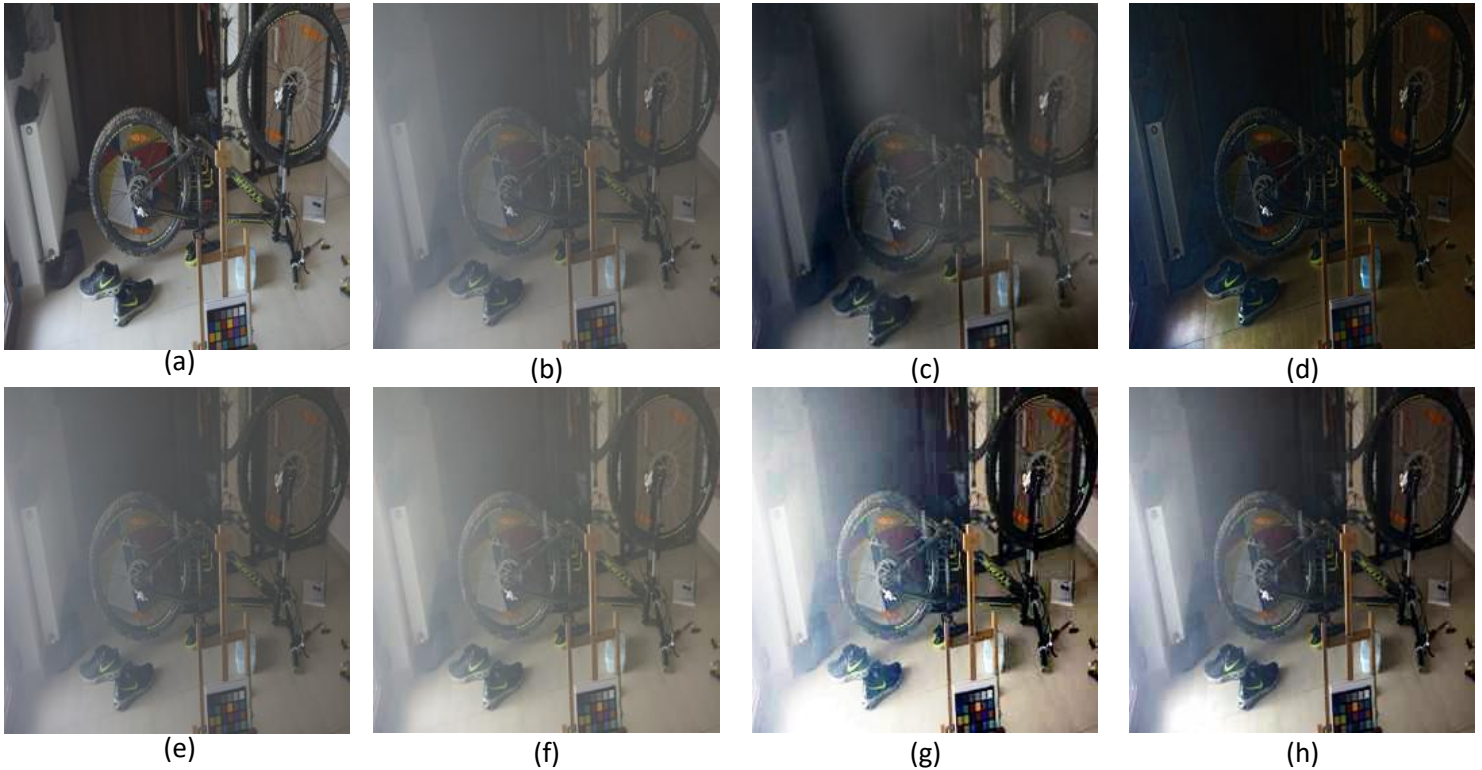


Figure 7. Comparative results for image number 5 from I-Haze dataset. (a) input image, (b) hazy image, (c) multi-scale fusion, (d) Dark channel prior, (e) Gray World, (f) White Patch, (g) Histogram Equalization, and (h) proposed approach

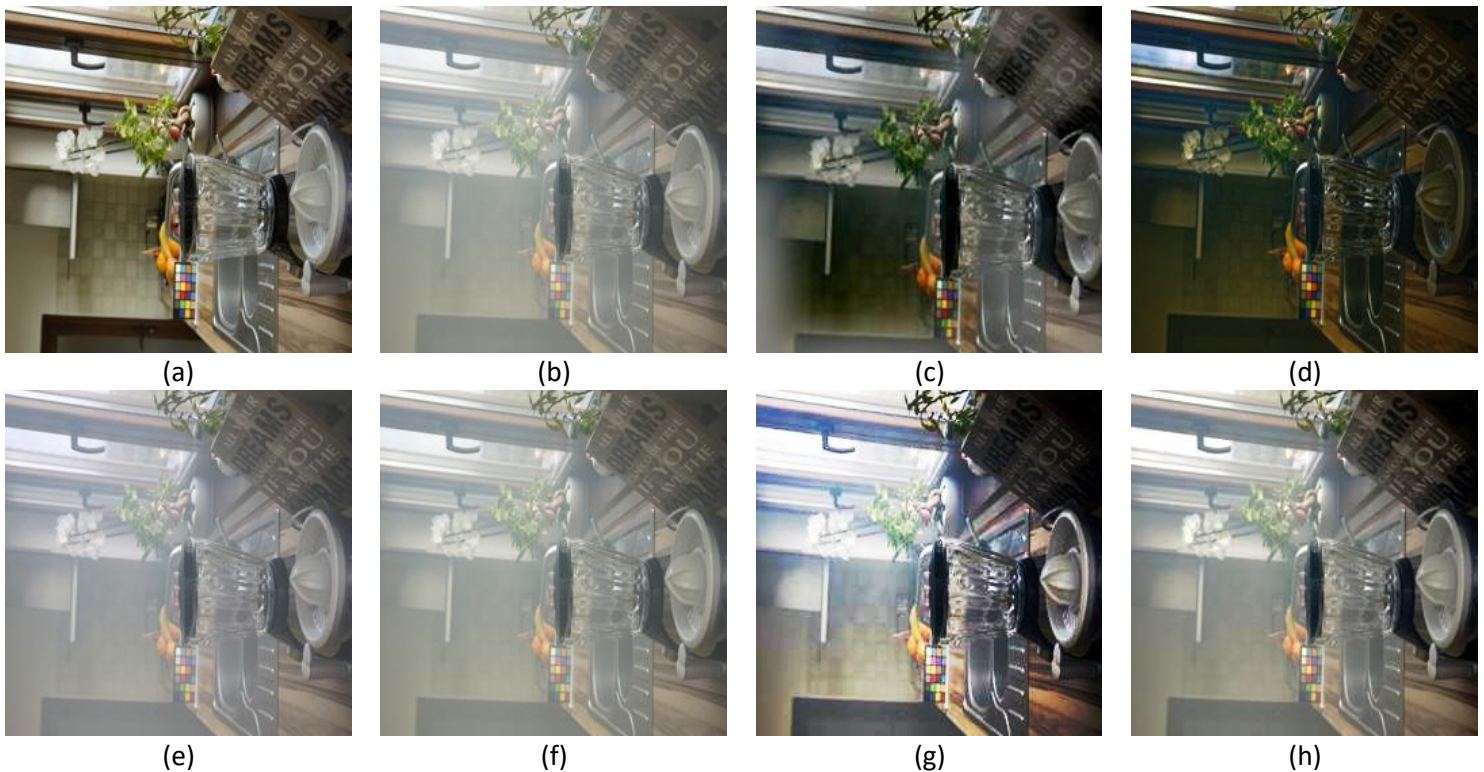


Figure 8. Comparative results for image number 9 from I-Haze dataset. (a) input image , (b) hazy image, (c) multi-scale fusion, (d) Dark channel prior, (e) Gray World, (f) White Patch, (g) Histogram Equalization, and (h) proposed approach

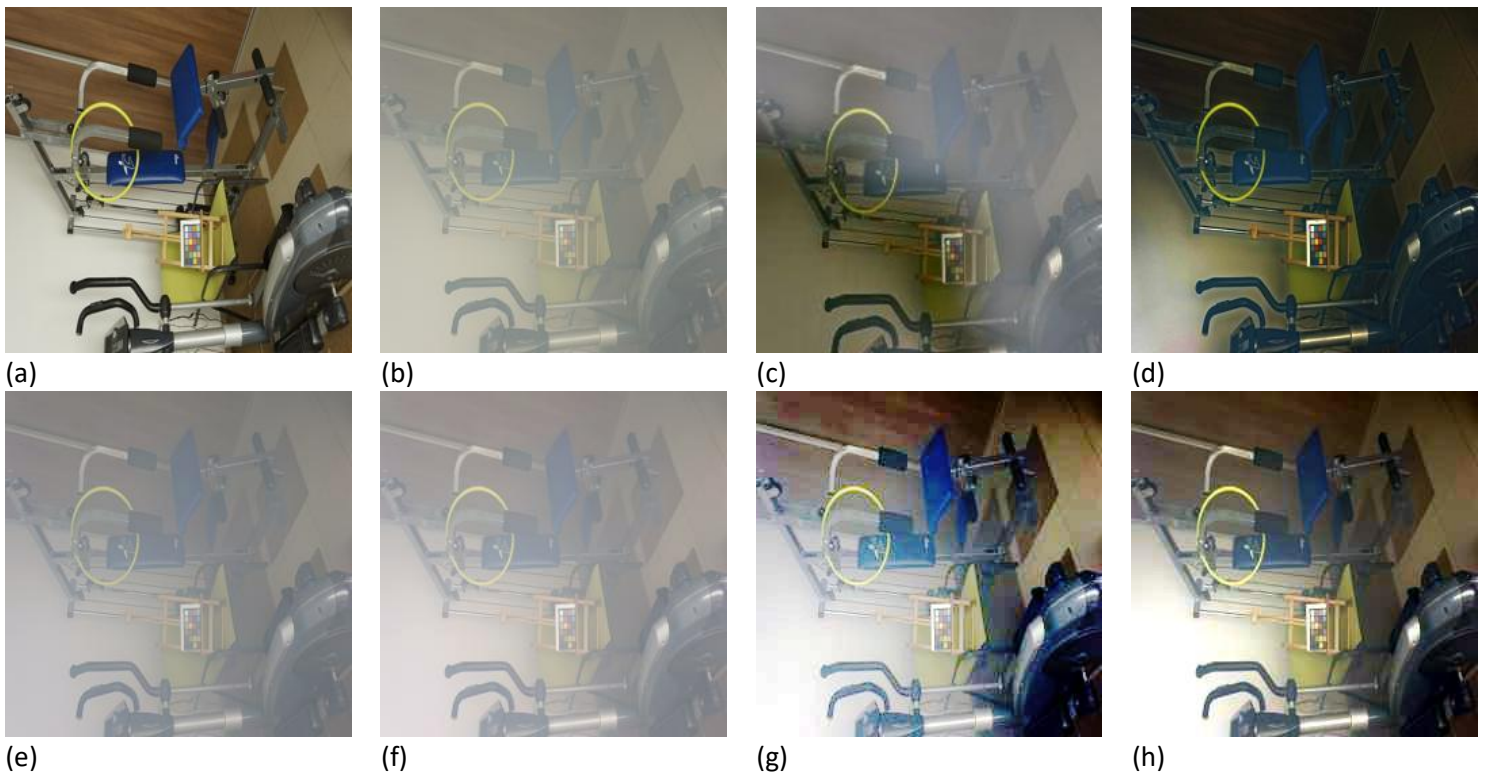


Figure. 9. Comparative results for image number 12 from I-Haze dataset. (a) input image, (b) hazy image, (c) multi-scale fusion, (d) Dark channel prior, (e) Gray World, (f) White Patch, (g) Histogram Equalization, and (h) proposed approach

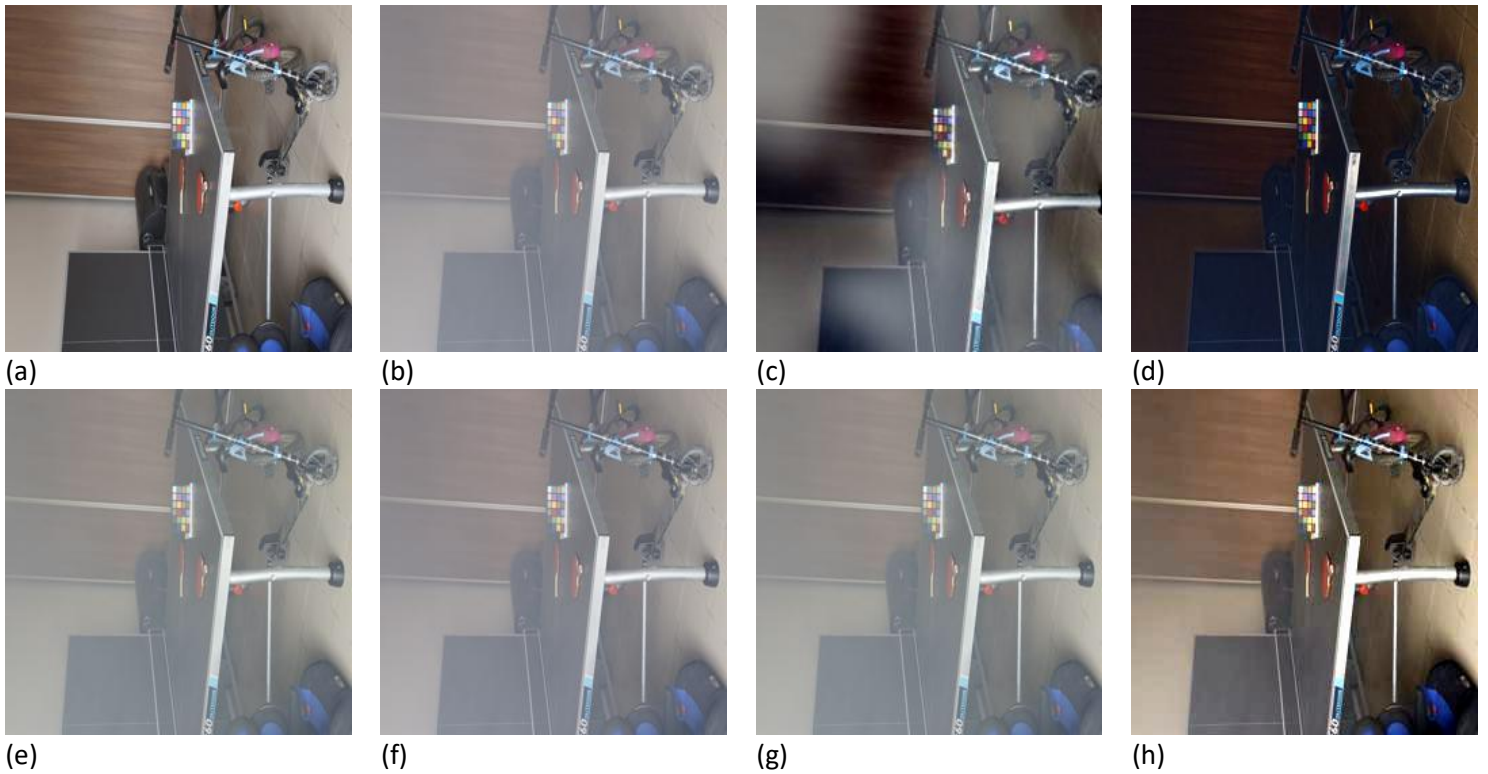


Figure. 10. Comparative results for image number 20 from I-Haze dataset. (a) input image, (b) hazy image, (c) multi-scale fusion, (d) Dark channel prior, (e) Gray World, (f) White Patch, (g) Histogram Equalization, and (h) proposed approach

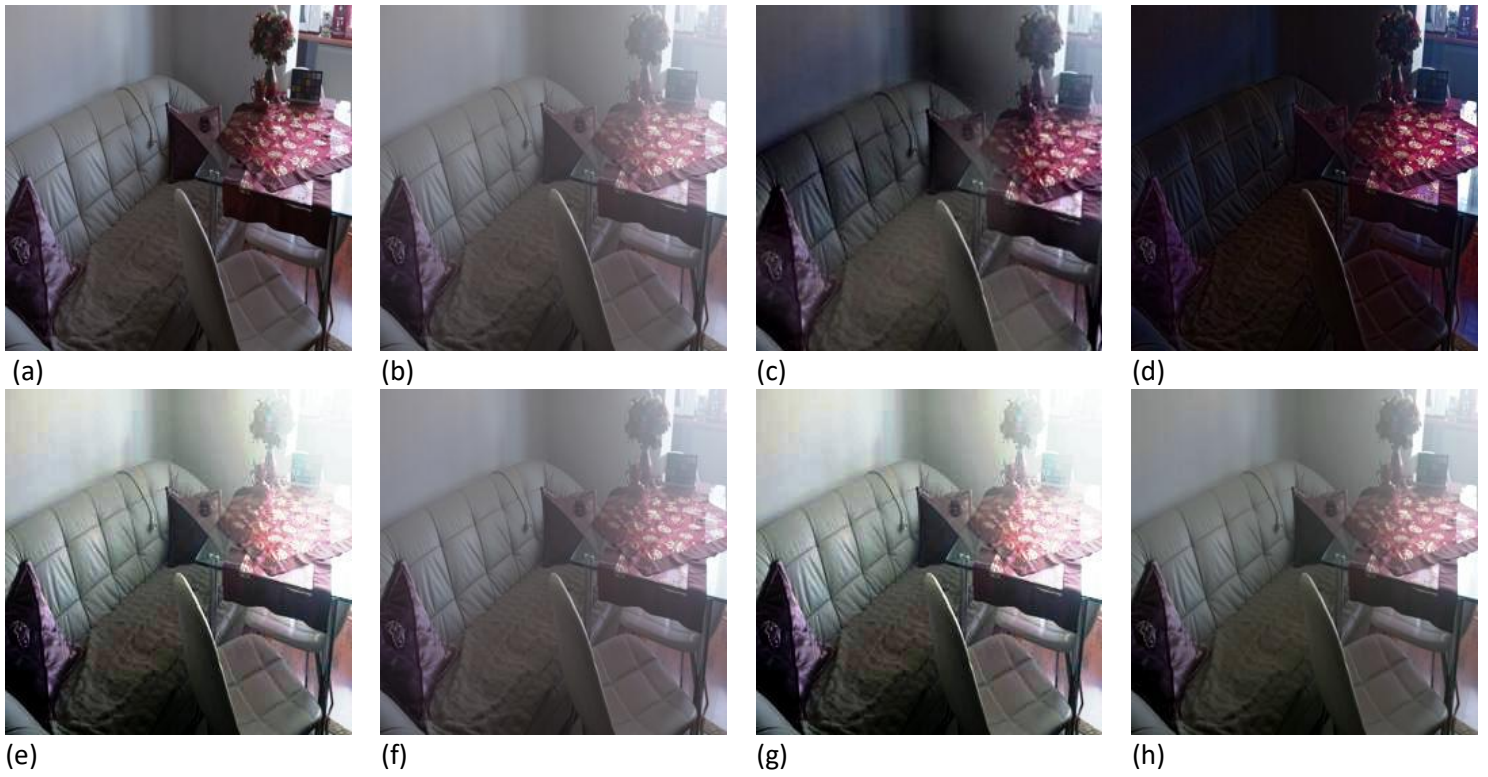


Figure. 11. Comparative results for image number 22 from I-Haze dataset. (a) input image , (b) hazy image, (c) multi-scale fusion, (d) Dark channel prior, (e) Gray World, (f) White Patch, (g) Histogram Equalization, and (h) proposed approach

Fire System for an Automated Electrical Substation via Programmable Logic Controller

Omar Freddy Chamorro Atalaya*, Dora Yvonne Arce Santillan, Martin Diaz Choque

Faculty of Engineering and Management, Universidad Nacional Tecnológica de Lima Sur, Perú

ARTICLE INFO

Article history:

Received: 06 September, 2019

Accepted: 01 December, 2019

Online: 16 December, 2019

Keywords:

Programmable Logic Controller

Fire System

Electrical Substation

ABSTRACT

This article presents the development of an automatism by means of a Programmable Logic Controller (PLC), for the Fire System of an Electric Substation; For this, the areas belonging to the electrical substation are initially described, where the automatism is developed, these being three; Patio area (Transformer location), Distribution board area and Control room. Then the components to be used in the automatism are identified, which are; 16 sensors (input elements), as well as 5 solenoid valves, 3 electro-pumps and 3 frequency inverters (output elements). Then the programming of the S71200 PLC is developed, through the contact scheme language, the automatic control guarantees the optimal operation of the system components. Once the system has been developed, the Cronbach Alpha test is carried out in the statistical program SPSS (Statistical Product and Service Solutions), which determines that the reliability is 0.794. Finally, the normality of the data was verified through the Shapiro Wilk test, obtaining as a result a significance of 0.60 for the pressure and 0.166 for the flow rate; being these data greater than the level of significance $\alpha = 0.05$, we can conclude that the variable pressure and flow follow a normal distribution, which is reflected in the normal QQ graph, in this way the correct operation of the fire system would be guaranteed. of the Electrical Substation..

1. Introduction

As is known, electrical energy implies risks for both entities and people, either directly due to the effect of an electric shock or indirectly, as a source of heat capable of generating a fire or explosion in certain environments of an installation. [1]

In the case of power transformers, when using highly flammable liquid insulation, such as mineral oil, the risk of fire is high, because it contains a large number of combustible elements that are in contact with live elements. Although the fire rate is not so high; Currently the surveys carried out indicate that the number of fires is growing significantly, generating very high economic consequences, and affecting the supply of consumers [2]

For this reason, in the industry fire systems are being considered using water spray, since, according to the studies carried out, it is the most beneficial, to extinguish electrical fires, due to the lack of continuity between water particles, which prevents Electricity can be conducted through them. That is why these systems are used effectively to extinguish, control, protect and / or prevent a fire. [3]

Considering the risk and the probability of occurrence of an accident in the different equipments of the substations, measures must be taken that meet the requirements effectively and safely; for this reason, the implementation of automatic control systems has emerged; that mitigate damage to facilities, personnel in charge or consumers.

Therefore, fire systems are currently operating through the use of technological innovations, one of them is the Programmable Logic Controller (PLC), with which multiple benefits are achieved, such as precise control of the entire system, reduction of accidents of work, reduction of equipment and material costs to replace and / or use, and use of man-machine times. [4]

In this sense, this article seeks to develop an automatism that optimally controls the Fire System of an Electric Substation.

2. Methodology

2.1. Kind of investigation

The research is level is descriptive; through which the development of the fire system automation of an electrical substation is described; In addition, the results of the pressure and flow of the sprinklers will be analyzed, which should be according to the design based on the NFPA standard.

*Omar Freddy Chamorro Atalaya. Jr. Los Damascos 986. Los Olivos, Lima, Perú, 968053089 & omar_chamorro1@hotmail.com

2.2. Population and Sample

For our study, the 24 sprinklers of the fire system of the electrical substation are considered as population.

Likewise, the sample will be the same as the population; since, according to Hernández cited in Castro (2003), he says that "if the population is less than fifty (50), the population is equal to the sample" (p.69). [5] The number of sprinklers contained in the design area, as well as the coverage area of the sprinklers, was determined by means of the NFPA-13 standard. Once these indicators were calculated, the number of sensors to be used could be determined.

It should be noted that in the present investigation our unit of analysis is made up of the measurements made in the fire system in relation to its pressure and flow parameters.

2.3. Instrument used in Data Coleccion

The instrument used is the data record data sheet, in which the measurement results of the pressure and flow parameters of the fire system have been collected.

3. Results

The electrical substation is divided into three areas; these are:

- Patio area (Transformer location)
- Distribution board area
- Control room

Likewise, the fire system will be of the type of water spray, these systems have spray nozzles, which allows the discharge to be in fine mist-type drops, these systems are the most appropriate for class C fire, in which they intervene fuels, in addition the discharge of this system does not conduct electricity. The water spray is used to extinguish fires caused by electrical equipment, since due to the lack of continuity of the water particles, which is why they prevent electricity from being conducted through each drop.

In addition, one of the advantages is that its components do not contain chemicals that affect the airways of the operators, it is also not a conductor of electricity, nor produces thermal or static shocks.

Described the areas of the substation and the type of fire system used, we will describe the sequence of the system to be automated. It should be noted that one factor is the scope to which we wish to reach and in turn the limitations that may arise. Thus, the use of the PLC is justified, since it will optimize especially the economic resources; It also controls an entire process, managing multiple devices simultaneously.

The control system will be activated when the smoke sensor detects the presence of visible and invisible combustion particles; The fire system has 16 smoke sensors, and 24 sprinklers the distribution of sensors and sprinklers is observed below:

Table 1: Sensor Distribution

Area	Spray Smoke	Sprinklers
Main playground	8	12
Boards	5	8
Control room	3	4

Source: Self made

The electric pump will then be activated and at the same time the solenoid valves will open; The solenoid pump has the function of boosting the water in the storage tank, while the solenoid valves will pass the water to the spray nozzles.

Also, there are 24 sprinklers, these will be activated independently, only in the area where the fire is taking place, that is, only the sprinklers will be activated, in the area where the sensor detects any anomaly; There are also three electric pumps, each of which will cover 8 sprinklers.

The following Table shows the characteristics of the components that are part of the automatic control of the fire system.

Table 2: Components of the System to Automate

Components	Features	Quantity
Sprinklers	K=5,6 gpm/psi T=79°C	24
Smoke sensors	9 VCC Brand FIKE 20mA 85db/3m 433,92 MHz	16
Solenoid valves	220 V 300PSI UL/FM	24
Electric pumps	4HP Elevation: 92m Suction Height: 8m Pumping capacity: 110 l / min	3

Source: Self made

Once the design of the automatism has been described, then the input and output elements of the control system are established:

Input Elements:

- Sensor a1, a2, a3, a4, a5, a6
- Sensor b1, b2
- Sensor c1, c2,
- Sensor d1, d2, d3
- Sensor e1, e2, e3

Output Items:

- Solenoid valve A, B, C, D, E.
- Electric pump 1, 2, 3.
- Drive 1, 2, 3.

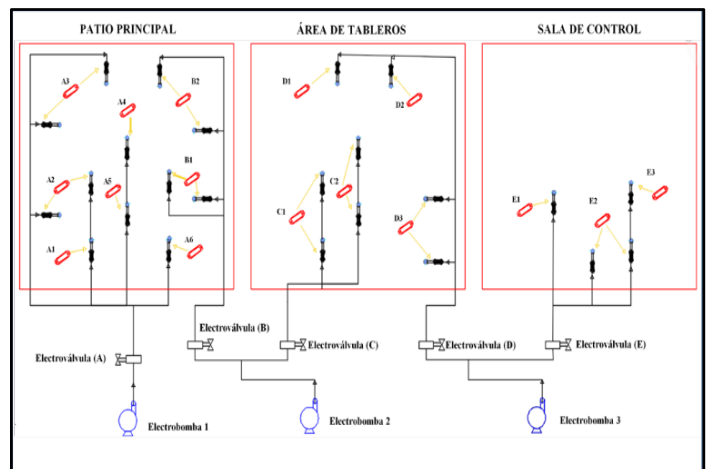


Figure 1: Automated fire system (Source: Own elaboration)

Once the input and output elements have been determined in the automatic control, the Programmable Logic Controller to be used in the Fire System is sized, which is the PLC-S71200, this controller will also be connected with 3 inverters, for every 8 sprinklers that are connected to a bomb.

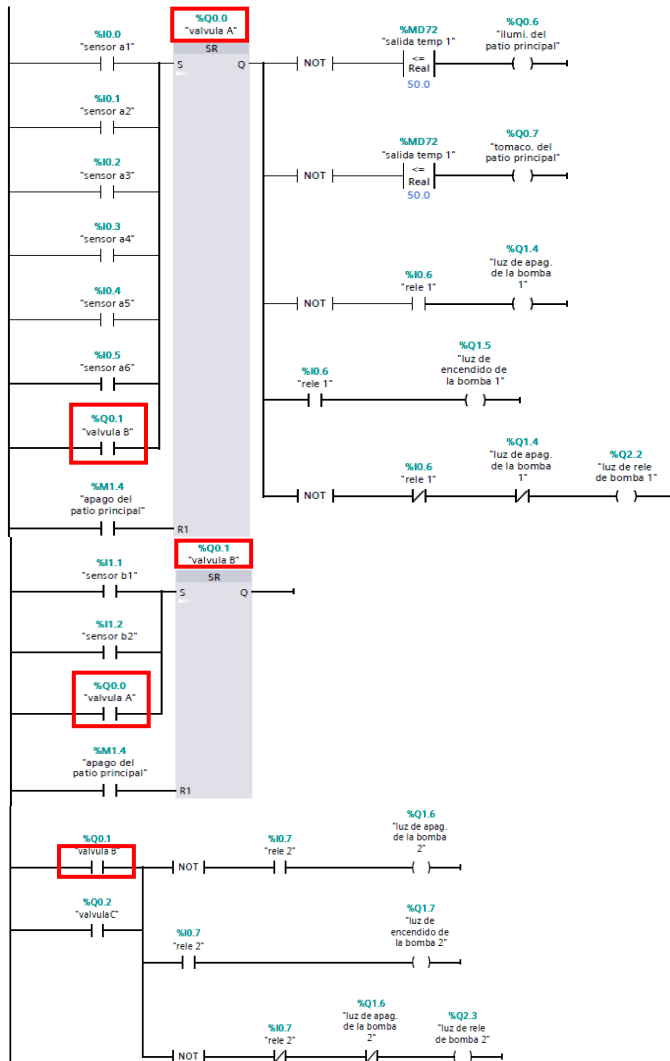


Figure 2: Segment 1 of the programming (Source: Own elaboration)

The automated fire system connection is shown below.

Next, the S71200 PLC programming is developed; in order to improve the pressure and flow regulation of the fire system.

In the main courtyard there are valves A (which has six sensors a1 to a6), B (which has two sensors b1 and b2, which send a signal to activate the solenoid valve A) with a switch and the temperature sensor; Valve B if it detects any active fire at solenoid valve A and is at the same time with another temperature sensor in which if it reaches 50 ° C it deactivates the lighting and outlet circuit.

Solenoid valve A and B activate pump1 and pump 2, respectively, these at the same time will operate at a maximum speed of 1700 rpm. It should be noted that the drive power system must be turned on in order for the drive to automatically start. It is possible to maintain a constant pressure, for this the use of a Honeywell frequency inverter; also the 3 drives to be used are connected to the PLC. The H2O level sensor for the pump has been considered, with an analog input (IW64 of integer type).

Next, the following figure shows segment 1: Valve, lighting, outlet and pump system plus the drive with segments 3 + 4 + 5 (1.1 / 2.1).

Likewise, its respective scaling is carried out for the pump1 with the Siemens commands (an int to real converter is used which is a MW15 that is connected in the MOVE, this sends the signal to the input of the conv., to later be an MD020 in the normalized (norm_X).

In the normalized parameters 0-1700 is placed; This normalized output enters the scaling input with parameters 0-27648 (PLC scanning) and its actual output is converted to a QW80 integer which is at the output of the SB120 module (is 0-10v) and is connect to the input of the drive that works with parameters 0-10v; This is the same for pump 2.

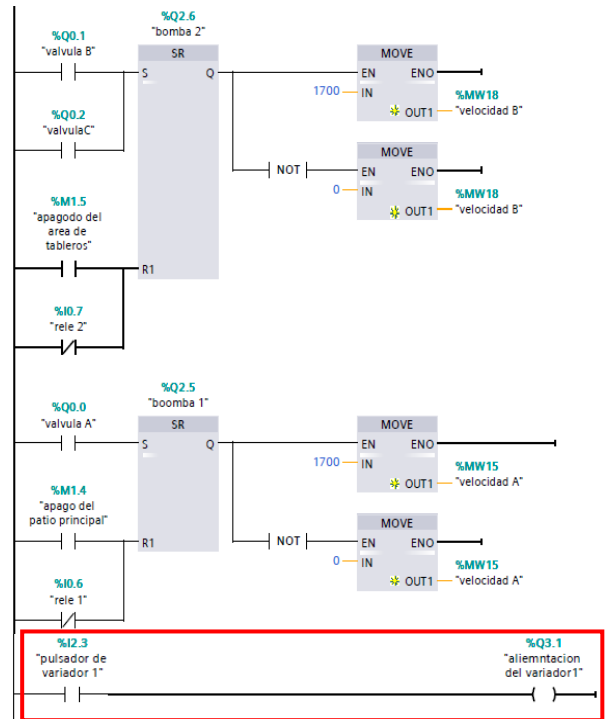


Figure 3: Segment 2 of the programming (Source: Own elaboration)

In the scaling of the temperature sensor 1, in the normalized one it sets parameters of 0-27648 and the output of the normalized one is connected to the entrance of the scaling with parameters of 0-100 ° C to be able to restrict its operation for the lighting system power outlet There is no relationship with the temperature level and the water pressure; as noted; The function of the temperature sensor is to deactivate the lighting system and outlet; when the heat parameters are outside the established range.

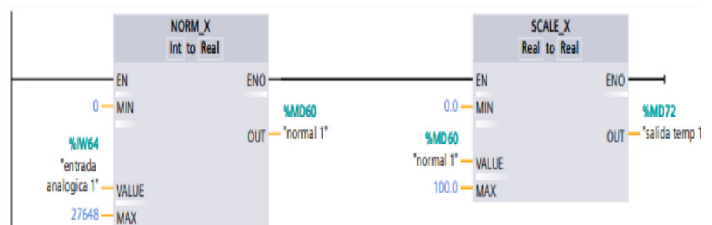


Figure 4: Segment 3 of the programming (Source: Own elaboration)

In the dashboard area there are the valves C (which has two sensors c1 and c2), D with a switch (which has three sensors d1,

d2 and d3, which sends a signal to activate the solenoid valve C) and the temperature sensor; valve D, if it detects an active fire at solenoid valve C and is at the same time with another temperature sensor in which if it reaches 50 ° C it deactivates the lighting and outlet circuit.

Solenoid valve C and D, activate pump 2 and pump 3, respectively; You will march at a maximum speed of 1700 rpm.

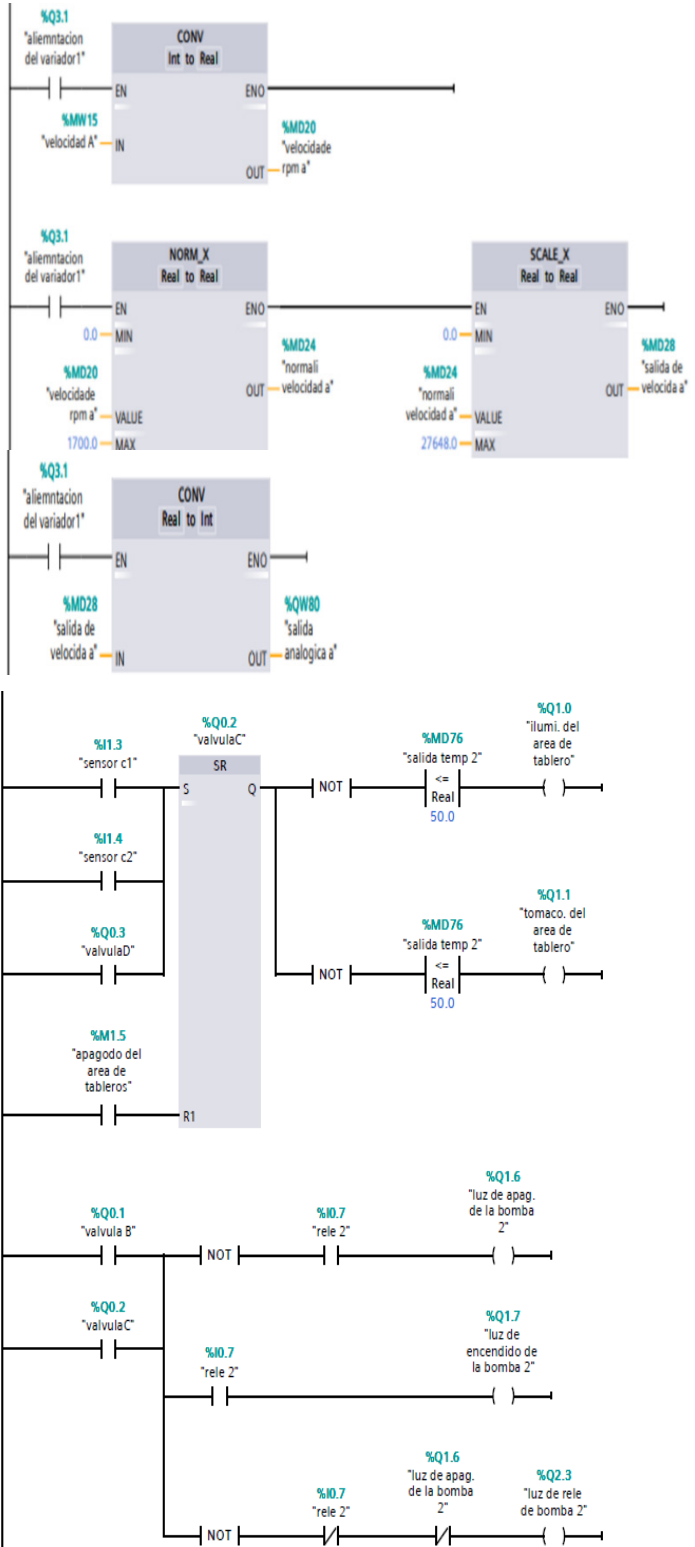


Figure 5: Segment 4 of the programming (Source: Own elaboration)

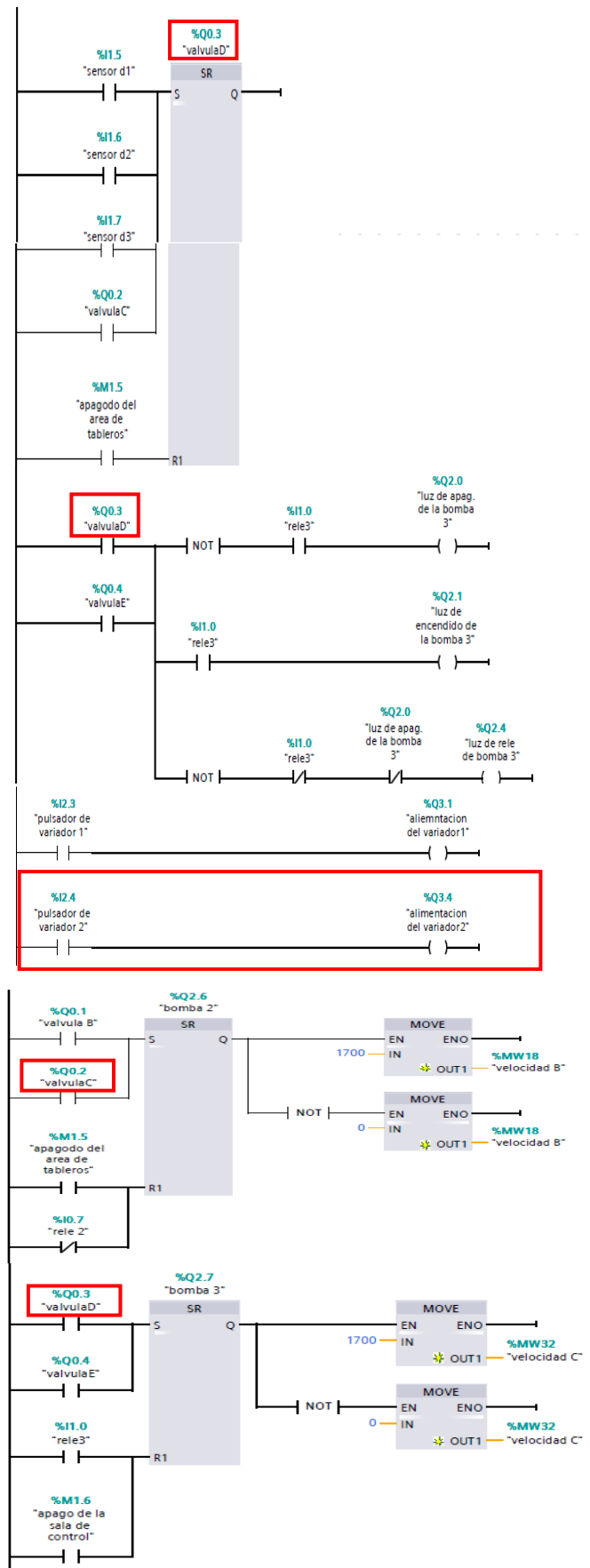


Figure 6: Segment 5 of the programming (Source: Own elaboration)

For this case, its respective scaling is also carried out for pump 2 with the Siemens commands (MW18 converter), when sending the signal to the input of the conv., It will become an MD034. The actual output is converted to an integer QW96, which is at the output of the SB-120 module and is connected to the input of the drive; this is the same for pump 3.

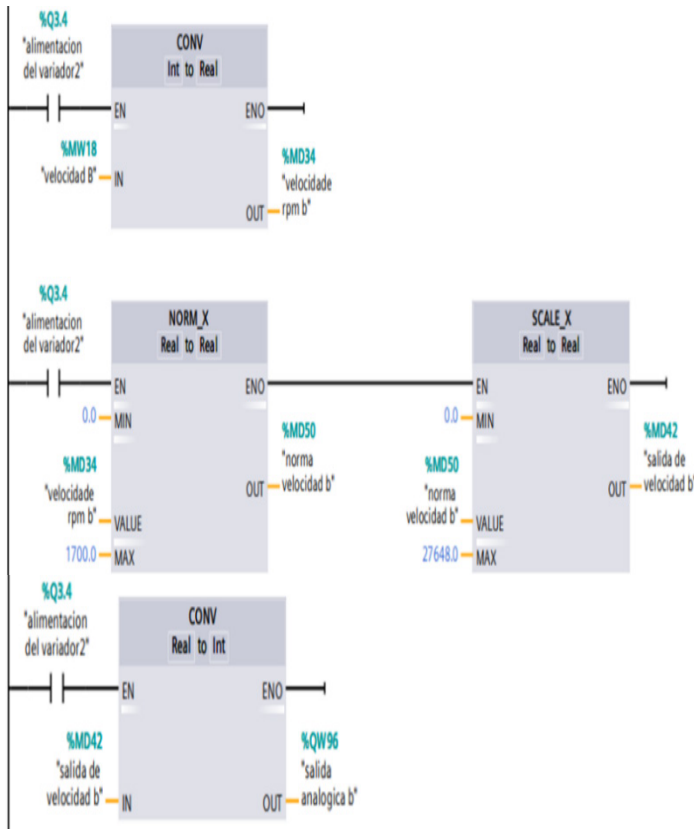


Figure 7: Segment 6 of the programming (Source: Own elaboration)

In the scaling of the temperature sensor 2, in its normalization the parameters of 0-27648 are set and the output of the normalized is connected to the input of the scaling with parameter of 0-100° C to be able to restrict its operation for lighting system and outlet.

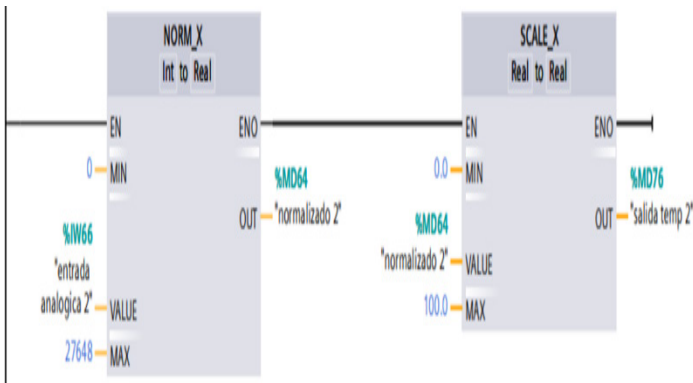


Figure 8: Segment 7 of the programming (Source: Own elaboration)

In control room is the E valves (which has three sensors e1, e2 e3), and the temperature sensor. The solenoid valve E activates the pump3, you are at the same time running at its maximum speed of 1700 rpm.

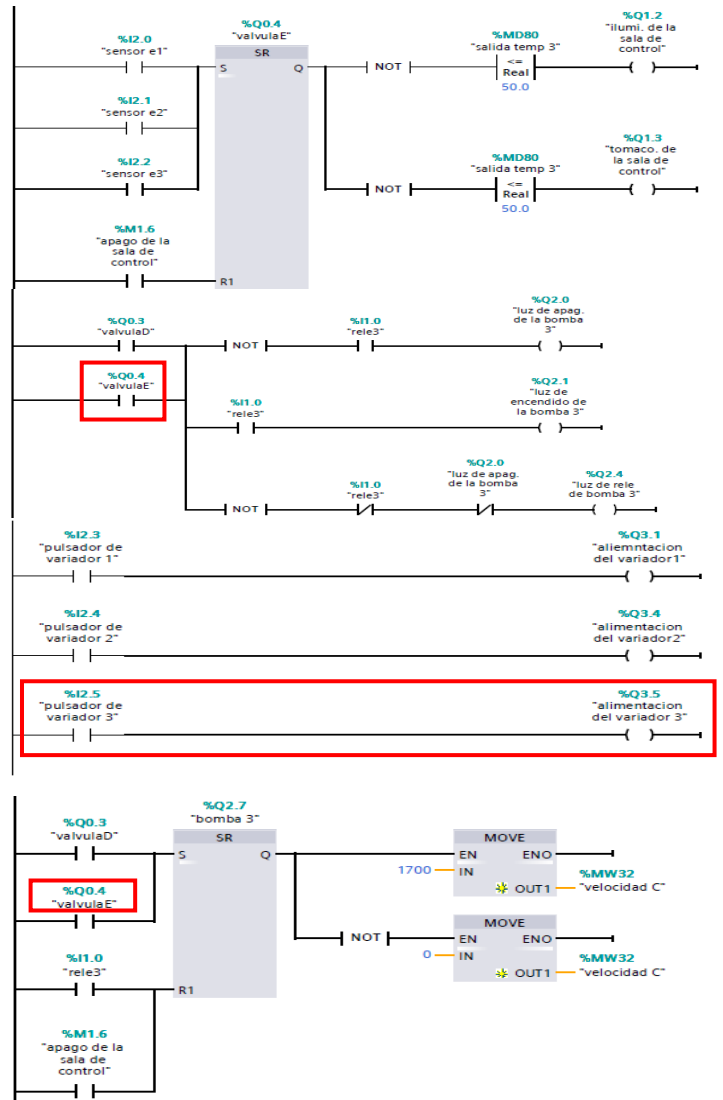


Figure 9: Segment 8 of the programming (Source: Own elaboration)

Its respective scaling is performed for pump 3 (when MW32 will be converted to MD038), the actual output is converted to an integer QW98.

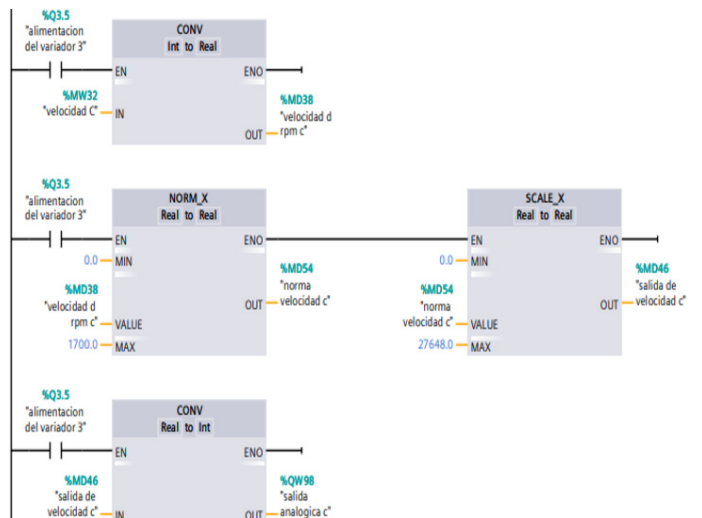


Figure 10: Segment 9 of the programming (Source: Own elaboration)

Finally, in the scaling of the temperature sensor 3, its normalized parameters are set to 0-27648 and the normalized output is connected to the scaling input with a parameter of 0-100 °C in order to restrict its operation for lighting system and outlet.

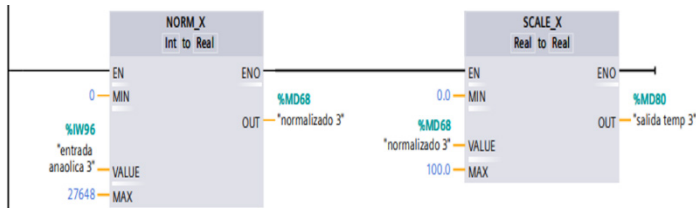


Figure 11: Segment 10 of the programming (Source: Own elaboration)

4. Statistical Analysis

Initially the Cronbach's alpha will be analyzed in order to determine the validity of my instrument, through this test the reliability of the flow and pressure measurements of the sprinklers will be established; To do this I will use the statistical program SPSS.

Table 3: Cronbach Alfa

Reliability statistics	
Alfa Cronbach	N of elements
,794	2

Source: SPSS

As seen in the previous table, the result of Cronbach's alpha is equal to 0.794; This means that the instrument is valid; since, according to Celina and Campo (2005) the minimum acceptable value must be greater than 0.7. [6]

The normality of the data will then be analyzed using the Shapiro Wilk test, this test is recommended for samples below 50.

Tabla 4: Normality Test

	Shapiro-Wilk		
	Statistical	gl	Sig.
Pressure_psi	,912	24	,060
Flow_gpm	,940	24	,166

Fuente: SPSS

As can be seen in both cases, the level of significance is greater than $\alpha = 0.05$, so it would be demonstrated that the variables present a normal distribution of their data.

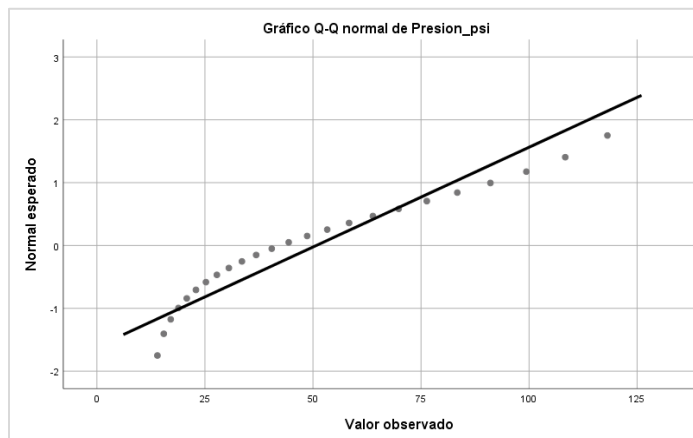


Figure 12: Normal Q-Q graph of each sprinkler pressure (Source: SPSS)

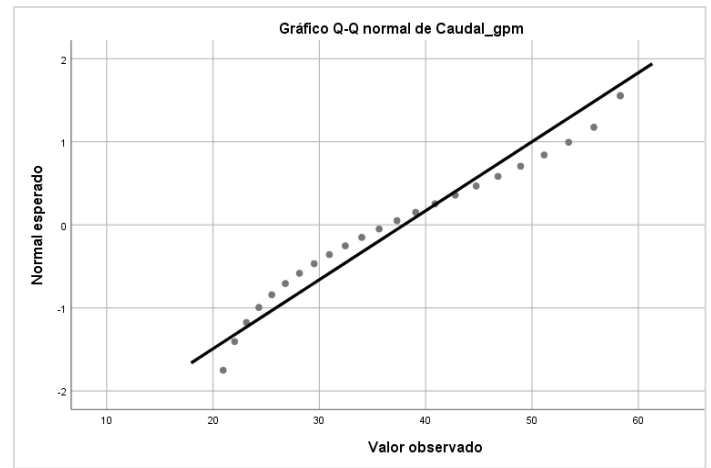


Figure 13: Normal Q-Q flow chart of each sprinkler (Source: SPSS)

The normal Q-Q chart ratifies the previous conclusion, since the observed values are placed on the diagonal, indicating the normality of the data.

Finally, we will observe the behavior of the pressure and flow parameters, obtained after performing the automation; which must comply with the NFPA standard, since, the greater the distance, the greater the pressure must be.

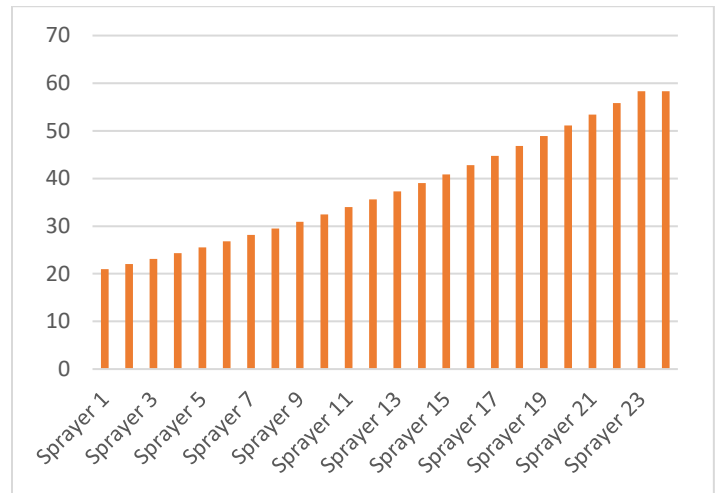


Figure 14: Result of the flow rate of each sprinkler (Source: Own elaboration)

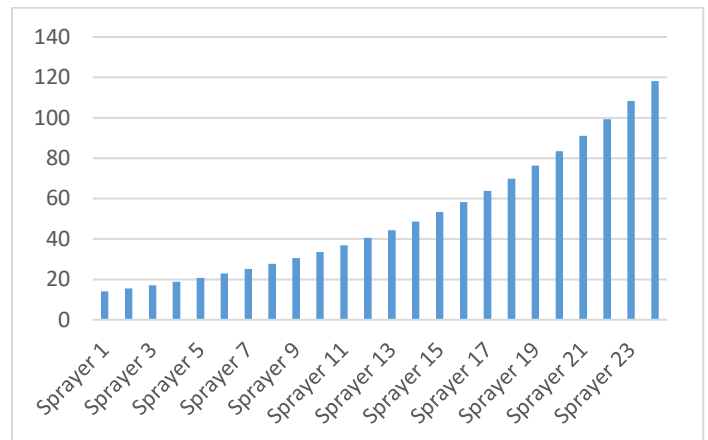


Figure 15: Result of the pressure of each sprinkler (Source: Own elaboration)

As it is observed, the results of pressure and flow, follow a correct behavior, this guarantees the optimal operation of the automation of the fire system of an electrical substation.

5. Discussion

Regarding the results obtained, these agree with those of Blum & Salazar, 2011; that in their investigation they conclude that: For the development initially the areas of greatest risk were identified, then the design was carried out and the analysis of the operability of the variables was carried out. Obtaining as a result that the system presents a quick and safe response to any incident, in addition the implementation of this system generates a profitability for the company of 14%. [7]

Regarding the results obtained, these agree with those of Ángeles & Vega, 2007; which in their investigation conclude that: To make the appropriate selection of the devices, the type of work area was initially analyzed, in order to design an effective and high quality control guaranteeing the required safety standards. With the use of technology such as that offered by a programmable logic controller, security is guaranteed, raising the degree of protection in terms of personnel integrity, as well as that of the devices that make up the system. [8]

Regarding the results obtained, these agree with that of Pachacama, 2012; which in his investigation concludes that: The development of automatism is based on the use of smoke or heat sensors mainly in cabinets, battery room and transformers; The design will prevent the spread of potential fires and minimize damage to transformers. [9]

6. Conclusions

It is concluded that it was possible to identify the programming of the S71200 PLC, using the contact scheme language; The automatic control guarantees the optimal operation of the system components.

It is concluded that it was possible to identify the components to be used in automatism, which are; 16 sensors (input elements), as well as 5 solenoid valves, 3 electro-pumps and 3 frequency inverters (output elements).

It is concluded that the project is reliable, since by means of the Cronbach Alpha test in the statistical program SPSS (Statistical Product and Service Solutions), a 0.794 reliability is determined. Likewise, the normality of the data was verified through the Shapiro Wilk test, obtaining as a result a significance of 0.60 for the pressure and 0.166 for the flow rate; these data being greater than the level of significance $\alpha = 0.05$, we can conclude that the variable pressure and flow follow a normal distribution, which is reflected in the normal Q-Q graph.

Conflict of Interest

The authors declare no conflict of interest.

Acknowledgment

The authors wish to recognize and thank the National Technological University of Lima South Lima for their support of this investigation.

References

- [1] Correa, M., & Licursi, R. (2010). Systems for fire protection in substations. CIER, 36-42.
- [2] Martín, V. (2009). Fire risk assessment of a transformer. (Undergraduate thesis). UNIVERSIDAD CARLOS III DE MADRID, Légeas.

- [3] Ybirma, L. (June 20, 2017). Counterfire. Obtained from <http://www.contraincendio.com.ve/sistemas-agua-pulverizada-proteccion-incendio/>
- [4] Quispe, D. (2011). Design and implementation of an automated system for the control and monitoring of the fire system for the process of extraction, storage and measurement of crude oil at the Paraiso station of ENAP Sipetrol Ecuador. (Undergraduate thesis). National Polytechnic School, Quito
- [5] Castro, M. (2003). The research project and its elaboration scheme. (2nd ed.). Caracas: Uypal.
- [6] Celina, H., & Campo, A. (2005). Approach to the use of Cronbach's alpha coefficient. Colombian Journal of Psychiatry, 572-580.
- [7] Blum, J. C., & Salazar, G. (2011). Redesign of the fire prevention and protection system for a food processing factory. (Thesis). Higher Polytechnic School of the Coast, Guayaquil.
- [8] Ángeles, G., Barbosa, L., & Vega, C. (2007). Control of the fire protection system of a mobile gas turbine. (Undergraduate thesis). National Polytechnic Institute, Mexico.
- [9] Pachacama, A. (2010). Design and proposal for the construction of an automatic fire detection, alarm and control system in the Cristiania N ° 18 substation of the E.E.Q.S.A. (Pregrao thesis). National Polytechnic School, Quito.

Experimental Analysis in Alternate Current and Direct Current of the Operating Parameters of a Universal Single-Phase Engine

Omar Freddy Chamorro Atalaya*, Nel Yuri Huaita Ccallo, Luis Enrique Rojas Vicuña, Rudy Jesús Capa Ilizarbe, José Arturo Pillco Torres, José Jean Franco Ramos Rupay

Faculty of Engineering and Management, National Technological University of Lima Sur, Lima, Perú

ARTICLE INFO

Article history:

Received: 08 October, 2019

Accepted: 01 December, 2019

Online: 16 December, 2019

Keywords:

Engine

Direct current

Alternate Current

Variac

Par motor

Efficiency

Torque

Power Factor

ABSTRACT

This article presents the experimental analysis of a rotary machine, Universal Motor Analysis; analysis that obeys the purpose of obtaining the almost perfect understanding of the electromechanical behavior of said unit of analysis; It should be noted that the variables to be analyzed were: voltage, current, power, torque, rpm, and power factor; specifically said data will lead to determine the regression model for each of the parameters measured, through the modification of its determination factor. Thus, an analysis of the correlational type was also performed among the variables collected above; finally, through a comparative analysis between engine efficiency during the alternative and continuous signal admission, the fuel efficiency of 91.03% will be determined in the first case, while in the second case, an efficiency of 96.66% was found; being able in this way to determine that the efficiency is greater in 5.63%, in Direct current (DC) compared to the application of Alternating current (AC).

1. Introduction

In recent decades, electric motors have increasingly become an element widely used in various applications. They are presented in a wide variety of use, going from the use generally in the industry to find them in homes, in addition to remote applications of research on land, in the air, in the water and, finally, in space, each with its own characteristics and specific protections. [1]

It is estimated that worldwide energy consumption in the industry due to the use of electric machines is in the range of 50 to 80% of the total. However, the operating conditions are increasingly demanding, therefore it is necessary to develop new proposals for operation, control and protection. [2] Electric motors are one of the main applications of Electric Power. Motors are the heart of machines and devices in general. [3]

Electric motors powered by direct current (DC: Continuous Current) have multiple applications and although they are already 125 years old, they have adapted very well to the demands of the market. [4] The electric motor operates through electromagnetic interactions, given its electromechanical characteristics. [5]

*Omar Freddy Chamorro Atalaya. Jr. Los Damascos 986. Los Olivos, Lima, Perú, 968053089 & omar_chamorro1@hotmail.com

The DC motor in certain applications require a large turning force at the start of the motor; In that sense DC motors due to their high starting torque are more suitable; Since their torque is high, they break the inertia that the load to displace during start-up can exert. [6]

The universal single-phase motor, specifically, is a very useful rotary electric machine in the industry and in daily life, for applications where more torque is required per amp and a speed control by voltage as it occurs in machining machines, drills, among others. [7]

In their small power design they are widely used in household appliances, with more powerful powers are used in electric traction at a frequency ranging from 50Hz to 60Hz. [8]

When an electromechanical system requires high revolutions, power and, above all, a high starting torque, the universal motor is usually selected. [9]

There are criteria in the motors in direct current and others in alternating current, which handle in different aspects both in the design of the structure, the variations in operating speeds, maintenance periods, among others. [10]

The appeal of this type of electric motor lies in the type of power available, be it VAC (alternating current voltage) or VDC (direct current voltage); reason for what is generally referred to as "Universal Motor". The constitution of this motor is of similar provisions that the DC series motor (direct current) with an armature (rotor or armature) and an inductor (stator), being able to control its speed using rheostats or any device that manages to control the voltage supplied as it comes in the DC motor. [10]

There are several analysis criteria involved in the operation of the universal motor that operate when operating this type of electric machine, this paper presents the experimental analysis of the internal behavior that this particular motor presents; by means of a raised electrical circuit that contains certain measurement and control devices, given a source of electrical network, part of the experimentation is carried out evaluating independent electrical parameters based on the modified supply voltage, considering the forms of motor operations in VDC and VAC. in a vacuum, identifying the expression of the function with respect to another study variable and the comparative analysis of efficiencies in both feeding systems.

2. Methodology

2.1. Data collection and analysis process

This research contains a series of guidelines the same that is based on three concrete stages for the process of collecting and analyzing data.

These stages are: previous considerations, alternating current experimentation and direct current experimentation.

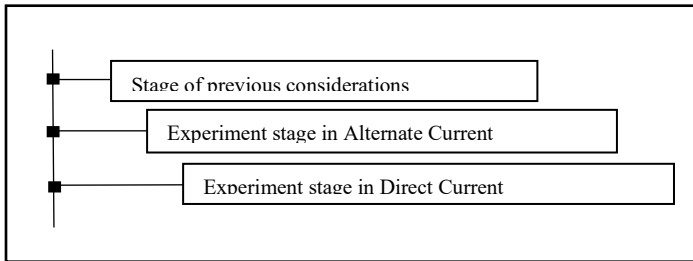


Figure 1: Stages of the data collection and analysis process.

The instrument used in the investigation was the technical data sheet, where the characteristics of the variables are detailed: voltage, current, power, torque, rpm, and power factor; of a rotary machine, called Universal Motor.

Table 1: Technical Characteristics of the Drill (Universal Engine in Analysis)

Percussion drill		
Nominal voltage	r.m.s	230
Nominal intensity	A	3,4
Nominal absorbed power	W	750
Useful power	W	380
Revolutions in vacuum	min ⁻¹	0-2800
Nominal revolutions	min ⁻¹	1750
Nominal frequency	Hz	50
Nominal turn torque	Nm	2,3
Efficiency or performance	%	51

2.2. Stage of previous considerations

It was considered a conventional hammer drill to which a VARIAC variable potential difference of alternating current www.astesj.com

(VAC) was applied, which was referred to throughout our analysis as an independent variable.

During this stage, relationships were established between independent variables vs dependent variables for the recording of electrical values by evaluating the degree of dependency ratio during the full period until establishing nominal electrical parameters, recommended in the data sheet of such a drill.



Figure 2: VARIAC voltage regulator.

For the connection it is considered an alternate power supply provided to us by the local network 220 VAC 60 Hz, however, for experimentation it is required to vary the voltage (r.m.s) gradually to extract samples from electrical parameters such as: voltage, intensity, power, power factor, rpm, between others; given this requirement, a VARIAC illustrated in Figure 2 was used, which is determined by a transformer.

At the output of this VARIAC is connected the load that would come to be the drill that in diagram is represented by: a resistance, an inductance and a rotor. Where the first two represent the stator fields representing and the last to the winding rotor. The instrumentation regarding data collection was considered a DT2235A digital tachometer, an oscilloscope, two measuring modules multifunctional, which allows permanent monitoring of parameters such as: voltage, intensity, power and factor.

Instrumentation respect to the connection of the measuring module are considered the typical connections of an Ammeter, Voltmeter, Wattmeter, Cosfimeter; where these readings are taken at the INPUT of the VARIAC and the second module is connected at the pre-load point.

2.3. Experiment stage in Alternate Current

A typical electrical circuit was developed, outlined in Figure 3.

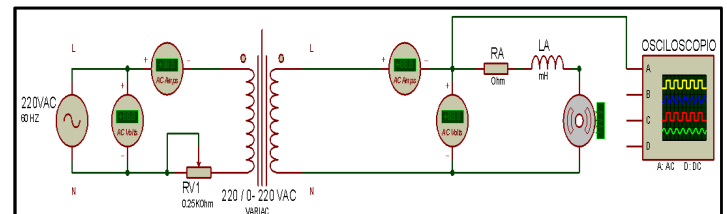


Figure 3: Universal motor diagram powered by AC.

Also, the connection of the oscilloscope is considered a typical connection where the channel is phased and the neutral is considered ground point of the instrument.

Exerting control on the universal motor of the drill by voltage variation; permanent control is obtained at all times of extraction of samples represented in Figure 4, it should be noted that the measured dependent parameters were: torque, power, rpm (revolutions per minute); correspondence tables are established after this to possess an order during the experimentation stage.

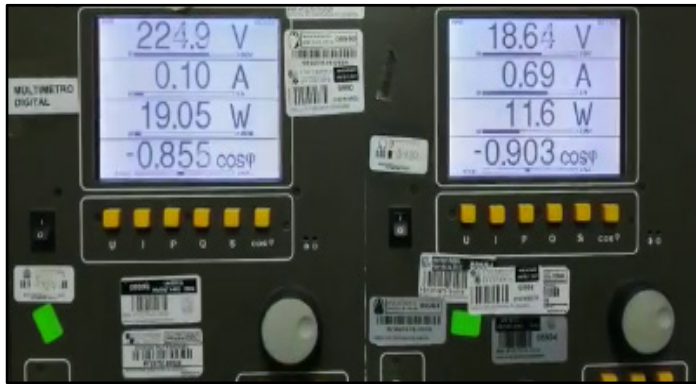


Figure 4: Electrical parameters per digital measurement module.

Regarding the values obtained from the rotational revolutions (rpm) of the drill, the digital tachometer was used to extract rotation data from the rotor, as depicted in the Figure 5.



Figure 5: Parameter of the revolutions obtained by tachometer.

The behavior of the sine wave in Figure 6, which represents the voltage when being altered by alternating current in the oscilloscope, was even contrasted.



Figure 6: Analysis of the motor with the application of an Alternate Voltage.

2.4. Experiment stage in Direct Current

A new source of variable potential difference was applied, but this time of continuous order (VDC) performing the same detailed analysis lines above.

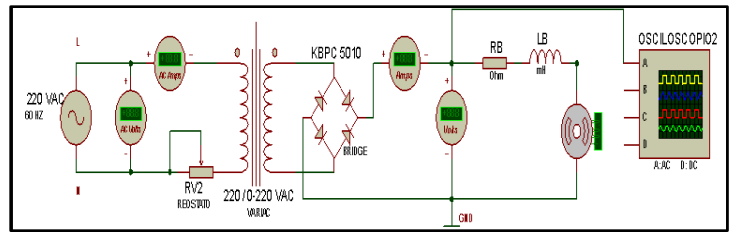


Figure 7: Universal motor diagram powered by DC.

In the VDC diagram in Figure 7, it is considered the same connections detailed above with the proviso that at the output of the VARIAC is connected a solid state component called bridge diode KBPC5010 rectifier and at the output of this polarities are set since you get a VDC voltage called pulsating continuous corrient, and the latter goes straight to load, that is the drill, however, between this section of bridge diode is connected the measuring instruments as detailed in the instrumentation point. [7]

With regard to the tachometer as detailed in instrumentation point, however, the oscilloscope, shown in Figure 8, is connected between channel to the positive rectifier diode and the negative to GND.

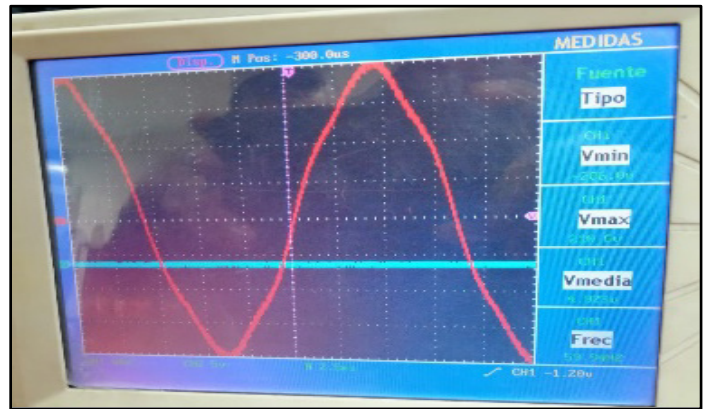


Figure 8: Engine analysis with the application of a pulsating Voltage.

3. Results

All electrical measurements, developed in both types of power supply, were established in the relevant modules and typical instruments; such results are exposed in tables using the Excel computing tool and the graph of the regression models obtained with the SPSS statistical software, for each parameter experienced electrical laboratory.

3.1. Electric parameters of the universal engine test

Before data representation, specific criteria presented by the firing hole are considered, as required in Table 1; the technical data of this percussion drill, presents a nominal torque of 2.3 N.m. and the useful power of 380 W. It should be noted that during the start-up of the universal engine in order to obtain its operating parameters, it was worked on the upper and lower margins of the torque and utility power; thus not to expose to possible damage to the drill in study.

In addition, the calculation of the torque of the "Tm" engine was performed, using the expression of mechanical power of the shaft, whose units expressed in the international system (N.m):

$$P_{eje} = \frac{T_m \times RPM \times \pi}{30} \quad (1)$$

Where:

- P_{eje} : Engine output power.
- RPM: Induced rotation speed.

The calculation of the power absorbed by the power grid in alternating current and direct current, if the case of pulsating VDC, its analysis is somewhat extended; therefore, it is considered quasi-alternative behavior.

$$P = V \times I \times \cos \phi \quad (2)$$

3.2. Universal Motor in alternate current

The register was detailed by the independent variable of the voltage regulated by the VARIAC with values from 10V to the rated voltage of the motor, the voltage data shown is the modified in full engine start.

Table 2: Electrical parameters obtained by modified voltage in AC

Drill electrical tests in AC.						
Item	Input (Supply) - AC				Axis	Value
	Voltage (r.m.s)	Current (A)	Power (W)	F.P. (cos)		
1	10.19	0.11	0.3	0.28	0	0.000
2	20.19	0.30	2.3	0.38	0	0.000
3	29.50	0.48	5.2	0.37	0	0.000
4	32.10	0.48	5.6	0.36	29	1.844
5	34.50	0.52	7.3	0.41	86	0.811
6	36.90	0.53	10.2	0.52	200	0.487
7	37.80	0.54	10.9	0.53	225	0.463
8	39.10	0.55	12.6	0.58	313	0.384
9	44.20	0.59	17.8	0.68	390	0.436
10	50.10	0.61	22.4	0.74	445	0.481
11	53.80	0.63	26.5	0.79	630	0.402
12	58.60	0.65	30.9	0.81	700	0.422
13	63.10	0.66	35.2	0.84	800	0.420
14	69.00	0.69	41.1	0.86	890	0.441
15	72.70	0.71	45.1	0.87	950	0.453
16	77.90	0.72	50.0	0.89	1000	0.478
17	82.70	0.73	54.4	0.90	1130	0.460
18	88.10	0.74	59.4	0.91	1210	0.469
19	93.30	0.77	66.4	0.92	1270	0.499
20	98.50	0.78	71.0	0.93	1380	0.491
21	107.70	0.81	81.3	0.93	1490	0.521
22	117.80	0.84	94.0	0.95	1630	0.551
23	126.90	0.89	107.5	0.95	1750	0.587
24	138.10	0.95	124.6	0.95	1850	0.643
25	146.60	0.99	138.2	0.96	1944	0.679
26	157.40	1.02	154.1	0.96	2060	0.714
27	168.50	1.05	170.7	0.96	2180	0.748
28	177.90	1.10	187.4	0.96	2265	0.790
29	187.00	1.14	204.8	0.96	2361	0.828
30	197.70	1.17	223.6	0.97	2439	0.876

3.3. Universal motor in direct current

The value register was similarly detailed by the voltage-independent variable regulated by the VARIAC applying the same voltage regulation criterion, the voltage data have also the modified voltage in engine operation.

Table 3: Electrical parameters obtained by modified voltage in DC

Drill Electrical Tests In DC						
Item	Input (Supply) - Dc				Axis	Value
	Voltage (r.m.s)	Current (A)	Power (W)	F.P. (cos)		
1	13.61	0.59	7.2	0.90	0	0.000
2	13.68	0.57	7.0	0.90	115	0.581
3	18.66	0.59	9.9	0.91	207	0.457
4	22.95	0.61	12.8	0.92	280	0.437
5	29.00	0.63	17.0	0.93	355	0.457
6	33.60	0.66	20.5	0.93	435	0.450
7	39.00	0.69	25.0	0.94	517	0.462
8	44.20	0.72	30.1	0.94	575	0.500
9	48.10	0.73	33.3	0.94	635	0.501
10	53.30	0.77	39.0	0.95	702	0.531
11	58.40	0.78	43.1	0.95	770	0.535
12	62.50	0.80	47.5	0.95	822	0.552
13	68.10	0.81	52.8	0.95	912	0.553
14	73.80	0.83	58.3	0.96	974	0.572
15	77.50	0.84	62.4	0.96	1040	0.573
16	82.10	0.85	66.8	0.96	1111	0.574
17	88.00	0.87	73.7	0.96	1190	0.591
18	92.20	0.88	77.8	0.96	1260	0.590
19	96.80	0.83	77.6	0.97	1370	0.541
20	107.00	0.87	90.7	0.97	1510	0.574
21	117.30	0.94	107.5	0.97	1630	0.630
22	126.80	0.99	122.1	0.97	1700	0.686
23	137.10	1.05	140.8	0.97	1800	0.747
24	145.70	1.08	153.7	0.97	1900	0.773
25	156.40	1.10	167.6	0.98	2040	0.785
26	166.00	1.13	183.4	0.98	2145	0.817
27	175.40	1.17	200.2	0.98	2230	0.857
28	186.70	1.23	224.4	0.98	2300	0.932
29	195.00	1.27	242.0	0.97	2380	0.971
30	204.70	1.32	264.0	0.97	2460	1.025

3.4. Regression trend lines using calculated electrical parameters

The values expressed in the Excel tables mentioned above allow you to perform adjustment charts of a regression type using the coefficient method of determination as a statistical instrument.

3.5. Regression Graphs in AC Behavior

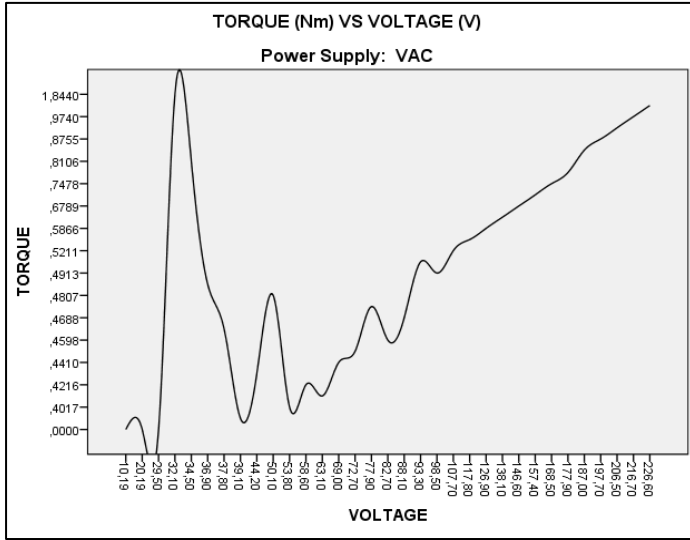


Figure 9: Analysis of Torque (N.m) and Voltage (r.m.s).

Table 4: Analysis of Torque (N.m) and Voltage (r.m.s).

Model Summary				
Model	R	R Square	Adjusted R Square	Std. Error of the Estimate
1	,496 ^a	,246	,221	,2976087

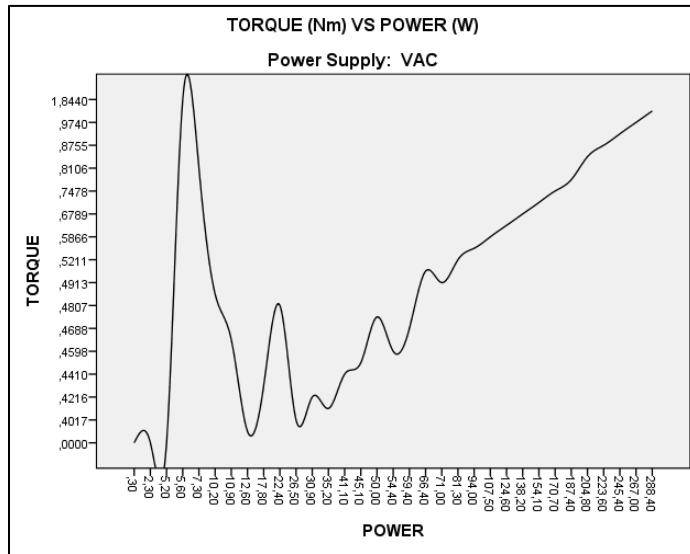


Figure 10: Analysis of Torque (N.m) and Power (W).

Table 5: Analysis of Torque (N.m) and Power (W).

Model Summary				
Model	R	R Square	Adjusted R Square	Std. Error of the Estimate
2	,499 ^a	,249	,224	,2970596

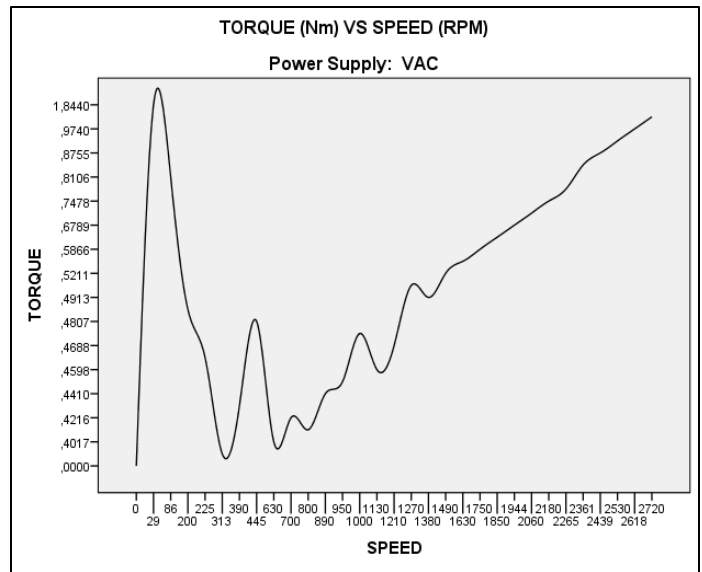


Figure 11: Analysis of Torque (N.m) and Rotation Revolution (RPM).

Table 6: Analysis of Torque (N.m) and Rotation Revolution (RPM).

Model Summary				
Model	R	R Square	Adjusted R Square	Std. Error of the Estimate
3	,436 ^a	,190	,164	,3084654

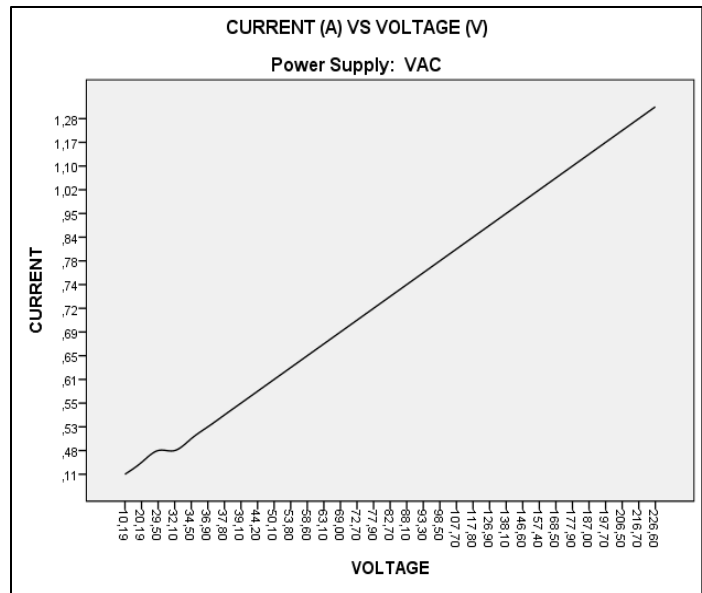


Figure 12: Analysis of Intensity (A) and Voltage (r.m.s).

Table 7: Analysis of Intensity (A) and Voltage (r.m.s).

Model Summary				
Model	R	R Square	Adjusted R Square	Std. Error of the Estimate
4	,976 ^a	,953	,952	,06255

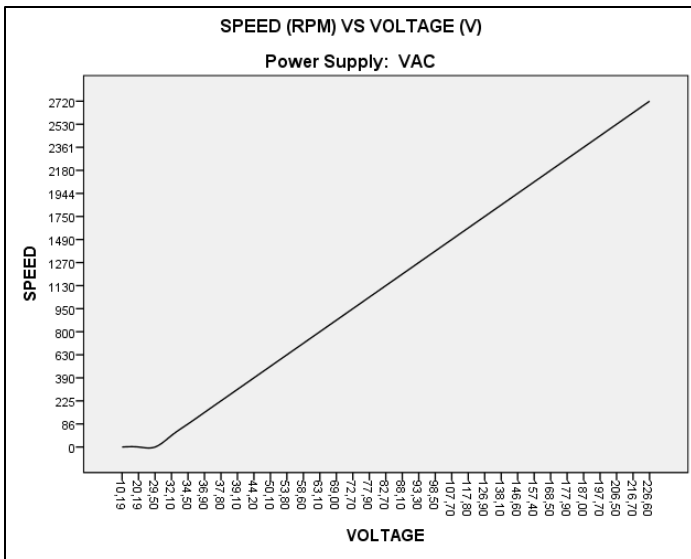


Figure 13: Analysis of Rotation Revolution (RPM) and Voltage (r.m.s).

Table 8: Analysis of Rotation Revolution (RPM) and Voltage (r.m.s)

Model Summary				
Model	R	R Square	Adjusted R Square	Std. Error of the Estimate
5	,987 ^a	,975	,974	143,388

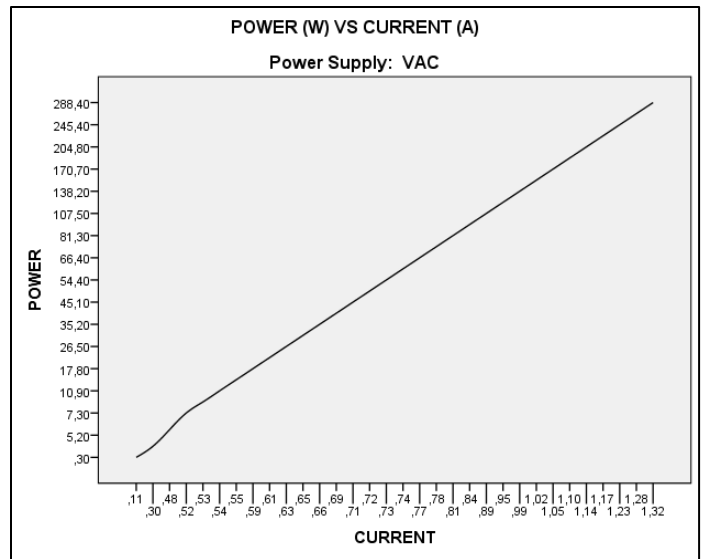


Table 10: Analysis of Power (W) and Intensity (A)

Model Summary				
Model	R	R Square	Adjusted R Square	Std. Error of the Estimate
7	,948 ^a	,898	,895	27,76831

3.6. Regression Graphs in DC Behavior

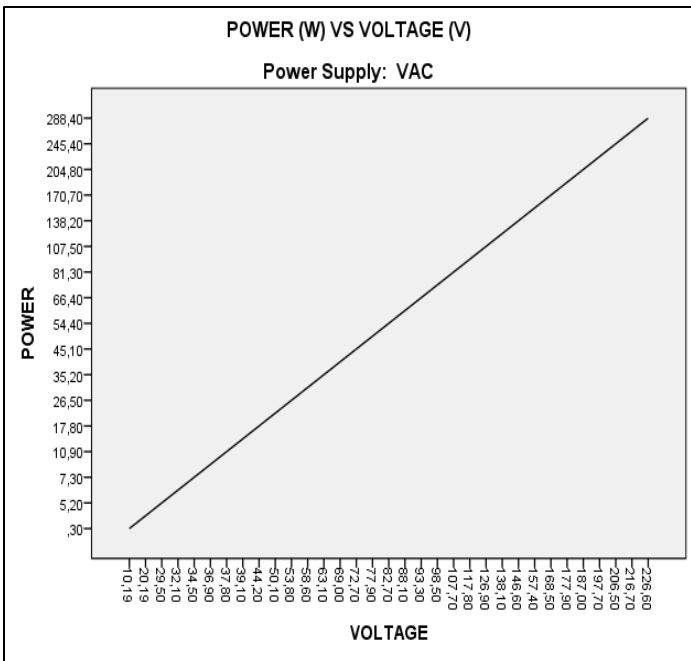


Figure 14: Analysis of Power (W) and Voltage (r.m.s).

Table 9: Analysis of Power (W) and Voltage (r.m.s)

Model Summary				
Model	R	R Square	Adjusted R Square	Std. Error of the Estimate
6	,987 ^a	,975	,974	13,74904

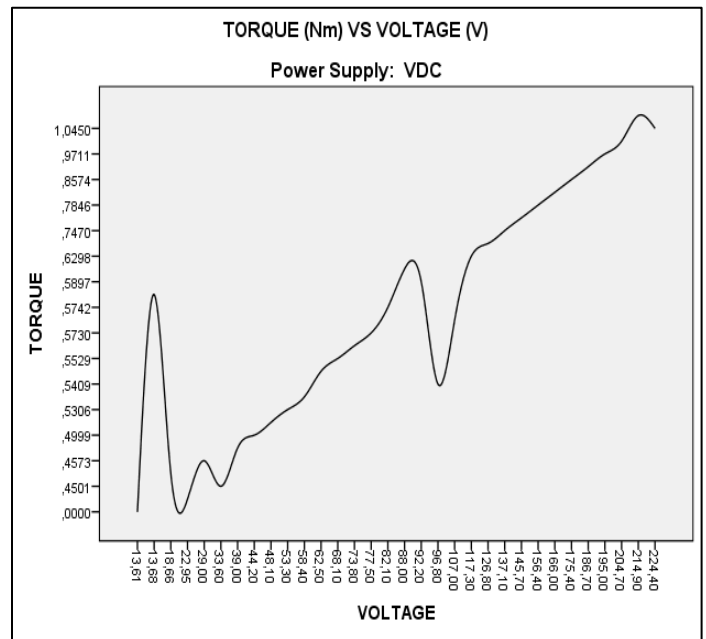


Figure 16: Analysis of Torque (N.m) and Voltage (r.m.s).

Table 11: Analysis of Torque (N.m) and Voltage (r.m.s)

Model Summary				
Model	R	R Square	Adjusted R Square	Std. Error of the Estimate
1	,922 ^a	,849	,844	,0870090

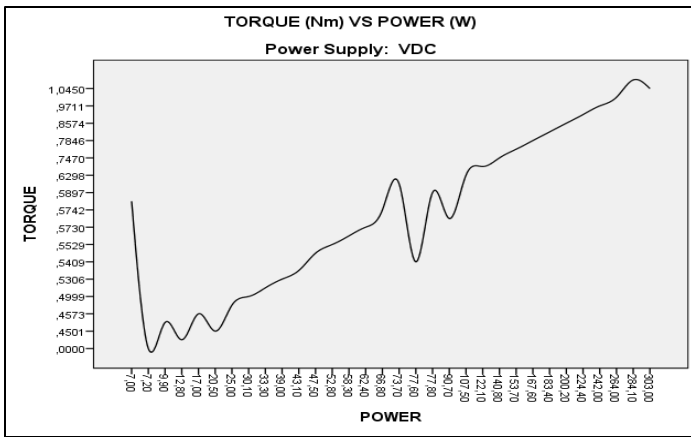


Figure 17: Analysis of Torque (N.m) and Power (W).

Table 12: Analysis of Torque (N.m) and Power (W).

Model Summary				
Model	R	R Square	Adjusted R Square	Std. Error of the Estimate
2	,924 ^a	,854	,849	,0856509

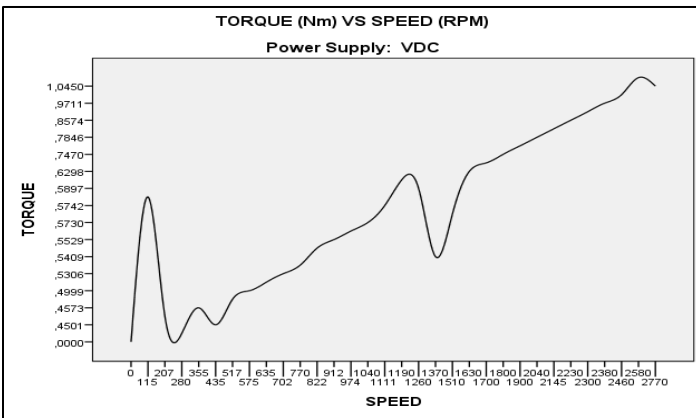


Figure 18: Analysis of Torque (N.m) and Rotation Revolution (RPM).

Table 13: Analysis of Torque (N.m) and Rotation Revolution (RPM).

Model Summary				
Model	R	R Square	Adjusted R Square	Std. Error of the Estimate
3	,915 ^a	,837	,831	,0905099

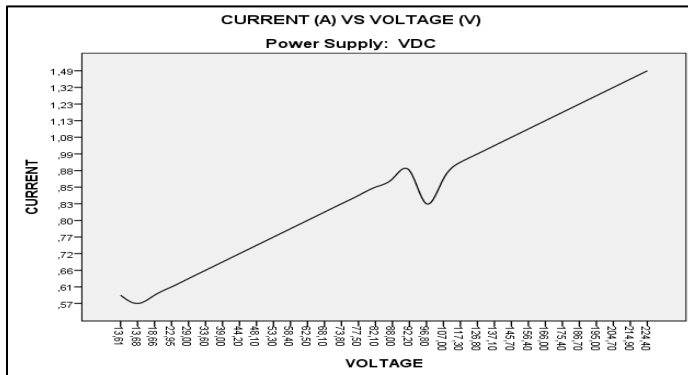


Figure 19: Analysis of Intensity (A) and Voltage (r.m.s.).

Table 14: Analysis of Intensity (A) and Voltage (r.m.s).

Model Summary				
Model	R	R Square	Adjusted R Square	Std. Error of the Estimate
4	,992 ^a	,984	,983	,03201

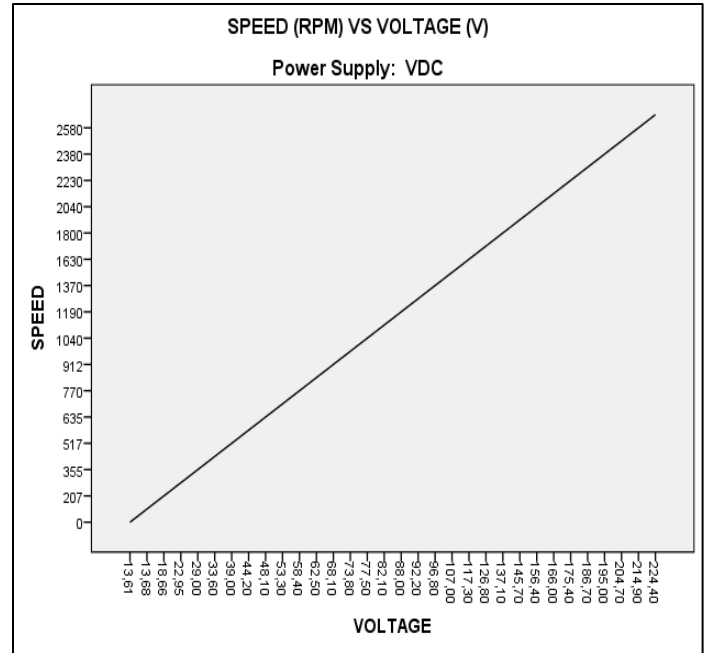


Figure 20: Analysis of Rotation Revolution (RPM) and Voltage (r.m.s).

Table 15: Analysis of Rotation Revolution (RPM) and Voltage (r.m.s).

Model Summary				
Model	R	R Square	Adjusted R Square	Std. Error of the Estimate
5	,995 ^a	,990	,990	80,165

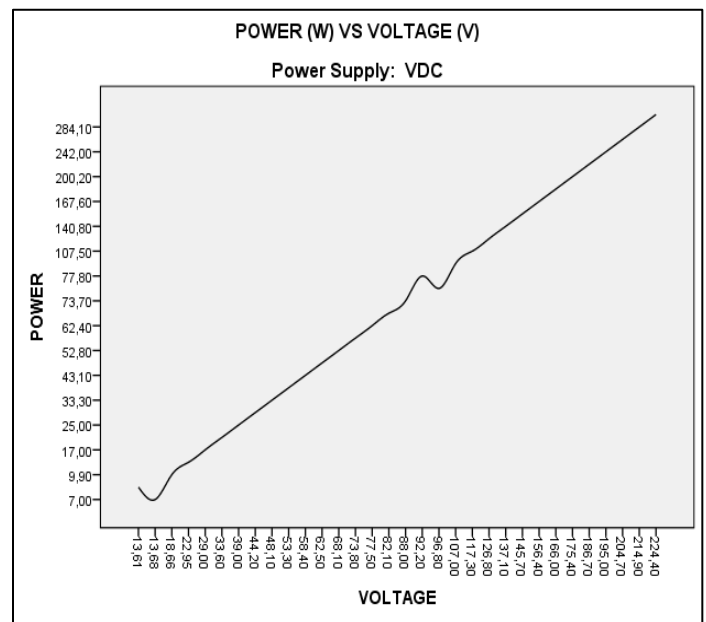


Figure 21: Analysis of Power (W) and Voltage (r.m.s).

Table 16: Analysis of Power (W) and Voltage (r.m.s).

Model Summary				
Model	R	R Square	Adjusted R Square	Std. Error of the Estimate
6	,986 ^a	,973	,972	14,81830

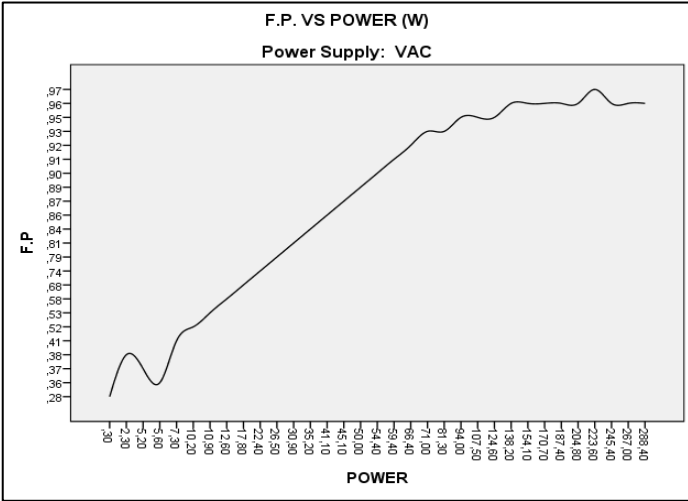


Figure 22: Analysis of Power (W) and Intensity (A).

Table 17: Analysis of Power (W) and Intensity (A).

Model Summary				
Model	R	R Square	Adjusted R Square	Std. Error of the Estimate
7	,989 ^a	,978	,978	13,23232

4. Analysis of results

The regression graphs for both Direct Current Voltage and Alternating Current Voltage behavior types presented above are analyzed.

Given the representations in AC behavior as shown in Figures 9, 10 and 11; as well as in DC behavior representations, in Figures 16, 17 and 18, one of its best virtues of this class of engines can be seen, which is a high starting torque, typical of this quality at the start moment requires greater resources and it is shown that during start-up this machine requires greater power and indirectly higher voltage or intensity; but since the first is an independent variable in addition to controlled, the second is the one that covers the requirement, until the inertia of the rotor expires, in the case of being empty and beating even the load that is subjected.

Given Figure 13 and Figure 20, the rpm is directly matched according to the electrical voltage. At the intrinsic increase of electrical voltage, the motor torque characteristics are dramatically increased and with this the intensity, until stabilized in time, expressed in Figure 12 and Figure 19.

The power is conditioned by very relevant electrical parameters in terms of electrical machines, such as voltage; this understanding is presented in Figure 14 and Figure 21.

Given the curve in Figure 10 and Figure 17, the inference can be performed on this type of rotating machines, the torque has a

direct ratio of increment to the power. According to the curve of Figure 11 and Figure 18, it can be inferred that these engines can reach high speeds and with these also reach high torque values.

According to Figure 23 and Figure 24, F.P. column can be inferred that these class of motors have better optimization of electrical energy in terms of active and reactive power; that is, when you are having a power supply in VDC.

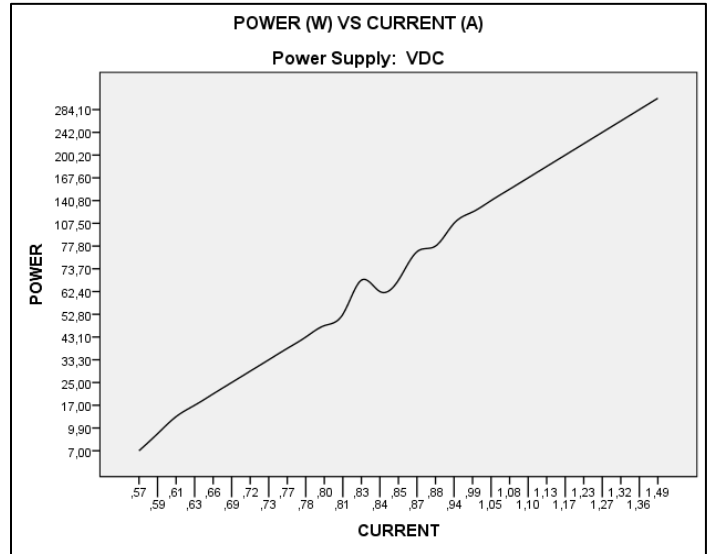


Figure 23: Analysis of F.P (cos φ) and Power (W).

Table 18: Analysis of F.P (cos φ) and Power (W).

Model Summary				
Model	R	R Square	Adjusted R Square	Std. Error of the Estimate
AC	,685 ^a	,469	,452	,16518

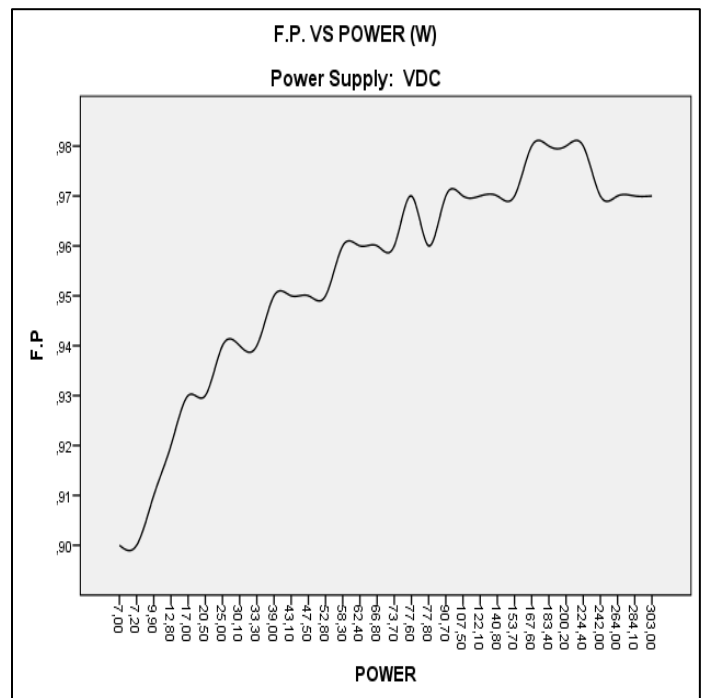


Figure 24: Analysis of F.P (cos) and Power (W).

Table 19: Analysis of F.P (cos)and Power (W).

Model Summary				
Model	R	R Square	Adjusted R Square	Std. Error of the Estimate
DC	,734a	,539	,524	,01576

Remember that alinear load can be inductive, the closer its F.P. is closer to the unit, it has a more efficient power consumption.

In addition, through theoretical concepts we can establish that efficiency is expressed:

$$\eta = \frac{P_{\text{useful}}}{P_{\text{absorbed}}} \quad (3)$$

Given the data sheet shown in Table 1, the efficiency value is obtained by Equation 3, this nominal factor is obtained when the drill is subjected to load:

$$\eta = \frac{380}{750} * 100\% = 50.6\%$$

By the first interpretation, efficiency is obtained, by applying a data relationship used by intuitive criterion, that result maintains a margin medium-reliability.

For analysis of the efficiency we resort to Table 2 and Table 3, where a section of items is used; segmenting the measurement in which the universal motor has the same RPM value, for the same voltage:

Table 20: Efficiency analysis in AC tests.

Drill Electrical Tests In AC.						
Item	Input (Supply) - AC				Axis	motor
	Tension (V)	Current (A)	Power (W)	Rpm	Torque (N.m.)	η (%)
22	98.50	0.78	71.0	1380	0.491	47.78
23	117.80	0.84	94.0	1630	0.551	46.65
24	157.40	1.02	154.1	2060	0.714	47.90

Table 21: Efficiency analysis in DC tests

Drill electrical tests in DC						
Item	Input (Supply) - AC				Axis	motor
	Tension (V)	Current (A)	Power (W)	Rpm	Torque (N.m.)	η (%)
20	96.80	0.83	77.6	1370	0.541	52.22
21	117.30	0.94	107.5	1630	0.630	53.35
22	156.40	1.10	167.6	2040	0.785	52.10

It is then derived from Equation 3, the expression:

$$\eta = \frac{P_{\text{vdc}}}{P_{\text{vac}} + P_{\text{vdc}}} \quad (4)$$

Given the case of 1630 RPM and 117 Volts, the calculation is proceeded.

$$\text{Efficiency with VDC power: } \eta = \frac{107.5}{107.5+94} * 100\% = 53.4 \%$$

$$\text{Efficiency with VAC power: } \eta = \frac{94}{107.5+94} * 100\% = 46.6 \%$$

By the second interpretation, you get the actual efficiency, which is obtained when the percussion drill is in operation, without considering applied load.

Table 22: Real efficiency in AC tests

Application - VAC			
Item	P. Useful (W)	P. Absorbed (W)	η
	P. Mechanical	P. Electric	%
1	0.00	0.31	0.00
2	0.00	2.27	0.00
3	0.00	5.18	0.00
4	5.60	5.55	1.01
5	7.30	7.32	0.99
6	10.20	10.17	1.003
7	10.90	10.82	1.008
8	12.60	12.47	1.010
9	17.80	17.73	1.004
10	22.40	22.62	0.991
11	26.50	26.78	0.990
12	30.90	30.85	1.002
13	35.20	34.98	1.006
14	41.10	40.94	1.004
15	45.10	44.91	1.004
16	50.00	49.92	1.002
17	54.40	54.33	1.001
18	59.40	59.33	1.001
19	66.40	66.09	1.005
20	71.01	71.45	0.994
21	81.31	81.13	1.002
22	94.01	94.00	1.000
23	107.51	107.29	1.002
24	124.61	124.64	1.000
25	138.21	139.33	0.992
26	154.11	154.13	1.000
27	170.71	169.85	1.005
28	187.41	187.86	0.998
29	204.82	204.65	1.001
30	223.62	224.37	0.997
31	245.42	243.84	1.006
32	267.02	266.28	1.003
33	288.42	287.15	1.004
Average total performance			91.03%

According to the experimental analysis these machines operate more efficiently when a VDC source is available, usually represented in Figure 25, with a variation of 5.63% from the AC power system; consequently motors working with VDC increase the life cycle of dynamic parts such as bearings, gears, collectors and their brushes; remember that an electrical disturbance can encourage the formation of harmonics and these instead trigger in mechanical vibrations, generating as a result of efforts in dynamic and statisticparts.

According to the above mentioned in addition to this last analysis you can be certain that under similar conditions such as rpm, voltage, power, and so on. This machine increases its performance when energized by VDC.

Table 23: Real efficiency in DC tests

Application - VDC			
Item	P. Useful (W)	P. Absorbed (W)	η
	P. Mechanical	P. Electric	%
1	0.00	7.23	0.000
2	7.00	7.02	0.998
3	9.90	10.02	0.988
4	12.80	12.88	0.994
5	17.00	16.99	1.001
6	20.50	20.62	0.994
7	25.00	25.30	0.988
8	30.10	29.91	1.006
9	33.30	33.01	1.009
10	39.00	38.99	1.000
11	43.10	43.27	0.996
12	47.50	47.50	1.000
13	52.80	52.40	1.008
14	58.30	58.80	0.992
15	62.40	62.50	0.999
16	66.80	66.99	0.997
17	73.71	73.50	1.003
18	77.81	77.89	0.999
19	77.61	77.93	0.996
20	90.71	90.30	1.005
21	107.51	106.95	1.005
22	122.11	121.77	1.003
23	140.81	139.64	1.008
24	153.71	152.64	1.007
25	167.61	168.60	0.994
26	183.41	183.83	0.998
27	200.21	201.11	0.996
28	224.42	225.05	0.997
29	242.02	240.22	1.007
30	264.02	262.10	1.007
31	284.12	283.50	1.002
32	303.02	324.33	0.934
Average total performance			96.66%

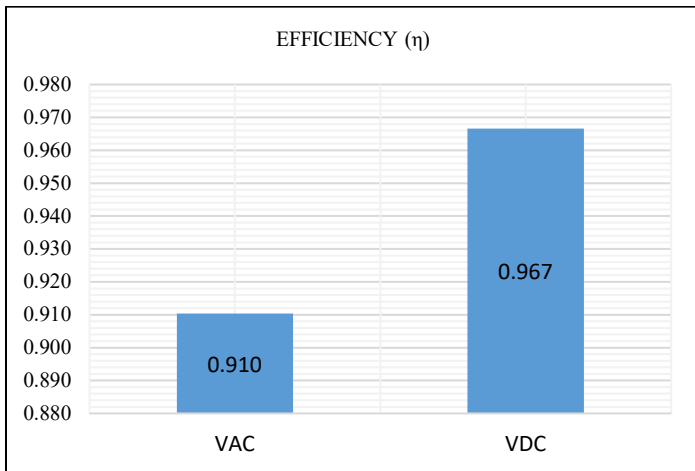


Figure 25: Representation of efficiencies in AC and DC tests.

5. Discussion

Given a source of energy to a reason of constant increase, it presents less electrical disturbance; however, if this increase doesn't obey any constant reason, this machine has radical torque increments coupled with the disturbances generated and include less efficiency in your life. [8]

Reaffirming Rosenberg's assertion, evidence throughout the experimentation a recession in what corresponds to the natural sizzle generated by the engines that have collectors; since it is proprio the rapid transition between delga and delga causes an electric arco small magnitude, however, this characteristic it is diminished how much it works with VDC which does not happen with VAC. This post-verification statement was made of the good condition of the brushes in addition to the correct adhesion between the dega and brush.

Remember that the proportion of the electric arco generated in the collector may also be caused by poor adhesion between brush and delga or also because of the speed. [5]

Universal motors are deficient in temperature, it is a cough to increase this variable of the maticte very quickly, however, to relatively short periods of use. Given the constitution of winding rotor with dolphins; In addition, the maintenance of these is very high. [5]

6. Conclusions

We will find that the good interpretation of the oscilloscope gives us greater reliability; in addition to the possibility of showing the complete shape of the wave, leading to the best analysis, as well as better accuracy in what the analysis is, in this instrument we can calculate the maximum effective voltage, frequency and period; in addition to so-called valley ridges and so on. Through this view of the function generator, we show the representative model of the VDC and VAC Power Supply; and the first called pulsating voltage and the second alternating voltage.

According to the figure of the oscilloscope is shown the representation of different wave qualities one complete sinusoidal and the other only half cycle, however, using measuring instruments it is shown that in both cases we observe the similar measurements of tension this in a similar revolution (rpm), this being that at all times a positive semicycle is always preserved throughout the period in VDC and a positive semicycle or a negative one in the case of VAC, however, they will always possess in both cases at similar effective tension.

The efficiency of this class of motors is directly related to the type of power supply by which it is used, in addition when we consider the reduction of network disturbances, the high starting torque, high rpm, longer service life given to a decrease in electrical distortions caused by its own induced winding rotor constitution; are all virtues of this type of motor during VDC operation.

Conflict of Interest

The authors declare no conflict of interest.

Acknowledgment

The authors wish to recognize and thank the National Technological University of Lima South Lima for their support of this investigation.

References

[1] Álvarez, J., Araque, O., & Merino, Y. (2017). Electronic device to control the frequency in a single-phase motor of alternating current. *Scientia et Technica*, 308-314X. Li, Principles of Fuel Cells, Taylor and Francis Group, 2006.

- [2] Dhinakaran, P., & Manamalli, D. (2016). Novel strategies in the Model-based Optimization and Control of Permanent Magnet DC motors. *Computers & Electrical Engineering*, 34-41.
- [3] Lechappé, V., Salas, O., De León, J., Plestan, F., Moulay, E., & Glumineau, A. (2016). Predictive control of disturbed systems with input delay: experimental validation on a DC. *IFAC*, 292-297.
- [4] Monroy, E., Garcia, A., Espinoza, E., Garcia, L., & Tapia, R. (2016). n Unmanned Ground Vehicles Experimental Setup for Image-Based Object Tracking. *IEEE Latin America Transactions*, 1-6.
- [5] Aguilar, O., Tapia, R., Valdarramo, A., & Rivas, I. (2016). Adaptive neural network control of chaos in permanent magnet synchronous motor. *Intelligent Automation & Soft Computing*, 2845-2850.
- [6] Bai, R. (2016). Neural network control-based adaptive design for a class of DC motor Systems with the full state constraints. *Computers & Electrical Engineering*, 34-41.
- [7] Chapman, S. (2016). *Electric machines (6ta ed.)*. D.F. Mexico: Mc Graw Hill.
- [8] Dionisio, O., Martín, D., & Díaz, A. (2016). Single-phase motor of shaded poles. Quantitative and comparative study. *Ciencia y Tecnología*, 25-41.
- [9] Wildi, T. (2015). *Electrical Machines and Power Systems*. Mexico D.F: Pearson Educacion.
- [10] Davidson, E., Lamola, J., Xia, X., & Gitau, M. (2015). Desing and permformance analysis of a universal motor for industrial alarm systems. Mexico D.F: Research Gate.

Design and Analysis of Frequency Reconfigurable Antenna Embedding Varactor Diodes

El Mustapha Iftissane¹, Moulay Driss Belrhiti², Seddik Bri^{*2}, Jaouad Foshi¹, Nawfal Jebbor¹

¹ Electronics, Instrumentation and Measurement Physics Team, Faculty of Sciences and Technics, Moulay Ismail University of Meknes, Errachidia, Morocco

² Material and Instrumentations Team, Electrical Engineering Department, ESTM, Moulay Ismail University of Meknes, Meknes, 50000, Morocco

ARTICLE INFO

Article history:

Received: 07 September, 2019

Accepted: 22 November, 2019

Online: 16 December, 2019

Keywords:

Reconfigurable antenna

Frequency shifting

Patch Slots

Varactor diode

HFSS

ABSTRACT

In this paper, we present a broadband frequency tunable antenna embedding varactor diodes. The reference antenna structure is a square antenna of patch dimensions $[39,2 \times 39,2]$ mm², operating at a single resonance frequency 2.45GHz. The recommended procedure to achieve the frequency shifting is to etch rectangular slots on the patch and to embed two varactor diodes with different values in the etched slots. When the integrated diodes have the same values, the simulated results of the proposed structure show good frequency flexibility by covering the $[2.5 - 2.88]$ GHz band with reflection coefficient value (-36 dB). To improve the frequency agility of the proposed antenna and its performances, the embedding varactor diodes are separately optimized. The optimized antenna geometry and the integration of the varactor diodes positions enhance the performances of the proposed antenna and thus exploit the frequency band which is not covered by the reference antenna. Therefore, the obtained results indicate an improved tuning frequency behavior of the designed antenna which will be adopted to the dynamic changes of the environment allowing a good exploitation of the frequency spectrum.

1. Introduction

The reconfigurability is an important desired feature of modern agile radio-frequency (RF) systems for wireless and satellite communications [1]. The research on reconfigurable antennas, including pattern, frequency and polarization has received increasing attention in modern wireless communication systems [2-6]. Compared to the traditional antennas, whose characteristics are fixed for specific functionalities and which severely limit the level of intelligence that can be introduced into multifunctional wireless systems [7], the reconfigurable antennas offer the advantages of compact size, and an ability to support more than one wireless standard and multifunctional capability [1]. Reconfigurable antennas can address complex system requirements by modifying their geometry and electrical behavior [8]. There are two kinds of approaches to construct the reconfigurable antenna. The first is to adopt discrete elements, such as the varactor [1], [3] or PIN diodes [8-10] and the microelectromechanical systems (MEMS) switch [9]. The second

is to use tunable materials, including ferro-electric film, graphene, and liquid crystal (LC) [11]. Frequency reconfigurable antennas are, in fact, useful for wireless applications that require an efficient use of the electromagnetic spectrum and low interference adjacent channels [1]. Tunable varactor diodes are usually used to design electrically frequency reconfigurable antenna [12]. In the literature [13], [14], various microstrip reconfigurable antennas using varactor diodes have been reported. The reference antenna (RA) subject of this investigation has been studied and well reported in [15]. The frequency agility has been achieved at frequencies lower than the single resonant frequency of (RA) by integrating a varactor diode in the corner of the patch. To improve the performances of the reference antenna structure (RA) and make it able to operate at higher frequencies, rectangular slots have been etched on the patch. The incorporation locations of the embedded varactor diodes are then optimized using the HFSS software. The frequency agility is obtained by changing the values of the integrated varactor diodes. The performances of the new proposed antenna structure under different values of inclusion elements are examined. A wide tuning range of frequency from 2.5 GHz to 3 GHz is achieved.

*Corresponding Author: Seddik Bri Electrical Engineering Department, ESTM, Moulay Ismail University, briseddik@gmail.com

This paper consists of two principal parts. The first one is dedicated to the exposition of the (RA) and its dimensions (section 2.1), while the (section 2.2) shows the parameters of the proposed antenna structure. The second one is devoted to present the simulated results using the proposed structure. These simulated results are then compared with the published measurement data in [15].

2. Key parameters of designed antenna structure

2.1 Reference antenna Parameters

The High Frequency Structure Simulator software (HFSS) is a high-performance full-wave electromagnetic (EM) field simulator for arbitrary 3D volumetric passive device modeling. It employs the Finite Element Method (FEM), adaptive meshing, and brilliant graphics. It can be used to calculate parameters such as S Parameters, Resonant Frequency, and Fields. The HFSS software has demonstrated incomparable efficiency in the simulation of microwave structures thanks to its reliability and reproducibility. In this approach, we use the HFSS as a simulation tool to implement the antenna structure. The (RA) is a square patch with the following dimensions (39.2×39.2) mm² printed on a Duroid™ substrate of permittivity $\epsilon_r = 2.2$, whose dimensions are ($80 \times 80 \times 1.6$) mm³. The (RA) is also fed by an inset microstrip line which provides impedance matching. The basic geometry of the reference structure antenna is depicted in Fig. 1. The Fig. 1(a) shows the front view, while the side view of the (RA) is presented in Fig 1 (b).

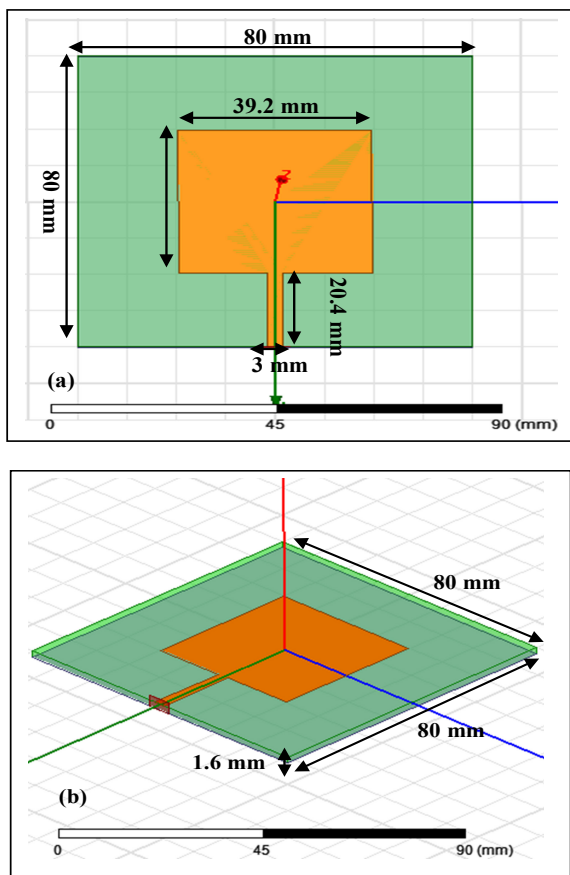


Figure 1: The basic geometry of the reference antenna (a): front view and (b): side view

As expected, the simulated reflection coefficient S_{11} of the (RA), using HFSS Software, indicates that the (RA) operates at a single frequency 2.45 GHz. The simulated value of S_{11} parameter is -17.02 dB. The bandwidth at -10 dB is 0.07 GHz. This result agrees well with the published measurement results in [15].

2.2 Proposed antenna structure

Admittedly, the goal of this paper is to achieve the shifting frequency exploiting the [2.45 – 3] GHz band because this part of the frequency spectrum is not exploitable by carrying out experimental measurements in [15]. To solve this problem, the proposed procedure for obtaining the frequency agility requires the integration of two varactor diodes on the square patch antenna. In order to insert the varactor diodes, the rectangular slots are etched on the radiating element and optimized using electromagnetic Ansoft HFSS software. The antenna design and performance parameters are discussed in the following sections. The proposed antenna structures are presented in Fig 2.

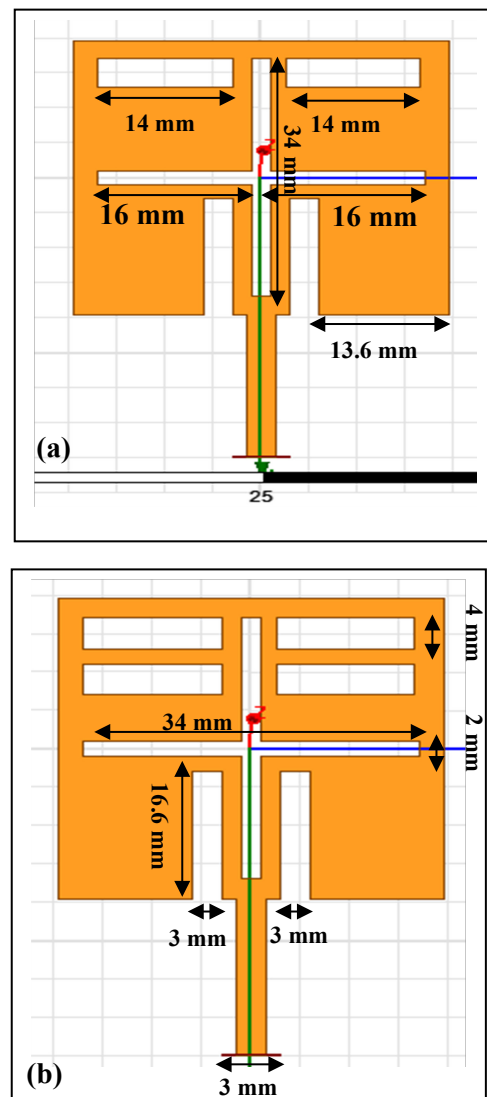


Figure 2: Proposed antenna structures with different dimensions of etched slots (a) patch with 2 slots in the superior part, (b) patch with 4 slots in the superior part

In order to study the mechanism of insulation and electromagnetic radiation in the two proposed structures, an analysis of surface currents is used. This analysis will enable us to adopt one of the two proposed structures as an investigation structure. It also makes it possible to locate the places of integration of the active elements in the adopted antenna structure. The current distributions on the radiated electric patches of the proposed structures are depicted in Fig 3. Note that, the current distributions in both proposed structures are presented at 2.45 GHz.

amplitudes of the current distributions on the radiated electric element patches of the two proposed structures, it is clear that the amplitude of the current distributions in Fig (3a) is higher than that in Fig (3b). This comparison justifies the choice of the structure shown in figure (3a) as the investigated structure.

3. Results and Discussion

3.1 Integration of varactor diodes in pair (i.e: Cd=Cg)

Since the varactor diode cannot be applied in the HFSS software, it is replaced by a lumped capacitor. Two varactor diodes are embedded on the radiated electric patch. The locations of the integrated active elements are optimized using HFSS. The positions are the two horizontal rectangles of dimensions (16 × 2) mm², as indicated in Fig 3a. The right varactor diode is noted by Cd, while the left diode is noted by Cg. By electronically controlling the biasing voltages distribution across the varactor loaded line, a reconfigurable frequency can be obtained. In order to show the achieved frequencies using the proposed antenna structure, the diagrams of reflection coefficient S₁₁ versus frequency for different values of the capacitances (same values of varactor diodes i.e. Cd=Cg) are presented in Fig 4.

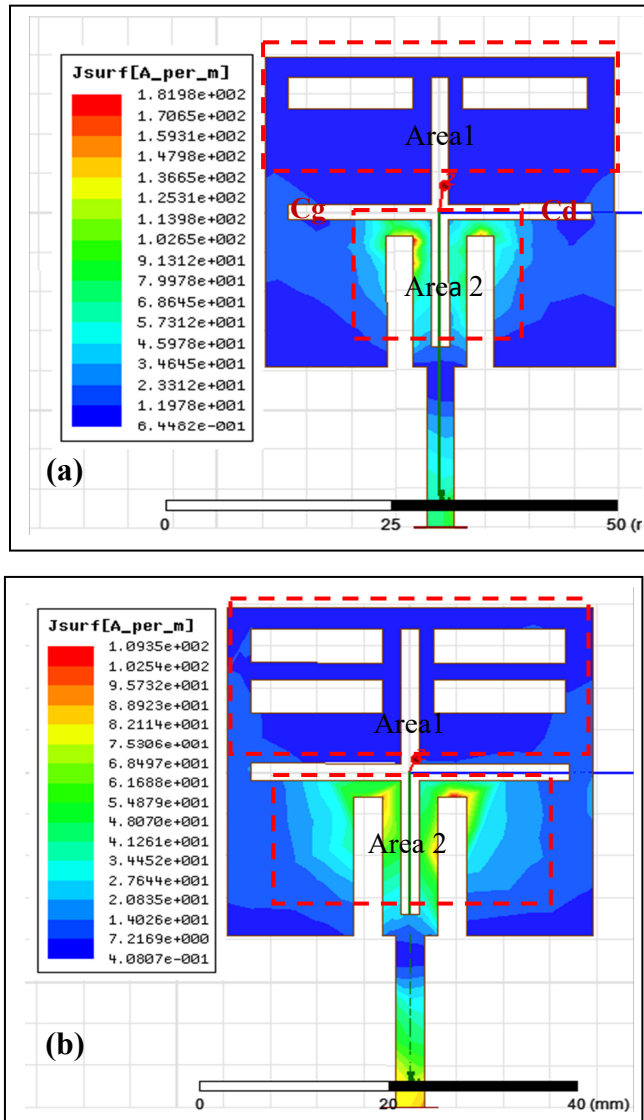


Figure 3: Current distributions on the radiated electric patches of the proposed structures at 2.45 GHz:

- (a) Current distributions of the patch with 2 slots,
- (b) Current distributions of the patch with 4 slots.

As presented in Fig 3a and Fig 3b, two areas can be identified on each structure. These areas are indicated in both Figs by two red dashed rectangles. On the one hand, the areas indicated by (area 2) are characterized by a very high distribution of excitation currents and they contribute to the radiation of the antenna. However, it is also clear that the areas indicated by (area 1) do not contain excitation currents. These areas are used for the integration of the varicap diodes. On the other hand, by comparing the

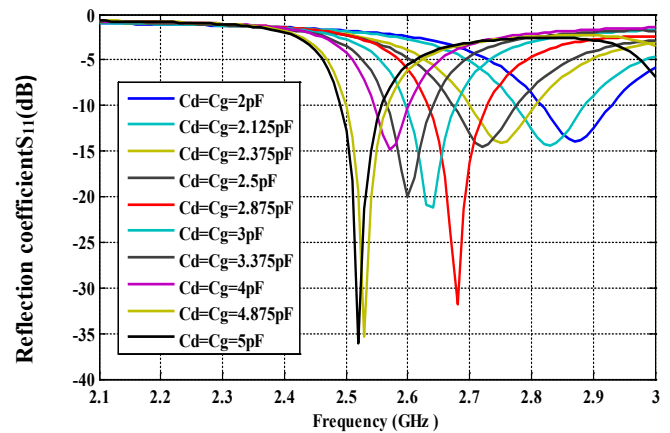


Figure 4: S₁₁ versus frequency for different values of varactor diodes (i.e: Cd=Cg)

The different values of the capacitances create different electrical lengths [16]. As a result, different resonance frequencies are obtained for the proposed antenna, which goes in line with the purpose of this article. As shown in Fig 4, frequency reconfigurability is achieved between 2.52GHz and 2.88 GHz. Many resonance frequencies with different bandwidths are achieved by changing the values of the pair varactor diodes i.e. (Cd=Cg). Table 1 displays the different achieved resonance frequencies as functions of the integrated capacitance values.

In this configuration, (i.e. the capacitances change the values in pair), the frequency agility is ensured in the frequency band [2.52 – 2.88] GHz and the reflection coefficient reach (-36 dB) for the operated frequency 2.52 GHz. It is also important to note that the evolution of the resonance frequency is inversely proportional to the values of the integrated diodes. For an experimental point of view, the integrated varactor diodes on the radiant element should be fed with the same reverse bias voltage.

Table 1: Different achieved resonant frequencies as functions of the integrated capacitance values

Capacitance value (pF)	Resonance Frequency (GHz)	Reflection coefficient S_{11} (dB)	Bandwidth (GHz) (-10dB)
$C_d=C_g=5$	2.52	-36.01	0.07
$C_d=C_g=4.875$	2.53	-35.42	0.07
$C_d=C_g=4$	3.57	-14.89	0.07
$C_d=C_g=3.375$	2.6	-19.99	0.08
$C_d=C_g=3$	2.64	-21.21	0.08
$C_d=C_g=2.875$	2.68	-31.79	0.08
$C_d=C_g=2.5$	2.72	-14.49	0.11
$C_d=C_g=2.375$	2.75	-14.12	0.11
$C_d=C_g=2.125$	2.83	-14.45	0.11
$C_d=C_g=2$	2.88	-13.81	0.11

3.2 Varactor diodes Effect on the antenna parameters

3.2.1 Effect on the radiation pattern

In an attempt to evaluate the effects of the integrated elements on the radiation pattern, the gain and the radiation efficiency, the evolutions of these parameters as functions of the integrated capacitance values are presented. For this purpose, the radiation patterns of the proposed antenna structure in the E($\varphi=0^\circ$) and H($\theta=90^\circ$) planes are simulated using HFSS software. The simulated radiation patterns at some achieved resonance frequency are shown in Fig 5a and Fig 5b.

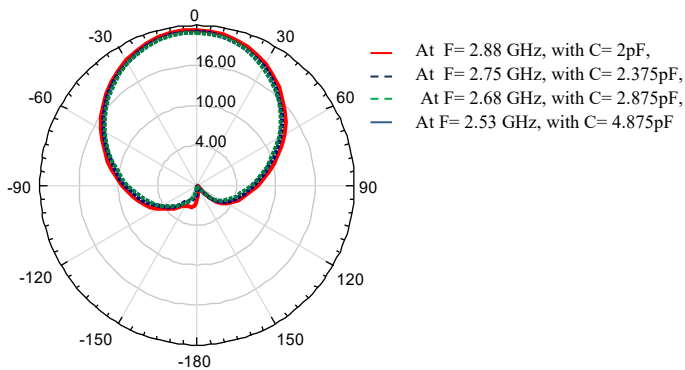


Figure 5 a : Simulated 2D radiation pattern E-Plan ($\varphi = 0^\circ$) at resonance frequencies of the proposed antenna

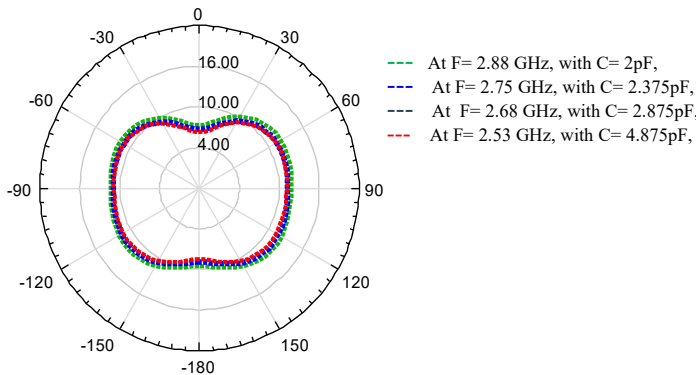


Figure 5 b: 2D radiation pattern on H-Plan ($\theta = 90^\circ$) at resonance frequencies of the proposed antenna

According to Figures 5a and 5b, it is clear that the diagrams in both planes E ($\varphi = 0^\circ$) and H ($\theta = 90^\circ$) are substantially identical. The radiation patterns in the two planes E and H show good stability despite the frequency agility achieved by the control of the integrated capacitance values.

3.2.2 Effect on the gain antenna

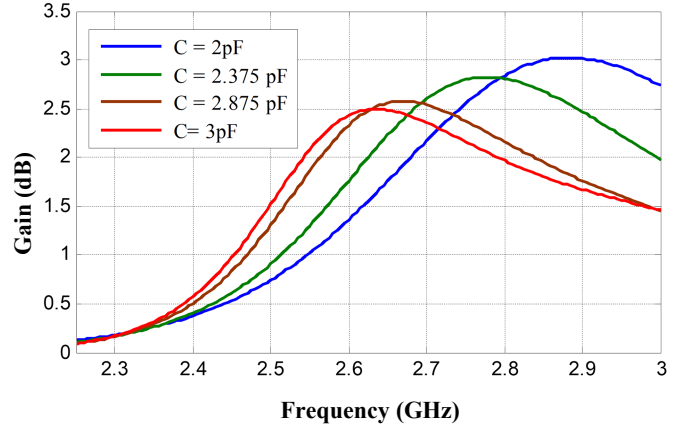


Fig 6 shows the gain (dB) of the proposed antenna structure at various achieved operating frequencies by the values control of the integrated capacities.

As indicated in Fig 6, the proposed antenna has an acceptable gain. The maximum gain is 3.02 dB when the capacitance value is fixed at $C=2\text{pF}$ with the resonance frequency $F=2.88\text{ GHz}$. It should be also noted that the gain value decreases as the integrated capacitance values increase. This increase is accompanied by a shift towards the resonance frequencies obtained close to 2.52 GHz.

3.2.3 Effect on the radiation efficiency

The radiation efficiency characteristics in (%) of the proposed antenna is calculated and illustrated in Fig 7.

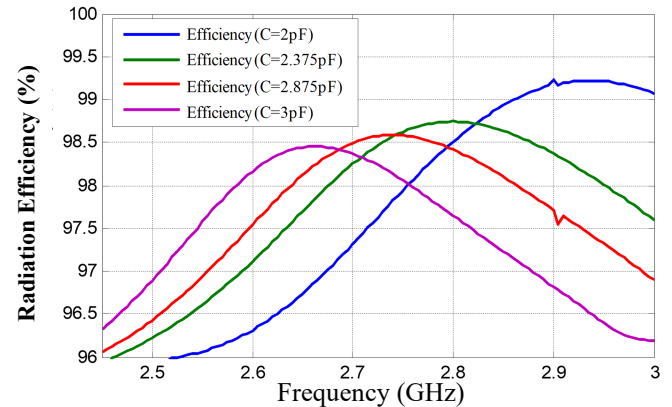


Figure 7: Radiation efficiency as function of integrated capacitance value

As depicted in Fig 7, the radiation efficiency of the proposed antenna resides within the range of 96 % and 99.25%. We also notice that when the capacitance value increases, the efficiency decreases. Note also that the radiation efficiency reaches its peak at each resonance frequency.

3.3 Integration of two varactor diodes with (Cd#Cg)

To shove the antenna to scan a large number of operating frequencies points, the values of the integrated varactor diodes are separately optimized (i.e. each diode may have a specific capacitance value). To this end, the simulated results of the reflection coefficient S_{11} as a function of frequency and capacitance values are presented in Fig 8.

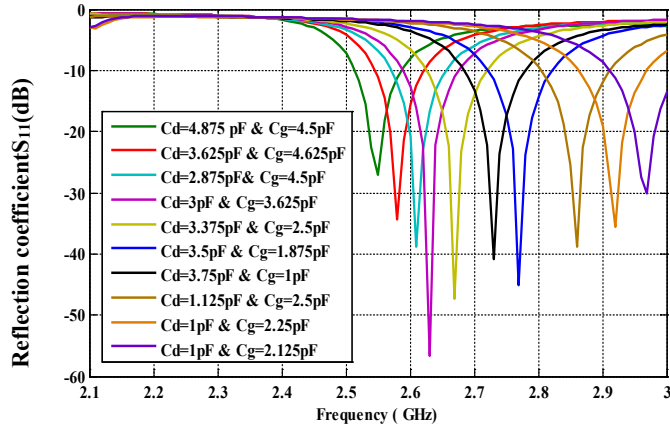


Figure 8: S_{11} versus frequency for different values of capacitance values

Fig 8 presents a good use of the frequency band which is ensured by varying separately the values of the integrated diodes. For the 2.63 GHz frequency, the S_{11} can reach a value of -56.04 dB. The obtained results show that the variation of the capacitance is more effective than the change of the physical size of the antenna. As indicated in Fig 8, each operated resonance frequency is associated with a specific capacitance value. To show the improvements assigned to the (RA), the simulated results (Table 2) of the proposed antenna are compared with the published measurements (Table 3) of the reference antenna [15]

Table 2: The achieved frequencies via simulation using proposed antenna

Simulation Results				
Capacitance value (pF)		Resonance Frequency (GHz)	Reflection coefficient S_{11} (dB)	Bandwidth (GHz) (-10dB)
Cd = 4.875	Cg = 4.5	2.55	-27	0.072
Cd = 3.625	Cg = 4.625	2.58	-34.38	0.076
Cd = 2.875	Cg = 4.5	2.61	-38.72	0.086
Cd = 3	Cg = 3.625	2.63	-56.04	0.087
Cd = 3.375	Cg = 2.5	2.67	-47.37	0.1
Cd = 3.5	Cg = 1.875	2.73	-40.48	0.097
Cd = 3.75	Cg = 1	2.77	-45.07	0.1
Cd = 1.125	Cg = 2.5	2.86	-38.81	0.107
Cd = 1	Cg = 2.25	2.92	-35.63	0.106
Cd = 1	Cg = 2.125	2.971	-29.3	+0.1

Hence, the results demonstrate that the separated optimization of the integrated varactor diodes, using the proposed antenna structure, yields good frequency flexibility on the frequency band [2.5 – 3] GHz. In addition, by comparing the obtained simulated results to the measurement results using the (RA), as indicated in table 2 and 3, the achieved frequencies are higher than the operated single frequency of the (RA), which are not obtained by the

measurement results in [15]. On the other hand, the bandwidths at -10 dB are larger than the measurement results. For an experimental purpose, it is necessary to feed each integrated varactor diode separately to obtain two different values of capacitances.

Table 3: Measurement Results of (RA) published in [15]

Measurement Results of (RA)			
Capacitance value (pF)	Resonance Frequency (GHz)	Reflection coefficient S_{11} (dB)	Bandwidth (GHz) (-10dB)
20	0.51	-42	0.05
9.6	0.75	-35	0.05
5.2	0.97	-16	0.05
3.1	1.17	-12	0.03
1.7	1.51	-10	0.025
1.3	1.7	-11	0.025
0.9	2.4	-12	0.05

To have the reliability of the obtained simulated results, we have compared them with references published in [16-19]. In this respect, Table 4 presents this comparison of the performances of our proposed antenna concerning the bandwidth, resonance frequency and reflection coefficient.

Table 4: Comparison of proposed antenna with published results

Antenna Ref	Bandwidth (%)	Resonance Frequency (GHz)	Reflection coefficient S_{11} (dB)
Antenna in [16]	4	2.5- 2.6	-15
Antenna in [17]	6.06	2.31	-20
Antenna in [18]	5.58	2.15 - 2.36	-20
Antenna in [19]	14.58	2.4 - 2.6	-45
Antenna in this work	28	2.5-3	-56.04

According to Table 4, we deduce that our antenna design can have a large band that can reach up to 28% [2.4 - 3.] GHz (UHF band), with a resonance frequency that varies between 2.5 GHz and 3 GHz; whereas other published structures do not exceed 15%. The proposed antenna has an important reflection coefficient (-56.04 dB) especially at the resonance frequency $f = 2.63$ GHz as well as a large band compared to the published antennas. The proposed structure allows varying its resonance frequency from 2.5 GHz to 3 GHz by controlling the integrated capacitance values.

4. Conclusion

This article has presented an analysis of the frequency reconfigurable square patch antenna. The proposed antenna structure achieves the desired frequency agility by integrating two varactor diodes on the rectangular slots that have been etched on the radiant element patch. The proposed antenna design has been examined for frequency reconfigurability; therefore, its performances have found a satisfactory comparison with the published results. When the two integrated varactor diodes are separately optimized, the frequency shifting allows a powerful sweep of the [2.5 – 3] GHz band. This part of the spectrum is not

exploitable by the reference antenna. This comparative study between our simulated results and the previously published results of the reference antenna will be completed in the next works by a real comparison between simulated and experimental results when we make a realization of the proposed structure.

References

- [1] Christos, G., Christodoulou, Y., Steven, A., and Scott, R.: "Reconfigurable Antennas for Wireless and Space Applications," *Proceedings of the IEEE*, 100, (7), pp 2250 – 2261. July 2012.
- [2] Qin P., Weily R., Guo, Y., and Liang, C., "Polarization Reconfigurable U-slot patch Antenna," *IEEE Trans. Antennas and Propagation*, 58, (10), pp 3383 – 3388, Octobre, 2010.
- [3] Bin, L., Benito S., Edward A. , and John, B., "A Frequency and Polarization Reconfigurable Circularly Polarized Antenna Using Active EBG Structure for Satellite Navigation," *IEEE Trans on Antennas and Propagation*, ,63, (1),pp 33 – 40, January 2015.
- [4] Qin, P., Guo, Y., Cai, E., Liang, C., "A Reconfigurable Antenna with Frequency and Polarization Agility", *IEEE Antennas Wireless Propagation Letters*, 10, pp 1373 – 1376, 2011.
- [5] Nghia, N., Leonard, H., Christophe, F., "A Frequency and Polarization-Reconfigurable Stub-loaded Microstrip Patch Antenna" *IEEE Trans. Antennas and Propagation*, 63, (11), pp 5235-5240, 2015.
- [6] Wei, L., Hang, W., "Polarization Reconfigurable Aperture-Fed Patch Antenna and Array," *IEEE Access*, April 2016, 4, pp 1510 – 1517.
- [7] Jay, Y., Pei-yuan, Q., Shu-lin, C., Wei, L., Richard W. Ziolkowski, "advances in reconfigurable antenna systems facilitated by innovative technologies," *IEEE*, 6, pp 5780 – 5794, 2018.
- [8] Chang, Y., Jea Hak K., Woo, J., Taejoon, P., Byungje, L., Chang, W., "Frequency-Reconfigurable Antenna for Broadband Airborne Applications," *IEEE Antennas and Wireless Propagation Letters*, , 13, (23), pp 189 – 192 , January 2014.
- [9] Shakhirul, S., Muzammil, J., Abdul Hafizh, I., Muhammad K., Philip, N., Mohamad, K., Rahim, M., Thennarasan, S., Mohamed, N., Jais, M., Ping, J., "Textile Antenna With Simultaneous Frequency and Polarization Reconfiguration for WBAN," *IEEE Access*, 6, pp 7350 – 7358, March 2018.
- [10] Rocktopal, B and Nidhi, S., "A Frequency Reconfigurable Meandered Slot Cut Rectangular Patch Antenna Using PIN Diodes *Progress In Electromagnetics Research C*,"77, pp 81–89, 2017.
- [11] Yamagajo, T, Koga, Y., "Frequency reconfigurable antenna with MEMS switches for mobile terminals," *IEEE-APS Topical Conference on Antennas and Propagation in Wireless Communications*, October, 2011.
- [12] M. T. Riaz, Y. Fan, J. Ahmad, M. A. Khan, and E. M. Ahmed, "Research on the Protection of Hybrid HVDC System," in *2018 International Conference on Power Generation Systems and Renewable Energy Technologies (PGSRET)*, 2018, pp. 1–6.
- [13] Seung-Bok, B., et al, "Reconfigurable Ground-Slotted Patch Antenna Using PIN Diode Switching," *ETRI Journal*, 29, (6), pp, 832 -834, December 2007.
- [14] Rouissi, I., Floc'h, J., Trabelsi, H., "Design of Frequency Reconfigurable Multiband Meander Antenna Using Varactor Diode for Wireless Communication, *International Journal of Advanced Computer Science and Applications*," 8, (3), pp, 159 – 164, 2017.
- [15] I Rouissi, I., Floc'h, J., Rmili, H., Trabelsi, H., "Design of a frequency reconfigurable patch antenna using capacitive loading and varactor diode, 9th European Conference on Antennas and Propagation," *EuCAP 2015*.
- [16] Sung Woo Lee, Youngje Sung, "A Polarization Diversity Patch Antenna with a Reconfigurable Feeding Network", *Journal of Electromagnetic Engineering and Science*, vol. 15, no. 2, 115~119, apr. 2015.
- [17] Seung-Bok Byun, Jeong-An Lee, Jong-Hyuk Lim, and Tae-Yeoul Yun, "Reconfigurable Ground-Slotted Patch Antenna Using PIN Diode Switching", *ETRI Journal*, Volume 29, Number 6, December 2007.
- [18] Suresh Kumar M and Yogesh Kumar Choukiker, "Study of Frequency and Polarization Reconfigurable on Square Patch Antenna ", *International Journal of Engineering and Manufacturing Science*. Volume 8, Number 1 pp. 145-149, 2018.
- [19] Mustafa Murat Bilgiç and Korkut YeLin, "Polarization Reconfigurable Patch Antenna for Wireless Sensor Network Applications", *International Journal of Distributed Sensor Networks*, 2013.

A Multi-Objective Voltage Optimization Technique in Distribution Feeders with High Photovoltaic Penetration

Temitayo Olayemi Olowu, Mohamadsaleh Jafari, Arif Sarwat *

Department of Electrical and Computer Engineering, Florida International University, Miami, FL 33174

ARTICLE INFO

Article history:

Received: 29 September, 2019

Accepted: 03 November, 2019

Online: 30 December, 2019

Keywords:

Multi-objective Optimization

Smart Inverters

Voltage Control

Photovoltaic Systems

Volt-VAR Optimization

ABSTRACT

With increasing photovoltaic (PV) penetration on distribution feeders, voltage functions is always a challenge. To control these variations due to the intermittent nature of PV generation, many utility companies use the traditional voltage regulating devices such as ON/OFF load tap changers, voltage regulators, switched capacitor banks and reactors. The use of smart inverters (SI) has been reported to provide a more effective and economical way of voltage regulation on distribution feeder. It then becomes necessary to optimally control the operation of these traditional voltage regulating devices and the SIs. This paper presents a multi-objective technique that minimizes the voltage fluctuation (by implementing conservative voltage reduction), the overall system active power losses and the amount of reactive power injection from the capacitor banks with various constraints on the smart inverter reactive power injection and voltage regulator switching. The proposed algorithm is tested on an IEEE 34 node system with six units of 300kW (400kVA SIs) PVs integrated using real data from an existing 1.4MW PV plant located at FIU. The Pareto optimization results of the proposed algorithm show the various optimal values of the PVs power factor, the voltage regulator settings and the capacitor reactive power injection. Using one of the Pareto optimal solutions, the results show that the system bus voltage profiles, total system power losses and capacitor reactive power injection were effectively optimized.

1 Introduction

For environmental reasons, there has been a consistent increase in global installation of photovoltaic (PV) systems. This is further facilitated by the declining cost of PV modules over the years [1–5]. The increase in PV installations is evident as the financial investments in PV installation globally is also on the rise. The increase in levels of PV penetration have lead to several challenges which include reverse power flow, voltage control issues, power quality issues [6–9] (voltage and current harmonics, flicker, momentaries), protection coordination problems, and possible increase in system losses. [3, 10–12]. Of these issues, voltage control is one of the most important and of concern to utility companies. Traditionally, utility companies uses the legacy devices such as reactors, voltage regulators (VR), ON/OFF load tap changers (OLTC), and switched capacitor bank for voltage control [13, 14]. With the integration of intermittent renewable energy resources such as PV systems, the need for fast and more effective voltage control becomes imperative. According to IEEE 1547-2018 [15, 16], inverter-based DERs such as PVs are allowed to participate in feeder voltage regulation. Ac-

ording to [11, 17, 18], the use of smart inverters (SIs) could provide a more effective and economical way of voltage control especially at high levels of penetration of inverter-based DERs. Voltage optimization can be carried out with the use of several components in a distribution network. Several devices such as voltage regulators, OLTC, switched capacitor banks, reactors, energy storages and recently smart inverters (SI). SIs can be used to make significant impact on the voltage profile of the distribution system using the power factor control mode or the Volt-VAR/Watt control mode. With all these devices simultaneously present in the distribution network, there is an obvious need for optimizing their operation and also their interaction in the system. Therefore the optimal coordination of the control operations of the smart inverter and these existing legacy devices becomes necessary. This paper presents a multi-objective voltage control an optimization algorithm which is an extension of a previous work done by the authors in [19]. In order to take the advantage of the reactive power injection by the smart inverter, the reactive power injection by the switched capacitor banks are minimized as one of the optimization objectives. The smart inverters are set to constant power factor mode with the optimal value selected

* Corresponding Author: Arif Sarwat, Department of Electrical and Computer Engineering, Florida International University, Miami, FL 33174, United States, Email: asarwat@fiu.edu

between 0.6 – 1 to allow for reactive power injection. The VR and OLTC switching constraints are set within ± 16 . The other objective functions are to flatten the nodal voltage profile towards the lower threshold of 0.95 pu and minimize the overall active power losses in the network. The rest of the paper is organized as follows: Section 2 presents a brief review of existing voltage control and optimization techniques; the proposed optimization algorithm and its formulation is presented in Section 3; Section 4 describes the feeder used as case study and the simulation set up; Section 5 presents the simulation results and their analyses; while Section 6 concludes the paper.

2 Voltage Control and Optimization Methods

Several voltage control techniques have been proposed and reported in literature. Active distribution networks allow for bidirectional flow of active and reactive power due to the integration of distributed renewable energy generators. An evolutionary-based algorithm for LTC and shunt capacitor Scheduling was proposed by authors of [20]. The study was done to minimize the active power loss of the system while keeping the operation of the voltage control devices and the total harmonic distortion within limits. An NREL report and publication by Ding et al [21, 22] developed an iterative optimization algorithm that coordinates the use of SI, LTCs and capacitor banks for optimal voltage regulation while implementing conservative voltage reduction technique as a means of mini zing the total system losses. The impact of the proposed optimization algorithm on the system’s power quality was also analyzed. Reference [23] developed three fuzzy logic controllers that control the OLTC switching, the reactive power sharing (to enable a relaxation of the OLTC switching operation) and reduce the active power curtailment from the integrated distributed generation. Similar to [23], authors of [24] proposed a Volt-VAR optimization (VVO) algorithm that relax the voltage regulators and LTC operations as well as minimizing the amount of PV generation curtailed. The proposed VVO multistage algorithm was compared to the multi-objective VVO. Most of the previously published papers did not optimally choose the SI setting such as its power factor, minimization of reactive power injection by the shunt capacitor banks by allowing more reactive power injection by the SIs, and flattening the system’s voltage profile and implementing conservation voltage reduction by pushing the nodal values to 0.95 pu. To address these research gaps, this paper proposes a multi-objective optimization algorithm that flattens the node voltage profile, minimizes the power loss in the network as well as minimizing the reactive power injection by the capacitor banks by optimally selecting the power factors of the SIs , the tap position of the voltage regulators and LTC as and the amount of reactive power to be injected by the capacitor banks.

3 Formulation of Proposed Optimization Algorithm

Objective functions

The first objective OF_1 of the proposed optimization algorithm is to flatten the voltage profile of the network as much as possible

and also to make the nodal voltages close to the lower boundary of the ANSI C84.1 voltage range of 0.95 pu. The benefit of this approach is to take the advantage of conservative voltage reduction which allows the total load on the network to be reduced by simply lowering the nodal voltages.

$$OF_1 = \min \sum_{j=1}^{N_n} \left| \left((V_j^{min} - V_{j,t}) + |\alpha V_{j,t} - V_j^{max}| \right) \right| \quad (1)$$

where V_j^{min} and V_j^{max} are the minimum and maximum allowable nodal voltages respectively as expressed in equation (4), while α is a factor which is used to make the nodal voltage $V_{j,t}$ close to V_j^{min} .

Objective 2 (OF_2) is minimizes the total active power losses in the network.

$$P_{loss}^{total} = P_{loss}^{trans} + P_{loss}^{lines} \quad (2)$$

$$OF_2 = \min |P_{loss}^{total}|$$

where P_{loss}^{trans} is the sum of the active power loss in the transformers and P_{loss}^{lines} is the sum of the active power loss in the lines.

The third objective (OF_3) of this work is to minimize the total amount of reactive power injected by the two capacitor banks connected to buses 844 and 848.

$$OF_3 = \min \sum_{cb=1}^{N_c} Q_{cb} \quad (3)$$

Where Q_{cb} is the capacitor bank reactive power injection and N_c is the total number of capacitor banks in the network.

Constraints Formulation

Bus voltage constrains is set to be within the ANSI C84.1 standards.

$$V_j^{max} \geq V_{j,t} \geq V_j^{min} \quad (4)$$

$$1.05pu \geq V_{j,t} \geq 0.95pu$$

Capacitor bank VAR and switching constrains is given as equation (5). The maximum reactive power injection by these capacitors are 300kVAR and 450kVAR according to the values in the feeder parameters.

$$|Q_{cbmax}^j| \geq |Q_{cb}^j| \quad (5)$$

Typical VRs and OLTCs have 32 tap steps. For each tap step, the change in voltage is typically 0.625%.

$$- 16 \leq Tap_{vr,t} \leq +16 \quad (6)$$

To enable the SIs inject some reactive power into the network in order to allow for some voltage control by the SI, the PF values of the SI are set as variable for the optimization in other to get their optimal values.

$$0.6 \leq PV_{PF} \leq 1 \quad (7)$$

Table 1: PV Specifications

PVs	Maximum Power (kW)	Inverter (kVA)	Phases	Default PF
PV1 and PV5	300	400	1	0.8
PV2, PV3, PV4 and PV6	300	400	3	0.8

4 Feeder Test Case and Simulation

In order to validate the effectiveness of the proposed multi-objective optimization technique, six PVs with specifications as shown in table 1 are integrated to an IEEE 34 node distribution feeder (as shown in figure 1). For each of the PVs, a minute resolution actual global horizontal irradiance and temperature data (as shown in figures 2 and 3 respectively) are used as input to estimate the power output of the six PVs. The PV locations were selected a little farther from the substation transformer where there is a potential for some voltage regulation issues.

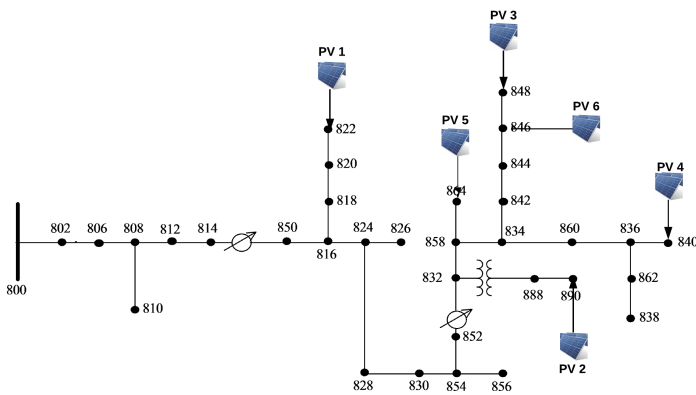


Figure 1: IEEE 34 node test feeder with PV locations

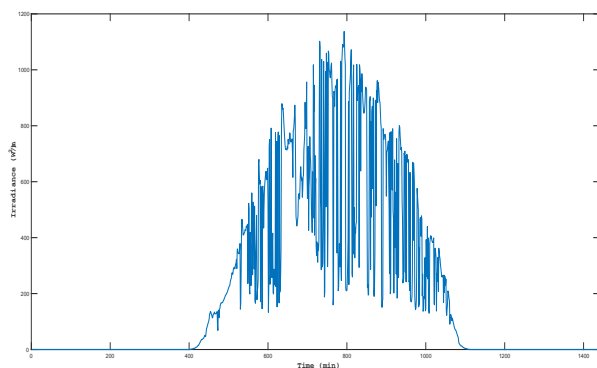


Figure 2: 1-minute resolution global horizontal irradiance profile of the location used for the simulation

5 Simulation results and Analysis

The PV integrated IEEE feeder was modelled using the OpenDSS software with the optimization algorithm developed with MATLAB. A time series simulation with a total time step of 1440 minutes was

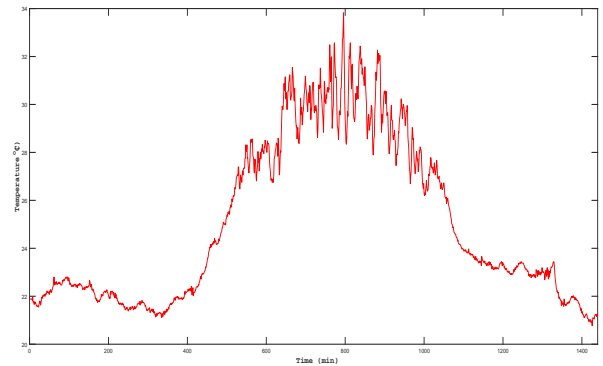


Figure 3: 1-minute resolution temperature data of the location used for the simulation

carried out. Based on the three objective functions formulated, the Pareto fronts for the 24 hour optimization are plotted as shown in figures 4, 5 and 6. The Pareto fronts show the several optimal solutions available for the multi-objective optimization.

Based on the objective of highest priority, the values of the variables which are the tap settings of the LTCs, power factor of the PVs, reactive power injection of the capacitor banks, can be selected. For example, if the objective of highest priority is to have the minimum amount of losses (OF_2) in the network the Pareto optimal values with their corresponding decision variables is as presented in tables 2 and 3. The loss minimization objective presented in tables 2 and 3 show the optimal values of the tap settings of the LTCs, power factor of the PVs, reactive power injection of the capacitor banks that will achieve the minimum amount of losses in the network. Using the optimal values acquired from the optimization algorithm, the nodal voltages of the network were simulated. The nodal voltages of buses (single phase buses) 822 and 864 are as shown in figures 9a-9b respectively while the nodal voltage for buses 840, 846, 848 and 890 are as shown figures 7, 8, 10 and 11 respectively.

The voltage profile on these buses clearly show the effectiveness of the proposed optimization algorithm. The bus voltage profiles were adequately reduced without going below the ANSI C84.1 standard voltage level of $0.95 pu$. As mentioned earlier, this was done to implement the benefits of Conservative voltage reduction which can be effectively used to reduce the total load on the network as well as minimize the total system power loss. Also, as shown in figure 11, the un-optimized voltage profile of bus 890 was increased from less than the minimum $0.95 pu$ to values above the minimum $0.95 pu$.

Figure 12 show the un-optimized and optimized total system losses. The figure clearly shows the there is consistent reduction in the overall system losses after optimization. Figure 13 shows the capacitor reactive power with and without the use of the proposed optimization algorithm. The value of the $kVAR$ injection by the capacitor banks were consistently reduced which further shows the effectiveness of the proposed optimization algorithm.

6 Conclusions

With the consistent rise in PV penetration on distribution feeders, effective voltage regulation and optimization using Volt-VAR control becomes very important. This paper presented a multi-objective optimization using the existing network legacy devices (switched

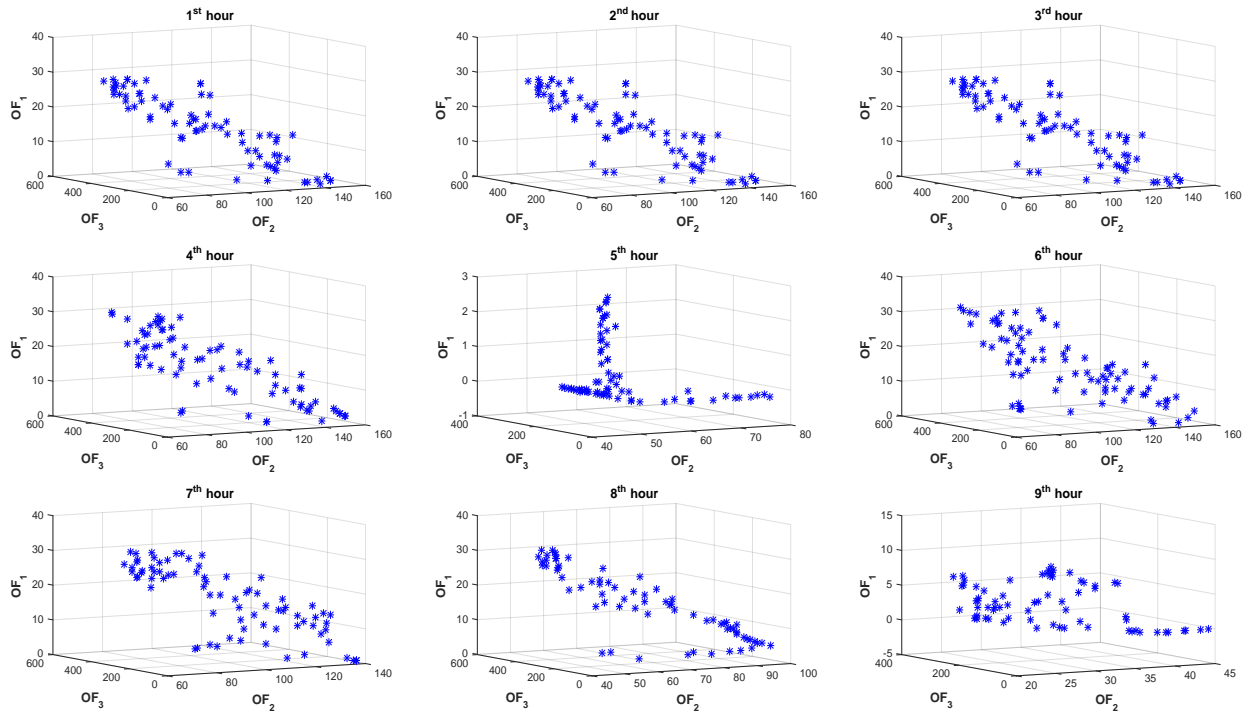


Figure 4: Hourly Pareto optimization curve for the optimized objective functions

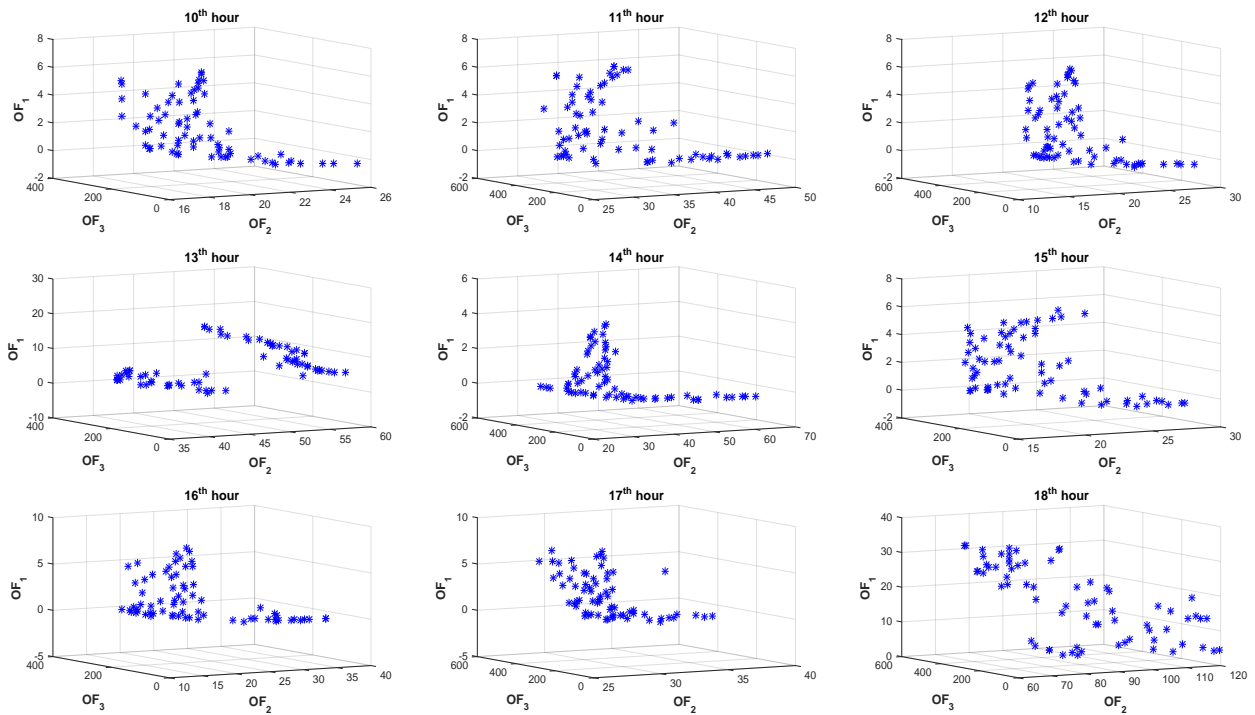


Figure 5: Hourly Pareto optimization curve for the optimized objective functions

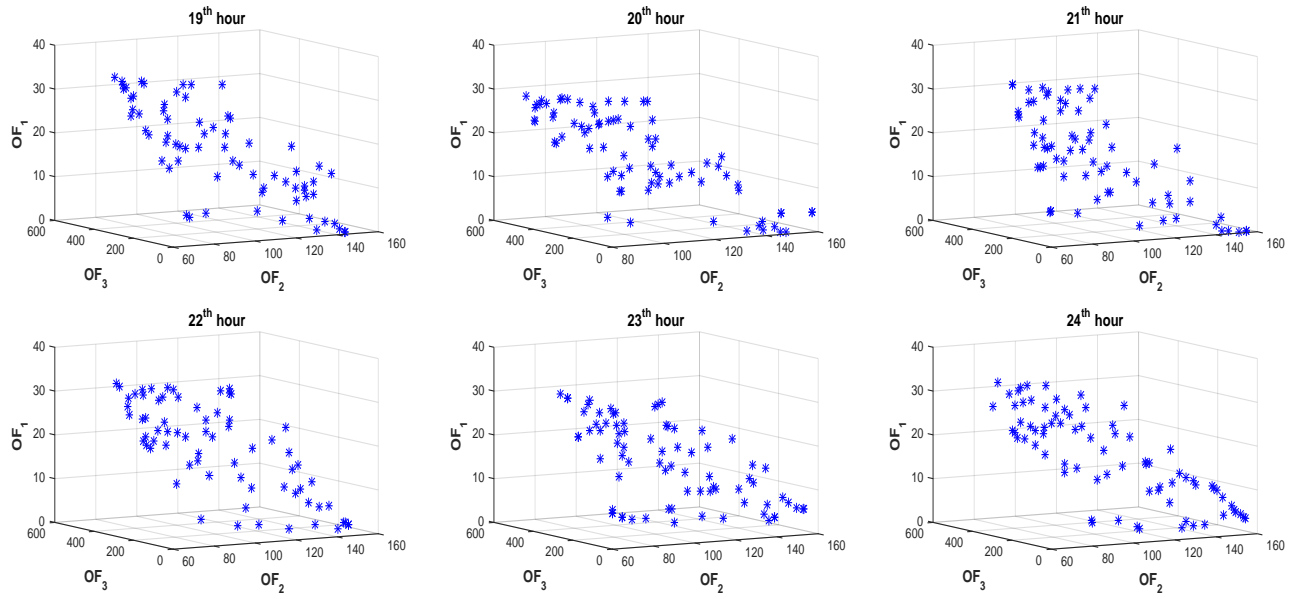


Figure 6: Hourly Pareto optimization curve for the optimized objective functions

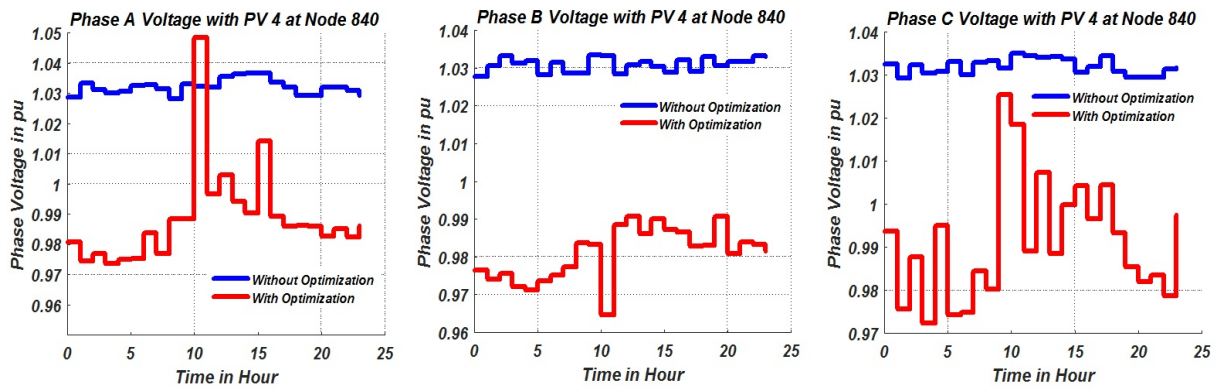


Figure 7: Voltage Profile of Node 840

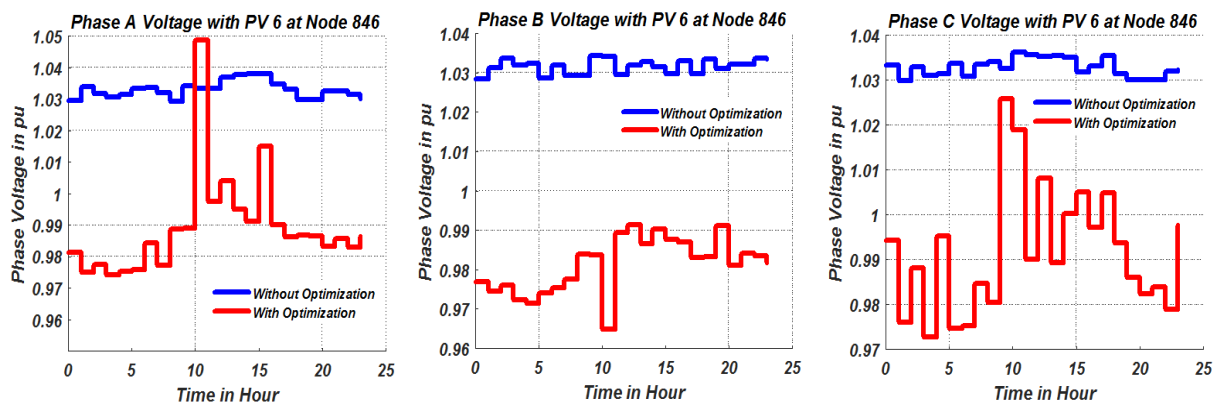
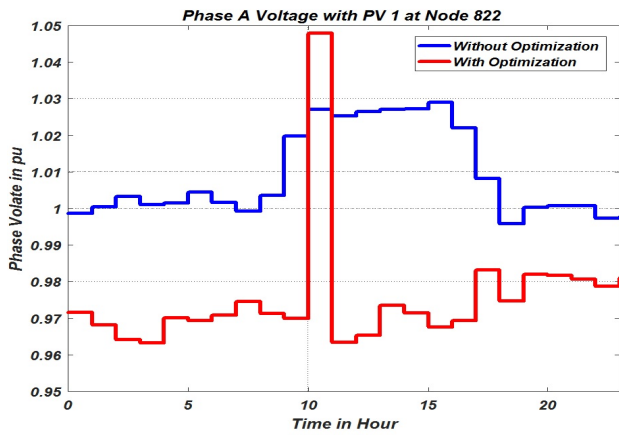
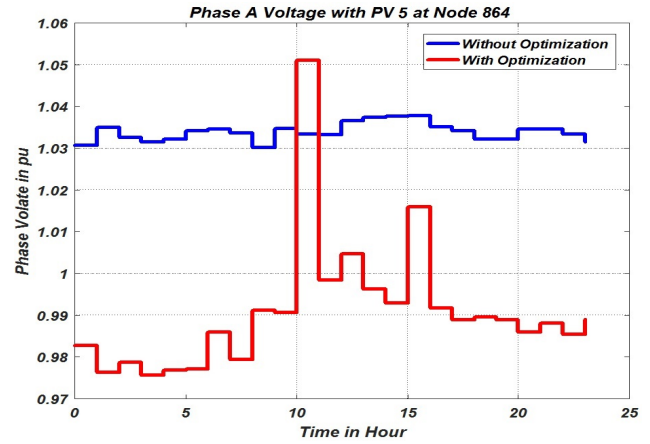


Figure 8: Voltage Profile of Node 846



(a) Voltage Profile of Node 822



(b) Voltage Profile of Node 864

Figure 9: Voltage profiles of Nodes 822 and 864

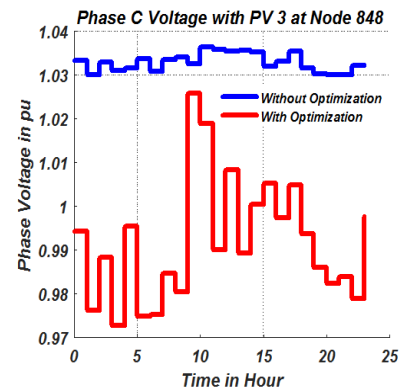
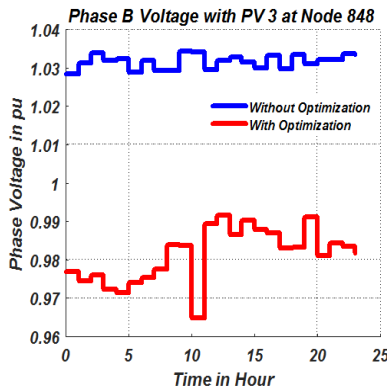
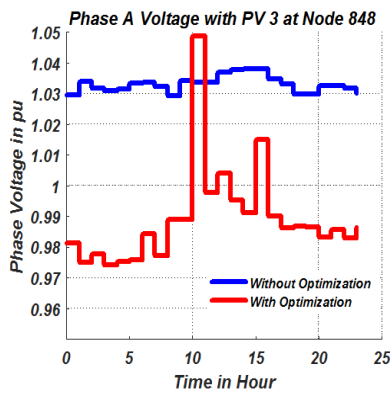


Figure 10: Voltage Profile of Node 848

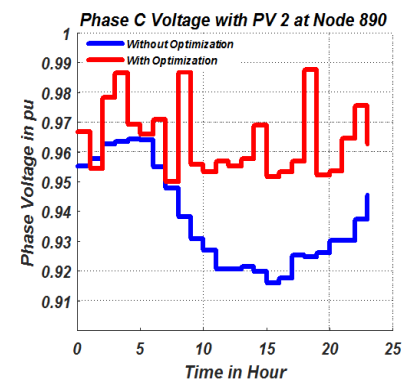
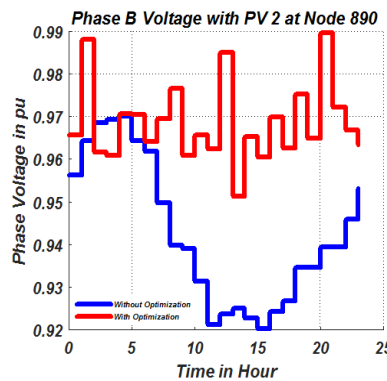
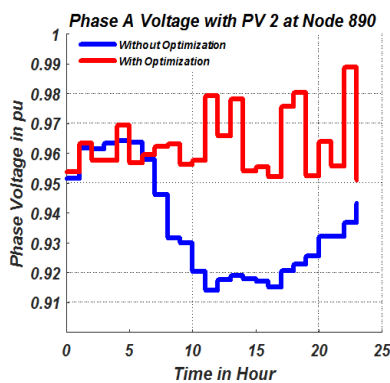


Figure 11: Voltage Profile of Node 890

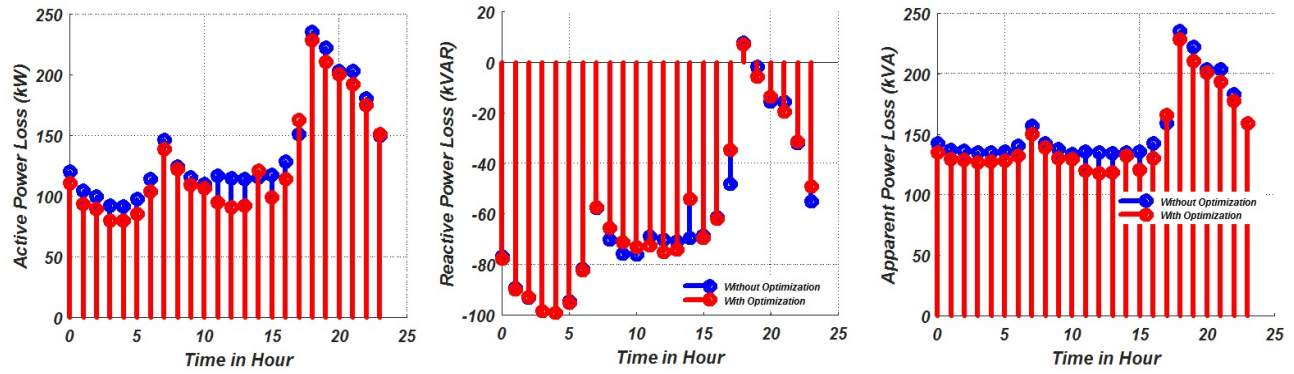


Figure 12: Hourly losses in the system

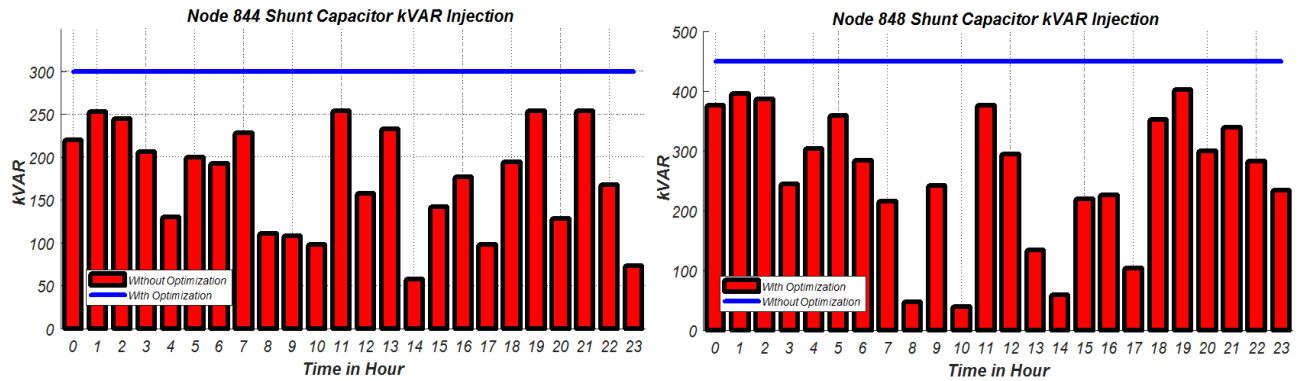


Figure 13: kVAR injection on nodes 844 and 848 by shunt capacitors

Table 2: Hourly Pareto optimal values with minimum system losses

Hour	OF ₁	OF ₂ (kW)	OF ₃ (kVAR)	VR ₁ (pu)			VR ₂ (pu)		
				Ph _A	Ph _B	Ph _C	Ph _A	Ph _B	Ph _C
1	29.2225	77.8766	483.3489	0.9250	0.9500	0.9563	0.9028	0.9083	0.9093
2	29.2225	77.8766	483.3489	0.9250	0.9500	0.9563	0.9028	0.9083	0.9093
3	29.2225	77.8766	483.3489	0.9250	0.9500	0.9563	0.9028	0.9083	0.9093
4	30.5524	76.6284	458.7750	0.9250	0.9563	0.9563	0.9043	0.9162	0.9114
5	2.6370	42.8064	26.2413	1.0063	0.9625	1.000	0.9913	0.9903	0.9771
6	32.0493	75.6853	560.9548	0.9000	0.9438	0.9063	0.9406	0.9186	0.9094
7	30.4924	78.3439	540.5442	0.9125	0.9125	0.9250	0.9487	0.9086	0.9580
8	31.9572	46.2742	424.1565	0.9125	0.9188	0.9000	0.9081	0.9156	0.9031
9	6.9547	23.7373	341.3215	0.9938	1.0063	0.9625	0.9567	0.9528	0.9406
10	5.5729	17.0715	282.4728	0.9875	0.975	0.9813	1.0312	0.9834	0.9344
11	6.2144	26.3293	291.0744	0.9750	0.9938	0.9750	0.9900	0.9558	0.9468
12	5.5438	14.4402	208.2059	1.0500	1.0000	0.9750	1.0365	0.9530	0.9344
13	5.9157	38.151	275.5213	0.9813	0.9938	1.0125	0.9844	0.9778	0.9341
14	3.6769	23.0707	109.9043	1.0188	0.9563	0.9938	1.0098	0.9844	0.9509
15	5.1211	15.9318	245.9954	1.0000	1.0063	1.0063	1.0099	0.9411	0.9156
16	5.797	12.5233	228.1546	1.0688	0.9688	0.9500	1.0213	0.9782	0.9541
17	6.4897	25.0358	299.8558	0.9813	1.0250	1.0188	0.9703	0.9342	0.9021
18	33.58	66.7876	466.7909	0.9000	0.9000	0.9000	0.9342	0.9468	0.9233
19	33.5301	75.1029	562.8816	0.9000	0.9063	0.9063	0.9594	0.9022	0.9405
21	32.9089	74.7385	494.4018	0.9063	0.9250	0.9188	0.9460	0.9031	0.9085
22	32.3954	77.4375	566.4084	0.9188	0.9063	0.9	0.9578	0.9219	0.9280
23	29.8817	79.9226	576.6802	0.9063	0.9438	0.925	0.915	0.9562	0.9154
24	33.4353	73.2124	496.9962	0.9000	0.9188	0.9313	0.9275	0.9086	0.9094

Table 3: Hourly Pareto optimal values with minimum system losses

Hour	Cap ₁ (kVAR)	Cap ₂ (kVAR)	PV ₁ (pu)	PV ₂ (pu)	PV ₃ (pu)	PV ₄ (pu)	PV ₅ (pu)	PV ₆ (pu)
1	224.9997	258.3492	0.7473	0.6684	0.7505	0.8664	0.7011	0.7987
2	224.9997	258.3492	0.7473	0.6684	0.7505	0.8664	0.7011	0.7987
3	224.9997	258.3492	0.7473	0.6684	0.7505	0.8664	0.7011	0.7987
4	251.9337	206.8413	0.7418	0.8002	0.7258	0.8058	0.7102	0.8987
5	14.2472	11.9942	0.9885	0.8909	0.9125	0.9063	0.9232	1.0000
6	245.1979	315.7568	0.8264	0.8950	0.6728	0.9998	0.6260	0.9511
7	214.3476	326.1966	0.7864	0.7001	0.6404	0.8971	0.7616	0.9258
8	274.3781	149.7784	0.7423	0.6425	0.9912	0.6334	0.8202	1.000
9	186.6092	154.7122	0.9425	0.6218	0.9984	0.9275	0.9818	1.0000
10	156.2404	126.2324	0.9636	0.7052	0.9941	0.917	0.9563	1.0000
11	162.369	128.7054	0.9503	0.6230	0.9753	0.8125	0.97	1.0000
12	109.2072	98.9987	0.9600	0.7317	0.9335	0.8969	0.9441	1.0000
13	122.0062	153.5151	0.9180	0.6195	0.8228	0.8295	0.9041	0.9102
14	26.4984	83.406	0.9811	0.8656	0.9427	0.9261	0.9378	1.0000
15	158.5989	87.3964	0.9625	0.7206	0.982	0.8842	0.9549	1.0000
16	141.6355	86.5191	0.9626	0.7743	0.9764	0.907	0.9592	1.0000
17	248.5619	51.2939	0.9468	0.6161	0.9694	0.8809	0.9735	1.0000
18	258.3798	208.411	0.7905	0.7331	0.9245	0.9227	0.6792	0.9354
19	239.9177	322.9638	0.9139	0.9348	0.8009	0.6829	0.9638	0.9188
20	273.3147	292.659	0.9998	0.9995	0.9999	0.9953	0.9777	0.9625
21	66.8531	427.5486	1.0000	0.9572	0.9994	0.7732	0.8599	0.9279
22	279.084	287.3244	0.9844	0.8301	0.9429	0.9452	0.898	0.9918
23	259.5105	317.1697	0.8380	0.8885	0.7520	0.6924	0.9566	0.7904
24	231.0427	265.9535	0.8280	0.7944	0.9795	0.9783	0.8495	0.9990

capacitor banks, voltage regulators and LTCs) and respective power injection from smart inverters. The proposed algorithm minimizes the voltage fluctuation (by implementing conservative voltage reduction), the total system losses, and the amount of reactive power injection by the switched capacitor banks. The Pareto optimization results showed that by selecting the objective of highest priority, the values of the voltage regulators' tap position, reactive power injection from the capacitor banks and the power factor value of the smart inverters can be effectively selected. Using one of the Pareto optimal solutions, the bus voltage profiles, system power loss and the capacitor bank reactive power injection were simulated. The results showed the effectiveness of the proposed multi-objective algorithm.

Acknowledgment The work is a outcome of the research supported by the U.S. National Science Foundation under the grant Numbers 1553494 and 1441223.

References

- [1] International Renewable Energy Agency. Data and Statistics - IRENA Resource. [Online]. Available: <https://www.irena.org/en/solar>
- [2] T. Olowu, H. Jafari, S. Dharmasena, and A. I. Sarwat, "Photovoltaic fleet aggregation and high penetration: A feeder test case," in *SoutheastCon 2019*, April 2019, pp. 1–6.
- [3] T. O. Olowu, A. Sundararajan, M. Moghaddami, and A. I. Sarwat, "Fleet aggregation of photovoltaic systems: A survey and case study," in *2019 IEEE Power Energy Society Innovative Smart Grid Technologies Conference (ISGT)*, Feb 2019, pp. 1–5.
- [4] A. Sundararajan, T. O. Olowu, L. Wei, S. Rahman, and A. I. Sarwat, "Case study on the effects of partial solar eclipse on distributed pv systems and management areas," *IET Smart Grid*, vol. 2, no. 3, pp. 477–490, 2019.
- [5] F. Ariyo, B. Famutimi, T. Olowu, S. Akintade, and A. Abbas, "Web-based application for the sizing of a photovoltaic (pv) solar power system," *American J. Eng. Res. (AJER)*, vol. 5, pp. 219–222, 2016.
- [6] S. Rahman, M. Moghaddami, A. I. Sarwat, T. Olowu, and M. Jafaritalarposhti, "Flicker estimation associated with pv integrated distribution network," in *SoutheastCon 2018*, April 2018, pp. 1–6.
- [7] A. Sundararajan, T. O. Olowu, L. Wei, S. Rahman, and A. I. Sarwat, "Case study on the effects of partial solar eclipse on distributed pv systems and management areas," *IET Smart Grid*, May 2019. [Online]. Available: <https://digital-library.theiet.org/content/journals/10.1049/iet-stg.2019.0002>
- [8] M. Jafari, T. O. Olowu, A. I. Sarwat, and M. A. Rahman, "Study of smart grid protection challenges with high photovoltaic penetration," in *2019 North American Power Symposium (NAPS)*, Oct. 2019, pp. 1–6.
- [9] A. I. Sarwat, A. Sundararajan, I. Parvez, M. Moghaddami, and A. Moghadasi, "Toward a smart city of interdependent critical infrastructure networks," in *Sustainable Interdependent Networks*. Springer, 2018, pp. 21–45.
- [10] T. Olowu, A. Sundararajan, M. Moghaddami, and A. Sarwat, "Future challenges and mitigation methods for high photovoltaic penetration: A survey," *Energies*, vol. 11, no. 7, p. 1782, 2018.
- [11] M. Chamana, B. H. Chowdhury, and F. Jahanbakhsh, "Distributed control of voltage regulating devices in the presence of high pv penetration to mitigate ramp-rate issues," *IEEE Transactions on Smart Grid*, vol. 9, no. 2, pp. 1086–1095, March 2018.
- [12] A. Anzalchi, A. Sundararajan, A. Moghadasi, and A. Sarwat, "High-penetration grid-tied photovoltaics: Analysis of power quality and feeder voltage profile," *IEEE Industry Applications Magazine*, vol. 25, no. 5, pp. 83–94, 2019.

- [13] M. Jafari, T. O. Olowu, and A. I. Sarwat, "Optimal smart inverters volt-var curve selection with a multi-objective volt-var optimization using evolutionary algorithm approach," in *2018 North American Power Symposium (NAPS)*, Sep. 2018, pp. 1–6.
- [14] T. Olowu, H. Hassan, M. Moghaddami, and A. I. Sarwat, "Physics-based design optimization of high frequency transformers for solid state transformer applications," in *2019 IEEE Industry Applications Society Annual Meeting (IAS)*. IEEE, 2019, pp. 1–6.
- [15] IEEE Standards Coordinating Committee 21, "IEEE standard for interconnection and interoperability of distributed energy resources with associated electric power systems interfaces," *IEEE Std 1547-2018 (Revision of IEEE Std 1547-2003)*, pp. 1–138, April 2018.
- [16] T. Olowu, S. Dharmasena, and A. I. Sarwat, "Bidirectional ac/dc converter topologies: A review," in *SoutheastCon 2019*, April 2019, pp. 1–6.
- [17] F. Ding, A. Pratt, T. Bialek, F. Bell, M. McCarty, K. Atef, A. Nagarajan, and P. Gotseff, "Voltage support study of smart pv inverters on a high-photovoltaic penetration utility distribution feeder," in *2016 IEEE 43rd Photovoltaic Specialists Conference (PVSC)*, June 2016, pp. 1375–1380.
- [18] A. Aghazadeh, M. Jafari, N. Khodabakhshi-Javinani, H. Nafisi, and H. Jabbari Namvar, "Introduction and advantage of space opposite vectors modulation utilized in dual two-level inverters with isolated dc sources," *IEEE Transactions on Industrial Electronics*, vol. 66, no. 10, pp. 7581–7592, Oct 2019.
- [19] T. O. Olowu, M. Jafari, and A. I. Sarwat, "A multi-objective optimization technique for volt-var control with high pv penetration using genetic algorithm," in *2018 North American Power Symposium (NAPS)*, Sep. 2018, pp. 1–6.
- [20] A. Ulinuha, M. A. S. Masoum, S. Member, S. M. Islam, and S. Member, "Optimal Scheduling of LTC and Shunt Capacitors in Large Distorted Distribution Systems Using Evolutionary-Based Algorithms," vol. 23, no. 1, pp. 434–441, 2008.
- [21] F. Ding, A. Nagarajan, S. Chakraborty, A. Nguyen, S. Walinga, M. McCarty, F. Ding, A. Nagarajan, and S. Chakraborty, "Photovoltaic Impact Assessment of Smart Inverter Volt-VAR Control on Distribution System Conservation Voltage Reduction and Power Quality Photovoltaic Impact Assessment of Smart Inverter Volt-VAR Control on Distribution System Conservation Voltage Reduction and Power Quality," no. December, 2016.
- [22] F. Ding, A. Nagarajan, M. Baggu, A. Nguyen, S. Walinga, M. McCarty, and F. Bell, "Application of Autonomous Smart Inverter Volt-VAR Function for Voltage Reduction Energy Savings and Power Quality in Electric Distribution Systems Preprint," no. April, 2017.
- [23] M. Abdelkhalik Azzouz, H. E. Farag, and E. F. El-Saadany, "Real-time fuzzy voltage regulation for distribution networks incorporating high penetration of renewable sources," *IEEE Systems Journal*, vol. 11, no. 3, pp. 1702–1711, Sep. 2017.
- [24] M. Chamana and B. H. Chowdhury, "Optimal voltage regulation of distribution networks with cascaded voltage regulators in the presence of high pv penetration," *IEEE Transactions on Sustainable Energy*, vol. 9, no. 3, pp. 1427–1436, July 2018.

Novel Cost Function based Motion-planning Method for Robotic Manipulators

Dániel Szabó*, Emese Gincsiné Szádeczky-Kardoss

Department of Control Engineering and Information Technology, Budapest University of Technology and Economics, H-1117, Hungary

ARTICLE INFO

Article history:

Received: 09 October, 2019

Accepted: 01 December, 2019

Online: 30 December, 2019

Keywords:

robotic manipulator

motion-planning

Rapidly-exploring Random Tree

Fuzzy-approximation

ABSTRACT

In this paper an offline motion-planning algorithm is presented for robotic manipulators. In this method to solve the path-planning task, the Transition-based Rapidly-exploring Random Tree (T-RRT) algorithm was applied, that requires a cost-function over the search space. The goal of this cost-function is to keep distance between the actual position and configurations that cause collisions. The paper presents two possible cost function generation methods. The first one is based on multidimensional Gauss functions and the second solution uses fuzzy function-approximation to determine the cost all over the configuration space. At last, the trajectory generator method will be introduced that calculates the desired shape of the function of joint variables and their derivatives. The algorithm is universal, the only restriction is that the manipulator and the environment are modelled by their bounding polyhedra. To demonstrate the presented approach, simulation were performed in MATLAB Simulink environment using the Mitsubishi RV-2F-Q robotic manipulator.

1 Introduction

Nowadays, automation is playing an increasingly important role in our daily lives, therefore is a growing need for the autonomous motion-planning of robotic manipulators.

Two types of path-planning methods can be defined, the offline and the online methods. In case of offline path-planning method, the calculation time does not mean a bottleneck, so more time can be spent on improving the found path. For example, in [1] an offline path-planning method is introduced, that can find an optimal collision-free path, where the optimality is based on the energy usage of the manipulator. These kind of methods can ensure the collision-freeness only with static obstacles or obstacles with known motions.

Online path-planning methods are used to avoid collisions with dynamic obstacles having unpredictable movements. These algorithms can be used in human-robot collaboration systems for example [2]. The environment of the robot can be observed with a depth camera. Besides, the image processing can be calculated with GPU, so the real-time calculation can be ensured [3]. In this paper, an offline path planning method will be described.

In our case, the minimization of cost-function is needed during the motion-planning algorithm, while avoiding configurations leading to collisions. There are numerous solutions in robotic applications to this problem.

Many of these are founded on the classical grid-based methods like A* or D* which can be used to find an optimal path limited by the resolution of the grid [4]. The main disadvantage of these algorithms is that the computation time grows exponentially with the number of dimensions. This effect is called as the “Curse of dimensionality”.

Another type of path-planning methods are the sampling-based algorithms like the Rapidly-exploring Random Tree (RRT). These algorithms can be used effectively with higher number of dimensions as well, but the optimality of the solution is not guaranteed [5].

These problems can be solved by the Transition-based RRT (T-RRT) algorithm, that incorporates the advantages of the grid-based and the sampling-based methods [6]. Thus, it can be used to find a path that minimizes a cost-function defined in the high dimensional search space.

Heuristics can be used to determine the meaning of cost. For example, in case of a human-collaboration, to ensure the safe operation and the security, the cost has to be high near by the person [7].

Another method could be that, when the dynamics of the system is used to minimize the time or the performed work during the motion.

In this paper, the goal is to maximize the distance between the path of the manipulator and the configurations that cause collisions with the help of defined cost function. In this case the result of the offline path-planning algorithm can be used by a reactive mo-

*Corresponding Author: Dániel Szabó, szabo.daniel0604@gmail.com

tion planning method, that will have more space to avoid dynamic obstacles.

The paper is organized as follows. Section 2 introduces the base of the kinematics of robotic manipulators. In Section 3, the T-RRT algorithm is presented, that was used for path-planning in this work. Then the collision-detection method is described, based on investigation of the feasibility of inequalities of bounding polyhedra, that are describing the manipulator and the obstacles (Section 4). Then, Section 5 describes two cost function approximation algorithms with Gauss-functions and with fuzzy function-approximation. The latter is more detailed. Subsection 5.5 describes the method that is used in this work for cost function evaluation. The trajectory generation method is explained in Section 6. The simulation results are presented in Section 7. Finally, Section 8 contains conclusions and possible developments in the future.

2 Robotic manipulators

Robotic manipulators are usually modeled as open kinematic chains. A manipulator contains links, which are connected by joints. Two basic types of joints exist: Revolute joints are used to apply relative rotation, and prismatic joints allow linear motion between two adjacent links. The relative movement between adjacent links is given by the joint variables q_i . In case of revolute joints, q_i gives the angular displacement, while for prismatic joints, q_i equals the amount of linear motion. The actual configuration q of the robot is defined by the vector containing actual q_i values of all joints.



Figure 1: Mitsubishi RV-2F-Q manipulator (used in the simulations)

An end effector is usually attached to the last segment of the manipulator. To determine the position and the orientation of the end effector in the workspace of the robot, the equations of forward kinematics can be used. A homogeneous transformation matrix belongs to each robotic joints. The position and orientation of the coordinate frame attached to the end effector (relative to the base frame) can be determined by multiplying these matrices.

The main parameters of a robotic manipulator can be defined by the Denavit-Hartenberg parameters [8]. Homogeneous transformation matrices can be calculated from these parameters using actual joint variables.

The task of the path-planning is to find a path, which moves the robot to a desired goal configuration. (This goal configuration is typically given by the desired orientation and position of the end-effector at the end of the motion.) The path-planning problem can be defined in the Euclidean space, but usually, the planning is performed in the configuration space \mathcal{C} of robot. The configuration space is spanned by the admissible configuration vectors (q), i.e. joint variables (q_i) are used as coordinates. For example the configuration space of the Mitsubishi RV-2F-Q manipulator with six degrees of freedom is a six-dimensional space. This robot has six revolute joints. Its 3D model is depicted in Fig. 1. The simulations presented in Section 7 were performed using this manipulator.

3 The Path-planning Algorithm

The traditional RRT algorithm is a stochastic sampling path-planning algorithm. In this method a search tree is grown from the initial q_{init} point to the q_{goal} goal configuration. In a given iteration, a randomly selected configuration is inserted to the tree [9].

In these days, the planning algorithms like the RRT method are very popular, due to their efficiency in exploration of the search space. There exist several improvements of the traditional method, for example the RRT* described in [10], which checks the available corrections in every iteration cycle, so it is able to find an optimal path to the goal point. The method presented in [11] called RRT⁺ can be used in very high dimensional spaces, such as the configuration space of hyper-redundant manipulators. In this work, the T-RRT algorithm is used, that is able to find a suboptimal solution defined by a cost function in high dimensional configuration spaces as well. This solution is called as high quality path in [6]. In our case the goal of cost function is to minimize the risk of collision.

Algorithm 1: Rapidly-exploring Random Tree (RRT)

Input: the configuration space \mathcal{C}
the root q_{init} and the goal q_{goal}

Output: the tree \mathcal{T}

- 1: $\mathcal{T} \leftarrow \text{INITTREE}(q_{init})$
- 2: **while not** STOPCONDITION(\mathcal{T}, q_{goal}) **do**
- 3: $q_{rand} \leftarrow \text{SAMPLECONF}(\mathcal{C})$
- 4: $q_{near} \leftarrow \text{NEARESTNEIGHBOR}(q_{rand}, \mathcal{T})$
- 5: $q_{new} \leftarrow \text{EXTEND}(\mathcal{T}, q_{rand}, q_{near})$
- 6: **if** NOCOLLISION(q_{new}) **then**
- 7: ADDNEWNODE(\mathcal{T}, q_{new})
- 8: ADDNEWEDGE($\mathcal{T}, q_{near}, q_{new}$)
- 9: **end if**
- 10: **end while**
- 11: **return** \mathcal{T}

In Algorithm 1 the traditional RRT algorithm is described. The inputs of the algorithm is the configuration space, where the path-planning method is evaluated, the initial and the goal configuration of the path-planning. The output of the method is the search tree. At first, the search tree is initialized with the initial configuration as its root node.

After that a uniformly distributed random configuration q_{rand} is generated in function `SAMPLECONF`.

This configuration is used by the `NEARESTNEIGHBOR` function to determine the nearest configuration (called q_{near}) to it in the search tree. In this method, distance from the edges is not examined, due to the higher computational demand, it is determined only from the previously added nodes.

A new point q_{new} is created in `EXTEND`, which is in the same direction as q_{rand} to q_{near} , but the distance between q_{new} and q_{near} is maximized with the parameter δ . In this method, the collision-freeness of the created q_{new} configuration is not examined.

The function `NoCOLLISION` returns true, if the q_{new} configuration does not lead to a collision. In this case, a new node and edge will be added to the tree.

The algorithm is succeeded, if the distance between the last inserted point and the goal configuration is less than a given parameter, or failed, if a maximum number of iterations has been reached. In the function `STOPCONDITION` are these conditions inspected.

Algorithm 2 describes the T-RRT method. As it can be seen, the method is based on the traditional RRT algorithm described in Algorithm 1. The main differences are the `TRANSITIONTEST` and `MINEXPANDCONTROL` functions (see Subsections 3.1-3.2), which are the conditions to extend the search tree with a new node and edge.

The cost of the found path can be evaluated by several methods, e.g. maximal cost, average cost or total cost along the path. However it will lead to a path, that avoids the areas of search space with higher costs, if the performed work is minimized along the path, as it is introduced in [6]. In this case, the positive variations of the cost function will be minimized.

Algorithm 2: Transition-based RRT

Input: the configuration space \mathcal{C}
the cost function $c : \mathcal{C} \mapsto \mathbb{R}_+^*$
the root q_{init} and the goal q_{goal}

Output: the tree \mathcal{T}

- 1: $\mathcal{T} \leftarrow \text{INITTREE}(q_{init})$
- 2: **while not** `STOPCONDITION`(\mathcal{T} , q_{goal}) **do**
- 3: $q_{rand} \leftarrow \text{SAMPLECONF}(\mathcal{C})$
- 4: $q_{near} \leftarrow \text{NEARESTNEIGHBOR}(q_{rand}, \mathcal{T})$
- 5: $q_{new} \leftarrow \text{EXTEND}(\mathcal{T}, q_{rand}, q_{near})$
- 6: **if** $q_{new} \neq \text{NULL}$ **then**
- 7: $d_{near-new} \leftarrow \text{DISTANCE}(q_{near}, q_{new})$
- 8: **if** `TRANSITIONTEST`($c(q_{near}), c(q_{new}), d_{near-new}$)
and `MINEXPANDCONTROL`($\mathcal{T}, q_{near}, q_{rand}$)
and `NoCOLLISION`(q_{new}) **then**
- 9: `ADDNEWNODE`(\mathcal{T}, q_{new})
- 10: `ADDNEWEDGE`($\mathcal{T}, q_{near}, q_{new}$)
- 11: **end if**
- 12: **end if**
- 13: **end while**
- 14: **return** \mathcal{T}

3.1 Transition-test

Algorithm 3 describes the `TRANSITIONTEST` function. In the first step, the number, how many times the transition-test failed previously, is queried by the `GETCURRENTNFAIL` function.

Thereafter if the cost in q_{new} point is higher than a c_{max} parameter, then the test will not be accepted, so the search tree will not be extended. In case of negative variation of cost function the transition test will return true.

After that in case of positive slope of the cost, the transition test will be successful in accordance with a probability based on the Metropolis criterion [12], defined as

$$p_{ij} = \exp\left(-\frac{\Delta c_{ij}}{K \cdot T}\right) \quad (1)$$

where $\Delta c_{ij} = \frac{c_j - c_i}{d_{ij}}$ is the variation of the cost, K is a normalization constant, it can be taken as the average cost of the query configurations.

The difficulty of success for a given transition is defined by the temperature parameter denoted by T . The goal of this parameter is to minimize the amount of positive slopes in the cost function along the path, but it allows to explore the whole reachable configuration space by its adaptive tuning. In case of higher temperature the acceptance of transition test is more probable for a transition with higher positive slope. To accept only very low positive variations at the start, T is initialized with a very low value. This functions similar to the simulated annealing algorithm.

The function `RAND(0,1)` gives a random number between 0 and 1 based on uniform distribution.

The $\alpha > 1$ variable is used to change the temperature adaptively. If the transition was successful then the temperature is decreased. And if the test failed $nFail_{max}$ times then the value of T is increased by multiplying with α . Thus if the $nFail_{max}$ parameter is high then the path will be more likely to go into the valleys, however finding a path over a region with high cost will be more difficult.

Algorithm 3: TransitionTest(c_i, c_j, d_{ij})

- 1: $nFail = \text{GETCURRENTNFAIL}();$
- 2: **if** $c_j > c_{max}$ **then**
- 3: **return** False
- 4: **end if**
- 5: **if** $c_j < c_i$ **then**
- 6: **return** True
- 7: **end if**
- 8: $p = \exp\left(\frac{-(c_j - c_i)/d_{ij}}{K \cdot T}\right)$
- 9: **if** `RAND`(0, 1) < p **then**
- 10: $T = T/\alpha$
- 11: $nFail = 0$
- 12: **return** True
- 13: **else**
- 14: **if** $nFail > nFail_{max}$ **then**
- 15: $T = T \cdot \alpha$
- 16: $nFail = 0$
- 17: **else**
- 18: $nFail = nFail + 1$
- 19: **end if**
- 20: **return** False
- 21: **end if**

3.2 Minimal Expansion Control

The transition-test can slow the exploration rate of high cost hills and the new configurations only refine the already known regions.

By specifying a minimum level of exploration, this can be prevented. Accordingly, a new node close to the closest search tree configuration will only be accepted if the refining node ratio is smaller than the ρ parameter. The minimal exploration control method will accept the exploring nodes automatically.

This function is introduced in Algorithm 4. The function UPDATENbNODETREE increases the number of nodes, while the UPDATENbREFINENODETREE function updates the number of refining nodes in the search tree.

The Euclidean distance between the q_{rand} (not the extended q_{new}) and the q_{near} configurations is used to determine the type of a given point. A point is an exploring node if the distance is high, otherwise it will be a refining node.

The path-planning will discover the entire configuration space very effectively with this complement, while trying to stay in the valleys of the cost function owing to the transition-test.

Algorithm 4: MinExpandControl($\mathcal{T}, q_{near}, q_{rand}$)

```

1: if DISTANCE( $q_{near}, q_{rand}$ ) >  $\delta$  then
2:   UPDATENbNODETREE( $\mathcal{T}$ )
3:   return True
4: else
5:   if  $\frac{NbREFINENODETREE(\mathcal{T}+1)}{NbNODETREE(\mathcal{T}+1)} > \rho$  then
6:     return False
7:   else
8:     UPDATENbREFINENODETREE( $\mathcal{T}$ )
9:     UPDATENbNODETREE( $\mathcal{T}$ )
10:    return True
11:  end if
12: end if

```

4 Collision detection

The effectiveness of a path planning method depends highly on the applied collision detection function, since it is called often (see Step 6 of Algorithm 1 or Step 8 of Algorithm 2) and it has to ensure that only collision-free configurations are used for planning. To calculate in real time, which robot configurations are in collisions, is a difficult problem. The task is not only to determine if there is any collision between the robot and the surrounding objects, but also the self-collision configurations of the robot has to be avoided.

Moreover, the goal could be not only to plan a collision-free path, but also to get a time-optimal motion. A solution for such a problem is presented in [1], but the computational demand of that algorithm is high, due to the solution of the optimization problem. However, the collision detection algorithm used by that method can be applied by other applications as well. The algorithm presented in this paper is also based on this collision detection.

4.1 Collision detection with polyhedrons

The basic idea of this collision detection method is that the geometry of the robot and the obstacles is approximated such that they are

represented by unions of convex polyhedrons. Fig. 2 and Fig. 3 illustrate how the bounding polyhedrons can be determined around the robot and the obstacles. For the sake of simplicity, it is supposed that the workspace of the robot contains only one obstacle. The presented collision detection method can be easily extended if more obstacles are present.

Let P denote the union of polyhedrons that represent the robot:

$$P = \bigcup_{i=1}^{n_p} P^{(i)} = \bigcup_{i=1}^{n_p} \{y \in \mathbb{R}^3 | A^{(i)}y \leq b^{(i)}\} \quad (2)$$

where n_p shows the number of polyhedrons in P . A polyhedron is bounded by faces. A face $P^{(i)}$ is defined by $A^{(i)}$ and $b^{(i)}$ parameters and p_i is the number of faces. Then $A^{(i)} \in \mathbb{R}^{p_i \times 3}$ and $b^{(i)} \in \mathbb{R}^{p_i}$ for $i = 1, \dots, n_p$.

Similarly, an obstacle Q can also be described by the union of polyhedrons:

$$Q = \bigcup_{j=1}^{n_q} Q^{(j)} = \bigcup_{j=1}^{n_q} \{y \in \mathbb{R}^3 | C^{(j)}y \leq d^{(j)}\} \quad (3)$$

where n_q denotes the number of polyhedrons in Q . q_j shows the number of faces in $Q^{(j)}$, hence $C^{(j)} \in \mathbb{R}^{q_j \times 3}$ and $d^{(j)} \in \mathbb{R}^{q_j}$ for $j = 1, \dots, n_q$.

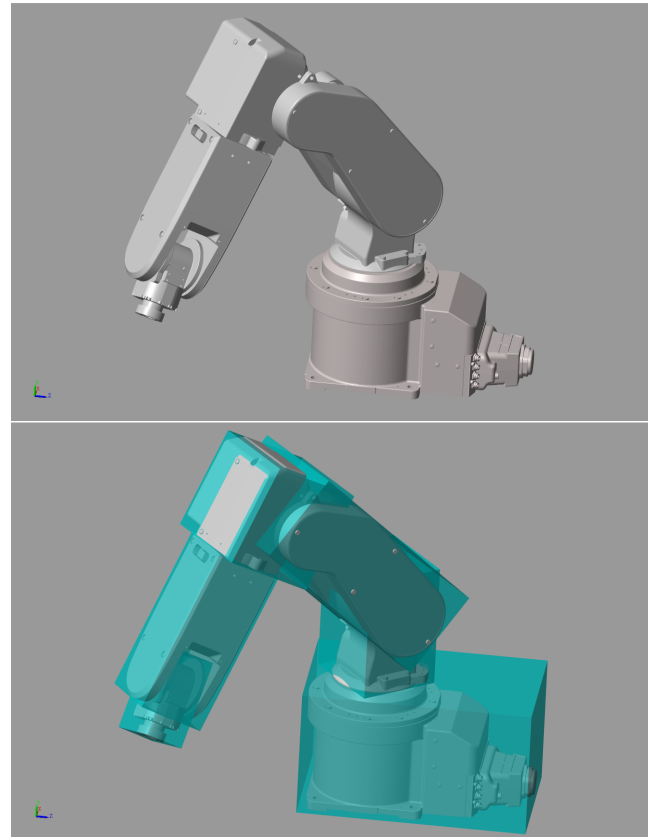


Figure 2: Bounding boxes of each segments were defined as the bounding polyhedrons of the manipulator

To avoid self-collisions, pairs of polyhedrons $P^{(i)}$ have to be checked, whether they collide with each-other. There exist such

pairs of $P^{(i)}$ where the collision detection is not necessary, since they cannot collide physically (e.g. adjacent segments). Therefore, the set of pairs (k, l) , $k \neq l$ has to be defined, such that k and l denote two polyhedrons $(P^{(k)}, P^{(l)})$ of the robot which could collide. This set is denoted by I . If $(k, l) \in I$, the collision check has to be performed for the corresponding two polyhedrons.

Suppose, that P is already calculated for a given configuration and Q is determined as well, then the configuration is collision-free if

$$P^{(i)} \cap Q^{(j)} = \emptyset \quad \wedge \quad P^{(k)} \cap P^{(l)} = \emptyset \quad (4)$$

$\forall i = 1, \dots, n_P$ and $\forall j = 1, \dots, n_Q$ and $\forall (k, l) \in I$.

One polyhedron of the robot $P^{(i)}$ and one of the obstacle $Q^{(j)}$ do not collide with each-other if the union of their system of inequalities has no solution. Formally, there exists no such $y^{(i,j)} \in \mathbb{R}^3$ point where

$$\begin{pmatrix} A^{(i)} \\ C^{(j)} \end{pmatrix} y^{(i,j)} \leq \begin{pmatrix} b^{(i)} \\ d^{(j)} \end{pmatrix} \quad (5)$$

Similar inequalities can be used to check self-collision.

To determine, whether an inequality similar to (5) has no solution, Farkas's lemma can be applied. The lemma says that there exists no solution for the linear system if and only if a vector $w^{(i,j)} \in \mathbb{R}^{(p_i+q_j)}$ can be found such that

$$w^{(i,j)} \geq 0 \quad \text{and} \quad \begin{pmatrix} A^{(i)} \\ C^{(j)} \end{pmatrix}^\top w^{(i,j)} = 0 \quad \text{and} \quad \begin{pmatrix} b^{(i)} \\ d^{(j)} \end{pmatrix}^\top w^{(i,j)} < 0 \quad (6)$$

Consequently, if given is a configuration q and a $w^{(i,j)}$ solution can be found for (6), then the q configuration can be marked as collision-free.

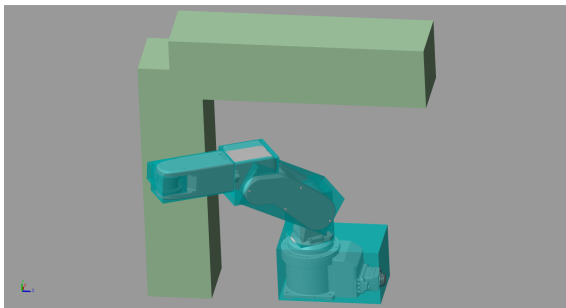


Figure 3: Bounding polyhedrons around the robot and obstacles (as used in the simulation)

4.2 Construction of polyhedrons

The face parameters $(A^{(i)}, b^{(i)})$ for some robot-polyhedron $P^{(i)}$ depend on the actual robot configuration q . This subsection describes how to calculate them.

First, $A_r^{(i)}$ and $b_r^{(i)}$ have to be determined for each segment of the robot in a reference coordinate system that is attached to the same segment. For example, the CAD model of the manipulator (e.g. shown in Fig. 1) can be used to measure the corresponding parameters in this frame. (For obstacles, the same process has to be performed.)

Then, a transformation is required to get these parameters in the base frame. Denote the resultant transformation matrix by $T^{(i)}(q)$. $T^{(i)}(q)$ can be used for the transformation from the base coordinate system to the reference frame of the i th segment, if the actual configuration of the robot is q .

The parameters in the base frame can be determined as follows

$$\begin{bmatrix} A^{(i)} & b^{(i)} \end{bmatrix} = \begin{bmatrix} A_r^{(i)} & b_r^{(i)} \end{bmatrix} [T^{(i)}(q)]^{-1} \quad (7)$$

During the collision-check algorithm, these parameters have to be used.

5 Cost-function approximation

The goal of cost-function is to keep distance from configurations leading to a collision. The approximation of this function is necessary, to decrease the computational demand of the algorithm. This cost-function is used by the T-RRT path-planning method, introduced in Section 3.

5.1 Cost-function approximation with Gauss-functions

At first, the approximation of cost-function was evaluated by taking enough sample of the configuration space and Gauss-functions were summed in every sampling point. The centers of Gauss-functions are the configurations causing a collision. There are several disadvantages of this method.

As it can be seen in the Fig. 4 the result is very hilly and a maximal value of the cost function can not be predefined, so the c_{max} parameter of the TRANSITIONTEST function in Algorithm 3 is difficult to determine.

In addition, the cost function has to be stored in every sampling point, moreover the interpolation is slow at any other point.

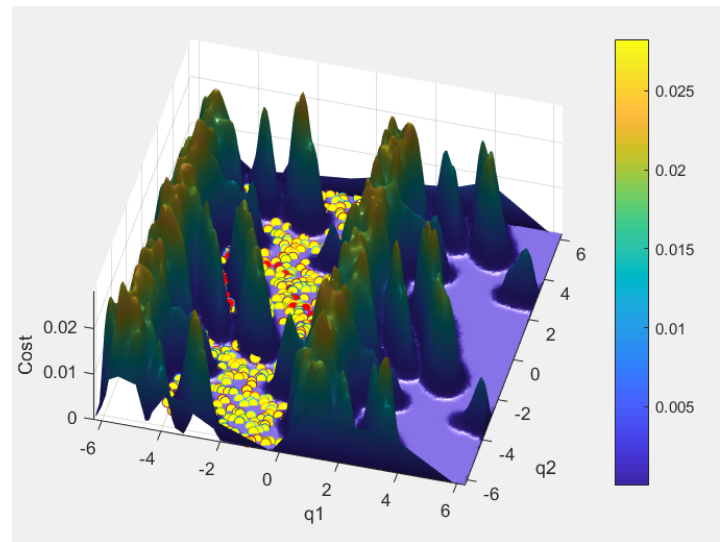


Figure 4: Cost-function approximation with Gauss-functions with the search tree found by the T-RRT algorithm

5.2 The base of fuzzy approximation

Another solution could be the fuzzy approximator systems.

Fuzzy systems have several uses in many areas such as decision making [13], system identification [14], control theory [15] etc. In addition, the approximation of nonlinear functions is possible as well, if enough teaching points are available. Teaching points are defined as $y_j = f(x_j)$, where f is the function that needs to be approximated, x_j is the position of the given teaching point and y_j is the value of f in x_j .

There are several advantages of fuzzy estimator systems. Depending on which type of inference method is used, their rules can be tuned adaptively and the approximation time is one of the benefits of these systems as well.

Singleton fuzzyfication, center average defuzzyfication, product inference and zero-order Sugeno model fuzzy systems with Gaussian membership functions are therefore the most widely used approaches [16].

Thus the fuzzy estimation of a nonlinear function is defined as

$$\hat{f}(x) = \frac{\sum_{l=0}^M \bar{y}^l \prod_{i=1}^n \exp(-(\frac{x_i - \bar{x}_i}{\sigma_i^l})^2)}{\sum_{l=0}^M \prod_{i=1}^n \exp(-(\frac{x_i - \bar{x}_i}{\sigma_i^l})^2)} \quad (8)$$

where n is the number of dimensions in the configuration space, \bar{y}^l is the output in the l th rule of the fuzzy inference system, \bar{x}_i is the location of the maximum value of the Gaussian membership function and with σ_i^l the width of this function can be modified.

The adaptive tuning of the fuzzy rules is feasible by modifying the \bar{y}^l , \bar{x}_i and σ_i^l values.

According to the Universal approximation theorem described in [16], for any given real continuous function f on the compact set $U \in \mathbb{R}^n$ and arbitrary $\epsilon > 0$ there exists \hat{f} in the form given in (8) such that

$$\sup_{x \in U} |f(x) - \hat{f}(x)| < \epsilon \quad (9)$$

Henceforth, two adaptive tuning method for fuzzy estimator systems will be introduced. In which bounded domain intervals of input vector x and output y are assumed.

5.3 Generating fuzzy rules by learning from examples

Details of the algorithm can be found in [17].

The input and output domain is divided into intervals, in each Gaussian membership functions are defined.

The possible fuzzy relations are determined exactly by the number of input membership functions. For example, in case of input variables x_1 and x_2 , if the number of membership functions are N_1 and N_2 then the number of possible rules is $N_1 \cdot N_2$. For each teaching point the relation and output membership function has to be selected that mostly fits the given teaching point.

In k th teaching step a generic form of fuzzy rules can be defined:

$$R^k : \text{IF } x_1 \text{ IS } F_1^k \text{ AND } x_2 \text{ IS } F_2^k \text{ AND } \dots \text{ AND } x_n \text{ IS } F_n^k \\ \text{THEN } y \text{ IS } G^k$$

where F_i^k is one of the input variable membership functions and G^k is one of the output variable membership functions.

In the k th step a given rule will be chosen, if it maximizes the following expression:

$$D(R^k) = \prod_{i=1}^n (\mu_{F_i^k}(x_i^k)) \cdot \mu_{G^k}(y^k) \quad (10)$$

where μ is the firing strength of the given membership function for the actual value of the teaching point.

There exist more possible solutions to that problem, if a new relation has to be added with the same condition part, but a different inference part as an already added relation. In this case, the relation with higher value can be selected by evaluating (10), or a weighted value of both inference parts can be specified.

The main disadvantage of this technique is that (10) has to be evaluated $N = N_1 \cdot N_2 \cdot \dots \cdot N_n$ times for every teaching points (where n is the number of dimensions of the space) to find the maximum value. As a consequence, with the number of dimensions the computational time grows exponentially.

5.4 Nearest neighborhood clustering

In this algorithm, teaching points are clustered depending on their position in the configuration space. A given cluster can be described by three parameter, the center of it x_0^l , the number of teaching points in it B^l and the sum of values of these points A^l [18].

A new point x_j ($y_j = f(x_j)$) is inserted to the cluster l , if it is closer to x_0^l than a given r radius. After that the other cluster parameters A^l and B^l will be updated. If the distance of the teaching point x_j is too high from all of the clusters then a new cluster will be created as $\{x_0^l = x_j; A^l = y_j; B^l = 1\}$. M represents the number of clusters that have been defined during the teaching process.

Therefore, the estimation of the nonlinear function can be defined as

$$\hat{f}(x) = \frac{\sum_{l=0}^M A^l \exp(-(\frac{x - x_0^l}{\sigma^l})^2)}{\sum_{l=0}^M B^l \exp(-(\frac{x - x_0^l}{\sigma^l})^2)} \quad (11)$$

5.5 Cost-function evaluation

Eventually, the cost-function for the T-RRT method was approximated with the Nearest neighborhood clustering algorithm, because it has a higher computational efficiency.

To determine the position of the teaching points, random sampling of the configuration space is needed, owing to the high number of dimensions.

The collision detection method described in Section 4 is evaluated in all of teaching points. If the x_j configuration causes collision, then one will be assigned as the value of the cost-function y_j in x_j , otherwise zero.

After that the rules of the fuzzy approximator are tuned with the Nearest neighborhood clustering algorithm. This method can be used for arbitrary robotic manipulators. An example for the cost function and path can be seen in Fig. 5 in case of 2-DoF manipulator (since it is not possible to depict the cost function in higher dimensions).

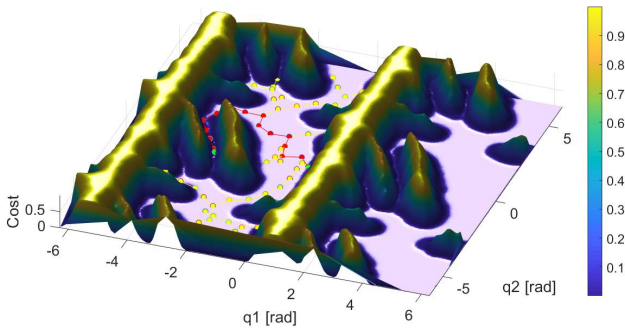


Figure 5: T-RRT method is able to find high quality path based on a cost-function. The cost-function is evaluated for a two degrees of freedom manipulator with the Nearest Neighborhood Clustering algorithm.

Table 1 shows the comparison of approximation with Gauss-function and the Nearest neighborhood clustering algorithm. As can be seen, both the training time and the evaluation time for one configuration in the case of Gauss-function approximation grow very fast by increasing the number of teaching points. In the case of Nearest neighborhood clustering, these values increased to a lesser extent. By using clusters, the evaluation time of the fuzzy function-approximation method did not increase significantly, which is ideal for applying the method in a path-planning algorithm.

Table 1: Comparison of fuzzy function-approximation and approximation with Gauss-functions

Num. of teaching points	Nearest Neighborhood clustering			Gauss	
	Training time	Number of clusters	Eval. time	Training time	Eval. time
1000	0.0481s	714	22μs	0.0402s	7.8μs
5000	0.207s	1649	45μs	0.3027s	28.8μs
10000	0.4554s	1974	52μs	1.4151s	58.2μs
50000	3.0962s	2431	65μs	22.88s	137.9μs
100000	7.045s	2521	76μs	155.26s	1632μs

6 Trajectory generation

The already presented methods can be used to find points in the configuration space, that by moving the robot between these points, the possible collisions can be avoided.

6.1 Trajectory generation for scalar values

In the following method y denotes one coordinate of the q configuration, in other words, one joint variable of the robot.

Let $\{y_k\}$ be the set of points founded by the path-planning algorithm and $\{t_k\}$ denotes the desired absolute time of reaching these points [19].

$$\begin{aligned} \{y_k\} &= \{\dots, A, B, C, D, \dots\}, \\ \{t_k\} &= \{\dots, t_A, t_B, t_C, t_D, \dots\} \end{aligned} \quad (12)$$

Due to the limits of torques, boundaries have to be defined for the acceleration of joints: $|\ddot{y}|_{max}$.

At first, $y(t)$ trajectory can be defined as a series of linear functions between adjacent points. In this case, the first derivative $\dot{y}(t)$ is constant between two points and it steps to another constant value in a given point. The acceleration $\ddot{y}(t)$ is zero in every point except the points where the slope of $y(t)$ trajectory is changing. In these points, the second derivative contains Dirac-delta functions, which leads to an unbounded control value, so this solution is not applicable. To overcome this problem, the acceleration of joints have to be changed continuously.

To reach the next point two kinds of phases can be defined: traveling phase and acceleration phase. In the former, we use a constant velocity and zero acceleration, while in the latter a continuous acceleration function has to be applied, to reach the desired constant velocity of the next traveling phase. The quadratic function can be chosen as the form of the function in the acceleration phase (Fig. 6).

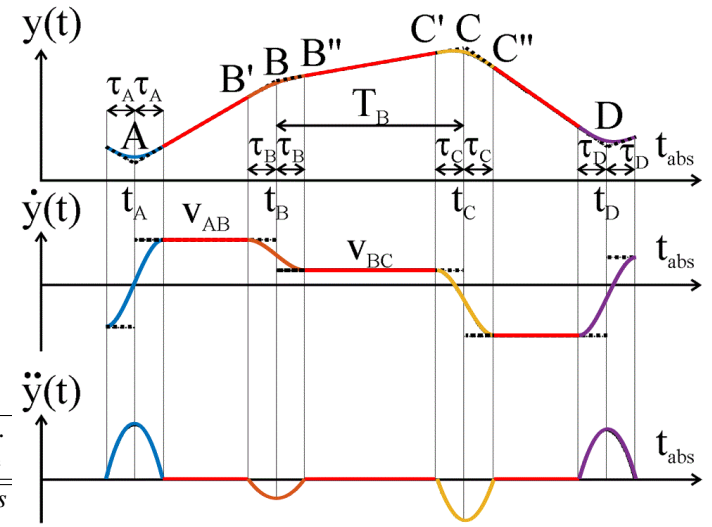


Figure 6: To ensure the continuity of the acceleration function, quadratic function can be applied in the acceleration phase. The form of the trajectories can be seen in the figure.

Let B and C be two adjacent points, while B' and C' are the beginning, B'' and C'' are the end of their acceleration phase. The relative time t can be defined as

$$t = t_{abs} - t_B \in [-\tau_B, T_B], \quad (13)$$

where t_B is the absolute time of reaching the point B , τ_B is the half of duration of acceleration phase in B and T_B denotes the time-interval of reaching point C from point B . This can be seen in Fig 7. The time-intervals between configurations can be determined by the boundaries of joint-velocities, for example $T_B = \frac{C-B}{|\dot{y}|_{max}}$.

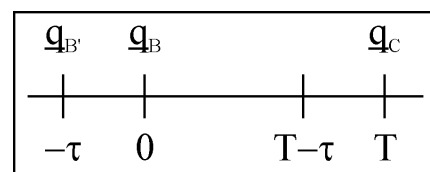


Figure 7: Relative time can be defined, where the zero value is in the q_B configuration. The zero point will be shifted with T , when the $T - \tau$ relative time is reached.

By integrating the quadratic acceleration during the acceleration phase, the velocity and position can be determined:

$$\begin{aligned}
 B'B'' : \quad & \ddot{y}(t) = a_0 t^2 + a_1 t + a_2 \\
 & \dot{y}(t) = a_0 \frac{t^3}{3} + a_1 \frac{t^2}{2} + a_2 t + a_3 \\
 & y(t) = a_0 \frac{t^4}{12} + a_1 \frac{t^3}{6} + a_2 \frac{t^2}{2} + a_3 t + a_4
 \end{aligned} \tag{14}$$

To determine the $a_0 \dots a_4$ parameters of the trajectory of position, five independent conditions have to be defined:

$$\begin{aligned}
 & \ddot{y}(-\tau_B) = 0 \\
 & \ddot{y}(\tau_B) = 0 \\
 & \dot{y}(-\tau_B) = v_{B'B} = \frac{B - B'}{\tau_B} \\
 & \dot{y}(\tau_B) = v_{BC} = \frac{C - B}{T_B} \\
 & y(\tau_B) = B + v_{BC} \cdot \tau_B
 \end{aligned} \tag{15}$$

The following linear equation system can be defined:

$$\begin{aligned}
 \begin{bmatrix} \ddot{y}(-\tau_B) \\ \ddot{y}(\tau_B) \\ \dot{y}(-\tau_B) \\ \dot{y}(\tau_B) \\ y(\tau_B) \end{bmatrix} &= \begin{bmatrix} \frac{\tau_B^2}{3} & -\tau_B & 1 & 0 & 0 \\ \frac{\tau_B^2}{3} & \tau_B & 1 & 0 & 0 \\ -\frac{\tau_B}{3} & \frac{\tau_B^2}{2} & -\tau_B & 1 & 0 \\ \frac{\tau_B}{3} & \frac{\tau_B^2}{2} & \tau_B & 1 & 0 \\ \frac{\tau_B^4}{12} & \frac{\tau_B^3}{6} & \frac{\tau_B^2}{2} & \tau_B & 1 \end{bmatrix} \begin{bmatrix} a_0 \\ a_1 \\ a_2 \\ a_3 \\ a_4 \\ a_5 \end{bmatrix} \\
 \mathbf{y} &= \mathbf{C} \cdot \mathbf{a}
 \end{aligned} \tag{16}$$

The solution of this linear equation system can be calculated as follows:

$$\mathbf{a} = \mathbf{C}^{-1} \cdot \mathbf{y} \tag{17}$$

In the traveling phase ($t \in [\tau_B, T_B - \tau_C]$), the form of the path of the scalar value will be a linear function:

$$y(t) = B + v_{BC} \cdot t \tag{18}$$

6.2 Trajectory generation for joint variables

The presented method for scalar values can be used for each joint variable separately, by taking into account the difference between the boundaries of velocities ($|\dot{q}_i|_{max}$) and accelerations ($|\ddot{q}_i|_{max}$) of some joints.

In addition, the minimal time needed to reach q_{Ci} joint value from q_{Bi} can be different as well, so just that joint have to be moved in maximal speed, that needs the most time to reach the next configuration.

The same τ parameter can be used for each joint variable and it is calculated as follows [19]:

$$\tau = \max_i \frac{3}{2} \frac{|\dot{q}_i|_{max}}{|\ddot{q}_i|_{max}} \tag{19}$$

The trajectory generation method can be seen in the Algorithm 5. The input of the method denoted by Q is the series of configurations contained by the found path.

Algorithm 5: TrajectoryGeneration(Q, τ)

```

1:  $q_C = \text{GETFIRSTCONFIGURATION}(Q)$ 
2:  $T = \tau$ 
3: while SIZE( $Q$ ) > 0 do
4:    $q_{B'} = q(T - \tau)$ 
5:    $q_B = q_C$ 
6:    $q_C = \text{GETFIRSTCONFIGURATION}(Q)$ 
7:    $T_i = \frac{|q_{Ci} - q_{Bi}|}{|\dot{q}_i|_{max}}$ 
8:    $T = \max\{\max\{T_i\}, 2\tau\}$ 
9:    $v_{AB} = \frac{q_B - q_{B'}}{\tau}$ 
10:   $v_{BC} = \frac{q_C - q_B}{T}$ 
11:   $\mathbf{a} = \mathbf{C}^{-1} \cdot \mathbf{y}$ 
12:   $t = -\tau$ 
13:  while  $t < T - \tau$  do
14:     $q(t) = \text{CALCULATETRAJECTORY}(\mathbf{a}, t)$ 
15:     $t = t + \Delta$ 
16:  end while
17: end while
18: return  $q(t)$ 

```

The GETFIRSTCONFIGURATION function gives the first element of the configuration queue and this element will be removed from the queue as well.

At first the variable T is initialized with τ calculated by (19), so in the first iteration the $q_{B'}$ variable will be the root configuration.

The equations in (14) are evaluated in the CALCULATETRAJECTORY function for each joint variable, consequently the dimension of the q variable is equal to the dimension of the configuration space.

Trajectories calculated with this method can be seen in Fig. 9.

7 Simulation results

The comparison of several path-planning algorithms can be seen in Table 2 in case of two degrees of freedom robotic manipulator. The result of planning with the T-RRT method can be seen in Fig. 8. The RRT* algorithm is a variant of traditional RRT method, that refines the search tree in every iteration to find the actual shortest path to the goal configuration [10]. In case of multi-directional RRT method an other search tree is started from the goal configuration [5]. The calculation time can be reduced by this method.

Table 2: Comparison of path-planning algorithms

Algorithm	Calculation time [s]	Length	Total cost	Performed work
RRT	0.039	10.54	0.415	0.896
Multi-directional RRT	0.019	10.54	0.396	0.822
Multi-directional RRT*	3.34	6.92	0.171	0.449
T-RRT _g	0.55	10.21	0.028	0.121
T-RRT _t	13.466	10.91	0.01	0.062

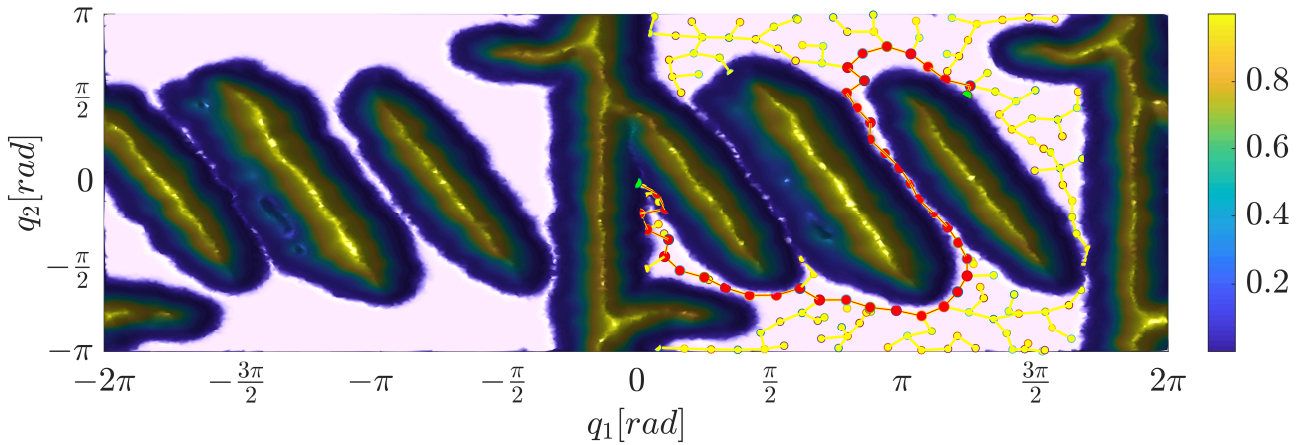


Figure 8: The result of path-planning for two degrees of freedom manipulator with the tempered version of T-RRT

Two parameter settings are examined for the T-RRT method, the first one (T-RRT_g) is a greedy version with $nFail_{max} = 10$, in the other case (T-RRT_t) $nFail_{max} = 100$, which will lead to a tempered version of T-RRT. The computation time in the first case is lower, but the found path has a lower quality as well. The other parameters were: $T_{init} = 10^{-5}$, $\alpha = 1.5$, $\rho = 0.2$, $c_{max} = 0.4$, $\delta = 0.3$. The parameters were chosen empirically.

As it can be seen, the path of the T-RRT algorithm is not equal with the shortest collision-free path.

To demonstrate the presented method, simulations were performed using the Mitsubishi RV-2F-Q manipulator as well. The task of the robot was to move to the other side of an obstacle, which is modeled by two polyhedrons. For implementation and simulation, MATLAB Simulink and Simscape Multibody toolbox were used. The running times were measured on a computer with Intel Core i7-7700HQ Processor.

For the cost function evaluation, the nearest neighborhood clustering method was applied. The parameters were empirically selected as follows: number of teaching points is $n = 20000$, radius of the cluster is $r = 1 \text{ rad}$ and deviation of the Gaussian membership functions is $\sigma = 0.5$. To determine the approximated cost function, $t \approx 120s$ computational time was required, what is appropriate, since these calculations have to be performed only once for a given robot and workspace.

The parameters of the T-RRT method were selected as $T_{init} = 0.01$, $\alpha = 5$, $nFail_{Max} = 10$, $\rho = 0.1$, $c_{max} = 0.8$ and $\delta = 0.4$. To get a solution for a path-planning problem, the average calculation time was $t \approx 7.3s$.

One solution is presented in Fig. 9–Fig. 10. Fig. 9 depicts the trajectories of the joint variables. The whole movement can be seen in a video: <https://youtu.be/t6G08LKG5js>. Some key configurations of the robot are also presented in Fig. 10. It can be seen, that the presented algorithm was able to plan such a motion, where colliding configurations can be avoided.

8 Conclusion

The method presented in this paper can be used to solve the offline path-planning problem for robotic manipulators. The algorithm is

based on the T-RRT method, which is able to calculate the reference motion for the robot, such that collision avoidance is guaranteed and suboptimal path is selected according to some cost-function.

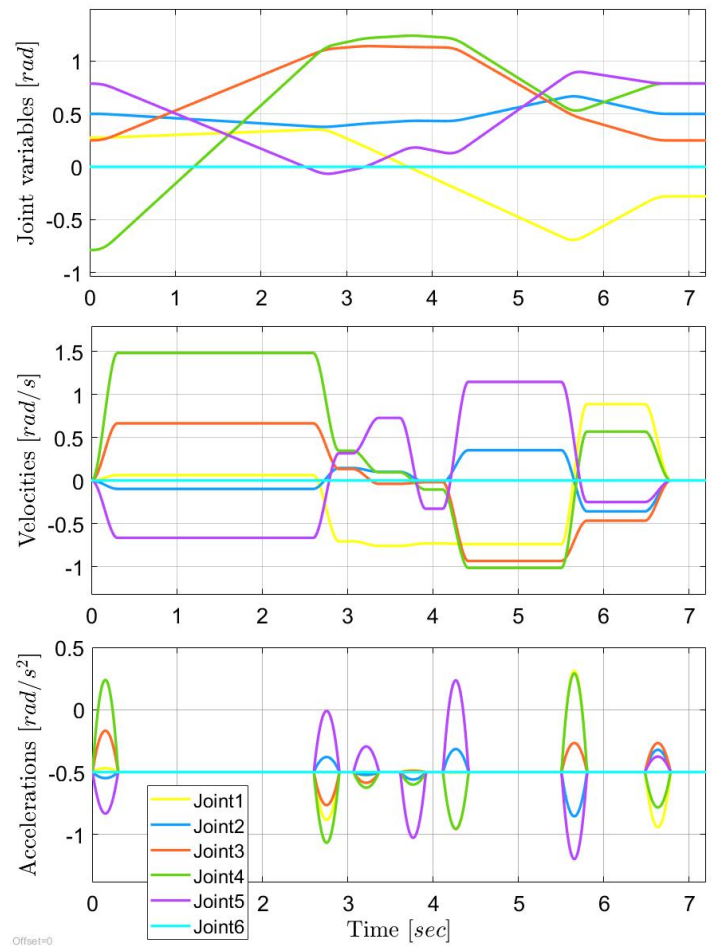


Figure 9: Trajectories of the joint variables

In this work such a cost-function was selected, which can ensure, that the distance between the path of the robot and the colliding configurations is large. Instead of the time-consuming determination of

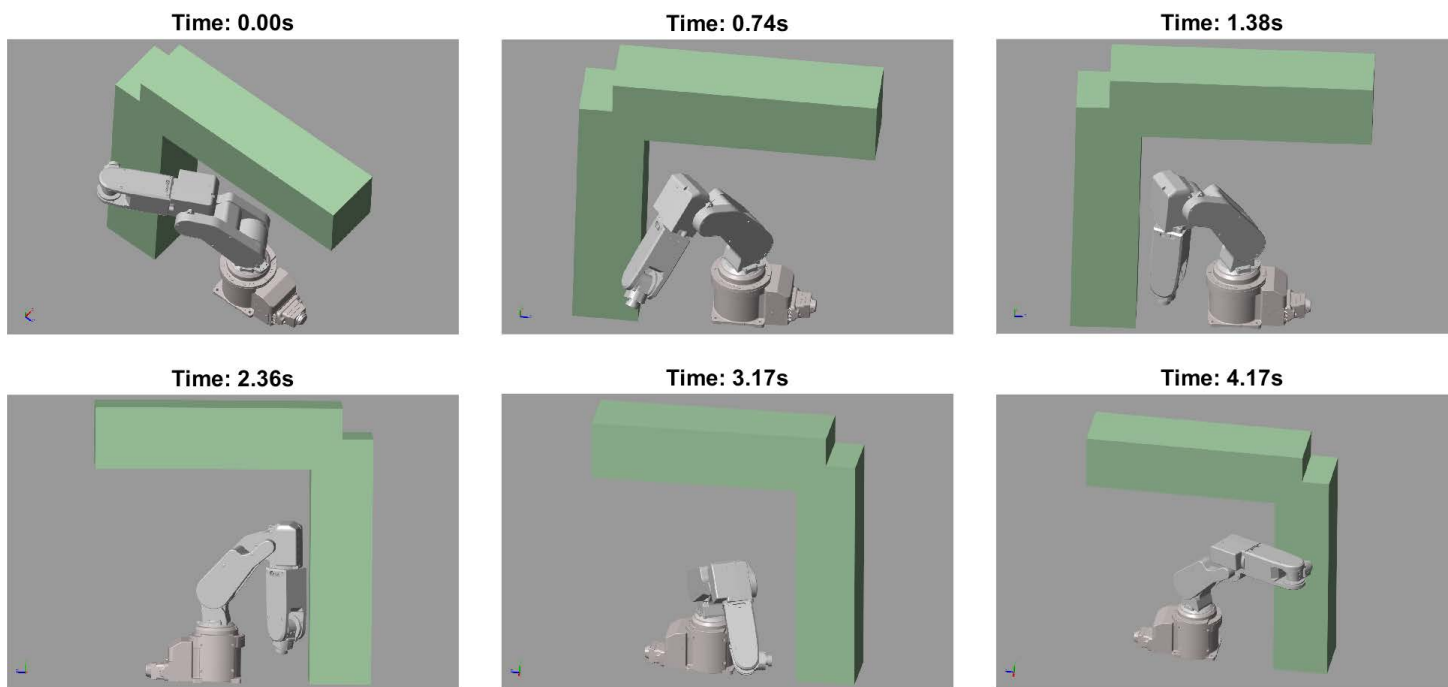


Figure 10: Robot configurations along the collision-free path

the exact cost values, a nonlinear-fuzzy approximation algorithm was suggested which uses the Nearest neighborhood clustering method.

For the collision checking of robot configurations, another approximation was applied. The segments of the robot and the obstacles can be modeled by sets of bounding polyhedrons. The collision of these polyhedrons was checked by the feasibility analysis of inequality systems.

Trajectory planning was also presented in the paper. To produce an input for a trajectory tracking and control method, time functions were determined for the joint variables and their derivatives using known bounds of the joint velocities and accelerations.

In the sequel, the goal is to develop an effective online motion-planning method, which can be used to plan a collision-free motion in such a workspace which contains obstacles with unpredictable movements as well. First, the reference motion can be determined by the presented T-RRT based method for the static environment, and additionally, a reactive planning method (similar to [20]) can be applied to ensure the avoidance of dynamic obstacles as well.

Conflict of Interest The authors declare no conflict of interest.

Acknowledgment The research reported in this paper was supported by the Higher Education Excellence Program in the frame of Artificial Intelligence research area of Budapest University of Technology and Economics (BME FIKP-MI/SC).

References

- [1] Chantal Landry, Matthias Gerdts, René Henrion, and Dietmar Hömberg. Path-planning with collision avoidance in automotive industry. In *IFIP Conference on System Modeling and Optimization*, pages 102–111. Springer, 2011.
- [2] Fabrizio Flacco, Torsten Kröger, Alessandro De Luca, and Oussama Khatib. A depth space approach to human-robot collision avoidance. In *2012 IEEE International Conference on Robotics and Automation*, pages 338–345. IEEE, 2012.
- [3] Massimo Cefalo, Emanuele Magrini, and Giuseppe Oriolo. Parallel collision check for sensor based real-time motion planning. In *2017 IEEE International Conference on Robotics and Automation (ICRA)*, pages 1936–1943. IEEE, 2017.
- [4] Anthony Stentz. Optimal and efficient path planning for partially known environments. In *Intelligent Unmanned Ground Vehicles*, pages 203–220. Springer, 1997.
- [5] Steven M LaValle. *Planning algorithms*. Cambridge University Press, 2006.
- [6] Léonard Jaillet, Juan Cortés, and Thierry Siméon. Sampling-based path planning on configuration-space costmaps. *IEEE Transactions on Robotics*, 26(4):635–646, 2010.
- [7] Ran Zhao. *Trajectory planning and control for robot manipulations*. PhD thesis, Université Paul Sabatier-Toulouse III, 2015.
- [8] Mark W Spong, Seth Hutchinson, Mathukumalli Vidyasagar, et al. *Robot modeling and control*. John Wiley & Sons, Inc., 2006.
- [9] Steven M LaValle. Rapidly-exploring random trees: A new tool for path planning. Technical report, Department of Computer Science, Iowa State University, 1998.
- [10] Sertac Karaman and Emilio Frazzoli. Sampling-based algorithms for optimal motion planning. *The international journal of robotics research*, 30(7):846–894, 2011.
- [11] Marios Xanthidis, Ioannis Rekleitis, and Jason M O’Kane. Rrt+: Fast planning for high-dimensional configuration spaces. *arXiv preprint arXiv:1612.07333*, 2016.
- [12] Peter JM Van Laarhoven and Emile HL Aarts. Simulated annealing. In *Simulated annealing: Theory and applications*, pages 7–15. Springer, 1987.
- [13] Dug Hun Hong and Chang-Hwan Choi. Multicriteria fuzzy decision-making problems based on vague set theory. *Fuzzy sets and systems*, 114(1):103–113, 2000.
- [14] Robert Babuška and Henk Verbruggen. Neuro-fuzzy methods for nonlinear system identification. *Annual reviews in control*, 27(1):73–85, 2003.
- [15] L-X Wang. Stable adaptive fuzzy control of nonlinear systems. *IEEE Transactions on fuzzy systems*, 1(2):146–155, 1993.

- [16] L-X Wang. Fuzzy systems are universal approximators. In [1992 Proceedings] *IEEE International Conference on Fuzzy Systems*, pages 1163–1170. IEEE, 1992.
- [17] L-X Wang and Jerry M Mendel. Generating fuzzy rules by learning from examples. *IEEE Transactions on systems, man, and cybernetics*, 22(6):1414–1427, 1992.
- [18] L. . Wang. Training of fuzzy logic systems using nearest neighborhood clustering. In [Proceedings 1993] *Second IEEE International Conference on Fuzzy Systems*, pages 13–17 vol.1, March 1993.
- [19] Lantos Béla. *Robotok irányítása (Robot Control)*. Akadémiai K., 2002.
- [20] MG Mohanan and Ambuja Salgoankar. A survey of robotic motion planning in dynamic environments. *Robotics and Autonomous Systems*, 100:171–185, 2018.

Multi-period Quadratic Programming Model for Sewon-Bantul Facultative Ponds Optimization

Sunarsih*, Sutrisno

Department of Mathematics, Diponegoro University, 50275, Indonesia

ARTICLE INFO

Article history:

Received: 30 September, 2019

Accepted: 12 December, 2019

Online: 25 December, 2019

Keywords:

Facultative pond

Quadratic programming

Wastewater treatment

ABSTRACT

Treatment plants have been developed in many countries to handle wastewater, therefore, many pieces of researches have been conducted in order to optimize the outcomes. In this article, a mathematical optimization model was developed using quadratic programming approach to optimize the pollutant degradation at the domestic wastewater facultative stabilization ponds. The data used in this research were obtained from Sewon, Bantul wastewater treatment plant (WWTP) located in Yogyakarta, Indonesia. The proposed mathematical optimization model was formulated by maximizing the total amount of domestic wastewater processed in four facultative ponds along with the efficiency index value of the biological oxygen demand (BOD) degradation. The corresponding quadratic programming problem was solved in LINGO 18.0 optimization tool by using the generalized reduced gradient algorithm. The result led to the optimal decision which is the value of the domestic wastewater processed in each facultative pond.

1. Introduction

The treatment of wastewater reduces its pollutant concentration through several processing levels. In Sewon, Bantul treatment plant, the process is conducted in three steps. It begins with the inception of the wastewater via inlet, following by filtering to remove its physical matters. It is further processed in the facultative pond to reduce pollutants, and processed in the maturation pond. In these steps, it is processed in order to reduce the pollutants such as bacteria, algae & zooplankton, due to prolonged storage time [1]. In order to observe, evaluate, and optimize the pollutant degradation process in facultative ponds, researches were conducted, for example, using the following approaches: a quantitative method for coefficient analysing [2], linear programming for BOD degradation [3], an economically viable natural adsorbent materials approach for wastewater treatment [4], dynamic model for sewage treatment [5], quantitative analysis for nitrogen removal mechanism [6], maturation pond analysis [7], and an optimization model approach developed for energy saving and mitigation [8].

Some advance researches were conducted to develop new approaches for wastewater treatment model using specific methods such as statistical analysis approaches [9], distillation column model approach [10], phosphorus content analysis [11], physio-chemical & micro-biological [12], oxygen electrode & biological approach [13], organism & organic matter analysis [14],

quadratic programming approach [15], a multi-objective particle swarm optimization for conjunctive use of treated wastewater & groundwater [16], fenton oxidation process optimization [17], data-driven in pumping station [18], WEST software approach for solid retention time optimization [19], integrated wastewater treatment for multiple input configurations, reuse, & disposal options [20], electrochemical oxidation for saline wastewater treatment [21], and wastewater treatment optimization using moving bed biofilm reactor method [22]. Furthermore, some articles in the literature were published on the utilization of wastewater residual, such as, for brick making [23], recycling [24], sludge for biodiesel [25], microbial fuel cells for power generation [26], etc. Conversely, numerous implementations of its optimization were reported in many areas, for example in textile bio-refractory treatment [27], municipal and piggery [28], [29], eco-industrial park [30], cutting oil on twisted tapes [31], brewery [32], sugar beet industry processing [33].

Unfortunately, the existing approaches mentioned above were modelled as a single period processing which means that the model can handle for single time processing only. In order to handle the wastewater processing in multi-period way, a new model which including the processing time variable is needed. In this paper, a multi-period mathematical optimization model approach is developed to determine the optimal decision for BOD degradation in facultative ponds. This model is developed from our previous research with data collected from Sewon, Bantul facultative ponds located in Yogyakarta, Indonesia.

*Corresponding Author: Sunarsih, Email: narsih_pdil@yahoo.com

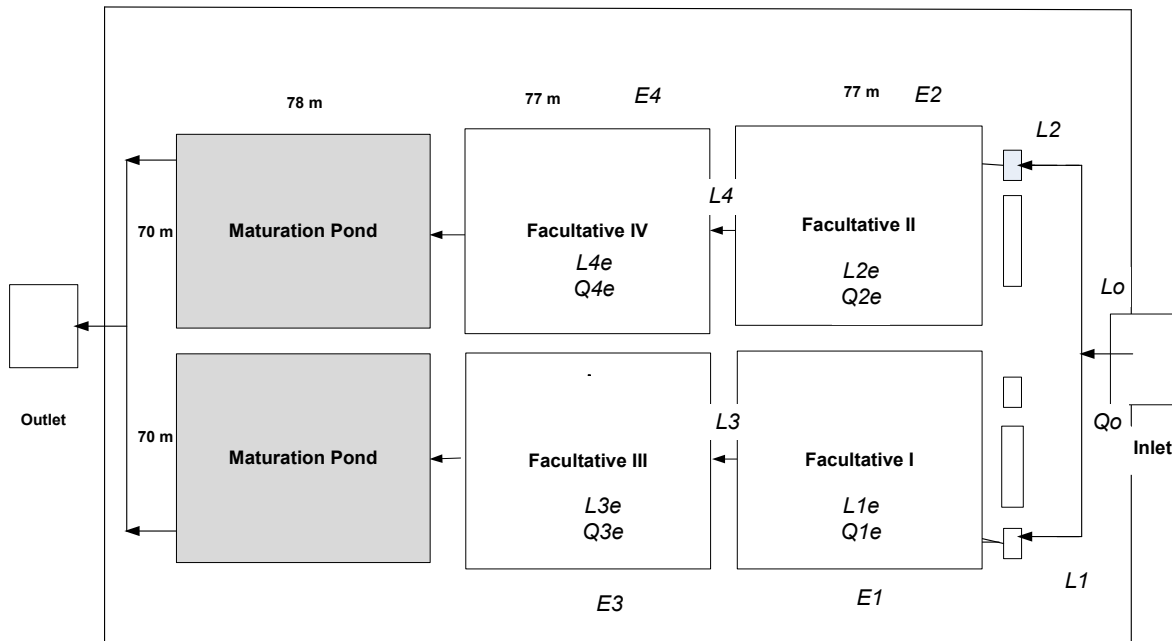


Figure 1: Sewon Bantul wastewater treatment plant [3]

2. Material and Method

2.1. Assumptions and Notations

The formulated mathematical model was considered under the following assumptions:

- (1) Optimizing wastewater processing only on four facultative ponds, we do not including the processing in the maturation pond;
- (2) The decision variable to be optimized is the BOD concentration parameter;
- (3) The data used in the model and the calculation were observed in Sewon, Bantul facultative ponds;
- (4) The data were taken from ponds I and II
- (5) The pollutant degradation process was assumed to be uniform in all ponds;
- (6) The quality standard value of the wastewater is taken from the government’s policy, Yogyakarta Province [34];
- (7) The formula to calculate the efficiency index value used in the model is based on our previous researches (see [3]);
- (8) The review period of time is assumed to be a day.

Sewon, Bantul WWTP facility contains inlet and outlet valve, as well as four facultative and two maturation ponds (see Figure 1). The following notations are used in the mathematical model:

index:

t : review period of time (day)

decision variables:

$L_p^e(t)$: Wastewater volume processed in pond p at review time period t (kg/period)

parameters:

L_0 : Initial wastewater load volume in inlet (kg/day)

$Q_0(t)$: Wastewater inflow rate in the inlet at review time period t (m³/period)

$Q_p^e(t)$: Wastewater inflow rate in facultative pond p at

- review time period t (m³/period)
- $L_p(t)$: Wastewater load volume prior to pond p at review time period t (kg/period)
- $C_p(t)$: Concentration of Biological Oxygen Demand at pond p at review time period t (mg/L)
- $L(t)$: Wastewater load for all ponds at review time period t (kg/period)
- $E_p(t)$: Efficiency value of the treatment at pond p at review time period t (in percentage)
- $E_{ref}(t)$: reference value for the efficiency value of the treatment in the pond at review time period t
- BM : Quality standards of wastewater decided by the local government (constant for all review time period)

2.2. Mathematical Model

We proposed the following mathematical model which was developed to maximize the load volume of the wastewater in all four facultative ponds and optimizing the efficiency index value of the BOD degradation by bringing it into a reference point decided by the decision maker. This was further formulated as a quadratic function of their difference, i.e.

$$\max Z = \sum_{t=1}^T \sum_{p=1}^P L_p^e(t) - \sum_{t=1}^T \sum_{p=1}^P (E_p(t) - E_{ref}(t))^2 \quad (1)$$

The following equalities/inequalities were formulated as the constraints to the model:

- (1) The efficiency index value of the BOD degradation at each review period per facultative pond need to satisfy the wastewater quality standard (BM):

$$E_p(t) \cdot C_p(t) \leq BM, \quad \forall p \in \{1, 2, 3, 4\}; \quad (2)$$

- (2) The wastewater load volume in pond p must not be exceeded:

$$L_p^e \leq L_p, \forall p \in \{1,2,3,4\}; \quad (3)$$

- (3) The wastewater load volume entering the facultative pond p is the flow rate containing BOD:

$$L_p^e(t) = \frac{(Q_p^e(t) \cdot C_p(t))}{1000}, \forall p \in \{1,2,3,4\};$$

- (4) The efficiency index value for facultative pond p at review period of time t is

$$E_p(t) = \frac{k \cdot S}{1 + k \cdot S}, \forall p \in \{1,2,3,4\}; \quad (4)$$

where k is the BOD degradation rate per day and S is the storing time (in day) of the wastewater in the facultative pond.

The above mathematical model is rewritten as:

$$\max Z = \sum_{t=1}^T \sum_{p=1}^P L_p^e(t) - \sum_{t=1}^T \sum_{p=1}^P (E_p(t) - E_{ref}(t))^2 \quad (5)$$

subject to:

$$E_p(t) \frac{(1000 \cdot L_p(t))}{Q_p^e(t)} \leq BM, \forall p = 1,2,3,4;$$

$$L_1^e(t) \leq L_1(t);$$

$$L_3^e(t) \leq L_1(t) - L_1^e(t);$$

$$L_2^e(t) \leq L_2(t);$$

$$L_4^e(t) \leq L_2(t) - L_2^e(t).$$

3. Results and Discussions

The optimal decision is calculated using the following scenario with some parameter values collected in Sewon, Bantul WWTP as reported by previous published articles. The domestic wastewater load in ponds P1 and P2 is half of the inflow rate in the value of $L_0 = 4.799,6$ kg/day, with a BOD degradation coefficient of 1.1% [3], a quality standard of 50 mg/L, and a wastewater inflow rate of 11238 m³/day in each facultative pond for one year [3]. The reference value for the efficiency of the treatment at the pond is decided to be 0.25 for ponds P1 & P2, and 0.5 for ponds P3 & P4 at any review time period t . To solve the optimization problem(5), the LINGO programming tool was run in a daily used personal computer. The optimization results are shown in Figures 2 and 3. First, the optimal decision value for the wastewater load in pond P1 & P2 is 11 2399 kg per day for each, and 1199.5 kg for P3 & P4 as shown in Figure 2 with a review time period 5, which is processed in each pond by 1199.5 m³ where the storing time is 0.25 day at pond P1, 0.25 day at pond P2, 0.57 day at pond P3, and 0.57 day at pond P4.

In order to simulate the problem in difference scenarios, the optimal decision was calculated with scenarios following the value of the wastewater load in facultative pond p at review time period t (m³/period) in Figure 2. The optimal decision, i.e. the wastewater volume to be processed in pond p at each review time t (kg/period) is shown in Figure 3. The optimal storing time is the same for all each review time i.e. 0.25 day at pond P2 & P3, and 0.57 day at pond P3 & P4.

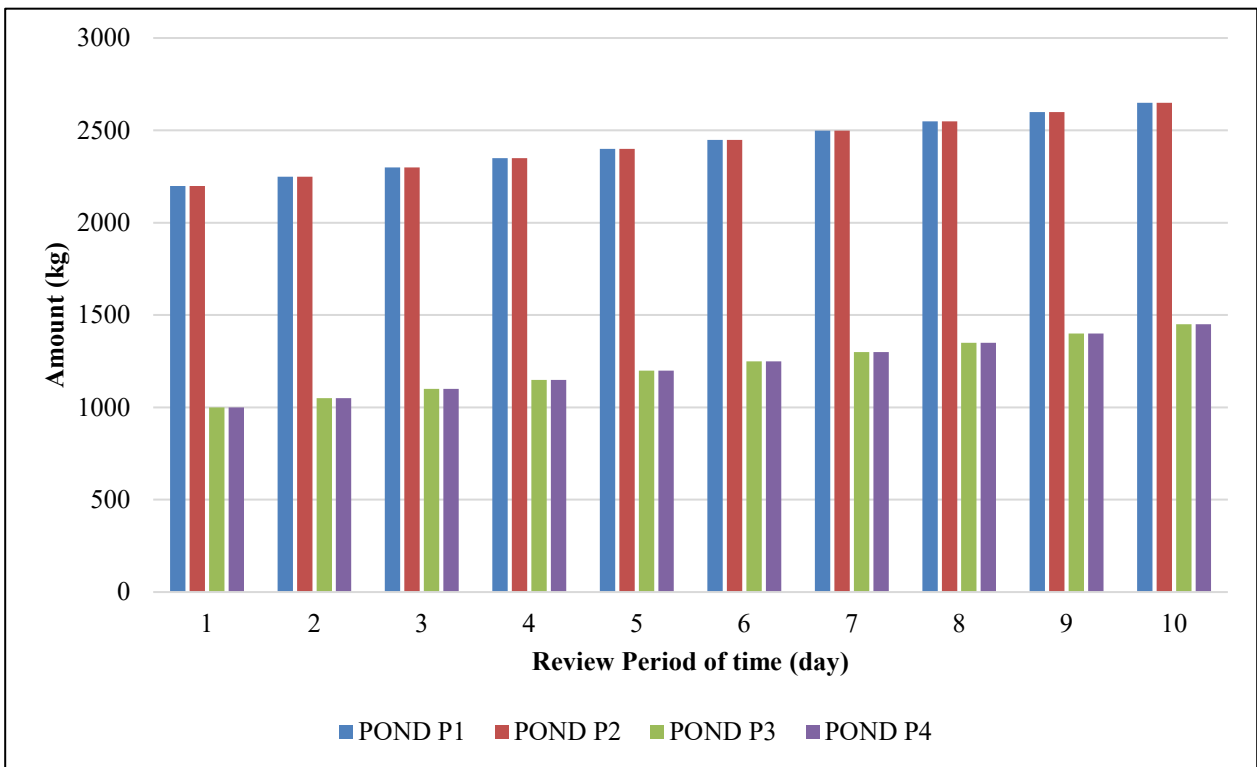


Figure 2: Wastewater load in facultative pond p at review time period t (kg/period)

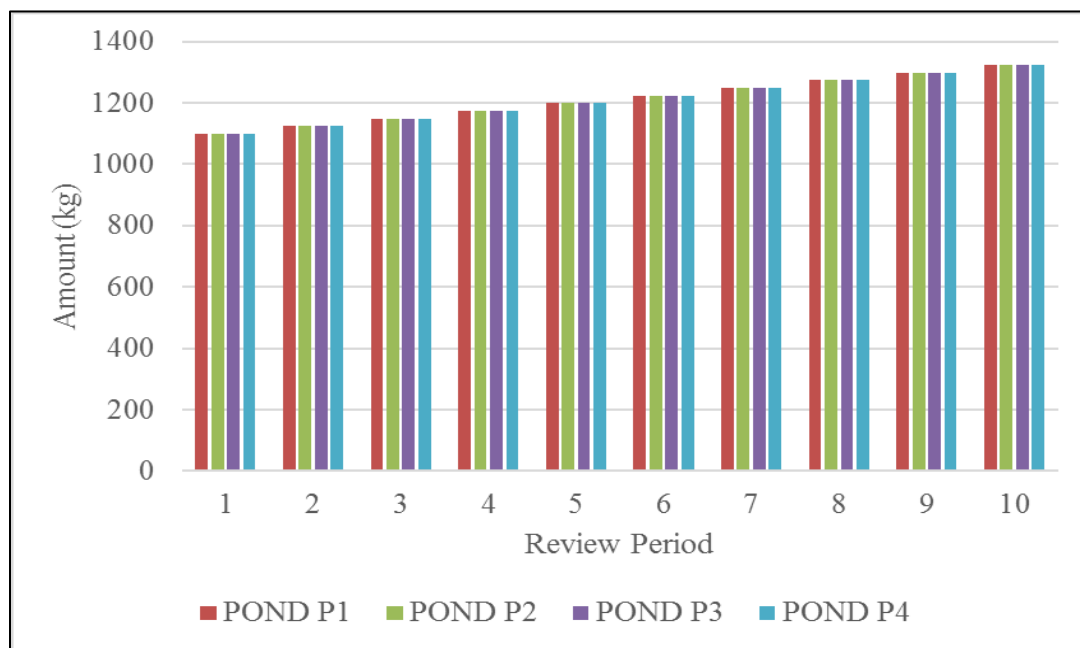


Figure 3: Wastewater volume processed in pond p at review time period t (kg/period)

4. Concluding Remarks

An optimization mathematical model in a quadratic programming was proposed in this paper which is used to calculate the optimal amount of domestic wastewater to be processed in facultative stabilization ponds. The model was solved using data collected at Sewon, Bantul WWTP, and from the computational experiment, the facultative pond was derived with the storing time at each pond.

The authors declare no conflict of interest.

Acknowledgment

Authors thank to LPPM Universitas Diponegoro for funding support under RPP Research Grant Contract No. 329-46/UN7.P4.3/PP/2019.

References

- [1] S. Sunarsih, P. Purwanto, and W. S. Budi, "Mathematical modeling regime steady state for domestic Wastewater Treatment facultative stabilization ponds," *J. Urban Environ. Eng.*, vol. 7, no. 2, pp. 293–301, 2013.
- [2] B. sheng Huang *et al.*, "Quantitative study of degradation coefficient of pollutant against the flow velocity," *J. Hydrodyn.*, vol. 29, no. 1, pp. 118–123, 2017.
- [3] Sunarsih, Widowati, Kartono, and Sutrisno, "Mathematical Analysis for the Optimization of Wastewater Treatment Systems in Facultative Pond Indicator Organic Matter," *E3S Web Conf.*, vol. 31, no. 05008, pp. 1–3, 2018.
- [4] A. Gopakumar, R. Narayan, S. A. Nagath, N. P. R. Mohammed. S, and S. Chandran .S, "Waste Water Treatment Using Economically Viable Natural Adsorbent Materials," *Mater. Today Proc.*, vol. 5, no. 9, pp. 17699–17703, 2018.
- [5] D. Recio-Garrido, Y. Kleiner, A. Colombo, and B. Tartakovsky, "Dynamic model of a municipal wastewater stabilization pond in the arctic," *Water Res.*, vol. 144, pp. 444–453, 2018.
- [6] A. W. Mayo and M. Abbas, "Removal mechanisms of nitrogen in waste stabilization ponds," *Phys. Chem. Earth*, vol. 72–75, pp. 77–82, 2014.
- [7] F. Cortés Martínez, A. Treviño Cansino, A. Sáenz López, J. L. González Barrios, and F. J. De La Cruz Acosta, "Mathematical modeling and optimization in the design of a maturation pond," *J. Appl. Res. Technol.*, vol. 14, no. 2, pp. 93–100, 2016.
- [8] S. Borzooei *et al.*, "Optimization of the wastewater treatment plant: From energy saving to environmental impact mitigation," *Sci. Total Environ.*, vol. 691, pp. 1182–1189, 2019.
- [9] F. Halters, E. Zondervan, and A. De Haan, "Integrated optimization of a waste water treatment plant using statistical analysis," *J. Hazard. Mater.*, vol. 179, no. 1–3, pp. 480–487, 2010.
- [10] F. Ferella, "Journal of Environmental Chemical Engineering Optimization of a plant for treatment of industrial waste solutions : Experimental and process analysis," *J. Environ. Chem. Eng.*, vol. 6, no. 1, pp. 377–385, 2018.
- [11] M. D. Sells, N. Brown, and A. N. Shilton, "Determining variables that influence the phosphorus content of waste stabilization pond algae," *Water Res.*, vol. 132, pp. 301–308, 2018.
- [12] L. T. Ho, A. Alvarado, J. Larriva, C. Pompeu, and P. Goethals, "An integrated mechanistic modeling of a facultative pond: Parameter estimation and uncertainty analysis," *Water Res.*, vol. 151, pp. 170–182, 2019.
- [13] M. Novak and P. Horvat, "Mathematical modelling and optimisation of a waste water treatment plant by combined oxygen electrode and biological waste water treatment model," vol. 36, pp. 3813–3825, 2012.
- [14] F. C. Martínez, A. T. Cansino, M. Aracelia, A. García, V. Kalashnikov, and R. L. Rojas, "Mathematical Analysis for the Optimization of a Design in a Facultative Pond : Indicator Organism and Organic Matter," *Math. Probl. Eng.*, vol. 2014, no. 1, pp. 1–12, 2014.
- [15] Sunarsih, D. P. Sasongko, and Sutrisno, "Process Improvement on Domestic Wastewater Treatment Stabilization Ponds by Using Mathematical Optimization Approach," *Mat. MJIAM*, vol. 35, no. 2, pp. 171–176, 2019.
- [16] M. Youse, M. Ebrahim, J. Soltani, and A. Roozbahani, "Multi-objective particle swarm optimization model for conjunctive use of treated wastewater and groundwater," *Agric. Water Manag. J.*, vol. 208, pp. 224–231, 2018.
- [17] M. Zhang, H. Dong, L. Zhao, D. Wang, and D. Meng, "A review on Fenton process for organic wastewater treatment based on optimization perspective," *Sci. Total Environ.*, vol. 670, pp. 110–121, 2019.
- [18] J. Filipe, R. J. Bessa, M. Reis, R. Alves, and P. Póvoa, "Data-driven predictive energy optimization in a wastewater pumping station," *Appl. Energy*, vol. 252, no. February, p. 113423, 2019.
- [19] R. Muoio *et al.*, "Optimization of a large industrial wastewater treatment plant using a modeling approach : A case study," *J. Environ. Manage.*, vol. 249, no. May, p. 109436, 2019.
- [20] M. S. Ang, J. Duyag, K. C. Tee, and C. L. Sy, "A multi-period and multi-criterion optimization model integrating multiple input configurations, reuse, and disposal options for a wastewater treatment facility," *J. Clean. Prod.*, vol. 231, pp. 1437–1449, 2019.
- [21] M. Darvishmotevalli and A. Zarei, "Optimization of saline wastewater treatment using electrochemical oxidation process : Prediction by RSM method," *MethodsX*, vol. 6, pp. 1101–1113, 2019.

- [22] R. K. Sonwani, G. Swain, B. S. Giri, and R. S. Singh, "A novel comparative study of modified carriers in moving bed biofilm reactor for the treatment of wastewater : Process optimization and kinetic study," *Bioresour. Technol. J.*, vol. 281, pp. 335–342, 2019.
- [23] L. P. Rodrigues, J. Nilson, and F. Holanda, "Recycling of Water Treatment Plant Waste for Production of Soil- Cement Bricks," *Procedia Mater. Sci.*, vol. 8, pp. 197–202, 2015.
- [24] S. Raghuvanshi, V. Bhakar, C. Sowmya, and K. S. Sangwan, "Waste water treatment plant life cycle assessment : treatment process to reuse of water," *Procedia CIRP*, vol. 61, pp. 761–766, 2017.
- [25] S. Mohseni and M. S. Pishvae, "Data-driven robust optimization for wastewater sludge-to-biodiesel supply chain design," *Comput. Ind. Eng.*, vol. in press, 2019.
- [26] H. Mehravanfar, M. A. Mahdavi, and R. Gheshlaghi, "Economic optimization of stacked microbial fuel cells to maximize power generation and treatment of wastewater with minimal operating costs," *Int. J. Hydrogen Energy*, vol. 44, no. 36, pp. 20355–20367, 2019.
- [27] A. Stéphane, K. Edmond, A. Emmanuella, K. Adouby, and P. Drogui, "In-situ generation of effective coagulant to treat textile bio-refractory wastewater : Optimization through response surface methodology," *J. Environ. Chem. Eng.*, vol. 6, no. 4, pp. 5587–5594, 2018.
- [28] L. D. S. Leite, M. Teresa, and L. A. Daniel, "Microalgae cultivation for municipal and piggery wastewater treatment in Brazil," *J. Water Process Eng.*, vol. 31, pp. 1–7, 2019.
- [29] J. Lu, X. Wang, H. Liu, H. Yu, and W. Li, "Optimizing operation of municipal wastewater treatment plants in China : The remaining barriers and future implications," *Environ. Int.*, vol. 129, no. March, pp. 273–278, 2019.
- [30] E. O. Dwyer, K. Chen, H. Wang, A. Wang, N. Shah, and M. Guo, "Optimisation of wastewater treatment strategies in eco-industrial parks : Technology, location and transport," *Chem. Eng. J.*, vol. 381, no. March 2019, p. 122643, 2020.
- [31] S. Popovi and M. Karad, "Optimization of ultra filtration of cutting oil wastewater enhanced by application of twisted tapes : Response surface methodology approach," *J. Clean. Prod. J.*, vol. 231, pp. 320–330, 2019.
- [32] R. Singh, P. Bhunia, and R. R. Dash, "Optimization of organics removal and understanding the impact of HRT on vermifiltration of brewery wastewater," *Sci. Total Environ.*, vol. 651, pp. 1283–1293, 2019.
- [33] S. Sharma and H. Simsek, "Sugar beet industry process wastewater treatment using electrochemical methods and optimization of parameters using response surface methodology," *Chemosphere*, vol. 238, p. 124669, 2020.
- [34] Gubernur DI Yogyakarta (Governor of Special Region Yogyakarta), *Surat Keputusan Gubernur Kepala Daerah Istimewa Yogyakarta (Decree of Special Region Yogyakarta Governor) No. 214/KPTS/1991*. 1991.

Performance Analysis of Routing Protocols in Resource-Constrained Opportunistic Networks

Aref Hassan Kurd Ali^{1,*}, Halikul Lenando¹, Mohamad Alrfaay¹, Slim Chaoui², Haithem Ben Chikha², Akram Ajouli³

¹Department of Computer Systems and Communication Technologies, Faculty of Computer Science and Information Technology, Universiti Malaysia Sarawak (UNIMAS), Kota Samarahan 94300, Sarawak, Malaysia

²Department of Computer Engineering and Networks, College of Computer and Information sciences, Jouf University, Sakaka 2014, KSA.

³Department of Computer Science, College of Computer and Information sciences, Jouf University, Sakaka 2014, KSA.

ARTICLE INFO

Article history:

Received: 19 October, 2019

Accepted: 09 December, 2019

Online: 25 December, 2019

Keywords:

Wireless Sensor Networks

Mobile Ad Hoc Networks

Delay Tolerant Networks

Opportunistic Networks

Routing Protocols

Analysis

Performance Evaluation

ABSTRACT

Recently, opportunistic networks are considered as one of the most attractive developments of ad hoc mobile networks (MANETs) that have emerged thanks to the development of intelligent devices. Due to the mobility-related instability of the paths between nodes and due to the limited buffer and energy resources, the ultimate objective of routing protocols in opportunistic networks is to enable the exchange of information between users. In such harsh environments, it is difficult to exactly pin down the services provided by these networks. To this end, we present in this paper a study on the performance analysis of six of the most popular routing protocols in opportunistic networks, namely, epidemic, PROPHET, MaxProp, Spray and Wait, Spray and Focus, and Encounter-Based Routing (EBR). We firstly described these protocols and presented their algorithms. Thereafter, we carried out a comparative study of these protocols using exhaustive performance testing experiments with different numbers of nodes, traffic loads, message lifetime, and buffer size. The results of this investigation are with an important role in helping network designers to improve performance in such challenging networks.

1. Introduction

Delay Tolerant Networks (DTNs) [1] are one of the most attractive progresses in Mobile Ad Hoc Networks (MANETs), which become dominant due to the emergence of the intelligent devices equipped with wireless communication facilities. Historically, DTN concepts were emerged in the interplanetary environment studies. After that, the DTN concepts grew to cover other types of networks. As examples of DTN networks we cite: disaster environments [2], under water communications [3], rural remote patient monitoring [4], animal habitat monitoring and network sensors for wildlife tracking [5], vehicular delay tolerant networks (VDTN) [6], surveillance for regions on the earth surface [7] and any network with frequent links disruptions due to environmental features changing. It should be noted that the

*Department of Computer Systems and Communication Technologies, Faculty of Computer Science and Information Technology, Universiti Malaysia Sarawak (UNIMAS), Kota Samarahan 94300, Sarawak, Malaysia. Mobile: +966503225673; Email: abhznk@gmail.com

routing in DTN is more difficult than in MANET. This is due to the lack of information about network topology in DTN networks. DTN Networks are characterized as intermittent connectivity with often end-to-end path interruption and topology alterations. Once a connection is established, there is no guarantee to maintain it until the end of the communication. This is caused by the mobility of the nodes, which can lead to instability of the paths between sources and destinations. To overcome this inherent problem, DTN networks rely on Store-Carry-Forward transport paradigm. In this paradigm, when a source node wants to transmit a message to a destination node, it sends the message to the neighboring nodes, referred to as relay nodes or candidate nodes. The relay nodes do the same until the message delivered finally to its destination. This paradigm is called opportunistic transport and the network on which is based is called opportunistic network. Despite opportunistic contacts, sporadic connectivity and limited resources, opportunistic networks attempt to facilitate the exchange of information between users (nodes). To this end, all internet and mobile Ad-hoc networks routing protocols need to be

redesigned according to this paradigm. For more than two decades researchers have developed many routing protocols for opportunistic networks. Some of these protocols are simple and rely solely on flooding the network with messages' copies in the hope that the messages will reach their destination. Intricate protocols try to forward copies of messages only to the nodes that are best placed to deliver messages to their destination at the lowest cost. In the literature, there are many classifications of routing protocols in opportunistic networks. Some of them are flooding-based and quota-based routing protocols [8]. In the flooding-based routing protocols, each node floods the network with messages' copies in the hope that one of them will reach its destination. In [9], Epidemic was presented as example of flooding-based routing protocols. Flooding-based routing protocols work very well if the network has unlimited buffer sizes and all nodes are rechargeable. However, in opportunistic networks with limited resources, flooding-based protocols are poor. To control flooding in these protocols, a lot of protocols have been proposed. These protocols are termed as guided-based routing protocols [10] and are considered as a subcategory of the flooding-based routing protocols. Guided-based routing protocols forward messages only to the nodes that are most likely to reach the destination. This is done by allowing the forwarding decision of the message to be based on a utility metric calculated according to certain criteria. Some of these criteria depend on the contact rate, as in PRoPHET protocol [11]. Some other utility metrics are calculated based on the path cost to the destination, as in the MaxProp routing protocol [12].

In the quota-based routing protocols, the router imposes an upper limit on the number of messages' copies in the network. For instance, we cite Spray and Wait (SaW) [13], Spray and Focus (SaF) [14] and Encounter Based routing (EBR) [8].

In this paper, we performed an analytical study on the performance of the most common routing protocols in opportunistic networks. These protocols are: Epidemic, PRoPHET, MaxProp, Spray and Wait, Spray and Focus and EBR. These protocols are selected precisely because of their outstanding performance and because they are often used as benchmarks in most studies. The experiments were conducted in resource-poor environments, non-rechargeable nodes, and limited memory. In such harsh environments, it is difficult to make a precise statement about what kind of services can be provided [15]. Therefore, our study serves to make comparisons and conclusions that help designers to improve performance in such challenging networks. To our knowledge, our work is one of the rare studies that could provide an in-depth analysis of the behavior of the most common routing protocols of resource-constrained opportunistic networks. The study also includes key recommendations for designing a high-performance routing protocol.

The remainder of this work is organized as follows: in section 2 the related works are presented. Opportunistic routing protocols explanations are presented in section 3. Section 4 introduces the used system model. Performance evaluation and the settings of the simulation are presented in section 5. In section 6, the results are presented followed by discussions. Design guidelines are presented in section 7. Finally, section 8 provides the conclusion of this work.

2. Related Works

Routing mechanisms in opportunistic networks are one of the most important elements that play a major role in their performance. Therefore, investigating the effectiveness of routing protocols in opportunistic networks is an important topic. Moreover, the store-carry-forward transport paradigm makes the routing performance analysis more complex and challenging than other networks. In view of the importance of the subject, we find in the literature a lot of researches that have addressed this topic.

Authors in [16] compared the performance of several routing protocols in opportunistic networks. The experiments were performed with different numbers of nodes at different speeds. However, this research did not take into account traffic loads, message lifetime, buffer size and energy consumption. Despite the valuable results of this research, it does not focus on opportunistic networks with limited resources.

Several representative routing protocols in opportunistic networks were investigated in [17]. The simulations performed with different numbers of nodes and traffic loads. The simulation time was 24 hours in all experiments and all nodes were rechargeable. However, this research did not highlight resource constraints in opportunistic networks.

In [18], authors perform a performance analysis research of eight routing protocols of delay tolerant networks. The eight protocols were compared in different traffic loads and message lifetimes. All nodes were rechargeable and equipped with buffers of 50 MB. in all experiments, simulation time was 6 hours. However, this study did not address the resource consumption issues which is a major concern in the limited resource opportunistic networks.

Authors in [19] highlight the energy consumption issue in opportunistic networks. they compared the performance of five of the most common routing protocols. The five protocols were compared in different numbers of nodes and hop counts. However, the study did not address the buffers consumption issue which is one of the most important resources in opportunistic networks.

Complexity and scalability was the main objective of comparison in [20]. The authors compared three routing protocols: Epidemic, PRoPHET and First Contact. Despite the valuable results, they did not take into account the consumption of network resources.

Authors in [10] compared the performance of four well-known routing protocols in opportunistic networks. the comparison was carried out by changing the values of message lifetime, buffers, traffic load and the number of nodes. In addition to the results of the comparisons, the authors addressed a set of guidelines to improve routing protocols. In spite of the beneficial results, the research did not include the effect of energy consumption on the performance of the routing protocol.

Our research differs from previous studies in that it mainly highlights the issue of the limited resources of opportunistic networks. Our study did not overlook the limitations of energy and memory in all analyzes. We firstly described the most common protocols and presented their algorithms. Thereafter, we carried out a comparative study of these protocols using

exhaustive performance testing experiments with different numbers of nodes, traffic loads, message lifetime, and buffer size.

3. Opportunistic Routing Protocols

3.1. Epidemic Routing Protocol

The authors in [9] propose the Epidemic routing protocol, which is classified as a flooding-based routing protocol. It is historically the first protocol in opportunistic networks. It works as follows: When a node encounters another node, it gives it a copy of the messages it has and is not in possession of the other node. In fact, both nodes exchange the so-called summary vector, which contains their respective message IDs. The messages remain in buffers until they are delivered to their destination or dropped due to their expired lifetime. The pseudocode of the Epidemic router is shown in Algorithm 1.

If all nodes in the network are rechargeable and have unlimited buffer sizes, the EPIDEMIC routing protocol theoretically achieves the highest transfer rate and lowest latency. However, in opportunistic networks with limited resources, EPIDEMIC is the neediest protocol for network resources in terms of energy and buffer consumption.

ALGORITHM 1. EPIDEMIC ROUTING PROTOCOL

```

1: Let  $n_x$  and  $n_y$  two nodes in an opportunistic network.
2: Let  $DropExpireMessages(n_x)$  a procedure for dropping expired messages in node  $n_x$ .
3: Let  $ExchangeSummaryVectors(n_x, n_y)$  a procedure for exchanging the summary vectors of both nodes.
4: if  $n_x$  meets  $n_y$  then
5:    $DropExpireMessages(n_x)$ .
6:    $ExchangeSummaryVectors(n_x, n_y)$ .
7:   for each message  $m_x$  in node  $n_x$  do
8:     if  $m_x$  did not exist in  $n_y$  then
9:       Forward a copy of  $m_x$  to  $n_y$ .
10:    end if
11:  end for
12: end if

```

3.2. PROPHET Routing Protocol

PROPHET stands for a Probabilistic Routing Protocol using History of Encounters and Transitivity [11]. In PROPHET, messages are routed based on the destination's encounter probability which is termed as *delivery predictability*, and denoted by $P_{(a,b)} \in [0, 1]$, where a is a node among nodes in the network and b is the destination node. Actually, the *delivery predictability* metric is computed according to three equations depending on the happened event. If the node a meets another node b , the *delivery predictability* metric is updated according to equation (1).

$$P_{(a,b)} = P_{(a,b)old} + (1 - P_{(a,b)old}) \times P_{(a,b)init} \quad (1)$$

where $P_{(a,b)old}$ is the previous *delivery predictability* value and $P_{(a,b)init}$ is the starting value.

The longer the interval between the two meetings between any two nodes, the less likely they will see each other in the future. Hence, the *delivery predictability* is aged (reduced) based on equation (2).

$$P_{(a,b)} = P_{(a,b)old} \times \gamma^k \quad (2)$$

where $\gamma \in [0, 1]$ is the aging constant and k is the number of time units that have elapsed since the last measurement was reduced.

Also, a transitive property is formed based on the observation that shows if a node a frequently meets a node b and node b frequently meets a third node c , then there is a high probability that node c will be a good choice for forwarding messages to node a . The *delivery predictability* is updated according to this transitive property as follows:

$$P_{(a,c)} = P_{(a,c)old} + (1 - P_{(a,c)old}) \times P_{(a,b)} \times P_{(b,c)} \times \beta \quad (3)$$

where β is a constant that decides how large the effect of the transitivity should have on the *delivery predictability*.

Now, the routing strategy that is followed is simple. When a node encounters another node, the messages will be forwarded (copied) to the other node only if the *delivery predictability* value for the message' destination of the encountered node is higher. The pseudocode for the PROPHET routing protocol is presented in Algorithm 2.

ALGORITHM 2. PROPHET ROUTING PROTOCOL

```

1: Let  $n_x$  and  $n_y$  two nodes in an opportunistic network.
2: Let  $DropExpireMessages(n_x)$  a procedure for dropping expired messages in node  $n_x$ .
3: Let  $ExchangeSummaryVectors(n_x, n_y)$  a procedure for exchanging the summary vectors of both nodes.
4: Let  $UpdateDeliveryPredictability()$  a procedure for recalculating the delivery predictability values for all known destinations.
5: Let  $n_D$  the destination node of the message  $m$ .
6: Let  $P(n, n_D)$  the value of the delivery predictability of  $n$  to deliver the message to its destination  $n_D$ .
7: if  $n_x$  meets  $n_y$  then
8:    $DropExpireMessages(n_x)$ 
9:    $ExchangeSummaryVectors(n_x, n_y)$ 
10:   $UpdateDeliveryPredictability()$ 
11:  for each message  $m_x$  in node  $n_x$  do
12:    if  $m_x$  did not exist in  $n_y$  then
13:      if  $P(n_y, n_D) > P(n_x, n_D)$  then
14:        Forward a copy of  $m_x$  to  $n_y$ .
15:      end if
16:    end if
17:  end for
18: end if

```

PROPHET is considered a guided-based routing protocol. This is because messages are routed to their destinations using the *Delivery Predictability* Metric. However, it still suffering from high overhead and high consumption of network resources.

3.3. MaxProp Routing Protocol

MaxProp [12] is motivated by the limitations of some existing systems, as they focus on short-range targets and can not remove obsolete messages from the network. Therefore, MaxProp removes outdated messages from the network buffers and prevents the double data spread on the same node. Each node in the network maintains a vector list which contains the estimation of encountering of all other nodes in the network. So, for any two nodes, denoted a and b , in a network of S nodes, the initial probability to meet each other is given by equation (4).

$$P_{(a,b)} = 1/(S-1) \quad (4)$$

If the node a meets the node b , the probability is updated by increasing $P_{(a,b)}$ with 1, and then all other probabilities of meeting between the node a and the other nodes in the network are normalized.

ALGORITHM 3. MAXPROP ROUTING PROTOCOL

```

1: Let  $n_x$  and  $n_y$  two nodes in an opportunistic network.
2: Let  $DropExpireMessages(n_x)$  a procedure for dropping expired messages in node  $n_x$ .
3: Let  $ExchangeSummaryVectors(n_x, n_y)$  a procedure for exchanging the summary vectors of both nodes.
4: Let  $UpdateDeliveryPredictabilities()$  a procedure for recalculating the delivery predictability values.
5: Let  $CostCalculation(n_D)$  a procedure to calculate the cost of the destination of the message  $m_x$ .
6: Let  $ExchangeAcknowledgments()$  a procedure to exchange the acknowledgments lists of the delivered messages.
7: if  $n_x$  meets  $n_y$  then
8:    $DropExpireMessages(n_x)$ 
9:    $ExchangeSummaryVectors(n_x, n_y)$ 
10:   $UpdateDeliveryPredictabilities()$ 
11:   $ExchangeAcknowledgments()$ 
12:  Delete acknowledged messages
13:  for each message  $m_x$  in node  $n_x$  do
14:    if (the message' hop counts < threshold) then
15:      if the message has the lowest hop count then
16:        Forward a copy of  $m_x$  to  $n_y$ 
17:      end if
18:    end if
19:     $CostCalculation(n_D)$ 
20:    if (A room is needed for an incoming message) then
21:      if ( $m_x$  has the biggest cost) then
22:        Delete  $m_x$ 
23:      end if
24:    end if
25:  end for
26: end if

```

Based on these probabilities, MaxProp computes destinations costs. Consequently, a message scheduling is done in each node based on these costs which will be used later for making the forwarding and dropping decisions. The pseudo code of MaxProp is given by Algorithm 3.

Although MaxProp can choose the optimal delivery path, the method of estimating delivery costs used in this work is fast and not considered accurate [21]. However, in terms of overhead and resource consumption, MaxProp is better than PProPHET [10].

3.4. Spray and Wait Routing Protocol

Spray and Wait (SaW) routing protocol is proposed in [13] to set an upper bound on the number of messages in the network. It is categorized as a quota-based routing protocol. The idea in SaW protocol is to associate a number L for each created message. This number defines the maximum number of copies that is allowed for the message in the network. the binary version of SaW protocol works as follows: When two nodes come together and exchange messages in their possession, the number L of copies of each message is equally distributed. The equally split process continues until the number of copies reaches one, then the node keeps a single copy of the message until it is delivered to its destination or it is dropped due to expiration. Therefore, this protocol is divided into two phases: *Spray* phase and the *Wait* phase. In the *Spray* phase, the number of copies is distributed until it reaches to one. In the *Wait* phase, a node waits until it meets the destination of the message. Algorithm 4 shows the pseudo code of SaW routing protocol.

Although SaW performs better than flooding-based routing protocols in term of overhead and resources consumption, performance degradation may occur because of the blind selection of the candidate node to carry the message.

ALGORITHM 4. BINARY SaW ROUTING PROTOCOL

```

1: Let  $n_x$  and  $n_y$  two nodes in an opportunistic network.
2: Let  $DropExpireMessages(n_x)$  a procedure for dropping expired messages in node  $n_x$ .
3: Let  $ExchangeSummaryVectors(n_x, n_y)$  a procedure for exchanging the summary vectors of both nodes.
4: Let  $L_{m_x}$  the initial number of the copies that are allowed for the message  $m_x$  in the network.
5: Let  $ExchangeAcknowledgments()$  a procedure to exchange the acknowledgments lists of the delivered messages.
6: if  $n_x$  meets  $n_y$  then
7:    $DropExpireMessages(n_x)$ 
8:    $ExchangeSummaryVectors(n_x, n_y)$ 
9:    $ExchangeAcknowledgments()$ 
10:  Delete acknowledged messages
11:  for each message  $m_x$  in node  $n_x$  do
12:    if ( $L_{m_x} > 1$ ) then
13:       $L_{m_x} \leftarrow L_{m_x} / 2$ 
14:      Forward  $m_x$  to  $n_y$ 
15:    else if ( $n_y$  is the destination of  $m_x$ ) then
16:      Forward  $m_x$  to  $n_y$ 
17:      Add  $m_x$  to the acknowledgment list
18:    end if
19:  end for
20: end if

```

3.5. Spray and Focus Routing Protocol

Spray and Focus (SaF) is proposed in [14]. SaF is similar to the SaW protocol. In fact, it uses the same first Spray phase, but it uses the phase of focus instead of the wait phase. In the Wait phase, the node that has a single copy of the message waits until it reaches the destination, or the message is expired. However, in the focus phase, the message will be forwarded to other nodes if only a single copy of the message remains in the node in order to accelerate the process of reaching the destination. The message forwarding decisions in the focus phase are made based on a utility metric that is estimated based on the contact history information. The pseudocode of the SaF routing protocol is shown in Algorithm 5.

ALGORITHM 5. SaF ROUTING PROTOCOL

```

1: Let  $n_x$  and  $n_y$  two nodes in an opportunistic network.
2: Let  $DropExpireMessages(n_x)$  a procedure for dropping expired messages in node  $n_x$ .
3: Let  $ExchangeSummaryVectors(n_x, n_y)$  a procedure for exchanging the summary vectors of both nodes.
4: Let  $L_{m_x}$  the initial number of the copies that are allowed for the message  $m_x$  in the network.
5: Let  $UpdateDeliveryPredictabilities()$  a procedure for recalculating the delivery predictability value.
6: Let  $ExchangeAcknowledgments()$  a procedure to exchange the acknowledgments lists of the delivered messages.
7: Let  $n_D$  the destination node of a message  $m$ .
8: if  $n_x$  meets  $n_y$  then
9:    $DropExpireMessages(n_x)$ 
10:   $ExchangeSummaryVectors(n_x, n_y)$ 
11:   $ExchangeAcknowledgments()$ 
12:  Delete acknowledged messages
13:   $UpdateDeliveryPredictabilities()$ 
14:  for each message  $m_x$  in node  $n_x$  do
15:    if ( $n_y$  is the destination of  $m_x$ ) then
16:      Forward  $m_x$  to  $n_y$ 
17:      Add  $m_x$  to the acknowledgment list
18:      Continue (break for loop)
19:    end if
20:    if ( $L_{m_x} > 1$ ) then
21:       $L_{m_x} \leftarrow L_{m_x} / 2$ 
22:      Forward  $m_x$  to  $n_y$ 
23:    else if ( $P(n_y, n_D) > P(n_x, n_D)$ ) then
24:      Forward a copy of  $m_x$  to  $n_y$ 
25:    end if
26:  end for
27: end if

```

Although SaW and SaF succeed in limiting the resource consumption, they still depending on the blind selection of the next hop in the *Spray* phase. Therefore, several solutions have been proposed to improve them in order to avoid blind selection of the relay nodes. As an example, we cite [22].

3.6. EBR Routing Protocol

An Encounter-Based Routing protocol (EBR) is proposed in [8]. Similar to SaW and SaF, EBR is considered a quota-based routing protocol because it limits the number of copies of the message in the network. Thus, the number of copies of a message m_x in the node n_x , is limited by a fixed threshold L . When a node x encounters a node y , the number of copies of the message m_x is distributed between the two nodes according to their previous encounter rate denoted by EV . To get more accurate EV values, the EBR protocol uses the concept of the exponentially weighted moving average. If CW stands for the current window, which is the number of encounters within the current time interval, EV is periodically recalculated using equation (5).

$$EV = \alpha \times CW + (1 - \alpha) \times EV \quad (5)$$

where α is a weighting constant. The pseudocode of the EBR routing protocol is presented in Algorithm 6.

ALGORITHM 6. EBR ROUTING PROTOCOL

```

1: Let  $n_x$  and  $n_y$  two nodes in an opportunistic network.
2: Let  $DropExpireMessages(n_x)$  a procedure for dropping expired messages in node  $n_x$ .
3: Let  $ExchangeSummaryVectors(n_x, n_y)$  a procedure for exchanging the summary vectors of both nodes.
4: Let  $L_{mx}$  the initial number of the copies that are allowed for the message  $m_x$  in the network.
5: Let  $ExchangeAcknowledgments()$  a procedure to exchange the acknowledgments lists of the delivered messages.
6: if  $n_x$  meets  $n_y$  then
7:    $DropExpireMessages(n_x)$ 
8:    $ExchangeSummaryVectors(n_x, n_y)$ 
9:    $ExchangeAcknowledgments()$ 
10:  Delete acknowledged messages
11:  if (CurrentTime > NextUpdateTime) then
12:     $EV_{nx} \leftarrow \alpha \times CW + (1 - \alpha) \times EV_{nx}$ 
13:     $CW \leftarrow 0$ 
14:     $NextUpdateTime \leftarrow CurrentTime + NextUpdateTime$ 
15:  end if
16:  for each message  $m_x$  in node  $n_x$  do
17:    if ( $n_y$  is the destination of  $m_x$ ) then
18:      Forward  $m_x$  to  $n_y$ 
19:      Add  $m_x$  to the acknowledgment list
20:      Continue (break for loop)
21:    else
22:      Send  $[L_{mx} \times EV_{ny} / (EV_{nx} + EV_{ny})]$  copies of  $m_x$  to  $n_y$ 
23:       $L_{mx} \leftarrow [1 - L_{mx} \times EV_{ny} / (EV_{nx} + EV_{ny})]$ 
24:    end if
25:  end for
26: end if

```

4. System Model

We consider an opportunistic network with the well-known Opportunistic Network Environment Simulator (ONE) [23]. ONE is a Java-based simulation program. It is designed primarily for opportunistic networks. Source codes are available in [24]. All experiments are conducted using real live mobility of the following patterns: pedestrians, bicycles, motorcycles, and drivers of faster

and slower cars. All nodes use Bluetooth as the communication medium. Each node is equipped with a battery with a limited power budget of 800 mAh. The size of the generated messages is 128 KB. The size of the world is 4500×3400 . No assignment to special routes or maps to a group. Downtown Helsinki (pedestrian streets and streets) is the environment of our experiments. We assume that all nodes employ the Shortest Path Map-Based motion model and all nodes are not rechargeable.

5. Performance Evaluation

Since we want to measure the performance of protocols in opportunistic networks with limited buffers and limited energy, the effectiveness of these routing protocols should be observed with different values of buffer sizes and their performance evaluated taking into account the continuous energy consumption over time.

5.1. Performance metrics

We consider four metrics to evaluate the performance of the routing protocols. The performance metrics are explained as follows:

- **Delivery Ratio:** It is the ratio of the total number of delivered messages D to the total number of created messages C. It is given by the equation (6).

$$\text{Delivery Ratio} = \frac{D}{C} \quad (6)$$

- **Overhead Ratio:** It reflects how many redundant messages are relayed to deliver one message. It simply reflects transmission cost in a network. It is given by equation (7).

$$\text{Overhead Ratio} = \frac{F - D}{D} \quad (7)$$

where F is the total number of forwarded messages by the relays nodes.

- **Average Latency:** It is the average of delay, i.e., the time between the creation of messages and their reception by the final destination. It is given by equation (8).

$$\text{Average Latency} = \frac{\sum_{i=1}^n (t_{Di} - t_{Ci})}{n} \quad (8)$$

where t_{Di} is the time at which the i^{th} message was delivered, t_{Ci} is the time at which the i^{th} message was created and n is the number of delivered messages.

- **Average buffer occupancy:** the percentage of memory fullness.

5.2. Simulation Settings

The network parameters used in all experiments are listed in Table 1.

6. Results and Discussion

Table 2 summarizes the obtained results from all experiments. The numbers listed in the table are the minimum and maximum values.

Table 1: Simulation settings.

Nodes	Pedestrian	Bicycles	Bikes	Drivers1	Drivers2
Speed range (m/sec)	0-1.5	4-10	16-32	33 – 65	65 – 120
Buffer sizes (MB)	2, 4, 6, 8, 10, 12, 14, 16				
Simulation Time (Hours)	12, 48				
Number of nodes	10,30,50,70,90				
Message generation rate (Msgs/Hour)	7, 18, 33, 103, 600				
TTL (Hours)	1, 3, 6, 9, 12				
Initial energy budget (mAh)	800				
Energy expenditure for scanning (j/hour)	0.1				
Energy expenditure for transmitting/receiving (J/hour)	15				
PRoPHET parameters	$P_{(a,b)_{init}} = 0.75; \beta = 0.25; \gamma = 0.98$				
SaW parameters	$L = 8$				
SaF parameters	$L = 8$				
EBR parameters	$\alpha = 0.85; CW = 30; L = 8$				

Table 2: Summary of results.

Impact of		Simulation Time & Buffer size	Number of Nodes & Buffer size	Traffic Load & Buffer size	TTL & Buffer size
Parameters		TTL=300 minutes TL=288 Messages/hour N=50 nodes BS = 2;4;6;8;10;12;14;16 MB ST = 6;12;18;24;30;36;42;48 Hours	TTL=300 minutes TL=288 Messages /hour ST=12Hours BS = 2;4;6;8;10 MB N=10;30;50;70;90 nodes	TTL=300 minutes ST=12Hours N=50 nodes BS = 2;4;6;8;10 MB TL = 7;18;33;103;600 Message/hour	ST=12Hours TL=288 Messages /hour N=50 nodes BS = 2;4;6;8;10 MB TTL =1;3;6;9;12 Hours
Delivery ratio	Epidemic	0.0271 - 0.2496	0.0536 - 0.46	0.0884 - 0.9951	0.1077 - 0.1512
	PRoPHET	0.0275 - 0.3026	0.0541 - 0.5105	0.0905 - 0.9873	0.1086 - 0.1938
	MaxProp	0.0378 - 0.5315	0.1514 - 0.5174	0.0962 - 0.9951	0.1506 - 0.267
	SaW	0.2124 - 0.9665	0.3772 - 0.9883	0.3763 - 0.9902	0.8313 - 0.8786
	SaF	0.4309 - 0.8817	0.4418 - 0.8538	0.5963 - 0.9814	0.7674 - 0.7782
	EBR	0.265 - 0.9708	0.4745 - 0.987	0.5255 - 0.9902	0.9669 - 0.9708
Overhead ratio	Epidemic	56.8929 - 61.5025	1.5646 - 226.7098	28.5933 - 675.697	44.4015 - 61.5
	PRoPHET	44.4575 - 62.8784	1.263 - 230.7487	29.0818 - 512.85	33.533 - 60.9436
	MaxProp	24.1285 - 52.0276	1.3028 - 65.9007	15.46 - 38.1538	24.303 - 53.4369
	SaW	4.9468 - 5.7475	1.2417 - 5.6081	4.8374 - 6.6602	5.0634 - 5.3531
	SaF	0.9022 - 1.2749	0.6812 - 1.4765	0.2589 - 1.3138	0.9069 - 1.2458
	EBR	3.7938 - 4.2563	0.7715 - 3.874	3.7783 - 4.3077	3.7938 - 3.8114
Average Latency (Second)	Epidemic	650.2969 - 1142.0538	620.9331 - 2373.1338	270.0485 - 1615.8364	598.9168 - 937.7454
	PRoPHET	751.1792 - 1177.0035	495.0259 - 2366.9254	520.7731 - 2391.2725	831.927 - 1082.0067
	MaxProp	464.6411 - 716.829	243.1398 - 3719.2038	270.2412 - 834.2565	455.9011 - 699.7181
	SaW	485.9072 - 783.5162	478.9431 - 2480.7165	450.6913 - 743.7702	521.8167 - 621.3069
	SaF	81.261 - 207.6359	41.8123 - 2051.7837	77.9121 - 235.7566	81.5913 - 205.8305
	EBR	636.2029 - 817.5432	584.2738 - 3422.6381	630.0306 - 821.7755	658.9494 - 673.6082

Note: N: Number of nodes; BS: Buffer size; TL: Traffic load; ST: Simulation time.

6.1. Impact of different buffer sizes on time

Figures 1 (a) - (c) show the comparison of the delivery ratio of flooding-based routing protocols, while Figures 1 (d) - (f) show the comparison of the delivery ratio of quota-based routing protocols. Obviously, the delivery ratio will be lowered over time. In fact, the number of dead nodes increases as the energy depletion increases. Note that the delivery ratio of the quota-based routing protocols is better than that of the flooding-based routing protocols. The reason for this is that the flooding-based protocols flood the network with messages and there is no upper limit on message processing. This results in exhaustion of the network resources due to the full memory and the large number of transmissions and receptions, thus consuming the energy of the nodes. Note that in the quota-based protocols, the number of copies of messages is limited. In addition, and in order to reduce the overhead in quota-based protocols, the destination notifies their relay nodes by sending acknowledgments so as to remove message copies from their buffers. As shown in Figures 1 (c), 1 (a) and 1 (b), the delivery ratio is better in the case of MaxProp protocol compared to the EPIDEMIC and PROPHET protocols and this is thanks to the use of acknowledgments by MaxProp protocol.

Figures 1 (a) - (c) show that delivery ratio is low for small buffer sizes and then gradually increases as the buffer size increases. Note that the increase in delivery ratio is almost constant at the value of 4 MB as seen in Figure 1 (c). This is can be explained by the fact that the delivery ratio stabilizes when the buffer size is larger than the traffic load. Of course, this behavior varies from one protocol to another and mainly depends on the protocol specifications.

Figures 1 (d) - (f) show that the quota-based protocols are not affected by the variation of the buffer size since they are conservative in terms of creating copies of messages. In other words, the buffer sizes are larger than the traffic load, so the delivery ratio is not affected as the buffer sizes change.

Figure 2 shows the average buffer occupancy of the protocols. It is noted that in all protocols, the average buffer occupancy decreases as the buffer sizes increase. Comparing Figure 2 (d) with 2 (f), we notice that the SaW protocol significantly occupies memory at the first period and then gradually decreases with time, whereas for the EBR protocol, the memory occupancy is small at first and then increases with time. In fact, in the EBR protocol the number of transfers is low at the beginning of the time since the calculation of the encounter rates has not yet stabilized. However, in the SaW, from the beginning of time, it begins with the Spray phase in which messages are quickly spread. However, for both protocols, the buffer occupancy decreases with the time due to the elimination of copies of redundant messages that have been delivered to their destination as explained earlier.

In Figure 2 (e), it is clearly shown that the buffer occupancy is high for SaF protocol. This result is normal since the SaF protocol continues to send messages in the Focus phase.

From Figure 1 and the results listed in Table 2, it can be seen that SaF achieves the highest output ratio with the lowest overhead ratio and the lowest latency. While the EPIDEMIC

protocol provides the lowest delivery ratio, the highest overhead ratio, and the longest delay period.

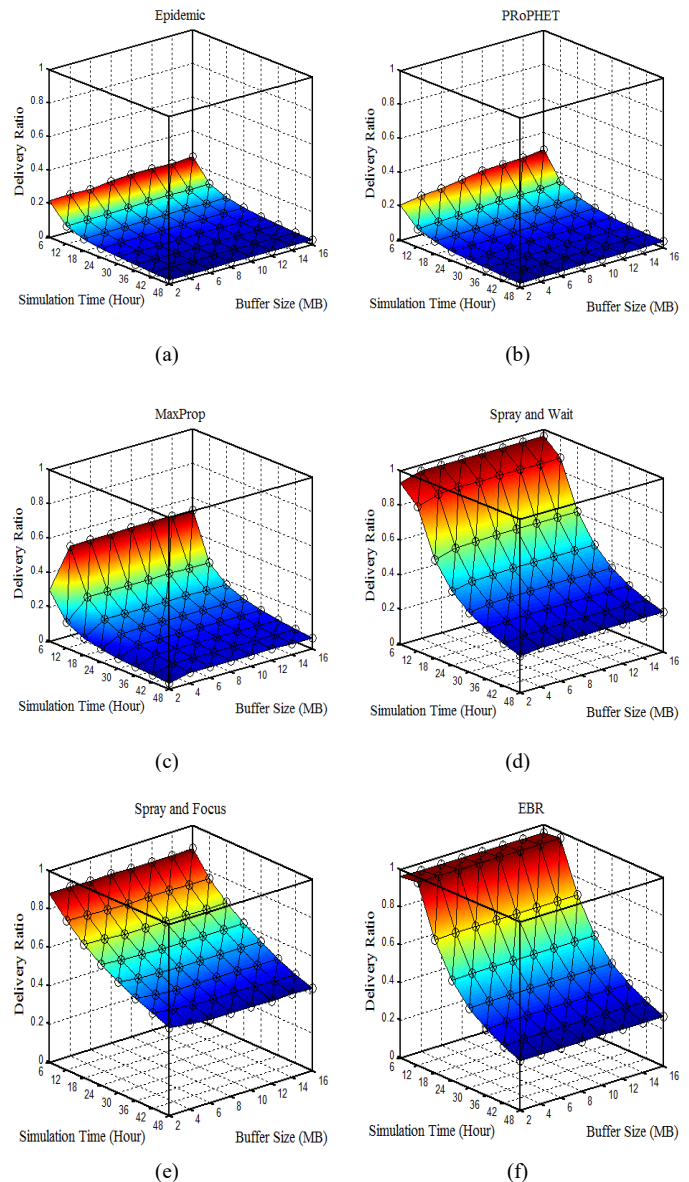


Figure 1. Delivery ratio comparison: (a) Epidemic; (b) PRoPHET; (c) MaxProp. (d) SaW; (e) SaF; (f) EBR.

6.2. Impact of Varying the Traffic Load

Figure 3 shows the variation of delivery ratios as a function of message generation rate. One can notice that all protocols are negatively affected when the rate of message generation increases. In fact, in opportunistic networks with limited resources in terms of memory and energy, increasing the rate of the generation of the messages will increase traffic load, and consequently will increase both the dropping rate and the exchange of messages (i.e., transmission and reception of messages). This consumes the energy of the nodes. Over time, the number of dead nodes increases and becomes permanently out of service.

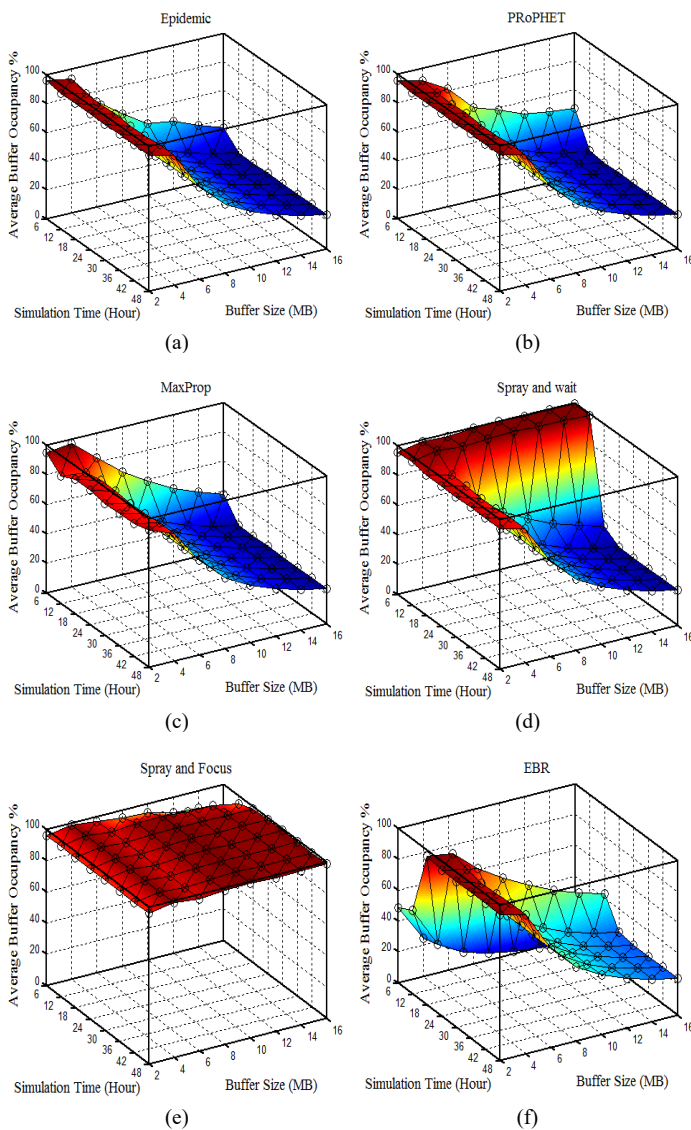


Figure 2. Average buffer occupancy comparison: (a) Epidemic; (b) PRoPHET; (c) MaxProp. (d) SaW; (e) SaF; (f) EBR.

Figures 3 (a) - (f) show that the delivery ratio of the MaxProp, SaW, SaF, and EBR protocols, which use acknowledgements to delete redundant messages, is better than of the EPIDEMIC and PRoPHET. Thus, as shown in Figures 3 (a) and (b), both EPIDEMIC and PRoPHET achieve the best output ratio at the highest buffer value and the lowest traffic load at the coordinates point (7, 10). Conversely, they achieve the worst delivery ratio at the lowest buffer value and the highest traffic load, at the coordinates point (600, 2).

Figure 4 shows the effect of the traffic load on the overhead ratio. As mentioned earlier, the overhead reflects the cost of transmission in the network. Figures 4 (d) - (f) show that quota-based protocols have a high overhead when the message rate generation is high. This means that the transmission costs are high and the delivery ratio is low. This is confirmed by the Figures 3 (d) - (f). In general, as shown in Figure 4, the overload in the quota-based protocols is much lower than the overload in the flooding-based protocols.

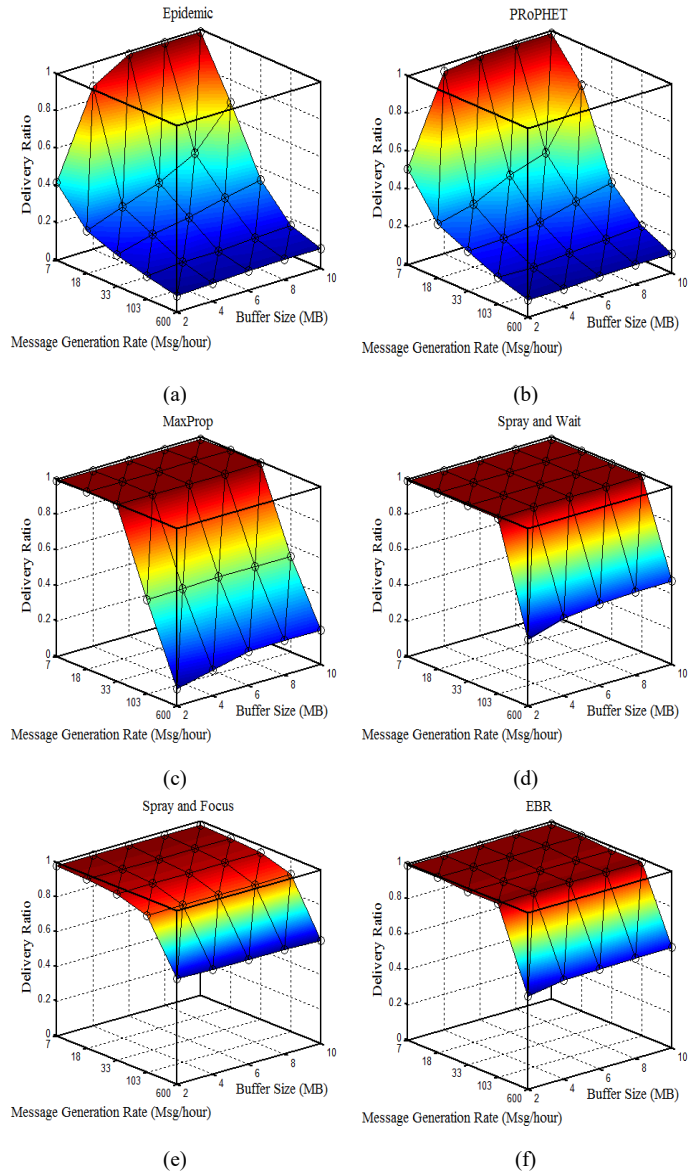


Figure 3. Delivery ratio Comparison for different traffic loads: (a) Epidemic; (b) PRoPHET; (c) MaxProp. (d) SaW; (e) SaF; (f) EBR.

Figures 4 (a) and (b) show that in the EPIDEMIC and PRoPHET protocols, at low levels of traffic load (i.e., 7, 18, and 33 Msgs / hour), the overhead gradually decreases as the buffer sizes increase, so the delivery ratio gradually increases too. This is confirmed by Figures 3 (a) and (b). However, unlike quota-based protocols, at high traffic load (that is 600 Msgs / hour) the overhead is low. The reason is that the high traffic load significantly affects the performance of the flooding-based protocols. Thus, the number of dead nodes increases resulting the decrease of the lifetime of the network. Hence, the overhead decreases. From the results given in Table II, at heavy traffic loads, both SaF and EBR have the highest delivery ratios, while SaF achieves the lowest overhead ratio and latency. On the other hand, the EPIDEMIC protocol exhibits the worst performance in terms of all the considered metrics.

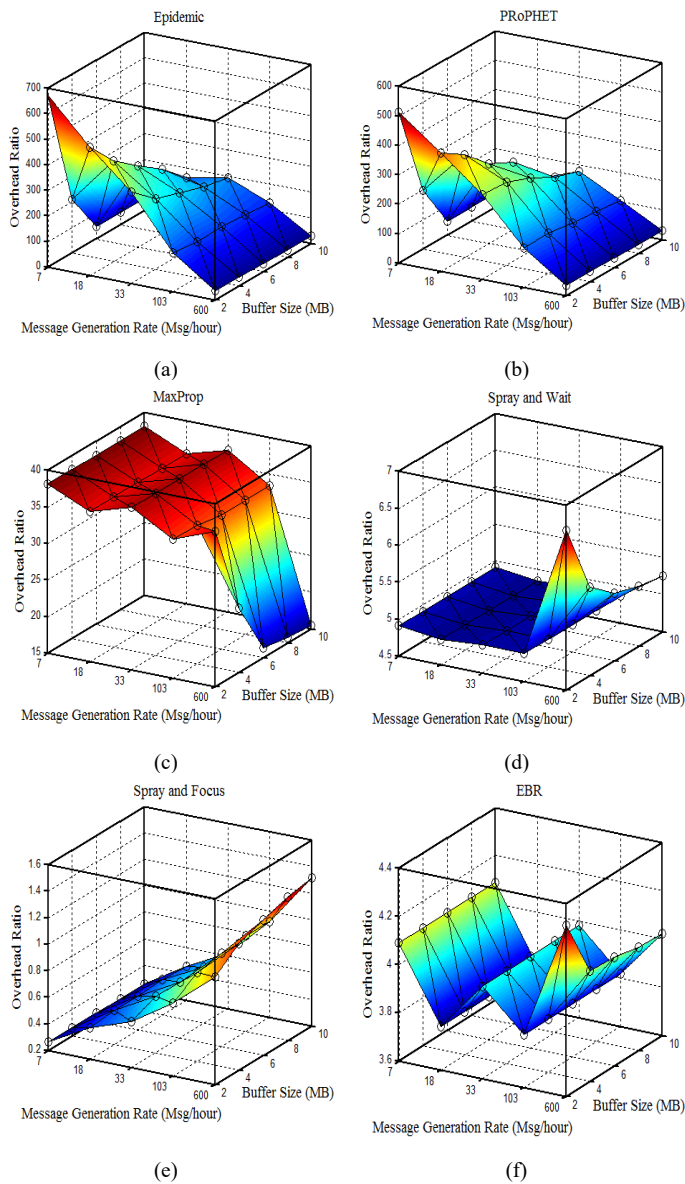


Figure 4. Overhead ratio Comparison for different traffic loads: (a) Epidemic; (b) PRoPHET; (c) MaxProp. (d) SaW; (e) SaF; (f) EBR.

6.3. Impact of Varying of number of nodes

Figure 5 shows that increasing the number of nodes while maintaining the rest of the parameters as listed in Table II, improves the delivery rate of quota-based routing protocols and greatly affects the delivery rate of flooding-based protocols. The reason is that in quota-based protocols, increasing the number of nodes increases the connectivity in the network and allows more messages to reach their destination. But, this will also lead to a large number of redundant messages that will roam the network and will drain its resources unless they are discarded. The inability to dispose of the redundant messages explains the low delivery ratio of the flooding-based protocols, as these messages will fill the buffers and will be frequently sent and received, which will drain nodes energy.

Figures 6 (a) - (f) depict the average latency time of the protocols. Obviously, the average latency at the nodes' high

density reaches its lowest value in all protocols. When the density of nodes is low, the average latency increases by increasing the buffer size. This is because message waiting times in the buffers increase, which in turn increases the delay.

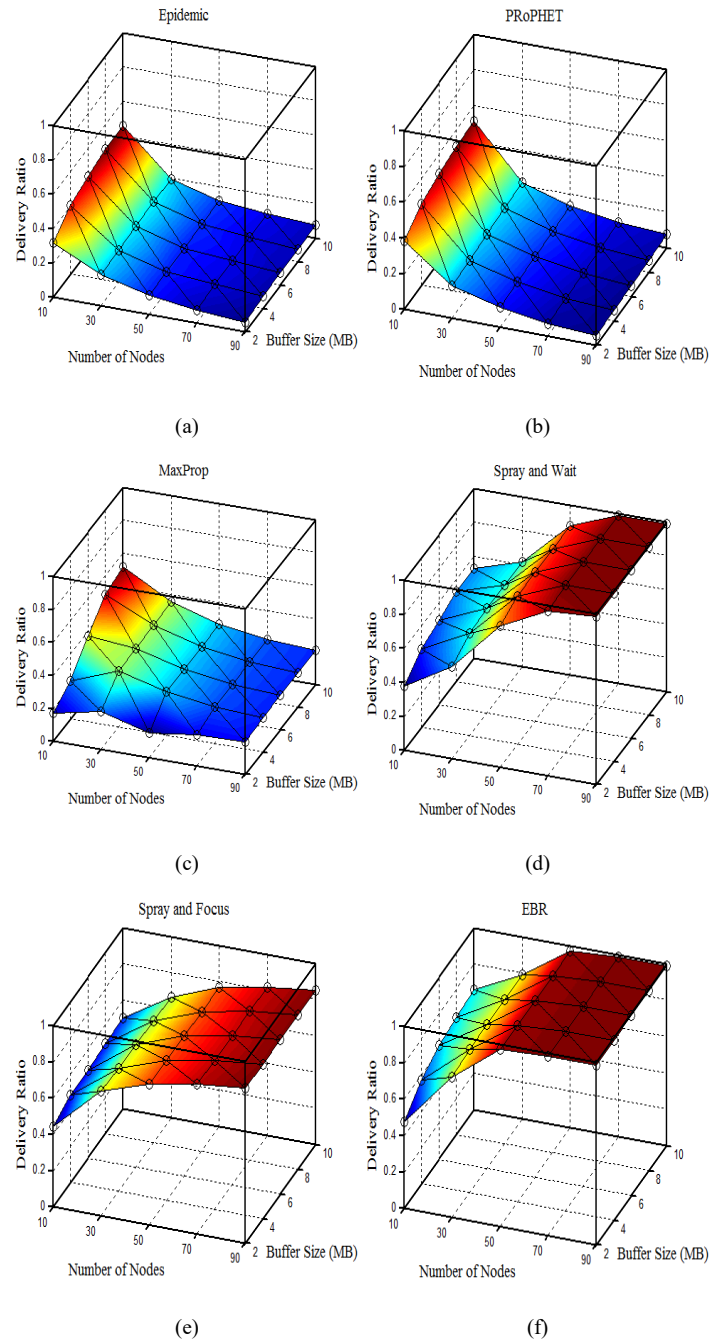


Figure 5. Delivery ratio Comparison for different number of nodes: (a) Epidemic; (b) PRoPHET; (c) MaxProp; (d) SaW; (e) SaF; (f) EBR.

As it shown from Figure 7, the overhead ratio increases in all protocols as the node density increases. This is due to the increase in the number of nodes that leads to an increase in connectivity among them. This in turn increases the relayed messages, and this causes the increasing in overhead ratio. From Figures 7 (a) and (b) we note that at the high density of the nodes, both protocols

EPIDEMIC and PROPHET are affected by buffer size. So that, the overhead decreases as buffer sizes increase.

Figure 5 shows that the EBR protocol achieves the best delivery ratio at the high node density. Figures 6 and 7 show that the SaF achieves the lowest overhead ratio and the lowest latency.

6.4. Impact of Varying of TTL

As presented in Table II, increasing message' time to life (TTL) increases the delivery ratio, the overhead ratio, and the average latency. However, the results show that in flooding-based protocols, the overhead ratio and the average latency dramatically increase as the message life increases. This is because the messages remain in memory until the expiration time of the message.

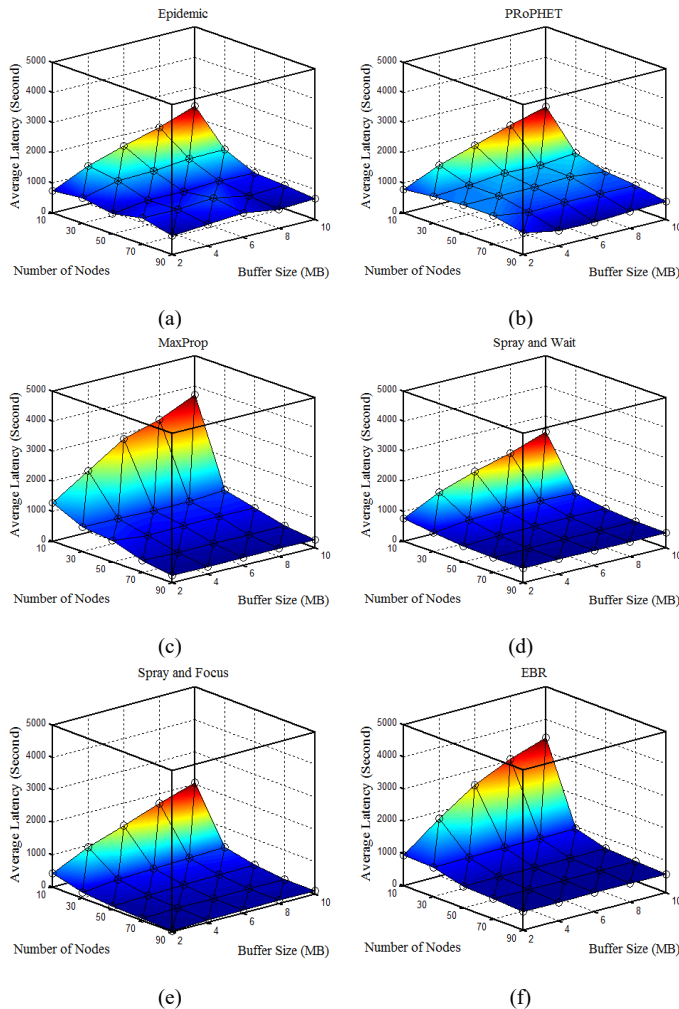


Figure 6. Average latency Comparison for different number of nodes: (a) Epidemic; (b) PRoPHET; (c) MaxProp; (d) SaW; (e) SaF; (f) EBR.

7. Design guidelines of routing protocols in the limited-resources Opportunistic Networks.

To design an effective routing protocol in resource-constrained opportunistic networks, the router should meet the following requirements: effective buffer management, impose an upper limit on message' copies, skillful selection of messages on

forwarding and deleting, skillful selection of the relay nodes by a utility-metric that includes the activity of the nodes and the contact history of the nodes.

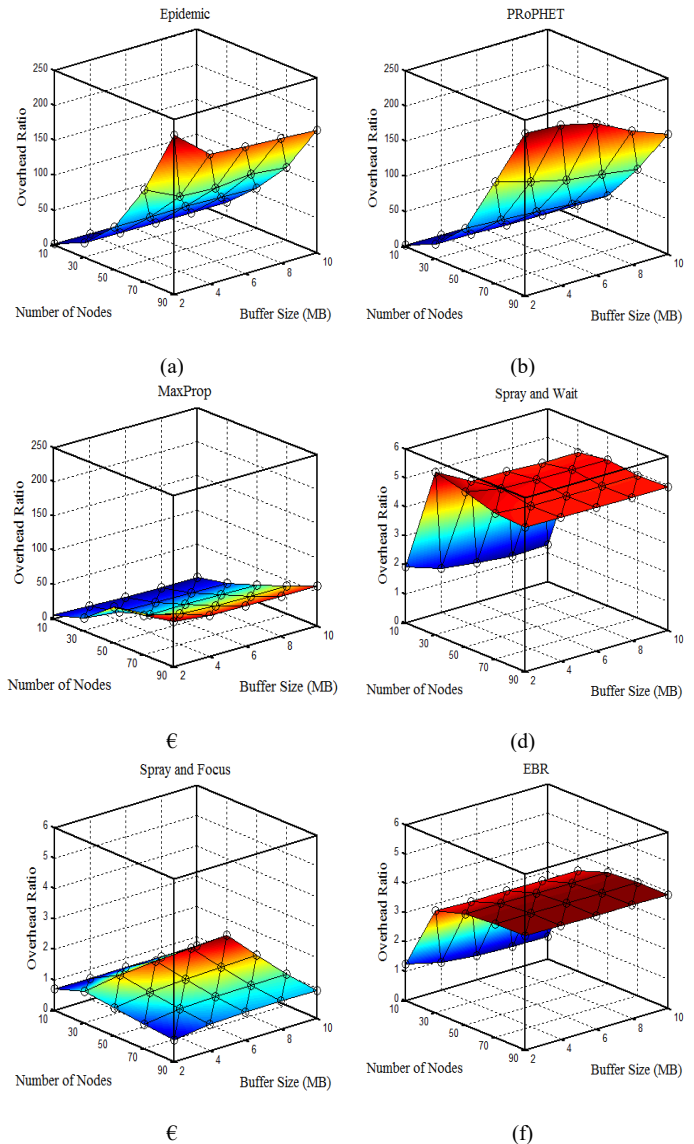


Figure 7. Overhead ratio comparison for different number of nodes: (a) Epidemic; (b) PRoPHET; (c) MaxProp. (d) SaW; (e) SaF; (f) EBR.

Based on the experiments results we deduce the following points:

- SaF routing protocol performs well in terms of all considered metrics against variations in traffic load and buffers size (see Section 6.2).
- SaF demonstrates superior performance in terms of overhead ratio and latency versus varying the density of nodes (see Section 6.3).
- EBR shows excellent performance in terms of delivery ratio against the variations in traffic load and density of nodes (see Sections 6.2 and 6.3).

- Quota-based routing protocols, which impose an upper limit on the number of messages' copies in the network, outperform flooding-based and guided-flooding protocols.
- Guided flooding protocols, which have a mechanism to drive the message to its destination, outperform flooding-based routing protocols.
- In limited-resource environments, flooding-based routing protocols deplete network resources and cause the worst performance.

Based on the results of the analytical study and the study of the functioning of the SaF and EBR protocols, we recommend the following points when designing a routing protocol in opportunistic networks in resource-constrained environments:

- Use acknowledgments to eliminate duplicate messages. Surplus copies of the messages occupy large areas in buffers and are continuously sent and received in the network, draining the energy of the nodes and reducing its lifespan.
- Implement efficient buffer management. The mechanism used in buffer management plays an important role in performance. Efficient buffer management involves deciding which message to delete or send. This must be based on justifications imposed by the nature of the limited-resources environments.
- The choice of the next-hop should be based on precise estimation. When the node encounters other nodes, it must select the appropriate nodes for message forwarding. Message forwarding decision should ensure that the message reaches its destination at lowest cost and time.
- Using nodes' contact history information to estimate forwarding decisions. Node' contact history information reflects the mobility pattern of the node and can be used to estimate the node's suitability to reach the message's destination.
- Exploit active nodes in routing decisions. The preference of active nodes over others when making routing decisions increases the likelihood that the message will reach its destination. However, the estimation of node activity must be based on justifications associated with resource-limited environments, such as residual energy, buffer occupancy, and the number of node encounters.

8. Conclusion

In opportunistic networks, where communication among users is intermittent and resources are limited, it is difficult to reveal a strong statement about the kind of services offered by these networks. For this purpose, we identified the most important requirements that should be met in the routing protocols and give the best possible performance in such harsh environments. In this

paper, we presented an analytical study on the performance of six of the most popular routing protocols in opportunistic networks namely: EPIDEMIC, PRoPHET, MaxProp, Spray and Wait, Spray and Focus and EBR. The results of the analysis showed that in order to design an effective routing protocol in resource-limited opportunistic networks, the router should effectively manage the buffer, set an upper limit on message copies, deftly select the messages on forwarding or deleting, and skillfully select the next hop based on a utility metric that includes the activity of the nodes and the contact history of the nodes.

Conflict of Interest

The authors declare no conflict of interest.

References

- [1] R. Nave, "Crossed Polarizers," in *Proceedings of the 2003 conference on Applications, technologies, architectures, and protocols for computer communications*, 2012, pp. 27–34.
- [2] K. Hazra et al., "A Novel Network Architecture for Resource-Constrained Post-Disaster Environments," in *2019 11th International Conference on Communication Systems and Networks, COMSNETS 2019*, 2019, pp. 328–335.
- [3] N. Rajpoot and R. S. Kushwah, "An improved Prophet routing protocol for underwater communication," in *Proceedings of the 2015 international conference on communication networks (ICCN)*, 2016, pp. 27–32.
- [4] E. Max-Onakpoya et al., "Augmenting Cloud Connectivity with Opportunistic Networks for Rural Remote Patient Monitoring," May 2019.
- [5] E. D. Ayele, N. Meratnia, and P. J. M. Havinga, "An Asynchronous Dual Radio Opportunistic Beacon Network Protocol for Wildlife Monitoring System," 2019, pp. 1–7.
- [6] P. Liu, C. Wang, T. Fu, and Y. Ding, "Exploiting Opportunistic Coding in Throwbox-Based Multicast in Vehicular Delay Tolerant Networks," *IEEE Access*, vol. 7, pp. 48459–48469, 2019.
- [7] P. Yuan, Z. Yang, Y. Wang, S. Gu, and Q. Zhang, "A Task-Driven Updated Discrete Graph Assisted Minimum Delivery Delay Routing for Remote Sensing Disruption-Tolerant Networks," *IEEE Access*, vol. 7, pp. 69351–69362, 2019.
- [8] S. C. Nelson, M. Bakht, and R. Kravets, "Encounter-based routing in DTNs," in *Proceedings - IEEE INFOCOM*, 2009, pp. 846–854.
- [9] A. Vahdat and D. Becker, "Epidemic routing for partially connected ad hoc networks 2000",.
- [10] T. Abdelkader, K. Naik, A. Nayak, N. Goel, and V. Srivastava, "A performance comparison of delay-tolerant network routing protocols," *IEEE Netw.*, vol. 30, no. 2, pp. 46–53, Mar. 2016.
- [11] A. Lindgren, A. Doria, and O. Schelén, "Probabilistic Routing in Intermittently Connected Networks," 2004, pp. 239–254.
- [12] J. Burgess, B. Gallagher, D. Jensen, and B. N. Levine, "MaxProp: Routing for vehicle-based disruption-tolerant networks," in *Proceedings - IEEE INFOCOM*, 2006.
- [13] T. Spyropoulos, K. Psounis, and C. S. Raghavendra, "Efficient Routing in Intermittently Connected Mobile Networks: The Multiple-Copy Case," *IEEE/ACM Trans. Netw.*, vol. 16, no. 1, pp. 77–90, Feb. 2008.
- [14] T. Spyropoulos, K. Psounis, and C. S. Raghavendra, "Spray and focus: Efficient mobility-assisted routing for heterogeneous and correlated mobility," in *Proceedings - Fifth Annual IEEE International Conference on Pervasive Computing and Communications Workshops, PerCom Workshops 2007*, 2007, pp. 79–85.
- [15] S. Palazzo, A. T. Campbell, and M. Dias de Amorim, "Opportunistic and Delay-Tolerant Networks," *EURASIP J. Wirel. Commun. Netw.*, vol. 2011, no. 1, p. 164370, Dec. 2011.
- [16] A. Socievole, F. De Rango, and C. Coscarella, "Routing approaches and performance evaluation in delay tolerant networks," in *Wireless Telecommunications Symposium*, 2011.
- [17] M. S. Hossen and M. S. Rahim, "Performance evaluation of replication-based DTN routing protocols in Intermittently Connected Mobile Networks," in *ICEEE 2015 - 1st International Conference on Electrical and Electronic Engineering*, 2016, pp. 101–104.
- [18] V. N. G. J. Soares, J. J. P. C. Rodrigues, J. A. Dias, and J. N. Isento, "Performance analysis of routing protocols for vehicular delay-tolerant

networks,” in *2012 20th International Conference on Software, Telecommunications and Computer Networks, SoftCOM 2012*, 2012.

- [19] A. Socievole and F. De Rango, “Evaluation of routing schemes in opportunistic networks considering energy consumption,” in *Simulation Series*, 2012, vol. 44, no. BOOK 12, pp. 41–47.
- [20] M. Alajeely, A. Ahmad, and R. Doss, “Comparative study of routing protocols for opportunistic networks,” in *Proceedings of the International Conference on Sensing Technology, ICST*, 2013, pp. 209–214.
- [21] N. Chakchouk, “A Survey on Opportunistic Routing in Wireless Communication Networks,” *IEEE Commun. Surv. Tutorials*, vol. 17, no. 4, pp. 2214–2241, Oct. 2015.
- [22] J. Cui, S. Cao, Y. Chang, L. Wu, D. Liu, and Y. Yang, “An Adaptive Spray and Wait Routing Algorithm Based on Quality of Node in Delay Tolerant Network,” *IEEE Access*, vol. 7, pp. 35274–35286, 2019.
- [23] A. Keränen, J. Ott, and T. Kärkkäinen, “The ONE simulator for DTN protocol evaluation,” in *SIMUTools 2009 - 2nd International ICST Conference on Simulation Tools and Techniques*, 2009.
- [24] “The ONE.” [Online]. Available: <https://www.netlab.tkk.fi/tutkimus/dtn/theone/>. [Accessed: 26-Nov-2019].

An Exploratory Qualitative Study of the Influence of Hospital Logistics Factors on Quality of Care and Patient Satisfaction at Public Hospitals in Morocco

Youness Fricchi*, Fouad Jawab, Said Boutahari

Industrial Technologies and Services, High School of Technology, Sidi Mohamed Ben Abdellah University, Fez 30 000, Morocco

ARTICLE INFO

Article history:

Received: 11 November, 2019

Accepted: 09 December, 2019

Online: 25 December, 2019

Keywords:

Hospital logistics

Quality of care

Patient satisfaction

ABSTRACT

The purpose of this qualitative research was to explore the influence of hospital logistics on quality of care and patient satisfaction. Hospital logistics was assessed by considering five factors in the patient pathway, namely: physical accessibility of care, waiting time, consultation time, administrative procedures and hospital hotel services. Semi-structured interviews were conducted, following an interview guide, with two categories of participants: patients and healthcare professionals. The interviews were transcribed and then a thematic analysis method was conducted using QSR NVivo 10 software. Results showed that hospital logistics has a direct impact on quality of care and patient satisfaction. All the participants' testimonies highlighted the critical and crucial role that hospital logistics plays in the perception of quality of care and patient satisfaction. It is recommended to pay great attention to hospital logistics activities in order to improve quality and satisfaction.

1. Introduction

This study is the extension of a previous study entitled "Elaboration of an association matrix of satisfaction factors in healthcare facilities and hospital logistics activities" in 2018 International Colloquium on Logistics and Supply Chain Management (LOGISTIQUA). The previous study examined the effect of hospital logistics factors on healthcare quality and patient satisfaction [1]. It was found, through a literature review, that patient satisfaction is influenced by several factors including hospital logistics factors [1]. The objective of this study is to support empirically these findings in order to better understand the effect of hospital logistics on quality of care and patient satisfaction. Given that the Moroccan Ministry of Health's new strategy (Ministry of Health (2018) "Plan Santé 2025", <https://www.sante.gov.ma/Pages/actualites.aspx?IDActu=276>) aims to ensure that healthcare services are of high quality and meet patients' needs, it was decided to conduct this empirical study in the Moroccan context. So, the contribution of this article is fully in line with this perspective by exploring the role of hospital logistics as a lever for quality and satisfaction. The health system in Morocco is structured in two sectors [2]:

- The public health sector: comprises healthcare services of the Ministry of Health, Defense department, and local authorities. Healthcare facilities under the Ministry of Health are Basic Healthcare Centers (BHC), Provincial Hospital Centers (PHC), Regional Hospital Centers (RHC), and University Hospital Centers (UHC).
- The private health sector: incorporates the private for-profit sub-sector that includes hospital clinics, dental surgery, pharmacies, etc., and the private not-for-profit sub-sector that includes healthcare services of the National Fund for Social Security, the National Fund of Social Welfare Bodies, the Moroccan Red Crescent, and non-governmental organizations.

The focus of this paper is on the public sector, particularly the healthcare services of the Ministry of Health provided at hospitals. The remainder of this article is organized as follows. Section 2 highlights the background of this research. Section 3 describes the methodology for data collection and analysis. Section 4 presents the results of the study. Section 5 provides a discussion of the main findings. Finally, the paper's limitation and future research, as well as conclusions are presented in sections 6 and 7 respectively.

* Corresponding Author: Youness Fricchi, BP 2427 Route d'Imouzzer Fez Morocco, Email: youness.fricchi@usmba.ac.ma

2. Background

2.1. Quality of care

Quality of care is defined in different ways in the literature. According to Donabedian [3], high-quality care is *the kind of care that is expected to maximize an inclusive measure of patient welfare after one has taken into account the balance of expected gains and losses that attend the process of care in all its parts*. From this definition, two aspects of quality of care might be distinguished: (1) technical quality that refers to medical practices and clinical outcomes; (2) quality of the care delivery processes and how the patient receives the service [4]. This second aspect can be assessed by measuring patient satisfaction [5]. However, some authors argued that patient satisfaction is not sufficient and must include other stakeholders' points of view [6]. In this paper, quality of care is considered only in terms of patient satisfaction.

2.2. Patient satisfaction

Patient satisfaction is defined as *an assessment that reflects the perceived differences between the patient's expectations and what is actually received during the process of care* [7]. It is considered to be the main indicator of quality of care. The objective of patient satisfaction studies is to understand the factors associated with satisfaction and whose improvement could enhance the quality of care [8]. Factors thought to be related to patient satisfaction include patient sociodemographic and health status characteristics [9], expectations concerning medical care [10], caregivers' attitudes and behaviors [11], waiting time [12], consultation time [13], healthcare accessibility [14], administrative procedures [15], and hospital hotel services [16]. It was concluded from previous studies that some of these factors fall within the scope of hospital logistics [17].

2.3. Hospital logistics

Hospital logistics is a *set of processes that exchange physical, information and financial flows in order to ensure all the necessary conditions to provide patients with a better quality service* [18]. This definition reflects the scope of hospital logistics, which includes all the support activities that are necessary for providing care: scheduling, forecasting, transportation, procurement, distribution, replenishment, information system, patient flow, catering, laundry, waste management, maintenance, etc. [19]. Over the last few decades, hospital logistics has received a great deal of interest from researchers. It is recognized to play an important role in improving the quality of care and patient satisfaction [20]. Indeed, many factors of patient satisfaction such as waiting time, consultation time, physical accessibility of care, hospital hotel services, and administrative procedures depend on the effectiveness of hospital logistics activities.

2.4. Interactions between hospital logistics and patient satisfaction

As mentioned above, several patient satisfaction factors fall within the scope of hospital logistics, including:

- Waiting time: is identified by most studies as a factor that has a strong impact on satisfaction. A long waiting time may

result from several causes, in particular, the inadequacy between the available resources (staff, operating rooms, hospital beds, drugs, equipment, etc.) and the patient flow [21,22]. This inadequacy is mainly due to a lack of planning and coordination in service delivery or because hospital resources are allocated in a way that is not dynamic and does not take into account the growing need for care [23,24].

- Consultation time: is the time spent with the caregiver. The longer the consultation time, the more satisfied patients are [13]. Consultation time is sometimes reduced because caregivers spend a huge amount of their time managing administrative and logistical matters, which reduces the time available for patients. Estimates indicate that a nurse spends between 30% and 34% of her time on logistical and administrative activities [25,26]. The availability of caregivers could be increased by freeing them from logistical and administrative tasks that consume a lot of their time [27].
- Physical accessibility: the physical accessibility of healthcare services depends on several logistics factors both outside and inside healthcare facilities. The patient's arrival is first ensured by adapted means of transportation such as ambulances. The availability of ambulances requires good management (maintenance, fuel allocation, human resources, equipment, etc.). Second, at the healthcare facility, access to care requires the availability of the right human resources with the right skills in the right place, which is conditioned by optimal time management, medical intervention planning, staff assignment, etc. [28]. Third, the availability of material resources such as operating rooms, medical analysis and radiology laboratories, technical equipment, etc., depends on the effectiveness of planning and scheduling operations, coordination between healthcare teams and maintenance activities. Also, the availability of medical supplies such as drugs and sterile medical devices (needles, syringes, gloves, etc.) is dependent on the effectiveness of procurement and inventory management systems [26].
- Hospital hotel services: such as catering, cleanliness, laundry, and accommodation conditions of patients stay at the hospital. Satisfaction surveys showed that the highest patient dissatisfaction was reported regarding hoteling services [7,29]. Adequate hospital hotel services require better planning and coordination between the different teams. For instance, the catering activity requires an efficient supply system to ensure fresh meals at the right time, as well as better coordination between the catering service and the care teams to consider the nutritional specificities of each patient. The cleaning activity is responsible for the cleanliness of the healthcare environment (e.g. wards, toilets, waiting areas, etc.). It assumes cleaning the hospital areas at regular intervals and whenever necessary, making cleaning supplies available in sufficient quantities in the right places, as well as adequate management of hospital wastes. The laundry activity provides care units with clean linens, towels, and staff uniforms, which ensures comfort, hygiene, and safety for hospitalized patients. In this respect, well-adapted logistics circuits are essential: definition of storage areas for clean and soiled linen, towels and linen transportation, operations' planning and sequencing (disinfection, washing,

rinsing, and drying) [30]. It is worth mentioning that hospital hotel activities are often outsourced, therefore their effectiveness depends on outsourcers' performance.

- Administrative procedures: administrative formalities related to patient admission, treatment, and discharge are associated with patient satisfaction [31]. These procedures can be optimized and simplified through better information flow management. The use of hospital information systems (HIS), including the implementation of electronic medical records is of great help [32].

Table 1: Semi-structured interview guide

Themes	Questions asked during the interviews
Quality of care	Can you describe what quality of care is all about?
Patient satisfaction	What makes a patient satisfied with hospital services? What are the determinants/factors of patient satisfaction?
Waiting time	Can you describe the importance of delay in medical care and its influence on patient satisfaction and quality of care?
Consultation time	To what extent is consultation time important for quality of care and patient satisfaction? Why is the consultation time sometimes reduced?
Hospital logistics factors	Physical accessibility How important is the ease of physical access to care? What are the factors that influence the physical accessibility of care?
Hospital hotel services	To what extent are hospital hotel services essential (cleanliness, laundry, comfort, catering, etc.)?
Administrative procedures	Can you describe the importance of organization, clarity, and ease of administrative procedures?

3. Methods

Given the exploratory nature of this study, a qualitative approach was employed. Qualitative approaches are appropriate for a comprehensive exploration of participants' perceptions and experiences. Some of the main techniques for collecting qualitative data in healthcare researches include individual interviews, focus groups, and observation [33]. In this study, semi-structured individual interviews are used. This choice is explained by the study's objective that consists of identifying and exploring the different perceptions of healthcare professionals and patients regarding the importance of the above-mentioned hospital logistics factors in ensuring quality of care and patient satisfaction. Data collection and analysis were based on steps described by Imbert [34]: development of the interview guide, participant selection, interviewing participants, and data analysis.

3.1. Interview guide

Semi-structured interviews collect data by interviewing participants face-to-face using an interview guide which contains the list of questions or topics to be covered. The interview guide developed here contained open-ended questions, that are structured in seven themes as shown in Table 1. Conversations

were initiated by asking general questions about the quality of care and patient satisfaction and then questions become specific about hospital logistics factors.

3.2. Participant selection

Two categories of participants were included in the study: the healthcare professional category and the patient category. The first includes physicians and healthcare managers, while the second is composed of former patients who have been hospitalized in public hospitals at least once in the last three months. In total, 5 participants from each category were included, they were from three types of public hospitals: University Hospital Center (UHC), Regional Hospital Center (RHC), and Provincial Hospital Center (PHC) (Table 2).

Table 2: Participants in semi-directive interviews

	Participant	Experience	Hospital	City
Healthcare professional category	ID1: Quality manager	13 years	RHC	Fez
	ID2: Head of Medical Affairs Department	17 years	RHC	Fez
	ID3: Logistics manager	16 years	RHC	Fez
	ID4: Head of Performance Evaluation Department	24 years	UHC	Rabat
	ID5: Emergency physician	6 years	PHC	Casablanca
	Patient category	ID6: Patient 1	3-day inpatient	UHC
ID7: Patient 2		2-day inpatient	UHC	Fez
ID8: Patient 3		3-day inpatient	RHC	Fez
ID9: Patient 4		2-day inpatient	RHC	Fez
ID10: Patient 5		3-day inpatient	PHC	Fez

3.3. Interviewing participants

The richness of semi-structured interview data depends on the trust relationship between the interviewer and the interviewees [34]. With this in mind, the interviews were started by an introduction to explain the objective of the study and to assure participants of the anonymity and confidentiality of their data, as well as to ask for permission to record the interviews. Healthcare professionals working in Fez city were met individually at their place of work. For those outside of Fez, the interviews were conducted by phone. Concerning the participants from the patient category, the exchanges were face-to-face.

All interviews were started by asking questions about the quality of care and patient satisfaction regarding hospital services. Subsequently, participants were asked for their opinions on hospital logistics factors as illustrated in the interview guide. Conversations were sometimes deepened for clarification purposes by asking *why* or *how* questions [35]. At the end of each interview, the interviewee was given the opportunity to add and discuss anything he or she thought was relevant or important and had not been discussed during the interview. Interviews took place during September and October 2019 and lasted between 30 to 60 minutes.

3.4. Data analysis

A thematic analysis was carried out for data analysis. It is the most common method for qualitative data analysis. It consists of identifying, analyzing, reporting patterns within data, and organizing them into themes, whether predefined or emerging themes [36]. In this study, themes are already defined and correspond to quality of care, patient satisfaction, and hospital logistics factors.

Recordings transcription is the first step in data analysis [36]. For that purpose, all interviews were transcribed using Google Docs' voice typing tool. The second step is coding interesting features of the textual data. It consists of assigning codes or labels, which are summative and essence-capturing attributes, for a portion of data [37]. Since the themes in this study are already defined, the coding method is a combination of *descriptive coding*, to describe and summarize the content of a sentence or a portion of the data, *sub-coding* to classify and categorize the codes into families, *themeing the data* to assign codes to predefined themes, and *attribute coding* to distinguish between healthcare professional participants and patient participants [37]. The coding process was performed using QSR NVivo 10 qualitative data analysis software.

4. Results

4.1. Quality of care

Participants from the healthcare professional category have defined the quality of care using criteria such as effectiveness, efficiency, and compliance with standards *"quality of care consists of providing healthcare according to standards and effective cost control"* (participant ID1). Other criteria were also mentioned including resource availability, accessibility, and responsiveness. For participants from the patient category, quality of care is attributed to good staff attitude and appropriate pain management within a short time frame *"quality of care requires a rapid healthcare delivery; the patient should not wait for a long time to be examined and treated"* (participant ID10). Participants have also insisted on the availability of skilled human resources, sufficient and functional material resources *"quality of care is conditioned by the availability of skilled doctors as well as technical equipment in sufficient quantity and quality"* (participant ID5).

4.2. Patient satisfaction

Interviewees from the healthcare professional category indicated that patients are satisfied when their expressed needs are met, which is not accurate. According to participants, caregivers should satisfy the real need resulting from the medical diagnosis *"to satisfy the patient, it is necessary to meet his or her expressed needs, which do not necessarily coincide with the real needs. The patient is unable to define the real needs"* (participant ID2). They claimed that patient satisfaction does not depend on the technical quality of care but tends to focus on the tangible aspects of the service *"from our experience in satisfaction surveys, we observe that patient satisfaction is not related to the technical aspects of care, but rather to support functions such as catering, cleaning, etc. This is mainly due to the fact that patients are unable to judge*

the technical care" (participant ID3). Interviewees from the patient category insisted on the staff attitude as a determinant of satisfaction *"patients are satisfied if they are physically and psychologically relieved, this depends on the behavior and attitude of the staff"* (participant ID6); *"patients are satisfied when they find a welcoming staff that soothe patients' anxiety and reduce the stress level"* (participant ID9). They also insisted on the importance of the availability of care providers, equipment and supplies, and the reduction of waiting times *"For the patient to be satisfied, healthcare must be available, staff behave well and treatment times are rapid"* (participant ID8).

4.3. Hospital logistics factors

To meet the objective of this exploratory study, we have reported in Table 3, the hospital logistics factors/themes and their corresponding codes.

Table 3: code categories of hospital logistics factors

Themes/ Factors	Code categories
Physical accessibility	Location of the healthcare facility
	Medical transportation
	Hospital reception
	Signs and architecture
	Availability of human resources
Waiting time	Availability of material resources
	Appointment scheduling
	Waiting time
	capacity-demand gap
	Patient flow
Consultation time	Non-compliance with the gatekeeping system
	Workload
Hospital hotel services	Performing non-professional tasks
	Cleanliness/ hygiene/ laundry
	Comfort
Administrative procedures	Catering
	Outsourcing
	Rules and regulations
	Clarity of procedures

These themes were raised by participants to different degrees. The frequency of codes under each theme according to their appearance in the corpus was generated by QSR NVivo and reported in the matrix in Figure 1. This matrix allows the content of qualitative data to be visualized and quantified.

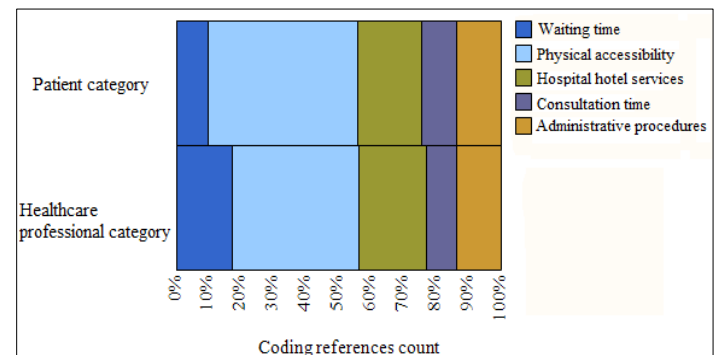


Figure 1: Matrix coding query – results preview

4.3.1. Physical accessibility

Figure 1 shows that the physical accessibility theme is the most discussed by both patient and healthcare professional participants. This theme includes a set of physical elements that are necessary to receive healthcare services. Participants agreed on the critical aspect of physical accessibility in relation to quality of care and patient satisfaction *"any accessibility problem prevents the patient from seeking care, which can worsen and harm his or her health status"* (participant ID1). Their perceptions are structured into six elements of the care pathway: location of the healthcare facility, medical transportation, hospital reception, signs and architecture, availability of human and material resources. Figure 2 shows the number of coded references for each of these elements. It can be seen that the availability of human and material resources are the most frequently mentioned elements.

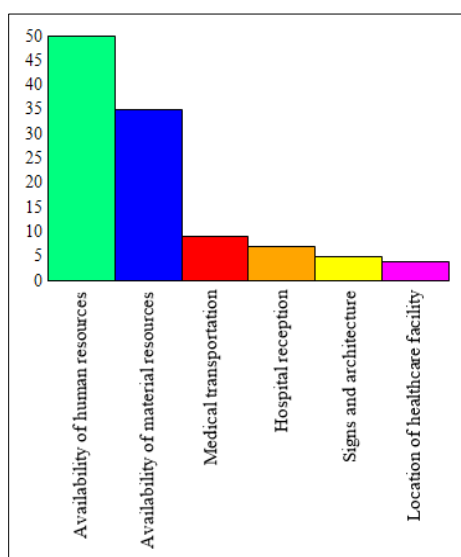


Figure 2: Physical accessibility - number of coding references per element

- Location of the healthcare facility

The first step towards receiving healthcare services is to access the healthcare facility, which depends on its geographical location. Participants believe that healthcare access is easier when the healthcare facility is accessible by public transportation *"obviously the geographical location of the healthcare facility can facilitate or hinder access to healthcare"* (participant ID5); *"If the hospital is located in the city center and accessible by public transportation such as buses and taxis, healthcare becomes easily accessible"* (participant ID 7).

- Medical transportation

Medical transportation ensures patient access to healthcare facilities. Despite its importance, medical transportation is considered to be the weakest link in the healthcare supply chain. Indeed, most participants made a negative assessment of medical transportation. It is criticized for its inefficiency, poor management as well as the multiplicity of the involved actors without a real coordination *"when I had my leg broken during a football match, my family did not call an ambulance because it is rare when ambulance services respond, and if they do, they are often late"* (participant ID7); *"the medical transportation system*

is ill at ease because it is poorly managed. Sometimes ambulances are available but inaccessible. There are several problems, including lack of coordination between actors, maintenance problems, insufficient fuel supply, regulations, etc." (participant ID4).

- Hospital reception

Patients' initial impression of healthcare services depends on the quality of the hospital reception. It is the first contact with the healthcare facility. At this stage, the patient or his/her family seeks information about the admission and treatment process. Therefore, a good hospital reception fosters patients' adherence to treatment and ensures continuity of care *"the quality of the hospital reception is very important, it is the first care. Upon his arrival at the hospital, the patient needs information and guidance that must be available at the hospital reception office"* (participant ID4). Information at the reception office is supposed to be delivered to patients by specialized and well-informed staff. However, some participants from the patient category reported that they were obliged to ask for information and guidance from the security agents because there was no reception staff. This led to patient dissatisfaction as the information was incomplete.

- Signs and hospital architecture

Inside the hospital, accessibility of care requires the existence of clear signs to locate, inform, and guide the patient through the hospital. All the interviewees recognized the importance of signs to ensure smooth patient flow. Signs allow patients to reach their destinations easily and quickly. Moreover, the fluidity and ease of circulation also depend on the architecture of the hospital *"even with the existence of clear signs, patient circulation remains difficult because of the architectural complexity"* (participant ID4). From the participants' point of view, the architecture of the healthcare facility should take into account both the movements of patients and staff to minimize their efforts and reduce the risks of contamination. For example, one of the participants points out that an inappropriate architecture could influence the patients' health status *"after a surgical operation, the patient is transported on stretchers for long distances to reach their room. However, in this case, the patient's health requires the minimum of movement to avoid post-operative complications"* (participant ID2).

- Availability of human resources

Patients' medical care requires the availability of adequate human resources, in terms of quality and quantity. In this study, all the participants revealed an insufficient number of physicians and nurses *"the number of doctors is very small compared to the number of patients. We were many in the waiting room, and there was only one doctor who has to treat everyone"* (participant ID10); *"for some specialties, we have only one specialist. When the latter gets sick or takes his leave, we face serious problems"* (participant ID2).

- Availability of material resources

The availability of sufficient and functional material resources (drugs, medical supplies, technical equipment, etc.) is critical to receiving care and satisfying patients *"it irritates me when my appointment day arrives and I discover that my appointment has been canceled because of material unavailability"* (participant ID8). From the participants' point of view, the unavailability of material resources can be due to several factors such as

dependence on other stakeholders. For example, the drug supply is carried out by the Ministry of Health, and the maintenance of technical equipment is managed through outsourcing contracts. Consequently, the availability of material resources depends on these stakeholders "when equipment breaks down, it is necessary to wait, between few days and several weeks, for the arrival of the repair company" (participant ID3).

4.3.2. Waiting time

The waiting time dimension includes the time it takes to obtain an appointment and the waiting time on site for consultation, medical analysis, and radiological examinations. All participants agreed that waiting times are critical for both quality of care and patient satisfaction "one more day would have a negative impact on the patient's health and well-being. Sometimes, the patient's case requires simple medical interventions if he/ she is treated on time. On the other hand, if he/ she waits several days before receiving care, his/ her health status may get worse" (participant ID2); "waiting times are the major disaster in public hospitals. In my case, I had to wait more than 5 months to get an appointment, and on the day of the appointment, I stayed in the waiting room for 5 hours before seeing the doctor" (participant ID8).

The main cause of waiting times revealed by the participants is the imbalance between capacity and demand. Capacity refers to the available human and material resources, and demand refers to patients' flow. Another reason cited for waiting times is the non-compliance with the gatekeeping system. Actually, the patient pathway should begin at basic healthcare centers, then provincial and regional hospitals and finally university hospital centers. The non-compliance with this pathway increases healthcare demand and causes long waiting times.

4.3.3. Consultation time

Participants stated that the longer the consultation time, the more satisfied the patient is. In addition, they have linked consultation time to the quality of medical diagnosis "long consultation times are synonymous with good medical decision-making" (participant ID5); "long consultation times give rise to in-depth discussions with patients, which makes it possible to accurately identify symptoms and signs of disease" (participant ID2). Some participants from the patient category stated that they have not been given sufficient information during the care process because the consultation time was short "the doctor had not given me enough time, he was fast. I left the hospital without understanding what I am suffering from" (participant ID9).

Participants explained the reduction of consultation time in different ways. Some have linked it to the workload "doctors are too busy, they have very long patient queues, so they do not have enough time to examine each patient thoroughly" (participant ID5), and to the caregivers' performance of non-professional tasks, such as organizing patient records and regulating the queue. Others have associated short consultation time with the lack of motivation "I insist much more on the lack of motivation because the salary is fixed and is not proportional to the work" (participants ID1).

4.3.4. Hospital hotel services

Hospital hotel services refer to the accommodation conditions of patients in hospitals. They include cleanliness, laundry, www.astesj.com

catering, and comfort during the hospital stay. While discussing hospital hotel services, participants have notified the important role of outsourcer companies because most of these activities are outsourced. The number of coded references corresponding to the hospital hotel services is given in Figure 3.

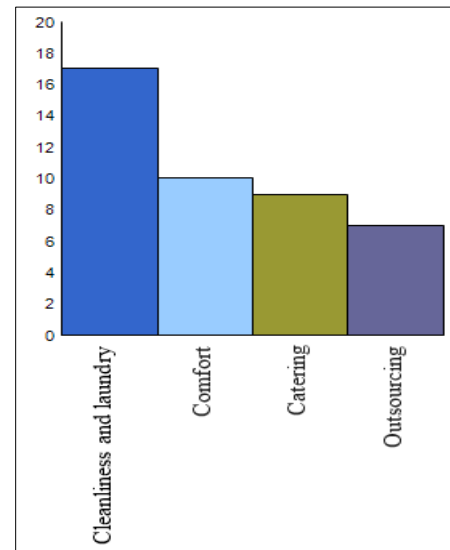


Figure 3: Hospital hotel services - number of coding references per element

Participants confirmed that it is essential to pay great attention to hospital hotel services in order to increase patient satisfaction "we concluded, from satisfaction surveys, that patients in some care units such as cardiology are very satisfied because hotel services are good. On the other hand, in hot units such as maternity and emergency departments, patients are dissatisfied, as the hotel services are poor" (participant ID3). For some participants, hotel services in the public hospitals are unsatisfactory, which reduces its attractiveness "I assume that most of the patients prefer private hospitals because of poor hotel services in public hospitals" (participant ID1); "the competitive edge of the health private sector lies in hospital hotel services" (participant ID2).

Hospital cleanliness was consistently mentioned by all participants as a fundamental criterion for the quality of care and safety "cleanliness is very essential because hospitals are full of germs, the risks of contamination are very high. Without cleanliness and hygiene, the hospital would be a place of infection rather than a place of care" (participant ID5). Concerning catering, participants argued that the effective provision of high-quality food is crucial for the well-being of patients. The interviewees revealed a lack of quality and quantity of the served meals. With regard to comfort, participants' observations focused on the lack of chairs in waiting rooms, lack of air conditioning, room heating, uncomfortable beds, noise during visiting hours, etc.

As hospital hotel activities are outsourced, the outsourcer companies are responsible for facilities maintenance, product supply (food, cleaning products, etc.), production and delivery of meals and clean linen, as well as ensuring the hospital cleanliness, etc. Thus, dysfunctions are attributed to the poor outsourcing management: lack of monitoring and control of service providers,

insufficient allocations of staff and products, non-respect of contractual obligations, etc.

4.3.5. Administrative procedures

Hospital administrative procedures are managed by hospital internal regulations and the Ministry of Health circulars. However, participants from the healthcare professional category reported that these regulations are obsolete and outdated. As for participants from the patient category, they generally expressed their dissatisfaction with the organization of administrative procedures. According to them, dysfunctions are diverse: complexity of administrative circuits, redundancy, lack of clarity and orientation, etc. *"the administrative formalities are too complicated; there are a multitude and redundancy of the required documents. In my opinion, all the required documents should be replaced by a single one"* (participant ID9); *"the procedures are not clear and patients and their families are victims of comings and goings"* (participant ID8). In particular, we noted that participants repeatedly raised issues of the RAMEM (Medical Assistance Scheme for the Economically Underprivileged), which is a health insurance regime for the poor and vulnerable population. They reported that the RAMEM procedure is cumbersome and results in a slow and lengthy care process. When we asked healthcare professionals about RAMEM procedure issues, they argued that these dysfunctions stem from patients' non-compliance with the gatekeeping system. However, for patients, the non-compliance with the gatekeeping system is due to a lack of guidance and difficulties in access to information.

All participants proposed to ease the administrative procedures by simplifying them and reducing redundancies, as well as through the use of Information & Communication Technology. Thus, would reduce the administrative burden and patient's frustration *"in my opinion the best way to overcome administrative documents redundancy problem is to use computerized and electronic procedures"* (participant ID3).

5. Discussion

Quality of care is a major issue for healthcare facilities that they are required to improve in order to comply with standards and to meet patients' needs [38]. Patient satisfaction is one of the important indicators of quality of care. According to previous studies, patients focus on tangible aspects of healthcare services and their administration to assess the quality of care, as they lack the necessary skills to judge the technical quality [39]. Satisfaction surveys revealed a variety of factors that influence patient satisfaction. In this exploratory study, we focused on the following logistics factors: physical accessibility, waiting time, consultation time, hospital hotel services, and administrative procedures. These factors were covered during semi-structured interviews with health professionals and patients from the public health sector in Morocco. The results highlighted the importance of the studied logistics factors for quality and patient-centered care. All study participants emphasized the critical aspect of hospital logistics in accessing healthcare and the management process from admission to discharge.

According to the results, the physical accessibility of healthcare is the logistics factor most often raised by the

interviewees. This can be explained by the scope of the elements it includes e.g. location of the healthcare facility, medical transportation, availability of human and material resources, etc., but also by the difficulties encountered by patients in accessing healthcare. Hospital logistics can help in different ways to mitigate patients' access to healthcare. For example, Frichi et al. [40] proposed to improve medical patient transportation in Morocco by increasing the availability of ambulances through collaborative practices in the healthcare supply chain. El Oualidi et al. [28], developed a mathematical model to optimize the assignment of nurses to emergency departments in a public hospital in Morocco, and thus improve the availability of nurses in these departments. Ben Kacem et al. [41] have suggested a hybrid algorithm to size needed medical resources in case of a massive influx of patients, so as to save maximum lives. In order to better manage drug provisioning in Moroccan public hospitals, Ibn El Farouk et al. [42] built a decision-making tool to select relevant indicators to better measure and manage the medicines supply chain. In the same context of dealing with pharmaceutical issues, El Mokri et al. [43] have developed a mathematical model for facility location problems to better locate pharmaceutical warehouses in order to serve all demand points such as hospital and basic healthcare centers and to minimize warehouses' opening cost.

Long waiting times lead to patient dissatisfaction and can affect their health status. One of the causes of waiting times raised by participants is the imbalance between demand and capacity. This is similar to the findings of Silvester et al. [44]. They assumed that failure to control variation in capacity and demand is the main origin of waiting times. Several works in hospital logistics have proposed actions to reduce waiting times. Indeed, Gupta and Denton [45] proposed to apply industrial engineering and operational research tools to optimize appointment planning. Golmohammadi [46] developed statistical and mathematical models capable of predicting the number of patients coming from the emergency department in order to prepare for their reception in the care units. The objective was to reduce the waiting time for preparing patients' reception.

The consultation time is considered one of the most essential features of healthcare services. Participants reported the benefits of extended consultation time on both satisfaction and quality of care. Similar results have been highlighted by quantitative surveys that have concluded that the length of time spent with the caregiver is strongly associated with patient satisfaction [47,48]. To increase consultation time, hospital logistics researches propose to decrease the workload of caregivers and increase their availability by freeing them from logistical and administrative tasks (e.g. organization of patient records, stock management in care units, transportation of laboratory tests, etc.). These tasks should be performed by dedicated and trained teams [20,49].

A very strong and recognized association is noticed between hospital hotel services (cleanliness, laundry, catering, comfort, etc.), patient satisfaction and quality of care. Given the tangible nature of hospital hotel services, they are easy to evaluate and to which patients are sensitive. These findings are in line with results from other studies. In fact, Sues and Mody [50], through a quantitative survey, have shown that hotel services in a hospital have a major influence on patients' well-being. Peters et al. [51]

discussed and proved the importance of cleanliness in reducing infections and promoting patient safety and satisfaction. Shirzadi et al. [52] reported that patients and their companions ranked highly the importance of hospital hotel services, which shows that they care about these issues. Their study has considered a large number of hotel services including esthetic of physical space, food services, cleanliness, availability of lifts and other services. Efforts to address and improve these nonmedical activities can have a profound positive impact on patient satisfaction and quality of care.

The last factor discussed in this paper concerns administrative procedures for patient admission, treatment, and discharge. Participants agreed on the decisive effect of administrative procedures on patient satisfaction. These results support previous studies [53]. In Morocco, a patient satisfaction survey conducted in a public hospital showed that more than half of patients (54.2%) found the administrative formalities complicated and 60% of them were not satisfied with the organization of their discharge [54]. The optimization of administrative procedures is necessary to reduce patient frustration and increase fulfillment. The existing procedures should be revised in depth to remove unnecessary and duplicate documents. Also, administrative circuits can be improved through the adoption of information technologies, which would help to reduce circuit redundancies and associated delays. Findings from previous research indicated that e-hospital systems increase clinical quality and enhance patient satisfaction and loyalty [55]. In Morocco, some hospital services use Information & Communication Technology e.g. web-based appointment systems [56]. But these applications are insufficient and not yet widespread.

6. Limitation and future research

This qualitative study explored the importance of hospital logistics factors in quality of care and patient satisfaction from the perspective of patients and healthcare professionals. However, this research has several limitations. It was restricted to a few public hospitals in Morocco and a limited number of participants. Therefore, study findings need to be confirmed by other studies on a larger population, using quantitative data collection methods. In particular, future studies would provide quantitative data on the impact of logistics factors on quality and satisfaction to see which of these factors is more preponderant.

7. Conclusion

Previous studies have stressed the vigorous association between quality of care and patient satisfaction on the one hand, and hospital logistics on the other hand. The aim of this paper was to gain a better understanding, through a qualitative study, of the effect of hospital logistics factors on quality of care and patient satisfaction. To this end, semi-structured interviews were conducted with five patients and five healthcare professionals. The combination of patients' opinions and healthcare professionals' opinions was of great value to capture different points of view. Results showed that participants gave considerable importance to hospital logistics factors when discussing quality of care and patient satisfaction. Thus, the hospital's role is not only to treat the disease but also to provide healthcare services that are

easily accessible, delivered on time, in a clean and comfortable environment in order to promote the well-being of patients and other service users. Therefore, it is suggested that healthcare planners and managers pay more attention to hospital logistics activities. Future research could be of great help to deepen and measure the impact of the studied logistics factors on quality and satisfaction in order to provide useful data to hospital managers to be able to make sound decisions and determine which factors need to be improved.

Conflict of Interest

The authors declare no conflict of interest.

Acknowledgment

The authors would like to thank the participants for their time and valuable contribution to this research.

References

- [1] Y. Frichi, F. Jawab, and S. Boutahari, "Elaboration of an association matrix of satisfaction factors in healthcare facilities and hospital logistics activities," in *2018 International Colloquium on Logistics and Supply Chain Management (LOGISTIQUA)*, 2018, pp. 32–37.
- [2] Y. Frichi, F. Jawab, and S. Boutahari, "Identification of health system stakeholders in Morocco," in *Proceedings of the International Conference on Industrial Engineering and Operations Management*, 2019, no. March 5-7, pp. 1193–1199.
- [3] A. Donabedian, *The definition of quality and approaches to its assessment. Volume 1. Explorations in Quality Assessment and Monitoring*. 1980.
- [4] Q. Nottingham, D. M. Johnson, and R. Russell, "A multi-year SEM model predicting the impact of behavior attributes on overall patient satisfaction," *Int. J. Qual. Reliab. Manag.*, 2018.
- [5] D. L. Frosch, "Patient-Reported Outcomes as a Measure of Healthcare Quality," *J. Gen. Intern. Med.*, vol. 30, no. 10, pp. 1383–1384, 2015.
- [6] Y. Frichi, F. Jawab, and S. Boutahari, "The Mixed-Method 5W2D Approach for Health System Stakeholders Analysis in Quality of Care: An Application to the Moroccan Context," *Int. J. Environ. Res. Public Health*, vol. 16, no. 16, p. 2899, Aug. 2019.
- [7] A. Mohd and A. Chakravarty, "Patient satisfaction with services of the outpatient department," *Med. J. Armed Forces India*, vol. 70, no. 3, pp. 237–242, 2014.
- [8] K. Park, J. Park, Y. D. Kwon, Y. Kang, and J. W. Noh, "Public satisfaction with the healthcare system performance in South Korea: Universal healthcare system," *Health Policy (New York)*, vol. 120, no. 6, pp. 621–629, 2016.
- [9] T. Verulava, R. Jorbenadze, L. Karimi, B. Dangadze, and T. Barkalaia, "Evaluation of Patient Satisfaction with Cardiology Services," *Open Public Health J.*, vol. 11, pp. 201–208, 2018.
- [10] S. Waters, S. J. Edmondston, P. J. Yates, and D. F. Gucciardi, "Identification of factors influencing patient satisfaction with orthopaedic outpatient clinic consultation: A qualitative study," *Man. Ther.*, vol. 25, pp. 48–55, 2016.
- [11] J. Fang, L. Liu, and P. Fang, "What is the most important factor affecting patient satisfaction – A study based on gamma coefficient," *Patient Prefer. Adherence*, vol. 13, pp. 515–525, 2019.
- [12] C. Bleustein, D. B. Rothschild, A. Valen, E. Valaitis, L. Schweitzer, and R. Jones, "Wait Times, Patient Satisfaction Scores, and the Perception of Care," *Am. J. Manag. Care*, vol. 20, no. 5, pp. 393–400, 2014.
- [13] J. G. R. Howie, M. D. Porter, D. J. Heaney, and J. L. Hopton, "Long to short consultation ratio: a proxy measure of quality of care for general practice," *Br. J. Gen. Pract.*, vol. 41, no. 343, pp. 48–54, 1991.
- [14] K. Pölluste, R. Kallikorm, K. Meesaar, and M. Lember, "Satisfaction with access to health services: The perspective of Estonian patients with rheumatoid arthritis," *Sci. World J.*, vol. 2012, 2012.
- [15] B. Mohamed and N. A. Azizan, "Perceived service quality's effect on patient satisfaction and behavioural compliance," *Int. J. Health Care Qual. Assur.*, vol. 28, no. 3, pp. 300–314, 2015.
- [16] H. D. SEVÍN, "Hotel Services In Hospitals," *J. Tour. Gastron. Stud.*, pp. 451–459, 2018.
- [17] Y. Frichi, F. Jawab, and S. Boutahari, "Patient satisfaction factors and their

- correspondence with hospital logistics activities,” in *Proceedings of the International Conference on Industrial Engineering and Operations Management*, 2018, pp. 1141–1147.
- [18] I. Ibn El Farouk, A. Talbi, and F. Jawab, “Chaîne logistique hospitalière : définition, état de l’art et pistes d’amélioration,” in *CIGIMS, FES/MAROC*, 2012.
- [19] F. Jawab, Y. Fricchi, and S. Boutahari, “Hospital Logistics Activities,” in *Proceedings of the International Conference on Industrial Engineering and Operations Management*, 2018, pp. 3228–3237.
- [20] S. Landry and R. Philippe, “How logistics can service healthcare,” *Supply Chain Forum An Int. J.*, vol. 5, no. 2, pp. 24–30, 2004.
- [21] T. Melo, “A note on challenges and opportunities for Operations Research in hospital logistics,” *Tech. reports Logist. Saarl. Bus. Sch.*, no. 2, pp. 1–13, 2012.
- [22] R. Khaldi, A. El Afia, and R. Chiheb, “Forecasting of weekly patient visits to emergency department: Real case study,” *Procedia Comput. Sci.*, vol. 148, pp. 532–541, 2019.
- [23] S. Villa, A. Prenestini, and I. Giusepi, “A framework to analyze hospital-wide patient flow logistics: Evidence from an Italian comparative study,” *Health Policy (New York)*, vol. 115, no. 2–3, pp. 196–205, 2014.
- [24] B. A. Ahmad, K. Khairatul, and A. Farnaza, “An assessment of patient waiting and consultation time in a primary healthcare clinic,” *Malaysian Fam. physician Off. J. Acad. Fam. Physicians Malaysia*, vol. 12, no. 1, pp. 14–21, 2017.
- [25] F. Lerebours et al., “Satisfaction des patientes traitées par chimiothérapie en hôpital de jour pour un cancer du sein : résultats de l’enquête TemporelLES,” *Bull. Cancer*, vol. 102, no. 4, pp. 316–323, 2015.
- [26] M. Beaulieu, “Une expérience de collaboration logistique,” *Gest. Hosp.*, no. 585, pp. 211–214, 2019.
- [27] S. Landry and M. Beaulieu, “The Challenges of Hospital Supply Chain Management, from Central Stores to Nursing Units,” in *Handbook of Healthcare Operations Management - Methods and Applications*, vol. 184, Springer, Ed. New York, 2013, pp. 465–482.
- [28] M. A. El Oualidi, J. Saadi, and A. Bellabdaoui, “Problème d’affectation des infirmières : un état de l’art et modélisation. Cas du service des urgences de l’hôpital Ibn Roch de Casablanca,” in *Congrès International en Génie Industriel et Management des Systèmes (CIGIMS 2012)*, 2012.
- [29] S. Chougrani and S. Ouhadji, “Les questionnaires de sortie et la place des usagers dans le projet qualité à l’Etablissement hospitalier universitaire d’Oran,” *Sante Publique (Paris)*, vol. Vol. 26, no. 4, pp. 499–508, 2014.
- [30] WHO, *Essential Environmental Health Standards in Health Care*. Geneva, 2008.
- [31] T. Schoenfelder, J. Klewer, and J. Kugler, “Determinants of patient satisfaction: A study among 39 hospitals in an in-patient setting in Germany,” *Int. J. Qual. Heal. Care*, vol. 23, no. 5, pp. 503–509, 2011.
- [32] L. Zemour, A. Belghitri, I. Damouche, K. Reguieg, R. Tedjani, and N. Midoun, “Mesure de la satisfaction des utilisateurs du dossier électronique médical au sein du système d’information hospitalier à l’établissement hospitalier et universitaire d’Oran, Algérie,” *Rev. Epidemiol. Sante Publique*, vol. 64, p. S260, 2016.
- [33] L. Kohn and W. Christiaens, “Les méthodes de recherches qualitatives dans la recherche en soins de santé : apports et croyances,” *Reflets Perspect. la vie économique*, vol. LIII, no. 4, pp. 67–82, 2014.
- [34] G. Imbert, “L’entretien semi-directif : à la frontière de la santé publique et de l’anthropologie,” *Rech. Soins Infirm.*, no. 3, pp. 23–34, 2010.
- [35] W. C. Adams, “Conducting Semi-Structured Interviews,” in *Handbook of Practical Program Evaluation: Fourth Edition*, K. E. Newcomer, H. P. Hatry, and J. S. Wholey, Eds. New Jersey, USA: John Wiley & Sons, 2015, pp. 492–505.
- [36] V. Braun and V. Clarke, “Qualitative Research in Psychology,” *Qual. Res. Psychol.*, vol. 3, no. 2, pp. 77–101, 2006.
- [37] J. Saldaña, *The Coding Manual for Qualitative Researchers - Second Edition*. SAGE, 2013.
- [38] E. A. Al-Shdaifat, “Implementation of total quality management in hospitals,” *J. Taibah Univ. Med. Sci.*, vol. 10, no. 4, pp. 461–466, 2015.
- [39] T. S. Dagger and J. C. Sweeney, “Service quality attribute weights: How do novice and longer-term customers construct service quality perceptions?,” *J. Serv. Res.*, vol. 10, no. 1, pp. 22–42, 2007.
- [40] Y. Fricchi, A. Ben Kacem, F. Jawab, O. Kamach, and S. Chafik, “Improving Interhospital Medical Patient Transportation in Morocco: A Forecasting Collaborative Approach,” in *Transportation, Logistics, and Supply Chain Management in Home Healthcare: Emerging Research and Opportunities*, J. Euchi, Ed. Pennsylvania, USA: IGI Global, 2020, pp. 136–162.
- [41] A. Ben Kacem, O. Kamach, S. Chafik, and M. Ait Hammou, “A hybrid algorithm to size the hospital resources in the case of a massive influx of victims,” *Int. J. Electr. Comput. Eng.*, vol. 10, no. 1, pp. 1006–1016, 2020.
- [42] I. Ibn El Farouk, A. Talbi, and F. Jawab, “Development of a Set of Indicators to Manage Medicines Supply Chain in Moroccan Public Hospital , Application of the SCOR Model,” *Int. J. Bus. Dev.*, vol. 3, no. 3, pp. 147–158, 2013.
- [43] A. El Mokrini, Y. Boulaksil, and A. Berrado, “Modelling facility location problems in emerging markets: The case of the public healthcare sector in Morocco,” *Oper. Supply Chain Manag.*, vol. 12, no. 2, pp. 100–111, 2019.
- [44] K. Silvester, R. Lendon, H. Bevan, R. Steyn, and P. Walley, “Reducing waiting times in the NHS: is lack of capacity the problem?,” *Clin. Manag.*, vol. 12, no. 3, pp. 105–109, 2004.
- [45] D. Gupta and B. Denton, “Appointment scheduling in health care: Challenges and opportunities,” *IIE Trans.*, vol. 40, no. 9, pp. 800–819, 2008.
- [46] D. Golmohammadi, “Predicting hospital admissions to reduce emergency department boarding,” *Int. J. Prod. Econ.*, vol. 182, pp. 535–544, 2016.
- [47] J. Ogden et al., “‘I want more time with my doctor’: a quantitative study of time and the consultation,” *Fam. Pract.*, vol. 21, no. 5, pp. 479–483, 2004.
- [48] N. Puri, A. Gupta, A. K. Aggarwal, and V. Kaushal, “Outpatient satisfaction and quality of health care in North Indian medical institute,” *Int. J. Health Care Qual. Assur.*, vol. 25, no. 8, pp. 682–697, 2012.
- [49] S. Landry and M. Beaulieu, “La logistique hospitalière : un remède aux maux du secteur de la santé?,” *Gestion*, vol. 26, no. 4, pp. 34–41, 2002.
- [50] C. Suess and M. A. Mody, “Hotel-like hospital rooms’ impact on patient well-being and willingness to pay: An examination using the theory of supportive design,” *Int. J. Contemp. Hosp. Manag.*, vol. 30, no. 10, pp. 3006–3025, 2018.
- [51] A. Peters, J. Otter, A. Moldovan, P. Parneix, A. Voss, and D. Pittet, “Keeping hospitals clean and safe without breaking the bank; summary of the Healthcare Cleaning Forum 2018,” *Antimicrob. Resist. Infect. Control*, p. 132, 2018.
- [52] S. M. Shirzadi, P. Raeissi, A. A. Nasiripour, and S. J. Tabibi, “Factors affecting the quality of hospital hotel services from the patients and their companions’ point of view : A national study in Iran,” *J. Res. Med. Sci.*, vol. 21, 2016.
- [53] F. Canoui-poitrine, H. Logerot, and M. Frank-soltysiak, “Évaluation de la satisfaction des professionnels et des patients d’une unité multidisciplinaire de chirurgie ambulatoire,” *Prat. Organ. des Soins*, vol. 39, no. 4, pp. 323–330, 2008.
- [54] K. Amazian, I. Toughrai, N. Benmansour, S. A. Laalim, M. E. A. El Alami, and K. Mazaz, “Enquête de satisfaction des patients atteints de cancer dans un hôpital universitaire au Maroc,” *Sante Publique (Paris)*, vol. 25, no. 5, pp. 627–632, 2013.
- [55] F. Kitsios, S. Stefanakakis, M. Kamariotou, and L. Dermentzoglou, “E-service Evaluation : User satisfaction measurement and implications in health sector,” *Comput. Stand. Interfaces*, vol. 63, pp. 16–26, 2019.
- [56] S. Bensbih, O. Bouksour, and S. Rifai, “On line appointment systems in a patient Centric Strategy: A qualitative approach in a case study for hospitals in Morocco,” *6th Int. Conf. Control. Decis. Inf. Technol. (CoDIT 2019)*, pp. 1735–1739, 2019.

Alleviation of Nonlinear Impact Using PAPR Hybrid Technique in CO-OFDM Systems

Liqaa A. Al-Hashime^{1,*}, Sinan M. Abdul Satar², Ghaida A. Al-Suhail¹, Osama Saied⁴

¹University of Basrah, Department of Electrical Engineering, 964, Iraq.

²University of Technology, Department of Electrical and Electronic Engineering, 964, Iraq

³University of Gharyan, Department of Electrical and Electronic Engineering, 218, Libya

ARTICLE INFO

Article history:

Received: 12 June, 2019

Accepted: 19 October, 2019

Online: 25 December, 2019

Keywords:

CO-OFDM

PAPR

BER

EVM

QF

CD

PMD

Nonlinear

ABSTRACT

Orthogonal Frequency Division Multiplexing (OFDM) is a modulation format that has recently attracted lots of consideration interior the long-haul fiber-optic transmission community. The most important advantage of optical OOFDM is its unlimited capability of canceling Inter-Symbol Interference (ISI) caused by Chromatic Dispersion (CD) and Polarization-Mode Dispersion (PMD). Specifically, Coherent OOFDM (CO-OFDM) presents a good and effective modulation method in modern optical communication systems. However, due to its high Peak to Average Power Ratio (PAPR), the performance of CO-OFDM is affected by nonlinear impairments. In this paper, we propose a new joint nonlinear technique; L3-by-3; with a distortion technique; clip-ping; that bypass the requirement for the use of any side information (SI) to minimize the high PAPR value of the transmitted signal and consequently improve various fiber nonlinear impacts through PAPR reduction. The simulation results reveal dependable and excellent signal recapture at the receiver and an effectively minimized PAPR level at the sender side.

1. Introduction

Because of the advantages and qualities of the OFDM system such as high spectral efficiency, this has led to its use in different modern communication applications. Furthermore, it is worthwhile noting that many authors have made the OFDM the first candidate for use in high-speed communications applications and high data rate systems. [1]. The OOFDM system is rated depending on the application in which it is used into two types, the first type is called Direct Detection OOFDM(DD), where a single photodiode is utilized for detection in the receiver. The second type is called Coherent Detection OOFDM (CO-OFDM) Which utilized an optical mixing is employed with a Local Oscillator (LO) in a coherent optical receiver. [2, 3]. The optical transmission system suffers from several disadvantages, especially when using a higher order of mapping M-PSK or M-QAM, where (M) is the order of mapping. these impairments have been discussed in many studies and articles and are classified as linear and non-linear. [4]. Nevertheless, coherent systems that utilizing Digital Signal Processing (DSPs) permits the compensation of system weakness. In addition, there are many ways to process the signal and compensate the impairments. Some of these processes are used in

the receiving transmitter side, some of them employed in the optical channel, while the others are used in the receiver side.

The synchronization and balance method is an example of the methods used to compensate impairments in the optical channel as demonstrated in [5, 6]. Moreover, there are other methods that can be utilized to compensate the impairments that have occurred to the signal in the optical channel, such as Optical Phase Conjugate (OPC) to reduce nonlinearity, and Dispersion Compensated Fiber (DCF) to mitigate the impact of CD on the signal [7, 8]. Additionally, some methods that based on DSP are utilized in the transmitter side, such as phase-conjugated twin wave method [5], where some of such methods depend on diminishing the Peak to Average Power Ratio (PAPR) of the transmitted signal. A worthy reduction can also be gained when using one of these techniques, such as Selective Mapping (SLM) [6], Partial Transmit Sequence (PTS) [7], and non-linear transforms [8].

In this paper, the primary objective is to mitigate the impact of phase noise and nonlinearity in a CO-OFDM system employing 4QAM and 16QAM modulation through PAPR reduction in the system using the VPI software. The novel contribution of this article the use of the nonlinear method; L3by3; joined with the clipping distortion technique; for the first time in order to produce

*Corresponding Author: Liqaa A, Email: newliqas@gmail.com

a new combining technique to lessen the nonlinear impact through PAPR reduction for two modulation order with 10 Gbps bitrate.

2. CO-OFDM System Principle

In general, the concept behind OFDM is that one stream with high data rate is converted into different streams with lower data rates. It has been evince that these streams can be sent in parallel, offering more extensive symbol periods than single bearer style. Moreover, in OFDM these parallel streams are modulated by using one type of modulation such as, QAM, BPSK, and QPSK. [9]. The main factor behind the use of OFDM In modern radio norms is the high spectral efficiency that provides due to the presence of subcarriers which are orthogonal to each other. Because of its normal flexibility to reduce the impacts of chromatic dispersion [2]. Although the CO_OFDM system It is complex in design from the transmitter side but provides spectral efficiency, future sensitivity and immunity to polarization dispersion. CO_OFDM system divides into five sections: Radio Frequency (RF) OFDM transmitter, optical transmitter, optical channel, optical receiver and RF receiver. Figure 1 shows the primary sections of a CO-OFDM system.

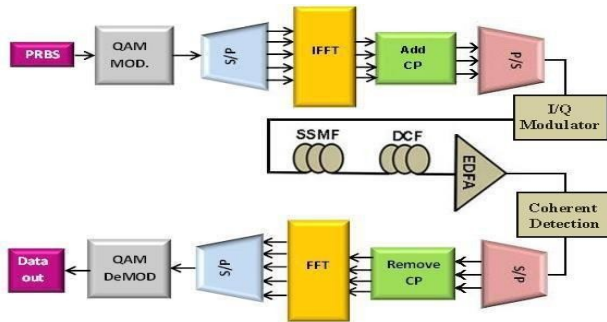


Figure 1 CO-OFDM system Block Diagram

In the transmitter, a serial binary data flow is obtained from a Pseudo-Random Binary Sequence generator (PRBS) and mapped into symbols using QAM mapping. In this study 4 and 16-QAM orders are considered where every two adjusted bits are mapped into one symbol in the case of 4-QAM, while in 16-QAM each symbol contains 4 bits. The serial data stream is converted to a parallel form before being passed to the Inverse Fast Fourier Transform (IFFT) block. In IFFT the block of data is transformed from the frequency domain into the time domain, and a cyclic prefix (CP) is added at the beginning of each time-domain OFDM symbol to eliminate Inter-Carrier Interference (ICI) and Inter-Symbol Interference (ISI) at the receiver. Afterward, the signal is converted from a parallel to a serial form (P/S) to send through the optical channel. The optical part of the system consists of an IQ modulator block which contains two Mach-Zehnder Modulators (MZMs) with a continuous wave (CW) laser that are utilized to up-convert the real/imaginary components of the signal, from the radio frequency(RF) domain to the optical domain.

In order to obtain the optical modulated signal, the signals that come from the two branches which have a phase difference of 90 are combined [10]. The subsequent part of the system is the fiber optic channel, which contains three processes: (i) Standard Single Mode Fiber (SMF) using to send optical signal.; (ii) compensating the dispersion in the optical channel using a Dispersion Compensating Fiber (DCF), where, the DCF, which is treated as a special kind of fiber optic that has a considerable negative dispersion, is used after the standard SMF [11] and (iii)

amplifying the strength of signals being carried through the fiber optic channel using an Erbium-Doped Fiber Amplifier (EDFA) as well as compensating the attenuation induced by the optical fiber. The third part of the system is the receiver, which contains a coherent reveal block with laser used as a local oscillator, which is used to convert the optical signal to an RF signal. The coherent receiver can convert an optical-signal to a baseband electrical signal, where the 90° phase difference between the I and Q components is generated by optical hybrids and producing a phase shift equals of 180° among balanced detection. The final part of the system is the OFDM decoder, which consists of a serial to parallel converter, where data is converted from a serial into a parallel form, removing CP and executing a Fast Fourier Transform (FFT). To retrieve the transmitted information, the FFT is first used to turn the signal into the frequency domain. The outgoing data from the FFT is then switched to a sequential order to perform the de-modulation process and obtained the original data. The OFDM signal is involve of a substantial number of subcarriers. the addition of the power of (N) subcarriers that have the same phase will give top power (N) by the normal power. However, a huge PAPR increases the Nonlinear (FNL) impairments, which diminish the performance of the optical system. the OFDM consist of (N) data sequences of vector $U(U_k (k=0,1,..., N-1))$, which will be sent in side by side. One OFDM data symbol is:

$$u(t) = \frac{1}{\sqrt{N}} \sum_{k=0}^{N-1} U_k e^{2j\pi f_k t} \quad (1)$$

where f_k is the subcarriers frequency spacing, U_k is the k_{th} information symbol vector and $u(t)$ is the baseband time domain OFDM signal after IFFT. the PAPR is relies upon the input information. As such, PAPR can be computed by finding the ratio between the peak power to the average power of the signal [12]. The equation of PAPR can then be written as:

$$PAPR = \frac{\max [|u(t)|^2]}{E[|u(t)|^2]} \quad (2)$$

where $E[|u(t)|^2]$ is the average power of the OFDM. The Cumulative Distribution Function (CDF) is the most frequently utilized parameters, and is utilized to gauge the performance of any PAPR technique. Regularly, the complementary cumulative distribution function (CCDF) is used when PAPR value exceeds the threshold. To find the probability that PAPR of an OFDM signal exceeds the threshold (p_0), assume the following complementary cumulative distribution function (CCDF) for non- overlapping sampling;

$$CCDF = p(PAPR > p_0) = 1 - (1 - \exp(-p_0))^N \quad (3)$$

3. Proposed Technique

Generally, the nonlinear method L3-by-3 was first discussed in [14] for wireless OFDM system. This method is based on the Sliding Norm Transform (SNT) based PAPR reduction method [15]. Here, we propose, for the first time, using a combination of clipping and L3by3 in CO-OFDM system. Let x be a real vector with N samples, $x=(x1,x2,x3, \dots, xN)$. The sliding norm transformer that can be used in the transmitter side is then defined as follows:

$$y_n = \frac{x_n}{\sqrt[3]{\alpha + x_{n-1}^3 + x_n^3 + x_{n+1}^3}} \quad (4)$$

The parameter (α) adjusts the PAPR of the transformed output. In other words, different values for PAPR can be obtained by changing α value, which indicates the possibility of setting a value

of PAPR by selecting the optimum value of α . The L3by3 transformer technique effectively lowers the PAPR of the CO-OFDM signals when compared with other techniques. The process of restoring x signals samples at the receiving end is done using the following Equation:

$$X = (+\sqrt[3]{x_n^3} \text{sign}(y_n)) \quad n=1,2,3,\dots,N \quad (5)$$

where $\text{sign}(0)$ is the Signum function. It can be noted that from Equation (5) data at the receiver can be recovered and the transmitted information can be obtained. The proposed hybrid technique is a combination between the clipping method and the L3-by-3 method and can be described by:

$$C(y_n) = \begin{cases} -A & \text{if } y_n < -A \\ y_n & \text{if } -A < y_n < A \\ A & \text{if } y_n > A \end{cases} \quad (6)$$

where $C(y_n)$ is the clipping signal, and A is a predetermined clipping level that can be defined as:

$$CR = \frac{A^2}{P_{in}} \quad (7)$$

where P_{in} represents the mean input power of the OFDM signals, and CR is the clipping ratio. The principle of clipping technique is based on setting the maximum value of the input signal to a predetermined value if exceeded it will be clipped, otherwise, the input signal is transmitted without any change. In general, the clipping ratio is used to determine the level of clipping. More specifically, the clipping method is considered as a non-linear process that causes (in & out) band distortion. In other words, the out-band distortion causes spectral extension and can be taken away by filtering out the signal after clipping. On the other hand, the in-band distortion limits the Bit Error Rate (BER) and can be disposed of by performing clipping with the adequately oversampled OFDM signals (e.g., $L \geq 4$ where L is the oversample factor), resulting in a less degraded BER performance. To achieve an excellent PAPR performance, the L3by3 technique is combined with the clipping technique, where despite the increase in the BER of the system due to the clipping technique such an adverse of in-band distortion impact is eliminated, through the L3by3 technique, which reduces the number of signals exceeding the threshold value.

4. System Setup and Simulation Results

This section introduces the simulation of a CO-OFDM system with PAPR reduction using the VPI Transmission-Maker and MATLAB software packages. The global parameters set for the simulations and their values are presented in the Table (1).

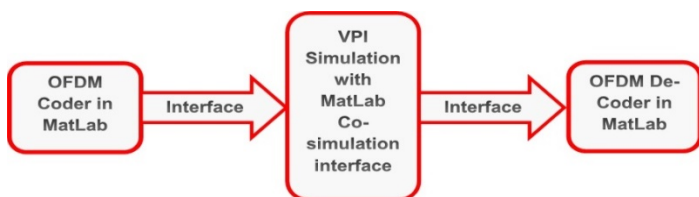


Figure 2 CO-OFDM system setup

Table1. The CO-OFDM system Simulation parameters

General parameters	
Bit-rate	10Gbps
Sample-rate	40Gbps
Sequence-length	8192
Samples-per-bit	2-bit
Mapping order	4QAM,16QAM
OFDM-parameters	
Sub-carriers	128
Cyclic-prefix	1/8
CW Laser & Local Oscillator	
Carrier freq.	193.1THz
Power in dBm	5dBm
Line-width	0.1MHz
SMF&DCF	
SMF length in km	50km
DCF length in km	5km
Number of loops	10
DCF attenuation	0.5dB/km
DCF dispersion	-160ps/nm/km
SMF dispersion	16ps/nm/km
SMF attenuation	0.2dB/km
Optical Amplifier DFA	
Gain	13dB
Noise Figure	4dB
α	0.2

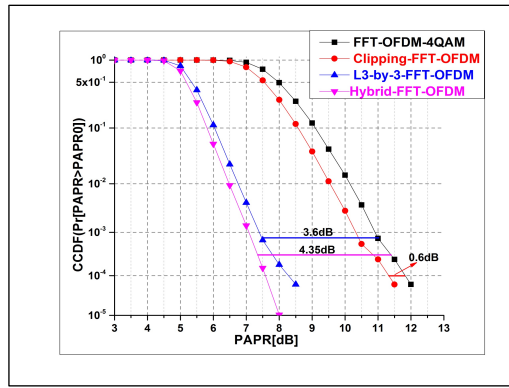
The OFDM signal generation and PAPR reduction were performed using MATLAB interfaced with VPI using the MATLAB Co-Simulation features, as shown in Figure (2).

First of all, referring to Equation (4) the control parameter α investigated for L3by3 for the 4-QAM and 16-QAM mapping orders. Table (2) shows the results obtained for PAPR at different values of α . The results show that α is directly proportional to PAPR. In other words, as α values change from 0 to 1, the value of PAPR increases, where the lowest PAPR value is obtained when the value of α is 0.1.

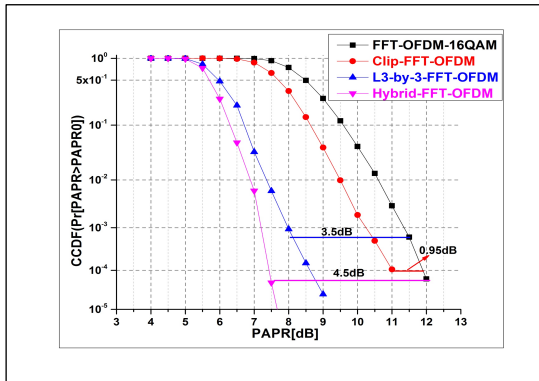
Table 2 PAPR values for different values of α

PAPR value in dB at probability of 10-4							
origina l	4QAM			11.5			
	16QA M			11.2			
α		0.1	0.2	0.4	0.6	0.8	1
L3by3	4QAM	6.35	7.75	8.4	9.1	9.4	10.1
	16QA M	6.75	7.6	8.5	9	9.55	10.2

Figure 3 (a) and (b) plot the CCDF as a function of PARP of the original signal without using any reduction technique for PAPR ; the CCDF when using a clipping for the signal at a clipping level 0.6, the CCDF when using L3by3 at $\alpha = 0.1$; and the proposed hybrid technique for 4-QAM and 16-QAM optical OFDM signals, respectively.



(a) 4QAM



(b) 16QAM
(c)

Figure 3 A comparison of the CCDF vs. PAPR performance of a CO-OFDM system using a variety of techniques

Table 3 summarizes the results of PAPR reduction using the proposed technique at CCDF probability values of 10^{-4} .

Table 3 PAPR for the proposed technique at CCDF probability 10^{-4}

PAPR Value in dB at Probability 10-4				
	original	clipping	L3by3	L3by3+clip
4QAM	11.9	0.6	3.6	4.35
16QAM	11.9	0.95	3.5	4.5

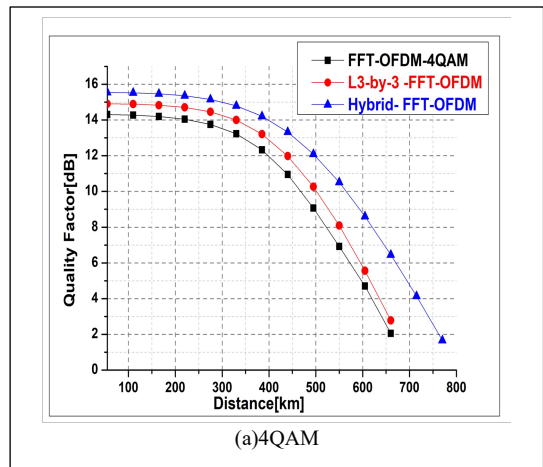
The table shows the efficiency of the proposed hybrid method in reducing the PAPR compared to using the L3by3 method and the clipping method separately. In addition, the suggested method has been compared with the other methods used to reduce PAPR in terms of their effectiveness in PAPR reduction as in table(4).

Table 4 Comparison between the suggested method and other PAPR reduction methods

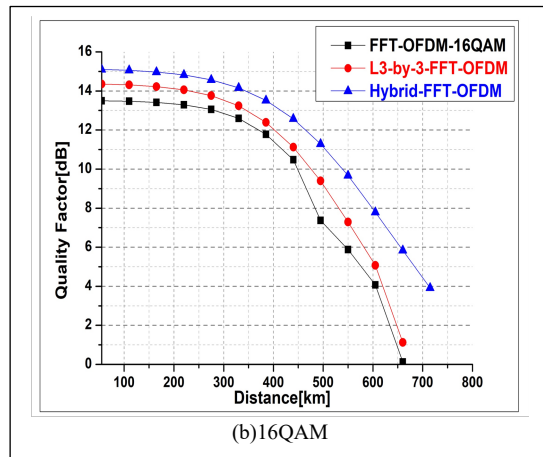
PAPR Value in dB at Probability 10-4				
Method	original	Hybrid	Reduction	Mapping
IPTS+CF[16]	10.5	7.32	3.18	QPSK
IPTS+MCF[16]	10.5	6.18	4.32	QPSK
Hadamard+m-law[17]	13.4	11.4	2	QPSK
L3by3+clipping	11.9	7.55	4.35	QAM

To check the efficiency and effects of the PAPR reduction on the system when changing distance, Figures (4) and (5) illustrate distance vs. Quality Factor (QF) and BER vs. distance respectively, for the system without using any technique to reduce PAPR ; for the system using the L3by3 ; and for the system using the proposed hybrid method. From figures, it is possible to deduce that the suggested hybrid method improves the QF and the BER for the system, where the results obtained for these parameters in the case of the hybrid method are better than those of the original system and those of system employing the L3by3 method. Table (5) summarizes the results obtained for QF from Figure (4).

As can be noted from Figure 4, the QF for the conventional CO-OFDM is good as well as the QF for both schemes at low distances (i.e. < 250 km), due to the reduction of the effect of chromatic dispersion as well as attenuation due to the presence of DCF that eliminates the effect of dispersion as well as the EDFA which minimizes the impact of attenuation. However, when we increase the launch power of the signal the distance will increase, thus increasing the nonlinear effects due to the Kerr effect, which reduces the performance of the system. As such for a larger distance (i.e. > 250 km), the proposed scheme outperforms the L3by3 method and the traditional CO-OFDM as it has the lowest PAPR, which reduces the fiber nonlinearity caused by the Kerr effect compared to the other two schemes (see Figure 3).



(a)4QAM



(b)16QAM

Figure 4 QF vs. distance for (a) 4-QAM and (b) 16-QAM

*Liqa Abdul Sattar, Email:newliqas@gmail.com

Table.5. QF for CO-OFDM at different distances using different PAPR reduction techniques

Quality Factor in dB				
Distance [km]	Mapping	Original	L3by3	Hybrid
275	4QAM	13.7	14.4	15.2
	16QAM	13	13.7	14.5
550	4QAM	6.9	8	10.5
	16QAM	5.8	7.2	9.6

The 4-QAM and 16-QAM constellation points for the three aforementioned schemes presented in Table 5 show the QF improvement when the proposed scheme is considered compared to the other two schemes. For example, a QF improvement of 1.5 dB and 0.8 dB is obtained for the proposed scheme compared to the traditional CO-OFDM and L3by3 schemes, respectively, when 4-QAM is considered as a modulation order at a distance of 257 km. The table also illustrates that increasing the distance to 550 km for the same modulation order (i.e. 4-QAM) results in a 4.5 dB and 2.4 dB QF improvement for the proposed scheme compared to the traditional CO-OFDM and the L3by3 schemes, respectively.

Figure 5 shows the received constellation points of the traditional CO-OFDM, as well as the L3by3 and the proposed hybrid schemes. As illustrate in Figure 5 (a) for the 4-QAM mapping order, it is shown that an excellent constellation diagram for the original system (i.e. CO-OFDM) is obtained for the short fiber length with excellent QF. However, the 4-QAM constellation points of this scheme becomes worse for long fiber distances, as its QF becomes low. In the case of the L3by3 and the proposed Hybrid method, the performance remains good with increased distances, where a good quality factor can be obtained for up to 550 km for the system with the L3by3 method, and for up to 660 km for the system with the proposed Hybrid technique.

Additionally, Figure 5 (b) shows the constellation points of 16-QAM with and without the use of the L3by3 method and the proposed Hybrid method. The figure shows that the constellation points of the traditional CO-OFDM system is excellent for low fiber distances, but with increasing the distance, the signal power must be increased, which means increasing the nonlinearity and degradation of the system's quality factor. However, if PAPR reduction methods are used, the negative effect of the nonlinearity on the system performance is reduced and consequently the quality factor is improved, thus allowing increasing the transmission distance to 55 km in case of using the L3by3 method, and up to 100 km in case of using the proposed Hybrid method.

Figure (6) shows the relationship between BER and distance for the 4-QAM and 16-QAM systems. For the system with 4-QAM mapping order, a distance increase of more than 120 km and 95km is achieved for the proposed Hybrid and the L3by3 method, respectively, compared to the original system. As for the system with the 16-QAM mapping order, a distance increase of more than 105 km and 65 km is achieved for the suggested Hybrid and the L3by3 method, respectively, compared to the original system.

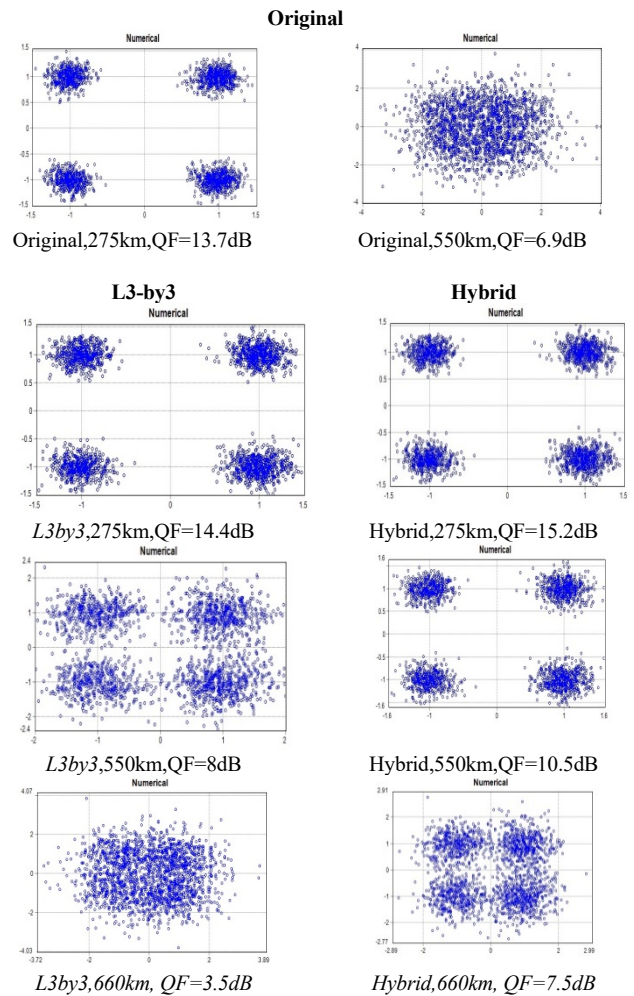


Figure 5 (a) 4-QAM Constellation diagrams of traditional CO-OFDM, L3by3and the proposed hybrid schemes at Different distance for 4-QAM

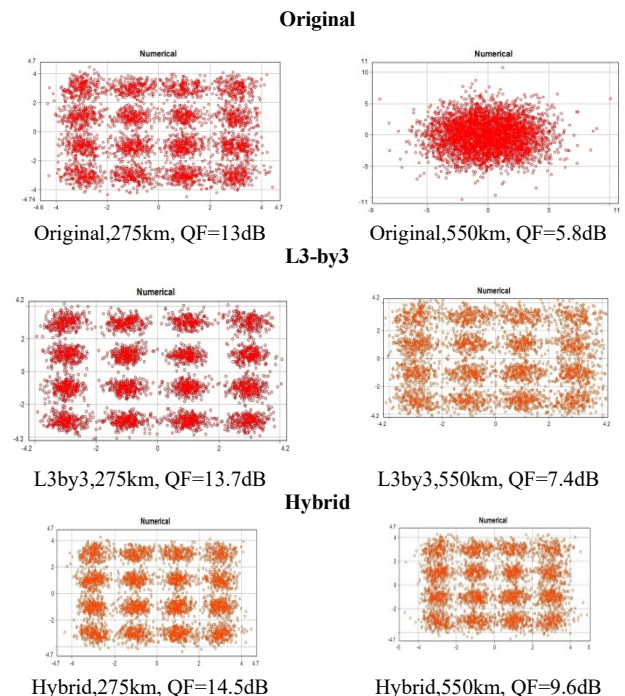
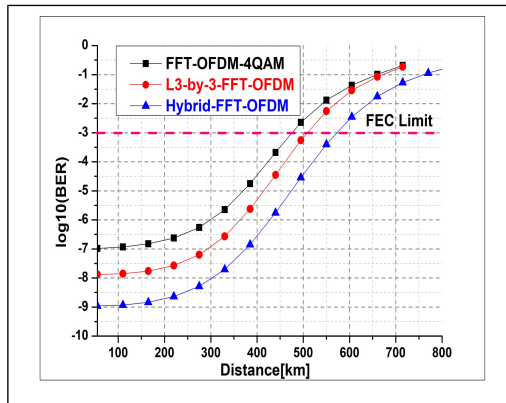
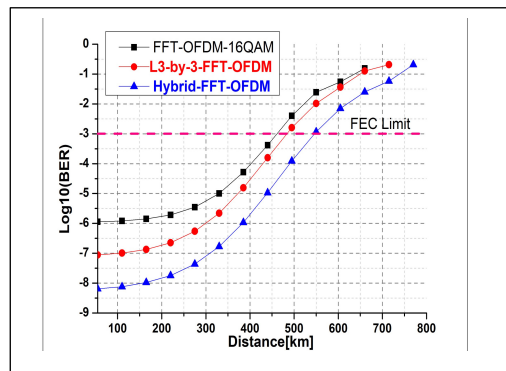


Figure 5 (b) 16-QAM Constellation diagrams of traditional CO-OFDM, L3by3and the proposed hybrid schemes at different distance for 4-QAM

Additionally, to examine the efficiency of the suggested Hybrid technique, the received power (RxP) and BER for the system with and without PAPR reduction techniques has been simulated. Figure (7) shows the results for the traditional system, the system with the L3by3 technique and the system with the proposed Hybrid technique at a distance of 550 km and launched laser power of 5 dBm. As shown in the figure, the best receiver sensitivity is obtained for the system with the Hybrid technique. Moreover, the figure demonstrates that the eye-opening of the system with the suggested combination technique is superior to the eye-opening in the case of using the L3by3 method or in the case of the primary system.



(a) 4 QAM



(b) 16 QAM

Figure 6 BER vs. distance

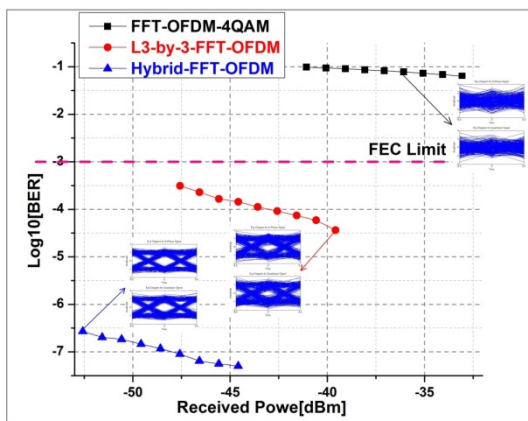
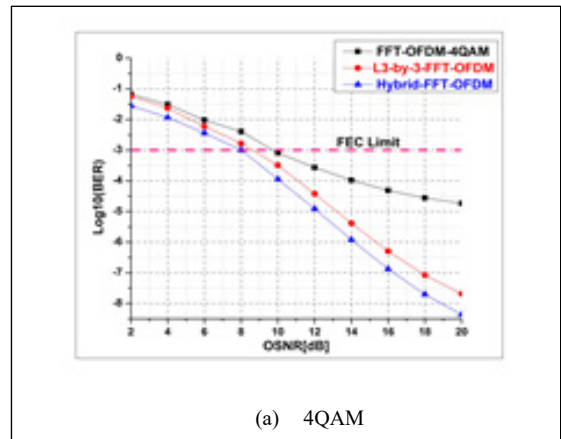
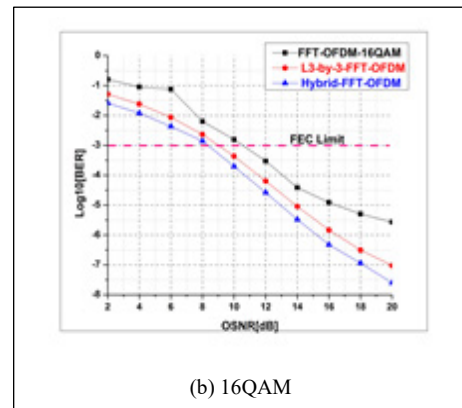


Figure 7 BER vs. received power at 550km for 4-QAM mapping order

Finally, Figure (8) shows the BER vs. OSNR for the traditional system, the system with the L3by3 method, and the system with suggested Hybrid reduction technique for PAPR at a distance of 550km and for 4-QAM and 16-QAM modulation orders. The results obtained show that when the value of the OSNR increases, the BER decreases.



(a) 4QAM



(b) 16QAM

Figure 8 OSNR vs. BER for (a) 4-QAM-(left), (b) 16-QAM-(right) at 550km

Table (6) provides a performance summary based on the BER vs. OSNR results for the 16-QAM and 4-QAM table.

Table.6 Received OSNR for 4-QAM and 16-QAM at a distance of 550km and BER of 10^{-3}

	OSNR in dB at 550km		
	original	L3by3	Hybrid
4 QAM	10	8.5	8
16 QAM	10.5	9	8.2

5. Conclusion

In this paper, an efficient and new hybrid method was proposed for PAPR reduction in CO-OFDM systems to lessen the impact of nonlinear effects and enhance the system performance. Both CO-OFDM with and without the proposed method were modeled using the VPI Transmission-Maker 9.5 and MATLAB software packages. The proposed scheme was shown to be an effective technique in reducing the PAPR. Furthermore, the scheme has low implementation complexity and no constraint on the system parameters because it does not need to send side information to the receiver. In addition, the results showed that the hybrid scheme can reduce the PAPR of the CO- OFDM by 4.35 dB and 4.5 dB for 4-

QAM and 16-QAM mapping orders, respectively. The hybrid scheme also achieved better QF and BER performance compared to the L3by3 and traditional schemes.

References

- [1] Shieh, W. and C. Athaudage, Coherent optical orthogonal frequency division multiplexing. *Electronics Letters*, 2006, vol. 42, issue10, p. 587-589.
- [2] Shieh, W., H. Bao, and Y. Tang, Coherent optical OFDM: theory and design. *Optics Express*, 2008. 16(2): p. 841-859.
- [3] Schmidt, B.J., A.J. Lowery, and J. Armstrong, Experimental demonstrations of electronic dispersion compensation for long-haul transmission using direct-detection optical OFDM. *Journal of Lightwave Technology*, 2008. 26(1): p. 196-203.
- [4] Nazarathy, M., et al. Recent advances in coherent optical OFDM high-speed transmission. In *PhotonicsGlobal@ Singapore*, 2008. IPRG IEEE.
- [5] Le, S., et al. Phase-conjugated subcarrier coding for fiber nonlinearity mitigation in CO-OFDM transmission. In *Optical Communication (ECOC)*, 2014 European Conference on, IEEE.
- [6] Goebel, B., et al. PAPR reduction techniques for coherent optical OFDM transmission. In *Transparent Optical Networks, ICTON'09*. 11th International Conference on. 2009. IEEE.
- [7] Dung, H.V.T., et al. PAPR reduction using PTS with low computational complexity in coherent optical OFDM systems. In *IEEE 2012 18th Asia-Pacific Conf. on Communications*.
- [8] Rishi, P. and S. Tamilselvi, Mitigation of Non-Linear Effects Using Non-Linear Transform in Dispersion-Managed Coherent Optical OFDM Systems. *Journal of Computational and Theoretical Nanoscience*, 2018. 15(2): p. 551-557.
- [9] Wang, Z., et al. Performance analysis of different modulation schemes for coherent optical OFDM system. In *Communications and Mobile Computing (CMC)*, 2010 International Conference on, IEEE.
- [10] Nehra, M. and D. Kedia, Design of Optical I/Q Modulator Using Dual-drive Mach-Zehnder Modulators in Coherent Optical-OFDM System. *Journal of Optical Communications*, 2018. 39(2): p. 155-159.
- [11] Gnanagurunathan, G. and F.A. Rahman. Comparing FBG and DCF as a dispersion in the long haul narrowband WDM systems. In *Wireless and Optical Communications Networks*, 2006 IFIP International Conference on, IEEE.
- [12] Kharagpur, B.K., U. Wali, and S. Bidwai. Novel technique to reduce PAPR in OFDM systems by clipping and filtering. In *Advances in Computing, Communications, and Informatics (ICACCI)*, International Conference on. 2013. IEEE.
- [13] Chen, L., et al. PAPR reduction in optical OFDM systems using asymmetrically clipping and signal scrambling technique. In *International Conference on Optical Instruments and Technology: Optoelectronic Devices and Optical Signal Processing*. 2015. International Society for Optics and Photonics.
- [14] Palanivelan, S.A.M., Modified Sliding Norm Transform based approach for PAPR optimization in OFDM Systems. *Australian Journal of Basic and Applied Sciences*, 2013: p. p. 10.
- [15] Grigoryan, A.M., S. Dursun, and M.M. Grigoryan. Method of sliding norm transforms for peak-to-average power reduction in OFDM systems. In *Industrial Electronics*, 2006 IEEE International Symposium on. IEEE.
- [16] Tong, Z.-r., Y.-n. Hu, and W.-h. Zhang, PAPR reduction in CO-OFDM systems using IPTS and modified clipping and filtering. *Optoelectronics Letters*, 2018. 14(3): p. 209-211.
- [17] Xiao, J. et al., Hadamard transform combined with a companding transform technique for PAPR reduction in an optical direct-detection OFDM system. *Journal of optical communications and networking*, 2012. 4(10): p. 709-714.

Linear Logic Synthesis of Multi-Valued Sequential Circuits

Nikolay Butyrlagin^{1,*}, Nikolay Chernov¹, Nikolay Prokopenko^{1,2}, Vladislav Yugai¹

¹Information System and Radio Engineering Department, Don State Technical University, Gagarin Sq. 1, Rostov-on-Don, 344000, Russia

²Institute for Design Problems in Microelectronics of Russian Academy of Sciences, IPPM RAS, Zelenograd, 124681, Russia

ARTICLE INFO

Article history:

Received: 02 October, 2019

Accepted: 10 December, 2019

Online: 25 December, 2019

Keywords:

Memory element

Logic operation

Linear representation

Truncated difference operation

Comparison operation

Circuitry implementation

ABSTRACT

The basics of unconventional design of current circuits of two-valued and multi-valued memory elements (ME) for storing current digital signals and flip-flops of the main types on their basis are considered. A nontraditional method of ME synthesis is proposed, which is based on the mathematical tool of linear algebra. Linear equations, structural and functional schemes of the main types of logic elements for the construction of ME are given. CMOS-circuitry of various versions of realization of linear logic elements of multi-valued MEs is considered. The comparative analysis is carried out and advantages and disadvantages of linear realization of current two-valued memory elements and flip-flops on their basis in comparison with potential (Boolean) realization are defined. The forecast of merits and demerits of linear implementation of multi-valued memory elements is given.

1. Introduction

Nowadays a potential logic and its mathematical tool, that is Boolean algebra, dominate in the world of logic synthesis of products of microelectronics. We sweepingly accept this fact and appreciate its contribution to digital electronics development.

However, as long as Boolean algebra exists, there have been attempts to replace it by another mathematical tool. It results in efforts to apply spectral transformations of Krestenson, Walsh, Haar [1-5], polynomial representations [6-9] for logic synthesis.

The authors of this article suggest applying mathematical tool of linear algebra for the aims of logic synthesis [10]. As a result of investigations, we have defined primary application domain of this tool that is current circuits of random valuedness. The Boolean algebra is not convenient to synthesize multi-valued digital circuits, so linear algebra is not an opponent to the Boolean algebra despite the specific nature of the logic synthesis process and multi-valued digital circuits circuitry [11-19]; it is rather an addition to Boolean algebra.

The authors have developed:

- Mathematical tool and methods of linear logical synthesis of two-valued and multi-valued digital structures;

- circuit solutions of the basic logic elements for constructing digital structures;
- circuitry solutions of some digital combinational two-valued and multi-valued structures (adders, decoders, multiplexers, digital components of the ADC, etc.);

In the process of research, the computer simulation of two-valued and multi-valued logical elements proved their operational integrity [20 - 27]. The effectiveness of linear algebra as a mathematical tool of logical synthesis is confirmed by patents RU2506695, RU2509412, RU2514789, RU2547225, RU2553070, RU2549144 and publications [20 - 27].

The results of research show the advantages of the proposed design methodology over the Boolean: it enables to suggest logic elements with improved characteristics compared to Boolean elements, as well as workable multi-valued elements. The purpose of this article is to demonstrate the possibilities of using current logic (linear algebra) as a mathematical tool for logical synthesis and circuit design of sequential two-valued and multi-valued digital structures using current flip-flops as an example.

2. Methodology

At the beginning, the well-known structural schemes of potential flip-flops of the main, widely used types are given. Then, structural schemes of their two-valued current analogues are

*Corresponding Author: Nikolay Butyrlagin, Don State Technical University, Russia | Email: butyrlagin@gmail.com

synthesized. Further, the features of the structural completeness of multi-valued flip-flops and their circuitry implementation are considered.

Two-valued potential flip-flops. Two-valued flip-flops have a quit wide classification [11, 12]. RS-, D-, T- and JK-flip-flops are the most commonly used two-valued flip-flops. A brief description of the structural implementation of these flip-flops is given below.

Asynchronous RS-flip-flop is a tandem amplifier with positive feedback. Its structural circuit, implemented on AND-NOT (OR-NOT) elements is in Fig. 1 a, and its logic symbol is in Fig. 1 b.

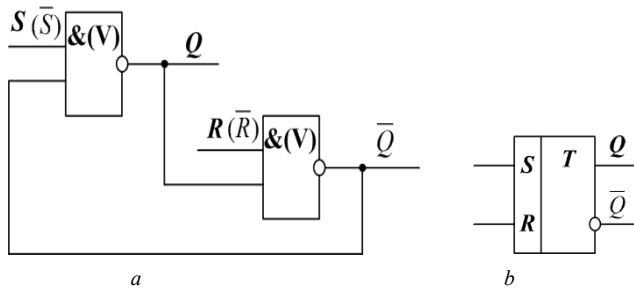


Figure 1: Structural circuit (a) and logic symbol (b) of RS-flip-flop on OR-NOT (AND-NOT) elements.

Its structural circuit, implemented on inhibit circuit (“implication gate”) is shown in Fig. 2 a, its logic symbol is shown in Fig. 2 b.

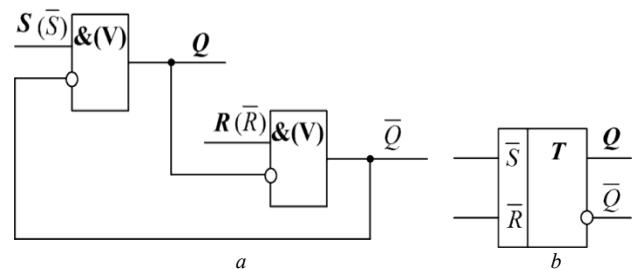


Figure 2: Structural circuit (a) and logic symbol (b) of RS-flip-flop on implication gates (inhibit circuits).

Single-ended synchronous RS-flip-flop is characterized by additional synchronization input. The flip-flop is switched to opposite state, if there is enabling level of signal at synchronization input. Its logic symbol is shown in Fig. 3.

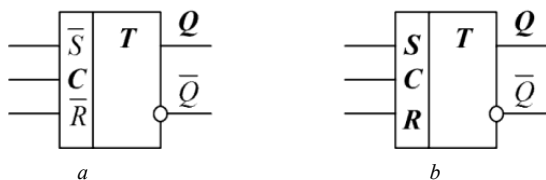


Figure 3: Logic symbol of single-ended synchronous RS-flip-flops: a – on OR elements, b – on AND elements

To eliminate disadvantages of single-ended RS-flip-flop’s switch [12] the push-pull circuits are used. Their structures, implemented on AND-NOT (OR-NOT) elements are in Fig. 4 a, b.

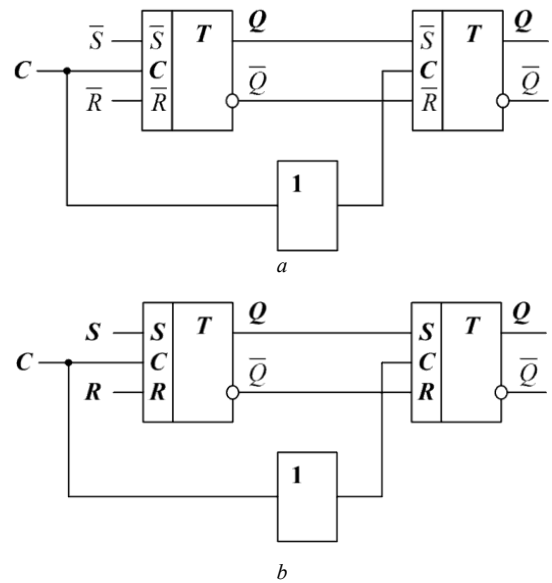


Figure 4: Structural circuits of push-pull RS-flip-flops.

The logic symbol of push-pull RS-flip-flops is in Fig. 5.

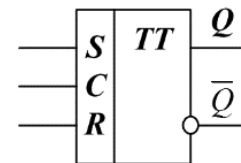


Figure 5: Logic symbol of push-pull RS-flip-flop.

Now let us show the structures of flip-flops of other popular types. The D-flip-flop structural circuit is shown in Fig. 6 a, its logic symbol is shown in Fig. 6 b.

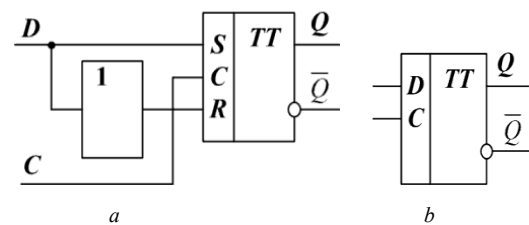


Figure 6: D-flip-flop: a – structural circuit, b – logic symbol.

The structural circuit of T-flip-flop is shown in Fig. 7 a and its logic symbol is shown in Fig. 7 b.

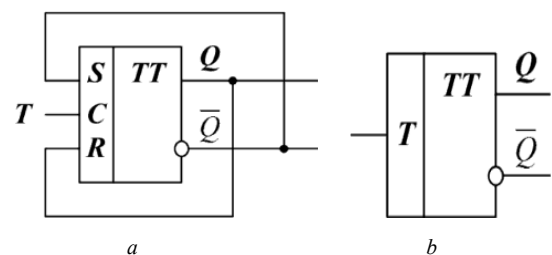


Figure 7: T-flip-flop: a – structural circuit, b – logic symbol.

And finally, the structural circuit of JK-flip-flop is in Fig. 8.

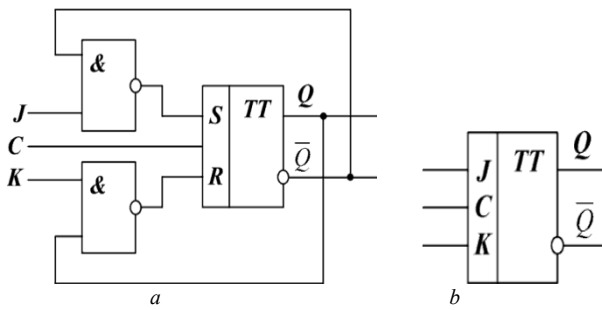


Figure 8: JK-flip-flop: a – structural circuit, b – logic symbol.

Two-valued current flip-flops. The potential flip-flops are similar to current flip-flops at system technology level, so it is possible to show the current asynchronous structural circuit of RS-flip-flop in the form, shown in Fig. 9, and its logic symbol - in the form, specified in Fig. 10 [21].

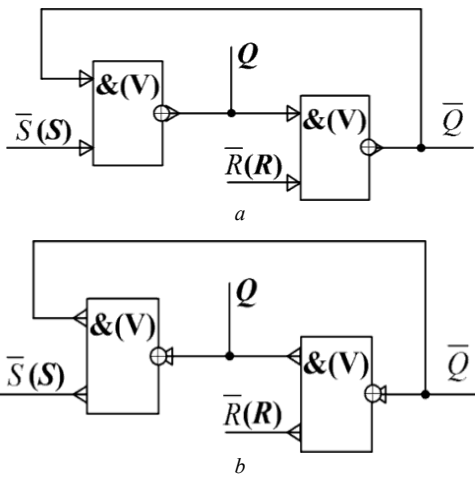


Figure 9: Structural circuit of two-valued asynchronous RS-flip-flop on AND-NOT (OR-NOT) current elements: a – output implementation, b – input implementation.

In the structural and functional diagrams given hereinafter, arrows indicate the directions of the current input and output signals: incoming arrows indicate input currents, outgoing arrows indicate output currents. The type of implementation of the element (incoming or outgoing) is determined by the direction of the output signal of the element.

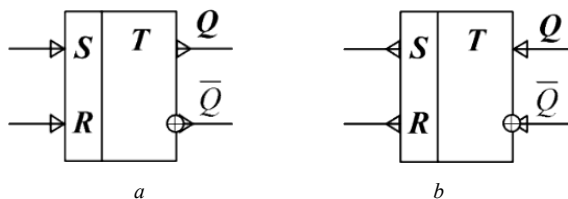


Figure 10: Logic symbol of two-valued asynchronous RS-flip-flop on AND-NOT (OR-NOT) current elements: a – output implementation, b – input implementation.

Possible differences in the options for implementing flip-flop circuits appear at the levels of functional and circuit design.

The structural circuit of synchronous RS-flip-flop is in Fig. 11 and its logic symbol is in Fig. 12.

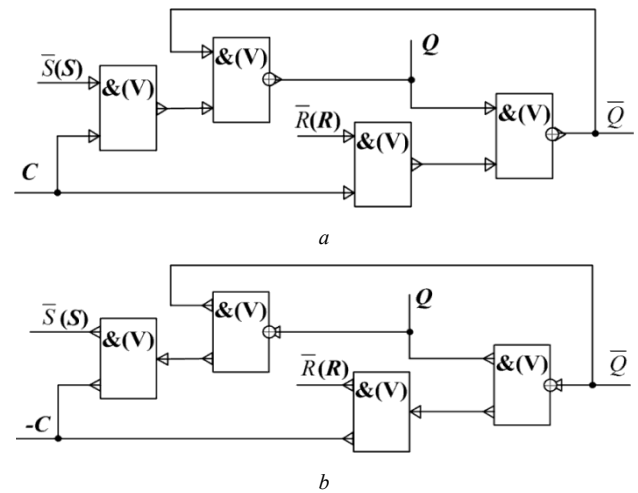


Figure 11: Structural circuit of two-valued synchronous RS-flip-flop on AND-NOT (OR-NOT) current elements: a – output implementation, b – input implementation.

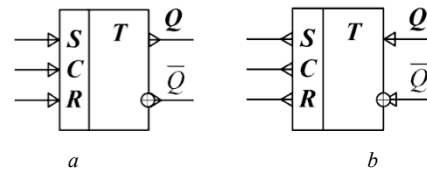


Figure 12: Logic symbol of two-valued asynchronous RS-flip-flop on AND-NOT (OR-NOT) current elements: a – output implementation, b – input implementation.

Similarly, structural implementation of push-pull current synchronous RS-flip-flop is similar to corresponding potential circuit. The structures of synchronous push-pull RS-flip-flops are in Fig. 13 and their logic symbols - in Fig. 14. The “+” element performs the function of an inverter.

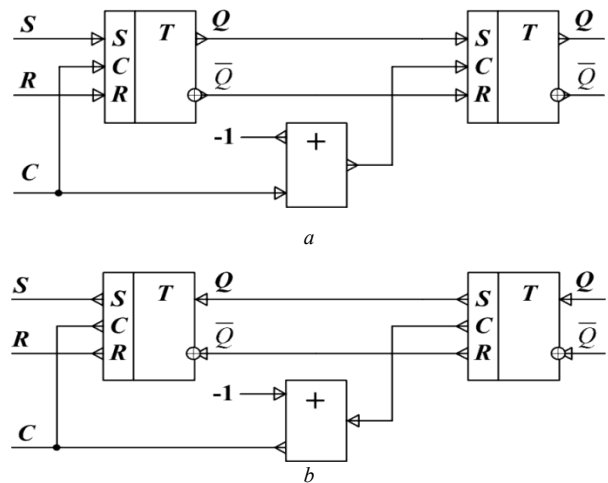


Figure 13: Structural circuits of push-pull synchronous current RS-flip-flops: a – output implementation, b – input implementation.

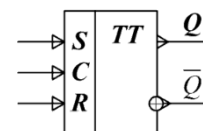


Figure 14: Logic symbol of push-pull synchronous current RS-flip-flops

The structural implementations for flip-flops of other types are also similar to implementations of corresponding potential circuits.

3. Three-valued flip-flops

Multi-valued flop-flops. Usually the multi-valued digital circuits are considered as generalization of corresponding two-valued circuits [1]. But bivalent logic degeneracy causes problems for such generalization. The primary difficulties of multi-valued flip-flop synthesis are the following:

- selection of logic valuedness, which is suitable to construct multi-valued memory elements;
- selection of multi-valued equivalents of logic operations, applied for logic synthesis of memory elements in two-valued logic;
- multi-valued interpretation of inversion.

Let us consider the above problems in details.

As to select logic valuedness to construct multi-valued flip-flops we should note the following. One uses concept of structural completeness (transition and outputs system completeness) for flip-flops, applied as automata memory elements for functional completeness of logic functions (basis) for combinational circuit in automata theory [9]. By default, the flip-flop is characterized by transition and output system completeness, if it is possible to assign some set of control signals to each output state, the said signals transit it from any previous state to the said state within finite number of steps. In two-valued case any known memory elements has this property.

The transition graph of two-valued flop-flop can be represented in the form shown in Fig. 15.

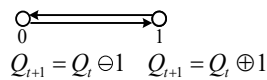


Figure 15: Transition graph of two-valued flop-flop.

In the multi-valued case, the situation is somewhat more complicated.

When $k = 3$ (Fig. 16), the multi-valued flip-flop can have transition graphs of direct (per neighboring vertex: $0 \rightarrow 1 \rightarrow 2 \rightarrow 0$ and through vertex: $0 \rightarrow 2 \rightarrow 1 \rightarrow 0$) and reverse (per neighboring vertex: $0 \rightarrow 2 \rightarrow 1 \rightarrow 0$ and through vertex: $0 \rightarrow 1 \rightarrow 2 \rightarrow 0$) type, which are opposite to each other. They are also complete graphs, covering all vertices, i.e. three-valued flip-flop has transition and output system completeness.

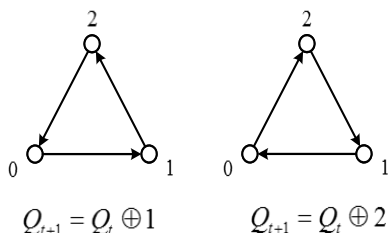


Figure 16: Direct and reverse transition graph for three-valued flip-flop.

When $k = 4$ (Figure 17), the multi-valued flip-flop can also have direct and reserve graphs.

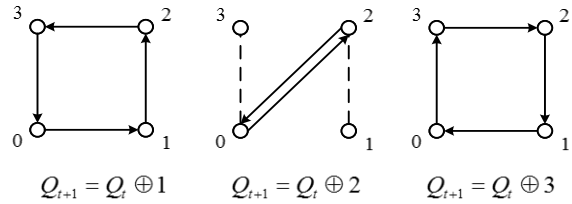


Figure 17: Four-valued memory element transition graphs.

However, from Fig. 17 it follows that the four-valued flip-flop does not have the completeness of the system of transitions and outputs: when passing through two vertices, the transition graph is looped. The transition graphs for $k = 5$ and $k = 7$ are in Fig. 18 and Fig. 19.

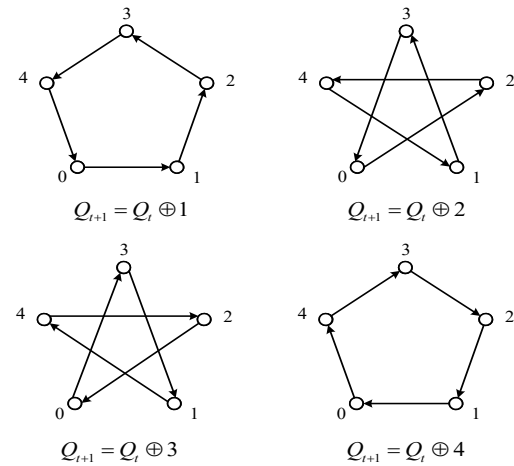


Figure 18: Transition graph of five-valued flip-flop.

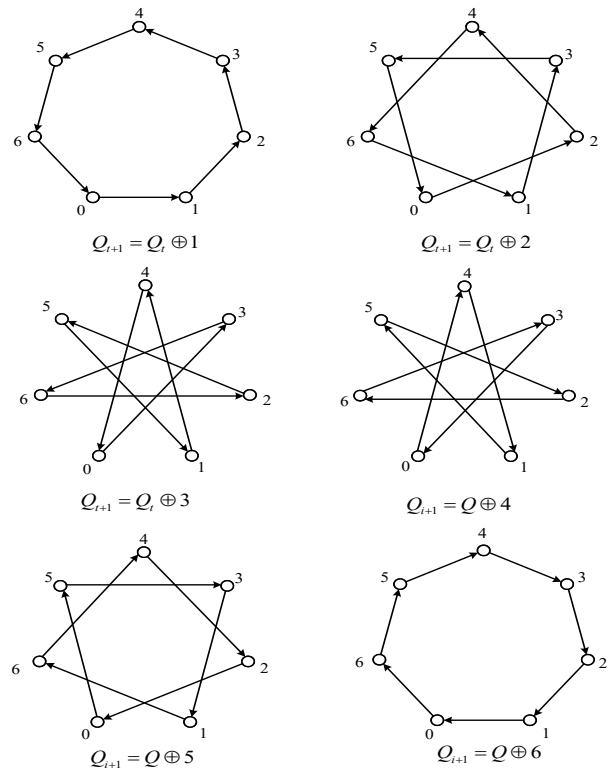


Figure 19: Seven-valued flip-flop transit graph.

The Fig. 15 – 19 show a confirmation of the known fact [9], that the transition and output system completeness of the flip-flop of random valuedness is provided, only when logic valuedness magnitude is a prime number.

Let us note the following, concerning selection of multi-valued equivalents of two-valued operations, used for memory elements synthesis. The most popular flip-flops for two-valued version are flip-flops, implemented on the elements realizing operations $\bar{\&}(x_1, x_2)$ (AND-NOT) and $\bar{\vee}(x_1, x_2)$ (OR-NOT).

The following operations are functionally close to these operations: $\bar{\&}(x_1, \bar{x}_2)$ (“Inhibit per x_2 ”) and $\bar{\vee}(x_1, \bar{x}_2)$ (“Implication from x_1 to x_2 ”). Generalization of these operations for multi-valued version results in the following representations:

$$\bar{\&}(x_1, x_2) \rightarrow \begin{cases} \min(x_1, x_2) \oplus i \\ (\min(x_1, x_2) \ominus i) \end{cases}$$

$$\bar{\vee}(x_1, x_2) \rightarrow \begin{cases} \max(x_1, x_2) \oplus i \\ (\max(x_1, x_2) \ominus i) \end{cases}$$

$$\bar{\&}(x_1, \bar{x}_2) \rightarrow \begin{cases} \min(x_1, x_2 \oplus i) \\ (\min(x_1, x_2 \ominus i)) \end{cases}$$

$$\bar{\vee}(x_1, \bar{x}_2) \rightarrow \begin{cases} \max(x_1, x_2 \oplus i) \\ (\max(x_1, x_2 \ominus i)) \end{cases}$$

In current circuits the authors use elements, implementing comparison operations $>(x_1, x_2)$, sum module $\oplus(x_1, x_2)$ and difference $\ominus x_1 x_2$ and truncated difference operations.

$$x_1 \dot{-} x_2 = \begin{cases} x_1 - x_2 & \text{when } x_1 \geq x_2 \\ 0 & \text{when } x_1 < x_2 \end{cases}$$

If to combine it with linear space operation, it is possible to have a variety of different presentations for multi-valued equivalents for main two-valued functionally complete system AND, OR, NOT. There are some possible versions of these operations in Tables 1-4.

Table 1: Primary operations, presented through truncated difference

Boolean representation	Linear difference representation
$\min(x_1, x_2)$	$x_1 \dot{-} (x_1 \dot{-} x_2)$
$\max(x_1, x_2)$	$x_1 + (x_2 \dot{-} x_1)$
$x_1 \oplus x_2$	$x_1 + x_2 - k[1 \dot{-} (k \dot{-} (x_1 + x_2))]$
$x_1 \ominus x_2$	$x_2 - x_1 + k\{1 \dot{-} [k \dot{-} (x_2 \dot{-} x_1)]\}$
$x \oplus i$	$x + i - k[1 \dot{-} (k \dot{-} (x + i))]$
$x \ominus i$	$i - x + k[1 \dot{-} (k \dot{-} (i \dot{-} x))]$

It is possible to synthesize more than 80 different flip-flops, using only set of operations, specified in the above tables, which are required to form logic elements, from which flip-flop memory elements are constructed.

It is necessary to note, that being fully equivalent to AND, OR, NOT operations in two-valued version, in multi-valued case some

of these expressions results in functions, different from multi-valued equivalents of AND, OR, NOT operations. This confirms the two-valued logic degeneracy, because multi-valued functional systems, different from traditional nature, are converged to it.

Table 2: Primary operations, presented through sum and difference module

Boolean two-valued representation	Linear-module representation
$\min_3^{M2}(x_1, x_2)$	$\frac{x_1 + x_2 - x_1 - x_2 }{2}$
$\max_3^{M2}(x_1, x_2)$	$\frac{x_1 + x_2 + x_1 - x_2 }{2}$
$\oplus_3^{M2}(x_1, x_2)$	$ x_1 + x_2 $
$\ominus_3^{M2}(x_1, x_2)$	$ x_1 - [(k - 1) - x_2] $
$\oplus_3^{M2}(x, i)$	$ x + i $
$\ominus_3^{M2}(x, i)$	$ x - [(k - 1) - i] $

Table 3: Primary operations, presented through comparison operation

Boolean representation	Linear-compared representation
$\min_3^{C2}(x_1, x_2)$	$x_1 - (x_1 > x_2)$
$\max_3^{C2}(x_1, x_2)$	$x_2 + (x_1 > x_2)$
$\oplus_3^{C2}(x_1, x_2)$	$x_2 - x_1 + k(x_1 > x_2)$
$\ominus_3^{C2}(x_1, x_2)$	$x_1 - x_2 + k(x_2 > x_1)$
$\oplus_3^{C2}(x, i)$	$i - x + k(x > i)$
$\ominus_3^{C2}(x, i)$	$x - i + k(i > x)$

Table 4: Primary operations, presented by threshold form

Boolean representation	Linear-threshold representation
$\min_3^{C2}(x_1, x_2)$	$[(x_1 > 0 + x_2 > 0) > 1] + [(x_1 > 1 + x_2 > 1) > 1]$
$\max_3^{C2}(x_1, x_2)$	$x_1 + x_2 - [(x_1 > 0 + x_2 > 0) > 1] - [(x_1 > 1 + x_2 > 1) > 1]$
$\oplus_3^{C2}(x_1, x_2)$	$x_1 + x_2 + 3[(x_1 > 1 + x_2 > 1) > 1] - 3[(x_1 > 0 + x_2 > 1) > 1] - 3[(x_1 > 1 + x_2 > 0) > 1]$
$\ominus_3^{C2}(x_1, x_2)$	$x_1 + x_2 - 2[(x_1 > 0 + x_2 > 0) > 1] - 3[(x_1 > 1 + x_2 > 1) > 1] + [(x_1 > 1 + x_2 > 0) > 1]$
$\oplus_3^{C2}(x, i)$	$x_1 + i + 3[(x_1 > 1 + i > 1) > 1] - 3[(x_1 > 0 + i > 1) > 1] - 3[(x_1 > 1 + i > 0) > 1]$
$\ominus_3^{C2}(x, i)$	$x_1 + i - 2[(x_1 > 0 + i > 0) > 1] - 3[(x_1 > 1 + i > 1) > 1] + [(x_1 > 1 + i > 0) > 1]$

Finally, on the multi-valued interpretation of inversion. In the two-valued case, the flip-flop consists of two identical logic elements, therefore, you can submit information to the input and “remove” it from the flip-flop output in a direct or inverse code. By controlling the process of recording information in a flip-flop, it is possible to process information by setting a direct or inverse value at the desired output.

A multi-valued flip-flop has k inputs and the same number of outputs. Here, the information processing function is much “richer” than in the two-digit case: controlling the process of recording information in such a flip-flop, it can be cyclically shifted left or right (“rotate”). In the process of information rotating, you must remember that

$$x \oplus i = x \ominus (k - i).$$

This ratio enables, if necessary, to replace one of the operations of the recorded ratio with another.

The synthesis of multivalued flip-flops should also be preceded by an agreement on the principles of generalizing two-valued flip-flops to a multivalued case. The agreement proposed by the authors of this article consists of the following main provisions:

- the number of flip-flop information inputs must be equal to the logic valuedness;
- at the outputs of the flip-flops there must be a full set of logic values (the number of outputs of the flip-flop must be equal to the valuedness of the logic);
- the valuedness of the output signals of the functional elements of the flip-flop should not exceed the valuedness of the logic used.

The listed provisions, as is easy to see, in the two-valued case are fully implemented.

RS flip-flop. A verbal description of the functioning algorithm of a multi-valued RS-flip-flop corresponding to the agreement on the principles of generalizing two-valued flip-flops to a multi-valued case is given below:

- the storage mode corresponds to the values of the input signals $S = SR = R = k - 1$ (or $S = SR = R = 0$);
- the signal S increases the flip-flop state index relative to the current state towards the state $k-1$, the SR signal decreases or increases the current one depending on the ratio of the current state index and the signal value at this input, and the signal R decreases towards the state 0 ; change of state in a cycle is impossible (let’s leave it for universal flip-flops!);
- the magnitude of the change in the state index is equivalent to the value of the input signal: a signal equivalent to 1 can increase (or decrease) the index of the current state by 1 , a signal equivalent to 2 by 2 , etc. ;
- to change the flip-flop state index relative to the current state i , signal S can take values from 1 to $k-1-i$ (larger values will be equivalent to $k-1-i$ in action), similarly, signal R can take values from 1 to $i - 1$ (larger values will be equivalent to $i - 1$);

- Allowed combinations of input signal values are all combinations in which one of the input signals is $k - 1$ (0) and the others take any of the possible values.

The meaning of the last paragraph of the algorithm is that to change the state of the flip-flop, the two inputs must have signals 0 or $k-1$, which passes the setting signal of any of the allowed values, and the third - the signal that sets the state.

Table 5: Logic symbols for “traditional” multi-valued equivalents of two-valued operations

Operation	Logic symbol	
	Two-valued	Multi-valued
$\min(x_1, x_2) \oplus i$		
$\min(x_1, x_2 \oplus i)$		
$\max(x_1, x_2) \oplus i$		
$\max(x_1, x_2 \oplus i)$		

4. Results and Discussion

Structural design. The above research results allow us to move to the structural design of current two-valued and multi-valued flip-flops.

In the following exposition, we will mainly confine ourselves to the synthesis of flip-flops with the valuedness $k = 2, 3$, since reasoning about flip-flops of greater valuedness practically repeats similar arguments about ternary flip-flops. In necessary cases, the features of flip-flops of greater valuedness will be specially discussed.

To construct the structural, functional and basic circuit diagrams of current flip-flops, the above current operations and their combinations, as well as linear space operations, will be used. Moreover, we restrict ourselves to the “traditional” approach, i.e. using operations generalized to the multi-valued case in the “conventional” way.

The logic symbols for “traditional” multi-valued equivalents of above operations are in Table 5.

A base of current operations is the following $[\min(\max)](x_1, x_2)$ and $[\oplus (\ominus)](x, i)$ operations with different representations, using various current operations. The most important representations (see Tables 1-4) are specified below:

- operation $\min(x_1, x_2)$:

$$\min(x_1, x_2) \Rightarrow \begin{cases} \frac{x_1 + (x_1 - x_2)}{2} \\ \frac{x_1 + x_2 - |x_1 - x_2|}{2} \end{cases};$$

$$[(x_1 + x_2) > 3] + [(2x_1 + x_2) > 2]$$

– operation $\max(x_1, x_2)$:

$$\max(x_1, x_2) \Rightarrow$$

$$\begin{cases} \frac{x_1 + (x_2 - x_1)}{2} \\ \frac{x_1 + x_2 + |x_1 - x_2|}{2} \end{cases};$$

$$x_1 + x_2 - [(x_1 + x_2) > 3] - [(x_1 + 2x_2) > 2]$$

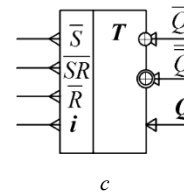
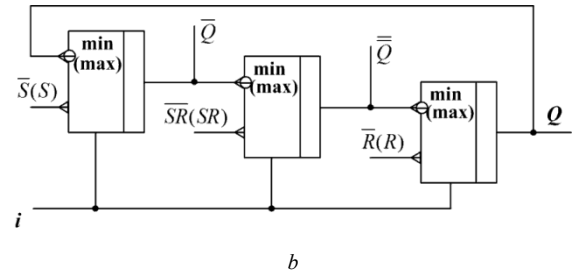
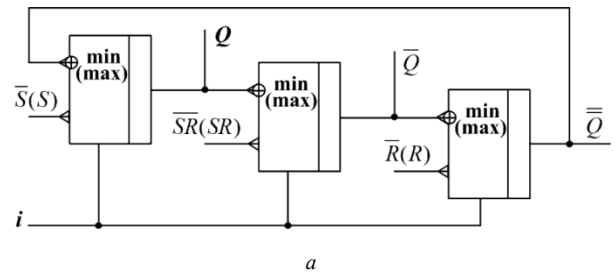
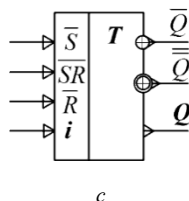
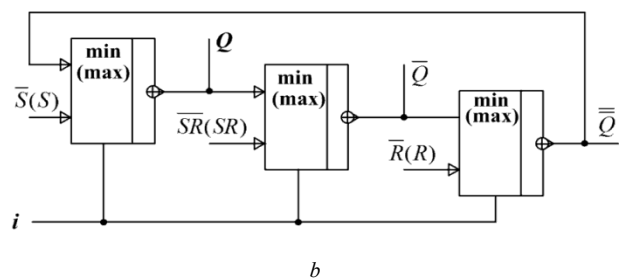
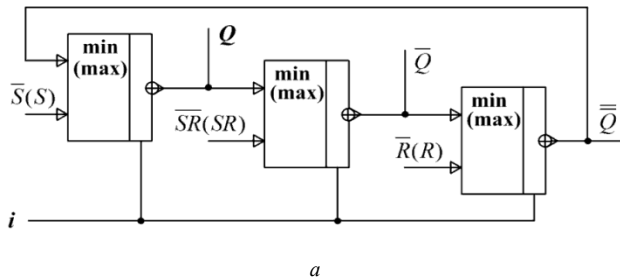
– operation $\oplus (x, i)$:

$$\oplus (x, i) \Rightarrow \begin{cases} i - x + 3(x > i) \\ x + i - k[1 + (k - (x + i))]; \\ |x + i| \end{cases}$$

– operation $\ominus (x, i)$:

$$\ominus (x, i) \Rightarrow \begin{cases} |x - [(k - 1) - i]| \\ x - i + 3(i > x) . \\ |x - i| \end{cases}$$

The logic elements, from which the analogues of conventional flip-flops are constructed, are consecutive connection of elements implementing $[\min(\max)](x_1, x_2)$ and $[\oplus (\ominus)](x, i)$ operations.



The structural circuit and logic symbol of three-valued asynchronous RS-flip-flop on equivalent elements AND-NOT (OR-NOT) are in Fig. 20-21.

Let us consider functioning of three-valued RS-flip-flop, which structural circuit is shown in Fig. 20 a. It is seen that state storage phase is provided by signals of level 2 (min – realization) or 0 (max – realization) at inputs S, SR, and R.

Let in *min* implementations of the RS-flip-flop (Fig. 20), at the beginning, the setup signal *i* is 0, which corresponds to a direct (i.e., without rotation) recording of the value of the input information. When the input signal is set $S = 0 - 2$ and $SR = R = 2$, the signal $\bar{Q} = S \oplus 1$ is formed at the output of the logic element D2, at the next (D3) - signal $\bar{\bar{Q}} = \bar{Q} \oplus 1$, at the last (D1) - signal $Q = \bar{\bar{Q}} \oplus 1$. For example, at $S = 0$, the signals $\bar{Q} = 1, \bar{\bar{Q}} = 2, Q = 0$ (state “0”) are generated at the outputs.

If the setting signal *i* is 1, which corresponds to the right cyclic shift of the signal by one in each logic element, then the signal $S \oplus 2$ is generated at the output of the first logic element D2, $\bar{\bar{Q}} = \bar{Q} \oplus 2$ at the output of the second element (D3), the output of the third (D1) is the signal $Q = \bar{\bar{Q}} \oplus 2$. For example, with $S = 0$ and $SR = R = 2$, the signals $\bar{Q} = 2, \bar{\bar{Q}} = 1, Q = 0$ (state “0”) are formed at the outputs.

If the setting signal *i* is 2, which corresponds to the left cyclic shift of the signal by two (to the left cyclic shift by one) in each logic element, then the signal $S \oplus 3 = S$ is generated at the output of the first logic element (D2), $\bar{\bar{Q}} = \bar{Q} \oplus 3 = \bar{\bar{Q}}$ at the output of the second element (D3), the signal $Q = \bar{\bar{Q}} \oplus 3 = Q$ at the

output of the third (D1). For example, with $S = 0$ and $SR = R = 2$, the signals $\bar{Q} = 0$, $\bar{Q} = 1$, $Q = 2$ (state "2") are formed at the outputs.

Let the flip-flop be in state "1". In this case, the input signal SR can transit it into any of the remaining states, since this signal determines the value of the output signal of the element D3 and propagates with a shift along the remaining elements of the flip-flop, the input state of the flip-flop cannot be changed, since the second input of the element D3 is 0, and the signal S can transit the flip-flop only in the state "0".

The graph of changes of the state, when $i = 1$ is in Fig. 22 a and the process of signal values change on the outputs of logic elements is in Fig. 22 b.

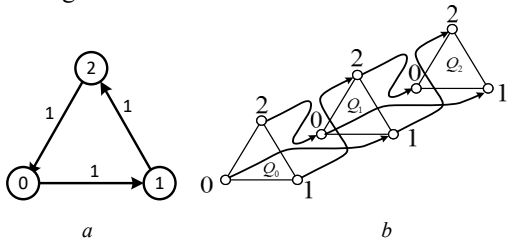


Figure 22: Three-valued RS-flip-flop graph, when $i = 1$: a – state change, b – output signal value change.

When $i = 2$, a switch process will go reverse. The graphs of three-valued RS-flip-flop for such case are in Fig. 23.

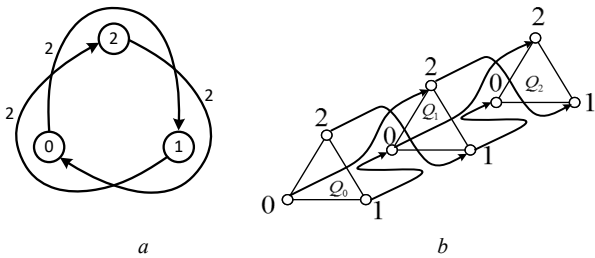


Figure 23: Three-valued RS-flip-flop graphs, when $i = 2$: a – state change, b – output signal value change.

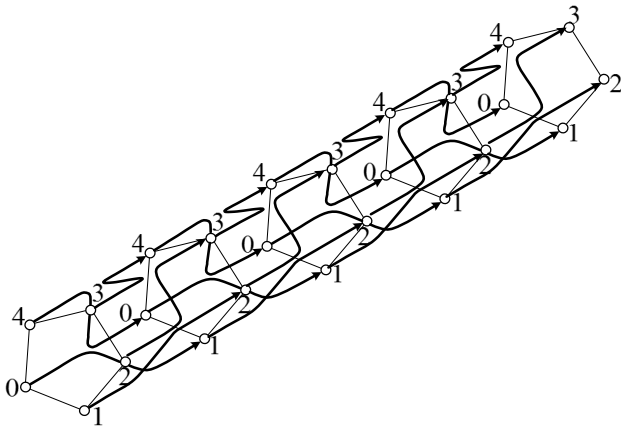


Figure 24: Graph of the value changes of the output signals of five-valued RS-flip-flop $i = 1$.

Similarly, it is possible to construct graphs for state change and values of flip-flop output signals of higher valuedness. The structure of the graph will change greatly at other values of k . The

graph of value changes of the output signals of five-valued flip-flop at $i=1$ is in Fig. 24 as an example.

Here visualization is lower than the one for three-valued case.

As in two-valued case synchronous single-ended RS-flip flops are characterized by wider functional possibilities. Their main difference from asynchronous flip-flops is an availability of additional synchronization input C , a signal on which defines a flip-flop state change moment, if there is a signal, which is able to result in such change, at informational input (inputs). An input signal is able to be from 0 to $k-1$ at any input, so signal C should take on value 0 ("lock" input of flip-flop, its state is not changed at any input signal change) or $k-1$ (any value signal comes to flip-flop input and it goes to the state, corresponding to the said value). It is in good agreement with two-valued flip-flops, if we understand synchronous signal inversion as $1 - C$, that is $(k - 1) - C$.

It is possible to describe k -valued single-ended synchronous RS-flip-flop as RS-flip-flop, where S -, RS - and R -inputs are connected to S -, RS - and R -inputs of memory element through min or max , where the synchronous signal C is supplied to second inputs.

The RSC-flip-flop structural circuit is in Fig. 25 and its logic symbol is in Fig. 26.

Push-pull circuit of three-valued RSC-flip-flop is constructed from two single-ended RSC-flip-flops similar to two-valued case. Its structural circuit and logic symbol are in Fig. 27.

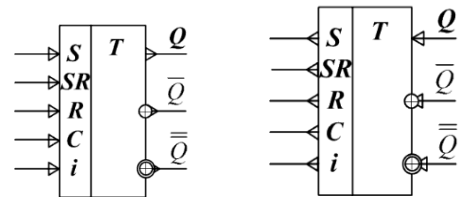
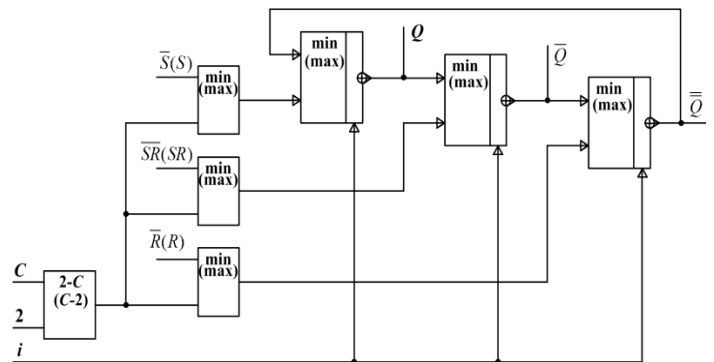


Figure 26: Logic symbol of three-valued synchronous RSC-flip-flops: a –output implementation, b – input implementation.

The tree-valued single-ended synchronous D-flip-flop is functionally similar to two-valued D-flip-flop: it is set to state, corresponding to input signal value by synchronous signal. In other words, it is possible to describe three-valued D-flip-flop as RS-flip-flop with input signals:

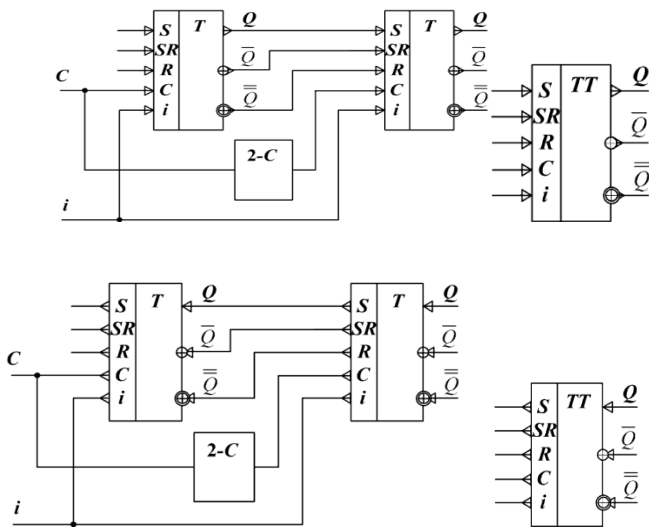


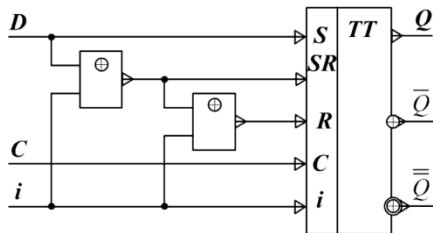
Figure 27: Structural circuit and logic symbol push-pull synchronous RS-flip-flop: a – output implementation, b – input implementation.

$$S = D;$$

$$RS = D \oplus i;$$

$$R = D \oplus i \oplus i.$$

The structural circuit of synchronous single-ended k-valued D-flip-flop (AND-NOT – equivalent) is in Fig. 28.



A structure of OR-NOT – equivalent of three-valued D-flip-flop is of similar form.

The three-valued T-Flip-Flop is also implemented on two single-ended RS-flip-flop and is counter module 3, an order of counting is defined by value of i. The structural circuit and logic symbol of T-flip-flop are in Fig. 29.

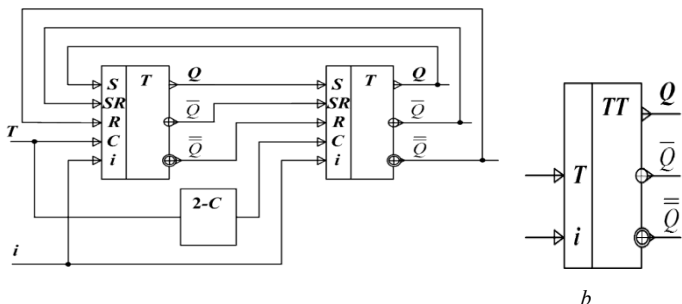
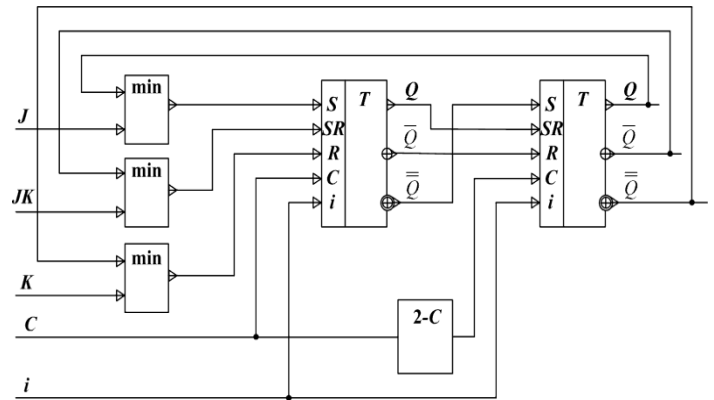


Figure 29: Three-valued push-pull synchronous T-flip-flop: a – structural circuit, b – logic symbol.

The structural circuit of synchronous three-valued push-pull JK-flip-flop is in Fig. 30.



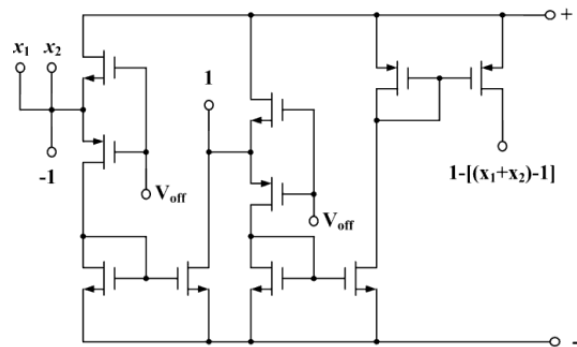
We perform circuit design via example of two-valued current flip-flops and their three-valued traditional generalization on the base of conjunctive function representation. Let us consider design of two-valued and three-valued logic elements and the simplest flip-flops. We do not consider circuits of multi-valued flip-flops of higher valuedness because it is quite difficult to show the said circuits within this article.

Two-valued flip-flops. All variants of basic operation representation, specified in Tables 1-4, are suitable for their synthesis.

The following operation is a current equivalent of OR-NOT operation in difference form:

$$1 \div [(x_1 + x_2) \div 1].$$

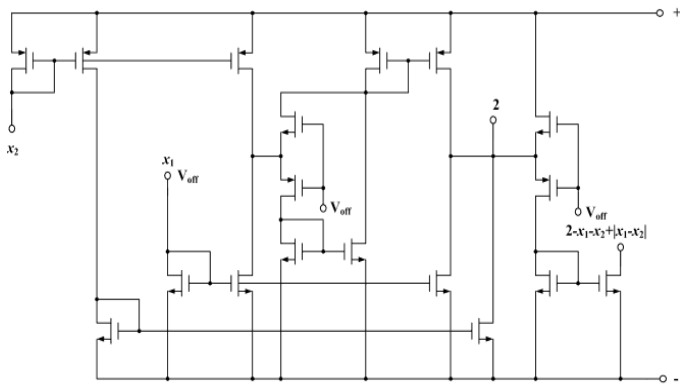
It is possible to verify its correctness by substitution. The basic diagram of logic element, which implements the said operation, is in Fig. 31.



Applying module form of current representation results in the following form of OR-NOT operation:

$$2 - x_1 - x_2 + |x_1 - x_2|.$$

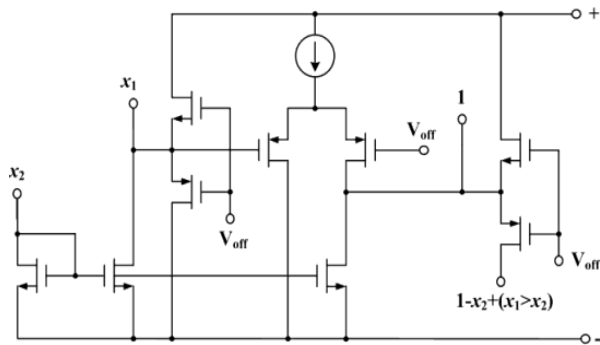
The basic diagram of OR-NOT operation implementation current variant in module form is in Fig. 32.



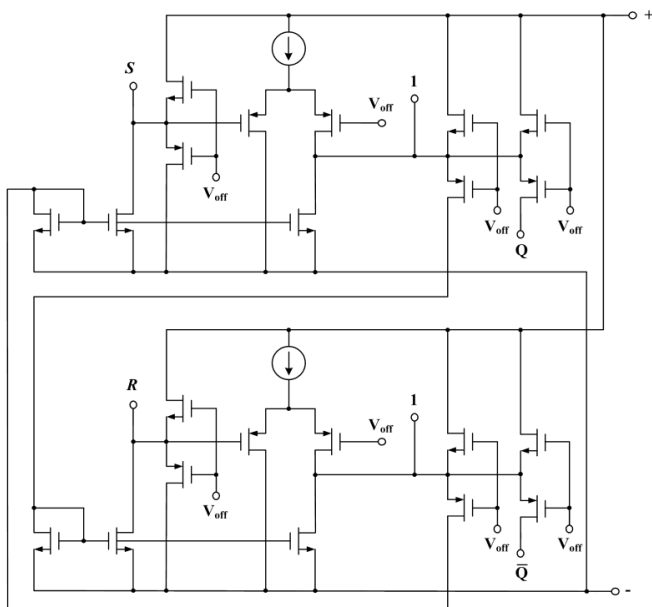
A comparison form of OR-NOT current representation results in the following form:

$$1 - x_2 + (x_1 > x_2).$$

Its circuit implementation is in Fig. 33.



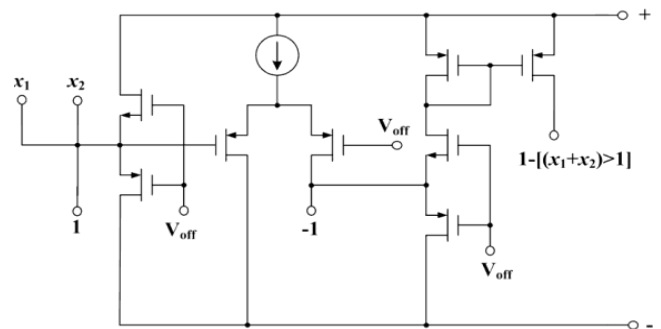
When combining two elements in amplifier circuit with positive feedback, it results in two-valued RS-flip-flop construction. Its basic diagram is in Fig. 34.



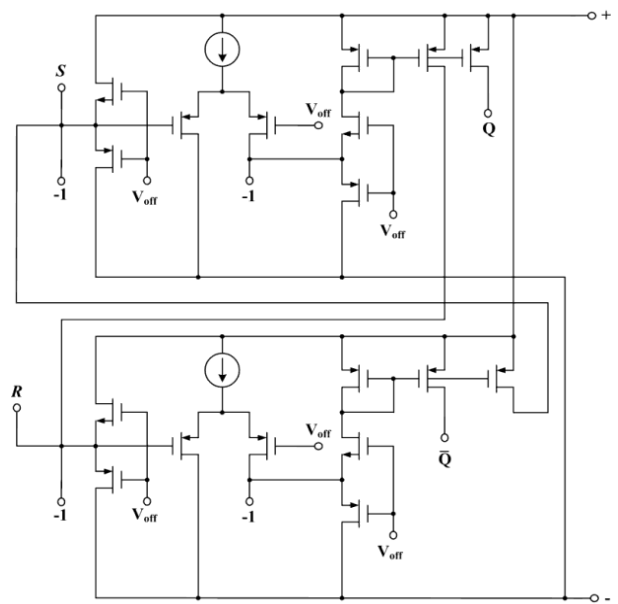
OR-NOT operation threshold current representation results as following:

$$1 - [(x_1 + x_2) > 1].$$

Its circuit implementation is shown in Fig. 35.



The simple current RS-flip-flop in threshold representation is in Fig. 36.



Multi-valued flip-flops are constructed on elements-generalizations of two-valued elements, which implement OR-NOT operation. As we have already said above, the traditional generalizations are consecutive connection of elements $[\min(\max)](x_1, x_2)$ and $[\oplus (\ominus)](x, i)$, that is $\min(x_1, x_2) \oplus i$, $\min(x_1, x_2 \oplus i)$, and two similar operations, based on \ominus . The operations, specified in Table 3, are not suitable for this purpose, because multiple generalizations are different from traditional ones here. It is better to consider them separately.

Difference representation of $\min(x_1, x_2) \oplus i$ is the following:

$$[x_1 \div (x_1 \div x_2)] + i - 3\{1 \div [3 \div [x_1 \div (x_1 \div x_2)] + i]\}$$

The implementation circuit for this expression is in Fig. 37.

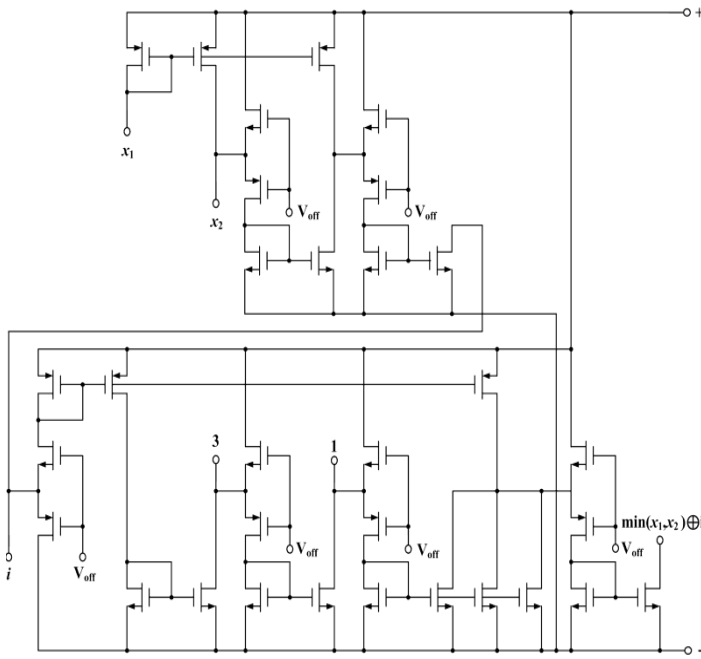
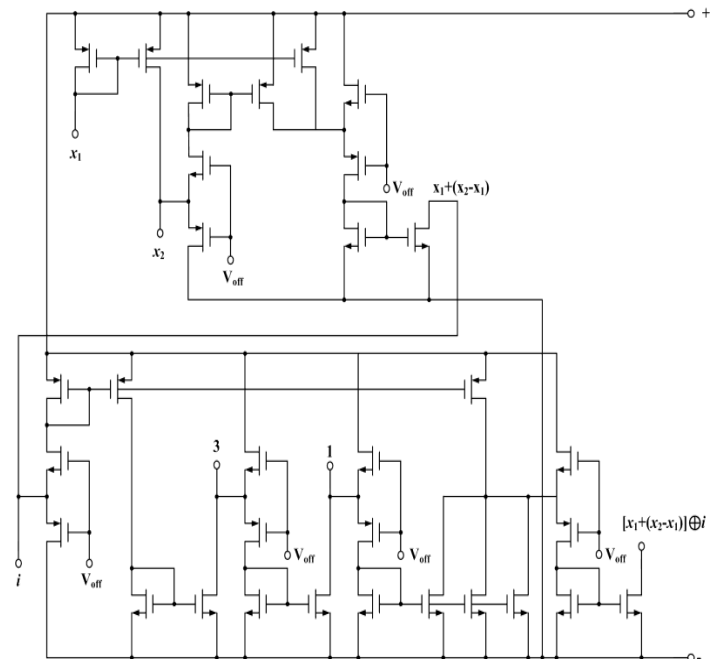
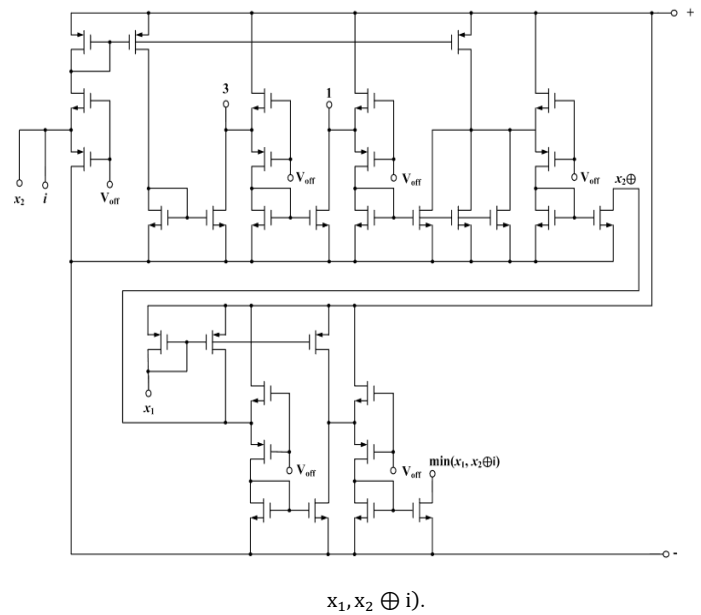


Figure 37: Basic diagram to implement difference representation $\min(x_1, x_2) \oplus i$.



a



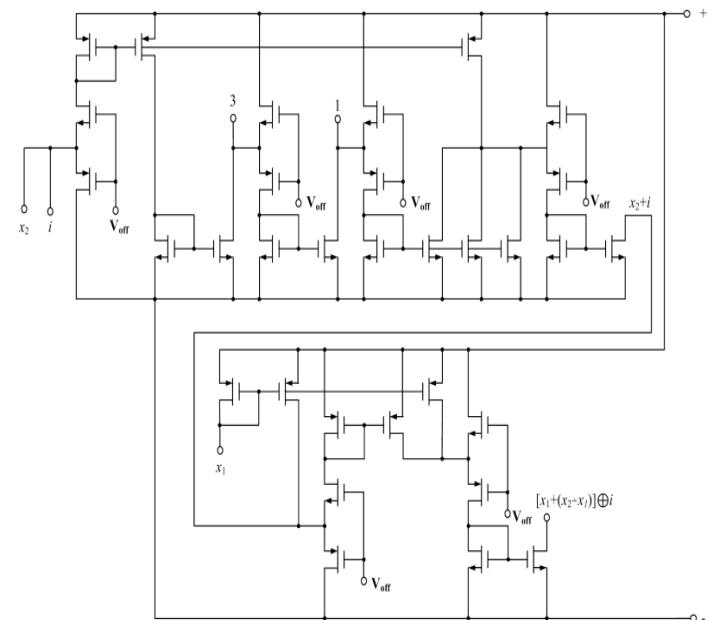
b

A difference representation of $\min(x_1, x_2 \oplus i)$ is the following:

$$i - [x_1 \div (x_1 \div x_2)] + 3\{1 \div \{3 \div [i \div [x_1 \div (x_1 \div x_2)]]\}}\}$$

It is visible that the last circuit is different from the previous one only by order of element sequence of $\min(x_1, x_2)$ and $x \oplus i$ operation implementation.

The circuit implementation of $\max(x_1, x_2) \oplus i$ and $\max(x_1, x_2 \oplus i)$ logic elements is in Fig. 39.



A module representation of $\min(x_1, x_2) \oplus i$ is formed from $\min(x_1, x_2)$ representation as following:

$$\frac{x_1 + x_2 - |x_1 - x_2|}{2}$$

$\oplus i$ which has the following form:

$$3 - x - i - 3|1 - i| + 3|x - |x - i||.$$

The basic diagram to implement logic element $\min(x_1, x_2) \oplus i$ is in Fig. 40.

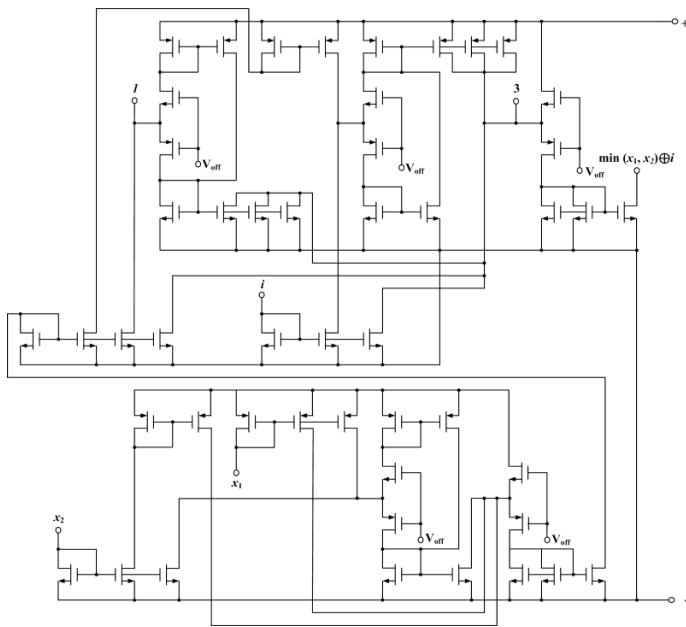


Figure 40: Basic diagram to Implement Difference representation of $\min(x_1, x_2) \oplus i$ operation.

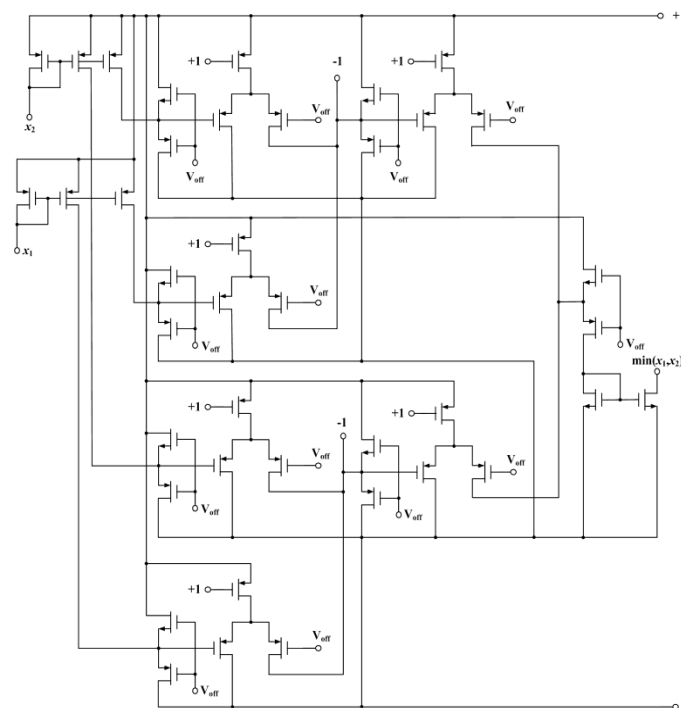


Figure 41. Basic diagram for threshold implementation of $\min(x_1, x_2)$.

$x_1, x_2 \oplus i$ is an interchange of $\min(x_1, x_2)$ and $x \oplus i$ implementations. Similarly, it is possible to implement $\max(x_1, x_2) \oplus i$ and $\max(x_1, x_2 \oplus i)$.

The threshold representation of $\min(x_1, x_2)$ consists of sum of two threshold functions and can be written as following:

$$x_1 > 0 + (x_2 > 0) > 1 + [((x_1 > 1) + (x_2 > 1)) > 1],$$

Its basic diagram is in Fig. 41.

We can describe $x \oplus i$ operation as following

$$x_1 + i + 3[((x_1 > 1) + (i > 1)) > 1] - 3[((x_1 > 0) + (i > 1)) > 1] - 3[((x_1 > 1) + (i > 0)) > 1].$$

The basic diagram of its implementation is in Fig. 42.

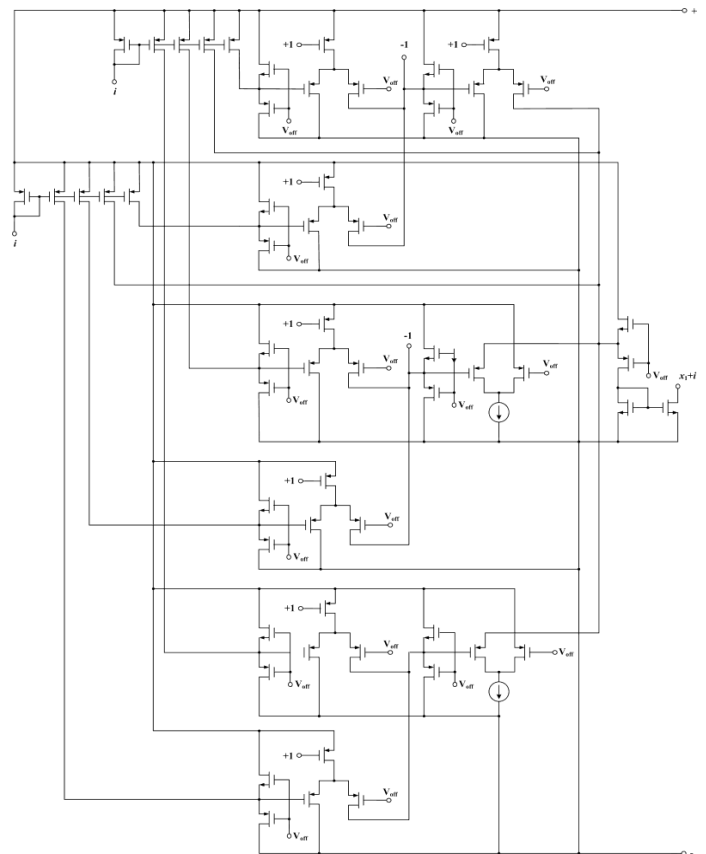


Figure 42: Basic diagram to implement $x \oplus i$.

It is possible to construct logic elements, from which the third-valued flip-flops are constructed, using the above schematic implementations. It is possible to construct flip-flops of different types, following the above structural circuits.

5. Conclusion

The advantages of using the proposed linear circuitry for the construction of flip-flops can be estimated on the basis that:

- all active circuit elements operate in unsaturated mode, therefore, they have higher performance and other frequency characteristics than potential elements;

- circuits contain only active components (transistors), therefore, they are more technological than potential elements; if, for example, to estimate the technological complexity of the elements of LSI contains one conductor, two transistors, three resistors, the technological complexity of the standard two-input potential inverter (11 links, 5 transistors, 5 resistors) is 36, and the linear threshold analog (6 links, 8 transistors) is 22, that is a third less!

- the basis for the construction of the equations of functioning of logic elements is their difference construction, in which the output signal of the element is the difference of the incoming and outgoing components, therefore, linear logic elements have better performance characteristics;

A possible negative indicator of linear circuits may be their energy characteristics: the condition for the operation of the circuits is a constant flow of current in their circuits. However, at high frequencies, these characteristics are likely to differ little from similar characteristics of potential circuits.

Multivalued current logic elements are a new class of elements, which has no analogue in potential logic and there is simply nothing to compare the characteristics of current elements with. Its advantages and disadvantages are all of the above positive and negative qualities of linear circuits, presumably a linear increase in hardware costs for the implementation of schemes with increasing valuedness, as well as the reality of creating a fully functional multi-valued logic elements and digital structures based on them.

Conflict of Interest

The authors declare that there is no conflict of interests regarding publication of this paper.

Acknowledgments

The reported study was funded by RFBR according to the research project No. 18-37-00061.

References

- [1] S.V. Yablonsky, "An introduction to mathematical mathematics," Textbook A manual for universities, 2nd ed, Moscow publ. Nauka, 1986, 384 p. (in Russian).
- [2] M.G. Karpovsky, E.S. Moskalev, "Spectral methods of analysis and synthesis of discrete devices," Moscow, Energy, 1973 – 144 p. (in Russian).
- [3] V.D. Efremov, A.A. Kuzmin, V.A. Stepanov, "Calculation of logical functions using the Rademacher transforms," Automation and Telemekhanics, 1984, No. 2. (in Russian).
- [4] V.P. Shmerko, "Synthesis of arithmetic forms of Boolean functions by means of the Fourier transform," Automation and Remote Control. 1989. No. 5. pp. 134-142. (in Russian).
- [5] T.I. Post, "Introduction to a general theory of elementary propositions," Math, 1921, 43, No.3, p.163-185. (in Russian).
- [6] L. A. Zalmanson, "Fourier transform, Walsh, Haar and their application in management, communications and other fields," Moscow, Nauka, Fizmatlit publ., 1989, 496 p. (in Russian).
- [7] V.L. Artyukhov, V.N. Kondratiev, A.A. Shalyto, "Realization of Boolean functions by arithmetic polynomials," Automation and Telemekhanics. 1988, No. 4, pp. 1-48. (in Russian).
- [8] V.D. Malyugin, G.A. Kukharev, V.P. Shmerko, "Transformation of polynomial forms of Boolean functions," Moscow, Institute of Management Problems, 1986. (in Russian).
- [9] V. Malyugin, "Implementation of Boolean functions by arithmetic polynomials," Automation and Telemekhanics, 1982, No. 4, pp. 84–93 (in Russian).
- [10] N.N. Prokopenko, N.I. Chernov, V.Ya. Yugai, "Base Concept of Linear Synthesis multi-Valued Digital Structures within Linear Spaces" Proceedings of The IS&IT13 Congress., The Scientific Edition in four volumes, Moscow, PhisMathLit, 2013, vol. 1, pp. 284–289. (in Russian)
- [11] E.P. Ugrumov, "Digital circuitry," BHV Publ, St. Petersburg, 2000, 528 p. (in Russian).
- [12] I.N. Bukreev et al, "Microelectronic circuits of digital devices," Moscow, Radio and communications, 1990, 416 p. (in Russian).
- [13] A.F. Gonzalez and P. Mazumder, "Multiple-valued signed digit adder using negative differential resistance devices", in IEEE Transactions on Computers, vol. 47, no. 9, pp. 947-959, Sept. 1998. DOI: 10.1109/12.713314
- [14] A. Morgul and T. Temel, "Current-mode level restoration: circuit for multi-valued logic", in Electronics Letters, vol. 41, no. 5, pp. 230-231, 3 March 2005. DOI: 10.1049/el:20056998

- [15] P. Gonga, "Quaternary logic and applications using Multiple Quantum well based SWSEETs", IEEE VLSICS, vol. 3, no. 5, pp. 27-42, Oct. 2012. DOI : 10.5121/vlsic.2012.3503
- [16] Ch. Babu Dara, T.Haniotakis, S.Tragoudas, "Delay analysis for an N-Input current mode threshold logic gate", Computer Society Annual Symposium on VLSI 2012 IEEE, DOI: 10.1109/ISVLSI.2012.34
- [17] K. Navi, "A Novel Current Mode Full Adder Based on Majority Function", World Applied Sciences, Journal 4 (5): 676-680, 2008.
- [18] N.K. Naware, D.S. Khurge and S.U. Bhandari, "Review of Quaternary Algebra & Its Logic Circuits", 2015 IEEE ICCUBE, 2015, pp. 969-973. DOI: 10.1109/ICCUBE.2015.204
- [19] B. Kishor, "Implementation of Ternary / Quaternary Addition using Multivalued Logic Digital Circuit", International Journal of Computer Application, vol. 118, no. 4, May 2015.
- [20] N.N. Prokopenko, N.V. Butyrlagin, N.I. Chernov, V.Ya. Yugai, "Synthesis of binary flip-flops in the apparatus of linear algebra," News SFU, Technical science, No. 2. 2015, pp. 115-125. (in Russian).
- [21] N.N. Prokopenko, N.I. Chernov, V.Ya. Yugai, N.V. Butyrlagin, "Linear synthesis of a k-digit digital element base with current logical signals: the principle of generalization," Problems of developing promising micro- and nanoelectronic systems, 2016 Proceedings under the general. ed. Academician of the RAS A.L. Stempkovsky, Moscow publ, IPPM RAS, 2016, Part I. P. 70-77. (in Russian).
- [22] N.I. Chernov, V.Y. Yugai, N.N. Prokopenko, N.V. Butyrlagin, "Basic concept of linear synthesis of multivalued digital structures in linear spaces," Proceedings of IEEE East-West Design and Test Symposium, EWDTs 2014, art. no. 7027045. DOI: 10.1109/EWDTs.2014.7027045
- [23] N.N. Prokopenko, N.V. Butyrlagin, N.I. Chernov, V.Ya. Yugai, "The linear concept of logical synthesis of digital IP-modules of control and communication systems," Proceedings of International Siberian Conference on Control and Communications, SIBCON 2015, art. no. 7147182. DOI: 10.1109/SIBCON.2015.7147182.
- [24] N.N. Prokopenko, N.V. Butyrlagin, N.I. Chernov, V.Ya. Yugai, "Basic linear elements of k-Valued digital structures," Proceedings of International Conference on Signals and Electronic Systems, ICSES 2016, pp. 7-12. DOI: 10.1109/ICSES.2016.7847763.
- [25] N.N. Prokopenko, N.I. Chernov, V. Yugai, N.V. Butyrlagin, "The element base of the multivalued threshold logic for the automation and control digital devices," Proceedings of 2017 IEEE International Siberian Conference on Control and Communications, SIBCON 2017, art. no. 7998508. DOI: 10.1109/SIBCON.2017.7998508.
- [26] N.N. Prokopenko, N.I. Chernov, V. Yugai, N.V. Butyrlagin, "The multifunctional current logical element for digital computing devices, operating on the principles of linear (not boolean) algebra," Proceedings of 2016 IEEE East-West Design and Test Symposium, EWDTs 2016, art. no. 7807723. DOI: 10.1109/EWDTs.2016.7807723.
- [27] N. Chernov, N. Prokopenko, V. Yugai, N. Butyrlagin "Linear algebra as an alternative approach to the synthesis of digital devices of automation and control systems", Advances in Science, Technology and Engineering Systems Journal, vol. 3, no. 1, pp. 168-190 (2018).

CSFs for the Implementation of the Hybrid Lean ERP System. Stakeholders Interactions

Mariam Houti*, Laila El Abbadi, Abdellah Abouabdellah

Systems Engineering Laboratory, National School of Applied Sciences of Kenitra, Ibn Tofail University, PoBox 241, Morocco

ARTICLE INFO

Article history:

Received: 21 October, 2019

Accepted: 12 December, 2019

Online: 25 December, 2019

Keywords:

Lean ERP

CSFs

Performance

Stakeholders

ABSTRACT

Lean ERP system is considered among the new trends of systems in the manufacturing sector, it has become one of the most widely adopted systems, thanks to its various benefits such as: a centralized database which gathers all the data of the enterprise in a single database which is accessible to all the departments, reduction in costs, high performance and best quality and many other advantages. However, many companies are starting the implementation of the hybrid Lean ERP system without prior study of the project. This may lead to its improper implementation which can impact negatively the enterprise and its stakeholders.

It is in this context that our study aims to help future companies wishing to implement the hybrid Lean ERP system, through identification, study and an analysis of critical success factors (CSFs) of Lean ERP necessary to this implementation, while focusing on different groups of stakeholders and their interactions with CSFs.

1. Introduction

As businesses in manufacturing and service sectors are increasingly subject to global competition, the highly variable demand from customers and the growing variety of products on the market [1], enterprises face several challenges in order to maintain their places in the market, which requires the improvement of their performance and competitiveness [2,3]. Otherwise, it encourages them to increase productivity and product quality, reduce costs and cycle times, be more flexible and respect delivery deadlines [4].

In order to cope with these fluid conditions, manufacturers often use two strategies to face these challenges: implementing Lean practices and integrating information and communication systems, in particular ERP systems "Enterprise Resource Planning" [3]. This combined implementation gave birth to the new hybrid Lean ERP system, that combines the entire database of all department in a centralized one.

A good implementation of the hybrid Lean ERP system offers several benefits to the enterprise and its stakeholders through a significant reduction in costs, operating time and a considerable increase in performance and quality (which could be traced from raw material to finished good) which leads to: responding quickly to customer's needs. However, if the implementation is not well achieved, it could lead to serious problems and losses. It is

therefore important to take into account the different parts of the company and critical success factors (CSFs) to ensure the successful implementation of the hybrid system.

The purpose of this Research is to identify Critical Success Factors (CSFs) for the implementation of the hybrid Lean ERP system, then study the degree of influence of the CSFs in order to extract the most decisive factors during implementation. Afterward, explore the role of stakeholders in the implementation of the hybrid system, in order to categorize which factors directly influence them, for the purpose of a successful implementation within the enterprise and its stakeholders.

2. CSFs For Lean ERP System

Critical success factors are all elements to consider when setting up or upgrading a new system, to optimize resources and effort by focusing on the important elements that contribute to successful implementation or upgrade. As a result, many researchers had shed more light on those factors (CSFs) and defined them according to their own points of view; the reason why we find different definition to CSFs in the literature.

Critical success factors usually vary from one industry to another, they define the elements influenced by the decisions of the top management and could affect the global competitive position of diverse sectors of an industry [5]. CSFs tend to relate more to how an organization approaches the change effort versus

*Corresponding Author: Mariam Houti | Email: Mariam.houti@gmail.com

change method specific factors. Even though certain authors bring up key aspects for the specific change method, most CSF are fairly general in nature [6]. Houti concluded that the concept of critical success factors is one of the important elements that influence the success of any organization. It should be used when implementing a system. As they are among the few elements that guarantee successful implementation in all phases: pre-implementation, implementation and post-implementation. While ensuring the sustainability of the system, through the use of factors of measurement of profitability and performance, as well as the respect of the different characteristics and conditions imposed in the specifications of the business [4]. Knowing that CSFs can have a direct positive or negative effect on the performance of the business. In fact, if they are well identifiable and applied, they can lead to the achievement of the business. On the other hand, if they are not used accurately they can lead to failure [4].

Several authors have discussed the critical factors whether success or Failure. Researchers have already identified according to the literature that CSFs affecting the implementation of both production systems, namely: Lean Manufacturing and ERP system. Our study is based on the work established by Houti and al., [4, 2] to gather the most critical success factors of Lean ERP system. It will be necessary to identify factors of success to guarantee an effective implementation of the combined system.

Our study allowed us to identify 20 different critical factors of success during the Implementation of the combined Lean ERP system. They cover the categories of management, resources and organizations, as well as the phases of implementation the Lean ERP system. The factors gathered are listed in the table 1:

Table 1. CSFs for Lean ERP implementation

N°	CSFs
C 1.	Top management support and commitment
C 2.	Project management and planning
C 3.	Change management / Organizational culture / Political issues;
C 4.	Business plan and a clear vision;
C 5.	Training and education;
C 6.	Effective Interdepartmental communication;
C 7.	Dedicated resources;
C 8.	Adequate ERP software selection and good Lean tools;
C 9.	Project monitoring and evaluation of performance;
C 10.	Active, strategic and visionary leadership;
C 11.	Suitable IT legacy systems;
C 12.	Interdepartmental cooperation;
C 13.	Skills and expertise;
C 14.	Involvement of stakeholders;
C 15.	Management of expectations;
C 16.	Implementation Strategies;
C 17.	Business Process Reorganization (BPR);
C 18.	Project selection and prioritization;
C 19.	On-going support (Customer, vendor);
C 20.	Motivation;

2.1. Degree of Influence Of Csf For Lean ERP Implementation

These 20 CSFs identified above have several interactions with each other. Our study is established thanks to an effective collaboration with a team of researchers and industrialists, in order to extract the different relations existing between each of these

factors, and which are visualized later using the vectograph drawing method, represented in FIG. 1, where:

- The “X” represents the factors on the columns influence the factors on the rows.
- The “O” represents the factors on the rows influence the factors on the columns;

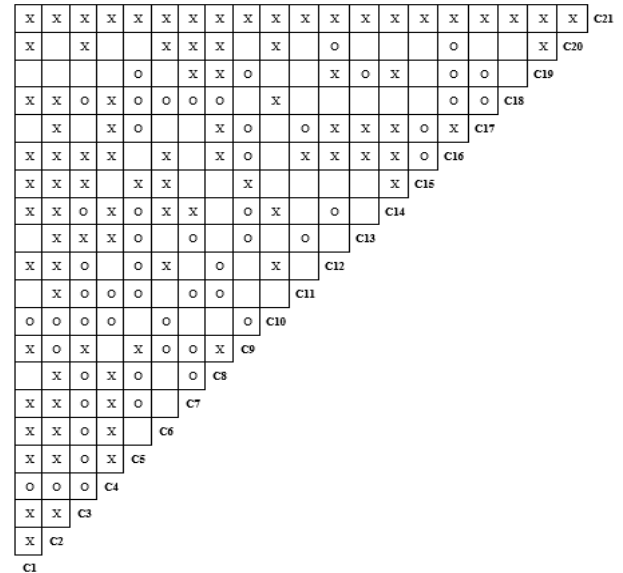


Figure 1. The influence among the different CSFs in Lean ERP implementation

The analysis of the figure 1 above, allowed us afterwards to draw the binary matrix [M] which is illustrated in figure 2, to better visualize the influence of each factor separately, Then, through calculating the degree of influence of each factor, the result matrix could be plotted, where: 1 represents an influence and 0 doesn't represent any influence;

By analyzing the resulting matrix [M], we can conclude that there are 11 levels of influence, distributed as follows in Table 2:

These CSFs's levels and degrees of influence will contribute to an easy implementation of the Lean ERP combined system; Starting with the first levels of influence (high influence factors), it will contribute indirectly to the establishment of other factors influenced factors; This will automatically facilitate the implementation of the other CSFs, and thus a quick implementation of the hole system.

3. Stakeholders Role in Lean ERP Implementation

Stakeholders could be defined as the different parts involved in a process, hence their positive or negative impact; depending on their degree of contribution and influence on the project. Knowing that close cooperation of stakeholders is necessary for the success of the project [7].

Identifying how stakeholders influence the success of project through a continuous development of their relationships, is an important and fundamental issue of stakeholder management, that remain an account for the success of projects [8], and an important issue in project management [9]. It is necessary to know how the stakeholders can be influenced, so they support and contribute to the project [10]; As a project can be seen as a temporary coalition of stakeholders pursuing an aim together [7,9].

	C1	C2	C3	C4	C5	C6	C7	C8	C9	C10	C11	C12	C13	C14	C15	C16	C17	C18	C19	C20	C21	
C1	1	1	1	0	1	1	1	0	1	0	0	1	0	1	1	1	0	1	0	1	1	} (13 14 6 13 4 7 6 8 5 11 7 6 8 9 1 4 5 8 7 3
C2	0	1	1	0	1	1	1	1	0	0	1	1	1	1	1	1	1	1	0	0	1	
C3	0	0	1	0	0	0	0	0	1	0	0	0	1	0	1	1	0	0	0	1	1	
C4	1	1	1	1	1	1	1	1	0	0	0	0	1	1	0	1	1	1	0	0	1	
C5	0	0	1	0	1	0	0	0	1	0	0	0	0	0	1	0	0	0	0	0	1	
C6	0	0	1	0	0	1	0	0	0	0	0	1	0	1	1	1	0	0	0	1	1	
C7	0	0	1	0	1	0	1	0	0	0	0	0	0	1	0	0	0	0	1	1	1	
C8	0	0	1	0	1	0	1	1	1	0	0	0	0	0	0	1	1	0	1	1	1	
C9	0	1	0	0	0	1	1	0	1	0	0	0	0	0	1	0	0	0	0	0	1	
C10	1	1	1	1	0	1	0	0	1	1	0	1	0	1	0	0	1	0	1	0	1	
C11	0	0	1	1	1	0	1	1	0	0	1	0	0	0	0	1	0	0	0	0	1	
C12	0	0	1	0	1	0	0	1	0	0	0	1	0	0	0	1	1	0	1	0	1	
C13	0	0	0	0	1	0	1	0	1	0	1	0	1	0	0	1	1	0	0	0	1	
C14	0	0	1	0	1	0	0	0	1	0	0	1	0	1	1	1	1	0	1	0	1	
C15	0	0	0	0	0	0	0	0	0	0	0	0	0	0	1	0	0	0	0	0	1	
C16	0	0	0	0	0	0	0	0	1	0	0	0	0	0	1	1	1	0	0	0	1	
C17	0	0	0	0	1	0	0	0	1	0	1	0	0	0	1	0	1	0	0	0	1	
C18	0	0	1	0	1	1	1	1	0	0	0	0	0	0	0	1	1	1	0	0	1	
C19	0	0	0	0	1	0	0	0	1	0	0	0	1	0	0	1	1	0	1	1	1	
C20	0	0	0	0	0	0	0	0	0	0	0	1	0	0	0	1	0	0	0	1	1	

Table 2. CSFs's Degree of influence

Level	Degree Of Influence	Factors
Level 1	14	C2
Level 2	13	C1 C4
Level 3	11	C10
Level 4	9	C14 C8
Level 5	8	C18 C13
Level 6	7	C11 C19 C6
Level 7	6	C12 C3 C7
Level 8	5	C17 C9
Level 9	4	C16 C5
Level 10	3	C20
Level 11	1	C15

The implementation of Lean ERP system is one of the complex project that need contribution and engagement of all part of the enterprises, due to the changes that will involve stakeholders.

These stakeholders typically have multiple and often conflicting interests and rarely agree on a set of common objectives [11].

3.1. Classification according to Stakeholders Group

Stakeholder involvement is essential when implementing a system such as Lean ERP; That provides high customer service and shorter lead times [12], which involves different parts of the enterprises. why is it important to consider the different categories of stakeholders to allow each group to focus on the relevant CSFs. Figure 3 shows the important groups of stakeholders. The Lean ERP implementation project involves all parts of the business. Therefore, the assessment of stakeholder groups is one of the important steps to establish when implementing the combined system.

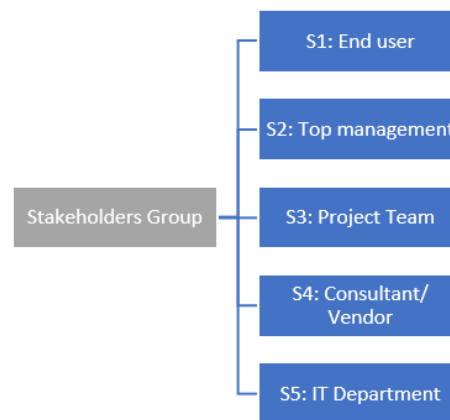


Figure 3. Classification of stakeholders groups

3.2. Stakeholder Assessments

Stakeholder assessments can assist planners to identify the interests, groups and individuals that are stakeholders in planning exercises, as well as their values, interests and relative power [13]. This can help to proactively determine ways to reduce negative impacts on the groups with less influence and power within the enterprise. A thorough stakeholder analysis can also identify potential conflicts or risks that could jeopardize the project, as well

Table 3. Analysis of Stakeholder assessments

Stakeholders	Role	Influence	Expectation	Issues
End user	<ul style="list-style-type: none"> Provide all the necessary business processes Effective communication of IT needs of the enterprise and its consultants 	Low influence	<ul style="list-style-type: none"> solved Business process Centralized system offering real and accurate information 	<ul style="list-style-type: none"> Lack of involvement in decision-making
Top Management	<ul style="list-style-type: none"> Provide the resources needed to implement the project Set up a road map and an execution plan Ensure stakeholders involvement 	Medium influence	<ul style="list-style-type: none"> Successful implementation of the combined system Minimize waste, reduce costs to increase profits 	<ul style="list-style-type: none"> Lack of support and ongoing commitment Implementation of other projects in parallel that minimize starting resources
Project Team	<ul style="list-style-type: none"> Application of business plans developed by Top Management Good use of available resources Adopt lean philosophy throughout the implementation of the Lean ERP system Ensure stakeholders involvement 	High influence	<ul style="list-style-type: none"> Accurate monitoring of the plans and processes put in place Provide relevant employees with the necessary information and documentation in real time, with precision. 	<ul style="list-style-type: none"> Anxious to be replaced by the new system
Consultant / Vendor	<ul style="list-style-type: none"> Work methodically with internal stakeholders Provide all the necessary documentation and training Ensure the successful implementation of the system 	High influence	<ul style="list-style-type: none"> Successful and efficient implementation of the combined system Collaboration and support of internal stakeholders 	<ul style="list-style-type: none"> Lack of cooperation from internal stakeholders
IT Department	<ul style="list-style-type: none"> Technical support Collaboration with consultant/ Vendor and Project Team to guarantee an effective implementation of the combined system 	Low influence	<ul style="list-style-type: none"> Consolidation of decentralized IT groups Creation of a centralized IT department 	<ul style="list-style-type: none"> Lack of cooperation Lack of involvement in decision making process

as opportunities and strategies for stakeholder engagement during implementation. Therefore, it is imperative to identify and engage all stakeholders early on in the project to ensure the proper measures are in place to manage the different characteristics of these stakeholders. Taking this initiative will increase the likelihood of successful implementation and adoption of the enterprise system [14]. Table 3 summarizes the assessment of stakeholder's groups including their role, degree of influence, expectations and issues related to Lean ERP implementation.

The stakeholder groups mentioned above have multiple interactions with each other within the organization, which is essential to the smooth running of the business, which has prompted our team of researchers and industrialists to draw the matrix [S](Figure 4) which standardize the degree of similarity and interactions over an interval of 0 to 1.

$$S = \begin{matrix} & \begin{matrix} S1 & S2 & S3 & S4 & S5 \end{matrix} \\ \begin{matrix} S1 \\ S2 \\ S3 \\ S4 \\ S5 \end{matrix} & \left\{ \begin{array}{ccccc} 1 & & & & \\ 0.9 & 1 & & & \\ 1 & 0.9 & 1 & & \\ 0.4 & 0.7 & 0.8 & 1 & \\ 0.9 & 0.5 & 0.9 & 0.7 & 1 \end{array} \right\} \end{matrix}$$

Figure 4. The binary Matrix [S]

Afterwards, we used the color-coding approach in figure 5 to illustrate the different interactions of the stakeholder network. The color ranges from turquoise to gray to indicate the degree of interaction of the stakeholder network. If the links colors are closer

to gray then we have a higher degree, which means that related stakeholders have a closer connection and stronger influence over each other. On the other hand, the colors closer to turquoise are not very marked, which means that the related stakeholders have a fragile relationship and a weaker influence on each other. Table 4 presents this classification that will help stakeholders of the enterprise to focus on factors that affect them.

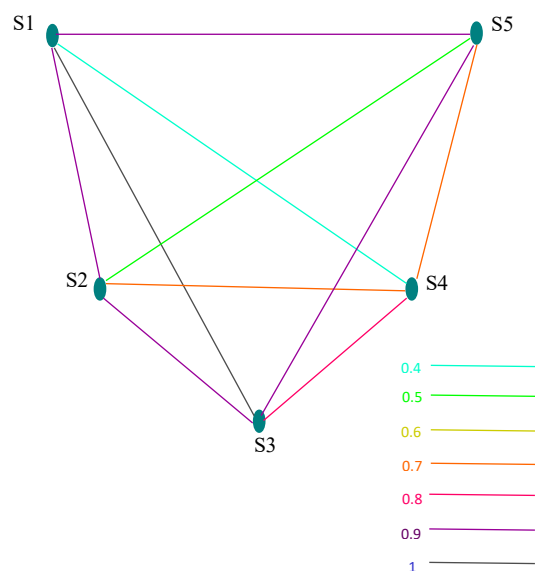


Figure 5. Relationships among Stakeholders network

Consequently, a classification according to Stakeholders Group of CSFs gathered during the previous study will be established to help further enterprises and its stakeholders to focus on CSFs that affect them directly in order to reach a better performance and a successful implementation of the hybrid Lean ERP system.

Table 4. Classification of Lean ERP CSFs according to stakeholders group

CSF \ Stakeholders Group	S1	S2	S3	S4	S5
C1.		X			
C2.		X	X		
C3.		X	X		
C4.		X			
C5.	X		X		X
C6.	X		X		
C7.		X			X
C8.		X		X	X
C9.			X		
C10.		X			
C11.					X
C12.	X		X		
C13.			X	X	X
C14.	X				
C15.		X	X	X	
C16.		X			X
C17.	X	X		X	
C18.		X		X	
C19.	X			X	
C20.		X	X		

4. Conclusion

The Lean ERP system has become the most widely adopted system by enterprises, as long as the many advantages that presents. However, the high cost of implementation and the risk of failure can lead to several critical issues within the enterprise and its different stakeholders, which could be solved by taking into account the CSFS and involving different stakeholders groups during the implementation of the hybrid system.

This article has enabled us to extract, 20 most CSFs to be used when implementing the hybrid Lean ERP system, thereafter study in more detail their degree of influence to further identify the factors to take into account as a priority, depending on their Level of influence, in order to simplify the implementation of other factors that affect them. Thereafter analyze the importance of the identified stakeholder groups (End user, Top Management, Project

Team, Consultant / Vendor, IT Department) and study their interactions to help future enterprises wishing to implement the hybrid system and their stakeholders to concentrate on the CSFs that directly affect each Stakeholder group in order to achieve better performance and successful implementation of the hybrid Lean ERP system.

5. References

- [1] Houti, M., El Abbadi, L., Abouabdellah, A., "E-Kanban the new generation of traditional Kanban system, and the impact of its implementation in the enterprise", Proceedings of the International Conference on Industrial Engineering and Operations Management, IEOM., Rabat, Morocco, (Apr, 11-13), 2017.
- [2] Houti, M., El Abbadi, L., Abouabdellah, A., "External critical successful factors for a successful implementation of ERP systems", Proceedings of International Conference on Computers and Industrial Engineering, CIE., Lisbon, Portugal, (Oct, 11-13), 2017.
- [3] Houti, M., El Abbadi, L., Abouabdellah, A., "Lean ERP: A hybrid approach Push /Pull", Proceedings of the 3rd IEEE International Conference on Logistics Operations Management, GOL 2016., Fez, Morocco, (May, 23-25), 2016.
- [4] Houti, M., El Abbadi, L., Abouabdellah, A., "Critical Success Factors for Lean implementation "Projection on SMEs", Proceedings of the International Conference on Industrial Engineering and Operations Management, IEOM., Pilsen, Czech Republic, (Jul, 23-26), 2019.
- [5] Hofer, C. W., Schendel, D. A., "Strategy Formulation: Analytical Concepts", West Publishing Company, Saint Paul, 1978.
- [6] Dag, N., "Lean and Six Sigma – critical success factors revisited", *International Journal of Quality and Service Sciences*, Vol. 5, N°.1, (2013), pp. 86 - 100.
- [7] Jepsen, A.L., Eskerod, P., "Stakeholder analysis in projects: Challenges in using current guidelines in the real world", *International Journal of Project Management*, Vol. 27, (2009), pp. 335–343.
- [8] McElroy, B.; Mills, C. "Managing stakeholders", In Gower Handbook of Project Management; Turner, R.J., Simister, S.J., Eds.; Gower: Aldershot, UK, 2000.
- [9] Andersen, ES., "Prosjektledelse – et organisasjonsperspektiv", Bekkestua: NKI Forlaget, Oslo, 2005.
- [10] Lund Jepsen, A., Eskerod, P., "Stakeholder analysis in projects: Challenges in using current guidelines in the real world", *International Journal of Project Management*, Vol. 27, (2009), pp. 335–343.
- [11] Sudevan, S., Bhasi, M., Pramod, K.V., "Interpreting Stakeholder Roles in ERP Implementation Projects: A Case Study", *International Journal of Computer Science and Information Technologies*, Vol. 5 (3), (2014), pp. 3011-3018.
- [12] Houti, M., El Abbadi, L., Abouabdellah, A., "How Could an Urgent Order Disturb the Supply Chain? Case S tudy of an Automotive Industry", *International Journal of Engineering & Technology*, Vol. 7(4.16), (2018), pp. 155-159.
- [13] Medeiros de Araujo. L., Bramwell. B., "Stakeholder Assessment and Collaborative Tourism Planning: The Case of Brazil's Costa Dourada Project", *Journal of Sustainable Tourism*, Vol. 7(3-4), (1999), pp.356–378.
- [14] McLaren, T., Jariri, I., "Stakeholder Assessment and Management for Enterprise Systems Implementation Projects", International Conference on Information Resources Management, CONF-IRM 2012 Proceedings, Association for Information Systems AIS Electronic Library (AISeL) (sep, 26), 2012.